R.A. Cushman

ANL-7520
Part I

ANL-7520
Part I

ARGONNE
NATIONAL LABORATORY

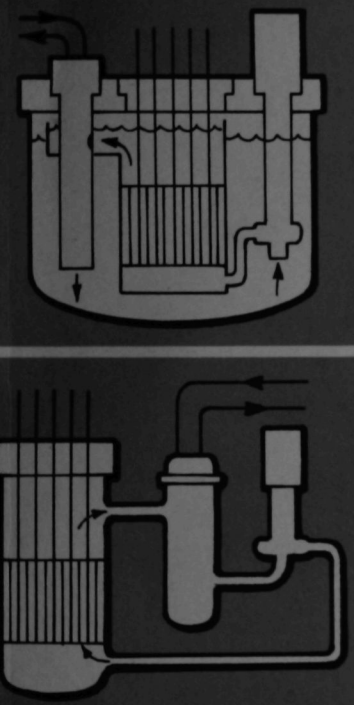

Proceedings of the International Conference on SODIUM TECHNOLOGY and LARGE FAST REACTOR DESIGN

November 7-9, 1968

Part I
Sessions on
Sodium Technology

The facilities of Argonne National Laboratory are owned by the United States Government. Under the terms of a contract (W-31-109-Eng-38) between the U. S. Atomic Energy Commission, Argonne Universities Association and The University of Chicago, the University employs the staff and operates the Laboratory in accordance with policies and programs formulated, approved and reviewed by the Association.

MEMBERS OF ARGONNE UNIVERSITIES ASSOCIATION

The University of Arizona
Carnegie Institute of Technology
Case Institute of Technology
The University of Chicago
University of Cincinnati
Illinois Institute of Technology
University of Illinois
Indiana University
Iowa State University
The University of Iowa
Kansas State University
The University of Kansas
Loyola University
Marquette University
Michigan State University
The University of Michigan
University of Minnesota
University of Missouri
Northwestern University
University of Notre Dame
The Ohio State University
Purdue University
Saint Louis University
Washington University
Wayne State University
The University of Wisconsin

LEGAL NOTICE

This report was prepared as an account of Government sponsored work. Neither the United States, nor the Commission, nor any person acting on behalf of the Commission:

A. Makes any warranty or representation, expressed or implied, with respect to the accuracy, completeness, or usefulness of the information contained in this report, or that the use of any information, apparatus, method, or process disclosed in this report may not infringe privately owned rights; or

B. Assumes any liabilities with respect to the use of, or for damages resulting from the use of any information, apparatus, method, or process disclosed in this report.

As used in the above, "person acting on behalf of the Commission" includes any employee or contractor of the Commission, or employee of such contractor, to the extent that such employee or contractor of the Commission, or employee of such contractor prepares, disseminates, or provides access to, any information pursuant to his employment or contract with the Commission, or his employment with such contractor.

Printed in the United States of America
Available from
Clearinghouse for Federal Scientific and Technical Information
National Bureau of Standards, U. S. Department of Commerce
Springfield, Virginia 22151
Price: Printed Copy $3.00; Microfiche $0.65

ANL-7520 Part I
Reactor Technology

Argonne National Laboratory
9700 South Cass Avenue
Argonne, Illinois 60439

Proceedings of the International Conference on SODIUM TECHNOLOGY and LARGE FAST REACTOR DESIGN

November 7–9, 1968

Part I. Sessions on Sodium Technology

Conference Chairman
D. Okrent

Program
J. E. Draley, Sodium Technology
L. W. Fromm, Large Fast Reactor Design

N. LONG
K. GOLDMAN
P. JONES

EXIT

G. DENELCU
M. NOZAWA
K. WIRTZ

Preface

This report is the proceedings of the fourth of a series of topical conferences sponsored by Argonne National Laboratory and the United States Atomic Energy Commission on specific topics related to the development of fast power breeder reactors. It is bound in two volumes: Part I contains papers presented at the Sessions on Sodium Technology, and Part II contains papers presented at the Sessions on Large Fast Reactor Design. The Table of Contents in each volume lists all of the papers presented at the conference.

The Proceedings of the first of these conferences, held in October 1963 and entitled "Breeding Economics and Safety in Large Fast Power Reactors," were issued as ANL-6792. The proceedings of the second, held in October 1965 on "Safety, Fuels, and Core Design in Large Fast Power Reactors," were issued as ANL-7120. The proceedings of the third conference, held in October 1966 on "Fast Critical Experiments and Their Analysis," were issued as ANL-7320. A related conference on "The Physics of Breeding" was held at Argonne in October 1959, with the proceedings issued as ANL-6122.

We at Argonne appreciate very much the assistance of all who participated in this conference. In particular, the open discussion and the willingness to examine controversial questions contributed to the value of these meetings. The cooperation and last-minute efforts of the speakers during the first informal session on Sodium Technology and in the final general discussion periods warrant special thanks. We wish also to express our appreciation to the U. S. Atomic Energy Commission and the participating organizations from abroad for making possible such meetings in which recent development on specific topics are reviewed and the basis for a cooperative effort on the remaining problems established.

These proceedings have been edited by J. E. Draley, L. W. Fromm, A. Glassner, Joyce Kopta, and D. Okrent, with the direct assistance of the scientific secretaries of the various sessions. In the interest of hastening publication, the speakers have not been given an opportunity to edit the discussions. The editors hope that a reasonable portrayal of the actual discussion has been accomplished.

I wish to acknowledge the able guidance and assistance provided by J. E. Draley and L. W. Fromm in formulating the Program. Finally, on behalf of all the participants, I express our appreciation of the efficient manner in which Dorothy Carlson, Gail Ahlvin, Rosalie Deskin, and Elizabeth Wallis handled the myriad of administrative details and thereby contributed to an effective meeting.

D. Okrent
Conference General Chairman

Table of Contents

SESSIONS ON SODIUM TECHNOLOGY

SESSION ST-I

November 7, 1968

Chairman: J. E. Draley, Argonne National Laboratory

Introductory Remarks 3
J. E. Draley, *Argonne National Laboratory*
Reports to the Conference on the November 5 and 6, 1968 IAEA Specialists' Meeting on Sodium-Water Reactions 4
R. H. Jones, Moderator, *U. S. Atomic Energy Commission*
Participants: D. A. Yashin, *International Atomic Energy Agency*
K. Furukawa, *Japan*
J. A. Bray, *United Kingdom*
K. Goldmann, *United States of America*
N. Lions, *France*
H. Mausbeck, *Federal Republic of Germany*
Sodium Boiling in Fast Reactors. A Review with Reference to the Ispra Conference 12
D. Smidt, *Karlsruhe*
INTRODUCTION: Impurities Expected in LMFBR Sodium and Their Significance 17
J. R. Humphreys, Jr., Moderator, *Argonne National Laboratory*
Impurity Considerations in the National Plan 18
J. M. McKee, *Argonne National Laboratory*
Estimation of Impurity Levels in LMFBR from Solubility Data, and Comparison with Impurity Behavior in Loops 21
J. R. Weeks, *Brookhaven National Laboratory*
Identification of Sodium-impurity Species by Analysis of Cold-trap Contents 25
S. J. Rodgers, *MSA Research Corp.*
Alkaline Earth Impurities in Sodium 33
L. F. Epstein, *Argonne National Laboratory*

SESSION ST-II

November 7, 1968

Chairman: J. H. DeVan, Oak Ridge National Laboratory

Effect of High-temperature Sodium on the Mechanical Properties of Candidate Alloys for the LMFBR Program 41
L. H. Kirschler and R. C. Andrews, *MSA Research Corp.*
Influence of Sodium and of Irradiation on the High-temperature Creep Behavior of Certain Stainless Steels 55
J. P. Andre, J. Beaufrere, L. Valibus, and A. Weisz, *CEA-EDF*
Creep under High Heat Flux and Stress-rupture Properties of Austenitic Stainless Steels in Elevated-temperature Sodium 74
J. H. Shively, D. F. Atkins, and W. T. Lee, *Atomics International*
Influence of Grain Size and Work Hardening on the Carburization of Austenitic Stainless Steels in Liquid Sodium 93
L. Valibus, *Electricité de France*
Carburization of Austenitic Stainless Steel by Sodium 104
M. Kolodney, *United Nuclear Corp.*
Friction and Wear in Liquid Metals 110
P. Barrau, J. P. Fontaine, *Electricité de France*, and B. Morin, *CEN-Cadarache*
Test Program for Components in Liquid Sodium 125
E. Arend and H. Wagener, *LUXATOM*

SESSION ST-IIIA
November 8, 1968

Chairman: J. R. Weeks, Brookhaven National Laboratory

Mass Transport and Corrosion of Stainless Steels in Flowing Sodium Systems at 1300°F ... 131
P. Roy, G. P. Wozadlo, and F. A. Comprelli, *General Electric Co.*
Mass-transfer Phenomena of the Austenitic Stainless Steels in the Loop of Sodium with a High Temperature and High Flow Velocity ... 143
K. Furukawa and I. Nihei, *Japan Atomic Energy Research Institute*
Kinetic Aspects of Corrosion of Steels in Flowing Sodium ... 150a
L. Champeix and O. Konovaltschikoff, *CEN-Saclay*
Preliminary Corrosion Results of Haynes 25 and Type 304 Stainless Steel with 4 and 12 ppm Oxygen in Sodium at Temperatures up to 760°C ... 151
A. J. Romano, S. J. Wachtel, and C. J. Klamut, *Brookhaven National Laboratory*
Corrosion and Fretting Corrosion in Sodium ... 153
A. J. Bogers, E. G. Chirer, J. W. Tichler, and A. W. J. deGee, *Metal Research Institute TNO*
Corrosion Studies of Stainless Steel in Flowing Sodium at High Heat Flux ... 163
J. Hopenfeld, *Atomics International*
The Effect of Oxygen in Sodium on the Compatibility of Sodium with Niobium ... 171
R. L. Klueh, *Oak Ridge National Laboratory*
Development of High-strength Vanadium-base Alloys with Improved Corrosion Resistance in Cold-trapped Liquid Sodium ... 177
H. Böhm and H. U. Borgstedt, *Karlsruhe*
The Corrosion of Vanadium and Vanadium-base Alloys in Sodium ... 182
W. E. Ruther, *Argonne National Laboratory*

SESSION ST-IIIB
November 8, 1968

Chairman: J. C. Biery, Los Alamos Scientific Laboratory

Characterization of Sodium Pool Fires ... 195
R. P. Johnson, M. Silberberg, J. Hopenfeld, and P. Beiriger, *Atomics International*
Cover-gas Impurities and Their Interactions with Sodium ... 206
G. B. Barton and H. P. Maffei, *Battelle Northwest Laboratory*
Sodium Sampling and Analytical Experience at EBR-II ... 213
C. C. Miles, E. R. Ebersole, and W. H. Olson, *Argonne National Laboratory*
Impurities in EBR-II Sodium and Cover Gas ... 222
W. H. Olson, C. C. Miles, and D. W. Cissel, *Argonne National Laboratory*
An Integral Full-flow Vacuum Distillation Sampling System for Use in a High-temperature Radioactive Sodium Environment ... 227
V. J. Rutkauskas, *Los Alamos Scientific Laboratory*
Impurity Monitoring in a Large Sodium Test Loop ... 233
J. E. Meyers and R. A. Hunter, *Atomic Power Development Associates*
Engineering Development and Performance of the UNC Carbon Meter ... 254
W. H. Caplinger and G. Stern, *United Nuclear Corp.*
An Electrochemical Meter for Hydrogen in Sodium ... 262
R. B. Holden and N. Fuhrman, *United Nuclear Corp.*

SESSION ST-IVA
November 8, 1968

Chairman: S. Lawroski, Argonne National Laboratory

Preparation of High-purity Sodium for Chemistry Studies ... 271
R. L. McKisson and R. L. Eichelberger, *Atomics International*
Analytical Methods for Determining Impurities in Sodium below 10 ppm ... 278
C. D. Bingham, J. M. Scarborough, and M. S. Maseda, *Atomics International*
A Direct Method for the Determination of Carbon in Sodium ... 284
E. Berkey and W. M. Hickam, *Westinghouse Research Laboratories*
Trace-element Behavior in Sodium ... 291
R. J. Meyer, C. E. Johnson, and L. E. Ross, *Argonne National Laboratory*

Solubilities of Nitrogen Gas and Sodium Cyanide in Liquid Sodium 295
E. Veleckis, K. E. Anderson, F. A. Cafasso, and H. M. Feder, *Argonne National Laboratory*
Solubility of Cobalt and Nickel in Sodium 299
P. K. Lee and E. Berkey, *Westinghouse Research Laboratories*
On the Solubilities of Cu, Ni, and Fe in Liquid Sodium 309
R. M. Singer and J. R. Weeks, *Brookhaven National Laboratory*
The Solubility of Cu, Mo, Nb, Fe, Ni, and Cr in High-purity Sodium 319
R. L. Eichelberger and R. L. McKisson, *Atomics International*

SESSION ST-IVB
Friday Afternoon, November 8, 1968

Chairman: G. W. Wensch, U. S. Atomic Energy Commission

Performance Limits of Materials for Sodium-heated Steam Generators 327
F. A. Comprelli, J. L. Krankota, and C. N. Spalaris, *General Electric Co.*
Tests of a Tube-in-Tube Sodium-heated Steam Generator 335
E. Büscher, W. Jansing, H. Knuth, and H. Mausbeck, *Interatom*
Detection of Small Leaks by Hydrogen Measurements in a Sodium-heated Steam Generator 345
J. Birault, A. Brachet, E. Cambillard, J. Coron, L. Lannou, and C. Rault, *CEA-EDF*
Status of Sodium-Water Reaction Test Work at INTERATOM 374
K. Dumm, H. Mausbeck, and W. Schnitker, *Interatom*
Wastage of Steam-generator Materials by Sodium-Water Reactions 384
H. V. Chamberlain, J. H. Coleman, E. C. Kovacic, and A. A. Shoudy, *Atomic Power Development Associates*
Evaluation of Sodium-removal Methods for Fuel Elements and Piping Systems 410
G. R. Bloom, *Battelle Northwest Laboratory*
Sodium Evaporation in an Argon Flow 418
J. Van Dievoet, A. Michel, and R. Lanckman, *Belgonucléaire*
Water Cleaning and Air Storage Effects on Sodium-exposed Fuel Clad Alloys, 304 and 304L Stainless Steel 426
F. A. Smith, E. L. Kimont, and L. H. Bohne, *Argonne National Laboratory*

SESSION ST-VA
November 9, 1968

Chairman: J. R. Humphreys, Jr., Argonne National Laboratory

An Evaluation of Carbon Activity Sources in Sodium 441
J. M. McKee and W. H. Caplinger, *United Nulcear Corp.*
Carbon Impurities in Sodium System Cold Traps 448
D. Dutina, J. L. Simpson, and R. S. Young, *General Electric Co.*
Carbon Transport in Liquid Sodium 455
C. Luner, H. M. Feder, and F. A. Cafasso, *Argonne National Laboratory*
A Study of Reactions between Oxygen and Impurities in Sodium 460
H. S. Isaacs, B. Minushkin, and F. J. Salzano, *Brookhaven National Laboratory*
The Determination of Oxygen Concentration and Mass-transfer Coefficients in Sodium Using Uranium 465
H. S. Isaacs, *Brookhaven National Laboratory*
Oxygen Transport in Sodium 471
C. C. McPheeters and J. C. Biery, *Los Alamos Scientific Laboratory*
Calculated Hydrogen-Oxygen Equilibria in Liquid Sodium 477
P. Vilinskas, *Argonne National Laboratory*
Some Effects of Hydrogen Compounds in Sodium Loops 481
J. L. Simpson, D. Dutina, and L. E. Pohl, *General Electric Co.*
The Reaction of HCl with Liquid Sodium and a Sodium-Barium Alloy 490
M. R. Hobdell and L. Newman, *Brookhaven National Laboratory*

SESSION ST-VB
November 9, 1968

Chairman: R. W. Dickinson, Liquid Metal Engineering Center

Design of FFTF Closed Loops 501
M. A. Vogel, *Battelle Northwest Laboratory*
Liquid Sodium Technology Development (II). Sodium Loop Components and Related Techniques 506
K. Furukawa, K. Yamamoto, I. Nihei, and M. Kamei, *Japan Atomic Energy Research Institute*
Status of Sodium Components Technology in Italy 515
G. Fogagnolo, F. Pierantoni, and A. Tarantini, *CNEN-Bologna*
The Distribution of Fission Products in LMFBR Sodium Systems 527
G. B. Zwetzig, J. Guon, and M. Silberberg, *Atomics International*
Radioisotope Transport and Deposition in Flowing Sodium 534
W. F. Brehm, E. A. Kovacevich, and D. W. Shannon, *Battelle Northwest Laboratory*
Fission Product Vaporization from Sodium Systems 540
A. W. Castleman, Jr. and I. N. Tang, *Brookhaven National Laboratory*
Vaporization of Fission Products from Sodium 549
B. D. Pollock, M. Silberberg, and R. L. Koontz, *Atomics International*
Behavior of Several Fission Products in the Atmosphere Surrounding Sodium-cooled Reactors in the Event of a Major Accident 555
Cl. Descamps, *Belgonucléaire*, C. Beaudet, and J. Rygaert, *S.E.R.A.I.*

SESSION ST-VI
November 9, 1968

Chairman: J. E. Draley, Argonne National Laboratory

General Discussion 565

Attendees 575

The following articles appear in Part II of this report

SESSIONS ON LARGE FAST REACTOR DESIGN

SESSION LFRD-I

November 7, 1968

Chairman: R. B. Duffield, Argonne National Laboratory

Sodium Technology Considerations in Fast Reactor Design 3
B. Wolfe and E. L. Zebroski, *General Electric Co.*

Status of Sodium Technology in France 20
J. P. Delisle, J. Faure, H. J. Gollion, J. P. Milliat, L. Vautrey, and J. Villeneuve, *CEA-EDF*

Operating Experience with EBR-II 24
G. E. Deegan, F. S. Kirn, H. Lawroski, and R. Neidner, *Argonne National Laboratory*

Remote Retrieval and Removal Operations in the Fermi Reactor 39
K. P. Johnson, *Power Reactor Development Corp.*, and J. Matte III, *Atomic Power Development Associates*

Rapsodie's First Year of Operation 52
G. Gajac, J. L. Ratier, M. Reboul, L. Reynes, and M. A. Valantin, *CEN-Cadarache*

SESSION LFRD-II

November 7, 1968

Chairman: M. Benedict, Massachusetts Institute of Technology

Safety Consideration in Setting the Design Criteria on the JAERI Design Studies 67
T. Iwaki, M. Nozawa, J. Takahashi, S. Terasawa, H. Shiozuka, and M. Fujita, *Japan Atomic Energy Research Institute*

Reference Concepts of the JAERI Large Fast Reactor Design Studies 77
M. Nozawa, T. Iwaki, J. Takahashi, S. Terasawa, H. Shiozuka, and M. Fujita, *Japan Atomic Energy Research Institute*

Special Engineering Problems Involved in the JAERI Design Studies 86
H. Shiozuka, M. Nozawa, T. Iwaki, J. Takahashi, S. Terasawa, and M. Fujita, *Japan Atomic Energy Research Institute*

Reasons for Choice of Major Mechanical Designs in the JAERI Design Studies 90
J. Takahashi, M. Nozawa, T. Iwaki, S. Terasawa, H. Shiozuka, and M. Fujita, *Japan Atomic Energy Research Institute*

Parametric Studies Leading to the Nuclear Characteristics of the JAERI Design Studies 99
S. Terasawa, M. Nozawa, T. Iwaki, J. Takahashi, H. Shiozuka, and M. Fujita, *Japan Atomic Energy Research Institute*

Plant System Parametric Study on Sodium-cooled Prototype Fast Breeder Reactor 110
H. Yoshimi, M. Nozawa, H. Shiozuka, Y. Nara, S. Terasawa, H. Yamamoto, J. Takahashi, and T. Iwaki, *Japan Atomic Energy Research Institute*

Testing of Feasibility of Ball Bearings in Liquid Sodium Environments 121
S. Iwai, M. Ishii, *Mitsubishi Atomic Power Industries*, M. Nozawa, T. Tamura, Y. Abe, *Japan Atomic Energy Research Institute*, A. Teramoto, and M. Akiyama, *Nippon Seiko K. K.*

Design Considerations and Experimental Program for the Common Development of a 300-MWe Sodium-cooled Fast Breeder Prototype SNR by a Belgian-Dutch-German Consortium 130
R. Harde, *Interatom*

The Sodium-CO_2 Fast Breeder Reactor Concept 147
J. P. Van Dievoet, *Belgonucléaire*

Plant Design Problems Associated with the Application of Vented Fuel to a Fast Breeder Reactor 154
L. Bruzzi, G. Gondoni, *CNEN-Bologna*, P. S. Lindsey, and R. E. Mueller, *Atomic Power Development Associates*

SESSION LFRD-III

November 8, 1968

Chairman: W. H. Zinn, Combustion Engineering, Inc.

Introductory Remarks on the 1000-MWe LMFBR Follow-on Study Program 169
L. W. Fromm, *Argonne National Laboratory*
Atomics International 1000-MWe LMFBR Follow-on Study Progress Report 171
R. E. Aronstein, E. B. Ash, D. F. Casey, S. Golan, and R. T. Lancet, *Atomics International*
Babcock & Wilcox 1000-MWe LMFBR Follow-on Study Reference Design 215
M. W. Croft, B. J. Goulding, D. R. Hostetler, and H. Honig, *Babcock & Wilcox*

SESSION LFRD-IV

November 8, 1968

Chairman: K. P. Cohen, General Electric Co.

Phenix: Status of the Design before Construction 243
R. Carle, J. P. Crette, J. Leduc, J. C. Moreau, M. Rozenholc, and J. Villeneuve, *CEA-GAAA-EDF*
Design Studies on the Reference Fast Power Plant (PCC-2) 254
G. Cicognani, G. Fogagnolo, F. Pierantoni, and A. Tarantini, *CNEN-Bologna*
PEC: Status of the Design before Construction 269
P. Aiello, G. Fogagnolo, F. Pierantoni, and R. Zona, *CNEN-Bologna*
Development and Evaluation of the Combustion Engineering Advanced 1000-MWe LMFBR Design 291
R. C. Noyes, J. C. Gilbertson, G. Menzel, J. J. Prabulos, Jr., and W. P. Staker, *Combustion Engineering, Inc.*
Transient Response of Heat Transfer and Thermal Stresses in Thick Walls of Sodium Components 331
N. Sagawa and S. Kawahara, *Hitachi, Ltd.*

SESSION LFRD-V

November 9, 1968

Chairman: W. J. McCarthy, Detroit Edison Co.

The Effect of Using Different Safety Criteria and Selected Safety Studies for a 1000-MWe Sodium-cooled Fast Reactor 345
P. M. Murphy, D. B. Sherer, and A. S. Gibson, *General Electric Co.*
Alternate Core Design Parameters and Economic Trade-offs for a 1000-MWe Sodium-cooled Fast Reactor 358
D. B. Sherer, W. A. Sangster, and F. W. Sciacca, *General Electric Co.*
Plant Design, System Optimization, and Equipment Selection for an Advanced LMFBR 369
A. S. Gibson, C. E. Boardman, and J. H. Germer, *General Electric Co.*
The Westinghouse 1000-MWe Follow-on Study 388
J. C. R. Kelly, Jr., A. Biancheria, C. A. Anderson, Jr., R. G. Hobson, and E. F. Beckett, *Westinghouse Electric Corp.*

SESSION LFRD-VI

November 9, 1968

Chairman: D. Okrent, Argonne National Laboratory

Panel Discussion 419

Attendees 431

SESSIONS ON SODIUM TECHNOLOGY

SESSION ST-I

Thursday Morning, November 7, 1968

Chairman: J. E. Draley
Argonne National Laboratory

Secretary: G. O. Haroldsen
Argonne National Laboratory

Introductory Remarks

J. E. Draley, Chairman

Argonne National Laboratory
Argonne, Illinois

Welcome to the Session on Special Topics in Sodium Technology. We have asked Ralph Jones from the U. S. Atomic Energy Commission to manage a review of the Proceedings of the International Atomic Energy Agency Panel on Sodium-Water Reactions. This panel meeting was held at Argonne yesterday and the day before. We have asked Dr. Smidt from Karlsruhe to summarize a meeting on Sodium Boiling which was held at Ispra in October, and we have asked Ross Humphreys of Argonne National Laboratory to organize a discussion which he has entitled "Impurities Expected in LMFBR Sodium and Their Significance."

Reports to the Conference on the November 5 and 6, 1968 IAEA Specialists' Meeting on Sodium-Water Reactions

RALPH H. JONES, Moderator

Division of Reactor Development and Technology
U. S. Atomic Energy Commission
Washington, D. C.

Introduction

RALPH H. JONES

Specialists' Meeting Chairman

Gentlemen, I am happy to see the turnout for our rather *ad hoc* panelist program.

As Chairman of the IAEA Specialist Meeting on Sodium-Water Reactions, I will hasten to explain several things. First, the Specialist Meeting was held on Tuesday and Wednesday of this week. Second, the Specialists representing each country participating in the meeting were endowed with their assignments on this panel just yesterday. Third, the Panelists prepared their statements last night and we have had no time to compare notes.

With this in mind, I believe we can proceed with what should be a very interesting exposé on a most interesting subject. Our plan is to have an official IAEA statement by Mr. Yashin, followed by reports by myself and representatives of each participating country giving appraisals of the meeting and summary reports on the subjects covered.

Purpose of IAEA Specialists' Meeting on Sodium-Water Reactions

DMITRI A. YASHIN, Scientific Secretary

International Atomic Energy Agency

Let me briefly refer to the history which has led us to the Specialists' Meeting on Sodium-Water Reactions.

About two years ago the idea of coordination of international meetings on the problems of fast reactors was initiated in the International Atomic Energy Agency. This idea was supported by a number of countries. As a result, the International Working Group on Fast Reactors was set up in March of this year under IAEA auspices to serve primarily as a collective adviser for the purposes of coordination of international meetings in the field and better exchange of information between the countries involved in the program. In particular, Dr. Wensch has made a great contribution in organizing the Group and identifying its terms of reference. Now he is the U. S. representative to this Group.

The Working Group has agreed that in addition to topical conferences, it would be most helpful to organize small meetings of specialists on specific aspects of fast reactors. Such meetings can provide an opportunity for thorough review and detailed discussions of a particular problem, which would be impossible to envisage within a large conference.

The idea of the meeting of specialists on sodium-water reactions, the first of its kind, has been unanimously supported by all members of the International Working Group on Fast Reactors.

The program of the meeting, drawn up in conjunction with participating countries, was too large for two days' discussion, but the high activity of participants and excellent chairmanship by Mr. R. Jones have made it possible to cover all the items.

In conclusion, I would like on behalf of the International Atomic Energy Agency to thank once again U. S. authorities and Argonne staff for the possibility of holding the meeting at Argonne.

Appraisals of IAEA Specialists' Meeting by Participants

Ralph H. Jones, Meeting Chairman

It was gratifying to me to observe, at this IAEA Specialists' Meeting, that all of the participating countries are actively working on the sodium-water reaction problem. From this I conclude that there is international acceptance of responsibility to find the necessary solutions to reactions occurring in sodium-heated steam generators.

In general, all participating countries are pursuing the single-wall-tube steam generator as the best approach for the LMFBR plants. All recognize that this approach is contingent upon safely accommodating a sodium-water reaction in the steam generator. This must be accomplished without communicating the trouble to the reactor primary system.

I conclude that the international exchange of ideas at this Specialist Meeting has been of service in assuring the success of the sodium-heated single-wall steam generator.

Kazuo Furukawa, Japan

Although Japan has not yet done much development work on the sodium-heated steam generator except for a few fundamental researches concerning sodium-water reactions and water-leak detections, we are now starting a big project of Fast Breeder Development to meet the National power demands. Therefore, we have heartily appreciated coming to this up-to-date Specialists' Meeting of IAEA, which was very useful to get the guiding knowledge in this field.

We are hoping for further international cooperation.

J. Alan Bray, United Kingdom

I would like to begin by saying how much I enjoyed meeting other members in the field of sodium-water reactions at the Panel. People engaged in this kind of safety study necessarily tend to plow a rather lonely furrow, and it is good to be able to meet now and then. We have had an interesting and fruitful exchange of information and viewpoints this week.

Kurt Goldmann, United States of America

It was a most valuable meeting.

Amongst safety problems in LMFBR power plants, I consider the problem of containing a sodium-water reaction in a safe and economic manner only second to the problem of containing a nuclear excursion. Admittedly the problem of sodium-water reaction is an order of magnitude less severe than the nuclear excursion problem, but it seems to me that the efforts spent on sodium-water reactions are less by more than an order of magnitude than those spent on nuclear excursions.

The meeting during the last two days represented a big step forward in the direction of rectifying this unbalance by giving recognition to the importance of this problem. If one cannot *safely* contain a sodium-water reaction in an *economic* manner, the utilities will not buy any LMFBR's. While we have reasonable assurance that sodium-water reactions can be contained safely, we are far from knowing what safety design criteria should be applied to LMFBR plants and what the costs of meeting such criteria will be.

For two days, we discussed all aspects of sodium-water reactions. Personnel from major installations around the world, which are actively engaged in this work, were represented. I would estimate that during these two days we collectively advanced the state-of-the-art to a point which might have taken years to reach on an isolated basis. Encouragement should be given to continue the free exchange of information in this special field in the future.

N. Lions, France

1. Discussions were very open.
2. There is a general agreement on instrumentation.
3. It seems that a secondary failure can occur in pool-type steam generators; less secondary failures are expected in the case of modular steam generators.
4. A leak of a size less than the total rupture of one tube may be more destructive than the full-tube leak.
5. No test has been run with more than one intentionally ruptured tube.
6. For detection of sodium-water reactions, development is being carried out on an electrolytic device, in addition to the nickel-membrane detector which is generally used.
7. Ferritic steel appears to suffer more damage by small water leaks than stainless steel.
8. Very few tests were made to determine the maximum pressure peak which a shell can withstand.

H. Mausbeck, Federal Republic of Germany

For all the different steam-generator designs, the study of the sodium-water reaction leads to many similarities in test work and mathematical description. Therefore, this meeting was highly valuable, since it gave a broad exchange of results and problems. I think it can be said that the meeting offered to a great extent the status of the technology in this field.

Especially, many areas of common understanding and interest were found, like:

definition of a maximum steam-generator failure;
codes for pressure propagation through the steam generator and the secondary system;
wastage of adjacent tubes or construction elements by tube failures, especially by small leaks;
necessity of measurement and identification of small leaks.

Summary Topical Reports on Sodium-Water Reactions

1. Statement of Problem

Ralph H. Jones, Specialists' Meeting Chairman

For acceptance in LMFBR plants a sodium-heated steam generator must be proven to be:

First — SAFE,
Second — RELIABLE, and
Third — ECONOMICAL.

To fulfill the first requirement: SAFETY, the LMFBR steam generator must have:

1. an undebatably high degree of assurance of safety to the general public;

2. nearly the same degree of assurance that a reaction in the steam generator will not be communicated to the primary reactor system;

3. an assurance of safety to plant personnel equal to, or better than, that in conventional steam plants;

4. a high degree of assurance that a minimum of damage is imposed on the steam-generator plant.

The second requirement: RELIABILITY, reflects the application of the LMFBR plant in the electric utility environment. In this commercial application, DEPENDABILITY, AVAILABILITY, and RELIABILITY spell the success or failure of the energy source, regardless of its origin. To meet its demands we must look into the realm of the designer-fabricator. Here the sodium-water technologist must be able to translate his data into a usable, understandable form for use by the designer in arriving at a safe and reliable steam-generator design. The designer-fabricator must have a knowledgeable awareness of the consequences of steam-generator failures. Only in this knowledgeable way can he institute the proper engineering-design and quality-assurance programs to fit the end-product application.

Last, but ultimately not least, the safe and reliable steam generator must not impair the economic acceptability of the LMFBR plant in the electric-utility market.

It is this spectrum of goals that we are faced with solving today. The technologists, designers, and fabricators that can work together to produce the SAFEST, MOST reliable, and MOST economical sodium-heated steam generator have SOLVED THE PROBLEM.

With this in mind, why has there been so little enthusiasm shown by industry to get in to help solve the problem?

2. Fundamental Studies of Sodium-Water Reactions

Kazuo Furukawa, Japan

The topic "Fundamental Studies on the Sodium-Water Reactions" has received rather little attention in this meeting. However, some comments can be classified into five categories as follows:

(1) Fundamental studies of reaction kinetics: Two presentations were made by UNC (United Nuclear Corporation) and by JAERI (Japan Atomic Energy Research Institute). UNC presented the status of a fundamental study conducted a few years ago. Following a literature survey, which was conducted in 1959, their group carried on a small-scale study of chemical reaction between sodium and water in the absence of air, concluding that the reaction is controlled by the mixing rate of sodium and water.

JAERI presented a movie showing a series of experiments on sodium-water reactions which was conducted at Tokai Research Establishment in 1967. Sodium of various forms, solid and liquid, was brought into contact with water of various states: steam, boiling, room temperature, or ice. The 23 experiments were made in air, changing the reactant weights and contact methods. These showed the very wide variety of reaction modes, from the case of a most violent explosion to the case of no reaction.

Already many papers on the sodium-water reactions are reported in the literature. However, in order to understand the problems associated with fast reactors, it is essential to continue to accumulate knowledge and information on these reactions.

(2) Thermodynamical properties of sodium-oxygen-hydrogen system: To deepen our knowledge of sodium-water reactions, there is a need for compilation of thermodynamic properties, particularly for the sodium-oxygen-hydrogen system, at a wide range of temperature and pressures, including solid and liquid regions as well as the gas region. Our knowledge in this field is still limited and was not discussed here.

(3) Corrosion and erosion studies: As another fundamental research field, there are the corrosion and erosion studies of structural materials in several prepared environments which have a relation to the small-water-leak wastage; for example, NaOH, NaOH/Na, NaOH/Na_2O/Na, Na_2O/Na, Na_2O/Na_2O_2, and others under changing temperatures, pressures and states, and also under changing flow velocities. These were not discussed in this meeting due to the limited time available.

(4) Fluid dynamics: A most important problem in fluid-dynamics concerned with the sodium-water reaction is the transient two-phase flow dynamics of sodium and the products of reaction, including steam and hydrogen. A fundamental research on this subject was reported by APDA. They used air or helium instead of steam and hydrogen, and water instead of sodium.

The reaction-simulation method, using a combination of fluid media other than sodium and water, is considered to be a very effective tool for the analysis of sodium-water reactions in a steam generator. By this method, the chemical reaction is separated from the hydrodynamics, and the two-phase flow phenomena can be visually observed by using high-speed motion pictures.

(5) Instrumentation: Reactions between sodium and water take place in less than 1 ms. Because of the very rapid reaction rate, it is difficult to apply ordinary instrumentation in experimental facilities. Therefore, very fast-response pressure, temperature, and structural-stress sensing devices are needed. These devices must be immersed in liquid sodium, which multiplies the difficulties. In this meeting some new improvements and refinements in transducers, thermocouples, strain gages, and water flowmeters received some comments.

This was a summary of the "Fundamental Studies" in sodium-water reactions, and I hope for further activity in this field.

3. Large and Small Leak Tests

J. Alan Bray, United Kingdom

The meeting considered the results of a considerable amount of test work carried out in the USA by Atomics International and APDA, in France by the CEA at Cadarache, in Germany by Interatom at Bensberg, and in the UK at Dounreay in Scotland. Nearly all the work was carried out with models representing particular designs of steam-raising units. The tests have all tended to strengthen confidence in the intrinsic overall safety of single-wall sodium-water heat exchangers.

Damaging sodium-water reactions in liquid-metal-heated steam generators may be divided broadly into two main types:

a) small water leaks which may arise from manufacturing defects, such as welding faults or flaws in tube material;

b) large water leaks resulting from the complete rupture of one or more water tubes. These might occur from fretting or vibration damage or possibly from water-side corrosion if there is inadequate control of water purity. Sodium-side corrosion resulting from unnoticed small leaks could also bring about complete tube failures.

In tests dealing with small leaks where an orifice size from $\frac{1}{16}$ to $\frac{3}{16}$ in. is involved, very rapid wastage rates have been observed for tube material in the path of the jet. Wastage rates of up to 3 mils/sec for 2¼ Cr-1 Mo steels have been reported in the APDA work, and similar rapid metal removal has been seen in tests at Dounreay. For a given spacing there seems to be an "optimum" rate at which maximum wastage occurs. There appears to be some relationship between the nickel content of alloys and their resistance to this kind of attack. Materials such as Incoloy 800 have suffered much less attack than stainless steels which, in turn, have behaved better than the ferritic steels. In an interesting but unexplained phenomenon, APDA has found that the rate of attack in a system in which sodium is flowing is increased by a factor of 10 over a static system.

The experiments seem to suggest that these rapid wastage rates are associated with the formation of a definite jet of water-steam fluid in the sodium. Where small leak tests have been carried out with tube-in-tube models, no large wastage has been reported, and it appears that the reaction bubble in this situation rapidly fills the cross section of the tube and pushes the reacting sodium-water interfaces apart so that an in-sodium jet does not form.

Where large "full bore" water-injection experiments have been carried out with orifice sizes up to ¾ in., the wastage effect has been completely absent in many tests. For example, in a series of 17 tests in a modular steam-generator mockup carried out by Atomics International, no wastage was observed. However, in some of the Dounreay tests secondary leaks in pressurized target tubes surrounding the injection point did occur within as short a time as 3 sec after initiation of the primary burst. The reason for these failures again could be associated with a jet. In the Atomics International module the shell was of comparatively small diameter (8 in.) and the reaction bubble would soon fill the cross section as in the tube-in-tube tests. The Dounreay tests were made in vessels of 2 to 3 ft in diameter, and the reaction bubble could have become detached from the jet itself, thus allowing the rapidly moving stream of reaction product particles at the sodium-water interface to bring about wastage of adjacent tubes.

Temperatures in the reaction zone of up to 1300°C were measured, and pressure peaks of up to 3000 psi were observed for short periods. Some pressure damage such as tube bowing in the reaction zone was reported, but no failures of the outer shell of any of the test rigs occurred. In one series of large-scale tests at Dounreay a vessel with a design pressure of 300 psi was used for ten tests without any detectable deformation or other damage. It is obvious that adequate pressure-relief devices were used in all of the tests, as damage to equipment due to shock or pressure waves seemed insignificant in all the work reported. Some data from AI indicated that transient pressures in adjacent modules may be as high as, or even somewhat higher than, in the reaction zone.

In large leak tests exact duplication of reaction conditions proved difficult, and good reproduction of results was not obtained. However, in small-leak

work a greater degree or reproducibility was possible. The same is true of tests with comparatively small modules of simple geometry.

Some experiments had brought about failure of adjacent pressurized tubes by high temperatures produced in the reaction zone, but as these tests did not have water flow they may not have been realistic.

Large-scale sodium-water tests highlighted the problems of dismantling and maintenance due to the formation of quantities of reaction products. These had a density about twice that of sodium and therefore settled at the bottom of the test vessel. There was no true melting point, but the material became liquid between 300 and 350°C. A typical analysis was NaOH 50%, Na_2O 40%, and NaH 10%. When cold, the material was rock hard and formed an effective cement, binding the components together. It could be removed by hot water.

In general, it was concluded that economic and safe operation of sodium-heated steam generators is entirely possible.

4. Leak Detection

Kurt Goldmann, United States of America

I have been asked to summarize specifically what we know about leak detection. I would like to do this in two parts:

a) detection of large leaks;

b) detection of small leaks.

First to the large leaks. You can't miss with the detection of large leaks. Pressure gages on the sodium side and in the cover-gas spaces will give immediate indication of large leaks. Continuity wires on rupture disks and shorting wires downstream of them will signal the rupture of a disk. Flow and level indicators may give additional confirmation of a large leak.

The second problem of detecting a small leak is much more severe. Since the leak is from the water to the sodium side (because of pressure differentials), we have to look for a leak on the sodium side. Sodium-water reaction chemistry tells us that we should look for hydrogen, sodium hydride, sodium hydroxide, or sodium oxide in the sodium, depending on temperature.

Since a small leak is <0.1 lb/sec of water and a typical sodium flow rate in a secondary loop may be 10,000 lb/sec, we are looking for a change of impurity level in the sodium of <10 ppm.

The most commonly used means for detecting a small leak is a hydrogen detector. Such detectors sense hydrogen in the cover gas or after diffusion from sodium through a membrane, which is frequently made of nickel. The membrane may be a flat disk, a small tube, or a bellows. The measurement may be made with a mass spectrometer, gas chromatograph, thermal-conductivity cell, or moisture indicator (after catalytic conversion of hydrogen into water). All of these devices require "measurable" amounts of hydrogen to diffuse through the membrane or into the cover gas. The variable amounts of hydrogen normally present in the cover gas make it difficult to recognize a genuine leak. A hydrogen meter, based on electrochemical principles, is under development and should not have some of these shortcomings.

The electrochemical oxygen meter has not yet been used to detect small leaks, but it should meet all requirements. The rhometer might, similarly, be useful.

Plugging meters have been used successfully, but their indication is not instantaneous.

If the leak is large enough to exceed the hydrogen-saturation limit of the sodium, hydrogen bubbles form. A hydrogen bubble meter, consisting of an induction coil in suitable geometry, has been used with success in Germany.

APDA has tried to sense a leak by sound detection, but efforts to date were hampered by background noise.

5. Calculational Methods and Applications to Steam-generator Designs

N. Lions, France

Two types of steam generators are now in operation or in design. The first type uses modules containing a few tubes in a small-diameter shell. The second type consists of a large-diameter shell surrounding many tubes; this is the pool-type steam generator. After the symposium held during the two last days, we can see that there is pretty good correlation between tests and calculations for the modular steam generator. This is reported in Dr. Mausbeck's paper presented at the symposium and in a paper of the French "Commissariat a l' Energie Atomique" presented at the "Aix-en-Provence Conference" in 1967. In both cases, calculations are made by using a computation model called "Piston-model," in which water diffusion through hydrogen, which was previously produced, is neglected. The main parameters of the phenomena (pressure pattern and sodium flow) are calculated to within 20% of the experimental values during the first 50 ms; after this time period, correlations are not so good.

The reproducibility of results of successive experiments was tested in France. It was found to be fairly good when the rupture of the water tube is reproducible.

Other correlations were shown to fit the test data obtained by Atomics International for another modular steam generator.

On the other hand, Mr. Hori from JAERI presented an interesting theoretical study concerning the slip between gas and liquid for the "Piston-model."

Calculations were performed by APDA and UKAEA for the pool-type steam generators. To date, the results of these calculations have not been checked by actual large-leak experiments.

As a conclusion, we shall say that one must be prudent when using computations of sodium-water reaction effects on steam generators and secondary sodium loops. The calculations are specific for the particular steam generator which was tested and cannot be applied to another type of steam generator.

When the calculations are in good accord with tests for a specific steam generator (tested with a part of the device at full scale), they can be used for the real steam generator and the secondary sodium loops of the reactor to predict the overpressures in any location of the loops and particularly in the intermediate heat exchangers.

6. Design of Steam Generators and Relief Systems

H. Mausbeck, Federal Republic of Germany

Among the problems covered during the meeting I should mention briefly the question of pressure relief in the case of a tube failure. This question is of common interest for all of the various designs of steam generators. At the moment, all steam generators under consideration are of the single-wall-tube, once-through design; they can generally be divided into modular and tube-in-shell types.

The problem of pressure relief is mainly dictated by the formation of hydrogen during the reaction. The entrance of high-pressure water-steam mixtures into the sodium system contributes to a minor extent. The design of the pressure-relief system influences the design pressure for the secondary sodium system. The questions to be solved can be arranged according to their importance in the following sequence:

Protection of the intermediate heat exchanger, since it is the safety interface between the primary and secondary loops. Therefore, its failure could cause core destruction; this means a nuclear incident.

Protection of the secondary loop and the steam generator itself to avoid secondary damage and large sodium spills.

Relief of the reaction products, the excess sodium, and the following steam and water entering through the leak, must be carried out without damage to the immediate surroundings and without risk to the general public.

All the different designs for a relief system use rupture discs as a primary means of depressurization. The number and locations of the rupture discs vary, depending on steam-generator design, expected reaction pressures, and size of the relief lines.

In all the modular designs the rupture discs are submerged in sodium. In case of the tube-and-shell designs, one often finds a gas space below the discs. In both cases, a most interesting question arises as to how to ensure an adequate and guaranteed lifetime of the rupture device. Additional test work is probably necessary in all cases. The relief line(s) leads to one or more reaction-products separation tanks to ensure that only the gaseous products are released to the atmosphere; these are mainly hydrogen and steam.

As a consequence of the high entrance velocities into the reaction-products separation tank, some sodium, sodium oxide, or sodium hydroxide escape with the gaseous products. Motion pictures shown at the meeting indicated the importance of an adequate design of the separation system. I conclude, from the material presented, that:

1. The reaction-products separation tank has to have a good separation efficiency, as is the case with a cyclone-type device; there is some indication that a separating device with two tanks in series improves the separation.

2. As to the measured data, a retention efficiency of about 95% was reported for a cyclone and more than 99% for two tanks in series with a water-spray system in the second one.

3. With respect to the location of rupture discs, two different locations were reported:

Directly at the steam generator unit; this gives the fastest pressure relief, but the action of isolation valves is normally needed.

Behind additional depressurizer tanks; this has enough additional sodium available not to depend on valve actions during the pressure-relief process.

In respect to the reliability, both of these systems should be adequate.

Participants in IAEA Specialists' Meeting on Sodium-Water Reactions

Held at Argonne National Laboratory November 5–6, 1968

IAEA

D. A. Yashin

Federal Republic of Germany

K. Gast, Karlsruhe
H. Mausbeck, Interatom

France

J. Leduc, CEA
N. Lions, CEA

Japan

K. Furukawa, JAERI
M. Hori, JAERI

United Kingdom

J. A. Bray, UKAEA
M. J. Watts, UKAEA

United States

J. Ford, APDA
K. Goldmann, UNC
L. Goodman, AI
R. Jones, USAEC
P. Probert, B&W

Discussion

Mr. Isbin (Univ. of Minnesota): Did I understand, Dr. Goldmann, that you said that you were not able to determine what the safety criteria should be during these meeting days?

Mr. Goldmann: That's right.

Mr. Isbin: Can you add a few more remarks as to what the problems are?

Mr. Goldmann: To start with, we know that sodium and water do react rather violently with each other. The question arises, first of all, can you allow such a reaction to take place; I think the obvious answer is yes. You cannot possibly design and build a steam generator in which you can guarantee that there will not be such a reaction. You are then confronted with the problem of deciding to what extent must you contain a reaction in order to safeguard many things. Perhaps one of the very first things that has to be prevented, as was mentioned briefly by some of the other speakers, is the sodium-water reaction leading to a nuclear excursion in the primary side of the system. However, today there are no statements in any of the designs of the steam generators or the secondary systems that say there must be a device that will assure that if there is reaction this reaction will not lead to a nuclear excursion. This is the most severe sort of thing that you certainly will have to guarantee some day.

Then there are other considerations, like what size of leak must you guard against. What is the probability for a single tube to leak or a whole bunch of tubes to leak all at the same time? What are the consequences to the surroundings in terms of how far you can get the reaction products spewed out into the atmosphere or the surrounding area? Such criteria have not been set, and I think it is very important to get working on this, to set them, and to realistically estimate what the cost is going to be to meet such criteria.

Mr. Eichelberger (AI): Dr. Goldmann mentioned detecting these leaks by measuring the hydrogen in the gas phase or in the sodium. Can you give us an idea of your detection levels in these media?

Mr. Goldmann: It appears that the normal hydrogen levels observed in cover-gas spaces of reactors are of the order of hundreds, possibly up to 2000 ppm. The problem is to identify a sudden change in hydrogen level due to a leak. The chances are that you will see a leak by a rate of change of hydrogen level rather than just a change of an absolute level. That was one of the perhaps significant experiences at APDA. In the sodium itself, the hydrogen levels are quite low, and I am really not prepared to give a number.

Mr. Jansson (W): I would like to know if the panel discussed the role of stress corrosion by hydroxide in the reactor system. Stainless steels are not exactly known to be very resistant to this. Especially at the point of a leak, you would expect a very high hydroxide concentration, and I would guess that you could get attack in the sodium loop as well as on the water side. The second question is to Dr. Bray. Is the reaction product with the melting point of 300–350°C sodium hydroxide, or does it also contain something else?

Mr. Bray: Perhaps I can answer the second question first. Yes, it is largely sodium hydroxide. It seems to be a mixture of sodium hydroxide, sodium oxide, and sodium hydride in varying proportions, according to the temperatures and the type of reaction. Stress corrosion of stainless steel was lightly touched upon in the meeting. I think that on the sodium side small amounts of sodium hydroxide will be removed by the conventional cleanup system provided in any sodium circuit. Caustic stress corrosion could arise during reclamation procedures, decontami-

nation, repair, and rebuilding. I think this is just a question of how much repair can be done to a damaged tube bundle, and how stringent can recovery procedures be made. Also, post-recovery inspection criteria have to be specified for a particular case.

Mr. Jones: I would like to ask that we amplify on that, since at the meeting we did cover another aspect of stress corrosion. John Ford, from APDA, could you say a few words about nitrite-nitrate corrosion?

Mr. Ford (APDA): What Mr. Jones is referring to is the corrosion on the inside of the steam-generator tubes, which was experienced at the Fermi plant due to improper cleaning procedures. This was stress corrosion of ferritic materials, 2.25 Cr-1 Mo, by a cleaning solution which was composed, among other things, of nitrites. The nitrites when exposed to air reacted to form nitrates; this, in combination with high temperature and some non-stress-relieved portions of the tubes, caused stress-corrosion cracking.

Mr. Jansson: May I ask if you do not think that stress corrosion could be a mechanism whereby a leak could grow and become more serious?

Mr. Bray: This question of leak growth is very difficult. Although it is purely a supposition, I wouldn't have thought that stress corrosion would be likely to affect leak growth because the sort of leak growth that we have seen is very rapid indeed. Very rapid wastage is associated with this kind of corrosion-erosion behavior. I would have thought that stress-corrosion attack of this type was more likely to be a long-term feature. This isn't to say that caustic stress corrosion in stainless steel components following decontamination couldn't be a problem if, for example, full washing procedures weren't followed, or if washing procedures weren't successful. I don't think this is a very real problem, for it is concerned with direct propagation in stainless steel tubes in operating heat exchangers with the tubes immersed in sodium anyway.

Mr. Isbin: With reference to the discussion of pressures, I believe by panelist Bray, the indication was that pressures up to 3000 psi were measured. This was discounted in part of your discussion in that you didn't find any damage. I am not sure whether you were implying, and perhaps the other panelists might want to amplify, are these pressures real, do you think? Are there measurement difficulties? Do you have a mechanism for generating such high pressures?

Mr. Bray: This puts me on a spot, as perhaps the weakest part of our experimental work has been in pressure measurement. With regard to pressure damage, we haven't seen very much. Pressure measurements have been made by Mr. Lions and by the Atomics International people. Mr. Goodman looks eager to answer this question. I wonder, would you like to say a word on this?

Mr. Goodman (AI): As far as our data are concerned, we have reason to believe the reality of the pressures. We have had ways of verifying the validity of the tapes so that we can be assured that the pressures were real. So far as not sustaining any damage is concerned, I can't speak with certainty about the other test programs, but in our test program we have designed a system to sustain pressures well in excess of 3000 psi. It came as no surprise that we saw no readily obvious accumulated damage after a series of tests. We were using schedule 80 pipe, and these tests only lasted for very short periods of time.

Mr. Lions: We measured peak pressures of about 100 bars in a shell of 10-cm diameter, 4 m in length, and 5 mm in thickness. After five runs, the shell was deformed but had not failed. That shell was of Type 316 stainless steel.

Mr. Probert (B&W): To make failure analyses on the basis of peak pressure is invalid. These analyses should be made on the basis of impulse-momentum calculations or work-energy type of calculations.

Mr. Mausbeck: We did some experiments in tube geometry. In this case we measured more than a thousand atmospheres but over a duration of less than 1 ms; the peaks lasted about ¼ ms, so the energy stored in the peaks was small.

Mr. Latzko (Delft): Dr. Mausbeck mentioned that in all modular designs the rupture discs were mounted under sodium. Is that correct?

Mr. Mausbeck: The discs were submerged under sodium.

Mr. Latzko: Well, I would like to know what materials were used, what was the maximum number of hours obtained with the rupture discs under sodium, and how were they mounted?

Mr. Mausbeck: It wasn't really much discussed during the meeting. I can only add our experience, that we have had them under sodium for, I think, about 6000 hr now.

Mr. Bray: I would like to add that the material used for this sodium work was nickel.

Sodium Boiling in Fast Reactors. A Review with Reference to the Ispra Conference

D. Smidt

Kernforschungszentrum Karlsruhe
Karlsruhe, West Germany

At the Conference on Fast Reactor Safety in Aix-en-Provence last year the liquid metal boiling group was established. This group, at that time, agreed to exchange progress letters and to have a meeting in about one year. This meeting took place on October 10 and 11 at Ispra, at the Euratom site, and the participants to this meeting came from Euratom, France, Italy, Belgium, Netherlands, United Kingdom, Japan, and Germany. I shall not give a point-by-point account of the Conference; I prefer to derive the present general understanding of sodium boiling and its importance for fast reactor safety, and to refer to specific Ispra papers at the proper place. Now, I was invited to give this talk only a few days ago and so I am sorry that I don't have any slides of any other group except ours. This doesn't mean we did all the work.

The general importance of sodium boiling for fast reactor safety has been discussed very widely. The present view as discussed at Ispra is that overall sodium boiling in the core is a very improbable event because many diverse and redundant safeguards have to fail before this event occurs. The designer can rely on these engineered safeguards and the complete design against sodium boiling over the whole core. More important is the single subassembly blockage of the Enrico Fermi type and subsequent blow-outs of the boiling sodium. The reactivity effect is negligible by itself, but rather large and short pressure pulses are observed, and these may lead to fast propagation of this failure to other subassemblies. I am saying fast propagation because slow propagation, as by fuel melting, to neighboring subassemblies is another case and has different safety aspects.

We have two causes for the pressure pulses: one is a sudden flashing of superheated liquid; the second is the recondensation of the vapor bubble with a water-hammer type of effect. Naturally, this also is, first, a problem of engineered safeguards and instrumentation, and we have to rely on the detection of any flow failure by thermocouples, flowmeters, fission gas detectors, etc., before boiling occurs. Then, second, the detection of boiling itself it possible, and we have to rely on reactivity meters or noise detectors. Here we are now in the field. These latter instruments naturally cannot help in preventing a propagation effect if it exists. Anyway, these provide a very valuable kind of instrumentation, and one very important paper was presented by the British on their work on boiling noise detectors.[8] They first tried these detectors in several loops and finally put a little test chamber with an electrically heated rod inside the Dounreay reactor. For the experiment this had to be insulated by some gas blanket around it; even so it was possible to hear the boiling noise among the general reactor noise by special filtering techniques. So this was a very impressive paper. So much for the instrumentation and the noise-detection side, I now turn to the boiling problem itself.

As already pointed out, we have two aspects, ejection and recondensation, and both are determined by liquid superheat. This is clear for ejection, but there is some evidence that also recondensation will be more violent if the vapour bubble has expanded very rapidly from the superheated state. The effects we are looking mainly for are the pressure pulses, because the designer's question is on its effect to the structure. Most of the experimental investigations started with single-channel equipment, because of its simpler technique, which is nevertheless already rather sophisticated, but we have to consider also the changes by the multichannel geometry as it refers to the reactor, although the experimental results in such overall mockups might be less detailed.

First, I shall say a few words on the present status of what has been said about superheat. Actually, the question of initial boiling superheat is a question of nucleation and influenced by the equilibrium between surface tension forces and vapour pressure of a nucleus, shown by the well-known Laplace equation $\Delta p = 2\sigma/r^x$. Naturally the main interest is centered on heterogeneous nucleation of boiling processes at heater wall cavities. Here we have a very difficult problem, which is not understood as yet, because sodium is a very wetting liquid and, therefore, the cavities may not stay active. Wetting experiments with austenitic surfaces have been reported in a Belgian paper.[1] At temperatures of more than 250°C the investigated surfaces have been totally wetted by sodium in less than one hour.

Therefore, at temperatures of 800°C and above we have to consider sodium certainly is a wetting liquid. Now, one experiment that was reported was especially directed to the effect of cavities (see Fig. 1).[2] In this assembly a small sodium pool was connected to hot- and cold-trap cleaning to get hold of the chemistry. The test section was a little cavity of 0.4-mm diameter and 2 mm deep. Quite a number of thermocouples was used to detect the events.

Figure 2 gives a more detailed view of the cavity and two of the thermocouples below it to measure the heat flux. The interesting result of this experiment was that this cavity stayed active as a nucleation center over more than six months, also under high operating temperatures. The size of the nucleus corresponding to a superheat of the order of 25°C was about the cavity diameter; even if afterwards it was detected and this cavity more or less was completely filled with sodium, it stayed active and a nucleus existed. Figure 3 shows the effect. The abscissa is the saturation temperature as determined by the pressure; as ordinate we have the measured superheat with the size of the nucleus as a parameter. One can easily calculate from the equations that superheat decreases for a given size with the saturation temperature. Now the oxide content of the sodium was changed between 33, 23, and 12

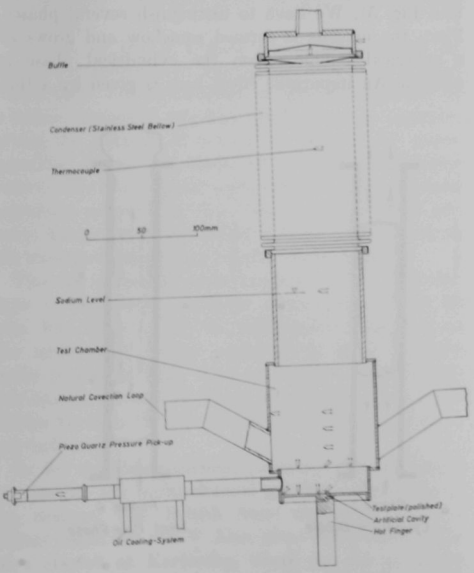

Fig. 1. Sodium Superheat Test Pool.

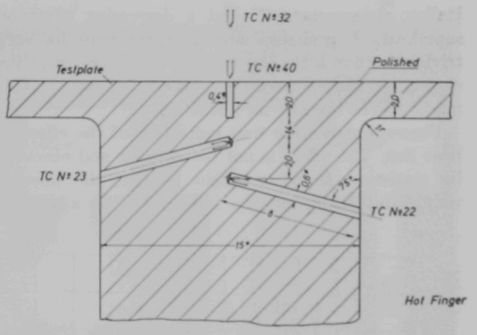

Fig. 2. Sodium Superheat Experiment: Dimensions of Test Section No. 1.

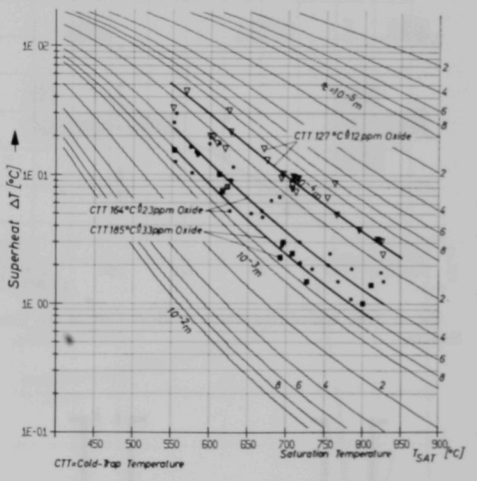

Fig. 3. Influence of Oxide Concentration on Sodium Superheat.

ppm to complete hot-trap cleaning. This had a clear effect on superheat. The highest superheat was measured with 12 ppm, and it fell to lower values with increasing oxygen content. If one expresses it by the size of boiling nucleus, the nucleus became larger with increasing oxide content. That is really not a true physical statement because all the qualities of the boiling sodium, especially the oxygen content, certainly will change. Especially the surface tension is not very well-known at these conditions right now.

Also with respect to chemistry, a French report told about some work on the effect of dissolved hydrogen.[3] The flow velocity according to some

Italian measurements[4] had a decreasing effect on superheat. A probable answer which may be very trivial, is that little gas bubbles are drawn into the system at higher velocities and act as nuclei. This might also be the case for a reactor.

Figure 4 shows the first indication of the effect of heat flux. The effect is not too distinct and obscured by statistics. A reason might be that the time in which the liquid at the surface is in a certain

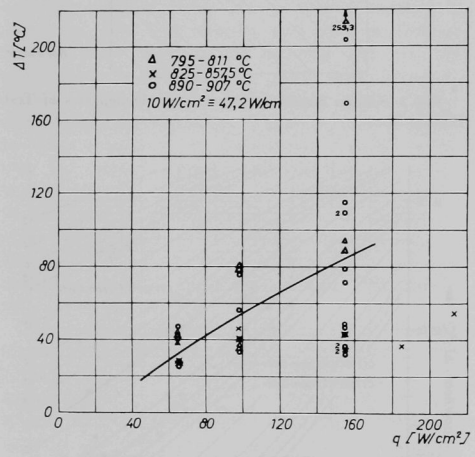

FIG. 4. NSK Sodium Superheat *vs* Heat Flux in the Test Section.

superheated stage decreases with heat flux. This may influence the flashing probability.

Now I come to the next point—the effect of history on superheat. Increasing superheat after repeated boiling often is reported. A theory developed by Holtz[5] gives the effect of the pressure-temperature history on superheat by a model in which the size of the nucleus is given by the pressure-temperature-dependent penetration of sodium in a conical cavity. Schultheiss[2] did not find evidence for this with his artificial cavity. He tried to put a stronger and stronger pressure on the sodium, but there was no change to the superheat. The Holtz theory may be too simple, and it doesn't take into account quite a number of other parameters.

From the practical standpoint superheat will certainly not present any problems in a reactor. You could apply this type of stable cavities I talked about before. For instance, this is possible between spacer and fuel rods, and experiments are prepared to prove this. Also, the tiny gas bubbles present in a system will certainly prevent superheat under reactor conditions.

Now I come to sodium ejection. There a sufficient understanding has been reached. A theoretical model based on single-bubble ejection has already been presented at the Aix Conference,[6] and now several groups have written codes according to this model (see Fig. 5). We have to distinguish several phases. First, the nucleus is formed somehow and grows as a spherical bubble. Then the cylindrical phase is reached. An important effect here is given by a thin

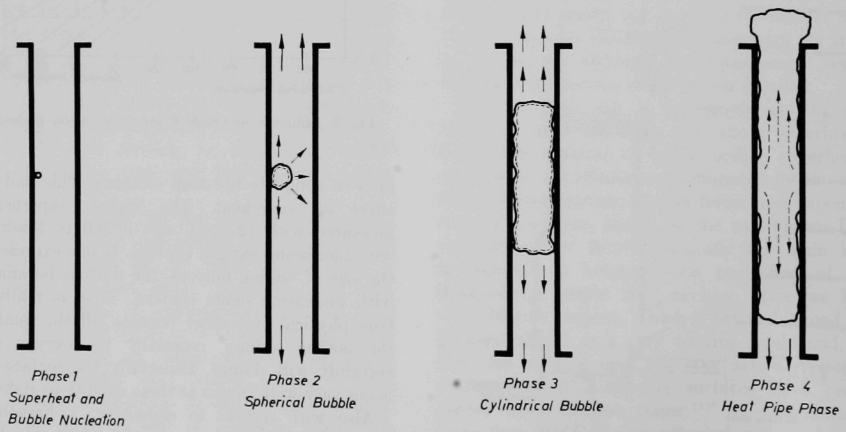

Fi . 5. Model of Coolant-channel Ejection.

layer over all the wall. This will supply sufficient vapour to the bubble even after some time has elapsed. Finally, the bubble touches the cold sodium of the plenum; this suddenly decreases the pressure in the bubble and will be followed by a rapid vaporization of the liquid film, with very good cooling of the wall. Therefore, we call this the "heat pipe phase."

There have been shown some experiments especially made at Ispra and Karlsruhe, and even a movie has been shown[7] which stated this very clearly. Figure 6 is an ideal picture of this experiment. Sodium was heated by conduction heating in a tube until it became bright red hot. The temperature went up until boiling started, and a rather low pressure peak occurred. Then the heat-pipe phase started. One could see quite clearly in the movies and in the experiment that suddenly the temperature decreased rapidly and that after some time the bubble collapsed. Even with a heat flux of the order of 200 W/cm² the wall temperature dropped rapidly and with it the glowing. This was repeated several times.

At present induction heating is the most powerful method to get high heat fluxes in the experiments. Peppler[2] has reached heat fluxes up to 700 W/cm² with this method. One interesting aspect is that because of the heat pipe effect a burnout in the channel becomes less probable. Eventually, after seconds, naturally, this repeated ejection may get unstable and suddenly a hot spot develops. But this may take some time.

Finally, in Fig. 7 I show the results of such an ejection experiment.[2] The acceleration b is plotted versus time. The acceleration as observed increases to a certain maximum and then finally becomes negative, giving the collapse. It is easy to calculate the corresponding driving superheat ΔT (which is the lower curve). The peak agrees quite well with the measured superheat at the wall. One has to consider that one never knows where the bubble actually occurs, and so the measurements have a certain range of error.

The single-channel recondensation gives, with this type of experiment, pressure peaks up to about 40 atm. But these are in the millisecond range, and so the mechanical energy contained in these pressure peaks is not too high. Also, no complete water hammer has been observed. There was always left a small bubble between the two columns of sodium approaching each other.

So for the single-channel geometry. Now we have to consider the multi-channel growth problem, as in the reactor. The British have developed a theoretical model for this.[8] Also, some experiments have been started at Karlsruhe, where we use an array

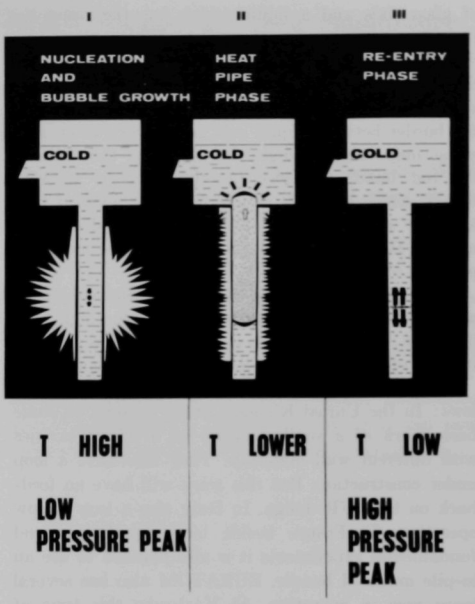

Fig. 6. Sodium Ejection.

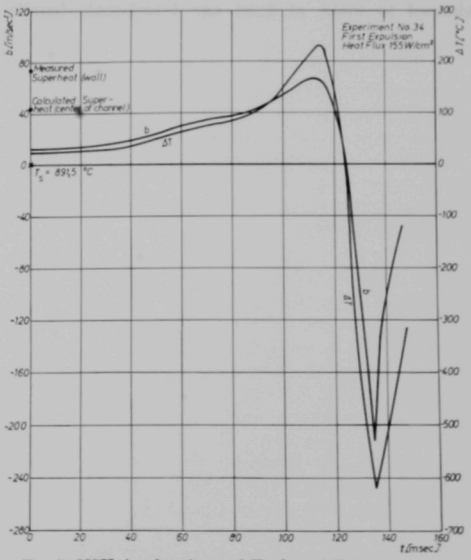

Fig. 7. NSK Acceleration and Evaluated Driving Superheat *vs* Time during First Expulsion.

of glass rods and a liquid which has the same refractory index as the glass rods. The assembly is thus quite transparent as long as it is filled with liquid. Then a gas bubble was created in this array and movies were taken. The evidence is that probably the border between liquid and gas moves rather as a plane only with a slight buckling, so that indeed the rod bundle behaves practically as if it were several single channels in parallel. It is planned that also the re-entry phase should be studied by this method. Here probably the geometry will be more important.

A large portion of the conference was concerned with the heater development necessary for high heat fluxes at high temperatures. I only mention this for it is not of too much interest to our present topic.

Future plans in the different countries are as follows: In the United Kingdom there is going on some basic work of a similar nature on artificial cavities with different wall materials. They also have a loop under construction. But this work will have no feedback on the PFR design. In Italy also a loop is now operating. In France beside loop experiments and fundamental experiments it is also planned to use an in-pile multirod bundle. EURATOM also has several loops now in operation. At Karlsruhe this type of work is going on as I described. Also there is planned to make at least one 1-to-1-scale bundle expulsion experiment just to see in natural size the effects on the structure, on the subassembly box, and the neighboring subassemblies. In this experiment we hope to use our knowledge from the more fundamental work, and so we shall employ a lower heat flux for practical reasons.

REFERENCES

1. Michel, A., *Wetting of Steel Pins in Sodium*, Belgonucleaire, Brussels Liquid Metal Boiling Working Group, Ispra, Progress Letters, Oct 1968, p. 3.
2. Peppler, W., and Schultheiss, G. F., *Liquid Metal Boiling Research*, Kernforschungszentrum Karlsruhe, KFK-874 (1968).
3. Taccoen, L., *Superheat Measurements in Sodium as a Function of Dissolved Gas*, Electricite de France, Chatou.
4. Pinchera, G. C., *Effect of Pressure, Velocity and Surface Roughness on Superheat*, CNEN, Casaccia di Roma; Liquid Metal Boiling Working Group, Ispra, Progress Letters, Oct 1968, p. 5.
5. Holtz, R. E., *The Effect of the Pressure-Temperature History upon Incipient-boiling Superheats in Liquid Metals*, ANL-7184 (June 1966).
6. Smidt, D., Peppler, W., Schlechtendahl, E. G., and Schultheiss, G. F., *Sodium Boiling and Fast Reactor Safety*, Kernforschungszentrum Karlsruhe, KFK-612 (Sept 1967).
7. Spiller, K. H., *Visualisation of Sodium Channel Boiling by Thermal Radiation*, S.E.T. Euratom, Ispra, Liquid Metal Boiling Working Group, Ispra, Progress Letters, Oct 1968, pp. 9–10.
8. Smith, D. C. G., and Sheriff, N., *Review of UKAEA Activities*. Liquid Metal Boiling Working Group, Ispra, Progress Letters, Oct 1968, p. 14 and p. 16.

INTRODUCTION: Impurities Expected in LMFBR Sodium and Their Significance

J. R. HUMPHREYS, JR., Moderator

Argonne National Laboratory
Argonne, Illinois

The subject for this portion of the program is "Impurities Expected in LMFBR Sodium and Their Significance." I would like to point out that we are going to discuss this; we are not going to solve problems. To stimulate and coordinate these discussions, we have invited four speakers to give their thoughts on various aspects of the subject. Each presentation will be followed by a discussion period. The audience will be invited to give opinions or experiences bearing on the subject area covered by the speaker. Our subject is a central one in sodium technology. Impurities in sodium coolant can significantly influence plant safety and reliability; they can limit operation temperatures and affect plant life. Many of the subsequent papers in both the plant design and sodium-technology sessions will deal with the subject much more specifically.

Our first invited prepared discussion is not on your schedule; last-minute changes allowed us to include it in our program, and we believe that it will serve to introduce our subject rather effectively. John McKee, Manager of the Sodium Technology Section, LMFBR Program Office, has agreed to summarize the Program Office's planning in this area and how this subject is treated in the LMFBR Program Plan.

Impurity Considerations in the National Plan

J. M. McKee

Argonne National Laboratory
Argonne, Illinois

The subject of impurities is indeed central to sodium technology, and many of the papers to be heard in the next few days will be dealing with it. Before you plunge into this rich, technical brew, it might be helpful to consider briefly how much more we *need* to know about impurities in sodium and how *soon* we need to know it. Some perspective on these questions is offered by the long-range plan for development of the LMFBR, issued in ten volumes by the U. S. Atomic Energy Commission in August of this year. By now I hope all of you have seen WASH-1105, which is Vol. 5. It describes a plan for developing the sodium technology needed to build and operate LMFBR plants in a utility environment, specifically plants with sodium outlet temperatures up to 1200°F. The latter requirement, of course, exercises an important effect on the size and cost of the plan.

Table 1 shows that impurities figure prominently in most of the nine task areas into which the sodium-technology element of the plan is divided. The problems addressed in these task areas are not new. What is new is an attempt to set limits on the time and money to be spent on them, the limits being derived from overall LMFBR needs and timing. Such an attempt implies that enough is now known about sodium technology to estimate realistically how much more government-supported work is needed in this area. Thus it signals, as Mr. Kintner noted in opening the conference, the "beginning of the end."

In the eyes of the LMFBR program planners, sodium technology is one of the base technologies needed by designers of LMFBR plants and components. It affects decisions on materials and temperatures which must be made early in the design process. Therefore, although the national plan covers a 12-year period through FY 1980, most of the output from the sodium technology program is needed within five or six years. The fast pace that results is apparent in a review of the schedule for major objectives associated with impurity levels in sodium.

Beginning with measurement of impurities, we have the exciting prospect that reliable on-line meters specific to oxygen, carbon, and hydrogen activities in sodium can become available for use during much of the compatibility testing as well as in reactors. Such monitors are much preferred over laboratory analysis for continuing measurements of impurity levels, for a number of reasons:

(1) They cost much less per measurement. For primary sodium, this difference is not trivial, since removing and analysing a single sample of radioactive sodium typically costs hundreds of dollars.

(2) They can measure oxygen and carbon activities, which are more significantly related to the effects of interest than are the total oxygen and carbon contents determined by laboratory analysis.

(3) They can measure things which laboratory analysis cannot, such as bubbles and plugging temperature.

(4) They eliminate sampling and handling errors.

(5) They provide rapid warning of abnormal impurity levels in the system.

The plan calls for development of six kinds of on-line monitors. In addition to monitors for oxygen, hydrogen, and carbon activities, development of an on-line monitor for radioactive impurities in sodium and of an improved plugging meter and resistivity meter is anticipated. Getting reliable monitors developed and into routine use in the experimental program is the most urgent immediate objective related to impurities. Efforts to evaluate existing meters should be accelerated. Development of improved or alternative concepts should be started promptly. AEC selection of concepts for development into prototype meters should be possible by the end of FY 1971. At this point, laboratory models should be ready for use in experimental work. Prooftested design and performance specifications for prototype on-line monitors are to be completed by the end of FY 1974. Further development from these specifications into on-line monitors commercially available for plant service is provided for in the Instrumentation and Control element of the Plan.

Sampling and analysis of sodium by laboratory methods also need further development. A substantial effort is schedules, both for the impurities already mentioned as well as for metallic impurities and others not measured by on-line meters. These laboratory methods are needed for support of experimental programs and for calibration on-line meters. The plan calls for development of laboratory methods to be complete by the end of FY 1973 and

for issuance of standard analytical procedures by the end of FY 1976.

The effects of impurities in sodium on material interactions are determined in the Materials Compatibility Task Area, which receives more than a third of the total effort called for on sodium technology. I propose to discuss just three of the major interaction problems briefly here: metallic mass transfer, carbon transfer, and refractory alloy corrosion.

Metallic mass transfer has traditionally received the most attention. The prominent role of oxygen is well-known and is beginning to be fairly well-explored. The plan calls for continuation of existing empirical corrosion testing, but it emphasizes a longer-range program intended to develop better understanding of the important mass-transfer mechanisms. These critical mechanisms are to be identified and characterized by the end of FY 1972. The end product of this task is a family of equations or curves for solution and deposition useful to a designer. These will include impurity effects as a prominent variable. They are to be fully developed by the end of FY 1975. The same end date applies for the technology of activity transfer and trace-metal transfer.

Carbon transfer seems to be causing designers more worry than metallic mass transfer. The plan calls for assuring control of carbon transfer within allowable limits by determining carbon-activity limits in sodium systems and monitoring with a carbon meter. The material pairs for which limits will be set include ferritic-austenitic steel and austenitic steel-refractory alloys. The preferred way to assure control of carbon transfer is to select material pairs that can be shown from thermodynamic equilibria to be permanently compatible. Essentially this means that their allowable carbon-activity ranges must overlap. It is also possible to use pairs of materials that are compatible within definable time-temperature envelopes, based on the kinetics of carbon transfer. In the plan, that kind of information is developed as a second choice. Quantitative models of carbon transfer are to be developed, and a preliminary check of the carbon control basis is to be completed by the end of FY 1975.

The crucial role of impurities in corrosion of refractory alloys in sodium is well accepted. The plan calls for identifying the rate-controlling corrosion mechanisms by the end of FY 1971. Corrosion equations or curves defining allowable impurity-temperature envelopes are to be available by the end of FY 1976. Other impurity effects evaluated in the plan but not discussed here include localized corrosion, effect of dissolved gas on cavitation, effect of particulate matter on erosion, corrosion of brazing alloys and metallic fuel, and corrosion of cladding by thermal-bond sodium.

TABLE 1. Organization of Sodium Technology Element

Task Area	Impurity Considerations
5-1 Materials compatibility	Determines effects of impurities on sodium-material interactions.
5-2 Sodium purification	Develops the technology for control of impurity levels in sodium.
5-3 Fission products in sodium systems	Fission products may be regarded as radioactive rather than chemical impurities.
5-4 On-line monitors	Develops methods for measuring impurities *in situ*.
5-5 Sampling and analysis laboratory methods	Develops methods for measuring impurities by laboratory analysis.
5-6 Fundamental properties of system sodium	Measures properties of impurities in sodium.
5-7 Cover-gas and maintenance atmospheres	Measures impurity distribution and transfer between gas and sodium.
5-8 Plant operations	Develops purity specifications for operating sodium systems.
5-9 General facility development	

The task area on fundamental property measurements includes, for impurities, determination of species, reactions, solubilities, solution kinetics, distribution coefficients, and diffusion coefficients in sodium. All of these measurements are needed in time to contribute to understanding the mechanisms of impurity damage discussed under materials compatibility.

In the task area on fission products, the plan calls for identifying the problem areas and developing methods of controlling fission products within allowable levels. The schedule here is more relaxed, calling for completion of that task area by the end of FY 1978.

Control of impurity levels in reactor sodium systems is to be developed in the purification task area, in which static and dynamic cold traps, soluble and insoluble getters of two types, and particle-removal methods will be evaluated. Impurity source rates in reactor systems are to be characterized by the end of FY 1972. AEC selection of purification concepts for development into prototype components is also scheduled at that time. Design and performance

specifications for purification components are to be completed by the end of FY 1975. The primary sodium-purification system developed in this task area must complement the system for fission-product removal developed in the fission-product task area. Substantial gains in performance and economy of purification components over those of current components are expected.

The final output of the plan, in addition to technologies for measuring and controlling impurities and design data on impurity effects, consists of specifications for allowable ranges of impurities in reactor sodium systems for all material combinations of interest. The Plant Operations Task Area calls for that to be done by the end of FY 1978.

This brief review of objectives and schedules shows that there is much to do and not much time to do it. In summary, the national plan spells out rather challenging goals in measuring impurities, determining their effects, and in controlling them, culminating in impurity specifications for LMFBR sodium systems. How well these goals and schedules are met will depend in a large measure on the people in the audience here today.

Discussion

Mr. Shannon (BNWL): Could you comment on what kinds of financing this plan is likely to require?

Mr. McKee: The plan does contain cost ranges, estimated by the Program Office, for each task. The total of these estimates for FY 1969 is about $12 million, at the center of the range. This amount is slightly more than the AEC expenditures now anticipated on sodium technology for FY 1969, but not seriously out of line. Substantial increases are called for in FY 1970, 1971, and 1972, and will obviously be necessary for the kind of scope and schedule just described. The AEC does anticipate increased budgets for sodium technology during this period. Whether such increases will match the plan and whether contractors' cost estimates will match those in the plan obviously cannot be stated with any certainty now, but I think the costs of the plan are not out of reach.

Mr. Zitek (ComEd): The program seems to be timed for the large commerical plants. What do we do for the demonstration plants that are supposed to be designed in 1971 and operating in 1974? Do we just have a plugging meter and go?

Mr. McKee: Some people representing potential reactor operators seem to believe that's all they need and want. I hope they will change their attitude. I mentioned briefly that there are current compatibility programs, which I think of as largely empirical. These are pretty much in direct support of the near-term plants. The mass-transfer program at General Electric in San Jose, one of the largest current programs, is actually being done at maximum temperatures higher than the primary coolant is likely to reach in near-term plants. That's because it is in support of the closed loops for FFTF. All of these programs measure compatibility as a function of temperature, so that it should be possible to estimate interaction rates at temperatures lower than the maximum used in the tests.

Estimation of Impurity Levels in LMFBR from Solubility Data, and Comparison with Impurity Behavior in Loops*

J. R. Weeks

Brookhaven National Laboratory
Upton, New York

Abstract

The types of impurities that might be found in an LMFBR are described. The lack of available data on their binary solubilities compounded with numerous probable or possible interactions between solutes in sodium makes impossible the estimation of impurity levels in LMFBR sodium from solubility data. The behavior of corrosion products in corrosion loops and of fission products in DFR is cited; at the present time, this information is believed to be more useful than the available solubility data in estimating LMFBR impurity levels.

In any stainless steel system containing sodium, there are invariably a number of impurities in the sodium which fall into two general classes: nonmetals such as O, N, C, H, and Cl, and metals such as Fe, Cr, Ni, and Mn. The solubilities of most of these impurities in pure sodium are not well-known at the present time, and their interactions in sodium with each other are even less known. In an LMFBR with vented fuel elements, a wide spectrum of fission products will also be present in the sodium. Adding these elements to the others already cited gives a system so complex as to make estimation of LMFBR impurity levels from solubility data a nearly impossible task, even if all the binary-solubility information were readily available, since a binary solubility implies that some form of the impurity is at unit chemical activity. This obviously will not be the case in an LMFBR. The purpose of this discussion is thus to cite the types of impurities likely to occur in sodium, their interactions in sodium that are either known or anticipated, and to compare the available solubility data with the behavior of impurities in sodium loops, and in fast reactors.

The concentrations of iron and nickel in the GE[1] and BNL[2] loops are compared in Table 1 with the solubilities of these metals in sodium at 500°C as determined at BNL.[3] The concentrations of iron are substantially higher than expected (500°C is an intermediate temperature in the GE loops and the minimum temperature in the BNL loops), whereas the nickel concentrations are more in agreement with the measured solubility. The concentrations of carbon in the sodium in both of these loops are considerably greater than the estimate of Luner *et al.* for the solubility of carbon in sodium at 450°C.

Metallic solutes are known to interact in liquid metals. An example of this type of interaction is shown in Fig. 1, as observed by the writer between iron and chromium in liquid bismuth solutions.[4] This figure represents the time dependence of the concentration of iron and chromium in bismuth held in a Type 410 stainless steel crucible after the temperature was raised from 410 to 600°C. Initially the iron and chromium dissolved in the bismuth at approximately their ratio in the steel. But, after the iron reached apparent saturation, the chromium, which is more soluble in bismuth than iron, continued to dissolve, displacing the iron from solution, so that the amounts of iron and chromium in solution after 350 hr were both approximately 25 ppm. This value bears little resemblance to either of the binary solubilities of iron (50 ppm) or of chromium (150 ppm) in bismuth at 600°C.[5] Similar interactions may occur in sodium.

Metal solutes in sodium are also known to interact with nonmetal solutes. Possible complexes of fuel-cladding metals with sodium and nonmetal solutes are listed in Table 2. Interactions between oxygen and metals in sodium are just beginning to be understood. Although most well-trapped sodium contains as much NaCl as it does Na_2O, we know very little about the effect of this dissolved chloride on either corrosion or solubilities of metals in sodium. Also, hydrogen, carbon, and oxygen in sodium possibly interact with each other and with metals. Several compounds that have been identified in cold traps or proposed to exist are also shown in Table 2. The fact that C-O or C-N compounds have been found in sodium, however, does not necessarily imply an effect of oxygen or nitrogen in the sodium on carbon transfer.[6]

The corrosion of steels or most refractory metals in sodium is directly related to the oxygen concentration in the sodium. All loops or reactors, built or proposed, use some kind of meter or device to control and/or measure the oxygen concentration of the sodium. These must all be calibrated against the solubility of oxygen in sodium. It is obvious from the above that

* Work performed under the auspices of the U. S. Atomic Energy Commission.

TABLE 1. Comparison between the Solubilities of Iron, Nickel, and Carbon in Sodium at 500°C with Their Concentrations Found in the GE[1] and BNL[2] Loops

Impurity	Solubility at ~500°C (ppm)	Amount in Loop Sodium (ppm)	
		GE[a]	BNL[a]
Fe	0.3[5]	2–5[b]	30–40[b]
Ni	1.0[5]	2.5	1
C	$<5 \times 10^{-3}$ [c] at 450°C	20–30	30–40

[a] Temperature ranges are approximately 650–370°C in the GE Loops, and 760–500°C in the BNL Loops.

[b] These numbers are not inconsistent with an estimate of the iron solubility at T_{max} as estimated by extrapolation of the results in (5).

[c] Luner, C., Cosgarea, A., Jr., and Feder, H. M., *Solubility of C in Na Alkali Metal Coolants*, IAEA, Vienna, 171 (1967).

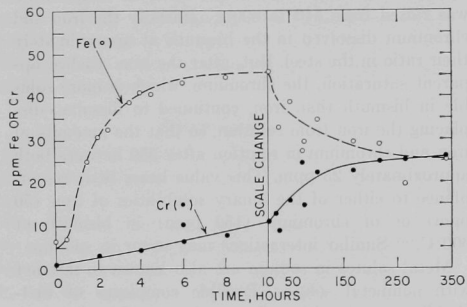

Fig. 1. Concentrations of Iron and Chromium in Samples of Liquid Bismuth Held in a Type 410 Stainless Steel Crucible as a Function of Time at 600°C after a Prior 24-hr Equilibration at 410°C. The binary solubilities of iron and chromium in bismuth at 600°C are 50 and 150 ppm, respectively.[5] Curve taken from Ref. 4.

solutions of Na_2O in sodium will react with many of the other impurities present, both dissolved or on surfaces in contact with the sodium, so that the conditions of the measurement may have substantial effect on the oxygen analyzed. This was demonstrated by Isaacs *et al.* at this conference[7] for Na-Cr-O interactions. These interactions may also effect measurements of the solubility of oxygen in sodium.

Table 3 lists five of the more recent attempts to determine, or to evaluate from other determinations, the solubility of oxygen (presumed to be as Na_2O) in sodium at 200°C. Thorley and Rutkauskas made measurements using loops, whereas Claxton and Eichelberger merely attempted to make sense out of the hodgepodge. They differ in the emphasis given to the low-temperature results of Thorley or Rutkauskas. Isaacs estimated the solubility from the emf of the cell: $Na\text{-}O_{diss} \| ThO_2\text{-}Y_2O_3 \| Na\text{-}Na_2O_{sat}$, with known amounts of Na_2O in solution. The reader can thus take his pick from a spread of values at 200°C between 8 and 30 ppm. Cold-trap temperatures, Na_2O analyses by amalgamation, and electrochemical oxygen-meter potentials in the BNL loops are all consistent with the Isaacs-Eichelberger-Rutkauskas values at low temperatures.[2] There is still disagreement over whether there is a change in slope of the solubility curve at approximately 330°C, with Claxton, Thorley, and Isaacs in favor of a change, and the others cited in Table 3 against it. In my opinion, when the interactions of Na_2O in sodium with metals, carbon, nitrogen, and hydrogen in solution are thoroughly understood, all of these experimental values will turn out to be right for the conditions in which they were measured. But, the important conclusion is that the true,

TABLE 2. Possible Complexes of Elements in Fuel-cladding Alloys with Sodium and Nonmetals, Either Identified or Presumed to Exist

Element	Complexes with Sodium and Oxygen
Fe	$(Na_2O)_2 \cdot FeO$,[a] $NaFeO_2$,[a] $Na_4Fe(CN)_6$,[a] $Na_4Fe(Cl)_6$ (?)
Cr	$NaCrO_2$,[a] $NaCrOCl_2$ (?)
Nb	Na_3NbO_4[a]
V	$Na_2O_{(x)} \cdot V_2O_{5(y)}$[a]
C—N—H—O	Na_2CO_3 (?), $Na_x(CO)_y$ (?), NaOH, NaCN

[a] Identified by one or more laboratories. $NaFeO_2$ may result from oxidation of $(Na_2O)_2 \cdot FeO$ during handling.

? Possible product.

TABLE 3. The Solubility of Oxygen (Presumed to be Na_2O) in Sodium at 200°C as Estimated by Recent Data or Correlations of Data

28.5	Claxton's Correlation[a]
22.0	Thorley's Try[b]
12	Isaacs' Isobar[c]
11	Eichelberger's Estimate[d]
9	Rutkauskas' Results[e]
$8 < ? < 30$	Weeks' Wild Guess

[a] Claxton, K. T., *Contribution to the Solubility of Oxygen in Liquid Sodium*, J. Nucl. Energy **21**, 351 (1967).

[b] Thorley, A. W., UKAEA R.M.L., Culcheth, Unpublished, Work Cited in (a).

[c] Isaacs, H. S., BNL, Upton, N. Y., in *Quarterly Prog. Rpt. for Work Sponsored by The Sodium Technology and Fuels and Materials Branches, Div. of R.D.T., USAEC*, BNL-50141, July–September (1968) pp. 28–31.

[d] Eichelberger, R. L., *The Solubility of Oxygen in Liquid Sodium: Recommended Expression*, AI-AEC-12685 (1968).

[e] Rutkauskas, V. J., *Determination of the Solubility of Oxygen in Na Using the Vacuum-Distillation Analytical Technique*, LA-3879 (1968).

binary Na_2O-Na solubility may not apply to the cold trap or plugging temperatures in an LMFBR.

Table 4 lists some of the types of impurities likely to be present in LMFBR primary sodium with fuel elements vented to the sodium. It is obvious that we know little of the binary solubilities of most of them at reactor temperatures. Their possible interactions are largely unknown in reactor sodium where none of them, with the possible exception of some of the corrosion products, are even close to unit activity. For example, the atom fractions of the rare gases argon and krypton that dissolve in sodium are 5×10^{-9} and 1.5×10^{-9}, respectively, at 480°C and 1 atmosphere pressure of rare gas.[8] As fission products, their partial pressure may be as low as $\sim 10^{-9}$ atm, so that their concentration in sodium may be $\sim 10^{-18}$ atom fraction, if true solutions exist at such concentrations.

The conclusion of this discussion is, therefore, that it is impossible to predict from the available solubility data the concentration of impurities to be expected in LMFBR sodium. The best guess on the behavior of fission products can come from examining their behavior in reactors, especially DFR, which uses vented fuel elements. During a visit to DFR in April 1967 (just before the leak caused shutdown), the writer discussed fission products in DFR with the DFR staff, especially R. A. Davies, V. M. Sinclair, J. Lyons, and J. Broadley. The following is a summary of their comments, taken from my notes. Cesium is difficult to determine in the cover gas, since it is stagnant and the sampler is quite remote from the sodium surface. The cesium activity in the DFR NaK is approximately 10 times greater than it was anticipated to be from recoil calculations; the cesium activity in the NaK was still rising at that time. There was also cesium activity in the cover gas, and the $^{137}Cs/Na$ ratio in the cold trap is higher than it is in the circuit NaK. Barium and lanthanum plate out all over the circuit; every solid material taken out of DFR has barium and lanthanum activity on it—specimen holders, NaK samplers, bypass loop sections, etc. An acid wash is required for their complete removal, suggesting a possible chemisorption of barium and lanthanum on the surfaces, if not diffusion of these metals into the steel surface.* Neither of the radiogenically produced calcium or magnesium ever built up in the primary NaK to their detection limit (~5 ppm). Calcium and magnesium were both found in the cold trap, and may have contributed to the gradual reduction with time of the oxygen activity of the NaK.

* Could this property of barium be responsible for its effectiveness in reducing mass transport of radionuclides from in-pile steel coupons to out-of-pile heat exchangers?[9]

TABLE 4. Types of Impurities Likely to be Present in LMFBR Sodium with Vented (or Ruptured) Fuel Elements Clad with Stainless Steel

Corrosion products:	
Fe, Ni, Cr, Mn	
Impurities always present in circulating sodium:	
O, C, H, Cl, N	
Fission products:	
Noble gases:	Xe, Kr
Alkali metals:	Cs, Rb
Halogens:	I, Br
Rare earths:	La, Ce, etc.
Alkali earths:	Ba, Sr
Noble metals:	Pd, Rh, Ru
Transition metals:	Zr, Nb, etc.
Radiogenically produced elements:	
Mg	

Acknowledgments

The writer is most grateful for the useful discussions he had at Dounreay. He also thanks J. R. Humphreys for inviting this discussion.

REFERENCES

1. Rowland, M. C., Plumlee, D. E., and Young, R. S., *Sodium Mass Transfer: XV. Behavior of Selected Steels in Flowing Sodium Test Loops*, GEAP-4931 (1965).
2. Romano, A. J. (Brookhaven National Laboratory), private communication (Oct 28, 1968).
3. Singer, R. M., and Weeks, J. R., *On the Solubilities of Cu, Ni, and Fe in Liquid Sodium*, THIS CONFERENCE.
4. Weeks, J. R., and Gurinsky, D. H., *Solid-Metal Liquid Metal Reactions in Bismuth and Sodium, Liquid Metals and Solidification*, Ed. Chalmers, B., American Society for Metals, Cleveland, 106 (1968).
5. Klamut, C. J., Schweitzer, D. G., Chow, J. G. Y., Meyer, R. A., Kammerer, O. F., Weeks, J. R., and Gurinsky, D. H., "Material and Fuel Technology for an LMFR," *Progress in Nuclear Energy*, Series IV, Vol 2—*Technology, Engineering, and Safety*, Pergamon Press, New York 433 (1960); 1958 Geneva Conference Paper P/2406.
6. Sinclair, V. M. (Dounreay Experimental Reactor Establishment, Thurso, Scotland) private communication (April 19, 1967).
7. Isaacs, H. S., Minushkin, B., and Salzano, F. S., *A Study of Reactions between Oxygen and Impurities in Sodium*, THIS CONFERENCE.
8. Veleckis, E., *et al.*, in *Chem. Eng. Div. Semiannual Reports*, ANL-6900 (Jan–June 1964) p. 125, and ANL-7325 (July–Dec 1966) p. 128.
9. Haag, F. G., "Material Transport in Sodium Systems, Liquid Metals Technology, Part 1," *Chemical Engineering Progress Symposium Series*, Number 20, Vol 53, p. 43 (1957).

Discussion

Mr. Zitek (ComEd): Where does the nitrogen come from? Is it a corrosion product or it is a cover-gas contaminant?

Mr. Weeks: Primarily from cover gas; in addition,

most metals contain nitrogen, which certainly can get into the sodium if the thermodynamics are proper for it to do so.

Mr. Zebroski (GE): I would like to comment a little on the fission products for the case of vented fuel. If you have an intentionally vented fuel instead of (unintentional) vented fuel by pin-hole failure, you can get a situation where essentially nothing shows up in the coolant except krypton. You don't have to contend with the xenon daughter products. Nonvented fuel may well lead to a nastier and harder-to-decontaminate system than vented fuel.

Mr. Weeks: I don't disagree.

Mr. Epstein (ANL): I was surprised by the occurrence of silver among the fission products. Silver has a very low yield as a fission product.

Mr. Weeks: I have no comment to make except that it was on a list of typical types of fission products. This is one, from our experience, which would be reasonably soluble in the sodium and probably stay there. That is the only reason I put it in.

Mr. Shannon (BNWL): I might add a comment on that point. We have recently seen radioantimony in sodium exposed to stainless steel. Antimony is not a very high constituent of stainless steel, but it is selectively leached and there results a fairly significant concentration of radioantimony.

Mr. Weeks: I have only one comment to make. Every single radiotracer sample that has seen sodium has had antimony in it. It is always there. We have taken a piece of zone-refined iron, pickled it, and hydrogen-fired it. We distilled sodium very carefully into it and sent the sample to the analysts. There was antimony. In other words, I agree with you, and I think it is a common observation. I know of no explanation for it.

Mr. Zitek: Could it be that it results from the analytical technique?

Mr. Weeks: The head of our analytical group is here, if he wishes to comment.

Mr. Newman (BNL): I don't think it can result from the analytical techniques since this is radioantimony. Nowhere along the line do we contact radioantimony other than from the sample.

Mr. Feder (ANL): I think it should be clear from the kinds of data that you have put on the board (and others that we will be discussing later this week) that it is unlikely that all species of the same element are necessarily in equilibrium with each other. Failure to distinguish among these species will of course cause variations in apparent solubility. On top of that, we have the obvious phenomenon that a great many of the materials we are looking at may not be in solution at all but are finely particulate. With these two considerations in mind, I think the situation overall can become much clearer.

Mr. Weeks: I agree with you. Actually Dr. Tyzack and I concluded at the Vienna Conference of 2 years ago that corrosion rates suggest the sodium is nearly saturated at the maximum temperature of each circuit. One of the conclusions that I will be talking about tomorrow, but I think I have to say it here because it is probably a different audience, is that the iron concentrations in sodium loops agree quite well with that postulate. I can't speak for carbon.

Mr. Humphreys (Moderator): Since the subject of particles came up, I think we should add that the complexity is very great. We have observed recently that immediately downstream of a particulate clean-up step there is a sharp increase in local corrosion rate. This indicates than an inventory of particles circulates and that some of them are in fairly rapid equilibrium with some of the solubility processes.

Mr. Weeks: Thank you. I had heard of that observation, but I haven't seen it on paper yet.

Mr. Humphreys: I think that does tend to clarify our present position on the application of solubility data for the prediction of impurity levels in sodium.

This leads us into the next topic, which is sampling sodium systems by looking at deposits that are taken from cold traps or other low temperature regions. This could be a potential system-sampling tool which could give information as to the impurity state that existed in the sodium from which these impurities were precipitated. Westinghouse has examined the Fermi cold trap; Mine Safety has examined their cold traps; EBR-II has cold traps ready for examination. It is quite conceivable that the information that is obtained in this way could lead to meaningful information as to the systems in which they were operated. The Program Plan that John McKee described earlier calls for the establishment of a cold-trap examination facility. Recently, Dutina, at General Electric, has attempted to go one step further by making specific sampling devices to gather such deposits and to analyze them. We have a program under way at Argonne, which is in the early stages, of making a model cold-trap device which again is designed to sample the precipitated deposits from a large engineering system.

Identification of Sodium-impurity Species by Analysis of Cold-trap Contents*

SHERIDAN J. RODGERS

MSA Research Corporation
Evans City, Pennsylvania

ABSTRACT

Two cold traps were removed from MSA Research Corp. operational loops and the contents were analyzed for O_2, C, N_2, H_2, carbon compounds, particle size, and metallic impurities. Cold Trap I-C had operated for 1400 hr and Cold Trap II-O_2 for 2300 hr. Loop I-C had operated with a high-carbon environment such that part of the mainstream flow passed through a bed of graphite rods at 1200°F. Loop II-O_2 had operated with a high-oxygen environment with the cold trap being operated at 700°F to provide oxygen concentration of ~300 ppm O_2.

The oxide was concentrated in the region below the mesh and in the first few inches of the mesh. Cold Trap I-C, which operated at 250°F, effectively removed hydrogen, whereas Cold Trap II-O_2 which operated at 700°F did not remove hydrogen. Carbon was found in both cold traps. Cold Trap I-C contained 0.05 lb carbon and Cold Trap II-O_2 0.01 lb carbon. It appeared that mesh must be used in a cold trap if carbon is to be removed effectively. Carbon dioxide, C_2H_2, and HCN were found in both traps at significant levels. Traces of methane, ethane, ethylene, carbonyl sulfide, hydrogen sulfide, cyanogen, and oxymonocyanogen were also found. Iron ranging to 1% was found in Cold Trap I-C; maximum iron concentration in Cold Trap II-O_2 was ~0.5%.

On the basis of the relative quantities of CO_2, C_2H_2, and HCN detected during analysis, it is assumed that Na_2C_2 or some acetylene-producing compound, such as a carbonyl, is responsible for carburization of austenitic steels.

1. Introduction

This paper describes the analyses of two cold traps removed from operational loops in service at MSA Research Corp. The contents were analyzed for oxygen, carbon, nitrogen, hydrogen, carbon compounds, metallic impurities, and particle size of insolubles. Cold Trap I-C was operated for 1400 hr and Cold Trap II-O_2 for 2300 hr. Loop I-C was operated with a high-carbon environment such that part of the mainstream flow was passed through a bed of graphite rods at 1200°F. Loop II-O_2 was operated with a high-oxygen environment with the cold trap being operated at 700°F to provide oxygen concentration of approximately 300 ppm O_2 in the main sodium stream.

Specimens for mechanical property test exposed to the sodium environment of Loop I-C underwent extensive carburization (up to 10,000 ppm in 168 hr) whereas others exposed in Loop II-O_2 showed no signs of carburization. One of the primary objectives of this study was to clarify the carburization mechanism of stainless steel in sodium based on the cold-trap contents.

2. Mechanical Property Test System

2.1. Description of Test Loops

Each loop contained 400 lb of sodium and was operated at 1200°F. Sodium flow was divided into seven parallel circuits, each containing a creep-test unit. An eighth parallel circuit included the necessary components for monitoring and controlling the impurity concentration of the sodium. Flow entered this circuit through a throttling valve and passed through a magnetic flow meter, an electromagnetic pump, an economizer, and a finned air cooler. Upon leaving the finned cooler, the flow was split by means of control and shutoff valves to allow a choice of flow through either the plugging indicator or the cold trap. Another parallel circuit was provided in Loop I-C where part of the stream was passed through the carbon bed.

2.2. Carbon Source

The carbon bed consisted of a Type 316 stainless steel tank containing 11.8 lb of spectrographic-grade carbon rod, ¼ in. in diameter and ¼ in. long. A micrometallic filter with a mean pore opening of 20 μ was installed at the discharge end of the container to prevent particulate carbon larger than 20 μ from being carried into the main stream. Resistance-type surface heaters were used to maintain the bed at the desired operating temperature. The carburization potential of the system was varied by appropriate selection of flow and/or temperature of the carbon bed. (Carburization potential is defined as the rate at which Type 304 stainless steel monitoring tabs will absorb carbon.)

2.3. Cold-trap Description

Figure 1 is a schematic of the cold traps, which were made of Type 316 stainless steel, Schedule 40, 8-in.

* Work performed under U. S. Atomic Energy Commission Contract AT(11-1)-765. Reported in greater detail in MSAR Topical Report No. 9, MSAR 67-203.

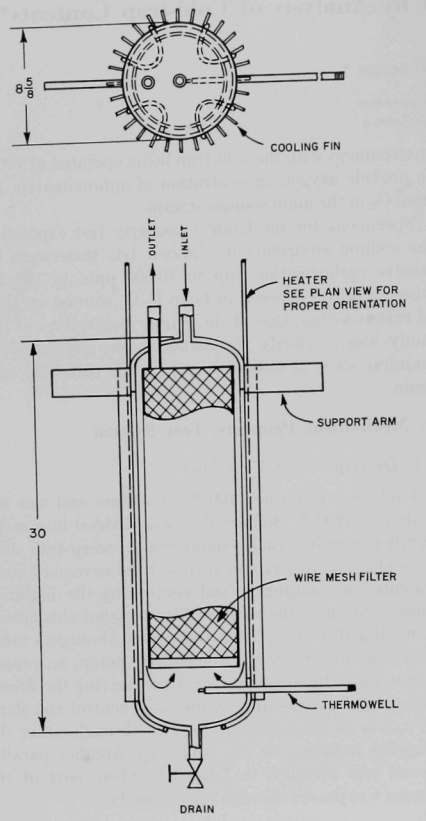

FIG. 1. Cold Trap.

pipe. Overall the height was 30 in. and the diameter 8 in. Wire mesh (11 mil, 316 stainless steel, 14 lb/cu ft) was packed in a tight cylinder, of 7-in. OD and 23 in. long. Sodium entered the top of the trap at 800°F, and flowed down an 0.49-in. annulus into a mesh-free region, up through the mesh, and out the top of the trap. Cooling fins were installed on the outside of the trap, and the temperature was adjusted and maintained by the air flow rate past these fins. The Loop I-C cold trap was operated at a temperature of 250 to 280°F and the Loop II-O_2 high-oxygen cold trap 700°F.

3. Procedures for Cold-trap Sampling

Figure 2 shows the cold-trap sample locations. Eighteen sample locations were chosen along the vertical length of the traps. Sample locations were alternated at 90° rotation to yield 9 sample locations in each of two planes. Number 1 sample location was at the bottom of the trap in the mesh-free region. Number 2 sample was in the mesh-free region also, and was rotated 90° from the number 1 sample. Each sodium core was sectioned into three equal parts representing a cross section of the cold trap. Thus, both vertical and radial distribution of impurities were determined.

The sampling technique consisted of drilling 1⅛-in. holes through the outer cold-trap wall and through the inner can, and then driving a 1-in.-OD sampling tube into the sodium. This method was used successfully for sampling both the Sodium Reactor Experiment sodium cold trap and the Enrico Fermi sodium cold trap. An argon atmosphere was maintained over the cold trap during the drilling and coring operation.

Figure 3 shows typical cores from the mesh-free section, the lower mesh region, and the higher mesh re-

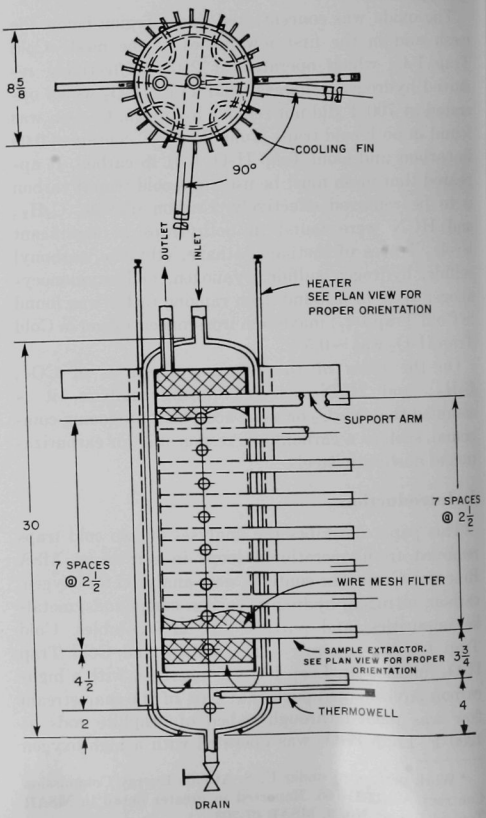

FIG. 2. Cold Trap and Sample Locations.

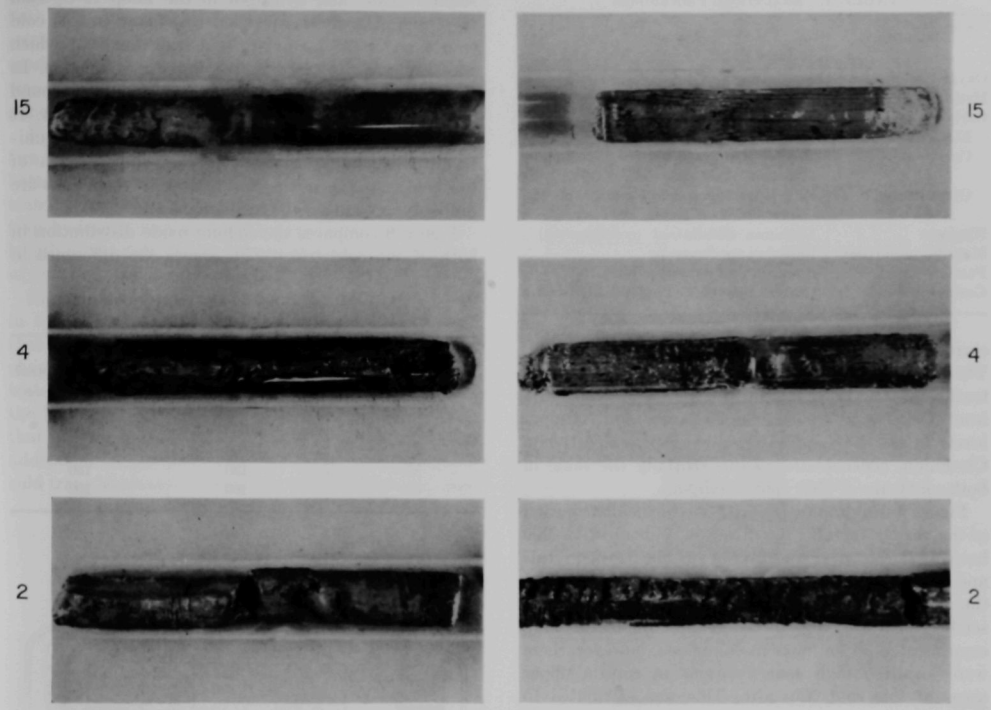

FIG. 3. Typical Sample Cores.

gion of both cold traps. The number 2 sample from Cold Trap I-C contained 20% sodium oxide and exhibited a metallic luster. The core when cut revealed a bright, shiny cross section with dark gray deposits and was harder than pure sodium. The number 2 sample from Cold Trap II-O_2 contained 67% sodium monoxide. The sample core was dark gray and had a coarse, grainy appearance. This material was hard and brittle, and visible examination of the cross-section cut indicated about 10% of this section to be bright and shiny sodium dispersed in a coarse, matrix material.

4. Analytical Procedures

The analytical procedures used in the analyses of the cold-trap residues are shown in Table 1. These procedures were originally established for analyses of relatively pure liquid metals; therefore some modifications were adopted to cover the full range of impurity concentration encountered in cold-trap sodium. For instance, high-oxygen sodium samples required more mercury extractions (typically 12 to 14 versus 6 for clean sodium) to obtain a sodium-free residue and 0.1 *N* acid was used in the final titration instead of the 0.01 *N* acid used for low-oxygen samples.

In most cases, a sample of 1 to 2 g of sodium was used for the procedures. A cross-section sample disc was sliced from the sodium core using a hinged cutting device. Any surface contamination on the disc was trimmed off with a knife. The cutting instruments were cleaned after each sample. The sample was ultimately placed in the appropriate analytical apparatus and removed from the glovebox; the analysis was then performed in the laboratory.

5. Results

5.1 Maximum Content of Metallic Impurities

Table 2 lists the maximum concentrations of the metals found in the cold trap. Iron, nickel, and chromium were transported to the cold trap as a result of

TABLE 1. ANALYTICAL PROCEDURES

Impurity	Method
Oxygen	Amalgamation
Hydrogen	Isotopic dilution
Carbon:	
Elemental	Combustion of dry chloride
Carbonate	Mass spectrography of results of acidification of off-gases
Other forms	Mass spectrography of results of dissolution of off-gases
Nitrogen	Ammonia distillation (colorimetric)
Metallic impurities	Emission spectroscopy
Particle size	Electron and optical microscopy
Carbon in mesh	Carbon analysis and optical microscopy

corrosion and/or erosion of the stainless steel system. The Loop I-C cold trap contained a maximum concentration of 1% iron, the Loop II-O_2 cold trap 0.5% iron. Nickel was found at the 2000-ppm and 700-ppm levels in the I-C and II-O_2 cold traps, respectively. Chromium concentration was essentially the same in both cold traps at 1500 ppm, maximum.

Figure 4 is a graphic presentation of the distribution of the various metallic impurities in cold trap I-C. The horizontal line near the bottom of the trap, in this and all subsequent figures, represents that area where the mesh started. The area below this line was a settling chamber. Most of the metallic impurities were concentrated in the lower mesh regions; however, there were localized high concentrations in certain upper areas of this cold trap also. This was attributed to thermal excursions that the cold trap had experienced; during these the impurities migrated from the lower part of the cold trap to the upper regions.

Figure 5 is a graphic presentation of the metallic impurities distribution in the cold trap II-O_2. Again, the major fraction of the impurities is located in the lower regions of the cold trap. It is interesting to note that in this cold trap a large portion of the impurities is also found beneath the mesh region in the settling chamber.

5.2. Distribution of Elemental Carbon, Sodium Oxide, and Hydrogen in Cold Trap I-C

Figure 6 shows the distribution of elemental carbon, sodium oxide, and hydrogen in the Loop I-C cold trap. Carbon appeared to be concentrated in the lower mesh region. Oxygen was also concentrated in the lower mesh region, but a significant quantity of sodium oxide was found in the settling-chamber region of the cold trap. Hydrogen was uniformly distributed in the lower mesh region and the settling-chamber area. Little hydrogen was found in the higher mesh regions.

Figure 7 shows the distribution of elemental carbon, sodium oxide, and hydrogen in the Loop II-O_2 cold trap. Significantly, less carbon was found in this cold trap than in the Loop I-C cold trap, but that which was found was located in the lower mesh region. In this cold trap, most of the sodium oxide was found beneath the mesh in the settling-chamber region. It is interesting to note that hydrogen was rather uniformly distributed throughout the whole length of this cold trap, suggesting that hydrogen compounds are probably unstable at the trap temperature, 700°F.

Figure 8 compares the sodium oxide distribution in both of the cold traps. This shows the difference in

TABLE 2. MAXIMUM CONCENTRATIONS OF METALLIC IMPURITIES

Element	Loop I-C (High Carbon) (ppm)	Loop II-O_2 (High Oxygen) (ppm)
Fe	10,000	5,000
Ni	2,000	700
Cr	1,500	1,500
Mo	150	150
Cu	100	100

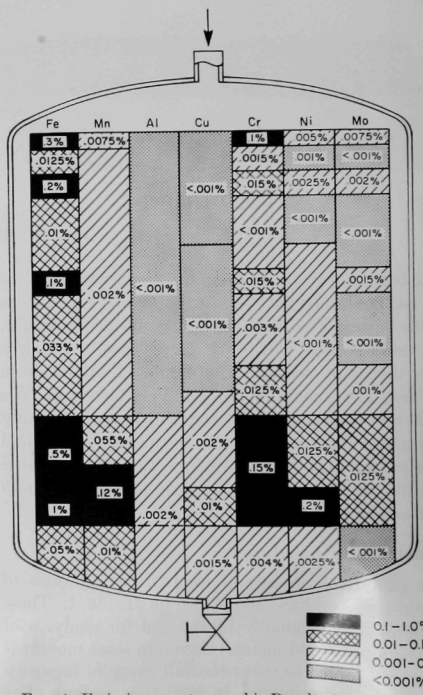

FIG. 4. Emission-spectrographic Results for Cold Trap I-C.

oxygen distribution in the two cold traps although both traps show that oxygen is concentrated in the settling-chamber region and in the first few inches of mesh. However, in the Loop II-O_2 cold trap, the oxide was more heavily concentrated in the settling-chamber region.

Figure 9 compares the hydrogen distributions in the two cold traps. In the Loop I-C cold trap, where the bottom was operated at 250°F, the hydrogen is concentrated in that region, whereas in the Loop II-O_2 cold trap hydrogen was uniformly distributed through the length of the cold trap, again indicating the instability of hydrogen compounds above 700°F.

Figure 10 shows the elemental carbon distributions in the two cold traps. It is interesting to note here that the carbon was not concentrated in the settling chamber as was the case with oxygen, but was concentrated in the first few inches of the mesh. This indicates the behavior of precipitated carbon is different from that of precipitated oxide in a cold trap and that additional design work may be required to optimize cold traps as cleanup devices for carbon. It should also

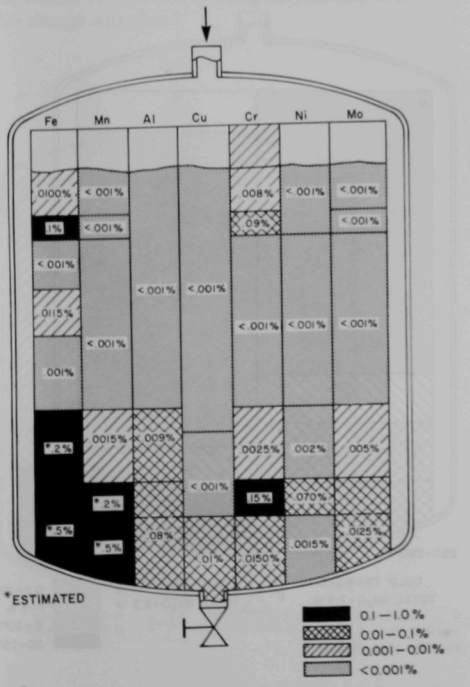

FIG. 5. Emission-spectrographic Results for Cold Trap II-O_2.

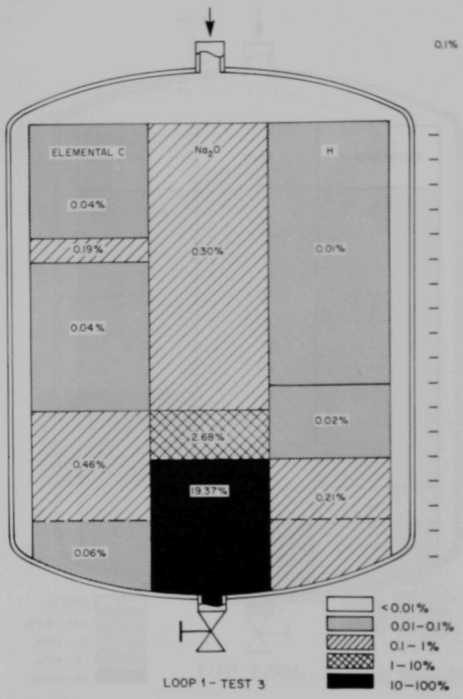

FIG. 6. Oxygen, Carbon, and Hydrogen Contents in Loop I, Test 3.

be pointed out that the wire mesh of the cold traps did undergo carburization. In the Cold Trap I-C carbon was nearly uniformly distributed throughout the length of the cold trap in the mesh at a level of about 1.39 wt %. In cold trap II-O_2 the average carbon content of the mesh was 0.45%, ranging from approximately 1% at the bottom of the mesh to approximately 0.25% near the top.

Particle-size analyses were made of materials which were insoluble after hydrolysis and digestion in acid. Both optical microscopy and electron microscopy were were used. In general, the individual particles ranged from 0.1 μ, with a mean particle size of ~0.3 μ. No particles smaller than 0.05 μ were found. Some agglomerates with relative particle sizes ranging to tens of microns were also observed.

5.3. Distribution of Carbon Species

Figure 11 compares the combined carbon distribution in both cold traps. In the Loop I-C cold trap, the combined carbon was concentrated in the settling chamber

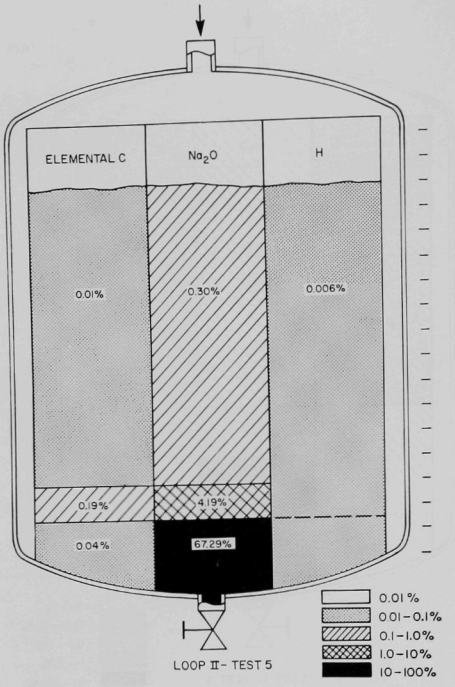

FIG. 7. Carbon, Oxygen, and Hydrogen Contents in Loop II, Test 5.

and in the first few inches of the mesh; in the Loop II-O_2 cold trap the combined carbon was concentrated in the settling chamber. The total combined carbon content of the Loop I-C cold trap was approximately 12½ times higher than that in the Loop II-O_2 cold trap.

Table 3 compares the carbon impurities in the two cold traps and may provide a clue as to the carbon species which causes carburization of stainless steel in 1200°F sodium. Stainless steel specimens exposed in Loop I-C underwent massive carburization while similar specimens exposed in Loop II-O_2 showed essentially no signs of carburization. The elemental carbon ratio of the cold traps was roughly 5 times higher in Loop I-C than in Loop II-O_2. However, chemical analyses of the sodium during the test showed the elemental carbon content to be essentially the same in both loops, that is, 30 to 35 ppm. Therefore, it is assumed that elemental carbon is not responsible for carburization. The ratio of HCN in the Loop I-C to the Loop II-O_2 cold trap was 0.66. Therefore it must be assumed that this could not have been responsible for carburization. The ratio of CO_2 concentration in the Loop I-C to the Loop II-O_2 cold trap was 17.5, which may suggest this as a potential means of carburization. However, recent work done in both this country and Great Britian indicates that carbonate added to 1200°F sodium does not cause carburization. Finally, the acetylene ratio of the Loop I-C to the Loop II-O_2 cold trap was 120. This is the highest ratio of carbon compounds in the two loops. This leads to the conclusion then that sodium carbide or an acetylene-producing compound is responsible for the mechanism of carburization of stainless steel in sodium.

In conclusion, the work on the analysis of cold traps has led to a better understanding of the fashion in which impurities are collected and distributed in the cold trap, and also an understanding of the difference in the behavior of these impurities, depending upon the cold-trap temperature and the nature of the impurities.

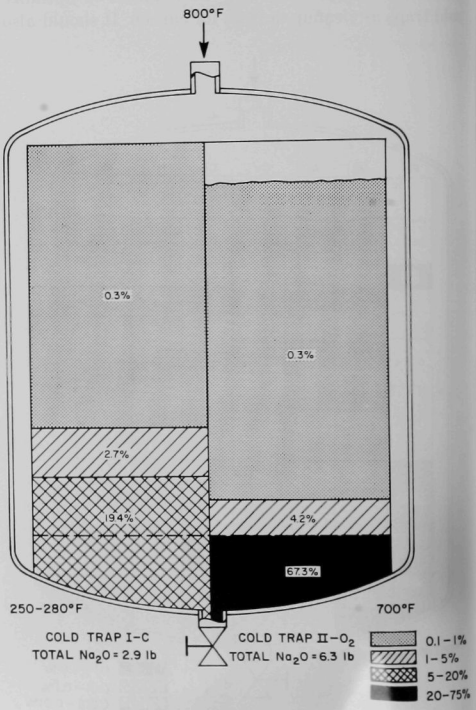

FIG. 8. Sodium Oxide Distribution in Cold Traps I-C and II-O_2.

The fact that many of the impurities, particularly oxide, appear to collect in the settling chamber beneath the mesh suggests potential designs could lead to an extended lifetime of a cold trap. Finally, the results indicate that a carbide type of material is probably responsible for carburization of stainless steel in sodium at 1200°F.

Discussion

Mr. Eichelberger (AI): You report a lot of hydrogen. Is the source of hydrogen your bed of carbon?

Mr. Rodgers: No, I have to go back and describe what we are doing in our system to explain the source of hydrogen. This is a mechanical properties test system, and we are continuously putting specimens into test pots and taking them out. Although we do make an effort to keep out air, we do get some air contamination. I believe our primary source of hydrogen is water vapor from the atmosphere.

Mr. D. L. Smith (ANL): In what form was the carbon that you put in the high carbon loop, and did this change with time? The second question refers to the carbon in the total system, not just cold trap. Did this change with time?

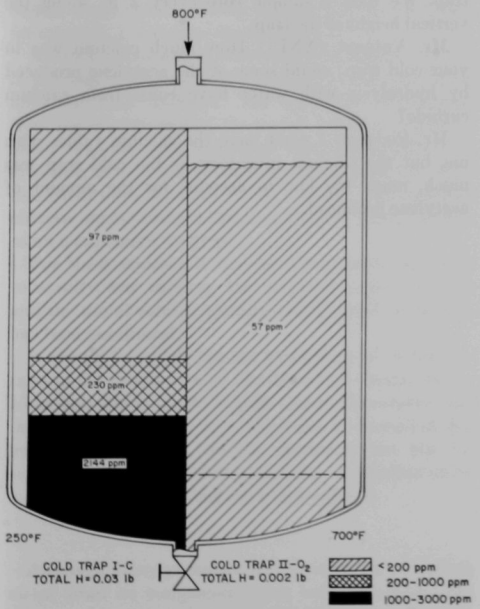

FIG. 9. Elemental Hydrogen Distribution in Cold Traps I-C and II-O_2.

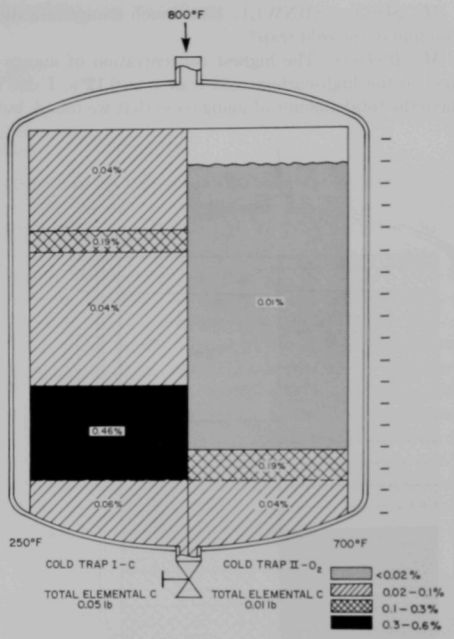

FIG. 10. Elemental Carbon Distribution in Cold Traps I-C and II-O_2.

Mr. Rodgers: The carbon that we added was in the form of spectrographic carbon rods. These were ¼ in. in diameter. They were broken into or cut into ¼-in.-long sections and packaged within a stainless steel vessel with a micrometallic filter downstream of the carbon bed to avoid the introduction of particulates. Whether we did or did not introduce particulates I do not know. In answer to your second question we analyzed primarily for elemental carbon during this period of operation, and in all honesty, we could not tell on the basis of elemental-carbon analysis the difference between loop one and loop two. Although the stainless tabs we exposed certainly showed that one had a high carburization potential and the other had essentially zero carburization potential.

Mr. Berkey (W): I was particularly interested in the high metallic impurity levels that you found and presumably this does not come from any reactions in the cold trap itself but constitute particles or material that was deposited from the loop. Did you study any particulate size distribution of metallic impurities?

Mr. Rodgers: No, we did not. The only size distribution that was performed was for the carbon itself.

Mr. Shannon (BNWL): How much manganese did you find in the cold trap?

Mr. Rodgers: The highest concentration of manganese in the high-carbon cold trap was 0.12%. I don't have the total amount of manganese that we found, but its concentration was 0.12% compared to 1% for iron, 0.2% for nickel. In the high-oxygen cold trap, the manganese concentration was about the same order of magnitude as was the iron concentration, approximately ½% max.

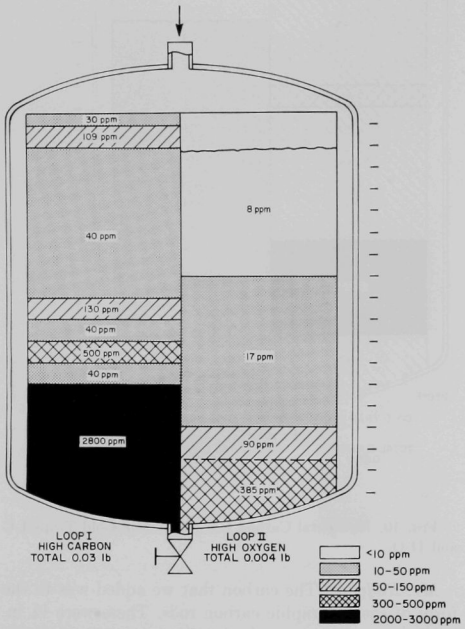

FIG. 11. Combined Carbon Distribution.

TABLE 3. COMPARISON OF IMPURITY INVENTORY

Impurity	Loop I-C High Carbon (lb)	Loop II-O_2 High Oxygen (lb)	Ratio (I-C/II-O_2)
O_2	2.9	6.3	0.46
C	5×10^{-2}	1×10^{-2}	5
CO_2	7×10^{-3}	0.4×10^{-3}	17.5
HCN	2×10^{-3}	3×10^{-3}	0.66
C_2H_2	2.4×10^{-2}	0.02×10^{-2}	120

Mr. Ramachandran (ANL): Did you introduce any impurities through your means of sampling?

Mr. Rodgers: I would hesitate to say that we didn't. There are so many impurities that they would have masked any small donation we may have had from the sampling technique itself. I doubt if the sampling technique added anything to the inventory.

Mr. Ramachandran: Did you sample the entire inventory inside the trap?

Mr. Rodgers: No, we did not analyze the whole trap. We took a sample core every 2 in. along the vertical height of the trap.

Mr. Natesan (ANL): How much calcium was in your cold trap; could some of the acetylene produced by hydrolysis with water have come from calcium carbide?

Mr. Rodgers: I don't have the calcium values with me, but the calcium inventory in the cold trap was much, much too low to account for the amount of acetylene produced.

Alkaline Earth Impurities in Sodium

Leo F. Epstein

Argonne National Laboratory
Argonne, Illinois

Abstract

Calcium is universally present in sodium because sodium is manufactured by the electrolysis of NaCl-$CaCl_2$ mixtures. Normally, the calcium content is of the order of 200 to 500 ppm by weight. For "reactor grade" sodium, this is reduced to 10 ppm or less. Low calcium values are achieved by taking advantage of the fact that when liquid sodium containing calcium is oxidized by air, insoluble CaO is formed preferentially and can be filtered off. Prolonged circulation of sodium containing calcium in a heat-transfer loop results in gradual reduction of the calcium content.

The alkaline earth metals thermodynamically can reduce Na_2O, forming relatively insoluble oxides like CaO and BaO. This is the basis for the use of these metals as "soluble getters." But the formation of brittle intermetallic compounds with the structural metals of the system, $CaNi_5$ with nickel-bearing alloys for example, is a serious disadvantage.

Another phenomenon observed with alkaline earths in solution in sodium is the reaction at the gas-liquid interface with nitrogen. The transport of nitrogen from the gas phase into the liquid, where it can bring about reaction with immersed materials sensitive to nitriding, is believed to depend markedly on the alkaline earth metal content of the sodium. This fact has obvious implications to the possibility of using nitrogen as an inexpensive cover gas.

For these reasons, it has been considered desirable to specify low calcium for "reactor grade" sodium, and the use of soluble alkaline earth metals as getters has been questioned.

It should be noted that the irradiation of sodium results in the production of Na-24, which decays with a 15-hr half-life to stable Mg-24. Calculation shows that the amounts of magnesium which can be formed in this way after extended reactor operation are not insignificantly small, and the problems of alkaline earth metals in sodium systems seem unavoidable.

Although many processes for the isolation of sodium metal from its compounds have been proposed since this was first accomplished by Sir Humphrey Davy in 1807, at the present time[1] virtually all large-scale production of sodium, in this country and abroad,* is carried out by the electrolytic dissociation of fused NaCl. Because of the high melting point of NaCl, namely, 800°C, calcium chloride ($CaCl_2$) is added to depress the operating temperature in order to prevent excessive corrosion of the cell walls and electrodes.† The NaCl-$CaCl_2$ eutectic (containing 66.8% $CaCl_2$, and melting at 505°C) might be expected to be the most desirable mixture; but in fact melts containing 58 to 59% $CaCl_2$, m. pt. 575–585°C, are used. This composition is a compromise between the decreased corrosion and the decreased cell efficiency observed at lower temperatures.‡ Normally, a steel cathode and a graphite anode are used in this process—a fact which has interesting implications as regards the impurities, particularly the carbon content, to be expected in sodium metal.

As a result of the use of this electrolyte, calcium is a ubiquitous impurity in commercially produced sodium. How much is present will depend largely on the care exercised in the collection of the molten metal at the cathode. All sodium manufacturers attempt to control the calcium content of their product and to keep it at a low level. This is achieved, among other procedures, by cooling the melt to a little above the melting point so as to precipitate out most of the calcium metal. As can be seen from Table 1, this should yield sodium containing some 250 to 500 ppm calcium by weight. So-called "reactor grade" sodium, to be used in nuclear systems, differs largely from run-of-the-mill material in its calcium content, largely because of the special

---

* Except in Japan and a few other locations, where Castner cell sodium, made by the electrolysis of fused NaOH, is produced. This material should be free of calcium and other alkaline earth metals. Also, it should be low in carbon, since a nickel anode is utilized, rather than the graphite used in the Downs process described above.

† Another important reason for using a melt with a lower melting point than that of pure NaCl is that the solubility of metallic sodium in liquid NaCl at about 800°C is so high that recombination cannot be prevented, and current efficiencies are impossibly low[2].

‡ The $CaCl_2$-NaCl eutectic is not used because at this level of $CaCl_2$ the Na^+ concentration cannot be maintained at a practical level in the cathode compartment. The electrolysis depletes the Na^+ to some level below the average bath composition depending on current density and bath circulation factors[2].

TABLE 1. SOLUBILITY OF CALCIUM IN SODIUM[13]

$\log_{10} w = 6.5629 - (1546.6/T_{(°K)})$

T (°C)	w (ppm by weight)
97.81 (m. pt. of Na)	250
100	260
125	480
150	820
175	1500
200	2000
300	7400
400	18,000
500	37,000

TABLE 2. FREE ENERGIES OF FORMATION OF OXIDES[12]

T (°K)	$-\Delta F°_T$ (cal/mole)				
	Na_2O	MgO	CaO	SrO	BaO
298	89,950	136,100	144,350	133,850	126,300
400	86,600	133,500	141,850	(131,450)	124,000
500	83,100	131,000	139,400	(129,100)	121,650
600	79,600	128,400	136,950	(126,750)	119,400
700	76,100	125,900	134,500	(124,400)	117,100
800	72,400	123,300	132,050	(122,250)	115,000
900	69,200	120,750	129,650	(120,000)	113,100
1000	65,700	118,050	127,200	(117,500)	111,100
1100	62,000	115,200	124,700	(115,200)	108,500
1200	(58,200)	112,600	(122,400)	(112,600)	(106,000)
Melting point (°K)	1190	3173	2873	2688	2186

precautions taken to prevent excess calcium from accumulating in the product.

Reactor-grade sodium contains much less than this equilibrium quantity of calcium, corresponding to saturation, of the order of 10 ppm or less. This comes about because of a very interesting chemical process: when liquid sodium containing calcium is exposed to air, the calcium appears to be preferentially oxidized. The resulting CaO is quite insoluble* in sodium and is normally removed in the first step in sodium purification: filtration. This reaction can be carried further, so that levels as low as 2 ppm calcium in sodium are not uncommonly achieved.

Furthermore, it has been observed that prolonged circulation of sodium in a heat-transfer system results in a steady and continuous decrease in the calcium content; for long-term operation, levels of 5 ppm and less are often obtained.† The primary mechanism of this process is believed to be the deposition of the CaO produced by preferential oxidation in system cold traps. Since calcium also reacts directly with nitrogen at elevated temperatures, some of the calcium may also be converted to the nitride, and end up precipitated in the cold traps along with CaO.‡ Another factor operating in such loops is the formation of a stable intermetallic compound between calcium and the structural metals in the loop, particularly with nickel.

Calcium and the other alkaline earth metals§ react with Na_2O present in sodium according to the equation

$$Ca + Na_2O \rightarrow 2\ Na + CaO,$$

as can be seen from the free energy data[12] in Table 2. The free energies refer to the standard states of the substances, solid or liquid for the elements, solid for Na_2O and the alkaline earth oxides. For the reaction of greater interest

$$Ca\ (\text{in solution in sodium}) + Na_2O\ (\text{in solution in sodium}) \rightarrow 2\ Na\ (l) + CaO\ (s),$$

the free energy change associated with the process is given by

$$\Delta F_T = [\Delta F_T°(CaO) - \Delta F_T°(Na_2O)] - RT \ln a_{Ca\ in\ Na}\, a_{Na_2O\ in\ Na},$$

where the $\Delta F°_T$ values can be derived from Table 2. The activities of the species in solution, which are proportional to their fraction at saturation, are often much less than unity. Thus the presence of the calcium and Na_2O in solution in sodium can be expected to lead to slightly different ΔF_T values for the reaction. The effectiveness of these materials as deoxidants apparently increases in going from lighter to heavier elements, probably largely due to the fact that the solubility of barium is so much greater than that of magnesium or calcium (see Fig. 1 and Table 3). The solubility of strontium in sodium has apparently not been measured. Elliott[15] constructed a phase diagram for the system Na-Sr from the data of Remy, Wolfrum and Haase[14] from which at 150°C a

* No quantitative data on the solubility of alkaline earth metal oxides exist, except for BaO[3]. The low solubility of CaO in sodium is inferred from the accumulation of calcium in sodium system cold traps.

† This conclusion is based largely on observations made in the G. E. Sodium Mass Transfer Program. See References 4 to 11 inclusive.

‡ Evidence for this is the strong odor of ammonia which has been observed occasionally on opening up cold traps and exposing them to moist air.

§ Beryllium is not considered in this discussion, although from its position in the periodic table it is also an alkaline earth metal. Radium, which similarly belongs to this family, is excluded as well.

value of 30 weight per cent strontium can be derived. This is probably the composition of the solid in equilibrium with liquid sodium at this temperature and is open to considerable doubt. These authors[14] also studied the Ba-Na system, and from their diagram (given in Ref. 15), a value of 70 weight percent barium at 150°C can be obtained, probably the solidus again. Kanda and King[18] have also studied the Ba-Na system, and their results do not agree with those of the other investigations.[3, 14] These discrepancies were also noted by Klemm and Kunze,[16] who concluded that future investigation would be required to resolve the differences. The relative solubilities of the alkaline earth metal oxides in sodium is also important, but data are lacking except for BaO, so far as is known. Gould[3] stated that "The solubility of barium monoxide in sodium tested at 500°C. for a period of six hours was found to be <0.05 wt. %." It would be extremely interesting to determine the solubility products of the alkaline earth metal oxides as a function of temperature; for the temperature values of greatest interest, cold-trap temperatures, the amount to be expected in solution is probably so small as to tax the ingenuity of the analytical chemists and will probably require rather refined trace-analysis techniques.

The reduction of Na_2O by alkaline earth metals in solution in sodium is the basis for the use of these materials as "soluble getters" to decrease the oxide content of the sodium, and thus the corrosive action of the coolant.[19] This process was first suggested at KAPL in the early '50's and has, somewhat spasmodically, attracted attention of workers concerned with sodium. A serious limitation of soluble getters which is frequently overlooked is that the alkaline earth metals form stable intermetallic compounds with many common structural metals, nickel for example (see Table 4). These compounds are quite brittle, and their formation results in the deterioration of the mechanical properties of the structural metal, particularly those depending on surface phenomena (fatigue, for example) and in thin sections such as fuel-element cladding. These effects have been noted in nickel-bearing alloys, the stainless steels for example.

In the use of alkaline earth metals as soluble getters, the insolubility of the oxides in sodium is also a source of difficulty. The use of these materials leads to the precipitation of the alkaline earth oxides and their deposition on the walls of the system. In some experiments, in which huge excesses of calcium or magnesium have been introduced into the melt, the quantities of precipitated oxides formed have been enough to result in decreased heat transfer (the oxides are poor thermal conductors) and even plugging.

There is another characteristic of alkaline earth

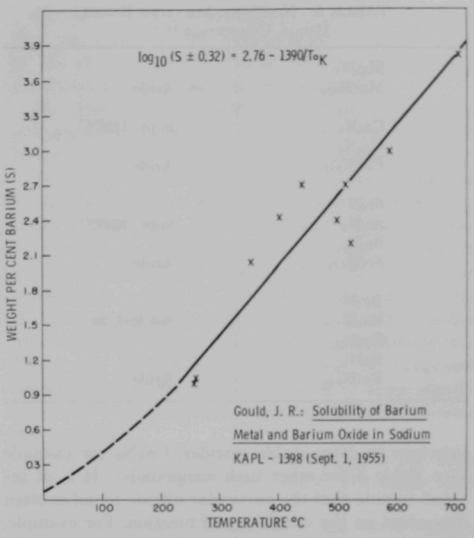

FIG. 1. Barium "Solubility" in Sodium.

TABLE 3. SOLUBILITY OF ALKALINE EARTH METALS IN SODIUM

Metal	Solubility (wt. %) at 150° C	Source
Mg	0.15	(3)
Ca	0.082	(13)
Sr	—	(14, 15)
Ba	0.60	(3, 14)

TABLE 4. NICKEL-ALKALINE EARTH METAL COMPOUNDS[13, 17]

Compound	Properties
Mg_2Ni (54.7% Ni)	Peritectic
$MgNi_2$ (82.8% Ni)	Stable, m.pt. 1145°C
$CaNi_5$ (88.0% Ni)	Stable

metals dissolved in sodium which is of extreme importance in reactor operation. In these systems there is a continuous inleakage of air, from which the oxygen is rapidly removed by the reducing action of the liquid. Since sodium does not combine directly with nitrogen at elevated temperatures, with pure sodium the residual nitrogen gas from the air is quite inert; in fact, nitrogen has been used as an "unreactive" cover gas in many sodium systems. But calcium (and other alkaline earth metals present) in solution in the sodium reacts directly with the nitrogen at the liquid-gas

TABLE 5. NITROGEN-ALKALINE EARTH METAL COMPOUNDS[15, 17]

Mg_3N_2	
$Mg(N_3)_2$	Azide
Ca_3N_2	m.pt. 1195°C
Ca_3N_4	
$Ca(N_3)_2$	Azide
Sr_2N	
Sr_3N_2	m.pt. 1030°C
Sr_2N_4	
$Sr(N_3)_2$	Azide
Ba_2N	
Ba_3N	See Ref. 20
Ba_3N_2	
BaN_2	
$Ba(N_3)_2$	Azide

interface to form stable nitrides, Ca_3N_2 for example (see Table 5 for other such compounds). It is of interest to note that the particular nitride found is often dependent on the conditions of reaction. For example, when nitrogen gas is passed over hot barium metal the product is normally Ba_3N_2. At high pressures, the stoichiometry can be varied towards BaN_2, and in vacuum the composition Ba_2N is observed. But if the reaction takes place between nitrogen gas and barium metal dissolved in sodium, the product of reaction is predominantly Ba_3N, as was found by Addison *et al.*[20] The nitrides thus formed appear to have an appreciable solubility in sodium, and in solution can move by normal transport processes (diffusion, convection, etc.) throughout the liquid. When these solutions encounter a material immersed in the sodium which is vulnerable to nitriding, the nitrogen moves from the liquid into the solid. Such effects have been noted with stainless steel, and to a pronounced degree with beryllium, zirconium, and other nitride-forming refractory metals.[21-26] In fact, the presence of a dissolved alkaline earth metal* has been considered essential[23] to the process of nitriding under sodium under normal reactor conditions.† The use of nitrogen as an inexpensive cover gas is obviously intimately associated with the alkaline earth metal content of the coolant and the role of these impurities as nitrogen carriers.

For the reasons indicated above: the embrittling action due to formation of an intermetallic compound, and the transport behavior of nitrogen, it has been considered desirable to specify a low content of calcium and other alkaline earths in "reactor grade" sodium. The use of soluble alkaline earth metal additives as "getters" has similarly been questioned; indeed, this technique has not been successfully used outside of laboratory studies.

It should be recognized that as a result of a neutron activation in an LMFBR, the sodium present will be converted to Na-24. This species decays with a half-life of 15.0 hr to yield stable Mg-24. Thus, even starting with sodium completely free of alkaline earth impurities, a significant concentration of magnesium will be built up after extended operation.

The maximum concentration of magnesium in sodium to be expected from this source can be derived from the value‡ computed for the specific activity due to Na-24 after many years of reactor operation, 0.05 Ci/g sodium. Multiplying this by the factor 3.7×10^{10} dps/Ci yields 1.85×10^{9} dps per gram of sodium. Since each disintegration gives rise to an atom of Mg-24, there will be 1.85×10^{9} atoms of magnesium formed per second for each gram of sodium present. This corresponds to

$$(1.85 \times 10^{+9} \text{ atom Mg/g Na-sec}) \times \frac{24 \text{ g Mg/mole Mg}}{6.06 \times 10^{+23} \text{ atom Mg/mole Mg}} = 7.33 \times 10^{-14} \text{ g Mg/g Na-sec.}$$

Thus in a year ($3.15 \times 10^{+7}$ sec), a concentration of

$$(7.33 \times 10^{-14}) \quad (3.15 \times 10^{+7}) \quad (10^{+6})$$

or about 2.3 ppm by weight of magnesium will be produced in the sodium. This concentration will increase linearly with the time of exposure of the sodium, and in older reactors the concentration of magnesium will reach levels of perhaps 10 to 100 ppm, by no means negligible in terms of the phenomena previously considered.

* Or possibly lithium.

† But the newly discovered facts on the high stability and solubility of NaCN in sodium may require modification of this conclusion.

‡ PNL calculation for FFTF, quoted in Ref. 27.

REFERENCES

1. Sittig, M., *SODIUM, Its Manufacture, Properties and Uses*, Reinhold Publishing Corp., New York (1956).
2. Letter, C. H. Lemke, Electrochemical Dept., E. I. duPont de Nemours and Co., Niagara Falls., N. Y. 14302, Nov. 21, 1968.
3. Gould, J. R., *Solubility of Barium Metal and Barium Oxide in Sodium*, KAPL-1398, (Sept 1, 1955).
4. Lockhart, R. W., *Sodium Mass Transfer: II* · · · , GEAP-3726 (April 1962).
5. Pohl, L. E., *Sodium Mass Transfer: X* · · · , GEAP-4437, (Feb 1964).
6. Lockhart, R. E., *Sodium Mass Transfer: XI* · · · , GEAP-4438, (Feb 1964).
7. Lockhart, R. W., *Sodium Mass Transfer: XII* · · · , GEAP-4439 (Oct 1964).
8. Rowland, M. C., Plumlee, D. E., Pohl, L. E., and Lockhart,

R. W., *Sodium Mass Transfer: XIX · · ·* , GEAP-4835 (May 1965).
9. Pohl, L. E., *Sodium Mass Transfer: XX · · ·* , GEAP-4836 (May 1965).
10. Lockhart, R. W., *Sodium Mass Transfer: XXI · · ·* , GEAP-4837 (Oct 1965).
11. Dutina, D., and Simpson, J. L., *Sodium Mass Transfer: XXIV · · ·* , GEAP-5020 (March 1967).
12. Wicks, C. E., and Block, F. E., *Thermodynamic Properties of 65 Elements—Their Oxides, Halides, Carbides and Nitrides*, Bulletin 605, Washington, D. C. (1963).
13. Jackson, C. B., Ed., *Liquid Metals Handbook, Sodium-NaK Supplement*, AEC—Dept. of the Navy, Washington, D. C. (July 1955).
14. Remy, H., Wolfrum, G., and Haase, H. W., Naturwissenshaften **44**, (534) (1957); Schweizer Archiv. **26**, (5) (1960).
15. Elliott, R. P., *Constitution of Binary Alloys, First Supplement*, McGraw-Hill Book Co., Inc., New York (1965).
16. Klemm, W., and Kunze, D., "Systems of Alkali and Alkaline Earth Metals, p. 3 in *The Alkali Metals*, Nottingham (July 19-22, 1966), The Chemical Society, London (1967).
17. Hansen, M., *Constitution of Binary Alloys*, 2nd Ed. McGraw-Hill Book Co., Inc., New York (1958).
18. Kanda, F. A., and King, A. J., TID-5691, pp. 46-49 (1960).
19. Haag, Fred G., Nucleonics **15**, 58 (Feb 1957).
20. Addison, C. C., Davies, B. M., Pulham, R. J., and Wallace, D. P., "The Liquid Alkali Metals as Reaction Media," p. 290 in *The Alkali Metals*, Nottingham (July 19-22, 1966), The Chemical Society, London (1967).
21. Brush, E. G., and Rodd, C. R., *Preliminary Experiments on the Nitriding of Reactor Materials in Sodium*, MEMO-EGB-21, General Electric Co.—KAPL, Schenectady, New York (Sept 22, 1955).
22. Brush, E. G., and Rodd, C. R., *Experiments in Sodium-Nitrogen Mixtures Report No. II. Interim Results at 1100°F*, MEMO-CRR-2 General Electric Co.—KAPL, Schenectady, New York (April 9, 1956).
23. Brush, E. G., *The Temperature Dependence of Some Nitrogen-Metal Reactions in Sodium*, MEMO-EGB-24, General Electric Co.—KAPL, Schenectady, New York (March 7, 1957).
24. Kendall, W. W., *Corrosion of Beryllium in Flowing Sodium*, GEAP-3333 (Jan 15, 1960).
25. Donaldson, D. M., *Chemical Experience with the Dounreay Fast Reactor*, Presented at the Symposium on Liquid Metals Aix-en-Provence and Cadarache, France (Sept 30 to Oct 2, 1963).
26. Babcock and Wilcox Tube Co., *Effect of Molten Sodium-Potassium Alloy and Its Vapor on Wrought Iron*, Reference No. F-99, Beaver Falls, Pennsylvania (Dec 17, 1946).
27. Strawbridge, L. E. and Edison, G. E., *Evaluation of Open Pool Operations in FFTF*, WARD-FRP-25 (Oct 1968).

Discussion

Mr. Miles (ANL): We have been running at EBR-II for quite a while and we find a magnesium content of only 0.14 ppm by weight. So there may be removal mechanisms.

Mr. Epstein: There certainly are. The removal mechanisms that I spoke of are oxidation of the metal and deposition in cold traps, nitriding, and perhaps deposition on the steel surfaces as an intermetallic compound.

Mr. Miles: True. Then how do you get this buildup that you mention—this concentration of several ppm of Mg-24 derived from Na-24. Did you consider depletion as well as production mechanisms?

Mr. Epstein: No, I did not attempt to. This is a straight nuclear calculation of the maximum that could be present. I did not try to evaluate removal processes.

Mr. F. A. Smith (ANL): I'd like to make a comment on an observation of long-term exposure of sodium to stainless steel. Data that have been developed by the U. S. Steel Co. identifies chrome-nitrogen compounds on the surface of the stainless steel. To excite your imagination a little bit, it appears from other work that we have done at Argonne that indeed the surface film may impede the dissolution of grain boundaries. There can be competitive processes of compound formation on surfaces which may be of some significance for very long-term operation of power plants, 20 years or so.

Mr. Epstein: I thought you were going to say these surface films may be of some benefit. This might very well be so.

Mr. Humphreys (Moderator): Are there further questions? Would anyone care to comment on the program by Borgstedt in Germany which calls calcium one of the principal impurities responsible for corrosion of vanadium alloys?

Mr. Epstein: The French people from Phenix were talking about the calcium problem yesterday. It turns out that the sodium used in France is much more like our commercial material than reactor-grade sodium and is much higher in initial calcium content than we are accustomed to. I believe that when one of the Rapsodie cold traps was opened up for the first time some years ago the smell of ammonia was rather overwhelming, probably due to the reaction of moisture in the air with the calcium nitride formed by the processes I was discussing.

Mr. D. L. Smith (ANL): In your discussion of the formation of calcium oxide from calcium metal and oxygen dissolved in sodium, did you infer that this would be more favorable than would the reaction between calcium and solid sodium oxide?

Mr. Epstein: Yes, because the free energy data that I gave were for unit activity. If the calcium and sodium oxide were in solution, the free energy for the reaction could be more negative.

Mr. Harms (ORNL): If you have all the calcium or magnesium present as the oxide, no nitriding will take place. Isn't that correct?

Mr. Epstein: That's certainly right if all the magnesium or calcium is present only in oxide form. But I don't know whether it will be or not. You know

lithium exposed to air preferentially forms the nitride, not the oxide. If you take an ingot of lithium and leave it around in air for some time and analyze the surface film, there is more nitride there than there is oxide. I simply don't know how this competition between the nitride formation and oxide formation will occur with the alkaline earth metals.

Mr. Harms: Yes, but to begin with the calcium isn't present as metal, but rather as the oxide because most of the sodium oxide has reacted. Right?

Mr. Epstein: After prolonged exposure this is correct. But in sodium as we get it from the manufacturer we believe that a significant amount still exists as the metal rather than as the oxide.

SESSIONS ON SODIUM TECHNOLOGY

SESSION ST-II

Thursday Afternoon, November 7, 1968

Chairman: J. H. DeVan
Oak Ridge National Laboratory

Secretary: S. Greenberg
Argonne National Laboratory

Effect of High-temperature Sodium on the Mechanical Properties of Candidate Alloys for the LMFBR Program

L. H. Kirschler and R. C. Andrews

MSA Research Corporation
Evans City, Pennsylvania

(PRESENTED BY L. H. KIRSCHLER)

Abstract

MSA Research Corporation (MSAR), under the auspices of the U. S. Atomic Energy Commission, has for several years been conducting out-of-pile high-temperature mechanical-property tests of candidate structural alloys for use in sodium reactor systems. These tests have been conducted in air, helium, and flowing sodium with varying degrees of oxygen and carbon contamination of the sodium. This report is limited to the most recent data generated on the tensile and creep-rupture properties of uniaxial test specimens for Type 304 and Type 316 austenitic stainless steels.

Two dynamic Type 316 SS loops were employed in performing preliminary unstressed excursions prior to the in-sodium mechanical-property tests. Exposures for 500 hr in high-oxygen sodium (50 ppm) at 1200°F and 1400°F were conducted in one loop, while 491- to 760-hr exposures in 1200°F sodium with varying degrees of carbon activity were conducted in the other loop. Subsequently, a third dynamic Type 316 SS loop was used to conduct up to 2000-hr instream creep-rupture tests following the various excursions. The mechanical testing was conducted in 1200°F sodium at a sodium velocity of ~20 ft/sec, an oxide content of the sodium at <10 ppm, and with a >70°F ΔT existing between the specimen test temperature and the coldest sodium-stream temperature.

Tensile tests were run at room temperature, 1200°F, and 1400°F on some of the test specimens following the excursions. These tests were conducted in air on a standard tensile machine at a strain rate of 0.1 in./min.

Curves of the creep-rupture life and creep strengths of Types 304 and 316 SS from the instream high velocity-ΔT-'clean' sodium tests following the excursions are compared with curves generated in earlier work. In this prior work, these same alloys were tested in air, helium, and sodium with the instream sodium rupture strengths being measured at isothermal conditions and at a low velocity, <1 ft/sec. Three sodium environments were investigated at that time: sodium with <10 ppm oxygen, sodium with 300 ppm oxygen, and sodium with an extremely high carbon activity.

Bar graphs were used to compare the yield strengths, the tensile strengths, and the ductilities of Types 304 and 316 SS specimens following the stress-free excursions in helium, in oxygen-contaminated sodium, and in carbon-contaminated sodium with the same properties of the as-received materials. This data was obtained from room-temperature, 1000°F, 1200°F, and 1400°F tensile tests conducted in air.

Introduction

MSAR's initial efforts under AEC Contract AT (11-1)-765 were to determine the effects of sodium and its normally anticipated contaminants on the mechanical properties of structural materials anticipated for use in nuclear power plants cooled with sodium and operating at a maximum temperature of 1200°F. The original materials considered were Type 316 stainless steel (SS) and 2¼ Cr-1 Mo ferritic steel with temperature limits of 1200 and 1100°F, respectively. Later, the program was expanded to include Type 304 SS as a candidate material for use at 1200°F. The environmental effects were to be evaluated through several tests of mechanical properties (creep, creep-rupture, fatigue, tensile and impact tests), as well as metallographic examinations. Environmental effects of 'clean' sodium, oxygen-contaminated sodium, and carbon-contaminated sodium were evaluated. Comparisons of data from tests in these respective environments with data from similar tests with the same heats in air and helium were made. This information was disseminated in the several topical reports listed in Table 1.

In the fall of 1966, the program was redirected toward support of the LMFBR program. In addition to the two existing Type 316 SS dynamic sodium systems (Loops 1 and 2) used in the earlier portions of the program, a third dynamic system (Loop 3) was constructed. The Loop 3 system was designed to be operated with a 'clean' sodium environment (<10 ppm oxygen) with added parameters of ΔT (50 to 150°F), velocities (15 to 30 ft/sec), temperature

TABLE 1. Topical Report Listing

Report No.	Title	MSAR Report No.
1	Test Facility Design And Operation Procedures, November 1963	63-161
2	Results Of Mechanical Properties Test Of 316 SS Specimens In 1200 F Sodium With Low Oxygen, March 1964	64-18
3	Results Of Mechanical Properties Test Of 2¼ Cr-1 Mo Steel Specimens In Sodium With High And Low Oxygen, Air, And Helium Environments At 1100 F, July 1964	64-81
4	Results Of Mechanical Properties Tests Of 316 SS Specimens In 1200 F Sodium Contaminated With Carbon, December 1965	65-194
5	Results Of Mechanical Properties Tests Of 316 SS Specimens In 1200 F Sodium Contaminated With Oxygen (~300 ppm), May 1966	66-78
6	Effect of Carburization On The Phases In Austenitic Stainless Steel, June 1966	66-119
7	Design Properties Of One Heat Of 2¼ Cr-1 Mo And 316 Stainless Steel In High Temperature Air, Helium And Sodium Environments, September 1966	66-174
8	Results Of Mechanical Properties Tests Of 304 SS Specimens Conducted In: 1. 1200 F Sodium Contaminated With Oxygen (~300 ppm); and 2. 1200 F Sodium Contaminated With Carbon, July 1967	67-103
9	Analysis Of High Oxygen And High Carbon Cold Traps, December 1967	67-203
10	A Limited Comparison Of The Relative Merits Of 304 Versus 316 Stainless Steel For Liquid Metal Service	67-216

(1400°F maximum), and variations in specimen thickness (15 to 60 mils).

Loops 1 and 2 are used to conduct the oxygen- and carbon-contaminated sodium excursions. A portion of the test specimens from these excursions are then tensile tested in air at room temperature, 1000, 1200, and 1400°F. Other specimens are then instream creep-rupture tested at various stress levels under the Loop 3 conditions of 'clean' sodium, high velocity, and with a system ΔT at a temperature of 1200°F. The data from these tests are then compared with thermally aged specimen test data and other environmental test data.

The present program is centered around the studies of candidate alloys for the LMFBR program. In the earlier testing of Types 304 and 316 SS, parameters such as ΔT, velocity, and material thickness were minimized and the sodium contaminants maximized to determine environmental effects. In the present program, these parameters approach the conditions anticipated in a reactor system.

Sodium chemistry of each of the sodium systems is monitored, using updated state-of-the art sampling methods and analytical procedures. Loop 3 is the most complete, including a bypass sampler, hot trap, and two UNC oxygen meters. Loop 1 has the first commerical UNC carbon meter. Post-test evaluations of the effects of stress and corrosion on the candidate materials are made metallographically, with microhardness, microprobe, X-ray diffraction, and spectrographic analyses employed to aid in the evaluation.

Summary

The heats of Types 304 and 316 SS used in conducting these tests were typical of standard heats and responded in a normal manner when thermally aged at 1200 and 1400°F in the helium atmosphere. The test specimens, exposed at 1200 and 1400°F for 500 hr in sodium containing 50 ppm oxygen prior to tensile testing, showed little change in tensile strength, small increases in yield strength, and large losses in ductility when compared to the thermally aged specimens.

Although there were only slight differences in the tensile and yield strengths between the 15- and 60-mil specimens, the ductilities of the 15-mil specimens were much lower than the 60-mil-thick specimens. A typical example would be in the 1400°F tensile tests of the Type 304 SS specimens from the 1200°F, 500-hr, 50-ppm-oxygen sodium excursions, where the total elongation of the 60-mil specimen was 66% and that of the 15-mil specimen was 23%. This latter fact pointedly demonstrates the more profound effect of surface embrittlement on thinner-wall materials.

Comparison of tensile data at room temperature, 1200°F, and 1400°F showed differences between oxidation and sensitization. In the 1200°F tests, both the helium and high-oxygen-exposed specimens showed a comparable decrease in ductility from the room-temperature tests. At 1400°F, however, the helium-exposed (no oxidation) specimen exhibited ductility recovery, whereas the sodium-exposed (oxidized) specimen showed only a partial recovery. Metallographic analyses supported these two observed effects (oxidation and sensitization).

Further effects of the 500-hr excursion in the 1200°F sodium with 50 ppm oxygen were noted when tested in 'clean' sodium at 1200°F with a sodium velocity of 20 ft/sec and a system ΔT of >70°F. In these tests, both the Types 304 and 316 SS showed losses in rupture strength and increases in creep

rates when compared to as-received material tested in air. The Type 304 SS material from these excursions had a loss similar to the as-received material tests in sodium containing 300 ppm oxygen. Likewise, the loss in rupture strength for Type 316 SS was not anticipated, since previous work had shown no effects on the rupture strength of as-received Type 316 SS when tested in 300-ppm-oxygen sodium, even though significant oxidation had occurred during the tests. These strength losses in both Types 304 and 316 SS cannot be assumed to be the result of the prior excursion alone, since other parameters, such as velocity and ΔT, were imposed by the test environment in Loop 3. Additional testing is in progress to resolve this question.

Examination of the tensile data from the 1200°F excursions in high-carbon sodium showed a general increase in tensile strength and yield strength (and decrease in ductility) for both Types 304 and 316 SS specimens, compared to those of the 500-hr thermal excursion in helium. The failure modes were reasonably consistent with those expected: brittle failure at room temperature and improving ductility with increasing test temperature. At 1400°F, however, even though there was substantial increase in ductility (elongation and reduction of area), the gage length showed extensive internal cracking and crack separation, which tend to detract from the validity of the elongation values. This particular behavior was not observed at 1200°F and, therefore, was not expected at 1400°F.

The additional carbon penetration between the exposure times of 491 and 760 hr in the high-carbon sodium environment was barely measurable and resulted in only an additional absorption of 20 ppm carbon. Also, these exposure times produced little difference in the mechanical test values for Type 316 SS and only a small separation in values for the Type 304 SS.

The lack of internal cracking of the base metal of the 15-mil material in room-temperature tests indicates that the effect of the carburization of the 15-mil material was significantly different from the 60-mil carburized material. This in itself would not appear to be important, but it is one additional observation to indicate that manner and rate at which carbon is added to the base metal dictates the effects it may have. Also, it may indicate that low carbon absorption by the base metal over long periods of time may be as detrimental as high carbon adsorption over short-time periods.

TABLE 3. Physical Properties of Test Materials

Type of Austenitic Steel	Heat No.	Tensile Strength, psi	Yield Strength, psi	Elongation, %	Hardness Rockwell B	Grain Size	Finish
304	322891	85,080	35,560	57.0	78	6	2B
316	880347	—	—	—	—	—	2B
316	19295	85,760	37,760	53.0	78	6	2B

Material Characterization of Test Specimen

The test specimens utilized throughout the test program were flat sheet and ½ in. x ~1 in. in gage length, as machined from standard mill runs of 16 gage sheet stock. The chemical composition and physical properties, as furnished by the supplier, is listed in Tables 2 and 3. The Type 316 SS, Heat No. 880347, was used in the earlier phases of this program. The nominal 60-mil specimens were taken directly from sheet stock. The 15-mil specimens were taken from sheet stock rolled down from the same 16 gage heats.

Tensile Strengths of Material Exposed to High-Oxygen Sodium

The Types 304 and 316 SS specimens of both 15 and 60 mils were exposed stress-free to a 50-ppm-oxygen sodium environment for 500-hr periods at temperatures of 1200 and 1400°F. During these excursions, additional specimens were submitted to the identical thermal histories while under a helium atmosphere. Loop 2, as discussed earlier, was used to conduct these excursions. The pertinent flow rates and temperature profiles around the system during these excursions are shown in Figures 1 and 2.

The specimens exposed to the high-oxygen sodium at 1200°F developed a surface scale with some grain-boundary oxide penetration. The average oxide penetration was of the order of 15 microns in the

TABLE 2. Composition of Test Material for MSAR-LMFBR Structural Material Program

Type of Austenitic Steel	Supplier	Heat No.	Cr	Ni	C	Mn	P	S	Si	Mo	Other
304	Allegheny Ludlum	322891	18.26	9.36	0.057	1.20	0.023	0.010	0.52	0.15	Cu = 0.16; Co = 0.090
316	Allegheny Ludlum	19295	17.64	12.72	0.048	1.68	0.019	0.011	0.56	2.85	Cu = 0.10
316	Armco	880347	18.00	12.84	0.045	1.94	0.019	0.012	0.48	2.33	

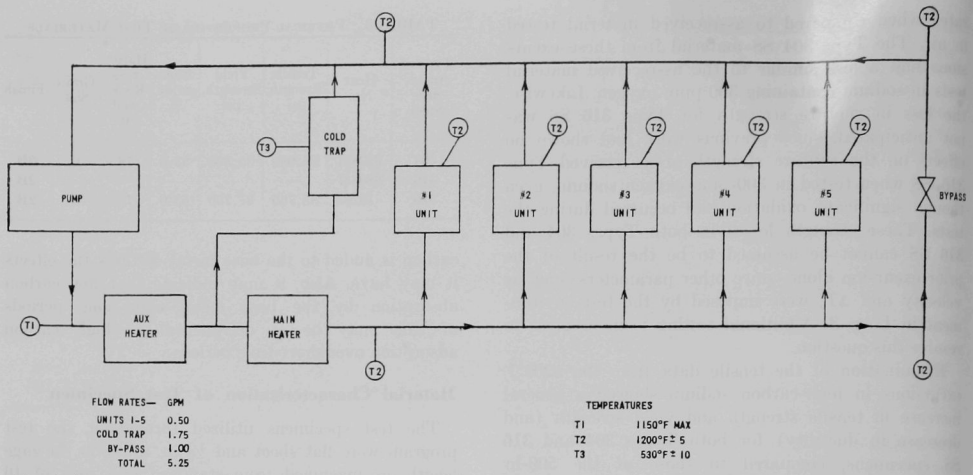

FIG. 1. Averaged Loop Conditions during the 500-hr, 1200°F, High-oxygen (50 ppm) Excursion of Types 304 and 316 Stainless Steel Specimens.

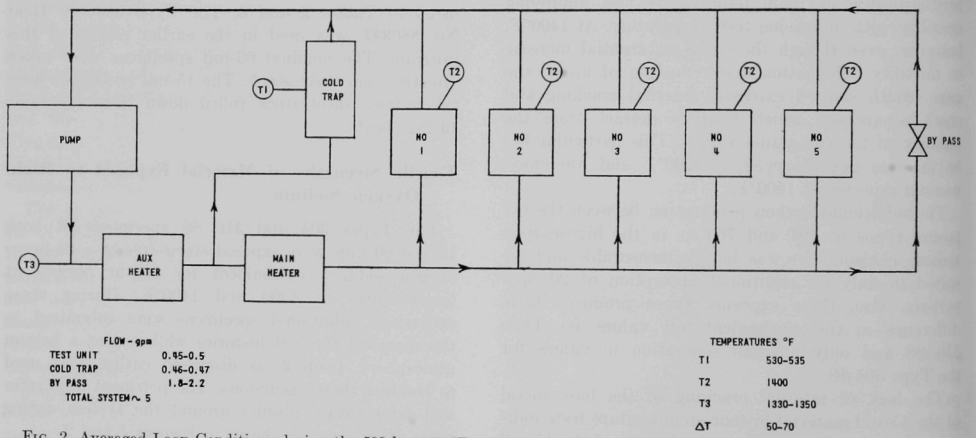

FIG. 2. Averaged Loop Conditions during the 500-hr, 1400°F, High-oxygen (50 ppm) Excursion of Types 304 and 316 Stainless Steel Specimens.

Type 304 SS (with maximum depth of 25 microns); the average depth of penetration in Type 316 SS was 10 microns (with maximum depths of 15 microns). This oxidation was independent of material thickness. Specimens from the high oxygen excursion at 1400°F, however, developed an almost immeasurable scale without the penetration of oxide into the grain boundaries. A change in the subsurface composition did occur which has not fully been defined at this time. The effects of this compositional change on the mechanical properties have not been determined.

Test specimens from these excursions were then used in conducting short-time tensile tests in air at room temperature, 1000, 1200, and 1400°F. Figures 3, 4, and 5 compare tensile-test results of the helium and high-oxygen (50 ppm) sodium-exposed specimens with the as-received material.

The data in Figure 3 show the two test materials to have room-temperature yield strengths slightly higher than typical heats. With Type 304, the yield strength of the test material was 45,000 psi (compared to a typical value of 33,000); the two Type 316

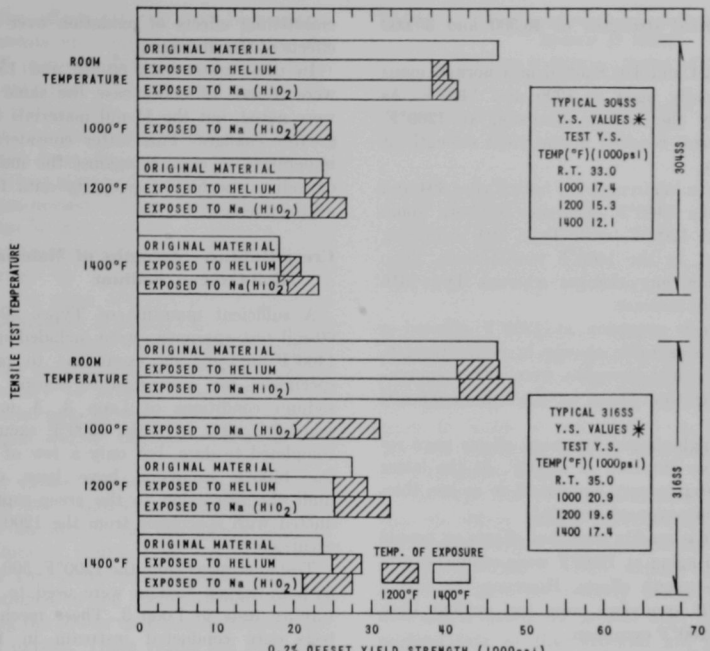

FIG. 3. 0.2% Offset Yield Strength of 60-mil Specimens after 500-hr Exposure to 1200 and 1400°F Helium and Sodium (50 ppm O_2).

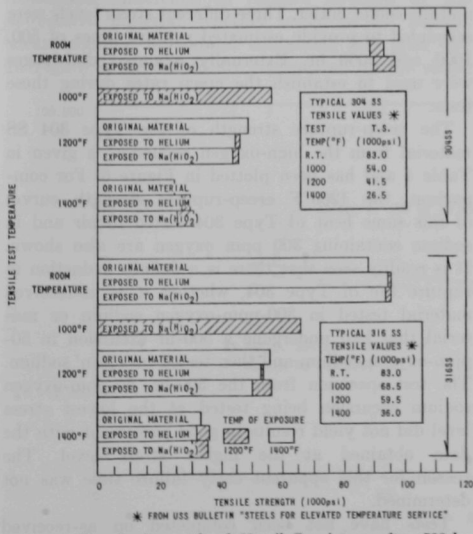

FIG. 4. Tensile Strength of 60-mil Specimens after 500-hr Exposure to 1200 and 1400°F Helium and Sodium (50 ppm O_2).

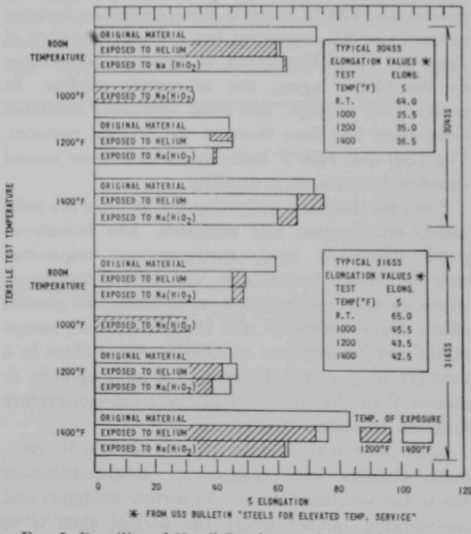

FIG. 5. Ductility of 60-mil Specimens after 500-hr Exposure to 1200 and 1400°F Helium and Sodium (50 ppm O_2).

materials had yield strengths of 46,500 and 35,000 psi.

Both Types 304 and 316 reacted in a normal manner when thermally aged at 1200 and 1400°F. As demonstrated by the helium excursion at 1200°F, only minor changes resulted in the yield strength at each temperature.

There was a loss in strength for both Types 304 and 316 SS from the 1400°F excursion at both room temperature and 1200°F, with Type 304 exhibiting the greatest loss. In the 1400°F tensile tests, Type 304 did not show any changes whereas Type 316 SS showed a slight increase.

The high-oxygen excursion at 1200°F effected a consistent and measurable change in yield strength. In all cases the yield strengths were either equivalent to or greater than those for the helium-exposed material.

The 1400°F high-oxygen excursion effects were reversed from those obtained at 1200°F. At the latter temperature strengths were equivalent to or less than those of the helium-exposed material.

In Figure 4, it is readily seen that effects on tensile strengths due to aging at 1200°F were commensurate with the yield-strength effects. However, the effects from the 1400°F excursions were less evident than those from the 1200°F excursion.

Of all the tensile properties measured, the ductility (particularly elongation) showed the greatest effect, but this was still small. Figure 5 shows that, in general, the 1200°F thermal aging caused an increase in the Type 304 elongation but a decrease in that of Type 316. Ductility would be expected to increase by the 1400°F aging, due to carbide solution. In general this is true, but some specimens exhibited elongations less than those of the original material. The 1200 and 1400°F high-oxygen excursions caused significant reductions in ductility.

From the data two competing mechanisms are indicated: sensitization and oxidation. The helium-exposed (thermally aged) specimens are responding only to carbide morphology. The 1200°F treatment, where carbide precipitation is occurring, in general effects higher strengths and lower ductilities, except at the test temperature of 1400°F, where there is a recovery in specimen ductility to a level equal to or greater than that observed in the room-temperature tests, due to carbide dissolution.

In the case of the sodium-exposed (oxidized) specimens, changes were exaggerated in embrittlement due to the additional feature of surface oxidation and considerably smaller where the normal shift is to higher ductility. This is a relative measure of the embrittling effects of oxidation over and above the effects of thermal aging.

In these tests, both 60-mil and 15-mil specimens were tested. In every case the same general trends were noted, but the 15-mil materials always suffered greater changes. This latter consideration makes it imperative to caution against the indiscriminate use of sodium mechanical-property data for materials of all thicknesses.

Creep-Rupture Strengths of Materials Exposed to High-Oxygen Sodium

A sufficient quantity of Types 304 and 316 SS 60-mil test specimens were included in the 1200 and 1400°F high-oxygen excursions to provide exposed specimens for creep-rupture testing in the 'clean' sodium conditions of Loop 3. A majority of the scheduled tests from the 1200°F excursion has been completed to date, but only a few of the tests from the 1400°F excursion have been completed. We limit the discussion to the creep-rupture tests conducted with specimens from the 1200°F high-oxygen excursion.

Test specimens from the 1200°F, 500-hr excursion in 50-ppm-oxygen sodium were used to conduct creep-rupture tests in Loop 3. These mechanical strength tests were conducted instream in 1200°F sodium containing 10 ppm or less oxygen. The sodium velocity across the test specimen was 20 ft/sec, and a minimum ΔT of 70°F existed between the test specimen and the cooler outlet. Three different stress levels were scheduled to provide estimated rupture times of 500, 1000 and 2000 hr. Externally mounted dial gages were used to establish the creep rates during these tests.

The creep-rupture strength of the Type 304 SS material from the high-oxygen excursion is given in Table 4 and has been plotted in Figure 6. For comparison, the 1200°F creep-rupture strength curves of this same heat of Type 304 tested in air and in sodium containing 300 ppm oxygen are also shown. It is readily seen that there is a definite reduction in rupture life of Type 304, whether it is as-received material tested in 300-ppm-oxygen sodium or material that had undergone a 500-hr excursion in 50-ppm-oxygen sodium and then tested in 'clean' sodium. The test specimen from the 500-hr, 50-ppm-oxygen sodium excursion being tested at the lowest stress level did not yield results in good agreement with the data obtained at the higher stress level. The reason for this apparent early failure time was not determined.

Tests have not been completed on as-received Type 304 in 'clean' sodium. One cannot say at this

time whether the effects of the two high-oxygen sodium environments are equivalent or whether the high-velocity-ΔT parameters of Loop 3 make them appear to be equivalent. Tests in progress are expected to resolve this question.

In Figure 7, the minimum creep rate, as determined for each specimen from dial-gage measurements, is plotted with curves generated during the previous air and 300-ppm-oxygen sodium tests. From this graph, it can also be seen that the weakening effects of the 300-ppm-oxygen sodium and the high-oxygen excursion, followed by testing in 'clean' sodium, are equivalent. The creep rate of the test specimen that indicated premature failure in the creep-rupture tests was also abnormally high when compared with those of other specimens of this test series. Again, it will be necessary to examine the data of the as-received material tests in 'clean' sodium in progress before the oxygen and/or velocity parameters are resolved.

The ductility values obtained during these tests of Type 304 SS are comparably higher than those obtained in the air and in the 300-ppm-oxygen sodium tests. Values of <30% total elongation were obtained in the two latter tests, whereas values of >40% were obtained in the 'clean' sodium tests of specimens having the 500-hr excursion in sodium containing 50 ppm oxygen. These values are from tests taken at equivalent stress loadings.

Previous tests of Type 316 SS did not show any measurable difference in rupture strength of the as-received material, whether tested in air, helium, 'clean' sodium, or sodium containing 300 ppm O_2. In Figure 8, these data are represented by the single curve shown. A different heat of Type 316 SS was used to conduct the tests in this portion of the program. It was therefore necessary to characterize this particular heat in air at 1200°F. These data—given in Table 5 and plotted in Figure 8—indicate this particular heat to be significantly stronger than the earlier heat.

TABLE 4. CREEP-RUPTURE DATA FOR TYPE 304 SS IN CLEAN SODIUM AT 1200°F

(Velocity = 20 ft/sec; System $\Delta T \leq 70°F$)

Specimen No.	Stress, psi	Rupture Time, hr	Reduction of Area, %	Elongation, %	Minimum Creep Rate, %/hr
A-30	21,000	324	45	—	0.106
A-29	19,500	598	48	—	0.0523
A-28	18,500	1165	52	44	0.0238
A-24	18,000	1131	51	58	0.0210

Note: All specimens from 500-hr, 1200°F, 50-ppm excursion.

The Type 316 SS test specimens that had undergone the 500-hr, 1200°F excursion in sodium containing 50 ppm oxygen were subsequently tested in Loop 3 under the 1200°F 'clean' sodium conditions, which include a 20-ft/sec velocity across the test specimen and a system ΔT greater than 70°F. The creep-rupture data of this material are given in Table 6 as well as in Figure 8. The test at the 22,000-psi level is still in progress. It is quite evident that there has been a reduction in the rupture strength from these test conditions. From the previous work, it was shown that there was no effect of 'clean' sodium or high oxygen-contaminated sodium on the rupture

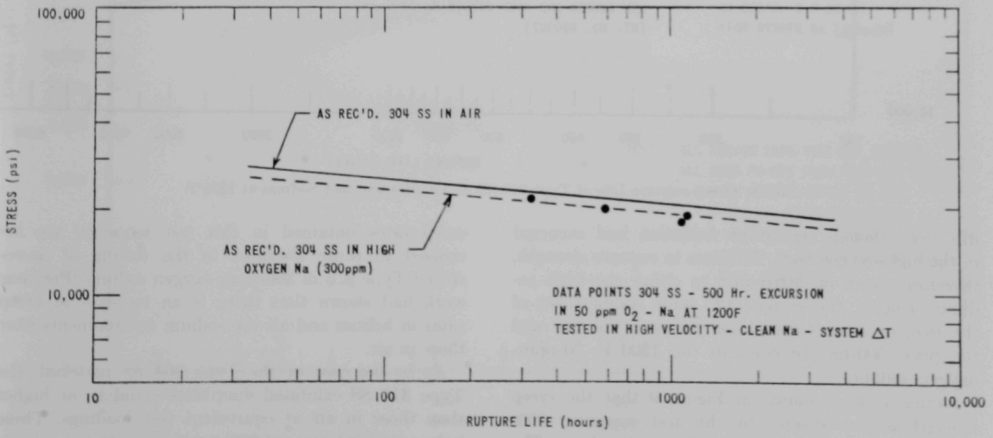

FIG. 6. Creep-rupture Life of Type 304 SS in Air and Sodium at 1200°F.

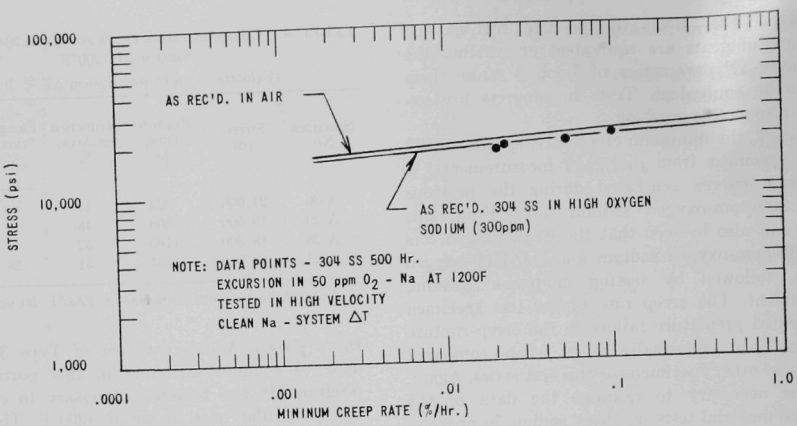

FIG. 7. Creep Strength of Type 304 SS in Air and Sodium at 1200°F.

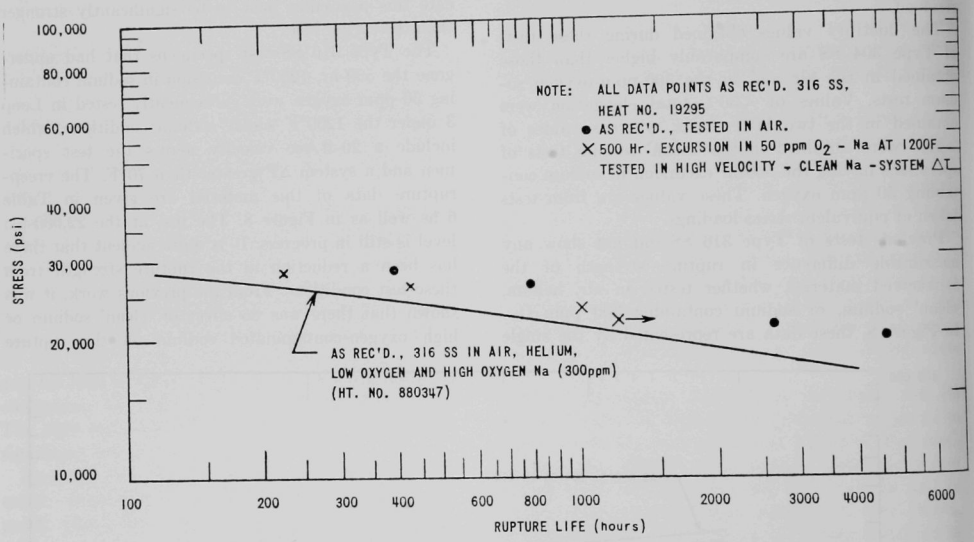

FIG. 8. Creep-rupture Life of Type 316 SS in Air, Helium, and Sodium at 1200°F.

life, even though significant oxidation had occurred in the high-oxygen tests. This loss in rupture strength, therefore, must be attributed to either the high sodium velocity, the system ΔT, some combination of the two, or some combination between the two and the prior 500-hr excursion in the 1200°F, 50-ppm-oxygen sodium.

Similarly, it is shown in Figure 9 that the creep strength is also affected by this test sequence: 500-hr excursion prior to testing in 'clean' sodium. The creep rates obtained in this test sequence are increased to those obtained in the testing of as-received Type 316 in 300-ppm-oxygen sodium. Previous work had shown that there is an increase in creep rates in helium and all the sodium environments over those in air.

As in the case of the Type 304 SS material, the Type 316 SS exhibited ductilities equal to or higher than those in air at equivalent test loadings. These values were in excess of 60% total elongation.

TABLE 5. Creep-rupture Data for Type 316 SS in Air at 1200°F

Specimen No.	Stress, psi	Rupture Time, hr	Reduction of Area, %	Elongation, %	Minimum Creep Rate, %/hr
B-192	28,000	392	39	68	0.0571
B-191	26,000	786	42	58	0.0278
B-149	21,500	2680	51	47	0.0055
B-148	20,000	4695	46	37	0.0015
B-150	18,500	Terminated at 2400 hr	—	—	0.001

Note: All specimens were as-received material.

TABLE 6. Creep-rupture Data for Type 316 SS in 'Clean' Sodium at 1200°F

(*Velocity = 20 ft/sec; System; T = 70°F*)

Specimen No.	Stress, psi	Rupture Time, hr	Reduction of Area, %	Elongation, %	Minimum Creep Rate, %/hr
B-24	28,000	225	65	72	0.157
B-26	26,000	425	67	78	0.075
B-25	23,500	1004	63	70	0.022
B-28	22,000	In progress 1210 hr	—	—	0.014

Note: All specimens from 500-hr, 1200°F, 50-ppm excursion.

Tensile Strengths of Material Exposed to High-Carbon Sodium

Three sets of 60-mil test specimens identical to those of the high-oxygen sodium excursions were placed, stress-free, in three of the exposure units in the high carbon-activity environment of Loop 1. The first unit was placed on-stream for a 491-hr period; the two remaining units were on-stream for times of 750 and 760 hr. All exposures were carried out at 1200°F. During this period, 5-mil Type 304 SS monitoring tabs carburized to a total carbon concentration of 7500 to 10,500 ppm carbon during a 162- to 165-hr exposure time. This carbon activity was considerably less than in previous work where similar tabs would carburize to total carbon levels of ~20,000 ppm in similar exposure times.

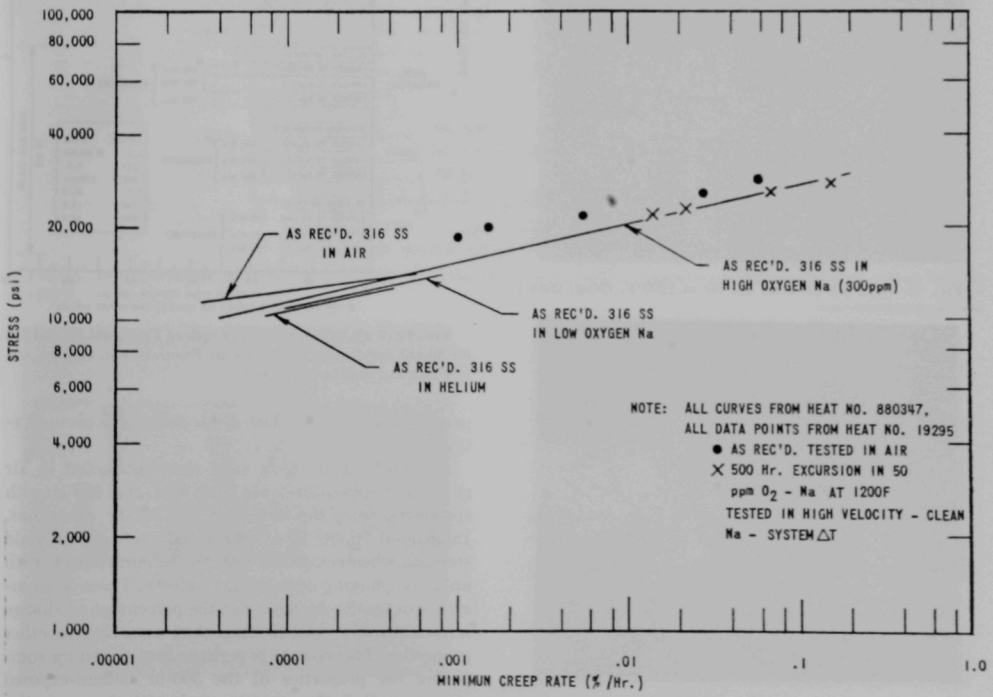

Fig. 9. Creep Strength of Type 316 SS in Air, Helium, and Sodium at 1200°F.

Figures 10 and 11 show that the test specimens of the 491-hr excursion attained a case depth of 1.5 to 2.0 mils in Type 316 SS, and of, 3.5 to 4.5 mils in the Type 304 SS specimens, with total carbon increases of 1000–1200 ppm. The 750- to 760-hr excursions showed only little additional carburization, which increased the carbon pickup to 1200–1400 ppm, with no noticeable increase in case depth. The case depths developed are typical of previously carburized specimens, i.e., there is a definite, heavily precipitated case in the Type 316 SS, with penetration into the grain boundaries ahead of it. In Type 304 SS, carbon tends to diffuse faster, providing a thicker case per unit of time than with Type 316. In addition, there is a less definite distinction between the case and the area ahead of it. In these exposures of relatively short time periods, the total carbon increases in Types 304 and 316 SS were nearly equivalent. However, Type 304 SS did experience a deeper penetration of carbon with a less dense case concentration of carbon.

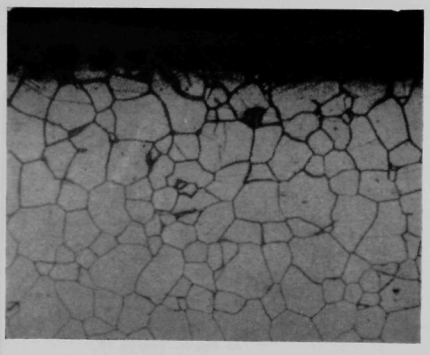

FIG. 10. Type 316 SS after 491 Hr at 1200°F. (Mag. 266×)

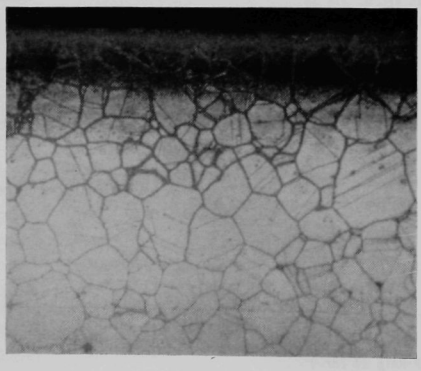

FIG. 11. Type 304 SS after 491 Hr at 1200°F. (Mag. 266×)

TABLE 7. PERCENTAGE CHANGE IN MECHANICAL PROPERTIES AFTER EXPOSURE AT 1200°F: 491 HOURS IN HIGH-CARBON SODIUM VERSUS 500 HOURS IN HELIUM

Test Temp, °F	Type 304 SS				Type 316 SS			
	Yield Strength	Tensile Strength	Elongation	Reduction of Area	Yield Strength	Tensile Strength	Elongation	Reduction of Area
R.T.	+25	−1.5	−58	−65	+20	+6	−55	−61
1200	+20	+8.0	−36	−30	+24	+10	−27	−25
1400	+14	+13.0	−31	−23	−1.4	+7.3	−31	−10

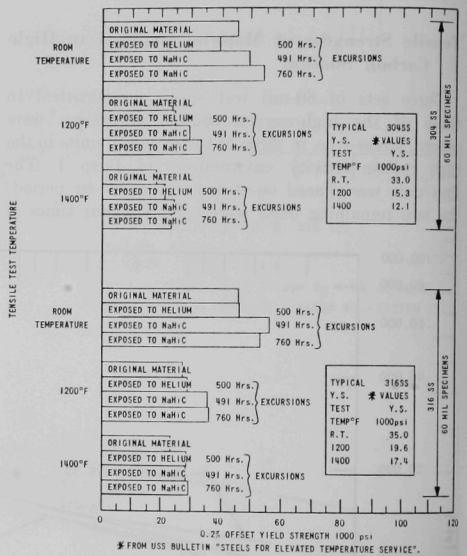

FIG. 12.,0.2% Offset Yield Strength of Types 304 SS and 316 SS 60-mil Specimens after Various Excursions in Helium and High-carbon Sodium at 1200°F.

Standard tensile tests were then conducted in air at room temperature, at 1200, and at 1400°F with specimens from the 491- and the 760-hr excursions. In general, there is a substantial increase in yield strength when compared with the helium control, with an accompanying decrease in ductility. There is an increase in tensile strength, but the percentage of change is considerably smaller than that occurring in other properties. This change is perhaps best shown by comparing the properties of the 500-hr helium-exposed specimens from the previous work with the properties

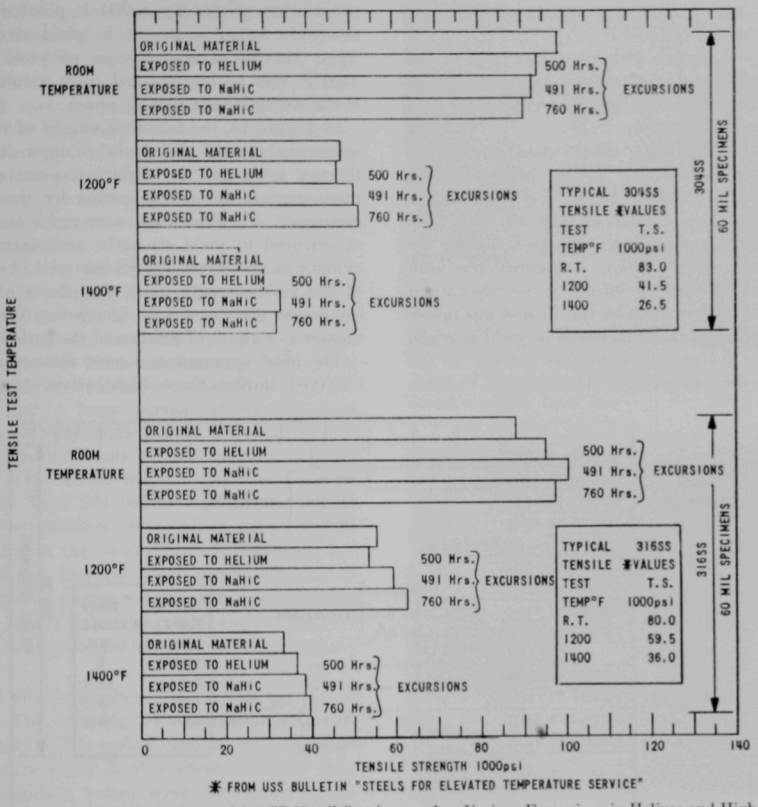

FIG. 13. Tensile Strength of Types 304 and 316 SS 60-mil Specimens after Various Excursions in Helium and High-carbon Sodium at 1200°F.

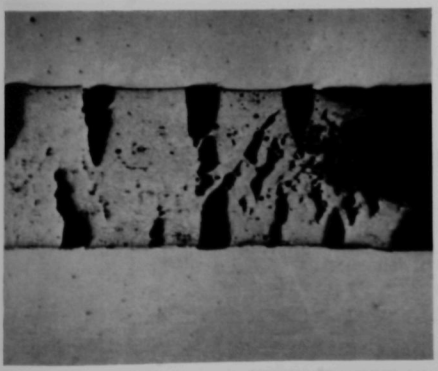

FIG. 14. Fracture Area of Type 304 SS Specimen Tested at Room Temperature. (Mag. 20×)

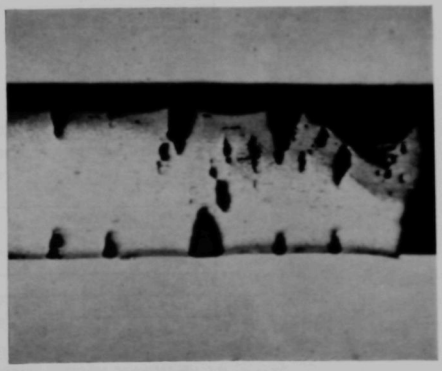

FIG. 15. Fracture Area of Type 316 SS Specimen Tested at Room Temperature. (Mag. 20×)

of the 491-hr high-carbon excursion specimens. This comparison is shown in Table 7.

The additional carbon pickup of 200 ppm in the 760-hr excursion did not change the percentage appreciably, but the changes that were noted were in the same general direction.

In Figure 12, the 0.2% offset yield strength is shown for the original and 500-hr helium-exposed material, as well as for the 491-hr and 760-hr high-carbon sodium-exposed material. At all test temperatures, only minor changes occurred during the 500-hr thermal aging (helium exposure) for both Types 304 and 316 SS. The effects of the two carbon excursions, are most evident in the room-temperature tests, for which substantial increases in yield strength are seen. (The increase becomes less evident as the test temperature increased.) The greater carbide penetration of the Type 304 is pointed out by the relatively larger increases in yield strength in the Type 316 SS. The reduction of yield strength at 1400°F was to be expected as a result of solution of the strengthening carbide phase.

In Figure 13, the tensile strengths of the same test specimens showed the minor changes due to 500-hr thermal aging and the slight increases (except in the room-temperature tests) caused by the two carbon excursions. These changes were much less than those experienced in yield strengths and again were most evident in the Type 304 SS material. As in the case of the yield-strength data, the effects of the carbon excursions decreased with increasing temperature increases as a result of solution of the carbide phase.

The most apparent and most discouraging changes observed during these high-carbon excursions con-

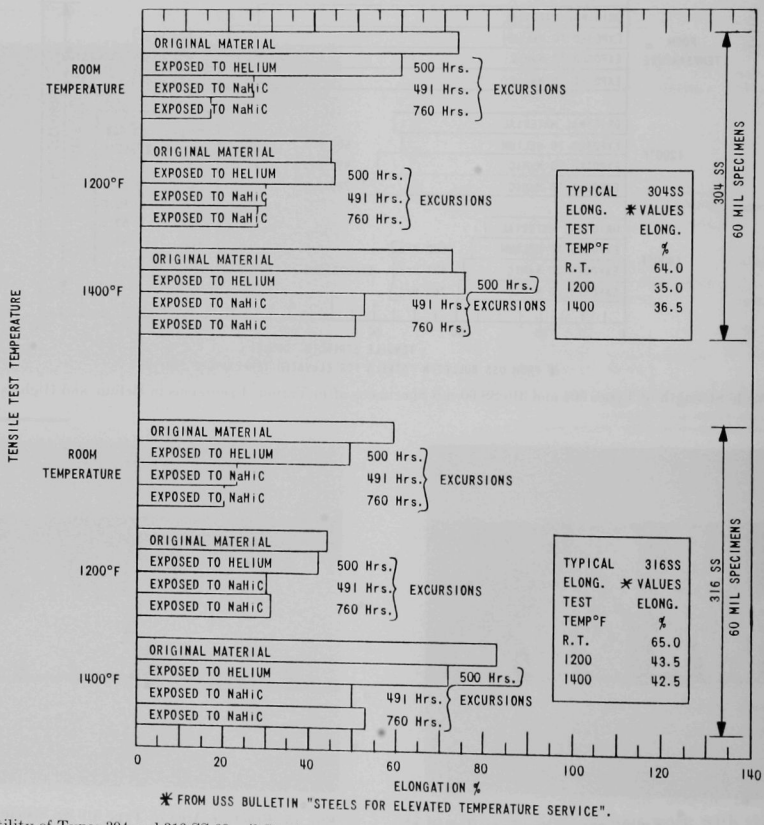

FIG. 16. Ductility of Types 304 and 316 SS 60-mil Specimens after Various Exposures to Helium and High-carbon Sodium at 1200°F.

cerned the reduction of ductility values. Although final ductility values of >15% are indicated in all the specimens from the high-carbon excursion, these data are somewhat misleading, since the stress-strain traces of each specimen indicated that the maximum test load and the breaking load were identical, typical of highly embrittled material. The photomicrographs of the Types 304 and 316 SS in Figures 14 and 15 show the extensive cracking that occurred during the room-temperature testing, with cracking in Type 304 SS the most extensive.

In Figure 16, the ductility values obtained from these tests are compared. As previously shown, there are small thermal-aging effects. The effects of the carbon excursions, however, are quite evident. Particularly in the room-temperature tests there were quite significant reductions in ductility values.

It is felt that a large portion of the measured elongation in both materials was in the cracking and crack separation, with only a small amount of metal deformation. This would indicate the 'true' elongation values of Type 304 might be somewhat <10% in the room-temperature tests, where brittle failure is occurring across the total specimen thickness. The Type 316 SS did, however, show metal deformation toward the center portion of the test specimen that would yield higher true elongation values than for Type 304. It is impossible, however, to assign specific values.

A different mode of failure prevailed in the 1200°F tensile tests. The cracking was confined to the immediate vicinity of the carbon case, as seen in Figure 17. The fracture mode is of a shear type. In these tests, the elongation values were not much greater than the room-temperature values, but the reduction-of-area values had increased measurably. Both Types 304 and 316 SS reacted similarly.

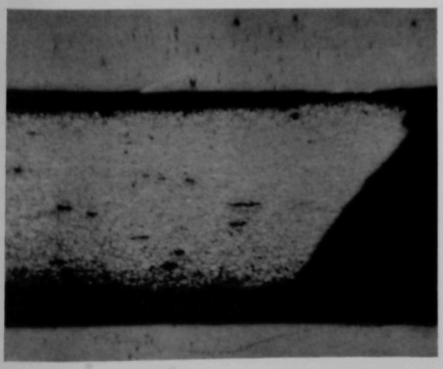

FIG. 17. Fracture Area of Type 316 SS Specimen Tested at 1200°F. (Mag. 26×)

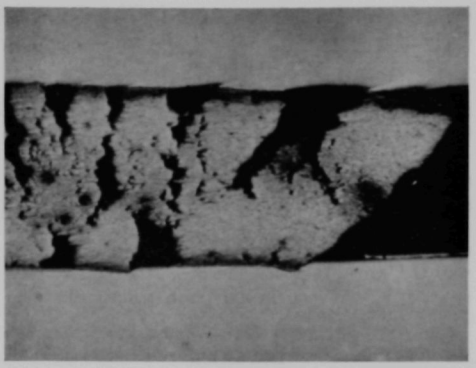

FIG. 18. Tensile Specimen Exposed in Loop 1 for 491 Hr and Tested at 1400°F. (Mag. 23×)

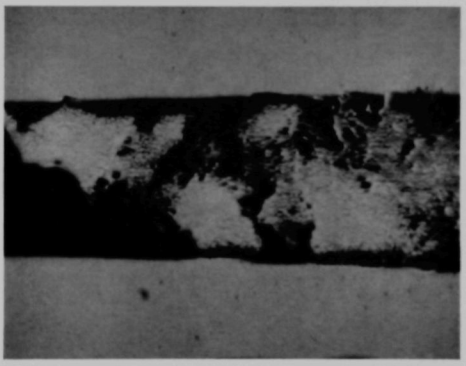

FIG. 19. Tensile Specimen Exposed in Loop 1 for 491 Hr and Tested at 1400°F. (Mag. 23×)

In the 1400°F excursion, the ductility values continued to show increases with the increase in test temperature. Again, the intense cracking and crack separation appeared quite similar to those observed in the room-temperature tests, which was not anticipated. Normally, as the test temperature rises, the effects of the brittle carbide case diminishes, wherein once cracking has proceeded through the brittle case depth, failure continues in a ductile fashion. Figures 18 and 19 show that, although extensive plastic deformation has occurred, the presence of cracking raises some question as to the validity of elongation data in the true sense of the word. The reappearance of this fracture mode, at temperatures for which

the effects of brittle cases would be expected to be diminishing, is unclear.

Similar tests were conducted with 15-mil specimens that had been carburized to similar case depths. These tests, in general, showed greater increase in strengths and losses in ductility than would be anticipated due to the area/volume ratio of the thinner cross sections. The only difference noted was that the 15-mil specimen failure-mode at room temperature was of a ductile nature once cracking through the carbon case depth occurred. This was the same behavior noted in the 60-mil tests at 1200°F, but not in the room-temperature and 1400°F tests.

Discussion

Mr. Comprelli (GE): In your high-oxygen runs, the data points you showed are very close to the so-called controls. You claimed a decrease, and I am wondering if the decrease is significant enough to bring it outside the error band for your controls. The second point I would like to ask would be with regard to your long-term testing. The microstructures that Dr. Zebroski showed this morning indicated that in an active system where mass transport is occurring there is a tendency to develop a surface-reaction zone. In the particular case illustrated this morning there was a zone around 4 mils in depth which had a modified structure because of loss of carbon along with the other major constituents. I am wondering if you saw this in your specimens.

Mr. Kirschler: In answering your first question, this point did appear to be significantly out of place as compared to the previous testing we had done in the low oxygen-sodium environments and in the air environments. We are currently repeating this test to see if this was a true deviation from the curve or not. In respect to your second question, we did not see this zone.

Mr. Comprelli: Was there any intensive mass transport in your testing at all?

Mr. Kirschler: No, not really.

Mr. Comprelli: How can you attribute this decrease in mechanical properties to some corrosion effect if you did not see any evidence of it?

Mr. Kirschler: It is a reduction in load-bearing area due to these oxide penetrations into the grain boundaries.

Influence of Sodium and of Irradiation on the High-temperature Creep Behavior of Certain Stainless Steels

J. P. Andre,* J. Beaufrere,† L. Valibus,† and A. Weisz*

(PRESENTED BY J. BEAUFRERE)

1. Introduction

The clads of the fuel elements of fast sodium-cooled reactors are subjected to rather high stresses during a long immersion in high-temperature sodium and under irradiations. These stresses are caused by the pressure buildup of fission gases, by the thermal gradient due to the heat flux, and to fuel swelling. Therefore, the basic characteristics of the materials of which these clads should be constructed are creep behavior and ductility. Now, while these characteristics are well-known for the common alloys at high temperature in normal ambience, we have very few results concerning the possible influence of the sodium and of the irradiations. Thus, EDF and CEA have cooperated in preparing test programs in order to evaluate these influence. EDF/SERNUTH is carrying on creep tests in sodium at its RENARDIERES laboratory, and CEA/SRMA creep tests in reactors and on irradiated specimens. The first results obtained bear on the steels Z 6 CND 17.13 (AISI 316), considered for the Phenix reactor clads.

2. Influence of Sodium on Creep Behavior

EDF has undertaken a general program of sodium creep tests bearing on materials intended for cladding for the critical points of the structures, and for the steam generator. (For the latter, special devices have been developed in order to study the possible influence of mass transfer between ferritic and austentitic steels.) The results given below bear only on AISI 316 stainless steels and derivatives.

2.1. General Conditions

The influence of sodium should be observed with respect to a reference atmosphere on specimens of a given form and for given sodium qualities.

Studies made by Shahinian,[1] Garofalo,[2] and Kramer[3] have shown that oxidation might play a part in creep behavior, of nickel and aluminum in particular, but that this effect should be small for stainless steels. Garofalo[2] and Andrews[4] have obtained close results in air, helium, or vacuum for an AISI 316 steel at 650°C and 700°C. Based on these studies, and on the fact that the proposed cover gas for fast reactors is argon, we have chosen this gas as the reference atmosphere. A few tests were also carried out in air.

Most of available results of creep in normal or special atmospheres have been obtained with rather heavy test specimens. In order to link our tests to the origins of these results and to obtain a first stage of rather general results not linked to a well-determined form, we have chosen solid cylindrical specimens of 4-mm diameter and of gauge length of 32 mm.

Andrews[4] has studied the effect of oxygen and carbon impurities contained in the sodium. We limited ourselves to nuclear-quality sodium containing about 20 ppm oxygen, which is the most likely industrial quality for fast reactors.

2.2. Test Equipment—Operational Procedure

2.2.1. The materials tested were Z 6 CND 17.13 (AISI 316), Z 8 CNDNb 18.12 (AISI 316 Nb stabilized), and Z 10 CNUDNbT 18.16 (AISI 316 with Cu), whose compositions are given in Table 1.

Tests were also performed with Hastelloy X.

2.2.2. The test specimens were supplied by CEA-SRMA. All had the same origins and heat treatments at those intended for grade-characterization tests and to tests of creep under irradiations. All the specimens of the same grade underwent the same heat treatments, and had the same grain sizes and the same surface states.

2.2.3. All the tests are performed at 700°C, the hot-point temperature planned for Phénix clad.

2.2.4. The creep tests in argon and in air were performed on conventional machines of two types: machines with continuous recording of elongations and with 1,000 amplification in "air" environment, and similar machines with 200 amplification in "argon" environment.

2.2.5. Creep tests in sodium: the creep to rupture tests were performed with 8 ADAMEL machines, EDF license[5] (see Fig. 1), of which the main characteristics are:

- continuous recording of elongations with 20 and 100 amplifications;
- maximum force of 450 kg;
- maximum temperature of 800°C with temperature regulation of ±1°C.

Six of these machines were mounted on static

* C.E.A., CEN Saclay, Gif-sur-Yvette, France
† Electricité de France, Chatou, France

TABLE 1. COMPOSITIONS OF THE TESTED STEELS

Grade	Weight %										Heat Treatment
	C	Si	Mn	Ni	Cr	Mo	Nb	Ti	Cu	B	
Z 6 CND 17.13 (AISI 316)	0.06	0.52	1.7	11.9	16.5	2.36				0.0015	35-mm forged bar; heat treatment at 1050°C.
Z 8 CNDNb 18.12 (AISI 316 st. Nb)	0.076	0.70	1.97	13.5	17.3	2.20	0.83				35-mm forged bar; heat treatment at 1,100°C
Z 10 CNUDNbT 18.16 (AISI 316 with Cu) FLUGINOX 140	0.109	0.52	1.80	14.48	16.49	2.58	0.50	0.35	2.98		25-mm forged bar; heat treatment at 1,175°C

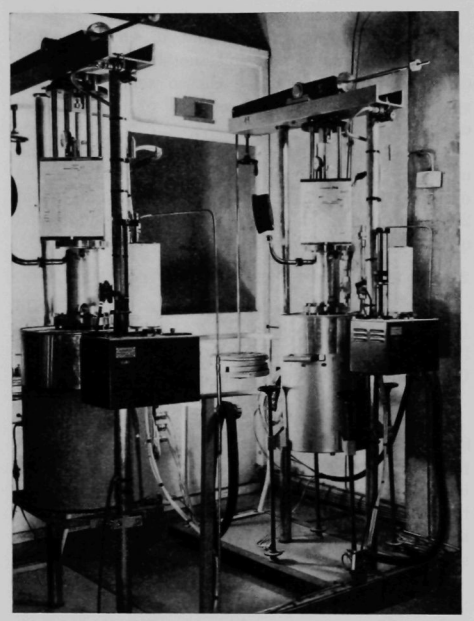

FIG. 1. Creep-rupture Machine on a Static Sodium Pot.

sodium pots and two on loops with a speed of the order of 1.5 m/sec along the specimens, a thermal gradient, and sodium treatment by diffusion cold trap.

The creep tests were performed on two ADAMEL machines, EDF license[6] (see Fig. 2), of which the main characteristics are:

- continuous recording of elongations with 500 and 1,000 amplifications;
- maximum force of 250 kg;
- maximum temperature of 800°C with temperature regulation of ±1°C;
- possibility of mounting in creep or in stress relaxation.

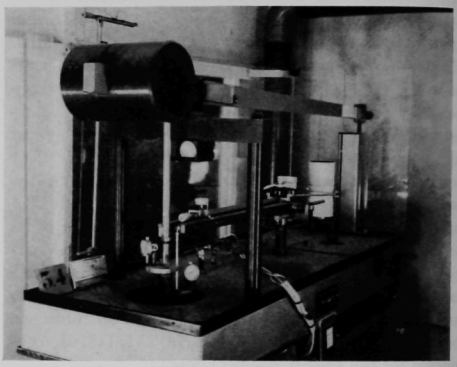

FIG. 2. Creep Machine on a Static Sodium Pot.

These machines were mounted on static pots in an air-conditioned room.

Special devices permitted the adaptation of conventional machines to sodium.

2.2.6. After their passage in environment, all the specimens were measured and analyzed in the metallurgy laboratory. Cracks, decohesions, and formation of surface coats and of precipitates were observed and analyzed under an optical microscope using X rays (above all in vacuum diffraction) and under CASTAING microprobe.

2.3. Experimental Results

Most results were obtained with the grade Z 6 CND 17.13 (AISI 316). The dynamic sodium tests have been performed only with this grade. Fragmentary results were obtained with Z 8 CNDNb 18.12 (AISI 316 Nb stabilized) and Z 10 CNUDNb 18.16 (AISI 316 with Cu). Furthermore, these are only preliminary results, the program being in progress in order to obtain numerous points for longer durations.

2.3.1. Comparison of the different characteristics

obtained in sodium with respect to those obtained in argon and in air were:

Rupture time (see Fig. 3) for the three grades; it is systematically a little longer in static sodium. On the other hand, there is no visible effect in dynamic sodium.

Time taken to reach a 1% elongation (see Fig. 4). It is less in static sodium for the 316 and the 316 Nb, while there is no visible effect for the 316 with Cu in static sodium and for the 316 in dynamic sodium.

Minimum creep rate (see Fig. 5). In static sodium, the behavior of 316 and of 316 Nb is not really altered. On the other hand, the 316 with Cu had a minimum creep rate that was slightly higher, and particularly when the stress was lower. In dynamic sodium, the behavior of the 316 was affected more clearly, and the minimum creep rate was lower for all the stresses.

Elongation at rupture (see Fig. 6). In static sodium, the elongation was a little greater for all the grades, and was more sharp for the 316. On the other hand, for the same steel in dynamic sodium, there was no visible effect.

Necking down at rupture (see Fig. 6). It seems slightly less in all the cases except for the 316 in static sodium.

2.3.2. Micrographic Observations

All the specimens showed an austenitic grain structure 4, with slip lines at the surface, due to parts machining.

Figure 7 shows the observations made with the 316 loaded at 8 kg/sq mm to bring out the appearance of the elongations and the necking-downs, the shape and distribution of cracks and decohesions, and the appearance of precipitates and surface coats. The results obtained with the other grades are less numerous, but have the same sense as those found with the 316.

Surface inspection: In the argon and dynamic sodium environments, a surface coat was formed. On the other hand, the metal appeared bare in static sodium. The composition of this layer was determined by X-ray diffraction under vacuum, by using the Kα chromium line. In argon, for durations of the order of 3,000 hr, there was found a layer 15 to 20 μ thick, composed mainly of Fe_2O_3 and Cr_2O_3. (The argon contained a few ppm of oxygen.) Below,

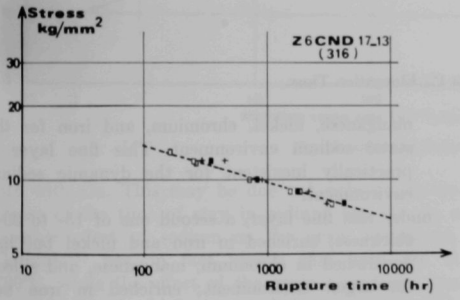

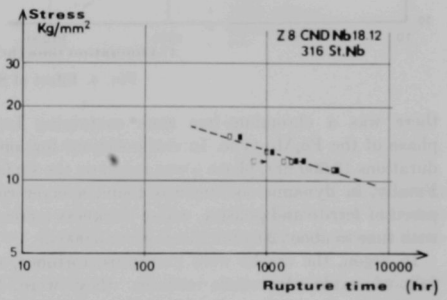

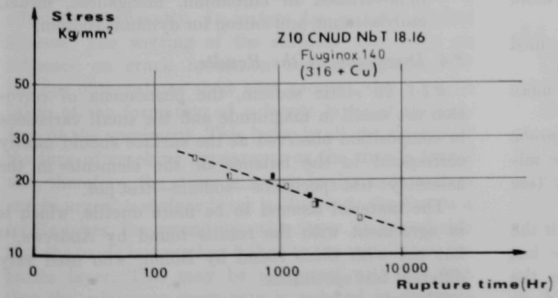

EXPOSURE AT 700°C

- Argon
- Static sodium
- Dynamic sodium

FIG. 3. Effect of Sodium on Rupture Time.

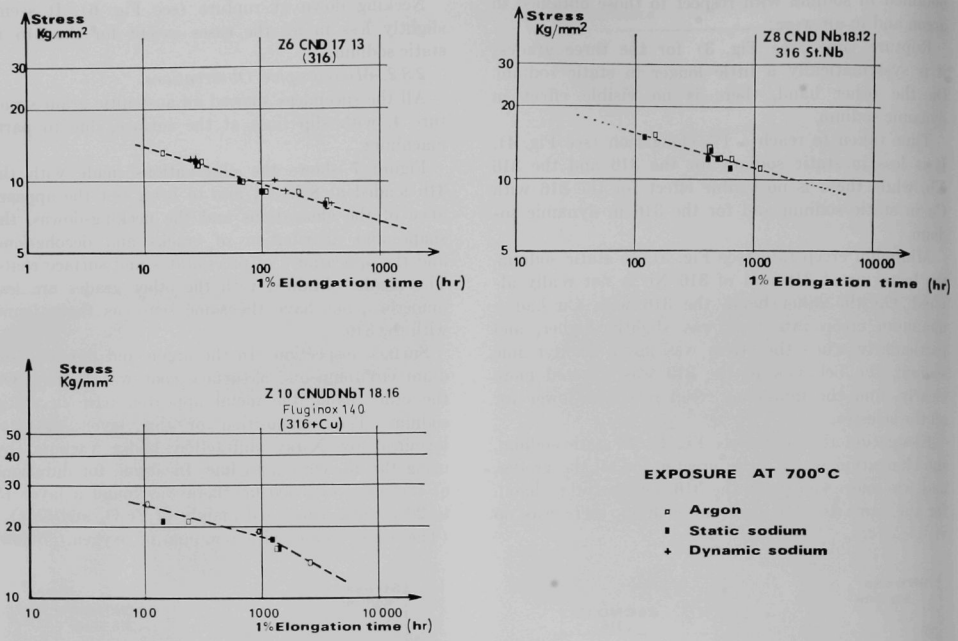

FIG. 4. Effect of Sodium on 1% Elongation Time.

there was a chromium-free zone containing Laves phase of the Fe_2Mo type. In static sodium for longer durations (3,000 hr), phase χ was found on the surface. Finally, in dynamic sodium was found a layer composed of ferrite and phase χ, whose thickness increased with time to about 20 μ for durations of 3,000 hr.

In argon, the cracks were numerous, tortuous, and full of oxide. In static sodium, they were less numerous, more open, and with sharply defined edges. In dynamic sodium, they were numerous and could be opened with difficulty since the ferrite layer, more ductile than the rest, filled them up in part.

Inspection of internal decohesions: They seemed greater in argon than in static or dynamic sodium.

Rupture inspection: The grains seemed to be more elongated at rupture in static sodium.

2.3.3. Examinations under CASTAING Microprobe

Quantitative analysis of the surfaces with the microprobe has brought out two successive layers (see Fig. 8):

a fine layer 2 to 3 μ thick at the contact with the fluid, enriched in chromium and manganese but impoverished in iron and molybdenum for the argon environment (oxide), and enriched in silicon and molybdenum but impoverished in manganese, nickel, chromium, and iron for the static sodium environment. This fine layer is practically inexistent for the dynamic sodium environment.

under this fine layer, a second one of 15- to 20-μ thickness, enriched in iron and nickel but impoverished in chromium, manganese, and silicon for argon environment; enriched in iron but impoverished in chromium, molybdenum, and silicon for static sodium; enriched in iron but impoverished in chromium, manganese, nickel, molybdenum, and silicon for dynamic sodium.

2.4. Discussion of the Results

2.4.1. In static sodium, the phenomena of corrosion are small in magnitude and the small variations in composition observed at the surface should mostly correspond to the balance of the elements in the assembly: test specimens—sodium—test pot.

The material seemed to be more ductile, which is in agreement with the results found by Andrews,[4] but not with those found by Böhm, who used very different test specimens.

The secondary creep rate tends to be somewhat greater, all the more as the stress is less for the

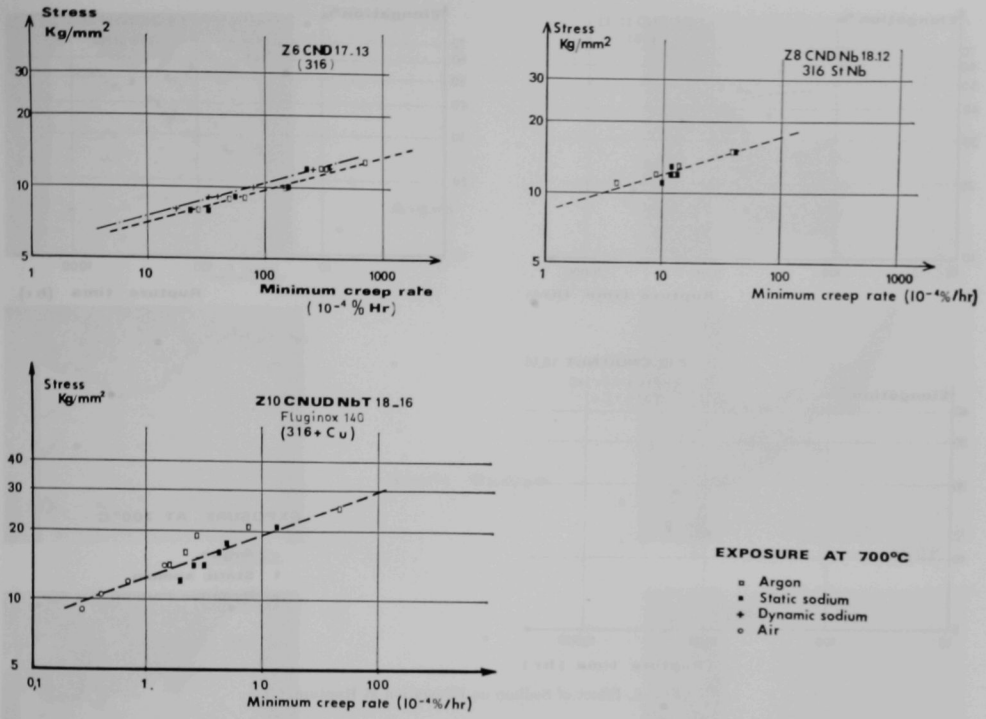

FIG. 5. Effect of Sodium on Minimum Creep Rate.

316 with Cu. This may be due not only to the increase of the time of stay in sodium, but also to a possible effect of sodium on the grain boundaries. Garofalo[7] has, in fact, shown that with 316 at 700°C, while the effect of the grain boundaries was very small under high stresses, it became appreciable below 10 kg/sq mm.

2.4.2. In dynamic sodium, only the creep rate is affected significantly. It is less for all the applied stresses. The wetting of the surfaces may have an influence on crack formation and propagation,[8, 9] but our observations show that account also must be taken of the formation of a ferrite layer at the surface of the specimens. This layer is all the thicker at the time of cracking appearance as the time is longer and, therefore, the stress is lower. In dynamic sodium and in argon, a surface layer is observed: the first is a ferrite layer, the second an oxide layer. It is probable that the oxide layer is less linked to the metal than the ferrite layer. This may be compared with the fact that the minimum creep rate is reduced in dynamic sodium, taking up the assumptions of Kramer.[3] A surface layer may render the escape of dislocations at the material surface more difficult and therefore delay the movement of dislocations and cause a hardening of the material.

The influence of stress on chromium solution[10] could not be verified by our analyses, since our tests were not performed at constant time, but were carried on mostly until rupture.

2.5. Conclusions

The main results obtained with the Z 6 CND 17.13 at 700°C are:

Rupture time and elongation were slightly greater in static sodium than in argon, air, and dynamic sodium.

Secondary creep rate was lower in dynamic sodium than in argon, air, and static sodium.

A surface layer developed in static sodium; an oxide layer developed in argon; a ferrite layer developed in dynamic sodium.

However, it should be noted that the tests were small in number and only endured for times of the

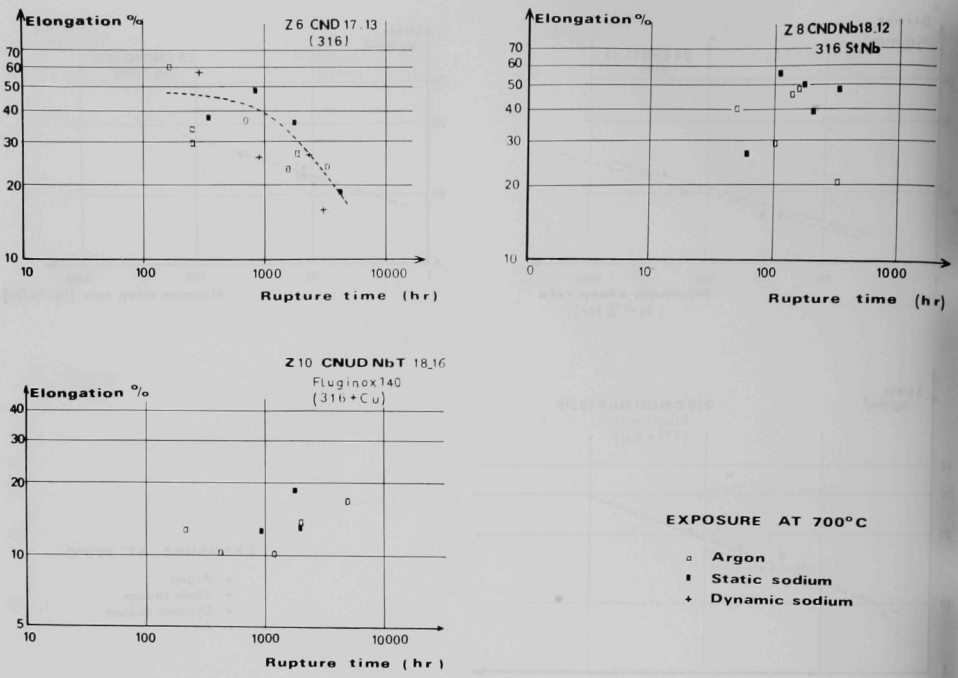

FIG. 6. Effect of Sodium on Elongation at Rupture.

order of 3,000 hr. Nevertheless, they are sufficient to enable us to say that, under these conditions, the influence of sodium on creep behavior of Z 6 CND 17.13 at 700°C is small, especially with respect to other effects that the materials might undergo in a fast reactor, particularly those due to irradiations.

The static sodium tests do not represent the effect of corrosion in reactors, and this may be very troublesome for thin parts and for long durations.

Therefore, it seems prudent to us to continue and to multiply our dynamic sodium tests, and to follow up this preliminary program by using specimens reproducing the real shape and subjected to stresses representing the real ones.

3. Influence of Irradiation on Creep Behavior

3.1. Introduction

The influence of irradiation on austenitic stainless steels has been mostly studied by mechanical tests performed after irradiation, such as tension tests or creep tests. Until now, we have few results concerning creep deformation in a reactor. It is known that creep at elevated temperature is a thermally activated process whose activation energy is often close to that of self-diffusion. This is attributed to the fact that the deformation rate depends on the dislocation climb rate. Qualitatively, one may then expect that the neutron flux has an effect on the creep rate because of the production of a large number of vacancies and interstitials as the result of the action of fast neutrons on the atoms of the lattice.

This reactor creep behavior of steel 304 has been studied by Williams and Carter[11] at Battelle Institute and by Bloom[12] at ORNL. These authors have conducted their studies within the temperature range from 550 to 750°C for stresses varying from 7 to 21 kg/sq mm. They found no change in the creep rate; on the other hand, they observed a large decrease in rupture ductility and a decrease in rupture life.

In our work, we have proposed to study creep characteristics in a reactor of steel 316, envisaged as cladding material in fast-neutron reactors, comparing them with those of a material subjected to creep before and after irradiation.

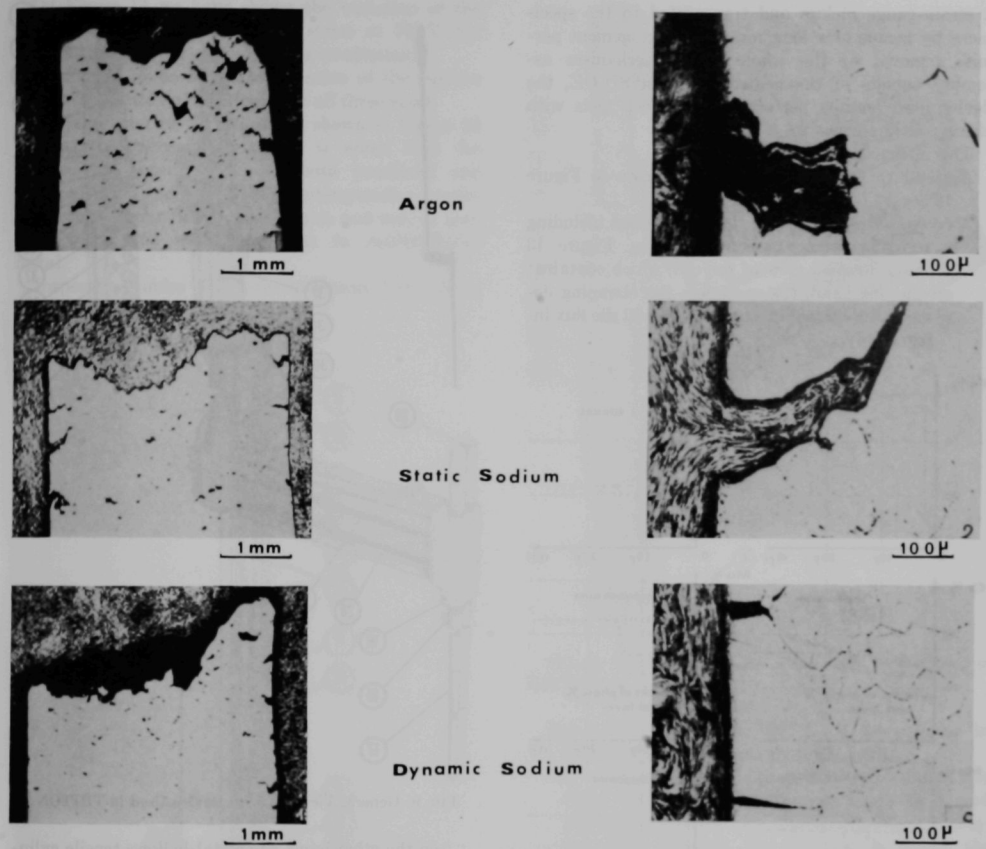

FIG. 7. Micrograph Showing Cracks, Decohesions, and Surface Layers in Z6CND 17-13 (316) Creep Specimens after Exposure in Sodium at 700°C.

3.2. Experimental Conditions

For our experiments, we used an austenitic stainless steel of Type 316, the composition of which is given in Table 1. The initial state was obtained by a solution treatment at 1050°C.

The tests were performed in the thermal reactors TRITON and SILOE. The respective fluxes in fast and in thermal neutrons are given in Table 2. The fast fluxes in the SILOE are of a higher order of magnitude than those in the TRITON.

Two creep facilities were used. In TRITON, we used a facility permitting simultaneous conduct of several creep tests under different stresses, without using strain gauges. Figure 9 shows an overall assembly view of the setup. It consists of two identical creep lines, juxtaposed but independent of each other from the point of view of tensile stresses and of temperatures. Figure 10 shows the part in the reactor in detail. Each test-specimen line is maintained at constant temperature by means of an electric furnace, fractioned into four elements regulated independently by means of thermocouples fastened on the test specimens. The two furnaces are immersed in water and placed against the reactor core. Their heat insulation is ensured by a gas layer, varying in accordance with test temperature.

The tensile mechanisms are shown in Figure 11. Their principle is as follows: the tensile stress is applied to each specimen line by means of a metal-bellows cylinder. This stress is measured by means of

a strain-gauge pickup and transmitted to the specimens by means of a long rod. This arrangement permits removal of the whole tensile-mechanism assembly outside of the neutron flux. In SILOE, the device used permits performance of creep tests with strain measurement.

This device includes:

A standard Chouca type furnace, shown in Figure 12,

A creep cell placed within the furnace and including a resonant-cavity measuring device. Figure 13 shows a detailed view of the cell, which contains: on the one hand, the specimen, the clamping devices, the control thermocouples, and the flux integrators;

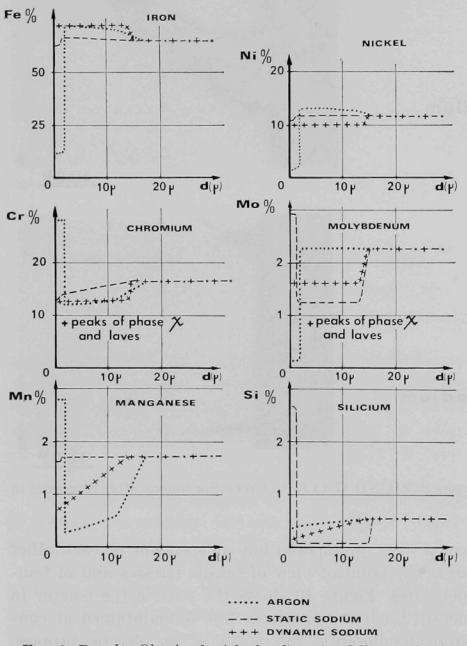

FIG. 8. Results Obtained with the Castaing Microprobe for Analyses of Surface Layers Formed in Z6CND 17-13 (316) Creep Specimens after Exposure in Sodium at 700°C.

TABLE 2. REACTOR'S CHARACTERISTICS

Reactor	Flux, n/cm²/s	
	Thermal	Fast
TRITON	0.9×10^{13}	0.95×10^{13}
SILOE	1.73×10^{14}	1.9×10^{14}

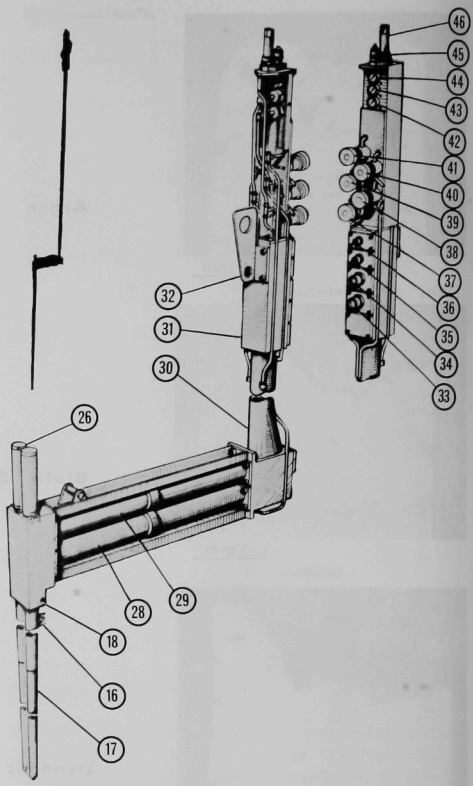

FIG. 9. General View of Creep Device Used in TRITON.

on the other hand, the metal-bellows tensile cylinder prolonged by a resonant-cavity displacement pickup, supplied by a wave guide.

The lower part of the capsule is filled with an eutectic NAK mixture in order to reduce the internal thermal gradient. Finally, the furnace is housed inside a water box inserted into the reactor core.

3.3. Results

All the creep-test results made before, during, and after irradiation are given in Table 3.

It is noted that:

The creep rate is not appreciably affected, regardless of flux value.

The life duration and ductility at rupture are the more affected as the flux is greater.

Finally, creep characteristics before and after irradiation are practically identical.

On Figure 14 we have shown the variation of the creep rate as a function of the stress at 700°C for each case: before, after, and during irradiation.

On Figure 15 we have the variation of the rupture time as a function of the stress, for all three cases.

The character of the rupture is shown in Figure 16 (micrographic observations). It is noted that the rupture was intergranular, on both irradiated and nonirradiated specimens. The intergranular cracks are perpendicular to the tension axis and are, in general, wider and more numerous in nonirradiated metal.

Inspections under electronic microscope have led to the following observations:

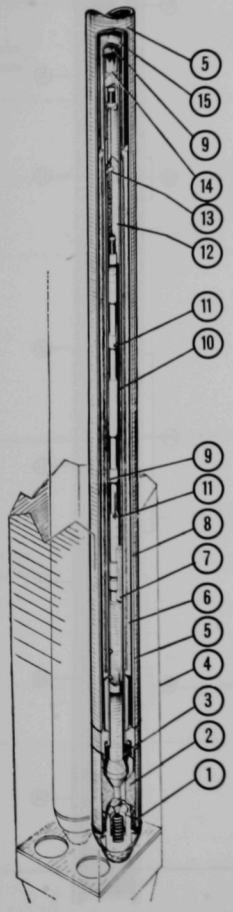

FIG. 10. In-reactor Part of the Creep Device Used in TRITON.

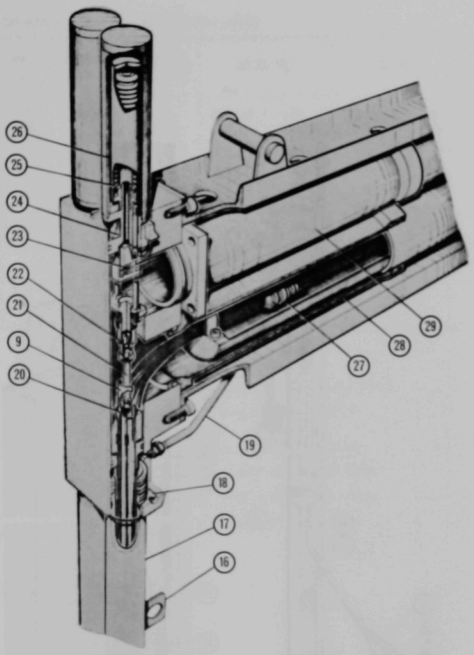

FIG. 11. Tensile Mechanisms of the Creep Device Used in TRITON.

For 0.15% elongation (700°C, 6 kg/sq mm in SILOE), there is no cavity in the joints,

For elongation greater than 1.5%, the joints are filled with cavities containing precipitates and serving as starters (see microfractograph of Figure 17). Between the cavities is noted the presence of cupules formed during rupture at −196°C (microfractograph on a sample placed within TRITON at 7.4 kg/sq mm).

On Figure 18 may be observed the fact that the cavities are found preferentially near triple edges.

Figure 19 shows the polyhedral appearance of these cavities, of which the facettes frequently show steps resulting from surface diffusion.

Figure 20 shows that, for orientations perpendicular to the tension axis, one observes cavities while, on a different orientation joint, only cupules are observed.

3.4. Discussion

In agreement with the results of the American researchers, we have brought out the fact that irradiation involves a large decrease in life duration and in ductility at rupture. These effects do not seem to be

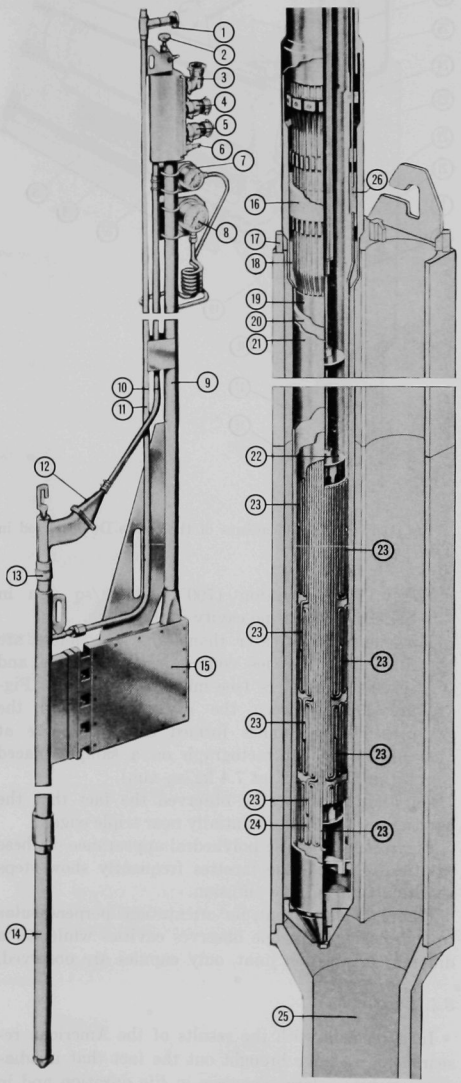

FIG. 12. General View of the Chouca-type Furnace Used in SILOE.

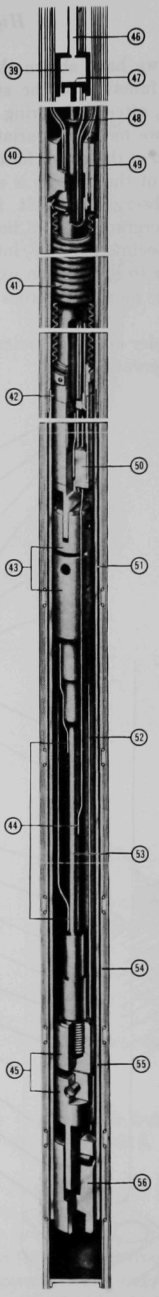

FIG. 13. Detailed View of the Creep Device Used in SILOE.

TABLE 3. RESULTS OBTAINED BEFORE, DURING, AND AFTER IRRADIATION

Reactor	Dose, n/cm²		Stress, kg/mm²		Rupture Time, hr		Minimum Creep Rate (10^{-4} % hr)		Δ1/1, %		Σ, %	
	Fast	Thermal	Out of Pile	In Pile	Out of Pile	In Pile	Out of Pile	In Pile	Out of Pile	In Pile	Out of Pile	In Pile
SILOE	4×10^{20}	3.8×10^{20}	6	6	600	>620*	0.6	<2.5*	>0.15*	>0.16*	—	—
SILOE	8.5×10^{20}	8×10^{20}	7	7	>1088*	1345	4	10.8	>1.28*	2.55	—	2.3
SILOE	7×10^{20}	6.5×10^{20}	8	8	4146	920	25	24	26.2	2.80	30	—
TRITON	4.8×10^{19}	2.8×10^{19}		6.8		>2160*				>0.56*		—
TRITON	8×10^{19}	4.5×10^{19}		7.4		>927*		14.5		1.35		
TRITON	8×10^{19}	4.5×10^{19}		8		927		36		3.34		—
BR II	1.08×10^{21}	2.05×10^{21}		7		1397		7		1.6		—
BR II	1.08×10^{21}	2.05×10^{21}		10		65		140		1.3		—

* Test stopped before rupture.

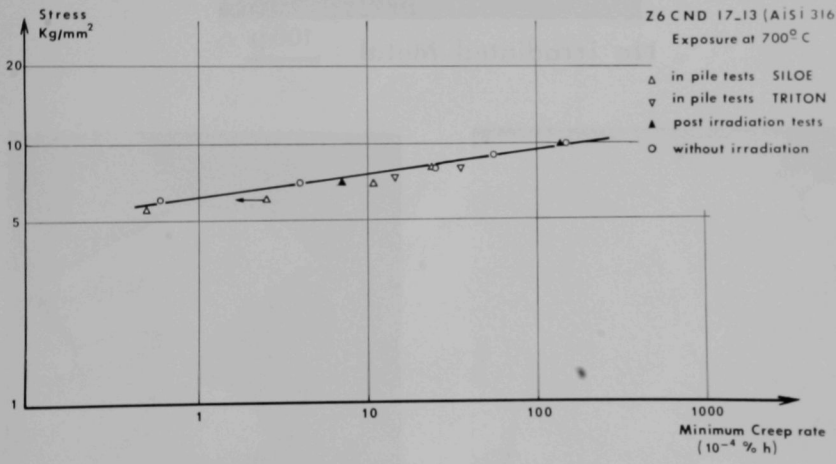

FIG. 14. Effect of Irradiations on Minimum Creep Rate.

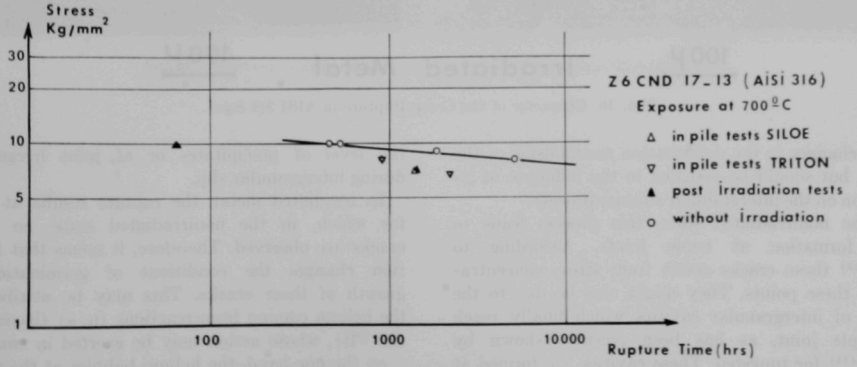

FIG. 15. Effect of Irradiations on Rupture Time.

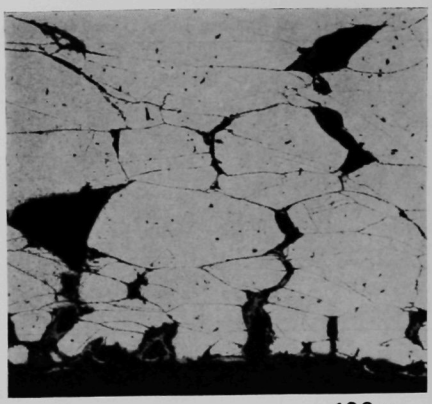

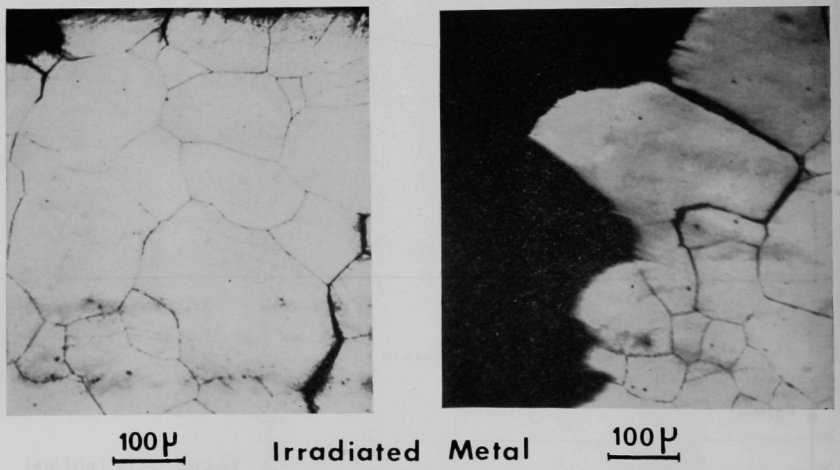

FIG. 16. Character of the Creep Rupture in AISI 316 Steel.

due to changes in the deformation mechanisms of the matrix, but should be assigned to the influence of irradiation on the intergranular rupture process.

In the nonirradiated state, this process leads to crack formation at triple joints. According to Zener,[13] these cracks result from stress concentration at these points. They might also be due to the growth of intergranular cavities which finally reach the triple joint, as has been recently shown by Stiegler[14] for tungsten. These cavities are formed at the level of precipitates or of joint irregularities during intergranular slip.

In irradiated metal, the rupture results at strains for which, in the nonirradiated state, no or few cracks are observed. Therefore, it seems that irradiation changes the conditions of germination and growth of these cracks. This may be attributed to the helium coming from reactions (n, α) (basically on the ^{10}B), whose action may be exerted in two ways:

on the one hand, the helium bubbles at the tip of a

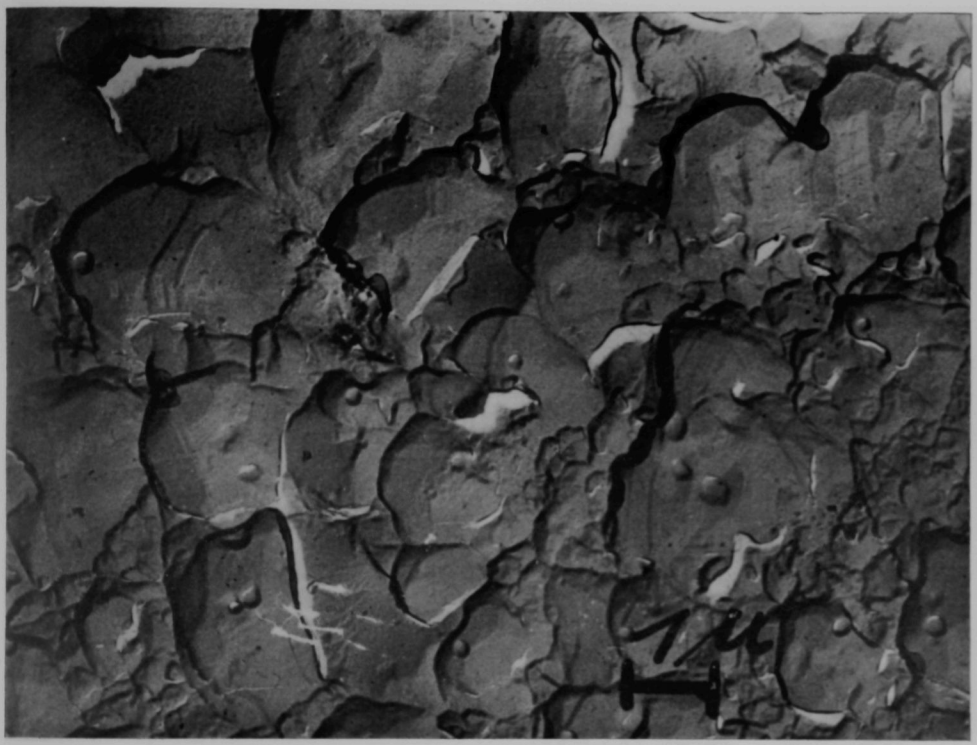

FIG. 17. Microfractograph Showing Cavities in Rupture after Irradiation.

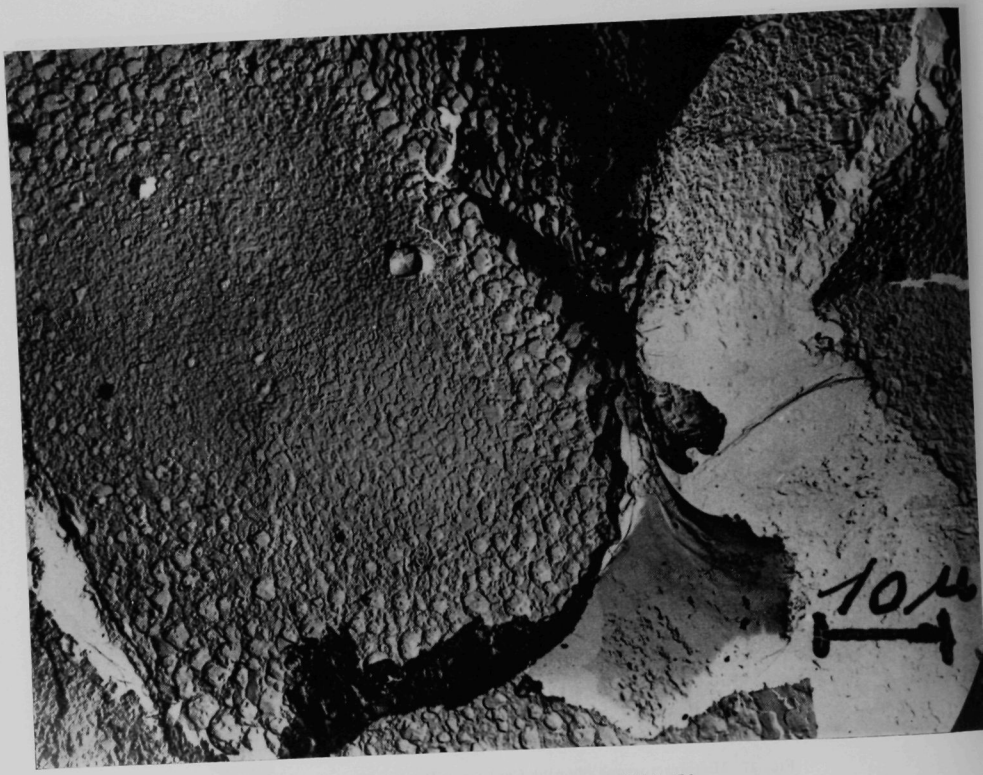

FIG. 18. Micrographs Showing Cavities at Triple Edges.

FIG. 19. Micrograph of Cavities.

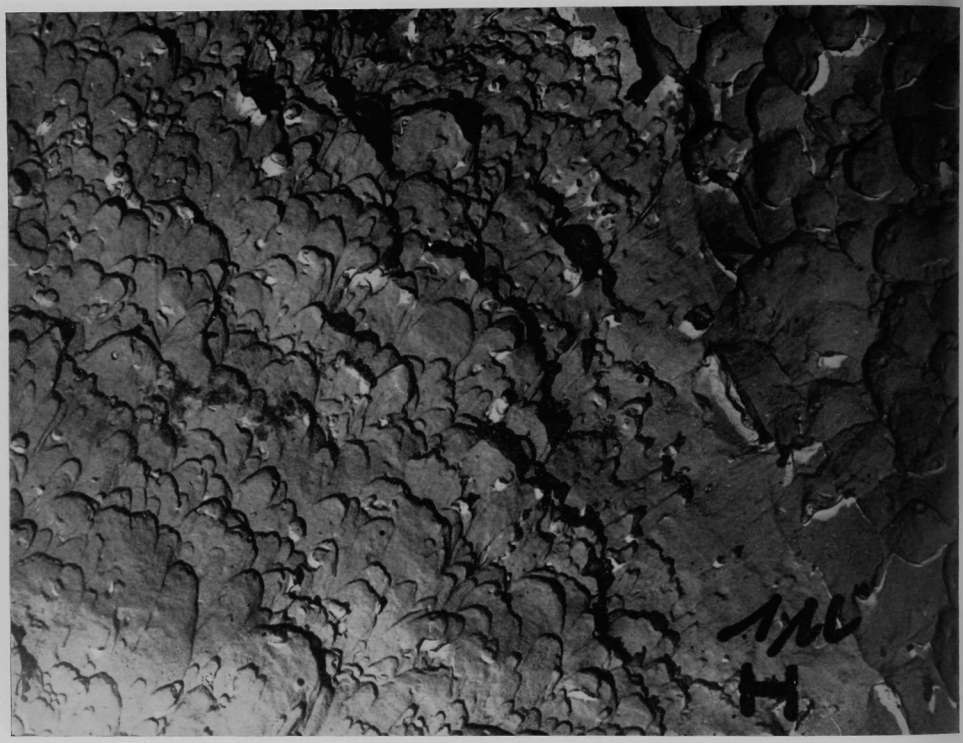

FIG. 20. Micrograph of Cavities.

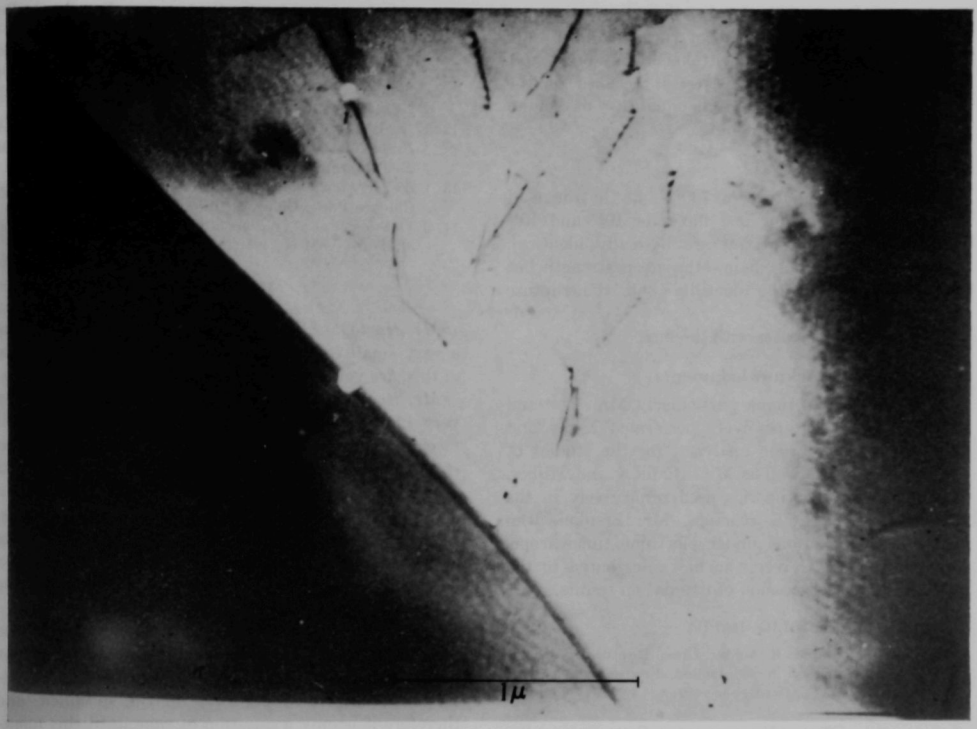

FIG. 21. Micrograph Showing Helium Bubbles.

crack may, through their growth under the effect of local stress concentrations, permit quick crack propagation;

on the other hand, the helium bubbles themselves may form cavities whose growth and subsequent coalescence might lead to intergranular cracking.

In fact, these bubbles have been observed in the joints and near the joints, as shown in Figure 21.

The absence of change in creep strength is coherent with the fact that, after irradiation at 1.3×10^{21} nvt, the 0.20% yield strength and the rupture load remain unchanged. In Table 4 are given the properties in tension at 700°C.

The creep behavior at 700°C in a fast reactor has not yet been studied. A rig within the "Rapsodie" reactor should be placed in service shortly. One may, however, make certain assumptions about this behavior on the basis of results of fast tension tests at 700°C after irradiation in a fast spectrum.

For small total doses of less than 10^{22} nvt, the strength characteristics in tension (0.2% yield strength and rupture load) are not appreciably changed. Under high stresses, it should be the same for creep strength, the embrittlement being less than in a thermal reactor, because of lesser helium production.

TABLE 4. MECHANICAL PROPERTIES OF AISI 316 STEEL AT 700°C IN AIR, IRRADIATED IN A FAST FLUX

Doses, n/cm²		Tensile Strength, kg/mm²	Yield Strength, E (0.2%), kg/mm²
Thermal	Fast		
1.70×10^{21}	1.31×10^{21}	25.1	16.2
0	0	25.1	16.1

For total doses greater than 10^{22} nvt, the yield strength and the rupture strength are increased. The result of this, in creep tests under low stresses, should be decrease in the creep rate, which is reached only after a certain length of time.

The hardening observed at this temperature should be due, in accordance with present assumptions, to the

presence of homogeneously distributed cavities, resulting from the precipitation of vacancies in a state of supersaturation. The embrittlement may be greater than in tests under high stresses, because of the double effect of increase in the quantity of helium formed and of matrix hardening.

4. Conclusions

For a test temperature of 700°C, in the range of stresses studied and for fast fluxes of 10^{13} and 10^{14} n/sq cm/sec, the properties are basically identical.

Irradiation does not change the creep strength but diminishes strongly the ductility and the rupture time.

This decrease increases with the flux.

Acknowledgments

We would like to thank particularly Mm. Ival and Pascal, who have respectively performed X-ray and CASTAING microprobe analyses, for the studies of creep in sodium, as well as Mm. Roulliay and Milhes, who have prepared the rigs used respectively in the TRITON and SILOE reactors, Mr. Frenkel, who made the observations under electronic microscope, and, finally, Mr. Calvet who has contributed to the presentation and discussion of irradiation results.

BIBLIOGRAPHY

1. P. Shahinian and M. R. Achter, Creep-Rupture of Nickel of Two Purities in Controlled Environment, *Joint International Conference on Creep (ASTM)*, London, 1963 è 7.49.
2. F. Garofalo, Effect of Environment on Creep-Rupture Behavior of Several Steels at Temperatures of 1000 to 1200F, *Proceedings of the American Society for Testing Materials Philadelphia*, Pa., **59** (1959).
3. I. R. Kramer, H. K. Shen, and S. E. Podlaseck, *The Influence of a Space Environment on the Mechanical Behavior of Metals*, SESA Spring Meeting held in Denver, Colo., on May 5–7, 1965.
4. R. C. Andrews, R. H. Hiltz, L. H. Kirschler, S. J. Rogers, and F. Tepper, Effect of High Temperature Sodium on Austenitic and Ferritic steels, MSAR Reports.
5. Beaufrere and L. Valibus, *Machine pour essais de fluage, notamment de fluage—Rupture*, Brevet FRANCE N° 1.524.301 (March 29, 1967).
6. J. Beaufrere and L. Valibus, *Machine pour essais de fluage*, Brevet FRANCE N° 1.524.300 (March 29, 1967).
7. F. Garofalo, O. Richmond, W. F. Domis and F. Von Gemmingen, *Strain-time*, Rate-stress and Temperature Relations during Large Deformations in Creep, Joint International Conference on Creep (ASTM), London (1963).
8. H. Böhm and H. Schneider, *Über das Zeitstand-und Kriechverhalten von austenitischen Chrom-Nickel-Stählen in Gegenwart von Natrium*, J. Nucl. Materials, **24** 188–197, (1967).
9. G. P. Dykova and V. I. Nikitin, *Effect of Liquid Sodium on Enduring Strength of Structural Materials*, Zhiekiye Metally Sbornik Statey, 292–299 (1963).
10. S. Kawahara, K. Furukawa, and K. Sako, *Sodium Technology in Japan*, London Conference on Fast Breeder Reactors (May 1966).
11. J. A. Williams and J. W. Carter, *The Creep of Annealed 304 Stainless Steel during Irradiation and Its Engineering Significance*, 69th Annual Meeting ASTM, Atlantic City, New Jersey, June 1966.
12. E. E. Bloom, *In Reactor and Postirradiation Creep-rupture Properties of Type 304 Stainless Steel at 650°C*, ORNL-TM 2130 (March 1968).
13. C. Zener, *Elasticity and Inelasticity of Metals*, University of Chicago Press, Chicago (1948).
14. J. O. Stiegler et al., *Nature of Creep Cavities in Tungsten et al.* Trans ASM **60**, 494 (1967).

Discussion

Mr. Horton (AEC): You said that the sodium has a very small effect on mechanical properties. In view of this, are you going to continue your tests?

Mr. Beaufrere: I have said that the sodium has a very little effect only on creep properties, not on all mechanical properties. Our tests are running now on specimens which are very thick, 4 mm thick, and 32 mm long. We think that the geometry can have a great importance; for the test of cladding materials, we will continue our tests with actual geometry using actual stress distribution. In fact we introduce a helium pressure inside our specimens to simulate the actual stress distribution.

Mr. Zebroski (GE): I have comments on the paper and on the last question. It seems to me your data showed that you basically were creating a different material at the surface of the specimen, and therefore it is only a question of time until this modified zone becomes thick enough to have very drastic effects on all the properties of that specimen. We see fairly sizeable effects on mechanical properties of specimens in sodium, but I will observe that we use specimens that have ⅓ the volume-to-surface ratio of the ones that you are using. I think that when you go on to your tubular specimen you will also see large effects on the mechanical properties.

Mr. Beaufrere: How long are your tests?

Mr. Zebroski: 3000 hours.

Mr. Coleman (APDA): I wonder if you can explain or have attempted to explain the difference between the data you saw in the flowing sodium and those from the static sodium system.

Mr. Beaufrere: I think it is an effect of corrosion. In the static sodium, corrosion is very low. In static sodium there is only a slight oxide layer, but in dynamic sodium there is diffusion of nickel and dissolution of nickel at 700°C. Although the appearance of the ferritic layer may be due to the nickel dissolution, there are only three points, and it is not possible to say definitely that diffusion of nickel controls the

formation of this layer, nor even the rate law of its formation.

Mr. Jansson (W): I notice that your argon wasn't very pure, since you have considerable oxidation going on. Do you expect that changes in composition of your surface layer could make the properties of this material different than it would have been in actual inert gas?

Mr. Beaufrere: That I have said in my paper. I think that it is only one hypothesis. I think that the ferrite layer on the surface of the material may prevent escape of dislocations. There are two different matrices, one austenitic and the other ferritic. Perhaps the escape of dislocations may be lower and the motion of dislocations inside the bulk may be reduced, so we can have a hardening effect by this process, but this is only one hypothesis.

Mr. Pfahler (LMEC): What were the velocities in your dynamic loop?

Mr. Beaufrere: 1.5 meters per second.

Mr. Bush (BNWL): How much chi phase were you seeing and were you detecting any effect on the ductility at lower temperatures due to the chi phase? I am really concerned if, in the thinner sections, you form enough chi phase by interaction to affect adversely your ductility under strain.

Mr. Beaufrere: Your question is "can the chi phase be correlated with a diminution or augmentation of ductility?" We have only a few observations of chi phase. I can't say definitely that chi phase has an effect on the ductility. We have observed too few cases of chi phase.

Mr. DeVan (Chairman): What is your interest in the Type 316 stainless steel plus copper?

Mr. Beaufrere: The creep characteristics are higher than the others. We have seen in the graphs the creep strain of the Type 316-copper is higher, comparable with Hastelloy-X.

Mr. DeVan: You didn't note any loss of copper from the material?

Mr. Beaufrere: We have tested the Type 316-copper in static pots. We have analyzed the sodium and even deposits around the pots, and we have seen nothing. We have analyzed for copper with the atomic absorption method and we have seen nothing, but it was in static sodium.

Mr. DeVan: Another point which I missed—what was the approximate time of the longest tests in the dynamic system for which you have data?

Mr. Beaufrere: We have tested for a maximum duration of about 3000 hr.

Mr. Comprelli (GE): In the 3000-hr test you say you measured the mass transport of several constituents. I didn't see the carbon data. Did you measure the carbon loss in this alloy, comparing the dynamic and the static systems?

Mr. Beaufrere: No, we have not measured in this test the loss of carbon from the material.

Mr. Comprelli: Were any changes in microstructure noticeable that might lead you to believe that there were differences in residual carbon?

Mr. Beaufrere: There is no carbon transfer because all our loops and our pots are made of the same grade of stainless steel. In static pots we have only an isothermal region and have not seen any carbon transport.

Mr. Comprelli: I might mention this will be discussed in a lot more detail tomorrow. In all-austenitic series loops we have seen as much as 40% carbon loss at 1300°F.

Mr. Beaufrere: In all-austenitic stainless steel?

Mr. Comprelli: Yes, in mono-metallic austenitic loops.

Mr. Beaufrere: But you have a very big ΔT between hot point and cold point.

Mr. Comprelli: 500°F.

Creep under High Heat Flux and Stress-rupture Properties of Austenitic Stainless Steels in Elevated-temperature Sodium*

J. H. Shively, D. F. Atkins, and W. T. Lee

Atomics International
A Division of North American Rockwell Corporation
Canoga Park, California

(PRESENTED BY J. H. SHIVELY)

Abstract

The purpose of the experimental effort described here was to define combined and separate effects of the non-nuclear LMFBR service conditions on the engineering properties of fuel cladding. Successful application of fuel cladding depends on adequate knowledge of the effects of temperatures from 700 to 1300°F, mechanical stresses from fission gases and fuel swelling, thermal stresses associated with high heat fluxes of the order of 1×10^6 Btu/ft²-hr, continuous exposure to sodium flowing at velocities as high as 30 ft/sec, and temperature cycling.

Stress-rupture tests were performed in static and dynamic sodium with Types 304 and 316 stainless steels. The tests in static sodium were performed on uniaxial and biaxial specimens between 900 and 1400°F. Creep tests were also performed in static sodium with specimens under uniaxial and biaxial stresses. The biaxial stress-rupture tests in dynamic sodium were made using an internal heater that produces a 1×10^6 Btu/ft²-hr heat flux through the cladding. Results of these tests are intended to serve a dual role: identification of the significant environmental effects, and quantitative determination of the relative magnitude in support of reactor fuel element design.

The results of tests in static and dynamic sodium have led to the following major conclusions:

1) High-purity static sodium does not influence the biaxial stress-rupture life of stainless steel.

2) The effect of stress state on stress rupture is best compensated for by use of the Von Mises effective stress relation.

3) The stress-rupture behavior of the two stainless steels is essentially the same in the annealed condition.

4) The strengthening benefits of cold work are more permanent in Type 316 than in Type 304 stainless steel.

5) Stress-rupture behavior of Type 304 stainless steel in flowing sodium under a steady heat flux correlated with the performance in static sodium for the temperature-stress conditions at the peak midwall position.

6) Stress-rupture life of tubes of Type 304 stainless steel in flowing sodium under a constant internal pressure and a cyclic heat flux is lower than that predicted using secondary creep data obtained in static sodium.

* Work performed under U. S. Atomic Energy Commission Contract AT(04-3)-701.

I. Introduction

The purpose of the experimental effort described here was to define the combined and separate effects of the non-nuclear LMFBR service conditions on the engineering properties of fuel cladding. Successful application of fuel cladding depends on adequate knowledge of the effects of temperatures from 700 to 1300°F, mechanical stresses from fission gases and fuel swelling, thermal stresses associated with heat fluxes of the order of 1×10^6 Btu/ft²-hr, continuous exposure to sodium flowing at velocities as high as 30 ft/sec, and temperature cycling.

The current scope of the program at Atomic International is limited to two stainless steels: Types 304 and 316. The technical approach taken by this phase of the LMFBR Cladding Program is to determine the effects of the LMFBR environment on the creep and stress-rupture behavior of cladding materials. The results are intended to serve a dual purpose: identification of the significant environmental effects, and quantitative determination of their relative magnitude in support of design analyses and design criteria. The current program includes an evaluation of the following:

1) sodium effects;
2) stress-state effects;
3) alloy type;
4) cold work;
5) thermal-gradient effects;
6) cyclic heat-flux effects.

II. Experimental Techniques

A. Static Sodium Tests

The test assembly for biaxial static sodium or helium tests has the capability of simultaneously testing

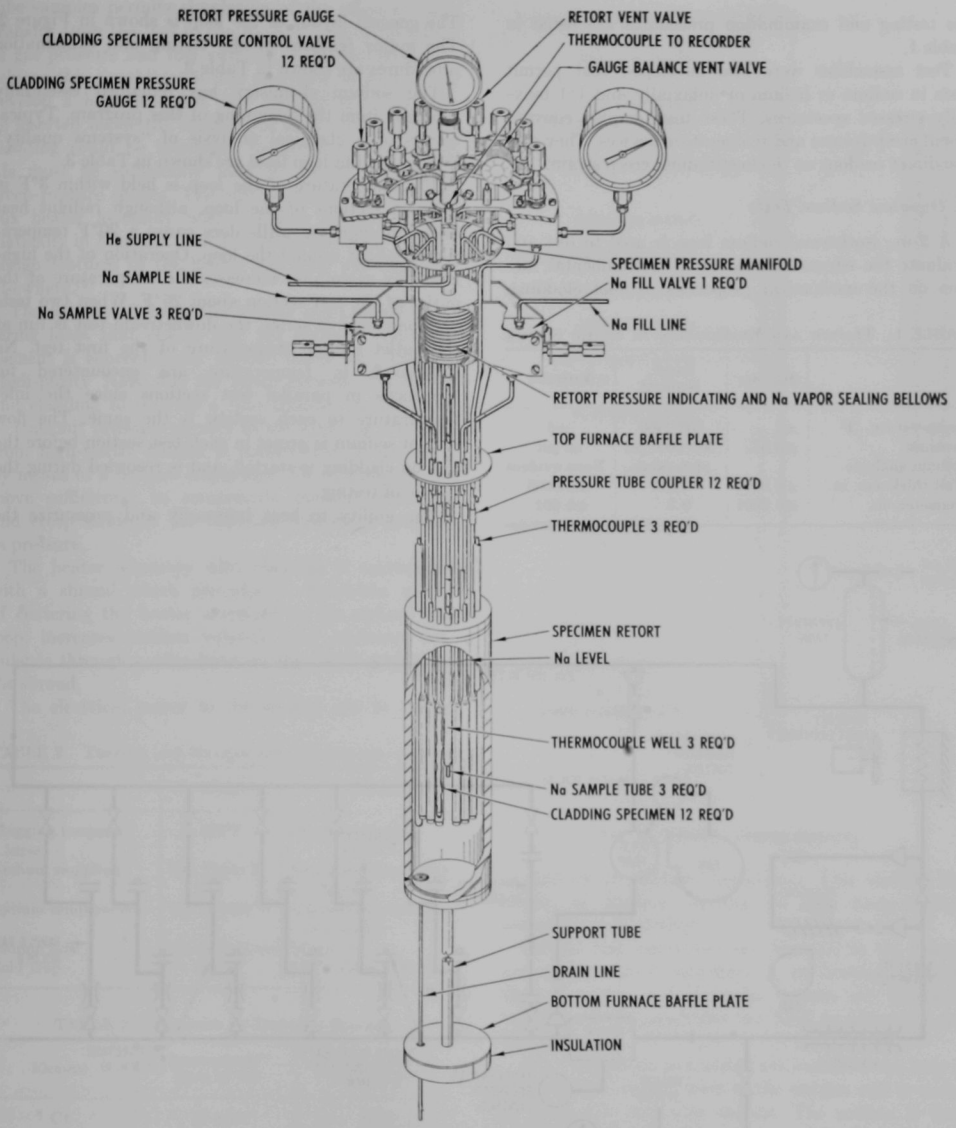

FIG. 1. Twelve-specimen Static Sodium Assembly for Biaxial Cladding Tests.

12 tubular samples (see Figure 1). The retort body was made of either Type 304 or Type 316 stainless steel, matching the material of the specimens. Provisions included are individual specimen pressurization and readout, sodium sampling on line, and thermocouple readout and calibration during testing. Detailed design, assembly, and test procedures have been reported previously.[1] The major features of

the testing and examination procedures are listed in Table 1.

Test assemblies were also developed that permit tests in sodium or helium of uniaxially and 1:1 biaxially stressed specimens. These tests employ conventional creep frames and temperature devices. They also use direct readout on the longitudinal creep strain.

B. Dynamic Sodium Tests

A 2-in., isothermal sodium loop is used to test and evaluate the effects of additional environmental factors on the mechanical properties of fuel cladding.

TABLE 1. TESTING AND EXAMINATION IN STATIC SODIUM

	Accuracy	Range, Nominal	Variation
Temperature, °F	±2	900–1400	±3
Pressure	±0.5%	500–6000 psi	50 psi
Sodium analysis		ppm range	None evident
Wall thickness, in.	±0.0002	0.010	±0.0005
Diameter, in.	±0.0001	0.3	±0.001

The general layout of the loop is shown in Figure 2. The major features of the testing and examination procedures are shown in Table 2.

The sodium chemistry has remained essentially constant from the beginning of this program. Typical results of a chemical analysis of "systems quality" sodium used in loop tests are shown in Table 3.

The temperature of the loop is held within 3°F in the test sections of the loop, although radiant heat losses through the walls does cause a 20°F temperature gradient around the loop. Operation of the high-heat flux assemblies increases the temperature at the outlet of the test section about 25°F. When two tests are conducted in series, the downstream test is run at the outlet sodium temperature of the first test. No differences in temperature are encountered for specimens in parallel test sections since the inlet temperature to each section is the same. The flow rate of sodium is preset in each test section before the test on cladding is started, and is recorded during the course of testing.

The ability to heat internally and pressurize the

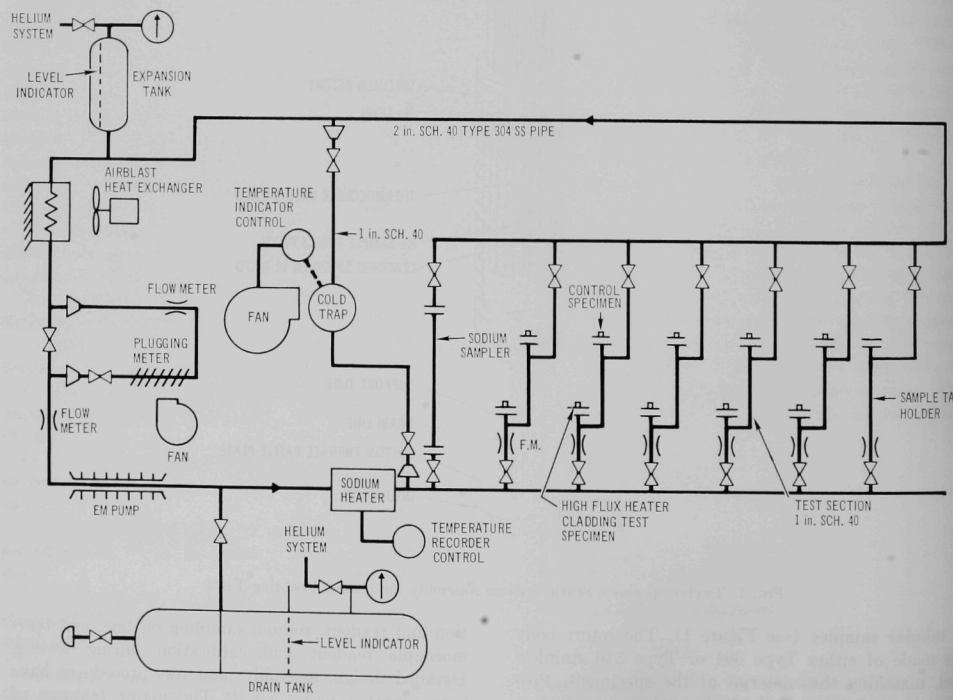

FIG. 2. Schematic of Sodium Loop for Test of High-flux Heater Assemblies.

tube samples permits simulation of the effect of heat transfer from the fuel to the coolant, and of the effect of gas pressure and fuel swelling on the cladding. To achieve this capability, it was necessary to design and develop a high-heat flux (10^6 Btu/ft^2-hr) heater to be inserted inside the cladding in such a way that the cladding could be internally pressurized. The heater life must be sufficiently long to obtain meaningful creep-rupture results. The current design of the high-flux heater assembly with cladding is shown schematically in Figure 3. The developmental work and the design features of the heater assembly are described elsewhere.[2]

The outside of the heater sheath contains two centering lobes that ensure that the graphite resistance element is concentrically located inside the cladding. High-purity NaK fills the space between the heater and cladding to provide a heat-transfer medium and to transmit pressure stresses to the cladding. Pressure from high-purity helium is transmitted to the NaK by means of a bellows diaphragm. The diaphragm can move sufficiently to compensate thermal expansion and creep strain of the cladding without a decrease in pressure.

The heater assembly with cladding is surrounded with a shroud which provides a convenient means of centering the heater assembly in the sodium test loop, increases sodium velocity, and promotes turbulence through a wire helix on the inside surface of the shroud.

The electrical power to the heaters can be cycled on and off at different frequencies. This enables the effects of thermal cycling on the creep-rupture properties to be studied.

Control test assemblies are identical to the heater assemblies, except that there is no heating element. Both geometry and hydraulic aspects are identical, and the control assemblies use NaK to pressurize the cladding.

After the heater assemblies are installed, the loop is evacuated to remove most of the oxygen and to assist in filling the loop with sodium. The sodium is then circulated at a low temperature while the sodium is cold trapped until the plugging run gives positive assurance that the plugging temperature is below 225°F. The bulk sodium temperature is brought to 1200°F and the test section flow to 20 ft/sec. The test is then started by setting the power to the heater for

TABLE 2. Testing and Examination in Dynamic Sodium

	Range	Method
Plugging temperatures	225°F	Plugging meter
Sodium sampling	See Table 3	Amalgamation; spectroscopic
Sodium temperature	Up to 1300°F	Chrome-Alumel thermocouples
Sodium flow	Up to 20 ft/sec	Magnetic
Cold trap	500°F	Circulating sodium

TABLE 3. Analysis of Dynamic Sodium

Element	Spectroscopic* (ppm by wt)	Typical Analysis (ppm by wt)
C†	12 max	10-6
Cr	5 "	<1
Fe	20 "	1
Ni	10 "	<1
O†	10 "	12-5

* ST0170NB0047
† Controlled values

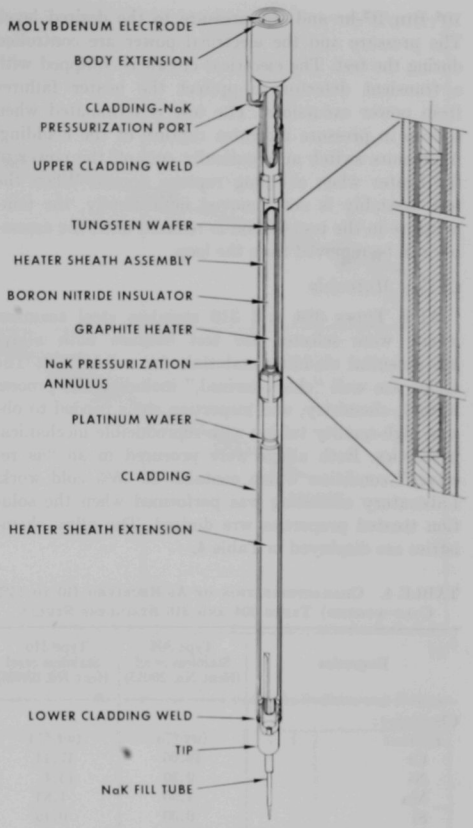

Fig. 3. High-flux Heater Assembly.

10^6 Btu/ft^2-hr and the pressure to the desired level. The pressure and the electrical power are controlled during the test. The electrical circuit is equipped with a transient detector to protect the heater failures from power excursions. The test is terminated when a drop in pressure indicates rupture of the cladding. A pressure switch automatically cuts off the power to the heater when cladding rupture occurs. When the test assembly is not removed immediately, the temperature in the test section is reduced until the assembly can be removed from the loop.

C. Test Materials

AISI Types 304 and 316 stainless steel seamless tubing were selected for test because both alloys are potential cladding materials for a LMFBR. The alloys are well "characterized," including the process history, chemistry, and inspection steps needed to obtain high-quality tubing with reproducible mechanical properties. Both alloys were procured in an "as received" condition which contains 10–15% cold work. Laboratory annealing was performed when the solution treated properties wre desired. The alloy chemistries are displayed in Table 4.

TABLE 4. Characterization of As-Received (10 to 15% Cold-worked) Types 304 and 316 Stainless Steels

Properties	Type 304 Stainless Steel (Heat No. 20013)	Type 316 Stainless Steel (Heat No. 65808)
Chemistry:		
Element	(wt %)	(wt %)
Cr	18.66	17.43
Ni	9.30	13.4
Mn	1.50	1.83
Si	0.30	0.45
Mo	0.22	2.5
Cu	0.20	0.09
C	0.06	0.012
P	0.03	0.004
S	0.03	0.002
Co	0.10	0.04
B	5 ppm	5 ppm
N_2	750 ppm	700 ppm
Room-temperature tensile properties:		
0.2% yield strength (psi)	89,000	89,000
Ultimate strength (psi)	118,000	108,000
Elongation (2-in. gage) (%)	29	35
Hardness (R_c)	23	23
Tube diameter (in.)	0.295 ± 0.001	0.295 ± 0.001
Tube wall (in.)	0.010 ± 0.0005	0.010 ± 0.0005
Grain size (ASTM)[a]	8	7
Annealing		
Temperature (°F)	1900	1950
Time (hr)	½	½
Environment	Dry H_2	Dry H_2

III. Results and Discussion

A. Sodium Effects

The early work in this program was concerned with the ability to maintain sodium purity in a static system. Zirconium foil was placed in each retort to absorb oxygen. (The getter was later found to be unnecessary.) Unfortunately, the zirconium also provided a sink for carbon. The stainless steel was decarburized during testing, which caused a substantial weakening of the alloy. Since sodium provides a convenient means of transporting carbon, care must be taken in any system design to avoid differences in carbon potential that could lead to decarburization and the associated weakening of fuel cladding.

In the static sodium without the zirconium getter, biaxial stress rupture shows no effect due to sodium when compared to similar tests performed in helium. Typical stress-rupture results in helium and in sodium are shown in Figure 4. The life under stress for biaxially stressed tubes is the same in sodium and helium for times up to 5000 hr and for temperatures between 900 and 1400°F. Thermal aging in static sodium prior to testing also had no effect on the stress-rupture life. These results show that sodium has no intrinsic effect on stress-rupture behavior over the range of LMFBR temperature conditions.

Static sodium did not influence the ductility exhibited under internal pressure. The strain at failure was the same in both environments. As can be seen in Figure 5, the stress sensitivity of the average strain rate, which is defined as the strain at failure divided by the time to failure, was identical in both static sodium and helium. Since the 2:1 biaxial stress state did not exhibit much diametral tertiary creep, the average creep rate was a fair indication of the secondary or minimum creep rate. Thus, static sodium when compared to helium does not alter strength, ductility, or creep rate of biaxially stressed thin-walled tubes of Types 304 and 316 stainless steel.

As further evidence of the absence of a static sodium effect, the microstructures after testing in sodium and helium for both uniaxial and biaxial tests were found to be identical. Cracking was intergranular and in a plane generally perpendicular to the largest stress. Carbide precipitation and sigma-phase formation also was similar in specimens from comparable tests. It should be mentioned that sodium provides an excellent medium in which to conduct tests in the absence of mass transfer since the temperature control is better than in gaseous environments.

Observations of biaxial stress rupture in flowing sodium for times up to 1000 hr correlate with those of stress rupture in static sodium. Although some evi-

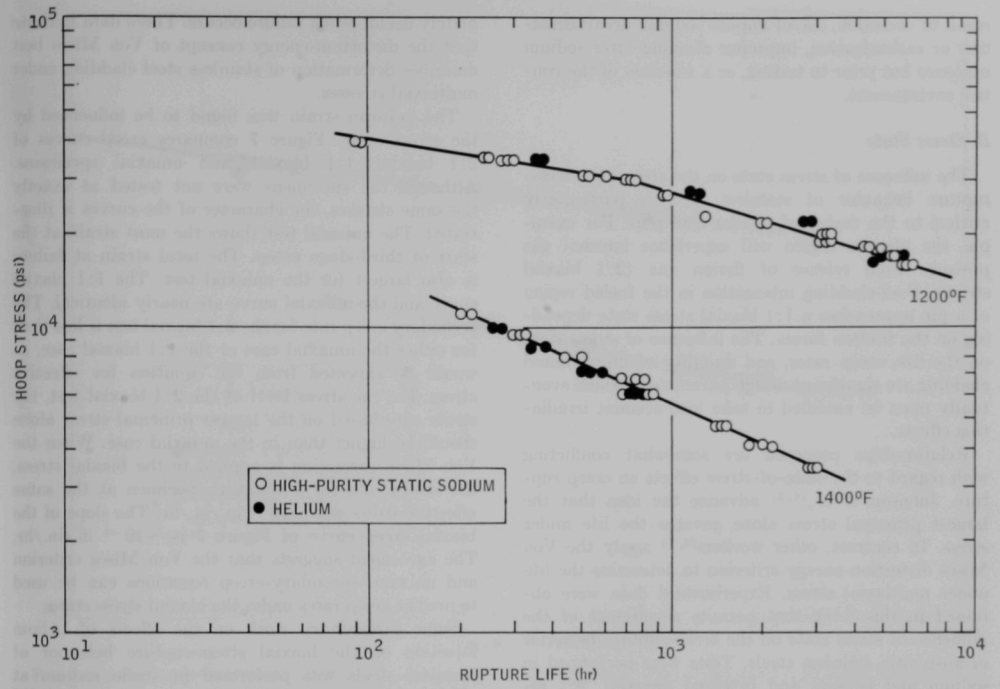

FIG. 4. Comparison of the Biaxial Stress-rupture Behavior of Cold-worked Type 304 Stainless Steel in Static Sodium and Helium.

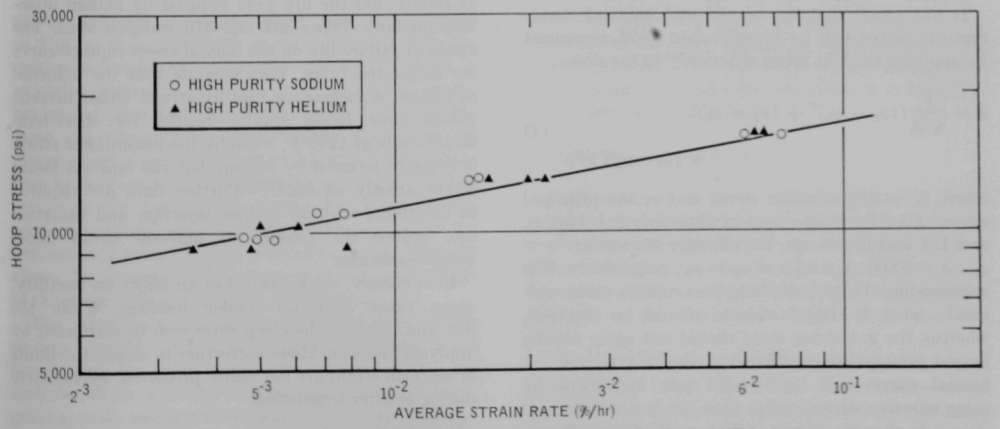

FIG. 5. Strain-rate Sensitivity to Stress of Cold-worked Type 316 Stainless Steel at 1400°F in Sodium and Helium.

dence of mass transfer was found, the amount was apparently too small to produce a detectable influence on the stress-rupture life.

Test results from this work have shown that high-purity sodium does not offer an intrinsic source of interaction that can observably influence biaxial stress rupture of stainless steel. The apparent effects, periodically reported in the literature, may be the

result of corrosion, use of impure sodium, decarburization or carburization, improper cleaning after sodium exposure but prior to testing, or a function of the control environment.

B. Stress State

The influence of stress state on the creep and stress-rupture behavior of stainless steel is particularly critical to the design of reactor fuel pins. For example, the plenum region will experience internal gas pressure from release of fission gas (2:1 biaxial stress). Fuel-cladding interaction in the fueled region of a pin approaches a 1:1 biaxial stress state depending on the friction forces. The influence of stress state on the life, creep rates, and ductility of unirradiated cladding are significant design parameters, which eventually must be modified to take into account irradiation effects.

Relationships proposed are somewhat conflicting with regard to the state-of-stress effects on creep rupture. Johnson *et al.*,[4, 5] advance the idea that the largest principal stress alone governs the life under stress. In contrast, other workers[6, 7] apply the Von Mises distortion-energy criterion to determine the life under multiaxial stress. Experimental data were obtained in this work that permits assessment of the influence of stress state on the creep-rupture behavior of austenitic stainless steels. Tests were performed in sodium and helium, and involved uniaxial, 2:1 biaxial, and 1:1 biaxial stress-rupture and creep tests.

It was found that the biaxial and uniaxial stress-rupture curves can be brought into good agreement by applying the Von Mises criterion[8] to the stress:

$$\bar{\sigma} = \frac{1}{\sqrt{2}}\left((\sigma_1 - \sigma_2)^2 + (\sigma_2 - \sigma_3)^2 + (\sigma_3 - \sigma_1)^2\right)^{1/2}, \quad (1)$$

where $\bar{\sigma}$ is the effective stress and σ, the principal stress. For the three cases of uniaxial, 2:1 biaxial, and 1:1 biaxial stresses, the effective stresses are $\bar{\sigma} = \sigma_1$, $\bar{\sigma} = 0.866\,\sigma_1$, and $\bar{\sigma} = \sigma_1 = \sigma_2$, respectively. The relationship (1) predicts that stress rupture under uniaxial and 1:1 biaxial stresses should be identical, whereas the 2:1 stress state should not agree for the largest principal stress. However, the uniaxial and 2:1 biaxial curves can be brought into agreement by using effective stress (rather than the largest principal stress) in the stress-rupture plots, as shown in Figure 6. The largest principal stress, σ_1, does not yield a correspondence in stress-rupture behavior for ductile failure. Cracks do lie in a plane perpendicular to the largest principal stress. However, the factors influencing the plastic deformation prior to rupture ultimately decide when failure occurs. These data indicate that the distortion-energy concept of Von Mises best describes deformation of stainless steel cladding under multiaxial stresses.

The uniform strain was found to be influenced by the stress state. Figure 7 compares creep curves of 2:1 biaxial, 1:1 biaxial, and uniaxial specimens. Although the specimens were not tested at exactly the same stresses, the character of the curves is illustrated. The uniaxial test shows the most strain at the start of third-stage creep. The total strain at failure is also largest for the uniaxial test. The 1:1 biaxial curve and the uniaxial curve are nearly identical. The secondary creep rate for the 2:1 biaxial test is less than for either the uniaxial case or the 1:1 biaxial case, as would be expected from the equation for effective stress. For the stress level of the 2:1 biaxial test, the strain rate based on the largest principal stress alone should be higher than in the uniaxial case. When the Von Mises correction is applied to the biaxial stress, the strain rate for a uniaxial specimen at the same effective stress was $\sim 10^{-4}$ in./in./hr. The slope of the biaxial creep curve of Figure 7 is $\sim 10^{-4}$ in./in./hr. The agreement suggests that the Von Mises criterion and uniaxial secondary-creep equations can be used to predict creep rates under the biaxial stress states.

Some preliminary work on the effects of helium injection on the biaxial stress-rupture behavior of stainless steels was performed in static sodium at 1200°F. In the case of the 2:1 stress state, the strain at failure and the life were reduced by helium injection for both Types 304 and 316 stainless steel. The strain at failure lies on the biaxial creep-rupture curve for uninjected tubes. This suggests that the influence of helium is largely on rupture strain. Other investigators have found similar results for short-term tensile tests at 1200°F, whereby the nonuniform strain is severely reduced by helium, but the uniform strain is not greatly affected.[9] Further data are required to determine whether helium injection and radiation also reduce the amount of uniform strain under creep conditions.

In summary, stress state has an effect on ductility, creep rates, and life under loading. While the life, and possibly the creep rates, can be estimated by applying the Von Mises correction to stress, the limits of uniform strain are not easily predicted, particularly during or after irradiation.

C. Alloy Type (Annealed)

This program has concentrated on a systematic comparison of the unirradiated mechanical properties of two potential fuel-cladding alloys, *viz.*, Types 304 and 316 stainless steel. A comparison of the stress-

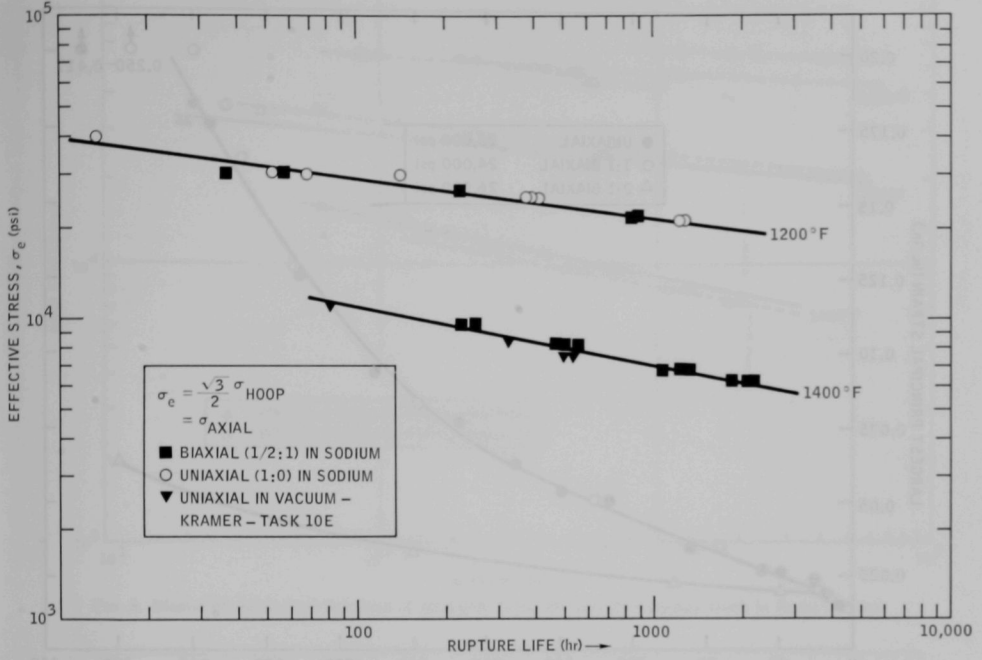

FIG. 6. Application of Von Mises' Yield Theory to Stress Rupture of Uniaxial and Biaxial Specimens of Annealed Type 304 Stainless Steel.

rupture behavior of the annealed alloys is displayed in Figures 8 and 9. Each of the two heats used for specimens represents a typical chemistry which is available commercially. The close agreement in behavior indicates that both alloys have essentially the same stress-rupture strength and ductility over the temperature range of interest to LMFBR's. An earlier heat to heat study showed that the variation in properties for the two alloys overlap.[10] Selection will certainly include other important criteria besides the unirradiated stress-rupture properties of the annealed alloys. No unusual features were observed with respect to the stress-rupture behavior of the alloys.

The microstructures of the annealed alloys after testing showed little void formation along grain boundaries. The grain boundaries were decorated with carbides. Some evidence of grain-boundary migration, grain growth, and serrations was seen. A small amount of sigma phase was present in Type 304 stainless steel, while none was found in Type 316 stainless steel.

In summary, the results of tests with annealed Type 304 and Type 316 are essentially the same, and there is very little justification for selecting one alloy over the other based on biaxial stress-rupture behavior of annealed tubing in static sodium. The good reproducibility and small scatter demonstrate an advantage of conducting the tests in a controlled environment such as sodium.

D. Alloy Type and Cold Work

Another aspect of alloy selection deals with effects of process history. The two alloys were initially obtained from the same vendor in a cold-worked condition (10–15% reduction on the last drawing pass). It is informative to compare the cold-worked material behavior to the annealed behavior of each of the alloys.

Figure 10 illustrates the effects of cold work on the stress-rupture behavior of Type 304 stainless steel. The stress-rupture curves show that the strengthening effect of cold work is temporary at these temperatures. Aging without stress produced no large effect on stress-rupture behavior. It therefore appears that weakening is promoted by stress-temperature-activated recovery processes. At lower temperatures, prior

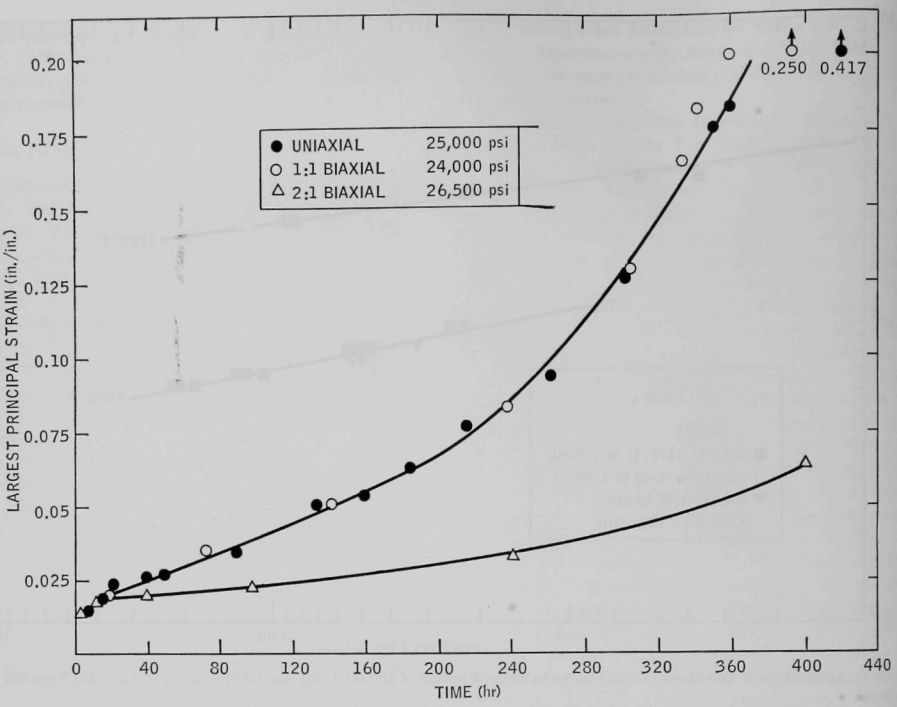

FIG. 7. Comparison of Creep Curves of Annealed Type 304 Stainless Steel under Three Stress States.

cold work persists longer, although convergence is projected for long times (>10,000 hr).

The behavior of cold-worked Type 316 stainless steel relative to the annealed state parallels that for Type 304. However, important differences exists, as may be seen by comparison of Figures 10 and 11. The strengthening benefits of cold work are retained longer for Type 316 alloy than for the Type 304 stainless steel at the same temperature. These observations indicate that the recovery processes are slower at the same temperature and stress in Type 316 than in Type 304 stainless steel. The recrystallization temperature to recover 50% of the annealed properties has been reported to be 100°F higher for Type 316 than for Type 304 stainless steel.[11]

The effect of cold work on the strain at failure is displayed in Figure 12. Clearly, the strain at failure as a function of time to failure is different for the two alloys at 1400°F. The convergence seen for Type 304 stainless steel has been seen by the British in a Type 316 steel at longer times and lower temperatures.[12] Thus, the ductility in a cold-worked alloy passes through a minimum with strain rate or time to rupture. The position of the minimum is not evident for Type 316 stainless steel because it occurs at times longer than tested thus far.

Microstructures of cold-worked samples of Types 304 and 316 exhibit similarity with respect to grain-boundary voiding; in both alloys, more grain-boundary voids have formed in cold-worked material than in the annealed counterparts. A large amount of sigma phase formed during testing of the cold-worked Type 316 stainless steel; little was found in the cold-worked Type 304 alloy.

To complete the comparison, the stress-rupture behavior of Types 304 and 316 stainless steel in the 10–15% cold-worked condition are presented in Figure 13. It is interesting that while the annealed behaviors were almost identical, the behavior of cold-worked tubes was not. Here Type 316 stainless steel was stronger at high temperatures near ~1400°F and weaker at ~1000°F than the Type 304 alloy. In any case, the two alloys studied are not identical in biaxial stress rupture in the as-received condition.

The amount of cold work introduced into cladding influences the stress-rupture behavior for uniaxially

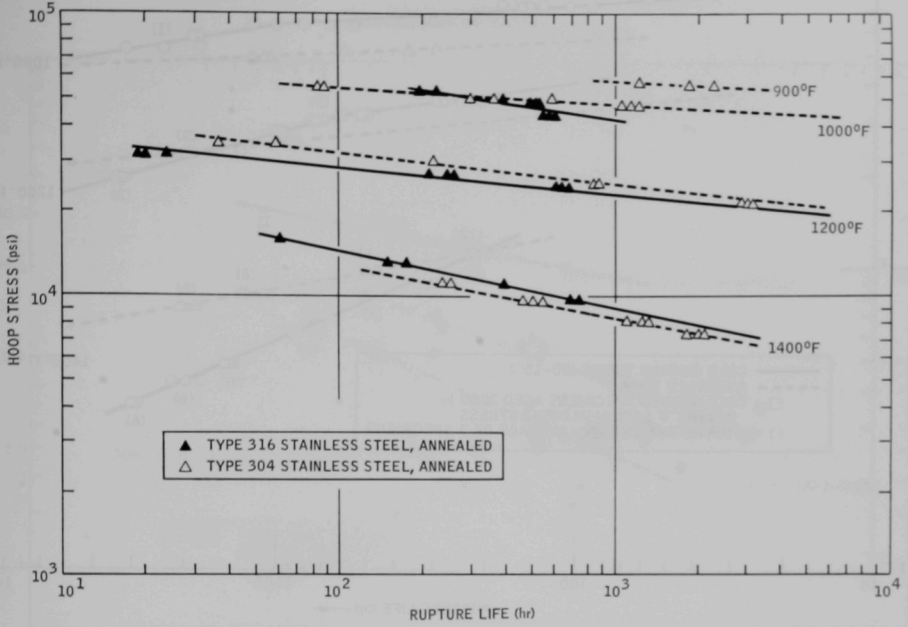

FIG. 8. Biaxial Stress-rupture Behavior of Annealed Types 304 and 316 Stainless Steels in Static Sodium.

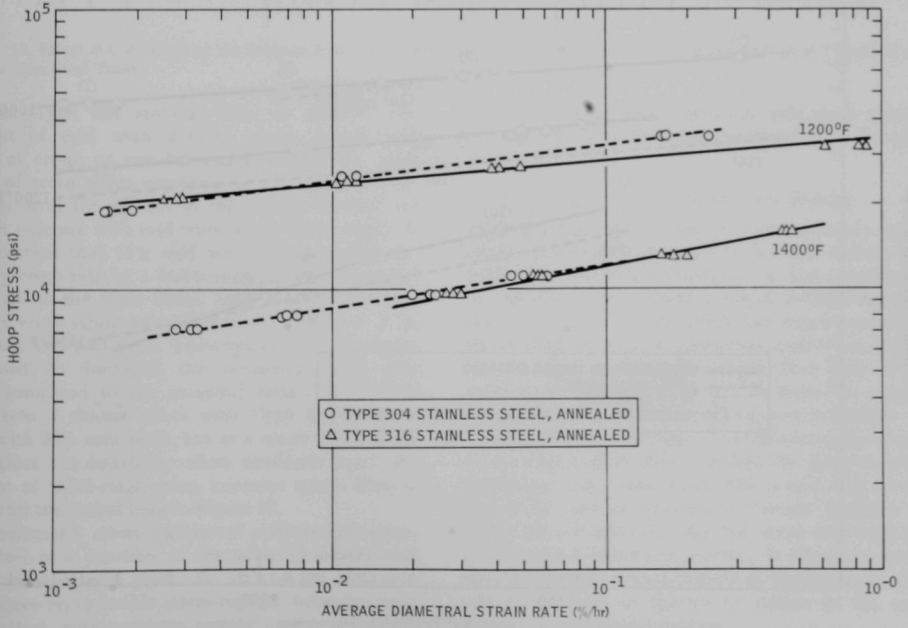

FIG. 9. Strain-rate Sensitivity to Biaxial Stresses of Annealed Types 304 and 316 Stainless Steels in Static Sodium.

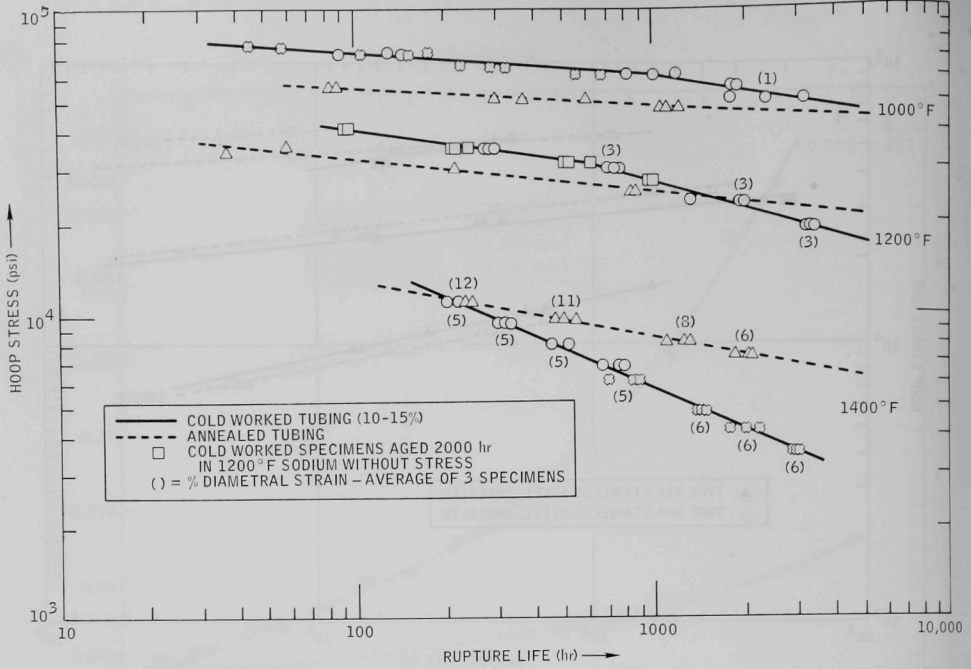

FIG. 10. Effect of 10–15% Cold Work on the Biaxial Stress-rupture Behavior of Type 304 Stainless Steel in Static Sodium.

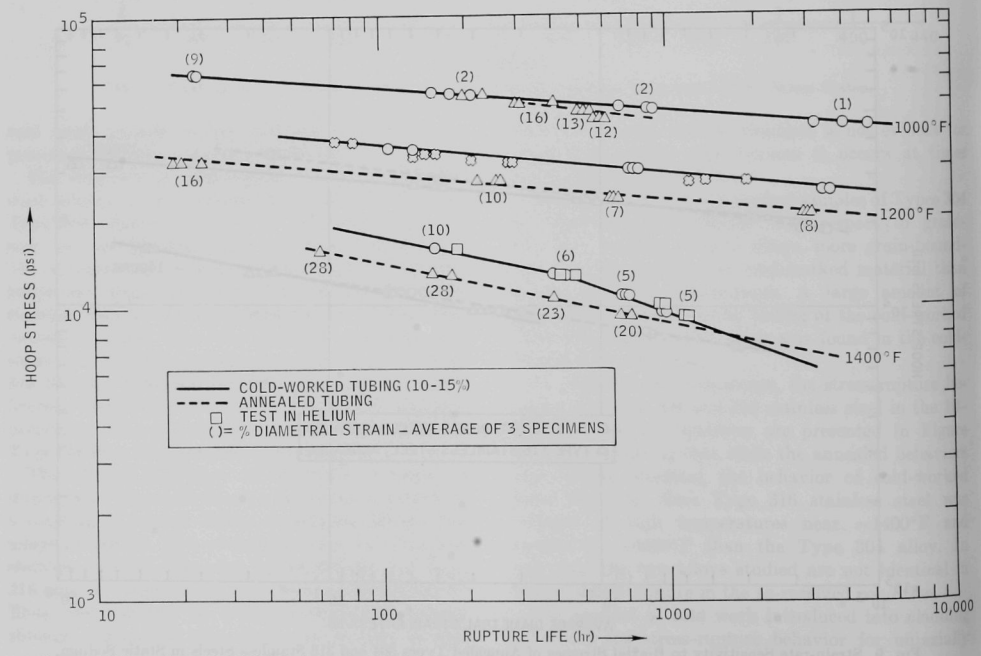

FIG. 11. Effect of 10–15% Cold Work on the Biaxial Stress-rupture Behavior of Type 316 Stainless Steel in Static Sodium.

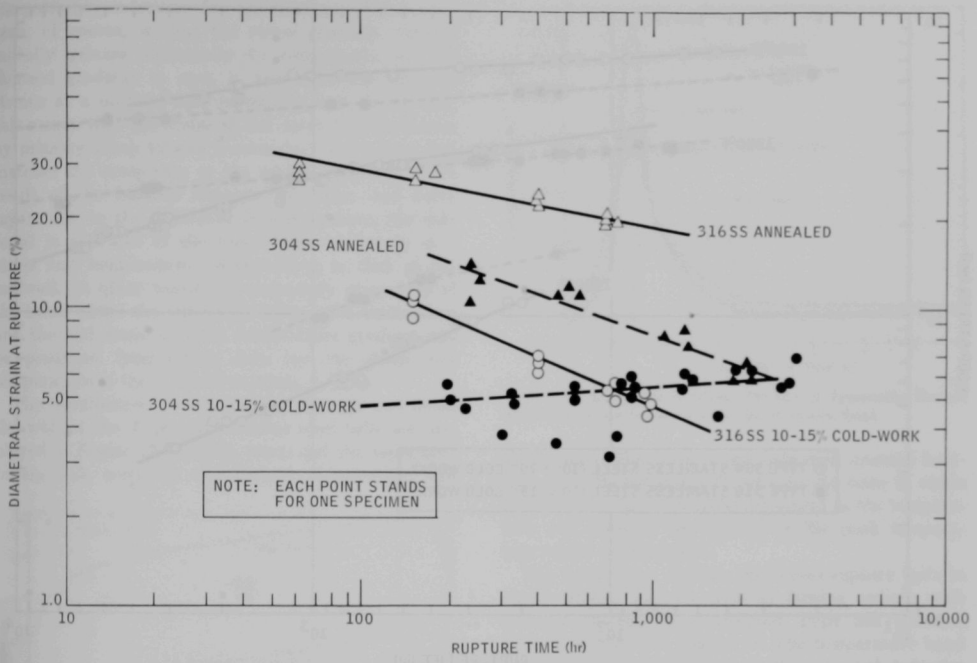

FIG. 12. Effect of Cold Work on the Rupture Strain as a Function of Time to Rupture in 1400°F Static Sodium of Types 304 and 316 Stainless Steel Tubes.

stressed Type 304 stainless steel in sodium. The amount of cold work governs strain during each stage of creep, as can be seen in Figure 14. Each stage of creep strain decreases as the cold work increases, with the amount of third stage showing the largest decrease with cold work of the three stages. It is important that 11% cold work decreased the secondary creep rate by a factor of $\frac{1}{20}$ that of annealed material at the same stress level, whereas the secondary creep strain was reduced by a factor of 2. In contrast, 38% cold work, depending on the stress level, increased or decreased the secondary creep rate when compared to the annealed rates. The British have seen a similar effect with Type 316 stainless steel with 20% cold work, but at a much lower strain rate. Once the instability effect manifests itself, the amount of third-stage creep increases again. This is shown by the dotted lines in Figure 14.

In summary, stress rupture of cold-worked stainless steel is a function of the alloy chemistry and the amount of cold work. As little as 10–15% cold work gave reproducible stress-rupture behavior from test to test, with no more scatter in the data than for the annealed state. Moreover, cold work reduces the ductility and the stress sensitivity of the secondary creep rate.

E. Stress Rupture under Steady-state Heating

The purpose of the tests of both internally pressurized and heated specimens in dynamic sodium was to simulate conditions anticipated in fast reactors for fuel cladding. As a direct result of internal heating, thermal stresses are generated and superimposed on the mechanical stresses, interstitials migrate inside the material, and mass transfer occurs. It is vital to the designer of fuel pins to be able to assess the magnitude of these effects both separately and in concert.

The mechanical stresses were calculated by means of the thin-wall-cylinder formula for internal pressurization. Tests were made with a heat flux of 10^6 Btu/ft^2-hr and an associated thermal gradient of 50°F; the corresponding thermal stress was 8300 psi at the peak temperature position. It should be noted that the thermal stress is tensile at the outside surface and compressive at the inside surface of the tube with no internal pressurization.

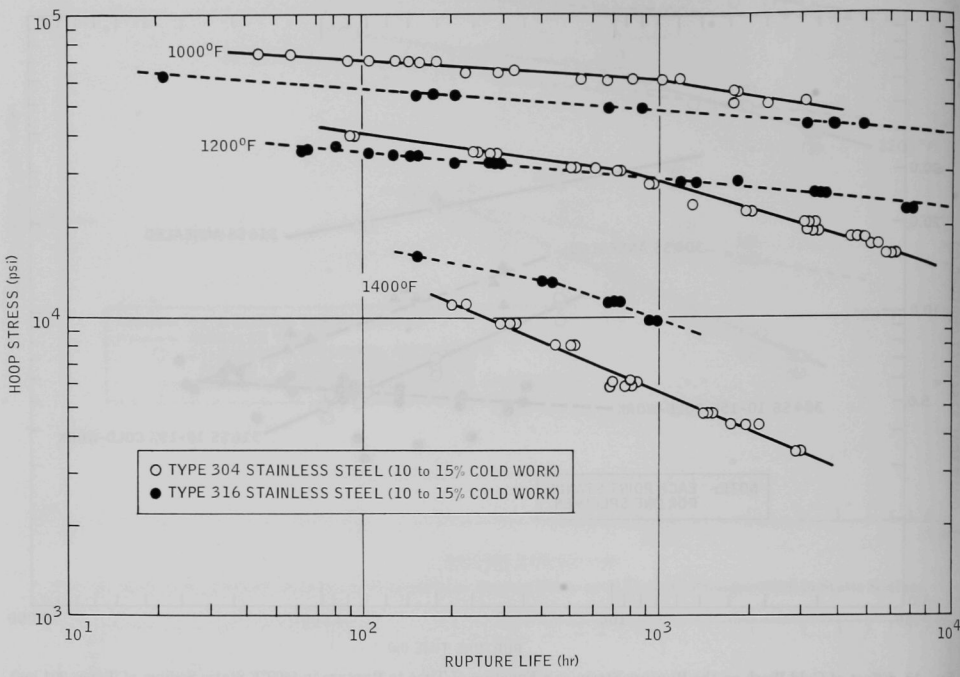

FIG. 13. Comparison of the Biaxial Stress-rupture Behavior of Cold-worked Tubes of Types 304 and 316 Stainless Steel in Static Sodium.

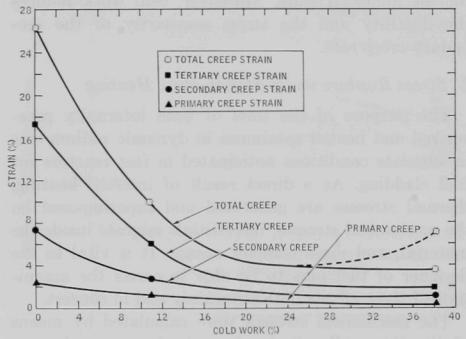

FIG. 14. Effect of the Amount of Cold Work on the Strain in Three Stages of Uniaxial Creep in Sodium at 1200°F.

For creep under combined mechanical and thermal stresses, it is to be expected that the thermal stresses will disappear due to stress relaxation. The amount of stress relaxation at the outer fiber due to secondary creep can be estimated from the creep equation. However, this estimate is too low because the initial loading from internal pressure and from the heat flux through the wall will produce a certain amount of primary creep. Since the strain associated with the creation of thermal stresses is small, $\epsilon_t \cong 10^{-5}$, almost all of the thermal stress is removed by deformation on loading. This gives rise to nonuniform straining across the wall of the tube. It is this strain gradient that plays a crucial role in the behavior of the thermally cycled specimens. This point will be discussed later. For the steady-state heating what is important is that the thermal stress is relaxed; creep then occurs under the combined action of the mechanical hoop stress generated by the internal pressurization and of the temperature gradient through the wall.

The influence of the temperature gradient complicates the creep behavior of the tubes. The hotter material on the inside layers of the wall should creep faster than the cooler surrounding material in the outer layers, providing these are stressed identically. From a standpoint of plasticity, this violates the

compatibility relations for plastic flow. What happens, of course, is that the stress gradient induced initially relaxes sufficiently to compensate for the thermal gradient in such a way that the material strains at a uniform rate across the wall. In essence, this means that the stress at the outer fiber decreases by primary creep to give a secondary creep rate that matches the creep rate at the midwall position. As a result of the balance between the inner and outer layers due to the difference in temperature, the material in the wall of the tube creeps uniformly at a stress and temperature corresponding to that at the midwall. In other words, the secondary creep rate of the tubes under the combined action of a mechanical and thermal stress and the temperature gradient can be predicted from creep data for the stress and temperature at the midwall position.

The distribution of temperature through and along the wall of the Type 304 stainless steel tube are displayed in Figure 15. Clearly, creep and the associated failure will occur at the highest temperature and

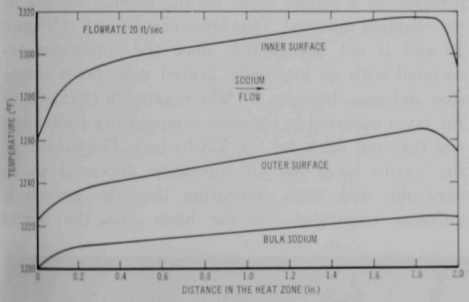

FIG. 15. Temperature Profiles in the Heat Zone along Cladding and under a Heat Flux of 10^6 Btu/ft^2-hr.

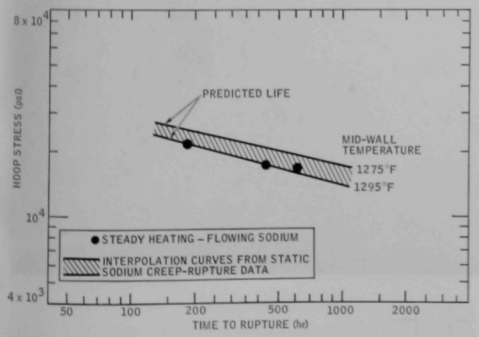

FIG. 16. Predicted Life *vs* Actual Life of Cold-worked Type 304 Stainless Steel Tubes under Constant Heating and Pressure in Flowing Sodium.

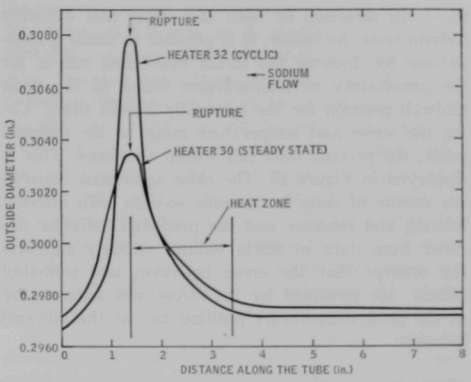

FIG. 17. Longitudinal Strain Profiles of Internally Heated and Pressurized Tubes of Type 304 Stainless Steel.

stress point. Therefore, if the tests with internal heating are to be compared directly to the tests in static sodium, then they should be compared at the temperature and stress at the midwall in the peak temperature region (peak strain).

The comparison between the stress-rupture tests in static sodium and the tests in flowing sodium with internal heating on as-received Type 304 stainless steel is displayed in Figure 16. The temperature band represents the uncertainty in the expected behavior based on data obtained in static sodium and was drawn by interpolating the static-sodium data for the limits of uncertainty in the peak midwall temperature of the internally heated tubes. On the basis of this interpolation, it appears that the behavior of the tubes under internal heating and pressure can be predicted from isothermal stress-rupture data for the peak conditions of temperature and stress described above. Thus, while the presence of a high heat flux complicates the interpretation of the behavior, in the last analysis creep is, under a steady-state thermal gradient, primarily a function of applied stress and temperature. If these two factors are known with some certainty, the behavior can be accurately predicted directly from isothermal-test data.

The strain profiles of tube tests with internal heating essentially follow the temperature profiles along the wall of the tube. This is illustrated in Figure 17. The failure occurred in the peak strain position, which is also the peak temperature position. This observation conforms with what is to be expected for creep deformation under a steady-state heating condition in flowing sodium.

It is instructive to compare the average strain rate (strain at falure divided by the time to failure) for

the hoop direction in both the static and dynamic sodium tests. As before, it is possible to make a comparison by drawing the strain rate-stress curves for the uncertainty in temperatures found at the peak midwall position for the internally heated tubes. Using the stress and temperature range at the midwall point, the present tests fall within the band. This is displayed in Figure 18. The close agreement between the results of tests in dynamic sodium with internal heating and pressure and the predicted behavior derived from data in static sodium strongly supports the concept that the creep behavior, and probably failure, are governed by the stress and temperature at the peak temperature position and at the midwall location.

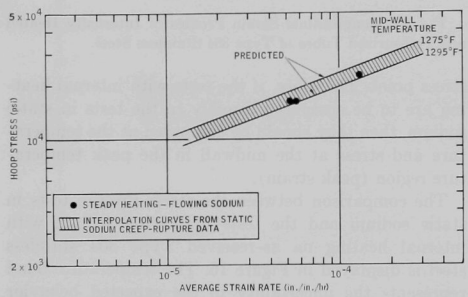

FIG. 18. Predicted *vs* Actual Strain-rate Sensitivity to Stress of Cold-worked Type 304 Stainless Steel under Constant Heating and Pressure in Flowing Sodium.

The microstructures of 10–15% cold-worked specimens tested with internal pressure in static sodium and the specimens tested with internal heating and pressure in dynamic sodium are essentially the same. The microstructures of the steady internally heated specimens are shown in Figure 19. In summary, the microstructures from both static and dynamic sodium exhibited:

1) intergranular failure,
2) void formation throughout the wall,
3) little or no sigma phase, and
4) carbide precipitate at the grain boundaries.

These observations are a further confirmation that internal heating does not radically change the behavior mechanically or metallurgically from that anticipated from isothermal tests. In addition, migration of interstitials under a temperature gradient is either absent or too small to be observed in the limited time of these tests.

One important observation concerning the microstructure of the steadily heated specimens was the presence of a ferrite layer on the outside surface of the cladding material. This layer can be seen in Figure 19 and is not unexpected, since the conditions associated with an internally heated tube favor corrosion and mass transfer.[13] The maximum thickness of the layer occurred in the peak temperature region and was 0.43 mil thick for the 558-hr test. The growth of the ferrite layer for all specimens appeared to be parabolic with time, indicating that the growth is diffusion controlled. On the basis that the ferrite

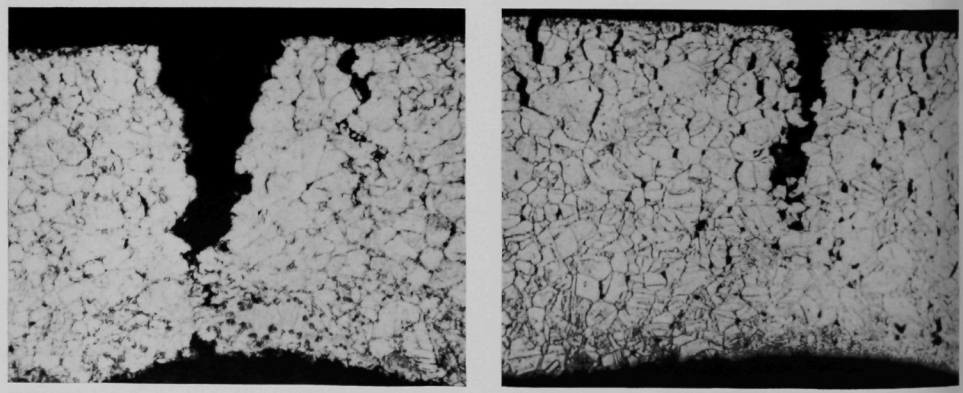

FIG. 19. Microstructures in the Rupture Area for Cyclic and Steady-state Heating at the Same Heat Flux.

layer does not contribute directly to the load-carrying capacity of the tube, it is possible to estimate the ferrite layer should reduce by 4% the stress-rupture life. This is too small to be seen in the comparison to the static sodium tests.

On the surface of the internally heated tubes, a polished zone was observed in the region of the heating element. This polished zone is undoubtedly associated with the removal of surface layer by corrosion. However, even for the longest testing time under the steady heat flux, the amount of surface removal was too small to be detected by measurements of the wall thickness. In fact, the extent of surface removal (polishing) was too small to even remove all of the surface scratches introduced in the mill cleaning treatment. Therefore, as was the case for ferrite-layer growth, the effect of surface removal was not observable in the stress-rupture behavior of the tubes tested under a steady heat flux. This does not mean that either surface removal of metal or growth of ferrite layers are not problems as far as the prediction of the long-term behavior of pressurized tubes with internal heating.

In summary, the stress-rupture behavior of tubes of Type 304 stainless steel under a steady internal heat flux of 10^6 Btu/ft^2-hr and with a high internal pressure parallels the same behavior of the same material under an internal pressure in static sodium for the appropriate temperature. In addition, the average strain rate of the heated tubes agreed with that predicted from tests in static sodium for the peak midwall temperature. The similarity in microstructures and cracking morphology coupled with the above indicates that the creep-rupture behavior can be accurately predicted directly from isothermal stress-rupture tests in static sodium when corrosion effects are small.

F. Stress Rupture under Cyclic Heating

The main goal of the stress-rupture tests in which tubes of as-received Type 304 stainless steel are pressurized and exposed to a cyclic heating is to simulate the variation in heat flux through the wall of the fuel cladding as a result of load variations to the reactor. In these tests, the heat flux is cycled off and on. This is the only difference between these and the steady-state tests. Therefore, it is useful to compare some of the observations of these tests with those of the steadily heated tests.

The strain profiles obtained for the tests under a cyclic heat flux exhibited some important differences when compared to those under steady heating. The strain at the peak temperature was 50% greater for the cyclic tests than for the steady heating tests. Also, the strain profile was much sharper for the cyclic heat-flux condition, indicating that deformation was more localized under these test conditions. This comparison is illustrated in Figure 15. It should be pointed out that the profiles for all the cyclic tests were almost identical in size and shape. It is highly likely that the observed plastic deformation occurred during the "heat on" portion of cycle, because both the temperature and the stress was larger during this time. This point will be discussed later. What is important here is that operating the internal heater in a cyclic mode brings about an accelerated rate of deformation above that obtained under steady heating.

The appearance of the microstructure and the cracking were different for the thermally cycled specimens in contrast to the steadily heated specimens. This can be seen by comparing the microstructures in Figure 19. For the cyclic heat-flux condition, the amount of void formation in grain boundaries is essentially limited to the region surrounding the failure in the tube. On the other hand, voids were present throughout the cross section of the steadily heated tubes. This perhaps means that most of the deformation took place in the region where the cracks were nucleated for the cycled specimens. The absence of extensive void formation except in the rupture area indicates that thermal cycling brings into play different deformation mechanisms than for steady conditions or isothermal tests in static sodium.

The thermally cycled and the steadily heated specimens did show some expected similarities. All failures occurred at the peak temperature position along the cladding. In the case of multiple ruptures, all cracks were at the same peak position but at different locations around the tube. The appearance of the microstructures, except for void formation, was the same for both the cyclic and the steady tests. There were:

1) carbides at the grain boundaries,
2) little or no sigma phase present,
3) slight evidence of recrystallization at the inner surface, and
4) a thin ferrite layer present on the outside surface. The ferrite layer was thinner for the cyclic specimens than for the steadily heated specimen which ran 500 hr. This is to be expected because the time at temperature is important in the growth of the ferrite layer in addition to the internal heating.

It is possible to make a direct comparison between the stress-rupture life under cyclic heating and that under steady-state heating. However, the results of steady-state tests compared directly with the data obtained in static sodium. Therefore, because the amount of data for the steady state is limited, it is

more fruitful to compare the cyclic tests with the static sodium tests.

An approach to the analysis of cyclic thermally stressed tubes under biaxial tension is that creep rate is a known function of stress and temperature. We may assume the average creep rate obeys a law of the form[14]

$$\dot{\bar{\epsilon}} = A\sigma^{n} \exp\,(\mathrm{kn}\ T/100), \qquad (2)$$

where $\dot{\bar{\epsilon}}$ is the average creep rate, A a material constant, n a stress parameter equal to 3, kn a temperature parameter equal to 0.9, and T an average temperature in °F. The specimen spends half its life at ΔT and $\Delta\sigma$ above some average condition and $-\Delta T$ and $-\Delta\sigma$ below; then the net creep rate is given by

$$\dot{\bar{\epsilon}} = \dot{\bar{\epsilon}}_0 \left\{ \left[1 + \frac{n(n-1)}{2} \left(\frac{\Delta\sigma}{\sigma} \right)^2 \right] \cosh \left(\frac{kn\Delta T}{100} \right) + \left(\frac{n\Delta\sigma}{\sigma} \right) \sinh \left(\frac{kn\Delta T}{100} \right) \right\}, \qquad (3)$$

where $\dot{\bar{\epsilon}}_0$ is the creep rate at the average temperature and stress. The parameters for this equation were derived from data obtained in static sodium. On the basis of the calculated temperature distribution and the secondary creep parameters in static sodium, the stress-rupture life of a cycled specimen can be estimated. This estimate is shown in Figure 20, in which a predicted life may be compared with the observed life. The difference between theory and experiment points out the danger in indiscriminate use of creep equations to predict fuel-cladding performance under reactor load cycling.

An increase in the cycle rate did reduce the life of the specimen a small amount. However, the life was not decreased by as much as the frequency was increased. If there were no cycling frequency effect, the tubes cycled at a higher rate would have had six times the number of cycles. This is not the case. Thus, the attendant rate of deformation has more to do with the time to failure than the number of cycles per hour. This observation is important because if thermal fatigue were operative, the frequency would be a large factor in the life of the specimen.[15]

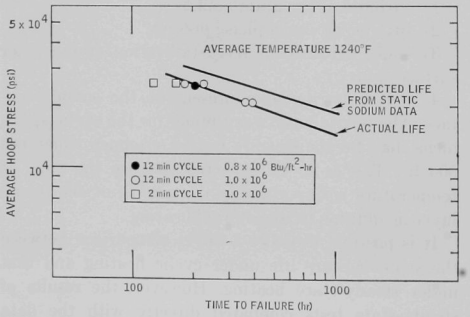

FIG. 20. Predicted Life *vs* Actual Life for Stress Rupture of Cold-worked Type 304 Stainless Steel Tubes under Cyclic Heating and Constant Pressure in Flowing Sodium.

If creep is operative, then the stress-rupture life should reflect the stress and temperature sensitivity of primary and secondary creep. As can be seen in Figure 20, the effect of a reduction in the internal pressure (hoop stress) is roughly parallel to the predicted behavior. This parallel slope is suggestive that creep is primarily responsible for failure and the deformation preceding it.

The tests under cyclic heating, in which the heater is turned off and on every 12 min, was performed at a lower heat flux (8×10^5 Btu/ft²-hr). This choice was based on the design prediction that the FTR will have a linear power rating of 18 kW/ft, whereas the previous tests with a cyclic heat flux of 10^6 Btu/ft²-hr correspond to a linear power rating of 23 kW/ft over the 2-in. heat zone. In addition, it is important to obtain some knowledge of the effects of heat flux on the stress-rupture behavior under cyclic heating.

The stress-rupture life under the lower heat-flux condition, compared to that at the higher condition, is displayed in Figure 7. The behavior at a lower heat flux is essentially that expected as a result of the lower thermal stress caused by the 20% reduction in the thermal gradient. Since the reduction in the total stress was small, the life of the cladding at a lower heat flux is not significantly different from that at a heat flux of 10^6 Btu/ft²-hr.

The enhancement of creep by a ratcheting mechanism is a possible mechanism by which the present observation on the cycled tubes can be explained. During the "on" portion of the heat cycle, the induced thermal stress relaxes by primary creep. This gives rises to a strain gradient in the wall of the tube. During the "off" portion of the heat cycle, only the mechanical stress due to internal pressure and the residual stresses created by the strain gradient are present. The strain-induced stresses are opposite to the thermal stresses created by internal heating. Thus, during the "off" half-cycle, the nonuniform stresses again relax by primary creep. Because of the lower average temperature during the off period, the extent of creep is less than during the on period. For the present tests, the relaxation is complete during the "on" period, but may not be complete during the off period. As a result, in the next heat cycle less thermal stress can be generated because the strain is present which reduces the stress. After a few cycles,

the extent of creep during each half-cycle is such that total strain per cycle is constant.

The mechanism described above can be extended to explain qualitatively the effects of frequency of cycling on the stress-rupture life of the internally heated specimens. In review, when the frequency was increased by a factor of 6, the strain per cycle decreased by a factor of 4. This simply reflects the influence of primary creep which is an exponential function of time. At the higher cycle rate, the period of time during which creep takes place was ⅙ that of the earlier tests. Since primary creep is nonlinear in time, proportionally more creep can occur during the one-minute half-cycle than during the six-minute half-cycle. This means that in one minute the amount of creep strain is more than ⅙ (actually ¼) that for a 6-min half-cycle. In fact, using the same creep data, it appears that the creep strain per cycle for the higher frequency is indeed one-fourth. If all the creep strain were due to secondary creep which is linear in time, then the higher cycle rate should result in one-sixth the creep strain per cycle and six times the number of cycles than for the slower cycle rate. This was not observed. In this work, the specimens experienced only 4000 cycles at the higher rate and ¼ the strain per cycle. Thus, it appears that while secondary creep may occur, most of the deformation is associated with primary creep during each cycle.

The influence of the mean pressure stress can also be explained by use of the creep equations described previously. The tests at lower mechanical pressure stress but at the same internal heat flux and cycle rate showed a longer stress-rupture life. This, undoubtedly, is a direct result of a smaller amount of primary creep during the off portion of the cycle. The decreased strain then limits the amount of creep due to increased thermal stress during the next period. The creep-rupture life under cyclic behavior paralleled that for the steadily heated specimens. The parallel behavior is perhaps a manifestation of the stress dependency of creep. Both secondary and primary creep are reported to have the same functional relation to stress.[16]

Cycling the heat flux through cladding under internal pressure increases the strain at failure and decreases the life when compared to that anticipated from isothermal secondary creep data. Stress relaxation by primary creep appears to be a more logical candidate to explain the observed behavior under cyclic heating. If this is so, then there is a definite need for biaxial creep data for these materials to account properly for the cycling effect in reactor-design efforts.

IV. Summary

The purpose of the program briefly reviewed here was to examine the non-nuclear aspects of the LMFBR environment in terms of stress-rupture and creep behavior of Types 304 and 316 stainless steel thin-walled tubing. The principal technical approach involves stress-rupture testing of stainless steel tubes in static and dynamic sodium. Tests in flowing sodium have been performed with steady-state and cyclic heat fluxes of 1.0×10^6 Btu/hr-ft^2. From these tests, it has been concluded to date that:

1) High-purity static sodium does not intrinsically influence biaxial stress-rupture behavior.

2) The stress-state effects on stress rupture are best compensated for by use of the Von Mises' effective stress relation.

3) The stress-rupture behavior of the two stainless steels is essentially the same in the annealed condition.

4) The strengthening benefits of cold work are definitely more permanent in Type 316 than in Type 304 stainless steel.

5) Cold work produces a minimum in the ductility as a function of strain rate or time to rupture, and the position of the minimum is at a lower strain rate or longer times in Type 316 stainless steel than for Type 304 stainless steel at the same temperature.

6) The amount of cold work has a large effect on uniaxial creep behavior, with tertiary creep showing the largest sensitivity to percent cold work.

7) Static sodium is an excellent environment in which to conduct biaxial stress-rupture tests because the environmental control gives reproducible results with little scatter.

8) The stress-rupture behavior of tubes of Type 304 stainless steel in flowing sodium under a steady heat flux of 1×10^6 Btu/ft^2-hr correlates with the performance in static sodium for the conditions at the peak midwall position.

9) The stress-rupture life of tubes of Type 304 stainless steel in flowing sodium under a cyclic heat flux is lower than that found under a steady heat flux. This behavior does not correlate with a life prediction based on secondary creep, but appears to be related to stress-relaxation phenomena associated with primary creep.

REFERENCES

1. W. T. Lee, *Biaxial Stress-Rupture Properties of Austenitic Stainless Steels in Zirconium-Gettered Sodium*, NAA-SR-12353 (Oct 1, 1967).
2. R. L. McKisson and E. L. Babbe, *High Flux Heater Design and Development*, AI-AEC-12681 (June 1968).
3. ASTM Standards, Part 31 (May 1967), p. 453.
4. A. E. Johnson, *Complex-Stress Creep of Metals*, Metallurgical Reviews 5(20), 447–506 (1960).

5. A. E. Johnson and N. E. Frost, *Fracture Under Combined Stress Creep Conditions of a 0.5% Mo Steel*, Engineer **191,** 434–438 (1951).
6. G. H. Rowe, J. R. Stewart, and K. N. Burgess, *Capped End Thin-Wall Tube Creep-Rupture Behavior for Type 316 Stainless Steel*, Trans. ASME, J. Basic Eng. **85,** 71–86 (1963).
7. H. R. Voorhees, C. M. Sliepcevich, and J. W. Freeman, *Thick-Walled Pressure Vessels*, Ind. Eng. Chem. **48,** 872–881 (1956).
8. G. E. Dieter, *Mechanical Metallurgy*, McGraw Hill, N. Y. pp. 60–64 (1961).
9. D. Kramer, H. R. Brager, C. G. Rhodes, and A. G. Pard, *Helium Embrittlement in Type 304 Stainless Steel*, NAA-SR-12601 (Dec 5, 1967).
10. K. E. Horton, R. C. Andrews, R. C. Werner, and D. F. Atkins, *Effect of Sodium on the Metallurgical and Mechanical Properties of Candidate LMFBR Alloys*, IAEA Symposium, Vienna, Dec 1966.
11. W. Siegfried, "Investigation into the Development of Intercrystalline Fracture in Various Steels under Triaxial Stress," in *Creep and Fracture of Metals at High Temperature*, HMSO, London (1956), p. 333.
12. H. K. Richardson and R. McDowell, *Elevated Temperature Stress-Rupture Properties of M316, FV548, and Nimonic PE16 PFR-Type Tubes*, TRG Report 1482(c), (1967).
13. J. Hopenfeld and D. K. Darley, *Dynamic Mass Transfer of Stainless Steel in Sodium under a High-Heat-Flux Condition*, NAA-SR-12447.
14. I. Finnie and W. Heller, *Creep of Engineering Materials*, McGraw-Hill Book Co., Inc., New York (1956), p. 264.
15. L. F. Coffin, Jr., "The Problem of Thermal Stress Fatigue in Austenitic Steels at Elevated Temperatures," in *Symposium on Effect of Cyclic Heating and Stress of Metals*, ASTM STP No. 165, Philadelphia (1964).
16. F. Garofalo, *Fundamentals of Creep and Creep-Rupture in Metals*, Macmillan Co., New York (1966), p. 10.

Discussion

Mr. Horton (AEC): Do you feel that this ferrite layer will continue to grow according to that parabolic function?

Mr. Shively: I am concerned about it. The evidence that I have read is rather old, but may be very good. It came from General Electric in an analysis of a report by Brush, I believe. The effect of the ferrite layer apparently saturated out at about 0.5 mil, and we are anxiously awaiting results of the test we have underway now which has gone beyond the 500-hr limit. We should have a ferrite layer thicker than this, if it continues to grow. I cannot see the curve bending over; if this bend-over occurs it must do it very sharply, very quickly.

Mr. Sutton (ANL): How do you define percent cold work?

Mr. Shively: By the gross reduction in area on a drawing pass.

Mr. DeVan (Chairman): I have a discussion point which I would like to throw out to see if it will elicit any comments. It concerns mechanical properties and the interaction with irradiation, and I wonder whether anyone else has been staying up late nights thinking about it. It has to do with the problem that Ed Zebroski discussed this morning, namely, the vacancy formation that results due to displacement damage at the temperature levels of certain parts of the cladding during reactor operation. As you know, this vacancy generation does result in formation of voids, and voids result in clad swelling and in effects on mechanical properties. The manufacture by mass transfer of a rather heavy ferrite layer and some rather appreciable concentration gradients in the metal underneath that layer is likewise a vacancy-generating process. Does anyone have any comments on what happens when you add these two processes together? I have had some comment from Jim Weir at Oak Ridge; he didn't think that the vacancy generation coming from the diffusion of substitutional elements could really keep up or amount to much compared to the displacement damage. I am just curious as to whether anybody else has given the problem any thought.

At the break an individual told me that he thought the concern with carbides is fine, but he has yet to hear anybody talk about the initial ferrite content of the austenitic stainless steel as a factor, either in corrosion or in strength. The question was: what do I think about the effect of the initial ferrite content; was it an important consideration in specifying the steel? Well, I honestly couldn't answer the question. I am curious about whether anyone else has any comments on that aspect of stainless steels for sodium service. (No comment)

We can only conclude, therefore, that it is not an important variable. If no metallurgist has been concerned about it, it cannot be important. Perhaps the question really needs to be part of another question which we have asked ourselves over and over again. Of what importance is sigma-phase formation in stainless steel for sodium service, and that question, as far as I know, still doesn't have an answer.

Influence of Grain Size and Work Hardening on the Carburization of Austenitic Stainless Steels in Liquid Sodium

L. VALIBUS

Electricité de France
Chatou, France

1. Introduction

The transfer of carbon by liquid sodium from the more carburized areas to less carburized ones is a problem of great practical importance in the study of the behavior of materials of the "fast neutron" reactors.

This phenomenon may be encountered in the following cases:

- a part of a circuit carrying sodium is made of austenitic steel and the other is of ferritic steel (for instance in the case of steam generator);[1-4]
- carbide-based materials in contact with sodium in the neighborhood of austenitic steels (for instance, carbide fuel clad with austenitic steel, or graphite-based protective material with B_4C also clad by austenitic steel).

In all these cases the mechanical properties of the materials may be altered.[5, 6]

The complexity of the phenomenon does not permit a completely satisfactory presentation of a theoretical model of the carburization kinetics of austenitic stainless steel,[3] since very often the metallurgical or stress condition to which the material is subjected plays a very important part.

At the surface of a sample exposed to sodium, the equilibrium level of the carbon is a function of its activity in the liquid metal, and there exists a carbon concentration gradient between the surface and the still intact matrix.[2, 3] The increased thickness of the carburized area is determined by carbon diffusion in the sense of the decreasing activity gradient.[7] In this area, carbide precipitation tends to balance the local carbon concentration with those of the different alloy elements.[8] However, the increase of places with high free energies or of defect densities (such as grain joints, slip lines, and dislocation) favors carbon penetration by creating preferential diffusion and precipitation localities.

In order to study the influence of such parameters, samples of titanium-stabilized austenitic stainless steel AISI 316, on the one hand with different grain sizes and, on the other hand, with several strain-hardening rates, have been subjected to aging in static sodium in the presence of a carbon source.

2. Experimental Conditions

2.1. Materials and Samples

2.1.1. Chemical composition of the materials studied: The average chemical composition of the titanium-stabilized austenitic stainless steel AISI 316 that was investigated is given in Table 1. The carburization of this steel was obtained either by placing it in the presence of ferritic steel AISI 430, whose chemical analysis is also given in Table 1, or by placing it in the presence of a small cube of nuclear-quality graphite, which is an impregnated "LIMA" coke.

2.1.2. Samples with different grain sizes: Our samples were in the form of 40 × 20-mm plates. They were taken from a 15/10 thick sheet. The different grain sizes were obtained by heat treatment lasting 15 min in high vacuum, the holding temperature being varied. The test specimens were cooled by helium sweeping; the first lot was treated at 1,000°C, the second at 1,100°C, and the third at 1,200°C.

2.1.3. Samples with different strain-hardening rates: Our samples were cut out of a 6-mm sheet in accordance with the plan given in Figure 1. In order to eliminate strain due to machining, our specimens were treated at 1,100°C during 30 min in a furnace under high vacuum, then helium hardened. The various strain hardenings (see Table 2) were measured with a "MORH & FEDERAHF" hydraulic tension machine at a uniform strain speed of 1% elongation per minute. The determination of the force required was theoretically derivable from the stress-strain curve of the metal used. In practice, it was necessary to correct this curve, obtained by recording, since the latter integrates the sliding of the clamping jaws to the elongation of the test specimen. Furthermore, we have recorded the yield-strength variations from one sample to the next. Therefore, systematic measurement of this yield strength, as well as the pertinent correction, was necessary.

In the rest of our report, the specimen strain hardening will be conventionally characterized by relative elongations, measured between gage marks after straining.

TABLE 1. MEAN CHEMICAL COMPOSITION OF THE STAINLESS STEEL STUDIED

Material	Chemical Composition (w/o)									Observations
	C	Si	Mn	S	P	Ni	Cr	Mo	Ti	
AISI 316 SS Ti	0.063	0.51	1.50	0.008	0.019	12.04	17.34	2.23	0.47	Material for the study of grain size
AISI 316 SS Ti	0.05	0.59	1.70	0.020	0.024	11.44	16.92	2.44	0.48	Material for the study of work hardening
AISI 430	0.068	0.34	0.43	0.01	0.02	0.14	16.97			

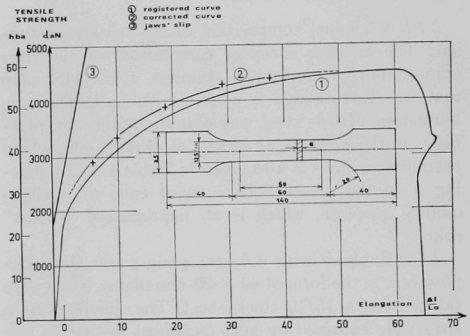

FIG. 1. Specimen and Stress-elongation Curve of AISI 316 SS Ti at Ambient Temperature.

TABLE 2. CHARACTERISTICS OF SAMPLES STUDIED BEFORE STRAIN HARDENING AND AFTERWARDS

σ: stress applied to the sample
σ_0: 0.2% yield strength
A: Relative permanent strain
H_{vi}: Vickers hardness of martempered samples (load: 30 kg)
H'_{vi}: Vickers hardness of samples after strain hardening (load: 30 kg)
H_m: Core microhardness of strain-hardened samples (load: 34.4 gr)

References	σ, kg/sq mm	σ_0, kg/sq mm	$\sigma - \sigma_0$, kg/sq mm	A, %	H_{vi}, kg/sq mm	H'_{vi}, kg/sq mm	H_m, kg/sq mm
4 D 1	0		0	0	136	136	195
4 D 2	37.5	22	15.5	5.8	138	177	201
4 D 3	43.3	21.85	21.4	10.7	136	198	210
4 D 4	49.9	20.6	29.3	18.9	134	218	219
4 D 5	54.9	21.25	33.7	28.9	136	265	242
4 D 6	57.3	21.2	36.1	37.1	138	265.5	250

2.2. Tests, Measurements, and Analyses

2.2.1. Description of carburization tests: After cleaning and weighing, the previously defined samples were placed in a test pot (diameter of 159 mm, height of 250 mm, and able to contain 2.4 liters of sodium) made of material of the same grade. A small graphite cube, 30 mm on each side, was included to maintain the carbon concentration very close to saturation. The casing was argon welded, and its sealing checked by a helium mass-spectrometer test. A filling circuit (see Figure 2) permitted introduction, under argon at 110°C, of a 2.4-l volume of nuclear-quality sodium in all the test pots. Before filling, the sodium at 110°C passed through a filter composed of 5-μ sintered stainless steel cartridge. Thus, for each test, the percentage of oxygen in the sodium was of the order of 20 ppm. The casings were then heated to 650 ± 5°C for 1,500 hr. When the desired test duration was reached, the casing was left to cool slowly down to about 200°C. The test pot was then connected to a tank and the sodium was drained by differential pressure. Each cell was then opened by a milling machine and the specimens were washed by a process that did not change the sample. The samples were weighed before being subjected to the planned measurements and analyses. For the carburization tests of samples strain-hardened in the presence of AISI 430 grade, the test pot, with 3 control samples, was made of ferritic steel.

In order to distinguish the influence of the temperature on the structural changes of the strain-hardened samples from that due to the carburization phenomenon, identical specimens were subjected to aging in an inert atmosphere (argon) at the same temperature and for the same length of time as for the static sodium tests.

2.2.2. Measurements and analyses performed on the samples after testing: After testing, we subjected all the carburized samples to gravimetric measurements, to chemical analyses for carbon by successive 0.1-mm samplings for specimens strain-hardened over a 6-mm thickness and, by global analysis, for those 15/10 mm thick, and, finally, to hardness measurements. In addition, the most representative samples were observed under an optical microscope and subjected to microhardness tests under a 34.4-g load. The latter samples were also subjected to X-ray diffraction, using the chromium Kα line under vacuum. They also were subjected to CASTAING microprobe analysis.

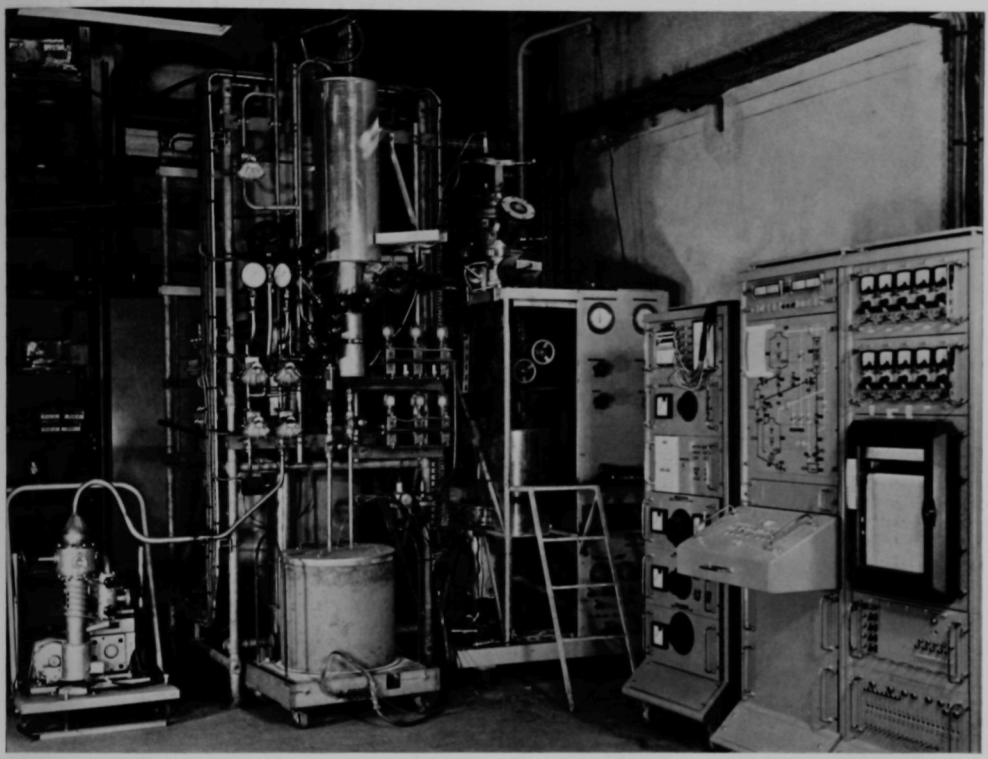

FIG. 2. Filling Circuit.

3. Influence of Grain Size on the Carburization of Austenitic Stainless Steel AISI 316 SS Ti

After holding for 1,500 hr in static liquid sodium at 650°C, we determined the grain-size indices in the core of the samples; for samples heat treated at 1000°C it was 8, for treatment at 1,100°C it was 5, and for 1,200°C it was 3 (see Figure 3). Irregular grain increase was noted, the mixed-grain structure obtained being characteristic of stabilized steel heated beyond a certain heat-treatment temperature. This phenomenon was undoubtedly connected with the dissolution of titanium carbides.[9]

We noted a weight increase of the specimens after testing. The weight and the overall carbon content, obtained by chemical analysis, both increased as a function of the grain-size index (see Figure 4). On the other hand, a slight diminution of the hardness increase occurred as a function of the same variable (see Figure 5). These results are in accord with the observations made by the optical microscope placed close to the surface (Figure 6). There was noted a widening of grain joints with very dense carbide precipitation and the existence of preferential attack areas in the neighborhood of the carbonitrides (see Figure 6d) and of the twins (see Figures 6a, 6b, 6c). The samples with grain-size indices of 5 and 3 were strongly attacked over a 10- to 20-μ surface area. The carburization evolution was followed by microhardness measurements (see Figure 7). There was noted a gradient between the surface and a depth of 300 to 400 μ for the samples with grain-size indices of 8 and 5. The sample with grain-size index 3 permitted a determination of the microhardness gradient on a grain directly in contact with the surface.

An X-ray-diffraction study enabled us to follow, parallel with the preceding study, the evolution of chromium carbide precipitation near the surface. The edges of all the specimens have shown large precipi-

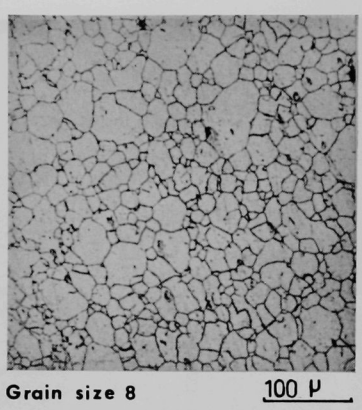

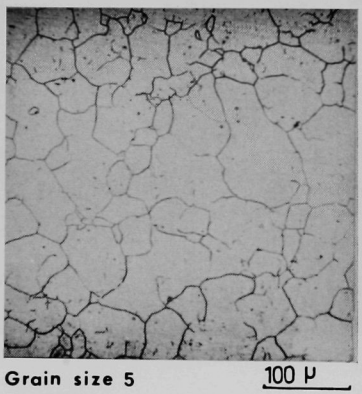

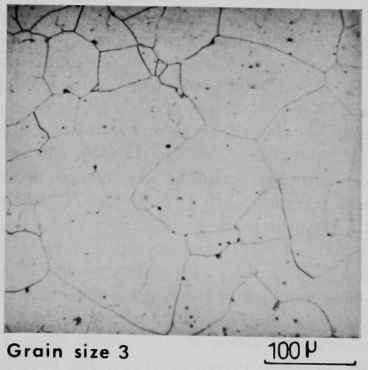

FIG. 3. Core Structures and Grain-size Indices of the Samples Studied after Aging in Liquid Sodium. (Electrolytic attack with oxalic carbon.)

tation of $M_{23}C_6$ carbides of the cubic $Cr_{23}C_6$ type. On one of the samples (that with index 8), we found two carbides with parameters $a_0 = 10.47$ Å and $a_0 = 10.56$ Å instead of 10.64 Å. This phenomenon may be explained by the greater content of iron in the carbide with the smaller parameter.[8] By means of successive polishing, we have followed the evolution of carbide precipitation from the edges of the test specimens. We noted (see Figure 8) that the depth at which the carbide precipitation (carbide peaks from background-noise pitch) was scarcely detectable was 200 μ for samples with index 8, 150 μ for samples with index 5, and 25 μ for those with index 3. For the latter, all the carbides were localized in the preferentially attacked area (see Figure 4d). This observation permits noting that the area involved in carbide precipitation is smaller than that with a microhardness gradient. It is likely therefore that carbon diffusion involves a larger metal thickness than that for which a detectable carbide formation is observed.

The electronic-probe study has enabled us to ana-

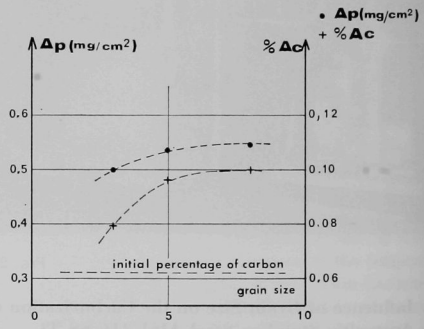

FIG. 4. Increase of Weight and of Overall Carbon Content as a Function of Grain Size.

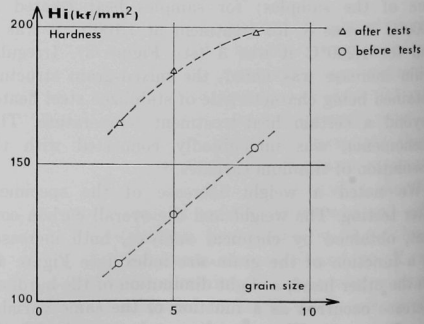

FIG. 5. Hardness Variation as a Function of Grain Size.

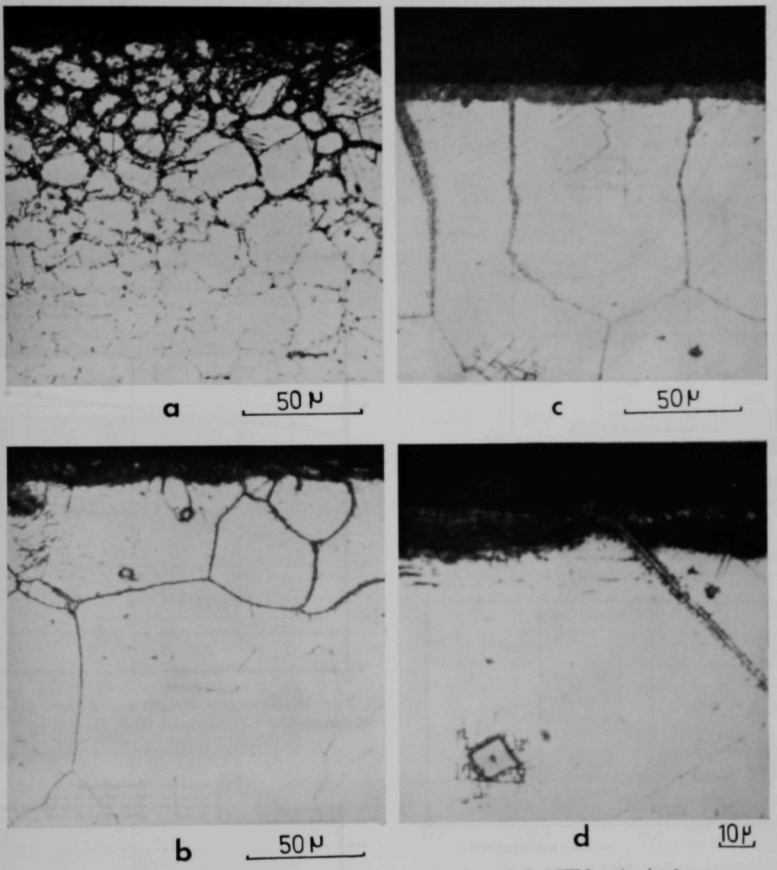

a. ASTM grain size 8
b. ASTM grain size 5
c. d. ASTM grain size 3

FIG. 6. Surface Carburization of Samples as a Function of Grain Size. (Electrolytic attack with oxalic acid.)

lyse the influence of grain size on carburization more completely and to check certain previously described observations. The analysis was made under an acceleration voltage of 10 kV with anticontamination by cold finger at −196°C and by oxygen jet.

The extent of the area enriched in free carbon or in carbides is 160 to 200 μ for index 8, is 60 to 80 μ for index 5, and is 12 to 15 μ for index 3. Carbon concentration on the edges was, respectively, 0.60, 0.65, and 0.80% for indices 8, 5, and 3. Figure 9 shows the intensity variation of the line Kα of carbon. The grain joints were enriched in carbon, but a quantitative measurement cannot be given since the thickness was less than one micron.

No marked variation of the other elements as a function of edge distance was noted. Only chromium enrichment in grain joints was observed.

4. Influence of Work Hardening on the Carburization of Austenitic Stainless Steel AISI 316 SS Ti

After holding in static liquid sodium at 650°C for 1,500 hr, we noted a weight increase.

The weight and the carbon content (obtained by chemical analysis after 1/10 mm sampling on the surface of the specimens) increased as a function of the strain hardening when graphite was the carbon source (see Figure 10). This increase was much less marked in the presence of ferritic steel AISI 430.

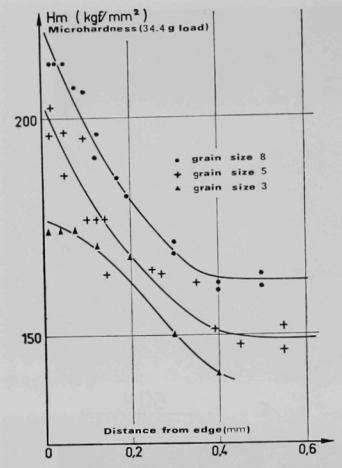

FIG. 7. Microhardness Variation with Respect to Sample Edge for Different Grain Sizes.

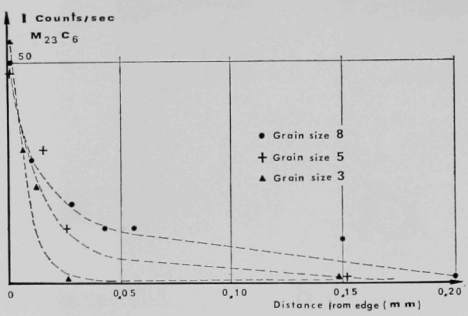

FIG. 8. Variation of $M_{23}C_6$ Content with Respect to Sample Edge for Different Grain Sizes.

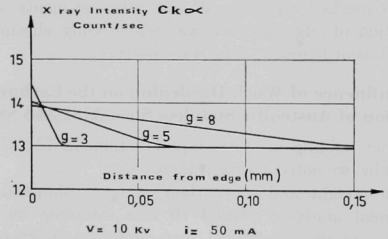

FIG. 9. Variation of the Intensity of Kα Carbon Line as a Function of the Edge Distance for Different Grain Size.

The hardness curve (see Figure 11) for the samples aged under argon lies above the control curve (for strain-hardened samples) up to a strain of approximately 25%. Beyond this, it is below the control curve. In fact, during aging at 650°C, part of the defects (mainly dislocations) created during cold strain hardening were eliminated, whence a decrease in hardness for a certain strain because of metal restoration. On the other hand, we have noted (see Figure 11) that

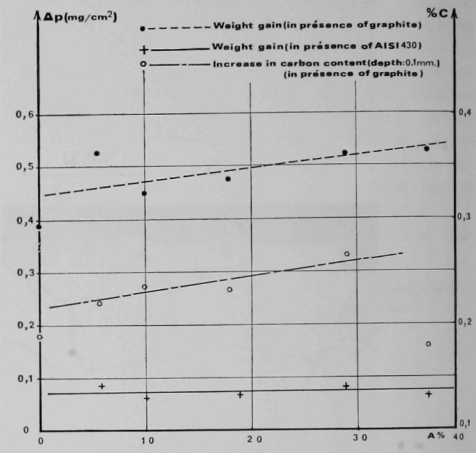

FIG. 10. Increase of Weight and of Surface Carbon Content of Samples as a Function of Work Hardening.

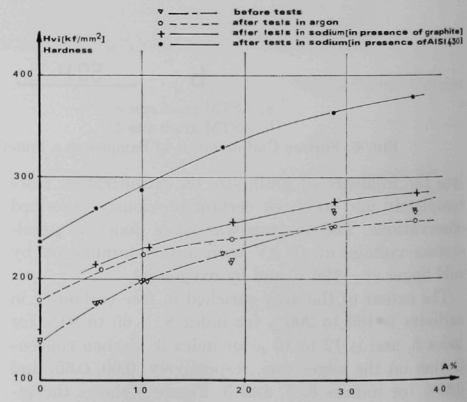

FIG. 11. Comparative Evolution of the Hardness of Control Samples, and of Samples before and after Aging in Static Sodium and Argon.

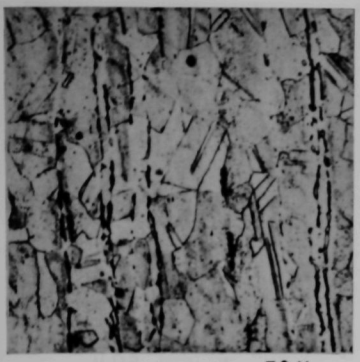

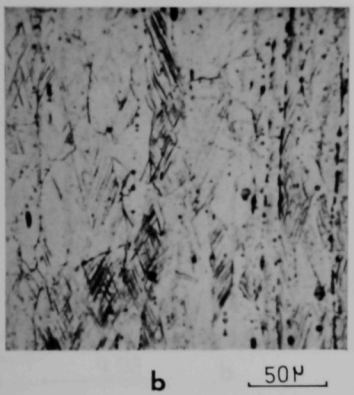

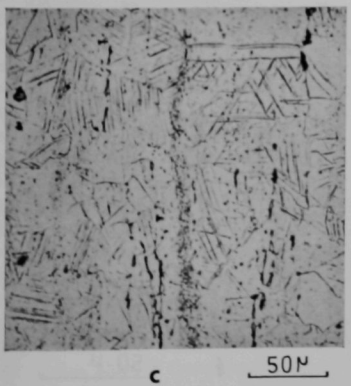

TABLE 3. Sample Hardnesses after being under Argon Atmosphere and in the Presence of Liquid Sodium as a Function of the Strain Hardening

H'_{vi} : Vickers hardness of samples after strain hardening (load: 30 kg)

H''_{vi} : Vickers hardness of samples after stay in ambient conditions (load: 30 kg)

References	A, %	Hardness	Test Conditions (1,500 hr at 650°C)		
			Argon	Static Sodium in the Presence of AISI 430	Static Sodium in the Presence of Graphite
4 D 1	0	H'_{vi}	136	136	139
		H''_{vi}	179	160	236
4 D 2	5.8	H'_{vi}	177	176	177.5
		H''_{vi}	209	214	269
4 D 3	10.7	H'_{vi}	198.5	197.5	197.5
		H''_{vi}	224	230	287
4 D 4	18.9	H'_{vi}	218	218	225.5
		H''_{vi}	239	255	329
4 D 5	28.9	H'_{vi}	265	268	250.5
		H''_{vi}	252	275	363
4 D 6	37.1	H'_{vi}	267	265	287
		H''_{vi}	257	285	379

the curves relative to carbided samples in the presence of liquid sodium are located entirely above the preceding curves. The hardness measurements of all the samples are summarized in Table 3. A very marked increase in surface hardness was observed as a function of the work hardening.

These results were confirmed by micrographic observations. The non-strain-hardened metal had a twinned-grain texture with numerous bands of precipitates due to rolling (see Figure 12a). The oxalic acid attack brings out slip lines on the strain-hardened samples. They are clearly visible beginning with 30% elongation (see Figures 12b and 12c).[10] The micrographs (see Figures 13b, 13d, and 13f) show that recrystallization after strain hardening and aging is effected without grain-size variation (samples with index 8). In fact, the critical strain hardening, for which one may observe a marked grain variation after recrystallization, is less than 5%, the smallest strain hardening that we have achieved. In the core, in the grain boundaries, and in the slip lines, one observes a coalesced sigma phase and finer pre-

Fig. 12. Control Strain-hardening Samples. Electrolytic attack with oxalic acid.

a. A = 0 longitudinal cutting
b. A = 37% longitudinal cutting
c. A = 37% transversal cutting

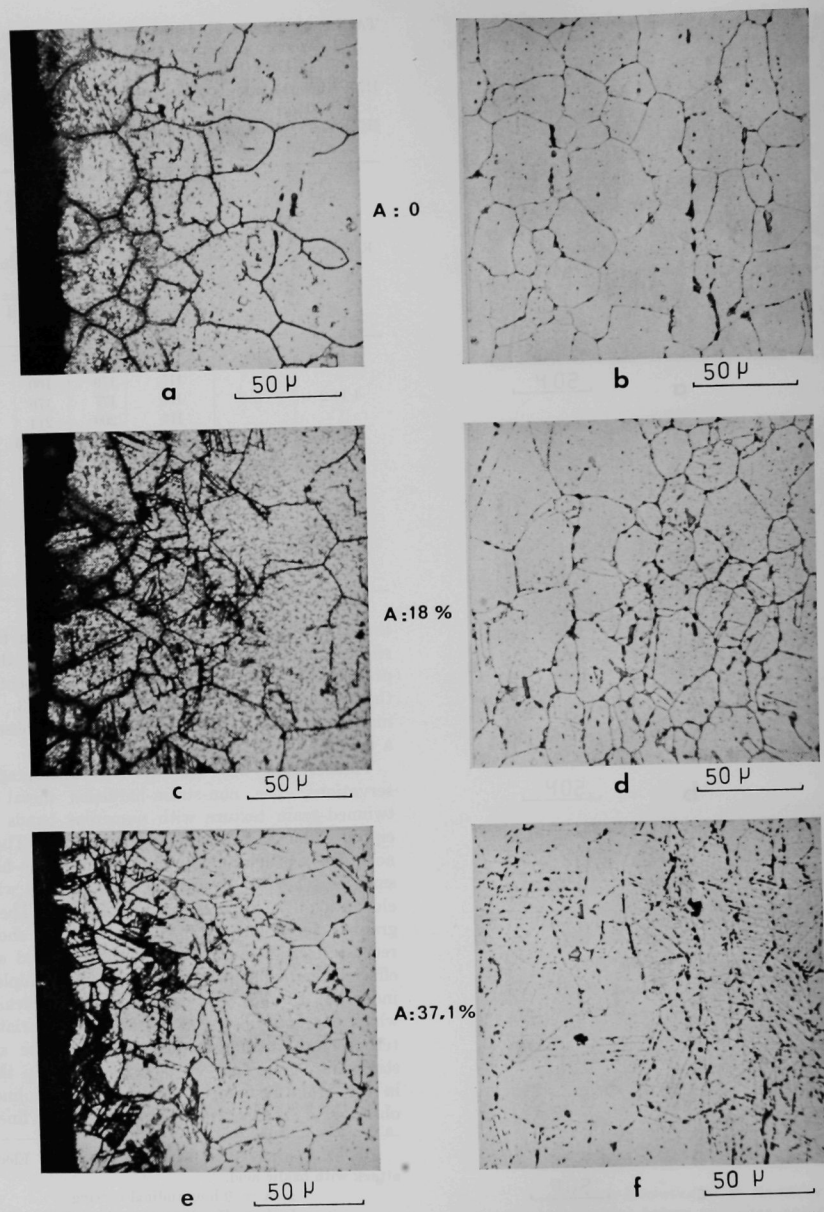

FIG. 13. Surface Carburization and Core Structure of Samples for different Work-hardening Rates: a, c, e: Surface Carburization; b, d, f: Core Structure. (Electrolytic attack with oxalic acid.)

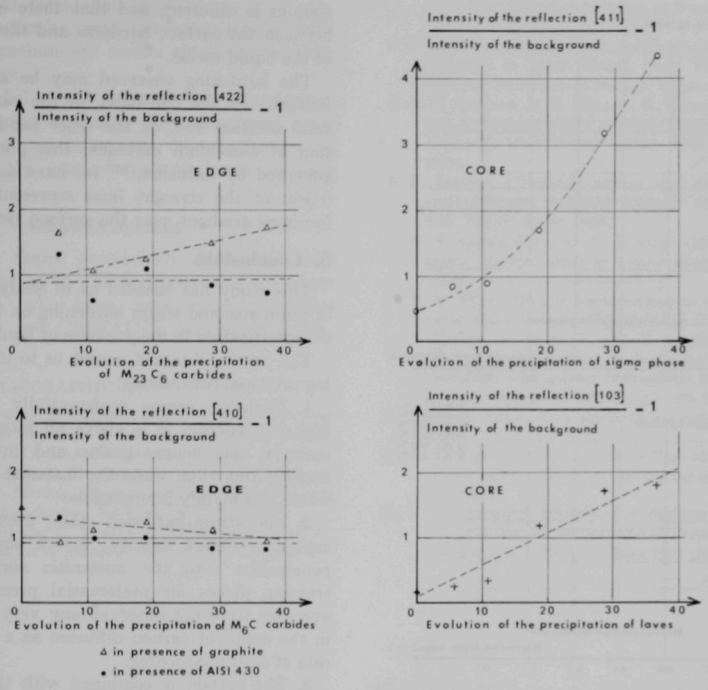

FIG. 14. Evolution of Precipitation at the Core and at the Surface of Samples as a Function of Work Hardening.

cipitates, more difficult to identify under the optical microscope.

The structure of samples aged in sodium has a region without sigma phase near the surface, and with carbide precipitation at grain boundaries and in the slip lines (see Figures 13a, 13c, and 13e). The width of this area is less for samples put in the presence of ferritic steel AISI 430 than for those in the presence of graphite.

The examination of control samples by X-ray diffraction shows that they are totally austenitic regardless of the degree of strain hardening. The possible precipitation of phase α (martensite) could not be detected by this method. On the other hand, we observe a widening of the austenite bands as a function of the strain. Radiocrystallographic examination of samples aged under argon has brought out the presence of a sigma phase in increasing quantity (see Figure 14). For a 37.1% strain, we noted a quantity of this phase 8 times greater than that relative to a non-strain-hardened specimen. We have also noted the presence of a Laves phase of the type Fe_2Mo, increasing with the strain hardening.

The core structure of specimens aged in static liquid sodium was analogous to that found with the samples described above. On the surface, we observed the presence of carbides of the type M_6C and $M_{23}C_6$ (see Figure 14). For greater strains, we noted the appearance of carbides of the type Cr_7C_3.[8] The slight decrease of intensities of the peaks of carbides M_6C and the increase of those of $M_{23}C_6$, with the appearance of those of Cr_7C_3, shows up well the increase in the quantity of carbides formed in function of the strain hardening.

The evolution of carburization has also been followed by microhardness measurements (see Figure 15). A microhardness gradient was noted near the outer surface. We have plotted, using semilogarithmic coordinates, the microhardness values as a function of the edge distance of the specimen in millimeters, in order to be able to extrapolate the values near the surface.[11] The core microhardness of the samples aged in static liquid sodium was identical for the same strain hardening to that of a sample aged under

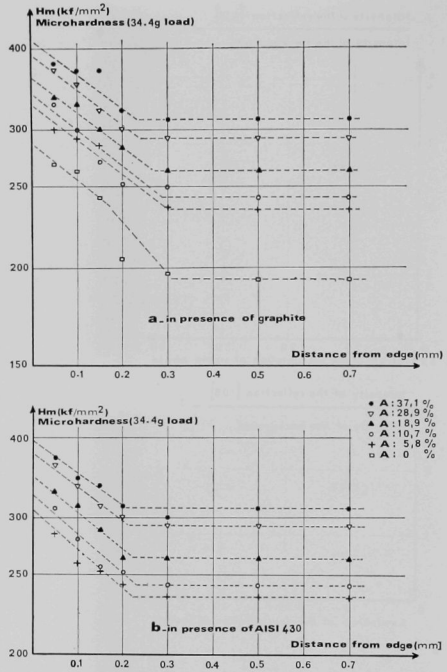

FIG. 15. Microhardness Evolution near the Surface of Strain-hardened Samples after Carburization in Liquid Sodium.

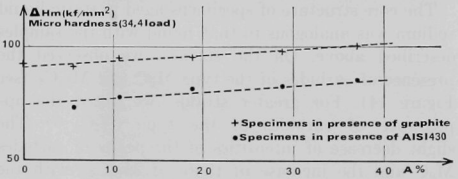

FIG. 16. Variation of Microhardness Deviation between the Core and Surface as a Function of Work Hardening.

argon. In this way, we could determine the microhardness variation between the values extrapolated at the surface (see Figure 15) and the core.

We have noted (see Figure 16) a slight augmentation of microhardness increase as a function of the strain hardening and two levels of values: one for samples in the presence of graphite, and the other for those in the presence of ferritic steel AISI 430. The latter fact shows, as believed by Holcomb,[11] that the quantity of carbon present in both cases in the sodium is different, and that there exists a relation between the surface hardness and the carbon content of the liquid metal.

The hardening observed may be attributed to an increase, on the one hand, of the carbon content in solid solution and, on the other hand, to the formation of chromium carbides; this phenomenon being governed by diffusion,[12] we have assumed a parallelism of the straight lines representing the microhardness gradient near the surface (see Figure 15).

5. Conclusions

This study has enabled us to analyse the influence of grain size and strain hardening on the phenomenon of carburization in the presence of liquid sodium.

The results obtained permit us to make the following principal conclusions:

1. Diffusion occurs preferentially in places with high free energy. It is above all intergranular if the material has coarse grains and involves a much smaller area than when the material has fine grains, where it is mainly intergranular.

2. The strain-hardened state, because of the increase in defect density, favors superficial carbon penetration into the austenitic stainless steel by creating places for preferential precipitation. However, we have not observed any very large variation in the depth of carbon diffusion as a function of the rate of strain hardening.

3. The carbon is combined with the alloying elements to give carbides more slowly than the rate at which it diffuses. The larger the carburization, the richer are the carbides in iron.

4. The microhardness measurements are very representative of the penetration of this impurity in the steel. They integrate both the carbide formation and the carbon in solid solution in the austenite. Nevertheless, the X-ray-diffraction study and the electronic-microprobe analysis have enabled us to follow the evolution of the phenomenon more accurately.

5. The microhardness deviation between the values extrapolated at the surface and those obtained at the core of the samples aged in neutral atmospheres has enabled us to follow the increase of the surface penetration of the carbon as a function of the strain hardening. There exists a relation between surface microhardness and the overall carbon content of the liquid metal. Since grain size and strain hardening play a great part in the mechanical characteristics of materials, we believe that our observations may bring a contribution to the knowledge of carbon-transfer phenomena when the steel is subjected to stress.

A more thorough study of the phenomenon re-

quires additional tests. This is what we have undertaken, in particular, with the nonstabilized grade AISI 316. The preliminary results obtained confirmed those given above.

Finally, parallel to this research on carburization, it seems of interest to analyse the influence of grain size and strain hardening on decarburization of ferritic steels, the two phenomena being in fact, closely linked.

Acknowledgment

We wish to thank particularly MM. Ival and Pascal, engineers at the EDF Materials Laboratory at Renardieres, who have respectively performed X-ray analyses and CASTAING microprobe analyses.

BIBLIOGRAPHIC REFERENCES

1. W. J. Anderson, G. S. Sheffield, and A. J. Birkle, *Development of Ferritic Steels for High Temperature Sodium Service (Part II)*, NAA-SR-7544 (Nov 1963).
2. W. C. Hayes and O. C. Shephard, *Corrosion and Decarburation of the Ferritic Chromium-Molybdenum Steels in Sodium Coolant System*, NAA-SR-2973 (Dec 1958).
3. C. S. Campbell and C. Tyzack, *A Preliminary Model for the Carburization of Stainless Steel at High Temperatures in Sodium Containing Carbon at Unit Activity*, UKAEA SM 85/19, Vienna (Dec 1966).
4. B. A. Nevsorov *et al.*, *Corrosion Resistance of Constructional Materials in Alkali Metals*, Proc. Third Intern. Conf. Peaceful Uses Atomic Energy, Geneva, 1964, **9**, 561.
5. R. C. Andrews, R. H. Hiltz, L. H. Kirschler, S. J. Rodgers, and F. Tepper, *Effect of High Temperature Sodium on Austenitic and Ferritic Steels*, MSAR Reports (1964–1966).
6. L. Valibus, *L'impureté carbone dans la corrosion par le sodium liquide*, Internal Reports EDF SERNUTH—HM. 3 31–62, 63, 64 (1965).
7. W. J. Anderson and G. V. Sneesby, *Carburization of Austenitic Stainless Steel in Liquid Sodium*, NAA-SR-5282 (1960).
8. R. H. Hiltz, *Effect of Carburization on the Phases in Austenitic Stainless Steel*, MSAR 66 119 (June 1966).
9. J. Dedieu, A. Sulmont, and T. Legrand, *Analyse de l' influence de la structure de la dimension du grain et du traitement thermique sur le fluage des tubes en acier 18/11 au titane*, Revue de Métallurgie, 229–241 (Mars 1965).
10. B. Jaoul, *Etude de la plasticité des mêtaux*, DUNOD 381 (1965).
11. W. F. Holcomb, *Carburization of Type 304 Stainless Steel in Liquid Sodium*, Nuclear Engineering and Design, **6**, 264–272 (1967).
12. O. C. Shephard, *The Effect of Carbide Precipitation and Carburization on the Mechanical Properties of Type 304 Stainless Steel*, NAA-SR-Mem-2576 (1958).

Carburization of Austenitic Stainless Steel by Sodium

Morris Kolodney*

United Nuclear Corporation
Elmsford, New York

Abstract

Measurements of the rates of carburization of austenitic stainless steels in sodium have been reviewed.

Models proposed to explain carburization rates have been examined. Emphasis has been placed upon a model in which the assumption is made that carbon from the sodium enters the steel and causes rapid precipitation of a stable carbide, reducing the chromium concentration in the surface. As chromium precipitates, the carbon activity in the stainless steel surface increases until it becomes equal to the carbon activity in the sodium. Thereafter, carbon diffuses into the interior of the steel, precipitating carbide along a front that moves inward.

Existing basic data on solubilities, diffusivities, and carbide compositions were employed to predict rates of carburization on the basis of the model and compared with measured values. In addition, the results of short-time carburizations have been correlated with the readings of the United Nuclear Carbon Meter.

Introduction

The exposure of austenitic stainless steels to high-carbon sodium results in extensive carburization and embrittlement of these steels. Thin sections may reach carbon contents in excess of one percent after relatively short times in highly contaminated sodium.[1, 2, 3] Since the austenitic stainless steels are preferred alloys for many applications in sodium-cooled reactors, their ease of carburization is a matter of concern. Yet, despite considerable experimental effort, two major questions remain unanswered. First, how much carbon and what carbon distribution are allowable before the steel becomes unfit for use? Second, what carbon concentration or carbon activity in the sodium is tolerable without excessive carburization damage during brief excursions or over long operating periods?

There does not yet appear to be a widely accepted specification for the maximum carbon content of austenitic stainless steel. In 1962, Sinizer and Pearson[4] predicted an infinite life for Type 304 steel if its surface carbon content remained less than 0.5%. This specification has been reinforced in a more recent review of sodium purity requirements.[5] Presumably, a uniform carbon content of 0.5% would also be acceptable. Thorley and Tyzack[6] have reported that carbon contents of 0.3–0.5% cause a loss at room temperature of about 75% of the original ductility in 18-8 steels. However, mean carbon contents of 0.6 to 1% may be tolerated for the same loss of ductility at 1200°F. On the other hand, recent work at MSA[1] has shown substantial loss of ductility in Types 304 and 316 steels with minor increases in carbon.

Even when a carbon limit for the steels becomes widely accepted, it will be most desirable to relate the rates of carburization to the carbon activity of the sodium. Only then will it be possible to predict carbon absorption by the steels during selected operating intervals. Unfortunately, until recently there has been no convenient method for measuring the carbon activity or "carburizing potential" of the sodium. Therefore, in the past, experimenters at Atomics International attempted to correlate carburizing potential with the surface carbon content of stainless steel and with the carbon content of the sodium.[3] Efforts have also been made to relate microhardness test results to carburizing potential.[3, 7] For a variety of reasons, these techniques are not as likely to succeed as the recently developed carbon meter that has been described elsewhere[8] and whose engineering development is reported in another paper at this conference.[9]

Carburization Measurements

The lack of a tool for the analysis of the carbon activity of sodium has not entirely prevented the measurement of carburization rates. The most comprehensive early series of measurements are those performed for periods up to 150 hr in capsules at AI[3] and for times in excess of 5000 hr in loop tests at MSA.[2] More recently, a series of 100-hr tests have been carried out by Holcomb[7] at ANL. As might be expected, in the absence of a good method for characterizing the carbon activity of the sodium, the most reliable measurements are those obtained from sodium "saturated" with carbon.

In order to compare the results obtained with different specimen thicknesses exposed for different

* Department of Chemical Engineering, College of the City of New York.

lengths of time, we may define a carburization rate parameter

$$P = \frac{(C_m - C_0)L}{t^{1/2}}, \qquad (1)$$

where

C_m = average concentration of carbon in the specimen, ppm;
C_0 = original concentration of carbon in the specimen, ppm;
L = total thickness of tab specimen undergoing diffusion from both sides, mils;
t = time, hours.

(This parameter is derivable from a simple diffusion model in which no carbide precipitation is assumed. Such a model was used at AI and MSA to calculate diffusivities of carbon. Although the calculated diffusivites have been challenged, it may be shown[10] that the form of the equation is approximately the same when carbide precipitation occurs, provided that the composition of the precipitate is constant with time. The particular units for the parameter have been chosen because they are in common use.)

In terms of this parameter at 1200°F, the MSA data yielded values of about 8500 ppm-mils/hr$^{1/2}$ for Type 316 steel and about 10,000 for Type 304 (see Figs. 42 and 49 of Ref. 2). By comparison, the AI data (calculated from Fig. 4 of Ref. 3) resulted in a P value of 11,000–12,000 units for Type 304 steel. This agreement is good considering the very different kinds of experiments and the large scatter of the data.

To set this carburization rate in perspective, one may estimate that a parameter of 10,000 means that a fuel clad thickness of 10 mils (diffusion from one side; L = 20 mils) would reach an average carbon concentration of 0.5% in 100 hr. Clearly, no reactor can operate in this manner. However, although this level of carbon contamination is unrealistic, it is of interest as an extreme. It is also of interest to estimate whether the damage may be significantly ameliorated by a decrease of temperature, particularly since the effect of temperature may be about the same at all carbon levels if the basic carburization process remains the same.

It may be assumed[10] that the parameter P varies with the square root of the diffusivity for both simple solution diffusion and for diffusion involving carbide precipitation. (This is approximately true if the concentration of carbon dissolved in the surface of the steel is independent of temperature.) Consequently, if the diffusivity may be expressed by the usual equation

$$D = D_0 e^{-Q/RT}, \qquad (2)$$

the effect of temperature may be determined if the activation energy Q is known. There have been a number of measurements of the diffusivity of carbon in austenite with activation energies reported between about 31,000 and 38,000 cal/mole. (The diffusivity data obtained at AI,[3] although they may be incorrect in absolute terms, yield an activation energy of about 31,000 cal/mole.)

A recent measurement by Smith[11] of carbon diffusion in gamma iron-nickel alloys appears pertinent because the surface of the stainless steels may resemble these alloys after depletion of chromium by precipitation. Use of an activation energy of 35,000 cal/mole from Smith's results produces the following expected changes in the carburization parameter based upon an experimental value of 10,000 at 1200°F for carbon-saturated sodium:

Temperature, °F	P, ppm-mils/hr$^{1/2}$
1400	27,700
1200	10,000
1000	2,750
800	485

Obviously, very substantial improvements in carburization rates may be achieved at a sacrifice of operating temperature.

Carburization rate measurements with sodium saturated with carbon may be of value for predicting the worst to be expected after a brief accidental excursion, but the information needed for long-term operation involves much purer sodium. Unfortunately, there are no measurements over long periods with sodium of known and constant carbon activity. There have been a few efforts to determine carburization rates at known concentrations of carbon,[3, 7] but these experiments cannot be considered reliable. Recently, MSA[1] attempted mild carburization of stainless steel by a series of carbon excursions, but without any expectation of constant carbon activity in the sodium. At UNC, a series of carburizations of Type 316 specimens were performed at 1400°F in termal convection loops. The carbon activity was measured by means of a carbon meter and was manually controlled by insertion of carburized iron tabs or by injection of carbon monoxide into the cover gas. Unfortunately, the test times were short—not exceeding about 30 hr and were not replicated. Nevertheless, it was found possible to correlate the carburization rates with the measured carbon activities[10] as shown in Fig. 1.

It is interesting to derive a carburization parameter from this correlation. The value found for P at 1400°F for the lowest meter readings (corresponding to nor-

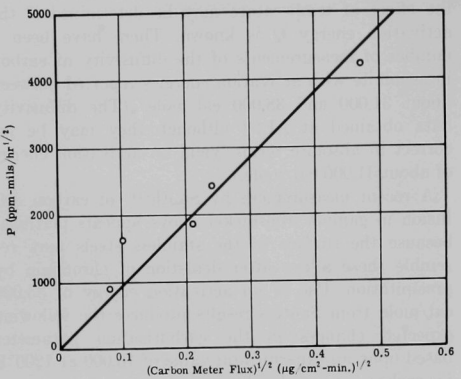

FIG. 1. Correlation of Carburization Parameter with Carbon-meter Reading at 1400°F.

mal operation of a "clean" loop) was about 740 ppm-mils/hr$^{1/2}$. If this may be translated to lower temperatures by means of ratios previously derived from diffusivity data, it would correspond to a P value of about 270 at 1200°F, compared with a value of about 10,000 under carbon saturation conditions. Calculating the lifetime (average carbon gain of 5000 ppm) of a 10-mil fuel clad in the "clean" sodium gave about 140,000 hr as against only 100 hr in heavily contaminated sodium. In view of the paucity of data, it cannot be too strongly emphasized that this calculation is little short of foolhardy. However, it points up the need for good carburization rate information at low levels of carbon activity.

Models for the Carburization of Stainless Steel

In the carburization models employed in connection with the earlier measurements, diffusion of carbon without phase change was assumed. By contrast, Campbell and Tyzack[12] have presented a detailed theoretical analysis of the carburization process based upon the assumption that chromium carbides precipitate in the steel. Taking the case of carbon saturation (activity of carbon = 1) and utilizing existing thermodynamic data for the carbides and for the activity of chromium in iron, they have recalculated the diffusivity of carbon as measured by Anderson and Sneesby.[3] However, the diffusivity so corrected appears still to be in error by about one order of magnitude.

The validity of the homogeneous solution and precipitation models has been tested using the sparse data obtained by McKee and Caplinger with the UNC Carbon Meter.[10] By making a substantial number of simplifying assumptions, it may be shown that the parameter P of Figure 1 should be proportional to the carbon-meter flux if homogeneous diffusion had taken place. On the other hand, it shoud be proportional to the square root of the meter flux if the precipitation model were correct. The results depicted in Figure 1 seem to lend credence to the precipitation mechanism. Indeed, it would appear that precipitation begins at very low carbon activities.

If the precipitation mechanism be accepted, it becomes possible to predict the rate at which the carbide precipitation zone moves into the steel. Thus, Darken[13] has treated diffusion accompanied by phase change. For carbon diffusion, the thickness X of carbide precipitation zone reached in time t should be given by the following equation:

$$\frac{X^2}{t} = 2D\frac{C_s}{C_p}\left[1 + \frac{C_s}{12C_p} - \frac{1}{240}\left(\frac{C_s}{C_p}\right)^2 + \cdots\right]^2, \quad (3)$$

where D is the diffusivity of carbon, C_s the surface concentration of dissolved carbon, and C_p the total carbon concentration in the zone of precipitation. Since C_p is much larger than C_s, the bracketed term is close to unity.

The total concentration, C_p, comprises (a) carbon precipitated by chromium originally present in the precipitation zone, (b) carbon precipitated by chromium that has diffused into the precipitation zone from the interior of the steel, and (c) the average concentration of carbon dissolved in the matrix of the zone. The concentration corresponding to (a) is equal to the weight percent of original Cr(C/Cr), where (C/Cr) is the ratio of carbon to chromium in the compound being precipitated. If the carbide is very stable, this ratio may be assumed constant as a first approximation.

The carbon concentration corresponding to (b) may be calculated if the diffusivity of chromium in the matrix is known. However, since chromium diffuses by a vacancy mechanism, while carbon diffuses interstitially, it may be assumed that chromium is stationary relative to carbon, i.e., that the contribution from source (b) is zero.

The carbon derived from (c) has been shown[14] to be equal to $C_s/3$. With these assumptions, equation (3) is reduced to

$$\frac{X^2}{t} = 2D\frac{C_s}{C_p}, \quad (4)$$

with C_p for a particular kind of carbide dependent only on the original chromium content and C_s. Equation (4) may be employed to calculate a value of X^2/t at 1200°F under saturation conditions for comparison with the AI data. The two carbides that have been found in carburized 304 stainless steel are $M_{23}C_6$,

and at higher carbon contents, M_7C_3.[15] These compounds contain both iron and chromium. An assumption that the ratio of iron to chromium is unity appears reasonable from the data. Hence, C_p may be computed on the basis of $Cr_{11.5}C_6$ and $Cr_{3.5}C_3$. By use of Smith's data for carbon diffusivity ($D = 1.4 \times 10^{-9}$ cm²/sec at 1200°F) and $C_s = 0.48\%$ C as the solubility in austenite at 1200°F, the results predicted are

for $M_{23}C_6$	for M_7C_3
$\frac{X^2}{t} = 3.2 \times 10^{-7}$ in.²/hr.	2.0×10^{-7} in.²/hr.

The data of Anderson and Sneesby (see Fig. 6 of Ref. 3) are equivalent to a value of 1.6×10^{-7} in.²/hr at 1200°F. In view of the many uncertainties, the agreement may be considered good. Since C_s may be related to the activity of carbon in the surface of the steel and since this is presumed equal to the activity in the sodium, the rate of growth of the precipitated zone may be calculated, at least approximately, for any activity of carbon in sodium.

An alternative approach would be based upon an experimental determination of the relationships between carburization rates and carbon activities, using an instrument such as the UNC carbon meter. This device is based upon the diffusion of carbon through an alpha-iron sensor. If this process of diffusion in the solid limits the flux of carbon, it becomes possible to provide a theoretical connection between the carbon activity of the sodium, a_C, and the meter reading.[16] If we utilize literature data for the solubility and diffusivity of carbon in alpha iron and assume that Henry's law holds, the equation obtained at 1400°F is

$$a_C = 0.114 \text{ (carbon-meter flux)}, \qquad (5)$$

where the carbon-meter flux is expressed as the flow of carbon through the sensor in $\mu g/cm^2$-min. Now the very tentative correlation shown in Figure 1 may be expressed as

$$P = 9570 \text{ (carbon-meter flux)}^{1/2} \qquad (6)$$

Combination of equations 5 and 6 yields

$$P \cong 28000\, a_C^{1/2}. \qquad (7)$$

While emphasizing once again the weak experimental foundation for this result, it is nevertheless interesting to observe that it leads to a value of $P = 28{,}000$ at $a_C = 1$ (carbon saturation). This is identical with the parameter obtained by translation of the MSA and AI data to 1400°F. Although this agreement upon a value derived from such widely different experiments is probably only fortuitous, it encourages additional predictions. For example, assume that a 10-mil sheet is to absorb not more than 0.5% carbon in 10,000 hr by carburization from one side at 1400°F. Equation (7) requires that the activity be little more than 10^{-3}. Although this seems exceptionally small, it may be approximately correct, for Campbell and Tyzack[12] have calculated that at about 1300°F the activity of carbon in an 18-8 stainless steel at the point of incipient precipitation of $Cr_{23}C_6$ lies between about 3×10^{-3} and 6×10^{-3}.

As a second example, one might predict that failure of a fuel element containing single-phase UC-PuC might not be disastrous. Thus, Holden and Fuhrman[17] have found that sodium in equilibrium with this fuel at about 1470°F reaches a carbon activity of about 0.02. If, as a result of a fuel-clad failure, a 10-mil sheet were exposed on one side to sodium of this high carbon activity for 24 hr at 1400°F, it would gain only 0.15% carbon. Ductility would not be seriously impaired. Hopefully, the failure would be discovered and the temperature reduced in less than 24 hr.

The estimates that have been made are speculative and may prove to be quite incorrect. They have been offered in the hope that they will spur the acquisition of better experimental evidence.

REFERENCES

1. Andrews, R. C., and Barker, K. R., *The Effect of High Temperature Sodium on the Mechanical Properties of Candidate Alloys for the LMFBR Program*, MSAR 68-77 (May 1968).
2. Andrews, R. C., Hiltz, R. H., Kirschler, L. H., Rogers, S. J., and Tepper, F., *Results of Mechanical Properties Tests of 316 SS Specimens in 1200°F Sodium Contaminated with Carbon*, MSAR 65-194 (Dec 1965).
3. Anderson, W. J., and Sneesby, G. V., *Carburization of Austenitic Stainless Steel in Liquid Sodium*, NAA-SR-5282 (Sept 1960).
4. Sinizer, D. I., and Pearson, E. N., *Relationship of Carburizing Potential to Operating Temperature Limitations in SRE*, NAA-SR-Memo-7804 (1962).
5. Hinze, R. B., *Sodium Purity Requirements*, NAA-SR-Memo-12394 (May 1967).
6. Thorley, A. W., and Tyzack, C., *The Corrosion Behavior of Iron and Nickel-Based Alloys in High-Temperature Sodium*, TRG Report 1356(C) (1966).
7. Holcomb, W. F., *Carburization of Type 304 Stainless Steel in Liquid Sodium*, Nuc. Eng. and Design, **6**, 264 (1967).
8. McKee, J. M., Caplinger, W. H., and Kolodney, M., *Continuous Carbon Meter for Sodium Systems*, Nuclear Applications (Oct 1968).
9. Caplinger, W., and Stern, G., *Engineering Development and Performance of the UNC Carbon Meter*, THIS CONFERENCE.
10. Kolodney, M., *Mechanism of Carburization of Stainless Steel in Sodium as Identified by a New Carbon Meter*, Nuc. Eng. and Design, **7**, 481 (1968).
11. Smith, R. P., *The Diffusivity of Carbon in Gamma Iron-Nickel Alloys*, Trans. Met. Soc. AIME, **236**, 1224 (1966).

12. Campbell, C. S., and Tyzack, C., "A Preliminary Model for the Carburization of Stainless Steel at High Temperatures in Sodium Containing Carbon at Unit Activity," in *Alkali Metal Coolants*, IAEA, Vienna, p. 159 (1967).
13. Darken, L. S., *Diffusion in Metal Accompanied by Phase Change*, Trans. AIME **150,** 157 (1942).
14. Rhines, F. N., Johnson, W. A., and Anderson, W. A., *Rates of High-Temperature Oxidation of Dilute Copper Alloys*, Trans. AIME **147,** 205 (1942).
15. Hiltz, R. H., *Effect of Carburization on the Phases in Austenitic Stainless Steel*, Topical Report No. 6, MSAR 66–119 (June 1966).
16. Kolodney, M., *Diffusion Limited Carbon Flux Through An Iron Wall*, United Nuclear Corporation, Internal Report (June 1967).
17. Holden, R. B., and Fuhrman, N., *A Fundamental Study of the Compatibility of Stainless Steel and Mixed Carbide Fuel*, To be presented at the ANS Winter Meeting, Washington, D. C. (November 10–15, 1968).

Discussion

Mr. Hiltz (MSA): I would like to clear the air a little bit.

1. AI can jump on me if they like, but AI's data don't say that a half percent carbon is allowable; they say the carbon in the sodium which gives them a carburization rate (of the stainless steel) of 5000 ppm in 100 hr is an allowable carbon concentration in the sodium; that is what we disagree with violently.

2. I am afraid that MSA does not believe in homogeneous carburization. As a matter of fact, we state that the thing is in constant change. The carbide chemistry is changing, the carbide is changing, the carbon concentration dissolved in the austenite is changing, constantly. So it brings me to two questions, although I cannot argue with your numbers—they all seem to come out close. In your first equation you have a term which relates to the thickness of the specimen and yet our data would say—this is for 5-, 15-, and 60-mil specimens—that until such time as the carbon concentration at the centerline of the specimen has exceeded the original carbon content, the carburization rate is the same regardless of specimen thickness. This relates back, I think, to something like an infinitely thick specimen.

The second thing that I wonder about is in going back to Wagner's data on diffusion, which you have taken from Darken, you are using a carbon solubility based on dissolved carbon in the stainless steel. In the carburization of stainless steel in sodium, I don't believe that the carbon concentration in the austenite is constant, but is a function of the chromium which is still dissolved in the austenite.

Mr. Kolodney: Am I supposed to answer that? I am really not trying to attack the MSA data at all. In fact I am a great admirer of the data; however, what MSA did was to calculate diffusivities on the basis of a homogeneous diffusion model.

Mr. Hiltz: That was based on earlier data, and we have repeatedly stated that is no longer our view.

Mr. Kolodney: The other things you said, of course, are true. The composition of the carbide does change, and I have said again I have made a lot of simplifying assumptions. The only way I can get any numbers at all from the little bit of data available is by making these simplifying assumptions. I pleaded for no one to believe the answers, but here they are.

Mr. Feder (ANL): Would it make any difference in your argument if you never invoked the concept of the activity of the carbon in the sodium, but spoke only of an arrival rate of carbon at the surface of your carbon meter and at the surface of the tabs that you are interested in?

Mr. Kolodney: I suspect it would. I think basic to a lot of the work that has been done at United Nuclear is the assumption that the surface of the steel has the same carbon activity as the bulk of the sodium and that is a weak point—something that we are not sure of. It depends upon the solubility of carbon in the sodium. It does depend upon the transport, and we have been told by people at Argonne that the solubility of carbon in sodium is extremely low. If it is extremely low, then the carbon meter may not read accurately.

Mr. Feder: That impression has gotten out. We never said that the carbon solubility in sodium was low. We said the *graphite* solubility in the sodium was low. We have never claimed and, I think people should not take it for granted, that there is any equilibrium among the various forms of carbon in sodium. And this is precisely the point I was trying to make—that if we do not attempt to assign an activity of carbon to the sodium, we will not be making the implicit assumption that the species which are present are in equilibrium.

Mr. Furukawa (JAERI): Dr. Hiltz told almost all, but I wish to add a little more to his statement. We should consider, I believe, the transfer effect-surface composition changes caused by mass-transport phenomena. Anyway, we are concerned with low carbon activity in practical systems, not with very high carbon activity. Therefore, we should spend more effort in examining the low-carbon activity range. In the high-temperature region we should expect some mass-transfer phenomena in all loops. I believe we should use pure metals for examination, for example, pure iron. I think you used stainless steel for your tests. But if you use pure iron, I think more reliable

data will be obtained relating carbon activity and carburization phenomena.

Mr. Jansson (W): It seems to me that the use of your parameter P, and consideration of carbon diffusion in the UNC iron membrane are basically the same. It isn't surprising, then, that you get this linear relationship if you have two membranes which are in the same carburizing medium. I would say that just shows that you have similar materials where carbon goes in and there doesn't seem to be much more to that. If you accept the feeling that the carbon solubility is low in sodium, then it would be better I think to speak about the availability of carbon just the way I understand the Argonne people do now. The carbon activity that the United Nuclear carbon meter measures, therefore, is the activity of carbon at the interface in the iron membrane at the surface. It is not, I think, the activity in the sodium itself.

Mr. Kolodney: I think I said that. We are not sure that it measures the activity in the bulk sodium, although that is what we had hoped it would measure and that does depend on the transport property. I don't make any claim for originality of the parameter. It's an old kind of relationship—the square root-time relationship. However, the carbon meter is a device in which diffusion occurs without precipitation, and here we are talking about precipitation in the stainless steel. I have combined the two and said that with enough assumptions you come out with a very similar kind of a relationship. I have also tried to take whatever numbers are available and to show what they mean in terms of time.

Mr. Jansson: You are precipitating, though, something which is more stable, so in fact there is no difference. In both cases you have lowered the carbon activity on the other side of the membrane. You can look on your stainless steel as a membrane.

Mr. Horton (AEC): Prof. Kolodney, why should we worry about carburization when we can de-carburize our stainless easily enough afterwards?

Mr. Kolodney: De-carburization of austenitic stainless? Decarburize it by using a hot trap? I don't know. You really are the people who ought to answer that. Do you expect to operate breeders with hot traps?

Mr. Horton: It's debatable. AI has shown rather by accident that they can easily de-carburize their stainless in sodium. No, I don't know if we are going to operate with a hot trap or not, but if carbon is going to cost so much money in research, it may be cheaper periodically to put a zirconium hot trap on line and de-carburize back to equilibrium amount.

Mr. Kolodney: Did I hear someone say today that if you overdo it you are going to lose the strength of the stainless?

Mr. DeVan (Chairman): There is another point. You first have to define your source. The SRE after the tetralin spill would have loved a trap that could have taken it down in a reasonable period of time. If you could have invented one, you could have become a rich man overnight. So, I, for one, would worry about a pump seal going and a gallon or so of oil hitting the system. This has happened more than once at the Laboratory, and you got cracked carbon everywhere—a tremendous amount of carbon—that you have to go back and retrieve. And until you have retrieved all that cracked carbon, you do maintain a carbon activity of saturation for that period of time. So it's relative to the source that you assume is going to be in there.

Friction and Wear in Liquid Metals

P. Barrau, J. P. Fontaine

Electricité de France
Chatou, France

AND

B. Morin

C.E.A., CEN Cadarache
Saint Paul lez Durance, France

(PRESENTED BY J. BEAUFRERE)

1. Introduction

Sliding and rolling friction in liquid metals or argon carrying sodium aerosols are important features for the good running of mechanisms, such as mechanical pumps, fuel-handling devices, and control rods, used in liquid metal fast breeder reactors. An experimental study of sliding friction in NaK has been carried out by the French Atomic Energy Commision (CEA) from 1960 to 1966 in Fontenay aux Roses research center.[1, 2] Tests have been done with liquid sodium in the Cadarache research center since 1966. At the same time, the research department of the French Electricity board (EDF) began similar tests but under different conditions and with different materials.

In this report, the main experimental results recently obtained by the two organisations are presented, an interpretation is proposed, and some practical applications of the results are presented.

2. Test Apparatus

2.1. Tests Realized in Plane Contact Geometry

2.1.1. CEA Apparatus

The device is presented in Figure 1. The elements in relative motion are (see Figure 2):

moving element: pins or ring;
fixed element: disc.

It is possible, with this device, to make tests under the following conditions:

sliding speed: from 0 to 5 cm/s;
specific load: 0 to 5×10^5 N/m^2;
temperature: from 20°C (NaK tests) to 600°C;
liquid metal purification by horizontal-convection cold trap (O_2 content < 30 ppm).

2.1.2. EDF—Devices

The test specimens are two circular rings: one rotating, the other one fixed. Two types of machines are used:

frictiograph for the exact measurement of the friction and wear coefficients for short-duration tests (1 hr);
machine derived from the first type for long-duration tests (100 hr) with previously selected materials.

The frictiograph,[3] shown on the block diagram 3 and on Figures 4 and 5, has a fixed test specimen (see Fig. 6), which is integral with the apparatus for measurement of the friction torque. The rotating test specimen is chamfered so as to get rid of the boundary effects and of a possible decentering of one specimen with respect to the other, the fixed specimen then behaving like an indefinite plane.

The devices for loading and measuring the torque are located in an enclosure containing purified cold argon. This eliminates the friction points on the measuring shaft. The load is applied by weights on the measuring shaft. A jack permits lifting the load and separation of the specimens from one another. The shaft is maintained in place by an elastic device with two degrees of freedom: axial for placing the specimens into contact, rotary for torque measurement. The applied load is controlled by a dynamometer, and the torque is measured by strain gages placed on metal blades stressed in tension. The measurements of the friction coefficient, unperturbed by the sealed outlets, are quite accurate, being 5% for small loads (5 to 10 × 10^5 N/m^2), and 10% for the heaviest loads studied at present (25×10^5 N/m^2).

The two test specimens (see Fig. 6) are placed within a crucible supplied with filtered sodium by a pot or by a loop. Immersion of the test specimen is signalled by means of a discontinuous level-measurement device, based on resistance changes and developed in our laboratories. The maximum operational temperature is 700°C. The movable specimen is driven by a variable-speed motor located in air (8 cm/sec to 4.6 m/sec in the present arrangement).

Sealing is ensured by a rotary joint developed by us. The operational principle of this device is identical

with that used by us in the long-duration testing machine and is described further on.

The specimens may be put in place without it being necessary to open the tank, thanks to a system of chambers and glove compartment under an argon atmosphere. The test rate is high because of the simplicity of changing the test specimens.

The long-duration testing machine, shown on the block diagram 7, also uses a fixed and a rotating specimen, of a size greater than that used in the frictiograph. The fixed specimen is mounted on the end of two concentric bellows between which a controllable argon pressure is maintained, while the movable specimen is driven in rotation, at a variable speed, by a motor and a hydraulic transmission system. The applied load depends on the pressure within the chamber located between the two bellows and is thus known. The friction torque is not measured, but the motor torque can be determined.

The test specimens are located in a crucible supplied with sodium (max temperature 600°C), static and purified by a cold trap (120°C). The specimens are placed before the sodium is directed into the device, and the test rate is low. On the other hand, this assembly operates automatically and is thus reserved for long-duration tests.

An identical device, composed of a rotary ring of solid tungsten carbide G1 (see Appendix) and of a leaded bronze ring ELCO 1 (see Appendix), is successfully used as a rotary joint (200°C maximum on the frictiograph).

2.2. Heavy-loaded bearings test apparatus

Tests are performed with radially loaded journal bearings to provide good simulation of the operation of real mechanisms. The principal parts of the test apparatus are (see Figure 8):

sodium vessel of 500-mm diameter;

on the bottom of the sodium vessel a nonrotating bearing set on a moving carriage (the carriage is driven by a shaft penetrating the sodium vessel via bellows);

a very strong shaft, centered with two roller bearings operating in air, penetrates the top plug of the vessel and drives the tested journal in the bearing set on the moving carriage;

drive shaft of the moving carriage is tightened to a force indicator and a screw-bolt system with which one can apply the bearing on the journal with a known force;

the shaft is driven by an electrical motor (a beam carrying strain gages used in torque measurement joins the electrical motor and driving shaft);

the shaft has two directions of rotation.

The journal and bearing tested are shown in Figure 9. The device allows the following test conditions:

relative contact sliding speed of 1.46 cm/sec;

radial contact load from 0 to 2×10^4 newton;

temperature from 150 to 600°C;

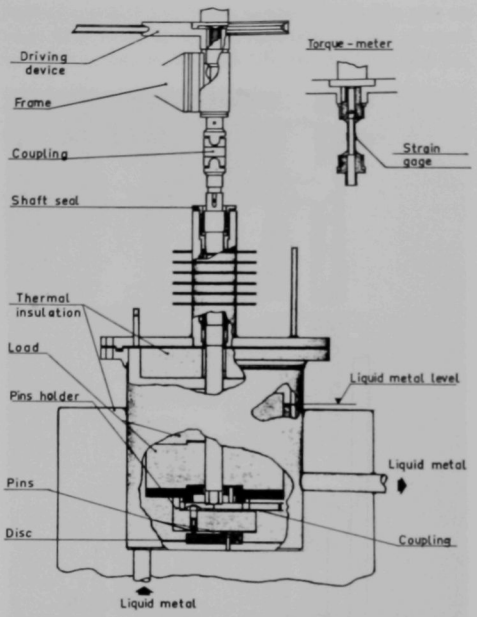

FIG. 1. Test Apparatus to Determine Friction of Materials in Liquid Metals.

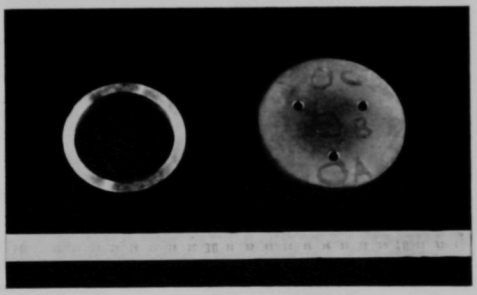

FIG. 2. Elements in Relative Motion for CEA Friction Tests.

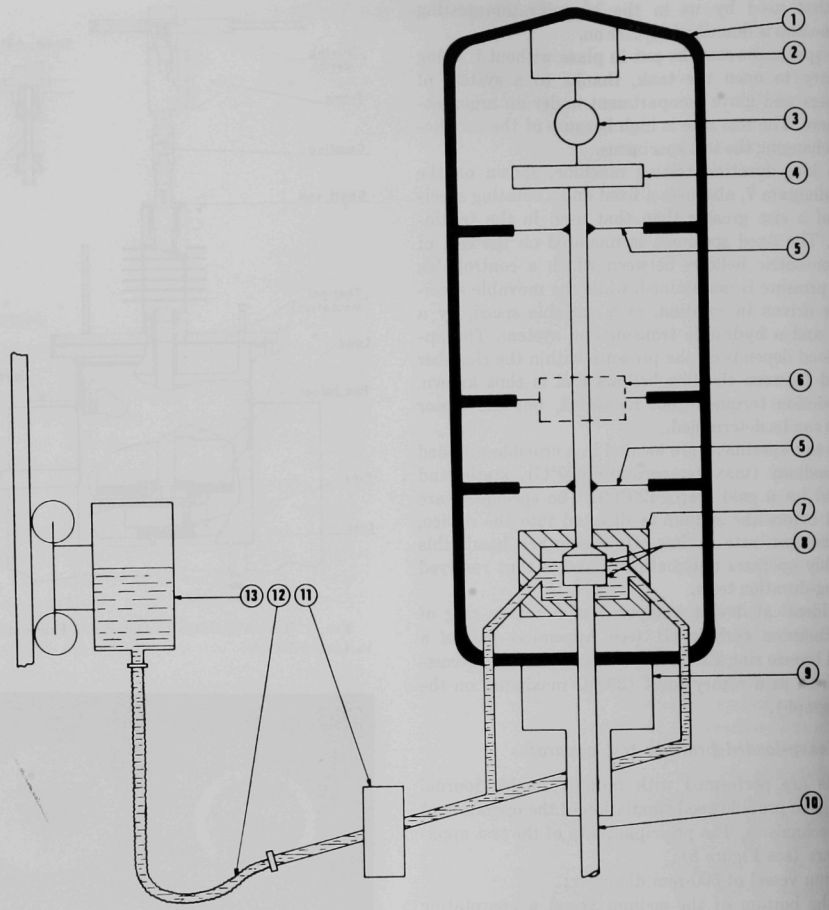

FIG. 3. Test Apparatus.

1. Air-tight chamber
2. Hydraulic jack
3. Dynametric ring
4. Loads
5. Elastic suspension
6. Friction-measuring blades
7. Furnace
8. Specimens
9. Turning seal
10. Rotating shaft
11. Filter
12. Flexible tube
13. Sodium mobile tank

sodium purification by vertical diffusion cold trap kept at about 150°C.

3. Results

3.1. EDF Test Results

3.1.1. Test Conditions

a) *Frictiograph.* We have considered the mechanisms operating at slow speed under varied ambient conditions (sodium at temperatures from 200 to 600°C; argon whether loaded or not in sodium vapours). For all the tests performed the conditions were the following:

unit load: 18×10^5 N/m^2;
speed: 8 cm/sec;
temperature of sodium or argon load in sodium vapours: 200 to 600°C;
oxygen content of sodium: 15 ppm;

O_2 and H_2O content of argon: 5 ppm;
test duration (friction): 1 hr;
time of prior immersion of specimens: 0 to 18 hr.

b) *Long-duration testing machine.* The tests were conducted in sodium at 400°C, without prior immersion. The sodium, purified by a diffusion cold trap, had an oxygen content less than 15 ppm. The total test duration varied from 600 to 800 hr, the duration of the friction tests being approximately 100 hr. The unit load was equal to 2×10^5 N/m^2. The rotation speed corresponded to a product of unit load by linear speed, identical with that obtained with the frictiograph.

3.1.2. Test Results

a) *Introduction.* We first sought a stainless steel that is as hard as possible, easy to use, and relatively cheap. Our choice was structural-hardening stainless steel Z5NCDTV 25-15. As antagonistic material we have chosen Stellite-type alloys based on nickel or cobalt, tungsten carbides, chromium, titanium (solid, pure or mixed in variable proportions with cobalt binder), high-speed steel ZNZ (the compositions of these materials is given in the Appendix). The friction combination which has given excellent results in CO_2 heated to 500°C (4): CaF_2 applied by plasma gun on steel Z5NCDTV 25-15 (see Appendix), Al_2O_3 sprayed by plasma gun on steel Z3 CN 18-10 (Type 304 L),

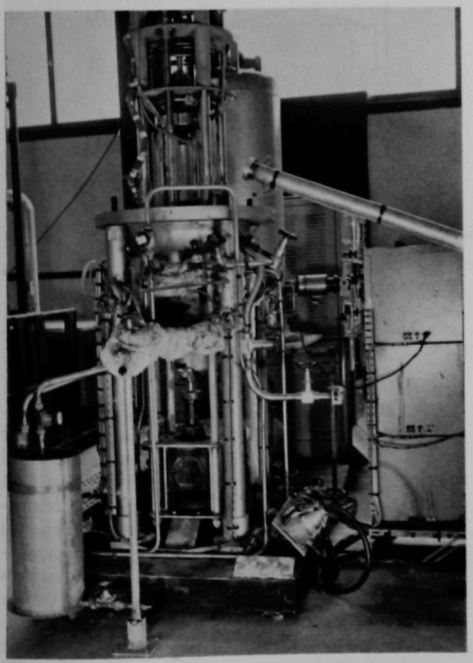

FIG. 4. General View of the Frictiograph.

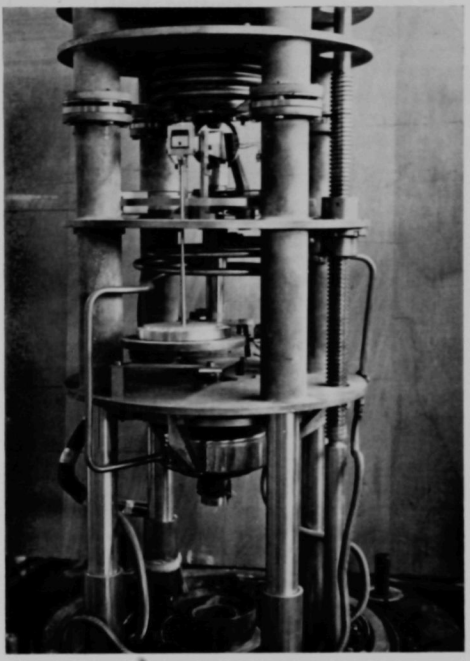

FIG. 5. Details of the Frictiograph, Showing the Crucible, a Test Specimen, and the Devices for Loading and Measuring the Torque.

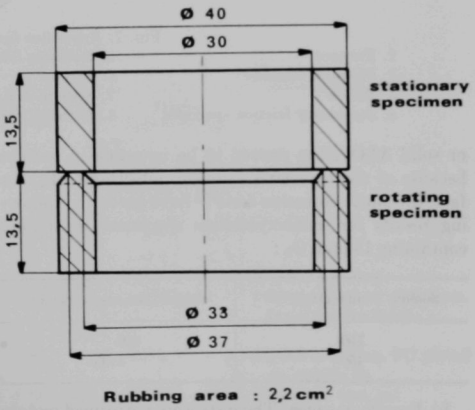

FIG. 6. Friction Specimens.

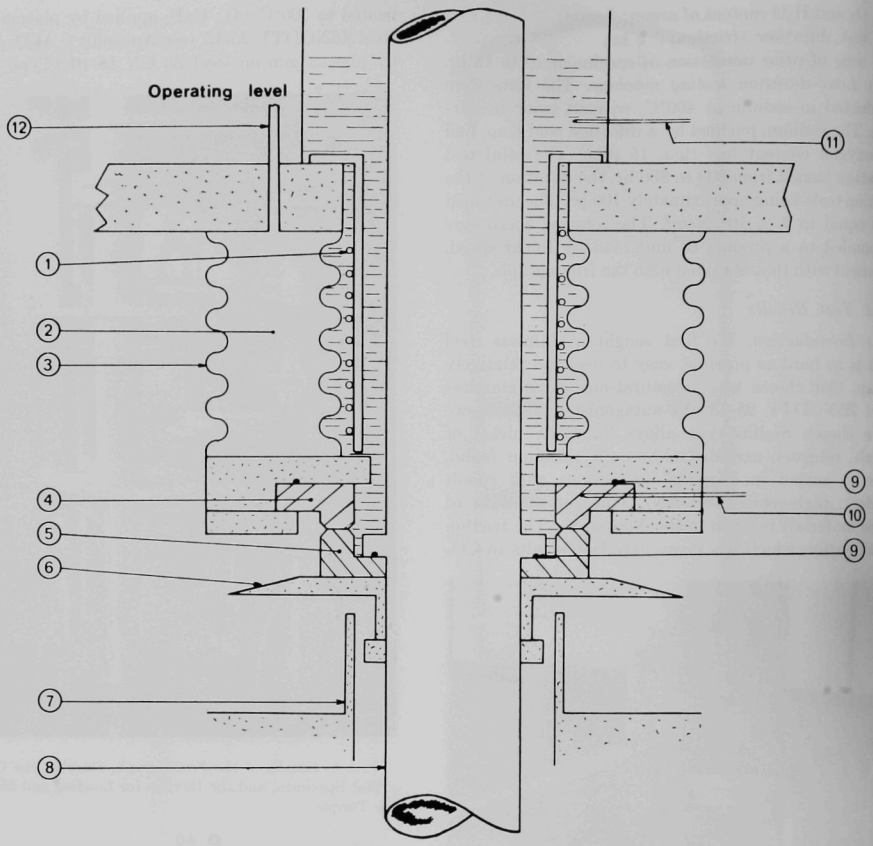

FIG. 7. Apparatus for Friction Endurance Tests.

1. Furnace
2. Pressure chamber
3. Bellow
4. Stationary friction specimen
5. Rotating friction specimen
6. Ejector
7. Sodium drain tank
8. Rotating shaft
9. Seal
10. Stationary specimen thermocouple
11. Sodium thermocouple
12. Argon

or solid Al_2O_3, has proved to be unusable in sodium because of the extensive corrosion affecting CaF_2. In fact, the static corrosion tests[5] have given the following results for monocrystalline specimens in sodium containing 15 ppm O_2 :

Sodium Temperature, °C	Weight Loss, mg/sq cm/mo
750	420
450	1.05

b) *Results in argon.* The tests were performed mainly at 400 and 600°C. Results are given in Table 1.

c) *Results obtained in sodium.* First, in order to explain the dispersion of the results obtained during our first sodium tests with the same combinations and under the identical experimental conditions, we have undertaken to study the influence of the prior immersion time of the test specimens. The combination chosen was Z5 NCDTV 25 on Virium 12 (see Appendix). Figure 10 shows the amplitude of the fluctuations of the friction coefficient of this combination at various friction temperatures with or without prior immersion at 600°C, this temperature having been chosen in order to accelerate the kinetics of the phenomenon. Figure 11 shows the influence of the duration of the immersion

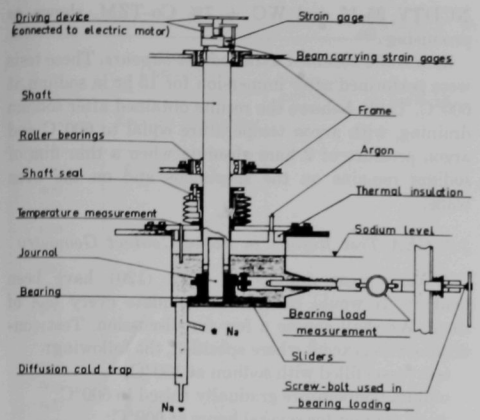

FIG. 8. Heavy-loaded Bearing Test Apparatus.

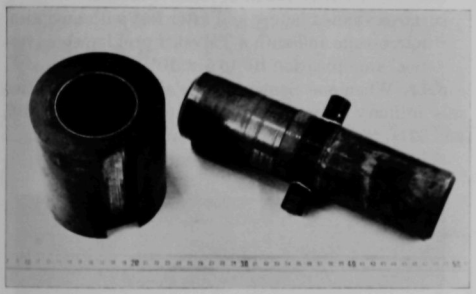

FIG. 9. Journal and Bearing Tested.

on the values of the friction coefficient at 600°C of the following combinations (compositions given in the Appendix):

Virium 12-Z5 NCDTV 25-15 (see Figs. 12 and 13);
WC + 7% Co-Z5 NCDTV 25-15;
Virium 12-Aerometal FC.

Figure 11 shows that an immersion of 10 hr in sodium at 600°C is sufficient to yield stabilized results. Table 2 groups the results used for the preparation of Figures 10 and 11. Table 3 shows the results obtained with a

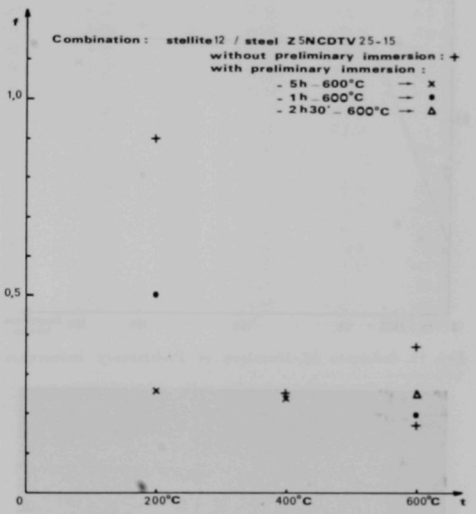

FIG. 10. Friction at Different Temperatures with Preliminary Immersion or Not at 600°C.

TABLE 1. FRICTION IN ARGON

Speed: 8 cm/s

Temperature, °C	Material Combination		Load, kg	Duration Exposed Period, min	Coefficient of Sliding Friction			Weight Variations, mg		Remarks
	Rotating	Stationary			Initial	Max	Stable	Static Specimen	Rotating Specimen	
400	Bronze Elco 1	Aérométal FC	21.0	60		0.24	0.20	0.0	−0.1	
400	Bronze Elco 1	Aérométal FC	59.8	60	0.20	0.41	0.33	0.0	−0.6	
400	Fer	Aérométal FC	28.0	60	0.62	0.62	0.38	−15.4	−5.2	Excessive galling
400	Bronze NS5	Chromium dur	56.9	60	0.60	0.83	0.7	−3.4	−1.1	Bronze plated on chromium. Good surface finish
400	CaF_2	Al_2O_3 (plasma)	28.9	60	0.44	0.44	0.36			
600	Aérométal FC	Carbide G_1	25.0	15	0.98	0.98		+2.4	−5.5	Excessive galling. FC plated on carbide G_1
600	Aérométal FC	Chromium dur	38.5	60	0.52	0.52	0.36	−155.9	−9.0	Chromium torn out
600	Aérométal FC	Aérométal FC	37.0	15	0.48	0.44		+2.3	−42.2	Excessive galling.

prior immersion of 10 hr. Table 4 gives the overall wear results obtained with the long-duration testing machine at 400°C for the combinations WC + 7% Co-Z5 NCDTV 25-15 and WC + 7% Co-TZM, shown as promising.[6]

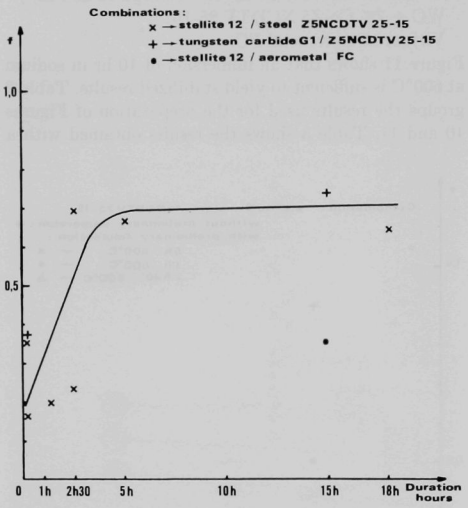

FIG. 11. Influence of Duration of Preliminary Immersion.

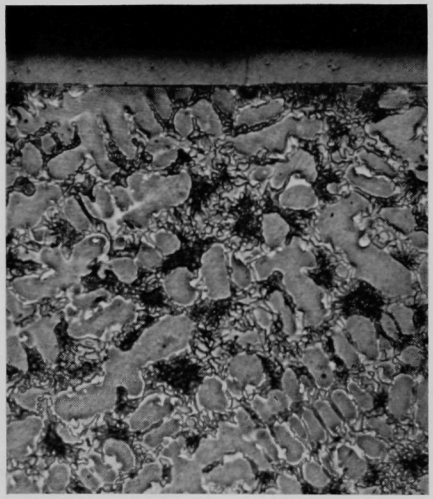

FIG. 12. Virium 12 after Friction with the Structural Hardening Stainless Steel Z 5 NCDTV 25.15 (× 400). Duration of immersion: 15 hr. Duration of friction test: 1 hr. Sodium temperature: 600°C. No work-hardening. The upper clear film is a nickel coating.

d) *Results obtained with sodium vapours.* These tests were performed after immersion for 15 hr in sodium at 600°C. Table 5 shows the results obtained after sodium draining, with argon temperature equal to 600°C and argon pressure of 2 bars absolute when a thin film of sodium remains on the specimens and on the oven walls.

3.2. CEA Test Results in Plane Contact Geometry

A very great number of tests (120) have been made.[1] It would be tedious to quote every one of them. We shall choose a few for discussion. Test conditions were, except where specified, the following:

test vessel filled with sodium at 150°C;
sodium temperature gradually raised to 600°C;
static contact for several hours at 600°C;
sliding motion at a relative speed of 1.46 cm/s under specific load equal to 4.6×10^5 N/m^2;
test stopped after 100 hr of relative motion;
surfaces studied before and after test with an optical microscope and with a Talysurf profilometer (vertical amplification 10^3 to 5×10^4).

3.2.1. When one element of the sliding configuration was ordinary austenitic stainless steel (Types 304, 316, and 321), results were always unsatisfactory.

3.2.2. Nitrided steel behaved unsatisfactorily.

FIG. 13. Z 5 NCDTV 25.15 after Friction with Virium 12 (× 400). Test conditions same as given in Fig. 12. Light work-hardening.

TABLE 2. FRICTION IN SODIUM

Temp, °C	Material Combination		Duration of Immersion at 600°C, hr	Load, kg	Duration Exposed Period, min	Coefficient of Sliding Friction			Weight Variations, mg	
	Rotating	Stationary				Initial	Max	Stabilized	Static Specimen	Rotating Specimen
600	F 130	V 12		41.3	60	0.28	0.28	0.16	+0.8	−2
400	"	"		40.0	60	0.37	0.37	0.25	0.0	−3
200	"	"		39.6	60	0.59	1.08	0.89	+4.2	−30.9
600	"	"		40.3	60	0.50	0.53	0.35	−2.4	+0.8
200	"	"	1	40.0	60	0.55	0.56	0.50	+1.7	−58.6
600	"	"	1	41.3	60	0.45	0.45	0.20	−2.1	+1.1
600	"	"	2½	39.9	60	0.28	0.28	0.25	0.0	+0.9
600	"	"	5	41.7	60	0.73	0.73	0.66	−6.9	+1.7
400	"	"	5	40.3	60	0.23	0.26	0.25	+2.8	+0.4
200	"	"	5	38.6	60	0.59	0.59	0.27	+0.2	+1.1
600	"	"	15	41.0	60	0.56	0.66	0.65	+1.2	−3.3
600	"	"	15	40.5	60	0.09	0.38	0.38	+1.3	−1.5
600	F 130	G 1		41.2	60	0.33	0.37	0.29	−1.3	−60.6
600	"	"	15	38.7	60	0.15	0.32	0.31	−1.1	0.0
600	"	"	15	40	60	0.38	0.73	0.72	−3.0	−0.1
600	F 130	Z N Z		41.2	60	0.39	0.46	0.32	−3.2	−31.3
600	"	"	15	40	60	0.12	0.12	0.10	−0.1	+1.7
600	F 130	FC		39	60	0.72	0.72	0.44	−1.5	−15.5
600	"	"	15	40.3	60	0.18	0.34	0.32	−4.0	+1.5
600	F 130	V 24		41.4	60	0.30	0.30	0.21	−5.4	−38.2
600	"	"	15	40.5	60	0.11	0.11	0.10	−15	+8.3

TABLE 3. FRICTION IN SODIUM AFTER PRIOR IMMERSION OF 10 HR IN SODIUM AT 600°C

Temp, °C	Material Combination		Immersion Duration, hr	Load, kg	Duration Exposed Period, min	Coefficient of Sliding Friction			Weight Variations, mg		Remarks
	Rotating	Stationary				Initial	Max	Stabilized	Static Specimen	Rotating Specimen	
600	F 130	WC	10	39	30	0.28	0.28	0.16	+2.5	−18.2	Leak on turning seal
600	F 130	TIC	10	39	15	0.15			+94.4	+8.3	Great vibrations; porous carbide
600	F 130	V 12	10	40	30	0.17	0.17	0.13	+2.2	+1.5	Leak on turning seal
400	F 130	G 5	10	40	60	0.66	0.34	0.31	−0.2	+4.4	
400	F 130	CK 45	10	40	60	0.43	0.58	0.43	−0.3	+3.4	
400	F 130	WC	10	39.5	60	0.49	0.49	0.28	−1	+2.5	
400	F 130	TiC	10	40	60	0.07	0.07	0.05	−4.6	+2.8	
400	F 130	G 1	10	39	60	0.44	0.37	0.35	−0.4	+1.2	
200	F 130	ZNZ	10	40	60	0.85	0.85	0.72	−6.2	+1.9	
600	G_1	G 5	10	40	60	0.35	0.64	0.56	−0.8	−1.1	
400	G_1	TZM	10	40	60	0.26	0.49	0.40	−12.5	−0.7	

3.2.3. Materials combinations using cobalt-cemented tungsten carbides. Wear induced by friction was not detectable by optical interferometry, but friction coefficients could reach as high as 0.8, for example, pins in Adram A5 (WC + 6% Co) or discs in Adram A6 (WC + 8% Co). The Surfaces of the materials before and after operation are shown on Figures 14, 15, 16, and 17.

3.2.4. Friction of Alloys Hardened with Cobalt. The materials made with Co, Cr, and W are usually flame sprayed onto Types 304 or 316 stainless steels to a thickness of about 1.5 mm. The compositions are reported in the Appendix.

Wear was usually quite low, but detectable. The friction coefficients were highly correlated with the exact composition of the alloys. The presence of boron and silicon usually induced low and no temperature-correlated friction coefficients. Examples are a ring of Type 304 stainless steel covered with Alacrite 554, or a disc of Type 304 stainless steel covered with Alacrite 602.

The time and temperature dependences of the fric-

TABLE 4. FRICTION ENDURANCE TEST

Material pairs:		
A.....	Z5 CNDTV 25.15	TZM
B.....	WC + 7% Co	WC + 7% Co
Test Conditions		
Test duration, hr, in sodium at 400°C; cold trap at 120°C	820	650
Friction duration, hr	100	80
Specific pressure times speed, $kg_f/cm\text{-}s$	160	160
Results		
Specific wear of material A, $cm^3/cm\text{-}kg_f$	3.32×10^{-11}	13×10^{-11}
Specific wear of material B, $cm^3/cm\text{-}kg_f$	1.1×10^{-11}	1.64×10^{-11}
Transversal rugosity, 10^{-3} mm		
Before test } A	0.1	0.09
After test } A	3	2.2
Before test } B	0.01	0.13*
After test } B	0.06	0.55
Stabilized coefficient of sliding friction (friction from short-term test)	0.35	0.40

* Necessary for very plane surface of material.

TABLE 5. FRICTION IN ARGON AT 600°C AFTER PRIOR IMMERSION FOR 15 HR IN SODIUM AT 600°C

Material Combination		Load, kg	Duration Exposed Period, min	Coefficientof Sliding Friction			Weight Variations, mg	
Rotating	Stationary			Initial	Max	Stabilized	Static Specimen	Rotating Specimen
F 130	V 12	39.2	60	0.12	0.12	0.09	−1.2	+2
F 130	ZNZ	40.9	60	0.12	0.12	0.09	−1.7	+0.4
F 130	G 1	40.8	60	0.12	0.41	0.37	+0.2	−2.5
V 12	F C	39	60	0.09	0.09	0.08	+0.7	+1.6

tion coefficients are shown in Figure 18. Surface profiles before and after testing are shown in Figure 19. Apparently some elastic distortion of the specimen, induced by different expansions of steel and Alacrite, occurred. This led to friction contact on the edge of the ring. In spite of this, wear was very low.

3.2.5. Friction of Alloys Hardened with Nickel. These alloys are very attractive in nuclear technology for they are not neutron activated. This is not true for cobalt alloys. Both nickel and cobalt can be deposited on stainless steels by arc spraying or powder projection and fusion. Two sorts of sliding configuration materials were tested: Ni-Mo-Cr-W on Ni-Mo-W and Ni-Cr-B-Si on Ni-Cr-B-Si. Results were very similar in each type of test:

FIG. 14. Surface of a Pin in Adram A5 before Friction Test (× 320).

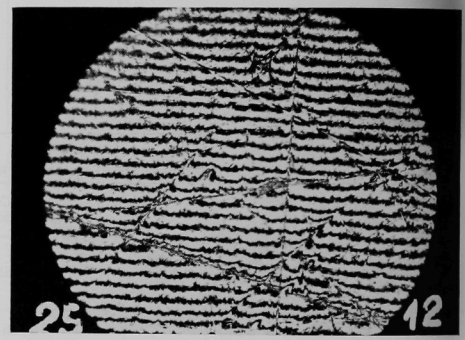

FIG. 15. Surface of a Pin in Adram A5 after Friction Test (× 320).

FIG. 16. Surface of a Disc in Adram A6 before Friction Test.

slight wear and metal transfer leading to slight modification of the surface finish of the sliding materials;

friction coefficient f quite low ($f < 0.4$) and not temperature-correlated.

Surface profiles before and after test are shown in Figure 20. Friction coefficients are shown in Figure 21.

3.2.6. Friction of Nickel-bonded Tungsten Carbides on Nickel Alloys. This sort of configuration leads to slight wear and low friction coefficient. Examples of such systems include a ring of Type 304 stainless steel covered with LW 5 (flame-plating deposition to a thickness of 0.1 mm; for composition see Appendix), and a disc of Type 304 stainless steel covered with Adnic 482 D. The wear evolution of the configuration is shown in time and temperature dependence of the friction coefficient in Figure 23.

FIG. 17. Surface of a Disc in Adram A6 after Friction Test.

3.2.7. Other Tests Showing Unsatisfactory Results. Molybdenum sliding on tungsten carbide (nickel or cobalt bonded) showed large wear of molybdenum. With Al_2O_3 plated on Type 304 stainless steel and sliding on Al_2O_3 plated on Type 304 stainless steel, results were good at 150°C, but Al_2O_3 showed a poor corrosion resistance to liquid sodium at 600°C.

3.3. Results for Journal-bearing Configurations

The tests performed are shown in Table 6. The results confirmed those obtained in plane contact geometry. Wear was classified according to the following criteria:

A: very good surface, no apparent groove;

B: some grooves, depth less than 15 μ;

C: numerous grooves, depth less than 60 μ;

D: surface showing cracks, metal transfer, or grooves more than 60 μ deep.

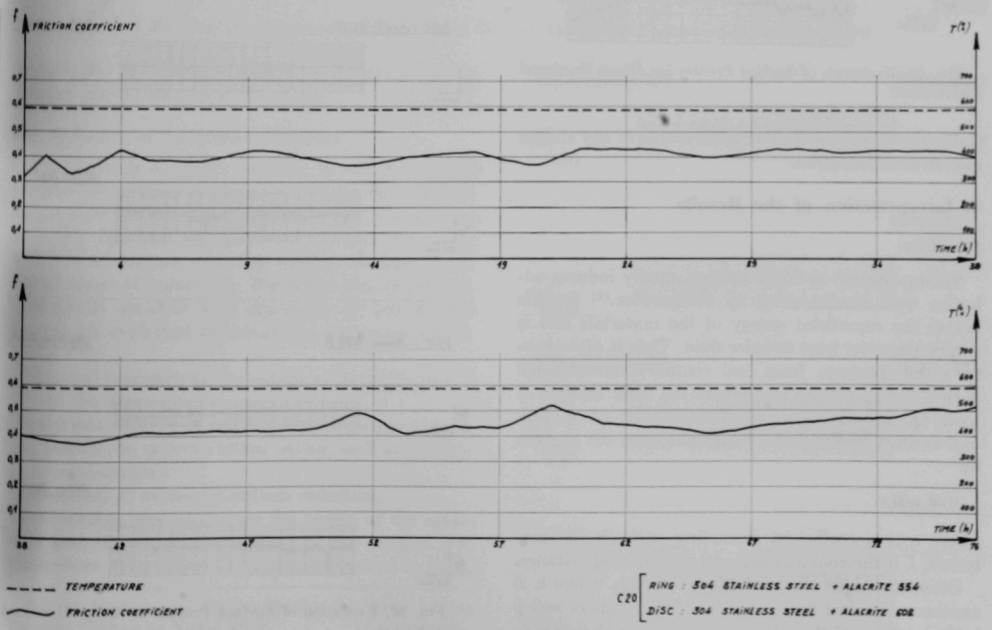

FIG. 18. Time and Temperature Dependence of Friction Coefficient in Sodium of Alloys Hardened with Cobalt.

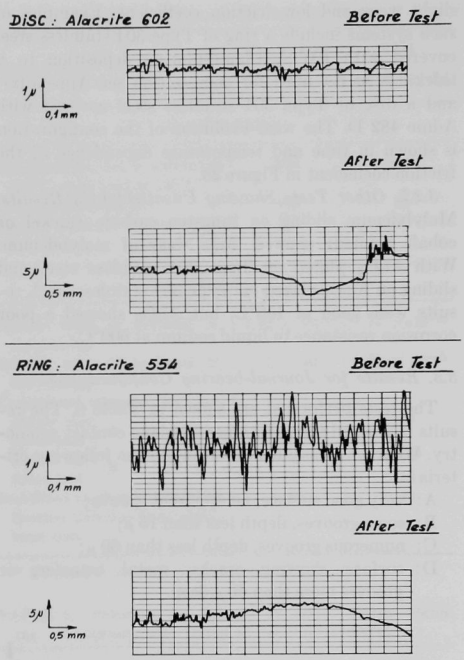

FIG. 19. Evolution of Surface Profiles for Alloys Hardened with Cobalt.

Galling or seizure leading to interruption of any sliding motion never occurred.

4. Interpretation of the Results

4.1. Wear

Sliding contact in liquid sodium usually induces adhesive wear, as described by Rabinowicz.[7] Sodium lowers the superficial energy of the materials and is a very powerful heat transfer fluid. Thus it often protects the specimen from real contact-area extension during sliding motion and lowers the total amount of wear. Quantitative laws of adhesive wear are usually well verified; the volume of material worn out is given by

$$V = c\,L\,x,$$

where c is a coefficient depending only on the materials, L is the contact load, and x the sliding distance.

Often it can be observed that $C = k/p$, where k is another coefficient not correlated with hardness and p is the hardness of the softer material of the sliding configuration. Important hardness differences between the materials of the sliding configuration often lead to abrasive wear. Polishing (CLA $< 0.30\ \mu$ in.) does not lead to wear reduction but to wear increase (extension of real contact areas and sodium effect lowered). The best surface finish seems to be grinding with oil circulation, giving CLA roughness equal to about 10 μin.

4.2. Friction Coefficients

Wear is not closely related to friction coefficients. For example, the friction of nitrided steel against nitrided steel leads to friction coefficients less than 0.40 and yet to a very important total wear; but friction of Adram A6 against Adram A5 gave no detectable wear, yet friction coefficients were as large as 0.8.

Friction coefficients were often in the range 0.25-0.5. They may be explained by sodium contamination of the specimens, providing boundary lubrication by oxides or double-oxide films. Roberts[8] has supposed that films of double oxides, such as Na_2MoO_4, Na_2WO_4, or Na_2CrO_4 existed on the materials containing Cr, W, and Mo. Other double oxides, such as Na_2SiO_4 or $Na_2B_4O_7$, may also be present and could explain the good results shown by "Colmonoy" (Ni-Cr-B-Si) or "Alacrite" (Co-Cr-W-Si-B) alloys. Reduction of the superficial energy of nickel alloys[9] by sodium may

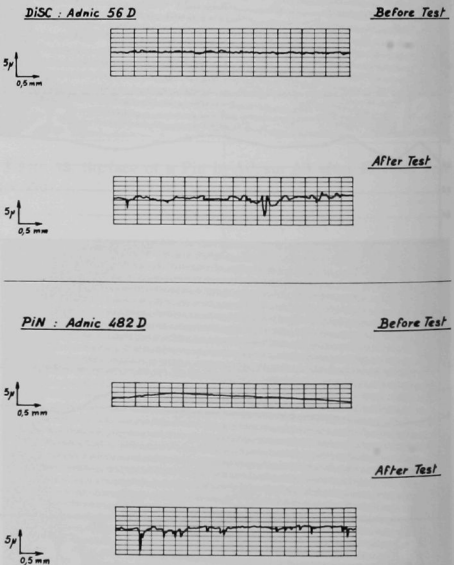

FIG. 20. Evolution of Surface Profiles of Alloys Hardened with Nickel.

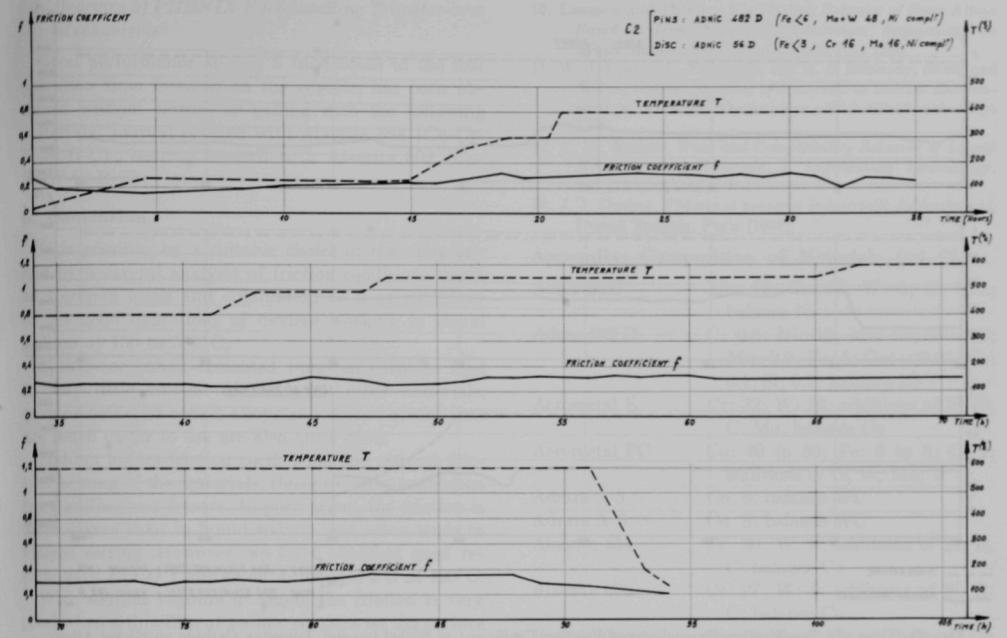

FIG. 21. Time and Temperature Dependence of Friction Coefficients of Alloys Hardened with Nickel.

explain the low friction coefficients observed during relative sliding motion of its alloys.

4.3. Influence of Immersion Duration

Most metals or alloys exposed to air at ambient temperature acquire a thin oxide film on their surface. In the tests that we have conducted, we consider that it is this film and not the metal or the alloy itself which is in contact with the sodium, at least in the initial phase of immersion. The dispersion of the friction results obtained with immersion of less than 10 hr may be explained by one of the following mechanisms:[10]

chemical reduction by the sodium of the oxide formed in the air;

cheminal interaction, causing the formation of compounds (in general, mixed oxides, such as sodium-metal-oxygen);

formation of oxides by sodium reduction.

These mechanisms depend on the nature of the materials and on the oxygen content of the sodium. For immersions longer than 10 hr, there appeared to be no

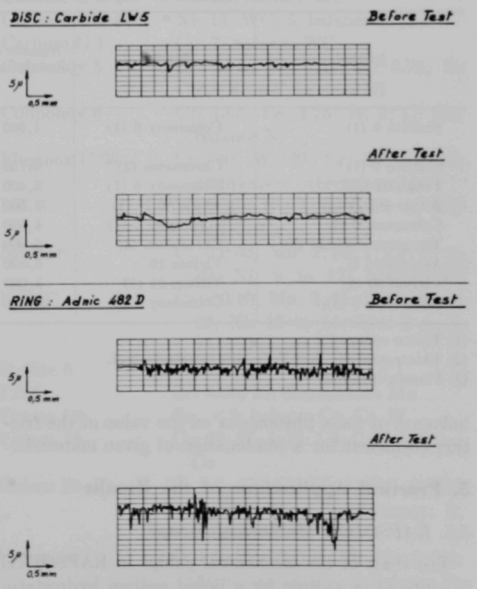

FIG. 22. Evolution of Surface Profiles for Nickel-bonded Tungsten Carbide on Nickel Alloy.

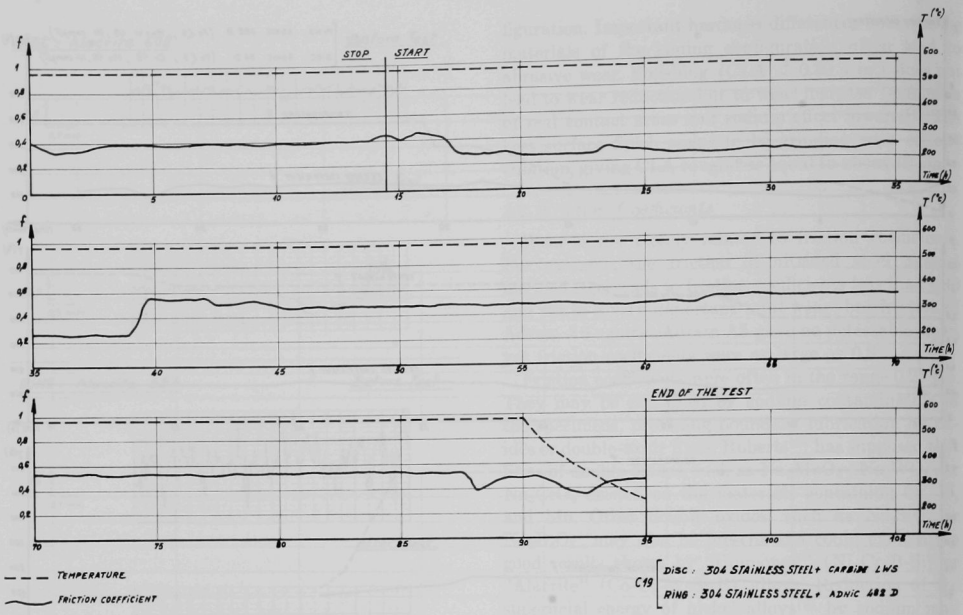

FIG. 23. Time and Temperature Dependence of Friction Coefficient of Nickel-bonded Tungsten Carbide on Nickel Alloy.

TABLE 6. TESTS OF JOURNAL-BEARING COMBINATIONS IN SODIUM

Journal	Bearing	Number of Revolutions	Load, N	Temperature, °C	Friction Coefficient			Wear Notation (see Text)
					Maximum	Mean	Minimum	
Stellite 6 (1)	Colmonoy 6 (1)	4,500	5,000 to 20,000	250–580	0.46	0.42	0.30	A
Stellite 6 (1)	Chromium (2)	6,750	"	"	0.70	0.55	0.35	C
Fluginox C35	Colmonoy 6 (1)	6,400	"	"	0.60	0.45	0.20	C
Adnic 482 D (1)	Adnic 56 D (1)	4,500	"	"	0.40	0.35	0.30	B
Colmonoy 6 (1)	Colmonoy 5 (1)	4,500	"	"	0.60	0.45	0.26	B
Tungsten carbide (3)	Chromium (3)	5,000	"	"	0.52	0.42	0.30	C
Aerometal E	Virium 16	5,000	"	"	0.50	0.39	0.20	B
Virium 30 (1)	Virium 24 (1)	5,000	"	"	0.42	0.35	0.28	B
Colmonoy 6 (1)	Colmonoy 5 (1)	18,000	"	"	0.60	0.35	0.19	B

(1) Flame sprayed
(2) Electroplated } on Type 316 stainless steel.
(3) Plasma-sprayed

influence of these phenomena on the value of the friction coefficient for a combination of given materials.

5. Practical Applications of the Results

5.1. RAPSODIE Mechanical Pumps

The shaft of the mechanical pumps in RAPSODIE is centered in sodium by a liquid sodium hydrostatic bearing. The journal is made with Type 316 stainless steel covered with Colmonoy 6 (see composition in Appendix). The bearing is of Type 316 stainless steel covered with Colmonoy 5 (see composition in Appendix).

The pumps have operated for 15000 hr. Hundreds of starts and stops have been made. Operation has always been quite satisfactory.

5.2. Bearings of PHENIX Fuel-handling Transfer-arm Mechanisms

Good performance, during a time equal to the real operation time foreseen on the reactor, has been obtained without seizure or galling with the following materials: journal covered with Alacrite 554 (Co-Cr-W-Si-B-C); bearing covered with Alacrite 602 (Co-Cr-W-Si-B-C).

6. Conclusion

It is possible, by a suitable choice of the materials and by a careful analysis of friction conditions (such as Hertzian loads and elimination of wear particles) to get good operations of devices working in liquid sodium at 150 to 580°C.

Nickel- or cobalt-cemented tungsten carbides lead to very little amount of wear, but other materials, such as nickel or cobalt alloys and special steels, that are much easier to use are also quite good.

Sodium lowers friction coefficients and reduces friction heating of the materials, thus providing protection from galling and seizure. In pure argon, the friction is more severe than in liquid sodium and often leads to violent seizing. However, we have obtained good results with ELCO 1 bronze on Aerometal FC at 400°C.

With sodium vapours in argon, the friction is very good when a thin film of sodium remains on the surface of the test specimens. In that case, the small quantity of sodium present may be rapidly saturated in oxygen, and the mixed oxides would appear more easily than in a bath of liquid sodium. This may explain identical or better behavior.

BIBLIOGRAPHY

1. J. Birault, *Essais de frottement dans le Sodium Potassium, le Sodium et l'Argon chargé de vapeurs de sodium*, CEA/DRP/EMTR/R. 212 (Jan 1968).
2. B. Morin, *Quelques aspects particuliers du frottement dans le sodium liquide*, CEA/DRP/EMTR/R. 543 (March 1968).
3. B. Blampin, *A Few Studies of Friction in Nuclear Ambience*, EDF/ERNUTH House report HC 042/68-023 (1968).
4. B. Blampin, *Lubrication by CaF_2 in Air and in Hot Carbon Dioxide*, Wear, **11**, (No. 6) (1968).
5. B. Blampin and L. Valibus, *Calcium Fluoride Corrosion in Liquid Sodium in View of Its Use as Lubricating Lining*, EDF/ERNUTH House report HC 042/68-034 (1968).
6. A. J. Baumgartner, *Mechanical Element Design for High Temperature Sodium Environment*, Symposium of lubrication in nuclear applications, Miami, ASME, June 1967.
7. Ernest Rabinowicz, *Friction and Wear of Materials*, John Wiley and Sons, New York (1965).
8. W. H. Roberts, *The Friction and Wear Behavior of Molybdenum-Tungsten-Chromium Alloys in High-Temperature Sodium Environments*, ASLE Trans. **8**, 109–122 (1965).
9. A. W. Thorley and G. Tyzack, *Corrosion Behavior of Steels and Nickel Alloys in High Temperature Sodium*, Proceedings of the Symposium on Alkali Metal Coolants, IAEA, Vienna, 28 Nov–2 Dec 1966.
10. Longson and Thorley, *The Wetting Behavior of Some Alloys Based on Iron, Nickel and Chromium*, Symposium on Alkali Metals, Nottingham, 19–22 July 1966.
11. W. J. Freede, L. Newcomb, and R. S. Kennedy, *Static and Sliding Contact Behavior of Materials in Sodium Environment at Elevated Temperature*, NAA-SR-12 446 (Sept 1967).
12. A. W. Wallace, *Wear and Compatibility Behavior of Liquid Metal Bearing Materials*, J. Lubrication Technology, 466–472 (Oct 1967).
13. J. J. Caubet, *Théorie et pratique industrielle du frottement*, Dunod Technic, Paris (1964).

Appendix: Composition of Materials (wt %)

Adnic 56D	Mo: 16; Cr: 17; W: 5; C: 0.15; balance Ni
Adnic 482 D	C: 0.8; Ni: 48; Mo: 36; W: 8.5; Mn: 0.9; Fe: 5; Cu: <0.01; Cr: 0.1; Si: 0.7; balance Ni
Aerometal E	Cr: 32; W: 13; additions of Si, B, C, Mo; balance Co
Aerometal FC	Co: 40 to 50; Fe: 5 to 8; C: 1; additions of G, W, Mo, V
Adram A 5	Co: 6; balance WC
Adram A 6	Co: 8; balance WC
Alacrite 554	Cr: 30; W: 8; additions of Si, B, C; balance Co
Alacrite 602	Cr: 27; W: 5; additions of Si, B, C; balance Co
Bronze Elco 1	Sn: 7; Pb: 6; Zn: 4; balance Cu
Bronze NS 5	Cr: 2; Ag: 0.5; balance Cu
Carbure G 5	Co: 25; balance WC
Carbure CK 45	Ni: 15; WC: 5, balance Cr_3C_7
Carbure G 1	Co: 7; balance WC
Colmonoy 5	Cr: 11.5; Fe: 4.25; Si: 3.75; B: 2.5; C: 0.8; balance Ni
Colmonoy 6	Cr: 13.5; Fe: 4.75; B: 3; C: 0.8; balance Ni
Fluginox C 35	Co: 40; W: 20; Cr: 20; Ni: 10; additions of other materials
LW 5	WC: 25; Ni: 5; mixture of WC and Cr_3C_2
NS 22 S	C: <0.03; Mn: 2; Si: 1; Cr: 17 to 20; Ni: 9 to 12; balance Fe
NSMC	C: <0.10; Mn: 2; Si: 1; Cr: 16 to 20; Ni: 10 to 14; Mo: 2 to 3; Ti: 5; balance Fe
Stellite 6	Co: 66; Cr: 26; W: 5; C: 1
TZM	Zr: 0.07; Ti: 0.5; balance Mo
Virium 12	Fe: <2; balance Co, Cr. W
Virium 16	Cr: 26; W: 4; Si: 1.8; C: 1; balance Co
Virium 24	C: 0.2; Cr: 15; W: 4; Co: 0; Fe: 2; Do: 16; otherelements: 2, balance Ni
Virium 30	C: 1.5; Cr: 15; Co: 16; Mo: 8; Ni: 20; other elements: 2; balance Fe

ZR NCDTV 25-15 (F 130)	C: 0.05; Cr: 15; Ni: 25; additions of Mo, V, Ti; balance Fe
ZNZ	Cr: 15 to 35; Mo: 2 to 20; W: 2 to 20; additions of Nb, Ta, Zr, Ni; balance Fe

Discussion

Mr. Horton (AEC): Are your results good enough now so you are not going to do any more wear-testing or friction-testing in sodium? Are you going to continue this type of testing or are you satisfied now that you have good bearings?

Mr. Beaufrere: We will continue our long-duration tests. We have many results for short durations like 10 or 20 hr, and we think that is not enough. We now have a machine to make very long-duration tests. We have selected the materials and will continue long-duration tests for wear measurement and surface destruction.

Mr. DeVan (Chairman): I have a question on the tungsten carbide cobalt-bonded materials. Have you been looking at the problem of attaching these materials to a substrate to be able to use them as a bearing? How do you plan to use these things—as solid blocks or as attached to a substrate?

Mr. Beaufrere: Flame-sprayed, but we have also used them as solid materials. We have obtained better results with solid materials than with flame-sprayed materials.

Mr. DeVan: If you use the solid, though, you will have to come up with a method of attaching it to something.

Mr. Beaufrere: There are problems of sealing because of different coefficients of thermal expansion. Brazing or welding is impossible. It is a very difficult problem. In some applications, such as fuel-element mechanisms, it is possible to use them as small parts.

Test Program for Components in Liquid Sodium

E. Arend

Gradel S.A.
Steinfort, Luxembourg

AND

H. Wagener

Arbed S.A.
Dommeldange, Luxembourg

(PRESENTED BY H. WAGENER)

Introduction

A research program is being conducted by the Luxembourg industry group LUXATOM to develop techniques for dismantling irradiated fast power reactor fuel assemblies and recover fuel pins.

This work is performed under contract with Euratom and forms part of the studies on a short fuel-reprocessing cycle. The aim of the program is to design a complete dismantling unit suitable for a 1000-MWe power reactor. In order to shorten the cooling time of the assemblies, the dismantling should be performed in a liquid sodium pool located in a special-purpose cell at the power-plant site.

This design calls for an appreciable number of mechanisms working immersed in liquid sodium at a reference temperature of 200°C for a prolonged time.

A component test program will be started before the end of this year in order to set up specifications for the mechanisms and to prove their feasibility.

Mechanism Test Rig

The static test rig is fitted with two test vessels, each having a useful capacity of 35 liters of sodium, and both mounted in an argon-filled glovebox. Test sections will be adapted to exchangeable vessel lids or to flanged ports of the vessel wall. Maximum temperature in the test vessels will be 300°C.

The test vessels are connected to a common sodium supply and purification system, consisting of a melting vessel, a purification vessel, and a storage vessel. Sodium movements are effected by differential pressure applied to the argon cover gas. The purification tank is used as a dump tank to which the test vessels can be drained by gravity. The maximum sodium load of the system is about 100 kg.

Purification is done by cold-trapping in the purification vessel and by the use of filters in the connecting piping. Discontinuous level control by vertical thermocouple thimbles is provided for on each vessel.

Test Program

The program, scheduled for a duration of about two years, intends to test mechanism components under conditions similar to those prevailing in a dismantling sodium pool and to define their design criteria.

1. Extensive tests of roller and journal bearings at slow speeds will help to define and solve material and clearance problems. A recirculating ball screw device will be included.

2. Spur and bevel gears are to be tried out under various conditions in order to set up speed and torque limits for different surface materials, and machining and fitting tolerances.

3. Testing of rotating shaft seals will examine the possibility of sodium to argon penetrations used for immersed motive components. A particular example of this application will be a membrane-gap magnetic coupling.

4. A bellows-sealed immersed cylinder operated by argon for small linear motions will be tested for bellows endurance, and for cylinder and piston material combinations.

5. Several position-sensing devices will be tried for feasibility and reliability, such as a bellows-sealed microswitch, a gas jet device, and an ultrasonic probe.

Conclusion

The under-sodium testing of mechanical components in the lower-temperature region, carried out by LUXATOM, is thought to be of general interest for the promotion of equipments working immersed in liquid alkali metals, despite the modesty of its scope.

Acknowledgments

This work is performed partially under the auspices of Euratom and partially under sponsorship of the Luxembourg Government.

Discussion

Mr. Zitek (ComEd): Are you saying that you are going to dismantle the fuel assemblies under sodium?

I am wondering how you are planning to do this. You must have some portion of the assembly out of the sodium or is this all going to be done remotely?

Mr. Wagener: As I said, this is a study of a rather long-term goal. At the moment we are thinking about milling or sawing the hex can inside the sodium pool. I must say, temperatures considered are rather low, about 400°F, and we plan to make tests with milling cutters at this temperature inside the sodium. The big problem naturally in this case is sucking off the cuttings, etc., formed by the operation, so as not to contaminate the sodium pool by continued milling. The problem that we consider is that rather a short time after reactor shutdown, the power of one fuel assembly is about 40 kW for a big power reactor. In order to be sure that under all circumstances the heat is removed, we rely only on conduction and natural convection for heat removal. That is why consideration is given to doing the work in the liquid sodium pool.

Mr. Zitek: Will this reprocessing be on the power site?

Mr. Wagener: The fuel assembly such as that having about 40-kW heat output could not be handled outside the sodium or even transported. But if you have individual fuel pins at the same moment, they can be brought out to the argon cover gas and the heat dissipated, by radiation and natural cooling, without getting too high surface temperatures. The idea is to cut up the fuel assembly after a rather short time to get to rows of pins. In several projects rows of pins are attached by ribs at their foot, and the object is to get these rows of pins out of the sodium, clean them, and transport them at a rather short time after reactor shutdown to a reprocessing facility.

Mr. Zitek: It will be a pyrometallurgical reprocessing?

Mr. Wagener: Yes, or a fluoridization process.

Mr. DeVan (Chairman): There are some summary conclusions that can be drawn out of today's session. I didn't want to do it earlier because I didn't know just how we would end up in time, but I think particularly in the investigations of mechanical properties in sodium, it is interesting to see where we are. There are two classes of problems to worry about insofar as mechanical properties are concerned, and I tend to think about them as nonattritive corrosion problems, if you will, and attritive corrosion problems. By attritive, I mean something is taken away from the material by sodium. Then, in the other class of nonattritive mechanisms, I would include the lowering of cohesive forces in the material, the classic stress corrosion-cracking problem in liquid metals, the problem of sodium invasion of the material, and carbon and/or nitrogen invasion of the material from sodium. These are the nonattritive mechanisms, and I think we are at a stage today where we can certainly rule out stress-corrosion cracking as much of a factor in the systems that we are talking about. Sodium invasion until recently was laid to rest. Apparently under some circumstances there is an ingress of sodium into the material—we don't understand exactly why this is. Some people believe that it is associated with the attack of carbides of the material, but it seems to be a rare happening rather than a routine happening, and I don't believe it has turned up yet in any of the mechanical properties. That leaves us, you might say, with carbon-nitrogen invasion in nonattritive mechanisms as the area that seems to be causing us the most concern and where we probably still need to do a considerable amount of work.

Attritive mechanisms can be categorized by thinking about the gross effects of wall thinning and intergranular grooving. These seem to be of minimal importance in sodium. I suppose there are conditions where mass-transfer rates get up above the one mil per year level, but normally we are talking a mil per year or less, and wall thinning itself has not been too important to us. The other aspect of this though is the selective diffusion problem which Ed Zebroski this morning classified as the metabolism change. I think that is a very good simile myself—sort of like myself—I feel like I still look the same but because of a lot of chemical changes I can't perform as effectively. And, that's about what happens to these steels—as a result of losing carbon, nitrogen, manganese, chromium, nickel. I might emphasize that at above 1200°F or 650°C these are quite considerable amounts. These don't have a tremendous effect on the mass of the material, but they certainly affect its chemistry and its mechanical properties. And I must say that this is one area in the mechanical-property studies that we haven't gotten to yet. We still aren't running tests in which we preferentially take away these constituents, that is, at high Δt's and high temperatures. I think that we are about ready to start some of these tests, but I think we should emphasize that we are not there yet; certainly these conditions are going to lead to a deterioration of properties. Ed Zebroski preached this point too today, and I must echo his sentiments. When you look at concentration gradients in these materials it just has to have an effect on mechanical properties.

The other aspects of the talks today which I thought were particularly interesting were that carburization in the stainless steel is a classic diffusion problem and it is a very interesting one to study. I was interested in Mr. Feder's remarks about arrival rate. I missed that argument completely, and I must say it seems incredible to me that arrival rate can any longer be

considered important in the carburization of stainless steels in these systems. Maybe I am missing something, but it seems to be totally a problem of either the precipitation-carbide reaction controlling, in which case it is mass transfer with chemical reaction, or it is not controlling, in which case it is just homogeneous diffusion. I thought that looking at it from the Darken model is long overdue and certainly, even though the data that Dr. Kolodney presented are quite preliminary, they bear looking into. It seems to me it would be a very reasonable model. The point that Ralph Hiltz made was "The chromium activity is equally as important as the carbon activity in the materials insofar as the precipitation of the carbide is concerned." The last point on bearing materials I think we have known for a long time—those of us who have been working at still higher temperatures with sodium—that the hard-on-hard bearing materials give us a very good system as far as friction, self-welding, and what have you is concerned. The problem is with the use of these materials in massive forms—how do you attach them, how you keep them from cracking up?

Mr. Zitek: I have heard a number of times now that we will not have to worry about stress-corrosion cracking. Do you feel that we have had enough operating test time to know whether or not we will be faced with something which is similar to stress-corrosion cracking in water systems? You mentioned the question of whether the ferrite content of austenitic stainless steel is going to play a part somewhere. Now, I don't profess to be a specialist in sodium technology, but I can readily see that these tests have not been run long enough to say really we do not have to worry about something similar to stress-corrosion cracking in sodium systems.

Mr. DeVan: I can't dispute that; all I can say is that the nucleation time is darn long if there is one.

Mr. Zitek: When you say long, how long?

Mr. DeVan: Well, I guess the longest-term systems have been the loops at General Electric which have run for a total time of about 3 years.

Mr. Zitek: We didn't run into our problem at Dresden for maybe four or five years.

Mr. DeVan: That's a good point. I also should emphasize that there could very definitely be a caustic-embrittlement problem in sodium. This is another area in which trouble can occur.

Mr. Zitek: Well, what do you do? Is there something you are proposing?

Mr. DeVan: There are studies on caustic embrittlement for sure; stress-corrosion cracking is an automatic outfeed of the creep tests that are going on, I think.

Mr. Zitek: I am surprised to learn that they are seeing chloride in the sodium. Does anyone know what concentration?

Mr. DeVan: 15 ppm was a number I have heard. I must admit I never worried about it.

Mr. Pfahler (LMEC): This is somewhat off the topic but relates to the subject. One area that hasn't been covered and which is very important to liquid metal systems is thermal fatigue. In at least the data that I am aware of there is a great lack, and I would like to see this covered somewhat.

Mr. DeVan: I am also surprised that somebody hasn't jumped up and said yes, and what about bellows. I tend somehow to feel that the bellows problem we still have with us is not really a mechanical-properties problem, but is sort of circumstantial and not really proved.

Mr. Greenberg (ANL): We agree with Jack about the effect of changing chemical concentration on mechanical properties. There is essentially a two-part program going on at Argonne. One is at relatively low temperatures. There are hydraulically stressed samples (they are close to the core) in EBR-II which are subjected to the temperature gradient of the reactor. At higher temperatures we have a loop very close to operation to check out just these things for vanadium alloys and presumably also for stainless steel alloys.

SESSIONS ON SODIUM TECHNOLOGY

SESSION ST-IIIA

Friday Morning, November 8, 1968

Chairman: J. R. Weeks
Brookhaven National Laboratory

Secretary: M. Ader
Argonne National Laboratory

Mass Transport and Corrosion of Stainless Steels in Flowing Sodium Systems at 1300°F*

PRODYOT ROY, GARY P. WOZADLO, AND FRANK A. COMPRELLI

General Electric Company
Advanced Products Operation
Sunnyvale, California

(PRESENTED BY P. ROY)

I. Introduction

Mass transport and corrosion of austenitic stainless steels in flowing sodium systems have been the subject of several investigations in the United States, the United Kingdom, and elsewhere. Broad correlations between materials behavior and experimental parameters have been observed, and all studies are in general agreement under nonlimiting conditions. Data are still sparse at conditions of time and temperature which limit acceptability for critical application.

In order to explore the limits of performance at potential hot-spot conditions, extended corrosion studies have been conducted at 1300°F involving the effects of alloy compositions and of heat transfer. A more detailed evaluation of the effects of velocity and downstream was also made. These studies were conducted in flowing sodium for periods up to 3000 hr with oxygen levels of less than 10 ppm.

Four alloys were included in this study: Types 304, 316, and 347 stainless steel, and Incoloy-800. Especially significant observations were made of the type and extent of microstructural changes induced in these alloys as a consequence of sodium exposure. These changes should result in appreciable degradation in mechanical properties at times $\geqslant$3000 hr at 1300°F. In addition to corrosion rates, the pattern of deposition of corrosion products in the low-temperature regions was determined, showing marked differences in the behavior of each alloying element.

II. Experimental Results

The alloys under study included Types 316, 347, 304, and Incoloy-800, with primary emphasis on Type 316. After sodium exposure, the samples were removed from the loop (see Figure 1) into an argon atmosphere, rinsed with alcohol and water to remove all accessible sodium, and subsequently weighed and microscopically examined.

The nominal loop-operating conditions for the corrosion experiments included exposures up to 3000 hr, a peak sodium temperature of 1300°F, a minimum of 800°F, and an oxygen content of less than 10 ppm, based on a plugging temperature (T_p) of 260–280°F.

In order to analyze and interpret the results of these experiments, a set of average exposure parameters was established for each specimen. Temperatures in various sections of the experimental facility were directly monitored and recorded. The recording of exposure time, however, did not commence until the system temperatures were within a few percent of the design values. Therefore, it was possible to accumulate appreciable exposure at temperatures slightly below the desired limits, especially during loop startup and periods of component difficulties. All such exposure at temperatures other than the design value was not considered in the corrosion correlation. Periodic chemical analysis of the sodium for oxygen showed variations between 4 and 8 ppm in any given experiment, consistent with a plugging temperature below 280°F. A limit on the precision of the corrosion rates is attributed to the variation in average oxygen concentration within and between experiments.

1. Effect of Velocity and Downstream on Corrosion Rate

The corrosion rate of Type 316 stainless steel at 1300°F is shown in Figure 2 as a function of velocity at several downstream† conditions. In the velocity range up to about 15 fps, the dependence of corrosion rate on velocity is approximately linear, in accordance with previous results. With increasing velocity, the deviation from linearity becomes more pronounced. For comparative purposes, available United Kingdom (U.K.) data at 1200°F[1] are included in Figure 2; they show similar trends of alloy corrosion with increasing velocity.

The effect of sodium velocity on corrosion rate suggests that the rate-determining step in the corrosion process is velocity-dependent in the low-velocity

* Work performed under the auspices of the U. S. Atomic Energy Commission under Contract AT(04-3)-189, Project Agreement 15.

† The term "downstream" is used to signify that the quantity of corrosion product in the sodium has increased an incremental amount, over a finite distance along the loop, corresponding to the driving force for corrosion at the point.

range. These data support the hypothesis[2] that up to approximately 15 fps, the diffusion of solutes and/or corrosion products across the liquid boundary layer is rate-determining. At higher velocities, the liquid boundary layer diminishes sufficiently so that a surface reaction rate becomes the rate-controlling step and is independent of velocity.

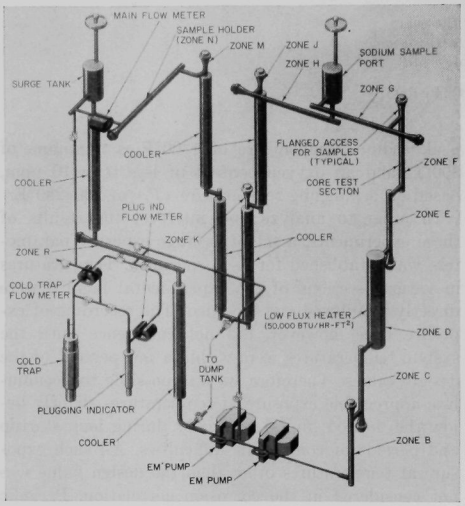

FIG. 1. Sodium Mass Transfer Corrosion Loop.

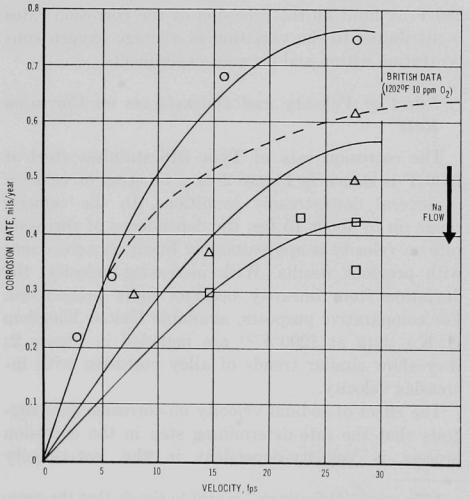

FIG. 2. Corrosion Rate at 1300°F as a Function of Sodium Velocity at an Oxygen Level of Less than 10 ppm. The influence of downstream (saturation) upon this correlation is also shown.

The corrosion and selective leaching of alloy constituents in flowing sodium are expected to be complex functions of temperature, oxygen, concentration, velocity, and various reaction-rate constants. Previous work[1, 3] indicates that the corrosion rate of austenitic stainless steel strongly depends upon the oxygen level in sodium. It was also observed[1] that the corrosion rate of high-nickel alloys, such as Nimonic-80A (75% Ni), does not depend on the oxygen concentration in sodium.

The above observations suggest that the removal of the chromium and iron from stainless steel involves a chemical reaction with oxygen at the surface. On the other hand, nickel probably corrodes by an atomic dissolution process. Since each of these processes (see Figure 3) involves several steps, the effect of velocity on the corrosion rates of various alloys and alloy constituents will be different, depending on the predominant corrosion mechanism.

The corresponding effect of downstream on corrosion rate at 1300°F is shown in Figure 4 at several velocity levels. The reduction in corrosion rate with increasing downstream can be attributed to the increase in the chemical activities of solute (corrosion products) elements in sodium as they are removed from the alloy steel.

2. Effect of Composition on Corrosion Rates

For comparative purposes, corrosion tests of Types 304, 316, and 347 stainless steel and of Incoloy-800 were performed. The alloys were positioned in a parallel flow channel arrangement so that comparable downstream or attenuation was present. The tests were conducted at 1300°F with a sodium velocity of 17 fps, and oxygen levels of less than 10 ppm. The results, shown in Figure 5, show that the corrosion rate for Incoloy-800 (32 Ni, 21 Cr, Fe) is considerably higher than for the three 300 series alloys. This observation is in qualitative agreement with UK[1] and Brookhaven (BNL)[4] data. The initial corrosion rates which were measured for these alloys under comparable exposure conditions were: 0.99 mil/yr for Incoloy-800, 0.51 mil/yr for Type 347, 0.44 mil/yr for Type 304, and 0.29 mil/yr for Type 316.

The higher corrosion rate of the high-nickel alloy is believed to be due to a faster selective dissolution rate for nickel. Since each of these alloys has approximately the same chromium level (18–21%), the contribution of this element to the weight loss should be fixed for a given temperature, oxygen concentration, and velocity condition. Therefore, the corrosion rate

of these alloys should be directly related to nickel content, and the atomic dissolution rate of the nickel should be the rate-controlling step. This analysis implies a balance between the mechanisms contributing to the overall corrosion. This balance is defined by and is characteristic of the temperature, velocity, and oxygen content through their influence in determining the rate-controlling step in the corrosion process.

For the conditions of this experiment, it appears that the dissolution of nickel would adjust the corrosion rate by some increment over the base rate associated with the Cr/Fe corrosion process. On the basis of this argument, the corrosion rate for Type 316 should be slightly greater than that for Types 304 and 347 because of the higher nickel content (13% vs. 9%). This apparent inconsistency is under further evaluation.

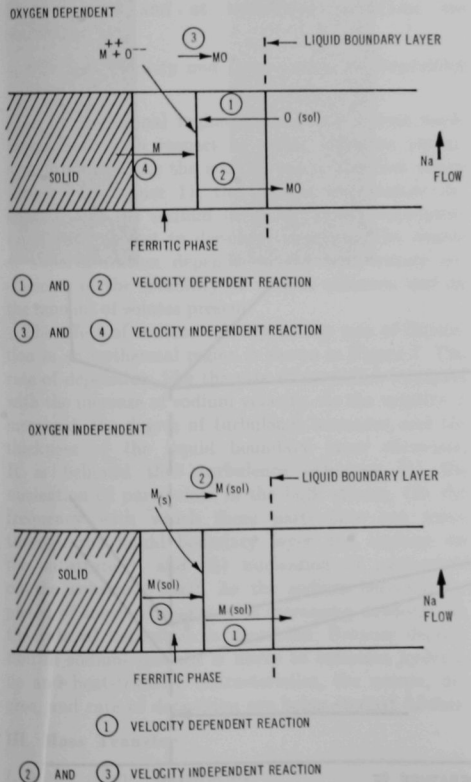

FIG. 3. Mechanisms Which Are Believed to be Active in the Process of Corrosion in Sodium at 1300°F.

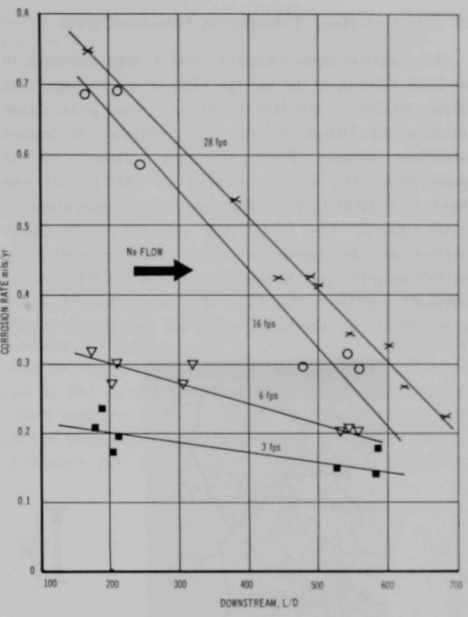

FIG. 4. The Effect of Downstream (Sodium Saturation) on Corrosion Rate over a Range of Velocities Is Shown for Exposure at 1300°F to Sodium with Less than 10 ppm Oxygen.

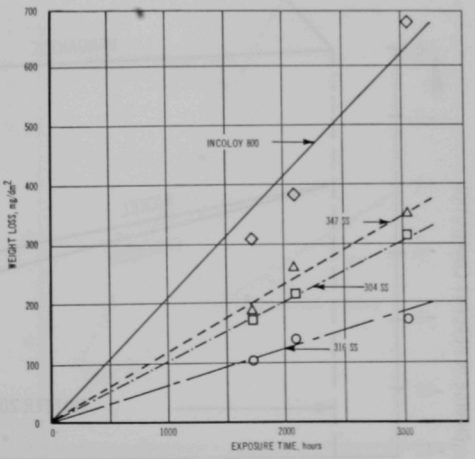

FIG. 5. Corrosion Behavior of Annealed LMFBR Materials in Sodium (Types 304, 316, 347, and Incoloy 800) at 1300°F with Less than 10 ppm Oxygen and a Velocity of 17 fps.

3. Effect of Heat Transfer on Corrosion Rate

An electron-bombardment heater was exposed to sodium flowing at 15 fps for 1725 hr at average heat fluxes of 0.8×10^6 Btu/ft^2-hr and local peak fluxes of 3×10^6 Btu/ft^2-hr to study corrosion of heated stainless surfaces. The heater had a 10-in. emitting zone which the sodium entered at 1000°F and was heated to 1200°F, with short periods of operation at 1100–1300°F. The Type 316 stainless steel anode served as the specimen which was evaluated by metallography and X-ray fluorescence (XRF) of the exposed surface. The basis for evaluation was by comparison to corrosion rates of specimens which corroded under isothermal conditions because weight-change measurements were not possible.

The results of the evaluation are shown in Figure 6. The linear temperature gradient (ΔT) of 200°F along the heated length produced a bulk microstructural change with the formation and growth of the ferritic surface phase. The bulk microstructural change followed the temperature along the emitter zone, and the depth of the ferritic surface phase increased with increasing corrosion rate and increasing temperature, as would be expected. The surface XRF results confirm the increasing corrosion rate by showing increasing losses of chromium, nickel, and manganese with increasing temperature.

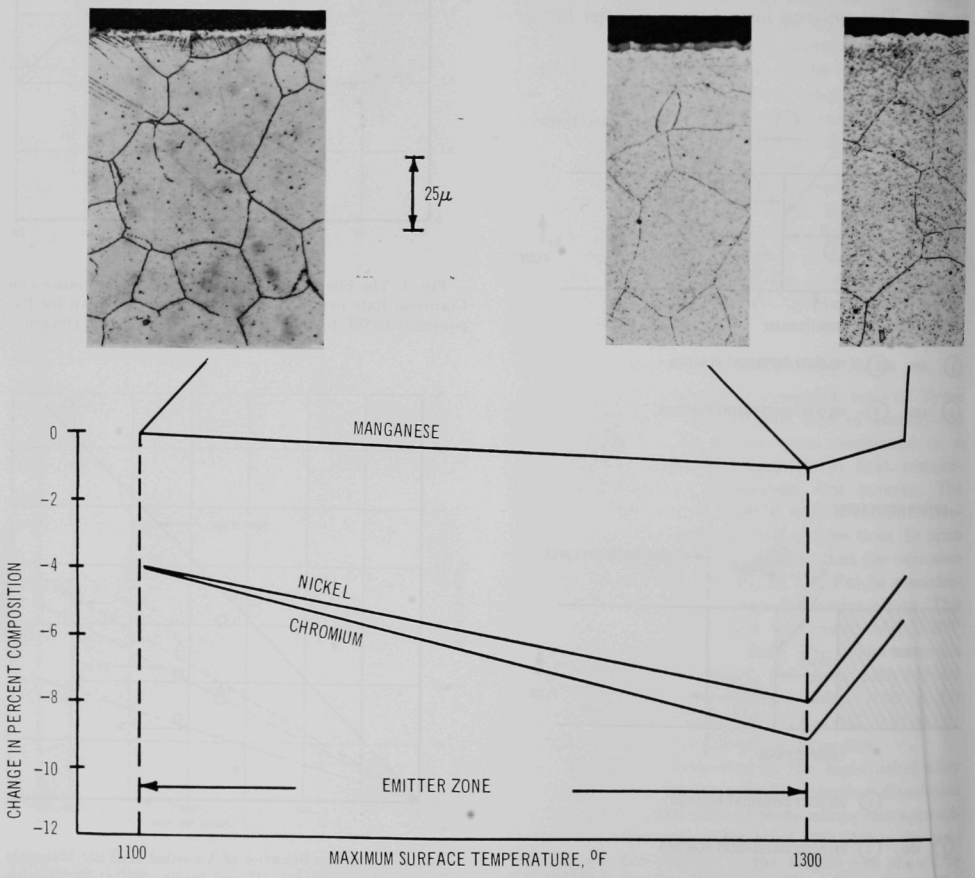

FIG. 6. The Effect of Heat Transfer upon the Corrosion Behavior of Type 316 Stainless Steel after 1700 Hr in Sodium with Less than 10 ppm Oxygen.

The metallographic examination of an isothermal area of the anode immediately downstream of the maximum temperature region showed essentially no ferritic surface phase, which was confirmed by the fluorescence results.

The proper basis of comparison between heat transfer and isothermal effects is equal metal temperature and loop position (degree of sodium saturation). At the peak heat fluxes of 3×10^6 Btu/ft^2-hr, flowing sodium at 1200°F corresponds to a metal temperature of approximately 1275°F. The comparison of the anode metallography and fluorescence data at 1275°F with those of the isothermal exposures at 1300°F (furthest upstream position) shows equivalent corrosion effects. Based upon these comparisons, the effect of heat transfer on corrosion rate appears to be one of increased metal temperature. At the same metal temperature, the corrosion rates under heat transfer and at isothermal conditions are equivalent.

4. Effect of Velocity and Downstream on Deposition Rate

In an isothermal region, the flowing sodium tends to saturate with respect to solute elements (corrosion products). As the sodium enters the first cooler (Zone J in Figure 1), the sodium temperature decreases, and the sodium becomes slightly supersaturated with respect to dissolved elements. The degree of supersaturation depends on the temperature coefficients of the solubility of various elements and on the amount of solutes present.

The effect of sodium velocity on the rate of deposition in an isothermal region is shown in Figure 7. The rate of deposition, like the rate of corrosion, increases with the increase of sodium velocity. As the velocity is increased, the degree of turbulence increases, and the thickness of the liquid boundary layer decreases. It is believed that turbulence enhances (1) the nucleation of particulate in the bulk stream, (2) the frequency with which these particulate can move through the liquid boundary layer and impinge on the substrate,[5] and (3) nucleation of particulate on the substrate itself. As the sodium becomes depleted of solute elements with increasing downstream, the rate of deposition is decreased. Because deposition in sodium systems is likely to influence hydraulic and heat-transfer characteristics, the nature, degree, and rate of deposition are being studied further.

III. Mass Transfer

1. Major Alloy Constituents

The movement of various alloying elements around the experimental loop was monitored by the X-ray fluorescence analysis of surface compositions of the hot- and cold-leg samples from all experiments.

After weighing, the samples were sectioned for fluorescence analysis on the exposed surface. Representative results are shown in Figures 8 and 9. The data show the change of the elemental compositions at the surface after exposure at various positions and temperature distributions in the loop. For comparative purposes, the total weight change is also shown.

In all experiments, selective leaching of chromium, nickel, and manganese was observed; this increased with the increase in total corrosion. Results show that the nature of the relative movements of alloy constituents in stainless steel will be sensitive to sodium velocity, oxygen level, and temperature. In Figures 8 and 9, the corrosion and deposition of various elements patterns for the two separate experiments are shown. Although the relative change in composition of chromium and nickel at the surface was radically

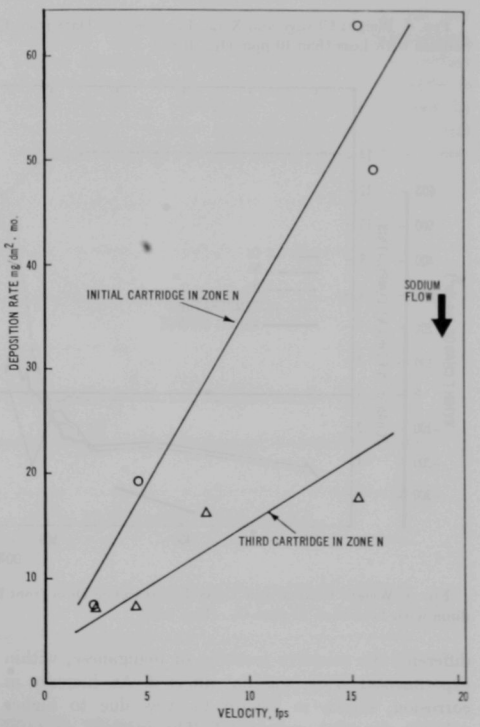

FIG. 7. The Rate of Deposition Is Shown as a Function of Velocity at Several Downstream Positions at 800°F.

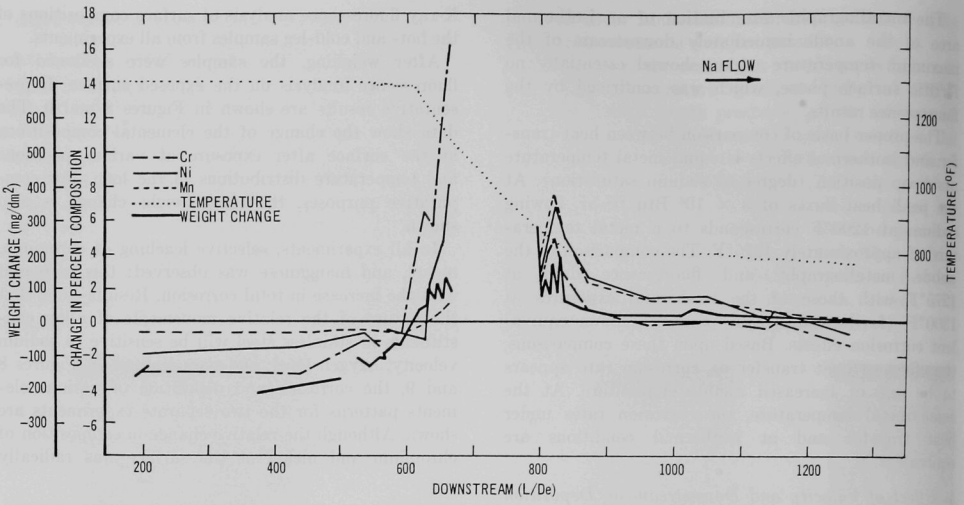

FIG. 8. Weight Change and X-ray Fluorescence Data from Exposed Surface as a Function of Position after 3000-hr Exposure to Sodium with Less than 10 ppm O_2. (Run 8-1.)

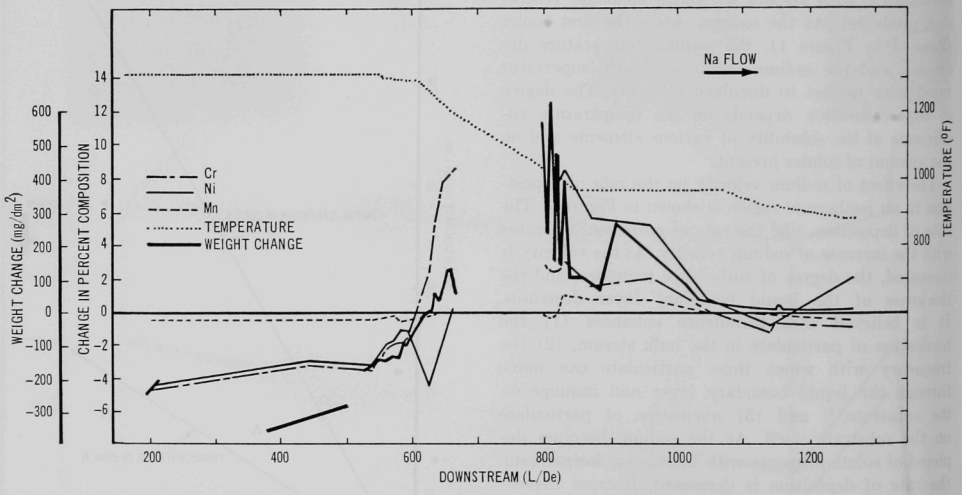

FIG. 9. Weight Change and X-ray Fluorescence Data from Exposed Surfaces as a Loop Position after 3000-hr Exposure to Sodium with Less than 10 ppm O_2. (Run 8-2.)

different, the selective leaching of manganese, within experimental error, was not affected. An increase in corrosion, shown in Figure 13, was due to higher velocity for that experiment. The increase in total corrosion for the high-velocity run resulted in an increase in nickel and chromium movement, but the increase of nickel movement was greater than that of chromium. Therefore, nickel loss due to corrosion is much more sensitive to velocity than chromium loss at equivalent oxygen contents.

2. Carbon Transport

When austenitic and ferritic steels are bridged by sodium, carbon is transferred from the ferritic to the austenitic steel. This is due to the fact that the activity coefficient of carbon is considerably higher in ferritic steels than in the austenitic steels, which contain higher percentages of chromium.[6] The carbon will, therefore, be transferred to the austenitic stainless steel in an attempt to bring the carbon activities into equilibrium.[7] Since the activity coefficient for carbon in austenitic steel increases with decrease in temperature,[6] one should expect from equilibrium considerations that the carbon would be transferred from the cold to the hot leg in an all-austenitic steel system.

The direction of carbon transport, observed in these all-austenitic systems, is seemingly contrary to the equilibrium considerations mentioned above. Carbon losses as high as 40% were measured from austenitic alloys at the highest temperature regions (see Figure 10). As the sodium flow continued downstream into regions of lower temperature, increases in carbon level were measured.

This direction of carbon transport suggests that, in a sodium-cooled reactor, the Intermediate Heat Exchanger (IHX) may carburize, whereas the core will decarburize. Carburization of the IHX tubes can change the mechanical properties considerably, in particular the ductility. The extent of the change is of importance to the design and the expected life of this component. Thus, carbon-transport effects on the properties of core and IHX materials warrant increased study.

IV. Compositional and Microstructural Changes

In general, three types of microstructural response have been observed in flowing sodium at 1300°F: (1) formation of a ferritic phase at the surface, (2) development of a zone adjacent to the surface in which the nature of the precipitation depends upon the composition gradients present, in particular carbon, and (3) severe depletion of selected elements in localized regions at the surface, in particular at the grain boundaries. The type of response and the extent to which it occurs are a function of corrosion rate and alloy composition.

The effects of flowing sodium after 3000 hr at 1300°F on the microstructure of Type 316 stainless steel are shown in Figure 11. In the initial test cartridge, FA (smallest downstream attenuation, highest corrosion rate), Type 316 forms a surface phase ~¼ mil thick and a zone of 4-mil depth in which the grain boundaries are not delineated by characteristic carbide precipitation as is the bulk material. Throughout this zone, large, blocky par-

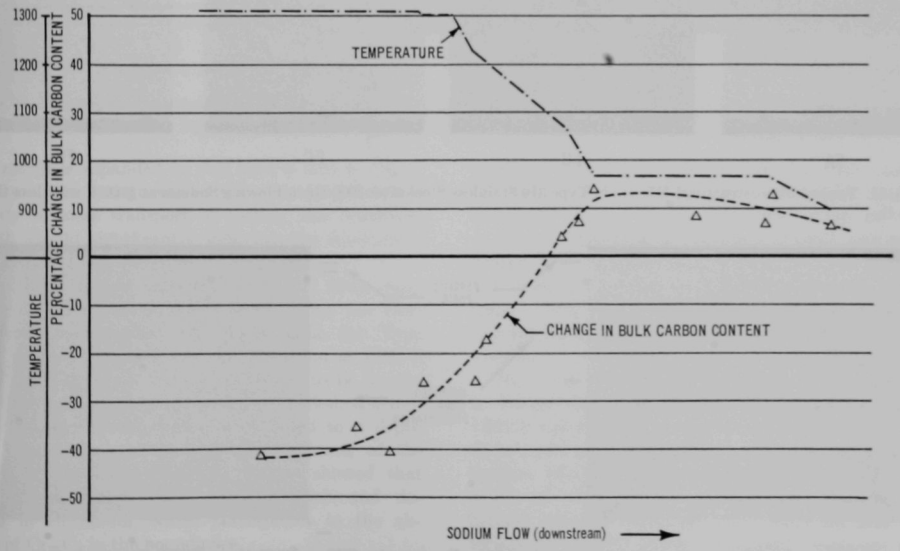

FIG. 10. Change in Bulk Carbon Content of Alloy Specimens as a Function of Downstream and Temperature.

ticles of sigma phase are common, both in the matrix and at the former grain boundaries. A Laves phase (Fe_2Mo) was also identified.

As the sodium progresses downstream, FA to FH in Figure 11, the surface phase diminishes and finally disappears, but the blocky sigma particles and the absence of grain-boundary carbides persist to a depth of about 4 mils.

The occurrence of sigma phase in Type 316 stainless steel has been previously observed. However, the fact that this precipitation occurred concurrent with the disappearance of grain-boundary carbides and the fact that the reference control specimens of this material (same time at temperature, but not in sodium) showed no sigma formation suggest that this microstructural modification is a direct consequence of the surface reaction. Of particular importance are nickel and carbon, both austenite formers, and, therefore, sigma suppressors. Loss of nickel from the surface has been discussed previously. Bulk carbon analysis of Type 316 exposed to 1300°F sodium has showed a loss as high as 79%. Therefore, carbon loss was rapid at the highest temperatures of these experiments. A graphic illustration of this effect upon the microstructure of Type 316 is shown in Figure 12. After 1750 hr in sodium at 1300°F, a surface phase, ¼ mil in depth, has been established along with a subsurface zone, 3 mils in depth, in which the large, blocky sigma particles have replaced the normal thermally activated precipitation at the grain boundaries. After continued exposure for 3000 hr, the surface phase remains at ¼ mil in depth, but the subsur-

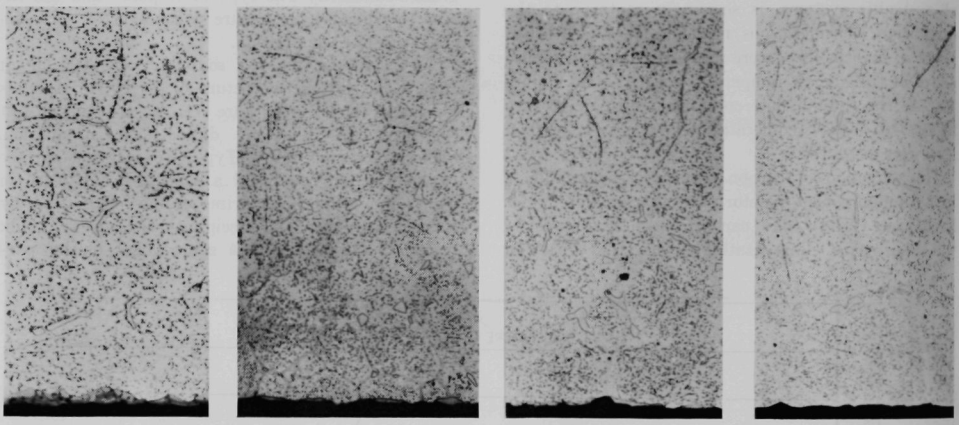

FIG. 11. Typical Microstructural Effects in Type 316 Stainless Steel after 3000 Hr in Flowing Sodium at 1300°F with less than 10 ppm O_2.

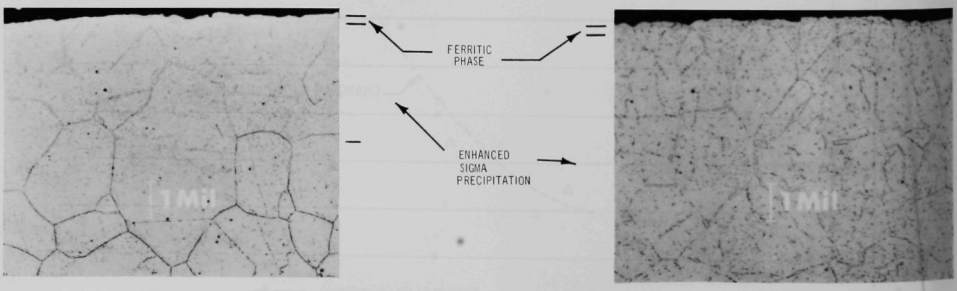

FIG. 12. Structural Effects in Type 316 Stainless Steel after Exposure for 1750 and 3000 Hr in 1300°F Flowing Sodium with Less than 10 ppm O_2.

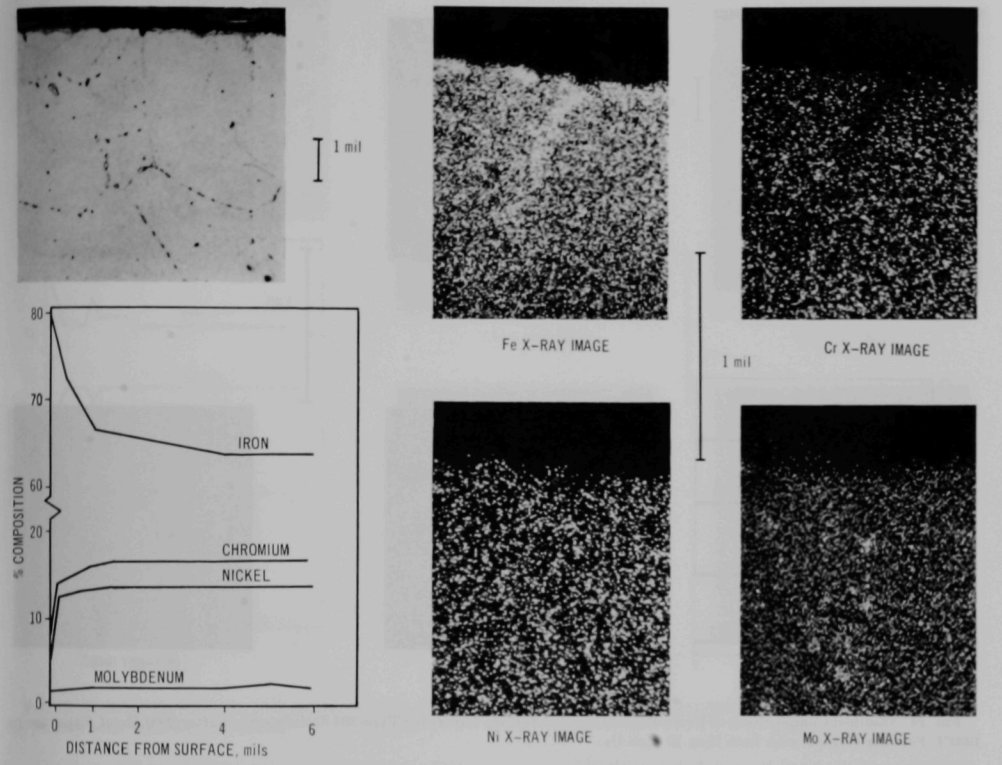

FIG. 13. Modified Compositions of Grain Boundaries and Surface Layers for Type 316 Stainless Steel after 2000 Hr of Exposure to 1300°F Flowing Sodium with Less than 10 ppm O_2.

face zone has expanded to well over 6 mils in depth. The formation and growth of this zone are attributed directly to mass transport of carbon, and continued growth should significantly influence the mechanical properties of these materials.

Additional insight into the nature of these compositional disturbances was obtained with the electron-beam microprobe. The probe data for Type 316 stainless steel after 2000 hr in sodium at 1300°F (see Figure 13) show the surface phase to be ferritic due to the loss of chromium and nickel. Further perturbations in composition were noted to a depth of 1.5 mils, far greater than the thickness of the ferritic phase. Beam scanning images showed that the grain-boundary areas were iron-rich and depleted in chromium, which corresponds to the absence of $Cr_{23}C_6$ in the boundaries.

The response of Type 304 stainless steel to this exposure (see Figure 14) is different than that of the Type 316. Very large areas of modified composition are present in the Type 304, which are rich in iron and depleted in chromium, nickel, and manganese. The composition gradients in Type 304 are not steep, but extend to a depth of 4 mils. Again, large, block sigma particles are apparent in the microstructure and are associated with the loss of carbon.

The most dramatic localized effect was observed in Incoloy-800 after 2000 hr in flowing sodium at 1300°F (see Figure 15). Severe depletion of chromium, nickel, and manganese was observed, not only at the surface, but proceeding along grain boundaries to a depth of about 2 mils. Incoloy-800 also had the highest average corrosion rate among all test materials at 1300°F under comparable exposure conditions.

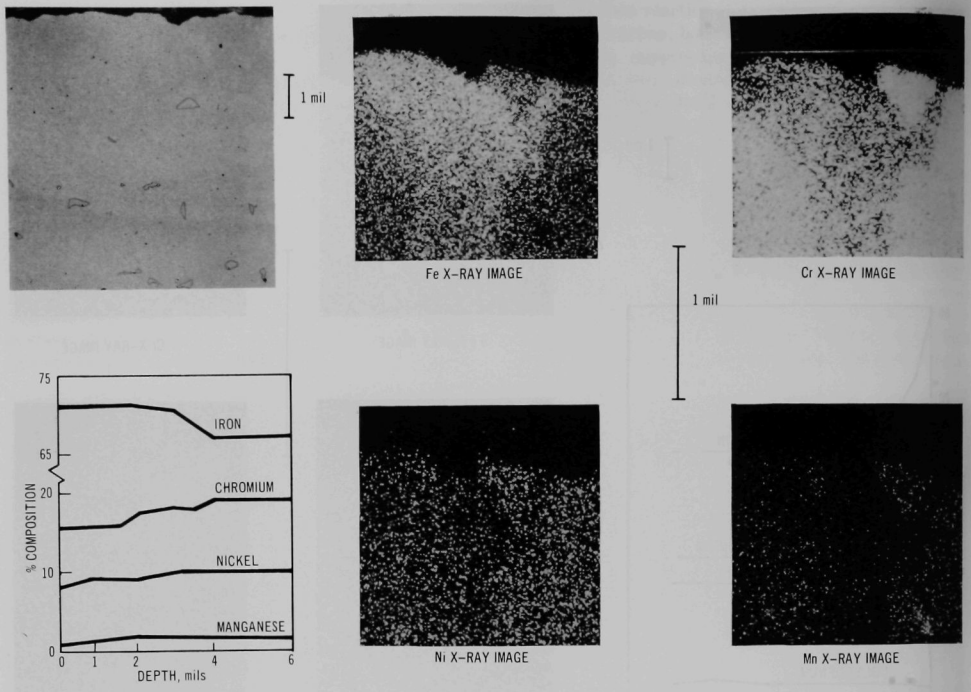

FIG. 14. Modified Compositions of Grain Boundaries and Surface Layers for Type 304 Stainless Steel after 2000 Hr of Exposure to 1300°F Flowing Sodium with Less than 10 ppm O_2.

V. Summary

1. The relationship between velocity and corrosion rate is approximately linear below 15 fps. With increasing velocity, less than linear dependence is observed, with the deviation from linearity increasing with velocity.

2. An interdependence was observed between the effects of velocity and downstream (sodium saturation) on corrosion rate. Decrease of local corrosion rates by 50–75% was observed at a single velocity over the range of downstream values studied.

3. Reproducible and significant differences in corrosion rates were measured at 1300°F for Incoloy-800 and Types 316, 304, and 347 stainless steel. The rates, measured under comparable conditions, were 0.99 mil/yr for Incoloy-800, 0.51 mil/yr for Type 347, 0.44 mil/yr for Type 304, and 0.29 mil/yr for Type 316.

4. The effect of heat transfer on corrosion rate appears to be adequately described as an increase in rate corresponding to an increase in metal surface temperature over the bulk sodium temperature. For equivalent metal surface temperatures, corrosion rates under heat transfer and at isothermal conditions are equal within the accuracy of present measurement techniques.

5. An increase in velocity (therefore, flow turbulence) has a strong influence in promoting deposition. The magnitude of this effect is also dependent upon downstream or loop position (degree of saturation).

6. Significant reductions in chromium, nickel, and manganese were observed on the surface of corrosion samples, the relative amounts of losses being dependent upon the exposure conditions.

7. Carbon transport was observed from higher- to lower-temperature regions, contrary to equilibrium considerations. Losses as high as 79% were measured for Type 316 stainless steel at 1300°F.

8. Microstructural changes were observed in all alloys, and appeared to be dependent upon corrosion rate and alloy composition. Three general changes

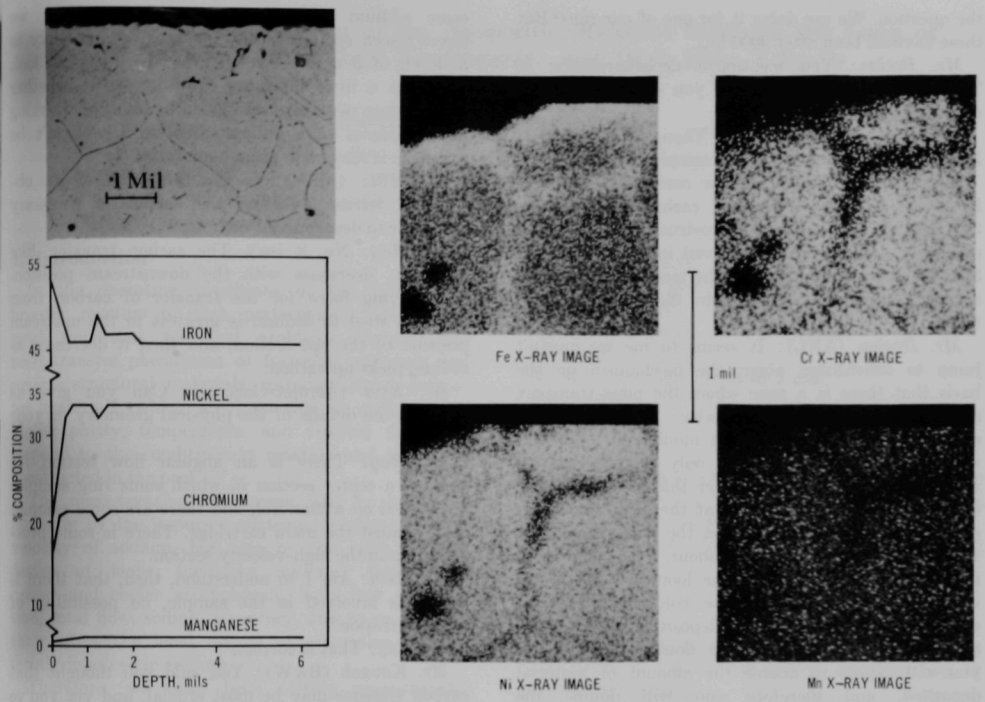

FIG. 15. Modified Composition of Grain Boundaries and Surface Layers for Incoloy 800 after 2000 Hr of Exposure to 1300°F Flowing Sodium with Less than 10 ppm O_2.

were seen: (1) ferritic surface phase, (2) a zone adjacent to the surface and depleted in carbon, and (3) localized and enhanced elemental leaching at grain boundaries.

9. Carbon movement had a profound effect on microstructural changes, by reducing the normal carbide precipitation and enhancing formation of intermetallic phases. Continued development of these changes implies major effects on long-term creep and rupture properties.

REFERENCES

1. Thorley, A. W., and Tyzack, C., *The Corrosion Behavior of Steels and Nickel Alloys in High Temperature Sodium*, IAEA Symposium on Alkali Metal Coolants . . Corrosion Studies and System Operating Experience, Vienna, Austria (November 28–December 2, 1966)
2. Epstein, L. F., *Static and Dynamic Corrosion and Mass Transfer in Liquid Metal Systems*, Chemical Engineering Progress Symposium Series 20, **53**, pp. 67–81 (1967)
3. Zebroski, E. L., Young, R. S., Comprelli, F. A., and Dutina, A., *Effect of Mass Transfer, and of Changes in Properties on Austenitic Steels in Flowing Sodium*, IAEA Symposium on Alkali Metal Coolants . . Corrosion Studies and System Operating Experience, Vienna, Austria (November 28–December 2, 1966)
4. Gurinsky, D. H., *Brookhaven National Laboratory Quarterly Progress Report*, BNL 50123 (T-501) (April 1–June 20, 1968)
5. Weeks, J. R., and Gurinsky, D. H., *Liquid Metal Solidification*, The American Society For Metals, pp. 106–161, Cleveland (1958)
6. Bodsworth, C., Davidson, I. M., and Atkinson, D., Trans. AIME, **242**, 1135–1143 (1968)
7. Campbell, C. S., and Tyzack, C., *A Preliminary Model For The Carburization of Stainless Steel at High Temperatures in Sodium Containing Carbon at Unit Activity*, IAEA Symposium on Alkali Metal Coolants . . Corrosion Studies and System Operating Experience, Vienna, Austria (November 28–December 2, 1966)

Discussion

Mr. Brehm (BNWL): You mentioned that chromium and nickel precipitate out in the first cooler. Did you ever notice a change in the deposition pattern of chromium and nickel as a function of time?

Mr. Roy: No. So far we haven't data to answer

the question. We are doing it for one of our runs. But these have all been after 3000 hr.

Mr. Brehm: You mentioned decarburization of Type 316 stainless steel. Did you observe any decarburization of Type 347?

Mr. Roy: No, we didn't. These mass-transport loops didn't have any Type 347 samples.

Mr. Comprelli (GE): In our mechanical-property loops, we did see evidence of carbon loss in Type 347, but on the basis of microstructure it was significantly less than that observed in Types 304 and 316. We did see what we call the modified zone in all alloys, but significantly less in the stabilized materials.

Mr. Draley (ANL): It seems to me we mustn't jump to conclusions about the mechanism on the basis that there is a zone where the mass-transport rate varies linearly with velocity. I'm sure that a clever person could think of a number of models in which that might be so; not only surface reaction control of some kind, but other things as well. One of the most evident ones is that there be a constant efficiency of deposition, so that the concentration of the material we are talking about, perhaps iron, is nearly constant throughout the loop. It precipitates efficiently and quickly in the cold zone as it is cooled, but most of it doesn't deposit; it remains suspended in the liquid. As you double the velocity, you will expect to double the amount of material deposited, and therefore you will double the amount of unsaturation when you heat it back up. I only suggest that as a quick one. Let's not pretend that we know more than we know on the basis of a straight line.

Mr. Beaufrere (EDF): You have seen intergranular attack in Incoloy-800 and a depletion of iron, nickel, and chromium?

Mr. Roy: No, a depletion of nickel, chromium, and manganese.

Mr. Beaufrere: Yes, that's right. Have you seen a slight penetration in these specimens?

Mr. Roy: Yes, we've had some. We tried to detect some sodium with our microprobe analysis; we haven't seen sodium to any great extent (possibly to a depth of 3 or 4 microns). We are trying to look into that a little bit more carefully, as to whether sodium does penetrate into grain boundaries. Looking at the places that sodium goes in, I wouldn't be surprised if they were grain boundaries.

Mr. Hiltz (MSA): Is the formation of an observable ferrite layer on the surface a necessary precursor to decarburization?

Mr. Roy: No, it isn't. The carbon transfer, like corrosion, decreases with the downstream position. The driving force for the transfer of carbon from stainless steel to sodium is greatest in the upstream position of the hot section, and then it decreases as sodium picks up carbon.

Mr. Reid (Aerojet-General): Can you give us more on the details of the physical geometry of your sample?

Mr. Roy: There is an angular flow section for sodium, a center section in which some ring samples are placed on a mandrel, and there are some samples flush against the main cartridge. There is some pressure drop in the high-velocity section.

Mr. Reid: Am I to understand, then, that there is no stress involved in the sample, no possibility of stress corrosion?

Mr. Roy: That is correct.

Mr. Kovach (B&W): You said you thought that carbon transfer may be most crucial, and yet you've spent most of your time talking about other effects. Do you intend to get back to the carbon problem?

Mr. Roy: This is one of our objectives at the present moment, to look at the nature of deposits and to develop a model for carbon transfer.

Mr. Beaufrere: Did you analyze the effect of sodium in the welded zone on Types 304 or 316?

Mr. Comprelli: Not in these experiments. We did not have welded and drawn materials; these are all seamless materials. We do not have any particular part of our program emphasizing examination of welded sections.

Mass-transfer Phenomena of the Austenitic Stainless Steels in the Loop of Sodium with a High Temperature and High Flow Velocity

KAZUO FURUKAWA AND ISAO NIHEI

Japan Atomic Energy Research Institute
Tokai-mura, Ibaraki-ken, Japan

(PRESENTED BY K. FURUKAWA)

1. Introduction

In the operating conditions of the future fast breeder reactors of high performance, one of the most important technical problems concerns the mass-transfer phenomena of fuel-clad materials and several structural materials, including steam-generator materials, which are immersed in sodium of a higher purity, temperature, and velocity than correspond to the conditions in reactors and test loops constructed in the past.

The mass-transfer phenomena will be influenced not only by the impurity contents, temperature, and velocity of sodium, but also by the more detailed design of loops, including material distribution, heater and cooler arrangement, local flow distribution, total flow, sodium inventory, and so on, because they affect the local degree of saturation of materials dissolved in sodium.

Therefore, we have been testing mass-transfer phenomena in a temperature gradient, using three special test loop stands as part of a phase-1 program. Two loops are monometallic, utilizing Type 304 stainless steel, and the other is bimetallic, constructed of Type 304 stainless steel and 2¼ Cr-1 Mo steel.

This is an interim report on the monometallic loop tests. One loop has been operated for about 3,000 hr and the other for about 1,400 hr.

2. Loop Design and Test Conditions

2.1 Brief Description of the Test Loops

In an attempt to simulate the conditions of the future fast breeder reactors, the following test conditions were chosen for the phase-1 test program:

(1) loop materials:	AISI Type 304 stainless steel;
(2) test-specimen materials:	2¼ Cr-1 Mo alloy steel. types 304 and 316 stainless steel; 2¼ Cr-1 Mo steels (Incoloy and high-nickel alloys).
(3) sodium purity:	5 to10 ppm oxygen.
(4) max and min loop temperatures:	600 and 380°C.
(5) sodium velocity:	1 to 10 m/sec.
(6) sodium flow rate:	4 or 6 liters/min.
(7) cold-trap flow	less than 5% of the toal flow.
(8) loop circulation time:	2.5 to 4.5 min.
(9) minimum gap of path:	about 1 mm.
(10) test duration:	about 10,000 hr.

To simplify intermediate and final comprehensive analyses of the data, the general shape of loop was "0" and not "8," with a heat economizer.

The actual test conditions are described in detail in the following.

2.2. Sodium Purity

As the impurity level of loop sodium, the plugging temperature of 120°C was chosen corresponding to about 5 ppm oxygen.

Our test loops were constructed as part of the Mother and Daughter Test Loop System,[1, 2] and sodium purity was controlled by the Mother Loop. The relation between the mass-transfer test loops and the Mother Loop is shown in Fig. 1. A total of 1,000 liters of loop sodium was cleaned and kept at a plugging temperature of 120°C by a forced-convection type of cold trap.

Each mass-transfer test loop has a sodium capacity of about 15 liters and was constantly supplied with fresh sodium corresponding to a few percent of the test loop flow from the Mother Loop.

With this loop system, several experiments in all daughter test loops were performed with the same sodium while other test conditions were varied.

2.3. Loop Construction Materials and Specimens

All parts of the Mother Loop and the mass-transfer test loops were made of Type 304 stainless steel, except for the valve sheet and disc, which were made of Stellite.

The specimen materials were Type 304 and 316 stainless steels, whose compositions are presented in Table 1.

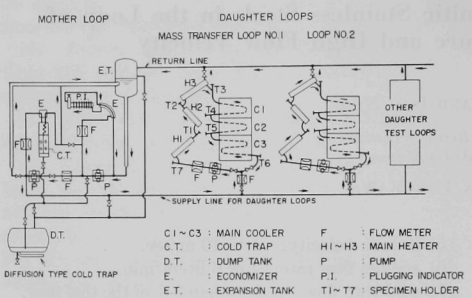

FIG. 1. Flow Sheet of the Mother and Daughter Test Loop System.

2.4. Testing Temperature

Maximum and minimum sodium temperature in both test loops were 600 and 380°C, producing a temperature difference (ΔT) of 220°C. There were three heaters (H1, H2, and H3) in series in the heating region, and three specimen-holder-inserting positions: T1 (500°C), T2 (550°C), and T3 (600°C), near the outlet of each heater.

In the cooling region there were three air-cooling tubes: C1, C2, and C3, and three specimen-holder-inserting positions: T4 (520°C), T5 (470°C), and T6 (400°C), near the outlet of each cooling tube. In the lowest temperature region near the inlet of heater H1, the specimen-holder-inserting position T7 (380°C) was placed (cf. Fig. 1).

TABLE 1. TEST-SPECIMEN MATERIALS

	Mechanical Properties				Alloying Elements, w/o								
	Tensile Strength, kg/mm²	Toughness, kg/mm²	Elongation, %	Hardness, H_RB	C	Si	Mn	P	S	Cr	Ni	Mo	Fe
Type 304 stainless steel	64.8	33.9	54	84	0.06	0.63	1.54	0.021	0.014	18.49	9.04	—	Bal
Type 316 stainless steel	59.0	28.4	54	77	0.06	0.61	1.41	0.033	0.006	16.75	12.04	2.33	Bal

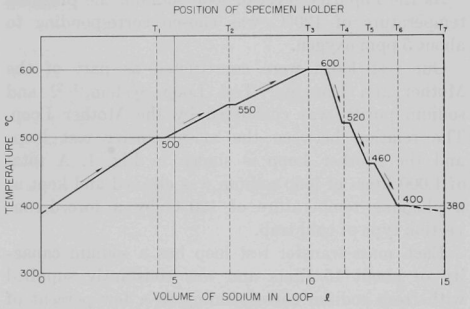

FIG. 2. The Temperature and Volume Distribution of Sodium in the Mass-transfer Test Loops.

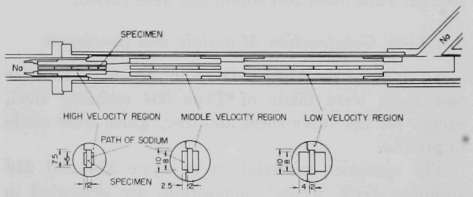

FIG. 3. The Specimen and Specimen Holder.

The distribution of loop temperatures is shown in Fig. 2 in relation to sodium volume.

2.5. Flow Rate and Velocity

The testing flow rates of loops No. 1 and No. 2 were 4 l/min and 6 l/min, respectively.

The mean flow velocity of sodium on each specimen surface was adjusted to a maximum value of 10 m/sec by varying the cross-sectional area of flow in specimen holders (see Fig. 3 and Table 2).

2.6. Loop Operation

Charging of sodium from the Mother Loop to the mass-transfer test loops was performed after the

TABLE 2. CONDITIONS OF SODIUM FOR TESTS

	Specimen Holder No.	Temp, °C	Velocity, m/sec	
			Loop No. 1	Loop No. 2
Heating region	T1	500	6.6, 1.7, 1.0	10, 2.5, 1.6
	T2	550	6.6, 1.7, 1.0	10, 2.5, 1.6
	T3	600	6.6, 1.7, 1.0	10, 2.5, 1.6
Cooling region	T4	520	1.7, 1.0	2.5, 1.6
	T5	470	1.7, 1.0	2.5, 1.6
	T6	400	1.7, 1.0	2.5, 1.6
	T7	380	1.7, 1.0	2.5, 1.6

sodium plugging temperature was at 120°C. To prevent the inclusion of dirty sodium in the initial operation period, the test loops were precleaned with 350°C sodium for 24 hr.

The removal and reinsertion of specimens from loops were done at room temperature after sodium drain. Any adhering sodium was dissolved with ethyl alcohol and the loop dried after washing with acetone.

3. Results

Test specimens were taken out at 386, 773, and 1,575 hr after insertion into No. 1 loop, and after 655 hr from No. 2 loop. Weight changes were measured, and then most were returned to the loop for continued test. Some specimens were used for detailed examination.

3.1. Weight Change

The mean weight changes of specimens inserted into No. 1 loop are given in Fig. 4 as a representation of the overall temperature-gradient mass-transfer phenomena. In the heating region, we confirmed that the specimen weight was decreased by a dissolution process that was very much stronger in the higher-temperature region. In the cooling region the specimen weight was increased by a precipitation process, which was most significant in the 400°C region (T6) but not so much in regions T4 and T5. This indicated that a weak dissolution remained in T4 (520°C).

3.2. Material Change

For the detailed analysis of the mechanism of the dissolution and precipitation processes, the microscopic structures were examined by X-ray microprobe and electron diffraction.

The resolving power of the X-ray microprobe was 2 to 3 μ, using a electron beam of 1-μ diameter. The distribution patterns shown in this report are typical of those measured at several different places.

The results for Type 304 stainless steel specimens inserted at T3 (600°C, 1,575 hr) are shown in Fig. 5, which includes the microscopic structure and microprobe composition analyses of a vertical section. Table 3 presents the composition change of the corroded surface measured by a microprobe having a beam of 40-μ diameter.

The results with Type 316 stainless steel specimens are given in Fig. 6.

Figure 5 indicates that the chromium content of Type 304 stainless steel is markedly decreased within a distance of 5 μ from the surface, but increased near the surface. The amounts of iron and nickel

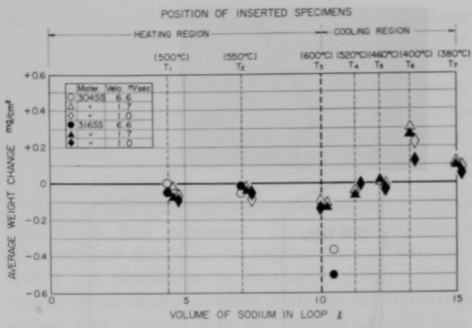

FIG. 4. The Relation Between the Weight Change and Specimen Position (Exposed Time: 1575 Hr).

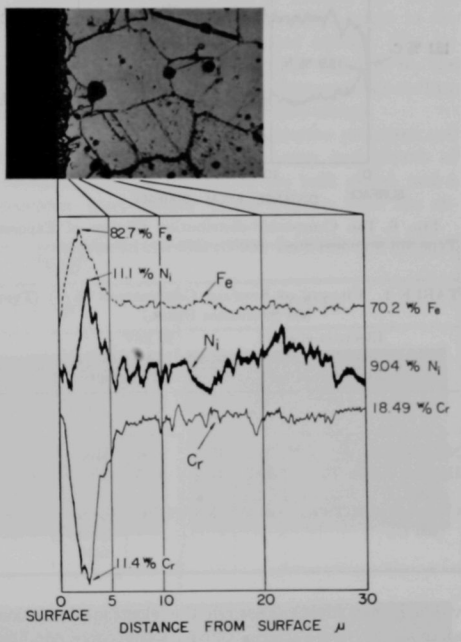

FIG. 5. The Component-distribution Change of Exposed Type 304 Stainless Steel (600°C, 1575 Hr; 1.7 m/sec).

increased corresponding to the decrease of the chromium content.

From Table 3 it is found that the oxygen content of the surface (T3) was not detectable, but the carbon and chromium contents increased considerably. (However, the accuracy of carbon content

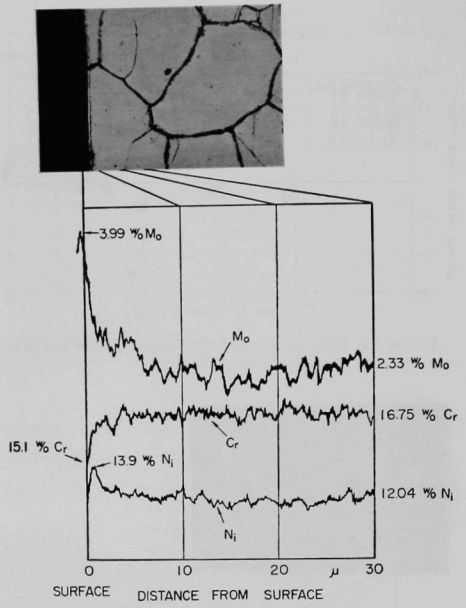

FIG. 6. The Component-distribution Change of Exposed Type 316 Stainless Steel (600°C; 1575 Hr; 1.7 m/sec).

TABLE 3. CHANGE OF SURFACE COMPOSITION (w/o) (TYPE 304 STAINLESS STEEL)

Electron energy: 10 keV
Absorbed electron current: 1.73×10^{-7} A
Effective range: 0.3 mg/cm²

	Fe	Cr	Ni	O	C
Nonexposed	70.2	18.5	9.04	Min	(0.06)
Heating region T3 (600°C)	42.3	41.9	8.75	Min	(0.13)
Cooling region T6 (400°C)	29.8	5.8	(11.0)	Large quantity	(0.03)

value is not high.) Through the electron-diffraction analysis of this surface, the patterns corresponding to a ferritic (bcc) metal phase and presumably carbide Cr_7C_3 were observed. Magnetic inspection verified that the specimens (T3) were transformed into the ferromagnetic structure, at least partially.

For Type 316 stainless steel inserted into the highest temperature region (T3, 600°C), iron, chromium, and nickel contents were scarcely changed, but molybdenum was significantly increased (see Fig. 6).

Specimens of Types 304 and 316 stainless steel inserted in the cooling region T6 (400°C) had no detectable change in the microscopic structure and composition of vertical section, as compared with these quantities before the sodium test. However, the surface exposed to sodium darkened, and a large amount of oxygen was detected by the X-ray microprobe (see Table 3). The strong lines of the electron-diffraction pattern of the above dark materials corresponded to Cr_2O_3.

3.3. Influence of Sodium Velocity

The relations between the sodium velocity and the corrosion rates of Type 304 and 316 stainless steel specimens inserted into the maximum temperature region T3 (600°C) are shown in Fig. 7. Although the duration of the tests was not long enough, it appears that the corrosion rate increases linearly with sodium velocity and does not depend on differences between the specimen species.

3.4 Relationship between Corrosion Rate and Test Duration

The weight losses of the Types 304 and 316 stainless steel inserted into the maximum temperature region T3 (600°C) are given in Fig. 8 in relation to the test duration. The metallographic structure change of a vertical section is shown in Fig. 9.

The weight loss increased linearly with the time. The modified layer (cf. Figs. 5 and 9) near the corroded surface had appeared after 386 hr, and became about 5 μ thick for Type 304 and about 2 μ thick for Type 316 after about 700 hr. Beyond this time the thickness of this modified layer seemed to stay constant.

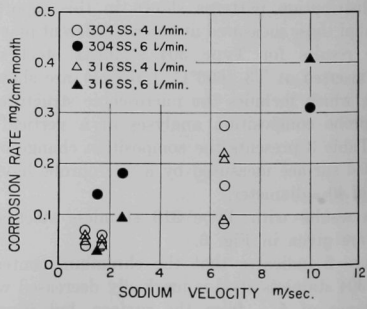

FIG. 7. The Effect of Velocity on the Corrosion Rate (Sodium Temp: 600°C; ΔT: 220°C, Sodium Flow Rate: 4 or 6 l/min).

4. Discussion

The most significant characteristics of the composition change of a Type 304 stainless steel specimen in our mass-transfer test results are (1) the change of chromium content in heating region, and (2) the formation of surface oxides in cooling region.

The amount of chromium in specimens placed in the heating region was decreased within about 5 μ from the surface and increased in the thin surface layer 1–2 μ thick (cf. Fig. 5). However, the width of this layer may be thinner than 1–2 μ, considering the resolving power of the X-ray microprobe. On the surface exposed to sodium, chromium carbides and ferritic metals of ferromagnetic character were coexistent.

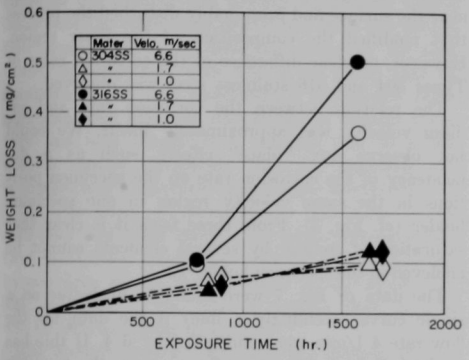

FIG. 8. The Relation Between the Weight Loss and Exposure Time (Sodium Temp: 600°C).

These abnormal phenomena may be explained by considering four processes: (a) stronger selective dissolution of chromium in sodium than of iron and nickel, (b) dissolution of iron and nickel, (c) retention of chromium carbides (possibly more inert to sodium than metals) near the surface, and (d) further slow decomposition of chromium carbides and/or scaling out of them by flowing sodium.

In the heating region, due to process (a) above, chromium activity in the metal matrix ought to decrease gradually near the exposed surface. The increase of iron and nickel contents depends on the depression of chromium content. Very near the surface the dissolution of iron and nickel also occurs.

Accerelated by the above dissolution processes and higher temperature, the precipitation and growth of chromium carbides proceed in the bulk metal, and a relatively inert carbide phase remains near the ex-

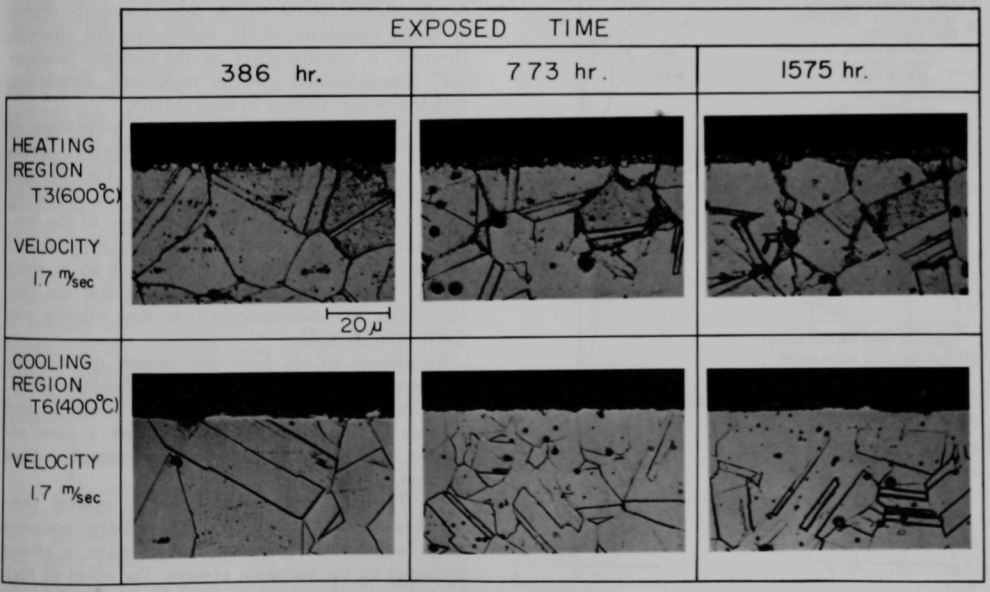

FIG. 9. Metallographic Structure of Type 304 Stainless Steel Exposed in Sodium.

posed surface. To advance corrosion beyond this stage, we can expect a slow (rate-determining?) decomposition process of carbide particles by sodium, although the decomposition process depends on the carbon activity of sodium. Parallel to this process may be a scaling-out caused by the fast-flowing sodium, especially by sodium of high carbon activity.

The formation of chromium oxide (Cr_2O_3) on the surface might be due to its stabilization in the colder condition or to an air oxidation after taking the specimen out of the loop, owing to the active surface structure of deposited materials. Evidence for this is provided by the dark colour.

The depression of nickel content near the surface has been reported previously.[3-6] However, we could not confirm this fact. It may be caused by several different test conditions, as for example, the sodium quality and design aspects of overall test loop.

The thickness of the modified layer was stationary after 700 hr. Therefore, in further tests the corrosion rate may have been constant. However, it should also be remembered that there was a possibly more complicated situation due to the slow composition-modification processes in the lower-temperature region.

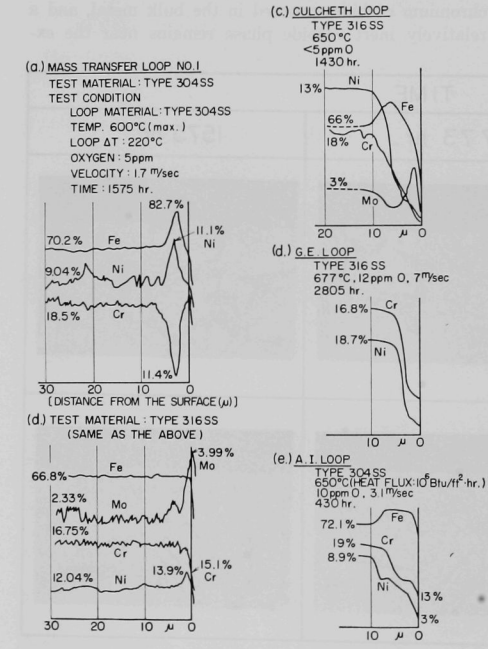

FIG. 10. Comparison of the Component-distribution Curves in the Several Mass-transfer Tests.

For Type 316 stainless steel specimens, test results in the cooling region were similar to those for Type 304 stainless steel, but the results for the heating region were quite different as regards the microscopic structure and composition change.

Because molybdenum has a smaller solubility than other alloying elements, molybdenum was enriched near the surface and presumably disturbed the process that modified the composition of the inner region. However, no clear difference of the corrosion rates of Types 304 and 316 stainless steel was observed.

The relation between the corrosion rate and sodium velocity was approximately linear. We could not observe any "place" effects, such as a dependency of the corrosion rate on the specimen positions in the same velocity region in one specimen holder (cf. Fig. 3). From these facts it is clear that saturation of sodium by several elements cannot be achieved in the specimen holder T3.

The data of Fig. 7 were found to fit better on a single curve (seemingly a line) if the data for the flow rate 4 l/min were multiplied by 6/4. If this has a physical basis, the total flow rate in the test section is an important quantity affecting the mass-transfer rate. Further, the effect of flow velocity on the dissolution process will be related with the degree of metal saturation of the sodium in this channel. However, a velocity effect on the possible "scaling-out" process should also be recognized, correlating with the carbon activity of used sodium.

Our data are not always consistent with those of others.[3-6] Various component-distribution curves for a sectional surface are shown in Fig. 10, and they differ widely from one another. (It should be pointed out that in these curves the sum of the concentrations of major components in any place should always be near to 100%, but it is not so in some figures.) Further, Culcheth[5] reported that the corrosion rate was constant when the flow velocity was faster than 10 ft/sec.

At present we do have not enough quantitative data based on longer tests to give further details. However, for each test we should compare and analyze on the following points to get a more effective understanding of the mass-transfer phenomena.

(1) *Testing temperature, including general temperature distribution in loop:* The relative positions with heaters and specimen holders have a strong incluence on the corrosion process. The effect of high heat flux on the metal surface should also be analyzed.[6]

(2) *Flow distribution in loop:* The degree of saturation of the several elements in sodium will depend on the successive flow and temperature distributions in loop.

(3) *Flow rate and circulation period:* Both the sodium velocity and the total flow rate are important factors controlling the dissolution capacity. The period of one circulation in the loop and residence times in the heating and cooling regions are also of importance in estimating departures from the saturation concentrations of dissolved elements. As mentioned in connection with Fig. 4, we found that the specimen at T4 still underwent a dissolution effect, suggesting the apparent importance of sodium inventory and loop length. It is possible that in a loop with a shorter circulation time the corrosion rate is smaller and apparently independent of velocity.

(4) *The mode of purification:* The ratio of the cold-trap and main flows is an important parameter that determines whether or not we can neglect this bypass flow in the consideration of the effects (1), (2), and (3). If the ratio is smaller than $\frac{1}{20}$, we will be able to neglect this effect.

(5) *Sodium purity:* Not only the content of oxygen in sodium, but also of carbon, hydrogen, nitrogen, calcium, magnesium, and metallic elements dissolved from structural materials themselves, affect the corrosion rate, modifying the activities and, therefore, the solubilities of several metallic elements.

(6) *Test duration:* The establishment of a steady-state metallographic structure near the corroding surface will be delayed in the lower-temperature region. The intensity of this effect for specimens in the highest-temperature region will depend on the loop design in general. It seems that the steady-state condition will be achieved more slowly in a loop with a shorter circulation period.

(7) *Construction materials and operational history of the test loop:* If the loop is reconstructed or repaired, the presence of new construction materials in contact with sodium affects the local chemical balances in the sense discussed in (3), (5), and (6). Thus a knowledge of the detailed design features and operational history of the test loop is of importance.

5. Conclusions

(a) The results of analyses of mass-transfer phenomena associated with Type 304 and 316 stainless steels inserted in the two monometallic mass-transfer test loops made of Type 304 stainless steel were presented as an interim report. Principal test conditions were: a sodium temperature of 600°C maximum and of 380°C minimum (ΔT = 220°C); sodium flow rates of 4 and 6 liters/min; mean flow velocity ranging from 1 to 10 m/sec; a sodium purity measured by a plugging temperature of 120°C, corresponding to about 5 ppm oxygen; and maximum exposed time of specimens of 1,575 hr.

(b) In the heating region, the significant corrosion process is a selective dissolution of chromium. In the region of highest temperature (600°C), a modified structure layer was formed, about 5 μ thick for Type 304 and about 2 μ for Type 316 stainless steel, this stationary condition being achieved in about 700 hr. Near the exposed surface, some chromium carbides (mostly Cr_7C_3) and a ferritic metal phase were found.

(c) In the cooling region, the existence of chromium oxide (Cr_2O_3) on the specimen surface was confirmed. However, a detailed analysis of deposited materials could not be obtained because of the small thickness.

(d) The corrosion weight loss at the highest temperatures increased almost linearly with the sodium velocity. Corrosion rates for 600°C and 10 m/sec were 0.3 mg/cm^2-month (or 4.6 μ/yr) for Type 304 and 0.4 mg/cm^2-month (or 6.2 μ/yr) for Type 316 stainless steel.

(e) This difference of corrosion rates was negligibly small.

(f) The general aspects of the temperature-gradient mass-transfer mechanism have been discussed in some detail. Further discussion should be based on the analysis of the several experimental results from the different test loops that consider the following effects;

(1) the influence of general loop-design feature, such as temperature and flow distribution in loop, sodium inventory and circulation period, and cold-trap flow;
(2) the effect of high heat flux;
(3) the effect of nonmetallic and metallic impurities, as well as the elements of structural materials, on the dissolution process, the carburization process, and their solubilities;
(4) the influence of coexistence of different materials.

Acknowledgments

We would like to express our gratitudes to the technical assistances of all members of Sodium Technology Laboratory, especially to Messrs. I. Sumiya, Y. Fukaya, K. Yamamoto, and E. Yamada.

Furthermore, we would like to acknowledge with appreciation, the advice and assistance of Mr. F. Watanabe of JAERI on design, and of Dr. K. Izui and Mr. S. Furuno of Jaeri for the X-ray microanalysis.

REFERENCES

1. Kazuo Furukawa, Ken Yamamoto, Isao Nihei, and Yae Iguchi, *Liquid Sodium Technology Development (I) Test Loops, Purification Methods and Supplmentary Techniques*, JAERI-1129 (March 1967).
2. Kazuo Furukawa, Ken Yamamoto, Isao Nihei, and Mitsuru Kamei, *Liquid Sodium Technology Development (II) Sodium Loop Components and Related Techniques*, THIS CONFERENCE.
3. E. G. Brush, *Sodium Mass Transfer: XVI, The Selective Corrosion Component of Steel Exposed to Flowing Sodium*, GEAP-4832 (March 1965).
4. E. L. Zebroski, R. S. Young, F. A. Comprelli, and D. Dutina, *Mass Transfer and Properties Changes Effects on Austenitic Steels in Flowing Sodium*, Symposium on Alkali Metal Coolants, SM 85/28, Vienna (Nov 1966).
5. A. W. Thorley and C. Tyzack, *The Corrosion Behaviour of Steels and Nickel Alloys in High Temperature Sodium*, Symposium on Alkali Metal Coolants, SM 85/18, Vienna (Nov 1966).
6. J. Hopenfeld and D. Darley, *Dynamic Mass Transfer of Stainless Steel in Sodium under High-heat-flux Conditions*, NAA-SR-12447 (July 15, 1967).

Discussion

Mr. Comprelli (GE): For the purpose of discussion, I'd like to refer to Figures 13 and 14 of the preceding paper by Roy *et al.* for Types 316 and 304 stainless steel, respectively. For Type 316, once again at 1300°F, in the positions in the loop at which the greatest corrosion occurs, we do not find nearly as much molybdenum movement as you did. We also find a concentration gradient of far greater depth than you do. Of course this may be due to the 100°F temperature difference also. In addition to that, in Type 316 we also see the localized problem. The grain boundaries, as you can see, were depleted in chromium and the iron content of grain-boundary regions was higher than normal. The molybdenum does not seem to be affected, nor does the nickel in the grain-boundary areas. For Type 304 we see a much shallower gradient, but a far greater depth. I believe you were talking of something like several microns; we see it as something like 4 mils, or 100 μ. Our gradient is not nearly so steep as with the other materials in Type 304 for the same loop position; however, we do see chromium leaving the material uniformly, as opposed to selective leaching at the grain boundaries, which has been mentioned for Incoloy 800 and Type 316 stainless steel. As you can see, we form massive phases at the surface of Type 304 to depths of 4 mils. We can see that this particular phase is rich in iron, depleted in chromium, nickel and manganese, and it follows very well the information shown by the microprobe traces on the left. The exposure was 2000 hr.

Mr. Horton (AEC): You showed the corrosion rate increasing with time. Do you think that would continue?

Mr. Furukawa: I do not know yet, but I am assuming that after some 700 hr we will expect a more constant rate.

Mr. Jansson (W): Do you understand why chromium diffuses to the surface to form the chromium carbide and the chromium-rich surface layer, rather than carbon diffusing in to form a chromium carbide at some depth? From the diffusion rates of carbon versus chromium we would expect the latter.

Mr. Furukawa: I'm not sure. I cannot measure the carbon content as yet.

Kinetic Aspects of Corrosion of Steels in Flowing Sodium

L. Champeix and O. Konovaltschikoff

C.E.A., CEN Saclay
Gif-sur-Yvette, France

(PRESENTED BY L. CHAMPEIX)

1. Introduction

As a rule, it is considered that steels offer a satisfactory resistance to the corrosion by liquid sodium. The austenitic steels, in particular, are frequently used in plants up to temperatures of 650°C. However, if the nature of the chief processes of corrosion are pretty well-known, the various studies that have been published don't enable us to state the value of the corrosion rate as a function of the main parameters that determine it, in particular, its progress in time[1-5]. The aim of this short report is to help towards a contribution to the understanding of this kinetic aspect of corrosion phenomena.

2. Experimental Technique

The study of corrosion kinetics has been pursued in two nonisothermal loops labeled Sophie and C_2. Figure 1 is a schematic diagram of Sophie. Beside the main circuit in which sodium can be conveyed by an electromagnetic pump, this plant includes a purifying bypass circuit with cold trap. The test chamber has been devised so as to receive at the same time four groups of samples fastened to adequate supports or gathered by screwed rods (see Fig. 2); a lock chamber enables their insertion or removal separately in a argon atmosphere.

Loop C_2 is a similar circuit, exploited under contract by the Ugine Kuhlmann Company (Mr. Graff). The test chamber, smaller than in Sophie, includes three canals, each equipped with a device on which six sample plates are attached (see Fig. 3).

The tests have been run under the conditions given in Table 1.

In both cases oxygen concentration has been determined by amalgamation[6] after taking samples into glass containers.[7] The samples, in the shape of small plates or test bars for mechanical tests (traction and impact strength), are taken out of sodium in a pure argon atmosphere, then carefully washed with ethyl alcohol and distilled water. They then undergo the following classical tests:

weighing;

micrographic examination of the surface and of the structure of the metal;

hardness determination;

titration for carbon;

impact strength and rupture change at room temperature.

The results as a whole cannot be reported here. We shall include but a few results about the kinetic aspects of the phenomena dealing with ferritic steels, on the one hand, and with austenitic steels on the other.

3. Kinetics of Corrosion of Ferritic Steels

Two kinds of ferritic steels, the former with 2.25% chromium, the latter with 9%, have been studied and compared with an austenitic steel of the Type 304L. The compositions are shown in Table 2.

The weight changes observed are shown in Fig. 4; every point corresponds to the average of measures taken on two or three samples. The variations between the values do not exceed 0.15 mg/cm². The curves are parabolic on the whole, but it is also possible to consider that after a first period spread over 1000 or 2000 hr, the kinetics becomes almost linear.

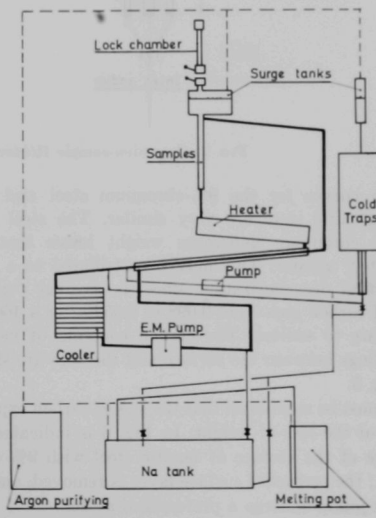

Fig. 1. Design of Sophie Test Loop.

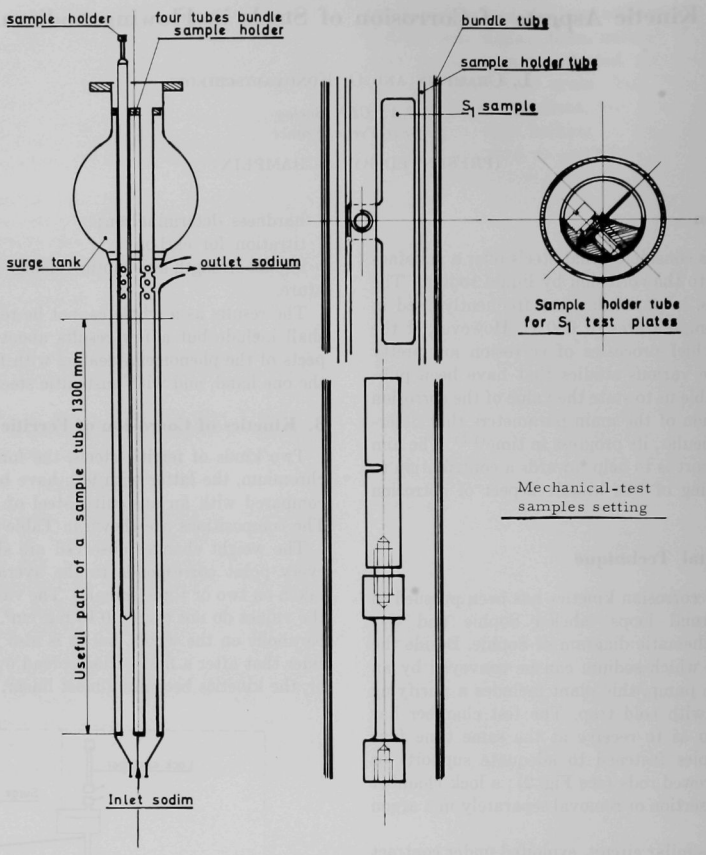

FIG. 2. Corrosion-sample Holder and Arrangement of Metallurgical Specimens.

The curves for the 9%-chromium steel and that of austenitic steel are very similar. The steel with 2.25% chromium undergoes weight losses that are definitely greater. This may be attributed to a very important decarburization, since the average percentage of carbon goes from 0.098 to 0.052 after a 4600-hr exposure to sodium. The carbon contents of various samplings between the surface and the core are shown in Fig. 5.

It must be mentioned that the loss of carbon explains most of the loss of weight. In Fig. 6 is indicated the change of the surface of ferritic steel with 9% chromium; the perturbed surface layer is removed, and the grains joints undergo a preferential attack.

4. Kinetics of Corrosion of Austenitic Steels

We have studied the kinetics of corrosion of 5 kinds of austenitic steel in the C_2 loop at a temperature of 700°C for 2000 hr. The compositions of these steels are shown in Table 3, and the weight-changes appear in Fig. 7.

Three remarks can be made about these first results:

a) The results were coherent and reproducible.

b) The stabilized steels of the 347 and 321 types showed greater weight losses than did nonstabilized steels.

c) During the 2000 hr, the rate of corrosion steadily decreased (see Fig. 8).

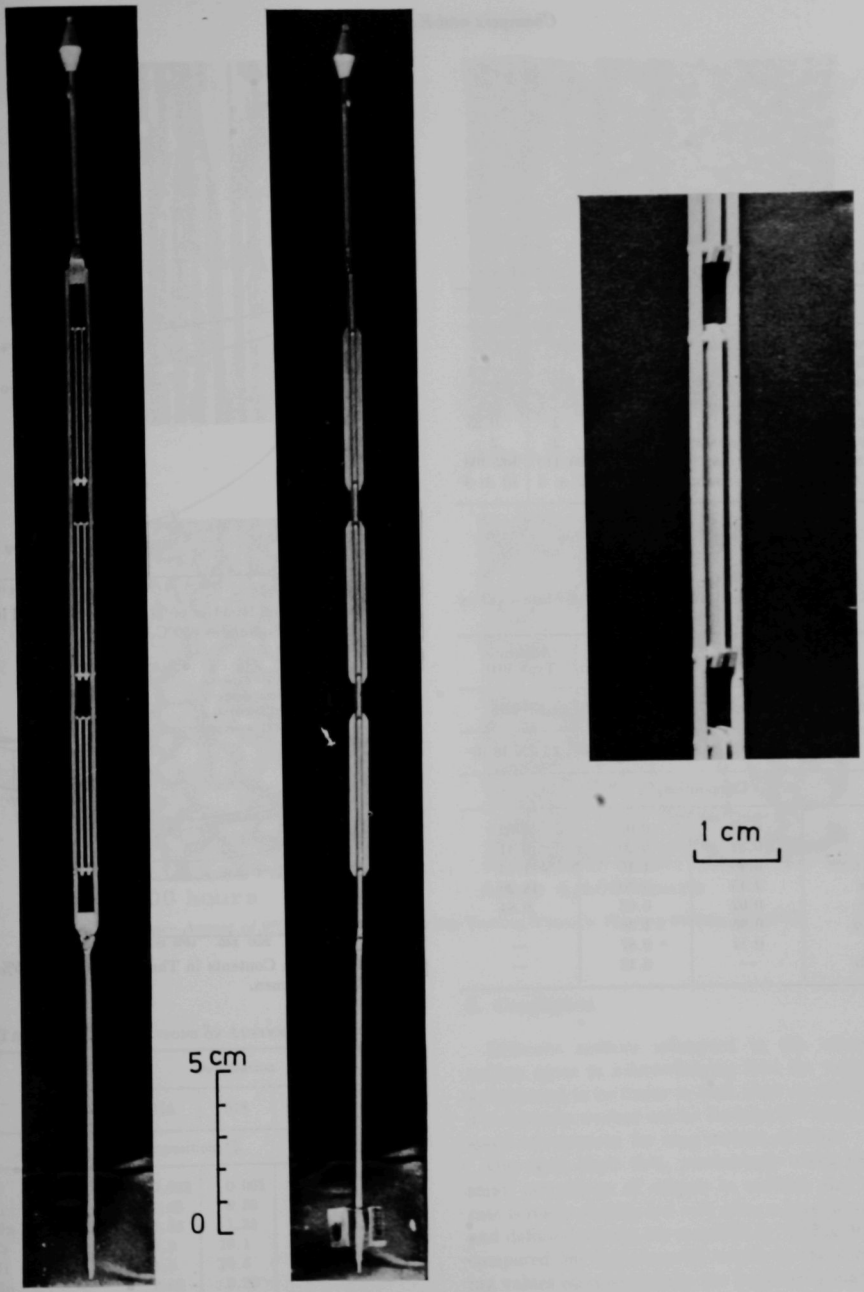

FIG. 3. Sample Holder in Loop C_2.

TABLE 1. Test Conditions for Sophie and C_2 Loops

	Sophie	C_2
Temperature of the sodium in the test chamber (°C)	650	700
Temperature of the sodium at the coldest point of the main circuit (°C)	300	300
Flowing of sodium (l/sec)	2	0.25
Velocity of sodium on the sample (m/sec)	2	2
Temperature of the cold trap (°C)	105–110	102–103
Oxygen concentration in sodium (ppm)	12 ± 3	10 ± 3

TABLE 2. Compositions of Ferritic and Low-carbon Austenitic Steels Studied

	2.25% Cr	9% Cr	Austenitic Type 304L
Designation.....	Chromesco 3	EM 12	NS 22 S
AFNOR rule....	10 CD 9	Z10 CD Nb V9	Z3 CN 18-10
	Composition, %		
C	0.10	0.07	0.02
Si	0.32	0.20	0.41
Mn	0.46	1.16	1.73
Cr	2.15	9.70	18.20
Ni	0.02	0.02	9.84
Mo	0.95	1.36	—
V	0.11	0.87	—
Nb	—	0.13	—

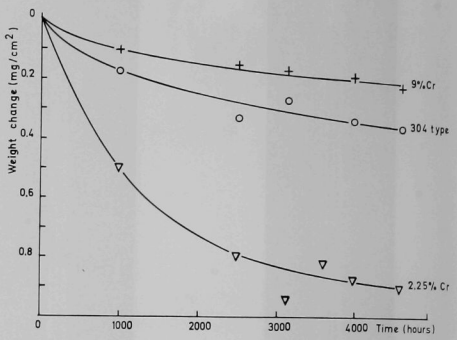

Fig. 4. Corrosion Kinetics of Three Types of Steel in Cold-trapped Flowing Sodium at 650°C.

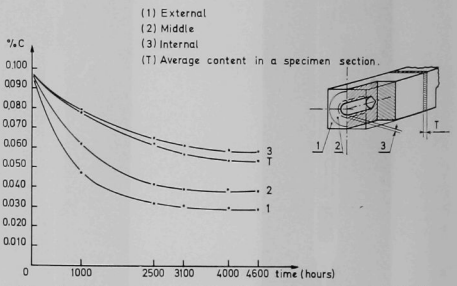

Fig. 5. Carbon Contents in Three Zones of a 2.25% Chromium Steel Specimen.

Initial

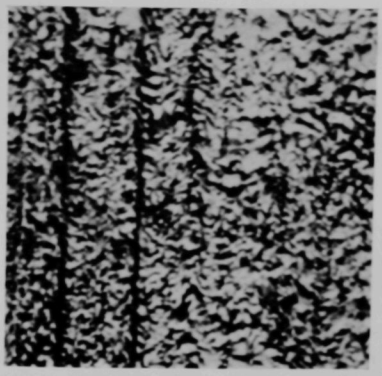

After 1,000 hours

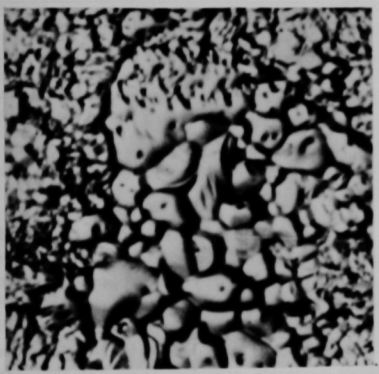

After 3,100 hours

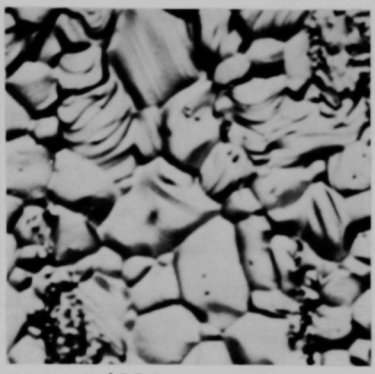

After 4,600 hours

FIG. 6. Surface Aspect of 9% Chromium Steel after Various Times in Flowing Sodium at 650°C.

TABLE 3. COMPOSITIONS OF AUSTENITIC STEELS

	Designation				
	304	316	318	321	347
	Composition, %				
C	0.028	0.028	0.061	0.068	0.051
Si	0.20	0.43	0.58	0.42	0.50
Mn	1.53	1.55	1.35	1.43	1.70
Cr	17.8	16.3	16.1	18.2	18.3
Ni	9.7	13.3	10.5	11.6	10.6
Mo	—	2.68	2.20	—	—
Nb	—	—	0.54	—	0.71
Ti	—	—	—	0.40	—

5. Conclusion

Different authors interested in the corrosion by sodium agree in acknowledging that the variations of weight tend to be linear in time after an initial period. The formula worked out by Lockhart[2] leads a steady speed of corrosion for long periods of time.

Our tests show that, particularly when there is a small percentage of oxygen in sodium, the corrosion rate is really steady, but only after a long lapse of time and definitely going beyond 2000 hr. In Fig. 9 we have compared our experimental results to the corresponding values calculated from the Lockhart equation with two values for the percentage of oxygen.

We believe that experimental researches are still

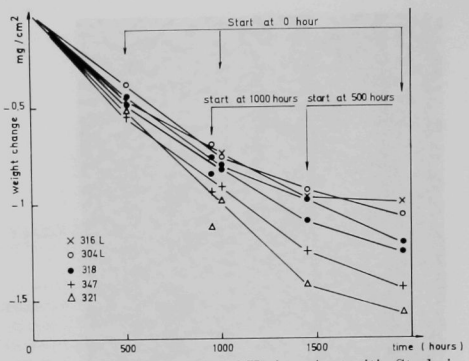

FIG. 7. Corrosion Kinetics of Various Austenitic Steels in Cold-trapped Flowing Sodium at 700°C (C_2 Loop).

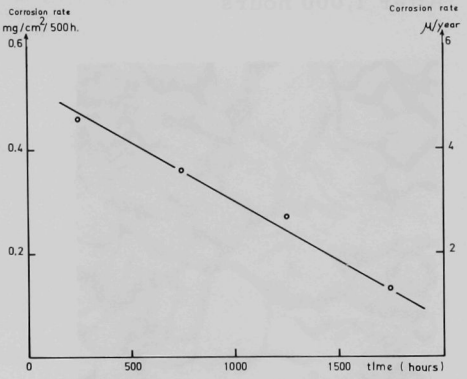

FIG. 8. Mean Corrosion Rate of an Austenitic Steel *vs* Time.

necessary to understand and define more accurately the kinetics of the phenomena of corrosion in sodium. We think that these kinetics are related to such factors as the percentage of oxygen and the speed of the fluid. Meanwhile, it is probably advisable to use discretion in the choice of the corrosion rates to be considered for very long periods.

Acknowledgment

We are most thankful to all those who took part in studying these problems and, in particular, to G. Cornec, R. Darras, D. Leclercq, and J. Sannier of CEA, and to W. Graff of Société Ugine Kuhlmann.

REFERENCES

1. L. Champeix *et al.*, CEA Report 2371 (1963).
2. H. C. Rowland, D. E. Plumlee, and R. S. Young, *Sodium Mass Transfer*, GEAP 4831 (1965).
3. K. Furukawa, J. Nucl. Sci. Tech. **3**, 501 (1966).
4. N. P. Agapova *et al.*, *Alkali Metal Coolants*, International Atomic Energy Agency, Vienna (1967), p. 85.

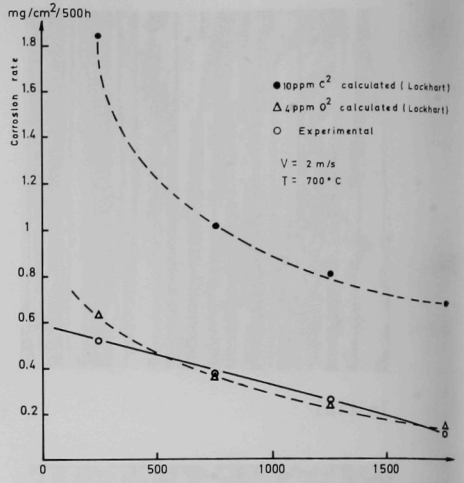

FIG. 9. Mean Corrosion Rate of an Austenitic Steel *vs* Time Compared with Results of the Lockhart Equation.

5. A. W. Thorley and G. Tyzack, *Alkali Metal Coolants*, International Atomic Energy Agency, Vienna (1967), p. 97.
6. J. Sannier and L. Champeix, *Alkali Metal Coolants*, International Atomic Energy Agency, Vienna (1967), p. 449.
7. J. Sannier and R. Vingot, CEA Report 2369 (1963).

Discussion

Mr. Weeks (Chairman): I'd like to use the chairman's prerogative to suggest that with the cold-trap temperature as low as yours, 4 ppm oxygen seems more reasonable than 10–12, don't you think?

Mr. Champeix: Probably.

Mr. Weeks: I also notice that you find a slightly higher corrosion rate for Type 321 than you do for Type 304 stainless steel, which is something that we also have been observing at Brookhaven.

Mr. Champeix: I saw also in a paper from the General Electric Co. this morning that there was more corrosion with Type 347.

Mr. Horton (AEC): Does your 9% chromium steel decarburize?

Mr. Champeix: No, no decarburization.

Mr. Weeks: But you also have a 2¼ chromium steel in the same loop. Is that correct?

Mr. Champeix: Yes.

Mr. Roy (GE): Do you think that final corrosion rates depend on the initial corrosion rate?

Mr. Champeix: I am not sure that we have final corrosion rates. It is possible to draw a very nice curve of parabolic form through the points.

Mr. Roy: Do you feel that in high-velocity sodium the rate will decrease faster?

Mr. Champeix: Perhaps, but I have no evidence.

Preliminary Corrosion Results of Haynes 25 and Type 304 Stainless Steel with 4 and 12 ppm Oxygen in Sodium at Temperatures up to 760°C*

A. J. Romano, S. J. Wachtel, and C. J. Klamut

Brookhaven National Laboratory
Upton, New York

(PRESENTED BY A. J. ROMANO)

Introduction

Potential fuel-cladding materials for advanced Liquid Metal Fast Breeder Reactors are currently under investigation at Brookhaven National Laboratory. The materials under test, at temperatures as high as 760°C, include refractory metal alloys, cobalt-base alloys, and stainless steels.

High-velocity (~22 ft/sec) corrosion studies are being carried out in two pumped loops fabricated entirely of stabilized stainless steels in which specimens are exposed to sodium in a 24-in.-long rising-temperature region. The specimens are periodically removed from each loop through an inert-atmosphere glovebox, cleaned by vacuum-distilling the residual sodium, rinsed in alcohol, and evaluated by measuring their weight changes and by metallographic examination. The weight-change measurements can subsequently be converted to mils/yr.

Results

In one of the loops, a 1655-hr test run with about 4 ppm oxygen in the sodium was concluded, and a portion (647 hr) of a second test run at about 12 ppm oxygen in sodium has been completed. Among the materials evaluated in these test runs were a cobalt-base alloy, Haynes 25, and Type 304 stainless steel. The specimens were not replaced by new specimens at the end of the run with 4 ppm oxygen.

The weight changes are plotted vs time at 760 and 710°C for the Haynes 25 alloy and the Type 304 stainless steel specimens in Fig. 1. The calculated corrosion rate (mils/yr) for the last incremental run at the two oxygen levels are also shown. The corrosion rate of Type 304 stainless steel shows a nearly linear dependence on the oxygen concentration in sodium. Haynes 25 does not show this dependence and, in fact, the corrosion rate decreases with increased oxygen.

During the test, specimens of these alloys were analysed by X-ray fluorescence. The results of the analysis of the 750°C specimens are shown in Fig. 2. The data are plotted as a ratio of counts of an element at the specimen surface to that of an unexposed specimen. Hence, values greater than 1 indicate enrichment of that constituent and values less than 1 indicate depletion.

During the run with 4 ppm oxygen in sodium, the surfaces of both alloys were depleted in nickel and chromium, and enriched with iron. When the oxygen content of the sodium was increased, the degree of enrichment and depletion of the constituents of Type 304 stainless steel decreased. Similar results were observed with respect to tungsten, cobalt, and chro-

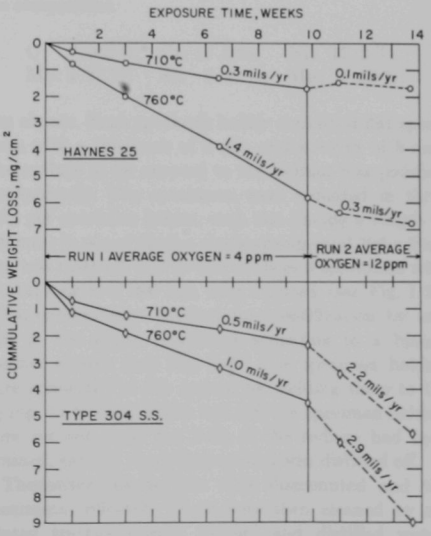

FIG. 1. Effect of Oxygen on Corrosion Rate of Haynes 25 and Type 304 Stainless Steel. (Sodium velocity = 22 fps.)

* Work performed under the auspices of the U. S. Atomic Energy Commission.

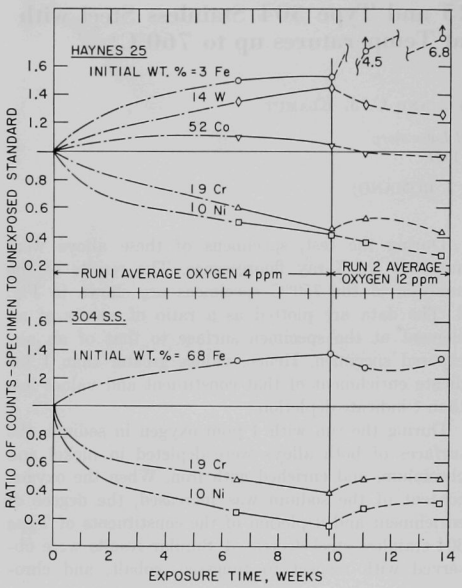

FIG. 2. Results of X-ray Fluorescence.

mium in the Haynes 25. However, the most striking change was the degree of enrichment of iron on the surface of Haynes 25; the ratio of counts increased from 1.5 at the conclusion of the low-oxygen run to 6.8 after 647 hr at the higher oxygen level. This increase in iron at the surface was contrary to the anticipated results based upon the stainless steel (Types 304 and 321) observations.

Preliminary metallographic examination of Haynes 25 after the 12-ppm-oxygen run showed the surface of the specimen to be porous to a depth of approximately 6 to 8 μ. There appears to be nonadherent particulate material on the surface, which may be deposition. Further identification of this material is being pursued.

Summary

Preliminary results show the cobalt-base alloy Haynes 25 appears to have better corrosion resistance than Type 304 stainless steel to sodium containing 12 ppm oxygen. However, the possibility of iron deposition on the surface of the Haynes 25 exists, which would certainly complicate corrosion measurements. Prolonged testing at these conditions should reveal whether the corrosion rate or the deposition rate will be predominant at equilibrium.

Corrosion and Fretting Corrosion in Sodium

A. J. Bogers, E. G. Chirer, J. W. Tichler, and A. W. J. deGee

Metal Research Institute TNO
Delft, The Netherlands

(PRESENTED BY A. J. BOGERS)

Summary

In the first part of the paper corrosion and mass-transfer tests carried out at temperatures up to 700°C in a dynamic sodium system with a thermal gradient are described. The material tested was austenitic stainless steel Type 316. The behaviour of this steel was studied in two tests lasting 3000 and 2500 hr, respectively, and with an oxygen content of the sodium of about 10 ppm. The results of weight analysis and of detailed metallurgical examination, including mainly metallography and X-ray micro-analysis, are given.

In the second part, wear tests under conditions of oscillatory relative motion (fretting wear or fretting corrosion) are described; these were carried out with a number of potential structural and canning materials. Results show significant differences between a number of generally accepted steels. Fretting tests were also performed with potential bearing materials. Preliminary results indicate that the relatively well-established material Stellite 6B may successfully be replaced by a sprayed tungsten carbide cermet. However, much work remains to be done before the composition of the hard facing layer is optimized.

I. Corrosion in Sodium

1. Introduction

Since austenitic stainless steel is very important as a structural material for fast breeder sodium systems, for fuel cladding as well as for core and component construction, the behaviour of such a material is being studied in a dynamic sodium system. It has already been established that the deterioration, expressible as the rate of metal loss per year, depends on the impurity content of the sodium, the sodium velocity, temperature, temperature difference, and time.[1, 2]

To investigate these influences within the Dutch Programme on Sodium Technology, a corrosion and mass-transfer facility was constructed. The results of the first two tests obtained in this installation will be presented in the first part of this paper.

2. Sodium System

The main characteristics of the sodium system, schematically given in Figure I-1, are as follows:

The circuit has been constructed of Type 316 stainless steel. It contains several electric heaters (H), cooling sections (C), regenerative heat exchangers (H.E.), an expansion chamber (E), an electromagnetic pump (EMP), and seven specimen holders (1–7) in the main circuit. Moreover, it contains a cold trap (CT), a plugging meter (PM), and a sodium-sampling device (S) in bypasses. There are, of course, a dumptank (D) and a number of electromagnetic flowmeters (F). The sodium content of the circuit is about 60 l. The piping of the main circuit has an inner diameter of 20 mm.

3. Specimens and Specimen Handlings

As a specimen material Type 316 stainless steel of the composition

C: 0.055%; Cr: 17.0%; Ni: 11.2%;
Mo: 2.78%; Si: 0.42%; Mn: 1.56%;

was chosen. Each specimen holder contained flat specimens with a thickness of 2 mm and a width of 8 mm. The surface to be exposed to the sodium was polished mechanically. The specimens were mounted in three slots per specimen holder, each slot having a length of 200 mm; in one of them a single specimen of 200 x 8 x 2 mm was inserted, and in two of them 6 specimens with a total length of 200 mm were inserted (see Fig. I-2). All specimens were marked for identification by saw cuts in the edges, positioned according to a binary number system (see Fig. I-3). The specimen holders were connected to the system by welding them to the piping. At the end of the test run the specimen holders were cut out, after the bulk of the sodium had been drained, and the remaining sodium was distilled off.

Thereafter the holders were dismounted and the specimens collected. These were then cleaned by repeated treatment with alcohol and distilled water, and finally dried before weighing.

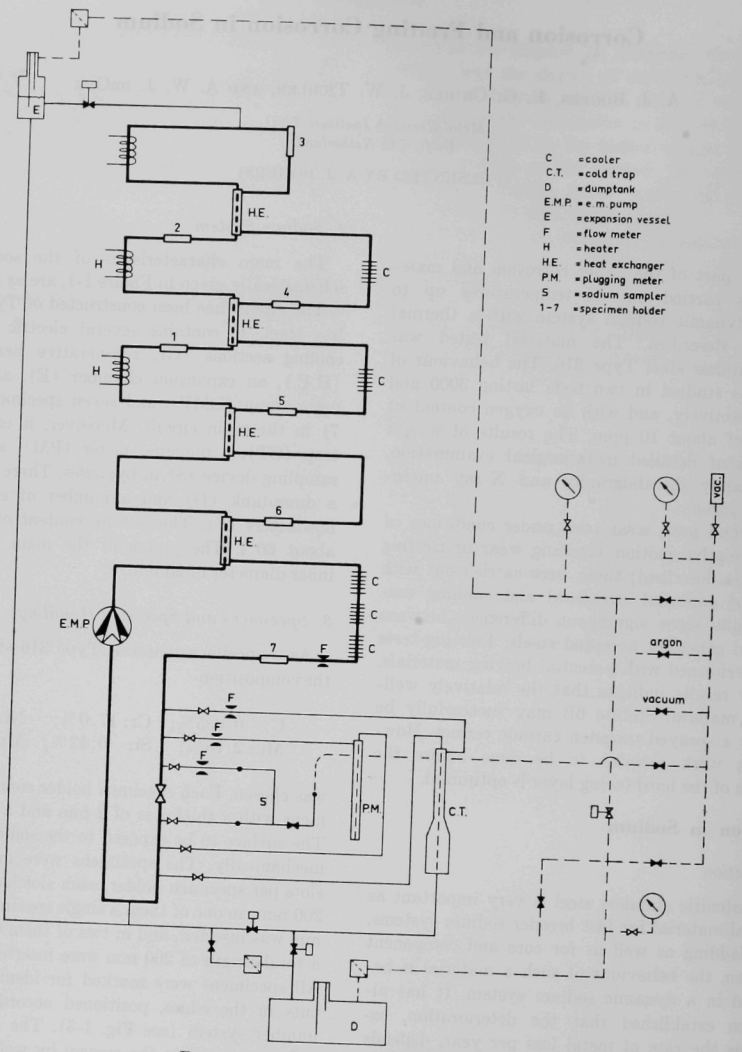

FIG. I-1. Flow Sheet for Corrosion Loop 2.

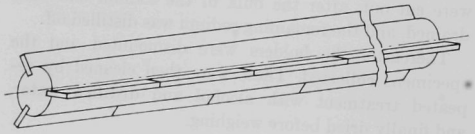

FIG. I-2. Specimen Arrangement.

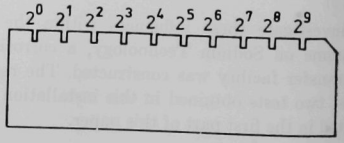

FIG. I-3. Marking of Specimen.

4. Conditions of Test Runs

First Test

The specimen holders were kept at the following temperatures (see Fig. I-1):

No. 1 at 550°C	No. 5 at 550°C
No. 2 at 600°C	No. 6 at 450°C
No. 3 at 650°C	No. 7 at 360°C
No. 4 at 600°C	

The sodium velocity was 2 m/sec, not only along the specimens, but throughout the system.

The cold-trap temperature was maintained at 250°C, and the oxygen content was checked by determining the plugging temperature as well as by chemical analysis of sodium samples. Probably as a consequence of a lack of oxide in the cold trap at that time, the oxygen content of the sodium did not correspond to a cold-trap temperature of 250°C and decreased during the test. For the greatest part of the test duration, the oxygen concentration was less than 100 ppm. The duration of the test was 3000 hr.

Second Test

The specimen holders were kept at the following temperatures (see Fig. I-1):

No. 1 at 600°C	No. 5 at 600°C
No. 2 at 650°C	No. 6 at 500°C
No. 3 at 700°C	No. 7 at 400°C
No. 4 at 650°C	

The sodium velocity was 6 m/sec along the specimens and 2 m/sec in the remainder of the system. For this test run the total specimen length was increased to 300 mm.

The average cold-trap temperature was 240°C, and the oxygen content measured by plugging meter and chemical analysis was about 15 ppm.

The duration of the test was 2500 hr.

5. Weight Analysis and Corrosion Rate

The measured weight changes have been transformed into changes in thickness, assuming that the same specific weight could be used both in case of metal gain and in case of metal loss. The mean corrosion rate is expressed in units of 10^{-3} cm/yr, and will be called positive in case of metal loss and negative in case of metal gain.

Since, with the first test, no significant difference was found between the specimens in one specimen holder, the mean corrosion rate for each specimen holder was calculated. The corrosion rates were plotted against the specimen-holder position as they were arranged from 1 to 7 (see Fig. I-1). The results are given in Fig. I-4.

In the second test, on the contrary, a significant difference in weight change was found between specimens in one holder, in such a way that always the weight change decreased according to the direction

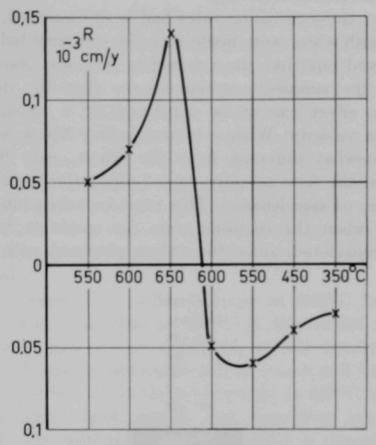

FIG. I-4. Corrosion Rate of Type 316 Stainless Steel *vs* Specimen-holder Location for Test I.

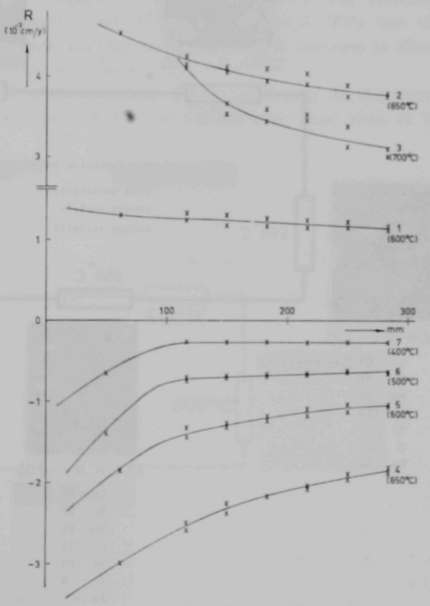

FIG. I-5. Corrosion Rate of Type 316 Stainless Steel *vs* Specimen Location in Holder for Test II.

of flow for the successive specimens in one slot. Otherwise stated, there was a marked downstream effect. This is demonstrated in Fig. I-5, where for each specimen the corrosion rate was plotted against its position in the holder (1).

After these corrosion rates had been measured, flow tests with water were made with the specimen holders. It turned out that the volumetric flow was constant along the successive specimens, so that the downstream effect cannot be explained by a change in sodium velocity. With specimen holder No. 3, which is somewhat different from the others, only 90 to 70% of the flow actually passed along the specimens because of side leakage. This must be taken into account when the corrosion rate for specimen holder 3 is considered, since the values obtained with this specimen holder at 700°C are lower than those obtained at 650°C (specimen holder 2).

From the determinations of corrosion rate given above, it is obvious that at least under the conditions of the second test run a very marked dependency on position in the loop exists.

6. *Metallurgical Examinations*

Although there was only very slight deterioration of the specimens of the first run (0.14×10^{-3} cm/year at 650°C), two methods were used to investigate observable effects, namely, microscopy of the sodium-exposed surface in the as-exposed condition without etching, and fluorescence of the exposed surface by means of defocusing the electron beam of an X-ray microanalyser, thus exciting X rays from an area of

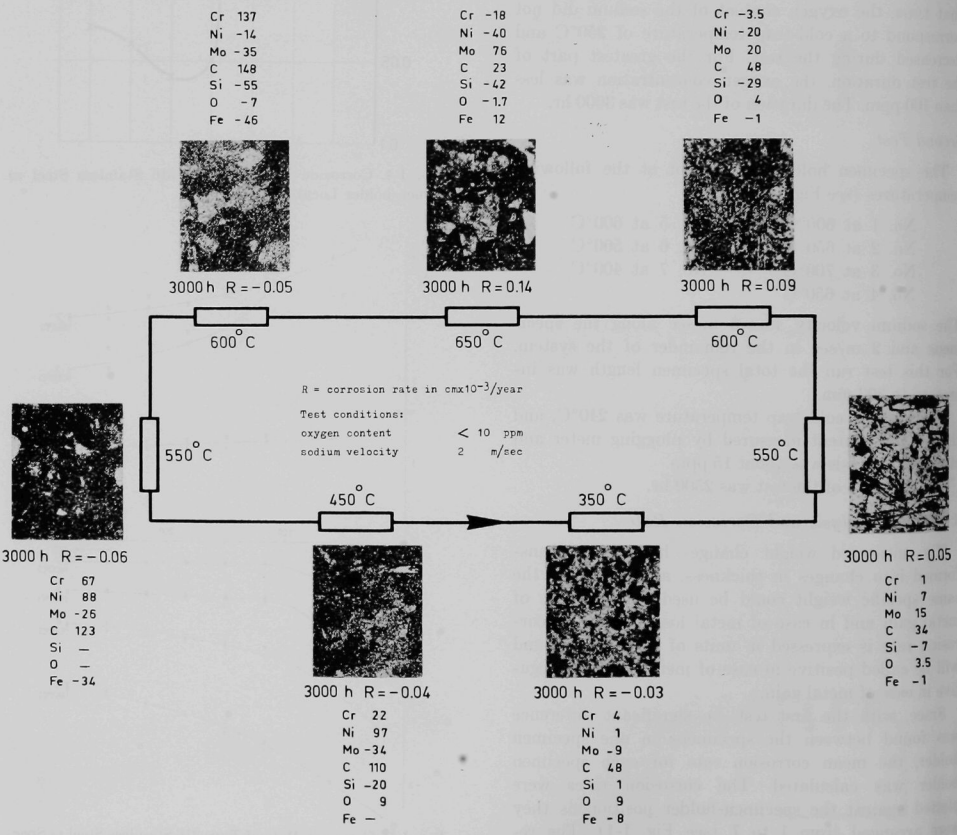

FIG. I-6. Microstructures of Sodium-exposed Specimens for Test I. (Mag. 80×)

200,000 square microns. The results of these examinations are given in Fig. I-6, where the characteristic micrograph is given for each specimen-holder position

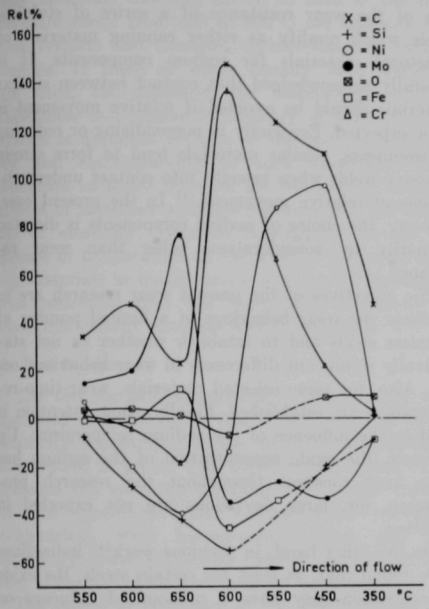

FIG. I-7. Distribution of Elements on the Surface of Specimens of Type 316 Stainless Steel for Test I.

in the loop and the results of the microfluorescence are tabulated in arbitrary units. (The percentage given for each element shows how much its concentration at the surface is higher or lower than in bulk material.)

In Fig. I-7 the microfluorescence data are given as a function of specimen-holder position. When the first position in the heated zone, i.e., at 550°C, is considered, a slight attack can be observed on the micrograph, for the surface looks as though it had been etched. The attack is a selective leaching of the various elements. At 600°C in the heated zone somewhat more attack is observed, and it should be noticed that increased amounts of chromium, nickel, and silicon were leached. At 650°C the strongest attack is observed; again these elements were strongly leached.

The situation is quite different at 600°C in the cooled zone from that at 600°C in the heated zone. A weight gain is now produced, mainly by deposition of chromium and carbon. Both attack and deposition are to be seen on the micrograph. At 550°C in the cooled zone, again attack and deposition are observed. The increased content of nickel is remarkable for this position. At 450°C still an increase in content of chromium, nickel, and carbon is found. At 350°C attack is no longer observed, but chromium and carbon are still being deposited. This was also the only position at which a slight increase in silicon content was measured.

The deterioration of the specimens of the second test run was considerably greater than that of the

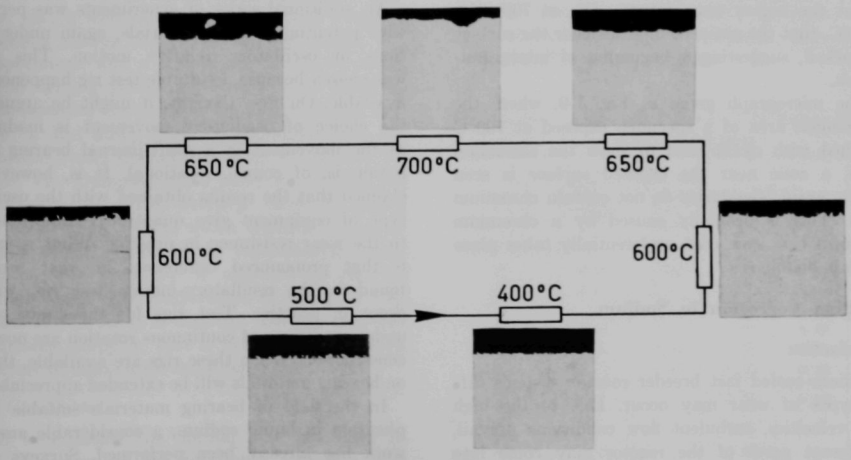

FIG. I-8. Micrographs of Specimens from Test II. (Mag. 215×)

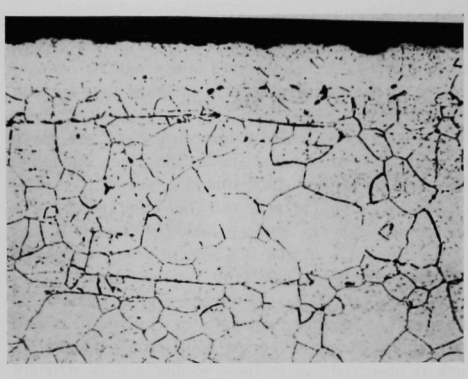

FIG. I-9. Specimen at 700°C (Test II) Etched with Oxalic Acid. (Mag. 280×)

first run being $\pm 4 \times 10^{-3}$ cm/yr at 650°C. The results of the X-ray micro-analysis are not available, but a number of effects are clearly visible on micrographs that were made of unetched cross sections of several specimens. A characteristic micrograph for each specimen holder position is given in Fig. I-8. It is observed that the attacked surface of the specimens at 600°C in the heated zone shows many indentations and dark matter. This configuration is less pronounced at 650°C and is no longer visible at 700°C.

At 650°C in the cooled zone a coarse, crystalline deposit is observed. This effect gradually disappears with lowering of temperature. It was generally observed at the higher temperatures, i.e., at 700, 650, and 600°C, that the grain boundaries near the surface were marked, suggesting a beginning of intergranular attack.

On the micrograph given in Fig. I-9, where the cross-sectional area of a specimen exposed at 700°C was etched with oxalic acid to show the chromium carbides, a zone near the exposed surface is seen where the grain boundaries do not contain chromium carbides. This is probably caused by a chromium depletion of this zone that preferentially takes place along grain boundaries.

II. Fretting Corrosion in Sodium

1. Introduction

In sodium-cooled fast breeder reactor systems different types of wear may occur. Due to the high coolant velocities, turbulent flow conditions prevail, and different parts of the reactor may come into oscillatory motion. This, in turn, may cause local wear phenomena. Furthermore, the sodium-pump bearing may cause troubles, especially during starting and stopping.

The present work has been associated with evaluation of the wear resistance of a series of stainless steels which qualify as either canning materials or structural materials for sodium components. It is generally acknowledged that contact between similar materials should be avoided if relative movement is to be expected. Especially in nonoxidizing or reducing environments, similar materials tend to form strong adhesive welds when brought into contact under conditions of relative movement.[3] In the present case, however, the choice of mating components is dictated primarily by considerations other than wear resistance.

The objectives of the present wear research are to evaluate the wear behaviour of a limited number of stainless steels and to establish whether or not statistically significant differences in wear behaviour occur. Also, for some selected materials, wear-time relationships are established. Finally, some attention is paid to the influence of the sodium temperature. Up till now, the oxide concentration of the sodium has been kept constant throughout the research programme, for, large deviations are not expected in practice.

On the other hand, in previous work[4] indications were found that, at least for certain steels, the oxide concentration may have a pronounced influence on wear in liquid sodium. This means that some additional experiments at higher and lower oxygen contents are to be performed in the near future.

An additional series of experiments was performed with potential bearing materials, again under conditions of oscillatory relative motion. This motion was chosen because a suitable test rig happened to be available. On first thought, it might be argued that the choice of oscillatory movement is inadmissible as the movement in a shaft-journal bearing combination is, of course, rotational. It is, however, not claimed that the results obtained with the oscillatory type of equipment give quantitative information as to the wear resistance in practice. What is expected is that pronounced differences in wear resistance, found in the oscillatory-motion test rig, will also occur in practice. Test rigs for the study of wear under conditions of continuous rotation are now under construction. When these rigs are available, the work on bearing materials will be extended appreciably.

In the field of bearing materials suitable for application in liquid sodium, a considerable amount of work has already been performed. Surveys of materials and methods are given by Anderson[5] and

Freede *et al.*[6] Anderson concludes that steels are never quite satisfactory at temperatures above 300°C. The same holds for nickel and nickel alloys as well as for chromium-tungsten-cobalt alloys. In fact, the only materials that can safely be used in the temperature range from 400 to 800°C are tungsten carbide cermets and titanium carbide-tungsten carbide cermets. If these or other equally hard materials are used, the necessity for maintaining extreme cleanliness and geometric accuracy in a liquid-metal system is apparent because of the poor embeddability and conformability of such materials. Thus, Anderson indicates the need for research on different classes of materials with low hardness and low modulus of elasticity. Detailed information on the influence of temperature on the wear of potential bearing materials in liquid metals is given by Roberts,[7] who concludes that the wear rate of variety of materials steadily increases with temperature.

2. *Test Equipment*

The test rig and sodium-supply system have been described in detail by de Gee *et al.*[4] In Fig. II-1 a schematic presentation of the essential components of the system is given. The experimental vessel (EV) contains the specimen assembly (S), which consists of four specimens: two moving upper specimens (cylindrical, with hemispherical tips) and two stationary lower specimens (which present flat surface to the tips of the mating upper specimens).

The radius of curvature of the hemispherical tips of the upper specimens is 2.5 mm. They are attached to a vertical shaft, which transmits the oscillatory motion. This motion is made up of two components, viz., a rotational vibration, which causes a reciprocating sliding movement between upper and lower specimens, and a superimposed normal vibration. The driving system is described in detail in (4). The essential elements of the sodium supply system are: a 30-l dump tank D, connected with the experimental vessel through the filter F and the filling valve V_F. Dumping takes place by opening the dumping valve V_D. The overflow valve V_O forms part of an overflow system which controls the maximum level of the sodium in the experimental vessel. A diffusion cold trap CT is attached to the experimental vessel. The temperature of this cold trap is kept at 150°C. As it is doubtful whether this cold trap functions properly, care is taken that the filling temperature of dump tank and filter is also 150°C.

3. *Test Conditions*

In all experiments the normal load has been 10 N, the frequency of the rotational vibration 30.0 sec^{-1}, and the normal frequency 23.3 sec^{-1}. The amplitudes of rotational and normal motion were 50 μm.

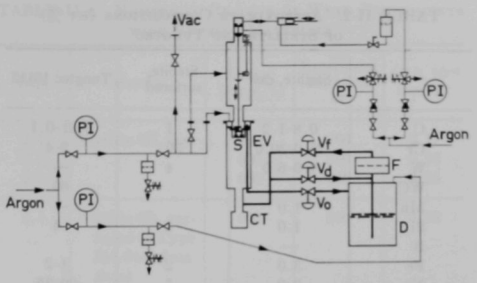

FIG. II-1. Test Rig for Testing Wear under Conditions of Oscillatory Relative Motion in Liquid Sodium (schematic).

The experimental temperatures varied from 500 to 650°C, dependent on the type of material tested.

4. *Materials Tested*

Until now, experiments were performed with five different steels, viz., 2.25Cr1Mo, Type 316 stainless steel, and three German grades of austenitic creep-resisting steels indicated as 4988, 4981, and 4961. The chemical compositions of these materials are given in Table II-1.

As potential bearing materials two hard-facing materials were tested, viz., Stellite 6B and Tungtec 10112. The chemical compositions of these materials are found in Table II-2. Both materials were surfaced on stainless steel, the Stellite by oxyacetylene welding, and the Tungtec 10112 by flame spraying and subsequent fusing. The Stellite has also been studied in the as-cast condition.

TABLE II-1. COMPOSITIONS (WT %) OF STEELS TESTED IN WEAR PROGRAMME

	2.25 Cr 1 Mo (7380)	Type 316 Stainless Steel (4401)	4988	4981	4961
C	0.10	0.06	0.05	0.06	0.04
Cr	2.38	17.0	16.15	16.30	16.2
Ni	—	11.4	14.30	16.30	13.2
Mo	1.01	2.62	1.27	1.86	0.15
Mn	0.49	1.28	1.32	1.31	1.10
Si	0.24	0.68	0.57	0.49	0.40
Nb } Ta }	—	—	0.55	0.92	0.59
V	—	—	0.71	—	—
N	—	—	0.10	—	—

TABLE II-2. Approximate Compositions (wt %) of Stellite and Tungtec

	Stellite, cast	Stellite, surfaced	Tungtec 10112
C	0.8–1.2	1	0.01–0.1
Cr	25.0–30.0	30	2–4
W	4.0–6.0	4	—
WC			60
Mn	1.0		—
Si	1.0	2	4
B	—		
Fe	3.0	2	1–2
Ni	3.0	1	30–35
Co	Bal	60	—

5. Results

5.1. Wear Mechanism of Steel in Liquid Sodium

It has been shown by de Gee *et al.*[4] that the wear of steel in liquid sodium proceeds by a mechanism of strong adhesive weld formation, particles of one specimen being transferred to the surface of the opposite specimen by the formation of microwelds between the surfaces. That the same holds in the present case is shown by Figure II-2, which shows details of cross sections through the upper and lower specimens of Type 316 stainless steel after termination of a 200-hr experiment in liquid sodium at a temperature of 600°C.

Figure II-2a shows a magnified picture of a middle section of a lower specimen, and Fig. II-2b shows an edge of the corresponding upper specimen. It can be seen that the worn surfaces are covered with a layer of transferred material which has a distinctly laminated structure. The welds between the transferred layer and the surfaces of lower and upper specimens are perfect. The laminated structure indicates that the transferred layer has been built up during many subsequent transfer operations. Figure II-2b shows how wear particles can be formed. Due to plastic shear in the transferred layer, transferred material bulges out at the edges of the upper specimen and, occasionally, a free wear particle is formed.

5.2. Numerical Results of Steel Experiments

Numerical results obtained so far are presented in Table II-3. As the research programme is not yet finished, a full statistical treatment is not possible and only tentative conclusions can be drawn.

The values of volume loss ΔV in the last column of Table II-3 were calculated on the basis of profilometric measurements, performed on the upper specimens. Each individual value is the sum of two readings which were obtained by measuring the two upper specimens available per experiment. It turns out that the reproducibility of the results is not unreasonable, taking into account the rough nature of the wear process. The average wear rate, calculated over the five 360-hr experiments performed with Type 316 stainless steel at 600°C (exp. 5 to 9), is 1.0×10^{-3} mm³/hr with a standard deviation of 39%. If the results of experiments 5 to 9 are compared with those of experiments 1 to 4 and 10 and 11, it is seen that the wear rate tends to decrease with increasing time. There is, however, not yet enough statistical evidence to support this.

The same applies for the influence of sodium temperature. Although the wear rate measured after termination of experiment 12 is rather high, there is no statistical evidence to show that the result obtained at 650°C differs significantly from those obtained at 600°C.

The results obtained with the niobium-stabilized

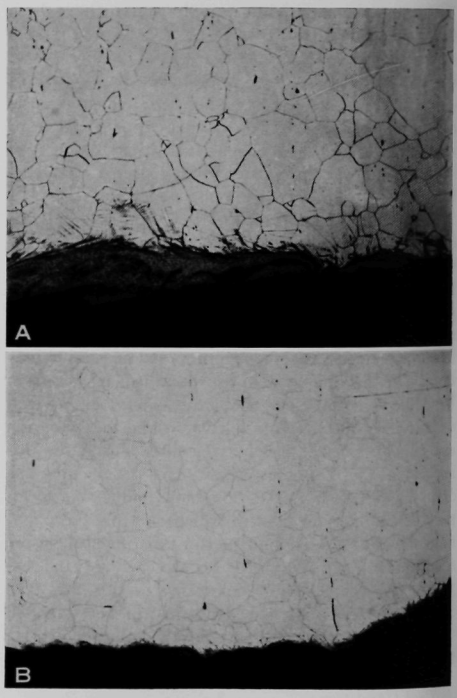

Fig. II-2. Transferred Layer on Type 316 Stainless Steel. (a) Middle section of lower specimen; (b) Corresponding edge of upper specimen.

austenitic stainless steels (experiments 13 to 18) show that there is probably no difference in wear behaviour between these three types of steel. This is expected inasmuch as the differences in chemical composition are rather small (see Table II-1). The results of the experiments performed with material 4988 (experiments 13–16) do not show a time dependency of the wear rate.

The wear rate, averaged over the results of experiments 13 to 18, is 2.8×10^{-3} mm³/hr, with a standard deviation of 28%. This value is significantly higher than the corresponding value for Type 316 stainless steel at 360 hr and 600°C.

Finally, consider the results obtained with the ferritic steel 2.25Cr1Mo (experiments 19 to 23). Of course, the number of experiments performed so far is much too small to predict the shape of the curve of wear rate versus time. An increase in temperature of 100°C (see exp. 23), however, causes a considerable increase in wear rate. This means that, when measured at 600°C, ferritic chromium steel has much less wear resistance than the austenitic stainless steels tested. Actually, the wear rates of 2.25Cr1Mo and Type 316 stainless steel measured at 600°C differ by a factor of about 10.

TABLE II-3. Numerical Results of Wear Experiments with Steels

Experiment	Material	Sodium Temp, °C	Experiment Duration, hr	$\Delta V/t$, 10^{-3} mm³/hr
	316 SS (4401)			
1.1		600	30	2.3
1.2		600	120	2.2
1.3		600	200	2.0
1.4		600	200	1.7
1.5		600	360	0.4
1.6		600	360	1.4
1.7		600	360	1.2
1.8		600	360	0.8
1.9		600	360	1.0
1.10		600	600	0.6
1.11		600	800	0.7
1.12		650	360	1.7
	4988			
1.13		650	130	2.1
1.15		650	360	3.4
1.15		650	590	1.6
1.16		650	1,050	3.5
	4981			
1.17		650	360	3.7
	4961			
1.18		650	360	2.5
	2.25 Cr-1 Mo (7380)			
1.19		500	200	1.8
1.20		500	400	1.7
1.21		500	600	1.5
1.22		500	800	0.9
1.23		600	200	9.8

TABLE II-4. Numerical Results of Wear Experiments with Bearing Materials

Exp.	Material	Sodium Temp, °C	Experiment Duration, hr	$\Delta V/t$, 10^{-3} mm³/hr
2.1	Stellite 6B, cast	600	360	0.17
2.2		600	360	0.25
2.3		650	360	0.25
2.4	Stellite 6B, surfaced to Type 316 Stainless Steel	500	360	0.28
2.5		650	360	0.08
2.6		650	720	0.58
2.7		650	858	0.77
2.8	Tungtec 10112	650	360	0.03
2.9		650	720	0.07

5.3. Wear of Hard Facing Materials

Microscopic study of the worn surfaces of Stellite and Tungtec specimens reveals that, again, wear proceeds by a mechanism of adhesion. However, transfer is less pronounced and, presumably, the average residence time of transferred particles is much shorter than in the case of steels.

The numerical results obtained with these materials are given in Table II-4. Again, the number of experiments performed has been too small to allow statistical data analysis. Nevertheless, the results suggest that:

There does not seem to be a difference between cast Stellite 6B and Stellite 6B, surfaced to Type 316 stainless steel. Nor can a distinct temperature effect be found.

The wear rate of surfaced Stellite 6B seems to increase steeply with time. This is a very undesirable effect; it is clear that the wear rate of Tungtec 10112 is lower by an order of magnitude than that of Stellite.

Conclusions

The results show that significant differences in wear resistance between austenitic stainless steels 316 at 600°C and stablized German grades at 650°C can be observed. The wear rate of 316 at 600°C seems to decrease with increasing time. More data are needed to support this. The same effect is not observed with the stabilized German grades. The wear rate of 2.25 Cr1Mo increases sharply with temperature between 500 and 600°C. The wear rate of surfaced Stellite 6B increases steeply with time.

Tungtec 10112, plasma sprayed and fused on Type 316 stainless steel, has a much higher wear resistance than Stellite 6B.

REFERENCES

1. E. L. Dunn, *Sodium mass Transfer VI. Statistical Correlation of Corrosion Data*, GEAP 4183 (1964).
2. A. W. Thorley and C. Tyzack, "Corrosion Behaviour of Steel and Nickel Alloy in High-temperature Sodium," *Proceedings of the Symposium on Alkali Metal Coolants*, Int. Atomic Energy Agency, Vienna (1966), pp. 97–118.
3. F. P. Bowden and D. Tabor, *The Friction and Lubrication of Solids*, Clarendon Press, Oxford (1950) pp. 82–111.
4. A. W. J. de Gee, C. P. L. Commissaris, E. G. Chirer, and A. J. Bogers, "Equipment for the Study of Wear under Conditions of Oscillatory Relative Motion in Liquid Sodium," *Proceedings of the Symposium on Alkali Metal Coolants*, Int. Atomic Energy Agency, Vienna (1966), pp. 415–426.
5. W. J. Anderson, "Lubrication of bearings with Liquid Metals," *Advanced Bearing Technology*, NASA SP-38, Washington, D. C. (1964), Ch. 14.
6. W. J. Freede, L. Newcomb, and R. S. Kennedy, *Static and Sliding Contact Behaviour of Materials in Sodium Environments at Elevated Temperatures*, NAA-SR-12446 (1967).
7. W. H. Roberts, Proc. Inst. Mech. Engrs. Conference of Non-conventional Lubricants and Bearing Materials, Manchester (1962), The Inst. of Mech. Engrs., London.

Discussion

Mr. Horton (AEC): What do you do with the numbers for the wear rate of austenitic stainless steel? How do they help your designers?

Mr. Bogers: We do not pretend to give any design data on these, but we do provide a type of merit rating between these different metals and alloys. You can also get an impression of certain things: for example, does the wear increase with time, does the wear rate increase with time for this particular material?

Mr. Horton: As a result of these tests would you not say go to those higher-strength steels in place of Type 316?

Mr. Bogers: We were looking at these types of steel under this particular kind of motion to see whether, for instance, degenerated tubes might be subject to real damage when they were in motion relative to support grids and things like that.

Mr. Beaufrere (EDF): There is confusion between your test and ours (which I explained yesterday). You have made fretting-corrosion tests and observed wear. But it is perhaps not a good test to observe wear. We have made friction tests, sliding tests, and vibrating tests. We also have done fretting-corrosion tests, and we have never observed, for durations up to 3000 hr, any fretting corrosion characterized by pitting.

Mr. Bogers: We happen to have had these fretting installations available, so we made our first experiment there. We now have sliding-wear installations especially for the study of the wearing material.

Corrosion Studies of Stainless Steel in Flowing Sodium at High Heat Flux*

J. Hopenfeld

Atomics International
A Division of North American Rockwell Corporation
Canoga Park, California

(PRESENTED BY J. H. SHIVELY)

Abstract

An experimental technique for the study of corrosion of stainless steel fuel cladding, with heat flux at the surface, in flowing sodium is described. The experimental results indicate that the sodium at the entrance to the heated section is saturated with respect to the corrosion products. This observation together with the well-defined hydrodynamic flow in the test section provides means for testing some of the prevailing hypotheses about the basic mechanism of corrosion in sodium.

Because of preferential dissolution of chromium and nickel, an activation technique was developed to measure individual corrosion rates of iron and chromium. After exposure to 1210°F, 20-ft/sec sodium for 387 hr at a heat flux of 0.8×10^6 Btu/ft^2-hr, the relative average losses of iron and chromium over the heated zone were found to be $0.57\% \pm 0.32\%$ and $2.39\% \pm 0.45\%$, respectively. Methods for improving the accuracy of these results and obtaining local measurements instead of average values for the entire heated zone are discussed.

Surface roughness measurements show that exposure to sodium under heat-flux conditions for less than 600 hr tends to smooth the surface in the heated zone and roughen the surface in the unheated zone. The available data are not sufficient to provide a complete explanation for these observations.

Introduction

The corrosion behavior of austenitic steels in flowing sodium have been studied by Young and Lockhart,[1] Thorley and Tyzack,[2] Agapova, Ioltukhovsky, and Romaneer,[3] and Weeks.[4, 5] The results reveal that corrosion is affected by many parameters and that at the present time there is no theory that will satisfactorily account for the experimental observations. There is not sufficient information about the behavior of steels under heat-flux conditions such as would be encountered by the fuel cladding during reactor operation. Therefore, a program was initiated at Atomics International to study the effect of internally generated heat flux on corrosion of stainless steel in flowing sodium so that an accurate corrosion allowance can be made for cladding thickness.

* Work performed under U. S. Atomic Energy Commission Contract AT-(04-3)-701.

When heat is flowing from the surface of the metal to the sodium, a local temperature differential exists between the metal surface and the liquid; the solubility of the metal in sodium at the hotter surface is higher than the solubility in the bulk of the liquid. If it is assumed that the surface-to-bulk concentration difference is the driving force for mass transfer, then the mass-transfer rate under heat-flux conditions would not obey the same correlation as obtained with isothermal specimens in ΔT loop experiments. There the surface-to-bulk concentration difference is established by the simultaneous dissolution and deposition of material in the hot and cold legs of the loop, respectively. When the deposition rate in these loops is much slower than the dissolution rate, the bulk sodium at the hot-leg isothermal specimen will be very near saturation with respect to the corrosion products. By contrast, because there is a heat flux at the specimen surface, the local bulk sodium concentration will always be less than that at the surface by an amount that cannot be smaller than that corresponding to the surface-to-bulk temperature gradient.

During the course of experimental planning it was found that the simulated, internally heated cladding is also suitable for yielding information about the basic mechanism of mass transfer, because the heated area is very small compared to the isothermal loop area and, therefore, the bulk sodium at the inlet to the heated zone is saturated with respect to the species undergoing mass transfer. This is in contrast to the conventional ΔT loop studies in which the bulk concentration at the inlet to the test section is unknown.

The purposes of this paper are to describe an experimental procedure that includes a unique method of measuring corrosion rates in sodium and to present some preliminary experimental results on corrosion rates under heat-flux conditions.

Apparatus and Method

A. Description of the Loop

Figure 1 is a schematic of the test loop, constructed of Type 304 stainless steel, Schedule 40 pipe with valves of Type 316 stainless steel. The loop contains 51 gal of sodium when filled to normal operating level. The surface area exposed to sodium is approximately 105 ft^2.

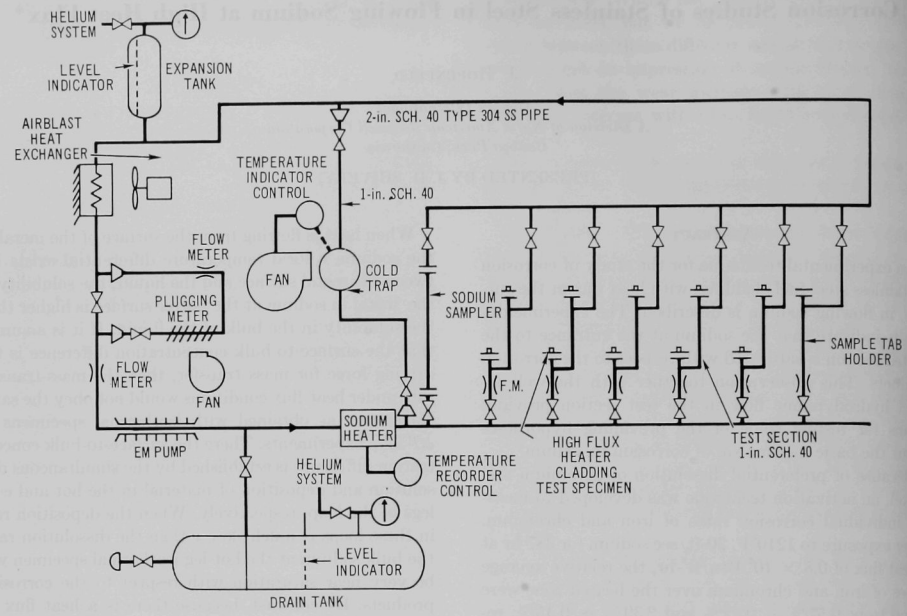

FIG. 1. Cladding Test Loop.

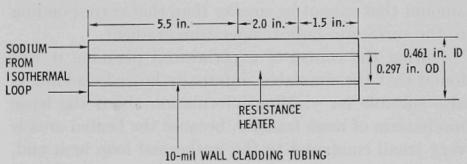

FIG. 2. Schematic of the Test Section.

There are five parallel legs, each with two sections. Excluding the test section regions, the sodium in the loop is maintained at approximately constant temperature.

Sodium purity is reduced to less than 10 ppm dissolved oxygen by use of a forced-circulation cold trap prior to a run. The oxygen concentration is monitored with a plugging meter. Sodium samples are taken weekly during operation to check on the impurity level in the loop.

B. Description of the Test Section

Figure 2 shows a schematic of the test section. The test section is a concentric annulus 9 in. long with outer and inner diameters of 0.461 and 0.297 in., respectively. The 2-in. heated portion of the cladding is positioned at a distance of 5.5 in. from the entrance to the annulus; this corresponds to a length of 34 hydraulic diameters. For turbulent flow, the velocity profile would, therefore, be fully established throughout the heated section.[6]

If the driving force for metal dissolution is the difference between the concentration of the dissolved metal in sodium next to the surface and of the dissolved metal in the bulk of the liquid, the mass flux per unit area, J, can be expressed by

$$J = K[C_w^\circ - C_b] \quad (1)$$

for a solution rate-controlled process and by

$$J = h[C_w^\circ - C_b] \quad (2)$$

for the diffusion rate-controlled process, where K is a reaction-rate constant, h is a mass-transfer coefficient in the liquid phase, and C_w° and C_b are the solubility of the metal at the surface and the concentration of the dissolved metal in the bulk liquid, respectively. Because the surface temperature of the heated portion of the cladding increases in the direction of the flow, C_w° will also increase in that direction. The constant K is independent of flow velocity and must be determined experimentally. However, for a diffusional process through the liquid (see Appendix), the local corrosion can be

expressed as

$$J = GAB\beta \int_0^X \frac{(X - \xi)^{-p}}{(\alpha + \beta\xi)^2} \exp\left(-\frac{B}{\alpha + \beta\xi}\right) d\xi, \quad (3)$$

where

G = constant depending upon velocity, dimension of annulus, and the diffusion coefficient of the metal in sodium;
X = distance from heated section;
ξ = dummy variable;
α, β = constants describing the variation of surface temperature along the heated section;
A, B = constant appearing in the equation which relate solubility to temperature;
p = constant depending on Reynolds number.

Equation 3 was derived for the case in which the bulk sodium is saturated at the start of the heated zone and the bulk enrichment in corrosion products is negligible compared to the local difference between solubility at the surface and bulk solubility at the entrance to the heated section. For corrosion rates of the order of 2 mils/yr this assumption is valid for the present system over a wide range of experimental variables.

Measurements of Corrosion Rates

A test of the validity of either Equation 1 or Equation 3 requires measurements of the local corrosion rates. In the case of an alloy such as stainless steel, the various species dissolve at different rates and, therefore, gross weight measurements of the sample before and after exposure to the sodium environment would not yield information about the dissolution of any of the individual species. What is needed, therefore, is a method of measurement capable of detecting separately the loss of iron, chromium, and nickel from the sample under examination. To this end, two identical cladding tubes are irradiated at a flux of approximately 10^{13} n/cm^2-sec for 2 hr. After irradiation, the gamma-ray spectrum of both tubes is measured with a counting detector. This spectrum consists of gamma rays from the isotopes of iron, chromium, and cobalt. (Because of the short half-life of nickel it is physically inconvenient to measure this species at the present time.) The samples are counted several times at various locations along their surface. One tube is then placed in the sodium loop and the other tube kept as a reference. The same counting procedure is repeated when the test sample is removed from the loop.

The activity loss due to corrosion is then obtained from the change in counts of the exposed sample after allowing for natural decay. The latter is established by the reference tube.

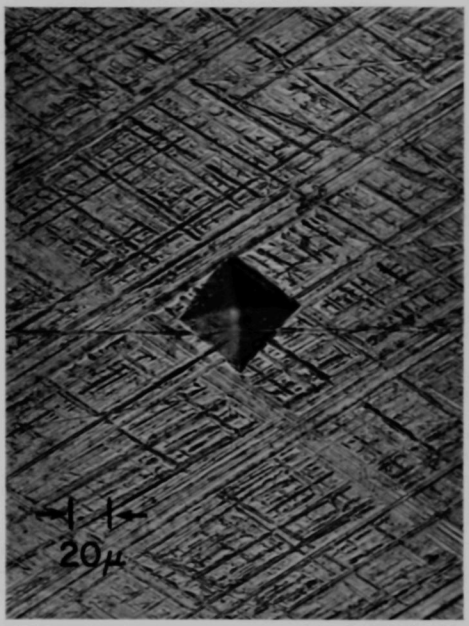

FIG. 3. Vickers Diamond (136°) Indentation Used for Surface Recession Measurements.

In addition to measuring corrosion by the activation method, each sample is indented along its surface with several indents as shown in Figure 3. The depth of penetration of such an indent is one seventh of its diagonal. The surface recession is thus calculated from the change in the dimension of the diagonal. Attempts to check the accuracy of this method by electrochemically removing a known amount of material failed because of rounding of the indent edges due to preferential metal dissolution at the sharp corners.

Results

A. Material Loss

1. Activation Method

Table 1 summarizes the activity change, as measured with a sodium iodide detector, for a test tube which was exposed to flowing sodium for 387 hr. It can be seen from the table that the loss of counts due to radioactivity decay and the total loss due to corrosion in the heated zone are of the order of 6×10^5 and 9×10^4 counts, respectively. The error in the count rate

TABLE 1. Results of Activity Change of Irradiated Type 304 Stainless Steel Cladding Tube after Exposure to Sodium for 387 Hours*

Distance from Entrance to Test Section (in.)	Initial Count of Test Sample (millions)		Change in Activity of Test Sample (millions)		Average Decay of Reference Sample (count ratio)		Loss of Counts of Test Sample Due to Natural Decay (millions)		Loss of Counts due to Corrosion (millions)		Average Activity Loss due to Corrosion (%)	
	Total	Cr	Total	Cr	Total	Cr	Total	Cr	Total	Cr	Total	Cr
2.24	16.508[a]	2.593[b]	6.240[c]	1.466[c]			6.256[c]	1.480[c]	−0.016[c]	0.014[c]		
Nonheated zone	16.045[b]	2.593[b]	5.946[d]	1.498[d]			5.985[d]	1.498[d]	−0.039[d]	0.000[d]	−0.214	−0.185
2.50	16.339	2.505	6.183	1.438			6.192	1.432	−0.009	−0.006		
Nonheated zone	15.905	2.505	5.910	1.465	0.621[c]	0.428[c]	5.932	1.450	−0.022	−0.015		
6.25	16.972	2.720	6.510	1.577	0.627[d]	0.422[d]	6.432	1.553	0.078	0.024		
Heated zone	16.537	2.720	6.238	1.622			6.168	1.570	0.070	0.052		
6.50	16.429	2.709	6.329	1.571			6.226	1.545	0.103	0.026	0.845	2.39
Heated zone	15.992	2.709	6.041	1.590			5.965	1.565	0.076	0.025		
6.75	17.242	2.898	6.639	1.665			6.535	1.655	0.104	0.010		
Heated zone	16.798	2.898	6.360	1.712			6.266	1.680	0.094	0.032		

* Sodium Velocity = 20 ft/sec; Heat Flux = 0.8×10^6 Btu/ft²-hr; Inlet Bulk Sodium Temperature = 1210°F.

Notes apply to whole column: [a] Count taken on 7-11-68.
[b] Count taken on 7-12-68.
[c] Count change during 7-11 to 8-15.
[d] Count change during 7-12 to 8-16.
[e] Count change during 7-12 to 8-15.

can be calculated[7] as follows:

$$\left(\frac{\sigma_s}{r_s}\right)^2 = \frac{1}{r_s\tau}\left[1 + \frac{2}{r}\left(1 + \sqrt{1 + r}\right)\right], \qquad (4)$$

where

σ_s = standard deviation of the net sample count rate;
r_s = sample counting rate change due to corrosion only;
r = ratio of sample to background count rates;
τ = total counting rate = counting time for background plus counting time for sample
= 15 min + 15 min.

If we assume the background count to be of the order of 12×10^6 counts,

$$r = \frac{9 \times 10^4}{12 \times 10^6} = 0.75 \times 10^{-2};$$

$$r_s = \frac{9 \times 10^4}{15} = 6 \times 10^3 \text{ counts/min};$$

$$\left(\frac{\sigma_s}{r_s}\right)^2 = \frac{1}{(6 \times 10^3)30}\left[1 + \frac{2}{0.75 \times 10^{-2}} \cdot (1 + \sqrt{1 + 0.75 \times 10^{-2}})\right]$$

$$= 2.69 \times 10^{-3};$$

$$\epsilon = \frac{\sigma_s}{r_s} = \pm 5.46 \times 10^{-2};$$

$$3\sigma_s = 3\epsilon r_s$$

$$= 3 \times 5.46 \times 10^{-2} \times 9 \times 10^4$$

$$= 1.47 \times 10^4 \text{ counts.}$$

Total count loss in the heated zone is

$$9 \times 10^4 \pm 1.47 \times 10^4 \text{ counts } (3\sigma),$$

and similarly, the total count gain in the unheated zone is

$$2.5 \times 10^4 \pm 1.46 \times 10^4 \text{ counts } (3\sigma).$$

With the exception of one location, the data indicate a slight activity gain (both total and chromium) in the unheated upstream section of the cladding. The magnitude of the activity loss in the heated zone is more than four times as large as the magnitude of activity gained in the unheated zone. As indicated above, the total count gained is larger than the counting error and on that basis cannot be disregarded; however, more data are needed before this gain in activity can be regarded as real and not a result of other system errors.

Each measurement in the heated zone was found

to be influenced by the total activity of the heated section, due to insufficient collimation. Thus, one must regard these readings as representing average loss rather than local differences. The measurements of heated and unheated regions were not influenced by each other, because the section between them was not irradiated and added shielding was used.

Measurements of iron and cobalt with a solid-state detector showed that the ratio of iron to cobalt before and after exposure to sodium remained the same. From the known amounts of iron, chromium, and cobalt in stainless steel (Fe: 70%, Cr: 18.9%, Co: 1%) and from the total and chromium activity loss, the loss in iron was found to be: 0.75% ± 0.32%. It is of interest to note that the relative loss in iron is small compared to the relative loss in chromium (2.39% ± 0.45%).

2. Indentation Method

The surface recession of the same irradiated cladding tube as measured by the indentation method is shown in Fig. 4. The extremes of each datum point represent two separate measurements of two different persons. The average diagonal of the indents before and after the test ranged from 56 to 60 μ and from 44 to 59 μ, respectively. With the microscope scale calibrated to 0.5 μ, and the depth of the indent being $\frac{1}{7}$ of the diagonal, the reading error is ± 0.071 μ. The relatively large difference between the two independent observations is attributed to the difficulty in locating the extremes of the diagonal. This uncertainty can be reduced by increasing the number of indents along the specimen surface.

The data on Figure 4 indicate that no surface recession occurs in the unheated region upstream of the heated area and that surface recession extends beyond the heated area in the downstream direction. Visual observations of the surface are consistent with the latter findings. Because of the uncertainty in the absolute measurements, the method is useful only as a qualitative indication of corrosion rates at various locations on the specimen.

Surface Characteristics

In a visual inspection of the test sample after exposure to sodium, a shiny appearance was observed from the start of the heated section extending throughout the length of the sample in the downstream direction. The upstream unheated portion of the sample exhibited a rather dull surface appearance. Figure 5 shows stereo-pair replicas of the (a) as-received surface, (b) heated surface, and (c) upstream-unheated surface after exposure to flowing sodium for 589 hr.

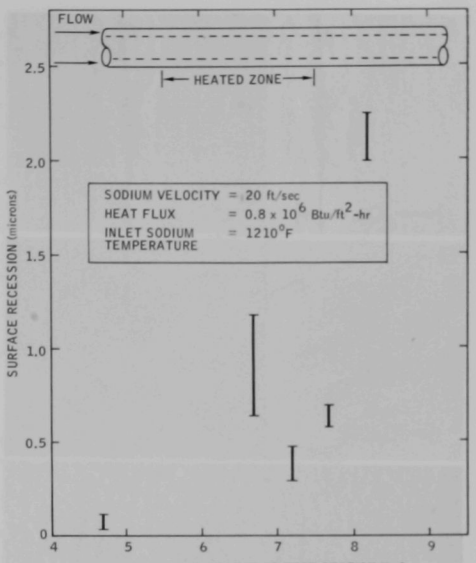

FIG. 4. Surface Recession as Measured by Indents.

To distinguish quantitatively between the three surfaces of Figure 5, profile measurements from the electron-micrograph stereograms were made. A Zeiss Stereotope plotter was used for that purpose. Briefly, the procedure employed was as follows:

After proper orientation of the photo pair on the instrument base carriage, parallactic values were read at closely spaced (2-mm) intervals along selected image profile lines. These parallactic values were then related to the surface-height differences by taking into account the angle of tilt between the two exposures of the stereogram and the image magnifications.

The height differences thus obtained along the three surfaces of Figure 5 are plotted in Figure 6. The arithmetic-average surface roughness of the as-received, heated, and unheated surfaces was found to be 0.21, 0.12, and 0.25 μ, respectively. This indicates an increase in roughness of the unheated zone and decrease in roughness of the heated zone. It is interesting to note that in Figure 5 the grain boundaries are lower with respect to the grain surfaces, indicating a preferential attack of a higher rate at the grain boundaries.

A heated sample held at 1250°F in vacuum (10^{-8} mm) showed no surface change after 200 hr, indicating that the observed phenomenon is not due to temperature alone.

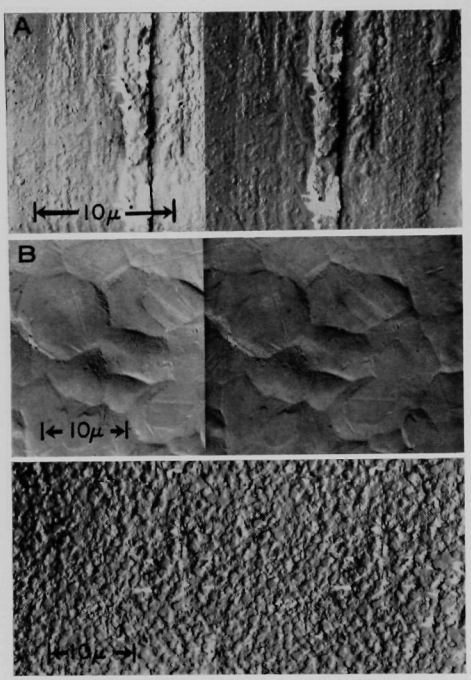

FIG. 5. Stereo-pair Surface Replicas. (a) As-received surface, 320 grit paper finish; (b) Heated-zone surface; (c) Upstream heated-zone surface.

Time of exposure	= 589 hr
Cladding surface heat flux	= 10^6 Btu/ft²-hr
Sodium velocity	= 20 ft/sec
Loop temperature	= 1210°F

Formation of Ferritic Layer

Electron-microprobe examinations revealed that in the heated region a thin layer near the surface of the alloy was relatively rich in iron, but depleted of chromium, nickel, and manganese. The thickness of this layer, referred to as the ferritic layer, changed along the surface of the cladding tube. Figure 7 shows that the thickness of the ferritic layer increased from zero upstream of the heated section to a maximum of 0.4 mil at the downstream end of the heated section. From there on, the ferritic layer still existed, but its thickness decreased.

Discussion

The success of the present experimental method used to yield information about the mechanism of mass transfer in sodium relies heavily upon the assumption that the sodium at the start of the heated zone is saturated with respect to chromium, nickel, and iron. The experimental observations that no material was lost in the upstream unheated section of the sample, as indicated by the indentation and activation measurements and the absence of ferritic-layer formation, substantiates this assumption. The surface appearance of the unheated zone indicates that some sort of material deposition takes place there. More data of activated specimens are needed before it can be ascertained that the small gain in activity in the heated zone is due to deposits of corrosion products originating in the heated zone.

The observations of material loss extending beyond the heated zone in the downstream zone would seem to indicate that the bulk sodium along the heated region is not saturated with corrosion products. To ascertain this point, however, it would be required to show experimentally that there is no temperature gradient between the surface and the bulk sodium downstream from the heated zone.

Since data from 400°F ΔT loops show corrosion rates of the same magnitude as those observed in the present experiment, it would seem to indicate that the driving force for mass transfer in these loops corresponds to a ΔT closer to 25°F (difference between the average surface temperature in the heated zone and inlet bulk sodium temperature) than to 400°F.

Because the degree of undersaturation in the sodium

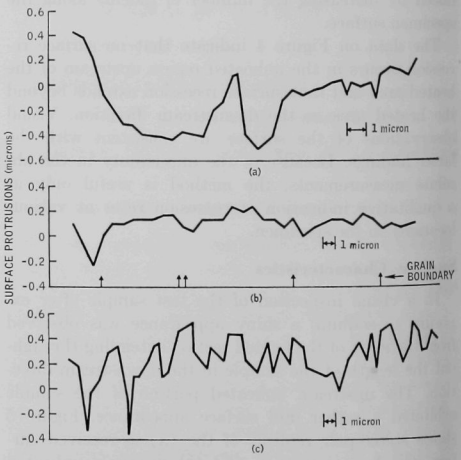

FIG. 6. Surface Roughness as Measured from Stereo-pair Replicas; (a) As-received Surface, (b) Heated-zone Surface, and (c) Unheated-zone surface.

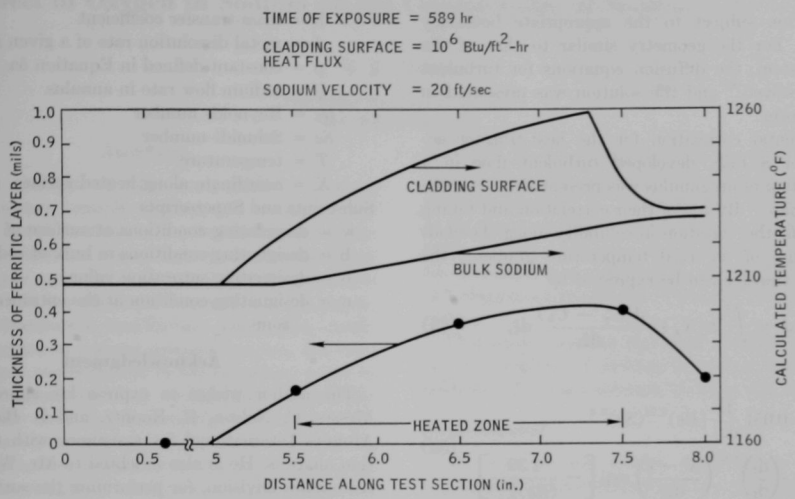

FIG. 7. Thickness of Ferritic Layer along Cladding As Measured from ×500 Photographs of Etched Cross Sections.

stream could be expected to depend upon the residence time of the sodium in the heat exchangers and on the size of the heat exchangers, one would expect variations in the corrosion rates at various loops as, indeed, is observed.

The present experiments promise to provide the means for determining the mass-transfer coefficient (h or k) and thereby to allow application of the appropriate scaling laws when experimental data from loop studies are applied to reactor systems.

Lack of sufficient experimental data on the effects of system parameters such as sodium velocity, impurity level, and temperature prevents a comprehensive comparison of the results with theoretical predictions. It is of interest to note, however, that use of solubility data for iron in sodium in the ppm range together with Equation 3 yields corrosion rates which are higher by more than two orders of magnitude than those presently observed.

Summary and Conclusions

1. An experimental test for studying mass transfer under heat-flux conditions has been described. The test results are amenable to theoretical analysis because, before reaching the heated zone of the specimen, the sodium is saturated with respect to the corrosion products and because the hydrodynamic flow in the test section is well understood.

2. A radioactive method is suitable to provide measurements of preferential dissolution rates of chromium and iron for short periods of exposure to sodium. The accuracy of the present results can be improved by (a) using a solid-state detector for the initial count to distinguish between the peaks of iron and cobalt, and (b) to section the exposed specimen before counting so as to minimize the interference from neighboring areas.

3. The average surface recession as measured by the indentation method (1.10 mils/yr) was found to be in fair agreement with the calculated value from iron loss as measured by the activation method (0.94 mil/yr).

4. The total loss of chromium and iron corresponds to a linear recession rate of 2.01 mils/yr, indicating that weight measurements when directly interpreted in terms of surface recession can introduce sizable errors.

5. Surface roughness measurements show that the roughness of the heated zone decreases while that of the unheated zone increases in comparison with the as-received surface. The available data are not sufficient to explain the reason for surface changes in the unheated zone.

6. More data are needed to yield information about the mass-transfer coefficient before the result can be applied to calculate corrosion rates of cladding in the actual reactor system.

Appendix

For a diffusion-controlled process, the mass transfer of dissolving species from the surface to the bulk sodium can be obtained by solving the convective-diffu-

sion equation subject to the appropriate boundary conditions. For the geometry similar to that of the present system, the diffusion equations for turbulent flow were solved[8] and the solution was presented in graphical form.

Experimental correlation for the heat-transfer coefficient for a fully developed turbulent flow in a heated section of an annulus was presented by Farman and Beckman.[9] By use of their correlation and taking into account the variation in solubility along the cladding because of an axial temperature gradient, the local mass transfer can be expressed by

$$J = \int_0^X h(X, \xi) \frac{d(C_w^o - C_b)}{d\xi} d\xi, \qquad (5)$$

where

$$h(X, \xi) = 0.051 \frac{D}{d_{eq}} (Re)^{0.78} (Sc)^{0.4} \cdot \left(\frac{d_2}{d_1}\right)^{0.45} \left(\frac{X - \epsilon}{d_{eq}}\right) \exp\left[-\frac{1.39}{(Re)_{d_{eq}}^{0.196}}\right] = G(X, \xi)^{-p}. \qquad (5a)$$

The solubility at the wall can be expressed in terms of the local temperature:

$$C_w^o = Ae^{-B/T}. \qquad (6)$$

If the variation of the surface temperature along the heated section may be taken to be linear, Equation 6 becomes

$$C_w = Ae^{-B/(\alpha+\beta\xi)}. \qquad (7)$$

For mass-balance consideration the bulk concentrations C_b is given by

$$C_b = C_{b,e}^o + \frac{J(\pi d_1)X}{Q} \qquad (8)$$

when the second term on the right of Equation 8 is very small compared with $C_w^o - C_{b,e}^o$ The above equations reduce to

$$J = GAB\beta \int_o^X \frac{(X - \xi)^{-p}}{(\alpha + \beta\xi)^2} \exp\left(-\frac{B}{\alpha + \beta\xi}\right) d\xi. \qquad (9)$$

Nomenclature

A, B = constants defined in Equation 6
C = concentration of a given specie in sodium
D = diffusion coefficient of a species in sodium
d_1 = outside diameter of clad tube
d_2 = inside diameter of annulus
d_{eq} = equivalent diameter
G = constant defined in Equation 5a
h = mass-transfer coefficient
J = metal dissolution rate of a given species
p = constant defined in Equation 5a
Q = sodium flow rate in annulus
Re = Reynolds number
Sc = Schmidt number
T = temperature
X = coordinate along heated surface

Subscripts and Superscripts

w = designating conditions at surface of cladding
b = designating conditions in bulk of sodium
o = designating saturation value
e = designating condition at the entrance to heated zone

Acknowledgment

The author wishes to express his appreciation to Messrs. C. Nelson, R. Koontz, and L. Baurmash of Atomics International for assistance with the activation analysis. He is also indebted to Mr. W. H. Cook, Autonetics Division, for performing the surface roughness measurements.

REFERENCES

1. R. S. Young and R. W. Lockhard, *General Electric Sodium Mass Transfer Program*, Conf. 650620 (1965).
2. A. W. Thorley and C. Tyzack, *The Corrosion of Iron and Nickel-Based Alloys in High-Temperature Sodium*, TGR 1356(C) (Nov 1966).
3. N. P. Agapova, A. G. Ioltukhovsky, and V. V. Romanneer, *Behavior of Stainless Steel in Sodium in the 600–900°C Temperature Region*, paper SM-85/51 presented at the IAEA Symposium on Alkali Metal Coolants in Vienna, Austria, November 28–December 2, 1966.
4. J. R. Weeks, "Sodium Corrosion Mechanism Program," *in Annual Progress Report of Work Sponsored by the Fuels and Materials Branch*, BNL-50092 (T-482) (January 1–December 31, 1967).
5. J. R. Weeks, C. J. Klamut, and D. H. Gurinsky, *Corrosion of the Aklali-Metals*, BNL-10800 (1966).
6. H. Schlichting, *Boundary Layer Theory*, McGraw-Hill Book Company, Inc., New York (1960).
7. M. A. Greenfield and R. L. Koontz, *A Universal Function for Computing Counting Performance*, International Journal of Applied Radiation and Isotopes, **8**, 205–210 (1960).
8. W. M. Kays and E. Y. Leung, *Heat Transfer in Annular Passage-Hydrodynamically Developed Turbulent Flow with Arbitrary Prescribed Heat Flux*, International Journal Heat and Mass Transfer, **6**, 537–559 (1963).
9. R. F. Farman and R. B. Beckman, *Entrance Region Heat Transfer in an Annulus*, Chemical Engineering Progress Symposium Series **63**, 57–65 (1967).

Discussion

As the result of defective tape, it was not possible to transcribe the discussion that followed the presentation of this paper.

The Effect of Oxygen in Sodium on the Compatibility of Sodium with Niobium*

R. L. Klueh

Oak Ridge National Laboratory
Oak Ridge, Tennessee

Abstract

Previous studies of the compatibility between refractory metals (mainly niobium and tantalum) and the alkali metals sodium and potassium have shown that the dissolution of the refractory metal in the alkali metal depends upon the concentration of oxygen in the alkali metal. It has also been observed that the experimentally determined equilibrium distribution coefficient for oxygen at a given temperature (i.e., the ratio of the oxygen concentration in the refractory metal to that in the alkali metal at equilibrium) is generally much smaller than the theoretically calculated value. These observations have generally been explained by postulating the formation of a ternary oxide containing refractory metal, alkali metal, and oxygen atoms.

As an alternative to the ternary-oxide hypothesis, it is proposed that at equilibrium a liquid ternary solution exists and that the oxygen affects the solubility of the refractory metal by decreasing the activity coefficient of the refractory metal in the liquid. The phase rule has been used to check this hypothesis in the niobium-oxygen-sodium system at 600°C. The interaction between niobium and oxygen in sodium has been characterized using the interaction parameters developed by Wagner, and these results were used to show how the discrepancy in distribution coefficient can be resolved.

Introduction

In recent years several investigators have examined the compatibility between the refractory metals (niobium, tantalum, and molybdenum) and the liquid alkali metals. Although the refractory metals are extremely resistant to attack by the alkali metals in the absence of impurities, this compatibility may be compromised if oxygen is present in either the refractory metal[1] or the alkali metal.[2]

It is generally found that increasing the oxygen concentration of the alkali metal increases the "apparent" solubility of the refractory metal in the alkali metal. For example, at 600°C the solubility of niobium in pure potassium is negligible, whereas it increases several hundredfold when the oxygen concentration of the potassium is increased to 100 ppm.[2, 3] Others have reported increased dissolution of refractory metals due to oxygen impurities in potassium,[4, 5] sodium,[6] and cesium.[7] Most explanations have assumed the formation of a ternary oxide containing alkali metal and refractory metal.[2, 4, 5, 8] The addition of more oxygen to the liquid would then result in the formation of more oxide. To date, however, the existence of such oxides has not been demonstrated at oxygen concentrations or temperature conditions of interest to reactor applications.

This paper examines the effect of oxygen in sodium on the solubility of niobium in sodium and the redistribution of oxygen between niobium and sodium.

Experimental

The experimental system used, shown in Fig. 1, consisted of a niobium specimen in contact with sodium in a container of the same composition as the specimen. The sodium was hot-gettered with zirconium foil before test, and the oxygen content was then adjusted by weighed additions of Na_2O. The capsules were filled and welded in a 1-atm pressure of argon and were sealed in an outer stainless steel container for protection during test (see Fig. 1).

After exposure of the specimen for 500 hr at 600°C, the capsule was inverted and quenched in liquid nitrogen. The oxygen concentration of the refractory metal specimens and capsules was determined by vacuum-fusion analysis, and the concentration of oxygen in the sodium was calculated by a mass balance. The sodium was dissolved in isopropyl alcohol, precipitated as the chloride, and then analyzed for niobium by spectrographic analysis with an accuracy of $\pm 10\%$.

Results

Niobium solubility determined at 600°C is plotted in Fig. 2 as a function of the oxygen concentration in the sodium at the end of each test. Extrapolation to 1 ppm oxygen in sodium gives a niobium solubility of about 10 ppm. No comparative data are available for the solubility of niobium in pure sodium.

Table 1 shows the change of oxygen concentration of niobium when oxygen was added to the sodium. The surfaces of the niobium specimens had an etched appearance, and only the specimen exposed to sodium with 2000 ppm oxygen showed any indication of a surface scale. This film was quite superficial, however, for when it was removed, no differences in the oxygen concentration of the niobium specimen could be de-

* Work performed under the auspices of the U. S. Atomic Energy Commission.

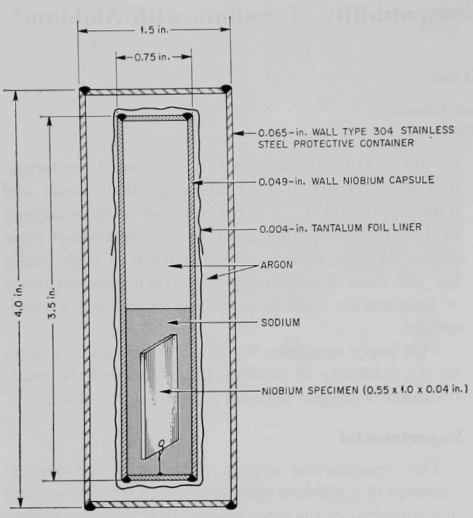

FIG. 1. Niobium-Oxygen-Sodium Test System.

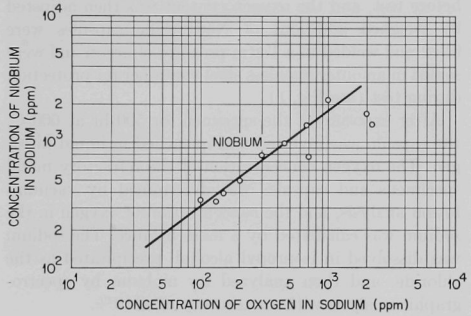

FIG. 2. The Effect of Oxygen on the Solubility of Niobium in Sodium at 600°C.

tected within experimental limits, and attempts to identify the film by X-ray diffraction techniques were unsuccessful. In view of the phase-rule analysis discussed below it was concluded that the scale formed during quenching.

Throughout this paper, the systems under discussion will be assumed to have reached equilibrium after 500 hr at 600°C. Considering the high mobility of atoms in the liquid phase, the slowest process in the approach to equilibrium should be the diffusion of oxygen in the niobium. Diffusion calculations indicate that after 500 hr the concentration of oxygen at the center of the niobium specimen should be within about 2% of its final value. In support of this, we could detect no microhardness gradients in the niobium after test.

Discussion

Phase-rule Analysis

As was previously done for the niobium-oxygen-potassium system,[3] we have tested the present results against the hypothesis that only two condensed phases are in equilibrium at the test temperature (i.e., the refractory metal that contains dissolved oxygen and the liquid alkali metal that contains dissolved oxygen and refractory metal). Exact atomic (or molecular) states of the species were ignored, and the problem was treated phenomenologically in terms of the activities of the solutes in the liquid ternary solution. Some investigators have inferred that the ternary oxide referred to in the "Introduction" is not a separate phase but a molecularly dissolved complex in the liquid. Such a possibility is not excluded by the present treatment, though at present it is not possible to verify the existence of such molecules. Thus, such speculations seem to be of dubious value.

The first point to be established is whether there are three condensed phases (ternary-oxide hypothesis) or two condensed phases (solution hypothesis of this paper) present under the test conditions. According to Gibbs' phase rule, if the ternary-oxide phase exists at equilibrium, the other condensed phases must be of fixed composition. Additions of oxygen to the system, therefore, would result in the formation of more of the ternary oxide, and the oxygen concentrations of the refractory metal and sodium would not change. For two condensed phases, however, there will be a redistribution of oxygen between the refractory metal and sodium when the oxygen concentration of the system is changed. The experimental results in Table 1 show that the oxygen concentration of the refractory metal changes continuously with increasing amounts of

TABLE 1. REDISTRIBUTION OF OXYGEN IN THE NIOBIUM-OXYGEN-SODIUM SYSTEM AT 600°C

Initial Oxygen Content of Sodium, ppm	Oxygen Content of Niobium,[a] ppm	
	After Exposure to Sodium	Change
50	59	−11
300	62	−8
700	64	−6
1000	83	+13
2000	88	+18

[a] Initial oxygen content of niobium specimens was 70 ppm.

oxygen added to the system. If the assumption that equilibrium was reached is valid, this implies that only two condensed phases were present in the system.

Interaction Parameters

Chipman[10] has shown that in a dilute solution of $(n-1)$ components, 2, 3, 4, $\cdots$, n, in a solvent metal 1 the activity coefficient of any solute may usually be expressed as a product of $(n-1)$ factors; the activity coefficient of component 2 may be represented by

$$\gamma_2 = \gamma_2^0 \gamma_2^{(3)} \cdots\cdots \gamma_2^{(n)}, \qquad (1)$$

where γ_2^0 is the activity coefficient of 2 in the 1–2 binary containing the same mole fraction of 2 as the n-component system and where the other factors are correction terms accounting for the presence of the other components.

Wagner[9] derived an equivalent expression by using a Taylor series expansion for the logarithm of the activity coefficient and obtained

$$\ln \gamma_2 = \ln \gamma_2^0 + N_2\left(\frac{\partial \ln \gamma_2}{\partial N_2}\right) + N_3\left(\frac{\partial \ln \gamma_2}{\partial N_3}\right) + \cdots + N_n\left(\frac{\partial \ln \gamma_2}{\partial N_n}\right) + \frac{1}{2}N_2^2\left(\frac{\partial^2 \ln \gamma_2}{\partial N_2^2}\right) + N_2N_3\left(\frac{\partial^2 \ln \gamma_2}{\partial N_2 \partial N_3}\right) + \frac{1}{2}N_3^2\left(\frac{\partial^2 \ln \gamma_2}{\partial N_3^2}\right) + \cdots, \qquad (2)$$

where N_2, N_3, $\cdots$, N_n are the mole fractions of the solutes, and where the derivatives are to be taken for the limiting case of zero concentration of all solutes.

After all but first-order terms are dropped, Eq. (2) is usually written as

$$\ln \gamma_2 = \ln \gamma_2^0 + N_2\epsilon_2^{(2)} + N_3\epsilon_2^{(3)} + \cdots N_n\epsilon_2^{(n)}, \qquad (3)$$

where the $\epsilon_i^{(j)}$'s (i.e., interaction parameters) are defined as

$$\epsilon_i^{(j)} = \left(\frac{\partial \ln \gamma_i}{\partial N_j}\right)_{\substack{N_i \to 0 \\ N_j \to 0}} \qquad (4)$$

and are constant by definition. Wagner has shown that

$$\epsilon_i^{(j)} = \epsilon_j^{(i)}. \qquad (5)$$

For a ternary system, it follows that Eq. (3) becomes[11]

$$\ln \gamma_2^{(1+3)} = \ln \gamma_2^{(1)} + N_2^{(2)}\epsilon_2 + N_3^{(3)}\epsilon_2. \qquad (6)$$

When Henry's law is obeyed by component 2 in the 1–2 binary, $\ln \gamma_2 = \ln \gamma_2^{(1)}$ is constant and $\epsilon_2^{(2)}$ is zero. A negative value of $\epsilon_2^{(3)}$ then indicates that the addition of component 3 increases the solubility of component 2 and vice versa when $\epsilon_2^{(3)}$ is positive.

If Henry's law applies for the niobium-oxygen-sodium system, the activity coefficient for niobium in the ternary liquid is given by

$$\ln \gamma_{Nb}^{(Na+O)} = \ln \gamma_{Nb}^{(Na)} + \epsilon_{Nb}^{(O)} N_O^{(Na+Nb)}, \qquad (7)$$

where $\gamma_{Nb}^{(Na)}$ is the Henry's law constant.

The activity of niobium in the sodium solution in equilibrium with solid niobium is unity relative to pure niobium, that is,

$$a_{Nb}^{(Na+O)} = 1 = \gamma_{Nb}^{(Na+O)} N_{Nb}^{(Na+O)} \qquad (8)$$

and

$$\gamma_{Nb}^{(Na+O)} = \frac{1}{N_{Nb}^{(Na+O)}}, \qquad (9)$$

where it has been assumed that small amounts of impurities do not significantly alter $a_{Nb}^{(Nb)}$, since there is no measurable solubility of sodium in niobium. As determined from Eq. (9) and the data of Fig. 2, Fig. 3 shows $\ln \gamma_{Nb}^{(Na+O)}$ plotted as a function of $N_O^{(Na+Nb)}$. By definition $\epsilon_{Nb}^{(O)}$ is the slope of the curve of Fig. 3 as $N_O^{(Na+Nb)}$ approaches zero:

$$\epsilon_{Nb}^{(O)} \cong -8 \times 10^3. \qquad (10)$$

It is quite obvious from Fig. 3 that at higher oxygen concentrations it will not be possible to describe $\ln \gamma_{Nb}^{(Na+O)}$ accurately by using only the first-order

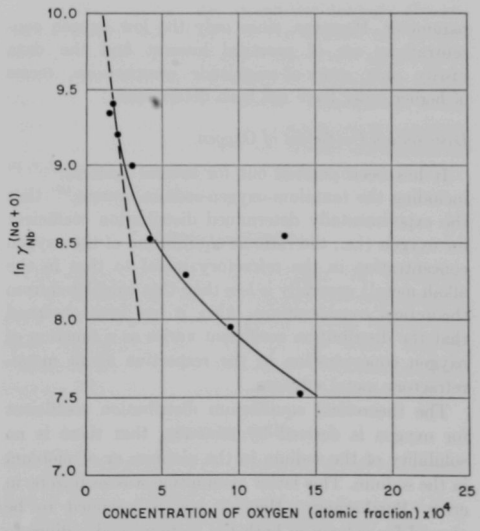

FIG. 3. The Variation of the Activity Coefficient of Niobium in the Sodium Solution as a Function of the Oxygen Concentration of the Sodium Solution.

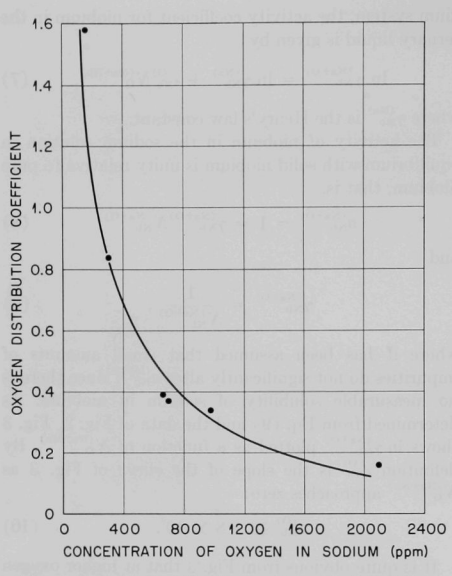

FIG. 4. The Effect of the Oxygen Concentration of the Sodium on the Oxygen Equilibrium Distribution Coefficient in the Niobium-Oxygen-Sodium System at 600°C.

parameter. However, since only the low oxygen concentrations are of practical interest and the data justify only order-of-magnitude comparisons, terms of higher order have not been determined.

Distribution Coefficient of Oxygen

It has been pointed out for several systems,[2, 3, 12] including the tantalum-oxygen-sodium system,[13] that the experimentally determined distribution coefficient for oxygen (i.e., the ratio at equilibrium of the oxygen concentration in the refractory metal to that in the alkali metal) generally is less than that calculated from theoretical considerations. Also, it has been observed that the distribution coefficient varies as a function of oxygen concentration in the respective alkali metal-refractory metal solvents.

The theoretical equilibrium distribution coefficient for oxygen is derived by assuming that there is no solubility of the sodium in the niobium or of niobium in the sodium. This latter assumption was seen to be in error. Furthermore, Henry's law is assumed to be obeyed for oxygen in both the niobium and sodium to saturation; the theoretical distribution coefficient at absolute temperature T is then[3]

$$\kappa_T \equiv \frac{(N_O^{(Nb)})}{(N_O^{(Na)})} = \frac{(N_O^{(Nb)})_{sat}}{(N_O^{(Na)})_{sat}} \cdot \exp\left(\frac{\Delta G^0_{Na_2O} - \Delta G^0_{NbO}}{RT}\right), \tag{11}$$

where $(N_O^{(Nb)})_{sat}$ and $(N_O^{(Na)})_{sat}$ are the saturation solubilities at T, and $\Delta G^0_{Na_2O}$ and ΔG^0_{NbO} are the free energies of formation of pure Na_2O and NbO from the pure metals and oxygen gas at 1 atm.

Equation (11) gives a theoretical distribution coefficient of about 600 for a temperature of 600°C, whereas the distribution coefficient determined experimentally was less than this and, as shown in Fig. 4, varies with the oxygen concentration of the sodium. Since oxygen in sodium affects the activity coefficient of niobium in sodium and since

$$\epsilon_{Nb}^{(O)} = \epsilon_O^{(Nb)}, \tag{12}$$

the activity coefficient of oxygen in the sodium is also affected by niobium.

Equation (11) can be rewritten as a function of the oxygen in the liquid (assuming that Henry's law is valid for the niobium solvent) as

$$\kappa_T(N_O^{(Na+Nb)}) \equiv \frac{N_O^{(Nb)}}{N_O^{(Na+Nb)}} \cong \gamma_O^{(Na+Nb)}(N_O^{(Nb)})_{sat} \exp\left(\frac{\Delta G^0_{Na_2O} - \Delta G^0_{NbO}}{RT}\right), \tag{13}$$

where

$$\ln \gamma_O^{(Na+Nb)} \cong \ln \gamma_O^{(Na)} + \epsilon_O^{(Nb)} N_{Nb}^{(Na+O)}. \tag{14}$$

Theoretically, it should now be possible to calculate $\gamma_O^{(Na+Nb)}$ for each value of $N_O^{(Na+Nb)}$ by substituting a value of $N_{Nb}^{(Na+O)}$ from Fig. 1 into Eq. (13) to calculate a distribution coefficient. When this is done for 200 ppm oxygen, an order-of-magnitude improvement is found. This is reasonable agreement, however, considering the simplifying assumptions and the accuracy of the method used for determining the solubility of niobium in sodium.

The distribution coefficient determined experimentally can be used for a more accurate determination of the interaction parameter; Eq. (11) can be rearranged to give

$$\gamma_O^{(Na+Nb)} = \frac{\kappa_T(N_O^{(Na+Nb)})}{(N_O^{(Nb)})_{sat}} \cdot \exp\left(-\frac{\Delta G^0_{Na_2O} - \Delta G^0_{NbO}}{RT}\right), \tag{15}$$

from which it follows that

$$\epsilon_O^{(Nb)} \cong \frac{\Delta \ln \gamma_O^{(Na+Nb)}}{\Delta N_{Nb}^{(Na+O)}} \quad (16)$$

when the slope is evaluated as the solute concentrations approach zero. It also follows from Eqs. (15) and (16) that

$$\epsilon_O^{(Nb)} \cong \frac{\Delta \ln \kappa_T(N_O^{(Na+Nb)})}{\Delta N_{Nb}^{(Na+O)}}. \quad (17)$$

Hence, measurements of κ_T and $N_{Nb}^{(Na+O)}$ at two oxygen concentrations will yield $\epsilon_O^{(Nb)}$. If the data of Table 2 are used,

$$\epsilon_O^{(Nb)} \cong -8.2 \times 10^3, \quad (18)$$

in good agreement with $\epsilon_{Nb}^{(O)}$. Since Eq. (18) requires $\Delta N_{Nb}^{(Na+O)}$ rather than $N_{Nb}^{(Na+O)}$, the interaction parameter determined in this manner should be the most accurate for the experimental technique used in this work. It is hoped that the accurate distribution-coefficient measurements at lower oxygen levels now in progress[14] will be accompanied by measurements of $N_{Nb}^{(Na+O)}$.

If the activity of oxygen in sodium in the sodium-oxygen binary were accurately known, $\epsilon_O^{(Na)}$ could be determined by extrapolation to $N_{Nb}^{(Na+O)} = 0$ as follows:

$$\epsilon_O^{(Nb)} \cong \frac{\ln \gamma_{O(1)}^{(Na+Nb)} - \ln \gamma_O^{(Na)}}{N_{Nb(1)}^{(Na+O)}}, \quad (19)$$

where (1) refers to a given oxygen concentration in the sodium solution. If Henry's law is again assumed to apply to oxygen in sodium to saturation, Eq. (19) can be used by picking an $N_O^{(Na+Nb)}$, determining $N_{Nb}^{(Na+Nb)}$ from Fig. 2, $\ln \gamma_O^{(Na+Nb)}$ from Eq. (15), and $\ln \gamma_O^{(Na)}$ from oxygen solubility data.[14-16] For 150 ppm oxygen, Eq. (18) gives (see Table 2)

$$\epsilon_O^{(Nb)} \cong 6 \times 10^4. \quad (20)$$

In theory, therefore, the interaction parameter can be determined by accurately determining the distribution coefficient and the niobium concentration of the liquid at one oxygen concentration.

Finally, the relatively small change in oxygen concentration in the niobium that accompanies a much larger change in the oxygen content of the sodium is consistent with the solution hypothesis. It can be shown[3] that

$$\frac{\Delta N_O^{(Nb)}}{N_O^{(Nb)}} \cong \frac{\Delta N_O^{(Na+Nb)}}{N_O^{(Na+Nb)}} + \epsilon_O^{(Nb)} \Delta N_{Nb}^{(Na+O)}. \quad (21)$$

At the low oxygen levels at which the first-order approximation is applicable, Eq. (21) indicates that a rather large percentage change in the oxygen concentration of the sodium will result in only a small percentage change in the concentration of oxygen in the niobium where $\epsilon^{(Nb)}$ is a large negative number, as in this work.

TABLE 2. DATA USED FOR CALCULATIONS OF INTERACTION PARAMETER

$c_O^{(Na+Nb)}$ (ppm)	$N_{Nb}^{(Na+O)}$ [a]	$\kappa_T(N_O^{(Na+Nb)})$ [b]	$\gamma_O^{(Na+Nb)}$ [b]
150	0.99×10^{-4}	1.58	0.353
300	1.98×10^{-4}	0.695	0.155

[a] Taken from Fig. 2.
[b] Taken from Fig. 4.

Summary and Conclusions

We have proposed that the effect of oxygen on the "apparent" solubility of niobium in sodium at 600°C is a result of the interaction between solutes (oxygen and niobium) in the liquid sodium solution rather than due to the formation of a ternary-oxide phase. The phase rule was used to show that at equilibrium at 600°C the niobium-oxygen-sodium system contains only the two condensed phases (i.e., the niobium containing dissolved oxygen and sodium containing dissolved refractory metal and oxygen).

For such a system, the interaction between the refractory metal and oxygen in the sodium can be described in terms of the Wagner interaction parameters. Theoretically it is then possible to explain the often-discussed distribution-coefficient discrepancy. The interaction parameter for the niobium-oxygen-sodium system was determined, and the revised calculation of the distribution coefficient was found to be much closer to the experimental value.

Acknowledgments

The author gratefully acknowledges the assistance of J. L. Griffith, Jr., for carrying out the experimental work: to J. H. DeVan for many helpful suggestions made throughout the course of this work: and to Frances Scarboro of the Metals and Ceramics Division Reports Office for the preparation of the manuscript.

REFERENCES

1. J. R. DiStefano, *Corrosion of Refractory Metals by Lithium*, ORNL-3551 (April 1966).
2. A. P. Litman, *The Effect of Oxygen on the Corrosion of Niobium by Liquid Potassium*, ORNL-3751 (July 1955).
3. R. L. Klueh, *Interactions in Alkali Metal Solutions Containing Oxygen I. The Niobium-Oxygen-Potassium System* (to be published).
4. C. M. Scheuerman and C. A. Barrett, *Compatibility of Co-*

lumbium and Tantalum Tubing Alloys with Refluxing Potassium, NASA TN D-3429 (May 1966).
5. R. E. Cleary *et al.*, *Solubility of Refractory Metals in Lithium and Potassium*, TIM-850 (Oct. 1965).
6. J. W. Mausteller and E. F. Batutis, *Effect of Oxygen on the Mass Transport of Stainless Steel Components in Sodium*, MSA Technical Report No. 36 (March 1955).
7. P. M. Winslow, "Synopsis on Cesium Compatibility Studies," *AEC-NASA Liquid Metals Information Meeting*, CONF-650411 (April 1965).
8. C. Tyzack, "The Behavior of Materials in Liquid Sodium," *Adv. in Materials* (Inter-Disciplinary Symposium), London, The Institution of Chemical Engineers (1964).
9. C. Wagner, *Thermodynamics of Alloys*, Addison-Wesley, Cambridge, Mass. (1952).
10. J. Chipman, "Atomic Interaction in Molten Alloy Steels," *J. Iron Steel Inst. (London)* **180,** 97 (1955).
11. The nomenclature for activities, activity coefficients, and concentrations in the solutions is as follows: $\gamma_2^{(1)}$ = activity coefficient of 2 in the 1-2 binary; $\gamma_2^{(1+3)}$ = activity coefficient of 2 in the 1-2-3 ternary.
12. J. R. DiStefano and E. E. Hoffman, *Corrosion Mechanisms in Refractory Metal-Alkali Metal Systems*, Atomic Energy Review **2,** 3 (1964).
13. G. E. Raines, C. V. Weaver, and J. H. Stang, *Corrosion and Creep Behavior of Tantalum in Flowing Sodium*, BMI-1284 (Aug 1958).
14. T. F. Kassner and D. L. Smith, *Calculations on the Kinetics of Oxygen Solution in Tantalum and Niobium in a Liquid-sodium Environment*, ANL-7335 (Sept 1967).
15. J. D. Noden and K. A. Bagley, *The Solubility of Oxygen in Sodium and Sodium-Potassium Alloy*, UKAEA Report TN-80 (1958).
16. These solubility measurements are usually carried out in stainless steel containers. The interaction between oxygen in sodium and the components of stainless steel—and thus their effect on the solubility of oxygen in sodium—are still uncertain.

Discussion

As the result of defective tape, it was not possible to transcribe the discussion that followed the presentation of this paper.

Development of High-strength Vanadium-base Alloys with Improved Corrosion Resistance in Cold-trapped Liquid Sodium*

HORST BÖHM AND HANS U. BORGSTEDT

Kernforschungszentrum Karlsruhe
Karlsruhe, Germany

(PRESENTED BY H. U. BORGSTEDT)

The program on vanadium-base alloys pursued in Karlsruhe for the past four years is concerned with the development and testing of high-strength alloys that are corrosion resistant in liquid sodium. Within this program, the influence of the alloying constituents on the creep and stress-rupture behaviour of the vanadium-base alloys was investigated systematically to assess the optimum compositions under the aspect of creep behaviour. The base was formed by the V-Ti-Nb alloys with which the dependence of the different creep parameters on the titanium and niobium contents was measured.[1, 2]

The most striking result of these investigations has been the overwhelming influence of titanium on the strength properties of vanadium-base alloys, with the dependency of strength on the titanium content strongly depending upon the strain rate. In Fig. 1 the high-temperature tensile strength and various creep strengths are plotted as a function of the titanium content. It is seen that the dependency of the strength on strain rate increases with increasing titanium content and that a definitive peak is established for the long-time strength at 1–3% titanium.

The very high strength values at low titanium contents are due to the interaction between titanium and oxygen atoms, according to our investigations so far. In Fig. 2, the values of the 1,000-hr stress-rupture strength of the V-Ti-Nb system are indicated in a space diagram. From this figure, also the strength maximum at low titanium content and the comparatively weak influence of the niobium content is clearly apparent.

The alloy screening performed simultaneously for the investigation of the corrosion behaviour in liquid sodium and results known from the literature clearly show that considerable addition of chromium is required to improve the corrosion resistance. Hence, further experiments were carried out to see to what extent the good strength properties will remain also in V-Ti-Cr and in V-Ti-Nb-Cr alloys, respectively, with the peak at low titanium contents. On the basis of V-3% Ti-15% Nb alloys in which niobium was substituted stepwise by chromium, it turns out that the short-time strength of V-3% Ti-15% Nb decreases slightly in the direction to V-3% Ti-15%Cr, but that stress dependency of the time to rupture is increased so that the creep values of the V-Ti-Cr alloy are even superior to the alloy containing niobium, as is borne out by Fig. 3.

In connection with studies of corrosion resistance, which will be dealt with in greater detail below, the substitution of titanium by zirconium was investigated. Results available up to now showed that in the range of concentration around 2% zirconium the corresponding alloys containing zirconium have a much lower stress-rupture strength than alloys containing titanium. It is being investigated at present whether or not there is a similar dependency on concentration of the stress-rupture strength in the V-Zr alloy as in those containing titanium. In this respect, it is not unlikely that there is one strength maximum at lower contents in the case of the V-Zr system.

The corrosion behavior in liquid sodium with very low oxide contents of Group VA elements of the periodic table is importantly related to their high affinity for oxygen. In the range of oxide concentration below 10 ppm Na_2O in sodium the composition of the vanadium-base alloys also plays a decisive part. Binary and ternary vanadium-base alloys with titanium or zirconium are sensitive to an oxygen-exchange reaction:

$$Na_2O + Me = MeO + 2\ Na, \qquad (1)$$

because of the high free enthalpy of formation of the oxides of both metals up to very low oxygen contents of sodium.

At a concentration of about 5 ppm oxide in the sodium, the free enthalpy of the reaction (1) is -20.5 to -22 kcal/mole in the range of temperature between 500 and 600°C, if the reacting metal (Me) is titanium. However, if the system consists only of sodium, sodium oxide, and vanadium, the exchange enthalpy is weakly positive, with values of about $+0.6$ to $+1.6$ kcal/mole, if thermochemical calculations by Tyzack[3] are used as the basis. In this

* Work performed within the association in the field of fast reactors between the European Atomic Energy Community and Gesellschaft für Kernforschung m.b.H., Karlsruhe.

case, there is no tendency of oxygen uptake from the sodium under experimental conditions. The fact that the free enthalpy of oxygen in sodium with 5 ppm Na_2O lies between the enthalpies of formation for the oxides VO and TiO, as is to be expected from theory, results in the phenomenon of internal oxidation of the vanadium-base alloys.[4] In addition to insignificant external oxide layers, internal zones of embrittlement often form in the V-Ti alloys; these zones will even cause material losses due to a breakaway mechanism in cases of extreme increases of hardness.[5]

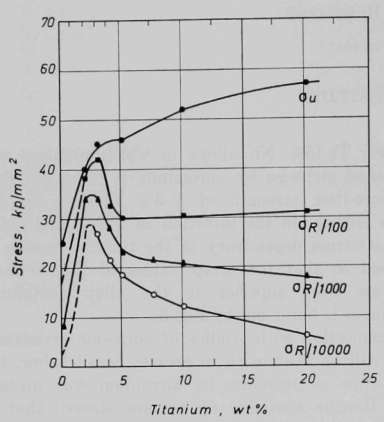

FIG. 1. Influence of Titanium on the Ultimate Tensile and Stress-rupture Strength of Vanadium at 650°C.

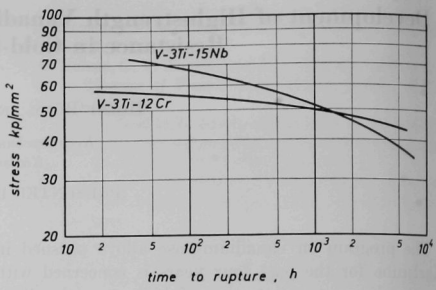

FIG. 3. Stress-rupture Strength of Vanadium Alloys at 650°C.

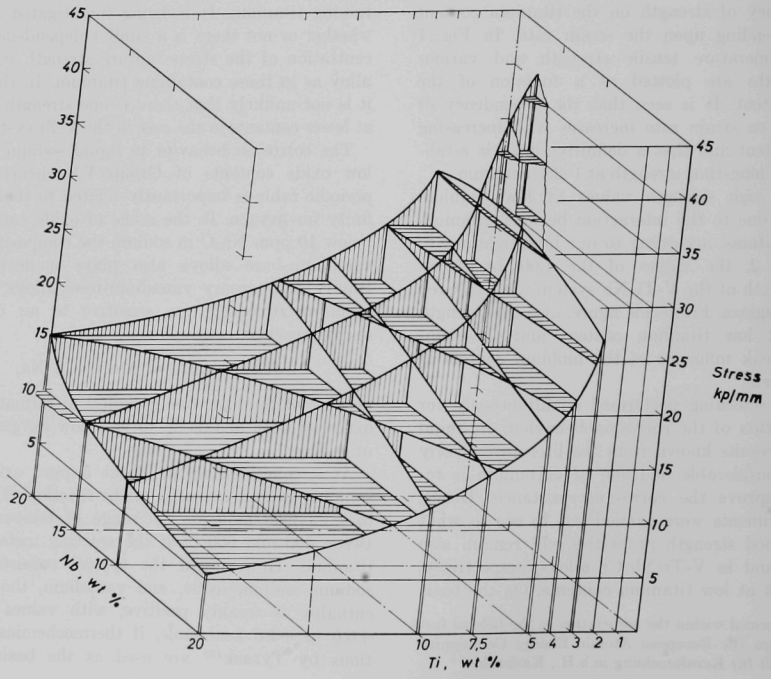

FIG. 2. 1,000-hr Stress-rupture Strength of V-Ti-Nb Alloys at 650°C.

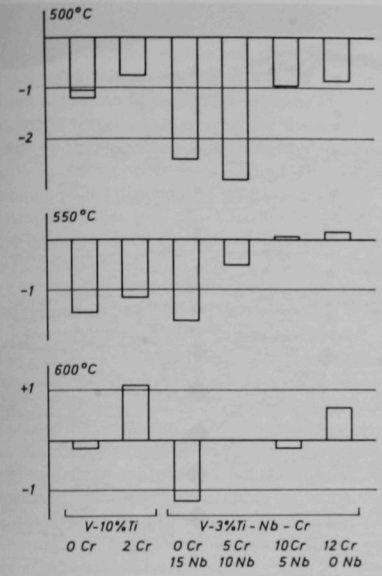

FIG. 4. Influence of Alloy Composition on Corrosion Rates (mg/cm²) of Vanadium-base Alloys in Liquid Sodium for 1000 Hr at 500, 550, and 600°C.

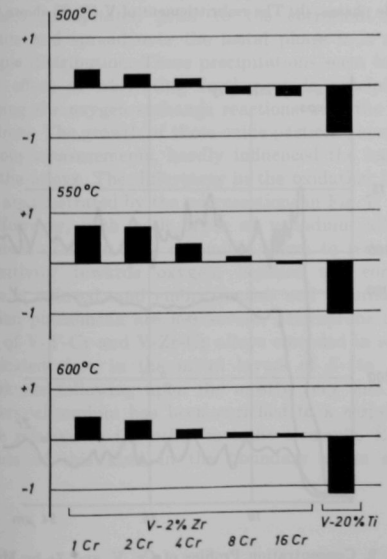

FIG. 5. Influence of Chromium Content of V-Zr-Cr Systems on Corrosion Rates (mg/cm²) in Liquid Sodium for 500 Hr at 500, 550, and 600°C. Comparison with V-20% Ti.

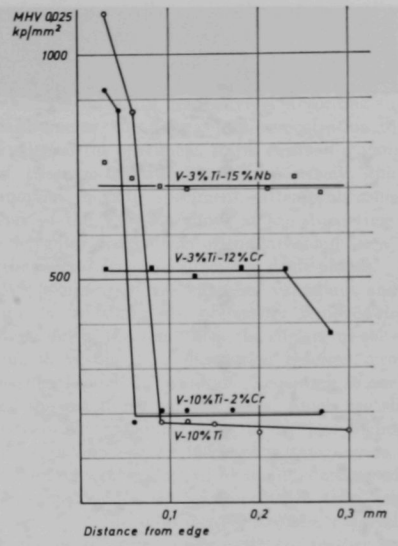

FIG. 6. Influence of Chromium Content of Vanadium-base Alloys on Internal Penetration due to the Oxygen Exchange with Liquid Sodium at 600°C. Test Duration: 500 hr.

Favorable effects on the corrosion behavior of vanadium alloys in liquid sodium as a result of the addition of chromium to the alloy were indicated in earlier work from the Argonne National Laboratory[6] and CEN Saclay.[7] A reduction of the weight changes due to the sodium action was also observed by us if titanium- or zirconium-bearing vanadium-base alloys contain additions of chromium or molybdenum. The influence of the chromiun content of the V-Ti and V-Ti-Nb alloys on the corrosion rates calculated from the weight changes is apparent from Figure 4.

A very clear picture of the effect of additions of chromium on the corrosion resistance of V-Zr alloys in sodium is given by the result of a series of experiments in which the same test contained specimens of V-2% Zr with additions of 1, 2, 4, 8, and 16% chromium in the test loop. Figure 5 shows that the weight changes at the three experimental temperatures will be reduced with increasing chromium content and that with rising temperature the weight changes of all specimens tend towards more positive values. No externally visible marks of corrosion were observed on the specimens with higher concentrations of chromium, and the specimens of the alloy V-2% Zr-16% Cr exhibted an unattacked, bright metal surface even after 1,000 hr in the test sections of the sodium test loop.

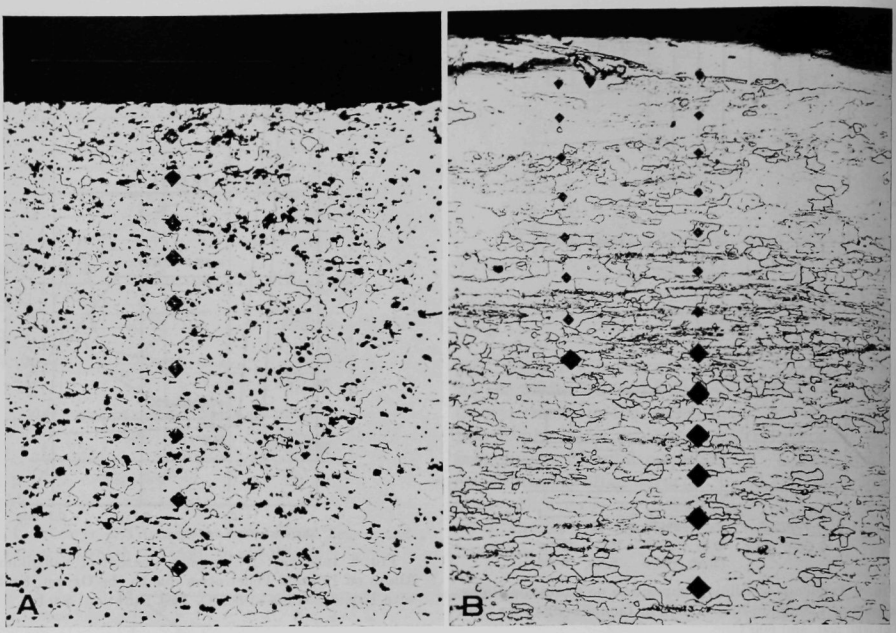

FIG. 7. Difference in Behaviour of V-4% Zr and V-5% Ti Shown by Metallographic Techniques. (a) V-4% Zr does not suffer remarkable embrittlement, but the microsection shows precipitations of oxide phases. (b) The embrittlement of V-5% Ti shows that the oxygen content is concentrated in areas near the surface.

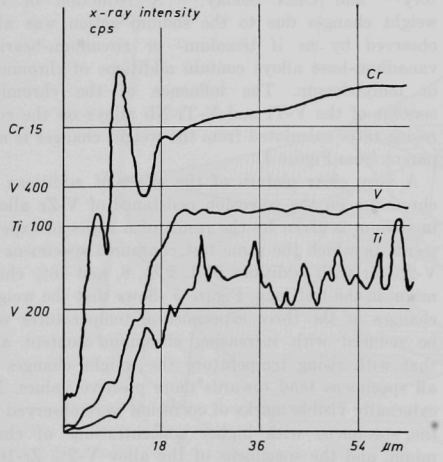

FIG. 8. Concentration Profiles of Cr, V, and Ti by Microprobe Analysis. Nominal Composition: V-3% Ti-12% Cr.

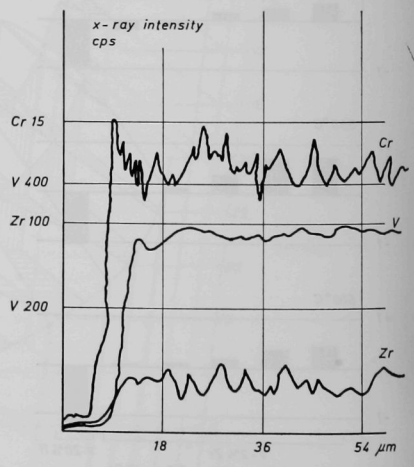

FIG. 9. Concentration Profiles of Cr, V, and Zr by Microprobe Analysis. Nominal Composition: V-2% Zr-16% Cr.

However, V-Ti-Cr alloys, just as the other vanadium-base alloys containing titanium, are attacked in the metal phase, even if the embrittlement caused by internal oxidation is not as strong as in the alloys without a chromium content. Diagrams of microhardness in the metal phase versus the distance from the surface of the specimens are compared in Fig. 6 for two V-Ti alloys with and without the addition of chromium. The dependency of the thickness of the penetration zones on the titanium content of the alloys corresponds to the laws of internal oxidation of binary alloys.[4, 5] With low titanium contents we have to expect a higher diffusion rate of oxygen, i.e., faster growth of the internal penetration zones, but the degree of embrittlement will be less severe.

The results of metallographic investigations of alloys with low titanium and zirconium contents indicate a different type of interaction with oxygen of both alloying elements. For thermodynamical reasons, both alloys take up oxygen from sodium whose oxide content is maintained constant as a result of the connection to the cold trap as an oxide reservoir. The quantity of oxygen taken up by binary V-Ti and V-Zr alloys in a test run of about 500 hr could be determined quantitatively.

With the V-Ti alloys the embrittlement zones described above are generated according to laws of time which are generally valid for internal oxidation.[4, 5] However, with the V-Zr alloys we observe oxide phases precipitated prior to the corrosion experiments and spread over the metal phase in a microscopic distribution. These precipitations seem to have the effect of nucleating further oxide precipitation during the oxygen-exchange reactions with the liquid sodium. The growth of these oxide particles, according to our measurements, hardly influenced the hardness of the alloys. The differences in the oxidation behavior are illustrated by the microsections in Fig. 7.

However, with both types of vanadium alloys a content of 15 to 20% chromium seems to reduce the sensitivity towards oxygen, because the corrosion rate is reduced, and embrittlement and external corrosion phenomena are less severe. Microprobe analyses of V-T-Cr and V-Zr-Cr alloys corroded in sodium indicated that, in the metal layers of 5- to 10-μm thickness following upon the mostly very thin oxide layers, chromium has been enriched to a certain degree relative to the other metallic elements. Enrichments of this kind in the boundary zones of the metal phase are shown in the intensity diagrams recorded with the CAMECA microprobe of the X-ray fluorescence radiation of the elements for the alloy V-3% Ti-12% Cr in Fig. 8 and for a specimen of V-2% Zr-16% Cr in Fig. 9, respectively. According to these measurements, the decrease of concentration towards the edge of the specimens starts earlier for vanadium and titanium or zirconium, respectively, than for chromium in both specimens. Microprobe measurements of the V-Zr-Cr alloys at the same time show the irregular distribution of the zirconium as a result of the precipitations of zirconium oxide phases.

We assume that the elements vanadium and titanium or zirconium are preferably removed by the sodium out of the zones near the surface of the vanadium alloys due to a dissolution reaction, probably occuring through an oxidation. According to our findings, the remaining surface zones, which are slightly enriched in chromium, seem to be less inclined to undergo a break-away mechanism than layers without any chromium or with small contents of this metal, and under certain conditions they seem to restrict the diffusion of oxygen into the material. The test results encourage us to carry out further work in the alloy systems vanadium-titanium-chromium and vanadium-zirconium-chromium.

REFERENCES

1. Böhm, H., and Schirra, M., J. Less-Common Metals **12,** 280–293 (1967).
2. Böhm, H., and Schirra, M., Z. Metallkunde **59,** 715–723 (1968).
3. Tyzack, C., "The Behaviour of Materials in Liquid Sodium," in *Advances in Materials*, 3rd, and 4th sessions, pp. 239–264 (1964).
4. Borgstedt, H. U., and Frees, G., Werkstoffe und Korrosion **19,** (1968)
5. Borgstedt, H. U., and Frees, G., Corrosion NACE **24,** 209–213 (1968)
6. Greenberg, S., Ruther, W. E., and Levin, H. A., "Corrosion of Vanadium-base Alloys in Sodium at 550 to 750°C," in *Alkali Metal Coolants*, Proc. Symp. IAEA, Vienna (1967) pp. 63–80.
7. Champeix, L., Darras, R., and Sannier, J., "Corrosion of Vanadium and its Alloys in Liquid Sodium," in *Alkali Metal Coolants*, Proc. Symp. IAEA, Vienna (1967) pp. 45–62.

Discussion

As the result of defective tape, it was not possible to transcribe the discussion that followed the presentation of this paper.

The Corrosion of Vanadium and Vanadium-base Alloys in Sodium

W. E. Ruther

Argonne National Laboratory
Argonne, Illinois

Abstract

Vanadium and certain stronger vanadium-base alloys (V-5 w/o Cr, V-10 w/o Cr, V-15 w/o Cr-5 w/o Ti, V-15 w/o Ti-7.5 w/o Cr, and V-20 w/o Ti) were exposed to sodium cold-trapped at two temperatures. The temperatures of exposure varied from 450 to 700°C. Linear rates of weight loss were noted at the higher impurity levels in the sodium (cold trap at ~175°C). Under optimum conditions, very low weight and dimensional changes were noted for vanadium and the vanadium-chromium binary alloys after exposure in sodium cold-trapped at ~110°C.

Postexposure chemical analyses indicated that oxygen was the major impurity transferred to the vanadium alloys. Titanium as an alloying additive caused increased impurity pickup and concentrated the impurities in a subsurface band 10 to 100 μm in thickness. The vanadium-chromium binary alloys were the most corrosion resistant at the lower cold-trap temperature, and appeared to offer promise as a reactor fuel cladding.

I. Introduction

Vanadium-base alloys containing less than about 25 w/o total alloying additives such as chromium and titanium possess favorable properties for use as fuel cladding in a liquid-metal-cooled, fast breeder reactor (LMFBR). Such properties include fabricability, retention of good mechanical properties at high temperatures, resistance to high-temperature radiation damage, and compatibility with many of the proposed fuel materials. In addition, the low nuclear cross section of such alloys permits useful breeding ratios in large power reactors. Of equal importance is the resistance of the alloy to the corrosive attack of reactor-grade sodium.[1-4]

The compatibility of unalloyed vanadium with continuously hot-gettered sodium to temperatures of at least 650°C is generally accepted. The very small vanadium weight changes reported (i. e., ±10 mg/dm² for 1000 hr at 600°C) and the unchanged sample appearance indicate the very slight interaction between pure sodium and vanadium.

However, considerations of economy and practical operation make it desirable that a sodium-cooled power reactor be operated with cold-trap impurity control rather than by hot-gettering. Unfortunately, widely different corrosion behavior has been reported by different investigators (see Table I) for vanadium exposed in sodium systems with cold traps at approximately the same temperatures.

Recently the corrosion behavior of vanadium and of selected vanadium alloys in cold-trapped sodium has been evaluated over the temperature range of interest to reactor designers. An effort has been made to characterize the impurity levels in the liquid sodium and to follow the movement of specific impurities into the solid alloy, as well as to provide the usual gravimetric corrosion data.

II. Experimental

The interaction of vanadium and vanadium alloys with reactor-grade sodium is a complex process, and no single method of evaluation is satisfactory under all conditions. Individual impurities in the sodium, such as substances containing oxygen, nitrogen, carbon, and/or hydrogen, interact with the specimen surface to form a layer growth of chemical compounds with a corresponding diffusion profile of the impurity element into the solid. The corrosion product may or may not adhere to the specimen. In binary and ternary alloys, metal-impurity phases can also form within the alloy by processes analogous to internal oxidation. Diffusion profiles of the nonmetallic elements into the solid may also occur in sodium of low impurity activities.

If one process clearly predominates, the progress of the reaction can usually be followed with reasonable precision by gravimetric means. Dimensional and metallographic checks are, of course, necessary to confirm the conclusions drawn from weight changes.

Oxygen-refreshed autoclave systems of the type shown in Fig. 1 were used for the static-corrosion exposures. The sodium was circulated slowly by a diaphragm pump through a cold trap previously loaded with an excess of sodium oxide; the controlled temperature of the cold trap thus established the oxygen level of the system. About one autoclave volume was pumped through the cold trap per hour. The system was constructed of Type 304 stainless steel with Type 316 fittings and valves.

A small dynamic test facility was constructed of

Types 318 and 316 stainless steels (see Fig. 2). A cold trap of adjustable temperature and loaded with excess sodium oxide was used for oxygen control. Commercially available electromagnetic pumps and flowmeters were used to regulate sodium circulation.

In all tests, the vanadium-alloy specimens were added and removed, and the sodium was sampled for oxygen analysis, while the system was at operating temperature. During the program the method of separation for analysis of oxygen in the sodium was changed from mercury amalgamation to vacuum distillation. Analytical samples of the sodium for the mercury-amalgamation method were removed in tubes of electropolished stainless steel or chemically polished nickel. A plunger within the sampling tube (actuated from outside the autoclave) permitted the inside of the tube to be flushed several times with bath sodium before retrieving a specimen. The sodium sample was extruded, amalgamated, and washed with mercury under vacuum ($\sim 4 \times 10^{-6}$ mm). Precautions were taken to minimize contamination during the analysis.

Samples for analyses by the vacuum-distillation method were obtained by directly attaching a pyrex distillation chamber to the sample part of the equipment. The sodium was withdrawn in a nickel dip crucible that had been electropolished and vacuum outgassed just prior to the distillation run. Distillation was accomplished by induction heating to a temperature of 300–325°C. In both analytical methods, the residue was titrated with 0.005 *N* HCl to a phenolphthalein end point.

The alloys used in this study were prepared by the Argonne Fabrication Group by multiple arc-melting, followed by extrusion and rolling into sheet form, usually 0.15 cm thick. The specimens were wet ground on standard 240-grit metallographic wheels before exposure.

The samples were cooled in dried argon after exposure, and the sodium was removed by reaction with ethyl alcohol. The surfaces were stripped of nonadherent corrosion product by vigorous brushing and ultrasonic cleaning. Most samples were then examined, weighed, and re-exposed. A single check at 650°C revealed no perturbation as a result of this method. Samples with the same total exposure, whether one continuous test or the sum of several shorter tests, gave the same results.

Standard methods of metallographic mounting and polishing were used to prepare the corroded specimens for microhardness traverses. This procedure provided a valuable method of measuring the extent of the internal penetration of interstitial impurity elements into the specimens.

TABLE I. Corrosion of Vanadium in Cold-trapped Sodium

Corrosion Media[a] Source	Temp, °C	Duration, days	Weight Change, mg/cm²	Cold-trap Temp, °C	Velocity, m/sec
Na[2]	650	69	0.25	110–120	6.1
Na[1]	600	41	−7 to −14	105	1.5
NaK alloy[5]	600	15	∼−45	120	1.6

[a] Reference numbers are given in parentheses.

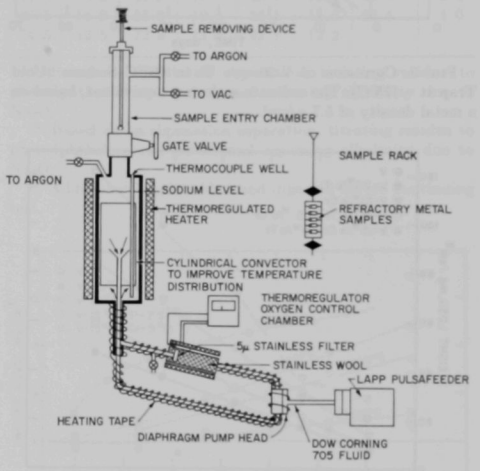

Fig. 1. Equipment to Study Corrosion in Sodium with Oxygen Control.

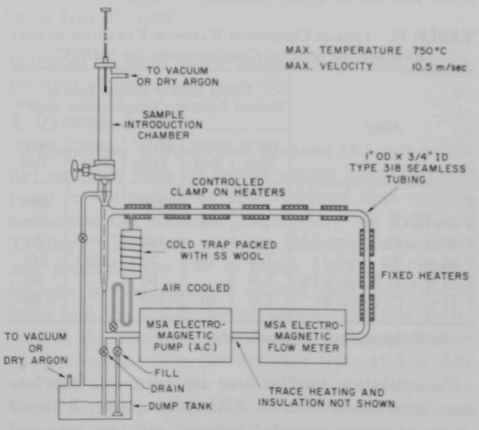

Fig. 2. Liquid-sodium Test Loop.

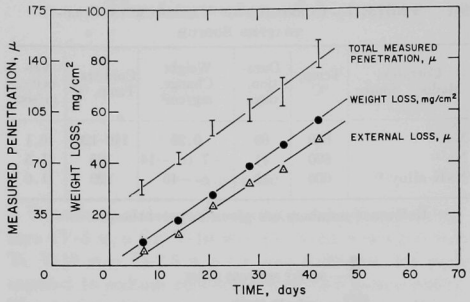

FIG. 3. Corrosion of V-20 w/o Ti in 650°C Sodium (Cold Trap at ~175°C). The ordinate scales are equivalent, based on a metal density of 5.7 g/cm³.

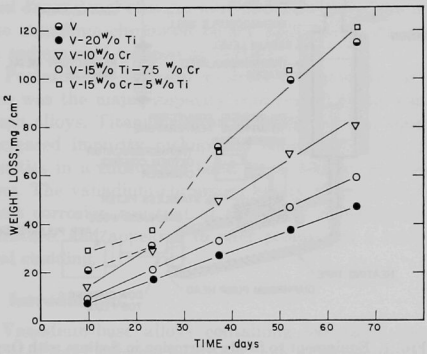

FIG. 4. Corrosion of Vanadium Alloys at 600°C (Cold Trap at ~175°C).

TABLE II. LINEAR CORROSION RATES OF VANADIUM ALLOYS EXPOSED TO SODIUM COLD-TRAPPED AT ~175°C

Alloy	Linear Rate of Weight Loss at Various Exposure Temperatures, mdd[a]				
	450°C Test	550°C Test	600°C Test	650°C Test	700°C Test
V			166		108
V-5 w/o Cr		64			
V-10 w/o Cr			133		54
V-20 w/o Ti	1.8	14	72	134	142
V-15 w/o Ti-7.5 w/o Cr	1.8		90		94
V-15 w/o Cr-5 w/o Ti	7.0	64	170		68

[a] Milligrams per decimeter²-day.

Concentration profiles near the corrosion interface were determined with an ARL Microprobe. A linear relationship was assumed between counting rate and weight percent. Calibration was accomplished by using standards of FeO (for oxygen) and carbon mounted adjacent to the corrosion specimen.

III. Data and Results

A. Corrosion Kinetics

1. Static Sodium

Oxygen analyses of the primary sodium in EBR-II gave values of 6–13 ppm (by the amalgamation technique) under conditions of infrequent cold-trap operation. Based on this information, two levels of oxygen in the sodium were chosen for this evaluation. The higher level, attained at a cold-trap temperature of ~175°C, represents the maximum level that presently might be expected to exist in the reactor for a protracted period. The lower level represents an oxygen content readily attainable by continuous cold trapping (cold trap at ~110°C).

Unfortunately, all of the alloys of interest were not available when the program started, but, as the alloys were prepared, they were added to the tests.

Initially, the corrosion of reference alloy V-20 w/o Ti was evaluated at 650°C (cold trap at 175°C) to determine if the rate of weight loss provided a valid measurement of the rate of total penetration. Total penetration was defined as the sum of the external dimensional loss (determined by micrometer) and the internal hardened zone (from microhardness traverses). As shown in Fig. 3, the relatively constant thickness of the internal penetration resulted in equivalent slopes of the curves of weight loss and total penetration. Thus, at least for this set of conditions, gravimetric data provided a reliable measure of the rate of total penetration.

A typical example of the gravimetric data of specimens exposed to sodium cold-trapped at ~175°C is is presented in Fig. 4. Roughly linear dependence of corrosion on exposure time was obtained for most alloys and exposure temperatures. Table II shows that the corrosion rate was quite rapid at temperatures above 450°C for all alloys exposed at the higher oxygen level. A comparison of these data suggests that titanium additions to vanadium become less useful and chromium additions more beneficial as the test temperature rises.

Figure 5 is an Arrhenius plot of the linear corrosion rate of V-20 w/o Ti (the only alloy tested at all temperatures) as a function of temperature; the resultant activation energy was 30,000 cal/mole. Except at the highest temperature (700°C), V-20 w/o Ti exhibited the best corrosion resistance. The corrosion rate obtained at 700°C, shown with a half-shaded circle in Fig. 5, is in error (probably low) due to the inability of the cold trap to supply oxygen to the samples at a

sufficiently fast rate. Table III compares the oxygen analyses for the exposure of V-20 w/o Ti at various temperatures and illustrates the difficulty at 700°C. A similar difficulty, but of much smaller degree, was noted for the 600°C test. No problem was noted in the 650°C experiment since fewer specimens were exposed simultaneously.

The corrosion behavior was more complex when the cold-trap temperatures were reduced to ~110°C. Both weight gains and losses were observed, sometimes in the same test, as shown typically in Fig. 6. The slope of the weight-change curves varied from protective kinetics (slope decreasing with time) through linear to accelerating-rate kinetics. The relative resistance of the alloys to corrosion also differed from the results with a 175°C cold trap. Except at the lowest test temperature, the V-20 w/o Ti binary now showed the poorest and the V-Cr binaries the best resistance to corrosion. In all tests, however, the weight changes were much smaller than those of corresponding tests at the higher oxygen level. Since internal penetration of the alloys is of greater relative importance under these conditions, less significance is attached to the gravimetric data.

Distillation analyses of the sodium for oxygen gave low values ranging from 0.5 to 1.8 ppm, with most values about 1.5 ppm (calculated from a phenolphthalein end point assuming only Na_2O contributing to the residue alkalinity). No general correlation was noted between weight gain or loss and the oxygen analyses. Nitrogen analyses by a Kjeldahl technique

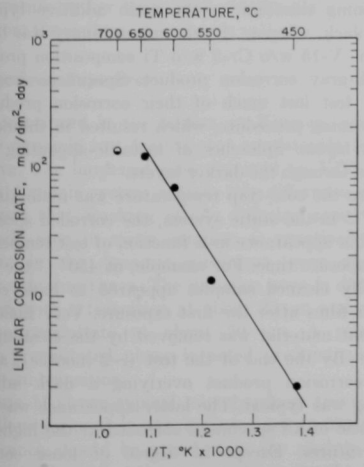

FIG. 5. Behavior of V-20 w/o Ti in Static Sodium Systems (Cold Trap at ~175°C).

TABLE III. OXYGEN ANALYSES OF SODIUM WITH A NOMINAL COLD-TRAP TEMPERATURE OF 175°C

450°C Test		550°C Test		650°C Test		700°C Test	
Days	Calc O, ppm[a]	Days	Calc O, ppm[b]	Days	Calc O, ppm[b]	Days	Calc O, ppm[a]
0	[c]	0	[c]	0	—	0	—
6.8	16.7	7.0	13.7	7.0	15.0	6.8[c]	4.2
13.8	13.2	13.9	13.1	14.0	15.0	20.8	10.2
27.8	16.3	27.9	11.5	21.1	13.6	34.8	10.4
43.8	16.2	41.8	11.0	28.1	15.6	48.6[c]	2.6
60.5	16.2	55.8	12.4	35.1	15.6	62.4	4.0
74.5	12.5	72.5	13.3	42.1	12.2		

[a] Based on distillation separation, titrating residue to phenolphthalein end point, and assuming alkalinity due to Na_2O.

[b] Based on amalgamation separation, titrating residue to phenolphthalein end point, and assuming alkalinity due to Na_2O.

[c] Additional Na_2O_2 added and digested before continuing test.

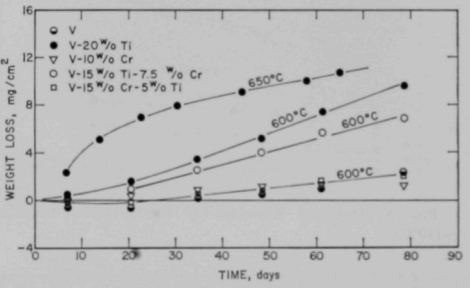

FIG. 6. Corrosion of Vanadium Alloys at 600 and 650°C (Cold Trap at ~110°C).

indicated the level in the sodium at less than 1 ppm, the limit of analytical sensitivity.

2. Dynamic Testing

Comparison of static and dynamic (6.1-m/s velocity) corrosion rates for modest oxygen levels (~15–20 ppm) in the sodium at 650°C showed that velocity accelerates the corrosion process for the V-20 w/o Ti alloy.[3] However, when the cold-trap temperature was reduced from 175 to about 110°C, the weight changes in the dynamic system were consistently lower and the sample appearance consistently better than in the static systems. Figures 7 through 9 show the gravimetric data for dynamic tests at 450, 550, and 650°C in sodium cold-trapped at 110°C. The V-Cr binary allows were the most resistant at all test temperatures. No dimension changes (limit of sensitivity was $\sim 2 \times 10^{-4}$ cm) were noted in samples

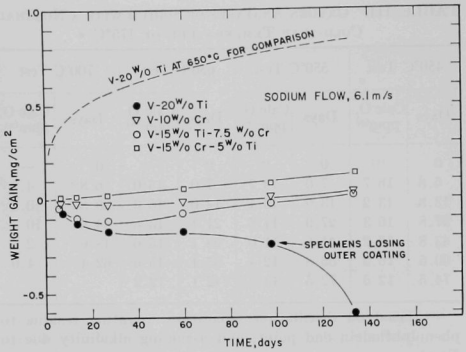

FIG. 7. Dynamic Exposure at 450°C (Cold Trap at ~110°C).

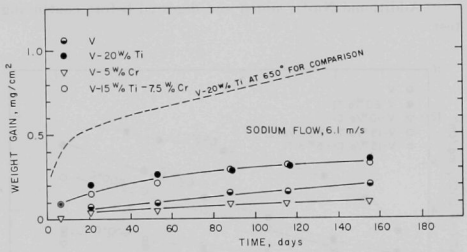

FIG. 8. Dynamic Exposure at 550°C (Cold Trap at ~110°C).

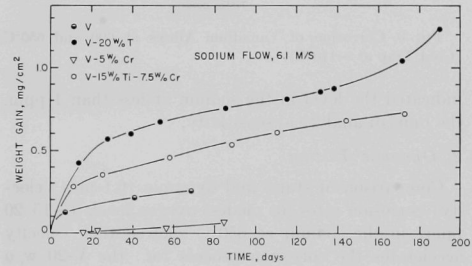

FIG. 9. Dynamic Exposure at 650°C (Cold Trap at ~110°C).

exposed at 550 or 650°C. (No dimensional measurements were made at 450°C.) This lack of dimensional change substantiates the inference that the low weight changes correspond to minimal corrosive attack.

In tests in which only weight gains were recorded for exposure periods of up to 4 months, the weight gain may be expressed empirically in the form $\Delta\omega = A(\text{Time})^B$, where A and B are constants depending on the alloy and temperature. For example, at 650°C with V-20 w/o Ti the relationship becomes[3] $\Delta\omega$ (mg/cm²) = 0.26 t(days)$^{0.24}$. The relationship was no longer valid (giving lower calculated values than actual values) after four months.

When a transition from weight gain to weight loss was noted, as, for example, with V-20 w/o Ti at 450°C, loss of corrosion product was obvious.

The results of oxygen analyses (by distillation) of the sodium in the dynamic experiments fell into the same range of values reported for static refreshed systems cold-trapped at ~110°C, namely, 0.5 to 1.8 ppm. The nitrogen level was also below the sensitivity (~1 ppm) of the technique used in the analysis. Qualitative peak measurements[6] of internal friction made with vanadium wires equilibrated in the static and dynamic systems indicated the level of oxygen and nitrogen in the dynamic system was less than half that for the static system.

B. Specimen Examination

1. Static Exposures

All specimens were covered with a loosely adherent, dark-gray coating after exposure in sodium cold-trapped at ~175°C. Removal of the outer layer by ultrasonic washing revealed a dark, firmly adherent corrosion product in most tests, except at 700°C. The color of the adherent layer varied with the alloy composition. The pure vanadium specimens and alloys containing titanium as the main additive typically were black, whereas the chromium binary was brown, and the V-15 w/o Cr-5 w/o Ti composition produced a dark-gray corrosion product. Specimens from the 700°C test lost much of their corrosion product in the cleaning procedure, which resulted in thinner adherent layers. Splotches of metallic-appearing areas showed through the darker layers.

When the cold-trap temperature was maintained at ~110°C in the static system, the corroded specimens varied in appearance as a function of test temperature and exposure time. For example, at 450° C the ultrasonically cleaned samples appeared to have colored temper films after the first exposure. Very little nonadherent material was removed by the cleaning procedure. By the end of the test (~2 months), a loose gray corrosion product overlying a dark adherent coating was typical. The latter appearance was characteristic of all specimens corroded at the higher test temperatures. Except in degree of loose corrosion product, these specimens resembled those corroded in sodium with a higher oxygen level.

Specimens in the dynamic system were covered with a thin, brown-tinted film, which did not change noticeably with time when only weight gains were recorded. This thin brown film spalled off in areas and revealed a dark underlying layer of corrosion product when a transition from weight gain to weight loss was recorded.

The binary vanadium-titanium alloys acquired a sharply defined subsurface diffusion zone upon exposure to high-temperature sodium. The metal under this zone appeared to be substantially unaffected by corrosion. The formation of this subsurface zone is of significance for practical applications of titanium-bearing alloys because the presence of the zone in sections of thin metal modified the mechanical properties of the section.[7] The depth of the hardened metal has been shown to be inversely related to the titanium content of a binary vanadium alloy[3] up to about 70 w/o titanium for constant exposure conditions. The sheet specimens (~1.5 mm thick) of unalloyed vanadium and the vanadium-chromium binary alloys did not develop a hardened layer in systems operating with a low cold-trap temperature, but were hardened uniformly when exposed for long periods in the static systems.

The addition of chromium to vanadium-titanium alloys made little change in the subsurface-hardened zone of corroded specimens when compared with a V-Ti binary of equivalent titanium content, but the hardness of the specimen center was increased somewhat. This may have been due to changes in internal microstructure resulting from the prolonged time at temperature rather than from penetration of impurities from the sodium.

2. Dynamic Exposures

As mentioned in the section on Kinetics, corrosion in the dynamic test facility was consistently less aggressive. The hardened zone obtained on V-Ti alloys in the dynamic system reflects this difference. Figure 10 shows that cracking of the diffusion zone, so extensively seen in static samples, is practically nonexistent in the dynamic specimens, even at much longer exposure times. The diffusion zone is distinctly layered, with a transition at about 25 μm and a band of fine precipitate at about 50 μm. A relatively coarse precipitated phase is noted predominantly at the 25-μm transition.

Figure 11 shows typical microhardness traverses of the alloys exposed in the dyamic test at 550°C. No significance should be attached to the slightly lower hardness values near the sample edges for the V and V-5 w/o Cr alloys. These values contain an error introduced by the microhardness tester because of the proximity of the poorly supported edge.

48668 212×

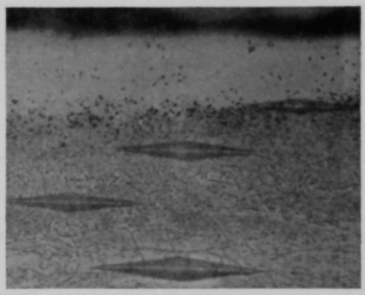

48669 (Brief Etch in Dilute Aqua Regia) 529×

FIG. 10. Corrosion Interface on V-20 w/o Ti Exposed 191 Days at 650°C to Sodium Flowing at 6.1 m/s (Cold Trap at ~110°C).

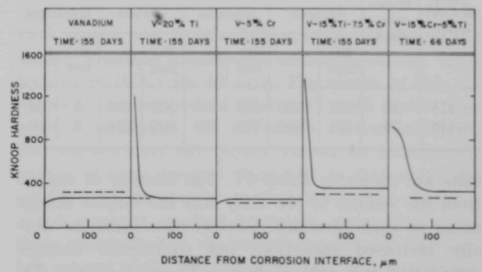

FIG. 11. Microhardness Profiles of Alloys Exposed to Flowing Sodium at 550°C (Cold Trap at ~110°C).

C. Specimen Chemical Analyses

1. Dynamic Experiments

Representative sections of corroded specimens from the dynamic experiments (including the thin corrosion coating) were chemically analyzed, and the re-

TABLE IV. Concentrations of Nonmetallic Impurities in Corroded Specimens[a] Exposed in the Dynamic System

Alloy	Exposure[b]		Results of Chemical Analyses, ppm							
	Days	Temp, °C	Oxygen		Nitrogen		Carbon		Hydrogen	
			After	Before	After	Before	After	Before	After	Before
V-20 w/o Ti	191	650	2630	575	362	250	620	305	5	5
	155	550	1660	575	362	250	116	305	13	5
	134	450	1400	575	166	250	413	305	13	5
V-15 w/o Ti-7.5 w/o Cr	173	650	1550	900	430	250	737	340	3	13
	155	550	1850	900	232	250	278	340	9	13
	134	450	1940	900	226	250	445	340	7	13
V-5 w/o Cr	85	650	1030		254		347		14	
	155	550	1020		176		327		8	
V-10 w/o Cr	134	450	1160	705	188	280	360	310	6	22
V-15 w/o Cr-5 w/o Ti	66	550	1330	815	196	190	320	234	10	47
	134	450	1270	815	162	190	417	234	4	47
V	69	650	770	390	434	250	552	420	11	50
	155	550	1000	390	157	250	294	420	16	50

[a] Pre-exposure values are average for the sheet supplied and not necessarily from adjacent specimens.
[b] Cold trap maintained at ~110°C.

TABLE V. Concentrations of Nonmetallic Impurities in V-20 w/o Ti Alloy Exposed at 600°C in the Static System

Temp of Cold Trap, °C	Exposure, days	Results of Chemical Analyses, ppm							
		Oxygen		Nitrogen		Carbon		Hydrogen	
		Before	After	Before	After	Before	After	Before	After
~175	66	575	3600	250	496	305	298	5	51
~110	79	575	7400	250	334	305	334	5	60

sults are shown in Table IV. The transfer of oxygen from the sodium to the alloy was the largest change noted in each specimen. Carbon concentrations usually increased somewhat, but substantial changes were noted only with V-20 w/o Ti and V-15 w/o Ti-7.5 w/o Cr exposed at 650° C. Nitrogen impurity levels tended to remain approximately constant, except for a slight increase after the 650°C exposure. Since the spread of the nitrogen values typically is wider than those of the other impurity elements before exposure to sodium (depending on sample position in the casting), a variation of 50–100 ppm may not be significant. Hydrogen levels were low (5–16 ppm) after corrosion exposure, even when the initial concentration was as high as 50 ppm. The removal of hydrogen from unalloyed vanadium by the corrosion exposure may account for the lower terminal hardness value shown in Figure 11.

2. Static Experiments

Representative V-20 w/o Ti samples with adherent corrosion coating were analyzed for changes in interstitial content as a result of corrosion exposure in the refreshed static system (see Table V). Oxygen, nitrogen, and hydrogen levels increased as a result of exposure, but carbon remained about constant. The higher oxygen value for the specimen exposed in the sodium of lower oxygen content is a result of the greater amount of retained corrosion product (presumably rich in oxygen) observed on this sample.

Comparison of the chemical analyses of the dynamic and static systems suggests that at comparable cold-trap temperatures the oxygen and hydrogen levels were much higher in the static system. Cold traps of similar size (1½-in. pipe by 12 in. long) and construction were used for both types of systems. The average flow rates were about 4 l/hr for the static system and roughly twice that for the dynamic loop.

D. X-ray and Microprobe Analyses

Corroded specimens of V and V-20 w/o Ti (exposed 80 days in 600°C sodium cold-trapped at 110°C) were examined with a slow-scan, X-ray diffractometer. All peaks obtained from the corrosion

produced correlated with those reported for γ VC ($VC_{0.4-0.5}O_{0-0.1}$). Similar results were obtained for powder patterns taken from the nonadherent corrosion products, except that a fainter pattern for either VC or possibly $VO_{0.9}$ was also present.

No corrosion-product peaks were obtained by the diffractometer for the specimen of V-20 w/o Ti corroded at 650°C for 191 days in the dynamic system. An attempt to obtain a powder pattern by filing the outer surface was not successful because of the high concentration of file metal in the resultant powder. (The outer surfaces of the specimens are very hard.)

The microprobe was used to examine the corrosion interface of the same V-20 w/o Ti specimen exposed at 650° C for 191 days in the dynamic system. Since precise standards were not available, the results are qualitative, particularly for nitrogen, because there is interference from the titanium present. The results for oxygen and carbon are shown in Figs. 12 and 13, respectively. A curve is not shown for nitrogen, but a substantial peak (twice the titanium interference level) occurred just inside the corrosion interface (at <8 μ). At a depth of 20 μ, the response due to nitrogen became equal to the titanium interference level.

Both the carbon and, to a lesser extent, the oxygen traces show double peaks. Simultaneous maxima in titanium suggest an interaction between the titanium and the impurities. Both carbon and oxygen are present in excess of their solid solubilities in pure vanadium.[10, 11]

E. Carbon Addition

The tentative X-ray identification of gamma vanadium carbide as a corrosion product led to an experiment to determine the effect on corrosion rate of an increase in the available soluble carbon in the sodium. The carbon donors were specimens of a high-carbon steel placed next to the V-20 w/o Ti samples in the holder. The unit was exposed to 650°C sodium (cold trap at ~110°C) for 16 days. The results of this exposure are compared in Table VI with those of a control experiment (no deliberate carbon addition). The carbon steel did supply carbon as anticipated; carbon content dropped from 0.91 to 0.14 w/o. The results were unexpected in that the carbon-contaminated exposure resulted in weight losses about half those experienced in the control experiment. The carbon content of the corroded specimens was up slightly, but the nitrogen content was sharply reduced when compared with the control experiment. Microexamination disclosed no differences between the control and contaminated specimens.

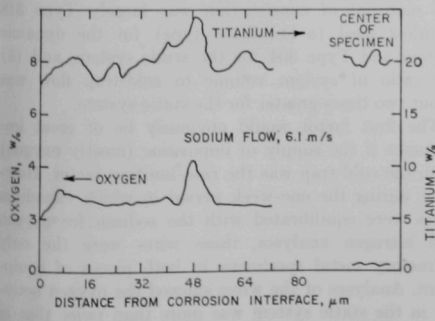

FIG. 12. Microprobe Traverse for Titanium and Oxygen on V-20 w/o Ti Exposed at 650°C to Flowing Sodium for 191 Days (Cold Trap at ~110°C).

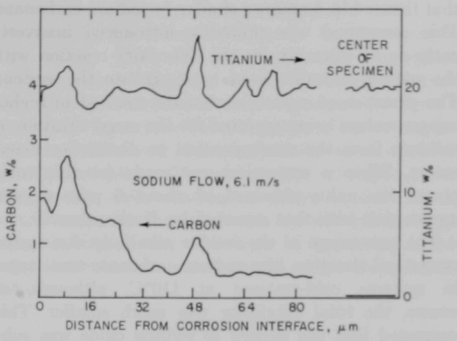

FIG. 13. Microprobe Traverse for Titanium and Carbon on V-20 w/o Ti Exposed at 650°C to Flowing Sodium for 191 Days (Cold Trap at ~110°C).

TABLE VI. INFLUENCE OF CARBON ON THE CORROSION OF V-20 w/o Ti IN SODIUM[a] AT 650°C

Conditions	Weight Loss, mg/cm²	Postexposure Chemical Analyses, ppm			
		C	O	N	H
Control (no deliberate carbon)	0.29	330	4750	380	55
	0.33				
Sample exposed with 0.9% carbon steel	0.13	405	4670	175	60
	0.15				

[a] Each sample was exposed for 16 days in sodium cold trapped at ~110°C.

IV. Discussion

The use of a cold trap to control the oxygen level in a sodium system tacitly assumes that the solubility of sodium oxide at a given cold-trap temperature will determine the oxygen level. The sodium cold-trapped at 175°C had a significant amount of a compound

that titrated in a manner similar to sodium carbonate. This compound was probably introduced inadvertently as an impurity by the CO_2 (air) reaction with the sodium peroxide used to oxygenate the system. The presence of sodium carbonate resulted in higher oxygen values being reported for the usual titration of residues from the amalgamation or distillation separation. When a correction was made for this compound the value obtained of about 6 ppm oxygen agrees well with that reported by Rutkauskas.[8]

The percentage of the residue alkalinity due to the compound titrating like sodium carbonate was larger in systems cold-trapped at 110°C, although, of course, the total alkalinity was much smaller. This suggested that the oxygen as sodium oxide was substantially below 1 ppm at this cold-trap temperature, again in agreement with the extrapolated data[9] of Rutkauskas and Noden-Bagley.

In general, these values are substantially lower than those reported in a previous paper[3] written before the sodium carbonate and sodium hydride contributions had been evaluated for the amalgamation-analysis technique.

Vanadium and all of the alloys exhibited great sensitivity to the impurity level in the test sodium. The V-20 w/o Ti binary demonstrated better relative behavior at the higher oxygen concentration and lower exposure temperatures, whereas the V-Cr binary alloys appeared best whenever the oxygen concentration was low. The ternary alloys, as might be expected, were intermediate in behavior, but the presence of as little as 5 w/o Ti resulted in the formation of a undesirable subsurface hardened zone during exposure to sodium cold-trapped at 110°C.

The apparent reduction in the linear corrosion rate for V, V-10 w/o Cr, and V-15 w/o Cr-5 w/o Ti alloys as the temperature increased from 600 to 700°C was probably largely due to the much lower oxygen level at 700°C.

A probable explanation for the behavior of titanium as an alloying additive for vanadium is the relative affinity of the metals for oxygen. At 650°C titanium is capable of forming titanium oxide in sodium containing $\ll$1 ppm oxygen, whereas vanadium does not form an oxide (carbo-oxide) phase until the oxygen level in the sodium exceeds $\sim$1 ppm. No oxide of chromium was found in sodium containing $\sim$20 ppm oxygen. In sodium containing an oxygen concentration of less than $\sim$1 ppm, the greater affinity of titanium for oxygen (in the V-Ti alloys) thus provided an added driving force for the pickup of oxygen. At oxygen levels significantly above about 1 ppm, the vanadium reacted rather rapidly to form a carbo-oxide layer. The presence of titanium in the alloy and the subsequent formation of titanium oxide in the corrosion coating apparently improved the protective character of the rather loosely adherent corrosion product and provided a better diffusion barrier to the corrosion reaction. The addition of titanium retarded the diffusion of oxygen into the bulk of the specimen, and a highly oxygen-enriched zone resulted near the surface.

Chromium also retarded oxygen diffusion in V-Cr alloys somewhat, and because of a lower chemical affinity for oxygen, chromium did not provide an increased driving force for oxygen pickup from sodium.

The vanadium alloys should only be considered for use at low oxygen levels ($<$1 ppm). Both the loss of metal-cladding thickness (strength) due to corrosion and the production of loose particulate corrosion product would cause difficulties in reactor operation at the 6-ppm oxygen (as Na_2O) level.

However, if a large reactor could be effectively cold-trapped near the melting point of sodium, then vanadium alloys should be useful (as demonstrated by the dynamic tests at 450, 550, and 650°C). Alloys of the V-Cr binary system gave the best corrosion results under these conditions; they had very low weight changes, no discernible dimension changes, and low nonmetallic-impurity content after exposure.

The better performance of all of the alloys in the dynamic system was fundamentally due to the lower impurity level in that system as compared with the low impurity level in the static system. The reason for the lower level is more difficult to rationalize. The cold traps were quite similar in construction for the dynamic and static systems, and tests were performed which indicated that an adequate amount of sodium oxide was stored in each trap. The dynamic and static systems differed in several aspects: (1) the ratio of exposed refractory-sample area to system volume was about five times greater for the dynamic system, (2) the material of construction was largely Type 318 stainless steel (a stabilized type) for the dynamic system and Type 304 for the static system, and (3) the ratio of system volume to cold-trap flow was about two times greater for the static system.

The first factor would obviously be of great importance if the supply of impurities (mostly oxygen) from the cold trap was the rate-limiting factor. However, during the one-week period in which vanadium wires were equilibrated with the sodium for oxygen and nitrogen analyses, these wires were the only refractory metal specimens in both pieces of equipment. Analyses of the wires showed the oxygen activity in the static system was more than twice that in the dynamic system under these circumstances.

The presence of stabilizing agents in the stainless

steel containment vessel was not expected to modify greatly the direct oxygen activity in the sodium, but their presence in the steel might possibly slow the mass transfer of carbon to the vanadium. Since the main corrosion product on vanadium was a carbo-oxide, carbon activity might play an important role in the overall corrosion process. However, an experimental check of this hypothesis in the carbon-contaminated test showed that it was not correct.

The elimination of the first two system factors leaves possibilities related to the relative cold-trap efficiencies to explain the differences in the levels of oxygen and other impurities between the dynamic and static systems. Since the two traps are similar, this suggests that a higher velocity of the sodium through the trap actually improved the trap efficiency. Experiments are being undertaken to check this hypothesis.

Chemical analyses of representative sections showed greater impurity pickup for the titanium-bearing alloys as compared with either pure vanadium or the vanadium-chromium binary alloys. Furthermore, the titanium-bearing alloys concentrated the impurities in subsurface zones ranging in thickness from 10 to 100 μm. Thus the average analysis would depend on the thickness of the specimen for this class of alloy. For very thin sections, as might be used in reactor fuel cladding, the average analyses would be much higher than reported for the 0.15-cm-thick corrosion specimens at the same exposure.

The increase of carbon in the sodium environment actually reduced the weight changes of the V-20 w/o Ti alloy somewhat as compared with control experiments. Combining this observation with the postexposure chemical analyses suggests that oxygen content of the sodium is the most significant variable in determining the corrosion behavior in this temperature range. However, the X-ray and microprobe analyses showed that the oxygen and carbon impurities interact concertedly with vanadium to form a compound layer of γ VC and again in the subsurface hardened zone with titanium to form an unidentified precipitated phase. The observation of a gold-brown tint on the outer coating on alloys exposed in the dynamic system combined with the microprobe result suggests that a very thin layer of vanadium nitride was present on the outer surface of the corrosion interface.

REFERENCES

1. L. Champeix, R. Darras, and J. Sannier, *Alkali Metal Coolants*, Proc. of IAEA Symp., Vienna, (1967) pp. 45–61.
2. M. Conte, Euratom-CEA Assoc. Report R3152 (March (1967).
3. S. Greenberg, W. E. Ruther, and H. A. Levin, *Alkali Metal Coolants*, Proc. of IAEA Symp., Vienna, (1967) pp. 63–84.
4. H. U. Borgstedt, Paper Presented at the NACE Meeting, Cleveland (March 1968).
5. M. David and A. Droycott, IGR-TN/C857 (1958).
6. D. L. Smith, Argonne National Laboratory, personal communication (1967).
7. F. L. Yaggee and E. R. Gilbert, *Alkali Metal Coolants*, Proc. of IAEA Symp., Vienna, (1967) pp. 215–229.
8. V. J. Rutkauskas, LA-3524-MS (1966).
9. T. F. Kassner and D. L. Smith, ANL-7335 (1967).
10. R. W. Thompson and O. N. Carlson, J. Less Common Metals **9**, 354–361 (1965).
11. A. U. Seybolt and H. T. Sumsion, J. of Metals, 292–299 (Feb. 1953).

Discussion

As the result of defective tape, it was not possible to transcribe the discussion that followed the presentation of this paper.

SESSIONS ON SODIUM TECHNOLOGY

SESSION ST-IIIB

Friday Morning, November 8, 1968

Chairman: J. C. Biery
Los Alamos Scientific Laboratory

Secretary: C. F. Cheng
Argonne National Laboratory

Characterization of Sodium Pool Fires*

R. P. Johnson, M. Silberberg, J. Hopenfeld, and P. Beiriger

Atomics International
A Division of North American Rockwell Corporation
Canoga Park, California

(PRESENTED BY M. SILBERBERG)

1. Introduction

The release of energy and effluents from a sodium fire, resulting from a major sodium spill in a Liquid Metal Fast Breeder Reactor (LMFBR), must be considered in the safety analysis of the plant. Such fires may occur, for example, when sodium which is sufficiently hot is discharged onto the floor of a primary-system equipment cell from a pipe rupture or inadvertently opened blocking valve during maintenance. A sodium fire in a primary cell which is open to the reactor building will result in the generation of pressure and the release of radioactive sodium aerosols within the building. The analysis of this accident determines the basis for the design pressure of the outer containment barrier in the LMFBR.

Experiments conducted in the past at Atomics International have been concerned primarily with small-scale fires, where sodium was burned in various containers, either in open air or in ventilated enclosures under steady, forced-flow conditions with air and reduced oxygen atmospheres.[1-4] These experiments provided information about some of the characteristics which affect the thermal behavior of sodium pool fires, such as dependence of the burning rate on oxygen concentration, surface condition behavior, and effects of prolonged burning periods in air. For example, Phase-I experiments in the sodium fires program, conducted with experiments with 3-ft^2 pools in a ventilated enclosure[5-9] show that sodium burning rates vary from 0.22 to 0.45 lb Na/hr-% O_2 per apparent square foot of surface area, over the range of sodium pool temperature (600 to 1300°F) and oxygen concentration (4, 10, and 21 vol %), for burning periods of up to a few hours. The highest burning rate observed for an air environment was 9.3 lb Na/hr-ft^2. Since a number of the detailed mechanisms of sodium burning are not well understood, the scaling laws for applying the results from the small-scale fire experiments to large-scale fire accidents which might occur in a reactor system are unknown. As a result, plans were formulated to design, construct, and conduct large-scale fire modeling experiments in an enclosure which simulates reactor system containment configurations. Because these fires are smaller in scale than those which may occur in the actual system, considerable effort is devoted to the instrumentation for these experiments, so that information about the basic mechanism of sodium burning can also be obtained.

The purposes of this paper are to describe the large sodium fire modeling test apparatus (Phase II) and the results of the initial test conducted in this facility, as well as some of the theoretical considerations associated with the development of a sodium fire accident model for the LMFBR. Release and transport characteristics of sodium oxide aerosols, generated during sodium pool fires, are described elsewhere.[8, 9]

2. Theoretical Considerations

In order to calculate the pressure rise in a given system in which heat is generated due to sodium burning, one must know the net amount of heat absorbed by the gas in the containment as a function of time. A heat balance for the gas requires the knowledge of the burning rate, a priori. However, if the burning rate depends upon the absolute temperature of the reaction region or upon the temperature gradients within the system, then the burning rate cannot be solved independently of the equations which describe the temperature distributions in the system.

The burning rate would primarily depend upon the following three processes:

1) rate of oxygen arrival to the burning region;
2) rate of reaction of oxygen with sodium;
3) diffusion of sodium vapor through the oxide layer to the burning region.

Any of these processes could be the limiting step, if it proceeds at a relatively slower rate than the others.

To clarify the essential features of the problem, consider the heat balance for a simplified sodium pool fire, as shown in Figure 1.

This simplified model consists of four regions:

1) liquid sodium pool;
2) porous sodium-sodium oxide layer;
3) reaction or flame zone, at which oxygen and sodium vapor combine to form sodium oxide;
4) gas containing sodium oxide aerosols.

* Work performed under U.S. Atomic Energy Commission Contract AT(04-3)-701.

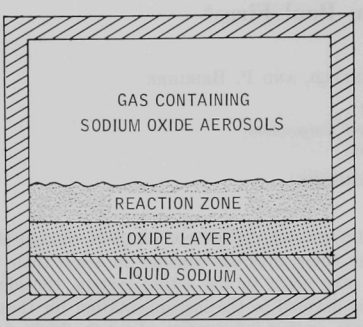

FIG. 1. Schematic of Sodium Pool Fire.

*2.1. Heat Balance for the Gas**

$$(Q_g)_{abs} = (Q_{fg})_{rad} + (Q_{fg})_{cv} - (Q_{gw})_{rad} - (Q_{gw})_{cv}. \quad (1)$$

This equation simply states that the amount of heat absorbed by the bulk gas equals the amount of heat received by radiation and convection from the reaction zone minus the amount lost to the walls by radiation and convection.

2.2. Heat Balance for the Reaction Zone

$$\beta\bar{Q}_c = (Q_{fg})_{rad} + (Q_{fg})_{cv} + (Q_{fs})_{rad} + (Q_{fs})_{cv}. \quad (2)$$

The amount of heat generated due to combustion equals heat losses by radiation and convection to the oxide surface and the gas. Additional terms, accounting for the radiation exchange with the walls, will be required if the gas is not a perfect absorber.

2.3. Heat Balance for the Oxide Surface

$$(Q_{cd})_{ox} = (Q_{fs})_{cv} + (Q_{fs})_{rad} - Q_v. \quad (3)$$

The total heat conducted from the oxide surface towards the liquid equals the total heat radiated and convected from the reaction zone minus the heat absorbed by the sodium vapor as it rises to the reaction region, again assuming the gas in the reaction region is a perfect radiation absorber.

2.4. Heat Balance for the Oxide Layer-Sodium Surface Interface

$$Q_{cd,Na} = (Q_{cd})_{ox} - Q_v - \beta\bar{Q}_{vap}. \quad (4)$$

The heat conducted downward towards the liquid equals the amount of heat arriving at the oxide surface from the reaction zone minus the heat absorbed by the sodium vapor as it rises through the oxide layer and the heat of vaporization.

* A nomenclature list is included at the end of this paper.

Finally, the problem is fully described when additional heat balances are written for the containment walls and the pool liquid sodium, and when Equations 1 through 4 are expressed in terms of temperatures and the appropriate physical properties of the media. This requires additional relationships for:

1) the burning rate β;
2) the emissivities of the gas and of the surface;
3) the thickness of the oxide layer;
4) the diffusion rate of vapor through the oxide layer.

It should be noted that these variables are not necessarily independent of each other (*e.g.*, the gas emissivity, which is related to the aerosol concentration in the gas, would be expected to depend upon the burning rate and the released fraction of sodium oxide).

The complexity of the problem at hand shows the need for experiments that will provide the necessary parameters and will point out whether further simplification of the theoretical equations is possible.

3. Description of Large Modeling Fires Test System

The system for the large sodium fires modeling experiments is located at the Atomics International Nuclear Development Field Laboratories, in the Sodium Fires Test Installation. The principal features of the Phase-II experimental apparatus are described in the following sections.

3.1. Test Vessel

The test vessel for the large sodium fires modeling experiments consists of a 10-ft-diameter, 31.7-ft-high, mild steel, cylindrical shell with ellipsoidal upper and lower head sections, certified for 40 psig at 700°F. The vessel body is assembled in three sections, the lower section being 10.9 ft high and the upper two sections each 8.5 ft high. Each ellipsoidal head section has a maximum height of 2.4 ft from the major axis. The cell, or lower section, is provided with a cylindrical skirt that allows attachment of the vessel to the facility pit floor. This skirt also places the lower ellipsoidal head section approximately 1 ft above the pit floor. The Phase-II test vessel is shown in Figure 2.

3.2. Atmosphere Control

The test-vessel atmosphere can be controlled, in both the cell and secondary sections, through the facility atmosphere mixing manifold. Either 100% air or nitrogen-diluted air may be introduced into the test vessel, at flow rates up to 200 cfm. This atmosphere supply can be used either to establish pre-test conditions or to supplement gas volume contraction due to

temperature decay or oxygen depletion. The pre-test oxygen concentration may be decreased within the cell section while maintaining a 100% air concentration within the secondary section, by opening a bypass line between the cell section and the vessel exhaust line. It should be noted that, during experiments that require a two-volume configuration (cell section and secondary section) with separate controlled atmospheres, a doughnut section is placed between the vessel sections. This doughnut assembly is provided with an opening to allow communication of gases between volumes during a cell-open-to-building model fire configuration, and may be closed initially or at any time during the test. The area of the opening between volumes may be varied from 1 to 28 ft², depending on test requirements.

Vessel exhaust can be accomplished through a 12-in.-diameter pipe, mounted in the center of the top ellipsoidal head section. A 12-in. gate valve is provided in this line for system closure. The exhaust gas is directed through this line to the facility gas bubbler-scrubber system, through an exhaust blower, and vented directly to outside atmosphere.

3.3. Spill Supply and Configuration

Two separate sodium-preheat and -transfer systems are provided on the test vessel. The primary system consists of a sodium drum melt station, an in-line filter, and a 1250-gal sodium-supply tank. The sodium-supply tank is provided with insulated 6- and 2-in. fill lines, directed to the test vessel. This primary supply tank and the dump lines are capable of delivering sodium at bulk temperatures from 350 to 1300°F. An auxiliary sodium-supply system, used for Phase-II experiments, delivers small, accurately determined quantities of sodium ($\leq$100 lb) to the test vessel. This system consists of a small-diameter preheat tank, an inert gas blanketing system, a transfer control valve, and a 1-in. insulated transfer line to the sodium burn pan.

The pool fire areas planned for the Phase-II sodium fires experiments will vary from about 3 to 60 ft². Typical burn pans will be cylindrical in configuration and will have depths ranging from 0.3 to 1 ft. Each burn pan is capable of being pre-heated to test conditions and/or completely insulated. The burn pan is supported on a stand above the ellipsoidal bottom of the vessel.

3.4. Instrumentation

In order to study the aerosol and energy-transport characteristics of sodium pool fires, an array of sodium oxide plating and fallout-sampling devices, and temperature, pressure, and heat-flux transducers are installed within the test vessel. Typical cumulative

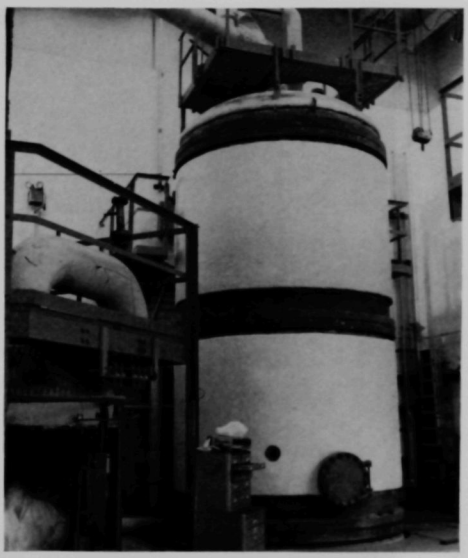

A. Photograph

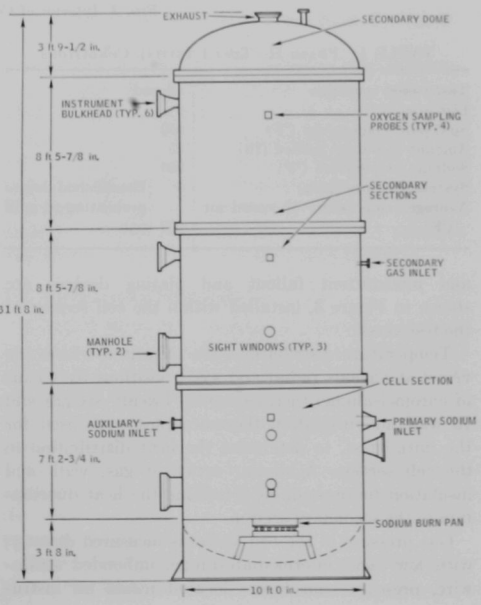

B. Line Drawing

FIG 2. Large Sodium Fires Modeling Experiment.

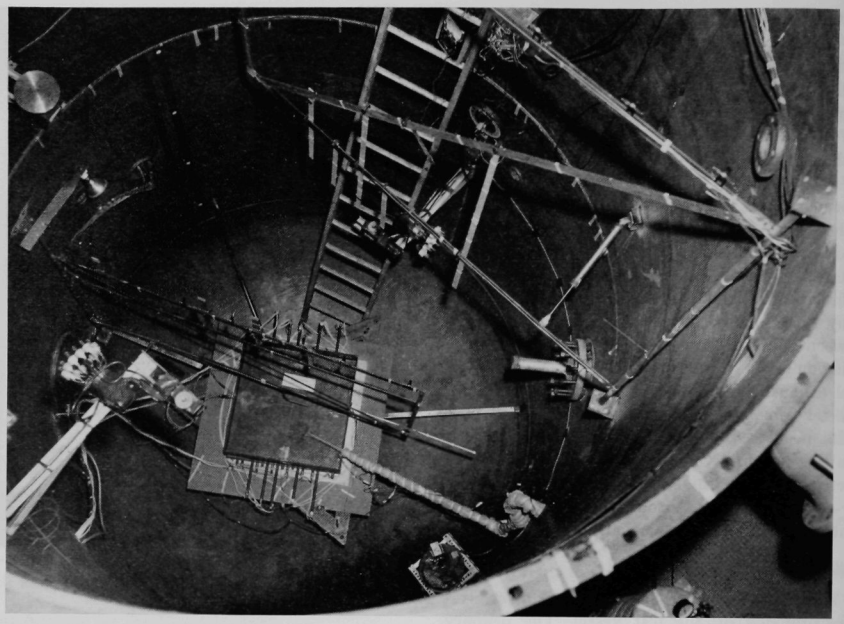

FIG. 3. Interior of Cell Section of Test Vessel.

TABLE 1. PHASE II—TEST-1 INITIAL CONDITIONS

Test vessel condition	Closed	
Fire area (ft^2)	6	
Spill-pan temperature (°F)	950	
Amount of sodium spilled (lb)	25	
Sodium temperature (°F)	950	
System pressure (psig)	5	Established due to preheating of spill pan
Average temperature of vessel air (°F)	210	

and intermittent fallout and plating devices are shown in Figure 3, installed within the cell section of the test vessel.

Temperature distributions are measured within the vessel at various radial and axial positions by means of chromel-alumel thermocouples. Twenty-six gas and 13 wall and insulation thermocouples were used for the initial test, to determine the heat distribution in the cell section. A similar array of gas, wall, and insulation thermocouples determine the heat distribution in the secondary section.

Gas pressure in the test vessel is measured directly, with low- and intermediate-range, unbonded strain-wire, pressure transducers located inside an instrumentation bulkhead. This bulkhead is located in the secondary section, at an elevation of 26 ft (from the bottom of the test vessel).

The sodium burning rate is obtained by determining the overall oxygen concentration within the test vessel, by sampling continuously the atmosphere at various locations. The oxygen-sampling stations available for the initial tests are noted in Figure 2b. At each selected oxygen station, a continuous flow of atmosphere (~200 cc/min) is pumped from the vessel, filtered, directed to an oxygen analyzer, and returned to the vessel for detector cooling.

The signals from each of the previously mentioned temperature, pressure, oxygen-concentration, and radiant heat-flux detectors are recorded directly on multipoint recorders and on a data-logger system at preselected time intervals. These digital data are processed by computer.

The test vessel is equipped with several view ports for visual observations. One of the view ports in the lower, or cell, section of the vessel is utilized for obtaining 16-mm motion pictures in the sodium-spill area during the initiation and progress of the fire.

4. Description of the Initial Phase-II Test

The initial Phase-II test involved 25 lb of sodium, introduced into the spill pan of the test vessel at a temperature of 950°F and an initial vessel atmosphere of about 100% air (21 vol % O_2).

The initial conditions for the test are summarized in Table 1.

Sodium, in brick form, was added to the auxiliary preheat tank, and a nitrogen blanket atmosphere was established within the tank. Initial heating of the tank was adjusted to melt the sodium. After the detector and recording instrumentation were completely checked, the initial conditions (see Table 1) were established.

The sodium was then introduced into the spill pan and the test was initiated. At the start of sodium transfer (T − 25 sec), the 16-mm motion picture camera was started. After all sodium had been transferred to the spill pan, T − 0 was marked and the data-logger system was activated to a mode which would scan 168 channels of data every 2 min.

5. Experimental Results

The data obtained from Phase II—Test 1 related to the salient features of some of the important characteristics, such as burning rate, gas temperature distribution, and radiant heat transport, are presented in the following section. A brief description is also given of the visual observations recorded by the 16-mm camera during the early stages of the fire (0 to 3 min).

5.1. Sodium Burning Rate

The oxygen concentration measured at three axial positions (1.5, 5.5, and 14 ft above the spill pan) in the test vessel as a function of time is shown in Figure 4. These data were used to compute the history of the sodium burning rate shown in Figure 5. This was done by first determining the volume-averaged oxygen concentration, from the various oxygen probes, and then taking differences of this concentration at successive time intervals. In converting the bulk oxygen decrease to the sodium burning rate per unit area, it was assumed that the sodium-oxygen reaction was

$$4\ Na + O_2 \rightleftarrows 2\ Na_2O,$$

and the physical area of the spill pan was used.

Figures 4 and 5 indicate that 90% of the sodium was consumed after about 20 min of burning. With the exception of an apparent high burning rate during the initial 2 min following the introduction of the sodium into the spill pan, the burning rate varies between about 8 and 12 lb/hr-ft², up to ~20 min, after which it drops sharply to 2 lb/hr-ft², continues at that rate for ~10 min, and eventually decreases to zero. Although the burning rate during the period from 2 to 20 min can be described fairly well by an average value of 10 lb/hr-ft², the data in Figure 5 suggest a steady rise, from 8 lb/hr-ft² at 2 min to a maximum of 12 lb/hr-ft² at about 12 to 14 min.

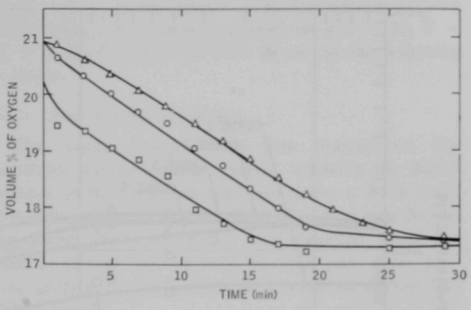

FIG. 4. Oxygen Concentration *vs* Time (Phase II—Test 1).

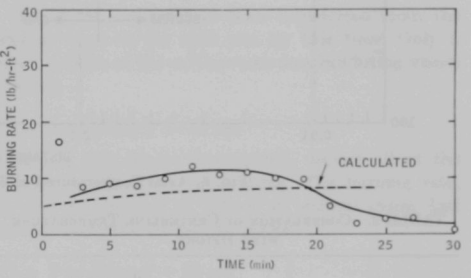

FIG. 5. Sodium Burning Rate *vs* Time (Phase II—Test 1).

5.2. Temperature Distribution

Figure 6 shows the variation of centerline temperature as a function of both height above the bottom of the pan and time. Curves 1, 2, and 3 represent the temperature distribution during the burning period, and Curve 4 represents the temperature during the postburning period.

The centerline temperature can be approximately represented by $T \sim Z^n$, where Z is a height above the sodium surface and n is a constant having the values as shown in Table 2.

Figure 7 shows the radial temperature distribution at an elevation of 4.3 ft above the spill pan. The

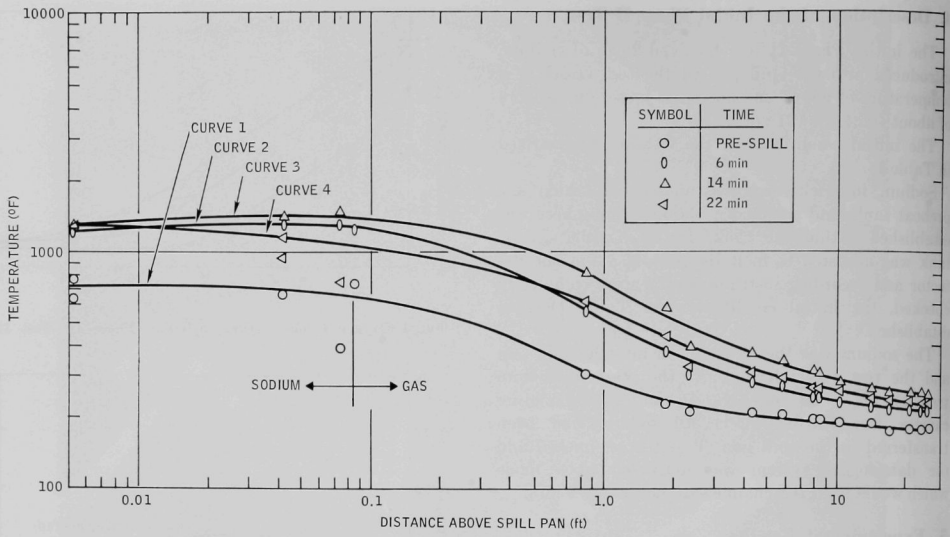

FIG. 6. Axial Temperature Profile for Various Times (Phase II—Test 1).

TABLE 2. CORRELATION OF CENTERLINE TEMPERATURE WITH HEIGHT

Time (min)	Curve	n			
		Zone 1 $Z = 0.08$ ft $\rightarrow 0.3$ ft	Zone 2 $Z = 0.3$ ft $\rightarrow 0.3$ ft	Zone 3 $Z = 0.8$ ft $\rightarrow 5$ ft	Zone 4 $Z = 5$ ft $\rightarrow 25$ ft
(Pre-spill)	1	0.23	0.45	0.243	0.0723
6	2	0.18	0.481	0.403	0.155
10		0.211	0.369	0.428	0.201
14	3	0.153	0.388	0.455	0.222
22	4	0.197	0.321	0.389	0.200

radial temperature distribution is approximately symmetrical with respect to the centerline, with the radial temperature gradient becoming steeper with time. The radial temperature gradients decrease at the end of the burning period. It is of interest to note that, at this elevation, the wall is hotter than the gas initially, with the trend reversing as burning continues.

Figure 8 shows the radial temperature distribution at various elevations, 6 min after the spill. Flattening of the temperature profile progresses as the distance from the heat source increases.

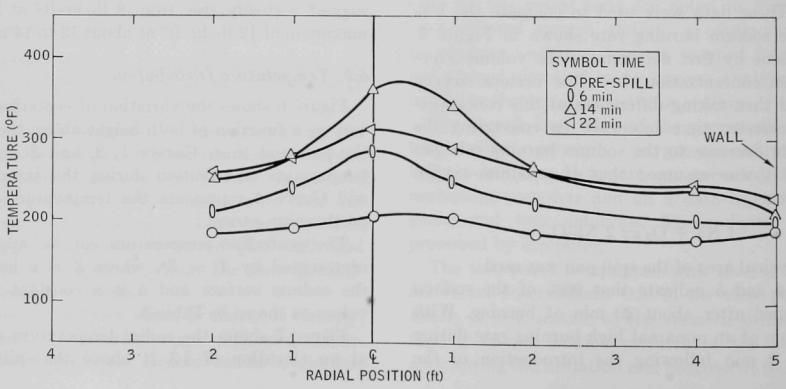

FIG. 7. Radial Temperature Distribution at 4.3 ft above Burn Pan.

5.3. Radiant Heat Transport

Since only one radiometer was available in this experiment, complete description of the radiant heat transport through the gas is not possible. The one radiometer was located ~10 ft above the pan. However, it is significant to state (see Figure 9) that during the period between 4 and 20 min after the spill, no apparent radiant flux can be recorded from the radiometer. Not until after about 20 min, at reduced burning rate, can the radiant heat flux be recorded from the radiometer.

5.4. Visual Observation from Motion Picture

Sixteen-millimeter motion pictures were taken of this test, through a viewing port located 4½ ft above the plane of the spill pan and at an angle of ~45°. Total test time recorded by the film was 2.2 min, including the sodium charging time, $T - 25$ to $T - 0$ sec, and ~1.8 min after $T - 0$. The sodium burning phenomena are described, at test times $T - 25$, $T - 0$, $T + 30$, $T + 60$, and $T + 90$ sec, in the following sections.

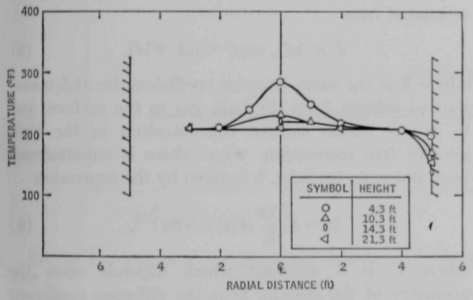

FIG. 8. Radial Temperature Distribution at Time = 6 min.

5.4.1. Test Time $T - 25$ sec

The sodium-dump valve was opened on the auxiliary sodium-preheat system, allowing the 950°F sodium to flow into the spill pan under a 10-ft head. Total transfer time for the 25 lb of sodium was 25 sec. An initial cloud of smoke was observed when the sodium stream first entered the spill pan. Also, partial ignition of the sodium pool occurred during this filling period.

5.4.2. Test Time $T - 0$ sec

All of the sodium had been transferred from the preheat tank to the spill pan by this time. Only a small portion of the surface area was exhibiting visual burning.

5.4.3. Test Time $T + 30$ sec

During this 30-sec time period, almost all of the sodium surface area was burning. The burning rate, as well as the rate of release of sodium oxide, had greatly increased during this period.

5.4.4. Test Time $T + 60$ sec

At an elapsed time of 1 min, the fire had definitely encompassed all of the 6-ft² area of the spill pan. The burning was also increasing in vigor. Since it became more difficult to see the sodium fire, it is apparent that the concentration of sodium oxide par-

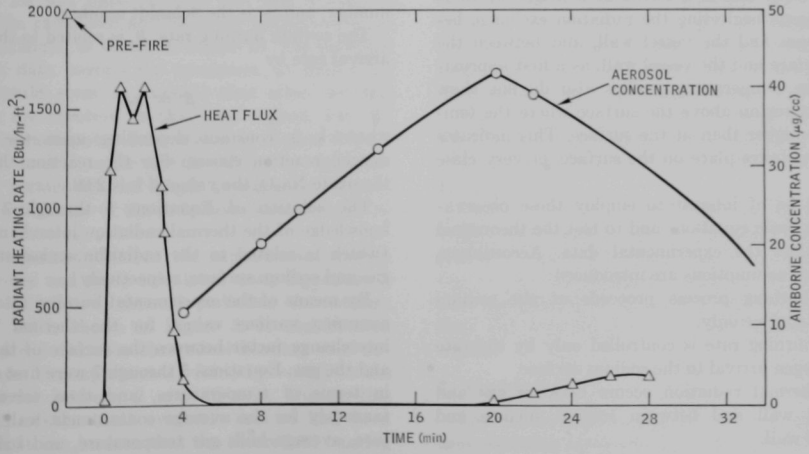

FIG. 9. Sodium Fire Radiant Heat Flux at 10 ft above Spill Pan, and Sodium Oxide Aerosol Concentration at 15 ft.

ticles above the spill pan had also greatly increased. It should be noted that the turbulence around the spill pan, caused by gas convection currents, had been well established during this period.

5.4.5. Test Time T + 90 sec

Full burning conditions, covering the entire surface of the spill pan, had been established. The density of oxide particles was such that now almost all the fire area was completely obscured.

6. Discussion

The magnitudes of the sodium burning rates (see Figure 5) observed during the period from 2 to 20 min were quite similar to those obtained in previous laboratory and ventilated-enclosure experiments with air atmospheres. In addition, the apparent increase in the burning rate, to a maximum during the period from 2 to 12 min, has been observed in a Phase-I air experiment, but over a longer time period and with a more pronounced change. The high apparent burning rate during the initial 2 min of the test, obtained from the oxygen-concentration data, appears to correlate with the pressure history during this time. Examination of the observed vessel gas pressure history, shown later in Figure 11, indicates a distinctly higher rate of pressure rise during the first 2 min, compared with later times. The motion pictures taken during the early history of the test show rather vigorous burning of the sodium during most of this period.

The observations that the bulk gas temperature (gas temperature averaged with respect to volume of the entire cell) is close to that of the wall and that no radiant heat flux is detected at a height of 10 ft or less suggests neglecting the radiation exchange between the gas and the vessel wall, and between the burning surface and the vessel wall, as a first approximation. The temperature profiles also do not show any distinct region above the surface where the temperature is higher than at the surface. This indicates that burning takes place on the surface, or very close to it.

It would be of interest to employ these observations in the basic equations and to test the theoretical results against the experimental data. Accordingly, the following assumptions are introduced:

1) The burning process proceeds at the sodium oxide surface only.
2) The burning rate is controlled only by the rate of oxygen arrival to the sodium surface.
3) No thermal radiation occurs between gas and vessel wall and between sodium surface and vessel wall.
4) The oxide layer is thin and of negligible thermal resistance.

Some justification for Assumption 2 can be found from previous experience, where strong dependence of the burning rate on oxygen content in the system was observed.

With the simplifications mentioned, the previous heat-balance equations (1 through 4) in Section II are reduced to the following:

Heat Balance for the Surface

$$\beta(\bar{Q}_c - \bar{Q}_{vap}) = (Q_{sg})_{cv} + (Q_{sg})_{rad} + Q_{cd}\downarrow \quad (5)$$

Heat Balance for the Gas

$$(Q_{sg})_{cv} + (Q_{sg})_{rad} = (Q_g)_{abs} + (Q_{gw})_{cv} \quad (6)$$

Heat Balance for the Walls

$$(Q_{gw})_{cv} = (Q_w)_{abs} + (Q_w)_{wr} \quad (7)$$

The rate of oxygen arrival at the surface can be estimated from

$$J = hC_o \exp[-(hA/V)t], \quad (8)$$

where h is the mass-transfer coefficient for the transport of oxygen from the bulk gas to the surface, and C_o is the initial oxygen concentration in the bulk gas. In free convection, where there is simultaneous heat and mass transfer, h is given by the expression

$$h = C\frac{D}{L}(Gr')^{1/3}(Sc)^{1/3}, \quad (9)$$

where C is a constant which depends upon the geometry of the system, D is the diffusion coefficient of oxygen in air, L is a characteristic length, and Gr′ is the combined heat- and mass-transfer Grashod number, and Sc is the Schmidt number.

The sodium burning rate, β, is related to the oxygen arrival rate by

$$\beta = kJ, \quad (10)$$

where k is constant depending upon the sodium-oxygen reaction chosen. For the reaction that forms the oxide Na_2O, the value of k is 2.88.

The solution of Equations 5 through 7 requires knowledge of the thermal radiation interchange factor (which is related to the radiation emissivity of the gas and sodium surface, respectively).

By means of the experimental burning rate, and by assuming various values for the thermal radiation interchange factor between the surface of the sodium and the gas, Equations 5 through 7 were first expressed in terms of temperatures, and then solved simultaneously for the average containment-wall temperature, average bulk gas temperature, and sodium sur-

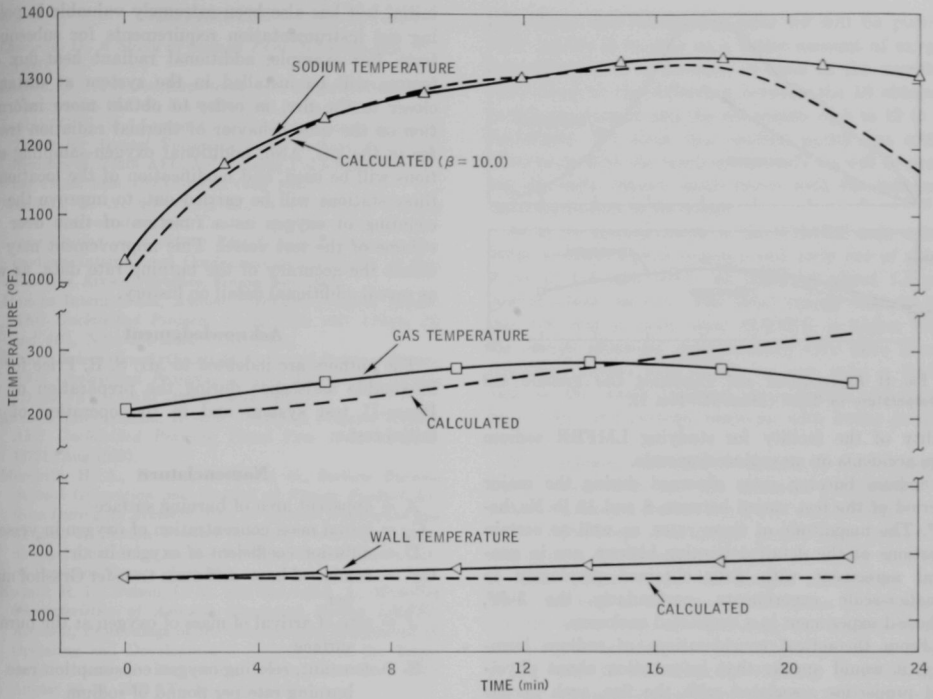

FIG. 10. Comparison of Calculated and Experimental Results for Determination of Radiation Interchange Factor (Phase II—Test 1).

face temperature. An interchange factor having the value of 1.0 was found to give the best agreement between the calculated and observed temperatures up to the maximum, as shown in Figure 10. The inability to fit the data beyond the maximum, as guided by theory, would seem to indicate that other thermal processes are involved in this time regime. For example, the radiometer data shown in Figure 9 indicate that heat transfer to the walls by radiation from the surface can no longer be neglected, due to an apparent change of the radiation characteristics of the gas.

The comparison between the experimental sodium burning rates and those calculated using Equations 5 through 10 with a thermal radiation interchange factor of 1.0 is shown in Figure 5. It can be seen from Figure 5 that the theoretical burning rate underestimates the experimental value by ~30% in the time interval between 2 and 16 min. During this time, 75% of the total available sodium had been consumed. It can be seen that the theoretical burning rate increases beyond 16 min, while the experimental rate decreases sharply. The generally good agreement between experiment and theory, in magnitude and trend, between 2 and 16 min, appears to indicate that, beyond the peak, the burning rate is controlled by a mechanism other than oxygen mass transfer to the surface. This effect has been observed previously in the Phase-I experiments, and is attributed to sodium oxide accumulation acting as a barrier between oxygen and sodium.

Figure 11 shows a comparison of the volume-averaged experimental gas temperature and the gas pressure with their theoretically predicted values (up to time of maximum pressure). It can be seen that the calculated maximum pressure rise is lower than the experimental maximum pressure rise by ~35%.

7. Conclusions

The initial test conducted in the large sodium fires modeling apparatus has demonstrated the capa-

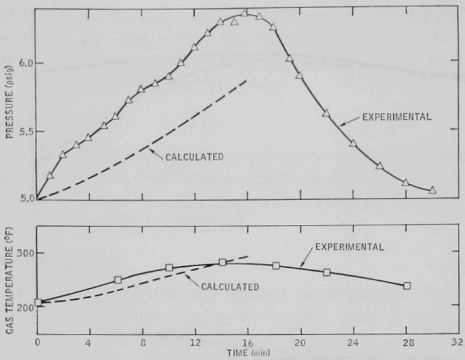

FIG. 11. Experimental and Calculated Gas Pressure and Temperature *vs* Time (Phase II—Test 1).

bility of the facility for studying LMFBR sodium fire accidents on an engineering scale.

Sodium burning rates observed during the major period of the test varied between 8 and 12 lb Na/hr-ft². The magnitude of these rates, as well as certain portions of the detailed burning history, are in general agreement with data obtained previously in smaller-scale experiments, particularly the 3-ft², Phase-I experiment in a ventilated enclosure.

From theoretical considerations of sodium burning, it would appear that information about physical properties associated with the fire, such as gas and sodium-surface emissivity and diffusivity of sodium vapor through the sodium oxide layer, are required for a rigorous solution of the problem. However, by means of a simplified model, based upon the assumption of a process controlled by oxygen mass transfer and a heterogeneous reaction, fair agreement with the overall experimental behavior is obtained, provided an empirical value is used for the effective emissivity for thermal radiation interchange between the gas and sodium surface.

Additional tests, conducted over a wide range of initial conditions which simulate postulated LMFBR sodium fire accidents, will be required to validate the simplified model presented here. These conditions include:

1) increased spill areas,
2) sodium temperature,
3) open cell-secondary volume configurations, interconnected by reduced access area, and
4) reduced oxygen atmospheres.

Modification of the theoretical equations, to account for additional details which the simplified model does not treat, will be investigated.

The evaluation of the experimental data from the initial test has also been extremely valuable in pointing out instrumentation requirements for subsequent tests. For example, additional radiant heat-flux detectors will be installed in the system at distances closer to the fire, in order to obtain more information on the time behavior of thermal radiation transfer to the gas. Also, additional oxygen-sampling stations will be used, and modification of the location of these stations will be carried out, to improve the accounting of oxygen as a function of time over the volume of the test vessel. This improvement may increase the accuracy of the burning rate data, as well as reveal additional detail on history.

Acknowledgment

The authors are indebted to Mr. S. R. Price for his invaluable assistance during the preparation of the Phase-II test system and in the operation of the initial test.

Nomenclature

A = apparent area of burning surface
C_o = initial mass concentration of oxygen in vessel
D = diffusion coefficient of oxygen in air
Gr' = combined heat- and mass-transfer Grashof number
J = rate of arrival of mass of oxygen at the burning surface
K = constant, relating oxygen consumption rate per burning rate per pound of sodium
L = characteristic length of pan
Q = heat quantity per unit time
$\bar{Q}$ = heat quantity per unit mass
Sc = Schmidt number
V = volume
β = burning rate, pounds of sodium per unit time

Subscripts

abs = heat absorbed in gas
c = heat of combustion
cd = heat flow by conduction
cv = heat flow by convection
fg = radiation exchange between flame region and the body of gas above it
fs = radiation exchange between flame and oxide surface
g = gas
gw = radiation exchange between gas and wall
ox = oxide layer
rad = heat exchange by radiation
v = vapor
vap = heat of vaporization
w = wall
wr = heat loss from wall to room

REFERENCES

1. Gracie, J. D., *A Study of Sodium Fires*, NAA-SR-4383 (Oct 1960).
2. Lauben, G. N., *Initial Experience with Large Sodium Fires Experiments (LF-1)*, NAA-SR-12041 (Aug. 1966).
3. Lauben, G. N., and Larson, C. L., *Characterization of Source Terms for Aerosol Transport during Sodium Fires*, Proceedings of Ninth AEC Air Cleaning Conference, September 13–16, 1966, CONF-66094 (Jan 1967).
4. Morewitz, H. A., Silberberg, M., *et al., Sodium Burning Aerosol Generation and Control of Fission Product Release During an Accident, Part I. Sodium Burning*, Proceedings International Conference on the Safety of Fast Reactors, Aix-en-Provence, France, Sept 1967.
5. Atomics International, *Annual Technical Progress Report, AEC Unclassified Projects, Fiscal Year 1967 (Tasks 6D and 6E)*, NAA-SR-12492 (Aug 1967).
6. Atomics International, *Quarterly Technical Progress Report, AEC Unclassified Projects, January–March 1968 (Tasks 6D and 6E)*, AI-AEC-12680 (May 1968).
7. Atomics International, *Annual Technical Progress Report, AEC Unclassified Projects, Fiscal Year 1968*, AI-AEC-12721 (Aug 1968).
8. Morewitz, H. A., Koontz, R. L., *et al., Sodium Burning Aerosol Generation and Control of Fission Product Release During an Accident, Part II. Aerosol Generation and Control of Fission Product Release*, Proceedings International Conference on the Safety of Fast Reactors, Aix-en-Provence, France, Sept 1967.
9. Koontz, R. L., Nelson, C. T., and Baurmash, L., *Modeling Characteristics of Aerosols Generated During LMFBR Accident*, Proceedings of the International Symposium on Operating and Developmental Experience in the Treatment of Airborne Radioactive Wastes, New York City, August 26–30, 1968 (To be published).

Discussion

Mr. Charak (ANL): I have two questions. First, why are the burning rates you are getting now considerably higher than those obtained in the past? Second, did you calculate the pressure in your cell with the SOFIRE code, and how do the results compare with the measured pressure?

Mr. Silberberg: Except during the first minute or so, the burning rates in the past varied between 8 and 12 lb/hr-ft^2. However, the accuracy of the burning-rate data is somewhat in question because of the limited number of probes we had in the chamber. In the second and subsequent tests we will be putting more probes in to give us a better account of oxygen concentration as a function of time in the vessel. I don't consider the difference between the 10 obtained in this experiment and the old results of 8 to 12 to be significant. We think that sodium purity has something to do with the burning rate, and we will be probing the early history much better with the increased instrumentation in the vessel.

As to the second question, the SOFIRE code calculation predicts a peak pressure and early rise of about 2 psi at 4–5 min, while we observed about 1.5 psi, lasting about 16 min. The total energy that is put into the system early from SOFIRE is higher than the energy observed experimentally. We have a new simplified model with which we can take a better look at the whole question of radiation absorption by the gas and perhaps come up with better predictions.

Mr. Coleman (APDA): I wonder if you've really looked into what are the realistic possibilities of actually getting a sodium fire inside an LMFBR?

Mr. Silberberg: The design people have looked at this quite a bit. People looking at the safety analysis of these plants make the simple assumption that while one loop is down for maintenance in the plant, and the other loops are operating, the equipment access plug in the floor is open. Therefore, there is air in the cell. If the blocking valve is inadvertently opened, sodium leaves from a large line and spills onto the floor. Actually, what we would have is not quite this situation; the simple situation is used to help us understand the problem. Let us say we have a hole of something of the order of 30 to 50 ft^2. The initial oxygen in the cell would be used up quite rapidly, and the further supply of oxygen to the sodium would now be restricted by this hole in the floor. Based on some calculations we made, it would result in even lower burning rates than this and taking place over a much longer period. These tests will be conducted shortly. The object is to predict the interchange of gas flowing to a restricted access from the secondary into the primary system.

Cover-gas Impurities and Their Interactions with Sodium*

G. B. Barton and H. P. Maffei

Battelle Memorial Institute
Pacific Northwest Laboratory
Richland, Washington

(PRESENTED BY H. P. MAFFEI)

The Fast Flux Test Facility (FFTF) includes a sodium-cooled fast test reactor (FTR) for irradiation of fast reactor fuels and materials. Because sodium is so reactive with air, special provisions must be included to provide inert gas to fill void spaces over the sodium and to blanket primary piping and components to prevent fires in the event of a sodium leak. For the conceptual design of FFTF, argon has been selected for the cover gas, although helium has been given serious consideration for some applications, such as experimental closed loops. Nitrogen has been selected to blanket equipment cells.

Since all cover gases will contain some impurities, specifications must be established for the maximum allowable impurity levels that can assure satisfactory operation of the plant and design life for the materials. Gas-analysis instrumentation is also required to indicate if the gas purity remains within established specifications. This paper will first present the results of a survey of cover-gas-analysis instruments and then will consider the initial results of studies of the reactions of impurities in cover gas with sodium.

Instruments for Analysis of Impurities

Since specifications for the allowable impurity levels in cover gas have not yet been established, it is necessary to make some assumptions on probable impurity content. First, it is desirable to keep the reactive impurity levels as low as can be measured. Second, inert impurities such as other rare gases and nitrogen need not be maintained at the low levels of the more reactive impurities. The reactive impurities are considered to be: water, oxygen, hydrogen, carbon dioxide, carbon monoxide, and organic compounds. Detection limits for these substances are of the order of 0.1 to 10 ppm, depending on the matrix gas and the measuring instrument.

The incoming cover gas (from a liquid argon supply) should be analyzed to assure that it is not contaminated with any of the above reactive impurities. This is probably the only point in the cover-gas system at which one might expect to find significant levels of oxygen and water vapor in the gas. All gas in contact with sodium should lose its oxygen and water rather rapidly.

The instruments applicable to cover-gas analyses may be considered in two classes, single-component and multicomponent. For the water and oxygen just mentioned there are several single-component instruments which we have examined. For water we have evaluated the electrolytic hygrometer and the alumina-film hygrometer. The electrolytic hygrometer uses a film of phosphorus pentoxide to absorb the water to form phosphoric acid, which is then continuously electrolyzed to decompose the water. The electrolysis current is proportional to the quantity of water introduced with the flowing gas stream. The alumina-film hygrometer is made from a strip of aluminum on which is formed a layer of alumina that is in turn overlaid by a thin film of gold. The whole forms a leaky electrical capacitor whose resistance and capacitance change with the change of a solid moisture content of the gas surrounding the sensor.

For oxygen we have evaluated the Hersch cell and electrolytic cell-type instruments. In the Hersch cell type of electrolytic instrument oxygen reacts at a silver cathode in an aqueous alkaline electrolyte to form hydroxide ions. In the cell the current produced is proportional to the oxygen content of the gas flowing through the cell. In the solid-electrolyte cell type of instrument the oxygen in the unknown gas acts as one side of a concentration cell, the other side being a gas of known oxygen concentration, usually air. The electrolyte is calcia-stabilized zirconia, which conducts oxygen ions when heated about 700°C.

For these instruments we have found that the electrolytic hygrometer gives a satisfactory measurement of the water content of the gas entering the instrument except at very low moisture levels (less than 1 ppm.). However, there may be considerable lag between changes in the moisture content of the source gas and the gas entering the sensing cell. This is due to the sorption effects in the sample transport system. One measurement we made will illustrate this. A clean 25-ft length of 0.25-in. stainless steel

* Based on work performed under U.S. Atomic Energy Commission Contract AT(45-1)-1830.

tubing was brought to equilibrium with air flowing at 200 cc/min and containing approximately 2 ppm water. The air stream was switched to a source introducing 600 ppm water. A delay of 8 min from the time of switching was observed. The instrument did not show a gradual increase of moisture with time, but a constant reading followed by a rapid increase after the initial delay period. (The volume of the tubing was about 125 cc, so that the delay considerably exceeds the volumetric delay.)

At low moisture levels the residual conductivity of the electrolytic cells varies with temperature. The individual cells vary in residual conductivity also. This means that at very low moisture levels it is necessary to have close temperature control and to correct the instrument reading for the specific cell in use.

The alumina-film hygrometer sensor is a probe that does not need to have a flowing gas sample brought to it. Rather, the sensor can be mounted in line. Our early experience indicated the sensor life might be a problem, but more recent probes have performed satisfactorily for a year or more. Because of its in-line character and its rapid response (less than 10 sec for initial response when in line), it appears the alumina-film hygrometer would be a good instrument to monitor the incoming argon for moisture. This instrument also has the virtue of a very wide range: from a −110°C frost point (less than 0.01 ppm) to a 10°C dew point (greater than 10,000 ppm).

The Hersch cell oxygen meters have been examined on several gloved boxes. For low oxygen concentrations (1–25 ppm) they have performed reasonably well. Slow approach to final equilibrium has been the major drawback. Calibration uncertainties at these low levels are also problems. These instruments appear to be unaffected by the presence of hydrogen in the gas stream.

The solid-electrolyte oxygen cell is rapid in response (within a few seconds) and covers a very wide range with the single sensor (from pure oxygen to less than 1 ppb). However, the electrolytic cell suffers from the disadvantage that it is measuring oxygen concentration in excess of any reducing agent that may be in the gas, since the cell operates at 750–800°C, at which the oxygen will rapidly combine with any fuel gas, etc., thus giving a low reading. A very common example of this problem is for the oxygen to combine with hydrogen in the gas.

For measurement of the other impurities in the cover gas, whether the incoming supply or that over sodium, a multicomponent instrument such as a gas chromatograph or a mass spectrometer is the prime candidate. We have used a gas chromatograph extensively for measuring trace impurities in helium. With a chromatograph utilizing a micro cross-section ionization detector we have been able to measure 0.2 ppm of oxygen, nitrogen, methane, and carbon monoxide in the helium and less than 1 ppm hydrogen. This type of instrument was used for the study of the rate of methane removal from helium by reaction with sodium, which will be reported later in this paper. When argon is substituted for helium the sensitivity of the detector is decreased by a factor of 10 to 20.

Methane or other organic compounds can be measured with the hydrogen-flame ionization detector on the chromatograph. Experiments preparatory to the study of the methane-sodium reaction with argon cover gas demonstrated the possibility of measuring less than 1 ppm methane in argon.

The other common gas-chromatographic detector, the katharometer or thermal-conductivity detector, must be used for nonorganic impurities in argon and was found to be less sensitive than the ionization detector. Thus, it appears the chromatograph may be limited to measuring greater than 5 ppm of the reactive impurities in argon.

The alternative multicomponent instrument is the mass spectrometer. We are in the process of evaluating a small time-of-flight instrument for measuring trace impurities in argon. The mass spectrometer is attractive for two reasons: (1) because it "looks" at all the ions that are generated from the sample, it is much more likely to "see" any unknown or unexpected impurities and to lead to identification of them; (2) because it can accept samples at high temperatures, its results may be less distorted by gettering in sodium vapor traps and sample lines than the results from the gas chromatograph and other instruments requiring samples at lower temperature.

The limits of detection of the mass spectrometer for impurities in argon appear to be of the order of 5–10 ppm. This is influenced by the background of the spectrometer and the overlapping mass patterns that arise from the cracking of the various molecules. With a low-resolution spectrometer this overlap of mass peaks is a particularly severe complication for nitrogen and carbon monoxide, since both have mass 28. If N_2 and CO are present in nearly equal quantities, their concentrations can be calculated from their cracking patterns. However, if one predominates, a supplementary measurement is needed.

One such supplementary measurement which has been investigated for the measurement of CO_2 is a nondispersive infrared analyzer. In this instrument the detector is sensitized by filling with the substance to be measured, and thus its specificity is made

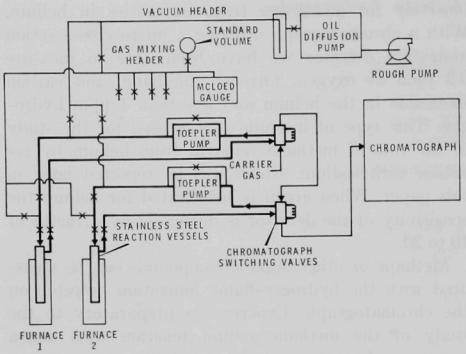

FIG. 1. Schematic of Cover-gas-interaction System.

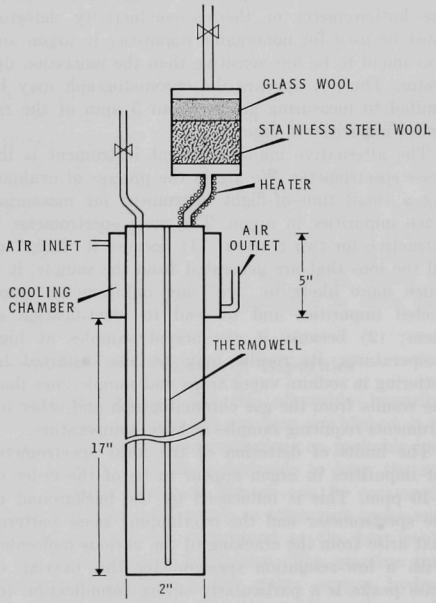

FIG. 2. Reaction Vessel.

high. We have tested an instrument with 0–100 ppm range and find it to perform reasonably well. The noise band is somewhat broad, so a lower limit of 5 ppm is about all that is measurable.

Interactions of Cover-gas Impurities with Sodium

The various parameters that have been investigated and that will be discussed include the following:

A. reaction of methane and sodium in helium cover gas;
B. reaction of methane and sodium in argon cover gas;
C. the effect of sodium volume and surface area on the reaction rates of methane with sodium;
D. initial results of the reaction of CO_2 and CO with sodium.

Experimental

The reaction of methane impurity in both helium and argon with molten sodium was measured at 800, 1000, 1200, and 1400°F. The tests were conducted in a glass, recirculating-gas system employing stainless steel capsules which contained the molten sodium. A diagram of the system is shown in Figures 1 and 2. Two liters of cover gas at a pressure of 760 mm Hg and containing nominally 100 ppm of methane were recirculated over the sodium in the stainless steel capsules and through a 10-cc sampling coil by means of a glass Toepler pump. Duplicate test loops were used for simultaneous runs. Except for the experiments to determine the effect of sodium volume and surface areas, each capsule contained 100 cc of sodium with a surface area of 14.1 cm^2. The resultant decrease in the methane concentration with time was measured by diverting the gas in the sampling coil to a gas chromatograph. A chromatograph employing a beta ionization detector was used for the helium cover gas, and a flame ionization detector was used for the argon cover gas.

Discussion

The reaction of methane in helium with molten sodium at the various test temperatures is shown in Figure 3. Evidently the reaction is temperature dependent. At 800°F the reaction proceeded very slowly and reached a value of approximately 70 ppm methane in 24 hr. At the higher test temperatures, the reaction proceeded virtually to completion in less than 24 hr at 1000 and 1200°F and in less than 4 hr at 1400°F. Figure 4 demonstrates that the methane-sodium reaction is similar in argon cover gas to that found in helium cover gas. At 800°F the reaction reached a value of 61 ppm in 24 hr, and at the higher test temperatures proceeded to completion in essentially the same time periods as for the helium cover gas.

It is believed that the reaction of methane with sodium proceeds most probably as follows:

$$2CH_4 + 10Na \rightarrow Na_2C_2 + 8NaH.$$

The reaction, being bimolecular, suggests a second-order kinetic reaction rate which may be expressed as

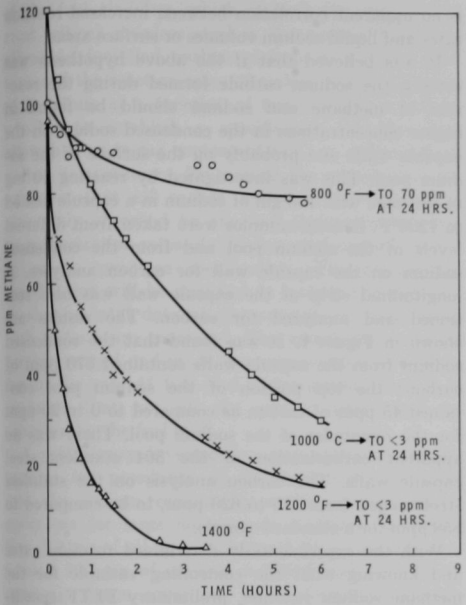

FIG. 3. Reaction of Methane and Sodium in Helium Cover Gas.

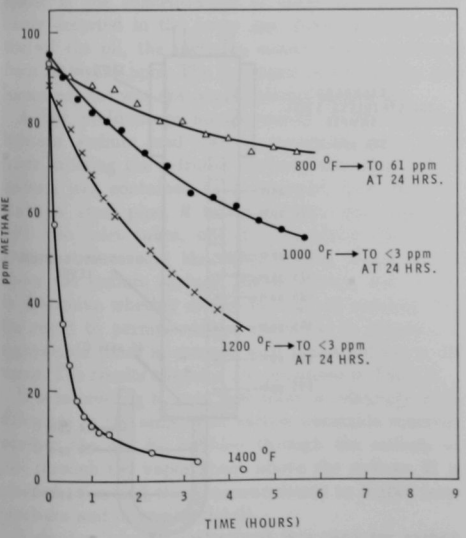

FIG. 4. Reaction of Methane and Sodium in Argon Cover Gas.

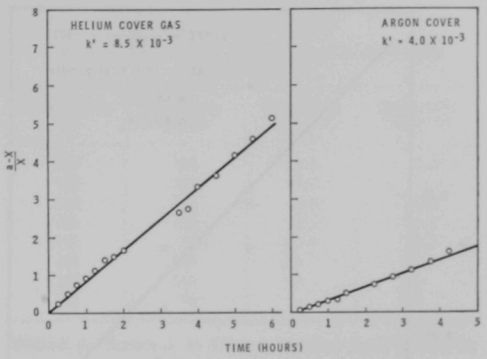

FIG. 5. Plot of $(a - x)/x$ *vs* t at 1200°F.

$$\frac{dx}{dt} = -k'x^2,$$

where x is equal to the methane concentration at time t. If this equation is integrated from zero time, when $x = a$, the original methane concentration, to any time t, the following expression is derived:

$$\frac{a - x}{x} = ak't.$$

A straight-line plot of $(a - x)/x$ vs. t would verify a second-order reaction for the process.

Figure 5 verifies that the methane-sodium reaction with both helium and argon at 1200°F is a second-order reaction. These plots are typical for the other test temperatures. The rate constants k′ derived by a least-squares fit from these plots are:

Temperature, °F	Rate Constant k′	
	Argon Cover Gas	Helium Cover Gas
800	5.38×10^{-4}	3.45×10^{-4}
1000	1.43×10^{-3}	4.02×10^{-3}
1200	4.04×10^{-3}	8.53×10^{-3}
1400	6.61×10^{-2}	5.2×10^{-2}

It can be seen that the rate constants are very similar for both the argon and the helium cover gas. These results indicate an activation energy for the methane-sodium reaction of 19.5 kcal/g-mol as determined from a plot of the variation of reaction rates with temperature, as shown in Figure 6.

The establishment of limits for the methane impurity for FFTF cover gas requires not only the determination of methane-sodium reaction rates, but also the determination of the controlling variable(s)

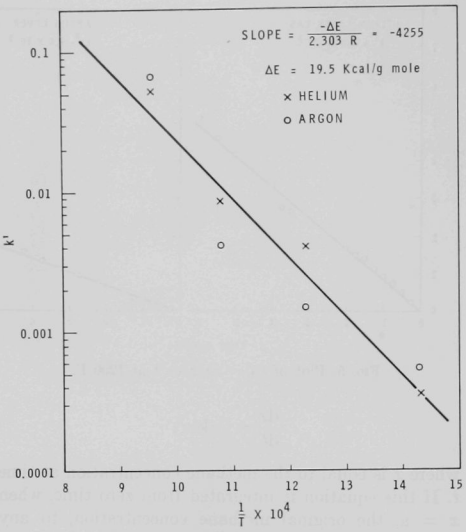

FIG. 6. Variation of Reaction Rate with Temperature.

TABLE 1. REACTION RATES OF METHANE AND SODIUM AT 1200°F

Gas Plenum Volume (Moles of Sodium Vapor)	Liquid Sodium Surface Area (cm^2)	Liquid Sodium Volume (ml)	Reaction Rate (Millimoles CH_4/hr)
4.8×10^{-4}	14.1	500	9.3×10^{-4}
6.8×10^{-4}	14.1	250	2.2×10^{-3}
7.3×10^{-4}	9.7	100	1.3×10^{-3}
7.7×10^{-4}	4.4	100	7.5×10^{-3}
7.9×10^{-4}	14.1	100	6.1×10^{-3}
3.5×10^{-3}	74.8	200	3.9×10^{-2}
3.5×10^{-3}	74.8	200	4.8×10^{-2}

for the reaction and the behavior of the carbon added to the sodium. Various investigations were performed at 1200°F to establish the reaction variables. The parameters investigated included sodium volumes, sodium surface areas, gas plenum volumes, and gas plenum surface areas. In addition, the disposition of the sodium carbide formed from the reaction of methane and sodium was also determined.

It was found that the gas plenum volume of the test capsule appears to be the controlling variable for the reaction of methane with sodium. The reaction rate is probably controlled by the amount of sodium vapor present and not the amount or geometry of liquid sodium. This is shown in Table 1. It can be seen that the reaction rates increase with an increasing volume of sodium vapor in the gas plenum. There is no apparent correlation between increased reaction rates and liquid sodium volumes or surface areas.

It was believed that if the above hypothesis was correct, the sodium carbide formed during the reaction of methane and sodium should be found in higher concentrations in the condensed sodium on the capsule walls and probably on the surface of the sodium pool. This was investigated by reacting 10 mg of methane with 100 gm of sodium in a capsule heated to 1200°F. Sodium samples were taken from different levels of the sodium pool and from the condensed sodium on the capsule wall for carbon analyses. A longitudinal strip of the capsule wall was also sectioned and analyzed for carbon. The results are shown in Figure 7. It was found that the condensed sodium from the capsule walls contained 370 ppm of carbon; the top portion of the sodium pool contained 45 ppm of carbon as compared to 0 to 20 ppm for the remainder of the sodium pool. There was no apparent carburization of the 304 stainless steel capsule walls. The carbon analysis on the stainless steel ranged from 575 to 620 ppm, to be compared to 858 ppm for a standard sample.

With the experimentally determined reaction rates and knowing what the controlling variable for the methane sodium reaction, preliminary FFTF specifications for methane in the cover gas may be established in the near future. The specification is expected to be based on the allowable carbon pickup

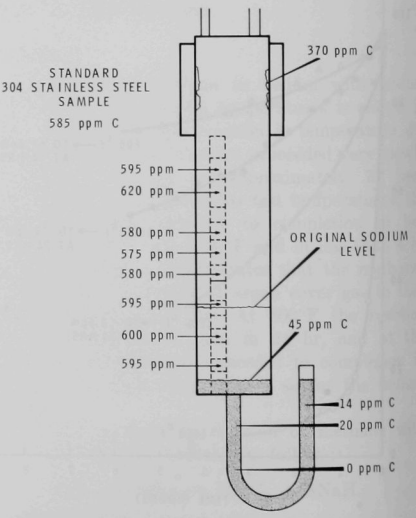

FIG. 7. Carbon Analyses for Sodium and Stainless Steel Capsule after Adding 10 mg CH_4 to Capsule.

of the fuel cladding, which is both the hottest and most critical stainless steel in the system. Given an allowable fuel-clad carbon pickup in a given lifetime and the reaction rates of carbon containing gases with sodium as a function of temperature, it will be possible to establish a specification for the total allowable cover-gas content of CH_4 as a function of sodium temperatures. By making the conservative assumption that all carbon added to the system is ultimately absorbed by the fuel clad, accurate data on carburization rates of stainless steel are not needed to set a cover-gas specification. The preliminary specification will be modified to include CO and CO_2 as experimental data on the reaction of these gases with sodium are generated. The specification can be further refined and made less conservative by factoring in the rate of fuel-clad carburization since it is probable that not all the carbon added will be absorbed by the fuel clad.

A preliminary investigation was conducted to determine the possibility of detecting small oil leaks into the sodium coolant by analyzing the sodium cover gas for large increases in methane concentration. 3.8 mg of oil were introduced into a capsule containing 100 gm of sodium at 900°F (38 ppm oil in sodium). Argon cover gas was recirculated through the capsule and analyzed by gas chromatography. Upon contact with the molten sodium, the oil was reduced to methane and hydrogen, and the large increase in the concentration of these two gases was easily detected in the cover gas. After the introduction of the oil, the methane concentration increased from 25 to 325 ppm. The hydrogen concentration also increased, but was not quantitatively measured.

A few preliminary measurements of the reaction between sodium and carbon monoxide have been made utilizing the infrared analyzer described above. Sodium was contained in a vessel of 2-in.-diameter stainless steel pipe, 8 in. long. This was equipped with two inlet tubes, one dipping below the liquid sodium surface and the other ending about ½ in. above the sodium surface. Measurements were made to determine whether or not the rate of reaction was too rapid to permit carbon monoxide to remain for appreciable times in contact with liquid sodium or its vapor. The results obtained are presented in Table 2.

It is interesting to note that there is relatively little difference in the amount of carbon monoxide removed whether the gas be bubbled through the sodium or just through the vapor space above the sodium. It is planned to extend these measurements to higher temperatures and in greater detail.

A similar infrared instrument was used for carbon dioxide measurements. Carbon dioxide is more strongly absorbing in the infrared, so the instrument is not being pushed as hard to cover the same 0–100 ppm range. It operated with a lower noise level so that 1–2 ppm could be measured. The results of a few measurements of the removal rate are presented in Table 3. Here we see that carbon dioxide is rapidly removed from the gas by sodium vapor when the temperature exceeds 150°C. It is possible that the temperature effect shown here is produced by the particular experimental configuration used.

TABLE 2. Removal of Carbon Monoxide from Argon by Reaction with Sodium

Volume of system: 300 cc. Initial concentration of carbon monoxide: 90 ppm

Temperature, °C	Flow Rate, cc/min	Removal by Liquid, %	Removal by Vapor, %
124	110	8.3	7.8
140	195	1.3	
140	144	5.5	3.3
140	115	6.7	3.1
140	75	10.5	6.7
195	130	45	39
255	116	62	56
255	75		100

TABLE 3. Removal of Carbon Dioxide from Argon by Reaction with Sodium

Initial concentration of carbon dioxide: 90 ppm

Temperature, °C	Flow Rate, cc/min	Removal by Vapor,[a] %
109	51	16
109	131	10
114	52	9.4
114	108	6.9
114	149	4.4
136	87	22
136	140	8.3
142	67	12
142	120	8.6
142	171	6.9
152	50	94
152	214	84
180	97	95
180	205	87

[a] At 109°C and 210 cc/min, liquid sodium removed CO_2 from the gas stream to a concentration below 1 ppm.

Discussion

Mr. Newman (BNL): Did you look for products in the gas phase?

Mr. Maffei: When we were passing helium through the chromatograph, we saw no increase in nitrogen, but a definite increase in hydrogen concentration. The hydrogen would increase and it would decay, paralleling and slightly delayed from the changes of

concentration. Probably methane reacts with sodium to form hydrogen and sodium hydride, and then the hydrogen diffuses through the capsule wall.

Mr. Shewmon (ANL): Hydrogen diffuses through steel pretty fast at these temperatures, so I wonder what the second decay proves. Are the stabilities of sodium hydride and sodium carbide well established at these temperatures?

Mr. Maffei: I would say so, but I am not sure.

Mr. Hobdell (BNL): Do you have any idea of the mechanism by which methane reacts with sodium?

Mr. Maffei: Very possibly methane reacts with sodium to form sodium carbide and sodium hydride.

Mr. Hobdell: It is possible that the methane just cracks?

Mr Maffei: We tried an empty capsule with no sodium present and introduced the helium cover gas with 100 ppm of methane at 1200°F. There was no decrease in the methane concentration for the same period of time; some of these tests were run for 24 hr.

Mr. Hobdell: Was hydrogen present in the cover gas?

Mr. Maffei: No.

Mr. Goldberg (ORNL): What was the oxygen contamination in your sodium?

Mr. Maffei: Probably 10 ppm of oxygen or less.

Mr. Hobdell: In answer to a previous question (by Dr. Shewmon), I think the thermal stability of sodium hydride is well established at the temperatures that we are concerned with. The sodium hydride-sodium equilibrium has been investigated.

Sodium Sampling and Analytical Experience at EBR-II

C. C. Miles, E. R. Ebersole, and W. H. Olson

Argonne National Laboratory
Idaho Falls, Idaho

(PRESENTED BY C. C. MILES)

Sampling

The problems in obtaining representative sodium samples are caused by four properties characteristic of sodium. Sodium is solid at room temperature, is chemically very active, has a high surface tension when molten, and impurities may not remain homogeneously distributed during sampling.

At EBR-II, we use common techniques for overcoming the first two properties, experiencing only minor difficulties with inert atmosphere or vacuum equipment and with plugs which form in heated lines. We discovered through repeated difficulties that sample lines should not be smaller than ⅜-in. OD for best results; however, ¼-in. lines may be used where absolutely necessary, but more than casual care must be used in applying heat to make certain there are no cold spots.

The high surface tension of sodium is a problem in filling small vessels, but this is easily avoided with flow from very small Type 304 stainless steel orifices, oxidized to prevent "wetting" by the sodium. Also, sodium should flow in a continuous stream rather than as discrete drops.

The major problem in sampling is the possible segregation of impurities in the sample so that extrusion aliquoting cannot be used.

Extrusion aliquoting of sodium samples has many advantages which make its use very valuable for sodium analyses.

First, it is possible to analyze a given sample many times to get a statistical value.

Second, within broad limits, almost any desired aliquot size may be taken.

Third, contamination of the sample in transport and handling can be easily eliminated, making interlaboratory analyses a valid possibility.

Fourth, sample weights can be obtained by measuring a length of extruded sodium slug, hence eliminating weighing-exposure in contaminating environments.

Fifth, flowing sodium readily cleans the extrusion vessel of any traces of impurities picked up in laboratory preparation of the vessel.

In all extrusion-vessel sampling at EBR-II, sodium is allowed to flow through the sampling vessel for sufficient time to clean the vessel thoroughly.

Because of these advantages we have been using extrusion-vessel sampling and aliquoting for carbon analysis for 2 yr at EBR-II. Also, we had no other way of getting uncontaminated samples, and we were not certain that carbon segregated in sodium.

Figure 1 shows an extrusion press and two extrusion vessels used with it. The vessel with the two ¼-in. stainless steel lines has a double wall through which liquid nitrogen can be forced for rapid cooling.

The history of suspected impurity segregation in sodium began during some work on carbon in sodium at the Chicago labs, where workers observed carbon concentrations near the walls of containing vessels which were higher than aliquots from the body of the sample. As a result, we looked for segregation of radionuclides that were easy to locate physically in the sample body by radiographic methods.

We found that ^{137}Cs segregates in any sample vessel of either ceramic or metal and that it collects at any interface of sodium with other substances contacting the sodium, including gas interfaces.

Figure 2 shows some radiographs of sodium surfaces in various vessels; the light areas represent local concentrations of ^{137}Cs:

(a) 10-ml pyrex beaker, lip of beaker at bottom, shrinkage hole at top;

(b) cross section through 1-in. aluminum tube, shrinkage hole at top;

(c) axial section through b;

(d) extrusion cup of Type 304 stainless steel; all light spots were voids in the sodium next to the filling adapter;

(e) Type 304 stainless steel cup with a ¼-in.-OD Type 304 stainless steel center post welded in; concentration of ^{137}Cs around post and inside cup surface.

To evaluate the extent of the ^{137}Cs segregation an extrusion partition method was used. Radioactive ^{22}Na is present in EBR-II coolant and does not segregate from the bulk sodium. With the ^{22}Na as a homogeneously distributed reference, both the ^{137}Cs and the ^{22}Na were counted to obtain a ratio of the two isotopes from aliquots provided by extrusion. Figure

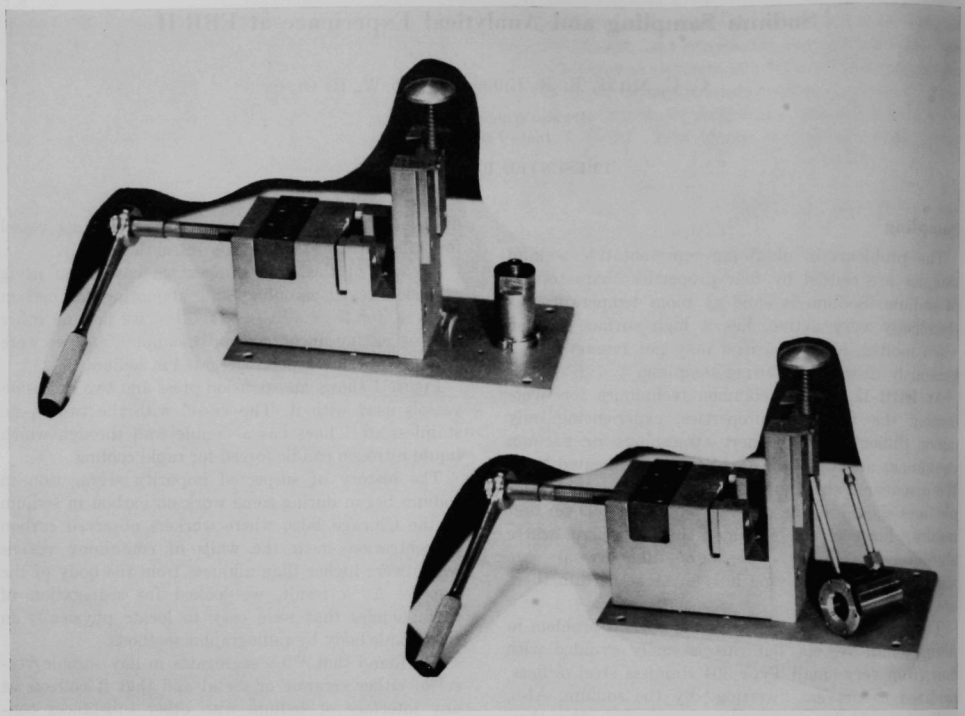

FIG. 1. Extrusion Press with Fast and Slow Cool Extrusion Vessels at EBR-II.

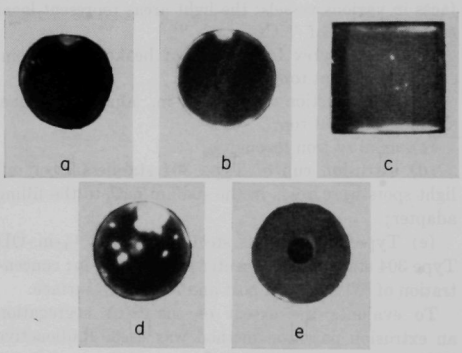

FIG. 2. Radiographs of Slow-cooled Samples of Primary EBR-II Sodium Containing ^{137}Cs.

3 shows schematically how the aliquots were provided. The vessel wall aliquot was obtained by washing with ethanol the 0.002-in. layer of sodium from the inside of the vessel. The other aliquots were counted as solid pieces. Quantitatively, the ^{137}Cs concentration in the 0.002-in.-thick wall layer left by the ram clearance ranged from 140 to 650 times what it was in the bulk of the sodium. Column two in Table 1 shows the results of the measurements on a normally chilled sample. We tried to stop segregation by various quick-chilling schemes, but none succeeded even though cooling times from hot flow to solid phase were as short as 25 sec. Columns three and four in Table 1 show the quantitative evaluation of a 98-sec and a 36-sec chill. The ratio $^{137}Cs/^{22}Na$ is different for the vessel walls in the three experiments because the amount of sodium left in digging out the bottom aliquot differed. Hence, in columns two and four the vessel-wall aliquot was somewhat diluted with interior material.

Figure 4 shows radiographs of cross sections through some quick-chilled samples with the usual ^{137}Cs segregation. In contrast to the radiographs in Figure 2, the dark areas represent the ^{137}Cs concentrations. Figure 5 shows the equipment in place for performing the quick chill. A pressurized stainless steel Dewar flask

is located to the left. The double-wall extrusion vessel is mounted in a quick-opening oven on the right. Sample flow was from bottom to top. These experiments were performed unshielded because the reactor plant had been shut down and ^{24}Na activity was not a problem at that time.

Since segregation could not be prevented, the only approach remaining was to take samples in scrupulously cleaned cup-shaped vessels of quartz, nickel, tantalum, etc., depending on allowable impurities. The sodium samples were than completely consumed in the analysis, thus avoiding the influence of inhomogeneity. In our local terminology we refer to these as total-consumption samples.

The apparently very rapid segregation of ^{137}Cs in cooling sodium led us to the belief that the segregation actually occurred in the liquid sodium whenever it was static.

An experiment proved that this was indeed the case and implies that an impurity layer may exist near every surface immersed in static liquid sodium. The experiment was performed using the same extrusion vessels as used for previous work. A piece of 20 mesh screen was fitted inside the extrusion vessel so that it was pressed tightly against the inside wall. This assembly was then placed in the sample line and

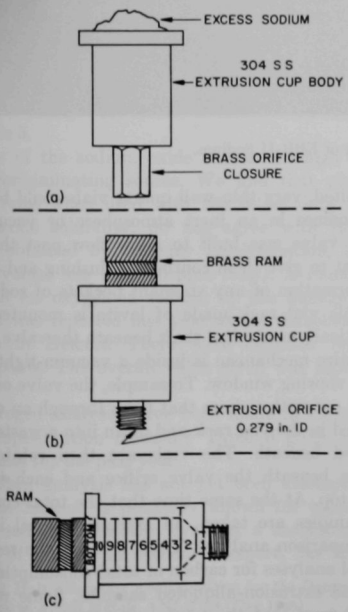

FIG. 3. Method of Estimating Distribution of ^{137}Cs in Aliquoted EBR-II Sodium.

TABLE 1. RATIOS $^{137}Cs/^{22}Na$ FOR EXTRUDER-PARTITIONED SAMPLES OF EBR-II PRIMARY SODIUM

Aliquot No.	1-hr Chill	98-sec Chill	36-sec Chill
1	0.06	0.05	0.06
2	0.08	0.07	0.05
3	0.09	0.07	0.07
4	0.09	0.07	0.07
5	0.07	0.08	0.07
6	0.07	0.08	0.07
7	0.09	0.06	0.08
8	0.06	0.06	0.05
9	0.06	0.03	0.03
10	0.03	0.02	0.03
Bottom	0.02	0.08	0.15
Vessel wall	12.9	28.9	12.7

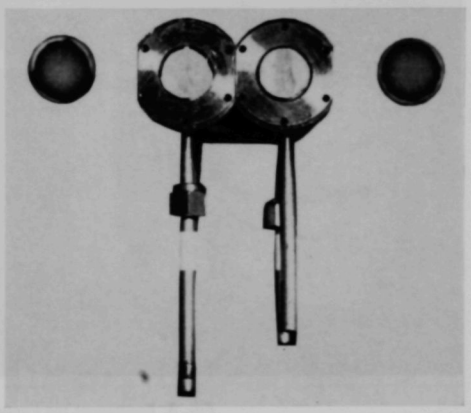

FIG. 4. Radiograph of Fast-cooled Samples of EBR-II Primary Sodium Containing ^{137}Cs.

the usual sample-stream flow established. After an hour or so the flow was stopped; after about 5 min, the molten sodium was blown with argon from the extrusion vessel. The sodium remaining on the screen and next to the walls had a ratio $^{137}Cs/^{22}Na$ almost as high as any observed in samples that were slowly cooled and aliquoted. Hence, the freezing of the sodium is not the mechanism involved in causing impurity segregation. We also found that ^{137}Cs could he redistributed in a sample by melting and mixing, indicating that the isotope was not strongly absorbed on the container wall but seemed to remain in the sodium.

The fact of ^{137}Cs segregation was a blow to extrusion-aliquoting for carbon because of the inference that if cesium segregated, all other trace impurities might also segregate. This belief was reinforced by finding that bismuth had segregated in historical sam-

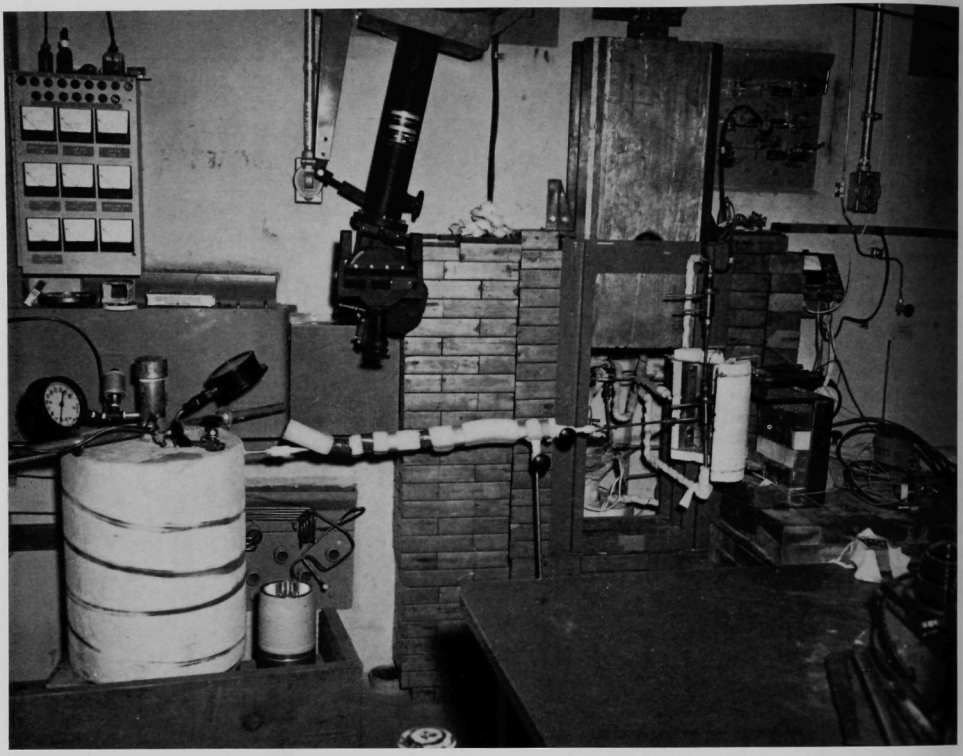

FIG. 5. Equipment for Fast-cool Sampling of EBR-II Sodium.

ples, wherein higher bismuth concentrations were found at the lower end of the sample. However, further work with tin, which does not segregate, proved that not all substances segregate during sampling.

Since one of our interests had been the possibility of carbon segregation, we checked the carbon concentrations of slow- and fast-chilled samples. Table 2 shows some such analyses. It is obvious that the cooling rate has not caused any significant changes. All the aliquots were taken by extrusion. The inferences are that suspected carbon segregation is not influenced by cooling rate and that the postulated segregation must be investigated and prevented by other means.

These experiments led us back to the total-consumption method of sampling, but with the requirement that the samples had to weigh one gram or less and that the containing vessel had to be free of impurities. The result was the development of a bypass stream sampler, shown in Figure 6, in which small, pre-ignited, very thin-wall quartz vials could be filled with sodium in an inert atmosphere or vacuum. A special valve was built to allow flow past the stem and seat to give them continuous flushing and to prevent formation of any stagnant pockets of sodium. A rotatable vial rack made of lavite is mounted on a magnetically controlled shaft beneath the valve orifice. The entire mechanism is inside a vacuum-tight vessel with a viewing window. To sample, the valve orifice is flushed out with sodium that flows through an opening provided in the vial rack and down into a waste vessel mounted beneath. The vials are then rotated into position beneath the valve orifice and each is filled to the top. At the same time that the total-consumption samples are taken, an extrusion vessel is filled for comparison analyses. Table 3 shows the results of parallel analyses for carbon of total-consumption samples and extrusion-aliquoted samples. Some recovery tests showed that the total-consumption sample gave

100% recovery of carbon spikes. Consequently, one can only conclude that, at these concentrations of carbon, significant segregation of carbon in sodium does not occur and that one may safely use extrusion vessels for sampling when carbon determinations are made.

Analysis

Both primary and secondary EBR-II sodium have been analyzed for carbon, hydrogen, oxygen, cyanide, chloride, sulfide, trace metals, and radioisotopes.

Carbon is determined by the oxyacidic flux method developed at EBR-II. This method was reported at the 10th Annual Conference on Nuclear Chemistry at Gatlinburg, Tennessee, in September 1966 and at the Anachem Conference in Detroit, Michigan, October 1967. In this method the sodium with impurities is burned in oxygen in the presence of potassium dichromate flux in a quartz bottle. Oxides of carbon pass over a platinum catalyst and copper oxide to complete the conversion to CO_2. The resulting carbon dioxide is determined chromatographically.

Carbon in EBR-II sodium has been determined by this method for the past 2 yr. Table 4 gives a summary of a few typical results obtained on aliquots from extrusion vessels.

Oxygen content of sodium has been approximated by the mercury amalgamation method.* This method is essentially a determination of sodium compounds insoluble in mercury and from which the oxygen content must be inferred by presuming the insolubles are all Na_2O. Some of the results of this method are shown in Table 5.

Some of the sodium oxide values are high due to some contaminating source. We find that plugging-meter runs, when used with the latest data for sodium oxide solubility, do not agree with the high values obtained by mercury amalgamation, but indicate values less than 10 ppm Na_2O. A round-robin analysis for oxygen in sodium by the amalgamation method was reported last year at the Anachem Conference in Detroit. There were eighteen reporting participants. The overall value given was 10.8 ± 4.9 at 1σ.

Hydrogen analyses have been made in Chicago by an isotope-dilution method.† Table 6 gives some of the results for the past year.

Nitrogen analysis has not yet been attempted. No adequate method is presently known for total nitrogen in sodium. However, cyanide, a carbon-nitrogen species of interest in carbon transport, has been determined at EBR-II in both primary and secondary sodium by use of a cyanide ion-specific Orion electrode.

TABLE 2. Carbon Analyses of EBR-II Primary-sodium Sampled at Various Cooling Rates

Sample Date	Aliquot	Carbon, ppm	Remarks
8/24/67	1	7.3	Sample slowly cooled for 1 hour
8/24/67	2	7.0	
8/24/67	3	8.9	
8/24/67	4	8.1	
8/24/67	5	7.4	
8/24/67	6	4.7	
8/24/67	7	5.5	
8/24/67	8	7.5	
8/24/67	9	4.0	
8/24/67	10	6.9	
8/24/67	11	10.4	
8/24/67	12	7.4	
		Avg.—7.0 ± 1.7 at 1σ	
9/20/67	1	6.0	Sample quickly chilled (35 sec)
9/20/67	2	5.1	
9/20/67	3	5.1	
9/20/67	4	6.7	
9/20/67	5	5.1	
		Avg.—5.6 ± 0.7 at 1σ	
9/21/67	1	5.6	Sample slowly cooled for 1 hour
9/21/67	2	4.6	
9/21/67	3	4.2	
9/21/67	4	5.9	
		Avg.—5.0 ± 0.8 at 1σ	
9/21/67	1	5.3	Sample quickly chilled (25 sec)
9/21/67	2	3.6	
9/21/67	3	5.6	
9/21/67	4	5.1	
9/21/67	5	4.2	
		Avg.—4.8 ± 0.8 at 1σ	

To adjust ionic strength to optimum values for the electrode without regard to sample size, we dissolved total-consumption sodium samples directly in water and distilled the cyanide out of an acidified solution into 1 *M* NaOH. The CN^- measurement was made simultaneously on the circulating absorbent base, with the final highest voltage taken as the value equivalent to the cyanide ion concentration.

Sulfide ion was analyzed in an exactly similar manner using a sulfide ion-specific electrode.

An attempt to analyze for chloride by this method gave inaccurate results due both to drift in the electrode system caused by the KCl bridge and to nontransference of Cl^- as HCl. Both faults in the chloride analyses have been corrected, but we have not pressed this work in the face of higher priorities. Our work to date has indicated that the chloride concentration is less than 5 ppm. The analyses for

* B. D. Holt, *Glovebox Amalgamation for the Determination of Oxygen in Alkali Metals*, ANL-7123 (Dec 1965).

† B. D. Holt, Anal. Chem. **31**, 51–4 (Jan 1959).

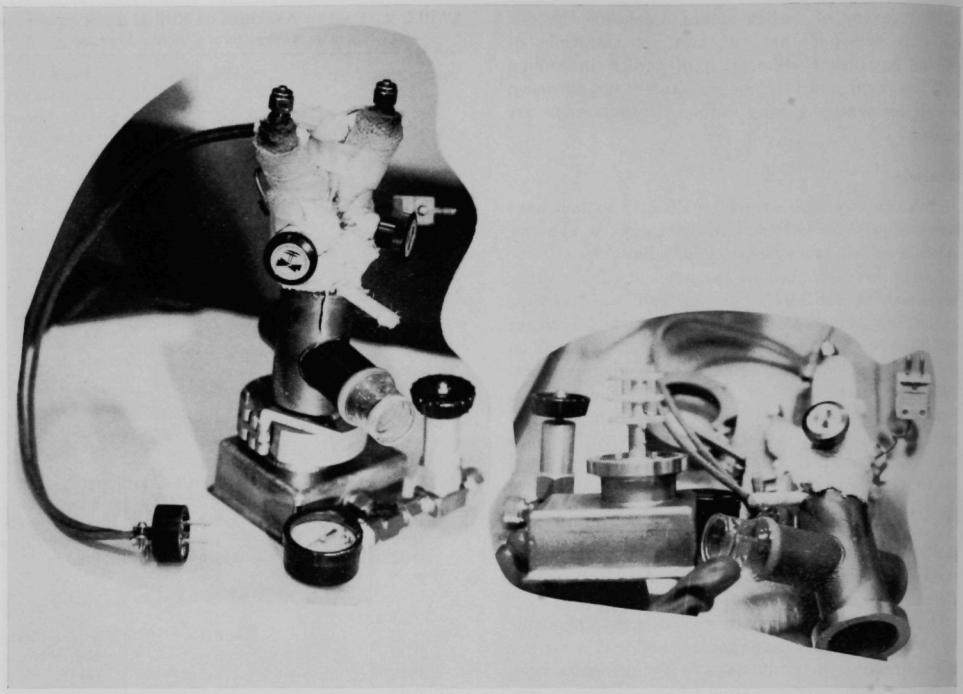

FIG. 6. Total-consumption Quartz-vial Sampler for EBR-II Sodium.

TABLE 3. CARBON CONCENTRATIONS OF EBR-II SODIUM BY TWO SAMPLING METHODS

Experiment No.	Extrusion Aliquots, ppm Carbon	Total Consumption, ppm Carbon
	2 runs per Value	4 runs per Value
1	2.2 ± 0.1	4.2 ± 2.0
2	2.1 ± 0.3	2.2 ± 0.5
3	—	3.5 ± 1.6
4	1.9 ± 0.3	0.9 ± 0.5
Mean Value	2.1 ± 0.2	2.7 ± 1.3

Standard addition tests with total-consumption samples gave 100% recovery.

TABLE 4. SUMMARY OF SOME CARBON VALUES IN EBR-II SODIUM BY OXYACIDIC FLUX METHOD

Primary Sodium			Secondary Sodium		
Sample Date	No. of Aliquots	Carbon, ppm	Sample Date	No. of Aliquots	Carbon, ppm
8–24–67	12	7.0 ± 1.7	11–8–67	4	4.8 ± 0.5
9–20–67	5	5.6 ± 0.7	11–16–67	4	3.5 ± 0.6
9–21–67	9	4.9 ± 0.8	12–4–67	7	4.8 ± 3.5
4–30–68	4	3.7 ± 0.6	2–12–67	8	4.0 ± 0.7
6–26–68	10	4.8 ± 1.8	2–1–68	5	3.4 ± 0.6
			6–4–68	7	4.4 ± 0.5
			7–22–68	3	3.3 ± 0.6

cyanide showed less than 0.2 ppm and for sulfide less than 0.1 ppb in both primary and secondary sodium.

Considerable effort has been devoted to analysis for trace metals. Qualitative emission-spectrographic analyses were made which showed that the metal concentrations were very low, with most below the detection limit of the method. Then wet chemical colorimetric procedures were used for quantitative analysis of trace metals. Since these methods were tedious, we converted to atomic absorption spectrometry. To avoid the effects of possible impurity segregation, unaliquoted 12-g samples were taken in quartz beakers and completely dissolved in a water-alcohol mixture. This solution was then acidified with nitric and/or hydrochloric acids, and the trace metals con-

TABLE 5. Oxygen Content of EBR-II Sodium by Amalgamation Method

Primary Sodium		Secondary Sodium	
Sample Interval	O, ppm	Sample Interval	O, ppm
10-26-66 to 12-7-66	7.8 ± 1.3 (six values)	11-17-66 to 12-28-66	6.2 ± 0.04 (four values)
1-26-67 to 6-21-67	8.4 ± 3.1 (eleven values)	1-25-67 to 7-18-67	8.0 ± 3.9 (eight values)
7-26-67 to 12-15-67	11.0 ± 5.2 (seven values)	4-8-68 to 8-23-68	12.0 ± 4.6 (seven values)
3-5-68 to 6-3-68	15.0 ± 5.8 (nine values)		

TABLE 6. Hydrogen Content of EBR-II Sodium by Isotope-dilution Method

Primary Sodium		Secondary Sodium	
Sample Interval	H, ppm	Sample Interval	H, ppm
10-26-66 to 12-7-66	3.0 ± 1.0 (six values)	11-17-66 to 1-25-67	4.06 ± 1.35 (six values)
1-26-67 to 5-29-67	5.0 ± 2.5 (ten values)	4-5-67 to 7-18-67	5.93 ± 1.74 (six values)
6-21-67 to 12-15-67	5.3 ± 2.9 (five values)	5-15-68 to 8-23-68	3.22 ± 1.26 (eight values)
3-5-68 to 6-3-68	1.76 ± 0.56 (eight values)		

centrated by coprecipitation with yttrium hydroxide or extracted by means of organic chelating agents. Extraction gives a better separation from sodium, which may interfere in the absorption spectrophotometry. After evaporation of the solvent and acidification, the metals were determined by atomic absorption. Table 7 gives a list of the elements determined for EBR-II sodium by atomic absorption. The source of the tin and bismuth in the primary sodium is the seal-trough alloy used to seal off the reactor cover gas from the atmosphere where the fuel-handling mechanisms penetrates the reactor vessel. Bismuth is low because it is efficiently trapped out by the cold trap. The source of the lead is unknown at this time.

All the less-than values indicate the limit of sensitivity of the method for that element in the size of sample taken to date. The main sources of errors in these analyses have been reagent contamination, sodium interference in the flame, sample contamination, and contamination of the flame by the burner construction materials. The latter have seriously interfered with iron analyses.

A vacuum distillation method for determination of impurity concentration is being tried for use with spark-source mass-spectrometric analysis. In this method a 12–15-g sample of sodium is taken in a tantalum crucible. The sodium is vacuum distilled from the crucible by induction heating, and the residue is taken up by aqua regia for analysis. Several experiments have been made to determine which elements may be lost in the distillation process. All the analytical work for these investigations was performed by atomic absorption. Table 8 shows the ele-

TABLE 7. Trace Metals in EBR-II Sodium by Atomic Absorption

Primary Sodium		Secondary Sodium	
Metal	Concentration, ppm	Metal	Concentration, ppm
Al	<0.5	Al	—
Bi	1.4	Bi	<0.2
Cd	<0.05	Cd	<0.05
Co	<0.1	Co	<0.1
Cr	<0.2	Cr	0.05
Cu	<0.4	Cu	<0.1
Fe	<0.1	Fe	<1
Mg	0.14	Mg	0.4
Mn	<0.04	Mn	<0.04
Ni	<0.1	Ni	0.1
Pb	11.1	Pb	1.0.
Sn	19.5	Sn	<4.0
Ag	<0.4	Ag	—

TABLE 8. Recovery of Metals in Residue from Sodium Distillation

Metal	Experiment I		Experiment II		Experiment III	
	Micrograms Added*	Percent Recovered	Micrograms Added*	Percent Recovered	Micrograms Added*	Percent Recovered
Al	60	100	60	100		
Bi	108	95	108	94		
Cr	20	100	20	99		
Co	40	97	40	99		
Cu	40	101	40	99		
Pb	20	*84*	120	*88*	120	*100*
Mg	20	96	20	99		
Mn	8	100	8	100		
Mo	58	101	58	100		
Ni	40	103	40	97		
Cd	10	*74*	10	*4*	10	*0*
Ca	11	*33*	54	*57*	54	*106*
Sn	209	*86*	104	*24*	209	*100*
Zn	10	*52*	10	*50*	10	*1.5*

* All elements added as chlorides.

ments investigated and their recoveries after distillation.

In two experiments, cadmium, calcium, lead, tin, and zinc were apparently lost to some extent in distillation when spiked into the sodium with the other nine elements listed. However, when these high-loss elements were used together in a third experiment, only cadmium and zinc were lost. Further investigation showed that the losses were spurious for the calcium, tin, and lead. Silica interference caused the atomic absorption method to give low results.

TABLE 9. Spark-source Mass-spectrometric Analysis of Vacuum Distillation Residue from EBR-II Secondary Sodium

Element	Spark-source Data, ppm in 10-g sodium sample	Results by Atomic Absorption, ppm
Ag	0.1	—
Al	0.006	—
B	0.02	—
Bi	0.04	<0.2
Ca	3	—
Cd	0.09	<0.05
Co	0.005	<0.1
Cr	0.9	0.05
Cu	0.03	<0.1
Fe	3	<1
K	0.04	—
Mg	0.3	0.4
Mn	0.05	<0.04
Ni	0.3	0.1
Pb	0.4	1.0
Si	1	—
Sn	0.04	<4.0
V	0.02	—
Zn	0.04	—

TABLE 10. Radioisotopes Found in EBR-II Primary Sodium

Isotope	Concentration, μCi/g	Source	Remarks
^{3}H	18×10^{-10}	Ternary fission product, $^{6}Li(n, \alpha)^{3}H$	Found in sodium samples
^{22}Na	1.8×10^{-2}	$^{23}Na(n, 2n)^{22}Na$	
^{137}Cs	1.6×10^{-2}	Fission product	
^{131}I	$\sim 5 \times 10^{-4}$	Fission product	
^{133}I	$\sim 1 \times 10^{-3}$	Fission product	
^{132}Te-^{131}I	Trace	Fission product	
^{113}Sn-^{113}In	Trace	$^{112}Sn(n, \gamma)^{113}Sn$	
^{117}Sn	Trace	$^{116}Sn(n, \gamma)^{117}Sn$	
^{54}Mn	Trace	$^{54}Fe(n, p)^{54}Mn$	Found in plugging valve
^{65}Zn	Trace	?	
^{51}Cr	Trace	$^{50}Cr(n, \gamma)^{51}Cr$	
^{60}Cr	Trace	$^{59}Co(n, \gamma)^{60}Co$	
^{58}Co	Trace	$^{58}Ni(n, p)^{58}Co$	
^{182}Ta	Trace	$^{181}Ta(n, \gamma)^{182}Ta$	
^{140}Ba-^{140}La	Trace	Fission product	

An exploratory run has been made with secondary sodium for trace metals using vacuum distillation followed by spark-source mass spectrometry. The results of the run are shown in Table 9.

Radioisotopes are generated in EBR-II primary sodium by the usual process of corrosion-product activation and fission-product release. These isotopes are determined in total-consumption samples to avoid possible segregation errors. Except for tritium, which requires liquid scintillation methods, gamma-ray analysis with a 512-channel analyzer with a 3-in. sodium iodide crystal and chemical separation techniques are used to make the analyses. Table 10 gives a list of isotopes found.

^{65}Zn and ^{140}Ba-^{140}La were found only in the primary-sodium plugging valve. These isotopes had not been observed in the bulk sodium but were concentrated in a copper deposit which had plugged the valve last September. They were found during the investigation of the plugging-valve failure.

The presence of these isotopes on the finely divided copper deposit in the plugging valve leads one to believe that the primary-sodium-purification cold trap also contains them as well as others which were found in the bulk sodium.

Future examination of the primary cold trap may reveal the presence of isotopes heretofore unsuspected.

Discussion

Mr. Dutina (GE): In Table 9 you compared results by atomic absorption and spark-source mass spectrometry. Iron, chromium, and nickel were 3, 0.9, and 0.3, respectively, by spark-source as compared to <1, 0.05, and 0.1 by atomic absorption. Your values by atomic absorption are lower than the ones we are accustomed to seeing in our systems.

Mr. Miles: We are afraid to say that our accuracy is so good that we can definitely call those real numbers; we just say that the difference isn't terribly great. I hate to make any real hard statements about this comparison.

Mr. Berkey (W): We have been doing spark-source mass spectrometry with sodium directly, not by going through the residue. One thing I can point out is that your spark-source results are plus or minus a factor of 3 for the particular type of analysis. You shouldn't be troubled by the lack of better comparison. The iron, chromium, and nickel values obtained by spark source are comparable to those that we have been seeing, going the direct route, and so it seems reasonable to us.

I also want to confirm Miles' observation with regard to cesium. We use an extrusion and dip technique to sample sodium, starting at approximately 100°C, in which case we only have a few degrees to cool before we get a solid sample. We still see cesium segregate to the walls over this time period. This type of surface effect is very reproducible, even though we use much lower temperature differentials and shorter times as compared to Miles' work. Furthermore, cesium is the only element that we have observed to show this surface effect. We have studied a number of other elements, and no visible segregation to the walls or anything of this nature has come out of the work.

Mr. Newman (BNL): I am still disturbed. You put up a number for iron of 0.1 ppm which, I think, is as low a cold iron analysis as I've ever seen. Do you or don't you believe this number?

Mr. Miles: As I said, we had a lot of trouble with iron analysis. I will not stand behind any number we can now report for iron. We expect to have more reliable numbers by the atomic-absorption method.

Mr. Goldberg (ORNL): On the migration of cesium to the walls, do you have any feel for whether you are dealing with dissolved cesium as against particulate matter?

Mr. Miles: I believe we are dealing with cesium in solution. The concentration is estimated to be 0.004 ppm.

Mr. Biery (Chairman): I would like to comment on the cesium segregation. We have run some capsule experiments in which we've kept the capsule isothermal, with cesium distributed throughout the capsule, and there seemed to be some, but very little, segregation of cesium to the walls. With a temperature gradient on the same capsule there would be heavy redistribution of the cesium to the gas-liquid interface and the capsule-to-sodium interface (probably liquid sodium) at the top of the capsule. Furthermore, radial scans of the capsule indicated a very definite redistribution of cesium to these stainless steel surfaces. It's not a simple problem and obviously involves such things as dropping surface tension or interfacial tension values by absorption of impurities at these surfaces.

Mr. Dutina: Newman said the lowest iron he had ever seen was the number you had up there; I believe that the carbon results are the lowest I've ever seen. Awhile back, people at Argonne were working to obtain high-purity sodium very free of carbon, and it seems to me the lowest value I've seen reported from that work was about 4 ppm. It looks to me like you've got a way of doing it.

Mr. Miles: I think I have.

Mr. Berkey: I was wondering two things about the carbon problem. First, have you confirmed your results using an independent carbon technique besides the one that you have developed? Second, you indicated that where you lacked precision this was due to a glovebox difficulty.

Mr. Miles: Almost every time our uncertainty has gone up, we've discovered something wrong with the glovebox atmosphere. We can't ship samples, so a comparison can't be interlaboratory yet; an independent check would involve setting up another method. We looked at all of them pretty closely, and we felt they needed improving; this is why we developed another method. I don't know what other method I would use—perhaps a technique using an accelerator.

Mr. Biery: Did you start with a bare orifice in the plugging-meter runs?

Mr. Miles: Yes.

Mr. Biery: The work done at Los Alamos indicates that if you start with a clean orifice, you will find a 10 to maybe 40°C temperature depression below the solubility curve before you will nucleate the material on the orifice. If you compare plugging-temperature data with the solubility curve you will get oxygen concentration considerably below, say, values obtained by vacuum distillation or amalgamation. That may explain why your plugging data indicated lower concentrations than your amalgamation data.

Impurities in EBR-II Sodium and Cover-gas

W. H. Olson, C. C. Miles, and D. W. Cissel

Argonne National Laboratory
Idaho Falls, Idaho

(PRESENTED BY W. H. OLSON)

Operating History of Primary-sodium Cold Trap

The original primary-sodium cold trap was removed from service in EBR-II in June 1968. It had been in the system for 5¼ yr, during which time it was in service approximately 630 days and processed about 23 million gallons of sodium. Figure 1 illustrates the cold-trap operating history. Cumulative days of operation and gallons of sodium processed are plotted against calendar time.

During the first year of operation, the cold trap was in service only 164 days (45% of the time), but processed nearly 12 million gallons of sodium. During the next 3 yr, operation was limited to 77 days (7% of the time) and processed only 5 million gallons of sodium. During the remaining 1¼ yr, the cold trap was operated 396 days (87% of the time) and processed about 7 million gallons of sodium.

The philosophy during the three years prior to March 1967 was to put the cold trap in operation when the plugging temperature approached 300°F, and operate it only until the plugging temperature was reduced to undetectable levels (<225°F). Following the discovery of copper in the primary sodium in March 1967 the philosophy was changed, and the cold trap was operated continuously except for short periods when it was secured for maintenance purposes.

Copper in Sodium

In late February and early March 1967, copper plating was discovered on interior surfaces of economizer, tubing, and valves of a primary-sodium plugging indicator. The plugging indicator had been removed from service to investigate the cause of a flow restriction. Copper plating was discovered in the process of removing sodium from loop components.

An extensive program of sodium sampling and analysis was initiated to determine the level and source of copper impurity in the bulk sodium. Historical (museum) samples of primary sodium, which had been taken and stored since the original charging of the system, were also analyzed to learn the history of copper in the sodium. Figure 2A illustrates the history of copper concentration in EBR-II primary sodium. It appears that the concentration never exceeded 1.5 ppm and most likely was not much greater than 1 ppm.

A large number of sodium samples were analyzed during March and April 1967 from both the influent and effluent streams of the cold trap. There was considerable scatter in the results of these analyses, but a least-squares fit to all the analytical data indicated a generally lower concentration in the effluent stream than in the influent stream, and a decreasing trend in the influent stream (see Fig. 2B). This is interpreted as verifying that copper is removed from sodium in the cold trap.

The results of analyses of monthly samples since June 1967 indicates that the copper concentration slowly dropped from ~0.5 to 0.2–0.3 ppm and appeared to reach equilibrium at that level.

The principle source of copper in the primary sodium was the auxiliary-pump bus bars. These bus bars were removed, inspected, and clad with stainless steel following the discovery of copper in the plugging-indicator loop. It was calculated from dimensions of the bus bars that approximately 10 lb copper had been lost.

In September 1968, a little more than two months after the purification system had been secured for the purpose of replacing the cold trap, another plugging valve located in the FERD (Fuel Element Rupture Detection) loop plugging indicator was removed, inspected, and found to be plugged with copper. The plugging indicator in the FERD loop was being used to monitor the primary-sodium plugging temperature during outage of the purification system. It was put in service in June 1968, when the cold trap and primary-purification-loop plugging indicator were secured. During the latter part of August and early in September, a progressive decrease in flow was observed under "hot conditions" (between plugging runs). The flow rate decreased to the extent that plugging runs could not be made. The FERD-loop plugging valve was then removed for inspection, and the copper deposit was discovered. Figure 3 shows the almost completely blocked flow passage in the valve body. Figure 4 shows the blockage of the flow passages on the valve plug.

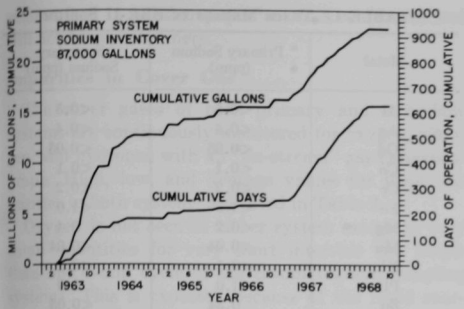

FIG. 1. Operating History of Primary Cold Trap.

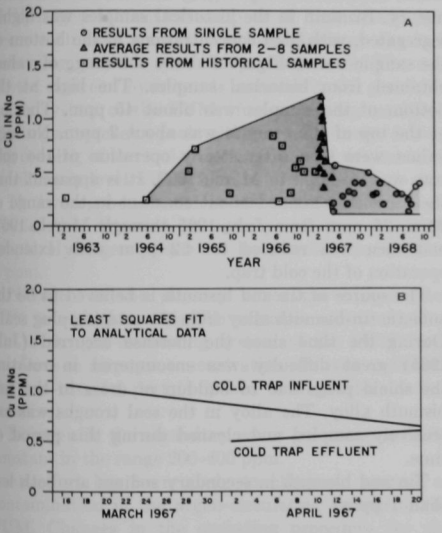

FIG. 2. A. Copper in Primary Sodium. B. Copper in Primary Sodium.

The plugging valve from the purification-system plugging loop, removed from service at the same time as the cold trap, was inspected and found to be free of deposits.

The plugging valve in the FERD loop operated at 450–550°F between plugging runs. The purification-system plugging valve operated at 650–680°F. The data for solubility of copper in sodium presented by Atomics International (Document AI-AEC-12671, May 31, 1968) show a solubility of 0.2 to 0.4 ppm at 500°F. The results of analyses for copper in primary sodium samples taken during the cold-trap outage are in the same range. Therefore, it is plausible that copper could precipitate in the FERD-system plugging valve but not in the purification-system valve which ran at higher temperatures.

Copper in the secondary sodium is less than 0.1 ppm.

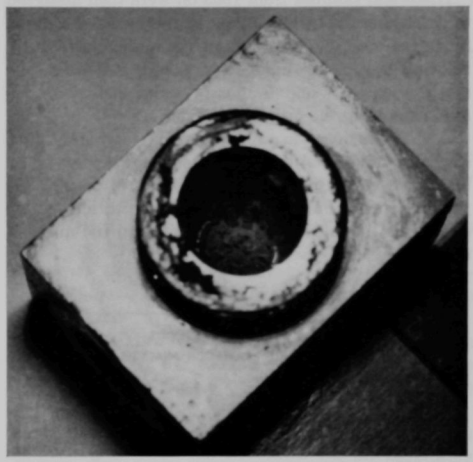

FIG. 3. Copper Deposit in Valve Body.

FIG. 4. Copper Deposit on Valve Plug.

Tin and Bismuth in Sodium

In August 1967, it was noticed that there were traces of ^{113}Sn and ^{113m}In in the primary sodium. In the belief that this came from activation of tin in the coolant, a number of sodium samples taken in September 1967 were analyzed for tin. Results showed that tin concentration in the sodium was 15 to 20 ppm.

Historical samples from 1963 on were then analyzed to determine the history of tin in the primary sodium. Since the most likely source of tin is the tin-bismuth rotating plug seals, analysis was also made for bismuth. Figures 5 and 6 illustrate the history of tin and bismuth in the primary sodium.

A sharp increase in tin occurred in early July 1965 and may have been increasing very slowly ever since. The increasing trend since July 1965 (~6 ppm in 3½ yr) may not reflect increasing concentration in the sodium as much as it does refinement in the analytical method.

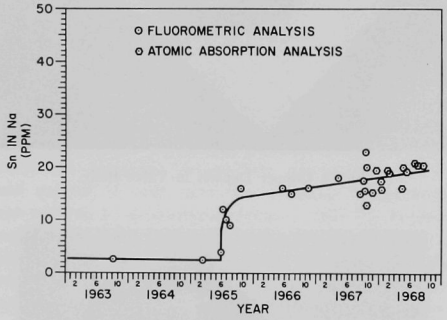

FIG. 5. Tin in Primary Sodium.

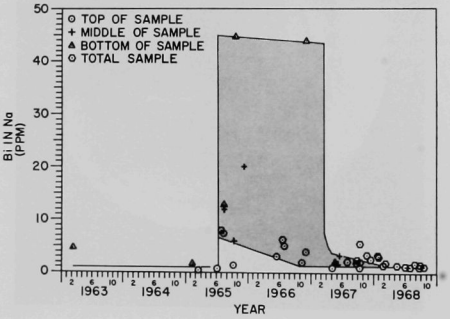

FIG. 6. Bismuth in Primary Sodium.

TABLE 1. TRACE METALS IN EBR-II SODIUM

Metal	Primary Sodium (ppm)	Secondary Sodium (ppm)
Al	<0.5	<0.5
Ag	<0.4	<0.4
Cd	<0.05	<0.05
Co	<0.1	<0.1
Cr	<0.2	<0.2
Fe	<1.0	<1.0
Mg	<0.2	0.4
Mn	<0.04	<0.04
Ni	<0.1	<0.1
Pb	11.0	1.0
Zn	0.34	<0.05

The bismuth history is not as well-defined as tin history. Bismuth in the historical samples was highly segregated, with high concentrations in the bottom of the sample vessel. Figure 6 shows the range of values obtained from historical samples. The high at the bottom of the samples was about 45 ppm. The low at the top of the samples was about 2 ppm. No high values were seen after steady operation of the cold trap was initiated in March 1967. It is apparent that the bismuth remained about constant in the range of 20 to 25 ppm from July 1965 through March 1967, and then was reduced to <2 ppm with extended operation of the cold trap.

The source of tin and bismuth is believed to be the eutectic tin-bismuth alloy from the rotating plug seals. During the time since the increase occurred (July 1965) great difficulty was encountered in rotating the shield plugs due to buildup of dross in the tin-bismuth alloy. The alloy in the seal troughs was extensively sampled and cleaned during this period of time.

Tin and bismuth in secondary sodium are both less than 1 ppm.

Other Metals in Sodium

Table 1 lists metals (other than copper, tin, and bismuth) which have been determined in primary and secondary sodium. Lead is the only one whose concentration differs significantly between the two sodium systems. Analyses of historical samples have shown that lead concentration in the primary sodium has been about 11 ppm since the original filling of sodium. The source of lead is unknown, but was most probably contamination in the primary system.

Other Impurities in Sodium

Routine analysis is made for oxygen, hydrogen, carbon, and various radioisotopes. Results have been

summarized in another paper* at this conference and will not be repeated here.

Impurities in Cover Gas

The cover gases of both primary and secondary systems are continuously monitored for oxygen, nitrogen, and hydrogen with an "on-stream" gas chromatograph. High, low, and average values for these impurities in both systems are listed in Table 2.

Oxygen is not seen in either system except in very small quantities for very short intervals (no longer than one 4-min cycle of the chromatograph sampling system). This is expected because of the rapid reaction of oxygen with molten sodium.

Hydrogen is seen in the primary cover gas continuously at levels ranging from 5 to 20 ppm. Peaks in hydrogen concentration up to as high as 400 ppm occur each time a transfer is made between the fuel-unloading machine and the primary tank. The suspected source of hydrogen is moisture in the gas-circulating system of the FUM (fuel-unloading machine). Hydrogen reaches a peak within a few minutes following opening of the fuel-transfer port, and returns to an equilibrium level within 2 hr.

No hydrogen is found in the secondary cover gas within the detection sensitivity of the chromatograph. Hydrogen would not be detected much below 4 ppm.

Nitrogen in the primary cover gas ranges from 0.1% to as high as 2%. The principle source of nitrogen is the gas-circulating system of the FUM. Step increases in nitrogen concentration are seen each time the fuel-transfer port is opened to the fuel-unloading machine.

Nitrogen in the secondary cover gas remains fairly constant in the range 200–400 ppm.

An effort has been made to eliminate sources of contamination in the argon-circulating system of the FUM. Changes in the operating procedure for the FUM have resulted in a reduction of the amount of hydrogen (moisture) and nitrogen (air) introduced to the primary cover gas during each transfer operation. However, the exact sources of air and moisture in the argon-circulating system of the FUM have not been identified at this time.

The FUM appears to be the principal source, but not the only source, of contamination of the primary cover gas. Air leakage through primary-tank nozzles is considered to be a potential source of nitrogen and hydrogen in the cover gas. A continuing effort is being made to identify all sources of air leakage into the primary tank, and to eliminate these, as feasible.

TABLE 2. Impurities in Cover Gas (*ppm*)

Impurity	Primary			Secondary		
	High	Low	Avg	High	Low	Avg
H_2	400	4	12	0	0	0
O_2	0	0	0	0	0	0
N_2	20,000	1,300	6,000	400	200	300

Discussion

Mr. Hill (APDA): Do you think it is possible to measure the hydrogen in the cover gas accurately with your system in the presence of sodium?

Mr. Olson: I would say so. I don't know what you might consider accurate. We certainly get good response on the instrument during fuel-transfer operations, when we believe we are introducing moisture to the cover gas.

Mr. Hill: How do you prevent hydrogen in the sample line and the sodium vapor from reacting to form hydride in the cold zones, thereby taking the hydrogen out of your samples?

Mr. Olson: The sample, of course, goes through air and vapor traps, and I presume you are suggesting that in these traps the presence of sodium and sodium vapor would remove the hydrogen. I don't know; maybe this happens to some extent. As I say, we run with a continual background in the primary of somewhere from 20 to 40 ppm. Maybe we are actually running a little higher because of something like this.

Mr. Hill: This is a caution that I wanted to make which apparently has not been recognized. Theoretically, you cannot determine hydrogen accurately, and it is not in equilibrium because you will always have a mass transfer of sodium. You can never determine exactly how much hydrogen-sodium interaction you will have until you've determined in some way the amount of hydrogen removal. You have no knowledge of whether that hydrogen reading you are getting is at all related to the hydrogen in the cover gas. I think this is a point that a lot of people ought to recognize, because I see people planning to put chromatographs on reactors to measure the hydrogen and other impurities in the cover gas. It simply is not possible to do it without solving that problem.

Mr. Olson: We have been bothered somewhat by the fact that we cannot see hydrogen in the cover gas in the secondary system. I believe that there has been shown to be some hydrogen migration through the

*C. C. Miles, E. R. Ebersole, and W. H. Olson, *Sodium Sampling and Analytical Experience at EBR-II*, This Conference.

steam-generator walls. We do not, at least within our detection capabilities, see hydrogen in the secondary cover gas.

Mr. Shannon (BNWL): This is one of the primary reasons we are looking with the time-of-flight mass spectrometer; it can work with a breakable inlet system so you do not have to reduce the temperature. We have seen the same thing that Hill referred to.

Mr. Dickinson (LMEC): Have you found any correlation between hydrogen and temperature? When you go up in temperature do you get a burst of hydrogen?

Mr. Olson: We don't see it in the secondary system. In the primary there is little opportunity to check, since it is always close to 700°F.

Mr. Young (GE): We have an on-line chromatograph on one of our loops, measuring hydrogen in the cover gas, and we suspect that we are getting a holdup of hydride in the vapor traps. There has been some indication that this not only holds up in the vapor traps, but also in the surge tanks in the gas phase due to changing levels of sodium. You can detect a change in plugging temperature as if there was hydride on the walls. Our plans are to do some heating in these areas and watch for bursts of hydrogen.

Mr. McSorley (W): Did you identify the composition of the copper where it was plugging on the plates?

Mr. Olson: It was metallic copper; I don't know the purity.

An Integral Full-flow Vacuum Distillation Sampling System for Use in a High-temperature Radioactive Sodium Environment*

V. J. Rutkauskas†

Los Alamos Scientific Laboratory
Los Alamos, New Mexico

Abstract

A laboratory model of an integral full-flow vacuum distillation sampling system is currently being used at the Los Alamos Scientific Laboratory for the routine analysis of oxygen in experimental dynamic sodium systems. This analytical method has a precision of ±0.5 ppm in the oxygen concentration range from 1 to 10 ppm, and the time required for a completed analysis is approximately 2 hr. The design of the laboratory system is being modified to enable it to be used in a radioactive sodium environment at LMFBR temperature conditions. The entire system is constructed of Type 304 stainless steel, and the separation of sodium from the nonvolatile impurities is accomplished with a high-frequency induction generator. The work coil for the induction generator is located within the metal envelope of the distillation zone. The system design eliminates the need for sample transfer, thereby eliminating potential atmospheric contamination. The sodium distillate is retained in a combination condenser and reservoir. A remotely operated sampling system will be installed in the EBR-II. The full-flow vacuum distillation sampling system is designed for the routine removal of sodium samples for oxygen analysis, and it has the potential for being used to identify other species present in a radioactive sodium environment.

1. Introduction

The characterization and control of impurities in high-temperature sodium systems is a basic requirement for the successful operation of a sodium-cooled, fast breeder reactor. The concentrations of interstitial impurities such as oxygen must be controlled within acceptable limits over the operating life of a system. Therefore, to ensure the effectiveness of purification methods, provisions must be made for the routine analysis of sodium. The vacuum distillation sampling technique is readily adaptable to this mode of operation.

Vacuum distillation sampling systems are currently being used at the Los Alamos Scientific Laboratory[1, 2] for the routine analysis of oxygen in experimental dynamic sodium systems. The sampling systems are incorporated as an integral part of the experimental facility. Sodium samples are removed from the system, after sufficient flushing to ensure the retention of a representative sample, and introduced into a nickel sampling cup where the sodium metal is separated from its nonvolatile impurities. The distillation is conducted under a dynamic vacuum of $<10^{-4}$ Torr, using an induction furnace as a heat source. The residue remaining in the sample cup following the separation is dissolved in dilute hydrochloric acid and analyzed with a flame emission spectrophotometer for sodium as an indirect measurement of the oxygen concentration, assuming the residue to be Na_2O. Although this method is not specific for the determination of oxygen in sodium, it has yielded reliable and reproducible data with a demonstrated sensitivity of 0.5 ppm in the concentration range from 1 to 10 ppm.[3, 4]

The laboratory model of an integral full-flow vacuum distillation sampling system currently being used at the LASL is being redesigned for use in a radioactive sodium environment at LMFBR temperature conditions. This modified engineering-loop version of the laboratory system is scheduled to be field tested in the EBR-II.[2] A remotely operated integral sampling and distillation system will be installed on the EBR-II primary sodium chemistry loop,[5] and a manually operated unit will be installed on the nonradioactive secondary-sodium system. The entire sampling system will be constructed of Type 304 stainless steel, and the separation of sodium from the nonvolatile impurities will be accomplished with induction heating. The work coil of the induction heater is located within the metal envelope surrounding the distillation zone. The sampling system is designed for the routine removal of sodium samples for oxygen analysis, but due to the elimination of the major source of radioactivity as a result of the sodium separation, it has the potential for providing samples for other analyses.

* Work performed under the auspices of the U. S. Atomic Energy Commission.

† Present address: Battelle Northwest Laboratory, Richland, Wash.

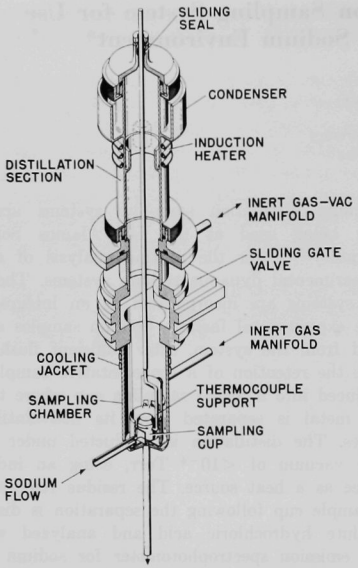

FIG. 1. Schematic of Full-flow Vacuum Distillation Sampling System.

2. Description of Apparatus

2.1. Vacuum Distillation Sampling System

The laboratory model of the full-flow vacuum distillation sampling system shown schematically in Figure 1 was incorporated as an integral part of a dynamic sodium system. The sampling system consists of a constant-flow sampling chamber, distillation section, and a vacuum/inert gas manifold. All components contacted by the flowing sodium were constructed of Type 304 stainless steel. A typical installation is shown in Figure 2.

The sampling chamber, constructed from a section of 2-in., schedule 10 pipe, was attached to the sodium system with 0.500 × 0.035-in.-wall tubing supply and return lines. Isolation valves were provided in the lines, and flow from the sodium system to the sampling chamber was regulated with a dc electromagnetic pump. The sampling chamber contains an inner sodium reservoir (of approximately 100-cm^3 capacity) which is positioned on a retaining spider. The sodium flow enters the reservoir tangentially, spills over the top, and drains back to the system by gravity. The tangential flow path provides a well-mixed sodium inventory, and the weir effect provides a means for mechanical separation of insoluble materials and floating scum. A small hole at the bottom of the reservoir provides a drain return to the system when the flow to the sampling chamber is terminated. Flow rates of up to 0.5 gpm could be obtained by regulating the current input to the pump from a 250-A dc rectifier. All components in contact with sodium were trace heated and maintained at or slightly above the sodium system temperature. The sampling-chamber volume below the sliding gate valve was always maintained under a positive helium pressure. A vapor trap, partially visible in Figure 2, was located in the inert gas line leading to the sampling chamber. The vapor trap was designed to prevent liquid sodium from entering the inert gas manifold through inadvertent flooding of the sampling chamber. A cooling jacket was located around the periphery of the sampling chamber adjacent to the isolation valve. This allowed the use of elastomer "O" ring seals and provided close coupling of components due to space considerations.

During the sampling operation, the distillation-section and sampling-chamber pressures are equilibrated, and the nickel sampling cup is lowered into

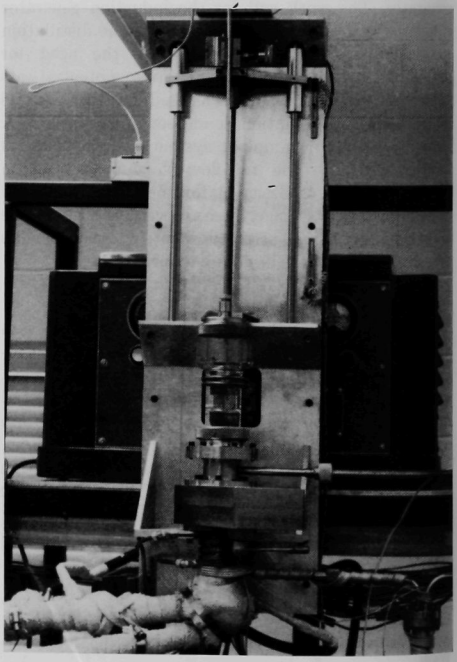

FIG. 2. Full-flow Vacuum Distillation Sampling System.

the sodium reservoir. After a short equilibration period the sampling cup containing a representative sample of system sodium is raised into a 2-in.-diameter Pyrex distillation section and isolated from the sampling chamber with a 2-in. sliding-seal gate valve. The cup is positioned in the work coil of a 1-kW high-frequency induction generator which is used as a heat source for distillation. The distillation section is evacuated and the distillation conducted under a dynamic vacuum of $<10^{-4}$ Torr, using the combination of a mechanical and molecular sorption pump. A thermocouple support for the sample cup provides temperature sensing during operations and allows distillation-rate data to be compiled.

On the completion of distillation, the entire distillation section is removed from the system and replaced. This is accomplished by backfilling the system above the sliding valve with approximately 2 psig helium and disconnecting the glass section at the lower metal-to-glass joint visible in Figure 2. The equipment exchange requires approximately 10 to 15 sec, and the flow of helium under pressure during this period minimizes the introduction of atmospheric contaminants. Following the exchange, the distillation section is evacuated and the sample cup pretreated at 500 to 525°C prior to receiving another sample.

The nickel sample cup was machined with a hemispherical radius and had a volume of 4.3 cm^3. With a normal meniscus the sample should contain approximately 5 g of sodium. The sample yields have been 5.0 g ± 2%, based on recovery of the distillate. The uniformity in sample size is attributed to several factors. Following a distillation the sample cups are abrasive and chemically cleaned, and prior to sampling the cup is preheated to 500 to 525°C under vacuum. Wetting is enhanced as the cup temperature is allowed to equilibrate with the system sodium temperature in the sampling chamber. In addition, as the cup shears the sodium surface when the sample is being withdrawn, the surface tension effect aids in removing excess sodium and enhances the maintenance of a uniform sodium volume.

Approximately 15 to 20 sec are required to raise the sample cup within the heater coils in the distillation section, isolate the sample chamber, and initiate the distillation at a pressure of $<10^{-4}$ Torr. A chilled water condenser located around the periphery of the distillation tube, shown in Figure 2, collects 95% of the distillate, and the rest is deposited on the lower portion of the tube. Slight heating of the glass with a torch in the region above the liquid level of the sample affords a window for visual observation of the distillation process. The distillations have always proceeded smoothly and without surface perturbations which could be attributed to gas entrainment, gas evolution, or superheating. The power input to the cup was adjusted to maintain a temperature of 355 ± 5°C throughout the distillation period of approximately 14 min. This has resulted in a distillation rate of 0.35 ± 0.02 g/min, based on the recovery of the distillate. A sharp increase in temperature without a change in power input to the cup marks the termination of the separation process. The cup temperature is then raised to 400 to 410°C, and heating is discontinued. The distillation section is backfilled with helium, cooled to ambient temperature, removed from the system, and replaced.

The sample cup is removed from the thermocouple support rod and the residue dissolved in 5 ml of 0.01 *N* hydrochloric acid. The sodium concentration in the solution is determined by flame emission spectrophotometry. When required, the sodium distillate is recovered and titrated with 1.0 *N* hydrochloric acid to determine the total inventory of sodium initially present in the sample.

When a clean glass distillation section is inserted into the system following completion of the previous sampling operation, it is isolated from the rest of the system and evacuated to $<10^{-4}$ Torr to remove any trace moisture and other volatile impurities. This is a precautionary measure against contaminating the surfaces of the sampling chamber. Preheating of the sample cup also helps to prevent contamination.

When not in use, sodium flow to the sampling chamber is shut off and the isolation valves are closed. The sodium in the sampling system is allowed to freeze, and a positive pressure of helium is maintained in the sampling chamber. The helium used has contained <10 ppm total impurities. The distillation section is maintained at a pressure of $<10^{-4}$ Torr or at the pressure of the sampling chamber, depending on where in the sequence of operations the system was shut down.

2.2. Remotely Operated Sampling System

The remotely operated integral full-flow vacuum distillation sampling system is shown schematically in Fig. 3. The features of this system and the sequence of operations are basically the same as the laboratory model. The modifications which set this unit apart from the laboratory system include the incorporation of a mechanism for sample-cut transfer and a condenser for the sodium. The entire system is constructed of Type 304 stainless steel. A nominal 3-in. bore is maintained in all horizontal and vertical components. All flanged connections are the high-vacuum type with metal-gasket seals. Elastomer gasket materials have been eliminated from the

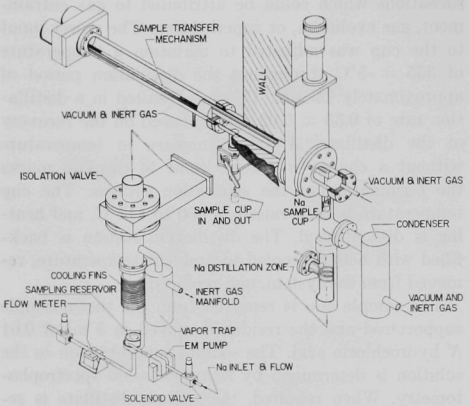

FIG. 3. Schematic of Remotely Operated Distillation Sampling System.

sections of the system exposed to sodium vapor. Radiation-resistant elastomers are used in the noncritical zones and where it is considered impractical to use metal-gasket seals. All operations are electronically controlled, and the sequencing of events are performed in a semiautomatic mode from a graphic display panel.

The sampling chamber contains the same features of internal flow as the laboratory model with the exception that there is a substantial increase in volume of the sodium reservoir. Isolation valves, electromagnetic flowmeter, and dc electromagnetic pump are an integral part of the sampling-chamber assembly. The sodium-supply and return lines are fabricated from ½-in. pipe. The sampling chamber and its associated equipment are being designed for 650°C sodium conditions. A cooling jacket is provided around the periphery of the sampling chamber well above the liquid sodium level in order to reduce the temperature requirements of the vapor trap and the isolation valve which separates the sampling and distillation sections.

The sodium separation from the nonvolatile impurities is accomplished with a 2½-kW high-frequency induction generator. The work coil for the induction generator is located within the metal envelope which comprises the distillation section of the system. A flange-mounted, high-vacuum rf feedthrough is used to introduce the work coil in the system. A thermocouple for monitoring the sample cup during the initial preheat and distillation is also an integral part of the distillation-zone flange assembly.

The condenser provides a reservoir for the sodium distilled from the sodium samples. The entire vertical section of the system above the isolation valve separating the sampling and distillation sections is trace heated to prevent vapor deposition on exposed surfaces during distillation, thereby effecting the flow of vapor to the condenser where it is retained. The condenser contains a series of internal flow baffles designed to maximize the collection efficiency. The vacuum/inert gas connection is located downstream of the flow baffles. The condenser can be heated periodically to remove the sodium deposited on the cold surfaces and redeposit the sodium in the reservoir (of approximately 1-l capacity) portion of the condenser. All vacuum and inert gas lines in the system are constructed of 1.00-in.-OD × 0.065-in.-wall tubing, so that pressure conditions can be established as rapidly as practicable.

The mechanism for sample-cup transfer is designed to accomplish both the vertical and horizontal travel needed to position the sample cup in the system properly. Horizontal travel is achieved with a movable rigid carriage assembly. The vertical travel is handled by a tape mechanism. The nickel sample cup (of 5- to 10-g sodium capacity) is cradled in a yoke fastened to the end of a 0.005-in. stainless steel tape, which in turn is passed through a slot in the movable carriage and fastened to a take-up reel at the rear of the carriage. The vertical and horizontal slo-syn motor drives required for accurate positioning are located external to the sample-cell shield wall pictured in Figure 3. The total amount of horizontal travel is only that which is necessary to accommodate a sample-cup transfer out of the radiation environment. Approximately 30 in. of vertical travel is involved between the horizontal transfer tube and the sodium reservoir in the sampling chamber.

A small-volumed access chamber is located as an appendage on the horizontal transfer tube. This provides access to the sampling system for the introduction and removal of sample cups while reducing the probability for the introduction of atmospheric contaminants into the system. By virtue of its design, the transfer tube and its mechanisms are not exposed to sodium vapor during the sampling and distillation sequence of operation. When a sample-cup transfer is being made the transfer mechanism is retracted, the large horizontal gate valve is closed, isolating both the horizontal and vertical segments of the system, and the horizontal tube is filled with inert gas prior to opening the isolation valve on the access port. A substantial gas flow out of the transfer chamber is maintained during the time required for transfer in order to minimize the quantity of at-

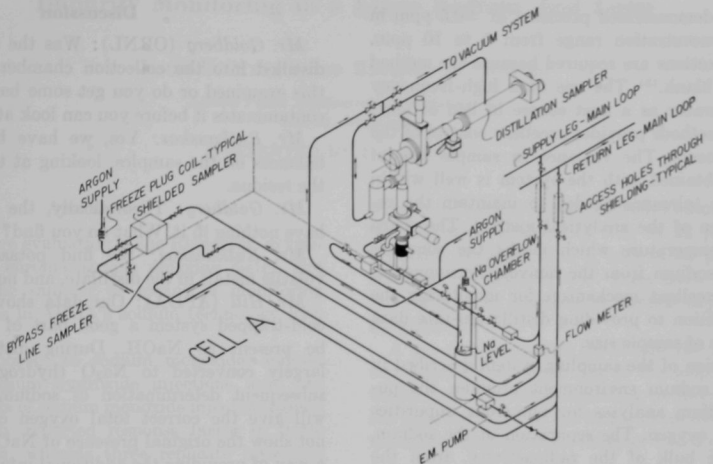

FIG. 4. Artist's Conception of EBR-II Sampler-system Installation.

mospheric contaminants back diffusing into the system. Following the sample-cup transfer, the transfer chamber is evacuated to remove trace moisture and other volatile impurities before the large isolation valve is opened. The transfer tube is maintained under vacuum or at a positive inert gas pressure and is exposed to the possibility of atmospheric contamination only when the access port is opened, whereas the distillation zone in the system is never exposed to atmospheric contamination, but only to a vacuum or inert gas environment.

2.3. EBR-II Installation

The installation for the integral full-flow vacuum distillation sampling system in the primary-sodium chemistry loop is shown pictorially in Figure 4. Only the all-metal sampling system is located within the shielded cavity, while the support equipment, such as the vacuum/inert gas system, induction generator, dc electromagnetic pump rectifier, and the data-acquisition and control circuitry, are located external to the shielded cavity.

A modestly sized sodium reservoir s located at the bottom of the shielded cavity. This provides a constantly refreshed sodium supply from the primary system of the EBR-II; it also affords all of the safety requirements necessary to comply with the operational requirements of the EBR-II reactor plant. The sodium from the intermediate reservoir is in turn pumped into the sampling chamber at a flow rate of approximately 0.5 gpm. Sample cups with a 5-g capacity will be used for oxygen analysis with provisions for an increase to 10 g if necessary for other types of analyses.

All moving parts within the shielded cavity have been reduced to a minimum. With the exception of a few cases, all critical components are readily accessible from outside the shield wall. Modular construction has been used throughout for ease of maintenance and component replacement. The system is being designed with a goal of 1000-cycle, maintenance-free operation. This results in a total of 500 sodium samples removed for analysis from the dynamic stream. The sampling system will be thoroughly tested and evaluated in a mockup of the actual EBR-II shielding-cavity configuration to assess the operating parameters and component-life expectancy prior to the actual installation in the EBR-II complex.

3. Summary

The laboratory model of the integral full-flow vacuum distillation sampling system as described in this paper is readily adaptable for remote operation in a high-temperature, radioactive sodium environment. The system provides representative sodium samples for analysis on a routine basis. The time required to run a complete analysis for the determination of oxygen in sodium is approximately 2 hr. The equipment design eliminates the need for sample transfer, thus eliminating the probability of sample contamination by atmospheric impurities. The vacuum distillation analytical method for oxygen in

sodium has a demonstrated precision of ±0.5 ppm in the oxygen concentration range from 1 to 10 ppm. No blank corrections are required because the method yields a zero blank.[3] The use of a high-frequency induction generator as a heat source in lieu of more conventional methods provides excellent control of the distillation process. The variance in sample size of 5.0 g ± 2% obtained with the system is well within the acceptable tolerance needed to maintain the required precision of the analytical method. The sharp rise in cup temperature which marks the complete separation of sodium from the nonvolatile impurities provides an excellent mechanism for monitoring the process in addition to providing distillation-rate data for estimations of sample size.

The adaptation of the sampling system described in a radioactive sodium environment provides the potential for sodium analyses for numerous impurities in addition to oxygen. The separation of the sodium, and hence the bulk of the radioactivity, from the nonvolatile residues provides samples for immediate analyses for all dissolved impurities, including most fission-product elements with a minimal shielding requirement on the sample cup containing the residues. Although the EBR-II temperature requirements are substantially more modest than the proposed LMFBR temperature conditions, the sampling system is being designed to meet the 650°C LMFBR sodium-temperature conditions. The modular construction of the sampling system using the fabrication and construction techniques adapted for high-vacuum systems affords a great deal of flexibility and versatility to the system for extension to other sodium systems.

Acknowledgments

The author gratefully acknowledges the support contributed by K Division members, especially Messrs. G. E. Meadows and W. R. Wykoff, who have expressed a keen interest in the fruitful conclusion on this project.

REFERENCES

1. *Quarterly Status Report on the Advanced Plutonium Fuels Program, April 1–June 30, 1967*, LA-3745-MS, Los Alamos Scientific Laboratory.
2. *Quarterly Status Report on the Advanced Plutonium Fuels Program, April 1–June 30, 1968*, LA-3993-MS, Los Alamos Scientific Laboratory.
3. V. J. Rutkauskas, *Determination of the Solubility of Oxygen in Sodium by Vacuum Distillation*, LA-3879 (1968).
4. K. S. Bergstresser, G. R. Waterbury, and C. F. Metz, *Determination of Trace Amounts of Oxygen Added to Metallic Sodium*, LA-3343 (1965).
5. *Reactor Development Program Progress Report for February 1968*, ANL-7427 (1968).

Discussion

Mr. Goldberg (ORNL): Was the sodium that you distilled into the collection chamber analyzed? Was this examined or do you get some back-diffusion that contaminates it before you can look at it?

Mr. Rutkauskas: Yes, we have been doing mass balances on the samples, looking at the distillate and the residue.

Mr. Goldberg: Theoretically, the distillate should have nothing in it. What do you find?

Mr. Rutkauskas: We find potassium and other volatile metals in the distillate, and not in the residue.

Mr. Hill (APDA): Our data show that in a well cold-trapped system a good part of the oxygen will be present as NaOH. During distillation, this is largely converted to Na_2O (hydrogen is evolved); subsequent determination of sodium in the residue will give the correct total oxygen content, but will not show the original presence of NaOH. Do you have a way of providing the additional information?

Mr. Rutkauskas: I don't know how you are going to get around the problem; it cannot be done simply by analyzing the distillation residue. The way we have been running the systems we can eliminate the NaOH simply by heating the system up to roughly 600°C and evacuating the cover gas. For most of the systems that we have been running we can really belch the NaOH out by this method. In a reactor system you have another situation. This is a problem that you have to face up to at some point in time.

Mr. Kovacic (APDA): Hill and I have discussed this many times. I think we have conclusive evidence that in a well cold-trapped system, on loops and in Fermi, there is about 1 ppm hydrogen as hydroxide.

Mr. Kanamori (APDA): How do you clean the nickel crucible?

Mr. Rutkauskas: Following the introduction of the dilute HCl, after washing the residue out, we then abrasively clean, chemically clean, and heat to roughly 500–550°C under vacuum (in the neighborhood 10^{-4} to 10^{-5} Torr) while in the system.

Mr. Haroldsen (ANL): We're to be the customer for this unit. One question we've been confused about is the head on the sample. In your model you have a tangential flow into the reservoir. Is this essential or would straight-through flow maintain an even head from sample to sample?

Mr. Rutkauskas: Tangential flow has the advantage that the liquid swirls to form a slight vortex which improves the mechanical separation for any insolubles. Flow straight in gives an impingement on the opposite wall and it isn't as effective.

Impurity Monitoring in a Large Sodium Test Loop

James E. Meyers and Raymond A. Hunter*

Atomic Power Development Associates, Inc.
Detroit, Michigan

(PRESENTED BY J. E. MEYERS)

Abstract

The quantitative evaluation of the Rhometer, oxygen meter, cover-gas chromatograph, plugging meter, and bypass freeze-tube sampler as means of monitoring sodium impurities in APDA's sodium technology loop is discussed.

Rhometer responses to sodium monoxide, sodium hydride, and sodium hydroxide injections were obtained. The results of sodium monoxide injection agreed with a previously reported response factor of 0.004 %R/ppm oxygen, whereas three replicate injections of 1 ppm hydrogen as sodium hydride gave response factors of 0.064, 0.049, 0.064 Δ%R/ppm hydride hydrogen. Rhometer response to three replicate injections of 1 ppm hydrogen as sodium hydroxide can be explained on the basis of total decomposition and on the assumption that the decomposition products (sodium monoxide and sodium hydride) contribute independently to the resistivity measurement.

Twelve oxygen-meter electrode assemblies have been evaluated since 1965. Calibration constants determined by impurity injections ranged from -19 to -40 V^{-1}. Sodium temperature coefficients varied from 0.56 to 0.04 mV/°F, and ambient temperature coefficients varied from -0.82 to -0.40 mV/°F. Gamma radiation caused response changes from 0 to more than 50 mV, depending on the cell. The time responses of electrode assemblies operating more than several months were prohibitively long.

The reliability of plugging-temperature measurement was studied. In 14 plugging-meter runs agreement was within 5°F. Regarding the relationship between plugging temperature and purity level, two interesting measurements were obtained: (1) an abnormally high plugging temperature (>500°F) for 900°F cold-trapped sodium and (2) essentially the same plugging temperature (≈365°F) for 600°F cold-trapped sodium following 1 ppm hydrogen replicate injections of either sodium hydride or sodium hydroxide.

Pinched nickel bypass freeze-tube samples were analyzed for oxygen impurities by the mercury amalgamation method at different oxygen levels. The results were as follows: at 7 ppm a relative standard deviation for individual analyses of 7%, at 22 ppm a relative standard deviation of 8%, and at 30 ppm a relative standard deviation of 6%. Data have been gathered for nonpinched samplers at various oxygen levels for comparison.

A gas chromatograph monitored the hydrogen concentration in the cover gas of the loop. This concentration was correlated according to Sievert's Law with the total hydrogen in the loop sodium over a hydrogen-in-sodium concentration range of 1 to 3 ppm.

1. Introduction

As part of the AEC's program to develop a sodium-cooled nuclear reactor, APDA has been engaged in a project to develop and evaluate inline instruments for detecting, monitoring, and controlling impurities in sodium. The quantitative evaluations of four of these instruments: the Blake Mark-I Rhometer, the UNC oxygen meter, the Thermco cover-gas chromatograph, and the APDA plugging meter, are discussed in this paper, as is the APDA freeze-tube sampler, an out-of-line device that collects sodium for laboratory analysis.

The loop being used for the development and evaluation of these devices is shown in Figure 1. This loop, which actually consists of a 4-in. main loop and a 1-in. test loop, has been described previously.[1] As can be seen from Figure 1, the loop contains sodium-purification apparatus in addition to the devices already mentioned.

In Reference (1), data were presented by APDA concerning the responses of both the Blake Rhometer and UNC oxygen meter, as well as sodium-sampling and analysis results for comparison. The data indicated that the three Rhometers installed in the loop were less sensitive to oxygen in the form of sodium monoxide that to sodium hydride and sodium hydroxide. The average response to the Rhometers to oxygen as sodium monoxide was about 0.004 %R/Δ ppm of oxygen at a base level of approximately 10 ppm and at sodium temperatures of about 600°F. Oxygen-meter response was found to be sensitive to perturbations of sodium temperature in the loop and possibly to changes in ambient temperature. In short, both Rhometer and oxygen-meter responses showed good qualitative agree-

* Now with U. S. Atomic Energy Commission, Division of Reactor Development and Technology, Washington, D. C.

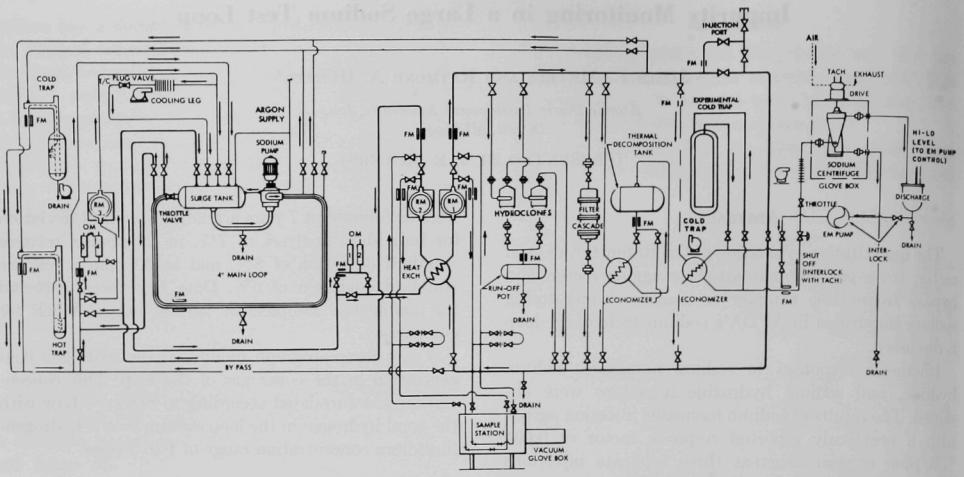

FIG. 1. Schematic of Sodium Technology Loop.

ment with impurity injections, but appeared quantitatively unreliable.

As regards the Rhometer, oxygen meter, plugging meter, and freeze-tube sampler, the information presented herein represents data acquired after evaluations reported in Reference (1) were made. Since the gas chromatograph has been evaluated only recently, the information given in this paper represents APDA's total experience with this instrument.

2. Rhometer

The initial APDA test results given in Reference (1) indicated the Mark-I Rhometer to be basically a sound instrument, but that further development and testing were required to make it sufficiently reliable for in-line monitoring of impurities. More recent results confirm the earlier work. As shown in Table 1, the average sensitivities found in recent tests were 0.0040, 0.0036, and 0.0046 $\Delta\%R/\Delta$ ppm measured oxygen for Rhometers 1, 2, and 3, respectively, with an average sensitivity for all three Rhometers combined of 0.0043 $\Delta\%R/\Delta$ ppm measured oxygen. This value agrees favorably with the 0.0045 $\Delta\%R/\Delta$ ppm measured oxygen obtained in similar sodium monoxide injection tests reported in the earlier work.

In Figure 2 are displayed typical responses of Rhometer 3 to injections of sodium hydroxide and sodium hydride to cold-trapped sodium, as well as the Rhometer responses to preinjection cold-trapping operations. It should be noted that the information in this figure is not the actual output from Rhometer 3, but rather a plot of hourly data points taken from recorder charts. The hourly data points, in addition to depicting the output, were used in statistical considerations for estimating the changes in percent resistivity resulting from the sodium hydroxide injections (see Table 2), the sodium hydride injections (see Table 3), and the cold-trapping operations.

As discussed later in this paper, there is definitely chemical interaction occurring within the sodium-oxygen-hydrogen system. This conclusion is essential to the interpretation of the Rhometer responses to the injections of sodium hydroxide. For the particular case of 100% decomposition (free-energy calculations indicate that the maximum equilibrium conversion of sodium hydroxide occurs near the loop operating temperature of 600°F), an injection of 15.05 g sodium hydroxide is equivalent to injecting 9.03 g sodium hydride and 23.2 g sodium monoxide. These quantities are equal to concentration increases in the loop of 1 ppm hydroxide hydrogen, 1 ppm hydride hydrogen, and 16 ppm oxygen, respectively. From the chemistry changes shown in Table 4 it could be concluded that the sodium hydroxide added to cold-trapped sodium did not fully decompose and also that sodium hydroxide was formed following injections of sodium hydride. However, the samples of the 600°F loop sodium were cooled to room temperature before analysis; from a thermodynamic standpoint, this would indicate hydroxide formation in the hydrogen-oxygen-sodium system. Thus, the presence of hydroxide in the samples at room temperature does not necessarily mean that it is present in the 600°F loop sodium.

As can be noted from Tables 2 and 3, the injections

TABLE 1. RHOMETER RESPONSES TO SODIUM MONOXIDE INJECTIONS

Injection No.	Date	Measured Initial Oxygen Conc,[a] ppm	Measured Oxygen Change,[a] ppm	Amount of Na_2O Injected, ppm	Change in Rhometer Output, Δ%R			Sensitivity, Δ%R/Δ ppm Measured O_2		
					RM-1	RM-2	RM-3			
1	4-27-66	11.5	19.0	25	0.065	0.062	0.060	0.0034	0.0033	0.0032
2	5-4-66	30.5	8.5	25	0.042	[b]	0.063	0.0049	—	0.0074
3	5-11-66	39.0	9.0	25	0.038	[b]	0.040	0.0042	—	0.0044
4	9-28-66	7.0	21.0	25	0.072	[b]	0.068	0.0034	—	0.0032
5	1-30-67	7.1	8.2	10	[b]	[b]	0.038	—	—	0.0046
6	2-3-67	15.3	8.5	15	[b]	[b]	[b]	—	—	—
7	9-13-67	12.8	NC[c]	8	0.017	0.043	NC	—	—	—
8	9-15-67	11.8	4.6	6	NC	−0.009	0.033	—	(−0.0020)[d]	0.0072
9	9-19-67	16.4	7.2	8	NC	0.027	0.031	—	0.0038	0.0043
10	9-21-67	23.6	2.0	10	NC	0.025	0.029	—	(0.0125)	(0.0145)
11	9-26-67	25.6	33.4	10	0.034	0.029	0.025	(0.0010)	(0.0009)	(0.0075)
12	2-7-68	6.0	16.0	16	[b]	[b]	[b]	—	—	—
13	2-14-68	6.0	20.0	16	[b]	[b]	[b]	—	—	—
14	2-21-68	7.5	18.5	16	[b]	[b]	0.070	—	—	0.0038
15	2-28-68	7.0	17.0	16	[b]	[b]	0.050	—	—	9.0029
				Average Sensitivity, $\bar{X}$				0.0040	0.0036	0.0046
				Grand Mean, $\bar{X}$				0.0043		

[a] Expressed as oxygen in Na_2O.
[b] No reading taken because of operational problems or because of Rhometer modifications.
[c] No change in response.
[d] Parentheses indicate value is not figured into the mean.

of sodium hydroxide to cold-trapped sodium gave percent resistivity increases larger than the three injections of 9.03 g sodium hydride, even though the amount of hydrogen added was the same in all cases. Such a result was anticipated on the assumption that all of the injected sodium hydroxide would decompose to form sodium monoxide and sodium hydride.

By use of the measured changes in oxygen and total hydrogen as given in Table 4 and the Rhometer response factors to oxygen and hydrogen as presented in Tables 1 and 3, the response of the Rhometer to sodium hydroxide was calculated, assuming that each species, sodium monoxide and sodium hydride, contributes independently to resistivity changes. A comparison of the calculated response of the Rhometer to sodium hydroxide with the actual Rhometer response to this impurity is presented in Table 2. With the exception of the first sodium hydroxide injection, all injections were made to cold-trapped sodium. This fact could account for the large difference between the calculated and the actual Rhometer response. However, for the remainder of the injection and subsequent cold-trapping operations for which data were available, the agreement between the calculated and actual Rhometer response is good.

The temperature-compensation range of the Rhometers installed in APDA's loop has been extended from 600 to 1000°F through the addition of transformers in the compensator circuit, as well as through the addition of variable resistors in the signal-summation circuit. As indicated in the summary of test results presented in Tables 1, 2, and 3, a number of problems have been encountered in the operation of the Rhometer at the APDA laboratories. Switch contacts have been a constant source of trouble. The platinum temperature resistors wound around the pipes for temperature compensation have exhibited resistance step changes, probably because the yield strength of the platinum wire is reached when the loop temperature is ramped to 1000°F. In addition, step changes in the Rhometer output of the order of 0.1 %R have been observed, but the causes have not been identified.

In spite of these malfunctions and because it is believed that the Rhometer is a promising in-line monitoring device, extensive modifications to the basic instrument have been made at APDA. These modifications consist of an automatic temperature compensator to operate over the range from 400 to 1000°F, and a redesign of the circuitry to reduce the signal-to-noise ratio and to eliminate base-line drift.

It is anticipated that APDA's modified Rhometer, which is scheduled for loop evaluation in November 1968, will be capable of exhibiting excellent base-line stability and be capable of detecting a change of impurity concentration equivalent to 1 ppm of oxygen or 0.1 ppm of hydrogen at a cold-trapped sodium purity level.

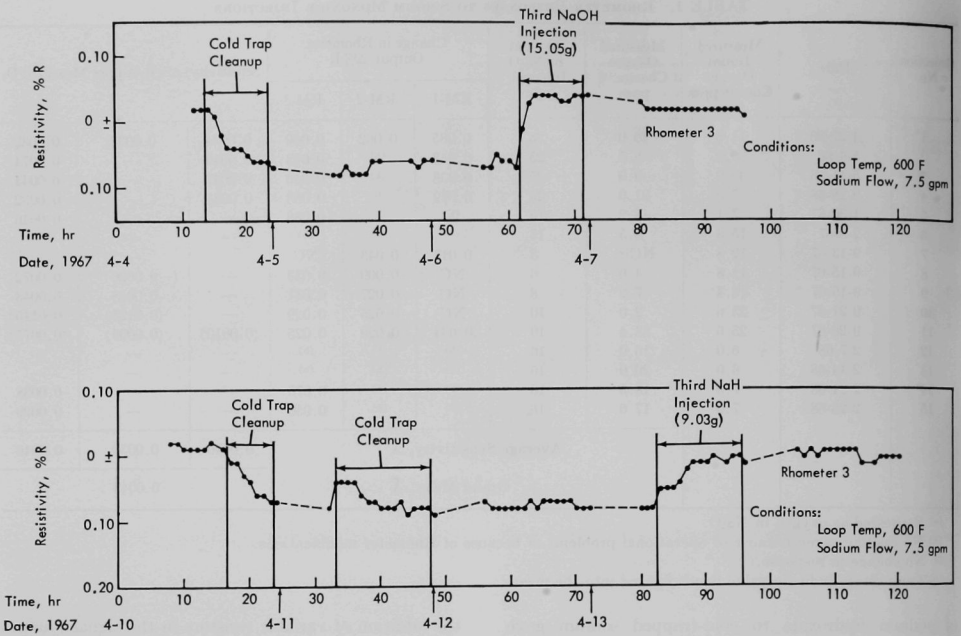

FIG. 2. Response of Rhometer 3 Before, During, and After Injections of Sodium Hydroxide and Sodium Hydride to Cold-trapped Sodium.

TABLE 2. RHOMETER-3 RESPONSE TO INJECTIONS OF SODIUM HYDROXIDE AND SUBSEQUENT COLD-TRAPPING OPERATIONS

Sequence of Loop Operations	Date	Measured Oxygen Change, ppm	Measured Total Hydrogen Change, ppm	Calculated Δ%R from Oxygen	Calculated Δ%R from Hydrogen	Calculated Rhometer Response, Δ%R	Actual Rhometer Response, Δ%R
1. NaOH injection	2-15-67	0.6	1.34	0.003	0.075	0.078	0.018
2. Cold trap		−34.4	−2.1	−0.158	−0.117	−0.275	−0.290
3. NaOH injection	3-30-67	13.6	1.17	0.063	0.065	0.128	0.097
4. Cold trap		−12.6	−1.1	−0.058	−0.061	−0.119	−0.140
5. NaOH injection	4-6-67	[a]	[a]	—	—	—	0.088
6. Cold trap		[a]	[a]	—	—	—	−0.097
7. NaOH injection	4-20-67	10.4	0.84	0.048	0.047	0.095	0.099
8. Cold trap		−9.8	−1.94	−0.045	−0.058	−0.103	[b]

[a] Samples were not taken because of scheduling difficulties.
[b] Erratic behavior of Rhometer after injection did not permit response to be measured.

3. Oxygen Meters

Since 1965, APDA has been evaluating in its sodium technology loop oxygen meters manufactured by the United Nuclear Corporation. Included in this effort have been studies to establish (1) meter response to injections of sodium monoxide, sodium hydride, and sodium hydroxide, (2) sodium and ambient temperature coefficients of the meters, and (3) effects of gamma radiation on meter performance.

In all, twelve oxygen-meter electrode assemblies have been in service at APDA, although only four are currently installed in the loop. Regarding cell life, or that period of time in which an electrode assembly produces meaningful information, only cell No. 1 (TP-15) has been tested extensively enough to state with confidence that capability exists for long-term quantitative performance (see Table 5). On the basis of the performance of this cell, however, as well as on

the basis of APDA's lack of oxygen-meter experience during the initial field testing, it is now believed that three of the first four cells installed [cells 2 (TP-19), 3 (TP-17), and 4 (TP-18)] were removed from service prematurely, thus making any judgment concerning the life of these cells impossible. Nonetheless, it is noteworthy that the original four cells evaluated by APDA were removed from sodium service, cleaned, inspected, and reinstalled without significantly affecting their performance. It should also be pointed out that the vendor has stated that the problem with those electrode assemblies which did not perform properly immediately was traceable to quality-control difficulties that arose during a geographical relocation of plant facilities.

To evaluate oxygen-meter response to various impurities, sodium monoxide, sodium hydride, and sodium hydroxide injections were made to an isothermal, circulating sodium loop maintained at 600 ± 5°F. The additions were performed using glovebox-enclosed sampling tubes as injection tubes. All of the oxygen concentrations, except where noted, were obtained by the mercury amalgamation method followed by titration of the residue.

Responses of oxygen meters 1, 2B, 3B, and 4B to sodium monoxide injections are shown in Figures 3, 4, 5, and 6.* The first three figures illustrate the responses of oxygen meters 1, 2B, and 3B to five successive sodium monoxide injections, equivalent to 8, 6, 8, 10, and 10 ppm of oxygen, starting with an initial concentration of oxygen in sodium of 5 ppm. The calibration curves for these successive injections are presented in Figures 7, 8, and 9. Although oxygen meter 1 responded as expected over the whole range of concentration changes, its calibration constant was sig-

TABLE 3. RHOMETER-3 RESPONSE TO INJECTIONS OF SODIUM HYDRIDE AND SUBSEQUENT COLD-TRAPPING OPERATIONS

Sequence of Loop Operation	Date	Response, $\Delta\%R$	Total Hydrogen, Δ ppm	Sensitivity, $\Delta\%R/\Delta$ ppm
NaH injection	2-24-67	0.043	0.67	0.0642
Cold trap		−0.034	−0.74	0.0459
NaH injection	3-10-67	0.057	1.17	0.0487
Cold trap		−0.065	−1.34	0.0485
NaH injection	4-13-67	0.081	1.27	0.0638
Cold trap		−0.060	−0.94	0.0638
Average sensitivity, NaH injection, $\bar{x}_1$				0.0589
Cold trap, $\bar{x}_2$				0.0527
Grand Mean, $\bar{\bar{x}}$				0.0558

* Responses of oxygen meters 1, 2, 3, and 4 to earlier sodium monoxide injections can be found in Reference (1).

TABLE 4. SAMPLING AND ANALYSIS RESULTS FOR THE SODIUM HYDROXIDE AND SODIUM HYDROXIDE INJECTION TESTS

Sequence of Loop Operations	Impurity Concentration, ppm											
	Total Alkalinity Measurements as Oxygen in Na_2O			Hydride Hydrogen			Hydroxide Hydrogen			Total Hydrogen		
	Pre-operation	Post-operation	Change[b]	Preop-eration	Postop-eration	Change	Preop-eration	Postop-eration	Change	Pre-operation	Post-operation	Change
1. NaOH injection (15.05 g)	44.2	44.8	0.6	0.93	1.5	0.57	1.53	2.3	0.77	2.46	3.8	1.34
2. Cold trap	44.8	10.4	−34.4	1.5	0.33	−1.17	2.3	1.37	−0.93	3.8	1.7	−2.1
3. NaH injection[a] (9.03 g)	10.4	11.0	0.6	0.33	0.80	0.47	1.37	1.57	0.2	1.7	2.37	0.67
4. Cold trap	11	8.0	−3	0.8	0.33	−0.47	1.57	1.3	−0.27	2.37	1.63	−0.74
5. NaH injection (9.03 g)	8	10.0	2	0.33	1.13	0.8	1.3	1.67	0.37	1.63	2.8	1.17
6. Cold trap	10	6.2	−3.8	1.13	0.3	−0.8	1.67	1.03	−0.54	2.8	1.33	−1.34
7. NaOH injection (15.05 g)	6.2	19.8	13.6	0.3	0.8	0.5	1.03	1.7	0.67	1.33	2.5	1.17
8. Cold trap	19.8	7.2	−12.6	0.8	0.30	−0.5	1.7	1.1	−0.6	2.5	1.4	−1.1
9. NaOH injection (15.05 g)	7.2	[c]	[d]	0.3	[c]	[d]	1.1	[c]	[d]	1.4	[d]	[d]
10. Cold trap	[c]	5.8	[d]	[c]	0.2	[d]	[c]	0.8	[d]	[d]	1.0	[d]
11. NaH injection (9.03 g)	5.8	7.4	1.6	0.2	0.70	0.5	0.8	1.57	0.77	1.0	2.27	1.27
12. Cold trap	7.4	6.0	−1.4	0.7	0.30	−0.4	1.57	1.03	−0.54	2.27	1.33	−0.94
13. NaOH injection (15.05 g)	6.0	16.4	10.4	0.3	0.77	0.47	1.03	1.4	0.37	1.33	2.17	0.84
14. Cold trap	16.4	6.6	−9.8	0.77	0.3	−0.47	1.4	0.83	−0.57	2.17	1.13	−1.04

[a] Visual inspection of injection tube showed solids remaining.

[b] Using the average values from two sample tubes, one taken prior to and one taken following a loop operation, changes of less than 3.5 ppm at the approximate 10-ppm level are not statistically discernible.

[c] No sample taken.

[d] Sample not taken; therefore, change cannot be calculated.

TABLE 5. HISTORY OF UNC OXYGEN METERS IN APDA'S LOOP

APDA Cell No.	UNC Cell No.	Months of Sodium Service as of November 1, 1968	Comments
1	TP-15	41.5[a]	Removed on March 25, 1966; cleaned, inspected, and reinstalled. Responsive to radiation; responsive to both ambient temperature and sodium temperature changes.
2	TP-19	13	Removed on March 25, 1966; cleaned, inspected, and reinstalled; 5% to 10% increase in output. Less sensitivity to Na_2O concentration change as compared to response of TP-15 and TP-18.
	TPE-1/160	1.5	Did not function properly; output in range from 100 to 400 mV with hourly variation as large as 100 mV.
2B	TPE-1/227	17[a]	Slightly responsive to radiation; unpredictable response to successive Na_2O injections. Sensitive to ambient and sodium temperatures.
3	TP-17	13	Removed on March 15, 1966; cleaned and inspected; 5% to 10% increase in output. Very sensitive to ambient temperature change.
	TPE-1/161	1.5	Did not function properly; output in range from 100 to 400 mV with hourly variation as large as 100 mV.
	TPE-1/162	3	Did not function properly; 20- to 30-mV variation in one hour, and as much as 100-mV change in 24 days. Output in range from 800 to 900 mV.
	TPE-1/198	3	Erratic behavior; found probe broken upon removal.
3B	TPE-1/216	19[a]	Appears to have undergone a calibration shift. Low sodium temperature coefficient. No response to radiation; unpredictable response to successive Na_2O injections; normal ambient temperature coefficient.
4	TP-18	21	Removed on March 15, 1966; cleaned, inspected, and reinstalled. Appeared to become less sensitive to Na_2O concentration changes than had been experienced in earlier testing.
	TPE-1/19	2.5	Erratic behavior; no meaningful response.
4B	TPE-1/258	11[a]	Very responsive to chemistry changes, but not responsive to sodium temperature changes; not responsive to radiation.

[a] Still in sodium.

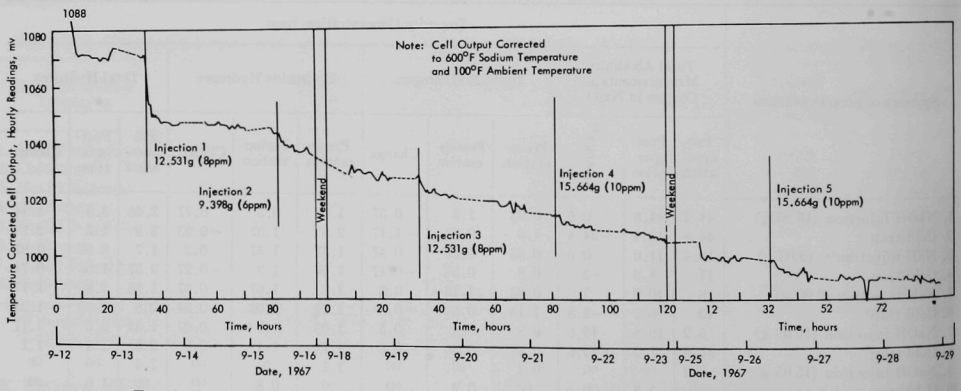

FIG. 3. Response of Oxygen Meter 1 (TP-15) to Five Successive Sodium Monoxide Injections.

nificantly lower than it had been previously (-27 V^{-1} compared to -36.8 V^{-1}). Oxygen meters 2B and 3B responded as expected, but only for the first three injections; they had essentially no response to the fourth and fifth injections. Calibration constants for these two meters over the range of oxygen concentrations where they appeared to be operating satisfactorily were -21.4 V^{-1} for oxygen meter 2B and -22.7 V^{-1} for oxygen meter 3B.

In Figure 10 is shown a calibration curve for oxygen meter 1 that was recently obtained while the loop was being used for a sampling and analysis program. During

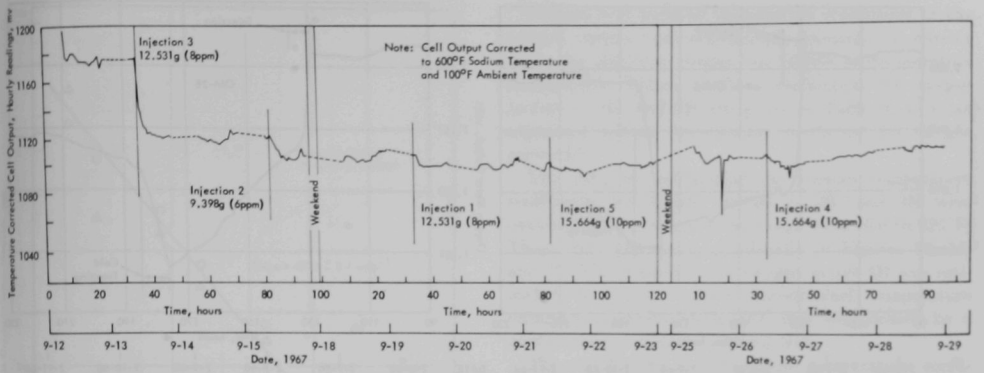

FIG. 4. Response of Oxygen Meter 2B (TPE-1/227) to Five Successive Sodium Monoxide Injections.

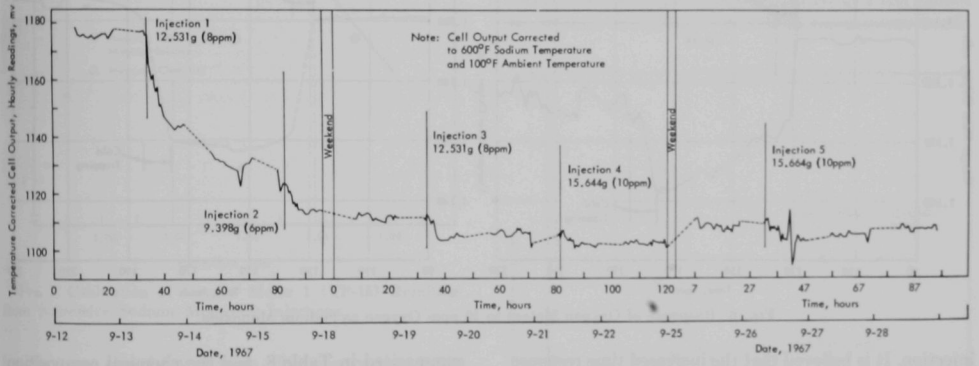

FIG. 5. Response of Oxygen Meter 3B (TPE-1/216) to Five Successive Sodium Monoxide Injections.

this same period, oxygen meters 3B and 4B were also in service, but zero drift in the electrometers (supplied to APDA by Keithley Instruments, Inc.) of the readout system for these meters was of such magnitude and frequency that the output could not be reliably interpreted.

Table 6 demonstrates the stability of the calibration of oxygen meter 1 over a long period of time. The only measure of the calibration constant significantly different from the rest was that obtained from the successive sodium monoxide injections 7, 8, 9, 10, and 11. Although this constant was obtained on the basis of calculated oxygen concentration rather than measured oxygen concentrations by the mercury amalgamation method, there was fair agreement between the two measures of oxygen concentration (see Figure 7). Therefore, the method used to obtain the calibration constant is not believed to be the reason for the difference between this measure of the constant and the other measures listed in Table 6.

Figure 6 shows the typical responses of oxygen meters 1, 2B, 3B, and 4B to a series of four replicate sodium monoxide injections to cold-trapped sodium. The results are presented here to point out the significance of the time response of the oxygen meter to sodium monoxide. At the time of this experiment, oxygen meters 1, 2B, 3B, and 4B were in service for approximately 33, 9, 10, and 2 mo, respectively. Since earlier experience indicated a solution rate of 1 ppm of oxygen per hour, it was anticipated that steady-state conditions would have been obtained 16 hr after the injections were started. Only oxygen meter 4B, however, displayed this behavior. Oxygen meters 1, 2B, and 3B drifted downward for as much as 40 hr following the

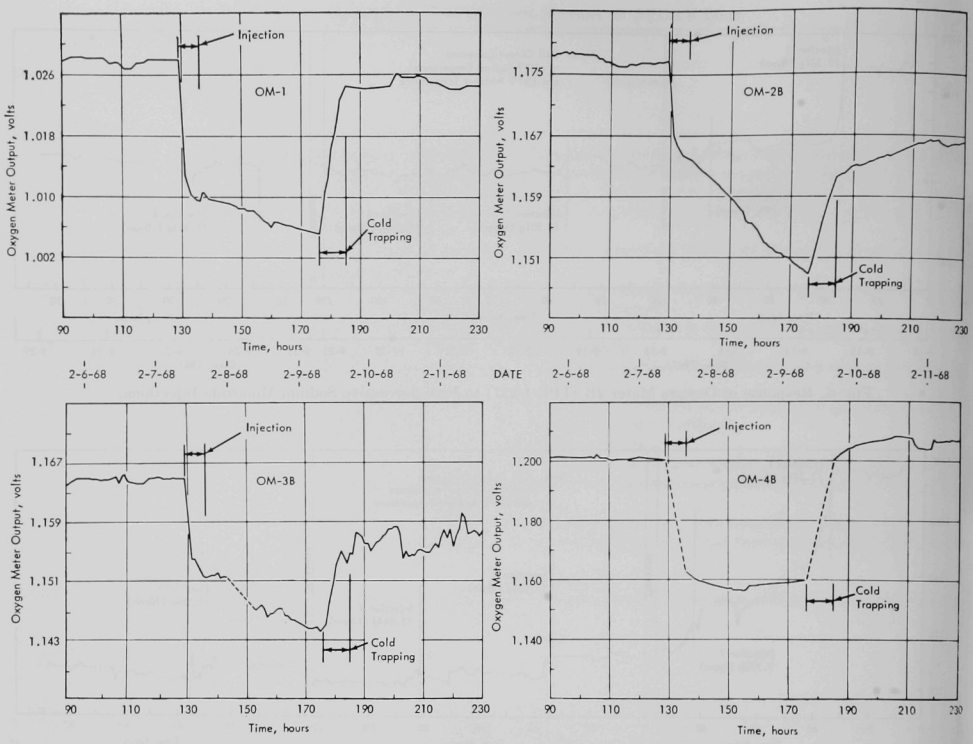

FIG. 6. Response of Oxygen Meters to 16 ppm Oxygen as Sodium Monoxide.

injection. It is believed that the increased time response was due to some aging phenomenon of the solid electrolyte in sodium.

Table 7 represents the extent of APDA experience with the response of the UNC oxygen meter to sodium hydride injections. These injections, equivalent to an increase in hydrogen of 1 ppm to cold-trapped sodium, were made to the loop at 600°F in the same manner as were the sodium monoxide injections. Response curves are shown in Figures 11 and 12, and the sampling and analysis results for the preinjection and postinjection periods for these tests are given in Table 4. It is clear from the data given in Table 7 that no conclusions can be made regarding the response of the oxygen meter to sodium hydride.

A typical response curve of a sodium hydroxide injection equivalent to 1 ppm hydrogen and 16 ppm oxygen is presented in Figure 13. Steady-state conditions were obtained about 10 hr after the injection was initiated. The results of four such injections are summarized in Table 8, and the chemical composition of the sodium for the preinjection and postinjection periods are given in Table 4. Only oxygen meters 1 and 3B were in service during these studies.

As given in Table 4, the first sodium hydroxide injection was made to sodium containing about 44 ppm oxygen. The remaining injections were made to cold-trapped sodium. Additional information from Rhometer response to sodium hydroxide injections 2, 3, and 4 support the conclusion that the sodium hydroxide completely decomposes to sodium monoxide and sodium hydride. These facts enable one to interpret the results given in Table 8. It is believed that because of the high contamination level which existed prior to the first injection, only a small amount of the sodium hydroxide decomposed. In the following three injections, however, all of the injected material appeared to have been converted to the monoxide and hydride.

It can be observed from Table 8 that the response of oxygen meter 3B is greater than that of oxygen meter 1

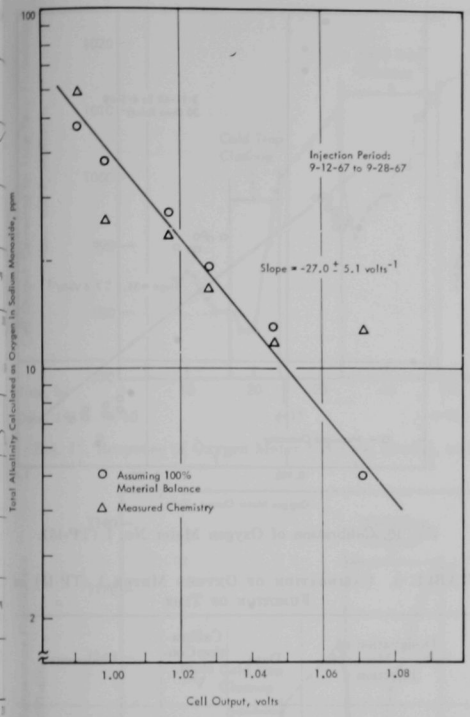

FIG. 7. Calibration of Oxygen Meter 1 (TP-15) Resulting from Successive Sodium Monoxide Injections.

for the same chemistry change. This observation leads to the conclusion, therefore, that oxygen meter 3B has a calibration constant algebraically larger than oxygen meter 1. By using the value -36.1 V^{-1} for oxygen meter 1, the value of the calibration constant for oxygen meter 3B is in the range from -19 to -25 V^{-1}.

The essence of the impurity injection results discussed in the preceding is as follows:

1. The oxygen meter responds to concentration changes in sodium monoxide in a quantitative and reproducible manner.

2. The calibration constant varies from electrode assembly to electrode assembly.

3. The time response of the cell increases with in-sodium service time.

4. The meter responds to sodium hydroxide impurity injections to sodium at 600°F.

5. The meter response to sodium hydride based on the data obtained thus far by APDA is inconclusive.

Sodium and ambient temperature coefficients of the oxygen meters were determined, primarily to remove from the observed output the effects of temperature fluctuations. Values of these coefficients for oxygen meters 1, 2B, and 3B are given in Table 9, as is an estimated sodium temperature coefficient for oxygen meter 4B.

The data for calculating the sodium temperature coefficients for oxygen meters 1, 2B, and 3B were obtained over a temperature range from 570 to 625°F. These data are shown graphically in Figures 14, 15, and 16. The coefficient for oxygen meter 4B was estimated from some minor uncontrolled temperature excursions approximating 10°F that were caused by a malfunction of a heater control unit.

The significance of the sodium temperature coefficients given in Table 9 is that the values change from cell to cell. Consequently, for those sodium systems in which sodium temperature fluctuations at a cell cannot be properly controlled, the sodium temperature coeffi-

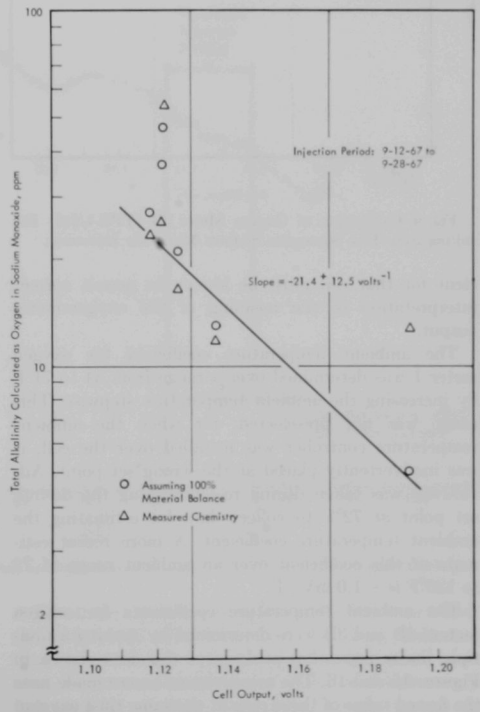

FIG. 8. Calibration of Oxygen Meter 2B (TPE-1/227) Resulting from Five Successive Sodium Monoxide Injections.

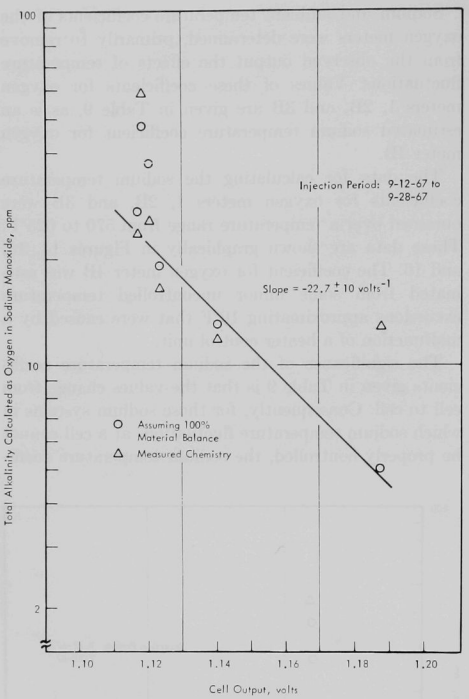

FIG. 9. Calibration of Oxygen Meter 3B (TPE-1/216) Resulting from Five Successive Sodium Monoxide Injections.

cient for that cell must be known to permit correct interpretation of the meaning of the oxygen-meter output.

The ambient temperature coefficient for oxygen meter 1 was determined over a range from 34 to 71°F by increasing the ambient temperature stepwise. This range was not preselected, for when the ambient temperature controller was installed over the cell, it was inadvertently placed at the wrong set point. Advantage was taken during re-establishing the desired set point at 72°F to collect data for estimating the ambient temperature coefficient. A more recent estimate of this coefficient over an ambient range of 72 to 130°F is −1.0 mV/°F.

The ambient temperature coefficients for oxygen meters 2B and 3B were determined by making a multiple linear regression analysis of the data shown in Figures 15 and 16. The measurements were made near the finned tubes of these cells at the same time oxygen-meter output and sodium temperature were being measured. Ambient-temperature controllers were not used to enclose the meters during the evaluation.

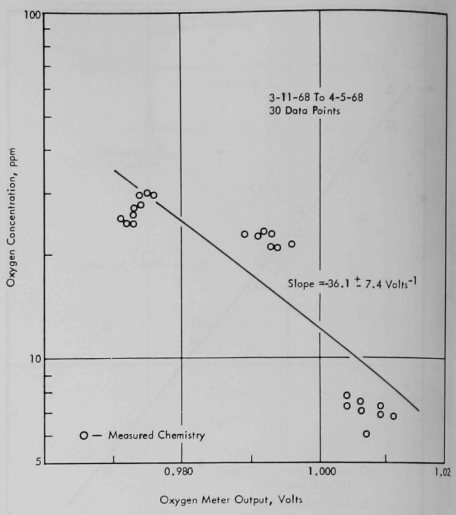

FIG. 10. Calibration of Oxygen Meter No. 1 (TP-15).

TABLE 6. CALIBRATION OF OXYGEN METER 1 (TP-15) AS FUNCTION OF TIME

Designation of Sodium Monoxide Injection	Date	Calibration Constant, V^{-1}	Comments
1	4/27/66	−36.8	Based on measured chemistry
5	1/30/67	−40.4	Based on measured chemistry
6	2/3/67	−40.0	Based on measured chemistry
7, 8, 9, 10, 11	9/12/67 to 9/28/67	−27.0	Based on calculated chemistry
Sampling and analysis program	3/11/68 to 4/5/68	−36.1	Based on measured chemistry

TABLE 7. RESPONSE OF OXYGEN METER TO SODIUM HYDRIDE INJECTIONS

Injection		Ambient-corrected Response of Oxygen Meter		Change in Total Hydrogen, ppm
No.	Date	OM-1, mV	OM-3B, mV	
1	2/24/67	+1	[b]	+0.67
2	3/10/67	0	[b]	+1.17
3[a]	4/13/67	+19	−7	+1.27

[a] Third injection had an ambient temperature change of 26°F.

[b] Not installed.

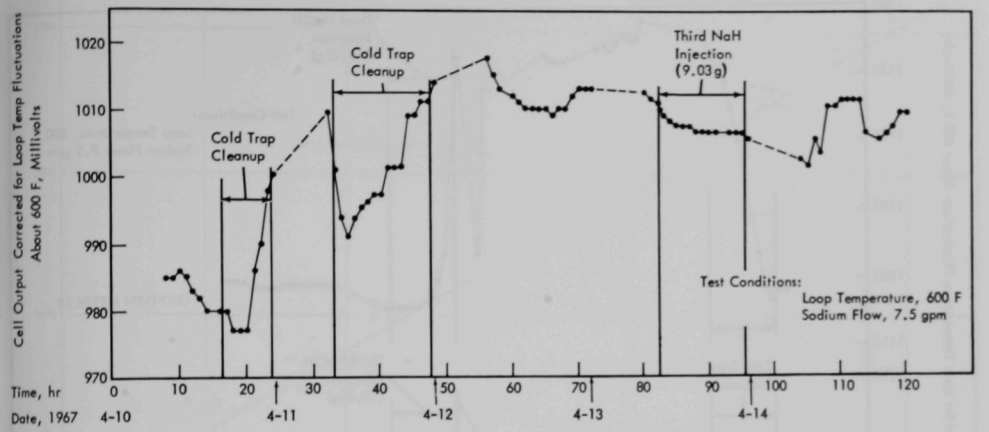

FIG. 11. Response of Oxygen Meter 1 Before, During, and After an Injection of Sodium Hydride to Cold-trapped Sodium.

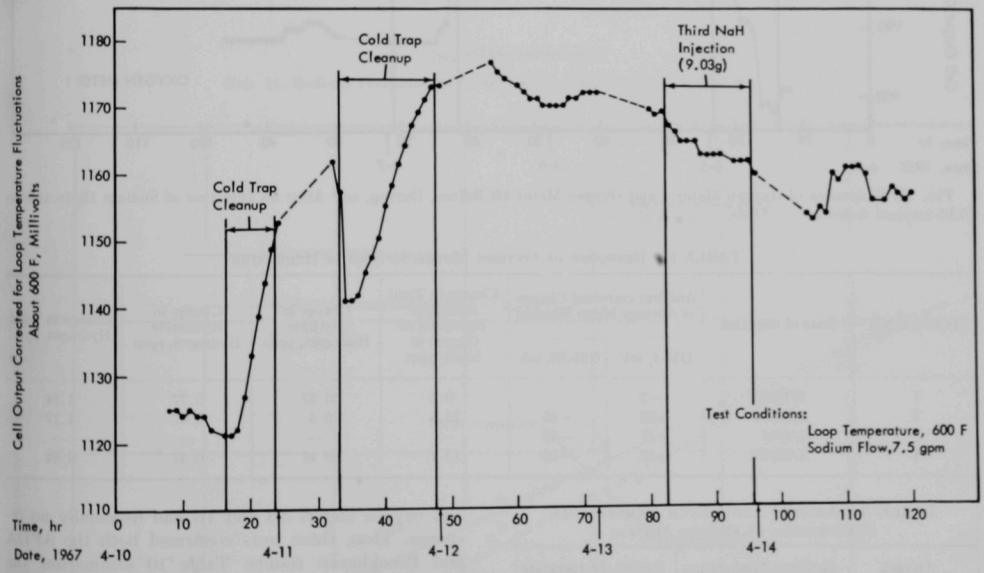

FIG. 12. Response of Oxygen Meter 3B Before, During, and After an Injection of Sodium Hydride to Cold-trapped Sodium.

As can be seen from the data presented, ambient-temperature fluctuations can affect oxygen-meter output significantly. APDA has chosen to eliminate this effect by housing the oxygen meters in a unit that provides an ambient-temperature-controlled environment.

Gamma-radiation tests with the setup shown in Figure 17 were conducted to determine cell response to radioactivity. Earlier test made by APDA,[1] in which an iridium-192 (28-Ci) source was used, indicated that oxygen meter 1 does respond to radiation; however, recent tests at Brookhaven National Laboratory indicated no response from their oxygen meters to radiation. To check these contradictory results, APDA subjected all four oxygen-meter cells now installed in the loop to radiation from iridium-192 (73 Ci) and

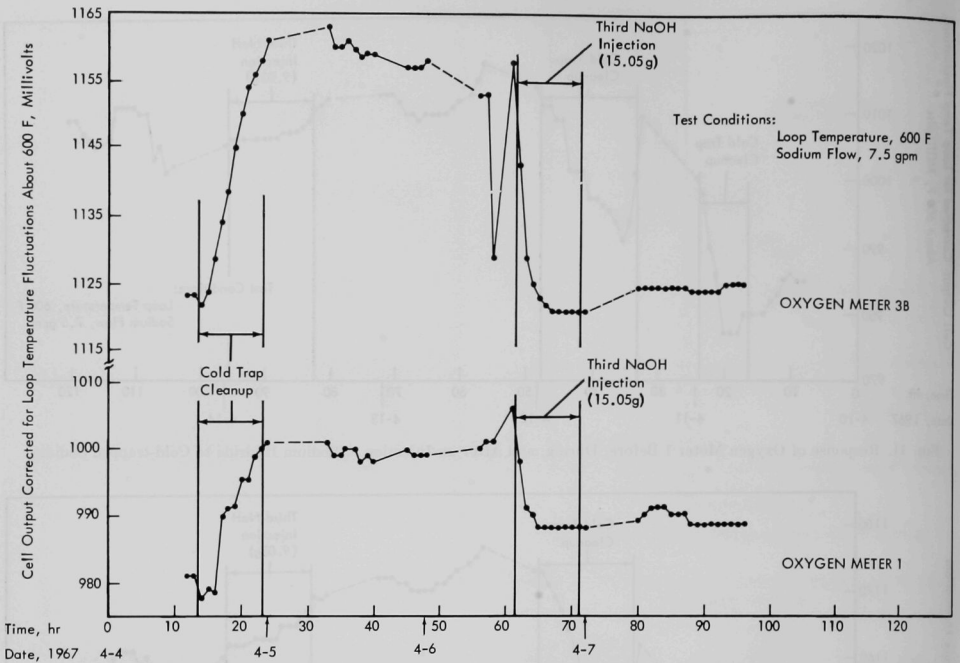

FIG. 13. Responses of Oxygen Meter 1 and Oxygen Meter 3B Before, During, and After an Injection of Sodium Hydroxide to Cold-trapped Sodium.

TABLE 8. RESPONSE OF OXYGEN METER TO SODIUM HYDROXIDE

Injection No.	Date of Injection	Ambient-corrected Change in Average Meter Reading		Change in Total Alkalinity Expressed as Oxygen in Na_2O, ppm	Change in Hydride Hydrogen, ppm	Change in Hydroxide Hydrogen, ppm	Change in Total Hydrogen, ppm
		OM-1, mV	OM-3B, mV				
1	2/15/67	−2	—	0.6	0.57	0.77	1.34
2	3/30/67	−29	−45	13.6	0.5	0.67	1.17
3	4/6/67	−17	−38	—	—	—	—
4	4/20/67	−36	−52	10.4	0.47	0.37	0.84

TABLE 9. AMBIENT AND SODIUM TEMPERATURE COEFFICIENTS OF OXYGEN METERS

Oxygen Meter	Ambient Temperature Coefficient, mV/°F	Sodium Temperature Coefficient, mV/°F
OM-1	−0.82	+0.56 ± 0.02
OM-2B	−0.52	+0.53 ± 0.02
OM-3B	−0.40	+0.29 ± 0.03
OM-4B	Not measured	Estimated at +0.04

cobalt-60 (12 Ci) sources. Again, as in the earlier APDA tests, oxygen meter 1 responded to radiation. Oxygen meter 2B responded only slightly, however, and oxygen meters 3B and 4B had essentially no response. Thus, these tests confirmed both the APDA and Brookhaven results. Table 10 summarizes the results of APDA's radiation tests.

By coincidence, or as an incidental result of the tests, the output of oxygen meter 2B began to drift upscale after exposure to radiation. The total drift for a period of about 180 hr after the test is shown in Figure 18.

4. Plugging Meter

The reliability of plugging-temperature measurements taken with APDA's variable-orifice plugging meter was studied from three standpoints: interpretive

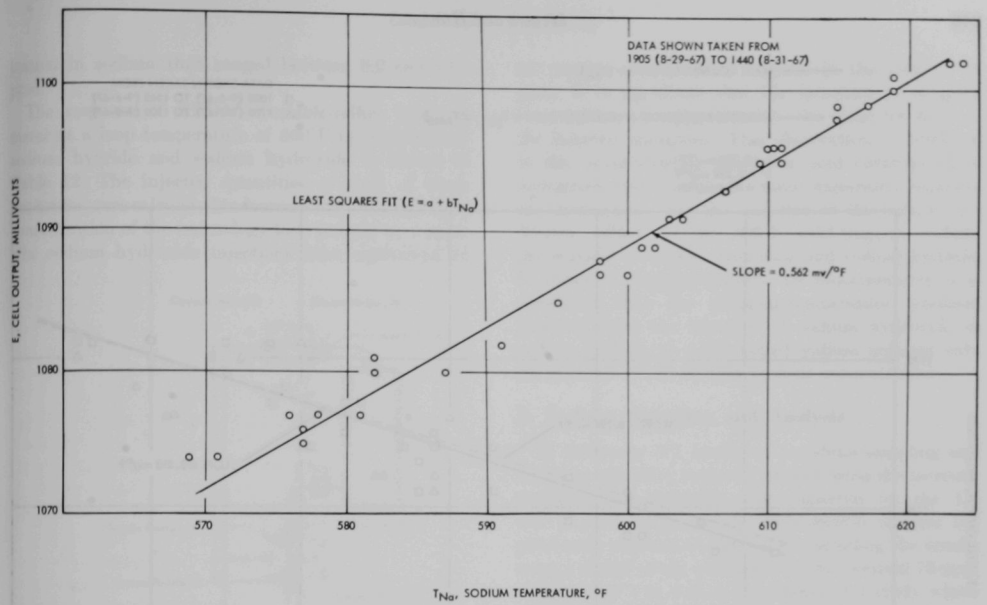

FIG. 14. Sodium Temperature Coefficient for Oxygen Meter 1 (TP-15).

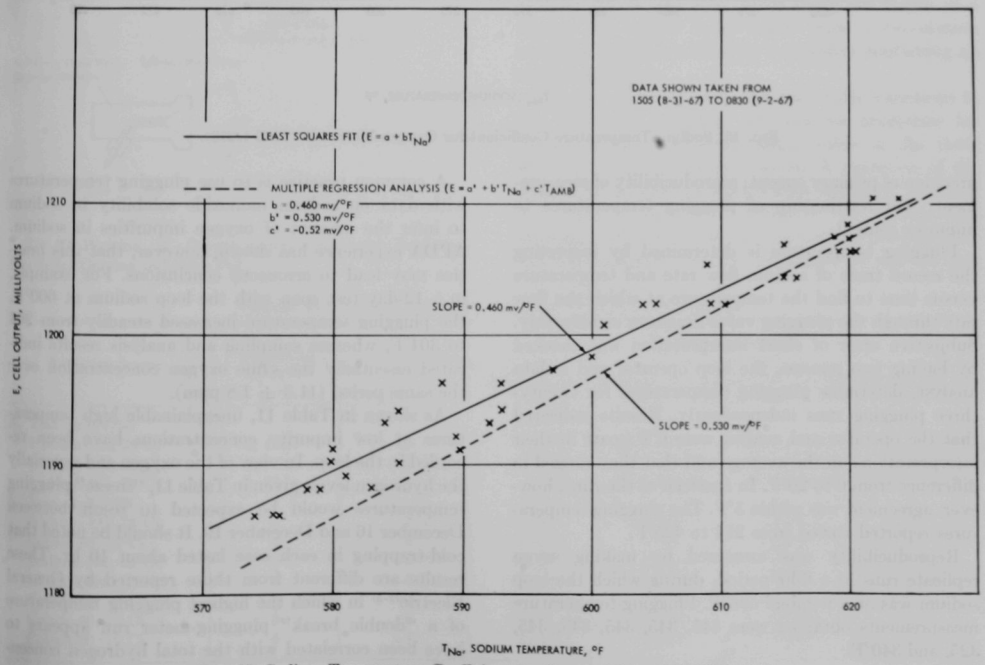

FIG. 15. Sodium Temperature Coefficient for Oxygen Meter 2B (TPE-1/227).

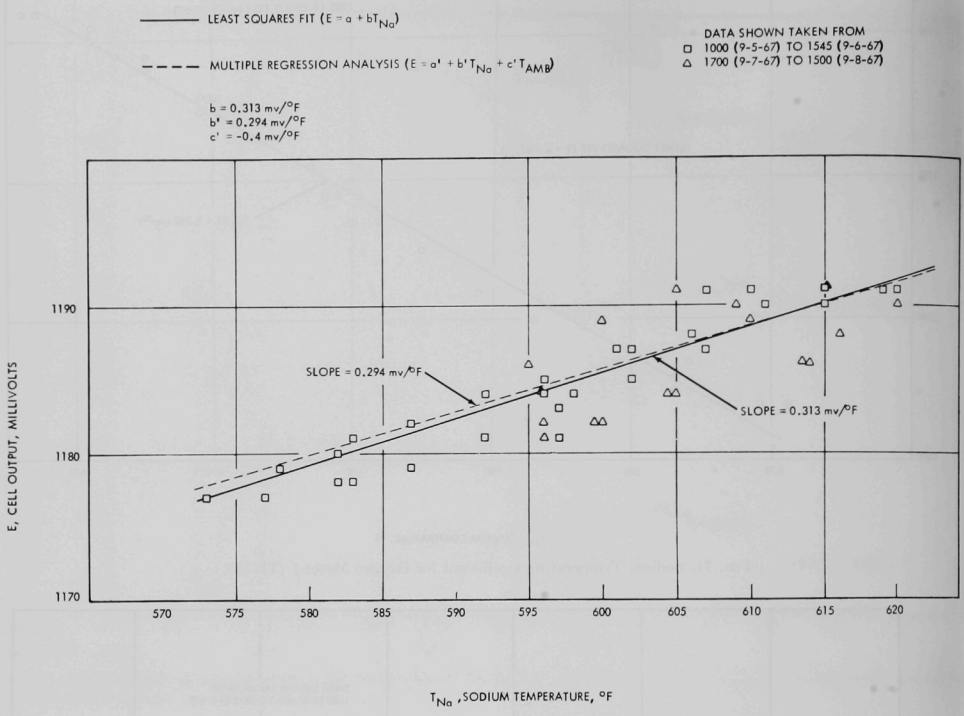

FIG. 16. Sodium Temperature Coefficient for Oxygen Meter 3B (TPE-1/216).

precision of primary output; reproducibility of measurement; and relationship of plugging temperatures to impurity content.

Plugging temperature is determined by inspecting the record trace of sodium flow rate and temperature versus time to find the temperature at which the flow rate through the plugging valve decreases significantly. Subjective error of chart interpretation was checked by having two persons, the loop operator and a data analyst, determine plugging temperatures for twenty-three plugging runs independently. Results indicated that the operator and analyst were 6°F apart in their interpretations on the average and that they ranged in difference from 0 to 20°F. In fourteen of the runs, however, agreement was within 5°F. The plugging temperatures reported varied from 214 to 425°F.

Reproducibility was measured by making seven replicate runs in a 6-hr period, during which the loop sodium was at a nominal 565°F. Plugging-temperature measurements obtained were 345, 345, 345, 343, 345, 325, and 340°F.

A common practice is to use plugging temperatures with data on sodium monoxide solubility in sodium to infer the amount of oxygen impurities in sodium. APDA experience has shown, however, that this practice may lead to erroneous conclusions. For example, in a 12-day test span with the loop sodium at 600°F, the plugging temperature increased steadily from 264 to 304°F, whereas sampling and analysis results indicated essentially the same oxygen concentration over the same period (11.3 ± 1.8 ppm).

As shown in Table 11, unexplainable high temperatures at low impurity concentrations have been recorded in the loop. In view of the oxygen and especially the hydrogen levels given in Table 11, "freeze" plugging temperatures would be expected to result between December 16 and December 19. It should be noted that cold-trapping in each case lasted about 10 hr. These results are different from those reported by General Electric[2-5] in which the highest plugging temperature of a "double break" plugging-meter run appears to have been correlated with the total hydrogen concen-

tration in sodium that ranged between 6.2 and 15.5 ppm.

The response of APDA's variable-orifice plugging meter at a loop temperature of 600°F to injections of sodium hydride and sodium hydroxide is shown in Table 12. The injected quantities of each of these impurities were calculated to increase the total hydrogen concentration of the technology loop sodium by 1 ppm. The sodium hydroxide injections were equivalent to an oxygen concentration increase in the loop of 16 ppm. It is significant that the increases in plugging temperature are approximately the same for both of the injected impurities. This observation, in addition to the oxygen-meter, Rhometer, and cover-gas-chromatograph responses to the same impurities, supports the assumption that the majority of the sodium hydroxide added to the 600°F cold-trapped sodium decomposed to sodium monoxide and sodium hydride. In terms of plugging-temperature measurements, it is concluded that the plugging-temperature increases resulting from the injection of sodium hydroxide or sodium hydride to cold-trapped sodium indicate only the increase in the sodium hydride concentration.

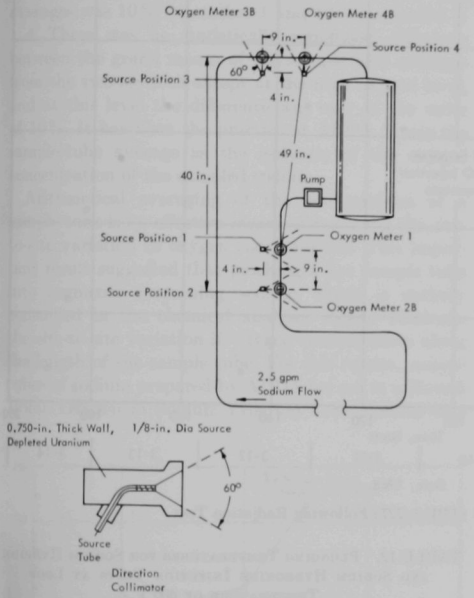

FIG. 17. Position of Oxygen-meter Cells and Radiation Source for Gamma-radiation Test.

5. Sodium Sampling and Analysis

In Reference (1), results of a sodium-sampling and -analysis reliability study for oxygen using the mercury amalgamation procedure were reported for the 11- and 47-ppm oxygen levels. This section updates the previously reported evaluation by including the results from a similar study conducted at the nominal 76-ppm oxygen level[6] as well as the results of a study which compares hot-pinched sample tubes to nonpinched sample tubes. In all of the investigations, multiple-site analyses for oxygen were made along the length of a number of sample tubes taken from a two-station sampling facility enclosed by a glovebox containing an inert atmosphere.

Figures 19 and 20 show the site-to-site variations in the combined sampling and analysis procedure for oxygen using nonpinched sample tubes at the three levels of oxygen mentioned above. A reduction of the same data in terms of sample-tube averages, standard and relative standard deviations for sample-tube averages, and individual site analyses are presented for the two sampling stations in Tables 13 and 14 (see

TABLE 10. GAMMA-RADIATION TESTS OF UNC OXYGEN METERS

Radiation Source	Position of Source	Exposure Time, min	Response to Radiation			
			OM-1, max mV	OM-2B, max mV	OM-3B, max mV	OM-4B, max mV
A. Test on 6/7/66						
Iridium-192, 28 Ci	1, 4 in.	5	−24.0	Not tested	Not tested	Not tested
Iridium-192, 28 Ci	1, 8 in.	5	−13.8	Not tested	Not tested	Not tested
Iridium-192, 28 Ci	1, 12 in.	5	−7.9	Not tested	Not tested	Not tested
B. Test on 3/7/68						
Iridium-192, 73 Ci	1	2	~−50	None	None	None
Cobalt-60, 12 Ci	2	5	−18.2	−1.7	None	None
Iridium-192, 73 Ci	3	5	None	None	None	None
Iridium-192, 73 Ci	4	5	None	None	None	None
Cobalt-60, 12 Ci	2	60	−31.5	−1.05	None	None
Cobalt-60, 12 Ci	3	5	None	None	−0.25	None
Cobalt-60, 12 Ci	4	5	None	None	None	−0.10

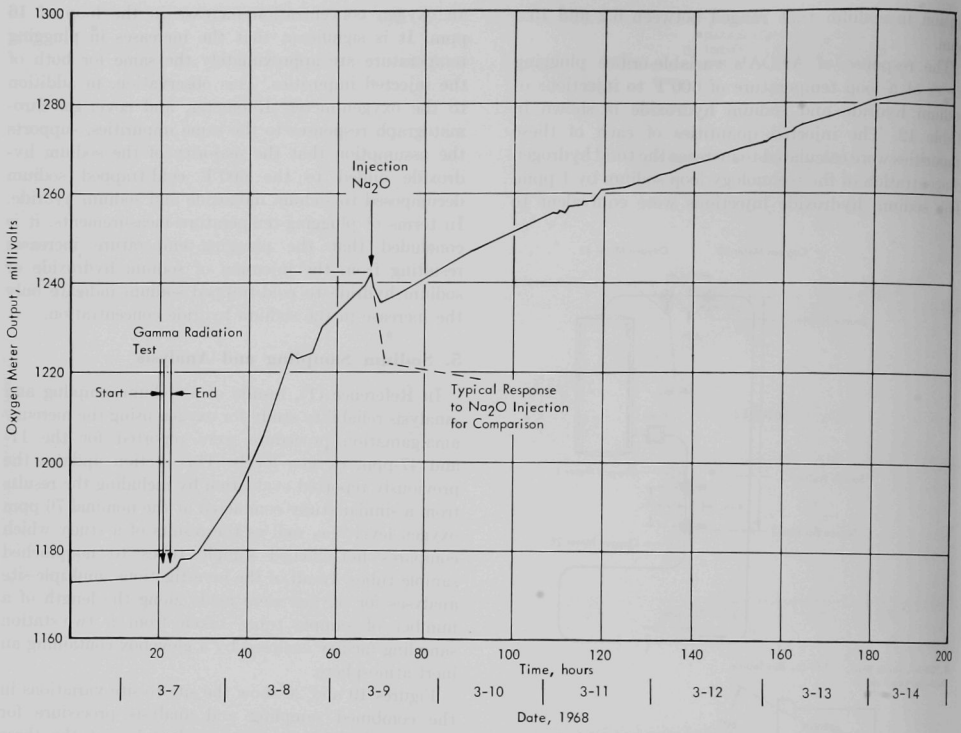

FIG. 18. Upscale Drift of Oxygen Meter 2B (TPE-1/227) Following Radiation Test.

TABLE 11. HIGH PLUGGING TEMPERATURES IN SODIUM TECHNOLOGY LOOP AT LOW IMPURITY

Date	Loop Temp, °F	Plugging Temp, °F	Oxygen Conc, ppm	Hydride Hydrogen, ppm	Hydroxide Hydrogen, ppm	Total Hydrogen, ppm
12-9-66	898	573, 577	35	2.4	1.7	4.1
12-12-66	897	577	27	3.1	1.5	4.6
12-13-66	898	—	Cold-trapping operation			
12-14-66	898	450, 490	—	—	—	—
12-15-66	883	510	10	1.0	1.5	2.5
12-16-66	895	529	—	—	—	—
12-16-66	895		Cold-trapping operation			
12-16-66	895	325, 335	5	0.7	1.4	2.1
12-19-66	879	518, 516	—	—	—	—
12-19-66	879		Cold-trapping operation			
12-19-66	879	310	5	0.4	1.2	1.6
12-20-66	875	492, 490	7	0.2	1.3	1.5
12-21-66	825	508	6	0.3	1.2	1.5
12-22-66	—	520	—	—	—	—

TABLE 12. PLUGGING TEMPERATURES FOR SODIUM HYDRIDE AND SODIUM HYDROXIDE INJECTION TESTS AT LOOP TEMPERATURE OF 600°F

Injection Test[a]	Date of Injection	Preinjection Plugging Temperature, °F	Postinjection Plugging Temperature, °F
1. NaOH	2-15-67	412	417
2. NaH	2-24-67	227	352
3. NaH	3-10-67	284	380
4. NaOH	3-30-67	223	350
5. NaOH	4-6-67	[b]	350
6. NaH	4-13-67	[b]	365
7. NaOH	4-20-67	224	365

[a] For each injection test, 15.05 g NaOH or 9.03 g NaH were added to the technology loop. Either amount is equivalent to a 1-ppm increase in the total hydrogen concentration of the loop.
[b] No plugging temperatures taken.

References (6), (7), and (8) for more detailed statistical data). From this study it was found that for nonpinched tubes:

1. A statistically significant site-to-site variation existed for all three oxygen concentration levels at

sampling station 1. The maximum difference between site averages was 26%, 17% and 71% for the low, medium, and high oxygen levels, respectively.

2. A statistically significant site-to-site variation occurred only at the 72.5-ppm oxygen level at sampling station 2. The maximum difference in site averages amounted to 30%.

3. A statistically significant difference among sample-tube averages from each station exists only at the high oxygen level. The maximum difference between tube averages was 10% for station 1 and 12% for station 2.

4. There was no statistically significant difference between the grand means of the sample-tube averages from the two stations except at the high oxygen level, and at this level the difference was only of the order of 10%. It has been the practice at APDA to use the sample-tube average as the estimate of the oxygen concentration of the sampled sodium.

Arithmetical averaging of the site analyses of a sample tube is an effective means of removing the site-to-site variation in oxygen concentration. This important result suggested that pinching a hot sample tube into segments containing sodium which is entirely consumed in the chemical analyses should eliminate the site-to-site variation in oxygen concentration along the length of the sample tube. For this reason, sample tubes of sodium prepared by APDA for use in a Round Robin Oxygen in Sodium Program were pinched into

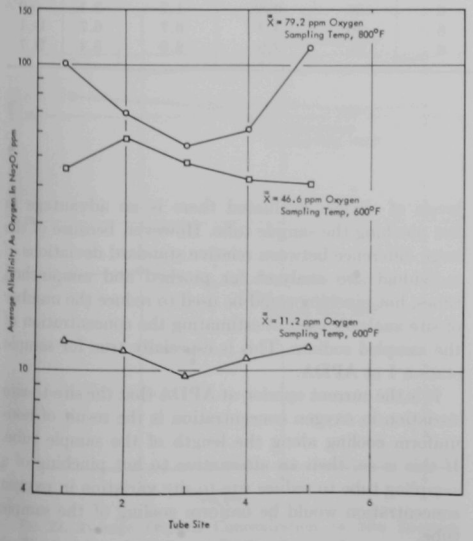

FIG. 19. Average Oxygen Concentration *vs* Site Location for Nonpinched Sample Tubes at Station 1.

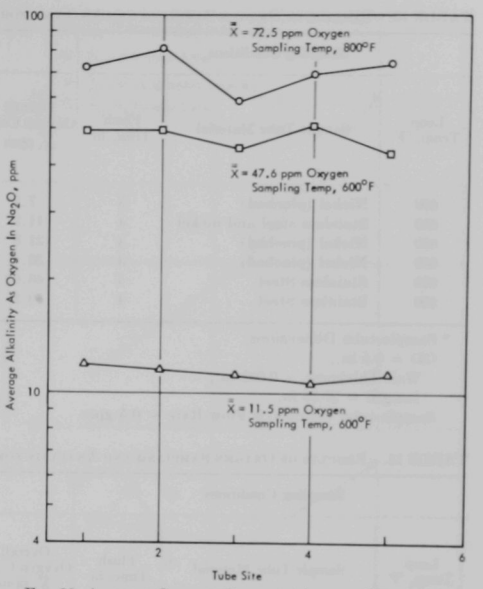

FIG. 20. Average Oxygen Concentration *vs* Site Location for Nonpinched Sample Tubes at Station 2.

six segments while hot (see Reference (9) for more detailed discussion of the preparation procedure).

Figures 21 and 22 show the site-to-site variation in the combined sampling and analysis procedure for oxygen using hot-pinched sample tubes. Tables 13 and 14 contain the same data for pinched sample tubes as mentioned previously for nonpinched sample tubes. (See Reference (6) for a tabulation of the individual site analyses.) From these data it was concluded that:

1. A statistically significant site-to-site variation exists at both sample stations at the nominal 30-ppm oxygen level. The maximum difference between site averages was 15% for station 1 and 11% for station 2. There was no statistically significant difference among site locations for either station at the other two oxygen levels.

2. A statistically significant difference exists among sample tube averages at station 2 for each of the three oxygen levels. The maximum difference between sample tube averages at station 2 was 14%, 15%, and 9% for the nominal 7-, 20-, and 30-ppm oxygen levels, respectively.

3. A statistically significant difference among sample tube averages for station 1 exists only at the nominal 20-ppm oxygen level. The maximum difference between sample tube averages for station 1 at this oxygen level was 15%.

TABLE 13. RESULTS OF OXYGEN SAMPLING AND ANALYSIS FOR PINCHED AND NONPINCHED SAMPLE TUBES* FROM SAMPLE STATION 1

Sampling Conditions			Sample Station 1						
Loop Temp, °F	Sample Tube Material	Flush Time, hr	Overall Oxygen Conc $\bar{\bar{X}}$, ppm	No. of Sample Tubes	Total No. of Analyses	Standard Deviation in Sample-tube Averages, $S_{\bar{X}}$, ppm	Standard Deviation in Individual Analyses, S_X, ppm	Relative Standard Deviation, %	
								$S_{\bar{X}}/\bar{\bar{X}}$	$S_X/\bar{\bar{X}}$
600	Nickel (pinched)	3	7.2	6	36	0.20	0.47	2.8	6.5
600	Stainless steel and nickel	4	11.2	5	25	0.49	1.5	4.4	13.4
600	Nickel (pinched)	3	21.8	8	47	1.4	1.8	6.4	8.3
600	Nickel (pinched)	3	30.4	5	29	0.51	1.8	1.7	5.9
600	Stainless Steel	4	46.6	8	40	1.3	9.2	2.8	19.8
800	Stainless Steel	4	79.2	6	30	6.2	23.9	7.8	30.2

* Sample-tube Dimensions:
OD = 0.5 in.;
Wall Thickness = 0.035 in.;
Length = 27.75 in.
Sample-tube Volumetric Flow Rate = 0.5 gpm

TABLE 14. RESULTS OF OXYGEN SAMPLING AND ANALYSIS FOR PINCHED AND NONPINCHED SAMPLE TUBES FROM SAMPLE STATION 2

Sampling Conditions			Sample Station 2						
Loop Temp, °F	Sample Tube Material	Flush Time, hr	Overall Oxygen Conc $\bar{\bar{X}}$, ppm	No. of Sample Tubes	Total No. of Analyses	Standard Deviation in Sample-tube Averages, $S_{\bar{X}}$, ppm	Standard Deviation in Individual Analyses, S_X, ppm	Relative Standard Deviation, %	
								$S_{\bar{X}}/\bar{\bar{X}}$	$S_X/\bar{\bar{X}}$
600	Nickel (pinched)	3	7.3	5	28	0.36	0.54	4.9	8.4
600	Stainless steel and nickel	4	11.5	4	20	0.42	0.86	3.7	7.5
600	Nickel (pinched)	3	21.8	8	47	1.1	1.8	5.0	8.3
600	Nickel (pinched)	3	28.4	6	36	0.88	1.7	3.1	6.0
600	Stainless steel	4	47.6	8	40	3.2	6.7	6.7	14.1
800	Stainless steel	4	72.5	6	31	3.9	8.5	5.4	11.7

* Sample-tube Dimensions:
OD = 0.5 in.;
Wall Thickness = 0.035 in.;
Length = 35.5 in.
Sample-tube Volumetric Flow Rate = 0.5 gpm

4. There was no statistically significant difference between the grand means of the sample-tube averages from the two stations except at the nominal 30-ppm oxygen level, and at this level the difference was only 7%.

5. The relative standard deviation of individual site analyses is much smaller for pinched tubes than for nonpinched tubes at both sampling stations (refer to Figures 23 and 24 and to Tables 13 and 14).

6. The relative standard deviations for sample tube averages are similar for both pinched and nonpinched sampling tubes.

If sample-tube averages computed from at least five individual site analyses are used to estimate the oxygen concentration of the sampled sodium, then for the levels of oxygen evaluated there is no advantage in hot pinching the sample tube. However, because of the large difference between relative standard deviations of individual site analyses for pinched and nonpinched tubes, hot pinching could be used to reduce the number of site analyses used in estimating the concentration of the sampled sodium. This is especially true for sample station 1 at APDA.

It is the current opinion at APDA that the site-to-site variation in oxygen concentration is the result of nonuniform cooling along the length of the sample tube. If this is so, then an alternative to hot pinching of a sampling tube to reduce site-to-site variation in oxygen concentration would be uniform cooling of the sample tube.

6. Gas Chromatograph

In late 1966, APDA installed a Thermco gas chromatograph to analyze the cover gas from the loop surge tank. Although mechanical problems prevented

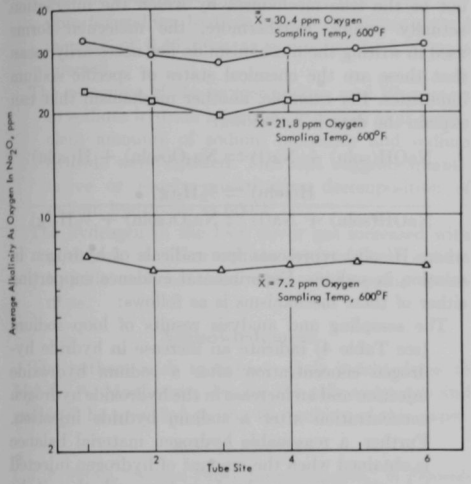

FIG. 21. Average Oxygen Concentration *vs* Site Location for Pinched Sample Tubes at Station 1.

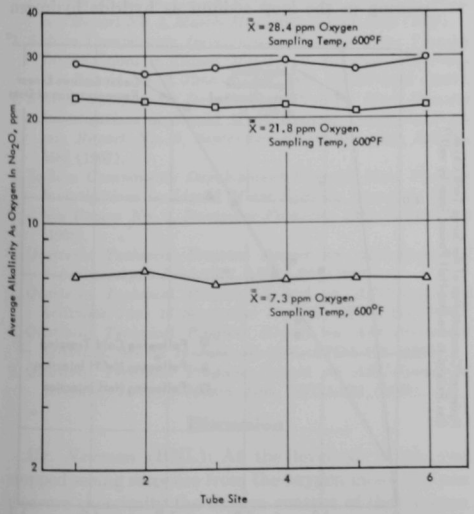

FIG. 22. Average Oxygen Concentration *vs* Site Location for Pinched Sample Tubes at Station 2.

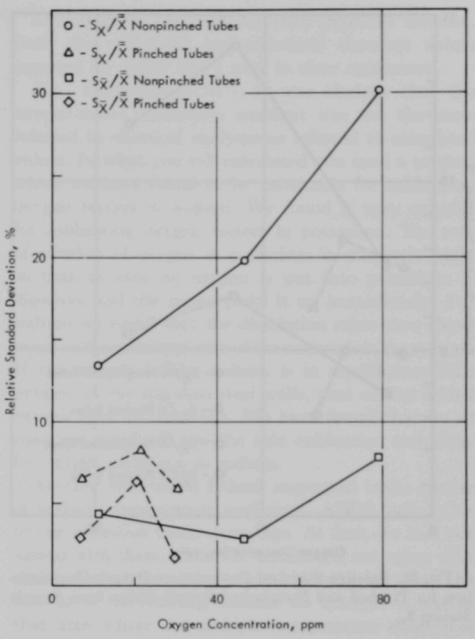

FIG. 23. Relative Standard Deviation *vs* Oxygen Concentration for Pinched and Nonpinched Sample Tubes from Sample Station 1.

the taking of hydrogen-concentration readings for all tests, data available from those tests in which the chromatograph was functioning indicated that hydrogen concentration increased with individual injections of both sodium hydroxide and sodium hydride. Cold-trapping operations subsequent to the injections, however, resulted in a decrease in hydrogen concentration in the cover gas.

Theoretical considerations indicate that the partitioning of hydrogen between the loop sodium and the cover gas should depend on the concentration of hydrogen in sodium, that is, either

$$NaH(soln) \rightleftharpoons Na(l) + \tfrac{1}{2}H_2(g)$$

or

$$H(soln) \rightleftharpoons \tfrac{1}{2}H_2(g),$$

depending on the form of hydrogen in solution; H(soln) represents free radicals of hydrogen in solution in sodium. For these relationships, the equilibrium constant expressed in ppm concentration units can be written as

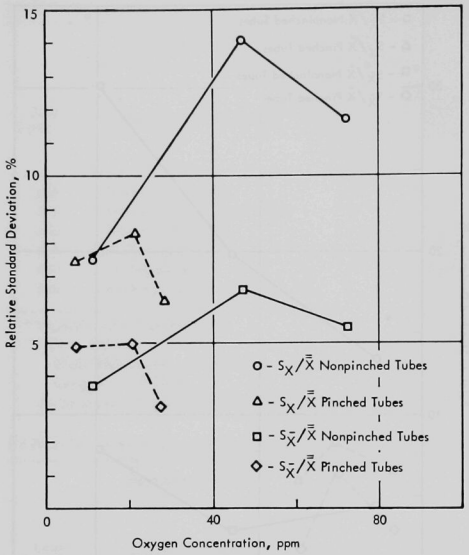

FIG. 24. Relative Standard Deviation *vs* Oxygen Concentration for Pinched and Nonpinched Sample Tubes from Sample Station 2.

$$\frac{C_{Na(l)}C^{\frac{1}{2}}_{H_2(g)}}{C_{H(soln)}} = K.$$

Since $C_{Na(l)}$ in ppm is approximately unity, the relationship becomes

$$C^{\frac{1}{2}}_{H_2(g)} = KC_{H(soln)},$$

where $C_{H_2(g)}$ is the cover-gas hydrogen concentration, ppm by volume, and $C_{H(soln)}$ the hydrogen concentration in sodium, ppm by weight.

A comparison of laboratory and loop hydrogen-equilibrium data is shown in Figure 25. According to the preceding relationship, the loop data should be correlated in a straight line passing through the origin. Although the line shown does not pass through the origin, a statistical evaluation indicated that the small nonzero intercept is not significant. The large difference between the data obtained in the laboratory and that obtained from the loop is believed to be attributable to hydrogen gettering in the sampling lines of the chromatograph by sodium vapor.

In addition to these gas-chromatograph readings, the discussed Rhometer responses, oxygen-meter responses, plugging-temperature measurements, and sampling and analysis results, as well as thermodynamic considerations, all indicate that chemical interaction occurs when sodium hydroxide is added to 600°F loop sodium. One mechanism that explains these data is as follows:

$$NaOH(soln) + 2Na(l) \leftrightharpoons Na_2O(soln) + NaH(soln)$$

$$NaH(soln) \leftrightharpoons Na(l) + \tfrac{1}{2}H_2(g)$$

$$NaOH(soln) + Na(l) \leftrightharpoons Na_2O(soln) + \tfrac{1}{2}H_2(g)$$

Although this mechanism correlates data, it may not be the true mechanism by which the interaction actually occurs. Furthermore, the molecular forms used in writing the mechanism do not necessarily mean that these are the chemical states of specific sodium impurities. For example, another mechanism that can explain the data is as follows:

$$NaOH(soln) + Na(l) \leftrightharpoons Na_2O(soln) + H(soln)$$

$$H(soln) \leftrightharpoons \tfrac{1}{2}H_2(g)$$

$$NaOH(soln) + Na(l) \leftrightharpoons Na_2O(soln) + \tfrac{1}{2}H_2(g)$$

where H(soln) represents free radicals of hydrogen in solution in sodium. Experimental evidence supporting either of these mechanisms is as follows:

The sampling and analysis results of loop sodium (see Table 4) indicate an increase in hydride hydrogen concentration after a sodium hydroxide injection and an increase in the hydroxide hydrogen concentration after a sodium hydride injection. Further, a reasonable hydrogen material balance is obtained when the amount of hydrogen injected into the sodium technology loop, whether it be in the form of sodium hydroxide or sodium hydride, is compared to the total amount of hydrogen appearing in the loop sodium as hydride hydrogen

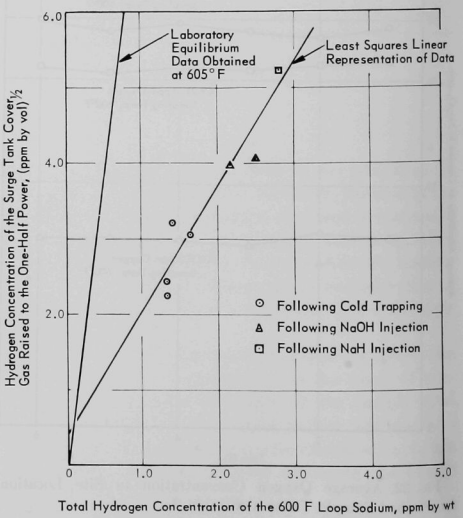

FIG. 25. Comparison of Laboratory and Loop Hydrogen-equilibrium Data.

and hydroxide hydrogen. In both sodium hydroxide and sodium hydride injections, for example, the amount of hydrogen injected was 1 ppm for each impurity. The sampling and analysis results for total hydrogen were 1.34, 1.17, and 0.84 ppm for sodium hydroxide injections and 0.67, 1.17, 1.27 ppm for sodium hydride injections, giving a total increase of 6.46 ppm as compared to 6.00 ppm injected.

The responses of the oxygen meters and Rhometers to sodium hydride injections correlate as if equivalent amounts of sodium monoxide and sodium hydride were injected. This fact suggests quantitative or nearly quantitative decomposition of sodium hydroxide at 600°F.

The hydrogen in the loop cover gas increased with injections of either sodium hydroxide or sodium hydride and decreased with cold-trapping operations.

Acknowledgment

The authors wish to express their indebtedness to Mr. W. A. MacLaurin, Jr., for the able assistance and guidance he provided during the writing of this paper.

REFERENCES

1. J. P. Petrek, "Sodium-Purity Instrumentation," in *Proceedings of the Symposium on Liquid Metal Instrumentation and Control*, ANL-7380 (1967).
2. *Sodium Components Development Program Mass Transfer Investigations in Liquid Metal Systems, Quarterly Progress Report No. 1, March–May, 1967*, GEAP-5508 (1967).
3. *Sodium Components Development Program Mass Transfer Investigations in Liquid Metal Systems, Quarterly Progress Report No. 2, June–August, 1967*, GEAP-5546 (1967).
4. *Sodium Components Development Program Mass Transfer Investigations in Liquid Metal Systems, Quarterly Progress Report No. 3, September–November, 1967*, GEAP-5582 (1967).
5. *Sodium Components Development Program Mass Transfer Investigations in Liquid Metal Systems, Quarterly Progress Report No. 4, December–February, 1968*, GEAP-5602 (1968).
6. *Quarterly Technical Progress Report on AEC-Sponsored Activities, April–June, 1968*, APDA-228 (1968).
7. *Quarterly Technical Progress Report on AEC-Sponsored Activities, June 15–September 15, 1966*, APDA-195 (1966).
8. *Quarterly Technical Progress Report on AEC-Sponsored Activities, March 15–June 15, 1966*, APDA-193 (1966).
9. *Quarterly Technical Progress Report on AEC-Sponsored Activities, January–March, 1968*, APDA-224 (1968).

Discussion

Mr. Newman (BNL): At the level at which you stopped seeing response from the oxygen meter did you measure chemically the oxygen content of that system at the same time?

Mr. Meyers: Yes, and saw the expected increase. Both the calculated and measured chemical values reported for meter No. 1 were in close agreement.

Mr. Goldmann (UNC): It was obvious that the oxygen-meter calibration constant was not the same referred to chemical analyses as referred to calculated values. In what you call calculated you used a method which we have found to be unsuitable for calibrating oxygen meters in sodium. We found it very suitable for calibrating oxygen meters in potassium. The rate of solution of oxygen in potassium is extremely high, so that as soon as oxygen is put into potassium it dissolves and the meter picks it up immediately. For sodium we found that the dissolution rates were about equal to the gettering rates of the materials in the system. If the oxygen in the sodium is in equilibrium with oxygen on the stainless steel walls, part of any added oxygen goes to the walls. We have found that in all cases we could not use the acid calibration technique for oxygen additions to sodium.

Another item which I think important is the matter of ambient temperature coefficient. APDA called this to our attention many years ago. At first, we had not agreed with them, since our results did not agree with theirs. Unfortunately, we were blowing air near the bottom of the housing because we thought it was in that area where the ambient temperature effect was occurring. Recently we started cooling the very top of the electrode assembly and discovered that when you cool the very top you do get an ambient temperature coefficient. This gave us a clue as to what the problem might be, and I think we have cured it. I think the next electrode assemblies, which we are making, will not show an ambient temperature coefficient.

Mr. Meyers: I would like to answer the question that was raised regarding the calculation and measured chemistry. Except for one point in Fig. 7 I believe that we had very good agreement in this particular evaluation between the calculated and the measured oxygen concentration.

Mr. Goldmann: You are absolutely right. There is excellent precision here but no accuracy. What is happening here is that the same thing is happening over and over again. The point is that you did not get all of the oxygen into the sodium, and at the same time some of the oxygen was getting to other places. Therefore the slope is 27, which is a lower slope than 36. That is also what we observed. It is exactly what you would expect if the mechanism which we are postulating is the right mechanism. For all of your other data, when you used measured chemistry, you did have a slope of 36 (see Fig. 10).

Engineering Development and Performance of the UNC Carbon Meter

Wayne H. Caplinger and George Stern

United Nuclear Corporation
Elmsford, New York

(PRESENTED BY W. H. CAPLINGER)

1. Introduction

UNC has developed a carbon meter capable of measuring the activity of carbon in liquid sodium. It operates by allowing carbon to diffuse from the sodium through a thin iron membrane into a decarburizing gas. An iron tube with a 10-mil-thick wall is immersed in flowing sodium at 1400°F. The inside of the iron tube is swept by a mixture of hydrogen, argon, and water vapor, which maintains a very low carbon activity. Carbon in the sodium diffuses through the iron and reacts with the moisture to form CO. The CO is converted to CH_4 by a ruthenium catalyst, and the carbon atoms of the CH_4 are counted in a Flame Ionization Detector. In this way, the concentration of CH_4 becomes a continuous measure of the carburizing potential of the sodium.

The UNC carbon meter is expected to fill a need for the continuous monitoring of the carburizing potential of sodium in large systems. It is well-known, for example, that austenitic stainless steel and refractory metals are embrittled by exposure to sodium of high carbon activity. The pickup of carbon from sodium by these metals lowers their ductility and impact strength, particularly at lower temperatures. This is serious for thin sections such as fuel cladding and bellows. On the other hand, ferritic steels such as 2¼% chromium-1% molybdenum may lose carbon to other materials in a flowing sodium system and be unacceptably weakened by decarburization, even though the sodium has a low carbon activity. The UNC meter should be useful in establishing operating guidelines for the protection of system materials.

Some hydrogen in the decarburizing gas diffuses through the iron diaphragm into the sodium. In clean sodium, the rate is about 15 mg H_2 per day, an amount that is insignificant in large systems.

The meter has already proven useful in laboratory studies of the interaction of oxygen and hydrogen with carbon in sodium. It will no doubt be quite helpful in further studies of the fundamental problems of sodium chemistry. Its main application, however, will probably be as a continuous monitor of the carbon level of the sodium in a reactor system.

2. Description of the Meter

2.1 General

The UNC carbon meter consists of four components:

1. carbon-meter probe;
2. side loop;
3. side-loop temperature-control console;
4. gas-supply and analysis console.

The package is rugged, self-contained, and capable of continuous semi-automatic operation. It can be installed in a system operating at almost any temperature up to 1400°F, since the side loop has its own heater to provide the proper temperature at the probe. The temperatures of the side loop are continuously recorded, and the side loop is automatically protected against overtemperature. The carbon flux level is read continuously by a meter and a recorder.

2.2 Carbon-meter Probe

The carbon-meter probe has the active sensor membrane and is immersed in 1400°F sodium, usually on a side loop. It is a cylinder slightly less than ⅜ in. in diameter by about 8 in. long. The top end has connections for two ⅛-in. (OD) gas lines. The bottom portion of the cylinder is the carbon-permeable iron membrane. The membrane is a high-purity iron tube with a 10-mil wall, 0.365-in. OD, and 1.35-in. length, having 10 cm^2 of active area. Inside the probe, two gas channels are provided by a heavy-walled ¼-in.-OD tube. The inlet decarburizing gas passes down the axial hole of the ¼-in. tube, sweeps over the inner surface of the membrane via a helical channel, and exits through the annulus between the OD of the ¼-in. tube and the inside of the ⅜-in. outer tube. The probe is sealed to the side-loop housing with a ⅜-in. Swagelok connector. Fig. 1 shows a probe.

2.3 Carbon-meter Side Loop

A side loop allows the meter to be installed on sodium lines operating at temperatures less than 1400°F. It provides the necessary 1400°F sodium at

the probe. Figure 2 is a photograph of a side loop. The side loop is intended to replace a 14.0-in. length of ½-in. IPS (Iron Pipe Size) vertical sodium line. The loop projects from the ½-in. IPS pipe as a trapezoidal-shaped thermal convection loop of ¼-in. IPS, Schedule 80, Type 304 stainless steel pipe. On the lower leg of the loop is a high-performance heater, which can provide 2400 W maximum or up to 1800 W continuously, to heat the inlet sodium to 1400°F. The short vertical leg at the end of the side loop houses the probe, and this chamber is heated by a separate guard heater to insure isothermal conditions near the probe. The top leg of the side arm is a ¼-in., Schedule 80, Type 304 stainless steel pipe which returns the sodium from the side loop back to the main stream through a mixing tee. The return leg is traced with a Calrod heater to provide thawing.

2.4 Side-loop Temperature-control Console

The side-loop temperature-control console shown in Fig. 3 is a cabinet about 48 in. high, 21 in. wide, and 22 in. deep. It controls the heater power to the side loop to provide and maintain 1400°F sodium automatically at the probe. The three heaters on the side loop: the trace heater, the guard heater, and the main power heater, receive power from the side-loop temperature-control console. A wattmeter is provided for continuous indication of the power consumption of the side-loop main heater. The console also has devices to protect against overtemperature; these automatically stop power to the side loop if the temperature exceeds the preset value. Should the preset temperature of the protection devices be reached, all power to the side loop stops, a horn sounds in the side-loop temperature-control console, and a light appears on the gas-supply and analysis console.

2.5 Gas-supply and Analysis Console

The gas-supply and analysis console provides decarburizing gas at the proper flow rate and composition to the probe and measures the carbon concentration, or counts the number of carbon atoms in the efflux gas from the probe. Figure 4 shows this console. The decarburizing gas originates at a cylinder of compressed argon-5% hydrogen. It is brought through the gas-supply and analysis console, where its flow rate is regulated to 12–½ cc/min. The gas then passes through a humidifier which contains a mixture of oxalic acid dihydrate and oxalic acid anhydride, held at 30°C (86°F), where it picks up 0.5% moisture. It then flows to the probe. In the probe, the moisture reacts with carbon to form car-

FIG. 1. Carbon-meter Probe.

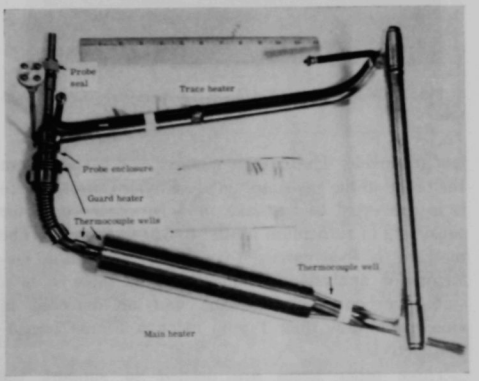

FIG. 2. Carbon-meter Side Loop.

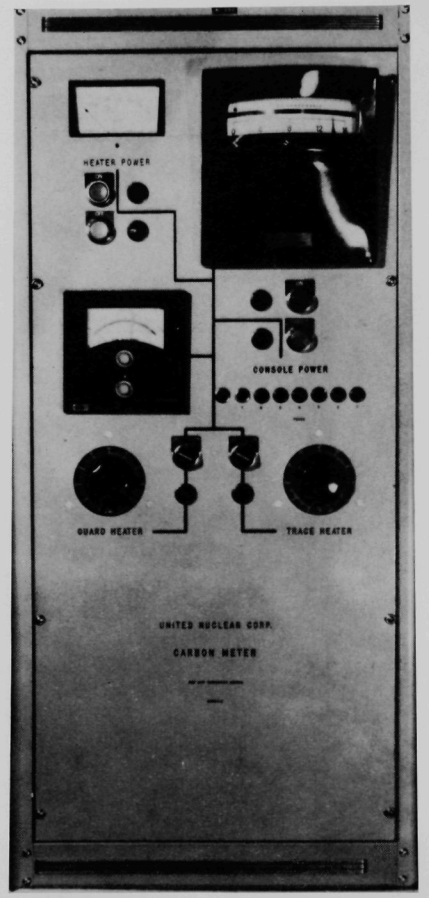

FIG. 3. Carbon-meter Side-loop Temperature-control Console.

bon monoxide. The carbon monoxide is carried from the probe to the gas-supply and analysis console where it is converted to methane in a catalytic converter consisting of ruthenium heated to 320°C (604°F). The methane is then carried to a Flame Ionization Detector for analysis. Methane is ideal since it is a stable carbonaceous gas and can be detected in amounts of less than 1 ppm using a Flame Ionization Detector.

Three other gases are needed to support the Flame Ionization Detector: hydrocarbon-free, ultrapure air; hydrocarbon-free, ultrapure hydrogen; argon plus 5% hydrogen plus a known amount of methane plus a known amount of CO. In the Flame Ionization Detector, a small hydrogen flame is maintained in the ultrapure air. An electric field imposed across the flame produces very little current in the absence of hydrocarbons. When hydrocarbons are burned, carbon ions are produced in proportion to the number of carbon atoms. The current through the flame is a measure of the methane concentration. A calibration gas of argon-5% hydrogen plus a known amount of methane is needed to calibrate the flame at a known concentration of methane. This gives one point on a curve relating methane concentration to electrometer reading. The second point is obtained from a zero gas, which is the decarburizing gas sent directly to the Flame Ionization Detector combustion chamber without going through a probe or converter. The detector is linear, and these two points determine a straight line

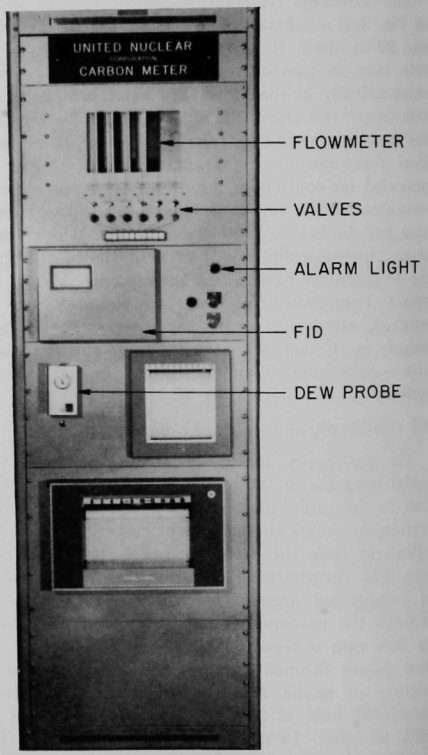

FIG. 4. Carbon-meter Gas-supply and Analysis Console.

relating concentration of methane to the detector output.

3. Instrument Performance

3.1 General

The carbon-meter probe measures the carburizing potential or carbon activity of the sodium, rather than the total presence of carbon. It responds within minutes to changes in the carbon activity, is reproducible, stable, has a long life, and is not affected by changes in sodium flow rate. The range of measured carbon activities extends from near unit activity to below that carbon activity present in commercial Type 304 stainless steel.

The instrument package is self-contained and semi-automatic. The gas-analysis unit is stable and reproducible, and the temperature control unit maintains 1400°F within ±5°F.

Detailed discussions of the form of carbon measured by the probe, its range and response characteristics, and a correlation of the meter flux with the carburization of stainless steel have been presented elsewhere.[1-3] The reproducibility, stability, and lifetimes of the probes and analyzers, the effects of sodium velocity on the side loop and carbon-meter readings, and the leakage of hydrogen from the probe will be discussed here.

3.2 Reproducibility and Stability of the Probes and Gas Analyzers

The carbon-meter probe and gas analyzer are reproducible and stable. Several probes exposed to the same sodium produced equal carbon fluxes and responded similarly to changes in carbon level of the sodium. The steady flux from a probe analyzed by different gas analyzers was read as the same value. Probes several thousand hours old produced equal fluxes and responded similarly to newly built probes. Some representative data are shown in Table 1. These data were taken from probes located in the test chamber of a thermal convection loop in which two or three probes were positioned within an

TABLE 1. Comparison of Carbon-meter Readings for Different Probes of Varying Ages

Probe No.	Age (hr)	Carbon Flux (μgm C/cm^2-min)	
L-11	700	0.007	
L-10	50	0.007	
L-10	350	0.005[a]	0.049[b]
L-11	1000	0.005[a]	0.045[b]
L-12	New	0.005[a]	0.048[b]
L-11	1200	0.11	
L-13	New	0.10	
L-6	3500	0.0037	
L-16	150	0.0038	

[a] Carbon flux at low carbon level.
[b] Carbon flux at higher carbon level.

TABLE 2. Comparison of Carbon-meter Probes Tested with Different Gas Analyzers

Probe No.	FID No.	Carbon Flux (μgm C/cm^2-min)
L-11	98	0.066
	141	0.065
L-13	98	0.023
	141	0.022

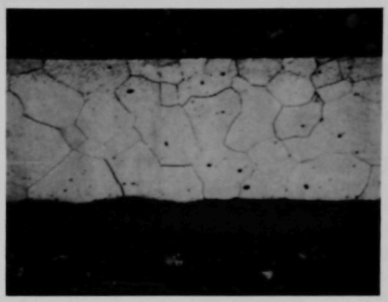

Nital 102×

Fig. 5. Microstructure of a Carbon-meter Probe Wall after 3500 hr of Operation.

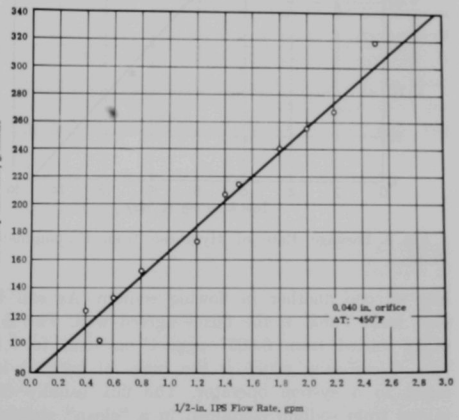

Fig. 6. Side-loop Flow Rate *vs* Main-line Flow Rate.

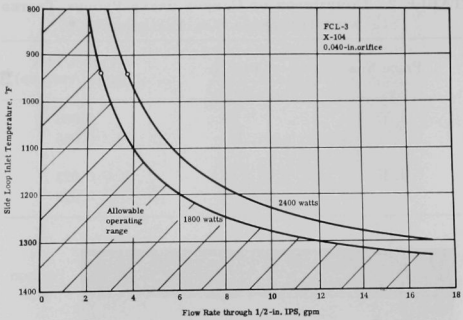

FIG. 7. Side-loop Sodium Inlet Temperature for the Allowable Flow Rate Past Side Loop.

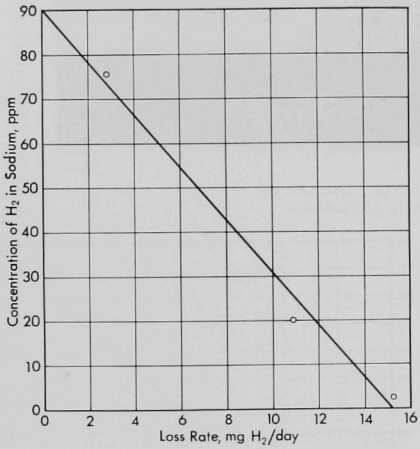

FIG. 8. Leakage Rate of Hydrogen from Carbon-meter Probe.

inch of one another in flowing sodium. As can be seen from Table 1, the fluxes agreed well. The flux range varied from 0.0037 μgm C/cm^2-min to 0.11 μgm C/cm^2-min, which is the range of greatest interest to a system operator. The flux usually obtained from sodium contained in a "clean" stainless steel system is about 0.007 μgm C/cm^2-min.

Typical data showing a comparison of gas analyzers is given in Table 2. The fluxes from probes L-11 and L-13 were analyzed by two Flame Ionization Detectors, Nos. 98 and 141. By transferring the gas line carrying a steady carbon flux from one analyzer to another, agreement within a few percent was obtained.

3.3 Life of the Probe and Other Carbon-meter Components

An accurate estimate of the life of the carbon-meter probe has not been made. It is likely to be quite long. Several probes were operated for thousands of hours during the program with no sign of failure. One probe was operated at a relatively high carbon flux for over 1400 hr. During this time, two atoms of carbon were transferred through the wall for each atom of iron in the wall. No change in the probe performance was noticed, and the test was stopped to allow metallography of the probe. The probe tested for the longest time accrued over 4500 hr without signs of deterioration.

Only one probe failed during the program. After 3500 hr of testing, it developed a hole in the 20-mil portion of the iron tubing, above the 10-mil-thick active area. The precise cause of the failure was not determined, but attacked appeared to have been from the inside. The metallographic structure of the wall of this probe is shown in Fig. 5. The layer on the gas side of the probe wall is believed to be the result of oxidation and subsequent reduction of the iron. This occurred when the probe gas consisting of hydrogen-water vapor-argon was inadvertently shut off. With no gas flow, the residual hydrogen diffused through the iron, leaving a wet argon which oxidized the iron. When the flow of the decarburizing gas was resumed, the hydrogen in the mixture partially reduced the iron oxide.

Some parts of the instrument package are consumed during operation. The four compressed gases for the gas analyzer last about six to twelve months for a size 1A cylinder. The humidifier contains enough water to supply moist decarburizing gas to one probe for at least 5 yr. With proper maintenance, the electronic components, such as recorders and temperature indicators, should last indefinitely. The four heaters on the side loop operate at relatively high power densities and are expected to last about 3–5 yr.

3.4 Effects of Sodium Flow Rate on Probe Flux and Side-loop Heater

The rate of sodium flow past the probe did not affect the carbon flux. Variations of ~100 gm/min to >300 gm/min through the side loop past the probe did not change the carbon flux of about 0.01 μgm C/cm^2-min. There are two sodium velocities of interest: (1) that past the probe, i.e., through the side loop, and (2) that past the side loop, i.e., through the ½-in. IPS main line. It was found that the flow rate through the ½-in. IPS main line of the side

loop (2) directly affects the flow rate through the side loop (1).

The fraction through the side loop [ratio of (1) to (2)] depends upon the size of the orifice used in the side loop. For an orifice with four 0.040-in.-diameter holes, the flow distribution between the ½-in. IPS main line and through the side loop is shown in Fig. 6. The portion that flows through the side loop is a linear fraction of that through the main line. When no sodium is pumped through the ½-in. IPS pipe, some sodium still circulates past the probe due to thermal convection. In the case shown in Fig. 6, the inlet temperature was 950°F and the flow due to the 450°F ΔT was 80 gm/min.

As the flow rate through the side loop increases or decreases, the heater power required increases or decreases similarly. Further, the total heater power required to maintain 1400°F at the probe depends upon the inlet sodium temperature. The flow rate through the side loop and the inlet temperature, i.e., the ΔT across the side loop heater, must be arranged so that the heater capacity is not exceeded.

Figure 7 shows the allowable operating range for two heater powers; 2400 W may be drawn from the heater for short times, but 1800 W is the maximum continuous power. The data shown in Figures 6 and 7 are taken from an early carbon-meter unit tested at United Nuclear Corporation. Following the tests, it was decided that the allowable operating range should be increased. To do this for subsequent units, the dimensional tolerances between the orifice and its seat in the side loop were tightened. This improved fit would shift the curve shown in Fig. 7 to the right, and allow a greater combination of flow rate and lower inlet temperature to the side loop.

The variation of sodium velocity through the side loop past the probe was investigated for its effect on the carbon-meter flux. During several tests in which the carbon-meter flux was in the range from 0.006 to 0.024 μgm C/cm^2-min, the flow rate was varied from about 100 to over 300 gm/min, and the carbon-meter fluxes were not affected. The flux of 0.006 μgm C/cm^2-min is "low" and is about that expected from a clean stainless steel-sodium system. The meter would be expected to be most sensitive to flow rate at low fluxes. The reasons are that the probe extracts some carbon from the sodium and local depletion could occur in stagnant sodium.

3.5 Hydrogen Leakage from Probe

The presence of hydrogen in the decarburizing gas allows some hydrogen to diffuse from the probe into the sodium. Since this would be viewed as a contaminant in the sodium, it is important to know the rate of hydrogen leakage from the probe. To obtain a quantitative measurement of the hydrogen leakage, a material balance of hydrogen in the decarburizing gas was used. The mass flow rate of decarburizing gas was 12½ cm^3/min, and the inlet concentration of hydrogen to the probe was determined by analysis to be 5.00%. By measuring the hydrogen concentration in the efflux decarburizing gas from the probe, the loss of hydrogen was calculated. To measure the hydrogen concentration or activity in the sodium, a diffusion-type hydrogen meter[3] was used. The loss rate of hydrogen from the probe was measured at three concentrations of hydrogen in the sodium. The results are shown in Fig. 8.

Although the hydrogen in the sodium is reported as a concentration, it should be kept in mind that these values were obtained from equating activities of the hydrogen in argon gas (inside the coil of the hydrogen meter) and in sodium by using the data of Savage *et al.*[4] The flow rate of the sodium past the probe during the determination of these three points was about 0.1 to 0.3 gpm. As can be seen from Fig. 8, the maximum loss expected for a sodium system with essentially zero hydrogen content, a clean system, is of the order of 15 mg of hydrogen per day. For a small system, this amount might present some problems if no efforts are taken to prevent its accumulation. However, in a system of reactor size, even assuming no loss to the outside, the total accumulation of hydrogen would be a few ppm per year.

4. Conclusions

A diffusion-type carbon meter has been developed for the measurement of carburizing potential in sodium. It reads continuously, has a rapid response, is reproducible, rugged, and possesses a long life. The range of carburizing potentials that the meter can measure extends from near unit carbon activity down to below the activity for carbon normally present in Type 304 stainless steel. Variations in sodium flow rate past the probe do not affect the carbon flux.

A semi-automatic, self-contained instrument package was designed and built consisting of a probe, a side loop operating at 1400°F, a side-loop temperature-control console, and a gas-supply and analysis console. This instrument package can be fitted into pumped loops.

Hydrogen leakage from the sensor will not be a serious contaminant in sizable sodium systems.

Acknowledgment

The work described was performed under Contract AT(30-1)-3665 with the United States Atomic Energy Commission. The contributions of J. M. McKee and M. Kolodney in the concept, experimental development, and final design of the carbon meter are gratefully acknowledged. The contribution of S. Lukasik in building the components as well as in performing development and test work in the laboratory is appreciated.

REFERENCES

1. McKee, J. M., Caplinger, W. H., and Kolodney, M., *Continuous Carbon Meter for Sodium*, Nucl. Appl., **5**, 236–246 (Oct 1968).
2. Kolodney, M., *Mechanism of Carburization of Stainless Steel in Sodium as Identified by a New Carbon Meter*, Nucl. Eng. Design, **7**, 481–484 (1968).
3. Caplinger, W. H., *Carbon Meter for Sodium, Final Report*, UNC-5226 (Oct 1968).
4. Savage, H. W. *et al.*, *SNAP-8 Corrosion Program Summary Report*, ORNL-3898 (Dec 1965).

Discussion

Mr. Rodgers (MSA): I thought the audience might be interested in an unbiased opinion of the carbon meter. We have the first carbon meter for fuel testing, and we have it installed in our high-carbon loop. We installed it about June of this year and have been getting some numbers from it. We have been doing this in our Loop 1 as described in a paper in yesterday's session entitled "Effect of High-temperature Sodium on the Mechanical Properties of Candidate Alloys for the LMFBR Program." We supply carbon to the system by bypassing some of our sodium stream through a bed of carbon rods. We therefore can vary the carburization potential of the system by varying either the temperature of the carbon bed or the flow through the carbon bed. We are attempting to calibrate the carbon meter in that system. I have tried to avoid using the words 'carbon activity' and to use the terminology 'carbon potential' or 'carburizing potential' as the rate at which Type 304 Stainless Steel tabs will carburize in the system. To date we have been trying to get down to a low level of carbon in our system. Our particular loop has been in operation for about 5 years under rather highly carburizing conditions, so we have not been able to get down to Caplinger's "clean" stainless steel system of 0.007 μmg/cm^2-min. But we have gotten down to a fairly constant level at about 0.012 μgm/cm^2-min carbon flux through the probe. We find that the temperature does have an effect on the carbon-meter output. I believe that the temperature-control console that United Nuclear supplies with the unit is satisfactory for the operation. We also see an effect of flow rate, which apparently United Nuclear does not. The orifice at the entrance to the carbon-meter probe can be adjusted to maintain a constant flow through the probe, so I don't consider either temperature or flow a problem.

We had a problem with the thermostatically controlled humidifier. It is recommended that you operate the humidifier at a dew point of about 27°F. This is fine if you have the console sitting in an air-conditioned laboratory or a constant-temperature laboratory. However, we have the console sitting in our loop area where in summer our ambient temperature varies from perhaps 60°F at night to 120°F in the day, so we have had to vary the thermostatic setting on the humidifier. I believe my biggest complaint about the UNC carbon meter is control of the flow rate. It seems we spend most of our time trying to get back to 12½ cc/min, and to adjust this flow rate and measure it.

We have had a couple of occasions now to determine whether or not the carbon meter does respond to a change in carburization potential. One of these was to introduce carbon impurities into the sodium system by changing the cold-trap temperature. When we did this, we saw an increase in the carbon-meter output, and we also saw a corresponding increase in the total carbon pickup by our monitoring tabs. Just in this past week we initiated flow through our carbon bed. We then found a change of carburization potential by about a factor of 10 by our tabs, while the carbon meter showed a corresponding increase by a factor of about 20. I don't think that these increases necessarily should agree, but the fact that the carbon meter gives quite a large response is very encouraging. At this point in time I am quite impressed with it.

Mr. Zebroski GE): You mentioned that there were a number of papers that discussed the phenomena and the species involved in the processes of the meters. I wonder if you could just mention two or three of the references that you feel to be most definitive.

Mr. Caplinger: Tomorrow morning John McKee will present a paper. You will find some references mentioned there. The final report is expected out before too long. I hope it will have a description of additional parameters for the carbon meter that I haven't discussed here. There is also a paper in the October 1968 issue of Nuclear Applications.

Mr. McKee (ANL): I believe there is one other publication in the open literature by Dr. Kolodney in Nuclear Engineering and Design, Vol. **7** (1968).

Regarding calibration of the meter in terms of carburization of stainless steel, I think Dr. Kolodney's paper is the best that has been published so far. I might say no great claims are made for it; there just are not yet any good data taken at constant carbon activities.

Mr. Dutina (GE): Have you ever considered using a galvanic cell to measure activity of carbon directly?

Mr. Caplinger: I think the galvanic cell has been considered.

Mr. Dutina: What was its fate?

Mr. Caplinger: We did no experimental work.

Mr. Dutina: Recently I saw a paper where a calcium carbide and calcium chloride mixture was used. The activity of carbon in iron agreed with gas-phase equilibrium measurements. Although we do not know the transfer number exactly, C_2^{-2} apparently is close to 100% ionic.

Mr. Caplinger: It has been suggested that we point out that we have a patent application on devices.

Mr. Holden (UNC): This is a question for Rodgers, not for Caplinger. When you pass the sodium flow through your packed bed of carbon, what actual numbers do you get for the carbon flux through the carbon-meter probe?

Mr. Rodgers: Before we started to go through the carbon bed we were getting fluxes of 0.012 to 0.014 μgm c/cm^2-min. Now that we have opened up the bed we are getting fluxes of about 0.3 μgm C/cm^2-min. We found an increase in carbon in our stainless steel tabs from 1000 ppm pickup in 48 hr to 10,000 ppm in 48 hr.

An Electrochemical Meter for Hydrogen in Sodium

R. B. Holden and N. Fuhrman

United Nuclear Corporation
Elmsford, New York

(PRESENTED BY R. B. HOLDEN)

1. Introduction

An on-line meter to monitor continuously the hydrogen activity of the sodium coolant in reactors such as the LMFBR is required for two basic applications: (1) to determine the hydrogen impurity level in the primary loop, and (2) to serve as an indicator of water leakage into the secondary sodium system. The latter is the more exacting application, requiring a sensitivity of 0.1 ppm hydrogen at the 1.0-ppm level and a response time of the order of 1 second.[1] United Nuclear Corporation is now developing an electrochemical hydrogen meter which shows promise of meeting these requirements.

The meter utilizes a hydrogen-sensor concept which is essentially an electrochemical concentration cell. The conceptual design of the sensor is shown in Fig. 1. It consists of a cylindrical reference electrode, within a concentric tube of a metal resistant to sodium, which serves as the sensing electrode. These electrodes are electrically insulated from each other except through their annulus, which contains an ionic hydride-bearing electrolyte such as, for example, LiH dissolved in LiCl-KCl eutectic. The active ends of the electrodes consist of thin metal septa, which permit transport of hydrogen, but separate the reference material and the sodium from the electrolyte. The reference may be a two-phase solid mixture whose hydrogen pressure is determined solely by temperature, such as Ca-CaH_2, or a flowing gas having a constant partial pressure of hydrogen. The outer septum comes to equilibrium with the sodium so that the hydrogen activity is the same in both. The inner septum similarly acquires the hydrogen activity of the reference material. The result is an electrolytic cell whose overall cell reaction involves the transfer of hydrogen from the sodium to the reference. The actual transfer of hydrogen is substantially zero, because the measurement is potentiometric with extremely low current flow.

Work on the electrochemical hydrogen sensor is now in the concept-development stage. The results of the initial feasibility tests of the principle performed in a gas environment at temperatures ranging from 370 to 650°C are presented below.

2. Theoretical Sensor Performance

To evaluate the performance of the experimental hydrogen sensors, the theoretical cell voltage vs temperature relationship and cell polarity based on a hydride-ion-electrolyte concentration-cell model were determined. The overall cell reaction can be expressed as

$$\underset{\text{Sensing}}{H_2(P_1)} = \underset{\text{Reference}}{H_2(P_2)}, \tag{1}$$

where P_1 is the hydrogen partial pressure at the sensing electrode, and P_2 the hydrogen partial pressure at the reference electrode. If the sensing electrode is in sodium, P_1 is simply the hydrogen overpressure in equilibrium with hydrogen in the sodium.

In accordance with electrochemical-cell convention, the cell representation is as follows:

$$\underset{\text{Reference}}{H_2(P_2)} \;\Big|\; \underset{H^-}{\overset{e}{\underset{H^-(a_{H^-})}{\rightleftarrows}}} \;\Big|\; \underset{\text{Sensing}}{H_2(P_1)}, \tag{2}$$

where (a_{H^-}) is the hydrogen-ion activity in the electrolyte. As is shown, when $P_1 > P_2$, hydrogen will be transported from right to left, electrons in the external circuit will move from left to right, the sensing electrode will be positive, and the emf will be positive. This is consistent with the cell reaction (Eq. 1) being spontaneous from left to right, producing a negative free energy change. For the electrode on the left, the oxidation reaction yields

$$H^-(a_{H^-}) = \tfrac{1}{2}H_2(P_2) + e, \tag{3}$$

and the electrode potential on the left, E_L, can be written as

$$E_L = -\frac{RT}{F}\ln\frac{P_2^{1/2}}{a_{H^-}}. \tag{4}$$

Similarly, for the reduction at the right-hand electrode,

$$\tfrac{1}{2}H_2(P_1) + e \rightarrow H^-(a_{H^-}) \tag{5}$$

and

$$E_R = -\frac{RT}{F}\ln\frac{a_{H^-}}{P_1^{1/2}}. \tag{6}$$

On adding Eqs. 3 and 5, the cell reaction (Eq. 1) is obtained; the cell voltage E is obtained on adding Eqs. 4 and 6:

$$E = -\frac{RT}{F} \ln \frac{P_2^{1/2}}{P_1^{1/2}} = -\frac{RT}{2F} \ln \frac{P_2}{P_1}, \qquad (7)$$

where

R = 8.315 J/°K-mol;
F = 96,500 coulombs/mol;
T = absolute temperature in °K.

As a function of T, P_1, and P_2, the cell voltage in volts is

$$E = -0.992 \times 10^{-4}\, T \log_{10} (P_2/P_1). \qquad (8)$$

By use of Eq. 8 the theoretical cell voltage vs temperature relationship for the initial gas-environment tests is plotted in Fig. 2. The hydrogen partial pressure P_1 of the reference gas was 0.05 atm and the hydrogen partial pressure at the sensing electrode, P_2, was varied from 0.01 to 1 atm.

3. Sensor Design and Construction

In order that the hydrogen sensor operate as a concentration cell, a reversible transfer of hydrogen between electrodes and electrolyte must be possible. The incorporation of hydride ions in the electrolyte permits such a reversible electrode process. It is known that the saline hydrides, i.e., the hydrides of the alkali and alkaline earth metals, are ionic, with crystal lattices composed of metal cations and hydrogen anions. When solid or molten lithium hydride (LiH) is electrolyzed, the hydrogen migrates to the anode and is converted to hydrogen gas.[2] The other saline hydrides cannot be melted, but if they, or LiH, are dissolved in molten halide mixtures, such as LiCl-KCl eutectic, hydrogen will form at the anode upon electrolysis.[2, 4]

Based on its availability as a verified electrolyte system, LiCl-KCl eutectic containing dissolved saline hydride was selected for the initial concept-feasibility tests. Because the eutectic melting point is 352°C, the electrolyte operated as a liquid in the testing temperature range of 370 to 650°C.

Table 1 lists the actual electrolytes tested as well as the other materials employed in the initial sensors. The choice of the sensor materials of construction was dictated in part by materials compatibility considerations. Iron and AISI 304 stainless steel are compatible with both the electrolyte and sodium. In addition, iron is highly permeable to hydrogen, and permeability is important because the sensor response time depends upon the speed of communication of a hydrogen change across the sensing-electrode septum to the electrolyte.

The details of construction of the test sensor are as

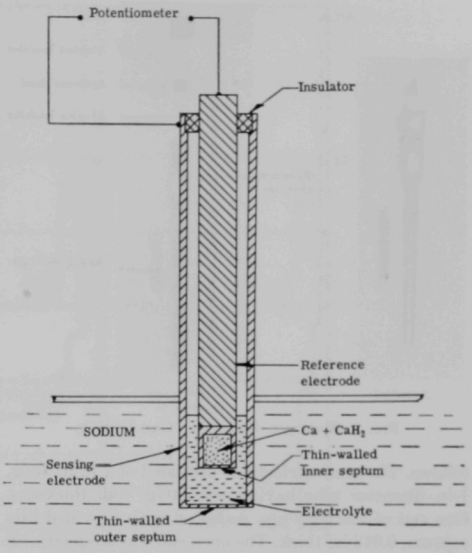

FIG. 1. Conceptual Design of Hydrogen-meter Sensor.

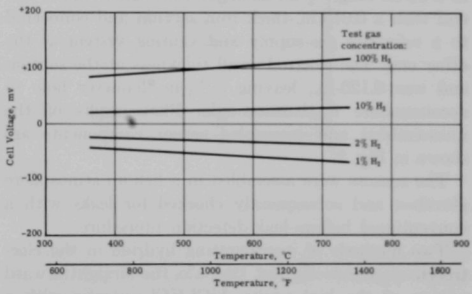

FIG. 2. Theoretical Cell Voltage *vs* Temperature (Reference Electrode: 5% H_2, 95% A).

TABLE 1. SENSOR MATERIALS FOR INITIAL TESTS

Electrolytes
LiCl-KCl eutectic + LiH
LiCl-KCl eutectic + NaH
LiCl-KCl eutectic + CaH_2
Septa
Iron
Reference Electrode Stem and Sensing Tube
AISI 304 Stainless Steel
Reference Hydrogen Source
5% Hydrogen-95% Argon Gas Mixture

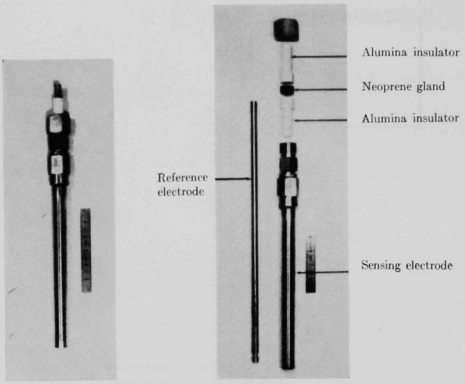

FIG. 3. Hydrogen Sensor for Gas Testing.

follows. The sensing electrode consisted of a 12-in.-long, 1-in.-diameter tube having a 0.120-in. wall thickness. One end of the tube was sealed off with a welded iron septum, 0.013 in. thick. The open end was adapted with a ½-in. Conax electrical feedthrough to accept and seal the reference electrode. The latter electrode consisted of a 15-in.-long, ½-in.-diameter tube sealed off at one end with a 0.013-in.-thick iron septum and connected to a reference gas-supply and venting system at the other end. The electrode wall thickness at the septum end was 0.120-in., leaving a ¼-in.-diameter hole to accommodate a thermocouple. Photographs of the unassembled and assembled sensor components are shown in Fig. 3.

The sensors were assembled in a helium-atmosphere glovebox and subsequently checked for leaks with a conventional helium-leak-detection procedure.

Two methods of incorporating hydride in the electrolyte were investigated. One was the straightforward mixing of the high-purity LiCl-KCl eutectic with a commercially available hydride, such as LiH. The other involved adding the precursor metal to the eutectic, then hydriding the metal *in situ* during gas testing of the assembled sensor above the melting point of the eutectic.

4. Gas Test Apparatus

The apparatus for sensor testing in a gas environment was designed to produce data for evaluation of the concept feasibility and for rapid screening of proposed sensor systems. It consists of a gas-supply system, an electrically heated stainless steel chamber accommodating three sensors, and a gas-analysis system.

The gas-supply system consists of an electrolytic hydrogen generator and a cylinder of compressed argon connected through pressure regulators, metering valves, flowmeters, and a mixing chamber to the test chamber. The generator produces ultra-pure hydrogen by utilizing the principle of purification by diffusion through palladium.

The gas-analysis system consists of a thermal-conductivity cell (Gow-Mac) sensitive to small changes of hydrogen level in hydrogen-argon mixtures. Gas from the chamber is passed through a metering valve and flowmeter into the cell for analysis. A similar line is provided for a calibrating gas.

5. Results

5.1. First Test Series

The first series of three sensors tested with 5% H_2-95% A gas reference electrodes were prepared with the following electrolytes:

Sensor A: LiCl-KCl eutectic + 2 m/o LiH;
Sensor B: LiCl-KCl eutectic + 2 m/o Li metal;
Sensor C: LiCl-KCl eutectic only.

In the case of Sensor B, the intention was to form LiH *in situ* during the initial testing in 100% hydrogen. The last electrolyte was included to determine whether extraneous electrode processes, not involving hydride, contribute to the sensor voltage response to hydrogen changes.

During a 6-day test period, the hydrogen level at the sensing electrodes was varied from 1 to 100% while the temperature ranged from 440 to 655°C. The temperature was increased in steps to 655°C and then reduced to the original levels to determine whether sensor behavior was reversible. The sensor voltage responses to the hydrogen concentration and temperature changes over the test period are plotted in Fig. 4 for two sensors: Sensor B, prepared with lithium metal in the eutectic, and Sensor C, prepared with eutectic only.

The significant results obtained from this test series may be summarized as follows:

1. The cell voltage of the sensors containing hydride responded to hydrogen-level changes, whereas that of the sensor containing LiCl-KCl eutectic only did not change with wide variations of hydrogen level at any temperature (see Fig. 4). This is considered strong evidence that the presence of ionic hydride in the electrolyte is necessary to detect hydrogen changes.

2. Sensor B responded to hydrogen changes after only several hours of exposure to 100% hydrogen, indicating that *in situ* hydriding is an effective method of constituting a working electrolyte.

3. Although the two sensors containing hydride did not exhibit the full theoretical voltage indicated in

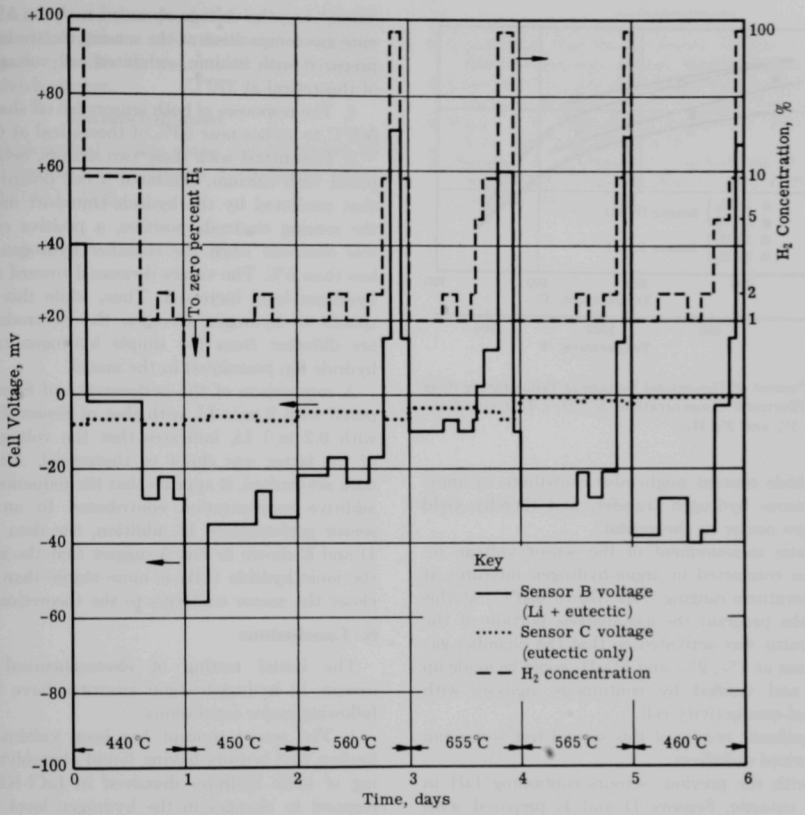

FIG. 4. Voltage Response of Hydrogen Sensor to H_2 Concentration and Temperature.

Fig. 2 as the chamber hydrogen concentration was varied, the expected reversal of cell polarity occurred near the 5% H_2 level, that is, with the sensing electrode positive, a positive emf was measured above 5% H_2 and a negative emf was measured below 5% H_2.

4. At 460°C on the sixth day, the voltage response of Sensor B (see Fig. 4) was quite high, approximately 70% of theoretical. However, at the higher temperatures the sensor was less responsive.

5. Initially, below 560°C, the voltage response of the two sensors containing hydride were similar. After the temperature increase to 560°C, Sensor A, prepared with LiH, exhibited a sharp reduction of sensitivity which was recovered, in part, after the temperature was lowered to 460°C.

The lower voltage response at the higher temperature is attributed partly to nonelectrolytic hydrogen transfer tending to equalize the hydrogen pressure at the two electrodes. One source of such hydrogen is the hydride in the electrolyte.

5.2. Second Test Series

With the above results in view, another set of three hydrogen sensors was tested to determine the effect of a variation in hydride stability on sensor behavior. The sensors were prepared with the following electrolytes, each containing the precursor metal additive to be hydrided *in situ:*

Sensor D: LiCl-KCl eutectic + 0.2 m/o Na;
Sensor E: LiCl-KCl eutectic + 0.2 m/o Li;
Sensor F: LiCl-KCl eutectic + 0.2 m/o Ca.

The 0.2 m/o metal added represents a reduction by a factor of 10 in concentration from the previous sensors. It was anticipated that the resulting lower metal-

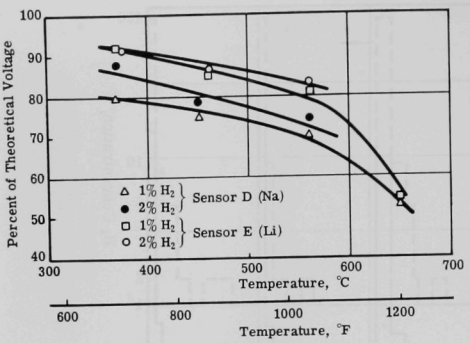

FIG. 5. Percent of Theoretical Voltage *vs* Temperature (Gas Reference Electrode Concentration: 5% H_2 ; Test Gas Concentration: 1% and 2% H_2).

metal hydride content might also contribute to limiting extraneous hydrogen transfer, and thereby yield cell voltages nearer to theoretical.

Systematic measurement of the sensor voltage response was conducted in argon-hydrogen mixtures at four temperatures ranging from 370 to 650°C. At this point in the program the gas-analysis portion of the test apparatus was activated so that the chamber-gas compositions at 1%, 2%, and 5% H_2 could be made up precisely and verified by continuous analysis with the thermal-conductivity cell.

The significant results of this second test series can be summarized as follows:

1. As with the previous sensors containing LiH in LiCl-KCl eutectic, Sensors D and E prepared with sodium and lithium, respectively, in the electrolyte tended to behave in accordance with the hydride-transport model. With the sensing electrode positive, a positive cell voltage was observed when the chamber hydrogen level was greater than 5% and negative cell voltage was measured below 5% H_2.

2. At a chamber hydrogen concentration of 5% (verified with the thermal-conductivity cell to be precisely the same as the reference gas composition) an emf of the order of 5 mV was observed. This nonzero value is attributed to a thermoelectric effect arising from nonisothermal conditions across the cell.

3. The cell-voltage data for these two sensors were not only reproducible from day to day, but tended to approach theoretical values as the temperature decreased. This can be seen in Fig. 5 in which the percent of theoretical voltage is plotted against temperature for Sensors D and E with 1% and 2% H_2 at the sensing electrode. The values were derived from steady-state voltage data and were referred to the sensor "zero," i.e., the voltage observed with the 5% H_2 reference gas composition at the sensing electrode. Sensor E, prepared with lithium, exhibited cell voltages of 92% of theoretical at 370°C.

4. The responses of both sensors fell off sharply above 560°C to values near 50% of theoretical at 650°C.

5. In contrast with these two sensors, Sensor F, prepared with calcium, exhibited a cell polarity opposite that predicted by the hydride-transport model. With the sensing electrode positive, a positive cell voltage was observed when the chamber hydrogen level was less than 5%. The values decreased toward zero as the hydrogen level increased. Thus, while this sensor responds to hydrogen changes, the electrode processes are different from the simple hydrogen transfer by hydride ion postulated in the model.

A comparison of the performance of Sensor B, prepared with 2 m/o Li, with that of Sensor E, prepared with 0.2 m/l Li, indicates that the voltage response of the latter was closer to theoretical. Although the data are limited, it appears that the reduction of metal-additive concentration contributed to an improved sensor performance. In addition, the data of Sensors D and E shown in Fig. 5 suggest that the more stable the ionic hydride (LiH is more stable than NaH) the closer the sensor conforms to the theoretical model.

6. Conclusions

The initial testing of electrochemical hydrogen sensors in hydrogen-argon mixtures have led to the following major conclusions:

1. The sensor concept has been validated by the finding that sensors having liquid electrolytes consisting of ionic hydrides dissolved in LiCl-KCl eutectic respond to changes in the hydrogen level of the gas mixture. Without hydride present the sensor is not responsive.

2. Preparation of a sensor by *in situ* hydriding of the precursor metal added to the electrolyte appears to produce a more responsive device than one prepared directly with the hydride.

3. Sensors operated with 5% H_2-95% A gas reference electrodes exhibit reproducible cell voltages from day to day. Although the full theoretical voltage is not achieved as the hydrogen concentration is varied at the sensing electrode, the expected cell-polarity reversal occurs at approximately 5% H_2. The observed polarity above and below 5% H_2 are in accord with a simple concentration-cell model involving hydrogen transfer by hydride ion.

4. In the case of such sensors prepared with lithium and sodium, the departure from theoretical voltage decreases with temperature, so that cell voltages on the order of 90% of theoretical are obtained at 370°C.

5. The unexpected polarity of the sensor prepared

with calcium, opposite that predicted by the hydride-transport model, indicates that there are other electrode processes possible in the present sensor design which involve hydrogen.

Acknowledgment

The work described in this paper was supported by the United States Atomic Energy Commission under Contract AT(30-1)-3908.

REFERENCES

1. *Liquid Metal Fast Breeder Reactor Program Plan*, Vol. 5, *Sodium Technology*, 193–196, WASH-1105 (Aug 1968).
2. Libowitz, G. G., *The Solid-State Chemistry of Binary Metal Hydrides*, W. A. Benjamin, Inc., New York (1965), p. 91.
3. Hurd, D. T., *Chemistry of the Hydrides*, John Wiley and Sons, New York (1952), p. 31.
4. Plambeck, J. A., Elder, J. P., and Laitenen, H. A., *Electrochemistry of the Lithium Hydride Cell*, J. Electrochem. Soc. **113**, 931–937 (1966).

SESSIONS ON SODIUM TECHNOLOGY

SESSION ST-IVA

Friday Afternoon, November 8, 1968

Chairman: S. Lawroski
Argonne National Laboratory

Secretary: T. F. Kassner
Argonne National Laboratory

Preparation of High-purity Sodium for Chemistry Studies*

R. L. McKisson and R. L. Eichelberger

Atomics International
A Division of North American Rockwell Corporation
Canoga Park, California

(PRESENTED BY R. L. EICHELBERGER)

A basic study of the interactions of materials with sodium requires the use of highly purified materials to ensure that the systems under study be as uncomplicated as it is possible to make them. The major problem in the purification of sodium is the removal of oxygen. Oxygen can be removed to a very low level by the use of an active metal getter such as zirconium, but the gettered product still has all of its original metallic impurities plus zirconium in solution. A more satisfactory purification process is the combination of hot gettering followed by vacuum distillation. The gettering reduces the oxygen content (and the carbon and nitrogen contents, too) in the sodium, which can them be separated from its metallic impurities by distillation. The effectiveness of this technique as practised at Atomics International is described below.

1. Process and Design Considerations

Since the work for which the purification of sodium is necessary involves the use of rather small samples (a few grams) of sodium, the process and design effort was directed toward the preparation of a product batch size of about 400 gm. This amount of material is sufficient for the needs of several experiments, and yet does not involve the construction of a large purification apparatus.

The essentials of the gettering process are to bring the nonmetallic impurities into contact with a reactive metal, to allow decomposition of any compounds which may be present, and finally to allow the elemental fragments to react with the getter. That compounds can exist in sodium is shown by the work performed at the Argonne National Laboratory[1] and at Dounreay.[2] These studies show that carbon monoxide can be absorbed in liquid sodium to form compounds such as sodium carbonyl ($NaOC \cdot CONa$) and tetrasodium tetraoxyquinone, $(NaO)_4C_6O_2$. One characteristic of these compounds is that in no case did these researchers find evidence of a Na—C bond. Because the CO appears to maintain some degree of identity in compounds such as these, there is some support for the view expressed by the Argonne National Laboratory workers[1, 3, 4] that carbon could not be separated from sodium by simple distillation because the carbon would separate from the sodium as CO during the distillation process, and would then be reabsorbed in the distillate. In their tests, the distillate was found to have about 50 ppm carbon. It is therefore necessary to ensure that any such compounds are destroyed and the products are absorbed in the getter before the sodium is distilled.

An examination of the relative chemical stabilities of CO, ZrC, and ZrO_2 shows that the reaction of CO (and probably of sodium-CO compounds) with zirconium to form ZrC and ZrO_2 (or oxygen-rich zirconium) is very strongly favored. The rate of decomposition is, of course, uncertain, but at the rather high temperature required for adequate oxygen gettering by zirconium (650–700°C), one would expect the decomposition to proceed rapidly. At this gettering temperature, oxygen has a reasonable rate of diffusion into zirconium metal, but the rate of diffusion of carbon into the zirconium is expected to be quite small. Therefore, it is necessary to provide a large area of zirconium metal surface to ensure that the getter can function for an extended time.

After undergoing the hot zirconium gettering treatment, the sodium is ready for distillation. Because the amounts needed are small, a batch distillation is appropriate. However, one must provide for the removal of elements more volatile than sodium as well as for those less volatile. Horsley[5] discusses in some detail the theoretical considerations of the separation from sodium of the principal contaminating elements. He shows that, with the exception of potassium, all of the usual metallic impurities in sodium are less volatile than sodium. Therefore, good separations of impurity metals by distillation can be readily achieved. The separation of potassium (and of rubidium and cesium, as well) can be effected by discarding the first fraction of the distillate in which these elements are enriched. The metals less volatile than sodium will tend to remain in the still, so that by saving the middle fraction of the distillate as product, a purification of sodium from both the more and the less volatile metals can be accomplished. The goal of the design study was thus to evaluate the volume of distillate that should be discarded before col-

* Based on work supported by the U. S. Atomic Energy Commission under Contract AT(04-3)-701.

TABLE 1. RELATIVE VOLATILITY VALUES
$\alpha = P^0(\text{Metal})/P^0(\text{Na})$

T (°K)	Cs	Rb	K	Na
600	96	60	18	1.0
700	40	28	11	1.0
800	21	16	6.9	1.0
900	13	10	5.1	1.0

T (°K)	Na	Mg	Li	Sr	Ca	Ba
600	1.0	2.3×10^{-3}	8.5×10^{-5}	7.3×10^{-5}	6.0×10^{-6}	3.5×10^{-6}
700	1.0	7.9×10^{-3}	3.9×10^{-4}	3.8×10^{-4}	4.7×10^{-5}	2.4×10^{-5}
800	1.0	2.0×10^{-2}	1.2×10^{-3}	1.4×10^{-3}	2.1×10^{-4}	1.1×10^{-4}
900	1.0	4.4×10^{-2}	3.0×10^{-3}	3.5×10^{-3}	6.8×10^{-4}	3.5×10^{-4}

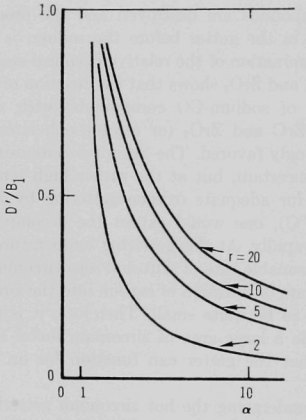

FIG. 1. D'/B_1 Values for a Still and Column for $\alpha > 1$ and $n = 0$.

lecting the product, and the volume of the "bottoms," which is also discarded.

The simple batch distillation process was first analyzed by Rayleigh[6] and, more recently, by Kirshbaum.[7] McKisson, Eichelberger, and Ott[8] have analyzed the performance of a batch process utilizing a distillation column and report the following expression:

$$\frac{B_1}{B_2} = \left(\frac{X_{B_1}}{X_{B_2}}\right) \exp\left(\frac{1}{\alpha^{n+1} - 1}\right) = r \exp\left(\frac{1}{\alpha^{n+1} - 1}\right), \quad (1)$$

where B_1 is the initial amount of the distilland, B_2 is the amount of distilland after operation of the still, X_{B_1} is the initial concentration of the more volatile component in the still, X_{B_2} is the concentration of the more volatile component in the still after operation of the still, α is the relative volatility of the more volatile component [equal to the ratio of the vapor pressure of a metal to that of sodium, $\alpha = P^\circ(\text{metal})/P^\circ(\text{sodium})$], and n is the number of theoretical plates in the column. The purification ratio r is given by the ratio X_{B_1}/X_{B_2}. The amount of distillate to be discarded, D', is given by

$$D' = B_1 - B_2', \quad (2)$$

where the primes indicate conditions at the end of the first "cut." Then the fraction of the distillate which is to be discarded is given by the ratio

$$D'/B_1 = 1 - (B_2'/B_1), \quad (3)$$

where the quantity B_2'/B_1 is merely the reciprocal of the value of B_1/B_2 from Eq. (1) evaluated at the conditions obtaining at the end of the first "cut." Table 1 shows the relative volatility values of a number of impurity elements for temperatures of interest. Figures 1, 2, and 3 show the values of D'/B_1 corresponding to values of α up to 20 and values of r up to 50, for distilla-

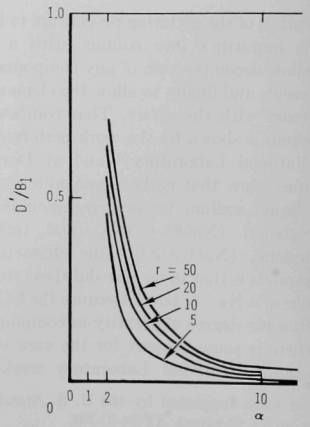

FIG. 2. D'/B_1 Values for a Still and Column for $\alpha > 1$ and $n = 1$.

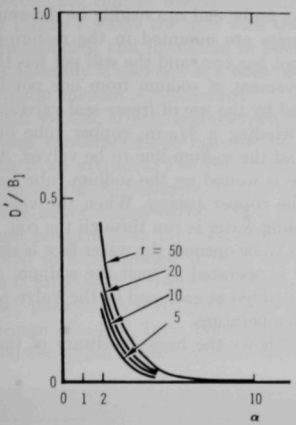

FIG. 3. D'/B_1 Values for a Still and Column for $\alpha > 1$ and $n = 2$.

tion systems having zero, one, and two theoretical plates, respectively. A comparison of Figures 1, 2, and 3 for $r = 20$ and $\alpha = 5$ shows the marked decrease in D'/B_1 values resulting from the use of a distillation column. For no plate, $D'/B_1 = 0.53$; for one plate, $D'/B_1 = 0.12$, and for two plates, $D'/B_1 = 0.025$. For larger values of α the D'/B_1 values are lower than those quoted above, so that it can be concluded that by using a distillation column having two theoretical plates and discarding at least the first 10% of the distillate, all of the more volatile alkali metals can be very adequately separated from sodium. Theoretically, at least a fifty-fold decrease in K, Rb, and Cs content should be achieved using such a process.

The separation of the impurities less volatile than sodium is effected by distilling the sodium away from them and allowing them to concentrate in the still bottoms. The overall material balance for an impurity less volatile than sodium at the end of the second (product) "cut" is

$$X_{B_1}B_1 = X_{B_2}B_2'' + \bar{Y}D'', \qquad (4)$$

where B_2'' is the amount of the distilland after operation of the still to the end of the second "cut," $\bar{Y}$ is the average concentration of the impurity in the distillate, and D'' is the amount of distillate at the end of the second cut. By dividing all terms in Eq. (4) by $\bar{Y}B_1$ and simplifying, one finds that

$$\frac{X_{B_1}}{\bar{Y}} = \frac{D''/B_1}{1 - (X_{B_2}/X_{B_1})(B_2/B_1)}. \qquad (5)$$

The quantity of $X_{B_1}/\bar{Y}$ is the ratio of the initial impurity concentration of the distilland to the average impurity concentration of the distillate and would exactly represent the purification ratio for the product if there were no first "cut." Although it is no longer a correct "purification ratio" for the product when a first "cut" is discarded, it is still a useful function in that it describes the effectiveness of the distillation process for the impurities less volatile than sodium. Equation (5) was evaluated using the relation given in Eq. (1); the results are summarized in Fig. 4 for the case of a simple pot still. This graph shows that for $\alpha = 0.001$, an $X_{B_1}/\bar{Y}$ ratio of 500 is effected by retaining 20% of the distilland as bottoms ($D''/B_1 = 0.80$). If 10% of the distilland is retained as bottoms, the ratio $X_{B_1}/\bar{Y}$ for $\alpha = 0.001$ is 390.

Because the α values of the metallic impurities less volatile than sodium are of the order of 0.001 or smaller, and because the separation ratios for a system having a distillation column will be greater than those shown in Fig. 4, no further analysis of the distillation process is warranted. The preferred distillation system consists of a two-plate column or its equivalent. The first 20% of the distillate is to be discarded, the product cut is the next 60 to 70% of the distillate, and the bottoms cut is thus the last 20 to 10% of the still charge.

The decision was made to use a packed column rather than to attempt to build a tray column. The required height of the column was estimated using the Height Equivalent to a Theoretical Plate (HETP) concept as described by Perry.[9] Based upon reported measurements for saddle-shaped packing materials in ¼- and ½-in. sizes, and an extrapolation based upon the expected mass flow rate of 30 lb/hr-ft² in a 1 ½-in. packed

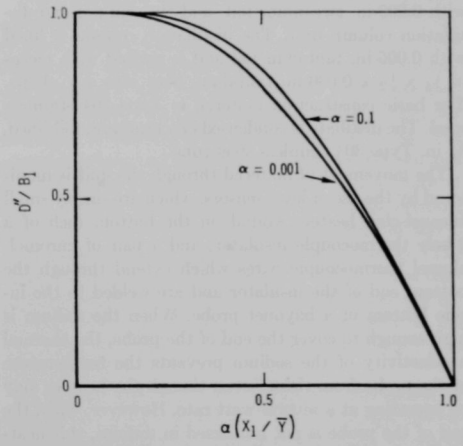

FIG. 4. Values of D''/B_1 for a Still and Column for $\alpha > 1$ and $n = 0$.

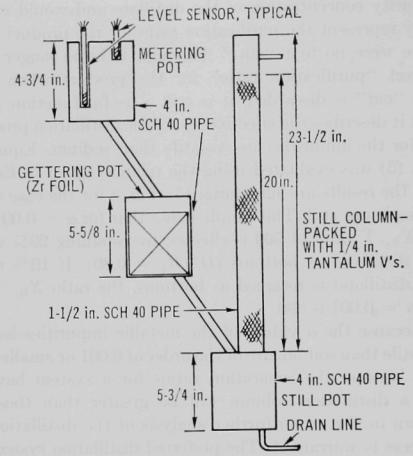

FIG. 5. Schematic Diagram of Sodium-purification Unit.

column, an HETP value of 0.7 ft was estimated. Thus a packed column depth of 1.4 ft is needed. In order to provide a modest contingency, a packed depth of 20 in. was chosen. The remaining design selection to be made was the amount of distilland to be treated. This value was based upon the desired amount of product per run, 400 ± 50 gm. For a 60% yield, about 650 gm is the amount of feed sodium needed per batch.

The apparatus designed to meet these requirements is shown in Fig. 5. It consists of a metering pot in which the batch volume is regulated, a gettering pot packed with 0.002-in. zirconium foil, and the still-pot-and-distillation column unit. The distillation column is lined with 0.005-in. tantalum foil and is packed with pieces of ¼ x ½ x 0.030-in. tantalum, bent into a V shape. The basic construction material is Type 304 stainless steel. The distillate is condensed in a tantalum foil-lined, ⅜-in. Type 304 stainless steel tube.

The movement of material through the unit is monitored by the use of level sensors, which are simply small Inconel-clad heaters wound on the bottom inch of a 2-hole thermocouple insulator, and a pair of chromel-alumel thermocouple wires which extend through the bottom end of the insulator and are welded to the inside bottom of a bayonet probe. When the sodium is high enough to cover the end of the probe, the thermal conductivity of the sodium prevents the temperature of the probe from rising, even though the heaters may be operating at a several-watt rate. However, when the end of the probe is not immersed in sodium, this heating rate is sufficient to cause the probe-end temperature to rise rapidly. Thus, the presence or absence of sodium at the probe end can readily be determined. Four of these units are mounted in the metering pot, the gettering pot has two, and the still pot has three.

The movement of sodium from one pot to another is controlled by the use of freeze-seal valves, which are made by winding a $^{3}/_{16}$-in. copper tube on a ¼-in. pitch around the sodium line to be valved. A sheathed heater wire is wound on the sodium tube between the turns of the copper tubing. When the valve is to be closed, cooling water is run through the coil, and when the valve is to be opened, the water flow is stopped and the heater is operated to melt the sodium. A thermocouple is mounted at each end of the valve to monitor the valve temperature.

Figure 6 shows the basic hardware of the purifica-

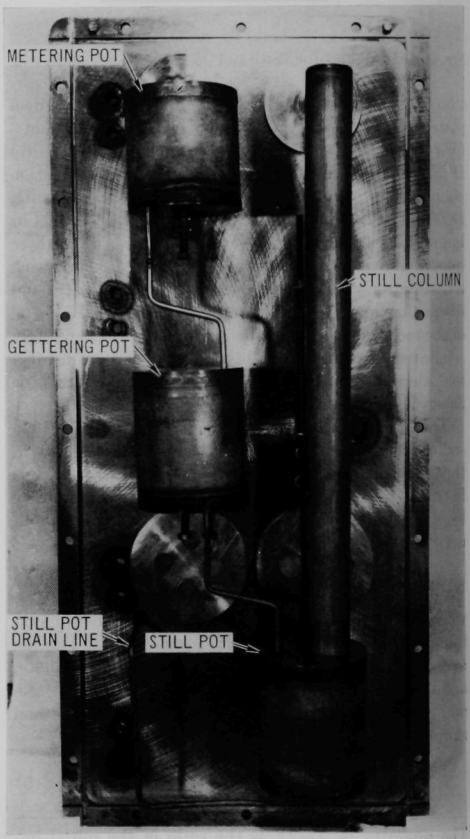

FIG. 6. Basic Structure of Sodium Purification Unit.

tion unit before the control instrumentation was installed, and Figure 7 shows the unit with the heaters, valves, thermocouples, and insulation in place. In operation, this assembly is enclosed in a housing in which a roughing pump vacuum is maintained.

The product sodium, after it is condensed in the tantalum-foil-lined condenser flows into the product collector, which is an extruder. The construction of this unit is shown in Fig. 8. Basically, it is a simple unit consisting of a heavy-walled barrel, and a piston. The liquid sodium product flows into the extruder and at first is allowed to flow through and out the discharge tube, which is fitted with a freeze-valve unit. The first distillate, D', passes into a container held in an ion-pumped vacuum of $\sim 10^{-7}$ Torr. Then the freeze valve is closed, and the liquid sodium product collects in the

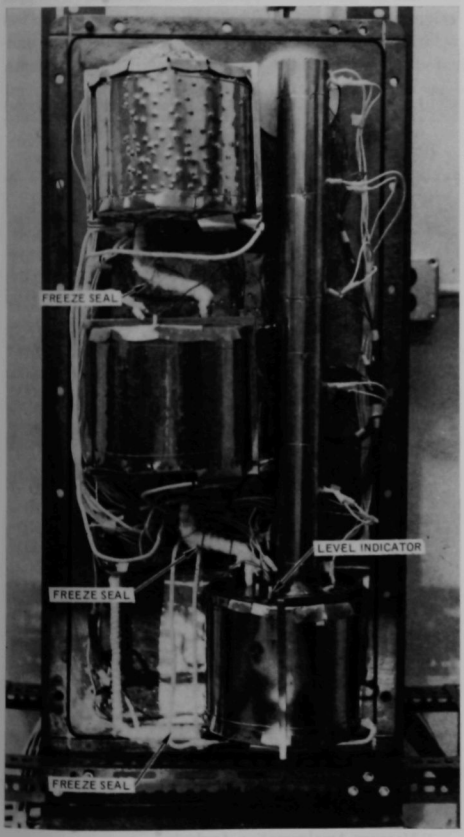

FIG. 7. Fully Assembled Sodium-purification Unit.

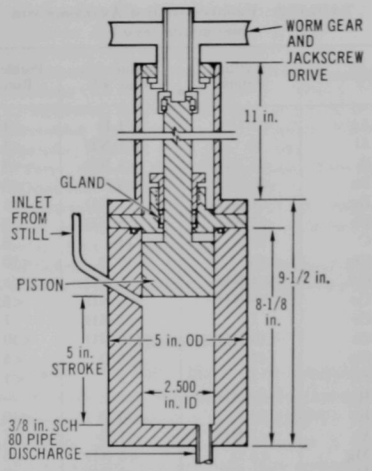

FIG. 8. Sodium Extruder.

extruder. The barrel is kept at about 125°C to prevent the sodium from freezing during the product-collection period. By maintaining the sodium as liquid, mixing occurs due to convection currents, so that the product sodium becomes essentially uniform in composition. When the product-collection is complete, the extruder is allowed to cool. When the sodium if frozen, the piston is run down against it to seal the purified sodium in the unit.

2. Procedure and Results

The purification apparatus described above has been operated to produce five product-sodium preparations. In these preparations, the operating technique involved filling of the metering pot with about 650 ml of sodium, and draining it into the gettering pot which was preheated to 650°C. The gettering process was carried out overnight at 650–675°C for a minimum of 16 hr. The gettered sodium was then drained into the still pot and distilled under high vacuum at a still temperature of 550 ± 5°C, at which temperature the vapor pressure of sodium is 9 Torr. The still column operated at 550°C at the bottom, and at about 525–530°C at the top. (The vapor pressure of sodium at 525°C is 6 Torr.) The temperature of the condenser was about 500°C at the beginning of the run and decreased to about 490°C at the end of the run. The distillation rate was about 1.5 to 2.0 ml/min.

In practice, the entire still system was precleaned by running one or two batches of sodium through the entire sequence without collecting any product to ensure that the internal surfaces were washed by fresh, clean

TABLE 2. PRODUCT-SODIUM ANALYSES FOR IMPURITIES (PPM)

Elements	Starting Material	Purification Run #1	Purification Run #3
Ag	<1 D[a]	<1 D	<1 D
Al	3	<1 ND	<1 ND
B	<1 ND[b]	<1 ND	<1 ND
Ba	<5 ND	<5 ND	<5 ND
Be	<1 ND	<1 ND	<1 ND
Bi	<5 ND	<5 ND	<5 ND
C	35	14	8
Ca	10	<10 D	<10 D
Cd	<1 ND	<1 ND	<1 ND
Co	<5 ND	<5 ND	<5 ND
Cr	1	<1 ND	1
Cs	<10 ND	<10 ND	<10 ND
Cu	17	<5 D	<5 D
Fe	4	1	<1 ND
H	<1 ND	—	—
K	50	<10 D	<10 D
Li	<1 ND	<1 D	<1 ND
Mg	<5 D	<5 ND	<5 ND
Mn	<1 ND	<1 ND	<1 ND
Mo	<1 ND	<1 ND	<1 ND
Ni	6	<5 ND	<5 ND
O	15[c]	5[c]	1[c]
Pb	7	<1 ND	<1 ND
Rb	<5 ND	<5 ND	<5 ND
Si	60	<10 D	<10 D
Sn	<5 ND	<5 ND	<5 ND
Ta	—	—	<1 ND
Ti	<5 ND	<5 ND	<5 ND
V	<1 ND	<1 ND	<1 ND
Zn	<100 ND	<100 ND	<100 ND
Zr	<10 ND	<10 ND	<10 ND

[a] D = Detected.
[b] ND = Not Detected.
[c] Mercury Amalgamation Analysis.

sodium prior to making the product run. This precaution is considered particularly important if the unit has been idle for an extended period between runs.

The operation of the unit has been rather routine, with the exception of the second purification run. Early in that run, a short circuit developed in one of the level probes and the resulting arc melted a hole in the probe wall. It was necessary to halt the run and to replace the probe, and, in doing so, the still appeared to have been contaminated, even though an argon purge was used during the repair period.[8]

The starting material for Runs #1, #2, and #3 was obtained from the Systems Quality Sodium supply loop,[10] which has a cold trap for control of the oxygen and a stainless steel-foil-packed hot trap for control of the carbon in the circulating sodium. The loop operates at 500°F with the hot trap at 1200°F. Two batches of material were obtained from the supply loop. The first was taken shortly after the loop was put into operation. This material was used in making preparations #1 and #3 as is shown in Table 2. The second supply batch was obtained after the operation of the loop had been stabilized and showed a markedly lower carbon content, as shown in Table 3. This material was used as starting material for Purification Runs #4 and #5.

An examination of Tables 2 and 3 shows the separation process to be effective and that the apparatus does produce product sodium in which the sum of the detected impurities totals less than 60 ppm. The oxygen content is reduced from a starting level of 15 ppm to 5 ppm and 1 ppm, and from a starting level of 8 ppm to 2 ppm and <2 ppm. All of these final values for oxygen content are at the limit of detection of the analytical procedure. Evidence that the column is performing is shown in the reduction of the starting levels of potassium of 50 and 75 ppm to the uniform <10 ppm values in the product. That the separation of the less volatile elements is also effective is shown by the indicated reductions in the Ca, Mg, Cu, Ni, and Si contents.

TABLE 3. PRODUCT-SODIUM ANALYSES FOR IMPURITIES (PPM)

Elements	Starting Material	Purification Run #4	Purification Run #5
Ag	<1[a]	<1 D	1 D
Al	1	<1 ND	<1 ND
B	<1 ND[b]	<1 ND	<1 ND
Ba	<5 ND	<5 ND	<5 ND
Be	<1 ND	<1 ND	<1 ND
Bi	<5 ND	<5 ND	<5 ND
C	8	9	6
Ca	10	<10 D	<10 D
Cd	<1 ND	<1 ND	<1 ND
Co	<5 ND	<5 ND	<5 ND
Cr	1	<1 ND	<1 ND
Cs	—	<10 ND	—
Cu	5	<5 D	<5 D
Fe	1	1	1
H	<1 ND	—	—
K	75	<10 D	<10 D
Li	<1 ND	<1 ND	<1 ND
Mg	<1 D	<1 D	<1 ND
Mn	3	<1 ND	<1 ND
Mo	<1 ND	<1 ND	<1 ND
Ni	5	<5 ND	<5 ND
O	8[c]	2[c]	<2[d]
Pb	1	3	<1 ND
Rb	—	<5 ND	—
Si	10	<10 D	<10 D
Sn	<5 ND	<5 ND	<5 ND
Ti	<5 ND	<5 ND	<5 ND
V	<1 ND	<1 ND	<1 ND
Zn	<100 ND	<100 ND	<100 ND
Zr	<10 ND	<10 ND	<5 ND

[a] D = Detected.
[b] ND = Not Detected.
[c] Mercury Amalgamation Analysis.
[d] Neutron Activation Analysis.

However, no quantitative comparisons with distillation theory are possible because of the very low levels of all the impurities.

The most puzzling aspect of the purification process is the apparent inability of the apparatus to reduce the carbon content of the product below a value of 8 ± 2 ppm. At first glance, Purification Runs #4 and #5 do not appear to have effected any decrease in carbon content. However, observations of other systems whose carbon content should be very low (such as in zirconium-gettered sodium) have also shown limiting carbon analyses of about 10 ppm.[11] This, therefore, suggests that these values may be arising from some analytical limitation rather than from the actual amount of carbon impurity in the sodium. However, this is only speculation at present.

The hypothesis of Argonne National Laboratory workers for carbon transport as CO in the sodium distillation process is not substantiated in this system, because the amount of carbon in the product is several times greater than the amount of oxygen. If CO were the transport medium, the amount of oxygen would have to be at least 16/12 as great as the carbon content.

3. Conclusions

The apparatus for preparing highly purified sodium for use in chemistry studies is quite effective. The impurity content of its product is very low, and the material is well-suited for the planned studies. An anomaly does exist, however, in that the carbon content of the sodium involved appears to approach an asymptotic value of about 8 ppm. No suitable explanation for this observation is now apparent.

REFERENCES

1. R. C. Vogel *et al.*, *Chemical Engineering Division, Research Highlights, May 1965–April 1966*, ANL-7175.
2. V. M. Sinclair, R. A. Davies, and J. L. Drummond, "Reaction of Carbon Monoxide with Sodium," *The Alkali Metals*, An International Symposium Held at Nottingham on July 19–22, 1966, Special Publication No. 22, The Chemical Society, London (1967).
3. R. C. Vogel *et al.*, *Chemical Engineering Division, Semiannual Report, January–June, 1964*, ANL-6900.
4. R. C. Vogel *et al.*, *Chemical Engineering Division, Semiannual Report, July–December, 1965*, ANL-7125.
5. G. W. Horsley, *The Purification of Sodium by Vacuum Distillation*, AERE M/R 1152 (May 12, 1953).
6. Lord Rayleigh, Phil. Mag. **8**, 534 (1904).
7. E. Kirschbaum, *Distillation and Rectification*, Chemical Publishing Co., Inc., Brooklyn, N. Y., (1948) p. 71 ff.
8. R. L. McKisson, R. L. Eichelberger, and J. B. Ott, *The Construction and Operation of a Sodium Purification Apparatus*, NAA-SR-12444 (July 15, 1967).
9. J. H. Perry, *Chemical Engineers Handbook*, Third Edition, McGraw-Hill, New York, N. Y. (1950).
10. E. W. Murbach, J. E. Bodine, and N. W. Heath, *The System Quality Sodium Loop Design, Construction, and Startup*, NAA-SR-12327 (1967).
11. D. C. Gehri and J. B. Ott, *The Solubility of Elemental Carbon in Sodium*, AI-AEC-MEMO-12686 (June 1968), p. 6.

Discussion

Mr. Mueller (APDA): Have you compared this method of purification with ion transfer through glass with a potential difference at around 1200°F? You can take relatively dirty sodium and transfer it through glass into a vacuum, and get very pure sodium on the other side.

Mr. Eichelberger: Do you have a problem with rate there? I haven't considered this method.

Mr. Mueller: I really don't know the speed, but I do know this is the main cause of our lighting problem when we are working in the reactor. We needed light down there to get the zirconium segments out, and we ran across this as one of our major problems.

Mr. Eichelberger: I would think your sodium would end up with quite a bit of silicon in it. I'm not familiar with this as a laboratory procedure.

Mr. Lemke (duPont): You didn't mention anything at all about reflux ratio in the operation of your still. Did you induce reflux or did you just take what reflux you got from radiant losses from your column?

Mr. Eichelberger: We are not able to measure reflux ratio, but I believe it is high.

Mr. Shannon (BNWL): Do you use an oil vacuum system for your rough vacuum? If so, the back-diffusion of oil vapor could provide carbon.

Mr. Eichelberger: We have a roughing pump vacuum on the outside container, but this never sees the sodium. The sodium region is pumped with ion pumps only.

Analytical Methods for Determining Impurities in Sodium below 10 ppm*

CARLETON D. BINGHAM, JAMES M. SCARBOROUGH, AND MARY S. MASEDA

Atomics International
A Division of North American Rockwell Corporation
Canoga Park, California

(PRESENTED BY R. L. EICHELBERGER)

ABSTRACT

In support of a program to measure the solubility in sodium of the elements potentially used in LMFBR cladding or structural material, it has been necessary to modify or develop methods to extend the sensitivity or improve the precision for measurement of the concentration of trace elements in high-purity sodium.

The methods for measuring trace quantities of iron, cobalt, nickel, chromium, manganese, copper, bismuth, niobium, and molybdenum will be described, and the results of statistical analysis of the data will be presented. The effect of the interfering elements investigated is included in the presentation. Those items of negative results will be given to provide other investigators with information to prevent their wasted efforts.

Potential new or improved methods for future research to further support basic solubility measurements are discussed.

1. Introduction

A requirement to provide high-sensitivity and high-precision chemical measurements of trace-level metallic impurities in small (~1 g) samples of sodium grew out of a program to acquire basic solubility data for potential LMFBR system materials in liquid sodium. Because of the design of the solubility experiments,[1] the quantity of impurity element available for measurement was in the range 0–10 μg. Many of the established spectrophotometric methods claiming low ppm-level impurity sensitivity require as starting material samples much larger than 1 g. Others suffer from imprecision in the measurement such that real differences in experimental data are masked out by statistical uncertainties. The potential matrix effect of sodium is not too well-documented for some methods. It therefore became necessary to verify and qualify new or modified procedures for selected elements in the 0–10 μg range in 1-g samples of sodium in the presence of other possibly interfering elements.

This paper will summarize our experience in developing these methods for Fe, Co, Ni, Cr, Mn, Mo, Nb, Bi, and Cu, and will present experimental data to support the claims made for them.

* Work performed under the auspices of the U. S. Atomic Energy Commission under Contract No. AT-(04-3)-701.

2. Methods

Results published last year by our laboratory[2] showed that the principal elements in structural stainless steels (Fe, Cr, Ni, Co, and Mn) used in sodium-cooled nuclear reactor systems could be measured as impurities in a 1-g sample of sodium by atomic absorption spectrometry (AAS) with lanthanum hydroxide-carrier precipitation. Figure 1 summarizes the results over the impurity range 0–1 ppm in solution in the presence of equal quantities of the other impurity elements, 1 mg/ml lanthanum and 500 ppm sodium. Each regression-line equation was generated from 24 data points (i.e., three points at each of the following solution concentrations: 0, 0.05, 0.10, 0.20, 0.40, 0.60, 0.80, and 1.0 ppm). Use of this technique therefore provides a 95% confidence limit for the precision of measuring the impurity content in 1 g of sodium of $\pm$0.1 ppm at the 1-ppm impurity level.

The conduct of the solubility experiments[1] introduces potentially interfering elements from the collector crucible into the sodium to be analyzed. These crucibles are fabricated from Nb-1Zr or Mo-½Ti commercial alloys or high-purity titanium. The collector material for a given series of experiments is chosen so as to minimize known interferences to the chemical analysis. In order, however, to demonstrate that the collector matrix offers no unsuspected interference to the determination of a given impurity, a series of qualifying experiments were performed, and the results obtained were analyzed statistically to discover if a bias was created.

2.1. Nickel

The possible effects of titanium on the AAS[2] and dimethylglyoxime spectrophotometric methods were investigated using synthetic solutions containing 1) 0–10 μg nickel only, 2) nickel plus 0.5 g. sodium, and 3) nickel plus 0.5 g. sodium and 500 μg titanium. Figure 2 shows results from the AAS determination of nickel. Over the concentration range investigated, the 95% confidence interval for a value estimated from a single

observation is equivalent to ±1 μg based upon pooled data. The presence of "noise" in the nickel lamp (since replaced) gave rise to slightly less favorable precision than previously reported.[2] Figure 3 summarizes the results of the spectrophotometric method in which pooled data were used to generate the regression line. Over the range 1–10 μg, the 95% confidence interval for a value estimated from a single observation is equivalent to ±0.5 μg.

2.2. Molybdenum

The possible effect of niobium or zirconium and sodium on the "standard" dithiol spectrophotometric method for molybdenum[3] was investigated using 1) solutions containing 1–10 μg molybdenum, 2) molybdenum + 13.6 μg zirconium, 3) molybdenum + 420 μg niobium + 500 mg sodium, and 4) molybdenum + 13.6 μg zirconium + 420 μg niobium + 500 mg sodium. Individual plots were prepared of optical density *vs* μg molybdenum/25 ml (see Fig. 4). Since there appeared to be no significant differences, visually, among the four curves, the regression analysis was performed using pooled data (N = 35). The 95% confidence interval of a value estimated from a single observation is equivalent to ±0.4 μg molybdenum over the range investigated.

2.3. Chromium

Initial attempts to apply the conventional diphenylcarbizide spectrophotometric method for chromium over the range 0–25 μg chromium/25 ml of final solution resulted in a lack of suitable precision for solubility measurements. The possible influence of niobium and/or zirconium on the lanthanum hydroxide-carrier atomic-absorption method[2] was therefore investigated. Chromium solution standards were aspirated directly into the AAS burner with no prior treatment (see Curve ○ of Fig. 5); chromium standards were precipitated with 10 mg lanthanum carrier, dissolved and aspirated (see Curve △ of Fig. 5), and chromium standards were spiked with 670 μg niobium, 70 μg zirconium, and 0.5 g. sodium, and precipitated with 10 mg lanthanum carrier, dissolved, and aspirated through the burner (see Curve ▽ of Fig. 5). No interference was evident. The precision measurement was essentially that observed and reported earlier.[2]

2.4. Niobium

The absence of interference of up to 1 mg titanium and 0.5 g sodium has been demonstrated over the range 0–10 μg niobium using a 4-(2-pyridylazo) resorcinol (PAR) spectrophotometric method. A series of parametric variations was applied to seven sets of calibration curves: 1) niobium + 8 drops conc HF, 2) niobium + 0.5 g sodium, 3) niobium + 0.5 g sodium + 500 μg titanium, 4) niobium in 4% tartaric acid, 5) niobium + 0.5 g sodium + 1 mg titanium, 6) niobium in 4% tartaric acid fumed down, and 7) niobium + 0.5 g sodium + 6 drops conc HF. For each set of data the regression curve was calculated, then a curve was calculated from the pooled data (N = 94). No attempt was made to exclude possible discrepant data points, thereby introducing the likelihood of some unfavorable statistical weighting. Only one of the seven curves, however, failed to be completely enclosed by the 2σ envelope (see Fig. 6). From the pooled data, the 95% confidence interval over the range 1–10 μg niobium for a value estimated from a single observation is ±0.65 μg.

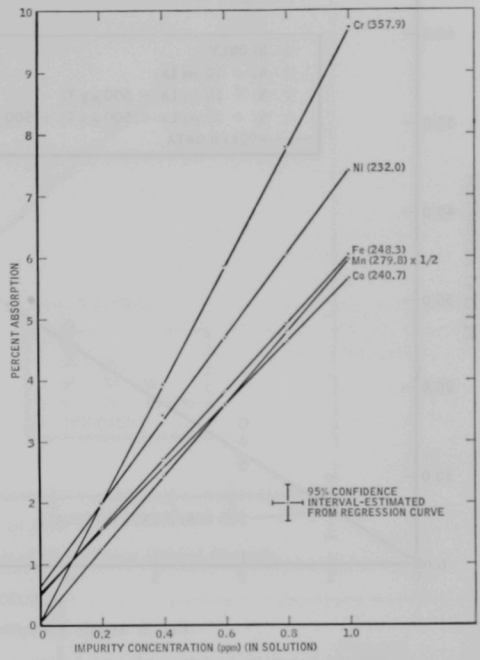

FIG. 1. AAS Responses for Impurities in Sodium (Lanthanum Carrier Precipitation).

2.5. Bismuth

Preliminary experiments with solutions containing 10–100 ppm bismuth, a range of stainless steel matrix materials and sodium as impurities indicate that bismuth can be determined without removal of the sodium matrix and with no interference from Fe, Ni, Cr, Co, or Mn at solution concentrations less than 5 mg sodium/ml and 20 ppm Fe, Ni, Cr, Co, and Mn.

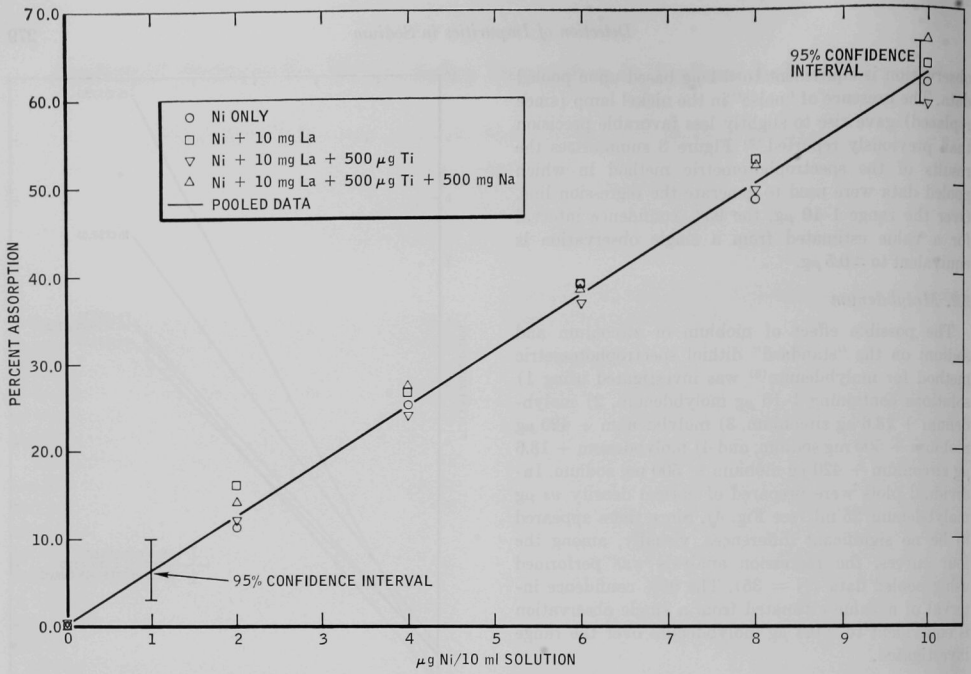

FIG. 2. Atomic Absorption Determination of Nickel.

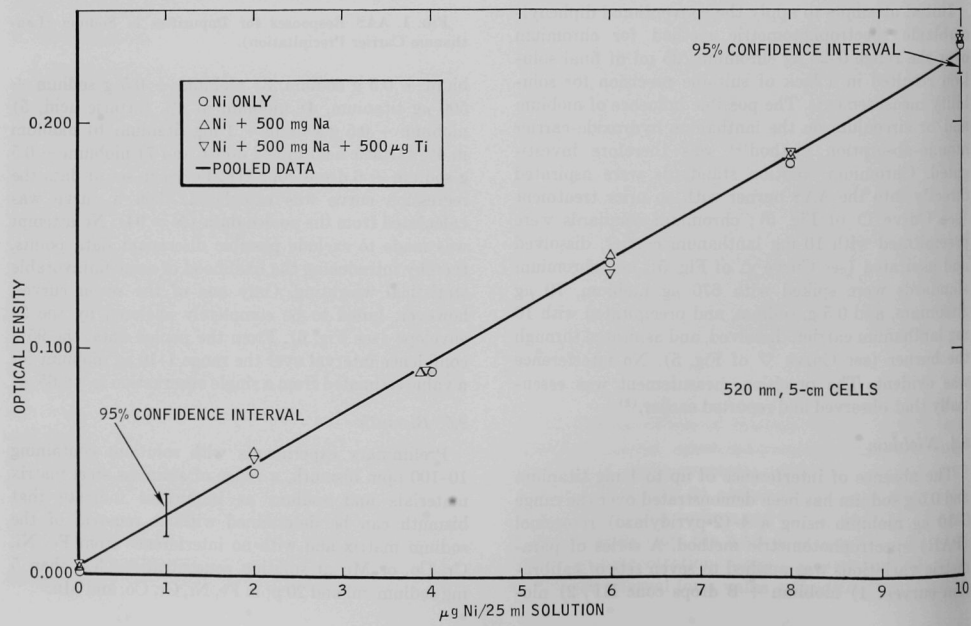

FIG. 3. Spectrophotometric Determination of Nickel (Dimethylglyoxime Method).

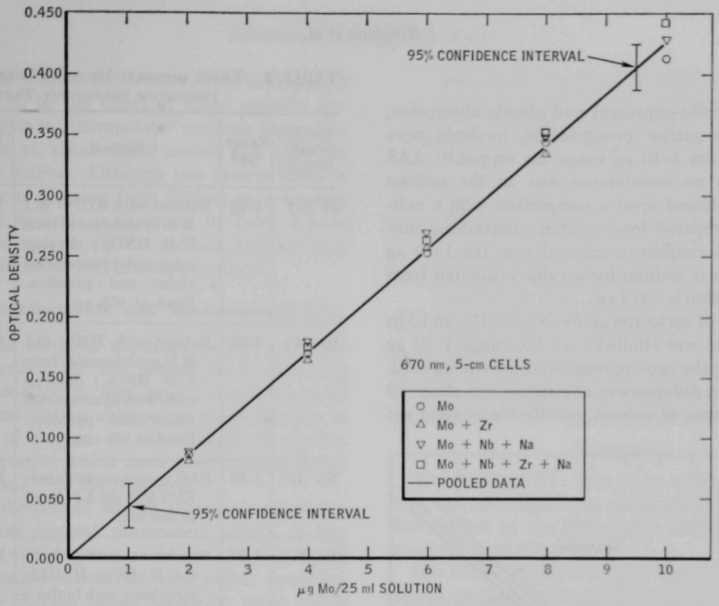

FIG. 4. Spectrophotometric Determination of Molybdenum (Dithiol Method).

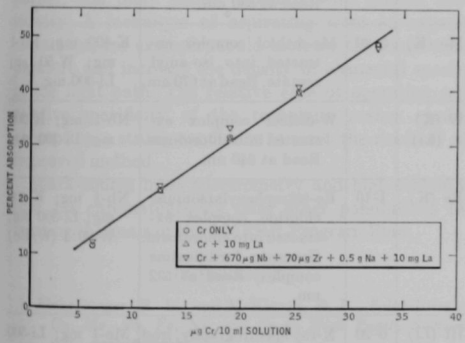

FIG. 5. Atomic Absorption Determination of Chromium.

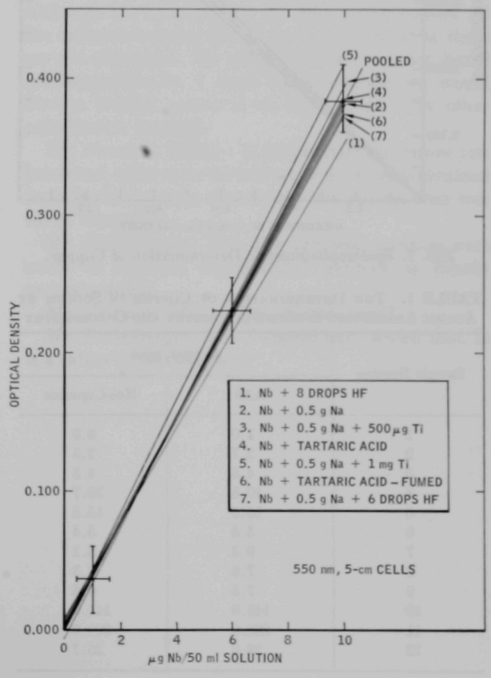

FIG. 6. Spectrophotometric Determination of Niobium Using PAR.

2.6. Copper

Colorimetric (neo-cuproine) and atomic absorption, with lanthanum-carrier precipitation, methods were compared over the 1–10 μg range for copper.[4] AAS results indicate no interference due to the sodium matrix residue. Based upon a comparison with a calibration curve prepared from solutions containing only copper, the 95% confidence interval over the 1–10 μg range for copper in sodium for a value estimated from a single observation is ±0.4 μg.

The influence of up to 100 μg Fe, Ni, Co, Cr, and Mn in 1 g of sodium was studied over the range 1–10 μg for copper using the neo-cuproine colorimetric method. Although a slight difference in absorption was observed due to the presence of sodium, no effect was apparent

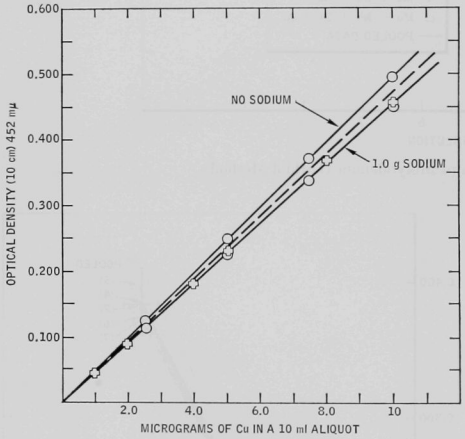

FIG. 7. Spectrophotometric Determination of Copper.

TABLE 1. THE DETERMINATION OF COPPER IN SODIUM BY ATOMIC ABSORPTION SPECTROPHOTOMETRY AND COLORIMETRY

Sample Number	Copper, ppm	
	AAS	Neo-Cuproine
1	7.0	6.9
2	2.7	2.3
3	4.5	4.3
4	10.8	10.7
5	16.3	15.8
6	5.5	5.4
7	9.3	8.1
8	7.6	7.3
9	7.5	6.6
10	149.0	141.0
11	208.0	209.0
12	24.6	25.7

TABLE 2. TRACE-IMPURITY METHODS USED IN LITHIUM AND POTASSIUM SOLUBILITY TESTS

Element Sought (matrix)	Range (μg)	Method	No Influence from Impurities
Zr (K)	3–50	Extract with TOPO (0.1 *M* in cyclohexane) from 7 *M* HNO_3; develop color with pyrocatechol violet and pyridine. Read at 655 nm.	Mo-1 mg; K-200 mg
Hf (K)	3–50	Extract with TOPO (0.1 *M* in cyclohexane) from 7 *M* HNO_3; develop color with pyrocatechol violet and pyridine. Read at 655 nm.	Mo-1 mg; K-200 mg
Nb (K)	1–10	PAR in acetate-buffered-EDTA at pH 5.8. Read at 550 nm.	K-200 mg; Mo-1 mg
Ta (K)	1–20	Hexone extraction from 0.4 *M* HF-6 *M* HCl; strip back with buffer + EDTA; develop color with phenylfluorone. Read at 530 nm.	Mo-100 μg; K-250 mg; Li-250 mg
Mo (K)	2–20	Mo-dithiol complex extracted into iso-amyl acetate. Read at 670 nm.	K-400 mg; Nb-1 mg; W-50 μg; Li-300 mg
W (K) (Li)		W-dithiol complex extracted into chloroform. Read at 640 nm.	Nb-1 mg; K-200 mg; Li-200 mg
Re (K)	1–10	Re-tetraphenylarsonium chloride complex extracted into chloroform. Generate furildioxime complex. Read at 532 nm.	Nb-1 mg; K-400 mg; Li-300 mg; W-20:1 (W/Re)
Hf (Li)	0–20	X-ray spectrography, iron hydroxide carrier, lutetium internal standard, Pt target X-ray tube.	Mo-1 mg; Li-500 mg

with the additional presence of the Fe, Ni, Co, Cr, and Mn impurities (see Fig. 7). Table 1 compares some of the results obtained by AAS and colorimetry in some early applications of these techniques.

Experience obtained from an earlier program to provide basic solubility data of elements in liquid potassium and lithium[5, 6] indicated that very few literature references treated the 1–10 μg range of refractory or transition metal impurities in alkali

metals or, if the subject was treated, little information was available as to the effect of other metallic impurities. Attempts to "extrapolate" methods from some other matrix to an alkali metal matrix met with less than complete success. Although less matrix effect is expected to occur in going from lithium or potassium to sodium, the methods summarized in Table 2 have not been tested specifically for sodium, and are only offered for information and first-choice guides.

3. Future Requirements and Recommendations

Although the methods described herein are marginally satisfactory for the present needs involving solubility measurements, they generally are not at all adequate for measuring changes in solubility due to the presence of oxygen or other chemical species. Methods are needed which have precisions of better than 0.1 μg at less than the 1-μg level.

Within the domain of atomic-absorption spectrometry there exist several parameters which, if improvements in performance could be effected, would result in increased sensitivity and better precision. Some of these include higher intensity, more stable source lamps, more stable, less "noisy" flame and burner, and more stable detectors with greater sensitivity. A technique of aspirating from an organic extractant, for example, could increase the flame temperature and increase the density of elemental species in the light path. The relative ease of operation and relative specificity of the technique makes atomic absorption a strong candidate to meet the needs of an improved method.

Spark-source mass spectrometry and high-temperature gas chromatography offer other possibilities for meeting the goals of the LMFBR Program Plan.

REFERENCES

1. Eichelberger, R. L., and McKisson, R. L., *Solubilities of Cu, Mo, Nb, Fe, Ni, and Cr in High Purity Sodium*, THIS CONFERENCE.
2. Scarborough, J. M., Bingham, C. D., and DeVries, P. F., *Determination of Trace Metallic Impurities in High Purity Sodium Using Atomic Absorption Spectrometry*, Anal. Chem., **39**, 1394–1397 (1967).
3. Sandell, E. B., *Colorimetric Determination at Traces of Metals*, Interscience Publishers, Inc. (1959).
4. Scarborough, J. M., *The Determination of Trace Level Copper in Sodium by Colorimetry and Atomic Absorption Spectrophotometry*, Paper presented at the 155th National Meeting of the American Chemical Society, San Francisco, California, April 1–4, 1968.
5. McKisson, R. L., Eichelberger, R. L., Dahleen, R. D., Scarborough, J. M., and Argue, G. R., *Solubility Studies of Ultra Pure Transition Elements in Ultra Pure Alkali Metals—Final Report*, AI-65-210 (also issued as NASA-CR-610) (March 21, 1966).
6. Eichelberger, R. L., McKisson, R. L., and Johnson, B. G., *Solubility Studies of Refractory Metals and Alloys in Potassium and in Lithium*, AI-68-110 (1968).

Discussion

Mr. Berkey (W): Was there any particular reason why the techniques you discussed in this paper were not applied to the high-purity sodium that you discussed in your first paper?

Mr. Eichelberger: Probably the only good reason is one of economics. We were convinced that our sodium was pretty good, and we were concerned with more precise measurements than the spectrograph could give. Although the last slide on the first paper showed all the detectable impurities in the sodium, most of them are not detectable. For example, nickel was not found spectrographically. I don't know whether we would have a fruitful answer if we tried to do it by other colorimetric methods.

Mr. Newman (BNL): Is it true that the curves you presented, other than the last set of data, were obtained from static samples, that it was not sodium that was taken through?

Mr. Eichelberger: Yes. The synthetic samples were made to simulate experimental samples as closely as was possible.

Mr. Newman: Was sodium chloride used?

Mr. Eichelberger: Yes. I should have stated that. It is a rather important point.

A Direct Method for the Determination of Carbon in Sodium

EDGAR BERKEY AND WILLIAM M. HICKAM

Westinghouse Research Laboratories
Pittsburgh, Pennsylvania

(PRESENTED BY E. BERKEY)

ABSTRACT

A new approach to the analysis of sodium for total carbon is discussed. The method employs spark-source mass spectrography and requires no chemical treatment of the sample. Past work in our laboratory had established its feasibility for sodium analyses. We have now shown that detection limits in the low parts per million range for carbon can be readily attained. The carbon blank of the instrument is limited by a combination of procedures which includes periodic baking, exposure only to argon during venting, cryo-pumping the source chamber, and a thorough pre-spark of the samples. The sodium is handled either under vacuum ($\sim 10^{-7}$ Torr) or in high-purity argon and is sparked directly while being cooled with liquid nitrogen. The analysis of 24 samples from a single batch indicates that the precision of the technique is of the order of 10–20% and that information on the heterogeneity of carbon in sodium can be obtained.

1. Introduction

Contact with liquid sodium can promote considerable carbon transfer among the structural components of a metallic containment system.[1-4] Some metals can be carburized, while others can be decarburized, and since either type of carbon transfer usually produces deleterious effects on the properties of the metals, there has been great interest in studying appropriate metal-sodium-carbon systems.[5-7] Concurrently, it has been necessary to develop suitable analytical techniques for determining carbon in sodium. These have the long-range purpose of establishing quantitatively the "carburization potential" of a given sodium sample. Techniques have been developed and are available in the literature that can variously determine "total" carbon, "elemental" carbon, or "dissolved" species" of carbon.[8-17]

Nevertheless, the "carburization potential" of sodium remains an elusive quantity to establish analytically. It is unclear which single species of carbon or which combination of such species is responsible for the phenomenon of carbon transfer. The analytical situation is further complicated by the paucity of good information on the sodium-carbon system and by the failure of two separate carbon round robins to achieve more than a modicum of agreement on the results between different laboratories and analytical techniques.[18] These round robins concluded that the variety of techniques employed seemed capable of determining carbon in sodium at levels above 10 ppm, but that there was apparent difficulty in providing homogeneous samples at a controlled level of carbon impurity. Some systematic differences between the results from distinct classes of techniques were also noted.

In view of the lingering uncertainties about sodium-carbon chemistry and the associated analytical questions, it is appropriate to discuss the application of spark-source mass spectrography (SSMS), an entirely new approach, to the determination of carbon in sodium. Previous work in our laboratory has demonstrated the feasibility of analyzing sodium quantitatively by this technique.[19] In this paper we discuss more thoroughly how it can be used for the determination of total carbon.

The major difference of SSMS from previous approaches to the carbon-in-sodium problem is that it provides a direct method to perform the analysis—chemical treatment of the sample is not required. Furthermore, only minimal sample handling and preparation is necessary. The analysis can be performed rapidly, and in addition to the average carbon concentration in the sample analyzed, information on the local heterogeneity of the sample can be obtained.

2. Previous Methods

Carbon can exist in many different chemical forms in sodium. The number and types of such forms depend on the history of the sample. Nevertheless, for most sodium it appears that the major part of the carbon is present as particulate matter in the uncombined elemental state having a size range in the micron region and below. (The solubility of carbon in sodium is not precisely known, but there are indications that it is quite low, $\ll 0.1$ ppm.[22]) Other possible types of carbon species include carbides, carbonates, cyanides, hydrocarbons, and carbonyl compounds.

Techniques intended for analyzing "total" carbon do not generally identify the contribution from individual species, unlike techniques aimed at indirectly

elucidating the "dissolved" species. Techniques for determining only "elemental" carbon are likely to miss a significant amount of the carbon present in a given sample.

In general, all carbon procedures available in the literature rely at some point on the oxidation or dissolution of the sodium to generate carbon-containing gases (CO_2, C_2H_2, CH_4, C_2H_6, etc.) which are subsequently collected and measured by some means. Typical drawbacks associated with these procedures include the possibilities of contamination from the prolonged chemical treatment required, the presence of sometimes large and erratic blanks, the incomplete release, conversion, or collection of all the contained carbon, and finally the possibility of loss from parasitic gettering.

There is no doubt that some procedures have in theory succeeded in overcoming some of these drawbacks. For example, the use of isotopic dilution or photo activation eliminates the blank problem.[11, 17] Nonetheless, the possibilities of systematic errors in the universally employed oxidation step remain, and the second carbon round robin concluded that the temperature at which this oxidation was carried out was critical to the complete conversion of the carbon.

By contrast, the use of SSMS obviates the need for oxidizing the contained carbon. The analysis is performed by detecting on a photographic plate the $^{12}C^+$ ions generated from the samples during the high-voltage spark discharge between the electrodes. For carbon in the low parts per million concentration range, only about 10^{17}–10^{18} atoms of material need to be consumed to produce a "just detectable" $^{12}C^+$ line. This limited sampling capability of the technique means that any gross sample segregation on this scale should be directly observable in the results. SSMS has the capability of determining "total" carbon most easily, but as the sodium-carbon system becomes more well-known, it may be possible to identify individual species. Most importantly, since SSMS is a multi-element technique, other impurities are detected simultaneously with carbon, and this gives it a unique capability compared with previous methods.

3. Experimental Procedure

The total experimental procedure employed in our laboratory for sodium analyses by SSMS has previously been published.[19] In the present paper, only those aspects of the procedure which have particular relevance to the determination of carbon will be elaborated.

The quantitative determination of parts per million levels of carbon in metals has been a long-standing analytical problem. It has already been established that SSMS can be successfully applied to such an analysis if sufficient care is taken to reduce the instrument blank, for example, by using a cryosorption pump in the source chambers.[20] Other procedures can also be used.

The carbon background in a typical spark-source instrument arises primarily from the ionization of CO_2 and various hydrocarbon molecules which are present in the source chamber. These contaminants can exist either as gaseous species or as adsorbed molecules on the walls of the chamber, which are spalled under the ion bombardment during sparking. The adsorbed molecules are generally thought to be the largest contributor. The contaminants are present in the source either because of their existence in the air normally used to vent the chamber, because of back diffusion of oil from the diffusion pumps, or because of unclean surfaces.

Since the nature of the SSMS analysis makes it extremely difficult to establish the carbon blank for any given run, definite measures must be taken to eliminate the contaminants at their origin. We employ a combination of three procedures to limit the carbon background and are the beneficiaries of another which results from the particular nature of the analysis.

1. After a thorough cleaning of all parts, the source chamber of the instrument is periodically baked under high vacuum at 150°C for a minimum of 8–10 hr. It is well known that such a procedure removes adsorbed gases (CO_2, H_2O, etc.) and hydrocarbons (C_xH_y) from the walls. Any small amounts of these substances not removed during the bakeout are unlikely to interfere in the subsequent analysis.

2. Secondly, once the adsorbed molecules have been removed from the walls, they are prevented from returning by never exposing the source to air until the next cleaning. The venting system of our mass spectrometer has been modified so that the source chamber is brought up to atmosphere with dried high-purity argon. A vacuum glovebox bolted to the front of the source when venting occurs completes the means by which atmospheric contaminants are excluded. Thus, all surfaces tend to absorb argon molecules during venting, and this inhibits the subsequent adsorption of any contaminants present in the gas. The pump-down time of the instrument is noticeably quicker with an argon vent system, and the resultant atmosphere and surfaces remain cleaner.

The oil diffusion pumps are baffled and trapped with liquid nitrogen, which further assures the maintenance of a high-purity environment.

3. Since the melting point of sodium (97.8°C) is relatively low and since substantial amounts of heat can be generated at the sodium electrodes during spark-

ing, we have found it profitable to cool the samples during an analysis by means of a liquid-nitrogen cold trap in the source which is connected by copper braids to the electrode holders. In addition to preventing melting of the sodium and limiting any preferential volatilization during sparking, the cooling system also serves as a convenient cryopump in the source. This provides additional pumping power in the immediate vicinity of the electrodes, which at liquid-nitrogen temperatures is quite effective in reducing the partial pressures of H_2O, CO_2, and the higher hydrocarbons (the ones most likely to arise from pump oil). Assuming a sticking coefficient near unity, the pumping speed of this cryopump is approximately 10 l/cm^2 sec,[21] and a surface area of several tens of square centimeters is available.

4. The sparking procedure followed in an analysis is also designed to minimize background contributions. After the samples have been loaded and the source pumped down to about 10^{-7} Torr, the liquid-nitrogen trap is filled and the samples are permitted to cool to their lowest temperature (~10–12 min are required for this). Then a thorough pre-spark is made. This has a double advantage. Not only are the samples cleaned of any surface contamination, but since the majority of ions produced do not pass the small entrance slit into the analytical regions of the instrument, a layer of sodium atoms is deposited throughout the interior of the source. These deposited atoms can act as a particularly effective chemical pump for many kinds of impurities, both because of the reactivity of sodium and because any thin layer of pure metallic atoms under vacuum is quite active chemically. A surface region on the order of tens of square centimeters is involved, and a significant portion of this is within millimeters of the sparking electrodes.

Typically, to reach a detection limit in the low parts per million range by a SSMS analysis of sodium requires a sparking period of less than a minute. Thus, the time at analytical temperature for the sample is substantially less in SSMS analyses than in normal combustion analyses. Since this ppm level is the normal range for carbon in high-purity sodium, a single carbon determination can be rapidly made by this technique once all preliminary parts of the procedure have been completed. Additional determinations can also be easily made by replicate exposures or by a series of graded exposures. Every exposure which produces a carbon line on the photographic plate with a density between about 15–80% transmission provides a separate determination. Thus, on a typical plate, an estimate of the average carbon concentration can be calculated from a number of determinations. Furthermore, since the material sparked for any one plate comes from a localized region of the electrodes, important information on the local homogeneity of the sample can be obtained by calculating the relative standard deviation of the several determinations. To obtain an even better estimate of the average carbon concentration, several separate analyses can be made using different plates, or analyses can be made with several different samples from the same batch.

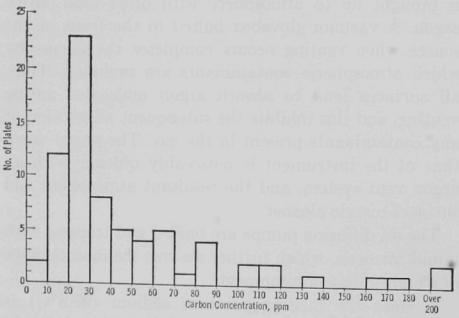

FIG. 1. Individual SSMS Results for Carbon from 74 Photographic Plates.

4. Results and Discussion

A single 10-lb container of high-purity, reactor-grade sodium obtained from Mine Safety Appliances Research Corp. (MSAR) was used as the source of material for the analyses reported in this paper. A carbon determination supplied by MSAR for the sodium in the container showed a result of 35 ppm. Twenty-four (24) separate pairs of electrodes, comprising about 0.5 g per pair, were taken from the container for SSMS analysis. All pairs of electrodes underwent multiple analysis, with an average of three photoplates being taken per sample. A dip-sampling procedure carried out in a glovebox with the sodium just above melting was used to form the samples as described in our previous paper. The sodium was transferred to the instrument sealed in a glass vial under vacuum (~10^{-6} Torr). The analyses were based on the detection of the $^{12}C^+$ line on the photographic plates. Unit sensitivity for carbon in sodium was assumed in the data reduction.

Figure 1 shows the distribution of results from all 74 photoplates comprising the analyses of the 24 samples. In the graph, the number of analyses showing a carbon concentration in a given interval is plotted as a function of concentration. The spread in the results is quite large, but there is a definite peak in the 20–30 ppm range. Furthermore, fully one-half of all the plates showed a carbon concentration of less than 30 ppm, and there were two results below 10 ppm. This demon-

strates that the technique has the ability to reach low carbon levels and that the carbon blank can be adequately controlled. Because of the systematic way in which the analyses were performed and the random manner in which the results varied, we believe that the spread in the data primarily reflects true differences in composition from sample to sample. The clustering of the results at low carbon levels is reassuring, and if the two values above 200 ppm are excluded, the average carbon concentration from the remaining analyses is 43 ppm, about 20% higher than the MSAR results.

Figure 2 shows the distribution of the average carbon concentration obtained from combining the replicate analyses of each of the 24 samples studied. As expected, the distribution is more compact when plotted in this manner. The median value is now above 40 ppm, and there are definite peaks in the 20–30 and 40–50 ppm ranges. Only one pair of electrodes showed an average carbon concentration appreciably above 100 ppm.

Using the same procedure as for Figures 1 and 2, in Fig. 3 is plotted the distribution of the relative standard deviation observed for each of the 74 plates. The spread is broad again, but there is an unequivocal maximum in the range 20–25%, and the distribution falls off sharply below 10%. This plot can be used to obtain an estimate of the precision of the analytical technique.

The overall variance (σ^2) associated with an analytical measurement can be exprressed as the sum of the variance associated with the experimental method (i.e., precision of measurement) and that associated with the sample because of possible inhomogeneities:

$$\sigma^2_{\text{meas}} = \sigma^2_{\text{meth}} + \sigma^2_{\text{sample}}. \qquad (1)$$

Since the variance from sampling is independent of that from the technique, the variances are additive. For a homogeneous sample, the precision of the final results is given only by the reproducibility of the method. In SSMS, it is well known that the variance associated with the technique does not undergo drastic changes from run to run, but rather assumes a fairly limited range of values. Thus, the spread in the distribution of Fig. 3 most likely arises from changes in the second term of Eq. 1 because of significant local inhomogeneities in the samples. The lower end of the distribution is attained when the samples are more homogeneous (i.e., when σ^2_{sample} is small). This end, then, represents the precision capabilities associated with a carbon determination on a locally homogeneous sample, and the indication is that ~10–20% is a reasonable value. This is within the normal range for precisions associated with generalized SSMS analyses of

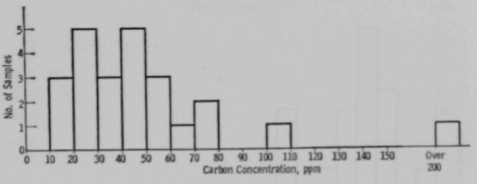

FIG. 2. Average SSMS Carbon Concentration of 24 Sodium Samples from a Single Batch.

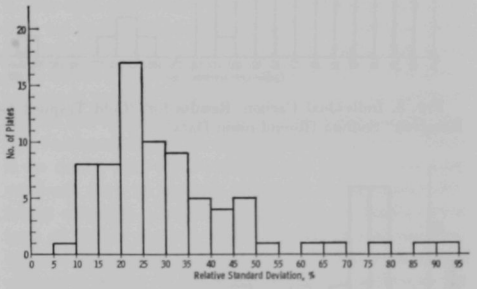

FIG. 3. Relative Standard Deviation of Carbon Concentration from Each of 74 Photoplates.

different materials, although somewhat better values (to ~4–5%) can be achieved in samples where all variables are more amenable to control.

It is interesting to compare the results achieved in this paper from a single batch of sodium with those obtained during the second carbon round robin[18]. Figures 4–6 plot the separate distributions of the results from the three batches analyzed by the 14 participating laboratories. All individual results reported by the analysts are included in the distributions. No attempt has been made to reject any data, since the determinations were all performed by laboratories experienced in sodium analyses. The broad distributions

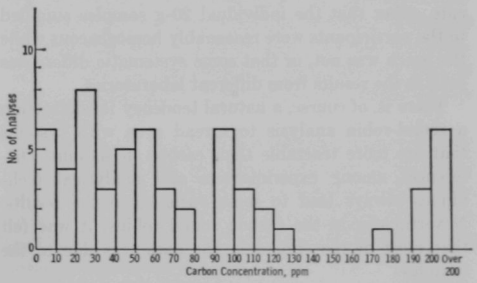

FIG. 4. Individual Carbon Results for "As Received" Sodium (Round-robin Data).

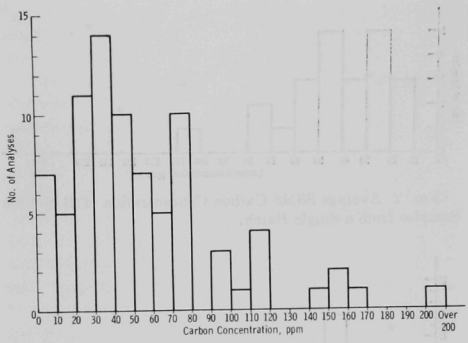

FIG. 5. Individual Carbon Results for "Cold Trapped-As Received" Sodium (Round-robin Data).

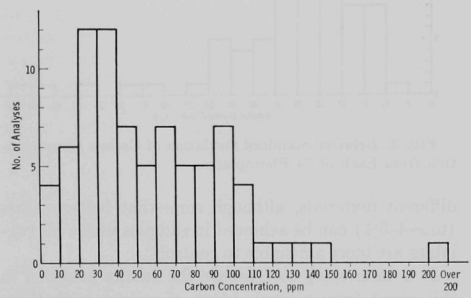

FIG. 6. Individual Carbon Results for "Carbon Addition" Sodium (Round-robin Data).

were interpreted in the round robin as indicating the lack of homogeneity in the batches, although the analytical variance exhibited by different laboratories for multiple analyses of the same sample was found to be substantially lower than that for the pooled results of all samples from the same batch. This would indicate either that the individual 20-g samples supplied to the participants were reasonably homogeneous while the batch was not, or that some systematic differences exist in the results from different laboratories.

There is, of course, a natural tendency for data from a round-robin analysis to spread even with systems that are more tractable than carbon in sodium. Differences among experimenters and analytical techniques always lead to some variance in the results. Nevertheless, in the carbon round robins, it was felt that most of the spread in the data was due to the samples.

Since the solubility of carbon in sodium is so low, the sodium-carbon system is at least partially two-phase, solid and liquid, and it is not surprising that gross inhomogeneities should occur. However, since the SSMS data presented in this paper were obtained in a single laboratory by a single set of experimenters following a specified procedure, non-sample variances tend to be minimized and the spread in the data is much more likely to reflect inhomogeneities in the sample. Figures 1–3 indicate that such inhomogeneities can be quite large, but the surprising thing is that even with the limited sample size treated by the spark instrument the distribution is not spread over several more orders of magnitude. Indeed, it appears that after a number of multiple SSMS analyses of a given batch, a pattern may develop which enables a good estimate of the average carbon concentration to be made. Nevertheless, considering the localized nature of the SSMS analysis and the inhomogeneities it reflects, the problems associated with determining a representative carbon value for a sodium sample by analyzing only a portion of it with any technique seem difficult indeed.

As has been mentioned, the SSMS results were calculated under the assumption of unit sensitivity for carbon. To test the accuracy of this assumption requires a well-characterized carbon-in-sodium standard. Unfortunately, no such standard can yet be prepared, and so no other assumption for the relative sensitivity factor (RSF) of carbon is yet justified. However, the results appear to indicate that the choice made is not wholly unreasonable. The use of a more correct RSF would affect only the accuracy of the results, not the precision.

Since the analytical sensitivity with which carbon can be detected in a SSMS analysis may well be a function of the initial chemical state of the carbon in the sample, at some future date it may become possible to distinguish different species of carbon as information about the system increases and the analyses improve. The pattern of observed lines on the photoplate may also become a clue in this respect. For example, the presence of Na_2CO_3 is likely to produce detectable $(CO_2)^+$ lines on the plate, whereas Na_2C_2 may produce lines corresponding to $(NaC)^+$, and so on. These eventual possibilities should be kept in mind for later SSMS analyses and the correlation of results with other analytical techniques.

Acknowledgments

The authors are grateful to Walter W. Weis, Jr., for his competent operation of the spark-source mass spectrograph.

REFERENCES

1. Hayes, W. C., and Shepard, O. C., *Carburization and Decarburization of Ferritic Chromium-Molybdenum Steels in Sodium Coolant Systems*, NAA-SR-2973 (Dec 1, 1958).

2. Anderson, W. J., and Sneesby, G. V., *Carburization of Austenitic Stainless Steel in Liquid Sodium*, NAA-SR-5282 (Sept 1, 1960).
3. Lockhart, R. W., and Billuris, IMD Special Report, Series No. 12, Nucl. Metall. AIME **IX**, 207 (1963).
4. *Effect of High Temperature Sodium on Austenitic and Ferritic Steels. Mechanical Properties of Materials. Quarterly Progress Report, Jan.–Mar., 1966*, MSAR (66-71).
5. Baerlecken, E., Lorenz, K., Kranz, E., and Schlegel, D., "Development of a Low Alloy Ferritic Steel for High Temperature Sodium Service with Special Regard to Carbon Transport," in *Alkali Metal Coolants*, IAEA, Vienna (1967).
6. Campbell, C. S., and Tyzack, C., "A Preliminary Model for the Carburization of Stainless Steel at High Temperatures in Sodium Containing Carbon at Unit Activity," in *Alkali Metal Coolants*, IAEA, Vienna (1967).
7. Zebroski, E. L., Young, R. S., Comprelli, F. A., and Dutina, D., "Effects of Mass Transfer, and of Changes in Properties, on Austenitic Steels in Flowing Sodium," in *Alkali Metal Coolants*, IAEA, Vienna (1967).
8. Pepkowitz, L. P., and Porter, J. R., *Determination of Elemental Carbon in Sodium*, Anal. Chem. **28**, 1606–7 (1956).
9. Mungall, T. G., Mitchen, J. H., and Johnson, D. E., *Gas Chromatographic Determination of Microgram Amounts of Carbon in Sodium Metal*, Anal. Chem. **36**, 70 (1964).
10. Kallmann, S., and Liu, R., *Determination of Total Carbon and Sodium Carbonate in Sodium Metal*, Anal. Chem. **36**, 590 (1964).
11. Eng, K. Y., Meyer, R. A., and Bingham, C. D., *Determination of Carbon in Sodium by Isotope Dilution Mass Spectrometry*, Anal. Chem. **36**, 1832–1834 (1964).
12. Bradley, H., and Meacham, S. A., *Determination of Carbon in Sodium by a High Temperature Combustion Method Utilizing Gas Chromatography*, APDA-164 (1964).
13. Sabol, W. W., Dutina, D., Rey, D. E., and Simpson, J. L., *Sodium Mass Transfer. XIII—The Determination of Total Carbon in Sodium*, GEAP-4540 (1964).
14. Boltz, D. F., and Meacham, S. A., *Determination of Carbonate Carbon in Sodium Metal*, APDA-166 (1965).
15. Sinclair, V. M., Drummond, J. L., and Smith, A. W., *The Analysis of Carbon in Sodium*, TRG-report-1185 (1966).
16. Hobart, E. W., Stevenson, R., and Kallmann, S., *Applicability of Low-temperature Ignition Methods for Determining Carbon in Various Alkali Metals*, Anal. Chem. **39**, 1659 (1967).
17. Lutz, G. J., and DeSoete, D. A., *Determination of Carbon in Sodium by Photon Activation Analysis*, Anal. Chem. **40**, 820–822 (1968).
18. Lockhart, R. W., Blair, R. C., Dutina, D., Jaech, J. L., and Sabol, W. W., *Results of the USAEC Round-Robin Analysis for Carbon Impurity in Sodium*, GEAP-4602 (1964).
19. Berkey, E., Sweeney, G. G., and Hickam, W. M., *Sodium Analysis by Spark Source Mass Spectrography*, Nucl. Appl. **5** (Nov. 1968).
20. Harrington, W. L., Skogerboe, R. K., and Morrison, G. H., *Quantitative Spark Source Mass Spectrometry Using Cryosorption Pumping*, Anal. Chem. **37**, 1480 (1965).
21. Dushman, S., *Scientific Foundations of Vacuum Technique*, 2nd Ed., Wiley, New York (1962).
22. Luner, C., Cosgarea, A., and Feder, H. M., "Solubility of Carbon in Sodium", in *Alkali Metal Coolants*, IAEA, Vienna (1967).

Discussion

Mr. Eichelberger (AI): First, I would like to ask how you read your photo plates, and second, do you think this method will be applicable to the low-ppm levels such as 5 to 10, or even less? This morning we heard about an oxyacidic flux method used by the EBR-II people. It seems pretty good down there. Can you compare them perhaps?

Mr. Berkey: Our photo plates are read by a Jarrell-Ash microdensitometer that has a precision drive on it. The data reduction is done with a computer program that we have written and employ on a general basis. The other part of your question is, of course, the much more subtle one. The only thing I can say at this point is there is nothing which bars the way for the application of this technique for low levels as long as the carbon background can be adequately controlled. There is no doubt that the technique can achieve low-ppm analyses, even in the ppb range for many, many different elements. Carbon is a problem no matter what type of matrix you are talking about. If you can control the background, you can do it. In the work that I alluded to before, in which the use of this technique for carbon analysis was studied, good results were obtained at the 1-ppm level for carbon in steel. Whether this can be done in sodium is a matter of carbon control.

Mr. Ramachandran (ANL): How did you prepare your standards for the mass spectrometer?

Mr. Berkey: The results were calculated on the basis of unit sensitivity, so no standard was utilized to compute the results. You see what they are, and can answer the question yourself as to whether you think this was a reasonable assumption or not. That is about all I can say.

Mr. Newman (BNL): The bulk of the samples appear to fall in a range of about 20%, which apparently you believe is due to inhomogeneity in your sample. However, this morning you commented on iron analyses that differed by a factor of 3 from mass-spectrometry technique versus conventional chemical techniques and you said, if I may quote you, "it is not unreasonable to get mass-spectrometry data that are plus or minus a factor of 3." Which of the two camps do you belong to?

Mr. Berkey: There are two elements involved here: one is precision and the other is accuracy. This morning I was talking about accuracy; this afternoon I was talking about precision. It is true that without a standard, one can be inaccurate to this factor of 3 which is generally conceded in the field, but the accuracy does not affect the precision at all. As long as all the variables (e.g., the instrumental variables and

other technique variables) are held constant, this 10 to 20% precision has been found true. The results that you allude to were the results of a residue analysis from a vacuum distillation of sodium, where the iron was at 3 ppm, whereas another technique saw it as much less than 1 ppm. This is wholly consistent with the accuracy argument; without a standard you really don't know that.

Mr. Newman: Then I am led to believe that the mass-spectrometry technique is only as good as our capability of preparing standards. There is no way of self-calibration.

Mr. Berkey: Our results are obtained without the use of standards. If the results or the unit-sensitivity assumption are not acceptable, then we will have to worry about standards, but at this point in time, no.

Mr. Newman: Am I to understand that the accuracy of the mass-spectrometry technique is of the order of a factor of 3?

Mr. Berkey: The differential volatilization and ionization efficiency of the different elements under the influence of the rf spark tends either to enhance or suppress the species roughly by about a factor of 3.

Mr. Newman: At this point can I rely on the numbers of mass spectrometry to better than a factor of 3 on an absolute basis?

Mr. Berkey: If I gave you a result using high-temperature combustion, I am sure you would not question it.

Mr. Newman: Let's say for iron, then.

Mr. Berkey: For iron in sodium, are we talking about a one-phase system or a two-phase system? If iron is at 100 ppm in sodium, do you have a homogeneous sample? Can you prepare a standard at this level? The only thing I can say is look at the results, and accept them or not; but don't be any more critical with this technique than you are with high-temperature direct combustion, because you saw those results. Laboratory A gets 10 to 20, laboratory B gets 50 to 100 on the same sample using large samples.

Mr. Rodgers (MSA): I got the impression that the average of all your analyses was about the same as ours. It costs me about $50 to run a sample. Can you give us some idea of the capital investment that this method takes and also the time to run a sample?

Mr. Berkey: The time to make a single exposure is less than 1 min. The time to analyze the sample, i.e., take 10 exposures, develop the plates, etc., can be brought down to 1–2 hr. In order to obtain results for more than one element, more time is required. The cost of this instrument is of the order of $100,000. This is a considerable amount of money. However, if we have to know trace impurities fairly well and at less than 10 ppm, and as easily as possible, then I heartily recommend that you give some consideration to this instrument.

Mr. Dutina (GE): Is there an application of the instrument for oxygen? I heard some early papers on spark-source mass spectroscopy where they were discussing oxygen, and I wonder if you have given it a try.

Mr. Berkey: There is a potential application, but we haven't demonstrated it. The background problem for oxygen is even tougher than for carbon, but we're working on it.

Trace-element Behavior in Sodium

R. J. Meyer, C. E. Johnson, and L. E. Ross

Argonne National Laboratory
Argonne, Illinois

(PRESENTED BY R. J. MEYER)

1. Introduction

This paper deals with the problem of segregation of trace constituents within sodium samples and the effects that this segregation can have on the reliability of analytical results. It is not within the scope of this paper to discuss the various methods of sampling sodium systems nor to discuss the behavior of specific elements in sodium. It is tacitly assumed that the experimenter and analyst are fully cognizant of the sampling methods available,[1] of the behavior of the elements of interest in sodium, and that the sample when taken is representative of the system.

The particular purpose of this paper is to point out that even if the liquid sample taken from the system is representative, there may also be a problem in sampling the solidified sodium. To sample a sodium system consisting of solid sodium in a container, it is imperative that the analyst understands (1) the behavior of the trace elements in liquid sodium between the time the sample is taken and solidification is complete and (2) that no one approach will be adequate for all sampling situations. Even the "safe approach" of dissolving the entire sample out of the container may at times be inadequate.

Three separate types of segregation which can occur during cooling and solidification will be discussed: precipitation, concentration at a surface, and wall absorption. Specific examples of ANL experience with these types of segregation will be given along with explanations, or possible explanations, for the behavior. Methods of predicting, detecting, and circumventing sample inhomogeneity will be given wherever possible.

2. Precipitation

Trace elements are known to segregate in sodium by precipitation. Illustrative of this type of segregation is the behavior of bismuth in EBR-II sodium. Large samples (~20 g) of liquid sodium were taken in aluminum cans and allowed to cool naturally over a period of 15 to 30 min. Analysis of sections of the solidified sample produced the following typical results:

Top portion	4 ppm
Middle portion	20 ppm
Bottom portion	40 ppm

This behavior is easily explained on the basis of solubility and density. Figure 1 summarizes the recent temperature-composition data for the sodium-bismuth binary system. The diagram shows two compounds, Na_3Bi, melting congruently at 848°C, and NaBi, undergoing peritectic dissociation at 443°C. In solutions dilute in bismuth, Na_3Bi is the only compound known to precipitate. Typical solubilities are: about 10^5 ppm bismuth at 500°C, and about 6 ppm at 125°C. As the temperature of a dilute bismuth-sodium sample is decreased, Na_3Bi will precipitate from the system. Extrapolation of available solubility data to 97°C (the expected eutectic temperature) indicates an equilibrium solubility of 1–2 ppm of bismuth. This is not greatly different from that found in the top portion of the sodium sample. Further, as the density of Na_3Bi is approximately three times greater than that for sodium, it is not surprising to find the bulk of the bismuth at the bottom of the sample cup.

Characteristics similar to those of bismuth are also to be expected for solutions of antimony[2] and tellurium in sodium because they form even more "salt-like" compounds than bismuth in sodium solutions. In general, any element above and to the right of bismuth in the periodic table can be expected to have "salt-like" characteristics similar to that of bismuth in liquid sodium.

From the above considerations, it is seen that sectioning of a sodium sample should be avoided whenever precipitation is suspected. Should sectioning be necessary, a longitudinal coring or drilling will provide a more representative sample than a slice off the end.

3. Surface Segregation

The concentration of trace elements at the surfaces of sodium metal can also cause sample inhomogeneity. This behavior is exhibited by cesium-137 (and presumably natural cesium) in EBR-II sodium. It was first observed when the cesium-137 content of an extruded sample of EBR-II sodium was compared

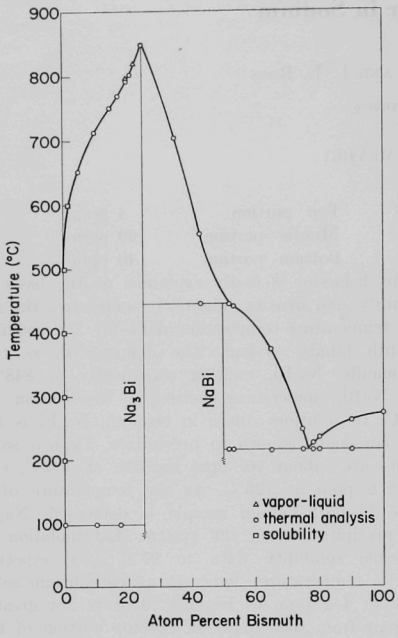

FIG. 1. Sodium-Bismuth Phase Diagram.

to the cesium-137 content of the sodium remaining in the extruder. The concentrations differed by orders of magnitude. Subsequently, it was found that in solid samples cesium was concentrated at all surfaces, both metal-wall and metal-gas. Furthermore, rapid quenching of the molten sodium samples did not alter the cesium distribution.

The explanation of this type of segregation is not nearly as clear-cut as it is in the case of precipitation. The possibility that wall adsorption is responsible for the cesium behavior was considered but rejected, as cesium is found not only at the metal-wall interface but at the metal-gas interface as well (this would not be the case if wall adsorption alone were responsible). Furthermore, Ebersole and coworkers[3] have remelted sodium samples and poured the sodium out of the vessel without major loss of the cesium to the container wall. The evidence thus accumulated suggests that the difference in surface tension between cesium and sodium liquids may be an important consideration. If this is the case, one might anticipate cesium to be inhomogeneously distributed in the liquid sodium as well as in the solid sodium. The above hypothesis might substantiate the observation that the segregation of cesium in quenched samples was the same as that in slowly cooled samples.

If one uses surface tension as a criterion for predicting the behavior of other metals in sodium, one might also expect rubidium, potassium, and possibly barium to exhibit surface segregation in sodium.

This type of sample inhomogeneity is best circumvented by dissolving the entire sample out of the sample container. In cases in which the container will be attacked during the dissolution, it would appear safe to remelt the sodium and pour it into a more suitable container before dissolution. Sectioning of the sample should be avoided, but should it be necessary, great pains should be taken to sample the surface and the bulk sodium in the proper proportions.

4. Wall Adsorption

Although to date there has been no confirmed observation of the reaction of a trace constituent in EBR-II sodium with the wall of a sample container, this phenomenon has been reported for other sodium systems. This experience and ANL experience in other liquid-metal systems indicate that this type of segregation should be considered as a likely sampling problem in sodium. It can be stated with certainty that if reaction with the container occurs in liquid-sodium systems, it can also be expected to occur in the sampling of sodium systems. However, it is also possible for an element to be "well behaved" in the large system and "misbehave" in the sampling system. This situation can arise in at least two instances: (1) if the sample container is made of a different material than that of the system, and/or (2) if the sample container is not properly equilibrated with the system prior to taking the sample.

Because the mechanisms which may lead to the adsorption of minor constituents from sodium onto the surfaces of a container have not been investigated and are therefore not understood, it is, at the present time, almost impossible to predict with which elements and/or under what conditions adsorption onto the walls of a sample container will occur. The fact that adsorption has occurred may indeed go undetected since the deposited species may not always respond in the dissolution in a manner characteristic of the deposited element.

This last point can be illustrated by discussing difficulties encountered with ruthenium in another liquid-metal system, zinc-magnesium. Samples of this system are customarily taken in tantalum tubes from a system in which the containing vessel is

tungsten. When a group of zinc-magnesium-ruthenium samples were dissolved, residues were obtained which contained ruthenium and which were initially presumed to be ruthenium metal. However, these residues did not dissolve in sodium hypochlorite (a normal chemical used for ruthenium dissolution). Not until the residues were pretreated with hydrofluoric acid and then subjected to sodium hypochlorite did they dissolve. All evidence indicates that the ruthenium reacted with the tantalum during the sampling operation. In these samples, it was fortunate that the reaction product separated from the container during dissolution and was of sufficient bulk to be observed. In other samples, ruthenium was deposited on the tantalum so effectively that it could be removed only by dissolving away part of the surface of the tantalum. Obviously, the "safe approach" of dissolving the entire sample out of the container was inadequate in this case.

Detection and circumvention of adsorption of an element onto the walls of the sample container requires close cooperation between experimenter and analyst. Very often the first clue to adsorption is an unexplained scatter in analytical results. Subsequent confirmatory experiments, often involving the use of radioactive tracers, are usually required. Finally, an effective method of circumventing wall adsorption has to be found. This circumvention might be a change in the dissolution method or it might involve changing the material of the sample container.

Two general practices which, if followed, will decrease the possibility of wall adsorption are: (1) whenever possible, the sample container should be of the same material as the container material of the system, and (2) the container should be equilibrated with the system before the sample is taken.

5. Conclusions

In view of the above discussion it should be obvious that sampling problems can exist not only in liquid-sodium systems, but also in the solid samples taken from the liquid systems. Unless the possibility of segregation in the solid sample is constantly kept in mind by both the experimenter and the analyst, a great deal of erroneous data may result. Solutions to these sampling problems are their joint responsibility. A strong cooperative effort between the two is necessary to discover sampling problems and to find satisfactory solutions to them.

REFERENCES

(1) F. A. Scott, *Sampling FFTF Sodium Coolant for Analytical Purposes*, BNWL-491.

(2) M. Okada, R. A. Guidotti, and J. D. Corbett, Inorg. Chem., **7**, 2118 (1968).

(3) E. Ebersole, Idaho Division, ANL, private communication.

Discussion

Mr. Brehm (BNWL): Could the segregation of manganese and cesium to the wall of your container be aided by oxygen on the container wall, which may result in the formation of a complex triple oxide?

Mr. Meyer: It is quite conceivable that manganese might have reacted with something on the wall. I can only say that if the cesium has reacted with any oxygen on the container wall it still remained in the sodium.

Mr. Brehm: I tried to rationalize this in the following manner. When you freeze your sample you form the oxide and when you remelt it, the complex triple oxide breaks up in the melt and you pour it out.

Mr. Meyer: I don't know that anybody has come up with a definite conclusion about this. The postulate that I like best is that in the case of cesium, the effect is due to differences in the surface tensions of the two metals. This is probably as good an explanation as the one you are offering here.

Mr. Olson (ANL): In the sodium samples taken from EBR-II, there was cesium on the voids formed by the shrinkage of the sodium upon freezing. I would expect a vacuum in a void, so that oxygen wouldn't be a consideration.

Mr. Newman (BNL): I would like to concur in this problem of segregation in the sample container. In the solubility study that Weeks will describe shortly, we found that iron in sodium segregated in buckets, and it was quite difficult to remove from the sample walls.

Mr. Castleman (BNL): In contrast to your conclusion that cesium is segregated in the liquid phase, tomorrow I will be presenting a paper on some of our transport results (vaporizing cesium from sodium); I think I can show that the cesium is not segregated in the liquid phase. I don't want to discuss those results today.

Mr. Larsen (ANL): The surface-concentration effect might be concentration-dependent. In the EBR-II sodium, it is estimated that the cesium (primarily fission product) concentration is only a few parts per billion. The result might be different in the ppm range.

Mr. Berkey (W): We observe the same phenomenon in the range of low parts per million, al-

though to a smaller extent than has been described for the more dilute solution.

Mr. Jansson (W): You started off by showing a phase diagram. Would you comment on how the concentrations from one region to another within the sample compare with the change in composition of the liquid that you would expect from continuous cooling and precipitation?

Mr. Meyer: I think the cooling-curve data and the EBR-II data agree very well. The extrapolated solubility of bismuth at the eutectic temperature is 1–2 ppm. The concentration in the upper portion of our samples was 4 ppm, and the present bismuth concentration in EBR-II sodium after extensive cold-trapping is reported to be between 1 and 2 ppm.

Mr. C. R. F. Smith (BNWL): I begin to suspect that a nice way to get cesium out of a radioactive solution would be to circulate through a material of large surface area, for example, metal sponge or shredded foil. Do you have any comment?

Mr. Meyer: I believe that the cesium is in the sodium but concentrated at an interface. You are proposing to enlarge the interface in order to get a concentration around this sponge or whatever it is. It's a possibility, but I doubt that it is that simple. It would depend on how big or porous the material was and whether the cesium would get to the large surface.

Mr. Smith: I am thinking about forced flow.

Mr. Lindhe (AB Atomenergi): Would it be possible to use this kind of segregation to get chromatographic partition of trace elements in sodium?

Mr. Meyer: I have no comment.

Mr. Feder (ANL): I regard the possibility seriously enough to propose this as one of the more effective means of fission product removal from sodium.

Solubilities of Nitrogen Gas and Sodium Cyanide in Liquid Sodium

E. Veleckis, K. E. Anderson, F. A. Cafasso, and H. M. Feder

Argonne National Laboratory
Argonne, Illinois

(PRESENTED BY E. VELECKIS)

Introduction

Structural reactor materials in liquid sodium systems are known to undergo corrosion by carburization[1] and nitridation.[2] As a first step in evaluating the role played in these processes by various carbon and nitrogen compounds, the solubilities of nitrogen gas and sodium cyanide in liquid sodium have been measured. These compounds are of particular interest because nitrogen may be present in the blanket gases of sodium-cooled reactors and because high concentrations of cyanide have been found in reactor cold traps.[3-5] To our knowledge there is no published information on the solubility of either compound in sodium.

Solubility of Nitrogen Gas

Nitrogen solubility was measured by adapting a method used by Grimes *et al.*[6] to determine the solubility of rare gases in eutectic mixtures of fused fluorides. Our measurements involved saturating approximately 2.5 l of reactor-grade sodium at a preselected temperature with nitrogen at 10 atm, stripping the dissolved nitrogen from ~2 l of sodium with helium, trapping the stripped gas on liquid-nitrogen-cooled molecular sieves, transferring it to a bulb, and, finally, analyzing it with a mass spectrometer.

The apparatus, shown in Fig. 1, consisted of three sodium-containing vessels interconnected by heated lines for sodium transfer. Vessel A was used for removing oxides from the sodium by cold trapping; vessel B, for saturating the sodium with nitrogen gas; and vessel C, for stripping the dissolved nitrogen from the sodium. The nitrogen used for saturation was stored in the reservoir assembly shown. The saturator and stripper vessels were parts of two separate gas-circulation loops. Each loop also contained a Lapp pump, a flowmeter, a pressure gauge, and a gas disperser (a perforated coil for the saturator, a sintered stainless steel disc for the stripper). The stripped gas was sampled in a section which was connected to the stripper loop and which was made up of a molecular sieves trap, a McLeod gauge, a manometer, and a sampling bulb.

The solubility experiments were carried out with the aid of nitrogen enriched with nitrogen-15. In this manner, the dissolved nitrogen could be distinguished from extraneous nitrogen. The measurements were made at 50° intervals between 450 and 600°C, with the results shown in Table 1. The solubilities are Henry's law constants expressed in parts per trillion per atm nitrogen pressure. The reliability of each solubility value was established by multiple determinations at each temperature. The data were fitted by the method of least squares to the linear equation, for the range 450–600°C,

$$\log S = -7.18 - 2780\ T^{-1},$$

where S is solubility in grams of nitrogen gas per gram of sodium per atmosphere, and T is temperature in degrees Kelvin. The heat of solution obtained from this equation is 13 ± 3 kcal/mole.

The use of nitrogen-15 tracer not only provided the requisite sensitivity for the solubility measurements, but also an insight into the nature of the dissolution process. The sodium was saturated with isotopically unequilibrated nitrogen having the typical composition 27.4 mole % $^{15}N_2$, 49.6 mole % $^{14}N_2$, and 23.0 mole % $^{14}N^{15}N$. If this nitrogen dissolved monatomically, then random recombination of the atoms on exsolution would be expected to give the equilibrated composition 15.2 mole % $^{15}N_2$, 37.3 mole % $^{14}N_2$, and 47.5 mole % $^{14}N^{15}N$. However, mass-spectrometric analyses of the stripped gas revealed only a small change in isotopic composition, to 25.7 mole % $^{15}N_2$, 46.1 mole % $^{14}N_2$, and 28.2 mole % $^{14}N^{15}N$, which is not consistent with purely monatomic dissolution. More likely, this change is catalytic, occurring at the hot steel surfaces of the apparatus. (Slow exchange between $^{15}N_2$ and $^{14}N_2$ over hot iron catalysts has been observed.[7]) The results, therefore, appear to be consistent with the mechanism of diatomic solution of molecular nitrogen in sodium. Past studies have shown that diatomic gases dissolve or react monatomically in liquid metals; this is the first to show that molecular dissolution also occurs.

Once the diatomicity of the dissolved nitrogen was established, its solubility in sodium was calculated according to the hard-sphere model of Reiss *et al.*[8] and Peirotti.[9] In this model the solubility is a

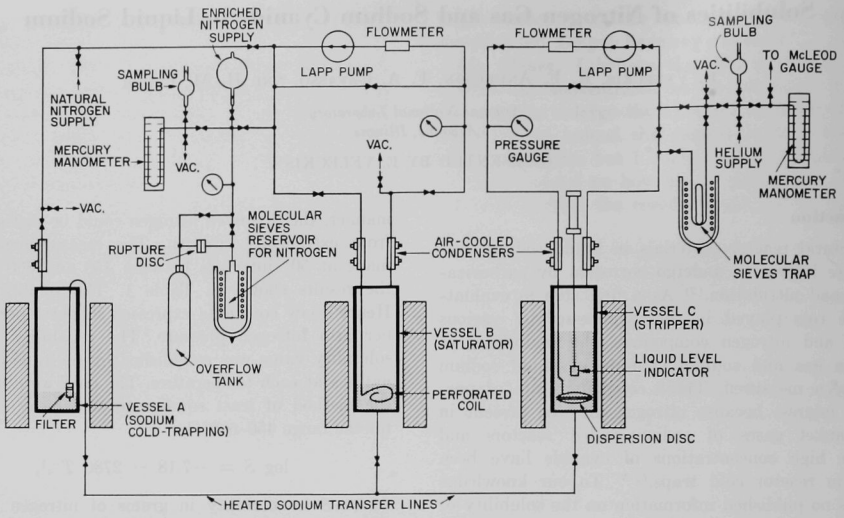

FIG. 1. Apparatus for Measuring the Solubility of Nitrogen Gas in Liquid Sodium.

TABLE 1. SOLUBILITY OF NITROGEN IN LIQUID SODIUM[a]

Temp (°C)	Mean Solubility (g N_2 per 10^{12} g Na per atm pressure)	Relative Standard Deviation (%)	Number of Determinations
451	10	78	7
502	17	44	6
550	25	31	7
600	44	21	6

[a] All solubilities were determined at a nitrogen pressure of ~10 atm.

sensitive function of the value selected for the hard-sphere diameter of sodium. The literature indicates that this diameter is 3.2 Å at 500°C,[10] for which the model predicts a solubility about 10^5 times greater than that measured. On the other hand, much better agreement (within 15%) was obtained for a diameter of 3.72 Å, the interatomic Na-Na distance in crystalline sodium. An explanation for this better agreement is being sought.

Solubility of Sodium Cyanide

The solubility of NaCN in liquid sodium was determined by direct sampling. The apparatus shown in Fig. 2 was used for these measurements. Excess sodium cyanide, purified by vacuum fusion, was equilibrated with reactor-grade sodium* at temperature in a tantalum crucible under helium at a pressure of 3 atm. The crucible and its contents were contained in an evacuable stainless steel furnace tube together with heat and vapor shields, a thermocouple well, a stirrer, and a sampler. Stirring was employed to equilibrate mixtures below 565°C (solid-liquid equilibrium), but not above 565°C (liquid-liquid equilibrium). The sampler consisted of a long stainless steel rod attached to the upper end of a tantalum sample tube (of 0.25-in. OD by 4 in.). Into the lower end of the sample tube was press-fitted a 0.25-in.-long, cylindrical, 5μ-porosity stainless steel frit. With this arrangement, the sample tube could be lowered past the ball valve into the melt and then withdrawn without significant contamination of the helium atmosphere. Sampling the melt involved stopping the stirrer, decreasing the pressure to 0.5 atm, immersing the sample tube in the melt, increasing the pressure to 3 atm, raising the sample tube above the ball valve, and closing the ball valve.

The samples, which contained ~1 g of the filtered melt, were assayed spectrophotometrically[11] for cyanide after being dissolved in water. Past experience had shown that during solidification of the

* The oxygen content (determined by the amalgamation method) of the starting sodium was 16 ppm; after completing all the solubility experiments it was 115 ppm.

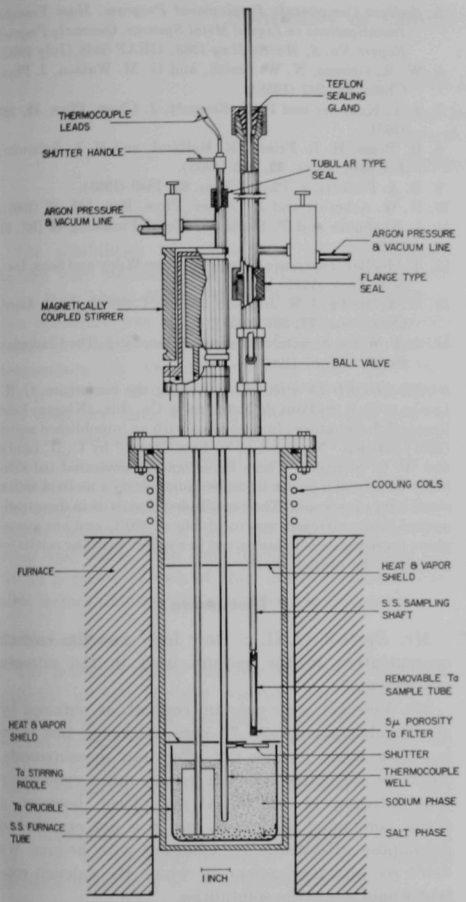

FIG. 2. Apparatus for Measuring the Solubility of Sodium Cyanide in Liquid Sodium.

melt in the sample tube ~16% of the dissolved cyanide segregated longitudinally and deposited on the filter. Also, it was known that the NaCN particles filtered from the melt were removed within the lower third of the frit. Therefore, to be certain that the entire sample, including the deposited NaCN, would be dissolved and analyzed, the lower portion of the frit was removed (and the surface of the sample tube was thoroughly cleaned) before placing the tube in the water solvent.

The results of the solubility experiments are given in Table 2. Solubilities were measured both below and above the monotectic temperature, which was found by thermal analysis to be 565 ± 2°C. A monotectic in the Na-NaCN system had been anticipated because cyanide ion is considered[12] to be a pseudohalide and monotectics have been observed[13] with the sodium-sodium halide systems. The reliability of each solubility value was established by multiple determinations. The data collected below the mono-

TABLE 2. SOLUBILITY OF SODIUM CYANIDE IN LIQUID SODIUM

Temp (°C)	Mean Solubility (ppm CN)	Relative Std Deviation (%)	Number of Determinations
402	0.70	69	12
425	4.2	111	8
450	4.2	123	12
500	40	25	8
525	160	14	14
549	108	18	10
575	500	28	8
600	780	27	8
650	1630	14	6

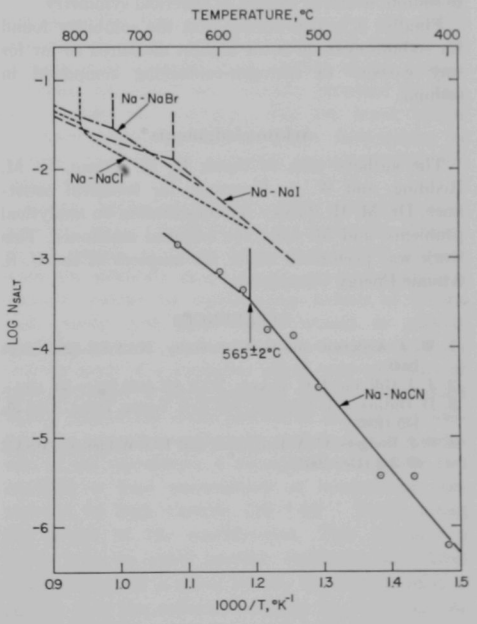

FIG. 3. Solubilities (Mole Fraction) of Sodium Cyanide and Sodium Halides in Liquid Sodium.

tectic temperature were fitted by the method of least squares to the linear equation, in the range 400–565°C,

$$\log (\text{ppm CN}) = 13.5 - 9140\ T^{-1}.$$

The heat of solution calculated from this equation is 42 ± 5 kcal/mole.

The variation with temperature of the solubility of NaCN in liquid sodium (on a mole fraction basis) is shown in Fig. 3 together with similar data for NaCl, NaBr, and NaI. The qualitative resemblance between the curves for cyanide and halide solubilities is consistent with the concept that cyanide ion is a pseudohalide. However, the solubility curves point to a significant difference in behavior: the solubilities of the sodium halides differ from each other to only a small extent, yet the solubility of NaCN is lower than that of any sodium halide by about an order of magnitude. From considerations of ionic size only, the solubility of NaCN would be expected to be closer to those of the sodium halides, since the radius of CN^-, assuming spherical symmetry, falls between those of Cl^- and Br^-.[14] Thus, one may speculate that the relatively low solubility of cyanide in sodium is due to its lack of spherical symmetry.

Finally, it is noteworthy that the solubility found for sodium cyanide is the highest measured so far for any carbon- or nitrogen-containing compound in sodium.

Acknowledgments

The authors wish to thank R. M. Yonco, G. M. Redding, and W. A. Kremsner for technical assistance, Dr. M. H. Barsky for consultation on analytical problems, and M. Ader for editorial assistance. This work was performed under the auspices of the U. S. Atomic Energy Commission.

REFERENCES

1. W. J. Anderson and G. V. Sneesby, NAA-SR-5282 (Sept 1960).
2. J. J. Gill and J. C. Bokros, NAA-SR-6162 (May 30, 1961).
3. D. Dutina, J. L. Simpson, and R. S. Young, Trans. ANS **10,** 145 (1967).
4. S. J. Rodgers, C. A. Palladino, and T. J. Wildeman, MSAR 67-203 (Dec 1967).
5. *Sodium Components Development Program. Mass Transfer Investigations in Liquid Metal Systems. Quarterly Progress Report No. 5, March–May 1968,* GEAP-5648 (July 1968).
6. W. R. Grimes, N. W. Smith, and G. M. Watson, J. Phys. Chem. **62,** 862 (1958).
7. J. T. Kummer and P. H. Emmett, J. Chem. Phys. **19,** 289 (1951).
8. H. Reiss, H. L. Frisch, E. Helfand, and H. L. Lebowitz, J. Chem. Phys. **32,** 119 (1960).
9. R. A. Pierotti, J. Phys. Chem. **67,** 1840 (1963).
10. N. W. Ashcroft and J. Lekner, Phys. Rev. **145,** 83 (1966).
11. I. Nusbaum and P. Skupeko, Metal Finishing **49** [10], 61 (1951).
12. T. Moeller, *Inorganic Chemistry,* John Wiley and Sons, Inc., New York (1952) p. 463.
13. M. A. Bredig, J. W. Johnson, and W. T. Smith, Jr., J. Amer. Chem. Soc. **77,** 307 (1955).
14. A. F. Wells, *Structural Inorganic Chemistry,* The Clarendon Press, Oxford (1962) p. 733.

NOTE ADDED IN PROOF: Following the conference, C. H. Lemke of E. I. du Pont de Nemours & Co., Inc. (Niagara Falls Research Laboratory) furnished us with an unpublished report (1958) entitled "Nitrogen in Sodium Metal" by C. H. Lemke and W. C. Sharples. These investigators measured the solubility of nitrogen gas in liquid sodium, using a method with a sensitivity of ~5 ppm. They concluded that, within this experimental limit, nitrogen was insoluble at 100°C and one atmosphere pressure—a conclusion not in conflict with the results reported in the present work.

Discussion

Mr. Epstein (ANL): How high was the calcium concentration in the sodium used in the nitrogen experiments?

Mr. Veleckis: Our calcium content, as obtained by atomic absorption, was 75 ppm. Although this value is pretty large, it does not affect our measurements. There is no doubt calcium reacts quite extensively with nitrogen in our initial gas phase; however, a stable compound is formed, and it is not expected to decompose afterwards by sparging with helium. We don't see any mechanism by which the calcium content would affect the solubilities.

Mr. Epstein: There could have been a great deal more nitrogen in the solution as the nitride.

Mr. Veleckis: This is another point that I would like to make. In this study, we did not measure the total nitrogen content of sodium; we only measured the nitrogen which is dissolved in sodium.

Solubility of Cobalt and Nickel in Sodium

PANG-KAI LEE AND EDGAR BERKEY

Westinghouse Research Laboratories
Pittsburgh, Pennsylvania

(PRESENTED BY P. K. LEE)

ABSTRACT

The solubilities of cobalt and nickel in liquid sodium were studied separately over the temperature range from about 280 to 500°C. A classical equilibration procedure was employed, exposing a high-purity cobalt or nickel crucible to sodium at the desired temperature. A vacuum chamber (at 10^{-6}–10^{-7} Torr) was used to protect the purity of the reactants. The solubility data were obtained by analyzing the resultant sodium by spark-source mass spectrography. The spread observed in the results can be attributed to local inhomogeneities in the solid samples analyzed. Both cobalt and nickel appear to have sodium solubilities in the low parts per million range and below, with experimental heats of solution within a factor of two of their heats of fusion. Possible factors affecting the solubility are discussed.

1. Introduction

The intended use of stainless steel as a structural material in fast breeder reactors has required extensive study of its corrosion behavior in liquid sodium systems. An important aspect of this effort has been to determine the solubility in sodium of the major elemental constituents of stainless steel. This information is essential not only to understanding the fundamental corrosion mechanisms involved, but also to assessing potential reactor operating problems which may occur as a consequence.

One such problem is the residual radioactivity in the sodium arising from the neutron activation of circulating corrosion products. This radiation could be objectionable or hazardous. The isotopes could be transferred by the coolant and deposited in the system outside the reactor proper. Some of the more important long-lived isotopes are formed by the reactions: $^{54}Fe(n,p)^{54}Mn$; $^{58}Ni(n,p)^{58}Co$; $^{59}Co(n,\gamma)^{60}Co$; and $^{50}Cr(n,\gamma)^{51}Cr$. The amounts of these transition metal species soluble in sodium are not yet sufficiently established.

Our work has sought to measure the upper limit concentrations or the equilibrium solubilities of several pure transition metals in high-purity sodium as a function of temperature. Because of the paucity of data for cobalt and the large discrepancies in the data for nickel, pure cobalt and pure nickel have been chosen as the initial materials to be studied.

Previous work on the solubility of cobalt has been done by Grand *et al.*,[1] using neutron activation analysis. Only three measurements over the temperature range 365–525°C were reported, ranging in value from about 21 to 1000 ppb. For nickel, there are two sets of data in the literature, those of Rodgers *et al.*[2] and of Kovacina and Miller,[3] which differ by about three orders of magnitude. Kovacina and Miller, using a tracer technique, showed that the nickel solubility in low-oxygen sodium (20–50 ppm oxygen) was in the low ppb range for temperatures between 200 and 600°C. They also showed that at 600°C the solubility increases as the oxygen concentration in the sodium rises appreciably above 100 ppm. The data of Rodgers *et al.* for the nickel solubility lie in the low ppm range and indicate no increase in level as the oxide content of the sodium increases. Anthrop[4] has critically reviewed the two sets of data and concludes that the lower values are more likely to be true. Other laboratories in addition to ours are currently re-determining the nickel solubility.[5, 6]

Several techniques besides those mentioned have appeared in the literature for measuring the solubility of metals in other liquid metals.[7-11] In our work, the solubility measurements are performed in a classical manner by equilibrating sodium of known high purity with pure metal (cobalt or nickel) crucibles over a wide range in temperatures. A crucible made of a dissimilar metal, pure tantalum or tantalum with a pure tungsten coating, is pressed tightly against the solute crucible in an inverted position and is used to collect the sodium at the conclusion of the experiment. A capsule containing the two crucibles is kept continuously at temperature surrounded by high vacuum (10^{-6}–10^{-7} Torr) during the course of the equilibration. This provides a buffer zone to avoid possible contamination. After equilibrating for a given period, the sodium melt is poured into the collector crucible by inverting the joined crucibles and is quenched with the help of a liquid nitrogen spray. The analytical data for the dissolved species are obtained with the use of spark-

source mass spectrography (SSMS). The application of this technique to sodium analyses has been previously discussed.[12] However, the present study represents the first attempt to use this method in the determination of solubility data. Its main advantage is the ability to perform a direct analysis of a solid sample. With a reactive element like sodium, this is particularly attractive in view of the contamination possible during extensive chemical treatment. Further details on the experimental conditions and the results obtained are presented and discussed.

2. Experimental

2.1 Materials

Ultrahigh-purity (3-pass electron beam zone-refined) cobalt rod (nominal purity 99.992%), nickel rod (nominal purity 99.997%), and tantalum rod (nominal purity 99.997%) of ½-in. diameter were obtained from Materials Research Corp. (Orangeburg, N.Y.). One piece of metallurgical-grade tantalum rod of ⅝-in. diameter was obtained from Kawecki Chemical Co. (New York, N.Y.). Cylindrical metal crucibles, of ⅜-in. inside diameter by 2-in. length, were machined from these rods by means of a Elox technique (spark machining). The inside surfaces of these crucibles were finished by electrochemical polishing. During the earlier experiments, a metallurgical-grade tantalum crucible coated inside and out by pure vapor-deposited tungsten was used as the collector. In later experiments, the high-purity tantalum crucible was used. The lip of the cobalt and nickel crucibles was tapered by 30°, whereas the lip of the tantalum collector was bevelled to match the crucible lips and form a tight tapered joint.

High-purity sodium was obtained from MSA Research Corp. (Callery, Pa.) in 2-g ampules. No further purification of the sodium was performed. Typical levels of impurities quoted by the supplier are given in Table 1, where typical SSMS results for the metallic elements are also included. Note that cobalt was undetectable in the blank, while nickel was quite low and variable.

TABLE 1. Typical Impurity Levels in High-purity Sodium (2-g ampules)[a]

Element	MSAR Analysis	SSMS Analysis
Cr	<3 ppm	0.5–7.0
Mn	<1	0.05–1.0
Fe	<5	1.5–8.0
Ni	<5	0.2–1.2
Co	<5	<0.03[b]
All others (except possibly Si and Ca)	<10	

[a] Supplied by MSA Research Corp. with the following specifications:

K <200 ppm
C <50 ppm
O <50 ppm (but usually <20 ppm)

[b] Upper limit; not detectable in samples.

2.2. Apparatus

The apparatus for the solubility measurements includes a capsule made of stainless steel or molybdenum for holding the solute and collector crucibles and isolating them from the environment, a resistance furnace, and a vacuum chamber which can be inverted. A schematic diagram of this equipment is shown in Fig. 1.

The solute crucible which contains the sodium metal and the joined collector crucible are inserted in a molybdenum capsule, of ⅝-in. diameter and 5⅛-in. length. The crucible and the collector are held in position and tightened together by means of two tungsten springs. The molybdenum capsule is sealed with a Swagelok cap, so that the force provided by the tightened cap compresses the springs and tightens the joint between the crucibles, assuring the integrity of the connection during the test.

During the test, the capsule is placed inside a cylindrical resistance furnace of 1¼-in. diameter and 4¼-in. height. The Swagelok cap is loosely supported on a stainless steel holder in such a way that when the system is inverted the whole capsule can slide down along the guide of the holder. The furnace is constructed by winding a 0.015-in.-diameter tungsten wire vertically on two tantalum wire loops which are insulated from the windings by ceramic beads. The tantalum wire loops are mounted on a stainless steel plate. A separate, flat heating coil is located at the bottom of the furnace. To increase the thermal uniformity of the furnace a molybdenum tube of ⅞-in. diameter and 0.007-in. thickness is placed inside the heating element. Three concentric cylindrical shields made of molybdenum with circular covers surround the heating elements to minimize heat loss by radiation. Two extra lower radiation shields are present underneath the furnace and inside the innermost cylindric shield. The main heating element of the furnace and the auxiliary heating element at the bottom of the furnace are separately controlled by two Pt-Pt 10% Rh thermocouples embedded near the heating elements, one at the midpoint of the furnace and one at the bottom of the furnace. The temperature of the furnace can be maintained constant to ±1° in the temperature range of the measurements.

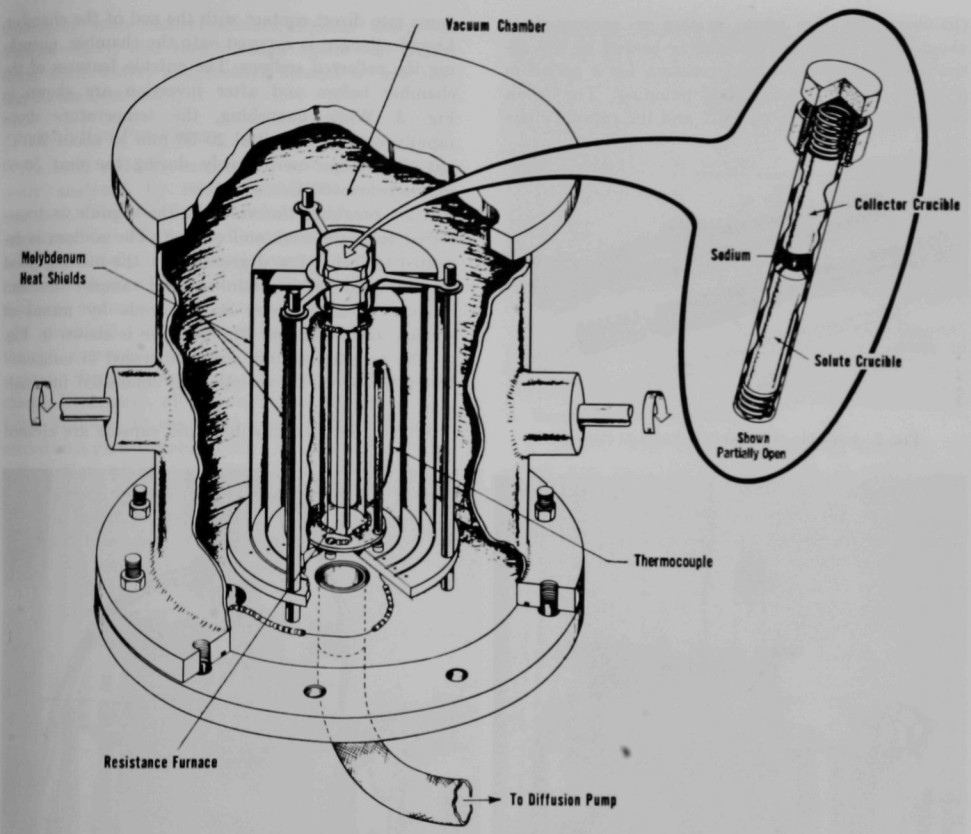

FIG. 1. Schematic Diagram of the Solubility Apparatus.

The temperature of the crucibles is measured by three sets of Pt-Pt 10% Rh thermocouples sheathed in alumina. Their junctions are situated adjacent to the outside wall of the molybdenum capsule near the bottom and the lid of the solute crucible and the midpoint of the collector crucible, respectively.

The stainless steel plate supporting the furnace is mounted on the base plate of a cylindrical vacuum chamber 8 in. in diameter and 8 in. high. The chamber is sealed by a gold O-ring. The pumping port is connected to a liquid nitrogen-trapped diffusion pump by a 1¼-in.-diameter flexible steel hose (45 in. long) and Curvac high-vacuum rotatable flanges, so that the entire vacuum chamber can be inverted 180°, while maintaining a vacuum of 10^{-6} to 10^{-7} Torr.

2.3. Procedure

During the preparation for a solubility run, the crucibles, springs, capsule, and Swagelok cap are successively rinsed with distilled water, acetone, and methyl alcohol, and then outgassed in the furnace under vacuum at 500 to 600°C for several hours. Then the components are transferred to an argon-filled (<1 ppm H_2O and <2 ppm O_2) glovebox where the components are heated for another hour on a hot plate at 150°C. Sodium samples, around 0.7 to 2.0 g in size, are loaded into the solute crucible, and the components are assembled in proper sequence as indicated in Fig. 2. The cap is screwed on tightly by means of two 12-in. wrenches.

The capsule is then transferred to the vacuum

chamber, and the whole system is evacuated to about 10^{-7} Torr. The furnace is heated to the desired temperature and held constant for a period of 4 to 25 hr with continuous pumping. The whole chamber is then inverted 180°, and the capsule slides down into direct contact with the end of the chamber. Liquid nitrogen is sprayed onto the chamber, quenching the collected sodium. The outside features of the chamber before and after inversion are shown in Fig. 3. While quenching, the temperature drops rapidly during the initial 20–30 min to about 200°C, but then drops more slowly during the next 50–60 min to below 100°C.

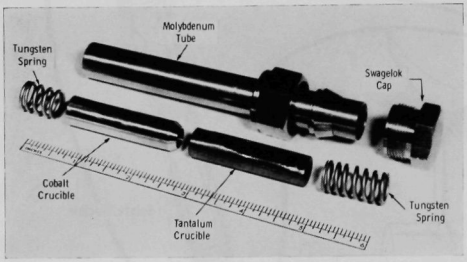

FIG. 2. Assembly of Metal Crucibles and Capsule.

After breaking the vacuum, the capsule is transferred to a glovebox and opened. The sodium is reheated to just a few degrees above the melting point and sampled with a stainless steel sampler that can produce ⅛-in.-diameter sodium rods by means of suction and extrusion. The sampler is shown in Fig. 4. The sampled sodium rods are sealed in outgassed Pyrex tubing under vacuum and submitted for analysis.

After a test, the crucibles and capsule are cleaned

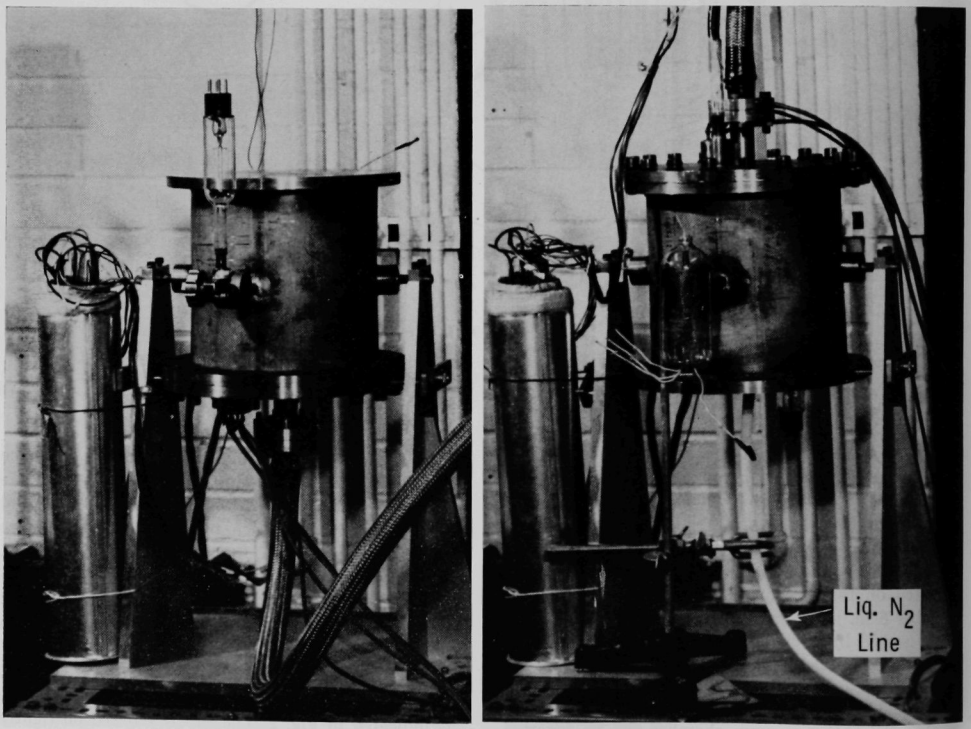

FIG. 3. The Solubility Apparatus in the Upright position during Equilibrium and Inverted 180° during Quenching.

thoroughly with methyl alcohol, flushed well with distilled water, and then cleaned again with dilute nitric acid, water, and methyl alcohol in preparation for the next test.

2.4. Analytical Procedure

The solid rod-like samples of sodium can be directly analyzed by SSMS without any chemical treatment. The detailed procedure employed in our laboratory for this type of analysis has been published.[11] Briefly, the samples are used as the electrodes between which a high-voltage (20 keV) rf discharge occurs to excite the constituent atoms. The ions produced are then accelerated and passed through successive electric and magnetic fields to separate them according to their ratio of mass to charge. Ultimately, all ions in the atomic mass range 7–240 (lithium to uranium) are simultaneously recorded on a photographic plate.

Protection of the samples at the instrument is accomplished by means of a glovebox. A vacuum glovebox bolted to the source chamber of the instrument and filled with high-purity argon is employed to limit any contamination of the samples while they are being affixed to the electrode holders. Furthermore, the samples are cooled during sparking by a liquid-nitrogen trap which is attached to the electrode holders with copper braids. This prevents melting of the samples and inhibits preferential volatilization.

Since the concentration of cobalt and nickel in the samples is extremely low, only a few very long exposures are placed on each photoplate. These exposures are separated by some distance on the plate to reduce any fogging effects on the image lines of interest ($^{58}Ni^{+1}$ and $^{59}Co^{+1}$). At least 5 or 6 short exposures on each plate are also included to calibrate the emulsion with $^{23}Na^{+1}$ lines, as is our normal practice.

The nickel and cobalt concentrations are calculated under the assumption of unit sensitivity. The comparison of our data with those of other experimenters using other analytical techniques will partially reflect the validity of this assumption. About 10 mg of sample are consumed in a single long exposure. In all cases, several plates were made with each pair of samples from a single solubility experiment. Whenever possible, more than one pair of samples was made from a run and duplicate analyses were performed.

The small analytical sample consumed by SSMS enables information to be gained on the possible local heterogeneity of the samples. This compares with the more usual case in solubility experiments, in which the analytical techniques consume larger samples.

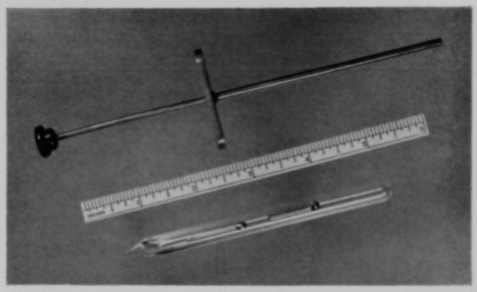

FIG. 4. Stainless Steel Sampling Device for Liquid Sodium. The rod-like samples produced are shown under vacuum in a glass tube.

3. Results and Discussion

A total of four experiments for the solubility of cobalt and three for the solubility of nickel have been carried out. These experiments covered a temperature range from 289 to 544°C and from 297 to 449°C, respectively. A summary of all the experimental conditions and the analytical results from SSMS analysis are given in Table 2. It is important to note that the table contains the observed concentrations from each long exposure on each separate photoplate. This provides some insight into the homogeneity of the samples.

To assess the possibility of significant oxygen contamination of the sodium during the experimental procedure, a sodium sample was placed in the nickel crucible and heated under normal operating conditions in the vacuum chamber for 8 hr at 380°C. A subsequent oxygen determination on the sodium by the amalgamation technique yielded a result of 14 ppm. Considering the accuracy of this analytical method, the result is within the normal oxygen range for the sodium used in the experiment, usually quoted at less than 10–20 ppm by MSAR. Thus, we believe that oxygen contamination during the course of the experiment was not a serious problem.

The solubility data obtained in this study for both cobalt and nickel are plotted separately as a function of temperature in Figures 5 and 6. At each separate temperature, note that all individual results from the appropriate photoplates have been plotted as distinct points and have been identified according to which plate in the series they appeared on. This portrays graphically the observed heterogeneity in the samples. No curve has been drawn through the results because of the limited number of points and their attendant spread. Nevertheless, some trend is apparent in each case, and the proper

TABLE 2. SUMMARY OF EXPERIMENTAL CONDITIONS AND SOLUBILITY MEASUREMENTS FOR COBALT AND NICKEL IN LIQUID SODIUM

Run	Sodium Weight, g	Temp, °C	Equilibration Time, hr	Analytical Results: Plate of Series	Analytical Results: Observed Conc for Each Exposure, ppm wt
Co #1	0.73	289	24	1	0.31
				2	0.52, 0.19, 0.22
				3	0.07
Co #2	0.80	347	5	1	1.6, 14.4, 12.2, 3.7
				2	2.7, 1.6, 1.1, 1.2
				3	0.13, 0.16, 0.11
Co #3	1.11	427	4	1	0.29, 0.28, 0.23
				2	0.28, 0.12
				3	6.6, 3.6
Co #4	1.14	544	4	1	0.49, 0.20
				2	0.43
				3	0.15
				4	0.14
Ni #1	2.04	297	25	1	0.92, 0.55
				2	0.38
				3	0.20
Ni #2	2.01	376	8	1	0.24, 0.17, 0.93, 0.73
				2	0.96, 1.7
				3	1.8, 0.45
				4	0.10, 0.54
Ni #3	1.22	449	5	1	4.9, 2.8
				2	3.1, 1.4
				3	2.3, 1.0

general behavior is displayed. Figures 5 and 6 also include the respective solubility data from the literature, and for the purpose of later discussion, Fig. 5 also includes the available data for iron in sodium.[2, 13]

At the higher temperatures, the present solubility data for cobalt are comparable to the result of Grand *et al.*[1] However, at lower temperatures, our cobalt results are significantly higher. This implies a lower value for the temperature coefficient of solubility from our data and consequently a smaller value for the heat of solution, ΔH_s. (In a semilog plot of solubility versus the inverse of the temperature, the slope of the theoretical straight line is given by $-\Delta H_s/2.30$ R, where R is the gas constant.) As Anthrop[4] points out, the data of Grand *et al.* lead to an extraordinarily high value for the ΔH_s of cobalt, 23,700 cal, which indicates a strong interaction between the cobalt and the sodium. By comparison, the heats of solution which have been observed for both iron and nickel in sodium are below 5000 cal,[4] more in line with their heats of fusion. The value of ΔH_s for cobalt reflected by this work is much closer to the iron and nickel values, and this is encouraging in view of the similarities between the three elements.

The spread in our data at a given temperature is indicative of inhomogeneities in the solid samples, since the variations observed are much larger than the precision of the spark-source technique (usually in the range 10–20%) when all parameters are being properly controlled. These inhomogeneities may have existed in the samples at the equilibration temperature, or they may have formed by precipitation during the cooling process. In the former case, the sample would not reflect true solubility, but rather the effects of particulate contamination or debris. In the latter case, the sample could still be analyzed to obtain a good average concentration by pooling the results of several duplicate analyses.

Unfortunately, our data cannot be divided with absolute certainty between these two possibilities, but there is evidence of some abnormal behavior in the cobalt data. As indicated in Fig. 5, all the points showing the highest cobalt concentrations are from

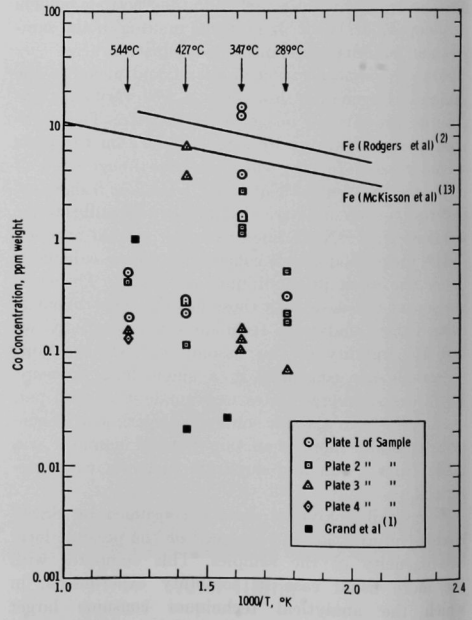

FIG. 5. Solubility Data for Cobalt in Sodium.

just three photoplates. This is some indication that perhaps a systematic effect was operating in these cases. The emulsion calibration line obtained for the three plates in question was normal, but the observed concentration of Fe, Ni, Cr, and Mn on all the plates was significantly higher than normal. Thus, these simultaneously high concentrations could be a result of some localized metallic contaminant in the sodium. Nevertheless, at this stage in our knowledge of solution processes in liquid sodium, to discard the data would be too subjective a judgment, and so they are included with the addition of these cautionary remarks. However, this situation serves to illustrate the type of information available with a multi-elemental analytical technique.

From Fig. 6, the trend of our solubility data places it between the two existing sets of results, about one order of magnitude below those of Rodgers *et al.*[2] and two orders of magnitude above those of Kovacina and Miller.[3] Furthermore, the slopes of the three sets of data are perceptibly but not radically different from one another. The heat of solution reflected by the present data indicates a result which is roughly as far above the heat of fusion as the previous results are below, 7500 cal versus 2600 cal and 1600 cal, respectively, with a heat of fusion of 4200 cal.

There was a low (<1 ppm) but variable nickel blank in the sodium used in our experiment. The variable nature of this blank prevents a constant correction from being applied to the data. However, the similarity in the slopes between our data and from previous work is some evidence that the blank problem was not overwhelming in our study.

It is interesting to note that there are no anomalous photoplates in our nickel data. In fact, the results from the separate plates for a given run are quite well intermingled. Moreover, no excessive Fe, Mn, Cr, or Co concentrations were recorded on any of the plates, the levels being generally low. There is little doubt, then, that the spread in our nickel data at a given temperature reflects local inhomogeneities in the solid samples arising from the solution and cooling processes.

To discuss further the validity of the data in this paper and to compare them to previous results, several additional considerations can be raised: 1) the analytical questions surrounding the use of SSMS to obtain the data, 2) the effects of metal surface cleanliness in the crucibles, and 3) the solubility trends expected from comparing the basic atomic-size factor of the different binary systems.

Since SSMS analysis has not previously been used to obtain solubility data, and since its application to

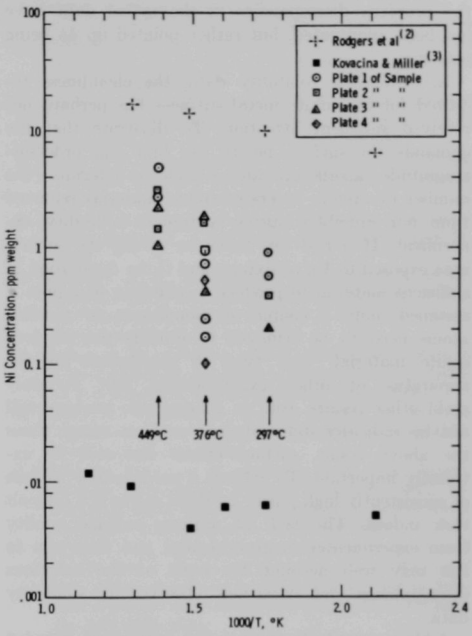

FIG. 6. Solubility Data for Nickel in Sodium.

sodium analyses in general is quite recent, there are some natural questions regarding the validity of its use. In a previous paper,[12] the overall feasibility of employing SSMS for sodium analyses was established. This involved showing that the technique was capable of detecting subparts per million levels of the important stainless steel group of elements: Fe, Ni, Mn, Cr, and Co. The precise accuracy with which these elements could be determined remained open to discussion, but it appeared that the correct results could be obtained within an order of magnitude. Since the accuracy of an SSMS analysis cannot be established without the existence of a suitable standard to correct for possible matrix effects, and since a sodium standard with known amounts of the stainless steel group of elements cannot yet be prepared, the opportunity to compare our solubility data with that of other experimenters provides a measure of the accuracy of the technique. The results achieved in this paper under the assumption of unit sensitivity for both cobalt and nickel confirm not only that SSMS can yield reasonable results compared with other analytical techniques, but also that unit sensitivity is a good assumption at this time. The cobalt solubility trend has been made more acceptable, and

the previous discrepancies in the nickel data have not been aggravated, but rather pointed up as being extremes.

In evaluating solubility data, the cleanliness required for the solute metal surfaces has perhaps not received sufficient attention. To illustrate that the demands for surface purity are high, an order-of-magnitude calculation can be made to determine the number of atomic layers of solute material removed from our crucibles during a typical solubility experiment. If 5 cm^2 are taken as giving the surface area exposed to 1 g of sodium and if the dissolution of sufficient material to produce a solubility of 1 ppm is assumed, only a couple of monolayers of crucible atoms need to be removed to provide the required solute material. This type of calculation for the apparatus of other experimenters will certainly yield other results. But, in general, the answers will not be radically different, and even at many times the above result, surface effects can still be extremely important. To achieve a good-quality surface of consistently high purity on these scales is a difficult task indeed. The lack of uniform surface quality from experimenter to experimenter and from run to run may well account for some of the notorious discrepancies and variations observed in solubility data.

Addison *et al.*[14] studied the wetting of abraded transition metal surfaces in liquid sodium and concluded that in the absence of any oxide film, pure liquid sodium would always spread to give a zero contact angle with a pure solid metal, and secondly, that any observed changes in the contact angle (when $\theta \neq 0$) as a function of time and temperature would be direct consequences of both the rate and the nature of chemical reactions between the sodium and a surface oxide film. For iron, nickel, and cobalt respectively, the oxide films are α-Fe_2O_3, γ-Fe_2O_3, Fe_3O_4, NiO, CoO (predominantly below 300°C), and Co_3O_4 (predominantly above 300°C). In terms of their free energies of formation, the stability of these oxides is much lower than that of Na_2O.[15] Addison *et al.*[14] found the critical wetting temperature to be 140°C for iron, 190°C for cobalt, and 195°C for nickel. Above these temperatures, they found that the contact angle for liquid sodium on these metals decreased with time to zero, corresponding to the reduction of the surface oxides previously formed in air.

With the present experimental procedure employed in our laboratory for solubility measurements, it is hoped that any surface oxide film does not pose a serious problem. The chemical reduction of such a film by sodium could produce finely divided particles of cobalt or nickel that might enter the sodium and possibly remain as local inhomogeneities in the liquid. But even if the reduced metal particles actually dissolved, the overall heat of reaction for all processes occurring would reflect the reduction of the corresponding oxide. Both of these processes could interfere significantly with the determination of good solubility data. The presence of a significant oxide film would lead to an apparent increase in the heat of solution and hence to an increase in the temperature coefficient of the measured solubility. No evidence of an excessive increase of this type is unequivocally discernible in our data. Since the solubilities of nickel and cobalt are quite low, in the absence of compound formation, the solution should behave ideally and the heat of dilution should be negligible. Consequently, the overall heat of solution should then be very nearly equal to the heat of fusion of the solute metal. The heat of fusion for cobalt is 4100 cal/g-atom, and for nickel 4210 cal/g-atom, and these are less than a factor of two from the values of ΔH_s reflected by our data in Figures 5 and 6.

If the metal surface of the crucibles is not perfectly smooth and clean, but contains minute particles or debris, the resultant sodium melt could be inhomogeneous from the occlusion of this material, which would not reflect true solubility. Scatter in the analytical data has plagued many investigators. The small analytical sample required by SSMS can point up the local inhomogeneities present in the sodium. Analytical methods which consume the sample in its entirety produce only an average value for the concentration and lose important information on the heterogeneity of the sample.

The final point to be discussed is the influence of the atomic-size factor. Strauss *et al.*[16] have presented a correlation between the temperature coefficient of solubility in dilute binary metallic systems and the atomic-size factor (defined as the atomic radius of the solvent atom divided by the atomic radius of the solute atom). They point out that the atomic-size characteristics of low-melting point solvent metals and high-melting point solute metals are such that the majority of binary systems formed by them have an atomic-size factor between 0.8 and 1.6. An interstitial solution process becomes energetically competitive with a substitutional solution process at size factors near 1.4. At higher values, the temperature coefficient decreases rapidly as the solute atom approaches the size of the unstrained interstices that might be expected to exist in

liquid metals. Taking the atomic radius for sodium as 1.896 Å[17] (which is approximately the same as the atomic radius of liquid sodium at 400°C[18]), and the atomic radii for iron, cobalt, and nickel as 1.165 Å, 1.162 Å, and 1.154 Å,[19] respectively, the size factors are 1.627, 1.632, and 1.643. From these figures, one would expect the temperature coefficients of solubility for iron and cobalt to be approximately the same, but slightly higher than that of nickel. Secondly, the solubility of cobalt in sodium should not differ appreciably from that of iron because in addition to the closeness of their size factors, their valencies, electronegativity, coordination number, and general chemical behavior are similar. For nickel, the problem is more complex because of differences in valence and coordination number, but its solubility should not differ excessively.

Obviously, all of the data on hand do not strictly conform to these theoretical arguments. There seem to be distinct differences between the solubilities of iron, cobalt, and nickel, but since the chance of systematic errors in past work is large, much more data will be required to make a more precise assessment. One note of encouragement is that the data do seem to be settling near slopes which indicate heats of solution that are not too far from ideal behavior. However, more detailed discussion on the points raised in this paper must await further experimentation. Some effort should be directed toward elucidating the role of other impurities on the solution process, and in this regard, a multi-elemental analytical technique like SSMS can offer many advantages.

Acknowledgments

The authors are grateful to William M. Hickam for his encouragement and technical insight, both of which contributed substantially to this work. Walter W. Weis, Jr., and William H. Reed also provided valuable assistance.

REFERENCES

1. Grand, J. A., Baus, R. A., Bogard, A. D., Williams, D. D., Lockhart, L. B., Jr., and Miller, R. R., *The Solubility of Tantalum and Cobalt in Sodium by Activation Analysis*, J. Phys. Chem. **63**, 1192–1194 (1959).
2. Rodgers, S. J., Mausteller, J. W., and Batutis, E. F., *Iron and Nickel Concentrations in Sodium*, MSAR-27 (NP 5247) (June 30, 1954).
3. Kovacina, T. A., and Miller, R. R., *The Solubility of Nickel in Sodium by a Tracer Technique*, Nucl. Sci. Eng. **10**, 163–166 (1961).
4. Anthrop, D. F., *The Solubilities of Transition Metals in Liquid Alkali and Alkaline Earth Metals, Lanthanum and Cerium—A Critical Review of the Literature*, UCRL-50315 (Sept 20, 1967).
5. Singer, R. M., and Weeks, J. R., *On the Solubilities of Cu, Ni, and Fe in Liquid Sodium*, THIS CONFERENCE.
6. Eichelberger, R. L., and McKisson, R. L., *The Solubility of Cu, Mo, Nb, Fe, Ni, and Cr in High-purity Sodium*, THIS CONFERENCE.
7. Horsley, G. W., and Maskrey, J. T., *The Determination of the Solubilities of Beryllium and Molybdenum in Liquid Bismuth*, J. Inst. Metals **86**, 401–402 (1957–58).
8. Teitel, R. J., *High-temperature Centrifuge for Niobium and Tantalum Solubility in Potassium*, Trans. ANS, Annual Meeting, June 21, p. 15 (1965).
9. Cleary, R. E., Schenck, G. F., and Blecherman, S. S., *Solubility Studies in Alkali Metals*, CNLM-6335 (April 21, 1965).
10. McKisson, R. L., Eichelberger, R. L., Dahleen, R. C., Scarborough, J. M., and Argue, G. R., *Solubility Studies of Ultra Pure Transition Elements in Ultra Pure Alkali Metals*, NASA CR-610 (Oct 1966).
11. Swisher, J. H., *Solubility of Iron, Nickel, and Cobalt in Liquid Potassium and Effect of Oxygen Gettering Agents on Iron Solubility*, NASA TN D-2734 (March 1965).
12. Berkey, E., Sweeney, G. G., and Hickam, W. M., *The Analysis of Sodium by Spark Source Mass Spectrography*, Nucl. Appl. **5** (Nov 1968).
13. McKisson, R. L., *et al.*, *Quarterly Tech. Prog. Report*, Atomics International (October–December, 1967), Information taken from High-Temperature Liquid-Metal Tech. Rev. **6** (2), Review No. 722 (April 1968).
14. Addison, C. C., Iberson, E., and Manning, J. A., *Liquid Metals. Part V. The Role of Oxide Films in the Wetting of Iron, Cobalt, and Nickel by Liquid Sodium, and by Solutions of Barium and Calcium in Liquid Sodium*, J. Chem. Soc. 2699–2705 (1962).
15. Olette, M., and Ancey-Moret, M. F., *Variation de L'Energie Libre de Formation des Oxydes et des Nitrures avec la Temperature*, Rev. Metall. **60**, 569 (1963).
16. Strauss, S. W., White, J. L., and Brown, B. F., *The Atomic Size Effect and Alloying Behavior in Liquid Metals*, Acta Met. **6**, 604–606 (1958).
17. Pauling, L., *Atomic Radii and Interatomic Distances in Metals*, J. Am. Chem. Soc. **69**, 542 (1947).
18. Gmelins Handbuch **21** (2), 558–559 (1965).
19. Pauling, L., *A Resonating-Valence-Bond Theory of Metals and Intermetallic Compounds*, Proc. Roy. Soc. (London) **A196**, 343–362 (1949).

Discussion

Mr. Weeks (BNL): Was each analysis that you showed that of an entire sample or only a portion of the sample?

Mr. Lee: Only a portion.

Mr. Weeks: I think that could account for a considerable portion of the scatter, as indicated by the talk we had a couple of hours ago. The second point I'd like to make is that I don't think the size-effect model applies at all. I think we should stop talking about it because there are more exceptions than there are actual confirmations when consistently accurate data are plotted.

Mr. Lee: I agree with that. But keep in mind we are assuming no compound formation. We were just talking about the dissolution process for either a substitutional or interstitial compound. For example, in the case of iron, we know this ternary compound, but we don't know about it in the case of cobalt.

Mr. Weeks: As many of you know, during the ten years we worried about the liquid bismuth reactor, we measured liquidus curves of practically all the constituents of steels, all the fission products that we could get our hands on, and a few other things to complete it. The systems that did not form intermetallic compounds were plotted in that manner in a summary paper I prepared about three years ago. It's just a random relationship when you plot the temperature coefficient of solubility as a function of the atomic ratio. The paper is published in ASM Transactions.

Mr. Berkey (W): I think it was clear from Dr. Lee's presentation that his data were based on extremely small analytical samples. Is it an analytical problem, or is it a sampling problem?

Mr. Weeks: I would think that if you could take a larger sample of sodium and dissolve it in a solution in which it will be homogeneous, such as an aqueous solution, and then take an aliquot of this, you might get far more reproducible results.

Mr. Berkey: Reproducible results are one thing, and accurate results are another. We were able to monitor continuously the concentrations of iron and nickel, that is, the important stainless steel elements. On this basis we were able to question data and reduce the scatter. If we take a sample and homogenize it and we still get a big scatter, what does that tell us about solubility? If inhomogeneities exist in the liquid state, is this really solubility that we're talking about? By this technique we have a possible means to get at inhomogeneity in the liquid state, whereas by a technique that consumes the entire sample, you wash out the data and may still end up with a wide spread.

On the Solubilities of Cu, Ni, and Fe in Liquid Sodium*

R. M. Singer and J. R. Weeks

Brookhaven National Laboratory
Upton, New York

(PRESENTED BY J. R. WEEKS)

Abstract

The solubilities of copper, nickel, and iron in sodium have been measured as part of a continuing program to obtain the solubilities of LMFBR materials. Copper solubilities in sodium have been determined to range from 0.2 to 60 ppm at temperatures between 255 and 547°C. The results are in excellent agreement with those of Humphreys[1] and of Eichelberger and McKisson.[2] The solubility may be estimated by the following equation:

$$\log_{10} S(\text{ppm Cu}) = 6.91 - (4200/T)(°\text{K}),$$

over the temperature range 315–700°C.

Nickel solubilities in sodium have been completed at temperatures from 446 to 600°C. Our results range from 0.6 to 1.8 ppm over this temperature range, and fall between those values reported by Kovacina and Miller[3] and by Rodgers *et al.*[4] The solubility may be calculated using the following equations:

$$\text{Ni(ppm)} = 0.0046T(°\text{C}) - 1.40$$

for the nickel content of the sodium samples, and

$$\text{Ni(ppm)} = 0.0076T(°\text{C}) - 2.76,$$

which include the nickel found on the samplers which cannot as yet be considered as a contaminant.

Iron solubilities in sodium were measured as a function of oxygen concentrations at 486 and 550°C. The iron solubility increases with oxygen content above an oxygen activity of approximately 0.2. Early experiments from 370 to 450°C in systems containing 10–20 ppm oxygen indicated the iron solubilities were below the analysts' detection limits. These lower limits varied from 0.05 to 0.1 ppm as a function of the ^{59}Fe decay. The present results are lower by a factor of 15 than those of both Rodgers *et al.*[4] and Epstein,[5] and higher by a factor of 85 than those of Bogard.[6]

1. Introduction

In any analytic equation for corrosion or mass transfer by a liquid metal there is a term representing the thermodynamic driving force for corrosion or deposition, $S_i - C_i$, in which S_i represents the solubility of the dissolving species and C the concentration in solution of this same species, both at point i in the system. The need for accurate values of S_i is thus obvious in the development of an analytic model for corrosion by liquid sodium.

Iron, chromium, and nickel as the primary constituents of stainless steels are the most important metals for which accurate values of S_i need to be determined in sodium. Previous attempts to measure these solubilities have yielded values ranging over a factor of more than a thousand; yet it is impossible to state conclusively which set of previous results are incorrect.

The present paper contains the results to October of 1968 of a continuing program on the determination of the solubility of LMFBR metals in sodium, and represents but another chapter in the problems of determining these frustratingly elusive quantities. The copper solubility was determined to assist in explaining the copper transfer in EBR-II and provided a means of demonstrating the reliability of the equipment. The data on nickel solubility are essentially complete, except for an evaluation of the effects of dissolved Na_2O on this property. The solubility measurements for iron are only partially completed at the present time.

2. Experimental

The apparatus designed to determine the solubilities of various metals in sodium is shown in Fig. 1. Hot-trapped sodium is passed through a 5μ stainless filter into a distillation pot. The sodium is then vacuum distilled through a Nb-1 Zr tube into a pure metal crucible contained in the apparatus shown in Fig. 1. The crucibles (Fe, Ni, Cu) are leak-checked and hydrogen-fired before insertion into the solubility chamber.

After the crucible and sampling cups are sealed into the solubility chamber, they are given another hydrogen treatment at 600°C for 1 hr. The molybdenum sampling cups and the molybdenum-lined solubility chamber are then outgassed for $\approx$24 hr at a temperature exceeding the highest anticipated experimental temperature. Previously hot-trapped sodium is vacuum-

* This work was performed under the auspices of the U. S. Atomic Energy Commission.

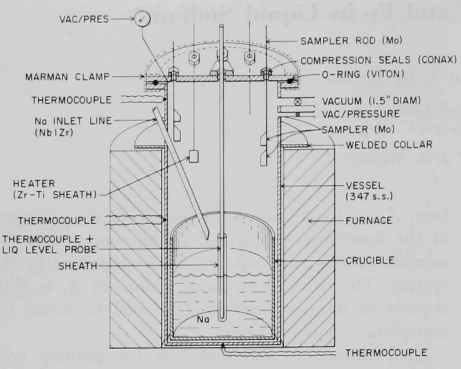

FIG. 1. Sodium Solubility Chamber.

distilled at 500°C; it condenses in the Nb-1 Zr tube at ≈200°C and drains into the crucible. The system is then pressurized with an ultrapure grade of helium that has been passed through our laboratory purification train.

The filled crucible and chamber are again pressurized, and raised to the desired experimental temperature and equilibrated for up to 24 hr. Twin molybdenum buckets were then lowered into the melt and held there 15 min to equalize their temperature with that of the liquid. They are then agitated to insure their being filled and raised. The temperature of the melt is then adjusted to another equilibration temperature, and the sampling procedure repeats. Duplicate samples can be taken at each of seven temperatures. The sealed solubility chamber is then delivered to the analyst's dry box where the duplicate samples are prepared for oxygen and metal analyses at each of the investigated temperatures. Preliminary experiments established handling procedures and eliminated the difficulties of providing filled sampling cups which hold approximately 2 g sodium.

The helium used for cover and transfer purposes is an ultrapure grade containing, upon purchase, 1.4 ppm O_2 and 2.1 ppm H_2O. The helium is passed through a Linde 4Å molecular sieve filter (capacity 125 g H_2O), a liquid-nitrogen-cooled Linde 5Å molecular sieve trap, and Zr-Ti (1:1) chips which are maintained at 600°C. The purified gas is finally passed through a stainless filter prior to use. A Lockwood and McLorie oxygen meter and a CEC moisture monitor are included in the purification assembly. The oxygen meter is calibrated with a known gas mixture. After purification the oxygen content of the helium is 0.45 ppm, and the moisture content is 0.8 ppm.

The fresh sodium distillate typically contains 1.0–2.0 ppm iron (spectrographic and colorimetric), <1 ppm nickel, 0.1–0.5 ppm chromium, and ~10–20 ppm O_2 (lower oxygen values are achieved by gettering with uranium foil).

3. Results

3.1. Copper

The solubility of copper in sodium was measured at temperatures between 255 and 547°C. The 99.999% copper sheet (Marz grade) was purchased from MRC and typically contained a 2-ppm total of oxygen, carbon, and nitrogen. The copper sheet was welded into a crucible 3 in. in diameter, 4 in. high, and 0.008 in. thick. It was then cleaned with a 10% aqueous solution of ammonium persulfate, washed, and hydrogen-fired at 500°C for 1 hr. The copper crucible was then loaded into the solubility apparatus which was outgassed at 600°C. Sodium was transferred from the hot-trapped MSA tank, and the apparatus was raised to the first experimental temperature, 500°C. After an equilibration period of at least 24 hr, duplicate samples were taken in molybdenum cups for analysis. This procedure was repeated at each of seven temperatures before the apparatus was unloaded in the analyst's dry box.

The results of the first run showed considerable scatter at temperatures below 300°C, and suggest that fine particulates were present in the sodium cooled to these temperatures. Also, the lower bucket occasionally contained ≈10 times as much copper as the upper bucket.

Consequently, a second run was made using the same copper crucible and sodium, in which, after an initial equilibration at 550°C, the apparatus was cooled to ≈250°C for 24 hr. All subsequent samples were taken after the melt temperature had been raised to the equilibration temperature. The results of the second run were more self-consistent than those of the first run, except for one high point (not shown) at 245°C, which contained visible particles of copper. During the 2 runs, oxygen analyses of 3 samples did not exceed 15 ppm (determined by the amalgamation technique). The samples were analyzed for copper by atomic-absorption spectroscopy. The results for all samples are given in Fig. 2, in which the copper concentrations are plotted against reciprocal absolute temperatures. The values range between 60 ppm at 547°C and <0.2 ppm (not detectable) at 245°C. The analytical reagent blank for these runs averaged <1 μg copper. There was evidence of precipitated copper in the high results at ~150 and 200°C in Fig. 2, most likely because the melt was cooled from higher temperatures prior to the runs in question.

As shown in Fig. 3, the results agree well with both

the magnitude and the temperature dependence of the results of Humphreys[1] from 500 to 700°C, and the results of Eichelberger and McKisson[2] above 500°C. Although the data are best represented by a curve, as shown, they can be approximated by the equation $\log_{10}$ (ppm Cu) = 6.91 − (4200/T(°K)) to within ±10% from 315 to 700°C.

3.2. Nickel

The nickel crucible was fabricated from material purchased from the United Mineral and Chemical Co. as 3-pass zone-refined ½-in. rod containing (on delivery) 16 ppm total metallic impurities and 58 ppm total oxygen, carbon, and nitrogen. The stock was rolled to 0.010 in. and annealed under argon prior to being fusion welded into a crucible, 3 in. in diameter and 4 in. high. The crucible was leak-checked and hydrogen-fired before insertion into the solubility chamber.

Preliminary experiments for nickel solubility at temperatures between 340 and 420°C produced widely scattered results. This scatter presumably resulted from two causes: the melt was alternately heated or cooled to the equilibration temperatures, possibly causing particulates to form; and the analytical blank was of comparable magnitude to the nickel solubility. The

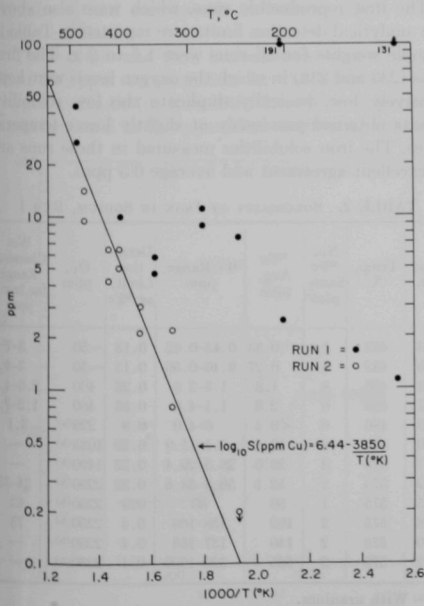

FIG. 2. The Solubility of Copper in Liquid Sodium as a Function of Temperature.

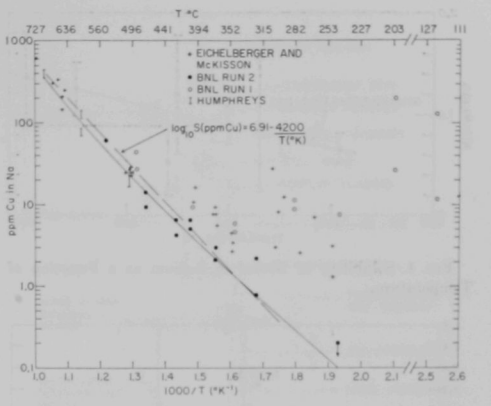

FIG. 3. A Comparison of Various Results for Copper Solubility as a Function of Temperature. References: Eichelberger and McKisson[2]; Humphreys.[1]

TABLE 1. SOLUBILITY OF NICKEL IN SODIUM

Temp, °C	No. of Samples	Nickel in Sodium, ppm	Nickel on Molybdenum, ppm	Total Nickel, ppm	Oxygen, ppm
446	5	—	—	0.67 ± 0.14[a]	21
474	4	—	—	0.76 ± 0.14	25
485	6	0.89 ± 0.66	1.35 ± 0.90	2.25 ± 1.46	220
525	5	1.19 ± 0.59	0.81 ± 0.83	2.00 ± 0.83	33
530	7	0.53 ± 0.33	0.93 ± 0.31	1.47 ± 0.54	31
575	2	1.24 ± 0.26	0.38 ± 0.12	1.62 ± 0.38	69
600[b]	9	0.89 ± 0.19	0.15 ± 0.09	1.04 ± 0.21	52
600	11	1.33 ± 0.48	0.51 ± 0.39	1.84 ± 0.67	46

[a] Average deviation.
[b] Temperature equilibrated at 500°C. Samples were taken after quickly increasing temperature to 600°C.

nickel solubility in this region as extrapolated from our higher temperature runs must be <0.5 ppm.

Measurements of the solubility of nickel at a series of temperatures from 446 to 600°C have now been completed. In this series, each equilibration temperature was higher than the previous temperature and many replicate samples were submitted for analysis at each temperature.

Table 1 lists the quantities of nickel found in the sodium samples and the additional quantities found on the molybdenum samplers by leaching them with 6 *N* HCl after the sodium has been removed. There is some experimental evidence that the nickel found on the molybdenum originated in the sodium; however, leaching experiments with clean molybdenum samplers with the same reagent have not resolved this problem conclusively. Therefore, Fig. 4 shows only the nickel found

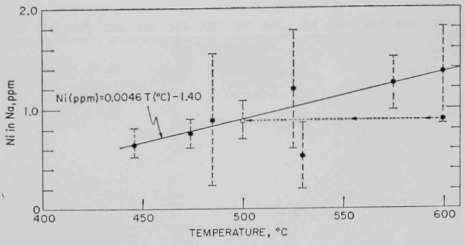

FIG. 4. Solubility of Nickel in Sodium as a Function of Temperature.

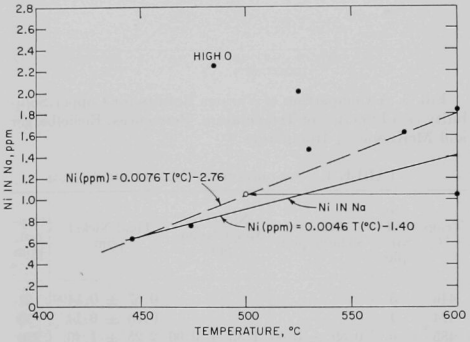

FIG. 5. A Comparison of the Total Nickel Found (Including the Nickel Leached from the Molybdenum Samplers) and the Nickel in the Sodium Poured from the Samplers (Data of Fig. 4).

in the sodium as a function of temperature. Figure 5 compares these values with the total of the nickel found on leaching the molybdenum buckets added to that found in the sodium that was melted and poured out of them.

The 600°C run for nickel was repeated because the first run (see Table 1, line 7) was actually equilibrated at 500°C for 24 hr and sampled immediately after raising the temperature to 600°C instead of the usual equilibration period at this temperature. The value for nickel for this run fits well with results for 500°C, as shown in Fig. 4.

Kovacina and Miller[3] found nickel solubilities to vary from 0.004 to 0.01 ppm over the temperature range from 200 to 600°C. Their technique consisted of equilibrating sodium with a ^{63}Ni-plated nickel crucible and counting the emitted (weak) beta particles after sampling. Their results at 600°C are 100–200 times lower than those of the present study.

Rodgers *et al.*[4] determined nickel solubilities (wet chemically) in both circulating and static nickel systems and in a static stainless pot. Their results ranged from 4 ppm at 200°C to 10 ppm at 540°C. Their extrapolated result at 600°C is higher by a factor of 6 to 10 than the result of the present study.

3.3. Iron

The iron used for the crucibles was triple-pass electron beam zone-refined material obtained from the Materials Research Corp., which typically contained 7 ppm each of O_2 and N_2, and 8 ppm of carbon. The stock was rolled in 2 stages to 0.005 in. and annealed under argon prior to fusion welding into the final form, using the tungsten inert-gas process without filler wire. The complete crucible was 3 in. in diameter and 4 in. high.

The fabricated iron crucibles, each with 2 iron standards, were irradiated in the Brookhaven Graphite Research Reactor for one month prior to their use in the solubility apparatus. In each case, excellent ^{59}Fe counting agreement was obtained between standards. As with early nickel runs, the early experiments with iron were also plagued with widely scattered results from precipitation problems generated by up and down equilibrium-temperature changes. Radiochemical techniques were complicated before the removal of ^{182}Ta and ^{124}Sb from the samples.

The first reproducible runs, which were also above the analytical detection limits, are reported in Table 2. Sample weights for all runs were 1.5 to 2 g. The first runs (233 and 238) in which the oxygen levels were kept relatively low, basically duplicate the low solubility results obtained previously at slightly lower temperatures. The iron solubilities measured in these runs are in excellent agreement and average 0.3 ppm.

TABLE 2. SOLUBILITY OF IRON IN SODIUM, RUN I

Run No.	Temp, °C	No. ^{59}Fe Samples	^{59}Fe Avg, ppm	^{59}Fe Range, ppm	Detection Limit, μg ^{59}Fe	O_2, ppm	Wet Chemical Range for Iron, ppm
233	482	5	0.33	0.13–0.62	0.13	~50	3–7
238	482	5	0.27	0.10–0.56	0.13	~50	3–4.5
250	486	8	1.8	1.3–2.9	0.28	460	2.6–4.2
257	486	6	2.0	1.1–4.0	0.35	460	1.2–7.6
273	486	6	$\leq$0.4	0–4.0	0.8	220[a]	3.1
280	486	2	10.5	9.1–11.9	0.22	1035[b]	—
281	525	3	29.0	28.5–29.4	0.22	1490[b]	—
282	575	2	52.1	50.3–53.8	0.22	2250[b]	34–35
285	575	1	80	80	0.3	2250[b]	62
288	575	2	162	158–166	0.4	2250[b]	73
290	575	2	146	137–155	0.4	2250[b]	—
292	575	2	685	320–1050	0.4	2250[b]	—

[a] With uranium.

[b] Saturated values interpolated from Eichelberger's estimate. 1% oxygen was added as Na_2O_2.

The same sodium melt was then doped with Na_2O_2 to raise the oxygen level to 460 ppm. Two series of samples (runs 250 and 257) were then taken. Iron solubilities increased, by a factor of $\approx$6, to 1.9 ppm, and were in excellent agreement, even though the melt was kept at room temperature for several days between the two runs.

The same sodium melt was then gettered with uranium foil to remove a sizeable amount of the previously introduced oxygen, using the technique described by Isaacs at THIS CONFERENCE. Run 273, which on analysis (by amalgamation) contained 220 ppm oxygen, was then started. At this point, however, the irradiated iron had decayed sufficiently to provide a detection limit of only 0.8 μg iron. This indicates an upper solubility limit of 0.4 ppm for each of the 2-g samples that counted $<$0.8 μg iron. The uranium foil was then chemically dissolved and counted for residual iron in an effort to locate the missing iron. The 3-g uranium sample analyzed $<$3.5 μg iron, the detection limit. The iron solubility must therefore be a function of the oxygen content.

The wet chemical iron content throughout the series of experiments remained unaltered at $\approx$3 ppm. This value is essentially the same as that found on analysis of sodium freshly distilled into quartz and molybdenum containers, and corresponds to $\sim$50 to 100% of the analytical blank.

The sodium was then increased in oxygen content from 220 ppm to saturation by the addition of 1% oxygen as Na_2O_2 (in Run 280). The ^{59}Fe concentration again increased to 10.5 ppm, thus reaffirming an oxygen dependence. At this point the temperature was elevated to 525 and 575°C, and samples were taken at each temperature. Values of ^{59}Fe increased to 50 ppm at 575°C. Additional samples were taken at 575°C over a period of one week (Runs 285–292). These runs showed continued large increases in iron concentration. Finally, the experiment was dismantled and the residue at the bottom of the iron crucible was found to contain milligram quantities of ^{59}Fe. However, the wet chemical analyses of the high-oxygen samples was lower than the radiochemical results in all cases. These results obviously do not represent true liquidus values.

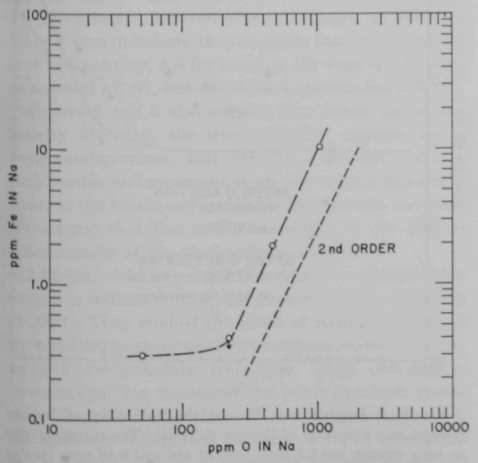

FIG. 6. Effect of Oxygen on the Solubility of Iron in Sodium at 486°C.

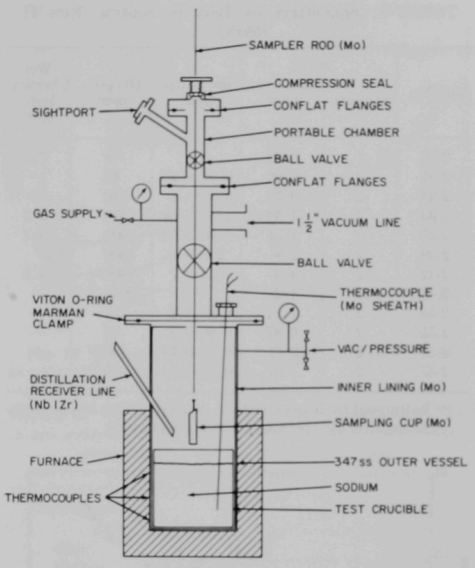

FIG. 7. Modified Solubility Apparatus.

The effect of oxygen on the radiochemical results for iron in sodium at 486°C is shown in Fig. 6. A close approximation to a second-order effect is apparent at oxygen concentrations above 200 ppm.

At this point, the experimental equipment was modified to include an "air-lock" sampling port (see Fig. 7) which fits the top of the experimental vessel. The sampling cups are introduced through a ball valve into a chamber capable of being evacuated and pressurized with purified helium prior to immersion of the cups into the sodium melt through a lower ball valve. The sampling port permits greater flexibility than heretofore possible. The sodium may be further oxygen-gettered with uranium or doped with a desired constituent at any point during an experiment. In addition, molybdenum sampling cups have now been prepared

TABLE 3. SOLUBILITY OF IRON IN SODIUM, RUN II (550°C)

Run No.	No. ^{59}Fe Samples	^{59}Fe Avg, ppm	^{59}Fe Range, ppm	Oxygen, ppm	Wet Chemical Iron, ppm
2-23	1	0.09	—	<1	7.3
2-31	2	0.66	0.57–0.75	85	—
2-34	2	0.73	0.31–1.1	340	—
2-35	2	1.54	1.44–1.64	570	2.1
2-37	2	1.51	1.40–1.62	1000	4.1
2-39	2	2.8	2.5–3.1	1600	13
2-42	2	3.6	3.5–3.7	1800[a]	4.2
2-45	1	4.2	—	2040	—
2-53	2	1.1	0.43–1.8	131	—
2-55	2	0.87	0.80–0.93	72	—
2-56	2	0.61	0.44–0.78	50[b]	—
2-57	2	1.07	0.83–1.3	25[b]	—

[a] Estimated by Na_2O addition. Amalgamation sample lost.
[b] Estimated by uranium gettering technique.

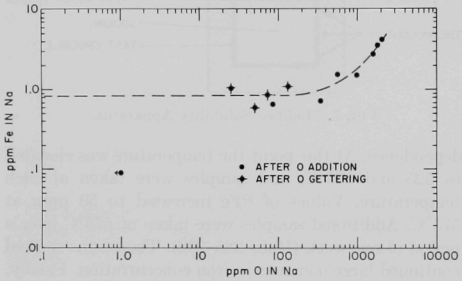

FIG. 8. Effect of Oxygen on the Solubility of Iron in Sodium at 550°C.

by boring out ½-in.-diameter molybdenum rod. The cups are suspended in the sodium melt via thin molybdenum wires. The many difficult welding operations required in the past to prepare cups from sheet stock has thus been eliminated. The surfaces of the new cups are smooth and no longer interfere with proper transfer of cup contents. These cups are cleaned with aqua regia and then rinsed in 6 *N* HCl until iron-leaching results are below the analysts' detection limits.

A freshly irradiated crucible prepared from 3-pass zone-refined MSA iron was removed from the Brookhaven Graphite Research Reactor and installed in the apparatus. After the crucible was filled with distilled sodium, the oxygen content of the sodium was further lowered by gettering with uranium, the temperature equilibrated to 550°C, and the melt sampled. Weighed additions of Na_2O were added to increase the oxygen content, and samples were taken. The oxygen in the system was gettered with uranium and sampled as oxygen levels were lowered. The results for iron solubility are shown in Table 3. In all cases the changes in the amalgamation results for oxygen agreed reasonably well with the added or gettered quantities of Na_2O. After an oxygen activity of 0.2 was reached, the ^{59}Fe values increased to ~4 ppm at the saturation value. The wet chemical results for iron were on occasion up to an order of magnitude greater than the radiochemical results. However, the relative constancy of the wet chemical results as the radiochemical iron changes (by oxygen additions and removals) implies that a major part of the iron found wet chemically in low-oxygen sodium may be due to contamination during subsequent handling to sampling.

Figure 8 shows the effect of oxygen on Fe in sodium at 550°C. Figure 9 shows the oxygen effect at both 486 and 550°C. It should be noted in Fig. 9 that the iron solubility appears to be oxygen independent below an oxygen activity of ≈0.2. Extrapolation to essentially zero oxygen yields solubility values of 0.3 and 0.85 ppm at 486 and 550°C, respectively. Figure 10 shows the same information plotted linearly. Table 4 compares the iron solubilities found for these 2 temperatures with those of previous investigators. At 550°C the present study gives results a higher by factor of 85 than those of Bogard[6] and lower by a factor of 15 than those of both Rodgers[4] and Epstein.[5]

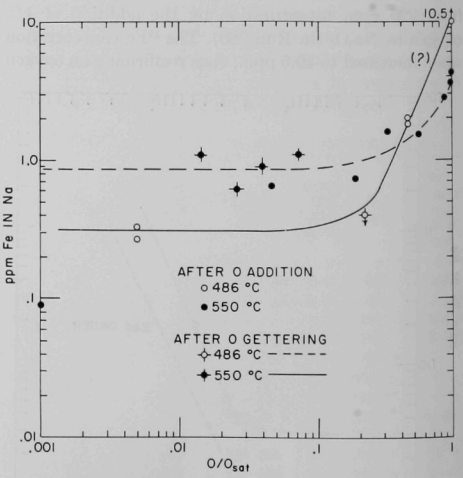

FIG. 9. A Logarithmic Plot of the Solubility of Iron in Sodium as a Function of Oxygen Activity. The extrapolations to zero oxygen are 0.3 ppm iron at 486 and 0.58 ppm iron at 550°C.

4. Discussion

The oxygen dependence of the apparent solubility of iron in sodium can be interpreted as arising from the following equilibrium:

$$Na_2O + Fe = FeO + 2Na(l), \qquad (1)$$

for which $\Delta F = 36{,}000 - 16.8T$; at 486°C ΔF is 23.2 kcal and at 550°C is 22.2 kcal. Also,

$$FeO + 2Na_2O = (Na_2O)_2 \cdot FeO, \qquad (2)$$

for which Thorley and Tyzack[7] give $\Delta H^\circ_{298} = -24.8$ kcal/mole FeO.

Assuming[7] that $\Delta F = \Delta H$ for reaction (2), we find an overall reaction

$$3Na_2O + Fe = (Na_2O)_2 \cdot FeO + 2Na, \qquad (3)$$

where $\Delta F_{486} = -1600$ cal/g-atom Fe and $\Delta F_{550} = -2600$ cal/g-atom Fe. These numbers correspond to activities of oxygen in sodium of 0.7 and 0.59, respectively, above which sodium ferrite of unit activity may form.

The present results, however, suggest that oxygen effects on the iron solubility occur at appreciably lower activities than those calculated. There are two possible explanations for this difference: $(Na_2O)_2 \cdot FeO$ may be present dissolved in sodium at less than unit activity, or the assumption[7] that for reaction (2) $\Delta F = \Delta H$ may be incorrect.

The data in Fig. 6 suggest that the effect of oxygen becomes pronounced at 486°C at an oxygen activity of ≈0.2. From this number, we estimate for equation (3) that $K_{(3)} = 125$, and $\Delta F_{486} = -7.28$ kcal/g-atom Fe. The present observed effect of oxygen on the solubility of iron in sodium thus suggests that, if the sodium is of unit activity, ΔS for reaction (2) must not be zero, as assumed by (7), but ≈+7.5 cal/g-atom Fe.

Figures 6 and 8 also suggest that below an oxygen activity of ≈0.2, the iron solubility appears to be oxygen-independent, and yet the corrosion rates of both ferritic and austenitic steels are oxygen-dependent down to the lowest oxygen levels that we can measure. We suggest that this is due to oxygen in the sodium concentrating at the steel-sodium interface.

Addison, Addison, and Kerridge[8] reported that oxygen in sodium reduces the surface tension of sodium at 200°C. They studied the effect of partial pressure of air in the argon cover gas on the sodium surface tension, using a vertical-plate technique. They observed a minimum surface tension at the point at which visible oxide films on the surface of the sodium formed. If one considers this partial pressure of O_2 to correspond to a saturated solution of oxygen in sodium, we can use

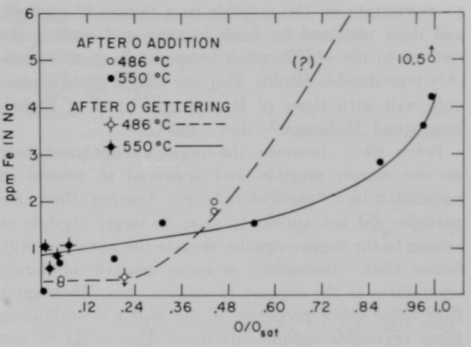

FIG. 10. A Linear Plot of the Solubility of Iron in Sodium as a Function of Oxygen Activity.

TABLE 4. A COMPARISON OF THE PRESENT SOLUBILITY RESULTS WITH OTHER PUBLISHED RESULTS, EXCLUDING THOSE PRESENTED BY OTHER WORKERS AT THIS CONFERENCE (ppm)[a]

Investigators	486°C	550°C
BNL	0.3[b]	0.85
MSA[4]	11.5	13
KAPL[5]	12.3	14
NRL[6]	0.006	0.01

[a] Culcheth reports a value of 7 ppm at 650°C with 10 ppm O_2 present (7).

[b] 50 ppm O_2 present.

Eichelberger's estimate[9] of 10 ppm for the oxygen solubility at 200°C, and Addison *et al.*'s measured surface tension depression of 8.5 ergs/cm² from 0 to 10 ppm oxygen to estimate the concentration of oxygen at the interface using Gibbs adsorption equation to be ≈10% for a 200°C saturated solution. Although this is obviously more than enough oxygen to catalyze dissolution of iron, the calculation could be grossly inaccurate, since Addison *et al.* added their oxygen through the cover gas—so that Na_2O is likely to be concentrated at the surface, rather than through the sodium. More accurate measurements at higher temperatures are obviously needed.

There is an obvious correlation between the difficulty in obtaining equilibrium (and reproducible data) in these experiments and the apparently (anomalously) low corrosion and/or precipitation rates of iron or nickel from steels into sodium. The behavior of the copper data suggest a clue to interpreting these low corrosion rates: when the copper-saturated sodium in the copper crucible was cooled to equilibration temperatures above 450°C, the dissolved copper appeared

to precipitate on the crucible in a "normal" manner, and data obtained by both heating and cooling the sodium to the equilibration temperature gave reasonably reproducible results. Also, our results agree reasonably well with those of Humphreys[1] and of Eichelberger and McKisson[2] above 450°C.

Below 400°C, however, the copper did not precipitate on the copper crucible and appeared to remain in suspension in a "particulate" form. Further, these fine particles did not appear to grow to larger crystals or adhere to the copper crucible despite the surface energy forces that "normally" promote growth of larger crystallites at the expense of smaller ones. We suggest that some other property of the liquid is stabilizing these crystallite-sodium interfaces. This could be one of two things:

(1) Adsorption on the crystallite surface of some impurity in the sodium, such as the oxygen adsorption on interfaces noted above, which prevents crystallite growth and grossly retards solid-solvent equilibration; this appears unlikely to occur in the case of copper because of the low stability of the copper oxides compared with the iron or nickel oxides, but may possibly be a contributing factor in iron, chromium, or nickel solutions;

(2) The solution may be so dilute at equilibrium that the probability of solute-solute interaction in the sodium solution approaches zero, and therefore the probability that a dissolved atom will precipitate also becomes very small. Since mass transfer of copper does occur through sodium, this probability can never be zero.

Neither of these two suggestions can be conclusively proved at the present time, but circumstantial evidence exists that either or both of them may be applicable. Repulsive forces exist between sodium and all three of the metals studied (iron, copper, and nickel), as demonstrated by their low solubilities and their large positive activity coefficients in sodium, deduced from the low solubilities, and the total absence of any intermetallic compounds between sodium and these solutes. Any impurity in the sodium such as oxygen or chlorine that has an affinity for the metallic solutes could stabilize the solid-sodium interface and inhibit precipitation of the solute when the solution is sufficiently dilute. Oxygen is known to catalyze corrosion and mass transfer of iron and chromium by sodium, but is not known to affect the corrosion of nickel and presumably of copper. If oxygen adsorption is the stabilizing mechanism, one would expect corrosion rates to increase in well-gettered systems; this has never been observed to our knowledge. An alternate "stabilizer" could be chlorine; there are a few ppm chlorine in nearly all commercial sodium. Little is known about the effects of chlorine in sodium on corrosion or mass transfer.

The theory of very dilute solutions of liquid metals is not well understood. From the available information, however, it seems unlikely that the disturbance caused by a solute metal atom to the structure of the liquid metal or to its electron cloud will extend to more than five atomic diameters of the solvent.[10] In the measurements of copper solubility, the change from short to long equilibration times on cooling the melt occurs at a temperature at which the copper solubility is $\approx$10 ppm, or $\approx$3 apm.*

In a 3-apm solution, the mean distance between solute atoms is $\approx$80 solvent atom diameters, or 8 times the likely maximum distance for solute-solute interactions. Further, all the nickel data and the low-oxygen iron data are below the 3-apm level. Although the liquid metal atoms are continuously in motion, the probability of solute-solute interactions may become quite small. Although in theory calculations of this probability could be made, they are in practice nearly impossible with the available computer programs for atomic motions in liquids.

If we accept a low probability of solute-solute interactions, we have a possible explanation for the long equilibration times in solubility measurements, and, more importantly, we have a possible interpretation for the low corrosion and mass-transfer rates of steels in sodium. When classic velocity-dependent mass-transfer theory was applied by Mottley[11] to corrosion of steels by sodium, using the GE data obtained to that time, he concluded that the solubility-differential term in the equation was a few ppb, or $\approx$100 to 1000 times smaller than one would estimate it to be if solute precipitation was as efficient from sodium as it has been found to be from bismuth.[12] Although mass transfer of iron in sodium appears to be oxygen-dependent, nickel transfer does not, and nickel-base alloys also corrode in a velocity-dependent but abnormally low rate.

Classic velocity-dependent mass-transfer theory depends on diffusion of solutes through boundary layers at both the hot and cold interfaces. The rate of diffusion of a solute down a concentration gradient (Fick's first law) depends on interaction between solute atoms. The important conclusion, then, is that classic diffusion equations (and therefore classic velocity-dependent mass-transfer equations) may not apply to solutions as dilute as those of iron and nickel in sodium at LMFBR temperatures. In the measurements of copper solubility we saw a change in behavior from reasonably fast equilibrations to remarkably long ones at 400 to 500°C.

* apm = atoms solute per million atoms of solution.

It would be most interesting to see how the corrosion rate of copper varies in small ΔT systems from $\approx$300 to $\approx$600°C.

Acknowledgments

The authors wish to express their appreciation to W. W. Becker and J. H. Sauls for their invaluable assistance in performing the experiments. Dr. L. Newman and his staff are due many thanks for their efficient handling of the varied analyses. Dr. R. W. Stoenner of the Chemistry Department is acknowledged for his spectrometric determinations of iron. The program of the Liquid Metal Corrosion Center is under the general supervision of Dr. D. H. Gurinsky.

Appendix

Analytical Techniques

(R. F. Doering)

The following general techniques were utilized for analysis of the solutes. Samples for copper, nickel, and iron are dissolved in butyl chloride. The cups containing the samples are leached with 6 *N* HCl for one hour at 100°C.

Copper is extracted with a $CHCl_3$-isopropyl alcohol mixture as the neocuproine complex. The organic phase is aspirated directly into a Perkin-Elmer Model 303 Atomic Absorption Spectrometer.

Nickel is determined as the dimethylglyoxime complex with a Beckman DU Spectrophotometer.

Cold iron is extracted into isoamyl alcohol as the bathophenanthroline and read on a Beckman DU Spectrophotometer. ^{59}Fe is dissolved in ethyl alcohol, and the cups are leached with 6 *N* HCl for 1 hour at 100°C. Ten mg iron carrier is added and $Fe(OH)_3$ is precipitated twice. ^{59}Fe is counted on a Technical Measurements Corp. 400-channel analyzer using the 1.1- and 1.3-keV photopeaks.

Oxygen is determined by amalgamation with 30 cc mercury, which is agitated for 20 min. The amalgam is allowed to settle, and the Na_2O is separated from the bulk amalgam in a separatory funnel. This procedure is repeated 10 times. The Na_2O is dissolved in H_2O and aspirated into an atomic-absorption spectrometer.

REFERENCES

1. Humphreys, J. R., Jr., Interdivisional Document K-3-774, Los Alamos Scientific Laboratory.
2. Eichelberger, R. L., and McKisson, R. L., *Solubility of Copper in Sodium*, AI-AEC-12671 (May 1968).
3. Kovacina, T. A., and Miller, R. R., *The Solubility of Nickel in Sodium by a Tracer Technique*, Nucl. Sci. Eng. **10**, 163–166 (1961).
4. Rodgers, S. J., Mausteller, J. W., and Batutis, E. F., *Iron and Nickel Concentrations in Sodium*, Technical Report 27, Mine Safety Appliances Co. Also NP-5241 (June 1954).
5. Epstein, L. F., Science **112**, 426 (1950). Also, KAPL-362 and *Liquid Metals Handbook, Sodium (NaK) Supplement*, TID 5277 (1955).
6. Bogard, A. D., *The Solubility of Iron in Sodium Metal, Sodium-Sodium Oxide and Sodium-Sodium Hydroxide*, NRL Report #4131 (March 1953).
7. Thorley, A. W., and Tyzack, C., "Corrosion Behavior of Steels and Nickel Alloys in High Temperature Sodium," *Alkali Metal Coolants*, IAEA, Vienna (1967) p. 97.
8. Addison, C. C., Addison, W. E., and Kerridge, D. H., *Liquid Metals, Part III. The Influence of Oxide Films on the Surface Tension of Liquid Sodium*, J. Chem. Soc. 3047 (1955).
9. Eichelberger, R. L., *The Solubility of Oxygen in Liquid Sodium—Recommended Expression*, AI-AEC-12685 (1968) (in preparation).
10. Dickey, J. M., (BNL) private communication (1968).
11. Mottley, J. D., *Sodium Mass Transfer: VIII. Corrosion of Stainless Steel in Isothermal Regions of a Flowing Sodium System*, GEAP-4313 (1964).
12. Weeks, J. R., and Gurinsky, D. H., "Solid Metal-Liquid Metal Reactions in Bismuth and Sodium," in *Liquid Metals and Solidification*, Ed. B. Chalmers, Am. Soc. Metals, Cleveland (1958) p. 106.

Discussion

Mr. Hickam (W): In regard to the contamination of the surface of the copper, I found that ordinary machine practices resulted in as much as one foreign atom per copper atom to depths of the order of 100 Å in the copper. These could not be reliably removed by cleaning and by electrochemical polishing. We effectively had to go to about 800°C to remove 50% of the foreign atoms. By going to the melting point, we found that we could then recover them as hydrogen and CO. It would appear from these measurements that there could be appreciable contamination if conventional machining practices were used unless approximately 100 Å were removed in some way without introduction of contamination.

Mr. Weeks: The copper crucible that we used was fabricated by electron-beam welding zone-refined copper sheet obtained from MRC. We then pickled the internal surface with ammonium persulfate solution until we got a visible crystalline structure. Then we hydrogen fired the crucible inside the apparatus and degassed at 600°C. This may not have removed the CO or all of the hydrogen, but that's what we did.

Mr. Hickam: Did you attempt to analyze the copper after this treating procedure?

Mr. Weeks: No.

Mr. Feder (ANL): My colleagues and I have been in the business of measuring solubility in liquid metals for about fourteen years. I can state with great confidence that there is nothing unusual with sodium in

this respect. The same phenomena that you see have been observed by us and others in mercury, zinc, cadmium, and a variety of liquid metals. When solubilities in liquid metals become very small there is indeed a difficulty which is not associated necessarily with analytical problems. It is associated with either the (possible) slow rate of precipitation or the minuteness of the nuclei and their lack of growth. In view of this fact, that we expect the nuclei to be extremely small and not to mature at any appreciable rate, it seems somewhat unreasonable to me to use the sophisticated techniques that have been applied for analyses, the sophisticated techniques of purification of the sodium, the use of monocrystals for the solid phase, and then to take a dip sample or a bucket sample which will not remove the suspended particles. I can't see the degree of sophistication in one area and the absolute lack in the other. Our own preference is always to filter.

Mr. Weeks: Mine is too, but I wasn't sure how to filter them satisfactorily in sodium at these temperatures. That's why I didn't do it. First, I'd like to point out some work done at the GE Research Laboratory by Laborski, in which he electrodeposited iron into mercury at essentially room temperature. He obtained fine particles that were stable for long periods of time and did not grow. The solubilities were down in the same range that we're talking about here. In our work with bismuth and mercury at higher temperatures, the solubilities were in the same range in parts per million, but in atoms per million they were higher by at least a factor of ten. Second, when GE runs a loop at 1200°F maximum temperature, they find 2 to 5 ppm iron in the sodium. The iron in the loop is very close to what we estimate saturation to be. We at Brookhaven run our sodium in Type 321 stainless steel loops at a maximum of 760°C. The solubility of iron at 760°C is a little over 30 ppm, and we did find 30 to 40 ppm iron in our loop. I think this is confirmation of two things. One, the precipitation rate must be the rate-controlling process in corrosion by sodium; two, the solubility data do reasonably well represent what we find in loops.

Mr. Vissers (ANL): You referred to the work of Laborski at GE, where he electrolyzed iron into mercury. Even though he reported that these particles were of the order of 100 Å, they can be easily filtered out with a 35-micron frit. As a matter of fact, if you take a system of iron and mercury that contains 0.1% iron and carry out a filtration, you'll find that you have less than a ppm in the mercury. This would indicate that the iron is not in solution and that it can be filtered out.

Mr. Weeks: I agree. I think in principle we could. At the temperature at which we are making our measurements, iron and sodium, or nickel and sodium, are known to react with almost any other clean metal surface with which they come in contact. Therefore, the question would be, if we filtered them would we actually lose dissolved as well as undissolved material. This is why we didn't do it. In principle, I think we should, but I didn't know how to do it.

The Solubility of Cu, Mo, Nb, Fe, Ni, and Cr in High-purity Sodium*

R. L. Eichelberger and R. L. McKisson

Atomics International
A Division of North American Rockwell Corporation
Canoga Park, California

(PRESENTED BY R. L. EICHELBERGER)

With the currently increasing potential use of sodium as the heat-transfer fluid for fast-breeder reactors, the importance of understanding its interactions with its environment is strongly emphasized. Of particular interest is the effect of liquid sodium on materials of construction for reactor heat-transfer systems, for example, the solubility of these materials in the sodium. It is generally acknowledged that the apparent solubility of many metals in sodium is strongly influenced by the presence of impurities, both in the liquid metal and in the solid solute. This effect has not been quantitatively described, however, nor is there very good agreement on the solubility of most metals in relatively oxygen-free sodium. The work described here was planned to study this latter area—the solubility in pure sodium—within reasonable limitations of time and expense.

1. Equipment and Materials

To preserve the original purity of the solute and solvent metals used in this work, a complex of ion-pumped and turbo-molecular-pumped vacuum systems was designed and built, as has been described by Eichelberger and McKisson.[1] This system provides for loading and sealing of capsule experiments in a vacuum of about 5×10^{-8} Torr. The sodium used was purified by gettering and fractional distillation, as described by McKisson, Eichelberger, and Ott,[2] and is exposed only to ion-pumped high vacuum after purification. Total detectable impurities in the sodium are less than 40 wppm, with carbon at 8 wppm and oxygen at about 2 wppm constituting the major impurities.

The copper used for solute was oxygen-free high-conductivity (OFHC) material that had been heated in hydrogen for one hour at 600° C to reduce any oxide. Other solute metals were ultra-pure materials produced by Materials Research Corporation. The Mo, Ni, Nb, and Fe were electron-beam floating-zone refined material, and the chromium was prepared by the decomposition of prepurified chromium iodide.

The solute metals were prepared for solubility experiments by either machining 0.5-in.-diameter rods into 2½- to 3-in.-long crucibles, or by threading the end of ¼-in.-diameter rods so that they could be screwed into matching threads in the bottoms of crucibles made from ½-in.-diameter tubing of commercial Cb-1% Zr alloy. Mo, Ni, Nb, and Fe were formed into solute crucibles, chromium was used as solute rods, and copper was exposed to sodium as both rods and crucibles.

The copper used has a guaranteed purity of 99.95% Cu. The other solutes are substantially purer, with nominal analyses provided by the manufacturer as shown in Table 1.

2. Experimental Methods

The experimental method is described in detail in Ref. 1. It provides for cleaning all components of a solubility experiment, final out-gassing at 10^{-7} Torr, followed by loading at $\sim 5 \times 10^{-8}$ Torr without removing any parts from the vacuum system, heating for the desired time at temperature, inverting the assembly to cause the sodium to drain away from the solute metal into the sample collector, cooling, opening, and, finally, analyzing the sodium for the solute concentration.

The time of heating for all experiments was 6 hr, as it had been determined previously[3] that equilibrium was obtained in 2 hr or less. Chemical analyses were made using methods described by Bingham, Scarborough, and Maseda.[4]

3. Results

3.1. Copper

The results for copper solubility have previously been reported in detail.[1] Figure 1 includes our results as well as the data of Singer, Becker, and Weeks[5] and of Humphreys.[6] The data from the three laboratories is best represented by the equation

$$\log_{10} S(\text{wppm Cu in Na}) = 5.957 - \frac{3430}{T(°\text{K})}. \quad (1)$$

Worth noting is the fact that the Los Alamos work[6] was done with irradiated copper foil, using

* Based on work supported by the U. S. Atomic Energy Commission under Contract AT(04-3)-701.

TABLE 1. Composition of Solute Metals

Nominal purity, %: ...	Chromium 99.996	Iron 99.996	Molybdenum 99.992	Nickel 99.997	Niobium 99.983
C	10	8	10	17	8
H	0.5	<0.1	0.9	0.2	0.4
O	5	7.2	4.3	18	4
N	2	7.0	0.5	3	23.4
Ag	—	<0.04	<0.7	<0.02	<0.3
Al	1	—	<0.025	0.3	0.15
Bi	—	<0.008	<0.015	<0.01	<0.007
Ca	3	2	0.04	0.1	0.02
Cd	—	<0.08	1.0	<0.08	<0.05
Co	—	0.3	<0.06	<0.1	<0.007
Cr	—	0.6	0.1	1.5	0.05
Cu	0.5	<0.02	<0.02	<0.04	<0.01
Fe	6	—	12	12	0.12
Hf	—	<0.025	<0.03	<0.03	<0.02
K	—	0.2	1.0	0.2	<0.04
Mg	1	8	<0.25	0.02	0.05
Mn	—	0.1	0.06	0.03	0.03
Mo	—	0.2	—	0.5	<0.7
Na	—	0.08	—	0.04	<0.03
Nb	—	0.03	1.0	<0.02	—
Ni	1	1.2	0.1	—	0.15
Pb	—	<0.015	<0.03	<0.02	<0.02
Pd	—	<0.08	<1.0	<0.03	<0.5
Pt	—	<0.025	0.06	<0.03	0.02
Rh	—	<0.03	<0.1	<0.01	<0.06
S	<10	1.2	1.0	<0.12	0.07
Si	—	0.5	0.08	0.2	0.6
Sn	—	<0.02	<0.4	<4.0	<0.3
Ta	—	<1	2.0	<0.5	100
Ti	—	0.5	—	0.15	<0.02
V	—	<0.1	0.02	<0.01	<0.8
W	—	<0.1	50	1.5	6.4
Zn	—	<0.8	0.02	<0.4	<0.015
Zr	—	<0.06	<0.04	<0.15	<0.3

a counting technique for analysis, whereas the other two laboratories used conventional analytical methods. In addition, the Los Alamos work was done about ten years prior to the work at BNL and AI, and the implication might be made that there was less concern at that time with the oxygen level of the solvent sodium. Neither of these factors has affected the rather good agreement among the laboratories.

Oxygen would not be expected to be involved in the solution of copper in sodium, since the stability of the copper oxides is much less than that of sodium oxide, and no evidence has been reported of copper-sodium double oxides.

The ΔH(soln) calculated from Eq. 1 is 15.7 kcal/gram-atom of copper.

3.2. Molybdenum

Data obtained from molybdenum solubility experiments are shown in Table 2 and plotted in Fig. 2. The line shown does not consider the lowest temperature point and is represented by

$$\log_{10} S(\text{wppm Mo in Na}) = 3.142 - \frac{3807}{T(°\text{K})}. \quad (2)$$

The ΔH (soln) calculated from Eq. 2 is 17.4 kcal/gram-atom of molybdenum.

3.3. Nickel

Data obtained from nickel solubility experiments are shown in Table 2 and plotted in Fig. 3. The figure also shows a line for nickel solubility reported in 1954 by Rogers, Mausteller, and Batutis.[7] The line shown for the data obtained at AI with the highly purified materials described here is expressed by

$$\log_{10} S(\text{wppm Ni in Na}) = 1.47 - \frac{918}{T(°\text{K})}. \quad (3)$$

The corresponding ΔH(soln) is 4.2 kcal/gram-atom of nickel.

3.4. Niobium

Data obtained from niobium solubility experiments are shown in Table 2 and plotted in Fig. 4, along with the data of Kovacina and Miller.[8] Although neither set of data shows very good internal agreement, all the data may be expressed by a tentative curve

$$\log_{10} S(\text{wppm Nb in Na}) = 4.16 - \frac{3530}{T(°\text{K})}. \quad (4)$$

Activation analysis was used to determine the niobium concentration in the NRL work,[8] and their solute was an alloy containing 1% zirconium. The sodium used in both sets of experiments contained less than 10 ppm of oxygen. The solubility values seem to be higher than would be expected for a simple solution process, but there is not enough oxygen available to explain the measured values in terms of double oxide formation. The ΔH(soln) value calculated from Eq. 4 is 16.1 kcal/gram-atom of niobium.

3.5. Chromium

Four chromium experiments were performed in the temperature range from 700 to 1000°C, giving results of 2 to 3 wppm. The same chromium rods were irradiated, and the results shown in Table 2 and Fig. 5 were obtained by counting the ^{51}Cr which was in the sample collector after the solvent sodium had been transferred to it. The sodium was subsequently dissolved from the collectors, the collectors etched, and the chromium determined by atomic absorption spectroscopy (AAS). The results are puzzling, since significantly less chromium was found by AAS analy-

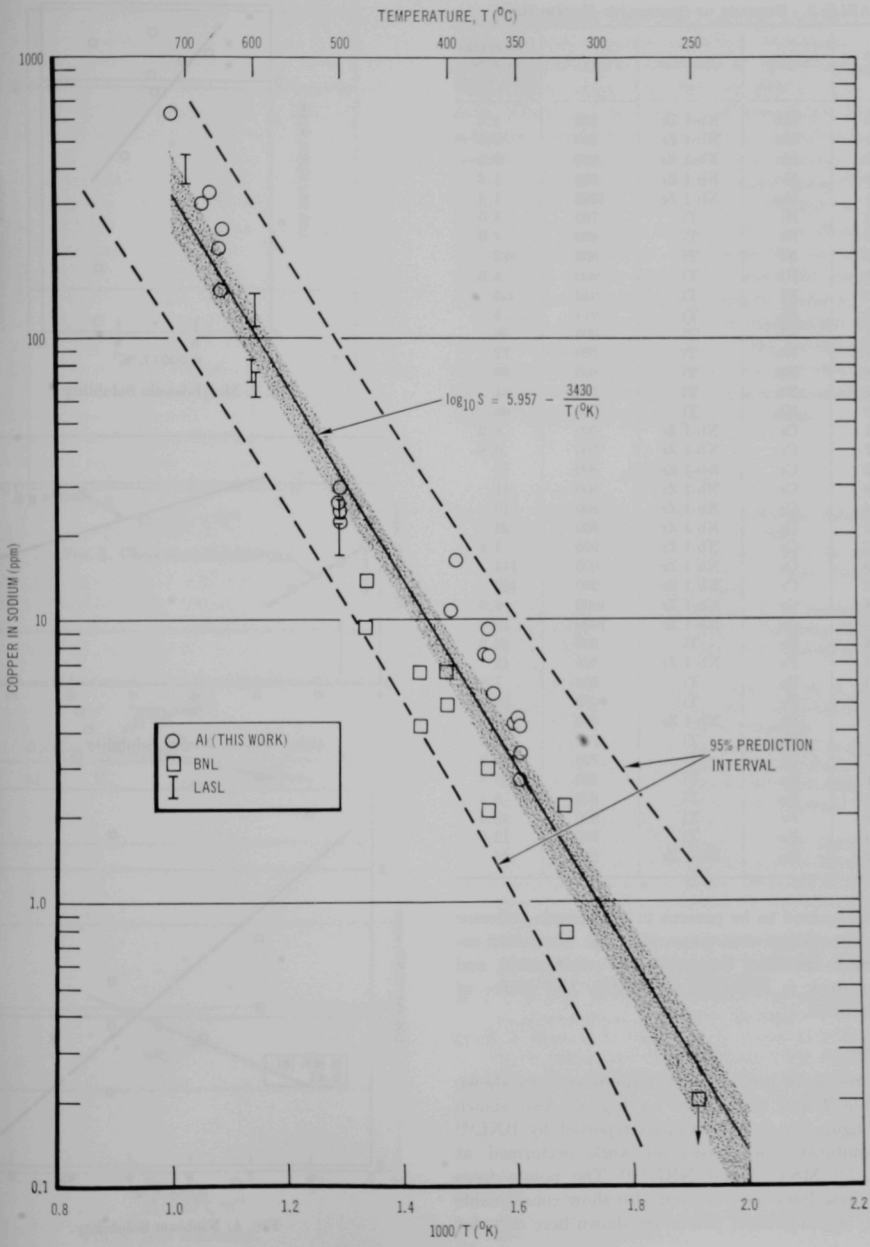

FIG. 1. Copper Solubility.

TABLE 2. RESULTS OF SOLUBILITY EXPERIMENTS

Run Number	Solute	Collector	Temp, °C	Concentration in Sodium, wppm
505	Mo	Nb-1 Zr	800	1.4
506	Mo	Nb-1 Zr	850	0.5
507	Mo	Nb-1 Zr	900	0.9
508	Mo	Nb-1 Zr	950	1.2
511	Mo	Nb-1 Zr	1005	1.3
299	Ni	Ti	700	3.0
300	Ni	Ti	800	4.0
258	Ni	Ti	800	<2
501	Ni	Ti	900	4.9
59	Ni	Ti	910	<5
60	Ni	Ti	914	<5
521	Nb	Ti	600	28
547	Nb	Ti	700	72
548	Nb	Ti	800	88
522	Nb	Ti	800	31
549	Nb	Ti	900	88
531	Cr	Nb-1 Zr	700	1.2
537	Cr	Nb-1 Zr	700	0.8
532	Cr	Nb-1 Zr	800	10
538	Cr	Nb-1 Zr	800	11
544	Cr	Nb-1 Zr	800	15
545	Cr	Nb-1 Zr	800	28
533	Cr	Nb-1 Zr	900	3.4
539	Cr	Nb-1 Zr	900	114
546	Cr	Nb-1 Zr	900	182
534	Cr	Nb-1 Zr	1000	6.9
540	Cr	Nb-1 Zr	1000	12.8
295	Fe	Ti	500	26.8
84	Fe	Nb-1 Zr	595	12
280	Fe	Ti	600	7.0
296	Fe	Ti	650	25.0
251	Fe	Nb-1 Zr	698	39
297	Fe	Ti	700	9.9
277	Fe	Ti	709	12.2
278	Fe	Ti	800	99.8
281	Fe	Ti	800	8.4
298	Fe	Ti	800	19.6
279	Fe	Ti	900	12.9
252	Fe	Nb-1 Zr	991	16

sis than seemed to be present in the sample collector before the sodium was removed. These chromium results must therefore be considered questionable, and further work is indicated to identify the source of disagreement.

3.6. Iron

The results of iron solubility experiments are shown in Table 2 and are plotted in Fig. 6. Also shown in the figure are iron solubilities reported by BNL[9] and solubility lines based on work performed at KAPL,[10] MSA,[7] and NRL.[11] The points from which these lines were derived also show considerable scatter, but individual points are shown here only for

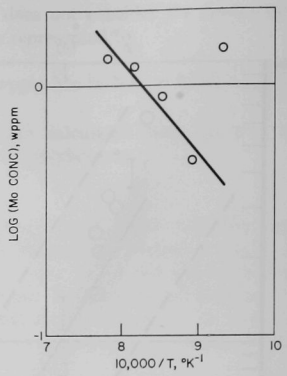

FIG. 2. Molybdenum Solubility.

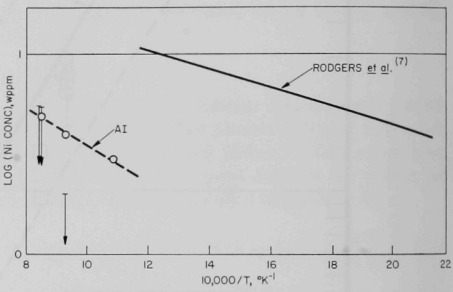

FIG. 3. Nickel Solubility.

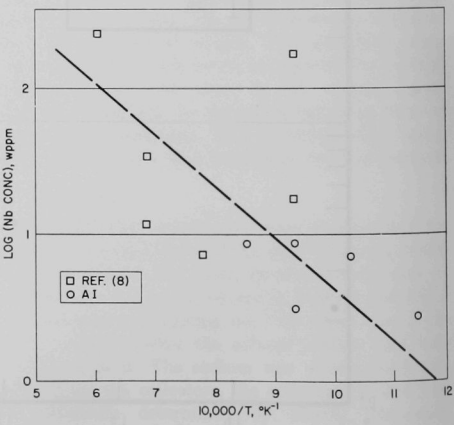

FIG. 4. Niobium Solubility.

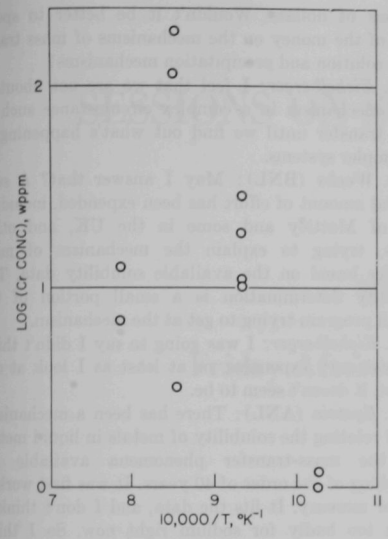

FIG. 5. Chromium Solubility.

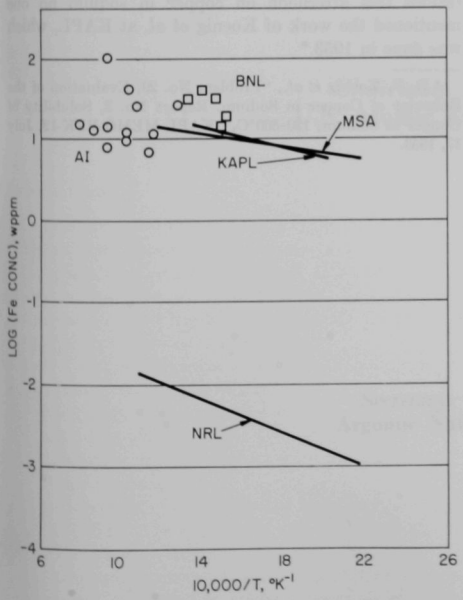

FIG. 6. Iron Solubility.

the recent results from BNL and AI. All the data obtained by wet chemical analytical techniques show a general clustering in the 5 to 40 ppm range in the temperature range, from 200 to 1000°C. The NRL data, which is 2 to 3 orders of magnitude lower in apparent solubility, resulted from radiochemical experiments. Recently, Weeks[12] has reported solubility values in the 0.3 to 1.9 ppm range, using ^{59}Fe as a tracer. This latter report also indicated a strong dependence on oxygen concentration, an effect which has been postulated to arise from the formation of sodium-iron double oxides ever since the compound Na_4FeO_3 was isolated from sodium by Horsley.[13]

There is as yet no satisfying explanation for the various observations reported in the Fe-Na system. Current work at several laboratories may well provide the key to understanding the apparent anomalies previously reported in this important system.

REFERENCES

1. R. L. Eichelberger and R. L. McKisson, *Solubility of Copper in Sodium*, AI-AEC-12671 (1968).
2. R. L. McKisson, R. L. Eichelberger, and J. B. Ott, *The Construction and Operation of a Sodium Purification Apparatus*, NAA-SR-12444 (1967).
3. R. L. McKisson, R. L. Eichelberger, R. C. Dahleen, J. M. Scarborough, and G. R. Argue, *Solubility Studies in Liquid Metals*, AI-65-210 (1965) (Also printed as NASA-CR-610).
4. C. D. Bingham, J. M. Scarborough, and M. S. Maseda, *Analytical Methods for Determining Impurities in Sodium below 10 ppm*, see paper THIS CONFERENCE.
5. R. M. Singer, W. Becker, and J. R. Weeks, in *Quarterly Progress Report of Work Sponsored by the Fuels and Materials Branch, April 1 to June 30, 1967*, BNL-50065 (1967).
6. J. R. Humphreys, Jr., Interdivisional Document K-3-774, Los Alamos Scientific Laboratory.
7. S. J. Rodgers, J. W. Mausteller, and E. F. Batutis, *Iron and Nickel Concentrations in Sodium*, MSA-TR-27 (1954).
8. T. A. Kovacina and R. R. Miller, *The Solubility of Columbium-1% Zirconium in Sodium by Activation Analysis*, NRL-6051 (1964).
9. J. R. Weeks (Compiler), *Annual Progress Report of Work Sponsored by the Fuels and Materials Branch, January 1–December 31, 1967*, BNL-50092 (1968).
10. L. F. Epstein, *Preliminary Studies on the Solubility of Iron in Liquid Sodium*, Science **112**, 426 (1950).
11. R. A. Baus, A. D. Bogard, J. A. Grand, L. B. Lockhart, R. R. Miller, and D. D. Williams, "The Solubility of Structural Materials in Sodium," Proc. First U.N. Intern. Conf. on Peaceful Uses of Atomic Energy, Geneva, **9**, 356 (1955).
12. J. R. Weeks (Compiler), *Quarterly Progress Report of Work Sponsored by the Fuels and Materials Branch, January 1–March 31, 1968*, BNL-50111 (1968).
13. G. W. Horsley, *The Corrosion of Iron by Oxygen-contaminated Sodium*, J. Iron and Steel Inst. **182**, 43 (1956); also AERE M/R 1441.

Discussion

Mr. R. A. Walker (ANL): Copper-sodium is one of the systems I have measured with Dr. Pratt at Birmingham. We measured the solubility of copper in sodium from 220 to 640°C; as you see in the figure, it

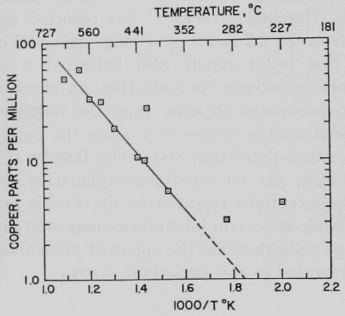

varies from about 2 to 60 ppm. The solubility data are in good agreement with those reported in the two previous papers.

Mr. Eichelberger: Apparently we had the same problem that you and the people at Brookhaven did at low temperatures. For all of us, some low-temperature points are quite high. We have thrown ours out and have done better work recently, I think.

Mr. Kolodney (UNC): Suppose you knew all these solubilities, what would you do with them? John Weeks said that you would have an analytical model for mass transfer, but it begins to look as though the business of determining solubilities goes on and on for millions of dollars. Wouldn't it be better to spend some of the money on the mechanisms of mass transfer in solution and precipitation mechanisms?

Mr. Eichelberger: I feel that we are not about to get a mechanism in a complex circumstance such as mass transfer until we find out what's happening in the simpler systems.

Mr. Weeks (BNL): May I answer that? A substantial amount of effort has been expended, including that of Mottley and some in the UK, and other places, trying to explain the mechanism of mass transfer based on the available solubility data. The solubility determination is a small portion of the overall program trying to get at the mechanism.

Mr. Eichelberger: I was going to say I didn't think this was very expensive, or at least as I look at our budget, it doesn't seem to be.

Mr. Epstein (ANL): There has been a mechanistic model relating the solubility of metals in liquid metals and the mass-transfer phenomena available for something of the order of 40 years. It was first worked out for mercury. It fits the data, and I don't think it works too badly for sodium right now. So I think there is justification for continuing to get the solubility data. I'd also like to make one other comment. I was quite surprised that with all the presentations this afternoon on copper in sodium no one mentioned the work of Koenig *et al.* at KAPL, which was done in 1953.*

* R. F. Koenig *et al.*, "Problem No. 29, Evaluation of the Behavior of Copper in Sodium. Report No. 3, Solubility of Copper in Sodium, 120–500°C," KAPL MEMO-RFK-12, July 17, 1953.

SESSIONS ON SODIUM TECHNOLOGY

SESSION ST-IVB

Friday Afternoon, November 8, 1968

Chairman: G. W. Wensch
U.S. Atomic Energy Commission

Secretary: G. A. Bennett
Argonne National Laboratory

Performance Limits of Materials for Sodium-heated Steam Generators

F. A. Comprelli, J. L. Krankota, and C. N. Spalaris

General Electric Company
Advanced Products Operation
Sunnyvale, California

(PRESENTED BY F. A. COMPRELLI)

Abstract

One of the critical technological requirements which must be met for the sodium-cooled fast reactor concept is the development of a reliable sodium-heated steam generator.

The desired operating conditions for the near-term steam generator are such as to permit the use of 2¼ Cr-1 Mo, an alloy with well-established performance (at ASME Code conditions) in steam and water environments. In addition to familiarity from use in fossil-fired plants, ferritic chromium-molybdenum steels are considered as an attractive possibility for sodium-cooled systems because they are resistant to stress corrosion, are less expensive pound-for-pound than stainless steel, have higher coefficients of thermal conductivity (20% higher), and lower coefficients of thermal expansion (28% lower).

The purposes of this paper are to: (1) discuss the corrosion performance and mechanical properties of 2¼ Cr-1 Mo steel with regard to extended service in the steam and sodium environment; (2) interpret this behavior and discuss performance limits related to the near-term needs of the steam generator.

Introduction

Selection of performance limits of materials for the sodium-heated steam generator must be made after considering the factors which may affect the performance of the unit in FCR systems. The following considerations were the foremost items that influenced the decisions made in our study:

a. the desired operating conditions of temperature, pressure, and length of use;
b. the "state of the art" for known materials with regard to fabricability and performance characteristics in systems closely resembling the steam generator;
c. construction materials for the units must conform to ASME Code criteria, or be amenable to coding under existing ASME procedures;
d. anticipated problems during performance, including repairability during maintenance periods.

Examination of the existing literature indicated that there are two broad categories of alloys that offer the highest probability of meeting the desired objectives: ferritic alloys and austenitic stainless steels, both of which meet all the conditions cited above. The choice of a ferritic material for the first sodium-heated generator was influenced primarily by anticipated problems in performance. The most serious problem in using austenitic alloys for an application which involves water and steam is that which has been classified in industry as stress-assisted localized corrosion. Its occurence has not been readily predicted in the past, and remedies to bypass it have not been available. The consequences of system failures by this mechanism are most serious, very difficult to repair, recurrent with high frequency, and often catastrophic from an economic point of view. The desire to achieve higher temperatures as it is envisioned in future systems will be dependent upon high-strength alloys such as the austenitic stainless steels. There have been many promising proposals for remedies to overcome localized corrosion in stainless steel, through design and alloy modifications. It is considered premature, however, to base our designs upon these modifications, because their effectiveness has not been evaluated by actual testing in operating systems. Improved grades of ferritics are also in contention for use in future system, specifically those which contain alloying elements to stabilize the carbon content. Stabilized grades of 2¼ Cr-1 Mo alloy are now being investigated and, in time, these will be available to the materials engineer and designer, especially when the appropriate code cases are established.

Selection of material is also predicated upon fulfilling stringent control of variables involved in fabricating the units. Some disadvantages of the alloy selected can also be overcome by choosing prudent design characteristics. Quality control of starting materials and the processes involved during fabrication and installation are part and parcel of the total problem regarding material selection and performance limits. It is with recognition of these ingredients that the selections were made, recognizing that satisfactory

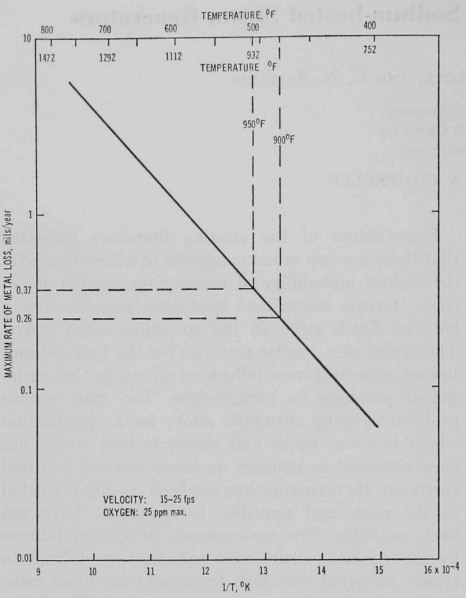

FIG. 1. Effect of Temperature on Maximum Rate of Metal Loss of Ferritic Steels in Flowing Sodium.

performance of the unit is the sum of total effort of which material selection is a part.

In this paper, basic properties of the 2¼ Cr-1 Mo alloy are discussed, which are pertinent to the design, fabrication, and operation of sodium-heated steam generator units.

Discussion

Before a material can be selected for an engineering application, many aspects of performance must be investigated to determine overall suitability. General corrosion, localized corrosion, and mechanical properties are considered in separate sections.

General Corrosion

A. *Sodium*

The sodium-heated steam generator will comprise the end of the "hot leg" and the beginning of the "cold leg" or cooling cycle of the secondary system. Existing experience indicates that corrosion (metal loss) will occur in the first part of the unit, and that deposition of material will occur in the remaining part.

Heated sodium has a corrosion potential which is characteristic of its oxygen content and the local temperature. The rate of corrosion of any structural component exposed to sodium is also dependent on coolant velocity and its relative position in the system. If the cumulative corrosion in the hot leg is not sufficient to utilize the full corrosive potential of the heated sodium, corrosion will continue into the cold leg until decreasing temperature neutralizes the remaining corrosion potential. From this point on, decreasing temperature promotes the deposition process. Empirical methods[1] for predicting the location of this area indicate that as plant operating conditions change, the location of the crossover from corrosion to deposition can shift. Therefore, it is considered reasonable to expect that the crossover zone will be in the superheater and that corrosion allowances must be made for this unit.

Experimental testing has been carried out in US[2] and UK[3] laboratories to determine the corrosion rates of alloys in flowing sodium. In these programs, the corrosion performance of ferritic and austenitic steels was determined as a function of sodium temperature, velocity, and mass flow, as well as of oxygen level, solute saturation (downstream), and system geometry.

In determining the maximum corrosion allowance for the steam generator, it is assumed, for comparative purposes, that the oxygen content of the sodium will be a maximum of 25 ppm during normal operation, sodium velocities will not exceed 15–25 fps, and the downstream, or saturation, effect does not apply. The available data, represented in Figure 1, indicate that general corrosion over a 30-yr lifetime (80% P.F.) will be 6.3 mils for the evaporator at a design temperature of 900°F and 8.9 mils for the superheater at a design temperature of 950°F. These values include peak uncertainty factors; a safety factor is not considered necessary because of the following built-in conservatism:

(1) Sodium velocities in the steam generator are expected to be ~5–8 fps. From General Electric data at 1300°F, a reduction in velocity from 15–25 fps to 5–8 fps can result in a reduction in corrosion rate of approximately 30%.

(2) Mechanistic studies at 1300°F have suggested that continual long-term operation of sodium facilities have the effect of reducing the effective oxygen content of the sodium to some low equilibrium value through reaction with the system materials. Therefore, if oxygen contamination of the system is kept to a minimum, the oxygen content of the sodium should be effectively lower than 25 ppm for a large portion of the unit lifetime. Since corrosion is known to be related to oxygen content, the ef-

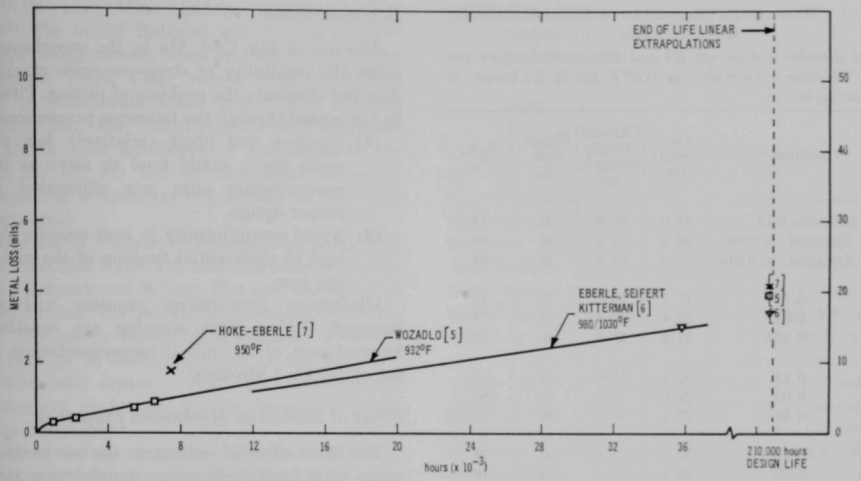

FIG. 2. Steam Corrosion of 2¼ Cr-1 Mo.

fective corrosion should be appreciably less than the allowance.

(3) No credit has been taken for the decrease in corrosion potential with increasing downstream or saturation.

B. *Steam/Water*

For 2¼ Cr-1 Mo in high-purity boiler-feedwater systems, Babcock and Wilcox[4] has established a corrosion allowance of 0.009 in. for 30 hr. This allowance consists of 0.003-in. corrosion, 0.003-in. loss during acid cleaning, and a safety factor of 1.5; this value is considered very conservative by Babcock and Wilcox. This rate appears reasonable for application at the FCR steam-generator conditions.

Ferritic steels usually display an oxide scale consisting of two layers of generally equal thickness, and no pronounced subscale penetrations. The outer layer of scale tends to have a lower density and significant porosity, which is thought to account for the observed flaking and exfoliation of scale, especially during thermal cycling, at these temperatures. The oxygen content of superheated steam can play a significant role in determining the corrosion behavior of these materials by influencing the adherence of the oxide scale (resistance to spalling) through control of the composition (therefore, of density) of each layer of scale.

The results of three corrosion studies (see Fig. 2) at the temperatures of interest, one in oxygenated steam (20 ppm O_2, 2.5 ppm H_2;[5] and two in high-purity steam (<10 ppm O_2),[6, 7] were analyzed to establish a steam-corrosion allowance. The study in oxygenated steam was used as a basis for extrapolation because descaled weight loss, instead of scale thickness, measurements were made. The metal loss rates, based on descaled weight changes, were not affected by scale spalling; rates determined by measurements of residual scale thickness are directly influenced by spalling history. Because of the sensitivity of metal loss rate to steam chemistry and spalling frequency, a linear, rather than logarithmic, extrapolation is considered more realistic and conservative over the design lifetimes of the steam-generator unit. It has recently been experimentally confirmed[8] that the corrosion behavior of 2¼ Cr-1 Mo does become linear after a relatively short period (<1 yr) and that long-term extrapolation over periods approaching design lifetimes can be based on the linear rate. The curve of descaled weight loss was determined through the initial transient region into the steady-state linear region, from which an extrapolation to the design life could be made.

Based on these studies, a design allowance for steam corrosion of 20 mils is envisioned for a 30-yr (80% load factor) superheater life at 950°F. This allowance does not include accelerated corrosion during and immediately following periodic acid cleaning. However, the frequency of cleaning is expected to be so low that the incremental metal loss accumulated during the cleaning and subsequent transient-rate periods can be accommodated within the corrosion allowance.

TABLE 1. Mechanical Properties of Decarburized 2¼ Cr-1 Mo Steel

Material decarburized in wet H_2 and heat treated before test
Heat Treatment: Normalize at 1742°F for ½ hr; temper at 1292°F for ½ hr.

Test Temp, °F	Condition, % C	Yield Strength, kpi	Ultimate Tensile Strength, kpi	Elongation, %	R.A., %
R.T.	As rec'd: 0.12	52.0	80.0	31	72
	Decarbd. to 0.03	34.2	51.4	43	80
	Decarbd. to 0.015	37.6	53.3	46	84
572	0.12	47.2	72.2	26	49
	0.03	23.4	49.6	35	78
	0.015	31.2	57.6	30	70
752	0.12	52.8	75.6	24	52
	0.03	22.8	54.6	33	80
	0.015	22.4	56.0	30	72
842	0.12	52.0	75.4	24	45
	0.03	22.4	52.4	33	78
	0.015	27.2	57.2	27	76
1000	0.12	46.4	61.6	26	65
	0.03	22.8	46.0	33	80
	0.015	20.8	45.8	33	80

Localized Attack

Localized attack can be defined as a nonuniform loss of effective wall thickness as a result of selective corrosion. The General Electric program is the only investigation to report the occurrence of this phenomenon in sodium-cooled systems.[9]

The metallurgical examination of the ferritic material in the bimetallic and all-ferritic loops showed intergranular attack. The depth of attack appeared to be temperature-dependent, the greatest depths of attack (2–3 mils) occurring in the highest temperature portions (1200°F) of the loops after 20,000–28,000 hr of exposure. In the lower-temperature regions (900–1000°F) no significant changes were observed in the 2¼ Cr-1 Mo pipe after equivalent exposure, except for a minor general surface attack and pitting to a depth of about 0.0005 in. Intergranular attack, if present, did not exceed this amount. The intergranular attack has not been found under normal operating conditions (10 ppm oxygen). Our present interpretation is that intermittent high oxygen levels (30 to 50 ppm) and localized stresses (≥½ yield stress) are necessary to produce such attack.

On the basis of these observations, an allowance of 5 mils for intergranular attack may be considered for a 30-yr lifetime (80% L.F.) at 900–950°F for 2¼ Cr-1 Mo.

B. *Steam/Water*

The use of 2¼ Cr-1 Mo in the superheater minimizes the possibility of stress-corrosion cracking, but does not eliminate the problem of pitting. Pitting may be minimized through the following precautions:

(1) Crevices and blind (relatively low velocity) spots which would tend to serve as impurity concentration sites are eliminated through proper design.
(2) Avoid nonuniformity in heat transfer that may lead to preferential flashing of the moisture in one area.

Minimizing atmospheric exposure and assuring thorough drying after cleaning are considered an integral part of the initial recommendations for the use of 2¼ Cr-1 Mo alloy.

Effect of Sodium on Mechanical Properties

The main effect of sodium on the mechanical properties of a ferritic chromium-molybdenum steel in a bimetallic system is decarburization with resultant loss of strength.

Decarburization of the ferritic steel in a bimetallic system has been observed in previous General Electric studies.[9, 10] Carbon loss from 2¼ Cr-1 Mo samples exposed in the cold leg of a bimetallic loop has been measured for times to 20,000 hr. The samples exposed to 1100°F sodium showed almost complete decarburization (from 0.105 to 0.025% carbon) in ~2800 hr of exposure. Lower rates of carbon loss were measured after 20,000 hr at 1000°F (from 0.105 to 0.05% carbon) and at 700°F (from 0.105 to 0.09% carbon).

The carbon loss was not confined to a shallow surface layer. Decarburization (to 0.025% carbon) had progressed completely through the wall (0.110 in.) of 2¼ Cr-1 Mo loop piping after ~21,000 hr at 1200°F.[10] It is interesting to note that the loop piping at 1200°F decarburized to the same lower limit of 0.025% carbon as the samples exposed at 1100°F.

UK experimenters[11] have observed changes in mechanical properties of 2¼ Cr-1 Mo with decreasing carbon contents (SPP Table 1). A significant reduction in tensile properties was associated with the lower carbon levels from room temperature to 1000°F. A limited amount of short-term rupture data for the 0.015% carbon material suggested a drop in rupture strength of 20% in 550-hr tests and over 3.1 reduction in rupture time at 1000°F at a stress of 27,000 lb/in.^{2}, i.e., 500 hr compared with 1700 hr.

The only US work oriented toward establishing design criteria for 2¼ Cr-1 Mo in high-temperature sodium has been conducted by Babcock and

Wilcox[12, 13] and Mine Safety Appliances Research.[14] The initial Babcock and Wilcox work[12] established design stresses based on 1962 ASME Boiler and Pressure Vessel Code values which had been adjusted to incorporate some unpublished Babcock and Wilcox data. The design stresses were developed within ASME code guidelines to accommodate the extended life (30 yr) and environmental considerations, including decarburization, known at that time for the material.

Construction of a model steam generator using both 2¼ Cr-1 Mo and Type 316 stainless steel was completed by Babcock and Wilcox. The unit was operated for 8,000 hr and the materials subsequently examined.[13] The results showed that exposure at 600 to 1000°F resulted in decarburization of the 2¼ Cr-1 Mo to detectable depths of 0.025 in. Unfortunately, the mechanical evaluation of this decarburized material was inconclusive.

The Mine Safety Appliance Research (MSAR) investigation[14] reported data developed from specimens which had been pre-exposed to sodium of various purities at 1100°F for 4,000 hr before the mechanical evaluation was initiated. Based upon the GE studies,[10] this exposure period should have been sufficient to induce a significant amount of, if not total, decarburization, with simultaneous degradation of mechanical properties.

The MSAR data provide a rough approximation of the long-term effect of decarburization upon high-temperature mechanical properties. The principal effect of sodium exposure was to reduce the stress required at 1100°F to produce a strain rate of 0.01%/1000 hr from 4000 psi, the ASME Code value, to 2500 psi.

Extrapolation of the most pessimistic MSAR rupture curve of 210,000 hr (30-yr lifetime at 80% L.F.) yielded a creep-rupture strength of 3300 psi at 1100°F. This value is still greater than the stress to produce a strain rate of 0.01%/1000 hr (2500 psi) and, therefore, the latter stress is the controlling parameter at temperatures greater than 800°F.

There is no doubt that extrapolation of this limited amount of data is subject to considerable uncertainty. However, these are the only data available and they appear reasonable as a first approximation.

The selection of an allowable stress for the 2¼ Cr-1 Mo will be based on the criteria defined in the ASME Code. The decarburized 2¼ Cr-1 Mo will be treated as a distinct alloy with characteristic properties. To set the allowable stresses at temperature below the creep range, the following asumptions are made:

(1) The creep range will start at 800°F as with normal 2¼ Cr-1 Mo.

(2) The ultimate tensile strength (UTS) at room temperature for this material is 52,000 psi, based on the English data[11] in Table 1. Therefore, the allowable stress at 800°F, and below, is 13,000 psi (25% of 52,000; ASME Code factor one).

Interpolation between the UTS criterion at 800°F and the strain-rate criterion at 1100°F is required to establish the value at the design temperatures. This interpolation is made more difficult by an incomplete definition of strain-rate criterion in the ASME Code. The criterion states that the allowable stress cannot exceed that required to produce a strain rate of 0.01%/1000 hr. For material which does not decrease in strength as a function of time, this criterion can be conservatively interpreted as the average strain rate over the useful lifetime of the material. However, the design of steam-generator tubing for a 30-yr life in sodium service must reflect: (1) increases in operating stress due to a decrease in wall thickness from corrosion and an increase in diameter due to creep, and (2) decreases in material strength due to decarburization and overtempering effects at temperature. Therefore, the criterion can be interpreted not only as the average strain rate over the lifetime of the unit, but also as the instantaneous strain rate at the beginning of operation, end-of-life, or at any intermediate time. These interpretations and their relative behavior as a function of time are schematically illustrated in Fig. 3.

For a conservative design within the confines of the ASME Code, it seems advisable that the Code strain-rate requirement (0.01%/1000 hr) be applied at the end-of-life as an instantaneous strain-rate condition. Since end-of-life conditions include effective decarburization, directly applicable information is not available. A first-level approximation can be made by assuming that the MSAR data for decarburized material can be interpolated to lower temperatures and extrapolated to extended-life conditions (an average strain rate of 0.01%/1000 hr over a test period of less than 10,000 hr at 1100°F in the MSAR study versus an instantaneous strain rate of 0.01%/1000 hr after 210,000 hr of service at 900°F or 950°F for the steam-generator unit).

The latest (1965) ASME Code allowable stresses for 2¼ Cr-1 Mo are shown in Table 2 as a function of temperature. These values represent the allowable stress levels when designing to an average strain rate of 0.01%/1000 hr. Modification ※1 in Table 2 represents potential allowable stress values for decarburized 2¼ Cr-1 Mo, determined by algebraic interpolation based on the 1965 ASME Code values, which the end points defined by the UK data at 800°F and the

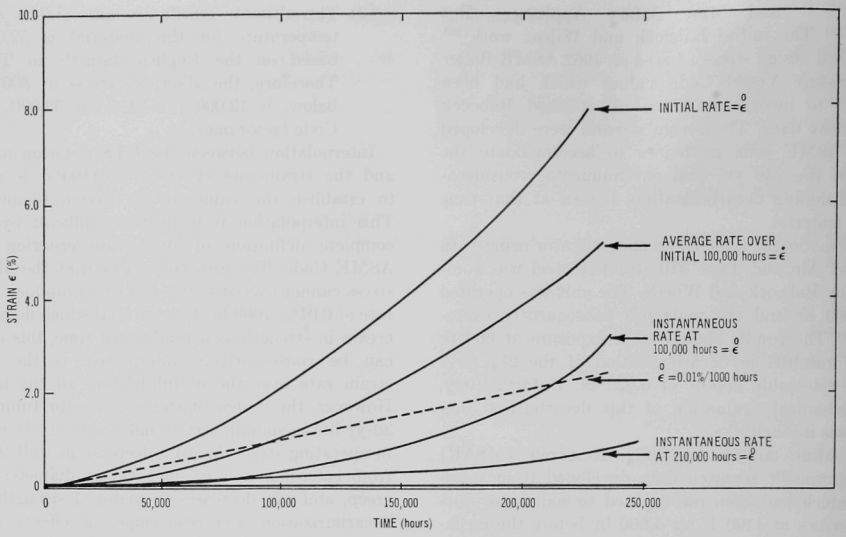

FIG. 3. Schematic Illustration of Strain-rate Criteria Permissible under ASME Code.

TABLE 2. DESIGN STRESSES FOR 2¼ Cr-1 Mo

Temp, °F	1965 ASME Code, psi	Modification №1,[a] psi	% of Code	Modification №2,[b] psi	% of Code
800	15,000	13,000	86.7	13,000	86.7
850	14,400	12,416	86.2	11,994	83.4
900	13,100	11,152	85.2	10,113	77.2
950	11,000	9,111	82.9	6,875	62.5
1000	7,800	6,001	77.0	4,863	62.4
1050	5,800	4,056	70.2	3,506	60.4
1100	4,200	2,500	59.5	2,500	59.5

[a] Interpolation between 800°F and 1100°F data based on 1965 ASME Code values.

[b] Interpolation based on Babcock and Wilcox extended-life criteria.[12]

MSAR data at 1100°F. Based on these data, which represent a design basis of an average strain rate of 0.01%/1000 hr, a uniform reduction of 70% of the ASME Code value appears to be a reasonable performance limit for temperatures less than 1050°F.

If the Babcock and Wilcox extended-life curve* is used as the basis for the algebraic interpolation, Modification №2 in Table 2 is developed for decarburized 2¼ Cr-1 Mo. As can be seen, the stress values, defined by this case, are substantially less than those associated with Modification №1, especially in the temperature range of interest to the steam-generator study.

Therefore, a range of stresses are defined which can be used to estimate performance limits. The selection of an initial allowable stress would then be directly dependent on the design philosophy, e.g., the strain-rate criterion. For the conservative application of the ASME Code criterion (0.01%/1000 hr) at the end-of-life (210,000 hr), an allowable stress of 6875 psi is envisioned at the design temperature of 950°F for the superheater and 10,113 psi at 900°F for the evaporator.

* Even though the Babcock and Wilcox extended-lifetime curve was based on adjusted ASME Code values, it appears to be reasonable. In addition, the strain-rate criterion for the Babcock and Wilcox curve (an average of 1% over the 210,000-hr projected lifetime) is a conservative upper limit for the design criterion selected in this study (an instantaneous strain rate of 0.01%/1000 hr at 210,000 hr).

Summary

(1) Performance limits have been estimated, on the basis of available information, for sodium and steam-water corrosion rates at the expected operating conditions for near-term steam generators. An allowance for localized corrosion was also estimated.

(2) In the evaporator and superheater, 2¼ Cr-1 Mo will decarburize to at least 25% of its original carbon content at projected operating conditions, resulting in significant reductions of creep-rupture strength.

(3) The allowable stresses for decarburized 2¼ Cr-1 Mo at temperatures of 900–950°F are based on

TABLE 3. PERFORMANCE LIMITS OF ALLOY

Component	Design Temp, °F	Corrosion Allowance		Allowable Stress, psi
		Water/Steam[a] mils	Sodium,[b] mils	
Evaporator	900	9	6.3	10,113
Superheater	950	20	8.9	6,875

[a] On steam side, allowances for periodic acid cleaning have not been specifically included, but may be accommodated within the 20 mils cited above, provided the frequency of cleaning is very low.

[b] General corrosion only during steady-state operation at 10 ppm oxygen in the sodium. Short-term operation with oxygen excursions can be accommodated in the allowance. An additional allowance of 5 mils may be added for localized-attack considerations.

interpolation between data points at 800°F and 1100°F and extrapolation to end-of-life strain-rate criteria. The stress limits are based directly on ASME Code criteria, are believed to be conservative, and reflect the degree of uncertainty associated with each extrapolation from known technology.

(4) Performance limits are listed in Table 3. The corrosion allowances are based on general corrosion characteristics only, and the allowable stresses are based on the ASME strain-rate criterion of 0.01%/1000 hr applied at the end of life. These limits are applicable for near-term requirements and must be revised as dictated by technological developments.

(5) Relatively large design margins must be allowed on the basis of present uncertainties in the data. A substantial amount of additional test work is required to establish actual usable properties within normal engineering tolerances.

REFERENCES

1. Lockhart, R. W., and Blair, R. C., *Sodium Mass Transfer: XXIII—Model for Corrosion Mockup for Sodium Cooled Reactors*, GEAP-4881 (July 1967).
2. Zebroski, E. L., Young, R. S., Comprelli, F. A., and Dutina, D., *Effects of Mass Transfer and of Changes in Properties on Austenitic Steels in Flowing Sodium*, IAEA Symposium on Alkali Metal Coolants—Corrosion Studies and System Operating Experience, Vienna, Austria (Nov 28–Dec 2, 1966).
3. Thorley, A. W., and Tyzack, C., *The Corrosion Behavior of Steels and Nickel Alloys in High-Temperature Sodium*, IAEA Symposium on Alkali Metal Coolants—Corrosion Studies and System Operating Experience, Vienna, Austria (Nov 28–Dec 2, 1966).
4. Clark, J. G., *Preliminary Design Report—Prototype Steam Generator*, BAW-1280-28 (Nov 1965).
5. Wozadlo, G. P., unpublished General Electric Data, personal communication.
6. Eberle, F., Seifert, J. W., and Kitterman, J. H., *Scaling of Ferritic Superheater Steels During 36,000 Hours Exposure in 980/1030°F Steam at 2350 psi with Particular Respect to Scale Exfoliation Tendency*, Proceedings of the American Power Conference, **26**, 501–510 (1964).
7. Hoke, J. H., and Eberle, F., *Oxidation of Superheater Materials by High Temperature Steam*, ASME Paper 57-A-175 (1958).
8. Lien, G. E., *Behavior of Superheater Alloys in High Temperature, High Pressure Steam*, ASME (1968).
9. Rowland, M. C., and Plumlee, D. E., *Sodium Mass Transfer: XXII—Metallurgical Examination of the Test Loops*, GEAP-4838 (Oct 1965).
10. Plumlee, D. E., Lockhart, R. W., Pohl, L. E., and Lauritzen, T., *Sodium Mass Transfer: XVIII, Extended Studies of Carbon Movement in Pumped Sodium Test Loops*, GEAP-4834 (June 1965).
11. Tyzack, C., and Thorley, A., *Interim Statement on Decarburization of Low Alloy Steels*, TRG Memorandum 2784 (March 1965).
12. Anstine, R. C., *The Combined Effects of a Sodium Environment and Extended Life on Type 316 Stainless Steel and Croloy 2¼ Alloy Steel Design Stresses*, BW 67-3 (Sept 1964).
13. Koch, D. W., and Kovach, P. J., *Materials Examination of a Model Sodium Heated Steam Generator*, BAW-1280-37 (June 30, 1966).
14. Andrews, R. C., and Kirschler, L. H., *Design Properties of One Heat of 2¼ Cr-1 Mo Steel and 316 Stainless Steel in High Temperature Air, Helium, and Sodium Environments*, MSAR-66-174 (Sept 14, 1966).

Discussion

Mr. Goodman (AI): In view of the design problem of having a steam generator last for some time, you have had to give a great deal of thought to the extended life mechanical properties of the material from the standpoint of accident conditions. Have you given any thought to what might be the properties of the material under extremely high loading rates and extremely short periods of time?

Mr. Comprelli: Extremely high loading rates from a stress standpoint?

Mr. Goodman: Yes, due to high pressures being generated as a result of a large-scale reaction. In other words, I am talking about high loading rate and short-term strength.

Mr. Comprelli: No, we did not.

Mr. Bishop (W): What allowances are made for the possibility of decarburization of the ferritic material and a resulting carburization of the austenitic material in the IHX?

Mr. Comprelli: In the IHX the stresses, of course, are significantly lower because the pressure of the sodium is significantly less, maybe 200 psi or something of that order. The temperature will be slightly higher. The main design problem in the IHX seems to be the loss of ductility due to carburization over an extended period of time. I believe, at least I hope, that there will be enough trade-off available to the designer with regard to loss of ductility and stress.

The stresses are going to be pretty low. We are thinking further about this.

Mr. DeVan (ORNL)*:* Have you looked at the problem of grain growth of decarburized 2¼ Cr-1 Mo at 950°F and do you think it could be a potential fatigue problem?

Mr. Comprelli: We have not done any of the experimental work to develop these correlations. They are all drawn upon from previous studies and published work, and appear to be reasonable assumptions for near-term steam-generator commitments. From the Phase-I work, in which we did get significant amounts of decarburization, I do not recall significant grain growth in the areas where decarburization occurred. With regard to fatigue, you know as well as I what happens.

Tests of a Tube-in-Tube Sodium-heated Steam Generator

E. Büscher, W. Jansing, H. Knuth, and H. Mausbeck

INTERATOM
Bensberg, Germany

(PRESENTED BY H. MAUSBECK)

1. The Test Facility

Since 1965 a 5-MW test facility of INTERATOM has been in operation. It was originally built as a part of the development program for the KNK reactor experiment.[1, 2, 3] During the first years it was operated exclusively for KNK.

An overall view of the test facility is shown in Fig. 1. Figure 2 is a simplified flow diagram, which is reduced by a scale factor of about 5 in flow rate, equivalent to one of the KNK heat-transfer systems. It consists of two sodium loops in series and the water-steam loop. The main heat-transfer components are the oil-fired sodium heater (1), the intermediate heat exchanger (2), and the once-through steam generator (5). The main sodium pumps (3 and 6) are of the free-surface centrifugal-pump type. For purification and purity control the two sodium loops contain separate cold traps (4 and 7) and plugging meters. Plugging temperatures of less than 120°C are normally reached. The purity of the argon cover gas is surveyed by a sensitive gas chromatograph. Normal impurity readings for the cover gas are: oxygen content, <5 vpm; nitrogen content, <500 vpm; hydrogen content, <30 vpm; methane content, <5 vpm.

In the water-steam system the superheated steam is depressurized to 10 atm by a control valve and condensed in a tank (10) which is connected with an air-cooled condenser (13). The piston pump (11) services as a feed-water pump. It delivers up to 10 m^3/hr of water through a high-pressure preheater (12) to the steam generator. Not shown in the figure are an air cooler on the primary sodium side and the reactor tank test mockup of the KNK reactor. The main layout data of the 5-MW test facility are compiled in Table 1.

The aim of the KNK test work can be divided into two parts:

gaining operating experience for the KNK reactor system, including the complete control system;
tests of the main components of the sodium system.

One of the most interesting components to be tested was the KNK steam generator, which is of the concentric tube-in-tube design. The two units consist of 28 tubes each with a maximum thermal output of 1 MW per tube. For the test work the design principle of this steam generator was advantageous since the reduction in power of the test unit did not change the characteristics of the steam generator markedly. Figure 3 shows the design principle of the test steam generator of the 5-MW loop. The feed water of 200 to 235°C flows up the central tubes of the steam generator. The superheated steam at 510°C and 84 atm is collected in the top-side steam header. The sodium flows downward in the surrounding annular tube. The pressure-relief system of the steam generator consists of the shutoff devices (2) at the entrances of the sodium tubes, the depressurizer with an orifice at its outlet (6), the rupture disc (4), the pressure-relief line (7), the reaction-products separation tank (8), and the quick-shut off valves (1) at both sides of the sodium headers. Table 2 shows the main data for the test steam generator.

The tube-in-tube design allowed a large number of different measurements to be made during the tests. Figure 4 shows a specially instrumented tube-in-tube unit. The hydrodynamic characteristics, in particular on the water-steam side, were investigated by pressure measurements, in part by means of nozzles at several points in the tube. By this means pressure drop in different parts of the tube system could be measured: pressure drop across the entrance orifice, pressure drop across the preheating zone, etc. The thermodynamic behavior was mainly measured by means of 26 thermocouples T at the outer wall of the sodium tube. Additional temperature measurements on the water-steam side were taken at the above-mentioned nozzles. Finally, the nozzles served for a survey of the corrosion behaviour on the water-steam side. Continuous hydrogen measurements and sample iron and oxygen measurements were taken. Additional bulk pressure, flow, and temperature readings at the sodium and water-steam sides were available.

2. Hydrodynamic Behaviour of the Steam Generator

2.1. Measurements of Pressure Loss

The pressure loss of the set of inlet orifices at each tube-in-tube unit and of the inner tube itself was measured

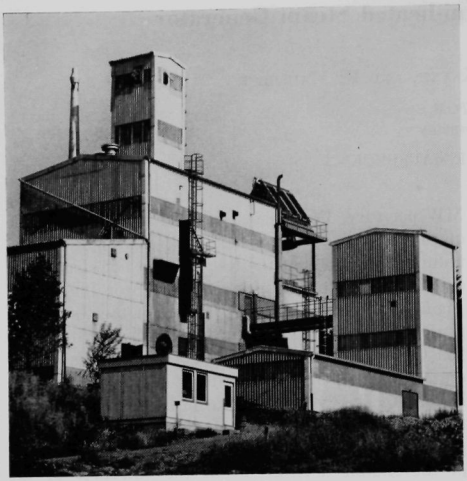

FIG. 1. Overall View of Test Facility.

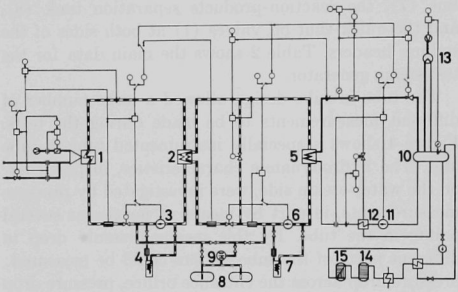

FIG. 2. Heat Transfer System of 5-MW Test Facility.

to check the design pressure of the feed-water pump;
to assure the uniform distribution of the flow rates;
to determine the surface roughness.

Pressure measurements were taken across the orifices and across the tubes by means of pressure differential cells (Barton cells). Special measuring nozzles were installed before and behind the orifices and behind each water-steam tube of the steam generator.

Three tubes were supplied with additional nozzles behind the boiling zone.

Figure 5 shows the result of the pressure-drop measurement of tubes 1–4. Tube 5 is not included since it failed after 68 hr of operation (see Sect. 5). The tube-and-orifice system has a pressure drop of approximately 25 atm at full flow (1.5 t/hr per tube); the orifices alone have a pressure drop of 18.5 atm. The differences in pressure loss of the tubes 2 to 4 are negligible even with a different number of measuring nozzles, which means also with a slight difference in the heated surface. The pressure drop of tube 1 is slightly lower than that of the other tubes. This is mainly due to a small difference in diameter and in minor part to a smaller roughness. As shown in Table 2, this tube is of a different material, namely, Inconel 600.

All readings of Fig. 5 are valid for an overall sodium-to-water ratio of 8.65. The pressure drop increases with the sodium-to-water ratio since the length of the preheating zone decreases with its smaller pressure drop. The increasing boiling and superheating zones have a higher specific volume and therefore a higher pressure loss.

Finally, it should be pointed out that the orifice

TABLE 1. PERFORMANCE DATA OF THE 5-MW TEST FACILITY

Primary and Secondary Sodium Pump	
Max operating temperature	580°C
Pump capacity	150 m³/hr
Total dynamic head	6.0 kp/cm²
Operating pressure	12.0 kp/cm²
Cycles per minute:	1500 min^{-1} for primary; 2900 min^{-1} for secondary
Materials	Type 347
Oil-fired Sodium Heater	
Duty	5.0 MW
Max inlet temperature	440°C
Max outlet temperature	580°C
Materials	2¼ Cr-1 Mo(Nb stabilized)
Main Pipes of Primary and Secondary System	
Pipe size	168.3 mm OD; 4.5-mm wall thickness
Materials	2¼ Cr-1 Mo (Nb stabilized)
Intermediate Heat Exchanger	
Duty	5 MW
Type construction	shell/helical tube
Number of tubes in parallel	20
Surface area	26.0 m²
Max operating pressure	12.0 kp/cm²
Max operating temperature	580°C
Materials	2¼ Cr-1 Mo (Nb stabilized)
Main Sodium Gate Valves with Freeze Seal	
Max temperature	580°C
Max pressure	12.0 kp/cm²
Materials	2¼ Cr-1 Mo(Nb stabilized)
Operating Time of the Main Components	
Sodium heater	8700 hr
Sodium pumps	10060 hr for primary; 8250 hr for secondary
Intermediate heat exchanger	6310 hr
Steam generator	3800 hr

pressure drop of 18.5 atm includes a safety margin with respect to uneven distribution.

2.2. Hydrodynamic Stability

2.2.1. Discussion of Flow Instability

The question of instability will be discussed as far as it proved to be of interest for this special sodium-heated steam generator. Generally two types of instability have to be considered:[4] steady periodic (oscillation), or aperiodic (decaying or diverging transient).

Figure 6 shows a typical example of a stable pressure drop-vs-flow characteristic. The curve describes the calculated 100% load case of one of our steam-generator units. Aperiodic instability is characterized by $d\Delta p/dG_{tw} < 0$ (Leddineg criterion). It can be seen in the figure that the tube without the orifice would be unstable under operating conditions. The strong stabilizing effect of the orifice is obvious. The stability criterion in Fig. 6 is often used with empirical numbers to describe a safety distance from the region $d\Delta p/dG_{tw} < 0$.

The second equation describes the influence of parallel tubes on stability. With respect to stability the lowest load was the most interesting case. The specified operational range of the steam generator was 30% to 100% of load. Figure 7 shows pressure drop-vs-flow curves calculated for different sodium-to-water ratios at 30% of load. The operating point turns into the unstable region between a sodium-to-water ratio of 7.25 and 7.79. This ensures an adequate safety margin as compared with the operating ratio of 8.65.

2.2.2. Measurement of the Stability Range

To determine the stability range at the lower load limit was the purpose of the stability tests. Among the different parameters which influence the stability

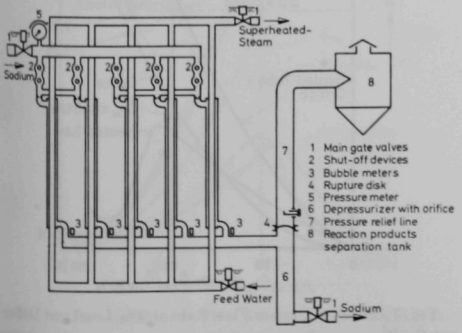

FIG. 3. 5-MW Steam Generator and Pressure-relief System.

TABLE 2. PERFORMANCE DATA OF THE STEAM GENERATOR

Type Construction: Once-through steam generator Concentric tube-in-tube 5 Tube-units in parallel	
Duty at Full Power	5 MW thermal
Feedwater flow rate	7.5 metric tons/hr
Sodium flow rate	64.9 metric tons/hr
Sodium-to-feedwater ratio	8.65
Feedwater temperature	238°C
Superheated steam temp	510°C
Superheated steam pressure	85.0 kp/cm²
Sodium inlet temperature	524°C
Sodium outlet temperature	308°C
Surface area	22.3 m²
Total length of one tube-in-tube	52.5 m²

	Tube size (mm) Wall thickness	Length (m)	Material
1) Econ. a. boiler region of inner tubes			
Size of tube Nr. 1	25.4 × 2.64	32.5	Inconel 600
Size of tube Nr. 2-5	25.0 × 2.90	29.0	2¼ Cr-1 Mo
2) Superheater region of inner tubes			
Size of tube Nr. 1	30.0 × 3.60	20.0	2¼ Cr-1 Mo (Nb stab)
Size of tube Nr. 2-5	30.0 × 3.60	23.5	2¼ Cr-1 Mo (Nb stab)
Outer-tubes Nr. 1-5	60.3 × 3.20	52.5	2¼ Cr-1 Mo (Nb stab)

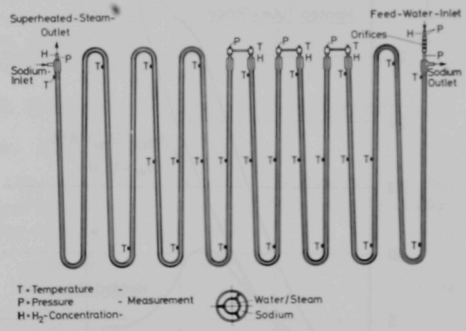

FIG. 4. Tube-in-Tube Unit for Steam Generator.

of the steam generator, the stabilizing effect of the inlet pressure drop (orifices) and the stabilizing effect of a different heat-transfer characteristic (sodium-to-water ratio) can be experimentally checked. Most of the tests were carried out with constant feedwater and decreasing sodium flow. Some tests with increasing

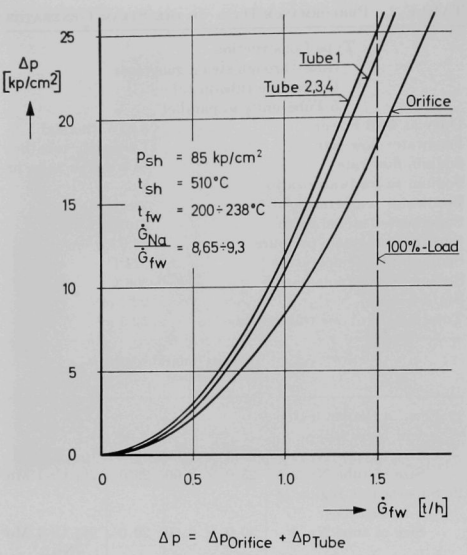

FIG. 5. Pressure Drops of Tubes 1–4 *vs* Flow Rate.

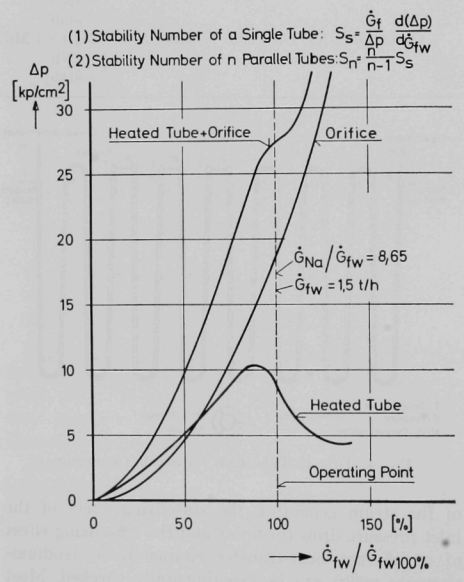

FIG. 6. Pressure Drop *vs* Flow Rate of One Tube-in-Tube Unit of the Steam Generator for 100% Load.

feedwater flow at constant sodium flow permitted direct comparison with the calculated pressure drop vs flow rate.

Figure 8 shows the flow-pressure characteristic for the 35% load case. Feedwater flow had been increased by stages up to 143% of the operating condition; pressure drops of the heated tubes and of the orifices were measured separately.

Within the accuracy of the measured values of Δp the pressure-drop curve of orifice and tube does not show a significant instability range in contrast to the calculated data. This was mainly due to the assumed surface roughness of 0.05 mm for the calculation. The experimental data were fairly well matched by using a surface roughness of 0.02 mm. This result of a stable behaviour was confirmed by the measurement of the steam outlet temperatures which decreased uniformly by decreasing the sodium-to-water ratio.

The tests with constant feedwater and decreasing sodium flow were performed at 20% and 30% of full load. Figure 9 shows the summary of the main parameters for a 20% load at different sodium-to-water ratios. The superheater outlet temperatures deviate markedly at a sodium-to-water ratio of about 7, but correspond typically to stable behaviour. Aperiodic instability normally means that some of the exit steam temperatures decrease extensively while the others increase slightly. In our case all steam temperatures decrease uniformly. This behaviour is due to the fact that the superheater zone is shortened

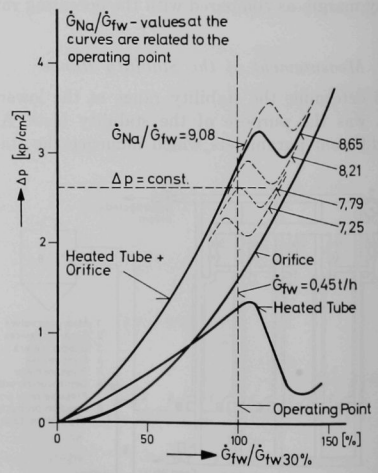

FIG. 7. Pressure Drop *vs* Flow Rate at 30% Load and Different $\dot{G}_{Na}/\dot{G}_{fw}$.

to a small tube area at the exit of the steam generator. This is shown in Fig. 10 where typical temperature curves for a 30% case of 8.92 and 6.34 as a sodium-to-water ratio are compared.

At the nominal sodium-to-water ratio the load has been reduced below the specified load limit of 30%. Under these test conditions the steam generator was stable down to less than 10%. The accuracy limitations of the measuring equipment did not allow a controlled further decrease of the load.

All the tests showed that the stability was guaranteed within the presumed range of operation. Moreover, under all circumstances there was a remarkable safety distance between the range of nominal operation and the point of extensive change of steam outlet temperatures. This safety margin is of value with respect to uneven flow and heat-transfer distributions which have been observed as a consequence of tube-diameter tolerances and a different roughness of the tubes.

The given pressure difference across the orifices at feedwater inlet effectively balanced out the temperature profile across the tube units during startup and shutdown. Therefore we had always uniform temperature distribution in the inlet and outlet headers,

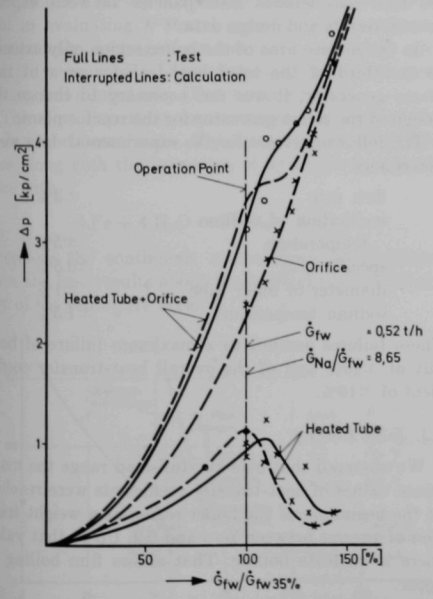

FIG. 8. Pressure Drop *vs* Flow Rate at 35% Load and Different $\dot{G}_{Na}/\dot{G}_{fw}$.

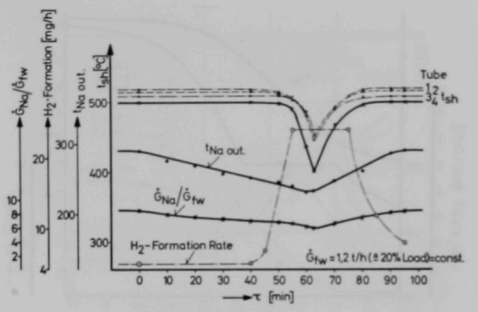

FIG. 9. Steam-generator Behaviour at Varying $\dot{G}_{Na}/\dot{G}_{fw}$.

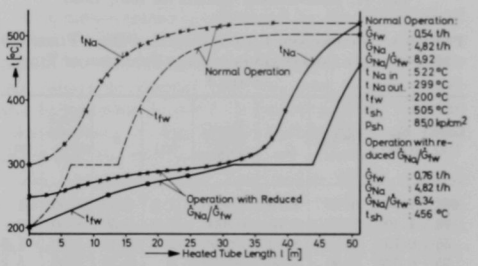

FIG. 10. Temperatures at Normal Operation and at Operation with Reduced $\dot{G}_{Na}/\dot{G}_{fw}$.

which allowed different startup methods of the steam generator. It could be started without difficulties at a sodium temperature of 200°C and also after shutdown of the test facility without cooling down the sodium, which is of interest for post-scram reactor restart.

3. Experimental Results on Heat Transfer

3.1. Instrumentation (see Fig. 4)

To determine temperature distribution, heat flux, and local overall heat-transfer coefficients, the following measurements were used:

sodium flow in the secondary system;
feedwater flow in the main tube and in each of the four units;
sodium inlet and outlet temperatures of all units;
surface temperatures over the length of the outer tubes of units 1 and 4 (26 measuring points);
feedwater inlet and superheated steam outlet temperature, both at the header and at each tube;
pressure and pressure drop on the water-steam side;
water-steam temperature at three points of unit 4.

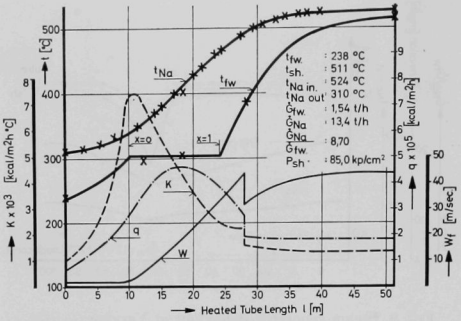

FIG. 11. Heat-transfer Results for 100% Load.

TABLE 3. VALUES AND LOCATION OF MAX HEAT FLUX AND MAX OVERALL COEFFICIENTS OF HEAT TRANSFER OF TUBE UNIT 4

Load (%)	$\dot{G}_{fw}$ (t/hr)	g_m (10^3 kg/m²-sec)	$\dot{G}_{Na}/\dot{G}_{fw}$	$q_{a\,max}$ (kcal/m²-hr)	l (m)	x	$k_{a\,max}$ (kcal/m²-hr-°C)	l (m)
101	1.54	1.46	8.70	466000	17.8	0.52	7500	11
73	1.10	1.05	8.70	432000	15.0	0.50	8350	9
53	0.75	0.76	8.70	360000	12.2	0.45	7800	7.5
35	0.525	0.50	8.66	285000	8	0.35	6850	5.2

3.2. Calculation of the Main Heat-transfer Data from the Experimental Data

The local heat flux is proportional to the differential of temperature vs length. It follows that

$$q_a(l) = \frac{\dot{G}_{Na} c_p}{d_a \pi} \left(\frac{dt}{dl}\right)_l .$$

The local overall heat-transfer coefficient is calculated by dividing heat flux and temperature difference between sodium- and water-steam side:

$$k_a(l) = \frac{q_a(l)}{t_{Na} - t_{H_2O})_l} .$$

Temperature on the water-steam side was determined by heat-balance calculations and by direct measurements on the water-steam side, respectively. The calculation of the heat-transfer coefficients on the sodium side with known heat-transfer correlations gave a first idea of heat-transfer coefficients on the water-steam side, with

$$\alpha_i(l) = \left[\left(\frac{1}{k_a(l)} - \frac{d_a}{2\lambda_{st}} \ln \frac{d_a}{d_i} - \frac{1}{\alpha_a(l)}\right) \frac{d_i}{d_a}\right]^{-1} .$$

By means of a data-evaluation program we calculated the desired data, including additional data of interest like velocity, pressure drop, and vapour content on water-steam side.

3.3 Discussion of Experimental Results

Figure 11 shows the most interesting curves of tube unit 4 at full load. The maximum overall coefficient of heat transfer is located at the beginning of the boiler region (this is practically identical with the maximum of the heat-transfer coefficient on the water-steam side). The maximum heat flux is located in the middle of the boiler region.

The discontinuities at a 28-m distance from the feedwater inlet are due to the increase of the diameter of the inner tube. We measured the interesting data of heat transfer over the full-load range down to less than 10% load.

Table 3 shows the values and locations of heat flux and overall heat-transfer coefficient at different loads. The maximum heat flux amounts to 466,000 kcal/m²-hr. The maximum overall heat-transfer coefficient is approximately 8,000 kcal/m²-hr-°C. The sodium-to-water ratio had a nominal value of about 8.7.

There was a good agreement between calculated and measured heat-transfer values in the economizer and superheater region. In the boiler region, however, we had considerable discrepancies between experimental results and design data.[5-7]

As the surface area of the boiler region only extends to one-third of the total heat-transfer area of this steam generator, it was not necessary to change the design of the steam generator for the reactor plant.

The following errors for the experimental data were determined:

flow rate	±3%
inclination of sodium temperature	±5%
specific heat	±0.5%
diameter of inner tube	±1%
sodium temperature	±1.5%

These failures amount to a maximum failure of heat flux of ±10% and of the overall heat-transfer coefficient of ±16%.

3.4. Film Boiling

We observed that over the full-load range the maximum values of heat-transfer coefficients were reached at the beginning of the boiler region at a weight fraction of vapour between zero and 0.2. Up to that value there is nucleate boiling. That allows film boiling to occur.

We therefore compared the measured heat fluxes with other experimental results in the literature[8, 9] and found that under such conditions of operation no

film boiling can exist, which was affirmed by the corrosion measurements and the metallurgical evaluations.

4. Corrosion Measurement at the Water-steam Side

4.1. Method

Corrosion measurement gives additional information about the status of the steam generator. In the case of ferritic steam-generator tubes the behaviour during the initial startup is dictated by the formation of a protective magnetite layer on the wall surfaces. After this formation is finished, the corrosion rate will be reduced to a small constant value, mainly due to the diffusion of iron atoms through the protective layer. The integrity of the magnetite layer can be disturbed. If this disturbance is a recurrent process, this may lead to the destruction of the steam-generator tube. Processes of this kind are:

steady periodic and aperiodic instability, as mentioned in Sect. 2;
stratified flow in the horizontal channels, which causes high-temperature stresses;
high heat flux;
deformation of the inner tubes by suppressed thermal expansion.

Therefore a survey of corrosion data is an additional tool in evaluating a steam generator. We measured continuously hydrogen concentration, electrical conductivity, and pH. Discontinuously measured were oxygen and diluted iron (Fe^{++} and F^{+++}).

The most important measurement was that of the hydrogen concentration. The formation of magnetite goes along with the formation of hydrogen in accordance with

$$3\,Fe + 4\,H_2O \rightarrow Fe_3O_4 + 4\,H_2\,.$$

Therefore the continuous measurement of hydrogen gives the best results about the buildup and the integrity of the protective layer.

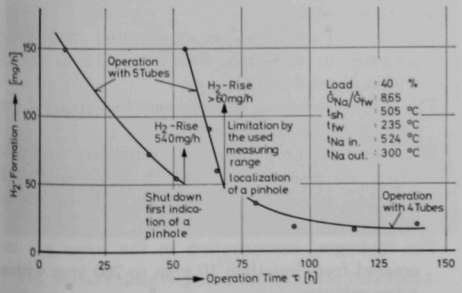

FIG. 12. Rate of Hydrogen Formation in the Steam Generator during Initial Startup.

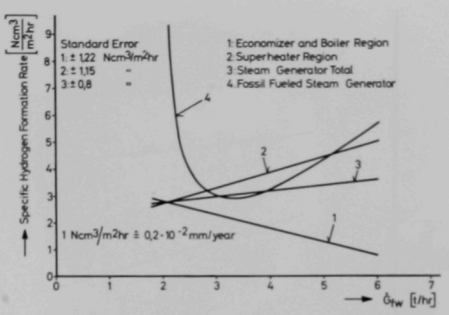

FIG. 13. Hydrogen Formation *vs* Load.

This measurement is influenced by the oxidation of diluted $Fe(OH)_2$ to Fe_3O_4, which is also accompanied by the formation of hydrogen. To eliminate this failure an Inconel tube was used as economizer and boiling zone in unit 1. It can be assumed that the corrosion rate of the Inconel is negligible as compared with the ferritic material.

The measuring nozzles, described in Fig. 4, allowed a small bypass flow to be directed to the measuring equipment. Especially the measuring points behind the boiling zone of units 1 and 4 allowed the reduction of the undesired effects of diluted iron.

4.2. Results

Figure 12 shows the development of the hydrogen concentration during the first time of operation of the steam generator. During the time of formation of the protective layer the hydrogen content is high. It decreases to a much smaller constant value within about 140 hr of operation. At that time the formation of the magnetite layer seems to be completed. The curve shows the hydrogen content behind the steam generator; the hydrogen value behind the Inconel tube is not yet eliminated.

The operation has been interrupted for 4 days after an operation time of 54 hr and for 12 days after an operation time of 68 hr. The interruptions were due to the failure of tube unit 5, which is discussed later.

In Fig. 13 the originally measured rate of formation of hydrogen has been reduced to a specific rate which allows a better comparison between different steam generators. Separate curves for the hydrogen-formation rate within the preheating and boiling zone and within the superheating zone are given and combined to form a third curve for the whole steam generator. These curves are compared with a fourth curve which shows the hydrogen development in a fossil-fueled once-through steam generator.[10] The economizer and boiler region of our steam generator show

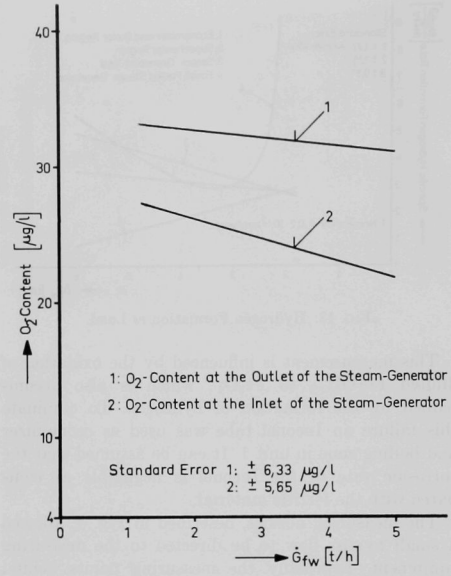

FIG. 14. Oxygen Content *vs* Load.

the expected lower corrosion rate as compared with the fossil-fueled boiler. The unexpected result is the higher corrosion rate of the superheater region. This is probably due to the fact that the elimination of other effects has only been done within the boiler and economizer region. An Inconel superheater region for comparison was not installed. Two different processes may be responsible for the higher corrosion rate of the superheater region:

1. some diluted $Fe(OH)_2$ may still be available for oxidation within the superheater region;

2. hydrogen may be formed by catalytic and thermal dissociation of steam.

This second process has been assumed by Freier and Kiekenberg.[11] In that case hydrogen formation would be accompanied by oxygen formation. Figure 14 shows the oxygen content before and after the steam generator as a function of the load. The maximum oxygen formation at a flow rate of 5 t/hr in the steam generator is 9 µg/l. This corresponds to a hydrogen formation of approximately 11 µg/l, if all oxygen formed in the steam generator originates from this dissociation process, which is doubtful. The hydrogen concentration of 11 µg/l of condensate corresponds to 5.6 mg/hr or, if it can be seen mainly as a surface effect, to 6.1 N-cm³/m²-hr. With these hydrogen numbers the hydrogen-formation rate in the super-heater region could even become negative. Therefore, the discussion of these fairly uncertain oxygen-formation processes is to show merely that the hydrogen-formation rate in the superheater region is probably much lower than is indicated in the figure.

The results of the electrical conductivity, pH, and iron measurements are not discussed in detail because the values are typical for normal feedwater. The measured oxygen content was slightly high, since the degasifier used was not effective enough.

5. Pinhole Failure in Tube-unit Five of the Steam Generator

5.1. First Shutdown of the Test Facility

After 54 hr of operation the test facility was automatically shut down. It was not possible to identify the initiating signal of the shutdown. However, we obtained two important indications:

The cover-gas pressure of the secondary and of the primary expansion tanks, which were connected together, increased from 1.31 to 1.64 atm within 13 min.

Before shutdown the gas chromatograph indicated a hydrogen concentration in the cover gas of the secondary expansion tank of about 5 vpm. After shutdown the concentration reached a value of more then 120 vpm, which was the end of the selected measuring range for this measurement, decreased for a short time to 50 vpm, and finally reached a constant value of 150 vpm.

A helium leak test was negative.

5.2 Second Shutdown of the Test Facility

The steam generator was started again. After 14 hr of operation we observed all symptoms of a pinhole in tube-unit five. During that time we had just tested the steam generator at a partial load of 40% with a sodium-to-water ratio of about 7.

The following indications pointed out a pinhole-leak in tube-unit five:

We observed a decrease of superheated steam temperature in tube-unit five from 511 to 300°C within about 8 min.

The bubble indicator of tube-unit five signaled the passage of gas bubbles.

The cover-gas pressure of the secondary and primary expansion tanks which were connected together, increased from 1.26 to 1.64 atm within 10 min.

The hydrogen concentration in the cover gas increased from less than 10 vpm to 700 vpm within a few minutes.

The revolution frequency of the secondary sodium

pump increased to its maximum value of 3,000 rpm; yet the pump capacity decreased to almost zero due to hydrogen bubbles in the sodium.

Inlet and outlet temperatures of the intermediate heat exchanger and the steam generator indicated flow disturbance, even reverse flow in the secondary system.

After shutdown of the system, a helium leak test indicated a pinhole leak in tube-unit five. The pinhole was located near a bend in the neighbourhood of a welding seam and at a distance of 29 m from the feedwater inlet. It had a diameter of about 0.25 mm, enlarged on the sodium side (see Fig. 15).

We found the pinhole was originated by a fault of the welder who ignited the welding electrode beside the welding seam. This caused small cracks in the ignition spot.

This process was proven by ignitions of different duration of an electrode on a tube of the same material and dimensions. The result of an ignition time of 3 sec is included in Fig. 15.

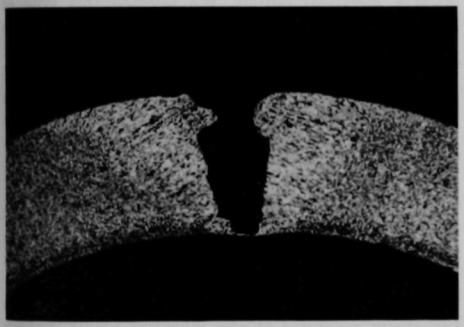

(a)

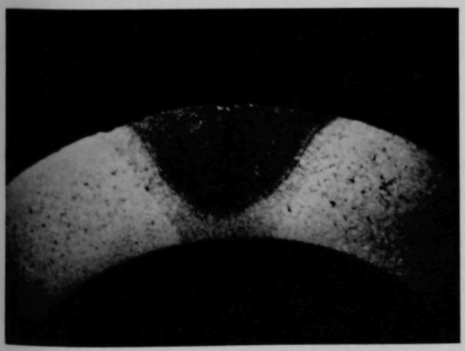

(b)

FIG. 15. (a) Failure Section of the Pinhole in Tube Unit 5. (b) Failure Section Caused by Ignition of the Electrode. (Magnification 8×, Polished.)

FIG. 16. Deposit of Sodium Hydroxide in the Annulus at the Sodium Side near the Pinhole.

Figure 16 shows deposits of sodium hydroxide at the outer tube wall in the downstream area behind the pinhole. As the melting point of NaOH is slightly higher (315°C) than temperatures at this point have been during the failure, it is possible that formation of NaOH at the outer tube wall had already started during operation with the leak. The outer tube wall opposite the failure showed only an increased surface roughness.

Two additional pinhole tests were performed to assure the phenomena discussed above are described correctly.

Symbols

c_p	(kcal/kg-°C)	specific heat of the sodium
d_a	(m, mm)	outer diameter of the inner tube
d_i	(m, mm)	inner diameter of the inner tube
g	(kg/m²-sec)	mass velocity
k, k_a	(kcal/m²-hr-°C)	overall coefficient of heat transfer
l	(m)	heated tube length
n	(—)	number of parallel tubes
p	(kp/cm²)	pressure
p_{sh}	(kp/cm²)	pressure of the superheated steam
q, q_a	(kcal/m²-hr)	heat flax at the outer tube surface
t	(°C)	temperature
t_{fw}	(°C)	feedwater temperature at the inlet of the steam generator

t_{sp}	(°C)	superheated steam temperature at the outlet of the steam generator
t_{Na}	(°C)	sodium temperature
$t_{Na\ in}$	(°C)	sodium temperature at the inlet of the steam generator
$t_{Na\ out}$	(°C)	sodium temperature at the outlet of the steam generator
t_{H_2O}	(°C)	water and steam temperature
w, w_f	(m/sec)	water and steam velocity
x	(—)	weight fraction of vapour
$\dot{G}_{fw}$	(t/hr, kg/hr)	feedwater flow rate
$\dot{G}_{Na}$	(t/hr, kg/hr)	sodium flow rate
S_s	(—)	stability number of a single tube
S_n	(—)	stability number of n tubes
α_a	(kcal/m²-hr-°C)	heat-transfer coefficient at the sodium side
α_i	(kcal/m²-hr-°C)	heat-transfer coefficient at the water and steam side
λ_{st}	(kcal/m-hr-°C)	thermal conductivity of tube wall material
τ	(min, hr)	operation time
Δp	(kp/cm²)	pressure drop

REFERENCES

1. Tebbert *et al.*, *Die Kompakte Natriumgekühlte Kernreaktoranlage Karlsruhe (KNK)*, Atom und Strom **9/10**, 117–129 (1967).
2. R. Harde *et al.*, *Die Kompakte Natriumgekühlte Kernreaktoranlage Karlsruhe (KNK)*, Atomwirtschaft-Atomtechnik **XI/7,8,9**, 354–360, 448–452 (1966).
3. R. Harde *et al.*, *A Contribution to the Advancement of Sodium Technology*, VIII Nuclear Congress, Symposium on Fast Reactors, Rome, June 17–19, 1963.
4. L. S. Tong, *Boiling Heat Transfer and Two Phase Flow*, John Wiley and Sons, Inc. New York (1965).
5. R. Herrick, *Liquid Metal Heat-transfer by Forced Convection*, United Kingdom Atomic Energy Authority, Risley, Warrington, Lancashire (1964).
6. O. E. Dwyer, *Recent Development in Liquid Metal Heat Transfer*, Atomic Energy Review **4** (1966).
7. H. Kraußold, *Wärmeübertragung bei turbulenter Strömung*, Forschg. Ing.-Wesen **4** (1933).
8. F. Mayinger, O. Schad, and E. Weiß, *Untersuchung der kritischen Heizflächenbelastung (burnout) bei siedendem Wasser*, EURAEC 1811, EUR 3347 (May 1966).
9. H. Herkenrath and P. Mörk-Mörkenstein, *Grundzüge der Probleme auf dem Gebiet der Blasenund Filmverdampfung*, EUR 2211.d (1964).
10. E. Ulrich, *Wasserstoffmessung im Hochdruckkesselbetrieb*, VGB-Mitteilungen 8/49 (1957).
11. R. Freier and H. Kiekenberg, *Betrachungen zum Fe_3O_4-H_2O-O_2-System des Dampfkessels*, BGB-Mitteilungen 10/50 (1957).

Discussion

Mr. Goldmann (UNC): I was wondering whether you actually observed any flow oscillations or sudden jumping from one regime to another.

Mr. Mausbeck: No, we didn't with this steam generator. According to the first calculations we expected to reach the instability range during our experiments, but didn't. In other experiments carried out with another steam generator we have seen such fast fluctuations, which are typical for a periodically unstable steam generator.

Mr. Zebroski (GE): I wonder if this unit was related to the plant design that Dr. Harde showed yesterday. What design relationship does the test unit have to a large unit that might bear on the same technology?

Mr. Mausbeck: This is the steam generator for the KNK reactor, which is an experimental reactor of 20-MW electrical output. We selected this type of steam generator very early. At that time we had to select a system that was safe and that we could show was safe with respect to sodium-water reactions and their effects. One of the main purposes was to choose a unit which could be fully tested with the equipment on hand at that time. When we went over to larger reactors, we also went over to a different steam-generator design as Mr. Harde mentioned in his paper.

Mr. Horton (AEC): What consideration do you give to the problem of tube vibration with the possibility, therefore, of high cycle fatigue? Did you make any attempts to figure this out?

Mr. Mausbeck: We couldn't find any vibration in this steam generator at any vibration points. I think that with the relatively thin walls in this tube-in-tube steam generator thermal-cycle fatigue is not a factor.

Mr. Kovach (B&W): Did you notice any difference in the steam-side scaling behavior of this modified 2¼ Cr-1 Mo material compared to the normal material?

Mr. Mausbeck: We saw some points of corrosion which were due to bad feedwater procedure during initial operation.

Mr. F. A. Smith (ANL): How long did it take to put the unit back into service?

Mr. Mausbeck: Twelve days.

Mr. Smith: What is a bubbler indicator?

Mr. Mausbeck: It is an electrodynamic device that is located at each sodium tube to measure bubble density.

Detection of Small Leaks by Hydrogen Measurements in a Sodium-heated Steam Generator

J. Birault,* A. Brachet,† E. Cambillard,* J. Coron,† L. Lannou,† and C. Rault†

(PRESENTED BY A. BRACHET)

INTRODUCTION

The study of the problem of detecting small water leaks in a steam generator heated by liquid sodium was undertaken in 1966 by the Heat Transfer Department of the EDF CHATOU Laboratory. In this paper are described all the studies and tests performed until now.

In the first stage, it was proposed to compare the different industrial methods of proportioning sodium impurities capable of being applied to the special case of hydrogen. Thus, it was sought to compare with the "conventional methods" (plugging indicator, nickel diaphragm associated with a Pirani gauge in accordance with the Atomics International principle,[1] and covergas chromatography) a new method based on a nickel diaphragm associated with a mass spectrometer for detection of the hydrogen. In addition, these preliminary tests were intended to bring out the main physicochemical mechanisms that might enter into a process of detecting a water leak in an industrial steam generator connected to a fast sodium-cooled reactor. The description of the tests performed and of the results obtained are given in Ch. I.

At the end of this first stage, the advantages of the new proportioning method were demonstrated. With the main mechanisms better known, it became possible to examine theoretically the advantages (basically sensitivity) of the various methods or processes of water-leakage detection in a steam generator. The corresponding theoretical considerations are covered in Ch. II.

In addition, these calculations have enabled us to evaluate the relative importance of the different parameters entering into the definition of detection sensitivity (the smallest detectable leak in a given item of equipment). It then appeared necessary to complete the already made experimental studies in order to improve the knowledge of certain important but badly known physical parameters. The experimental studies undertaken for that purpose and the results obtained until now are covered in Ch. III.

Although there still remain certain unknowns (particularly with respect to the physicochemical interpretation of the phenomena), the results acquired during these studies permit the design and dimensioning of a leakage-detection system for an industrial application. In this connection, there are described in Ch. II the solutions proposed for two steam-generator testing installations (1.5-MWt CHATOU circuit and 50-MWt RENARDIERES circuit (C.G.V.S.)).

While waiting for industrial experience to be obtained with these installations, a short-duration test was performed, in cooperation with the CEA, with the thermal testing installation of GRAND QUEVILLY.

The tests described in Ch. IV have confirmed, on the whole, the first conclusions of Ch. I relative to the general detection problems in a complex industrial circuit. In addition, they have supplied fundamental physical data for the NaK alloy used in the secondary circuit of that installation. Finally, they have permitted clarification of certain unknowns, like the normal diffusion rate of hydrogen through the heat-exchange walls of the steam generator (hydrogen due to aqueous corrosion of steels).

CHAPTER I

PRELIMINARY TESTS AT CHATOU

I.1 Test Installation

The test installation is described in detail in Ref. (2), and Fig. 1 gives its general scheme. Its main characteristics are summarized as follows:

	Sodium Loop	Water-steam Loop
Capacity, kg	150	10
Flow, kg/sec	0.6	Circulation by thermosiphon
Heat power, kW	60	—
Max temperature, °C	600	565
Pressure, bar	10	170

The steam-generator model has the following characteristics:

water tube: diameter = 28 mm; thickness = 2.6 mm; length = 3 m; material = ferritic steel with 2.25% Cr-1% Mo.

annular sodium space: diameter = 60 mm.

* C.E.A., CEN Saclay, Gif-sur-Yvette, France

† Electricité de France, Chatou, France

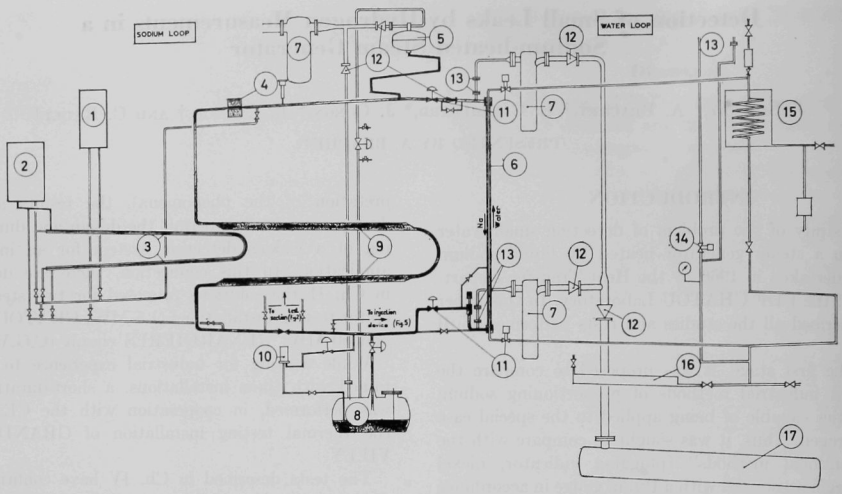

FIG. 1. The Test Loop. 1. Plugging indicator; 2. Cold trap; 3. Cold trap economizer; 4. E. M. pump; 5. Expansion tank; 6. Steam generator model; 7. Separator; 8. Storage tank; 9. Electrical heater; 10. Filter; 11. Pneumatic valves; 12. No-return valves; 13. Rupture discs; 14. Safety valve; 15. Cooler; 16. Water storage and expansion tank; 17. Gas products expansion tank.

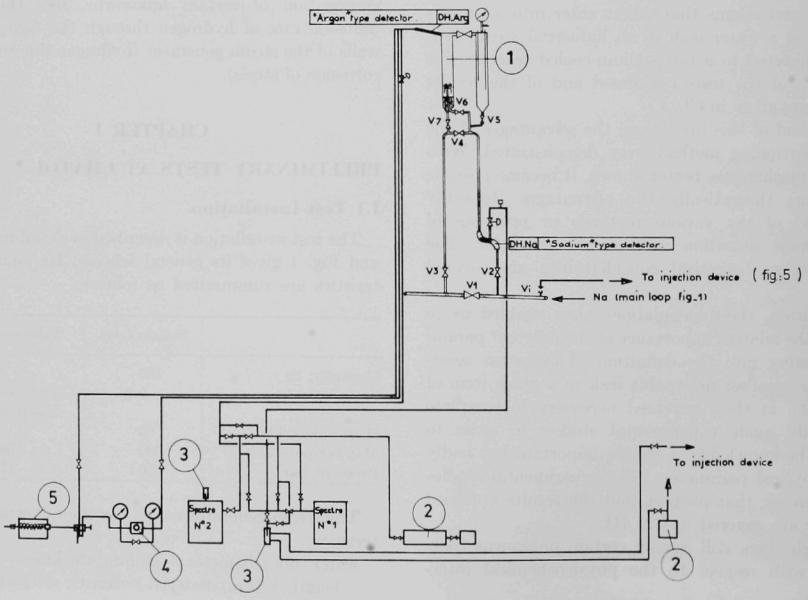

FIG. 2. The Test Section. 1. Argon "pot"; 2. Vacuum pumps; 3. Hydrogen calibrated leaks; 4. Argon compressor; 5. Chromatograph.

I.2 The Test Section

The different equipments to be compared, other than the plugging indicator, were arranged within the sodium loop in a special by-pass (see Fig. 2). The plugging indicator, of the manual type described in Ref. (2), was placed in another by-pass.

I.2.1. The Nickel-diaphragm Hydrogen Detector of the "Sodium" Type.

This detector consists (see Fig. 3) of thin nickel tubes within which sodium circulates. The instrument may be completely purged and does not include any dead area where the sodium is renewed slowly. The detector is connected to a vacuum circuit including a Pirani gauge and a mass spectrometer adjusted to mass 2 (hydrogen). The leaktightness of the detector welds was helium tested at temperature and pressure.

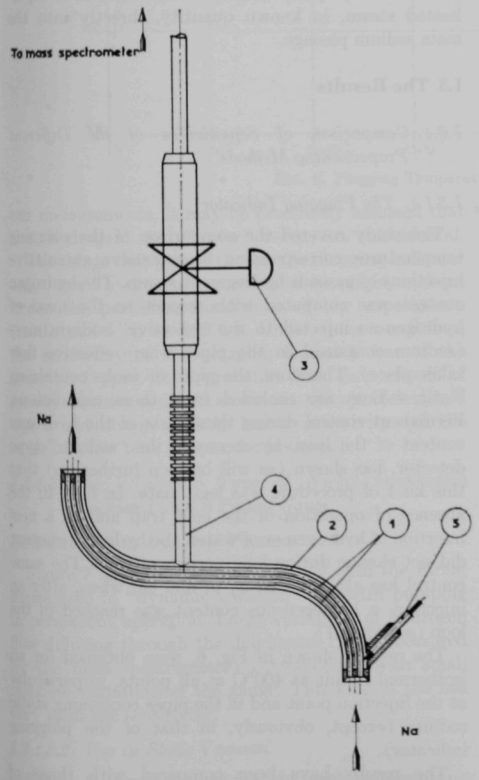

FIG. 3. Sodium Type of Detector (scale ¼). 1. Nickel tubes (0.2 mm thick); 2. Stainless steel tube; 3. Valve actuated by 5; 4. Vacuum pipe; 5. Sodium leak detector.

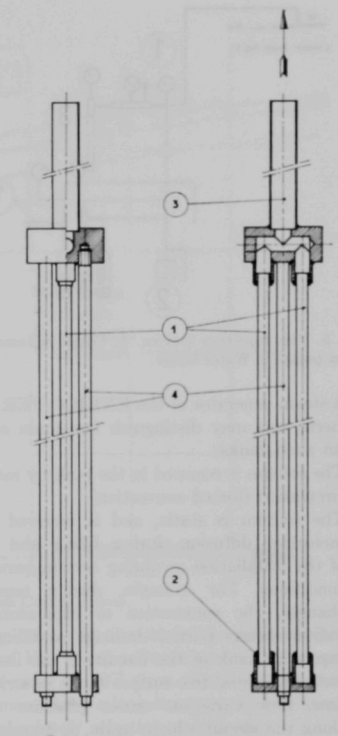

FIG. 4. "Argon" Type of Detector (scale ½). 1. Nickel tubes (0.2 mm thickness); 2. Plugs; 3. Vacuum pipe; 4. Stainless steel rods.

I.2.2. The Nickel-diaphragm Hydrogen Detector of the "Argon" Type

This device (see Fig. 4) is placed in a tank called the "sodium circulation pot," designed for the study of detection in the circuit cover gas (argon). It reproduces in "miniature" the different configurations that might be found in an industrial sodium circuit for a tank, including a free sodium surface, and in which one might analyze the argon in order to find out its hydrogen content. Such a tank in an industrial circuit may be, for instance: an expansion tank, the shell of a free-surface mechanical pump, the upper part of an intermediate heat exchanger of the RAPSODIE type

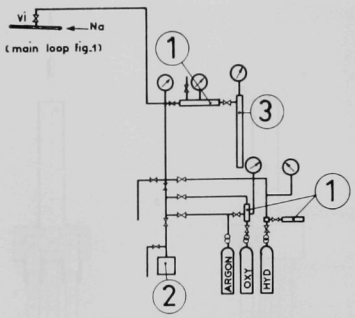

FIG. 5. The Injection Device. 1. Gauge volume tank; 2. Vacuum pump; 3. Water boiler.

or of a steam generator of the ENRICO FERMI type. In general, one may distinguish two main configurations in such tanks:

1. The sodium is renewed in the tank by maintained circulation (forced convection).
2. The sodium is static, and is renewed only by molecular diffusion during filling and draining of the installation or during certain variations of conditions. For example, during temperature changes, the contraction or expansion of the sodium causes partial drainage or filling of the expansion tank of the circuit. If the installation includes several free-surface tanks in series in the flow, flow variation causes pressure variation along the circuit which, again, is translated into partial draining or filling of the tanks.

Furthermore, the "pot" is designed in order to make possible a varied range of thermal conditions in the one or the other of the preceding configurations. In particular, through suitable heating, one may make the pot isothermal at circuit temperature or at another one; or make the pot anisothermal, the upper part being colder or hotter than the lower part.

Finally, when sodium is made to circulate in the "pot" (valves V_6 and V_7 open, and valve V_4 closed), one may, by acting on the height of the free sodium surface in the "pot," achieve the two following states:

1. Strong turbulence and large sodium-argon contact surface: the free level is lower than the upper end of the sodium-entrance pipe which, in that case, discharges a free sodium jet into the argon;
2. Small turbulence and smaller sodium-argon contract surface at the straight section of the "pot;" the free level is higher than the deflection plate of the jet, which is submerged.

The tank supplied by the valve V_5 is equipped with level probes which reference the position of the free surface of the "circulation pot" itself before the experiment. Subsequently, this tank is isolated (valve V_5 closed).

In the upper part of the "circulation pot" is placed an "argon" type of nickel-diaphragm detector connected, like the "sodium" detector, to a vacuum circuit and to a mass spectrometer.

Since the two spectrometric circuits are independent of each other, it is possible to observe the phenomena in the pot and in the dynamic sodium simultaneously.

In addition, in this "pot" two nozzles have been connected in an initial phase of the tests with a chromatograph. Later, following the results described further on, these nozzles were shut off.

I.2.3. The Hydrogen- or Water-injection Device

This device is shown schematically in Fig. 5. It permits the injection, in the form of a short-duration (about 30 sec) "puff," of gaseous hydrogen or of superheated steam, in known quantity, directly into the main sodium passage.

I.3 The Results

I.3.1. Comparison of Sensitivities of the Different Proportioning Methods

I.3.1.1. The Plugging Indicator

The study covered the comparison of the plugging temperatures corresponding to successive cumulative injections of gaseous hydrogen or steam. The hydrogen content was computed with respect to the mass of hydrogen so injected to the "effective" sodium mass (sodium contained in the pipes where effective flow takes place). Therefore, the pipes or tanks containing static sodium are excluded from these calculations. Permanent control during these tests of the hydrogen content of the loop, by means of the "sodium" type detector, has shown (as will be seen further on) that this kind of procedure was legitimate. In fact, in the absence of operation of the cold trap and of a new insertion of hydrogen or of water, the hydrogen content did not change during long periods of time. The same control has also allowed us to find out when, after an injection, a homogeneous content was reached in the loop (see Fig. 11).

The results, shown in Fig. 6, were obtained for an isothermal circuit at 400°C at all points, in particular at the injection point and in the pipes containing static sodium (except, obviously, in that of the plugging indicator).

The results have been compared with those of Subbotin and Kozlov.[3] There was good agreement for hydrogen but less so for water. However, in the latter case, it should be noted that, within the accuracy of

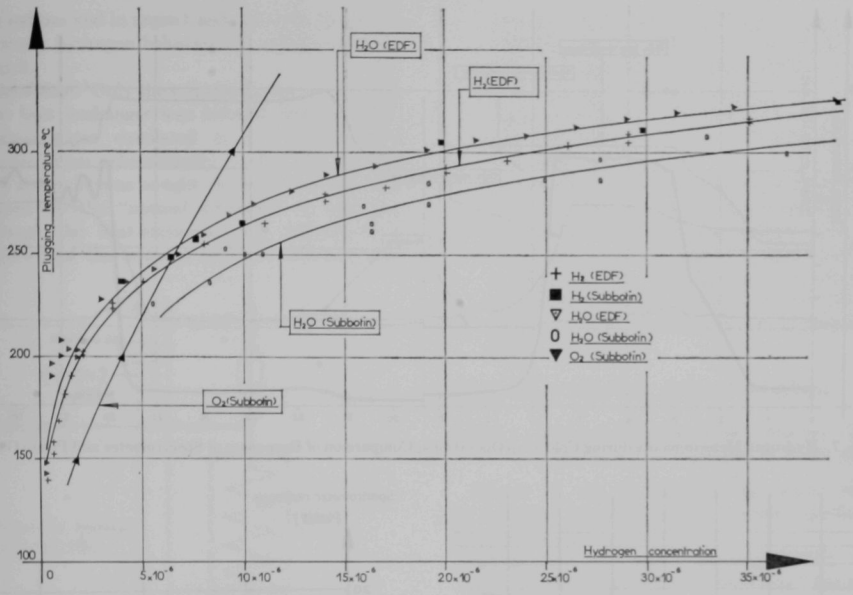

FIG. 6. Plugging Temperature *vs* Hydrogen Concentration.

our measurements, it may be practically assumed that the "hydrogen" and "water" curves are coincidental.

The things that passed though the plugging indicator only "saw" hydrogen, regardless of its origin, at least under the particular conditions of our experiments (isothermal loop at 400°C). Under these conditions, the sensitivity of the plugging indicator was of the order of 1 ppm. It is probable that, in a circuit of greater capacity and with an automatic type of device,[4] one would obtain slightly higher sensitivity (of the order of a few tens in ppm, for instance).

I.3.1.2. The "Sodium" Type of Nickel Diaphragm Associated with a Pirani Gauge

I.3.1.2.1. Use in Dynamic Vacuum

Figure 7 shows the results obtained with the Pirani gauge used in "dynamic vacuum," i.e., with pumping in permanent operation. Large variations of hydrogen flow diffusing through the diaphragm (flows measured by the mass spectrometer) corresponded with small response variations of the gauge. This kind of use has very mediocre sensitivity.

I.3.1.2.2. Use in Static Vacuum

Figure 8 shows the results obtained by observing the "vacuum rise" in the detector isolated from the pumping unit. The test conditions are identical with the preceding ones. Sensitivity is better than in the preceding case. For the device in question (the diaphragm of Fig. 3 and a Pirani gauge), this sensitivity is of the order of 10^{-1} ppm. On the other hand, the measurements take a long time, are discontinuous, and are not absolutely selective of hydrogen.

I.3.1.3. The "Sodium" Type of Nickel Diaphragm Associated with a Mass Spectrometer

Figure 9 shows the result obtained, still under the same conditions as before. The field of the device used in the version in question (diaphragm of Fig. 3 with spectrometer of the helium-leakage type of industrial detector) is between 0 and 1 ppm. For very small contents, of the order of 10^{-2} ppm, the sensitivity of the system may reach a few 10^{-3} ppm.

In addition, the use of the spectrometer presents several other advantages: specificity to hydrogen, short response time, and possibility of continuous measurement. Therefore, this method was adopted for the subsequent studies bearing, in particular, on the determination of the dominant mechanisms in a process of water-leakage detection.

I.3.2. Study of the Main Physicochemical Mechanisms Entering into a Process of Water-leakage Detection

For the main part, these tests have been conducted in the installation described in ¶I.1. The proportioning method was spectrometry. These tests were performed in three main stages:

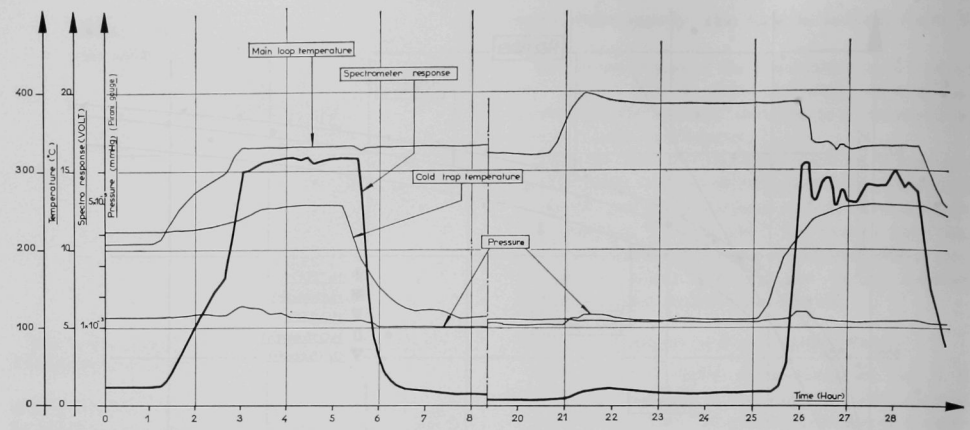

FIG. 7. Hydrogen Measurements during Cold-trap Operations; Comparison of Responses of Spectrometer and Pirani Gauge.

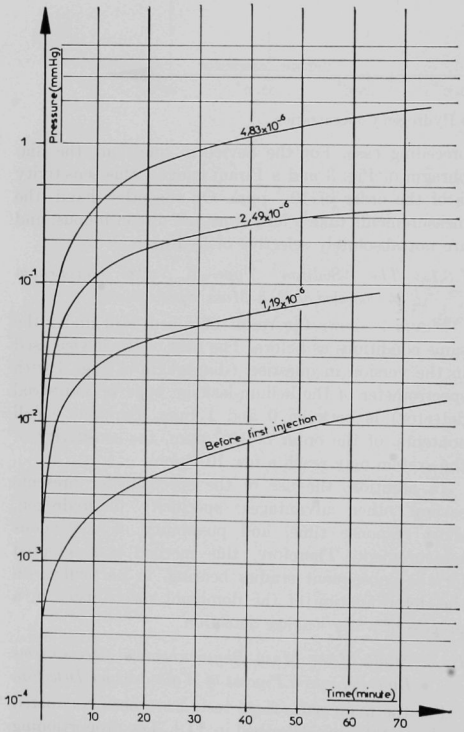

FIG. 8. Pressure *vs* Time in Isolated Detector.

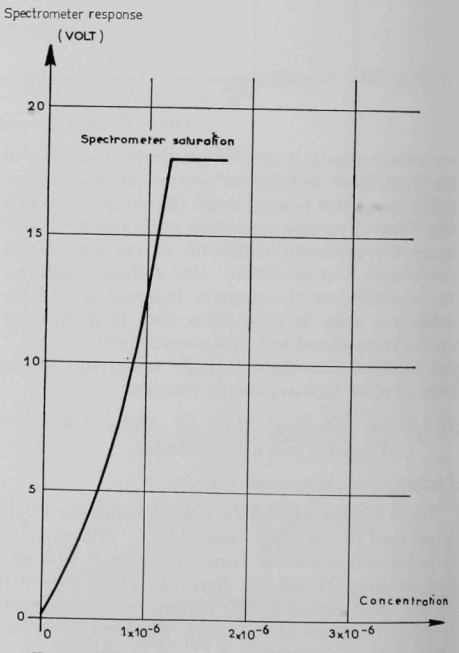

FIG. 9. Calibration of "Sodium" Type of Detector.

1. *First stage:* Only the sodium loop of Fig. 1 was operational (the water-steam part being filled with argon). It was sought in these tests to study the various possible arrangements of the detectors

(in sodium and in argon) and, generally speaking, to study hydrogen behavior in a complex sodium circuit.

2. *Second stage:* Only the water loop was operational. The heat exchanger was isolated, and the pressurized water circulated in the instrumented bypass given schematically in Fig. 10. In this test series, it was sought to bring out the part played by the "normal diffusion" of hydrogen through the heat-exchange wall. Indeed, it is known that the aqueous corrosion of steels frees hydrogen which, in the "nascent" state is particularly apt to diffuse and, consequently, to penetrate into the sodium, which is thereby contaminated. The presence of this "normal" hydrogen creates a background noise in which the signal due to hydrogen, as a result of a possible leak, may be lost.
3. *Third stage:* The two sodium and water loops were in operation and interconnected by the intermediary of the steam-generator model. These tests were to check results obtained previously. In addition, in a test phase now in preparation, one will study the behavior in time of real microleaks (due, for instance, to manufacturing defects).

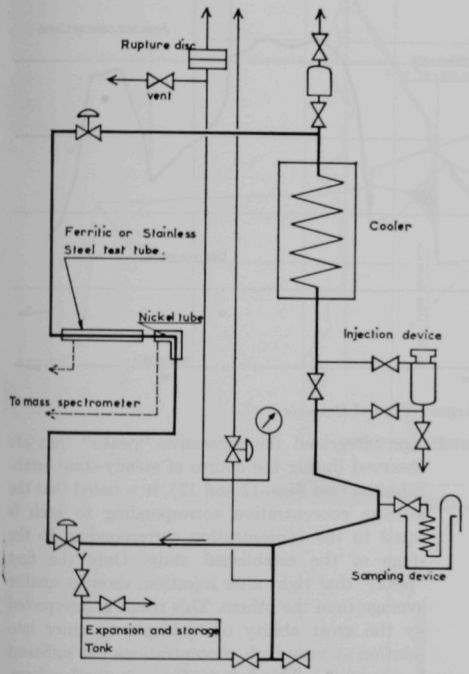

FIG. 10. Water Test Loop (Phase 2).

I.3.2.1. First-stage Tests: Sodium Circuit Only

I.3.2.1.1. Study of Response of the "Sodium" Type of Diaphragm to a Hydrogen or Water Injection

Figures 11 and 12 illustrate the results obtained for hydrogen injection and for a water injection. The initial test conditions were:

isothermal temperature of the loop: 400°C;

a prior purification stage by "cold trap" has reduced the "plugging temperature" to a nonmeasurable value (less than 140°C) and the response of the spectrometer to a value close to the intrinsic background noise of the device (when it is isolated from the detector);

the "cold trap" and the "plugging indicator" are isolated (there is no flow through them), and the main flow of the loop circulates fully in the instrumented bypass (valve V_1 closed, as well as V_5, V_6, V_7; valve V_4 open).

A known mass of hydrogen or of water is injected by V_1, at constant flow, for about 30 sec at ambient temperature. The water, on the other hand, is injected in the form of steam superheated to 400°C and under a pressure of a few bars.

The testing procedure was as follows: The passage of the "puff" of hydrogen is felt by the "sodium"

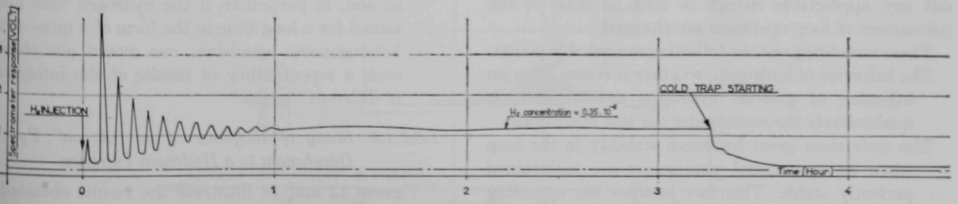

FIG. 11. "Sodium" Type of Detector and Hydrogen Injection.

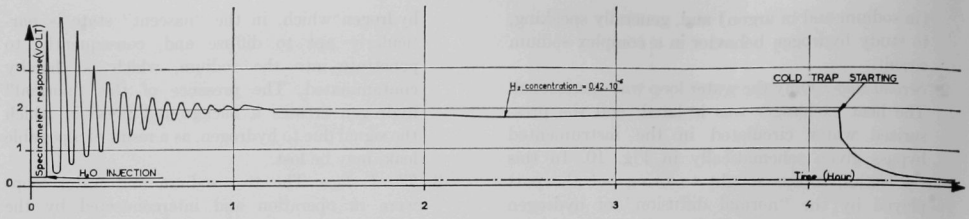

FIG. 12. "Sodium" Type of Detector and Water Injection.

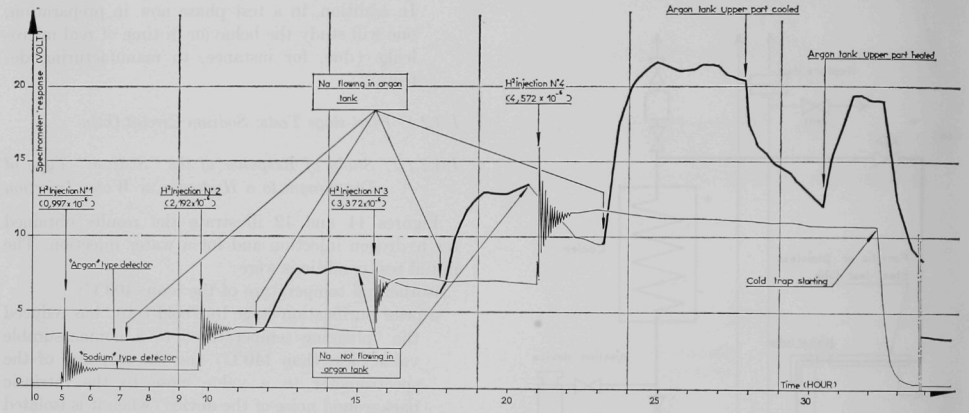

FIG. 13. Test No. 1 with "Argon" Type of Detector.

(DH_{Na}) detector after a period of time corresponding practically to the time of sodium passage between V_i and DH_{Na}. The amplitude of the response is relatively small. Then the response of the detector becomes again equal to the background noise before injection. Subsequently, the detector responds to each of the successive passages of the hydrogen "puff" with a periodicity equal to the passage time of the sodium loop. The turbulent diffusion tends gradually to dilute the "puff" until a steady state is reached (at the end of about one hour under the conditions of our tests). Then, the response of the spectrometer is stable in time. Constant hydrogen content will be maintained practically without any appreciable change so long as none of the parameters of loop operation are changed.

These tests bring out the following remarkable points:

The behavior of hydrogen, whether it comes from an injection of gaseous hydrogen or of water, is qualitatively the same under our test conditions.

The tests show great hydrogen stability in the loop when its operational parameters are maintained perfectly stable. This fact justifies the operating procedure we have used during the "plugging temperature" tests.

If one integrated the successive "peaks" that are observed during the course of steady-state establishment (see Figs. 11 and 12), it is noted that the average concentration corresponding to each is equal to the concentration corresponding to the stage of the established state. Only the first "peak," that right after injection, shows a smaller average than the others. This result is interpreted by the great ability of hydrogen to enter into solution at very high concentrations (at sufficient temperature). This fact confirms, in another form, the results relative to the plugging temperature. In fact, it may be believed that, if this were not so and, in particular, if the hydrogen were maintained for a long time in the form of a more or less heterogeneous emulsion, one would not observe such a repeatability of results of the integration of different "peaks."

I.3.2.1.2. Study of Response of an "Argon" Type of Diaphragm to a Hydrogen Injection

Figures 13 and 14 illustrate the results obtained in the comparison of operation of "sodium" (DH_{Na}) and "argon" (DH_{argon}) diaphragms. The initial testing

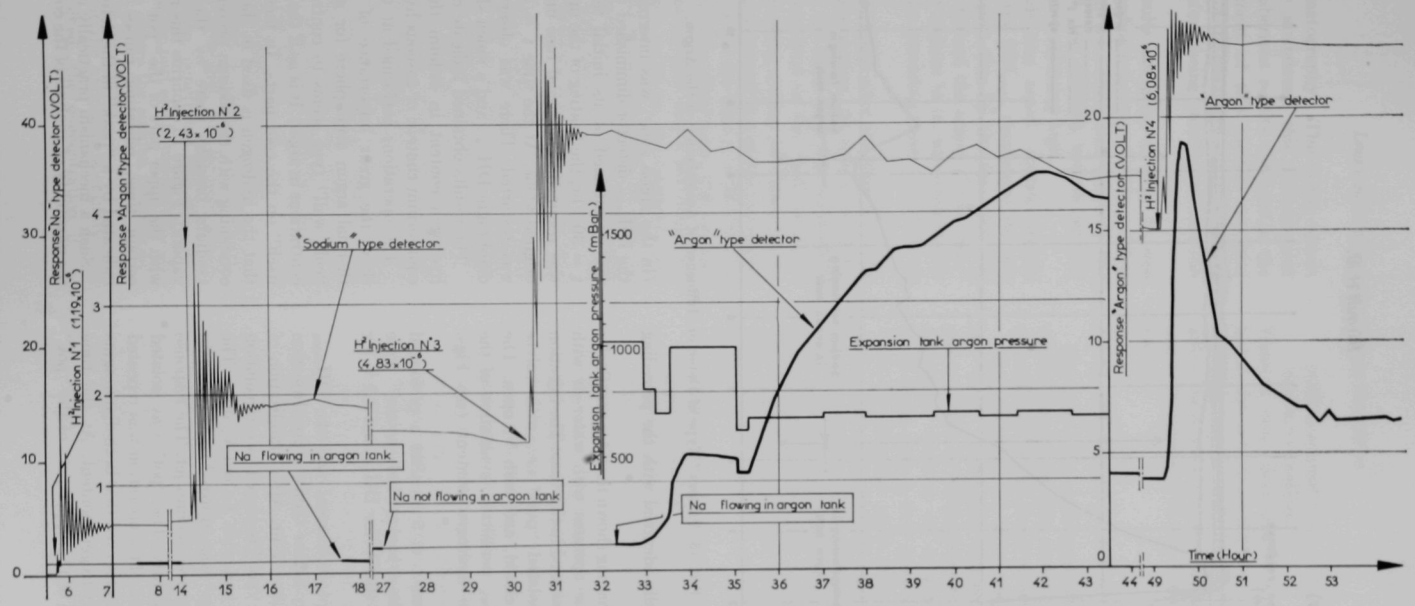

Fig. 14. Test No. 2 with "Argon" Type of Detector.

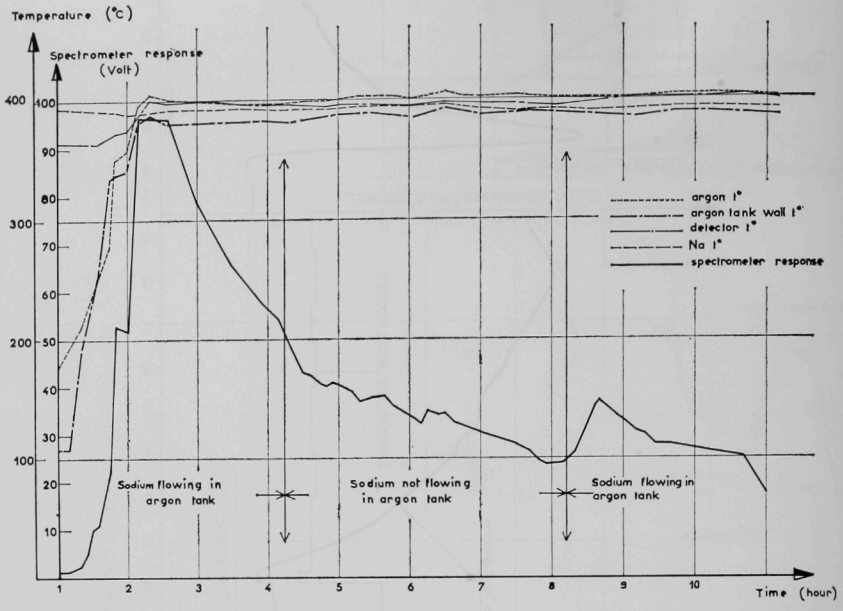

FIG. 15. "Argon" Type of Detector: Influence of Anisothermy of the Argon.

conditions were basically identical with the preceding ones.

The preceding tests having shown that it is practically indifferent whether one operates with water or with hydrogen; hydrogen was used in this case. The injection was made with an isolated "pot," i.e., with valves V_1, V_5, V_6, and V_7 closed, and with V_4 open. The observation with DH_{Na} permitted evaluation of the homogenization of the hydrogen content (see Figs. 11 and 12).

In Fig. 13, at a time t = 5 hr after a prolonged purification stage, the "background noises" were reduced to low values (0.2 V for DH_{Na} and 3.5 V for DH_{argon}).

The "pot" was kept isothermal and the DH_{argon} diaphragm at a slightly higher temperature. Injection was made at the time t = 7 hr. After stabilization of the sodium signal, the "pot" is placed into circulation with V_4 and V_5 closed and with V_6 and V_7 open. The sodium level in the "pot" was adjusted so as to obtain strong turbulence of the free sodium jet. The response of DH_{argon} increased slightly. The "pot" was isolated again for a new injection. This operation was repeated several times. It may be observed that both diaphragms recorded the rise in hydrogen content. At the time t = 28 hr, the heating of the upper part of the "pot" (in the argon zone) was interrupted; the response of the DH_{argon} detector diminished (while this diaphragm was maintained at its initial temperature). At time t = 30.5 hr, the heating of the upper part of the "pot" was resumed. The signal rose until it again found its original value. At the time t = 32.5 hr, the cold trap was restarted. There was observed a quick drop of diaphragm DH_{Na}, and a much slower one of DH_{argon}.

The results obtained indicate clearly that with each hydrogen content in sodium there corresponded an equilibrium content of gaseous hydrogen in argon.

The operations performed at the time t = 30.5 hr show the great importance of maintaining an isothermal argon atmosphere for a phenomenon of the "cold wall" type seems to control the hydrogen concentrations in argon. It is as if the hydrogen "condensed itself" on the cold parts. In fact, it may be believed that the hydrogen is fixed in the form of hydride, by combining with the sodium present in these cold zones (sodium brought there by the condensation of its vapors). Figure 15 confirms this result in another way: with the upper part of the "pot" remaining cold for a certain time, reheating causes hydrogen liberation, indicated by a "peak" in the detector.

Such a mechanism practically condemns in principle the possibility of analysis of the cover gases by sampling

(for instance by chromatography). This is the reason why, in phase 1, we abandoned this measurement method. In fact, the aberrant results obtained in the experimental development of this method are now explained. The sample of the gas taken was transformed during its cooling before being introduced into the chromatograph.

The test whose results are given in Fig. 14 was identical with the preceding one except for the position of the sodium level in the "circulation pot." In the first part of this test, the entering sodium jet was submerged, the sodium level being high.

The following result was noted: despite several successive injections, the DH_{argon} diaphragm did not react. One may interpret this by the fact that the diffusion of hydrogen toward the argon of the "pot," despite the renewal of sodium in it, was considerably smaller than during the preceding tests, for which we had a free sodium jet.

The maneuvers undertaken after the time t = 32.5 hr confirmed this interpretation. At time t = 33 hr, the argon pressure of the main loop was diminished. As a result, the sodium level in the "pot" dropped, which uncovered the entering sodium jet. Immediately, the response of DH_{argon} increased in a manner comparable with that of Fig. 14. At the time t = 33.5 hr, the argon pressure returned to its initial value. The response of DH_{argon} was blocked at once and a new stage was observed. At the time t = 35 hr, the operation performed at time t = 33 hr was repeated. At once the response of DH_{argon} began to increase until a stage was obtained comparable with those observed in Fig. 14, since, this time, the pressure was not brought back to its initial value.

It should be noted that during these tests the argon zone of the "pot" served as a receiver of hydrogen. We wanted to check the reversibility of the phenomenon and, to do this, at time 49.5 hr, a new injection was made. The initial conditions of this injection were different from the preceding ones: the "pot" was left in the circulation state (valve V_4 closed, and V_6 and V_7 open). The result observed was the following: the detector DH_{argon} showed a sharp rise followed by a very slow diminution, comparable with that observed at time t = 33 hr on Fig. 14.

This result may be interpreted in two ways:

1. During the injection, a "puff" of noncombined or nondissolved hydrogen, for instance in the form of an emulsion, penetrated into the "pot." The "pot" played the part of a liquid-gas separator and, thus, there occurs the sudden presence of a lot of hydrogen in the argon.
2. By assuming that the hydrogen is entirely combined and dissolved, the concentration in the sodium is greater than the equilibrium concentration in the sodium.

There is then liberation of hydrogen from sodium. Later, the inverse phenomenon occurs, since the concentration in the sodium has become equalized at a value lower than the equilibrium concentration; the excess of hydrogen in the argon is recombined with sodium.

I.3.2.2. Second-stage Tests: Water-steam Circuit Alone

The tests were performed with the previously described water loop. The model of the steam generator was replaced by the circuit shown in Fig. 10.

The conditions of these tests remained basically the same: isothermal temperature of pressurized water = 200 to 300°C; pressure = about 80 bars; no degassing, therefore no oxygen elimination; adjustment of pH value to 9 by ammonia injections.

The ferritic-steel pipes were subjected, before assembly, to a conventional leaching treatment. Before being introduced into water during the first test, these pipes were degassed under vacuum at 300°C, and their leaktightness was checked by helium mass spectrometry. Figure 16 gives the results of one of the tests performed. The following remarkable points should be noted:

1. At the first insertion into water, the ferritic-steel pipes liberated very high flows of hydrogen, corresponding, undoubtedly, to the initial intense corrosion due to the formation of a magnetite layer.
2. The subsequent protective role of the magnetite layer appears clearly: there is a quick decrease with time of the hydrogen flux. Furthermore, the variations of the pH of the water appear to have little effect on the diffusion flow.
3. It seems that the magnetite layer plays the role of a barrier for the diffusion of hydrogen (when it is of different origin than that from corrosion). Thus, injections of gaseous hydrogen directly into the water are indicated by an imperceptible rise of the signal of the spectrometer connected to the ferritic-steel pipes.
4. For the austenitic steels (and nickel) the phenomenon is distinctly different. There does not seem to be any protective layer analogous to the magnetite. The corrosion phenomenon goes on regularly. The gaseous hydrogen injected into the water diffuses without any apparent difficulty. These tests thus bring out the fact that "nascent" hydrogen produced by corrosion of the pipes is particularly apt to diffuse through the pipes. Besides, it seems that the ratio between the

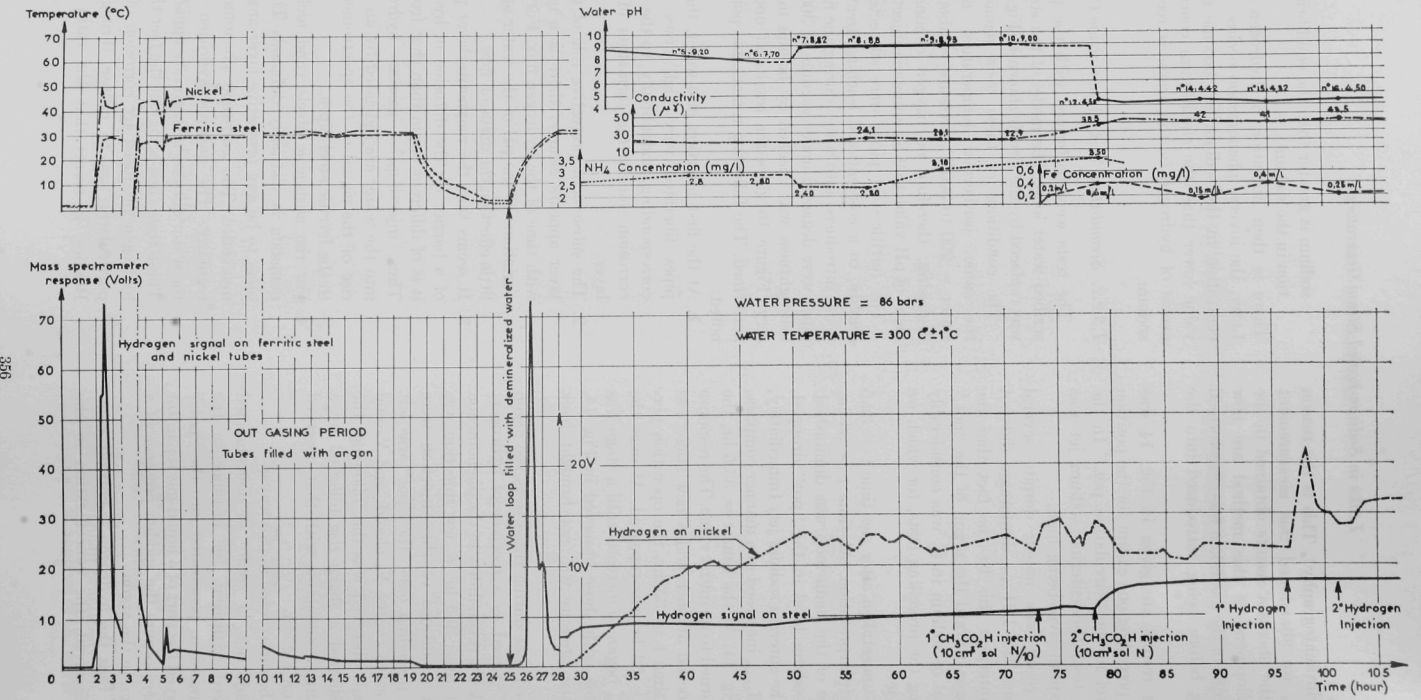

FIG. 16. Study of Diffusion of Aqueous Corrosion-generated Hydrogen.

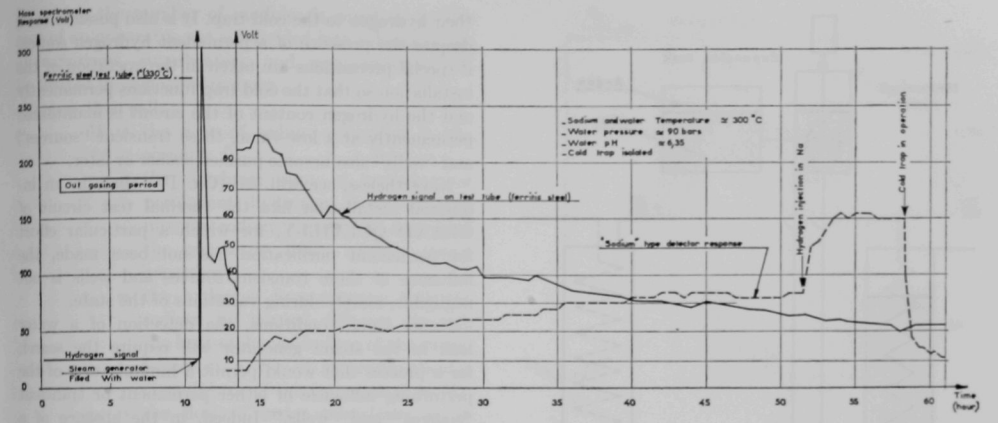

FIG. 17. Sodium-loop Contamination by Aqueous Corrosion-generated Hydrogen.

diffusing hydrogen and the hydrogen dissolved in the water is very high.

Thus, it should be assumed that the steam generator, in the absence of true leaks, constitutes a permanent hydrogen source for the sodium circuit.

I.3.2.3. Third-stage Tests: Sodium and Water-steam Circuits Connected by the Intermediary of the Steam Generator

This test was intended essentially to check that the "normal diffusion" hydrogen due to the aqueous corrosion of steels is actually found in the sodium. It was also desired to check whether the presence of sodium, in the place of vacuum in the experiments of the preceding paragraph, changed the results.

The test was performed in the installation described in ¶1. However, on the water loop, there was mounted, in series, ferritic-steel control pipes similar to the pipes constituting the exchange surface of the steam generator. These pipes were placed under vacuum (and connected to the spectrometer) by their outside face, like in the stage described previously. One could then compare, at any time, the hydrogen flow from the control pipes to the hydrogen flow entering into the sodium circuit and calculated from the sodium detector.

Figure 17 gives the general results of this test. After calculation, the hydrogen flow rate per unit of control pipe area and of steam-generator area proved to be identical within about 5 %.

In a test phase that is being prepared, the same installation should permit studying the detection of real microleaks. The pipe constituting the heat-exchange surface will include a real microleak (manufacturing defect, for instance). Its evolution will be followed in time, from the triple point of view of the detection of the leak proper, the study of kinetics of leak evolution, and the influence of the leak on the environment (corrosion, for instance).

CHAPTER II

THEORETICAL STUDY OF THE DETECTION PROCESSES OF A WATER LEAK IN A STEAM GENERATOR AND OF DETECTION SENSITIVITY

II.1. Status of the Problem

On the basis of the main experimental results described in Ch. I, it is possible to imagine, qualitatively at first, the principal mechanisms involved in the process of detection of a water leak.

Let us consider, for instance, the secondary circuit of the reactor, shown schematically in Fig. 18. Although simplified with respect to reality, this circuit nevertheless includes the essential constituent components that are ordinarily encountered. One may assume in such a circuit the existence:

1) of a permanent hydrogen "source" composed of the steam generator which, either by the diffusion of hydrogen due to corrosion or by water microleakage, permits a continuous flow of hydrogen into the sodium;
2) of a permanent hydrogen "well" composed of the cold trap of the secondary circuit (and, possibly even, by that of the primary circuit, thanks to possible hydrogen diffusion through the intermediate heat exchanger);
3) of various transient hydrogen "sources" and "wells" localized in the various tanks, including

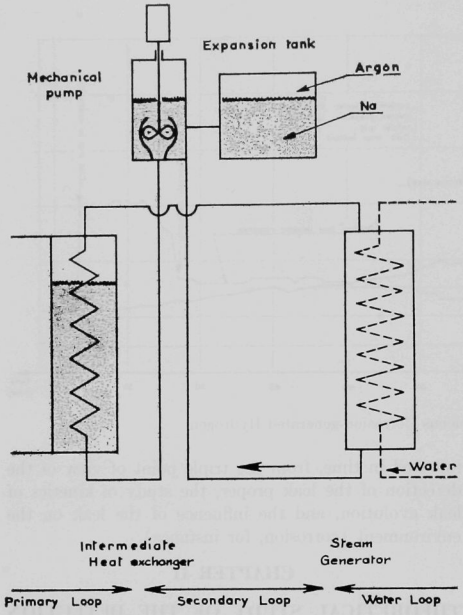

FIG. 18. Scheme of a Power Plant Secondary Circuit.

a free surface (expansion tank, intermediate exchanger according to its design, etc.) or including dead zones of more or less static sodium (bypass and various tanks, etc.). These capacities either trap or liberate hydrogen, in quantities, flows, and durations that depend on a large number of factors such as, in particular, those that the previously described experiments have brought out: tank volumes, argon-zone volumes, degree of agitation of free surfaces, degree of anisothermy of static-sodium zones or of argon zones, etc. In addition to these phenomena, there should be added the operational conditions of the whole installation (transient states of power, temperature, and flow), of which the consequences are large variations in tank levels and the placing into circulation of previously static sodium, loaded with a hydrogen content that is obviously very different from that of the main loop itself.

However, it should be remarked that these "sources" and "wells," which are transient, really play a part only because there exists elsewhere a permanent hydrogen source capable of supplying these "capacities" constantly. One may, in fact, believe that, in the contrary case, these capacities should sooner or later lose their hydrogen to the cold trap. It is also possible that, despite the presence of a permanent hydrogen source, if special precautions are taken in the operation of the installation so that the cold trap functions permanently and the hydrogen content of the circuit is maintained permanently at a low value, these transient "sources" and "wells" also become purified sooner or later.

Nevertheless, we will see (Ch. IV) that, in an industrial installation like the thermal test circuit of GRAND QUEVILLY, for which a particular effort for permanent purification has not been made, the influence of these transient sources and wells is not negligible, mainly during variations of the state.

Under these conditions, the detection of a water leak in the steam generator will require the search for a process that would permit a minimization of the perturbing influence of either permanent or transient "sources" and "wells." Indeed, in the absence of a leak, they might get one to believe in their existence, or vice versa; in the case of a leak, they might hinder its detection or even make it completely impossible.

In what follows, it is proposed to evaluate the detection sensitivity (the smallest leak detectable in a given installation) as a function of parameters defining this sensitivity.

II.2. Simplification of the Problem: The Types of Steam Generators Studied

Taking into account the experimental work described previously and the remarks made in the preceding paragraph for the whole secondary circuit, one may consider two cases of steam generators:

1) The steam generator does not have any free surface nor any large dead zone in which the sodium is likely to stagnate.
2) The generator does not meet the preceding condition. For instance, it has a free surface. In the latter case, a general theoretical study of the problem is difficult a priori; each device is a special case requiring a special study. Furthermore, it will be noted that the present designs of steam generators in France are all of the first category, and we will therefore limit our calculations to it.

In addition, we assume:

1) The steam generator is subdivided into three subassemblies: superheater, resuperheater, and vaporizer;
2) Each subassembly has itself a modular structure, i.e., it is subdivided into several identical items supplied in parallel by the same sodium manifold (see Fig. 19).

The case of a subassembly with a nonmodular (unitary) structure will therefore form a special case

for which the number of modules is equal to 1. The case of an apparatus not subdivided into subassemblies of vaporizers, superheaters, and resuperheaters will be treated in analogous manner.

Let us then call:

M = the mass of sodium contained in the circuit;

ϵ_H = the algebraic sum of transient or permanent hydrogen flows entering into the sodium circuit, but outside of the geometric limits of the steam generator;

q_{Hi} = the hydrogen flow entering into the sodium by normal diffusion through the heat-exchange surface of the superheater (i = S), of the resuperheater (i = R), or of the vaporizer (i = V);

q_{fi} = the flow of water microleaks or of steam in one of these subassemblies;

C, C_i, C_f = hydrogen concentration in sodium, respectively, at the entry of the steam generator, at the outlet of the different devices, and at the outlet of the cold trap;

Q_{pf} = sodium flow in the cold trap;

Q_i = sodium flow in the different devices.

Because of the relative slowness of hydrogen storage phenomena by the transient "sources" and "wells," one may, by simplification, assume that the concentration at the outlet of the steam generator, for instance, is governed by eq. (1) below, which expresses the conservation of the hydrogen mass. In the same way, between concentration at the intake and concentration at the outlet, we have equations (2), (3), and (4) for the different subassemblies:

$$\Sigma \frac{1}{g} q_{fi} + \epsilon_H + \Sigma q_{Hi} - (C_V - C_f) Q_{pf} = M \frac{dC_V}{dt}; \quad (1)$$

$$C_V = C + \frac{[\Sigma q_{Hi} + \Sigma(q_{fi}/g)]}{Q_V}; \quad (2)$$

$$C_R = C + \frac{[q_{HR} + (q_{fR}/g)]}{Q_R}; \quad (3)$$

$$C_S = C + \frac{[q_{HS} + (q_{fS}/g)]}{Q_S}. \quad (4)$$

II.3. The Proposed Detection Processes

It is possible to envisage a large variety of detection processes. We have chosen three principal ones, which we call:

1) process by accumulation;
2) process by instantaneous balance;
3) process by comparison.

It will be noted that the first two processes are applicable to steam generators of either modular or unitary type. The third one is applicable only to modular generators.

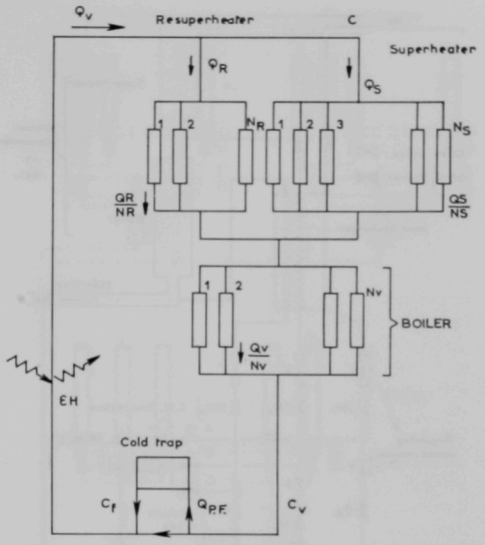

FIG. 19. Arrangement of the Steam Generator and Secondary Circuit for Theoretical Studies.

II.3.1. Process by Accumulation

At a point of the secondary circuit (for instance, at the generator outlet) is placed a single hydrogen detector (or a single stage for sodium sampling directed to a detector). At this point, the hydrogen concentration is governed by eq. (1), in which the various terms are poorly known functions of time. A knowledge of C_V can permit the detection of a leak only with difficulty unless the leak has a strong flow. To diminish the uncertainty concerning the different terms, a convenient method of procedure is:

1) to cancel those terms which it is possible to neglect in practice; this is the case of the term linked with the cold trap ($Q_{pf} = 0$);
2) to minimize the other terms if possible: this is the case for ϵ_H when one maintains the operational state of the installation as stable as possible (see Ch. I). Under these conditions, during a time T, the concentration passes from C_V to C'_V, so that

$$C'_V - C_V = \frac{1}{M} \int_0^T \left(\Sigma \frac{1}{g} q_{fi} + \Sigma q_{Hi} + \epsilon_H \right) dt$$

or, by assuming that the different terms are then constant during that time,

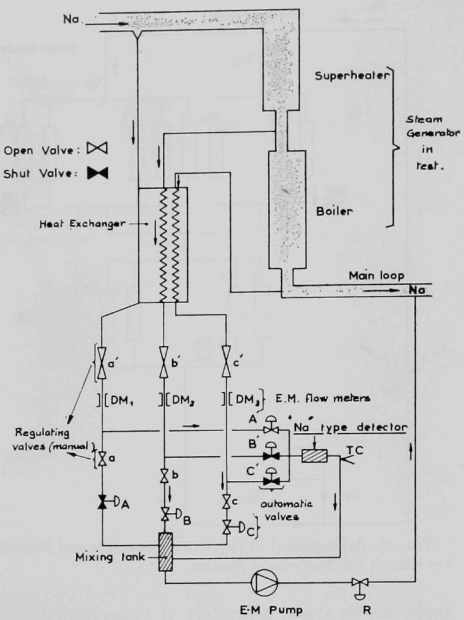

FIG. 20. Leak-detection Method by "Instantaneous Balance." "Chatou 1-MW Test Facility" Detection Device.

$$C'_V - C_V = \Delta_t C_V = T\left(\Sigma \frac{1}{g} q_{fi} + \Sigma q_{Hi} + \epsilon_H\right) t .$$

The method will consist in comparing this expression (with leakage) at time t with that obtained in the absence of leakage at another time t':

$$\Delta_{C'} C_V = T(\Sigma q_{Hi} + \epsilon_H) t'.$$

In practice, one compares the slopes of the two curves of concentration evolution. However, it seems that the smallest detectable leak will depend mainly on the terms ϵ_H and q_{Hi}, which enter directly into the balance.

We will see in Ch. IV a tentative application of this method for the evaluation of the term Σq_{Hi}, which will bring out the difficulties of this method.

II.3.2. Process by Instantaneous Balance

In order to eliminate the influence of the term ϵ_H, a method is employed in which a detector is placed at the inlet and another at the outlet of the steam generator (or of a subassembly), or sodium is sampled at each of these points and the samples directed to the same detector.

The concentrations between these different points are given directly by the equations (2), (3), and (4), whence the terms external to the steam generator are eliminated. The detector sensitivity depends on q_{Hi} nevertheless.

This method is probably the most sensitive of the methods applicable to a nonmodular steam generator.

This is why we have based on this principle the hydrogen-detection device of the 1.5-MW steam-generator testing circuit of CHATOU (installation described elsewhere). The operation of this leak-detection device is shown in Fig. 20. Samples of sodium are taken permanently and at constant flow at different points of the steam generator (for instance: sodium intake, superheater outlet, and vaporizer outlet). The samples at different temperatures are brought to a basically identical temperature, by means of an antimethodic heat exchanger with large exchange surface. The flow taken at the intake of the generator serves to reheat the colder sodium taken at the outlet. Then, the samples are directed one after another, by a set of valves controlled sequentially, to the hydrogen detector.

With the samples thus brought to the same temperature and compared to one another in the same detector, the signals transmitted by the spectrometer are immediately usable in order to judge the existence of a leak.

Taking into account the characteristics of the 1.5-MW loop, we hope, through the use of this device in the course of construction, to reach a detection sensitivity on the order of mg/sec.

II.3.3. "Process by Comparison"

This method, applicable only to a modular apparatus, is the most sensitive one theoretically. This is why it has been considered for industrial tryout on the steam-generator testing installation of 50 MWt of RENARDIERES ("CGVS 50 MW) (installation described elsewhere). This is also why we have tried, for this method, to refine our calculations in order to evaluate its sensitivity as accurately as possible. In addition, these calculations, for this and for other methods, bring out important parameters quantitatively.

Figure 21 gives the general principle of the devices, of which the operation is as follows:

II.3.3.1. General Operation

The sodium samples taken at the outlet of N_i modules of the same superheater subassembly (i = S), resuperheater (i = R), or evaporator (i = V) are, firstly, assembled in P_i groups (of N_i/P_i samples each). Through a set of appropriate valves (or a selector), the sodium of each of these groups is directed succes-

sively to the hydrogen detector. Then, the different sodium passages are reinjected into the main circuit.

II.3.3.2. Operation in the Absence of Leakage

Because of the "normal diffusion" of corrosion hydrogen, the sodium, as it progresses along the heat-exchange surface, takes up more and more hydrogen. The hydrogen flow diffused by a unit of heat-exchange surface depends on the temperature of the surface element in question. Consequently, at corresponding points of exchange surface in two modules in parallel, the hydrogen content in the sodium should be the same.

Under these conditions, it can be seen that, at different sampling points, at the outlet of the same subassembly (superheater, resuperheater, or evaporator), there should be the same hydrogen content.

II.3.3.3. Operation in the Presence of Leakage

If a leak appears in a module, an increase in hydrogen content occurs at the module outlet. After a sodium sample is taken and mixed as it comes from the leaking module with sodium samples coming from the non-leaking modules, the hydrogen content will increase for the sample group corresponding to the defective model. When scrutinized, the detector response will show a positive variation of the content at each passage by the direction corresponding to the group in question.

According to this measuring scheme, the smallest detectable leak will be the one causing an appreciable variation of the detector response with respect to the mean level (which we call "background noise"). This mean reference level is given, during scrutiny, by the response of the detector when it is connected to the nonleaking modules.

II.3.3.4. Detection Sensitivity

Equations (2), (3), and (4) show that, by this method, the influence of the term q_{Hi} can be eliminated systematically. It is therefore more sensitive than the balance method, which requires knowledge of q_{Hi}.

One cannot, however, assume that, in practice, the smallest variation of measurable concentration is independent of the mean value of this concentration. In fact, the measurement is made with a certain measuring accuracy and, consequently, the smallest measurable concentration variation is of the form $\Delta C = \beta C$.

In fact, the problem may be decomposed in two:

1) *Sodium circuit aspect:* It may be assumed that, in a given circuit, the smallest measurable concentration variation has the form $\Delta C = \beta C$, where β has a double significance:

a) the concentrations from the different sampling points are not absolutely identical because of various uncertainties concerning the geometry of the devices, the flows, the temperatures, etc. The coefficient β must take these uncertainties into account.

b) β is given the significance of a safety factor, i.e., it is assumed that there is a leak if a significant concentration variation is recorded (for instance, equal to 50% of the mean observed concentration).

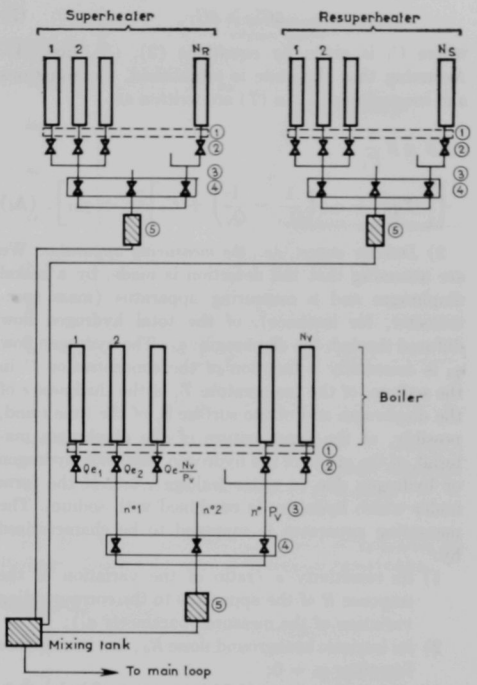

FIG. 21. Leak-detection Method by Comparison. 1. EM flowmeter; 2. Regulating valves (manual); 3. Mixing pipes; 4. Automatic valves (or selector); 5. Hydrogen detector.

Let us then call ΔC_i the concentration variation of a module outlet in which a leak q_{fi} has appeared. We have

$$q_{fi} = 9\Delta C_i \, (Q_{i/N_i}). \tag{5}$$

After mixing the sodium sample taken from this leaking model with the sodium samples coming from non-leaking modules of the same group, the concentration at the detector level, when it is connected to the same sample group, varies by $\Delta C'_i$ so that

$$\Delta C'_i = \Delta C_i \left(\frac{P_i}{N_i}\right). \tag{6}$$

With the preceding assumptions, this concentration variation will be detected if

$$\Delta C'_i \geqslant \beta C_i , \qquad (7)$$

where C_i is given by equations (2), (3), and (4). Assuming that the state is established, the equations and inequalities (1) to (7) are written as

$$q_{fi} \geqslant g\, \beta \frac{1}{P_i} \cdot \left[\left[(\Sigma q_{Hi} + \epsilon_H) \left(\frac{1}{Q_{pf}} - \frac{1}{Q_v} \right) + C_f \right] Q_i + q_{Hi} \right]. \qquad (A_i)$$

2) *Detector aspect, i.e., the measuring apparatus:* We are assuming that the detection is made, by a nickel diaphragm and a measuring apparatus (mass spectrometer, for instance), of the total hydrogen flow diffused through the diaphragm: q_d. The hydrogen flow q_d is essentially a function of the concentration C in the sodium, of the temperature T, of the thickness e of the diaphragm and of the surface S, of the time t and, possibly, of the exact nature of the diaphragm material, of the origin of the hydrogen (diffusion hydrogen or hydrogen due to water leakage), i.e., of the form under which hydrogen is combined with sodium. The measuring apparatus is supposed to be characterized by:

1) its sensitivity σ (ratio of the variation of the response R of the apparatus to the corresponding variation of the measured parameter q_d);
2) its intrinsic background noise R_0, i.e., its response for a flow $q_d = 0$;
3) the smallest appreciable response variation ΔR, which may be assumed to have the form $\Delta R = \alpha R_0$.

Under these conditions, the measuring apparatus capable of appreciating the leak q_{Hi} must meet the following conditions [with $q_d = f(T, C, e, t, S)$ and $\Delta C'_i$ defined previously]:

$$\sigma \Delta q_d \geqslant \alpha R_0 \text{ with } \Delta q_d = \frac{\partial f}{\partial C} \Delta C'_i ,$$

whence

$$\sigma \frac{\partial f}{\partial C} \Delta C'_i \geqslant \alpha R_0 . \qquad (B_i)$$

The inequalities A_i and B_i define the problem completely as a rule. Indeed, if one assumes known the maximum leak acceptable in a given apparatus, or q_{fi}, the inequalities A_i will, for an installation characterized by Q_i, q_{Hi}, C_f, Q_{pf}, ϵ_H, and β, permit us to calculate P_i. The q_{fi} then permits a dimensioning of the diaphragm, assuming known the characteristics of the spectrometer or of the apparatus measuring the flow $q_d(R_0, \sigma, \alpha)$. It may be that the problem in this form does not have a solution even if $P_i = N_i$. In that case, it means that the size of the modules is excessive or that the performance characteristics of the cold trap (Q_{pf}, C_f) are insufficient, etc.

It should be added that these inequalities bring out the main parameters of the problem. Among them, some are linked to the dimensional characteristics of the installation, others are unknown (or poorly known) physical parameters [C_f, q_{Hi}, ϵ, the function $f(T, C, e, t, S)$]. Therefore the study of these parameters was undertaken and is covered in the following chapter.

CHAPTER III

QUANTITATIVE EXPERIMENTAL STUDY OF THE MAIN PHYSICAL PARAMETERS ENTERING INTO THE DETECTION PROCESS

To try to provide responses to the principal questions raised in the preceding chapter, we have on the one hand tried to express the results of the tests described in Ch. I in a quantitative form and, on the other hand, have undertaken new tests intended for the specific study of each parameter.

For the sodium part, these latter tests have been performed in the installation described in Ch. I and in another testing installation of far larger capacity (300 kg) described in detail in Ref. (5). In the latter, a hydrogen- and water-injection circuit (see Fig. 5) has been put in place, as well as a bypass for detector placement. This bypass differs from that of Fig. 2 only by the presence, at the inlet, of a heat exchanger-economizer followed by an electric heater that permits the bypass to be maintained at a temperature different from the rest of the main loop.

For the water-steam part, tests were performed in the loop described in Ch. I and with the help of a thermal testing installation with high steam pressure, "IHPV" of the CHATOU testing center. Figure 22 shows the scheme of the testing device used in this case.

Quantitative measurements were made in every case by calibrating the spectrometers by means of hydrogen calibration leaks. Some measurements were made with a Pirani gauge and "pressure rises."

The particular points that have been studied and the results obtained are now described.

III.1. "Argon" Type of Detector

Measurement of diffused-hydrogen flux (flow per unit area) for a nickel diaphragm, 0.2 mm thick, is a function of the hydrogen concentration in the sodium after injection of gaseous hydrogen. The temperature conditions are the following: isothermal temperature of the loop is 400°C; temperature of the detector and of the isothermal argon tank is 400°C. The equilibrium partial pressure of hydrogen in the argon and solubility in the sodium were reached. The results are given in Fig. 23.

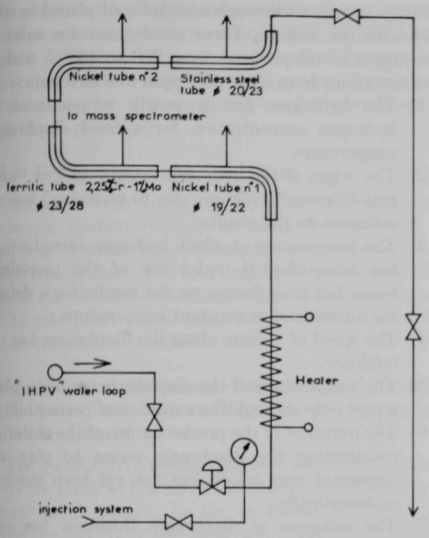

FIG. 22. Study of Corrosion-generated Hydrogen Diffusion with the IHPV Test Section.

III.2. "Sodium" Type of Detector

III.2.1 Measurement of diffused-hydrogen flux for 2 different nickel diaphragms (M_1 and M_2), 0.2 mm thick, is a function of hydrogen concentration in the sodium after injection of gaseous hydrogen or of steam. The temperature conditions were the following for the two detectors studied:

III.2.1.1. The sodium temperature of the main loop was 400°C; the temperature of detector M_1 was identical.

III.2.1.2. The sodium temperature of the main loop was 350°C; the temperature of detector M_2 was 400°C.

III.2.1.3. The sodium temperature of the main loop was 250°C; the temperature of the detector M_2 was 400°C.

The results are given in Fig. 24. No influence of sodium speed was noted in the range of Reynolds numbers between 1000 and 7000. This result confirms that observed by Subbotin[3] and is given below in Fig. 42.

On the other hand, a marked difference was noted between the results obtained with the different diaphragms. These diaphragms came from different nickel heats and were, besides, in different work-hardened condition. This might account for the results noted in Fig. 24.

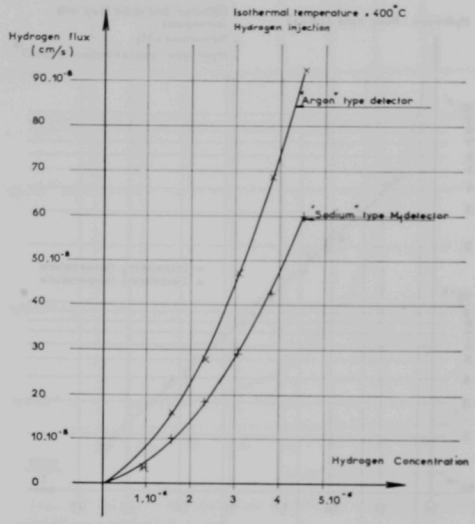

FIG. 23. "Argon" and "Sodium" Detector Responses for Hydrogen Flux as a Function of Hydrogen Concentration.

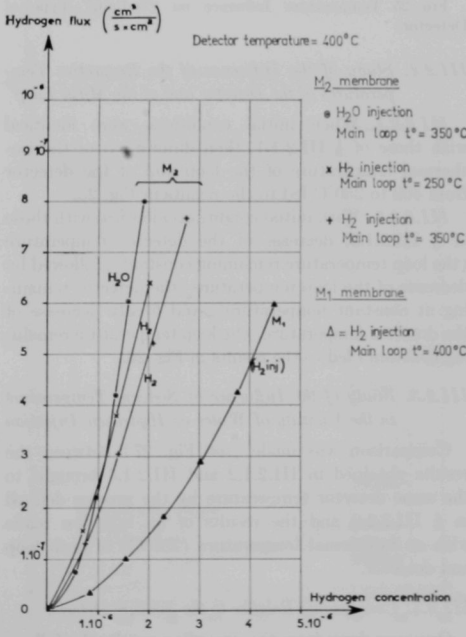

FIG. 24. "Sodium Type" Detector Responses for Hydrogen Flux as a Function of Hydrogen Concentration.

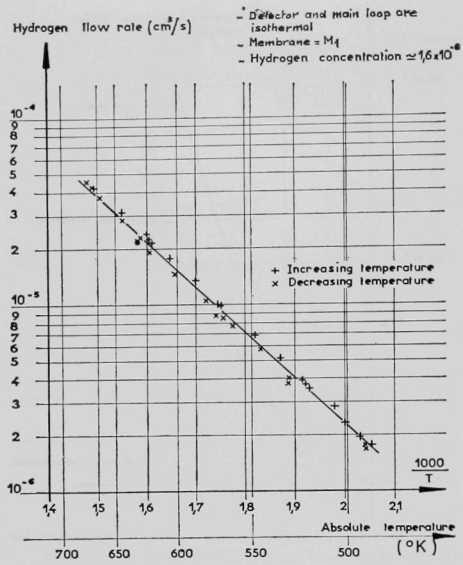

FIG. 25. Temperature Influence on "Sodium" Type of Detector.

III.2.2. Study of the Influence of the Respective Temperatures of the Detector and of the Main Loop

III.2.2.1. When initial conditions were identical with those of § III.2.1.1, then diminution of the isothermal temperature of the loop and of the detector from 400 to 250°C led to the results in Fig. 25.

III.2.2.2. With initial conditions identical with those of § III.2.1.2, decrease of the detector temperature (the loop temperature remaining constant), followed by decrease of the loop temperature (the detector remaining at constant temperature), and finally decrease of the detector temperature (the loop temperature remaining constant) led to the results in Fig. 26.

III.2.3. Study of the Influence of Sodium Temperature in the Vicinity of Water or Hydrogen Injection

Comparison was made (see Fig. 27) between the results obtained in III.2.1.2 and III.2.1.3 brought to the same detector temperature by the process defined in § III.2.2.2 and the results of an injection made with an isothermal temperature (250°C) of both loop and detector.

III.2.4. Conclusions Relative to the Sodium Detector

One may draw from the preceding results the following conclusions relative to the diffusion of hydrogen in solution in sodium through a nickel wall placed in contact with the sodium. These conclusions are valid in the ranges of temperature from 250 to 400°C, and in concentrations from a few 10^{-2} ppm to 4 or 5 ppm:

1) The hydrogen flux is nearly proportional to hydrogen concentration for a fixed diaphragm temperature.
2) The origin of the hydrogen (steam, gas, or "normal diffusion" hydrogen due to corrosion) has no influence on the results.
3) The temperature at which hydrogen introduction has been effected under one of the preceding forms has no influence on the results for a detector maintained at constant temperature.
4) The speed of sodium along the diaphragm has no influence.
5) The temperature of the diaphragm seems to play a part only through the variation of permeability.
6) The influence of the precise nature of the material constituting the diaphragm seems to play an important part which has not yet been studied systematically.
7) The influence of diaphragm thickness has not yet been studied.

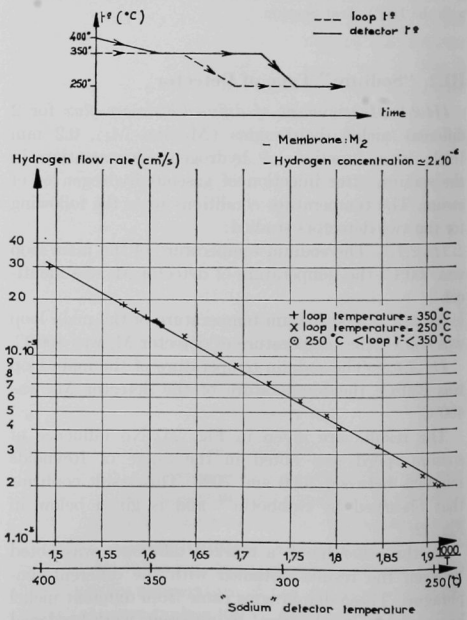

FIG. 26. Temperature Influence on "Sodium" Type at Detector.

In addition, the plugging-temperature measurements, which were carried out in correlation with the hydrogen content measurements, seem to show that this apparatus is also sensitive only to hydrogen, and it is possible to formulate for this apparatus conclusions identical with those preceding.

III.3. Performance of a Cold Trap

Attempts were made to measure the minimum hydrogen content capable of being reached with a cold trap of which the coldest point is maintained at a given temperature. The cold trap, described in Ref. (5), was of the air-cooled circulation type. The temperature of its cold point varied from 101 to 130°C. Figure 28 shows the results obtained.

III.4. Flow of Hydrogen Diffiused per Surface Unit of Steam Generator (Corrosion Hydrogen)

The quantitative results obtained during the various tests are given in Fig. 29. The results are relative, for a given metal sample, to the evolution with time of hydrogen flux (or of corrosion rate), beginning with the

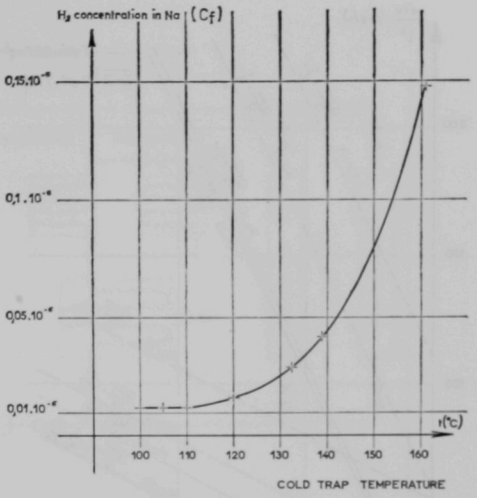

FIG. 28. Ability of Cold Trap to Reduce Hydrogen Concentration in a Sodium Loop.

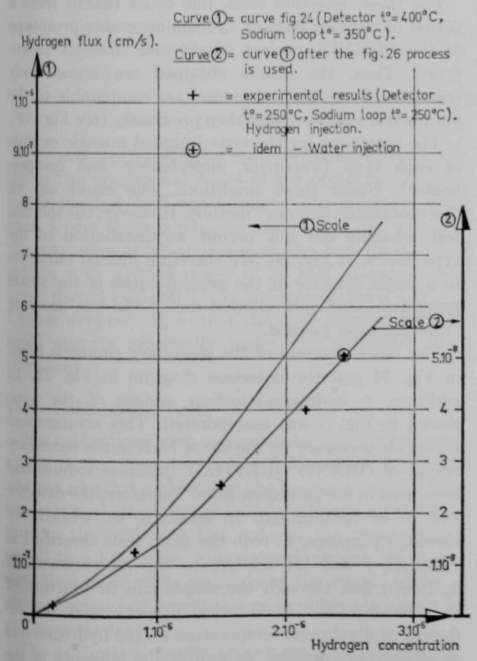

FIG. 27. Influence of Injection Temperature.

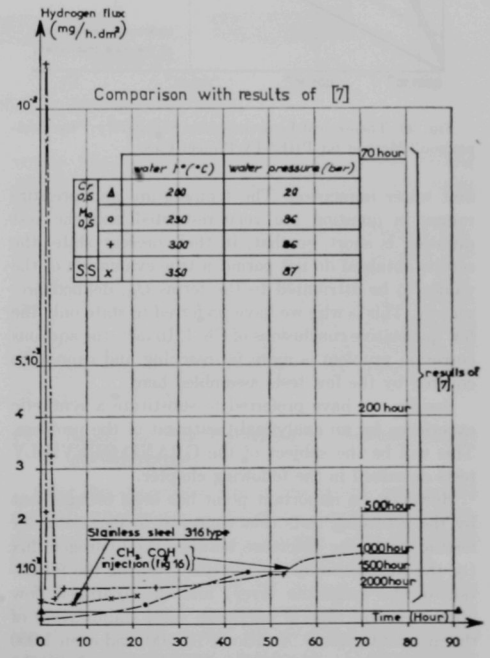

FIG. 29. Aqueous Corrosion-generated Hydrogen Flux. (Tests performed in facilities of Fig. 10 and Fig. 22.)

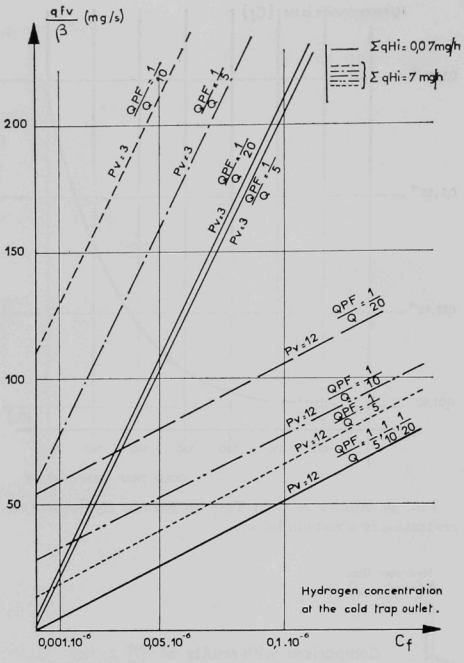

FIG. 30. Theoretical Leak-detection Sensitivity: "by Comparison" Method for PHENIX Project Case.

first water immersion. The temperature and pressure ranges in question are very restricted and the test duration is short, so that, in their present state, the results obtained do not permit a true evaluation of the values to be attributed to the terms Q_{Hi} defined previously. This is why we have preferred to state only the few qualitative conclusions of Ch. I. In fact, the aqueous corrosion problem is more far-reaching and cannot be covered by the few tests assembled here.

Besides, we have preferred to substitute a synthetic experience for an analytical treatment of the problem. This will be the subject of the GRAND QUEVILLY tests described in the following chapter.

However, an important point has been brought out by the preceding tests that concerns, in particular for ferritic steels, the difference between the hydrogen flux (or the corrosion rate) at the start (during the formation of the magnetite layer) and the hydrogen flow after a certain time of operation (and stabilization of the magnetite layer). A ratio of 10, 100, and even 1,000 may exist between these flows. In order to evaluate the influence of such a disparity of flows, a parametric study of the minimum detectable leak in the steam generators of the PHENIX project (the so-called "comparison method") was conducted by considering the Σq_{Hi} flows varying from 1 to 100 (see Fig. 30). It appears clearly in Fig. 30 that the conditions for detection of a given leak may be profoundly modified in the installation between its starting and its normal operation, according to the real importance of the term Σq_{Hi}.

CHAPTER IV

FIRST INDUSTRIAL TESTS AT GRAND QUEVILLY

In order to try to obtain an order of magnitude for "normal" hydrogen flows diffused through the exchange surface of a steam generator, i.e., an evaluation of the parameter q_{Hi} (which can play an important part), tests were undertaken, in cooperation with the C.E.A., in the thermal testing installation of GRAND QUEVILLY.[6]

In addition, the more industrial dimensions of this circuit should permit evaluation of the real importance in such a circuit of parameters other than q_{Hi} that the previous analytical studies have brought out.

For these detection tests, one could benefit from a period of thermal tests of a steam-generator prototype of the PHENIX project (Stein and Roubaix prototype). Thus, the results obtained are immediately transposable to the project and are comparable to the parametric studies undertaken previously (see Fig. 30).

The prototype for the tests included a single module of each type (vaporizer, superheater, and resuperheater). Under these conditions, one could use an "instantaneous balance" method. However, the thermal test schedule did not permit an installation of the type shown in Fig. 20. We therefore limited ourselves to a single detector at the general outlet of the steam generator. This only allowed use of the less accurate "accumulation method."

The block diagram of the secondary circuit is given in Fig. 31 and the detection diagram in Fig. 32. In addition, a hydrogen-injection system of the type shown in Fig. 5 was incorporated. This arrangement was made necessary by the use of NaK in the secondary circuit of GRAND QUEVILLY, whereas sodium had been used in the preceding tests. Therefore, the detector had to be recalibrated. In addition, we wished, for checking purposes, to redo the main tests described in Chapters I and III relative to the measurement of hydrogen flux through the diaphragm in function of the concentration (calibration proper), and the influence of diaphragm temperature on the hydrogen flux at given concentration, as well as the influence of the speed at given concentration and temperature.

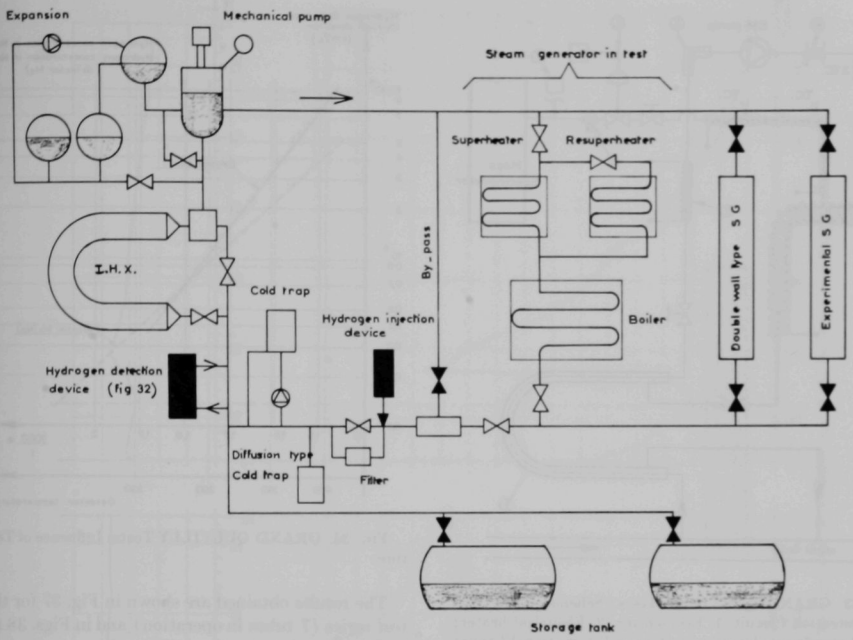

FIG. 31. GRAND QUEVILLY Test Facility (Secondary NaK Loop).

Two successive test series were performed corresponding to two operational states of the prototype generator. In the first, all 7 water tubes of the generator were used. Under these conditions and taking into account the maximum thermal power of the test circuit, the module with a rated power of 15 MW operated only under partial load (30%). In the second series, 4 of the 7 tubes were cut off, so that the three remaining tubes could operate practically under the maximum load conditions.

IV.1. Calibration Tests

The calibrations were conducted by a procedure very similar to that described in Ch. I. The steam generator was not supplied with water; the secondary circuit was basically isothermal; before hydrogen injection, purification by the cold trap had reduced the "background noise" to a low value. Successive hydrogen injections were then made while maintaining the circuit under a stable operational conditions as possible (in order to minimize the term ϵ).

The calibration results proper are given in Fig. 33. The influence of the detector temperature is brought out in Fig. 34. Figure 35 gives the general testing diagram and Figs. 41 and 42 the results of the study of speed influence.

During these tests, measurements of plugging temperature were made by means of the manual-type plugging indicator in the secondary circuit. The plugging temperature is plotted as a function of hydrogen content in Fig. 36, which shows that the plugging indicator is capable of giving a valid indication of hydrogen content up to contents on the order of a few 10^{-1} ppm (with NaK).

IV.2. Study of NaK Pollution by Normal Diffusion Hydrogen

After the steam generator is placed into service and a circuit stabilization as perfect as possible is obtained, the cold trap is stopped and isolated. Then the rise of hydrogen signal is observed as a function of time.

If we assume that there are no leaks in the steam generator (one check of this assumption was to vary the steam pressure during the test) and that the term ϵ is sufficiently small and constant, eq. (1) gives directly the flow of hydrogen, Σq_{Hi}, entering into the circuit.

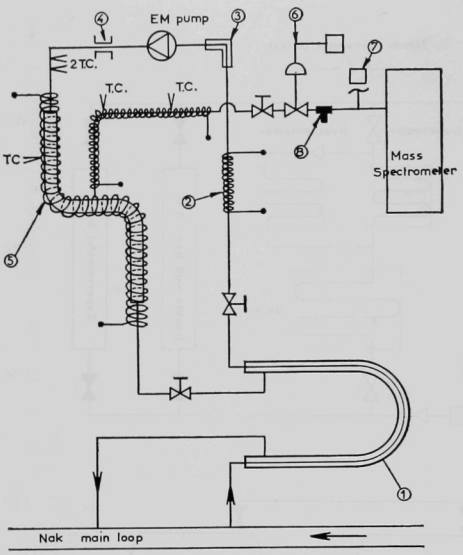

FIG. 32. GRAND QUEVILLY Tests: Scheme of the Hydrogen-detection Circuit. 1. Economizer; 2. Electrical heater; 3. Nickel membrane detector ("Atomics International" type) 4. EM flow meter 5. Sodium type nickel membrane detector (Fig. 3); 6. Automatic valve; 7. Pirani gauge; 8. Sodium leak detector.

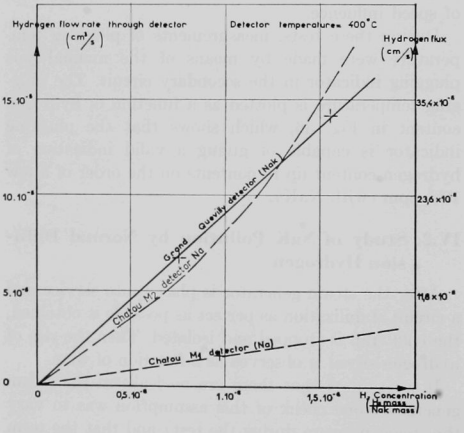

FIG. 33. GRAND QUEVILLY Tests: Hydrogen Flux *vs* Hydrogen Concentration. Comparison with Chatou M_1 and M_2 detector in sodium.

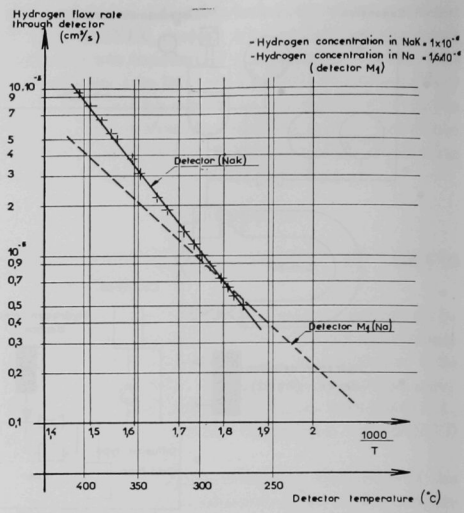

FIG. 34. GRAND QUEVILLY Tests: Influence of Temperature.

The results obtained are shown in Fig. 37 for the first test series (7 tubes in operation) and in Figs. 38 and 39 for the second test series (3 tubes in operation).

This last series was itself conducted twice. The first, short-duration series was ended when a quick increase in the rate of hydrogen seemed to occur. In the second, intended to confirm or to invalidate these results, the tests were of longer duration, but the operational states of the installation were very variable. There was a complex evolution of hydrogen content. One should note in particular in Fig. 39 the decrease in hydrogen content during the period of power drop. Translated into diffusion hydrogen flow, this negative evolution of the concentration brings out negative diffusion flows. In fact, it is more likely that this evolution is due to the intervention of the term ϵ. A hydrogen "well" has been "opened" during the power drop (the "well" may be due to the cooling of the pipes or of the static tanks).

If one considers only the periods during which relative stability of the circuit was maintained, it is found that the normal hydrogen flow Σq_{Hi} oscillates between 10 and 30 mg/hr. However, it will be noted in the first test series and at the very beginning of the tests, flows Σq_{Hi} were practically 10 times higher (a peak at 400 mg/hr). This phenomenon corresponds to the observations made in Chapters I and III.

It should be noted that the steam generator was operated for 2,000 hr during the testing. In accordance with the results of Chapters I and III, there should

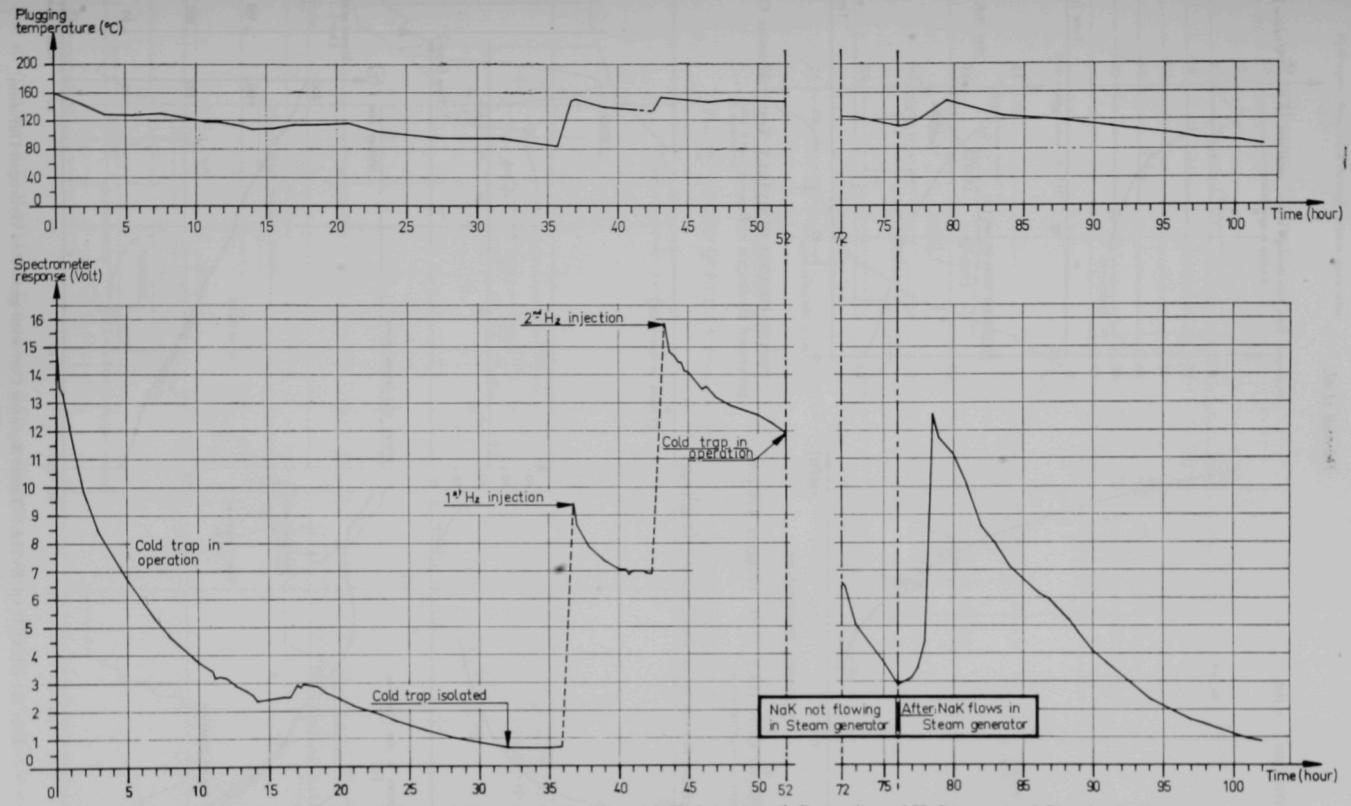

FIG. 35. GRAND QUEVILLY Tests: 1) Detector Calibration with H_2 Injection; 2) Comparison of H_2 Detector and Plugging Indicator.

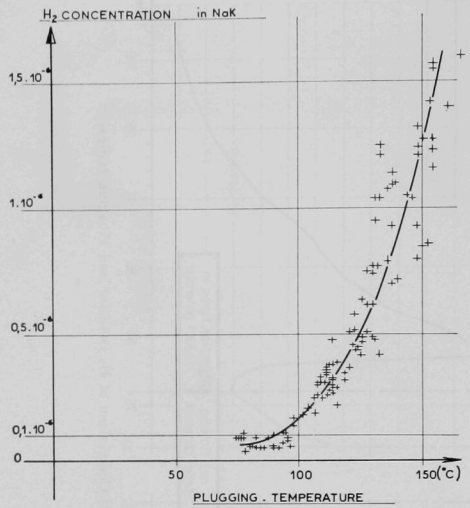

FIG. 36. GRAND QUEVILLY Tests: Plugging Temperature *vs* Hydrogen Concentration.

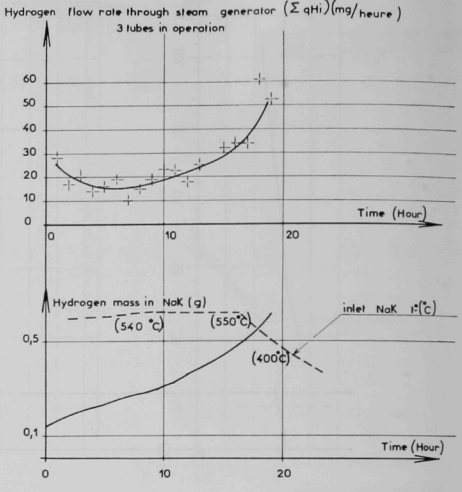

FIG. 38. GRAND QUEVILLY Tests: Aqueous Corrosion-generated Hydrogen Diffusion.

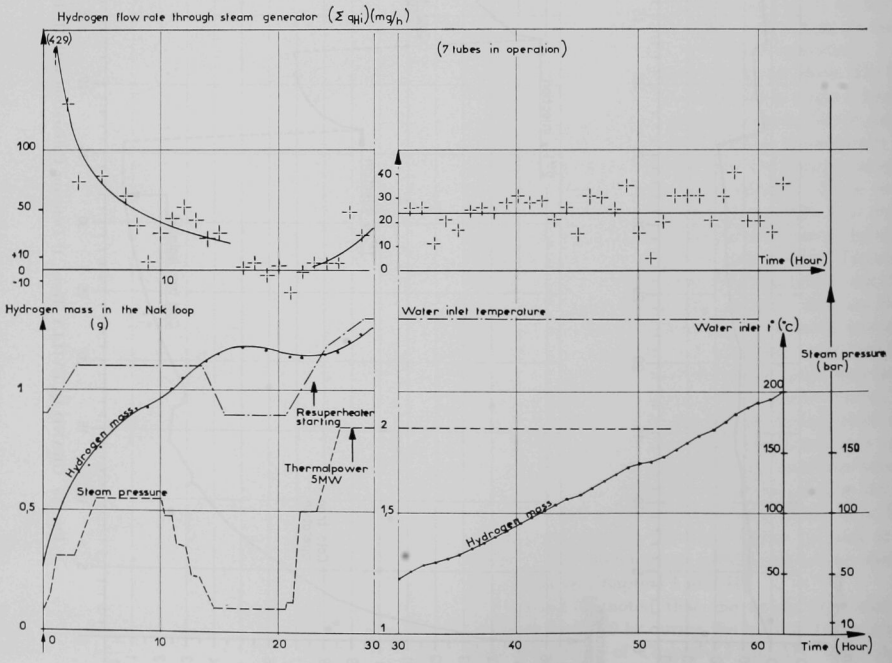

FIG. 37. GRAND QUEVILLY Tests: Aqueous Corrosion-generated Hydrogen Diffusion.

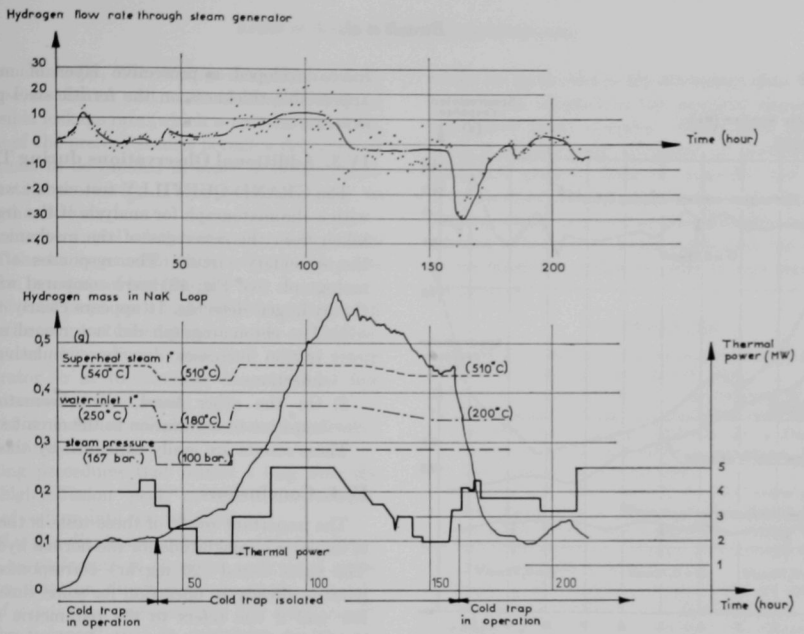

FIG. 39. GRAND QUEVILLY Tests: Aqueous Corrosion-generated Hydrogen Diffusion.

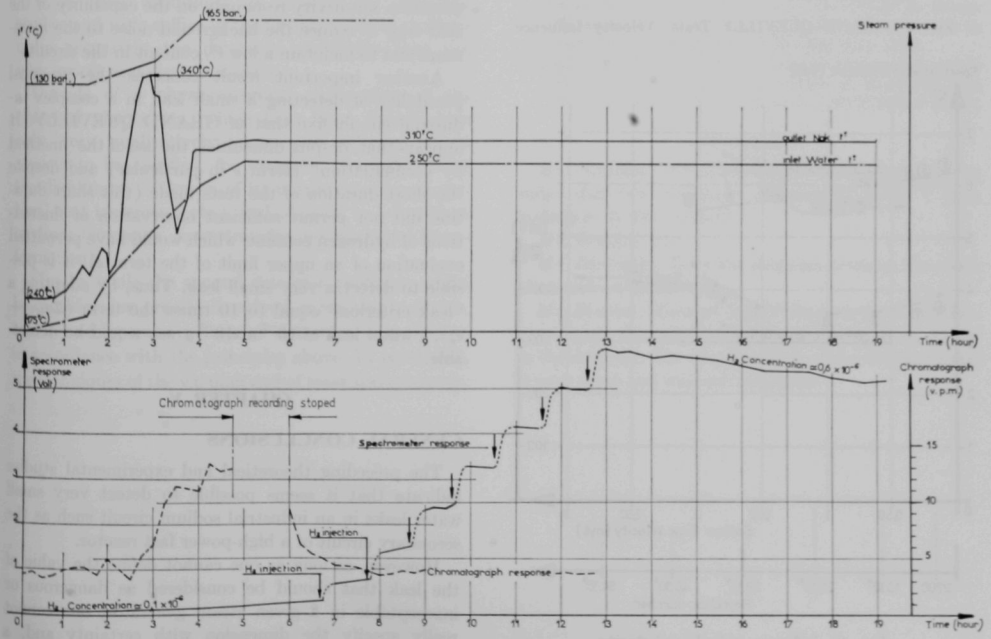

FIG. 40. GRAND QUEVILLY Tests: Comparison of Chromatograph and H_2 Detector (Cold Trap is Isolated).

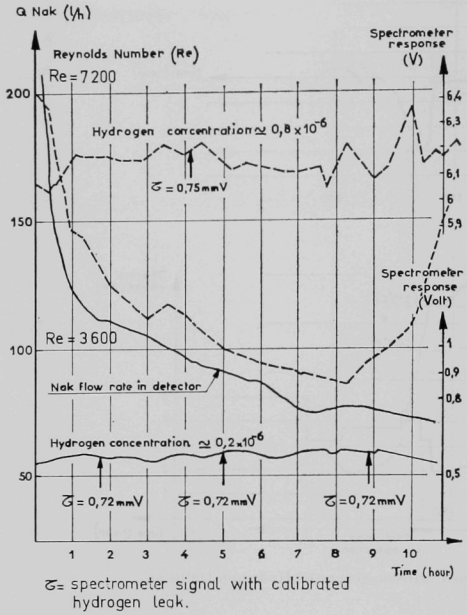

FIG. 41. GRAND QUEVILLY Tests: Velocity Influence.

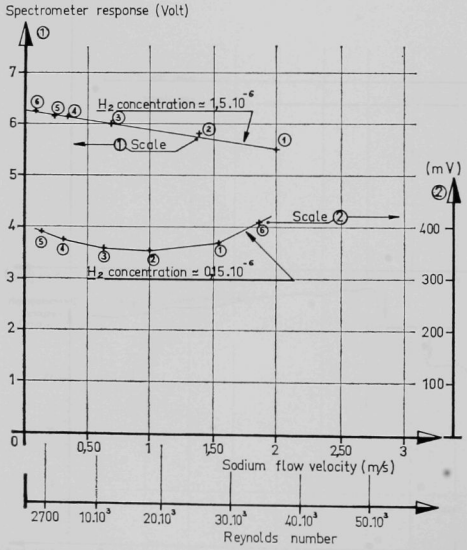

FIG. 42. Influence of Sodium Velocity.

have developed a protective layer of magnetite of appreciable thickness on the ferritic-steel pipes of the evaporator.

IV.3. Additional Observations during These Tests

The GRAND QUEVILLY test circuit was equipped with a chromatograph for analysis of the argon samples taken from the cover gas of the mechanical pump of the secondary circuit. The responses of this chromatograph (see Fig. 40) were compared with those of the hydrogen detector. It appears clearly that:

1) The chromatograph did not record any concentration increases due to cumulative hydrogen injections.
2) On the other hand, the chromatograph was sensitive to a variation in the circuit state.

These results are easily explained by those of Ch. I.

IV.4. Conclusions

The important result of these tests is the evaluation of an order of magnitude for the normal hydrogen flow. The value found (20 mg/hr) corresponds to an apparatus already in operation for some time. It is very low and if one refers to the parametric study summarized in Fig. 30, it appears clearly that the normal hydrogen flow Σq_{Hi} is completely negligible. The detection sensitivity rests only on the capability of the cold trap to reduce the background noise to the maximum and to maintain a low C_f content in the circuit.

Another important result concerns the practical possibility of detecting a small leak in a complex industrial circuit like that of GRAND QUEVILLY. It appears that, despite difficulties, the use of the "method by accumulation" (term ϵ in particular) and despite the short duration of the tests made (this short duration did not permit sufficient observation of fluctuations of hydrogen content, which would have permitted evaluation of an upper limit of the term ϵ), it is possible to detect a very small leak. Thus, by adopting a "leak criterion" equal to 10 times the term $(\Sigma q_{Hi} + \epsilon_\mu)$, a water leak of 10^{-3} at 10^{-2} g/sec would be detectable.

CHAPTER V

GENERAL CONCLUSIONS

The preceding theoretical and experimental studies indicate that it seems possible to detect very small water leaks in an industrial sodium circuit such as the secondary circuit of a high-power fast reactor.

However, as long as one cannot define the value of the leak that should be considered as dangerous or inacceptable in a given steam generator, one cannot really specify the dimension with certainty and, a

fortiori, economically, the leakage-detection system. Under these conditions and while waiting to find out the admissible leakage rate (which is another problem), the results of the present studies permit a definition of the conditions to be fulfilled in order to obtain maximum detection sensitivity. These conditions may be summarized as follows:

1) permanent control of the plugging temperature or of the hydrogen content in order to keep the sodium in a state of high purity;
2) use of cold traps with high retention power and with the temperature cold point as low as possible;
3) design of the sodium circuit and of the steam generator so as to minimize the extent of free surfaces and of dead zones;
4) use of a modular steam generator, preferably with unitary solutions;
5) starting procedures that permit a leap over the first high diffusion "peak" so as to avoid introduction of sodium into the installation;
6) use of nickel-diaphragm detectors of the "sodium" type, in preference to those for analysis of argon (argon detector, direct chromatography, etc.);
7) use of a detection process of the "by comparison" or "by balance" type in preference to "by accumulation" type.

When these conditions are fulfilled, the preceding studies and tests suffice in the present state to evaluate quite accurately the detection sensitivity that one may expect in a given installation.

Outside of a physicochemical explanation of the observed phenomena, which have been treated here only very qualitatively, there still remain certain aspects to be clarified, for example, the influence of the diaphragm thickness, of its nature (exact composition, heat treatment, etc.), and of aging in hot sodium medium (corrosion, mass transfer, metallurgical transformation).

Finally, while the general detection problems might be considered as practically solved, it remains to design, build, and operate industrial detection installations in accordance with the principles above. In particular, the techniques of the vacuum and of mass spectrometry, which are more close to the laboratory than to industry, have to be adapted to the practical requirements of the power plant operator. While such development work is already very advanced, in particular for the PHENIX project, tests of longevity and reliability of a detection device remain to be made. Furthermore, the important question of the allowable leakage rate remains to be solved. A new orientation has been given to our detection studies in order to face this aspect of the problem.

REFERENCES

1. Strahl, H., *A Device for Continuous Detection of Hydrogen in Sodium*, NAA-SR-6986 (May 31, 1962).
2. Lannou, L., *Application de la spectrométrie de masse à la détection et au dosage de l'hydrogène dans un circuit de sodium liquide*, E.D.F.—Bulletin de la Direction des Etudes et Recherches—Série A (Nucléaire, Thermique, Hydraulique)—**4**, 161–185 (1967).
3. Subbotin, V. I., and Kozlov, F. A., *The Control of Hydrogen and Oxygen Concentration in Sodium*, IAEA Symposium on alkali metal coolants, corrosion studies and system operating experience, Vienna, 28 November–2 December 1966, Paper SM 85/49.
4. Delisle, J. P., *Expérience d'exploitation des indicateurs de bouchage automatique*, *ibid.*, Paper SM 85/4.
5. Brachet, A., *Le transfert thermique par métaux liquides—Description d'une installation d'essais*, L'industrie chimique belge, **1**, 23–34 (1964).
6. Robin, M. G., *La station d'essais thermiques de Grand-Quevilly—Circuit de sodium du 5 MW avec générateur de vapeur surchauffée à 545°C*, CEA-2520 (July 1964).
7. Sonnen, C, and Warzee, M., *Influence du traitement de surface sur la corrosion d'aciers au carbone et inoxydable dans l'eau et la vapeur à haute température*, EUR-1735. F (1967).

Discussion

Mr. Dickinson (LMEC): I noticed on several of the slides that you indicate a response at about 1 ppm hydrogen. Is this correct?

Mr. Brachet: Yes.

Mr. Dickinson: Does the response occur in the order of seconds or minutes?

Mr. Brachet: Minutes. This is the time for the hydrogen to pass through the loop from the injection device to the detector. The response time of the detector itself is very short and was not measured.

Status of Sodium-Water Reaction Test Work at INTERATOM

K. Dumm, H. Mausbeck, and W. Schnitker

INTERATOM
Bensberg, Germany

(PRESENTED BY H. MAUSBECK)

1. Introduction

For several years INTERATOM has performed experimental and theoretical investigations with respect to the tube-rupture behaviour of sodium-heated steam generators (due to Na-H_2O reaction) and to the development of adequate pressure-relief systems. In an extensive series of tests the interest was originally directed to sodium-water reactions in tubes as related to the tube-in-tube steam generator which was selected for the KNK reactor experiment (KNK is a compact, sodium-cooled, zirconium hydride-moderated reactor). A large number of fundamental experiments was carried out in order to study the phenomena of the reaction mechanism in a simple geometry permitting comparison with theoretical models.[1] Finally a model of the anticipated pressure-relief system was subjected to some confirming tests.

In accordance with the design of the sodium-cooled fast breeder reactor the interest in sodium-water reaction tests was changed to reaction studies in different vessel geometries (tube-in-shell and modular steam generators). Again the first stage of tests was directed to fundamental experiments in a very simple reaction vessel without internals.

To obtain a larger flexibility in future test work, a new test facility has been constructed and put into operation. In this facility a wide range of tests can be carried out, such as pinhole tests, large leak tests with steam-generator models of different size, and leak-detection tests.

2. Test Work with Tube-in-tube Steam Generator

The KNK reactor experiment is equipped with two tube-in-tube steam generators. Figure 1 shows the design in principle of a KNK steam generator with its adjacent pressure-relief system. The steam generator consists of 28 tube-in-tube units in parallel. The inner tube contains the upstreaming water and steam. Sodium flows downward in the surrounding annular tube.

The pressure-relief units are connected at both the sodium inlet and outlet header. The pressure-relief system consists of a depressurizer vessel with an outlet orifice and a rupture disc at the top. The rupture disc opens to the pressure-relief line that connects with the reaction products-separation tank. A second relief line behind the orifice is connected with the same reaction products-separation tank. In case of a large leak the sodium will be accelerated mainly by the hydrogen formation. The orifice protects the adjacent sodium loop with respect to pressurization by the increased pressure drop across the orifice. The second relief line serves for a fast increase in the sodium flow since the sodium mass to be accelerated is small. The volume of the depressurizer itself has been selected to assure sodium flow at the orifice during the whole pressure-relief process, that is to say, during the flow time of the sodium plug into the reaction products-separation tank. This type of pressure-relief system is inherently safe without the use of shutoff valves.

This steam generator with its pressure-relief system has been checked in three stages: fundamental experiments in a straight short tube, experiments in a shortened meander-shaped tube, and experiments in a simplified model of steam generator and pressure-relief system. The results of the tube tests have been reported earlier.[1]

Figure 2 shows the test model used. Because of the small test facility available, a constant scaling factor could be reached only in cross sections, not in volumes. Measurements taken were pressures at P_1 to P_{14}, temperatures at T_1 to T_4, and sodium levels at Z_1 to Z_4. The main information was received from the pressure pickups of the piezoelectric quartz type. Temperature readings were taken by means of fast thermocouples only in the depressurizer vessel. The level indicators signalized the break of the rupture discs.

A typical test result is shown in Fig. 3. The reaction starts with high-pressure pulses at the leak, which propagate with decreasing amplitudes through the whole system. At the measuring point P_{12} behind the orifice no pressure pulses can be observed; this is due to the many cross-section changes in the system, especially at the orifice itself. A considerable pressure rise in header and depressurizer tank (at P_7 and P_8) was recorded 30 ms after the reaction has started; this was due to reactions between the water and the sodium of the adjacent tubes within the header itself. The entrance of the water front into the depres-

surizer vessel is indicated by a much smaller pressure peak. Pressure readings behind the orifice (at P_{11} and P_{12}) are low during the whole pressure-relief process. The pressure loadings of the system have become rather unimportant when the temperature starts to rise. The temperature reached its maximum of 1,300°C about 400 ms after the reaction started. This high temperature within the vessel is nearly without importance for the wall temperature, the maximum increase of which is only 50°C.

The main test results are:

1. The upper limit of the pressure within the steam generator and the pressure-relief system is given by the initial water pressure, which, in fact, is almost reached in some parts of the steam generator.

2. The lay-out pressure of the adjacent loop is not largely influenced by the sodium-water reaction.

3. The reaction temperatures do not influence the lay-out of the system.

3. Tests in Simple Vessel Geometries

As a first step toward tube-in-shell and modular steam generators as anticipated for the fast breeder program, sodium-water tests in simple vessel geometries without internals were carried out. Figure 4

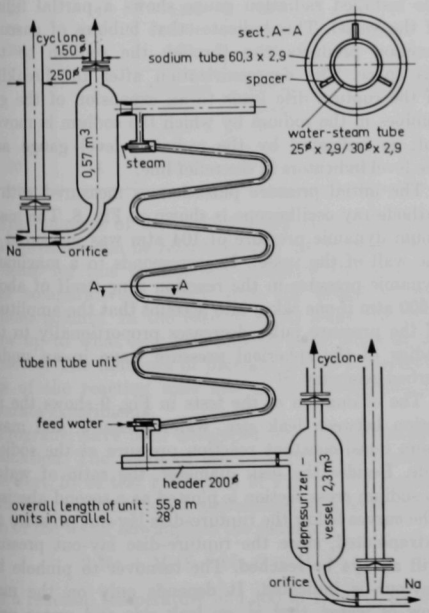

Fig. 1. Scheme of KNK Steam Generator.

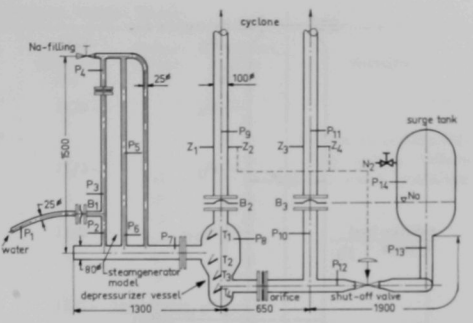

Fig. 2. Test Setup for KNK Pressure-relief System.

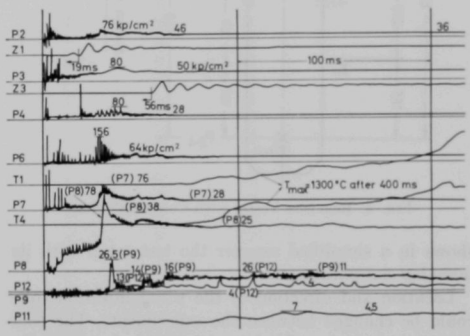

Fig. 3. Model KNK Pressure-relief System.

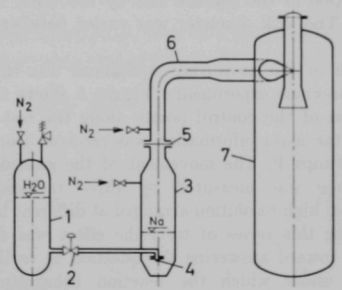

Fig. 4. Test Setup for Reactions in a Vessel.

1	Water container	120 kp/cm², 330°C, 75 ℓ
2	Quick action valve	25 diam
3	Reaction vessel	224 diam, 55 ℓ
4	Injection point	18 diam—1 diam
5	Rupture disc	100 diam, 15 kp/cm²
6	Pressure relief line	100 diam/250 diam
Cyclone		10 m³

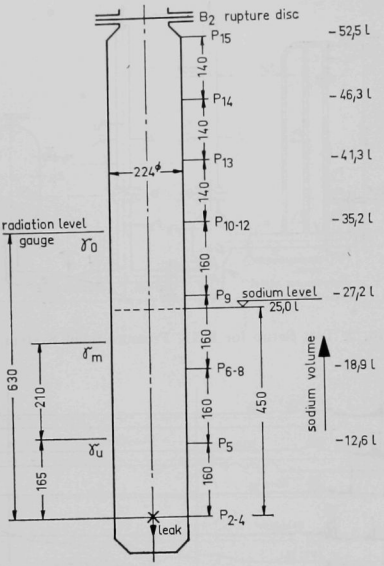

FIG. 5. Reaction Vessel with Control Points.

shows in a simplified manner the test setup with its main lay-out parameters.

Location and direction of the water-injection tube could be changed between the experiments. The leak diameter could be varied by insertion of changeable orifices which were closed by small rupture discs. Therefore, the start of the reaction was given by the destruction of the rupture disc by the water streaming in. The leak diameter was varied between 1 and 18 mm.

Much of the measuring equipment was the same as in previous experiments. Figure 5 shows the distribution of the control points along the test vessel. Again, the main information was received from pressure pickups P. The movement of the gaseous reaction zone was measured by three radiation-level gauges of high resolution arranged at different heights.

During this series of tests the effort was directed mainly toward answering the question as to the conditions under which the reaction behaviour turns over from a typical pinhole to a large-leak behaviour. In this connection pinhole behaviour is defined as a stationary reaction zone, and large-leak behaviour as a piston-type movement of the sodium column above the reaction zone. Under those conditions the parameters mainly to be varied are leak size, water pressure, and sodium filling.

Thirty tests have been carried out. The main test parameters are shown in Table 1. For comparison, one test was done with water instead of sodium and with nitrogen instead of the formed reaction products (mainly hydrogen).

Figure 6 describes the results of a typical large-leak test. The pressure pickups below the sodium level show the expected pressure pulsation immediately after the beginning of the reaction, as known from the reactions in tubes, but of much smaller amplitudes. Pressures at P_{13} and P_{14}, which are located in the gas space, show a first maximum at the break pressure of the rupture disc and a second, higher maximum when the sodium reaches the exit of the vessel. The quasi-constant pressures rise to approximately 40 atm, which is small compared with the water pressure of 120 atm. The radiation-level gauges indicate a velocity of the sodium column of about 8 to 10 m/s in the vessel. The level gauges in the relief line (Z_1 to Z_5) show a sodium velocity of 75 m/s in the relief line. The maximum temperature measured in the reaction zone amounts to 770°C.

Small-leak behaviour is shown in Fig. 7. The leak size during this test was 2 mm. The pressures at the sodium side rise continuously to the break pressure of the rupture disc within 1.430 ms. During that time the installed radiation gauge shows a partial filling of the vessel. This indicates that bubbles of gaseous reaction products rise through the sodium to the gas space. The depressurization after the breaking of the rupture disc leads to an expansion of the gas bubbles in the sodium by which the sodium is moved out, as indicated by the radiation-level gauge and the level indicators in the relief line.

The initial pressure pulsation as measured with a cathode-ray oscilloscope is shown in Fig. 8. The maximum dynamic pressure of 104 atm was measured at the wall of the vessel. It corresponds to a maximum dynamic pressure in the reaction zone itself of about 1,600 atm if one takes into account that the amplitude of the pressure pulse decreases proportionally to the radius of the spherical pressure wave in an undisturbed geometry.[2]

The evaluation of the tests in Fig. 9 shows the relation between leak size, water pressure, and maximum quasi-constant reaction pressure at the sodium side. Besides the leak diameter, the ratio of water-to-sodium cross section is plotted as a second abscissa. The curves below the rupture-disc lay-out pressure are extrapolated, since the rupture-disc lay-out pressure will always be reached. The turnover to pinhole behaviour is indicated. It depends only on the mass flow of water, that is, on leak size and water pressure.

TABLE 1. INITIAL CONDITIONS FOR VESSEL TESTS

Test	Leak Size, mm	Water Pressure, atm	Water Temp, °C	Injection Direction	Sodium Temp, °C	Sodium Pressure, atm	Sodium Volume, liter	Rupture Disc, atm	Remarks
1	18	120	200	down	250	2	25	15	
2	16	120	200	down	250	2	?	15	Failure in sodium-filling system; failure in water container
3	12	120	200	down	250	2	?	15	
4	12	120	200	down	250	2	25	15	
5	10	120	200	down	250	2	25	15	
6	14	120	200	down	250	2	25	15	
7	8	120	200	down	250	2	25	15	
8	6	120	200	down	250	2	25	15	
9	4	120	200	down	250	2	25	15	
10	3	120	200	down	250	2	25	15	
11	2	120	200	down	250	2	25	15	
12	1	120	200	down	250	2	25	15	Obstruction of leak
13	1	120	200	down	250	2	25	15	
14	2	60	200	down	250	2	25	15	Failures in measuring lines
15	2	60	200	down	250	2	25	15	
16	4	60	200	down	250	2	25	15	
17	10	60	200	down	250	2	25	15	
18	14	60	200	down	250	2	25	15	
19	18	60	200	down	250	2	25	15	
20	14	100	200	down	250	2	25	15	
21	14	80	200	down	250	2	25	15	
22	14	120	200	down	250	2	35	15	
23	14	120	200	down	250	2	45	15	
24	14	120	200	down	250	2	50	15	
25	3	60	200	down	250	2	25	15	
26	14	120	320	down	250	2	50	15	
27	14	120	200	up	250	2	35	15	
28	18	80	200	down	250	2	25	15	
29	3	60	200	up	250	2	25	15	
		Nitrogen press, atm	Nitrog. temp, °C		Water temp, °C	Water press, atm	Water volume, dm^3		
30	14	120	20	down	20	2	35	15	Test for comparison

The influence of the sodium filling of the vessel on peak pressure can be read from Fig. 10. It shows that at least for this undisturbed geometry the pressure rises comparatively slowly with the height of the sodium column. In the case of small leaks the tests show up to what leak size pinhole behaviour can be expected. The influence of pinholes on the sourroundings of the reaction zone has to be investigated in separate experiments.

Programs have been developed for a more detailed evaluation. The result of the code POOL evaluation (see Sect. 5) of test 1 is shown in Fig. 11. We started with the previously used assumption of a total reaction of the water flowing into the sodium:

$$2\,Na + H_2O \rightarrow Na_2O + H_2\,,$$

and a reaction temperature of 1,300 to 1,400°C, as related to the boiling or sublimation temperature of Na_2O. This assumption leads to a much higher quasi-constant pressure than observed. With the reaction

$$Na + H_2O \rightarrow NaOH + \tfrac{1}{2}\,H_2$$

and about the same temperature the pressure was substantially reduced because of the smaller extent of hydrogen formation, but the resulting pressure was still too high. The second reaction mechanism combined with a reaction temperature of 750°C gives the best fitting of the experimental and theoretical curves of the experiment, shown in Fig. 11. For all evaluated tests this mechanism gave the best comparison between theory and experiments with assumed reaction temperatures from 650 to 1,000°C. The measured values varied between 770 and 920°C. Lacroix *et al.* measured similar temperatures during their experiments.[3]

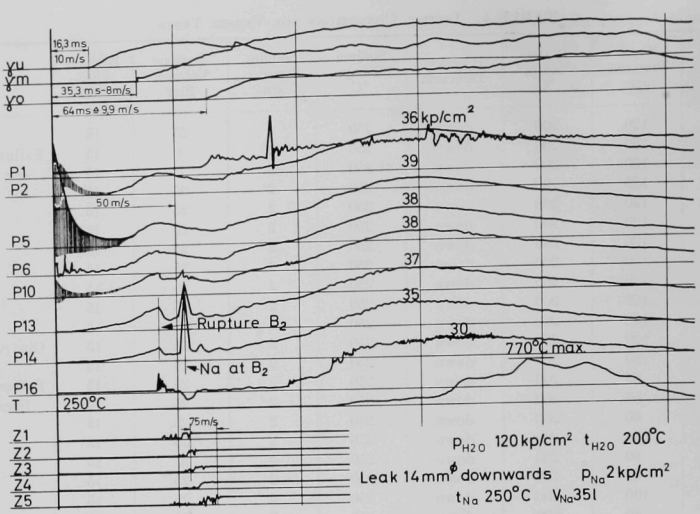

FIG. 6. Test 22.

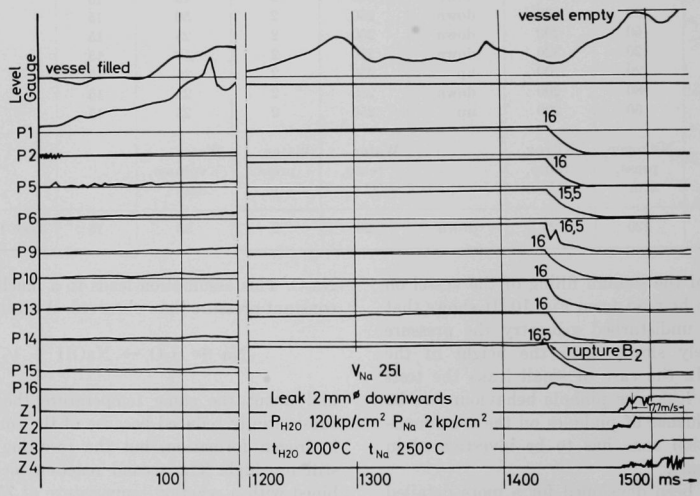

FIG. 7. Test 11.

4. ASB Test Facility and First Test Results

The tests described in the previous section were carried out in the same small test facility that served for the KNK test work. The fast breeder steam-generator concept requires additional test work in the direction of large model tests on the one hand, and pinhole behaviour on the other. The ASB (a facility for safety tests for the fast breeder reactor) has been built for this purpose.

Figure 12 shows the ASB building and Fig. 13 the sodium loop. Figure 14 gives a simplified flow diagram of the ASB. The loop can be divided into three

main sections which are located in separate parts of the building and partitioned from one another by concrete walls: the sodium loop, the test section itself, and the water system.

The sodium loop can be operated separately by bypassing the test section. Its main parts are a free-surface centrifugal pump of 120-m³/hr capacity (1), a surge tank with a volume of 2.5 m³ (2), a sodium heater-cooler with a heating capacity of 150 kW and

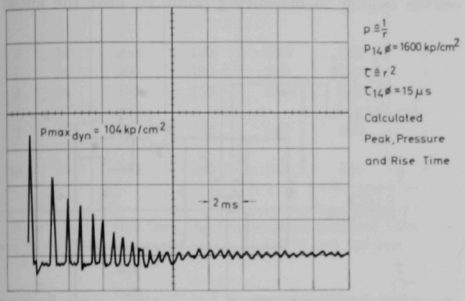

FIG. 8. Initial Pressure Pulses due to Reaction in Vessel.

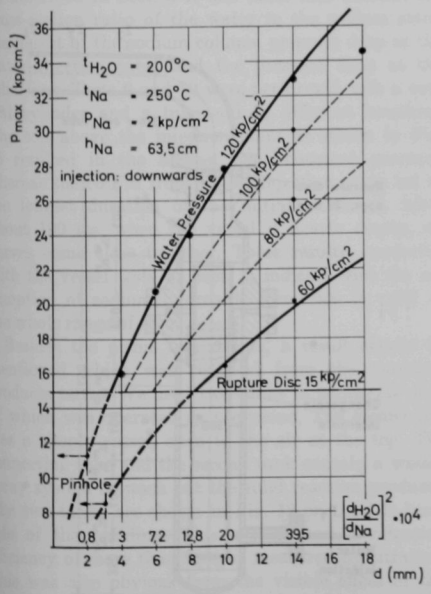

FIG. 9. Maximum Reaction Pressure P_{max} *vs* Leak Size d in a Vessel.

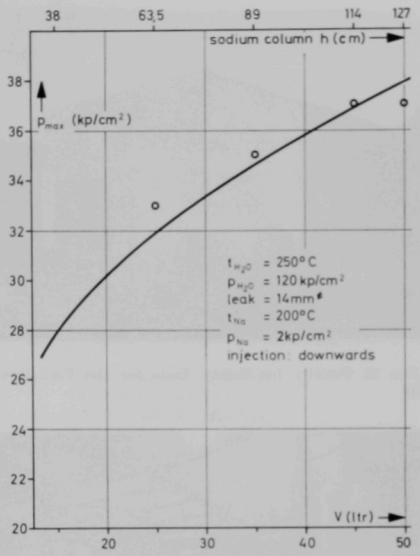

FIG. 10. Maximum Reaction Pressure P_{max} *vs* Sodium Volume V in a Vessel.

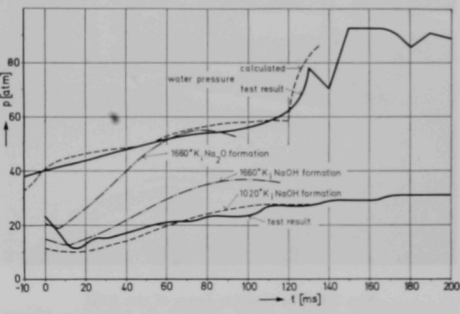

FIG. 11. Code POOL Evaluation for Reaction Pressure at the Sodium Side for Test 1.

a cooling capacity of 100 kW (3), four cold traps (4), and storage tanks with an overall capacity of 15 m³ (5). The main lay-out data are 550°C, 30 atm, and 10,000 hr of operation.

The main components of the water-steam system are 2 pressure vessels of 500-l (6) and 30-l (7) capacity, respectively, and the temperature-gradient section (8). The gradient section serves for a better simulation of the water-steam conditions. The main lay-out data are 280 atm and 370°C.

The test section consists of a large model section (9),

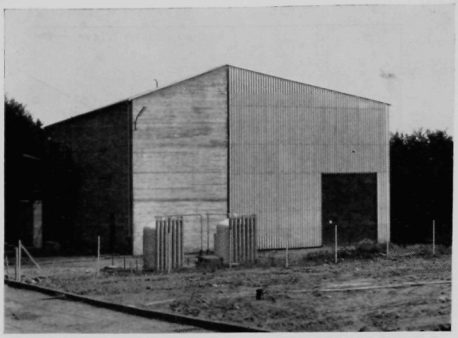

FIG. 12. Facility for Safety Tests for the Fast Breeder ASB.

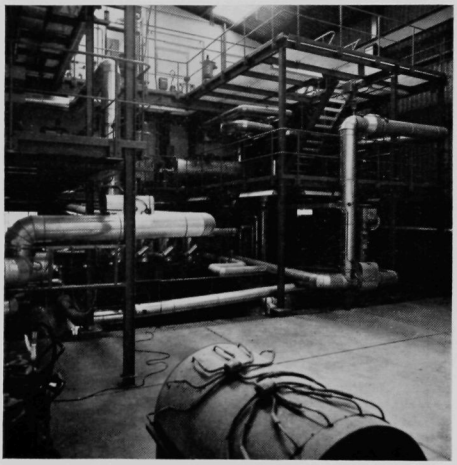

FIG. 13. The Sodium Loop of the ASB.

two small leakage test sections (10), and the reaction-products tanks (11).

With respect to model tests different steam generators are under consideration for the fast breeder plant: a 50-MWt model type and, as a back-up solution, a 5-MWt tube-in-shell type of steam generator. The model being tested now is adapted to the 5-MWt steam generator.

Figure 15 shows the test vessel with its removable internals and the plan of control points. The vessel has a total length of 2,450 mm, an inner diameter of 350 mm, and a diameter of the pressure relief line of 200 mm.

With this model 10 tests have been performed (see Table 2). The tests aimed at completing the information gained during the tests with simple vessel geometries (see Sect. 3). Especially the assumptions of sodium hydroxide formation and the comparatively low reaction temperatures were to be confirmed in a different geometry and under different pressures and temperatures.

The evaluation has not yet been completed. Some experimental results are compiled in Fig. 16. The curves belong to measuring point P_2 near the initial

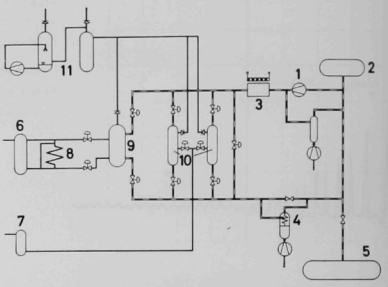

FIG. 14. Simplified Flow Diagram of the ASB Test Facility.

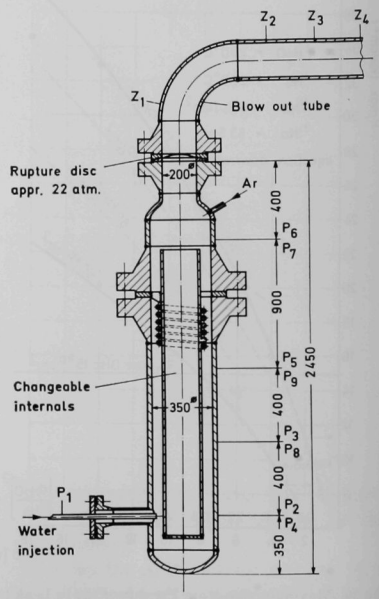

FIG. 15. Reaction Vessel and Control Points.

TABLE 2. INITIAL CONDITIONS FOR ASB TESTS

Test	Leak Size, mm	Water Temp, °C	Water Pressure, atm	Sodium Volume, liter	Sodium Temp, °C	Sodium Pres, atm	Argon Volume, liter	Rupture Disc, atm	Vessel Geometry	Remarks
1	14	200	120	50	250	2	195	23	Without internals	
2	14	200	120	150	250	2	95	23	Without internals	Failure in fill system; test not executed
3	14	200	120	150	250	2	95	23	Without internals	
4	14	200	120	210	250	2	35	23	Without internals	
5	14	200	120	210	250	2	35	23	Without internals	Failure at injection valve; no measurements taken
6	14	200	120	230	250	2	15	23	Without internals	
7	14	300	180	240	330	3	5	23	Without internals	
8	14	340–300	150	240	330	3	5	23	Without internals	See note
9	14	300	160	240	330	4	5	23	With internals, tube coil in highest position	
10	14	300	180	240	330	4	5	23	With internals, tube coil in leak area	

Note: During this test, the temperature-gradient tube was used; lowest water temperature was 300°C; the water slug of 5.35 l was followed by saturated steam at 340°C and 150 atm.

reaction zone. Tests 7 and 8, made without internals in the vessel, show a quasi-constant pressure adequate to the values found with the smaller test vessel as described in Sect. 3 if one takes into account the cross-section ratio of the water to the sodium sides, the height of the sodium column, pressure drop at the water-injection tube, and the pressure drop at the relief line. Tests 9 and 10 were performed with a central cylinder and a tube coil in different locations. The coil above the injection point as shown in Fig. 15 resulted in the highest quasi-constant pressure, whereas the coil in front of the injection point led to the longest duration of the initial pulsation. After about 100 ms, when the vessel is nearly empty, all curves come close together. These results, compared with the vessel tests of Sect. 3, indicate that the assumption of sodium hydroxide formation is valid in the whole range of tests.

Besides the prime test results, a result should be mentioned which was received from the reaction-products tanks. We used two tanks in series, the first of which was operated as a cyclone. The second one was a simple vessel, open to the air at the top. The connecting tube and the second tank contain a water-spray system to wash out the solid reaction products. The two tanks are shown in Fig. 12 on the left-hand side of the building. This system had a retention efficiency of more than 99% as measured by titration. This was also obvious from the visible effect of the small amount of fume loading of the escaping hydrogen (see Fig. 17). Earlier experiments with much

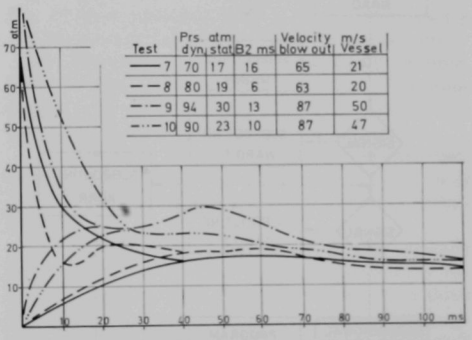

FIG. 16. Reaction Pressure at P_2.

smaller amounts of sodium were always accompanied by a large flame at the outlet of the reaction-products tank, even though the titration of the sodium residue in the cyclone always gave retention efficiencies of more than 95%.

5. Mathematical Description of the Sodium-Water Reaction in Vessels

For the description of the system behaviour in case of a sodium-water reaction, three computer codes have been developed. The main code, called POOL, is similar to the equation systems developed and used by Salmon,[4] Chase *et al.*,[5] and Lacroix *et al.*[3] Figure 18 shows a block diagram of the pro-

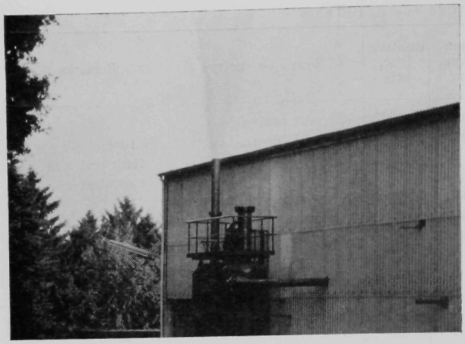

FIG. 17. Fumes Accompanying Escaping Hydrogen.

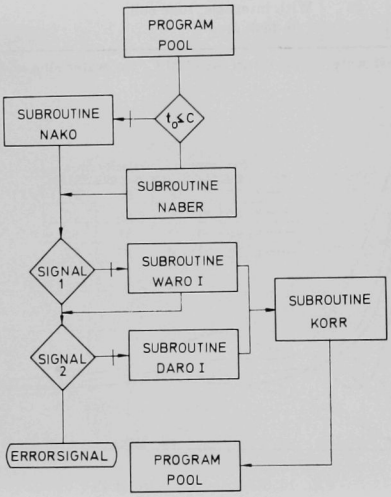

FIG. 18. Block Diagram for Program Pool.

gram and its subroutines. The program itself consists mainly of the law of ideal gases:

$$pv = MRT, \tag{1}$$

the description of the formation of H_2:

$$2\ Na + H_2O \rightarrow Na_2O + H_2 \tag{2}$$

or

$$Na + H_2O \rightarrow NaOH + \tfrac{1}{2}\ H_2, \tag{3}$$

and additional orders.

The volume v is the result of the subroutines which describe the sodium flowing off the reaction zone. The mass M is given by the mass of water streaming in (measured in kmol), which reacts instantaneously and completely with the sodium, forming hydrogen. The temperature T is an input value, whose theoretical upper limit is given by the sublimation temperature of Na_2O (1,663°K).

Subroutine NAKO calculates the sodium flow under the assumption of a one-dimensional geometry. Sodium is supposed to be compressible. The main equation is the equation of pressure waves in liquids:

$$\Delta p = \rho c \Delta u. \tag{4}$$

The pressure and velocity waves are reduced by reflection at all points of cross-section changes within the steam generator itself (e.g., the parallel tube bundle of the steam generator). This has been taken into account by the use of reflection factors at all these points, and the calculation of the pressure and velocity waves for every interval. The switchover from NAKO to NABER (the latter works with incompressible sodium) is ordered when the primary wave reflected at the end of the vessel comes back to the point of origin. NABER is based on the equation of motion of the liquid:

$$p_h - p_E - \zeta \rho \frac{u^2}{2} = \rho l \dot{u}. \tag{5}$$

The subroutine contains a number of logical elements to describe the changes in flow of the sodium column. In particular, the column length l and pressure-drop coefficient are functions of the changing geometry of the sodium flow path.

While NAKO and NABER give the volume which is available for the hydrogen to be formed, the subroutines WARO and DARO give, by way of the water- and steam-flow rate, the amount of hydrogen. WARO calculates the acceleration of the water by an equation similar to (5). In this case the driving power is given by the difference between the pressure in the water tank and in the hydrogen bubble. If the saturation pressure of the water at the outlet of the water tube is higher than the pressure in the hydrogen bubble, the hydrogen pressure is replaced by the saturation pressure.

DARO describes the steam side of the broken tube. In principle it is similar to WARO. In it is included the fact that a water slug with a temperature gradient is accelerated by the following steam. As soon as the water slug is pushed out of the tube, the steam flow is calculated, taking into account the possibility of critical flow. With respect to the experimental setup it is possible to shut off one of the two subroutines WARO or DARO. If the saturation pressure is higher than the hydrogen pressure, the sub-

routine KORR, describing the flashing of the water, is called for. If the flashing does not increase the water-side mass flow, KORR is not called.

A second code, DRUWA, has been developed in order to calculate the pressure propagation in the whole secondary loop. Usually in the literature only the pressure rise in the steam generator itself has been discussed, but the pressure development in the intermediate heat exchanger is also essential. The result of POOL in the steam generator is the input function of DRUWA. The loop is a manifolded system of tubes. The acceleration of the sodium in the single tubes is calculated by a system of equations similar to (5). At each branching the equation of continuity must be considered. This system of equations gives the pressure distribution in the loop. The change of the sodium column length due to penetrating hydrogen is taken into account. This is necessary only for the steam generator and pressure-relief system. Lacroix *et al.* used this method to calculate pressure propagation in their test facility.[3]

The third program, NAWA 3 D, is still under test. In the code POOL the movement of the different fluids is supposed to be one-dimensional. This gives errors in the description of the behaviour in approximately the first 10 ms. Therefore in NAWA 3 D pressure waves in the sodium are calculated in cylindrical geometry. The water-steam mixture penetrates into the hydrogen bubble and reacts with the sodium contacted. A part of the water may be evaporated. Compared with POOL, the program has the more complicated geometry. The action of the primary pressure wave on the surrounding tubes can be calculated with this program, too.

Symbols

c	= velocity of sound of sodium	m/s
l	= length of sodium column	m
M	= mass of gas	kg
p	= pressure	kp/m²
p_h	= pressure of the hydrogen bubble	kp/m²
p_E	= pressure at the end of the pressure relief line	kp/m²
R	= gas constant	m-kp/kg-°C
T	= absolute gas temperature	°K
u	= flow velocity of the sodium	m/s
v	= volume	m³
ρ	= specific gravity of sodium	kp-s²/m⁴
ζ	= factor of flow resistance	—

REFERENCES

1. K. Dumm *et al.*, *Experimental and Theoretical Investigations of Sodium-Water Reactions in Tubes*, CREST Meeting, Ispra, Italy, June 26–29, 1966.
2. H. Holtbecker *et al.*, *The Response of a Vessel to an Internal Blast Loading*, CREST Meeting, Ispra, Italy, June 26–29, 1966.
3. A. Lacroix *et al.*, *Etudes de Sûreté des Générateurs de Vapeur Sodium-Eau Méthode de Calcul et Résultats Expérimentaux*, Conférence Internationale sur la Sûreté des Réacteurs à Neutrons Rapides, Aix-en-Provence, France, September 19–22, 1967.
4. M. A. Salmon *et al.*, *Effects of Tube Leaks in Sodium Heated Steam Generators*, NAA-SR-8140 (April 15, 1963).
5. W. L. Chase *et al.*, *Analysis of the Babcock & Wilcox Full-Size Steam Generator for a Sodium-Water Reaction*, APDA-176 (Nov. 30, 1966).

Discussion

Mr. McCarthy (Commonwealth Associates): In Fig. 17 there appeared to be a lot of flame coming out. Do you inert your relief line and your separator?

Mr. Mausbeck: Yes, it was inerted by nitrogen. However, the jet of hot hydrogen mixed with some sodium and sodium oxide, so that it ignited immediately on reaching the exit of the relief line.

Mr. Chamberlain (APDA): Did you observe wastage in either of the units at the size of leak rates you were using? How was the leak injection terminated?

Mr. Mausbeck: The leak injection was normally terminated by closing the entrance valve after a few tenths to some seconds, depending on the test. I think you shouldn't expect wastage in case of these large leak tests. I would expect more wastage with small leaks. On two occasions we terminated the water flow because of increasing temperature in the outer vessel surrounding the reaction zone. With respect to temperature, it might be that small leaks are more dangerous than large leaks; the latter are of more importance for the pressure of the whole unit, including relief lines as well as for the secondary system.

Wastage of Steam-generator Materials by Sodium-Water Reactions*

HARRY V. CHAMBERLAIN, JOHN H. COLEMAN, EVAN C. KOVACIC, AND ALBERT A. SHOUDY

Atomic Power Development Associates, Inc.
Detroit, Michigan

(PRESENTED BY H. V. CHAMBERLAIN)

I. Introduction

The successful development of the sodium-heated steam generator is an essential requirement of the sodium-cooled fast breeder reactor program. If a number of sodium-cooled fast reactors are built, it seems certain that some leaks in steam generators will occur during their operating lifetime; therefore the consequences of leaks of the steam generator for the secondary heat-transport system and for the surrounding plant must be understood. The consequences of large leaks (that is, of single-tube and of simultaneous multiple-tube ruptures) in terms of deformation or rupture of the steam-generator shell has been a principal concern. Another major concern is corrosion and erosion of shell and internals by the sodium-water reaction.

In late 1962 a large leak occurred in one of the EFAPP steam generators as the result of a vibration-induced tube failure. Areas of general corrosion and tube-wall thinning were observed on several tubes in the region where the sodium-water reaction had occurred. This was unexpected because corrosion and erosion had not been observed in sodium-water tests involving single-tube ruptures. As a result of the experience with the EFAPP steam generator, the Detroit Edison Company conducted an investigation of wastage of Croloy 2¼ from sodium-water reactions associated with leaks that are relatively small compared to a single-tube rupture; some results of these investigations indicated that small leaks can cause rapid thinning of Croloy 2¼.

In early 1964 APDA initiated a project sponsored by the USAEC to determine the dominant parameters for materials wastage during small leaks and to establish a means of predicting wastage rates. Subsequently the project scope was broadened to include basic investigations of the wastage mechanisms and of the sodium-water reaction phenomena associated with needle-like jets of high-pressure water into a sodium pool.

* Work performed under U. S. Atomic Energy Commission Subcontract AT(11-1)-865.

II. Wastage Studies

A. Facilities and Procedures

The materials wastage tests at APDA were conducted in two different test apparatus designated Rig 10 and Rig 43. Rig 10 is a large test rig for investigating the effects of small leaks under conditions simulating the environment of a steam generator. A description of Rig 10 has been reported previously.[1] A schematic diagram is shown in Fig. 1. Prior to starting a test a measured amount of water is added to the injection-water storage tank, the circulating-water system is filled, and both systems are pressurized to 2650 psig with nitrogen. The sodium system is brought to temperature of 400°F and filled with approximately 7000 lb of sodium. With the sodium circulating, the system temperature is gradually increased to the test temperature of 625°F. During this period the sodium is cold trapped until the plugging temperature is below 400°F. The injection water and the circulating water are heated by the sodium to 625°F. The circulating water flows through the tube bundle by natural circulation.

A cross-sectional view of the tube bundle (see Fig. 2) shows the relative position of the water-injection nozzle and the target tube. The injection nozzle, which simulates a leaking tube, can be positioned between ¼ to 1½ in. from the target tube. The leak is initiated by breaking off the carburized capillary tube of the injection nozzle. Thermocouples swaged down to 0.040-in. diameter at the tips are located throughout the tube bundle, with a circular array of six thermocouples mounted on the target tube in the target area. Signals from the thermocouples are fed to an optical oscillograph for fast response temperatures and to indicate when the test is initiated and completed.

Rig 43 is a small test apparatus for basic studies of the sodium-water reaction.[2] A schematic diagram is shown in Fig. 3. The reaction vessel is a 12-in.-diameter by 42-in.-long carbon steel vessel; the sodium loop is of 1-in. Type 304 stainless steel pipe. The water-injection system is very similar to that used in Rig 10. A pressure-control valve normally vents the hydrogen from a sodium-water reaction, but for abnormal conditions a rupture disc is pro-

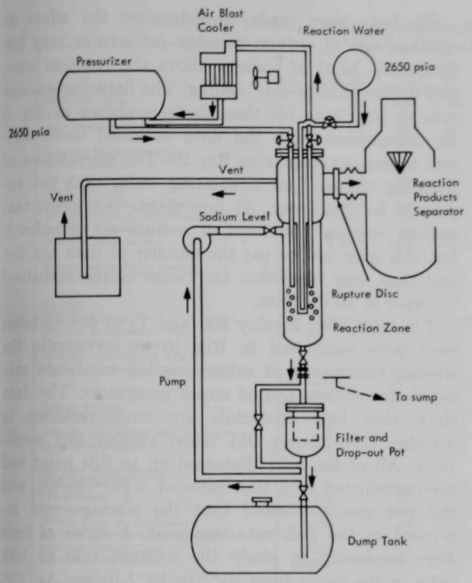

FIG. 1. Sodium-Water Reaction Test, Rig 10.

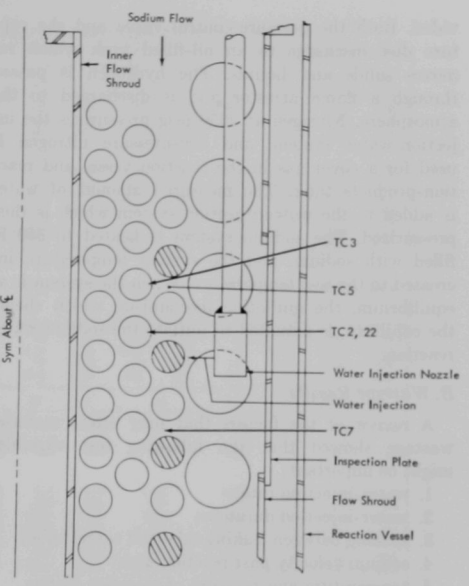

FIG. 2. Elevation Cross Section of Tube Bundle Assembly for Rig 10.

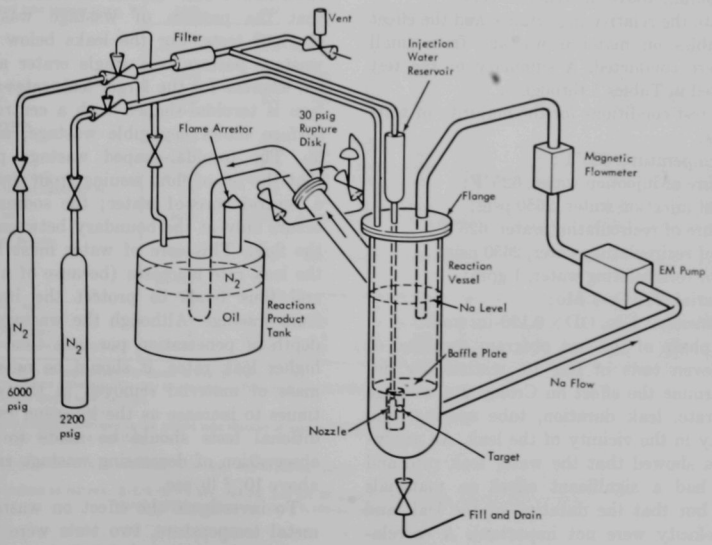

FIG. 3. Flow Diagram for Rig 43.

vided. Both the pressure-control valve and the rupture disc discharge to an oil-filled tank which removes solids and liquids. The hydrogen is passed through a flame arrestor and is discharged to the atmosphere. Nitrogen at 2650 psig pressurizes the injection-water system, and low-pressure nitrogen is used for a cover gas in the reaction vessel and reaction-products tank. The measured amount of water is added to the water-injection system which is then pressurized. The sodium system is heated to 350°F, filled with sodium, and the system temperature increased to the test temperature. When the system is at equilibrium, the guillotine mechanism, which shears the capillary, is actuated to initiate the sodium-water reaction.

B. Wastage Results

A review of the factors that may affect material wastage showed that the following test variables might be important:

1. water-injection rate;
2. water-injection duration;
3. spacing between leaking tube and target tube;
4. sodium velocity past reaction area;
5. temperature and pressure of injection water;
6. sodium temperature;
7. target-tube material;
8. target tube-side coolant;
9. head of sodium above the reaction zone.

To investigate the relative importance and the effect of these variables on material wastage from small leaks, tests were conducted. A summary of the test data is presented in Tables 1 through 3.

The general test conditions for the majority of tests were as follows:

1. sodium temperature, 625°F;
2. temperature of injection water, 625°F;
3. pressure of injection water, 2650 psig;
4. temperature of recirculating water, 625°F;
5. pressure of recirculating water, 2650 psig;
6. flowrate of recirculating water, 1 gpm;
7. tube material, 2¼ Cr-1 Mo;
8. tube dimensions: 1-in. OD x 0.120-in. wall.

The initial phase of the test program consisted of a series of eleven tests in Rig 10, statistically designed to determine the effect on Croloy 2¼ wastage rate of leak rate, leak duration, tube spacing, and sodium velocity in the vicinity of the leak. An analysis of the data showed that the water leak rate and tube spacing had a significant effect on materials wastage rate, but that the duration of the leak and the sodium velocity were not important. A correlation of leak rate, spacing, and wastage rate is shown in Fig. 4.

Six tests were made to determine the effect on wastage rate of sodium velocity (at zero or very low flowrates), head of sodium above the reaction zone, and degree of tube-side cooling. The data for wastage rate vs leak rate for these tests is shown in Fig. 5 for comparison with the data obtained under normal testing conditions in Rig 10. The substitution of stagnant nitrogen for circulating water does not appear to be significant. At first glance it appears that sodium velocity and head of sodium are significant, but this may not be so: the number of data are few and they may be within the range of the statistical variance of all the data.

Ten tests with Incoloy 800 and Type 304 stainless steel were conducted in Rig 10 to investigate the wastage resistance of other possible candidate materials for sodium-heated steam generators. The data show that both materials are more resistant to wastage than Croloy 2¼ under similar test conditions. All of the tests discussed up to this point had been conducted with leak rates of $<10^{-2}$ lb/sec, and the test results showed that the wastage rate increased as the leak rate increased. A series of tests were conducted to study the wastage rate at leak rates in the range from 10^{-2} to 10^{-1} lb/sec. As. Fig. 4 shows, negligible wastage of Incoloy 800 and stainless steel was obtained at leak rates of 10^{-1} lb/sec, and the wastage rate of Croloy 2¼ decreases at leak rates above 10^{-2} lb/sec. In these tests it was noted that the pattern of wastage was different from previous tests. For the leaks below 10^{-2} lb/sec the wastage pattern is a single crater as shown in Fig. 6a, whereas for the larger leak rates the wastage pattern is toroidal-shaped with a central plateau whose surface shows negligible wastage, as shown in Fig. 6b. The toroidal-shaped wastage pattern indicates that the jet of fluid issuing from the leak consists of a central core of water; the sodium-water reaction occurs only at the boundary between the sodium and the fluid. This core of water must become larger as the leak rate increases (because of a larger hole size) and thus tends to protect the impingement point from wastage. Although the wastage rate defined as depth of penetration per unit time decreases at the higher leak rates, it should be noted that the total mass of material removed in the wasted area continues to increase as the injection rate increases. Additional tests should be made to substantiate the observation of decreasing wastage rates at leak rates above 10^{-2} lb/sec.

To investigate the effect on wastage of the initial metal temperature, two tests were made with a sodium temperature of 680°F instead of the nominal 625°F. This was the maximum temperature that

TABLE 1. DATA SUMMARY FOR DYNAMIC SODIUM TESTS WITH APDA RIG 10

	TEST NUMBER												
	1	2	3	4	5	6	7	8	9	10	11	12	13
Sodium System													
Flowrate, gpm	400	400	420	395	400	200	400	400	200	200	400	400	200
Velocity past target tube, ft/sec ~	2	2	2	2	2	1	2	2	1	1	2	2	1
Bulk Temperature, F	632	618	611	615	625	608	605	605	610	603	613	628	605
Injection Water System													
Water added, lb	0.88	0.88	0.24	0.60	0.48	0.24	0.24	0.48	0.24	0.30	0.11	0.24	0.14
Temperature, F	632	618	611	615	625	608	605	605	610	603	619	628	605
Pressure, psig	2650	2650	2650	2650	2650	2650	2650	2650	2650	2650	2650	2650	2650
Orifice size, in. (nominal)	0.008	0.008	0.006	0.006	0.006	0.006	0.006	0.006	0.006	0.004	0.004	0.004	0.004
Injection point-to-target spacing, in.	1-1/4	1.0	1.0	1.0	1.0	1.0	1/4	1.0	1/4	1.0	1.0	1/4	1/4
Injection duration, sec	(a)	322	98	269	290	104	107	230	125	235	78	196	125
Injection rate, lb/sec	(a)	0.0029	0.0025	0.0022	0.0017	0.0023	0.0022	0.0021	0.0019	0.0013	0.0014	0.0012	0.0011
Recirculating Water System													
Pressure, psig	2650	2650	2650	2650	2650	2650	2650	2650	2650	2650	2650	2650	2650
Wastage													
Target Material	C.S.	←						2-1/4 Cr-1 Mo Steel					→
Depth of penetration, mil	16	(b)	25	100	13-15	19	80	28	72	0	2	38	24
Wastage rate, mil/sec	0.05	-	0.25	0.37	0.05	0.18	0.75	0.12	0.58	0	0.03	0.19	0.20
Wastage rate, mil/lb water	1.8	-	97	167	29	79	330	58	298	0	7	158	175
Maximum measured tube temperature, F	(d)	~800(c)	930	1030	947	1042	1075	892	970	778	777	1214	1030

	TEST NUMBER												
	14		18	19	19A	20	21		23	24	25	26	27
Sodium System													
Flowrate, gpm	400		400	400	400	400	400		400	400	400	400	400
Velocity past target tube, ft/sec ~	2		2	2	2	2	2		2	2	2	2	2
Bulk Temperature, F	610		610	610	604	600	400		602	625	602	610	605
Injection Water System													
Water added, lb	0.24		1.3	1.3	1.3	1.3	1.3		0.24	0.65	0.24	0.24	1.3
Temperature, F	610		608	613	604	600	600		602	625	603	610	605
Pressure, psig	2650		2650	2650	2650	2650	2650		2650	2650	2650	2650	2650
Orifice size, in. (nominal)	0.006		0.006	0.004	0.004	0.006	0.006		0.006	0.010	0.004	0.006	0.016
Injection point-to-target spacing, in.	1/4		1	1/4	1/4	1/4	1/4		1/4	1/4	1/4	1/4	1/4
Injection duration, sec	133		799	856(f)	861	691	570		145	103	208	619	100
Injection rate, lb/sec	0.0012		0.0016	(g)	0.0015	0.0019	0.0023		0.0017	0.0063	0.0012	0.0021	0.0013
Recirculating Water System													
Pressure, psig	75(e)		2650	2650	2650	2650	2650		2650(e)	2650	2650	2650	2650
Wastage			Incoloy	Incoloy	Incoloy	Incoloy	Incoloy		2-1/4 Cr-1 Mo	Incoloy			Incoloy
Target Material	2-1/4 Cr-1 Mo		800	800	800	800	800		-	800	321 SS	321 SS	800
Depth of penetration, mil	38		0	0	0	0	12		41	4	0	17	0
Wastage rate, mil/sec	0.20		0	0	0	0	0.02		0.28	0.04	0	0.03	0
Wastage rate, mil/lb water	158		0	0	0	0	9.2		170	6.2	0	13.1	0
Maximum measured tube temperature, F	1240		1020	1190	1150	1186	1341		940	1621	1081	1526	1803

	TEST NUMBER												
	28		29A	30	31	32	33		35	36	37	38	39
Sodium System													
Flowrate, gpm	400		400	400	400	400	400		400	400	400	400	400
Velocity past target tube, ft/sec ~	2		2.0	2.0	2.0	2.0	2.0		2.0	2.0	2.0	2.0	2.0
Bulk Temperature, F	622		610	600	600	600	605		605	615	600	680	680
Injection Water System													
Water added, lb	1.3		1.3	1.3	0.065	0.24	0.96		0.96	0.96	0.197	0.20	0.49
Temperature, F	622		610	600	608	600	605		605	615	600	680	680
Pressure, psig	2650		2650	2650	2650	2650	2650		2650	2650	2650	2900	2900
Orifice size, in. (nominal)	0.040		0.016	0.043	0.016	0.006	0.016		0.043	0.016	0.010	0.010	0.014
Injection point-to-target spacing, in.	1/4		1/4	1/4	1	1/4	1/4		1/4	1-9/32	1/4	1/4	1/4
Injection duration, sec	23		150.5	11	2.5	150.4	41		11	42.1	20.9	60(h)	74(h)
Injection rate, lb/sec	0.0565		0.0086	0.118	0.026	0.0016	0.0234		0.087	0.0233	0.0094	0.0033	0.0066
Recirculating Water System													
Pressure, psig	2650		2650	2650	100(e)	2650	2650(e)		2650	10(e)	2650	2650(e)	2650(e)
Wastage	Incoloy												
Target Material	800	←	304 SS	→					2-1/4 Cr - 1 Mo Steel				→
Depth of penetration, mil	0		21	0	0	79	36		6	21	63	122(h)	122(h)
Wastage rate, mil/sec	0		0.140	0	0	0.525	0.88		0.55	0.50	3.0	2.1	2.1
Wastage rate, mil/lb water	0		16.2	0	0	329	37.5		6.25	21.9	320	600	245
Maximum measured tube temperature, F	1793		1600	2016	1773	1000	1705		1770	1615	1580	1247	1605

(a) Unknown; assumed to be approximately equal to that in Test No. 2
(b) Tube failed by pressure following thinning by wastage. Tube wall was 0.120-in. thick.
(c) Temperature before target tube rupture.
(d) No thermocouples in wastage area.
(e) Test was run with stagnant nitrogen in the target tube instead of recirculating water.
(f) Test terminated due to plugged capillary.
(g) Unknown.
(h) Tubes completely penetrated in 58 seconds. Tube wall was 0.120-in. thick.

NOTE: Target dimensions as follows: 2-1/4 Cr - 1 Mo, 304 SS, and 321 SS targets were 1.0-in. OD x 0.120-in. wall; Incoloy 800 was 0.84-in. OD x 0.109-in. wall.

TABLE 2. TESTS IN RIG 10 SIMULATING CONDITIONS IN RIG 43

	Test No.					
	14	15	16	17	22A	23
Sodium System						
Flow rate, gpm	400	0[a]	0[a]	20[b]	0[a]	400
Velocity past target tube, ft/sec	2	0	0	.1	0	2
Bulk temperature, °F	610	610	620	610	600	602
Sodium level above target tube, ft	8.4	8.4	1.25	8.4	8.4	8.4
Water-injection System						
Water added, lb	0.24	0.24	0.24	0.24	0.24	0.24
Temperature, °F	610	610	620	605	600	602
Pressure, psig	2650	2650	2650	2650	2650	2650
Orifice size, in. (nominal)	0.006	0.006	0.006	0.006	0.006	0.006
Injection point-to-target spacing, in.	¼	¼	¼	¼	¼	¼
Injection duration, sec	133	125	153	145	236	145
Injection rate, lb/sec	0.0012	0.0019	0.0016	0.0017	0.0010	0.0017
System for Recirculating Water						
Pressure, psig	No Water[c]	2650	No Water[c]	2650	2650	No Water[c]
Wastage						
Material	2¼ Cr-1 Mo Steel					
Depth of penetration, mils	38	12	27	35	21	41
Wastage rate, mils/sec	0.20	0.10	0.18	0.24	0.09	0.28
Wastage rate, mils/lb water	158	50	113	146	87.5	170
Maximum measured tube temperature, °F	1240	1380	1180	960	1780	940

[a] Sodium pump turned off.
[b] Nominal flow rate; actual flow rate estimated to be between 0 and 40 gpm.
[c] Test was run with stagnant nitrogen in the target tube.

TABLE 3. DATA SUMMARY FOR TESTS WITH APDA RIG 43

	Test No.						
	1	2	3	4	5	6	8A
Sodium System							
Flow rate, gpm	0	0	0	44	23.5	25	0
Bulk temperature, °F	630	630	630	705	602	600	605
Sodium level above injection point, ft	1.5	1.5	1.5	1.5	1.5	1.5	1.5
Water-injection System							
Water added, lb	0.24	0.24	0.24	0.24	0.24	0.24	0.24
Temperature, °F	630	630	630	680	602	603	605
Pressure, psig	2650	2650	2650	2650	2650	2650	2650
Orifice size (nominal), mil	6	6	6	6	6	6	6
Injection point-to-target spacing, in.	¼	¼	¼	¼	¼	¼	¼
Injection duration, sec	70	61	52	23[a]	122	162	103
Injection rate, lb/sec	0.0034	0.0039	0.0047	[a]	0.002	0.0014	0.0023
Wastage							
Material	Croloy 2¼						
Dimensions							
Outside diameter, in.	1	1	1	1	1	1	1
Wall thickness, in.	0.120	0.120	0.120	0.120	0.120	0.120	0.120
Depth of penetration, mils	[b]	[b]	[b]	10	62	32	[b]
Wastage rate, mils/sec	[b]	[b]	[b]	0.43	0.50	0.19	[b]
Maximum measured tube temperature, °F	1440	1390	1610	747	1039	1385	1040

[a] The injection duration was much shorter than expected. The test temperature inadvertently exceeded the water saturation temperature, and it is quite likely that some of the water that was added to the injection system evaporated and condensed out in the cooler portions of the system. Because of this, the actual quantity of water injected is questionable; therefore, a meaningful injection rate cannot be determined.
[b] Negligible.

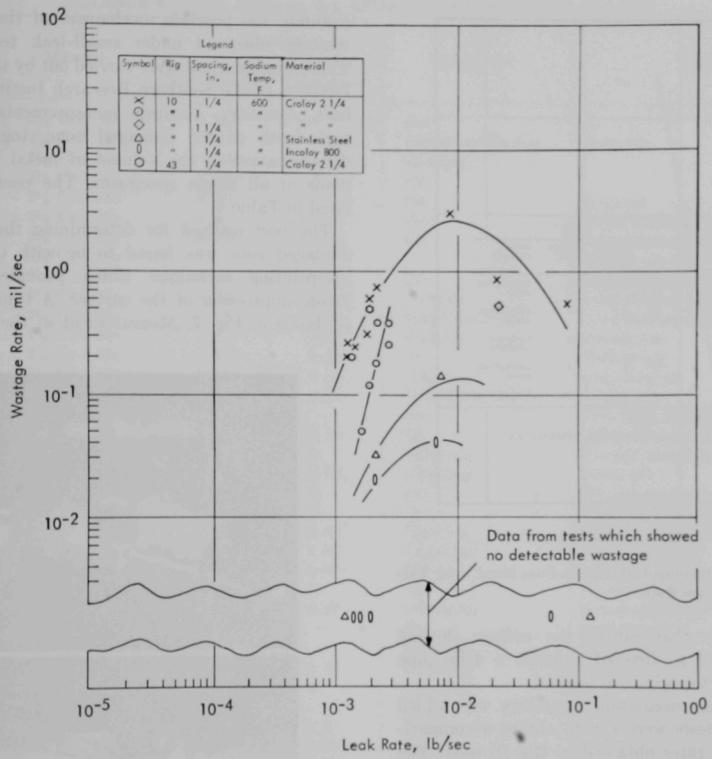

FIG. 4. Materials Wastage Rates Obtained in Dynamic Sodium Systems.

could be achieved with the existing high-pressure nitrogen system while still maintaining a water phase in the injection system. The leak rates were approximately 10^{-2} lb/sec. The wastage results were not significantly different from those obtained with sodium at 625°F.

To minimize the number of material evaluation tests in Rig 10, a materials screening program was initiated in Rig 43, which at the time was not equipped with the system for sodium circulation. The target consisted of a 2-in.-long piece of 1-in.-diameter tube sealed at the ends. Two thermocouples were attached to the surface near the impingement area. Prior to doing the materials screening tests, three tests with Croloy 2¼ target tubes were run to establish the reproducibility of the experiment and to establish the correlating factor between Rig 10 and Rig 43. Negligible wastage was obtained in each of the three tests, whereas tests conducted in Rig 10 under comparable conditions led to approximately 70 mils of penetration. Three major differences between Rig 10 and Rig 43 were: 1) velocity of the sodium past the target material, 2) sodium head above the reaction zone, and 3) configuration in the target region, that is, an unrestricted region with the single tube target versus a congested region for the tube bundle. As discussed earlier for the Rig 10 tests, the effect on wastage rate of low sodium velocity and low sodium head above the reaction zone was inconclusive; nevertheless, appreciable wastage was obtained with no sodium flow past the target tube. At this time it was decided that Rig 43 would be provided with means for circulating sodium. To minimize the size of the sodium-circulation system and still be able to achieve the desired sodium velocity, the internals of the Rig 43 reaction vessel

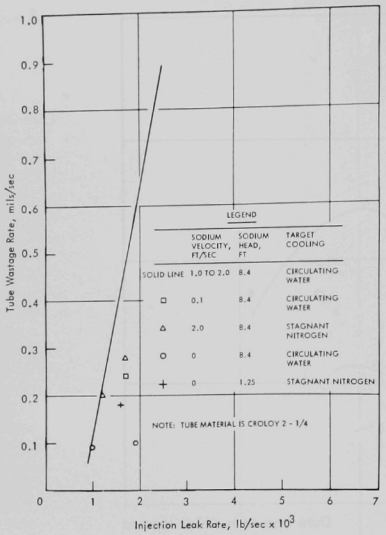

FIG. 5. Effect of Sodium Velocity, Sodium Head, and Target Cooling on Wastage Rate.

were modified so that all of the sodium flowing through the vessel is directed through a 4-in. pipe in which the target specimen is located.

After the sodium-circulation capability was added to Rig 43, three tests were run to obtain a comparison with wastage rates obtained in Rig 10 tests. The results of these tests, performed under essentially identical test conditions to establish reproducibility, showed that significant wastage occurred and that the wastage rates had a one-to-one correspondence with Rig 10 wastage rates for similar test conditions. The data are shown in Fig. 4. The wasted region of the three target tubes exhibited a pit-type pattern that is consistent with previous patterns obtained in Rig 10 tests at the lower leak rates. In a fourth test, run in stagnant sodium, negligible wastage was observed, verifying test results obtained prior to the Rig 43 modification. The results of the Rig 10 and Rig 43 tests definitely show that wastage rates in static sodium are significantly lower than in flowing sodium. The difference between wastage rates observed in Rig 10 and in Rig 43 in static sodium indicates there may be a geometry effect.

C. Post-test Examination of Target Tubes

Extensive examination of the target tubes was performed 1) to provide accurate data on the area, depth, and volume of the damaged zone, and 2) to evaluate the possible mechanism of the rapid metal wastage observed under small-leak test conditions. These examinations were carried out by the Metallurgy Division of the Southern Research Institute, Birmingham, Alabama. Accurate measurements of the area and depth of the damaged zone, together with a determination of the volume of metal wastage were made of all target specimens. The results are tabulated in Table 4.

The best method for determining the area of the damaged zone was found to be with the use of an ink-printing technique which provided a mirror-image impression of the surface. A typical ink print is shown in Fig. 7. Measurement of the depth of the

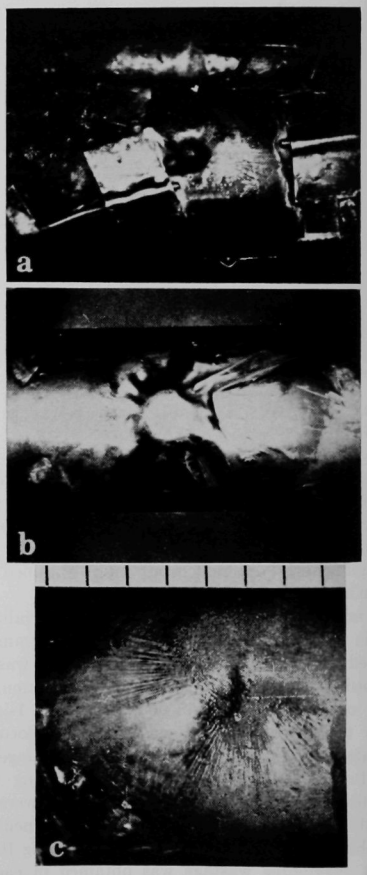

FIG. 6. Typical Wastage Patterns.

TABLE 4. DATA SUMMARY FOR APDA RIG 10 TARGET-TUBE ANALYSES

Test No.	Material	Wastage		Position[a]	Comments
		Data Area, in.^{2}	Volume, in.^{3}		
3	2¼ Cr-1 Mo	0.107	0.583×10^{-3}	On	—
4	2¼ Cr-1 Mo	0.158	4.14	Center to grazing	Deep pit
5	2¼ Cr-1 Mo	0.145	0.658	Grazing	—
6	2¼ Cr-1 Mo	0.0586	0.538	On	—
7	2¼ Cr-1 Mo	0.387	3.77	On	Deep pit
8	2¼ Cr-1 Mo	0.143	1.54	On	Broad shallow depression
9	2¼ Cr-1 Mo	0.300	2.58	On	Deep narrow depression
10	2¼ Cr-1 Mo	—	0	—	Erosion too faint and too little
11	2¼ Cr-1 Mo	0.109	0	On	Erosion too shallow
12	2¼ Cr-1 Mo	0.406	2.07	Grazing	Long shallow depression
13	2¼ Cr-1 Mo	0.190	1.30	Slight grazing	Long shallow depression
14	2¼ Cr-1 Mo	0.661	2.46	Grazing	Double pit
15	2¼ Cr-1 Mo	0.638	0.61	On	Shallow pit
16	2¼ Cr-1 Mo	0.718	1.36	Glancing	Deep long pit
17	2¼ Cr-1 Mo	0.534	1.23	Center to glancing	Triple pit
18	Incoloy-800	—	—	On	Very light frosted area
19	Incoloy-800	0.106	0.19	On	Sharp side pitted
19A	Incoloy-800	0.084	0	Glancing	Frosted area only
21	Incoloy-800	0.103	0.36	Glancing	Broad pit
21A	Incoloy-800	0.079	0	On	Frosted area only
22	2¼ Cr-1 Mo	0.116	0	On	Eroded tool mark
22A	2¼ Cr-1 Mo	0.536	0.42	Glancing	Shallow, broad pit
23	2¼ Cr-1 Mo	0.681	1.48	Glancing	Deep, broad pit
24	Incoloy-800	0.205	0.07	On	2 shallow pits
25	321 SS	0.009	0	On	Frosted area only
26	321 SS	0.203	0.27	Off center	Broad shallow pit
27	Incoloy-800	—	—	On	Light frosting
28	Incoloy-800	—	—	Glancing	Light frosting
29A	304 SS	0.769	1.62	Glancing	Shallow pit, little erosion
30	304 SS	0	0	Glancing	Only "stain"
31	2¼ Cr-1 Mo	0.934	—	On	Broad shallow "polish"
32	2¼ Cr-1 Mo	0.552	1.9	Slightly off center	Deep, steep-sided pit
33	2¼ Cr-1 Mo	1.516	13.96	On	Multiple pits around "mesa"
35	2¼ Cr-1 Mo	1.472	2.01	Off	2 broad shallow areas well separated
36	2¼ Cr-1 Mo	2.063	10.6	On	Large area central hump
37	2¼ Cr-1 Mo	1.079	2.61	Glancing	Off-center pit
38	2¼ Cr-1-Mo	0.284	1.94	Slightly off center	Full penetration in center of narrow jet
39	2¼ Cr-1 Mo	0.900	10.2	On	Full penetration 2 spots, central mesa

[a] Position relative to target point.

damaged regions was made with a standard 1-in. depth micrometer modified to provide four-point support. The maximum depth of the damaged region was measured with a cone-tipped spindle while manipulating both the specimen and the micrometer under a stereomicroscope. The area of the wasted region was measured with a planimeter, and the volume of the wasted region was determined using a positive epoxy replica weighed to a precision of 0.1 mg.

In almost every case the wastage area of the tube had a semi-matte appearance consistent with that frequently observed as a result of erosion. In addition, several target tubes showed a series of ridges radiating outward from the central portion of the damaged region (shown in Fig. 6c). In no case was there evidence of corrosion products remaining in the general area of the damaged zone. In some instances, there was a minor degree of staining observed, but this was believed to be associated with the post-test cleaning.

III. Mechanisms of Wastage

The injection of a high-velocity jet of water into sodium, such as is done in the small-leak sodium-water tests, produces a violent chemical reaction with

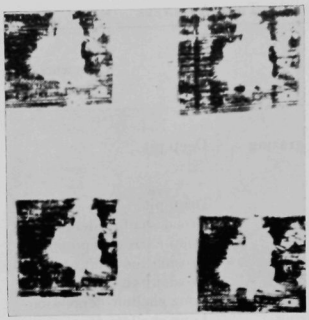

FIG. 7. Ink Print of Specimen No. 7 for Obtaining Area of Damaged Zone.

the formation of corrosive reaction products (e.g., sodium hydroxide and sodium oxide), the generation of heat, and the formation of particles and/or jets of the reactants and products moving at high velocities. A metallic surface in close proximity to the sodium-water reaction zone would be subjected, to some degree, to the reaction heat and to the blast of the reactants and reaction products. It is postulated that the wastage of a surface in the proximity of a sodium-water reaction could be the result of a combination of both erosion and corrosion by the reactants and the reaction products, and that the wastage is further accelerated by heating of the surface as a result of the heat generated by the sodium-water reaction.

Studies were conducted to determine the contribution of corrosion and erosion to the wastage process. Since both phenomena are temperature-dependent, tests were also conducted to determine the reaction temperatures occurring during small leaks of water into sodium.

A. Reaction Temperatures

The calculated adiabatic temperature for the sodium-water reaction is approximately 3000°F. Temperatures above 2000°F have been reported in tube-rupture tests with leak rates of pounds of water per second.[1, 3, 4, 5] However, no data had been available for smaller leaks.

APDA investigated temperatures in the reaction region and on adjacent metal surfaces for pinhole-sized defects with leak rates of the order of 10^{-3} lb/sec. The reaction temperatures were measured with fast-response, low-heat-capacity thermocouples. The tests to measure reaction temperatures were conducted in Rig 43. One of the target assemblies used consisted of sixteen $\frac{1}{16}$-in.-diameter, Type 304 stainless steel-sheathed thermocouples swaged down to 0.040 in. at the hot junction. The thermocouples were mounted in a 3-in.-diameter rim similar to spokes on a wheel, and the sixteen hot junctions formed a plane target approximately ¾ in. in diameter. In the tests, the spacing between the leak and the plane target assembly was varied between ¼ and 1½ in. During a test, temperatures were recorded on a high-speed oscillograph.

Figure 8 shows a plot of the maximum temperatures recorded during these tests versus the injection point-to-target spacing. The curve represents the maximum temperatures in tests with a needlelike jet of water from 8-mil-diameter capillaries. The temperatures are the maximum measured during a particular test, but may not be the maximum reaction temperature, although measurements by adjacent thermocouples suggest that they are within 100°F of the maximum reaction temperature. The maximum temperatures vary from 1580°F at a spacing of ¼ in. to 700°F at a 1½-in. spacing. The decrease in the maximum temperature as the spacing is increased can be expected for two reasons: 1) the fraction of unreacted water in jet decreases with in-

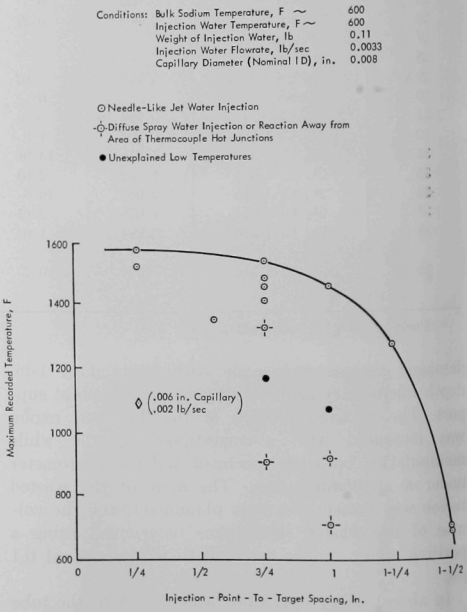

FIG. 8. APDA Small-leak Studies for Sodium-Water Reaction Temperatures.

creasing distance from the leak, and 2) the heat-transfer rate to the bulk sodium from the reaction zone increases due to the increased surface area as the jet spreads out.

All maximum temperature values are much lower than the adiabatic reaction temperature and also lower than maximum temperatures measured in tests at higher injection rates. We believe that this is caused by the low injection rate of 3×10^{-3} lb/sec. This belief was substantiated by the data point which was obtained at a flow rate 40% lower than in the balance of the experiments, yielding a maximum temperature 30% lower. The data also show that lower temperatures are obtained with a spray-injection pattern similar to an aerosol spray, as contrasted to a needlelike jet. This could be caused by several factors, as follows: 1) the reaction zone might be confined to a volume close to the injection point due to diminished penetration capability, 2) the reaction may be occurring only at the water vapor-sodium interface as discussed earlier, and the thermocouple hot junctions were contained within this volume and cooled by vaporization, 3) there is a lower density of reactants per unit volume in the reaction zone, and 4) a much heavier buildup of reaction products occurred on the target than with a needlelike jet, insulating the target thermocouples. The spray pattern is caused by bits of metal projecting into the jet at the point where the injection capillary is sheared off.

The test results indicate that the spatial orientation of the jet was very stable and that the cross section of the reaction zone was quite small. In more than 50% of the experiments the value of the maximum temperature varied less than ±10% throughout the test. The high stability of the reaction zone is inferred from the observation that the location of the maximum temperature remained within an area less than 0.1 in. in diameter at a distance of ¾ in. from the leak. The cross section of the reaction zone for a 0.008-in. defect is believed to be approximately ¼ in. in diameter at a distance of 1¼ in. from the defect.

The reaction appears to take place in an extremely thin layer between the bulk sodium and water phases. This is illustrated by a temperature gradient of 240°F over a distance of 0.060 in. from the maximum temperature location, which is equivalent to a temperature gradient of 4000°F per inch.

Another observation which indicates the extremely thin reaction layer is the comparison of temperatures measured by two adjacent thermocouples. One thermocouple, apparently located in the bulk water phase, indicated a temperature 300°F below the bulk sodium temperature, whereas a thermocouple 0.030 in. away measured 1300°F. This represents a temperature gradient of over 30,000°F per inch. After considering these temperature measurements we concluded that the reaction is taking place in a layer 30 mils thick. These data indicate that the sodium-water reaction takes place on the surface of a bubble containing a steam-water mixture and has a geometry somewhat like a flame. These conclusions are consistent with the wastage patterns observed in the Rig 10 and Rig 43 tube-wastage tests.

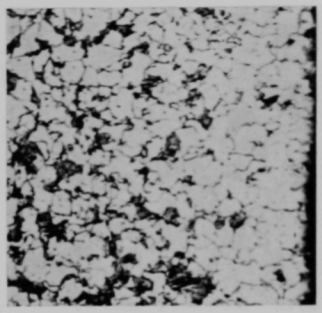

FIG. 9. Microstructure of Croloy Specimen No. 4.

B. Target-metal Temperatures

An effort was made to establish target-tube temperatures reached during the wastage tests. This was done both by observation of the microstructure of the Croloy material and by detailed hardness surveys. Microstructural examinations of cross sections of specimens Nos. 3, 4, 7, 22a, 32, 33, 38, and 39 were carried out. With the exception of specimen No. 32, which is discussed later, the general microstructure of the Croloy material adjacent to the damaged zone consisted of a mixture of ferrite and what is considered to be upper Bainite. There was no evidence of residual cold working of the tubing. In most cases, the outer surface was decarburized to a depth ranging from 0.001 to 0.005 in., probably resulting from mill-annealing. A typical example of this structure is shown in Fig. 9. The photomicrograph shows a fairly coarse carbide segregation, which subsequently made the determination of the temperature history of the specimens during test more difficult and less precise than would have been the case had the carbon distribution been more uniform.

A microstructure at the maximum depth of penetration of specimen No. 4 is shown in Fig. 10. The surface to the right of the microstructure is the outer surface of the target tube. It can be seen that there is no evidence of intergranular corrosion and that

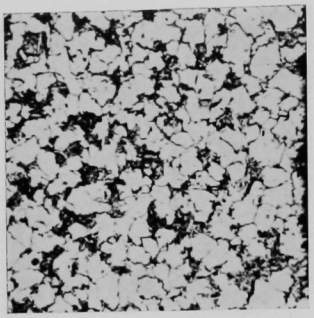

FIG. 10. Microstructure of Point of Maximum Depth of Damaged Zone.

essentially the microstructure is unchanged from that of Fig. 9. Figure 10 is representative of the surface condition of all target tubes examined metallographically.

A complete lack of change in microstructure or hardness established that in many cases the target-tube temperature during the wastage tests did not exceed the final mill-anneal temperature of 1200°F. To provide further insight into the actual temperatures achieved during the wastage tests, a study was conducted of the time-temperature-hardness relationship in Croloy 2¼. It was hoped that such relationships would provide a means of establishing temperature isotherms around the damaged region of the target tubes. A special target tube was prepared by heat treating at 1700°F for ½ hr, water quenching, and then tempering at 600°F for 6 hr, the nominal sodium temperature during the wastage tests. A piece of this tube was removed for use in tempering time-temperature-hardness studies, and the remainder of the tube, identified as specimen No. 32, was used as the target tube in Test No. 32 in Rig 10. In the tempering studies specimens of the material were tempered in a salt bath at temperatures ranging from 700 to 1400°F, for times ranging from 10 to 3600 sec. All specimens were then subjected to Knoop microhardness measurements and microstructural examination. The 50-sec tempering curve and the average of the 100- and 250-sec curves are shown in Fig. 11.

A series of 12 hardness traverses across the thickness of the tube in the damaged region were made of the tube exposed to the leak test. The hardness values were then compared with those obtained by the time-temperature-tempering studies, and a series of isotherms were developed. The general temperature profiles thus obtained are shown in Fig. 12. In the case of this target tube, maximum temperature achieved during tests were concluded to be in the neighborhood of 1500°F. It is pointed out that, due to uncertainty of the actual time at temperatures, these isotherms can only be considered approximate.

Further insight into the temperatures achieved was gained on the basis of microstructure changes at temperature. These were determined by subjecting specimens from target tube No. 39, well away from the damaged region of the tube, to annealing temperatures of 1350, 1400, 1450, 1500, 1550, and 1600°F for 15 min and water quenching. The point-count method was used to determine the fraction of austenite thus formed. Shown in Fig. 13 is the relationship between hardness and volume fraction of austenite formed under the various annealing temperatures. These data were used to estimate the temperature achieved in specimens Nos. 33 and 39.

The temperature profiles derived both on the basis of hardness measurements and volume fraction of austenite are shown in Figures 14 and 15. In the case of specimen No. 39 (see Fig. 14), it can be seen that the temperature isotherms based on microhardness and volume fraction of austenite are reasonably consistent. However, for specimen No. 33 (see Fig. 15) such consistency is not seen.

The major conclusions that were reached from the metallographic examinations were:

1. No evidence could be found to indicate that corrosion contributed to metal removal. However, the possibility exists that corrosion could have taken place and that the corrosion products were either dissolved in the media or eroded away. The examination carried out under this study did not preclude this possibility.

2. The metal wastage could apparently result from simple erosion, since there was no evidence of intergranular corrosion and since the surface appearance of the wasted area is consistent with that observed under erosion conditions.

3. In cases for which water was used as the cooling medium inside the target tube, there was no evidence either microstructurally or by change in hardness to suggest that temperatures in excess of 1500°F were reached. In the case of target tubes 33 and 39, for which gas was used as the cooling medium, temperatures in excess of 1500°F were achieved, and possibly as high as 1800 and 2300°F, respectively. The higher temperatures could have been expected, however, since most of the gas-filled tubes were used at the higher leak rates.

C. Studies of Caustic Corrosion

Severe corrosion of Croloy 2¼ has been produced by molten caustic and concentrated caustic solutions at temperatures from 700 to 2400°F in tests performed by APDA and B&W. In the B&W tests,[6] a corrosion rate of 3 in./yr for Croloy 2¼ was obtained with a 98.5% caustic solution at 900°F. However, this is much too low to account for the wastage rate of over 6×10^4 in./yr obtained in some of the small-leak sodium-water reaction tests in Rig 10. In the APDA scoping tests made in 1966[1] a corrosion rate

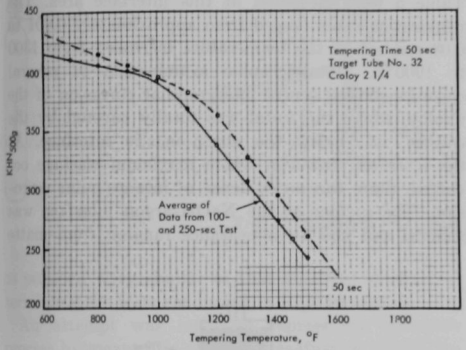

FIG. 11. Smoothed Hardness Data.

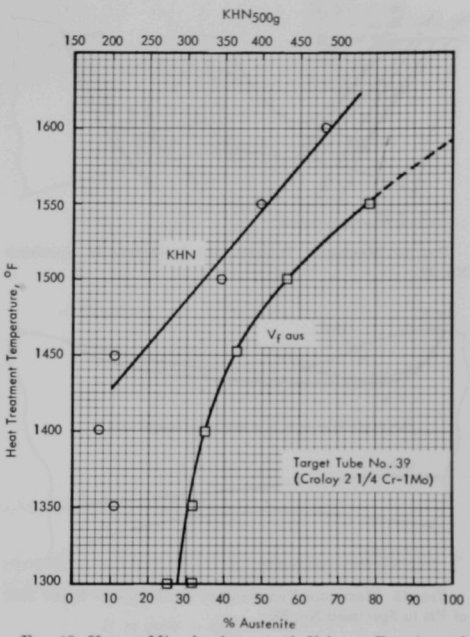

FIG. 13. Knoop Microhardness and Volume Fraction of Austenite.

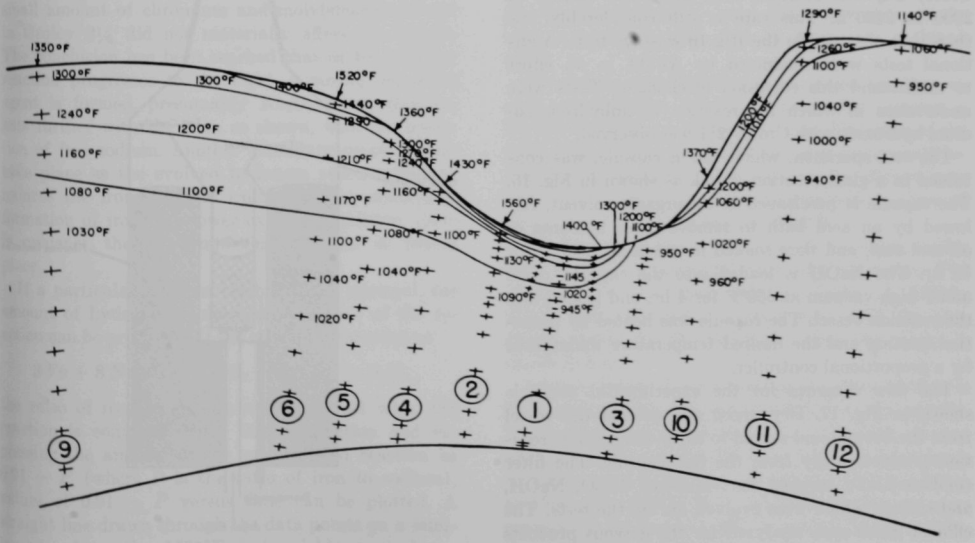

FIG. 12. Maximum Temperature Isotherms, in Specimen No. 32 as Estimated by Knoop Microhardness Measurements.

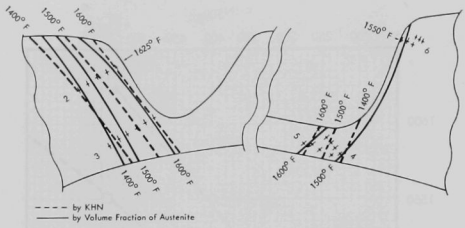

FIG. 14. Maximum Temperature Isotherms in Specimen No. 39.

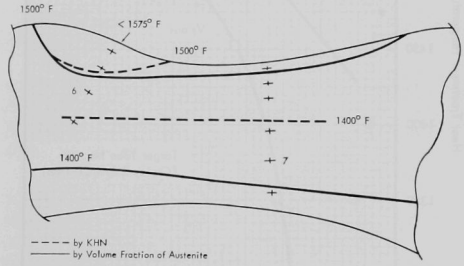

FIG. 15. Maximum Temperature Isotherms in Right Side of Pit in Specimen No. 33.

of 100 to 1000 in./yr (0.003 to 0.03 mil/sec) for Croloy 2¼ was obtained with anhydrous caustic at 2200 to 2400°F. This rate is still considerably less than that observed in the Rig 10 wastage tests. Additional tests were conducted by APDA in an effort to understand this corrosion mechanism. Tests were undertaken in which the reaction of anhydrous sodium hydroxide with Croloy 2¼ was observed.

The test specimen, which was a capsule, was contained in a glass reaction vessel, as shown in Fig. 16. The capsule is precleaned in an organic solvent, followed by an acid bath to remove gross amounts of oil and rust, and then soaked in argon at 2200°F for ½ hr. The NaOH is loaded into the capsule, dried under high vacuum at 650°F for 4 hr, and loaded into the reaction vessel. The capsule was heated by induction heating and the desired temperature maintained by a proportional controller.

The flow diagram for the experimental setup is shown in Fig. 17. Dry argon gas entered the vessel from the bottom and served to carry the gaseous reaction products away from the test capsule. The filter condensed and trapped the vaporized Na_2O, NaOH, and sodium which were evolved during the tests. The effluent gases were analyzed for the gaseous products by either an MS-10 mass spectrometer or a gas chromatograph (F&M 720). Continuing experimental difficulties with the mass spectrometer led to use of the gas chromatograph.

The primary test data for each temperature studied were: 1) the hydrogen concentration of the effluent argon stream, 2) time at temperature, 3) composition of the residue, 4) weight loss of the capsule, and 5) depth of penetration. A summary of the data is presented in Table 5. When measurable corrosion was observed, the maximum wastage always occurred at the interface of the NaOH and the argon cover gas. The depths of penetration reported in Table 5 were measured at this interface area. The penetration rates ranged from approximately 0.001 to 0.08 mil/sec as the temperature increased from 1300 to 1900°F. Metallographic examination of several capsules showed severe intergranular corrosion of the Croloy, where the metal was totally covered by the caustic, i.e., below the argon-caustic interface. At the interface, however, where maximum wastage occurred, there was no evidence of intergranular corrosion. The surface at the NaOH-argon interface was smooth and had an appearance ranging from matte

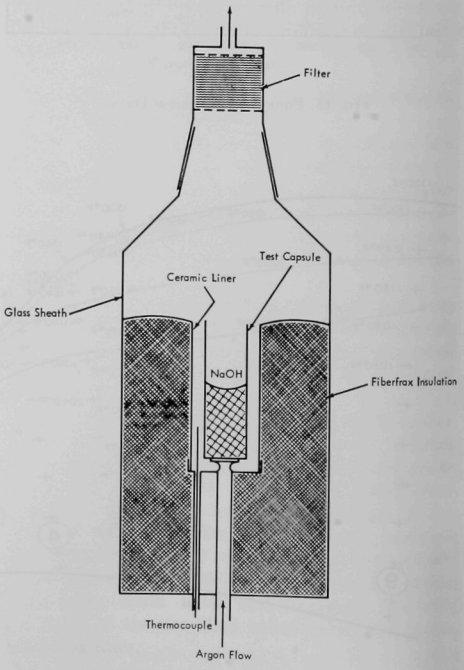

FIG. 16. Sectional View of the Reaction Vessel.

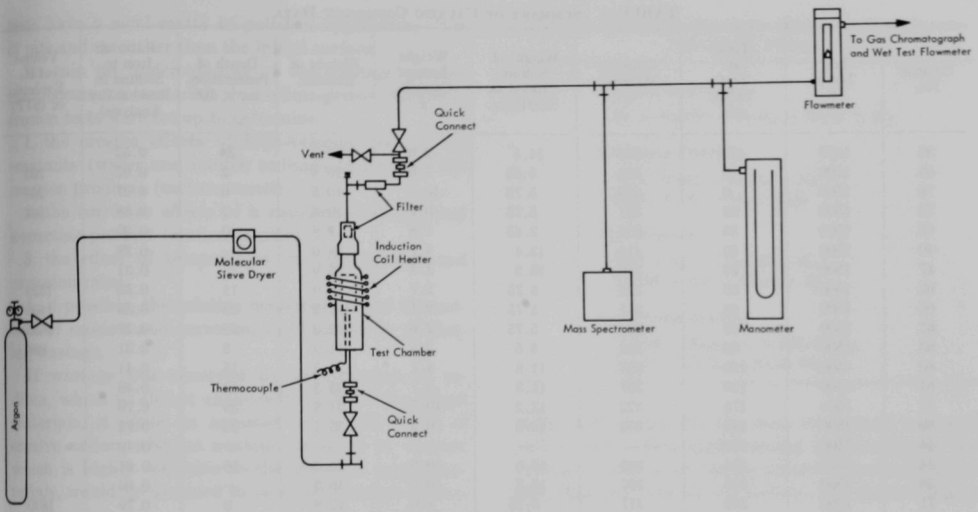

FIG. 17. Schematic Flow Diagram for Corrosion Test Equipment.

to polished, very similar to that observed in the material wastage tests conducted in Rigs 10 and 43.

An attempt was made to express the corrosion process by means of a chemical reaction. A partial list of the general reactions which may have occurred is given in Table 6, based on the assumption that the small amount of chromium and molybdenum present in Croloy 2¼ did not materially affect the results. The conclusion has been reached that as the primary reaction progresses to the right, a second corroding agent is formed, presumably Na_2O, which then reacts further with the iron, as shown, with the evolution of free sodium. Another secondary reaction may take place as the evolved hydrogen reacts with and reduces the iron oxide to iron, with the subsequent formation of iron or a lower oxide. In addition, there is evidence that a complexing reaction is taking place.

If a particular reaction mechanism is assumed, the amount of hydrogen evolved and the rate of the reaction can be predicted. If the reaction proceeded as

$$3\,Fe + 8\,NaOH \rightarrow Fe_3O_4 + 4\,Na_2O + 4\,H_2\,,$$

the ratio of iron to sodium would be 0.91 when the reaction is complete. With this assumption and expressing the amount of the uncompleted reaction as $0.91 - P$ (where P is the ratio of iron to sodium), values of $0.91 - P$ versus time can be plotted. A straight line drawn through the data points on a semi-log plot from the 1500°F tests yields a good approximation of the data. The equation expressing P as a function of time at 1500°F is

$$P = 0.91 - 0.81\,e^{(-4.21 \times 10^{-3}\theta)},$$

where θ is the time of test. The intercept of P at $\theta = 0.1$ occurs because the reaction has started during the time it takes to raise the temperature to the test temperature, and thus it represents a blank value.

The reaction at 1700°F was too rapid to allow an easy representation by this method. The reaction is 75–90% complete in the first 15 min. The slope of the data at this temperature has not been determined because of the rapidity of the reaction. Insufficient data have been taken at the other temperatures to allow an analysis similar to the data at 1500°F.

As mentioned above, the rate of hydrogen evolution can also be predicted from this expression. The treatment of this data may be found in APDA-214.[7] The comparison of test data with the predicted values for H_2 evolution using the model is shown in Fig. 18.

Another check of the proposed chemical reaction is by analysis of the residues remaining in the capsule. The residue analysis is shown as a function of time and temperature in Fig. 19. Note the high dependence on temperature in the first few minutes of the reaction at 1500 and 1700°F. If the assumed reaction goes to completion the ratio of iron to sodium in the residue should be 0.91. As the data in Fig. 19 show, this as-

TABLE 5. SUMMARY OF CAUSTIC CORROSION DATA

Capsule No.	Test Temp, °F	Time at Test Temp, min	Capsule Weight, g	Weight of Sodium (Added as NaOH), g	Weight Loss of Capsule, g	Weight of Residue, g	Depth of Penetration, in. × 10^3	Ratio of Iron to Sodium in Residue (by Analysis)	Volume of H_2 Evolved, cc (STP)
39	1300	429	319	14.5	9.0	32.5	28	0.52	
69	1500	0	321	5.65	1.0	10.8	2	0.07	205
70	1500	0	323	5.75	10.6	10.5	0	0.07	263
72	1500	30	321	5.75	0.7	10.6	2	0.18	594
65	1500	30	305	3.45	1.8	7.8	0	0.25	
40	1500	60	316	13.4	4.7	28.0	—	0.28	
47	1500	60	310	18.3	4.4	35.9	—	0.31	
62	1500	60	322	5.75	2.7	10.9	11	0.55	1539
66	1500	60	317	5.75	2.1	11.9	19	0.38	1406
67	1500	60	322	5.75	2.6	12.2	16	0.37	1655
63	1500	60	323	5.5	2.5	11.9	3	0.31	898
60	1500	120	324	11.8	4.7	24.5	15	0.41	
61	1500	120	307	11.5	5.7	25.5	13	0.48	
31	1500	175	322	13.2	10.7	31.8	20	0.70	
30	1500	180	318	14.9	10.2	35.1	26	0.72	
44	1500	180	—	—	—	—	—	0.49	
34	1500	274	322	15.0	10.6	36.6	16	0.61	
36	1500	276	307	15.3	10.3	36.5	—	0.66	
71	1500	360	317	5.75	4.0	12.8	9	0.79	1830
28	1500	405	323	14.2	10.8	34.8	27	0.79	
43	1500	420	321	16.0	8.6	36.5	30	0.77	
45	1500	420	—	—	—	—	—	0.76	
77	1700	0	311	5.69	0.6	10.5	2	0.28	1173
81	1700	15	305	5.63	4.7	14.3	3	0.69	581
78	1700	30	310	5.69	3.0	12.8	19	0.72	1104
79	1700	60	314	5.69	4.9	14.7	19	0.80	1470
46	1700	120	321	13.9	11.5	34.9	27	0.82	
22	1700	135	304	12.1	8.9	29.7	41	0.84	
42	1700	180	319	15.5	13.7	36.3	30	0.88	
26	1700	191	310	11.4	11.0	30.1	48	0.99	
25	1700	273	313	12.1	10.3	29.6	43	0.96	
24	1700	300	314	14.5	13.4	37.4	47	0.89	
27	1700	367	317	11.9	11.0	29.8	36	1.01	
37	1900	148	302	14.8	4.4	28.6	21	1.01	
35	1900	150	333	5.18	36.8	45.6	40	1.06	
48	1900	180	312	13.5	3.9	26.8	—	1.09	
38	1900	210	321	14.5	5.9	23.5	24	1.09	
49	2200	60	323	13.7	10.9	33.3	—	1.31	
50	2200	180	323	12.2	6.8	28.0	—	1.88	

sumed reaction appears to be valid up to approximately 1500 to 1700°F. Above 1700°F, this ratio exceeds 0.91, indicating that a secondary reaction occurs. This has been substantiated by the presence of free sodium in the cooler parts of the reaction vessel in those tests in which the iron-to-sodium ratio approached or exceeded the value of 1.0. Water was also noticed in the effluent argon stream in many tests.

X-ray diffraction analysis of the residues shows the presence of compounds which cannot be identified. The diffraction pattern gave no evidence of Na_2O, and this fact suggests that a complex sodium oxide-iron oxide compound has been formed.

D. Erosion Studies

Analysis of data from numerous references[8-13] about surface damage and wastage by liquids (metal and other) revealed that the pattern and mode of wastage produced by cavitation, high-velocity jet impingement, and impingement by water drops, as in rain erosion on aircraft and condensate erosion of steam turbine blades, were all somewhat dissimilar to that produced in the small-leak sodium-water tests. The surface of metal damaged by cavitation and liquid-drop impingement have a dulled, roughened, and pitted appearance, whereas the wastage surfaces from the small-leak sodium-water reaction

tests have a semi-matte to polished appearance, free of pits and smoother than the initial surface.

To gain an understanding of the wastage process that occurs on materials in sodium-water reactions, erosion tests were set up to determine:

1. the erosive effects of high-velocity jets of the reactants (water and molten sodium) and one of the reaction products (molten caustic);
2. the corrosive effects of a reactant (sodium) and a reaction product (molten caustic);
3. the effect of temperature on both erosion and corrosion rates;
4. if possible, the relative contribution and interaction of erosion and corrosion mechanisms in producing wastage.

If wastage was observed by impingement of sodium, which is almost chemically inert to the target materials, it could be assumed to be the result of erosive action, whereas wastage produced by caustic, which is highly corrosive to the proposed target materials, would be assumed to be a combination of corrosion and erosion. For the same amounts of impinged sodium and caustic under similar test conditions, the wastage produced by caustic should be more extensive than that produced by the sodium. The greater degree

TABLE 6. PROPOSED CHEMICAL REACTIONS FOR CAUSTIC-CROLOY 2¼ SYSTEM

Primary Reaction

$$Fe + NaOH \rightarrow Fe_xO_y + Na_2O + H_2$$

Secondary Reactions

$$Fe + Na_2O \rightarrow Fe_xO_y + Na$$
$$Fe_xO_y + H_2 \rightarrow Fe + H_2O$$

Side Reactions

$$H_2O + Na \rightarrow NaOH + H_2$$
$$NaOH + Na \rightarrow Na_2O + H_2$$

Complexing Reaction

$$NaOH + Fe_xO_y \rightarrow NaOH \cdot Fe_xO_y$$
$$Na_2O + Fe_xO_y \rightarrow Na_2O \cdot Fe_xO_y$$

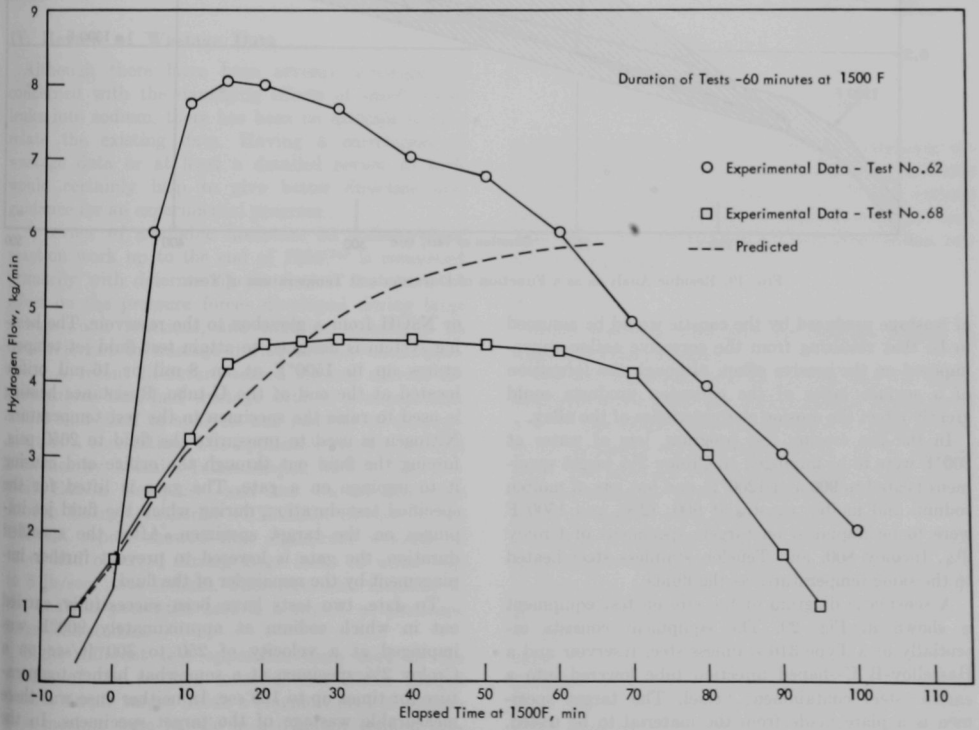

FIG. 18. Comparison of Predicted and Experimental Data for H_2 Evolution.

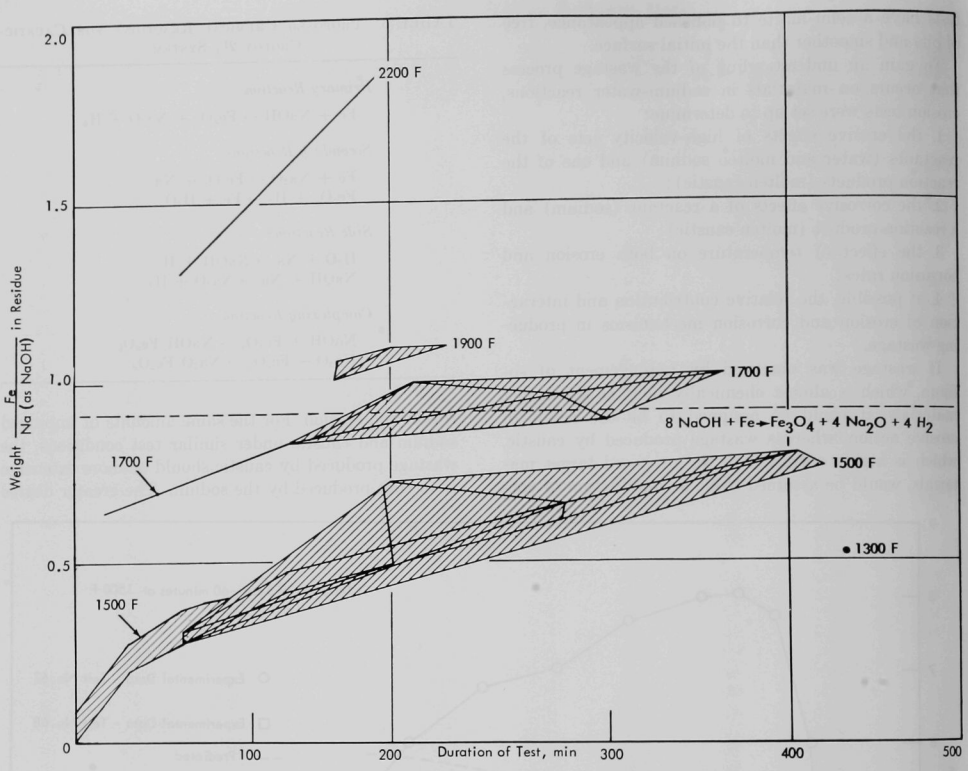

FIG. 19. Residue Analysis as a Function of Duration and Temperature of Test.

of wastage produced by the caustic would be assumed to be that resulting from the corrosive action superimposed on the erosive effect, although the formation of a surface layer of the corrosion products could greatly affect the erosion characteristics of the alloy.

In the hot erosion test program, jets of water at 200°F were to be impinged on Croloy 2¼ target specimens heated to 900 and 1200°F, and hot jets of molten sodium and molten caustic at 900, 1200, and 1500°F were to be impinged on targets specimens of Croloy 2¼, Incoloy 800, and Tenelon stainless steel heated to the same temperatures as the fluids.

A schematic diagram of the erosion test equipment is shown in Fig. 20. The equipment consists essentially of a Type 316 stainless steel reservoir and a Hastelloy-B U-shaped injection tube lowered into a carbon steel containment vessel. The target specimen is a plate made from the material to be tested. A preheat pot is used to liquefy and transfer sodium or NaOH from a glovebox to the reservoir. The heating system is designed to attain test fluid jet temperatures up to 1500°F at an 8-mil or 16-mil orifice located at the end of the U-tube. Resistance heating is used to raise the specimen to the test temperature. Nitrogen is used to pressurize the fluid to 2650 psig, forcing the fluid out through the orifice and causing it to impinge on a gate. The gate is lifted for the specified test duration, during which the fluid jet impinges on the target specimen. After the specified duration, the gate is lowered to prevent further impingement by the remainder of the fluid.

To date, two tests have been successfully carried out in which sodium at approximately 900°F was impinged at a velocity of 250 to 300 ft/sec on a Croloy 2¼ specimen at a somewhat higher temperature for times up to 120 sec. In neither case was there measurable wastage of the target specimens. In the water-impingement tests, very rapid cooling of the

targets occurred, and it was impossible to maintain the target temperature; again, there was negligible wastage on the specimen.

The lack of wastage in these tests suggests:

1. The 250–300-ft/sec velocity of the water and sodium jets, which are comparable to the velocity of the water jets from the capillaries in the Rig 10 tests, was too low to produce erosion of the target specimens in the short impingement time of the tests and at the temperatures achieved.

2. The cooling effect of the water jet on the target was so pronounced that the erosive effect of the water on the target area (temperature approximately 200°F during impingement) was negligible in the short time of impingement. With no wastage data from molten caustic impingement, conclusions cannot be made as to the relative or combined effects of erosion and corrosion on wastage. However, water by itself impinging on a target area with its concurrent drastic cooling effect is incapable of producing the wastage experienced in the small-leak sodium-water reaction tests.

IV. Review of Wastage Data

Although there have been several investigations concerned with the damaging effects of small water leaks into sodium, there has been no attempt to correlate the existing data. Having a correlation of wastage data or at least a detailed review of such would certainly help to give better direction and guidance for an experimental program.

A review of available literature on sodium-water reaction work up to the end of 1964[14] is concerned primarily with determining the factors that have an effect on the pressure forces developed during large sodium-water reactions, and contains essentially no data relevant to wastage during sodium-water reactions. A recent literature search showed several investigations that had wastage data of a nature that would lend itself to analysis and possibly to development of a correlation. The applicable reports covered activities by Atomics International, APDA, The Detroit Edison Company, and the United Kingdom Atomic Energy Authority (UKAEA). Review of the UKAEA report showed that significant wastage of tubes had occurred during large leaks of water (up to 8 lb/sec) into sodium. Therefore, also included in the analysis presented here is a review of pertinent large-leak studies.

Eight different test apparatus were used in the studies of the various investigators. These ranged from a simple target inside a stagnant pool of sodium to a mockup tube bundle in a dynamic sodium system. Three of the test apparatus were equipped for

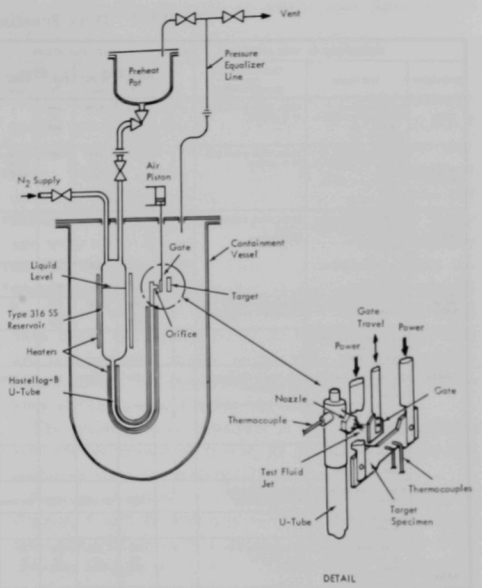

FIG. 20. Hot Erosion Test Equipment.

conducting studies in flowing sodium. Additional information on the test apparatus is presented in Table 7 and in the discussion that follows of the various factors that may contribute to material wastage rates. Also, more detailed descriptions are given in the reference documents.

A. Systems

Seven test rigs were used for wastage studies in stagnant sodium systems.

The test apparatus used by the UKAEA for corrosion tests was a small pot with a sodium inventory of 3 lb.[4] The target material consisted of rings of material specimens on a stringer rod or an "L"-shaped plate. The injection device consisted of a tube with a 0.100-in.-diameter orifice at the end. Water was injected by means of a small metering pump.

Next in complexity were the Detroit Edison Company Rig[15] and the APDA Rig 33.[3] These apparatus were quite similar and will be discussed together. The APDA Rig 33 reaction vessel was 10 in. in diameter by 6 ft long and contained 75 lb of sodium. The Detroit Edison Company Rig was 12 in. in diameter by 4 ft long and contained 50 lb of sodium. Both rigs used essentially the same type of target, which consisted of a target tube contained in a cluster of tubes about 4 in. in length and held together by

TABLE 7. DATA SUMMARY FOR STAGNANT SODIUM SYSTEMS

DESCRIPTION OF TEST APPARATUS			Number	TEST CONDITIONS				WATER INJECTION DATA					REACTION DATA		
Investigator	Test Target	Test Vessel Size and Sodium Inventory	of Tests	Water		Sodium		Nozzle Diam, in.	Spacing from Nozzle to Target, in.	Injection Rate, lb/sec	Duration of Injection, sec	Total Water Injected, lb	Maximum Temperature, °F	Depth of Penetration, mil	Wastage Rate, mil/sec
				Temp., °F	Press., psig	Temp., °F	Press., psig								
DECo	3 x 3 tube array 5/8-in. OD x 0.042-in. wall Croloy 2-1/4	12-in. diam x 4-ft long 50 lb sodium	4 1 2	450 to 480	1300	450 to 480	1	No Data	3/8	0.033 to 0.042 0.46 1.0 to 1.25	26 to 120 8.7 1.0 to 4.0	1.0 to 4.0 4.0 1.0 to 5.0	900 to 1400[1] 1420[1] No Data	ND to >12 37 ND	ND to ~3.35 4.25 ND
APDA (RIG 33)	3 x 3 tube array 5/8-in. OD x 9.075-in. wall 1-in. OD x 0.109-in. wall Croloy 2-1/4	10-in. diam x 6-ft long 75 lb sodium	2 2 2	350	2950 to 3000	350	atm (Nominally)	0.016 0.025 3/32	3/8 to 1-1/2	0.01 to 0.04 0.007 to 0.082 1.1	16 to 180 15 to 49 3.7	0.6 to 2 1.0 to 4.0 4.0	1000 to 1286[1] 640 to 1261[1] 1551 to 2014[1]	2.6 to 23.7 ND to 1.7 ND to 3.4	0.13 to 0.16 ND to 0.11 ND to 0.92
APDA (RIG 43)	0.040-in. OD thermocouples sheathed with 0.007 in. of 304 SS clad	12-in. diam x 42-in. long 60 lb sodium	1 8 4 3	600	2650	600	1 to 2	0.008	1/4 9/16 to 3/4 1 1-1/4 to 1-1/2	0.0036 0.0031 to 0.0041 0.0027 to 0.0034 0.0031 to 0.0032	28 27 to 36 26.5 to 33.5 34.5 to 35.0	0.11	1590[2] 1175 to 1545[2] 713 to 1464[2] 693 to 1279[2]	ND	ND
	1-in. OD x 0.122-in. wall 2-1/4 Croloy		3 1	630 605	2650 2650	630 605	1 to 2 1 to 2	0.008 0.006	1/4 1/4	0.0034 to 0.0047 0.0023	52 to 70 103	0.24 0.24	No Data 1040	ND ND	ND ND
APDA (RIG 10)	5/8-in. OD x 0.122-in. wall	36-in. diam x 16-ft long 550 to 3400 lb sodium	3	600 to 620	2650	600 to 620	10	0.006	1/4	0.0010 to 0.0019	125 to 236	0.24	1180 to 1780[1]	0.012 to 0.027	0.09 to 0.18
	5/8-in. diam x 0.085-in. thick Croloy 2-1/4		1 1 1								4.5 4.5 9.0	35 35 70		85 ND ND	19 ND ND
UKAEA	5/8-in. diam x 0.085-in. thick Croloy 9	2-ft diam x 8-ft long 700 lb sodium	2 1 1	570	2000	570	No Data	1/2	No Data	7.8 (nominal)	4.5 9.0 9.0	35 70 70	No Data	ND 85 ND	ND 9.5 ND
	5/8-in. diam x 0.085-in. thick 316 Stainless Steel		2								9.0	70		ND	ND
	1/8-in. thick mild steel wire; 0.020-in. SS tube		1							1.0	2	2		62.5 20	31 10
	Plate (L-shaped mild steel	Stainless Steel Pot with 3 lb sodium	3	932	No Data	932	No Data	0.1	0.10	0.000037	1800	0.067	No Data	16 to 23	0.009 to 0.013
	Rings of Croloy 2-1/4 0.060 thick		1								7200	0.26		60	0.083
APDA	7 Tube Array 1-3/16-in. OD x 0.065-in. wall Croloy 2-1/4	12-in. diam x 8-ft-8-in. long (l) 280 lb	4	285 to 350	900 to 1100	400 to 500	5 to 7	Full-size tube	NA[2]	16	~28	~450	1475 to 1950	ND	ND
AI-ESADA	36 Tube Array 5/8-in. OD x 4-ft long or 5/8-in. OD x 14-ft long	8-in. diam x 16-ft long 300 lb	2 3	970 to 1038 455 to 480	2060 to 2180 2650 to 2750	757 to 917 900 to 920									
		8-in. diam x 46-ft 600 lb	4	467 to 472	2690 to 2780	919 to 922		Full-Size Tube	NA	~10	~40	415	1200 to 2500	ND	ND
			5	400 to 478	2650 to 2770	674 to 691									
		8-in. diam x 46-ft 700 lb	3	468 to 476	2740 to 2760	886 to 933									
DECo	(4)	(4)	4 1 2	←		(4)	→	(3)	←			(4)	→	3 to 22 2.5 ND	0.08 to 0.90 0.39 ND
APDA (RIG 33)	(4)	(4)	2 3 2	←		(4)	→	(3)	0.01 to 0.040 0.067 to 0.01 1.1	←		(4)	→	2.1 to 6.1 2.3 to 4.5 ND to 2.6	0.03 to 0.13 0.09 to 0.96 ND to 0.70

(1) Had a 3.5-ft diam × 3-ft-high gas chamber on top.
(2) Not applicable.
(3) Wastage on tubes located adjacent to target tube.
(4) Same data as shown above.
(5) ND—Not Detectable.

end plates. The water-injection tube contained an orifice at its tip with a rupture diaphragm on the outside. The leak was initiated by suddenly increasing the pressure on the water side to the test pressure; this caused the diaphragm to burst, and the water began to flow into the sodium. Termination of the injection occurred when the fixed volume of water had been injected.

The APDA Fermi Rig contained a reaction vessel, 12 in. in diameter by 8 ft long, and contained approximately 280 lb of sodium.[16] The internal structure was a bayonet-type tube bundle consisting of 7 water-steam tubes with the water tubes fitted inside the steam tubes. The center tube of the bundle was the injection tube, and it contained a spring-operated plug valve that sealed the end of the steam tube. The leak was initiated by suddenly opening (remotely) the plug valve and allowing the water to flow into the sodium. Termination of the injection occurred when the fixed volume of water had been injected. Attached to the top of the reaction vessel was a 3.5-ft-high cover-gas chamber.

The main reaction vessel of the AI-ESADA Rig was 8 in. in diameter by 16 ft long and contained approxi-

mately 300 lb of sodium.[5] In some tests the reaction-vessel length was extended to 46 ft, in which case it contained approximately 700 lb of sodium. A 36-tube array was used for the internals and for most tests was 4 ft in length; the length was extended to 14 ft for a few tests. The center tube of the array was the injection tube. Two methods of injection were used: the first consisted of milling the surface of the tube to provide for a weak spot, and the second consisted of a rupture disc located at the end of the center tube. Injection of water in both types was initiated by suddenly increasing the water-side pressure to the test pressure, thereby causing the milled tube to rupture or the rupture disc to burst. Termination of the injection occurred when the fixed volume of water had been injected.

Although the UKAEA-NOAH Rig(s)[4] had a capability for circulating sodium, the description is included under stagnant sodium systems because sodium was not circulated in the majority of tests. The NOAH reaction vessel consisted of a 24-in.-diameter by 8-ft vessel containing approximately 700 lb of sodium. Two types of internal structure were used in this rig. One was a $\frac{1}{6}$-scale model of a preliminary design of a UKAEA Prototype Fast Reactor (PFR) heat exchanger and the other was a full-scale model of a segment of a PFR tube bundle. The $\frac{1}{6}$-scale model consisted of water-filled tubes, perforated plates having approximately the same volume and resistance to flow as the tube banks, and $\frac{1}{8}$-in.-diameter mild steel rods in the reaction area. These tubes, plates, and rods were laid horizontally in the vessel. The injection tube was part of a circulating-water system, and was provided with a sealed orifice that was located in the bottom portion of the vessel, with the orifice oriented vertically upward. The leak was initiated by breaking off the end of the tee orifice with a guillotine. Termination of the reaction occurred by actuating a quick-acting shut-off valve after a predetermined time interval.

The other types of internal structure used in the UKAEA-NOAH rig was a segment of a vertical full-scale tube bundle. The injection device consisted of a tube with an orifice at the end and sealed with a rupture diaphragm. Initiation of the reaction was caused by introduction of the high-pressure water into the injection tube through a quick-opening valve. The rapid increase in the pressure in the injection tube caused the diaphragm to burst. Termination of the reaction occurred by actuating a quick-acting shut-off valve.

Two test rigs were used for wastage studies in flowing sodium. These were the modified APDA Rig 43 and APDA Rig 10, both of which were described in Sect. II.A.

B. Wastage Results

The wastage data obtained by the various investigators are summarized in Tables 1, 3 and 7: Table 7 includes the data obtained in stagnant sodium systems; Tables 1 and 3 include the data obtained in dynamic sodium systems. Only those test results are tabulated for which measurements of materials wastage were made in terms that could be related to penetration rate. In some instances the investigators reported materials wastage in terms of specimen weight loss or in terms of weight loss per unit area. Such data could not be converted to penetration rate and are not included in the tables. The reference documents should be consulted for a more extensive review of the data and of the test details.

The wastage data obtained in the stagnant sodium systems are presented in Fig. 21 and those for the dynamic systems are presented in Fig. 4.

Special attention is directed to the data points of Figures 4 and 21 that are shown in the broken band near the bottom of the figures. These data are from tests in which there was no detectable penetration of the target material. Because the tests were of such short duration and because the measurements in most cases could not detect penetrations of 0.001 in., it would be misleading to state that the wastage rate was zero. However, in these instances it is possible to estimate that the wastage rate was less than a particular value.

As shown in Fig. 21, wastage-rate data obtained in the stagnant sodium systems have a large scatter. For example, at leak rates of approximately 4×10^{-2} lb/sec, the wastage rates reported by one investigator ranged from not detectable to almost 2 mil/sec; at leak rates of approximately 7.5 lb/sec there was no wastage in 8 of 11 tests conducted in the UKAEA-NOAH rig with the tube bundle, and in one test the rate was greater than 18 mil/sec.[4] The Detroit Edison Company data and the APDA Rig 33 data also are scattered. The APDA data obtained in Rig 10 show fairly good consistency. Generally, the wastage data obtained with tests made in stagnant sodium systems has very poor reproducibility at leak rates greater than approximately 10^{-2} lb/sec.

As shown in Fig. 4, the wastage data obtained in the dynamic sodium systems show very good reproducibility. These data are from tests in the APDA Rig 10, with the exception of two data points obtained from tests in the APDA modified Rig 43. At leak rates above 10^{-2} lb/sec there appears to be some data scatter; however, there are insufficient data to

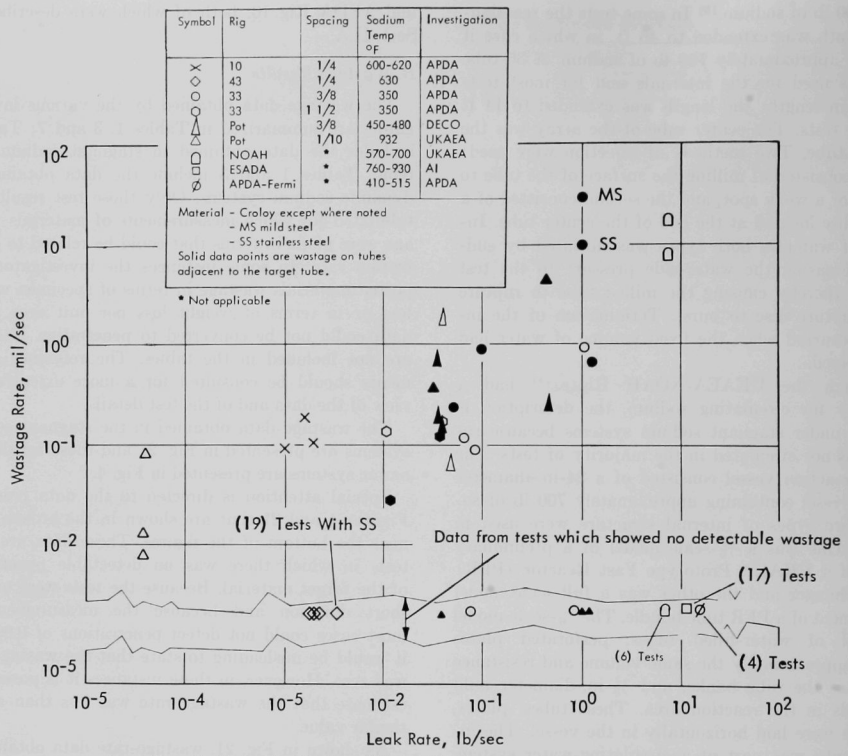

FIG. 21. Materials Wastage Obtained in Stagnant Sodium Systems.

establish the degree of reproducibility at these higher leak rates. It is possible that in dynamic systems the scatter in the wastage data will be greater at the higher leak rates, as it is in the data obtained in stagnant sodium systems.

1. Variables Affecting Material Wastage

The various investigators considered nine variables that could have an effect on material wastage rates: a) leak rate, b) spacing between the leak and the target material, c) leak duration, d) sodium velocity, e) type of leak, f) conditions of sodium and water, g) configuration in the reaction area, h) depth of submergence of the target material in sodium, and i) target-material coolant. The effect of these various factors on material wastage rates is discussed below.

a. Leak Rate

The leak rates in the wastage tests conducted in stagnant sodium range from approximately 10^{-5} to 16 lb/sec. The data for the stagnant sodium systems, shown in Fig. 21, show an increasing wastage rate as the leak rate increases, with increasing scatter in the data at the higher leak rates. The maximum wastage rates range from approximately 10^{-1} mil/sec at a 10^{-5}-lb/sec leak rate to over 20 mil/sec at a 10-lb/sec leak rate. It is very noteworthy that in such a large number of tests there was no detectable wastage. The reason for this is not known.

Most of the data in Fig. 21 are from tests in which the water leak is directed normal to the target material. In the UKAEA-NOAH test rig, some injections of water were made at right angles to the target tube and some parallel to the target tubes. In these tests, there was no detectable wastage of the target tubes; however, in some of the tests, wastage did occur with adjacent tubes. Wastage also occurred for adjacent tubes in both the APDA Rig 33 and the Detroit Edison Company tests; these data are also shown in Fig. 21. As is indicated in Fig. 21, all of the solid data points

are for wastage that has occurred for tubes other than the target tube.

The leak rates in the tests that were conducted in dynamic sodium systems are in the range from 10^{-3} to 10^{-1} lb/sec. As seen in Fig. 4, the leak rate is a very significant factor affecting rates of material wastage. For the test conditions indicated in Fig. 4, the wastage rate is increased by increased leak rates up to 10^{-2} lb/sec; but as the leak rate is increased beyond 10^{-2} lb/sec, there is a decrease in the wastage rate. This was not observed in the tests conducted in the static systems. Additional data at leak rates greater than 10^{-2} lb/sec are needed to complete the definition of the wastage rate curves.

In conclusion, the wastage data obtained in the stagnant sodium systems have much more scatter than that obtained in the dynamic sodium systems. In steam generators there will be regions of sodium stagnation; therefore, knowledge of wastage rates in stagnant sodium system tests is important. Because data reproducibility in the stagnant sodium systems is so poor, considerably more testing will be required to obtain significant correlations. Also, more testing is required in the dynamic sodium systems to establish definitely the effect of larger leak rates on wastage rates.

b. Spacing

The leak-to-target material spacing in the various studies ranged from 0.1 in. in the UKAEA pot tests to several inches in the UKAEA-NOAH rig. It is not possible to estimate the effect of spacing on material wastage rates in the stagnant sodium systems because of the scatter in the data. For the dynamic systems, only the APDA Rig 10 tests included a study to investigate the effect of spacing on the material wastage rate. A statistically designed experiment of 12 tests showed that increasing the spacing from 0.25 to 1 in. reduced the wastage rate significantly. The range of leak rates in this study was 1.3×10^{-3} to 2.9×10^{-3} lb/sec, and inspection of Fig. 4 shows the significance of spacing in that leak-rate range. The data, however, show that the curves are tending to converge as the leak rate increases. Only one test was made at a larger spacing, approximately 1.25 in., with a higher rate of approximately 2×10^{-2} lb/sec. The wastage rate obtained is somewhat lower than that obtained with a 0.25-in. spacing; however, considering there are only two data points, the difference may not be significant.

c. Duration of Injection

The duration of injection covered in the various studies ranged from about 1.5 sec to 2 hr; if the corrosion tests conducted by the UKAEA are not included, the maximum duration was approximately 300 sec. The UKAEA corrosion tests were conducted by injecting steam at a velocity of approximately 30 ft/sec against the targets, whereas in the remaining investigations the velocities were hundreds of ft/sec for the water phase and over 1000 ft/sec for the steam phase. Thus, it is believed that the wastage observed in the UKAEA pot tests is primarily due to corrosion; in any case, there is not sufficient data given to establish the effect of duration at these very low leak rates.

One of the most significant observations on the effect of duration is the high wastage rates obtained in the tests of very short duration; for example, in the one UKAEA test made in NOAH with circulating sodium, the penetration exceeded 0.062 in. in a 2-sec test. This result indicates that essentially zero induction time is required for wastage to begin.

A statistical test program conducted by APDA in Rig 10 indicated a negligible effect on wastage rates of leak duration time over the range from 100 to 300 sec. In later APDA Rig 10 tests it was demonstrated that wastage rates obtained in tests of 10-sec duration at the high leak rates correlated well with the data obtained at lower leak rates and much longer durations.

d. Sodium Velocity

All of the APDA tests with dynamic sodium systems were conducted in Rig 10 and Rig 43. These results, discussed in Sect. II.B, demonstrate the significance of sodium velocity on material wastage, at least at very low sodium flows. Additional data are needed to establish a quantitative relationship between wastage rate and sodium velocity.

e. Type of Leak

Three basic types of injection devices were used in the various studies. In all devices, except for that used in the UKAEA corrosion test pot, the flow through the orifice was controlled by the friction loss of the high-pressure fluid forced through an orifice. In the UKAEA corrosion tests, the steam flow rate was controlled by a mechanical pump.

The bursting of the rupture disks in the APDA Rig 33 tests was not very consistent, so some of the scatter in wastage data could have been caused by the variation in the burst patterns of the rupture disk, i.e., the way the rupture disk burst could have affected the flow pattern of the injected fluid.

The experience of APDA with the use of capillary tubing for orifices has been quite good. In almost all cases, a sharp, needlelike water jet is obtained. Due to

manufacturing tolerances for capillary diameters the actual leak rates are in the range of ±20% of the predicted rate; however, post-test flow checks provide a more accurate measure of the leak rate. In the UKAEA corrosion pot tests, where the leak rate was so low, the shape of the jet was not known; however, the patterns of the wasted areas indicate that the jet was not needlelike. The pattern of the jet from the other UKAEA tests is not known.

f. Conditions of Sodium and Water

The sodium temperature in the various tests ranged from a low of 350°F in the APDA Rig 33 tests to a high of 1132°F in the UKAEA corrosion pot tests. Water and steam temperatures are not available in all instances, but it is presumed that they were essentially equal to the sodium temperature. The injected fluid ranged from a water phase with very little steam to superheated steam. Considering the overall scatter of the data as shown in Fig. 21, it cannot be said that temperature affects the wastage rate. Only in the UKAEA corrosion test[4] was the effect of temperature studied; in these tests, increasing the sodium temperature from 660 to 842°F increased the material loss rate by a factor of 150. However, these tests were made with steam injected onto the plate at a low velocity and at a rate of 3.7×10^{-5} lb/sec; the wastage was typical of a general corrosion as compared to the erosive-type wastage at higher leak rates.

In general, the temperature of the injected water was essentially the same as that of the sodium. Thus, the effect of water temperature by itself cannot be determined. The only effects the pressure of the water could exert are related to the type of jet issuing from the orifice and the amount of vaporization occurring at the exit of the orifice. Insufficient data are available to determine how meaningful these factors may be.

g. Configuration in the Reaction Area

The brief description of the test apparatus given previously showed that the sodium-water reaction was occurring in many different configurations ranging from a "pool" of sodium to a tightly congested tube bundle. Comparison of the wastage data obtained in the UKAEA corrosion test pots cannot be made with other test apparatus because of the very low leak rates used in it. Comparison can be made, however, between APDA Rig 43 and APDA Rig 10 data. In this comparison, wastage data were obtained at comparable leak rates.

Comparison of the APDA Rig 43 and Rig 10 data shows that in stagnant sodium there was no detectable wastage in Rig 43 whereas in Rig 10 the wastage rates were in the range from 0.1 to 0.2 mil/sec. In Rig 10, the target tube is part of a tightly congested tube bundle. In Rig 43, negligible wastage was obtained in tests made in both an open pool of sodium and inside a 4-in.-diameter pipe (shown in Fig. 3). The reason for this difference is not known.

In tests conducted in these rigs with sodium circulation there was no significant difference in wastage rates.

h. Submergence

The depth of submergence of the target material in sodium ranged from less than 1 ft to a maximum of 8.5 ft in the various test rigs. The tests conducted by APDA showed no significant difference in wastage rates in Rig 10 under static sodium conditions. The wide spread in data obtained in the other static sodium tests makes it impossible to estimate the effect of submergence on wastage rates.

i. Target Coolant

In the various studies, target coolants included sodium, gas, and water. Tests were conducted in Rig 10 by APDA at leak rates of approximately 2 to 3×10^{-3} lb/sec showed no difference in wastage rates for target tubes containing recirculating water and those containing stagnant nitrogen. Higher wastage rates might be expected with the gas-filled tube since the tube surface would presumably become hotter and this would enhance corrosion and erosion; but the test results do not support this.

j. Method of Operation

Examination of the data presented in Fig. 21 for the static sodium systems shows that only 2 out of the 31 tests conducted at leak rates greater than 5 lb/sec had significant wastage. Of the 31 tests, negligible wastage was obtained in two of the test rigs: APDA-Fermi Model (4 tests) and the AI-ESADA units (17 tests); only in the UKAEA-NOAH rig was significant wastage obtained in 2 out of 10 tests.

A review of the experiments conducted in the three test rigs: APDA-Fermi Model, AI-ESADA, and UKAEA-NOAH, showed a significant difference in the manner which the sodium-water reaction was terminated. In both the APDA-Fermi Model and the AI-ESADA rig excess water was injected into the system, i.e., water (or steam) injection continued after the main reaction occurred. Invariably, most of the sodium either reacted with the water or was ejected from the reaction zone. Continued injection of water (or steam) beyond this point would flush the corrosive products of the reaction out of the unit and would also cool the surfaces of the tubes and shell. Both actions inhibit

wastage. The tests in the UKAEA-NOAH rig, however, were conducted in a different manner: termination of the water injection occurred immediately upon closing isolation valves in the water-injection system after a predetermined duration, thus leaving the hot, corrosive reaction products in contact with the tubes. Since there would be no cooling action on the tubes, wastage would be enhanced by the high temperatures produced in the reaction.

Although the reaction vessel of the NOAH rig is larger in diameter than those of the other two rigs (24 vs 12 and 8 in.) this is not thought to be a significant factor.

2. Comparison of Materials

In the majority of the tests described here the Croloys were used as the target materials. The UKAEA tests included mild steel, and the APDA and UKAEA tests included stainless steels and the Incoloys. The UKAEA tests, conducted in the corrosion pot, showed that the austenitic steels were more resistant. These data are not shown on Fig. 21 because it was reported on a weight-loss basis with no indication of penetration rates. APDA's wastage rates for stainless steels and Incoloy 800 are shown in Fig. 4. The data indicate that the stainless steels are more resistant to wastage than Croloy 2¼ by a factor of 20 to 30, and that Incoloy 800 is more resistant to wastage than Croloy 2¼ by a factor of 30 to 80. These data, in general, agree well with the UKAEA data. No information is available at this time to indicate why these two materials are more resistant to wastage than are the ferritic steels.

3. Wastage Mechanisms

A complete study was not made by any of the investigators to establish the mechanism of wastage occurring during small-leak sodium-water reactions. There have been some suggestions that the wastage is due to a combination of corrosion and erosion. The UKAEA investigators have shown in corrosion-pot studies that corrosion rates are appreciable; however, as Fig. 21 shows, these rates are considerably lower than those obtained at higher leak rates. The metallurgical examinations of the target tubes made by APDA have shown no evidence of intergranular corrosion and the surface features observed, being bright and semimatte in appearance, were consistent with an erosion mechanism for the removal of metal in the target area. It is concluded that more information is required before the mechanism of wastage can be established.

4. Conclusions

a. Comparison of Tests Made in Stagnant and Dynamic Sodium Systems

Reproducibility of experiments is much better in the dynamic sodium systems than in the stagnant sodium systems.

Tests in the dynamic sodium systems produced more information on the effect of the various factors that were thought to have an influence on wastage of materials.

b. Effect of Various Factors on Material Wastage Rates

The wastage rate in stagnant sodium systems appears to increase continuously with increasing leak rate over the entire range of the various investigations, i.e., from 10^{-5} to 10^{1} lb/sec.

The wastage rate in dynamic sodium systems appears to increase continuously with increasing leak rate up to a critical leak rate which appears to be approximately 10^{-2} lb/sec, and then decreases at still higher leak rates.

Increasing the leak-to-target spacing reduces the wastage rate. Studies of the effect of spacing on wastage rate need to be extended to higher leak rates.

The wastage rate is linear with time for a given leak rate over the entire range of investigation, i.e., up to 300 sec. Also, if there is a period needed for initiation of the wastage process, it is less than 1 sec.

Flow of sodium past the target material definitely has an effect on wastage rate in the leak-rate range from 1×10^{-3} to 3×10^{-3} lb/sec. Increasing the flow from zero to 1.0 ft/sec has a very significant difference. The effect of higher velocities is not known.

The influence of temperature on wastage rates is not known.

The effect of configuration within the reaction area is not known. Available data give conflicting indications.

The depth of submergence of the target material in sodium does not have a significant effect on wastage rate over the range of investigation, i.e., from 1.3 to 8.5 ft, in either stagnant or dynamic sodium systems.

Cooling of the target tube material appears to have no effect on the wastage rates.

At large leak rates (>5 lb/sec) continued purging with water or steam after main reaction has occurred appears to inhibit wastage by cooling of the tubes and by removal of reaction products.

c. Materials Evaluation

The stainless steels are more resistant to wastage than Croloy 2¼ by a factor of 20 to 30.

Incoloy 800 is more resistant to wastage than Croloy 2¼ by a factor of 30 to 80.

d. Wastage Mechanism

Erosion and corrosion are believed to contribute to the wastage process; however, insufficient data are available to verify this belief. Metallurgical examination of wasted areas of Croloy 2¼ by APDA indicated that target material which was adjacent to the wasted area and had temperatures up to 2000°F exhibited no evidence of corrosion; the material had the appearance of metal loss by an erosion mechanism.

e. Wastage Correlation

Although it was possible to establish the effect of some of the factors on wastage rates, insufficient data exist in most areas to establish a correlation that includes all the variables. There are too many variables and geometries in the tests evaluated. There is also lack of data in some areas necessary for a complete comparison of the stagnant and dynamic sodium systems.

5. Recommendations for Additional Data

Based on the evaluation of the various studies of sodium-water reactions and on the conclusions discussed in the previous section, development of the following additional data is recommended:

Obtain more wastage data at higher temperatures.

Obtain more wastage data at higher leak rates in the dynamic sodium systems.

Obtain more wastage data at larger leak-to-target spacings with the larger leak rates.

Obtain more wastage data on the effect of water and/or steam conditions of pressure and temperature.

Obtain more wastage data at low leak rates for which the leak is of a weeping type rather than a jet type.

Perform more tests at higher leak rates to establish the frequency and type of secondary failures, i.e., the failures or wastage on other than the target tube.

Perform tests to establish the effect on wastage rates of various orientations of the water and/or steam jet relative to target materials.

Perform more tests to establish the effect of configuration in the reaction area on wastage rates to verify that testing in small test rigs will produce data applicable to large units.

Perform additional corrosion and erosion tests to establish their relative contribution to the wastage process.

REFERENCES

1. H. O. Muenchow and W. L. Chase, "An Investigation of Tube Wastage Caused by Small Leaks of Water in Sodium-Heated Steam Generators," in *Symposium on Alkali Metal Coolants—Corrosion Studies and System Operating Experience*, Vienna, November 28 to December 2, 1966.
2. *Quarterly Technical Progress Report on AEC-Sponsored Activities, June 15–September 15, 1966*, APDA-195 (1966).
3. W. L. Chase *et al. Analysis of the Babcock and Wilcox Full-Size Steam Generator For a Sodium-Water Reaction*, APDA-176 (Nov. 1965).
4. R. A. Davies *et al.*, United Kingdom Atomic Energy Authority, "Corrosion of Steels in the Vicinity of a Sodium-Water Reaction," in *Symposium on Alkali Metal Coolants-Corrosion Studies and System Operating Experience*, Vienna, November 28 to December 2, 1966.
5. L. Goodman *et al., Effects of a Sodium Water Reaction in a Modular Steam Generator, an Experimental Study*, AI-66-152 (Sept. 24, 1966).
6. M. M. Rubright, *The Corrosion of Croloy 2¼ Steel in the Products of a Sodium-Water Reaction; Systems of NaOH in Water and in Molten Sodium*, BAW-1280-30 (Nov. 1965).
7. *Quarterly Technical Progress Report on AEC-Sponsored Activities, September 15–December 15, 1967*, APDA-214 (1968).
8. F. G. Hammitt, *Two-Phase Material Attrition Problems for Rankine Cycle Liquid Metal Power Plants*, Document No. NP-15431.
9. R. S. Carey, *Evaluation of Turbine Rotor and Nozzle Material*, Document No. AGC-2822, **2**, 36–40.
10. H. Derow and B. E. Farwell, *Snap-8 Report for January-June 1964 Vol. II, Development of Component Materials*, Document No. NASA-CR-54717 (1964).
11. F. G. Hammitt, *Observation on Cavitation Damage in a Flowing System*, J. Basic Engrg., Document No. JBAE-85-347-63.
12. F. G. Hammitt, *Damage to Solids Caused by Cavitation*, Proc. Roy. Soc. (London), **A260**, 245–255 (1966).
13. M. T. Pitek and F. G. Hammitt, *Hypervelocity and Fluid Impact Studies*, Tech. Report No. 1, A Literature Review, Univ. of Mich. Document No. 08153-1-T (Sept. 1966).
14. J. A. Ford, *Literature Review of Sodium-Water Reactions*, APDA-167 (March 15, 1965).
15. "Reply to Division of Reactor Licensing Request for Additional Information Dated May 27, 1964", Power Reactor Development Company, Enrico Fermi Atomic Power Plant, Docket 50-16, Addendum No. 2, Attachment No. 1, September 8, 1964.
16. "Technical Information and Hazards Summary Report, Section III: System Verification Programs," Power Reactor Development Company, Enrico Fermi Atomic Power Plant, Docket No. F-16, Volume 5.

Discussion

Mr. Bray (UKAEA-Dounreay): I would be very surprised if shutting off the water injection in the NOAH rig would have any significant effect on the wastage, because it's certain the wastage does not occur during the water injection. I am more inclined to the view that the actual metal removal takes place as a result of this fast-moving stream of highly aggressive reaction products that occurs at the interface between the water jet and the sodium. For example, in NOAH test #1, a great deal of wastage occurred. The overall

sodium temperature was only raised, I think, from about 300 to about 450°C, and the water-injection time was only 2 sec. I would have thought that would be a most unlikely mechanism for prolonged wastage because of the large convection currents inside the vessel, which was 2 ft 6 in. in diameter. So I don't really think shutting off the water injection would have very much influence on whether or not wastage took place.

Mr. Chamberlain: As I recall, the comment made about the NOAH rig tests that were described in your Vienna paper was that no wastage was observed on the tubes that were closest to the injection point, whether the injection was against the tube or parallel to it, and that the wastage that was observed was in tubes located in other parts of the NOAH rig.

Mr. Bray: That was in some cases. I think you can explain this effect also as a jet phenomenon if you assume that a hydrogen bubble or a reaction-product bubble occurs around the injection orifice. There can be circumstances in which you get a large reaction bubble with just a steam-water mixture passing through it. By some mechanism it could be that this will penetrate the bubble at a point remote from the orifice and thus bring about the jet effect on the other side of the bubble. I think this is the reason, or one possible explanation, for the bursting or wastage of tubes remote from the orifice. Another possible cause is flow deflection, as by a deflector plate above the jet, so that the water stream strikes a remote tube. I believe this is a likely explanation of the result in the Vienna paper.

Mr. Chamberlain: At least in our own tests we can certainly say that a needlelike stream or jet is more destructive that a spray-type injection. In some of our rig 10 tests, and also in our basic studies of reaction temperatures, we found that with a spray rather than a jet the wastage rate was very much reduced and the reaction temperatures which we had measured were also considerably reduced. So I guess it is possible that even in large rigs, such as the NOAH rig, the deflection of the jet in some way or another could produce the wastage in other areas.

Mr. Bray: Let me make one final point. We did carry out some tests and I can't remember whether they were reported in the paper or not, in which, as it were, samples of target tubes were cooked up in reaction products for long periods. We didn't observe anything like the corrosion attack that occurs during an actual sodium-water reaction which is taking place live.

Mr. Clayer (GAAA): How do you explain the maximum in the curve of wastage versus flow rate?

Mr. Chamberlain: We only observe that maximum in the dynamic system tests, and we do have limited data there. The factor that we have used for wastage rate is the penetration, the depth of the wastage area. We find this correlates much better with the injection rate, say, than if we were using the mass of material removed per unit time per mass of water injected. So, when using the depth of penetration as our wastage rate factor, we find that we get a change in the wastage pattern when we get up to approximately 10^{-2} lb/sec. At that point the penetration rate starts to decrease because the wastage now is occurring over a larger area, i.e., there is an inner plateau, if you will, that does not see as much wastage. I think the volume of material that is being removed does generally continue to increase. We certainly feel that much more data should be obtained at those leak rates and greater to substantiate that the phenomenon we see is a true one.

Mr. Clayer: Did you vary the diameter of the injection holes?

Mr. Chamberlain: Our tests were conducted with 2650 psi pressure on the water-injection system. The variation in injection rate was produced by changing the hole size of the orifice.

Evaluation of Sodium-removal Methods for Fuel Elements and Piping Systems*

G. R. Bloom

Battelle Memorial Institute
Richland, Washington

Summary

Effects of three sodium-removal procedures and subsequent reinsertions into high-temperature sodium have been determined for samples of Type 304 stainless steel. Sodium-removal procedures used were: (1) mercury amalgamation, (2) Dowanol EB reaction, and (3) argon-steam reaction. Samples of Type 304 stainless steel were single specimens, crevice specimens, and simulated FFTF fuel pins. Sodium exposures were in isothermal, stagnant sodium capsules at 800, 1000, 1200, and 1400°F for 500 hr. Metallographic and microscopic examinations after one and two sodium exposures following sodium cleaning showed no intergranular attack on the fuel-pin samples exposed to 1200°F sodium. Burst tests conducted with samples of ¼-in.-diameter fuel cladding at room temperature before sodium exposure, after one sodium exposure and one cleaning cycle, and after two sodium exposures and two cleaning cycles, showed no change in burst stress. Very thin, black to light brown (and blue) colored films were formed on some of the samples exposed to 800°F sodium and on others cleaned by the mercury process. Neither the cause of the film nor the nature of the film has been determined.

Introduction

The Fast Flux Test Facility (FFTF) will test fuels for the LMFBR using sodium as a heat-transfer fluid. Maximum operating temperatures will vary from 800°F for the initial bulk outlet temperature of the reactor to 1400°F for the eventual closed-loop outlet temperature. Structural materials of Types 304 and 316 stainless steel will sensitize when used in such environments. Unless proper care is taken, the sensitized fuel elements, components, and piping system could experience intergranular corrosion.

Sodium removal will be an essential step in fuel examination, major repair, or aqueous decontamination of equipment. However, procedures for removal of sodium expose the sensitized stainless to environments that could cause intergranular corrosion. Unremoved sodium hydroxide from some processes could result in caustic corrosion of fuel elements and components during storage or after exposure to hot sodium. The retention of sodium hydroxide after cleaning is most likely to occur in crevices. One critical crevice is the wire wrap-fuel-cladding crevice on the fuel pin. The cladding is relatively thin and any structural damage to the clad would result in a failure much more rapidly than in more massive pieces such as pipes. Consequently, sodium-cleaning processes for fuel elements are being evaluated.

Sodium reactor sites such as EFAPP,[1] EBR-II,[2] SRE[3] and HNPF have successfully used some form of inert gas-steam or inert gas-moist air process for sodium removal from fuel elements. These reactors did operate or now operate below 1000°F,[4] and the applicability of their procedures for sodium removal for 1400°F sodium-temperature operation is not assured. The purpose of this work is to provide experimental data on sodium-removal processes for materials exposed to sodium temperatures up to 1400°F.

Argon-steam reaction and Dowanol EB (n-butoxy ethanol) were selected as candidate cleaning processes. Since both processes are caustic-forming processes, a noncaustic-forming mercury amalgamation process was selected as a control. Sample selection included simulated FFTF fuel pins to evaluate any effect of the wire-wrap crevice on the FFTF fuel pin during reinsertion. Crevice samples were included to determine what size of crevice could actually be cleaned of sodium and reinserted back into sodium. Single samples were included to provide weight-change data and to study the effect of sodium exposure on uniform surfaces such as pipe walls.

Experimental

Laboratory tests were conducted with Type 304 stainless steel as single samples, crevice samples, and simulated FFTF fuel pins. These samples were exposed in 800, 1000, 1200, and 1400°F sodium and cleaned by mercury amalgamation, Dowanol EB, or argon-steam. They were then reinserted into sodium and cleaned again. Measurements performed were (1) weight change for single samples after each cycle, (2) bursting pressure of fuel pins, (3) residual sodium remaining in the crevice samples after each cleaning cycle, and (4) sodium analysis to assure purity during sodium exposures. Examinations performed were (1) microscopic examination of sample surfaces for localized attack and (2) metallography to show any in-

* Based on work performed under U. S. Atomic Energy Commission Contract AT(45-1)-1830.

TABLE 1. CHEMICAL AND PHYSICAL PROPERTIES OF TYPE 304 STAINLESS STEEL

Description	Dimensions	Heat No.	Chemical Constituents, wt %							Physical Properties		
			C	Mn	P	S	Si	Ni	Cr	Yield Point, psi	Tensile Strength, psi	Elongation, % in 2 in.
Crevice- and Single-sample Sheet Stock	0.0625 in.	3341645	0.063	1.73	0.027	0.010	0.63	9.35	18.05	42,250	87,660	56.5
Fuel-pin Clad Tubing	0.2495- to 0.2512-in. OD; 0.015- to 0.0161-in. wall	20191	0.05	1.65	0.013	0.011	0.48	9.33	18.74	46,000	95,600	54.0
Fuel-pin End Cap Rod	0.250-in. OD	FX 409	0.06	1.47	0.032	0.018	0.58	8.62	18.25	50,600	92,800	62
Fuel-pin Wire Wrap	0.031-in. OD	A926	0.050	1.32	0.022	0.025	0.42	11.88	18.69		95,500	43

tergranular attack and relative carbide precipitation at grain boundaries.

All tests were conducted with Type 304 stainless steel specimens. Crevice samples and single samples were fabricated from the same stainless steel sheet. The fuel pins were fabricated using rod, wire, and tubing stock. Chemical and physical analyses of as-received materials are in Table 1.

Simulated 5½-in.-long FFTF fuel pins were fabricated by the FFTF Fuel Development Section using prototypic fabrication techniques. The clad had a ¼-in. outside diameter and a 16-mil wall thickness. End caps were welded onto the cladding in a helium atmosphere. All cladding end-cap welds were X-rayed, and welds with penetrations less than 16 mils thick received another weld pass and were reexamined. A 31-mil-diameter wire wrap was welded to one fuel-pin end cap, placed under tension, and welded to the other end cap, the wire wrap wound around the clad making ⅛ of a turn in 4 in. A fuel pin is shown in Figure 1. Single-material samples were one-inch machined squares of 0.0625-in.-thick sheet stock. These samples were polished with number 320 grit emery cloth, degreased with ethanol, and weighed to the nearest 0.1 mg. The fuel pins were placed in wire racks and the single samples in machined sample holders. The fuel pins, single samples, sample holders, and the capsule are shown in Fig. 2.

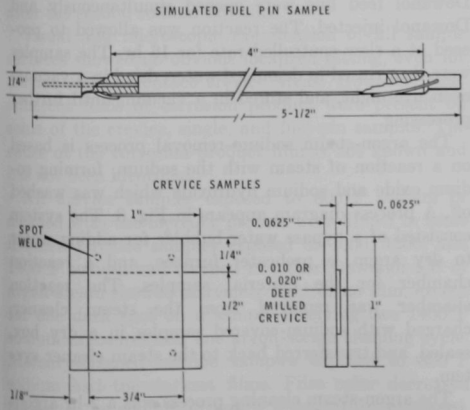

FIG. 1. Samples of Type 304 Stainless Steel.

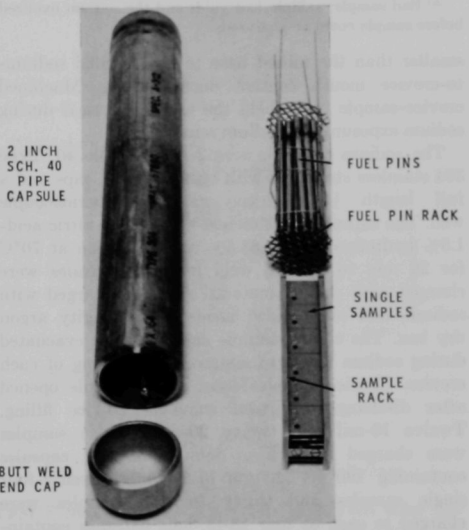

FIG. 2. Capsule, Fuel Pins, and Single Samples Prior to Charging.

The crevice samples were fabricated from the same stainless steel sheet stock as the single samples and are shown in Fig. 1. The crevice-sample top plate was

TABLE 2. Oxygen Analysis (wt ppm) of Capsule Sodium

	Crevice Samples					Fuel Pins and Single Coupons				
	Make-up Sodium for Capsule	Capsule Temperature, °F				Make-up Sodium for Capsule	Capsule Temperature, °F			
		800	1000	1200	1400		800	1000	1200	1400
1st sodium exposure	3[a]	9	11	7	[b]	4	14	11	7	7
2nd sodium exposure	6	6	6	3	1	14	5	5	4	12

[a] Average of 2 samples.

[b] Bad sample; sample had voids and the sodium oxidized before sample could be analyzed.

smaller than the milled base to assure good sodium-to-crevice mouth contact during filling. Machined crevice-sample racks held the crevice vertical during sodium exposure and sodium removal.

The sodium capsules were 2-in. Schedule 40, Type 304 stainless steel pipe with butt weld end caps and a full length ¼-in. heavy-wall-tube thermocouple well. The capsules were etched with a 15% nitric acid-1.5% hydrofluoric acid-83.5% water solution at 70°C for 20 min to remove weld residue. Capsules were charged with racked material samples, charged with sodium, and seal welded inside a high-purity argon dry box. The crevice-sample capsules were evacuated during sodium filling to assure sodium filling of each crevice. Crevice samples from every capsule opened after discharge confirmed complete crevice filling. Twelve 10-mil and twelve 20-mil crevice samples were charged to each of four 10-in.-long capsules containing 190 to 220 gm of sodium. Twenty-four single samples and thirty fuel-pin samples were charged to each of four 18-in.-long capsules containing 390 to 430 gm of sodium during the first sodium exposure.

High-purity sodium was piped directly from a sodium-purification loop to the dry box. Oxygen concentrations were 14 ppm or less by the mercury amalgamation technique for the makeup sodium and sodium discharged from each capsule. The detailed oxygen concentrations are given in Table 2. The carbon concentration in the makeup sodium was 11 ± 5 ppm carbon by high-temperature combustion.

Sodium-exposure temperatures were 800, 1000, 1200, and 1400°F. Vertical tube furnaces kept the capsules at temperatures during the 500-hr exposures. Calibrated thermocouples were located at the sodium-level midpoint for temperature data. Time to temperature was from 2 to 24 hr, and cooling time at the completion of the sodium exposure was about 8 hr down to 200°F. The temperatures were held within ±10° of the 800, 1000, 1200, and 1400°F control points.

Capsule discharge was performed in the argon dry box. Capsules were cut open, the sodium sampled, and the material samples placed in glass capsules to avoid sodium contamination during handling delays. All the single and fuel-pin samples were cleaned with either mercury, Dowanol EB, or argon-steam. Three sets of crevice samples from each crevice-sample capsule were not cleaned. One set was opened inside the dry box to check for complete filling with sodium; all samples were completely filled with sodium. Two crevice sample sets were reinserted into the second sodium cycle uncleaned.

The mercury process involved mercury amalgamation and mercury removal. A twenty-four crevice-sample batch or a thirty-two single-sample and forty fuel-pin batch were cleaned with 60 lb of high-purity mercury. The crevice samples were left in overnight, and the single samples and fuel pins were left in 0.5 hr. Mercury wet the stainless steel and could not be shaken off. Therefore, the mercury was boiled off by heating the samples to 200°C in a vacuum for 24 to 48 hr. Samples cleaned in mercury and recycled to sodium were not exposed to air, and any residues were mostly sodium oxide with small amounts of sodium hydroxide.

The Dowanol EB removal process was conducted in small capsules, as shown in Fig. 3. The capsule was charged with material samples while in the dry box, sealed, removed from the dry box, and connected to a Dowanol reservoir in a hood. The capsule vent and Dowanol feed line were opened simultaneously and Dowanol injected. The reaction was allowed to proceed at a slow controlled rate for 16 hr. The samples were then rinsed in deionized water, dried in a vacuum oven overnight, and stored in a vacuum until further processing.

The argon-steam sodium-removal process is based on a reaction of steam with the sodium, forming sodium oxide and sodium hydroxide which was washed off. A process diagram appears in Fig. 3. The system consisted of a bypass water bubbler for adding water to dry argon, a preheater furnace, and a reaction chamber for the material samples. The reaction chamber was removed from the steam cleaner, charged with sodium-covered samples in a dry box, sealed, and transferred back to the steam cleaner system.

The argon-steam cleaning process was a 2-hr argon-steam reaction followed by a 20-min rinse with de-

ionized water. The argon flow rate was 60 to 80 SCFH, and the argon reaction-chamber temperature normally ranged from 140 to 160°C. Problems were experienced with temperature control of the bulky furnaces which were used to heat the reaction chamber. A temperature rise to 200°C was observed during the first crevice-sample cleaning cycle, and one to 185°C was observed during the first single-sample and fuel-pin cleaning cycle. The gas concentration in stream water ranged from 1.2 to 4.0 vol % water, and the oxygen concentration ranged from 3.0 to 25 ppm O_2 for all the argon-steam cleaning runs. A 1.4-gpm deionized-water rinse for 20-min removed residual sodium hydroxide and sodium oxide. Samples were then dried in a 100°C vacuum oven and stored in a vacuum until further processing. Any sodium residue would be sodium hydroxide.

Selected samples were stored in vacuum until examination and testing. A second sodium exposure was conducted with the remaining cleaned samples and new replacement samples. Recycled samples were exposed to sodium of the same temperature as during their first sodium exposure. All material samples were cleaned at the conclusion of the second sodium exposure. Recycled samples were cleaned with the same sodium-cleaning process they received after the first sodium exposure.

Results and Discussion

The cleaned samples were tested for effects of sodium exposure and sodium cleaning. Crevice samples from all sodium-exposure temperatures and cleaning-procedure combinations are shown in Fig. 4. The samples receiving 1½ cycles were exposed to the first and second sodium exposures but were cleaned only after the second sodium exposure.

Visual and microscopic examination of all sample surfaces showed no obvious localized pitting, even for crevice sample-contact crevice areas. However, thin, adherent films of corrosion product were present on some of the crevice, single, and fuel-pin samples. The cause of the corrosion-product film is not known and has not been identified.

All crevice samples exposed to 800°F sodium or cleaned with the mercury process were filmed in some manner. Crevice samples exposed to 1000, 1200, and 1400°F sodium and cleaned in either Dowanol EB or argon-steam showed extremely light or no film, except for one dark spot on a sample receiving two 1400°F sodium exposures and one argon-steam cleaning cycle. Mercury-cleaned crevice samples exposed to 800°F sodium had the darkest films. Film color decreased markedly as sodium-exposure temperature increased, and the mercury-cleaned crevice samples exposed to

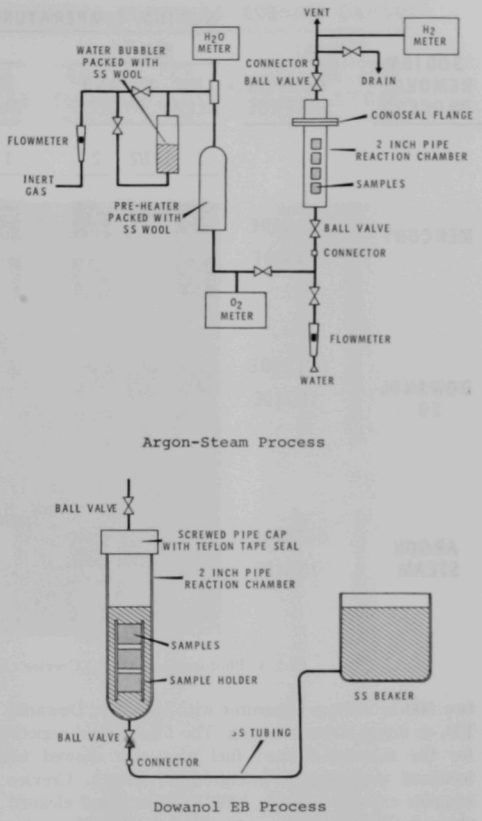

FIG. 3. Schematics of Sodium-cleaning Process.

1400°F sodium had a very light film. Film color decreased with cleaning process in the order mercury, Dowanol EB, and argon-steam. Samples with one sodium-exposure cycle and cleaning cycle were filmed much less than samples receiving two sodium exposures and cleaning cycles. Film color of samples with two sodium exposures and only one cleaning cycle were intermediate. The films were reproducible, but were much more apparent after the second sodium cycle.

Single samples and fuel pins showed similar film-color trends but were generally much less apparent, as seen in Fig. 5. The fuel-pin end-cap weld-region films were much more apparent than that on the clad at the center of the fuel pin.

Limited metallography examinations completed to date have demonstrated no localized corrosion of fuel-pin clad or intergranular attack after one and

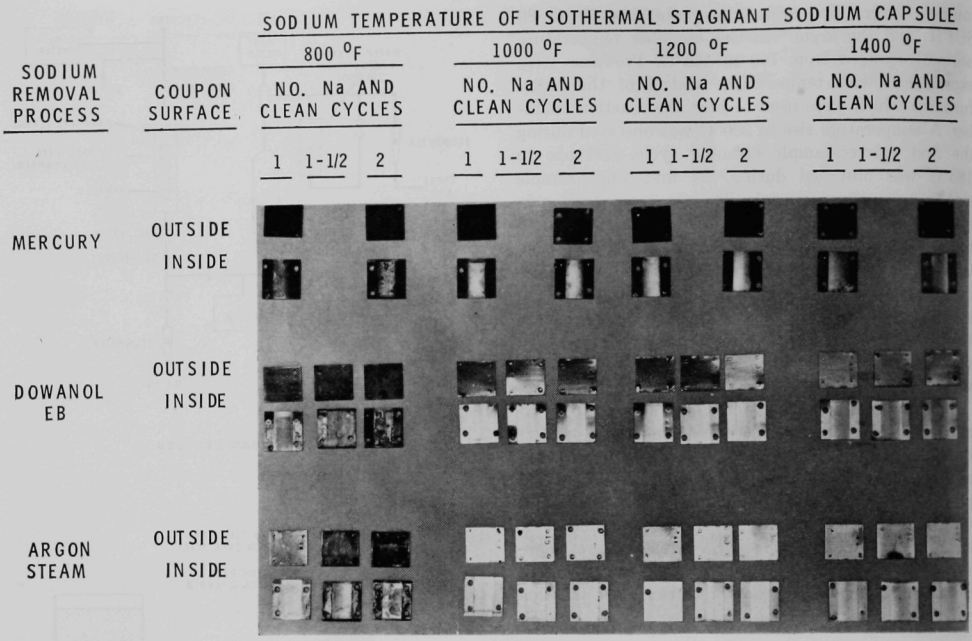

FIG. 4. Photograph of 10-mil Crevice Coupons after Sodium Exposure and Cleaning.

two 500-hr sodium exposures with mercury, Dowanol EB, or argon-steam cleaning. The filmed weld regions for the mercury-cleaned fuel pins also showed no localized corrosion or intergranular attack. Crevice samples exposed once to 1200°F sodium and cleaned showed no intergranular attack in the 10-mil crevice region or the contact crevice region. Samples exposed to all combinations of temperature, cleaning processes, and number of exposure cycles are presently undergoing metallographic examination.

The single specimens were weighed and total weight loss calculated. The average calculated weight losses are given in Table 3. The maximum average weight loss was 4 mg/dm^2, so no really significant weight loss was observed. Sample weights were measured with a four-place analytical balance having a precision of ± 0.03 mg. The samples had an area of 0.145 dm^2, so all weight change data had a precision of ± 0.2 mg/dm^2.

The fuel pins were burst tested to measure any gross effects of sodium exposure and cleaning on material physical properties. The burst test was conducted at room temperature with high-pressure helium with a pressurization rate of 5,000 psig/min. Test results, given in Table 4, show no significant decrease in burst pressure as a result of increasing sodium-exposure temperature or change of the sodium-removal process. There was a slight decrease in bursting pressure for the Dowanol EB-cleaned fuel pins exposed to 1200°F sodium. The small difference could be attributed to variations in burst-test conditions, since fluctuations in pressurization rate as great as 25% were observed. The average burst pressure was about 10,300 psi, which was a 78,400-psi burst stress. The burst stress was calculated by the expression.

$$S = \frac{P(R_o - 0.4t)}{t},$$

where R_o is the outside radius, t the wall thickness, P the burst pressure, and S = burst stress.

Crevice samples were analyzed for residual sodium oxide and sodium hydroxide after sodium cleaning. Calculated results are given in Table 5. The residual sodium was most likely in the form of sodium oxide for the mercury process and in the form of sodium hydroxide for the argon-steam cleaning process. The mercury process was the least efficient on the average. All cleaning processes were less efficient after the second sodium exposure than after the first. Sodium-ex-

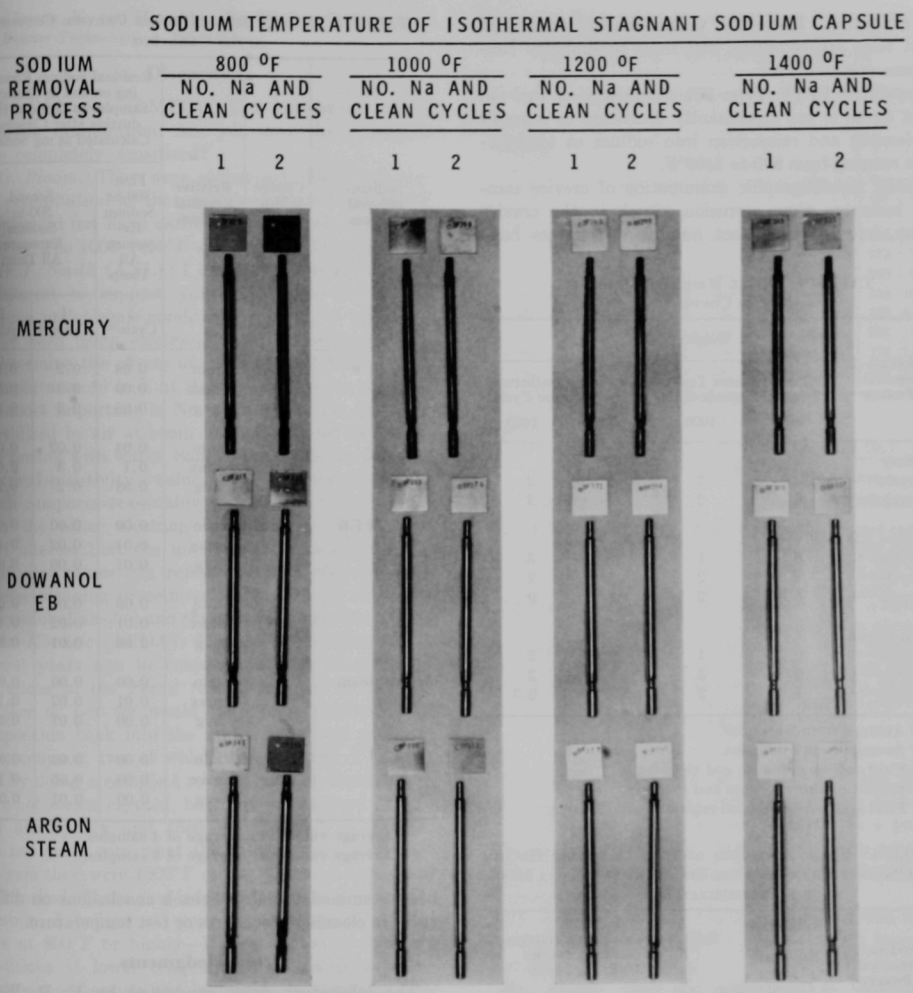

FIG. 5. Photograph of Single Coupons and Fuel Pins after Sodium Exposure and Cleaning.

posure temperature had no measurable effect on cleaning efficiency.

The residual sodium was measured by a nitric acid titration. Spot welds on crevice samples were drilled out and the sample broken into two pieces. The sample parts were placed in a 30-ml volume of water having a known pH as measured with an expanded-scale pH meter to the nearest hundredth of a pH unit. Any sodium oxide or sodium hydroxide on the sample immediately increased the pH. The sample and solution were then titrated with standard 0.005*N* nitric acid until the pH dropped to the original level. The major determination error was the conversion of NaOH to $NaHCO_3$ by exposure to CO_2 in the air, which caused measured values to be low.

Conclusions

All tests are not complete; therefore, an evaluation based on all data cannot be presented at this time. Metallographic examination of crevice samples must still be completed before the effect of sodium cleaning and reinsertion of the crevice samples into sodium can

be evaluated. However, weight-change tests and burst tests are complete, and some preliminary conclusions can be made:

Simulated FFTF Type 304 stainless steel fuel-pin burst stress is not significantly decreased as a result of cleaning and reinsertion into sodium at temperatures ranging from 800 to 1400°F.

Initial metallographic examination of crevice samples indicates some corrosion attack in the crevice region, but an insufficient number of samples have been examined to date to reach conclusions on differences in cleaning procedures or test temperature.

TABLE 3. Total Weight Changes for Single Coupons

Sodium-removal Process	Weight Loss, mg/dm²			
	Sodium-exposure Temperature (°F) in Isothermal Stagnant Capsule during 500-hr Exposure Cycles			
	800	1000	1200	1400
Mercury				
1 cycle[a,d]	2	2	3	2
2 cycle[b,e]	0	2	2	2
Dowanol EB				
1 cycle[a,c]	0	1	1	3
1 cycle[b,d]	2	2	4	2
2 cycle[a,e]	0.3	2	2	0
Argon-Steam				
1 cycle[a,c]	0.3	1	2	2
1 cycle[b,d]	2	3	3	2
2 cycle[a,e]	1	2	3	0.3

[a] Average from 2 samples.
[b] Average from 6 samples.
[c] First sodium exposure and cleaning.
[d] Second sodium exposure and cleaning.
[e] First and second sodium exposure and cleaning.

TABLE 4. Burst Pressures of Fuel Cladding: Helium Gas Pressure (psig) on Fuel Pin at Burst Using a 5,000-psi/min Pressurization Rate[a]

Sodium-removal Process	Number of Sodium Exposures and Cleaning Cycles	Sodium-exposure Temperatures (°F) in Stagnant Capsules during 500-hr Exposures			
		800	1000	1200	1400
Mercury	1[b]	10,350	10,325	10,350	10,200
	2	10,400	10,200	10,400	10,300
Dowanol EB	1[b]	10,325	10,200	10,225	10,050
	2	10,300	10,250	10,400	10,050
Argon-Steam	1[b]	10,375	10,250	10,475	10,200
	2	10,300	10,200	10,350	10,200

[a] Burst pressure of fuel pins unexposed to sodium were 10,325 psig.
[b] Average value of two samples.

TABLE 5. Sodium Remaining on Crevice Coupons after Cleaning

Sodium-removal Process	Crevice Width, mil	Relative Residual Sodium	Residual Sodium Remaining on and in Crevice Samples as Oxide or Hydroxide after Cleaning, Calculated as mg Sodium		
			First 500-hr Sodium Exposure All Temp	Second 500-hr Sodium Exposure All Temp	
			1 Cycle[a]	1 Cycle[a]	2 Cycle[b]
Mercury	10	min	0.08	0.2	0.1
		max	0.09	0.5	0.5
		avg	0.08	0.3	0.3
	20	min	0.04	0.02	0.01
		max	0.1	0.3	0.6
		avg	0.08	0.2	0.2
Dowanol EB	10	min	0.00	0.00	0.00
		max	0.01	0.02	0.4
		avg	0.01	0.00	0.06
	20	min	0.00	0.00	0.00
		max	0.01	0.02	0.1
		avg	0.00	0.01	0.03
Argon-Steam	10	min	0.00	0.00	0.00
		max	0.01	0.02	0.1
		avg	0.00	0.01	0.04
	20	min	0.00	0.00	0.00
		max	0.00	0.06	0.1
		avg	0.00	0.01	0.05

[a] Average values are average of 4 samples.
[b] Average values are average of 8 samples.

Acknowledgments

The laboratory work conducted by E. R. Wood and A. P. Bohringer making this paper possible is gratefully acknowledged.

REFERENCES

1. Rateick, R. G., and Stader, J. E., *Fuel and Repair Facility at the Enrico Fermi Atomic Power Plant*, ASME Winter Annual Meeting and Energy Systems Exposition, Pittsburgh, Pennsylvania (Nov 12–17, 1968).
2. Bernstein, G. J., Chilenskas, A. A., and Malecha, R. F., *Interbuilding Fuel Transfer Coffin for the EBR-II Reactor*, ANL-6934 (Sept 1964).
3. Deegan, G. E. *et al.*, *Design Modifications to the SRE During FY-1960*, NAA-SR-5348 Rev. (Feb 1961).

4. Goldmann, K., and Minushkin, B., "Sodium Technology," *Reactor Technology*, p. 326 (1965).

Discussion

Mr. Dickinson (LMEC): You mentioned metallographic examination. Are you sure these samples were completely sensitized?

Mr. Bloom: They were carburized. They had carbon precipitation at the grain boundaries. The 800°F samples did not have carbide precipitation even after 1000 hr. The 1000–1400°F samples did. They all did.

Mr. F. Smith (ANL): I have a table that might be of interest to support your conclusion that steam cleaning under some conditions certainly is adequate. We've been using electrical-resistivity measurements to determine the effects of cleaning, and I think it is of importance to look at the four techniques we used. The most important is No. 4, in which the specimen is oxidized in air at room temperature for 24 hr before rinsing with water. Sample No. 4 has an effective electrical-resistivity value of 66.3 microohm-cm, which compares reasonably well with values obtained after the other cleaning techniques were used. It is of interest that the microstructure and electrical-resistivity values are relatively unaffected by very adverse cleaning procedures, as well as by the more conventional alcohol and water-rinse procedure.

Mr. Kovacic (APDA): I might just comment that several years ago in conjunction with some repair operations in the Fermi reactor we had to consider whether or not we would take some steam-cleaned components back into the system. We had prepared some coupons, two of which were stressed, I believe, just by doing a complete reverse bend on them. These were not steam cleaned, but they were stored in normal atmosphere and then re-immersed in sodium. I'm not quite sure what the temperatures were, but I'm sure they were 1000°F or less. Of the 6 specimens, one cracked. That's just information. Now I do have a question. I believe all your re-exposures in sodium were at 800°F or higher—I suggest that re-exposure conditions at lower temperatures might possibly be more severe because the hydroxide wouldn't be converted to monoxide and might not be leached out of the crevices as fast. Have you had any tests at less than 800°F? My third comment, which you've already answered, is that I certainly think you ought to run stressed specimens.

Effects of Techniques for Removal of Surface Sodium on Resistivities of Type 304 Stainless Steel of Samples of 0.495-in. OD and 0.018-in.-wall Tube

Time in Strauss Solution (min)	Sample No. 1		Sample No. 2		Sample No. 3		Sample No. 4	
	R, 10^{-5} ohm-cm	ρ, 10^{-6} ohm-cm	R, 10^{-5} ohm-cm	ρ, 10^{-6} ohm-cm	R, 10^{-5} ohm-cm	ρ, 10^{-6} ohm-cm	R, 10^{-5} ohm-cm	ρ, 10^{-6} ohm-cm
0	155	63	148	63	161	64	163	66.3
15	192	78	175	75	189	75	175	72
30	215	88	193	83	215	85	205	83.5
45	265	108	233	100	278	110	255	104
60	291	119	259	110	Sample used		278	113
75	295	121	259	110	for micro-		278	113
90	293	120	259	110	scopic in-		278	113
120	293	120	259	110	spection		278	113

$$\text{Resistivity } \rho \text{ in ohm-cm} = \frac{R \text{ (ohms)} \times \text{Width (in.)} \times \text{Wall (in.)}}{\text{Width Probe Contacts (in.)}} \times 2.5$$

Sample	*Cleaning Techniques*
No. 1 (0.283 in. wide)	Remove from sodium and cool in argon atmosphere. Soak sample in alcohol for slightly less than 2 hr. Rinse in tap water.
No. 2 (0.297 in. wide)	Removal same. Soak sample in alcohol for 4 hr before rinsing.
No. 3 (0.275 in. wide)	Removal same. Soak sample in alcohol for 18 hr before rinsing.
No. 4 (0.283 in. wide)	Removal same. Oxidize in air at room temp for 24 hr before rinsing.

Mr. Bloom: It should be pointed out that these tests are very preliminary and that we don't even try to say that they're true prototype tests. As a prototype test one would try, with one cleaning process, to get all these conditions—all types of reinsertions, all temperatures.

Mr. Zitek (ComEd): I'm a neophyte in this field. What effect do you expect radiation might have on your tests?

Mr. Bloom: They did some tests at EBR-II in which they looked at irradiation effects. Some, I think ½-inch stainless steel tubes, samples were exposed to radiation. They saw no effect for the types of tests run but the effect could depend on the length and type of the radiation.

Sodium Evaporation in an Argon Flow

J. Van Dievoet, A. Michel, and R. Lanckman

Belgonucléaire
Brussels, Belgium

(PRESENTED BY A. MICHEL)

1. Introduction

A general study of fuel conditioning was carried out in Belgium in the framework of the Euratom-Belgium Association for fast breeder reactors. The fuel conditioning concerns all the operations included in the fuel cycle from the reactor fuel unloading to the fuel introduction in the reprocessing plant, that is, fuel-subassembly dismantling, fuel cleaning, fuel transportation, and fuel storage.

During the fuel conditioning, the fuel rods are transferred from a sodium environment to a gas environment, usually argon. This transfer can even be accomplished in the reactor itself during the fuel handling, when the latter is performed under argon.

Anyhow, an argon circulation is used during this transfer to remove the decay heat from the spent fuel. It is obvious that at the same time some of the sodium remaining on the fuel element is entrained in the cooling gas either through drainage or through evaporation.

It is very important for the cooling system and for the subsequent conditioning operations to determine the amount of remaining sodium. It was found that very little was known about the amount of sodium entrained with the fuel during the unloading operation, and also that no quantitative figures could be given for the distribution of this sodium among the argon coolant, the filters, and the cask car. Scarce information has been published on the remaining amounts, which would have to be removed during the cleaning operation. Some attention was given to the possibility of subassembly dismantling before transportation, either under sodium or in argon, in which case there was some probability that the cleaning operation of single rods could be avoided, draining and evaporation being sufficient.

A literature survey was done and some contacts taken with reactor operators. It showed that in EBR-II, for example, the sodium is drained and evaporated during unloading in an argon down flow and the assembly is later flooded with water.

Some values were given for entrained sodium in the case of the Fermi reactor (5 mg/cm^2). A systematic study was performed for SEFOR,[1] but since the purpose was mostly to investigate the possibilities of cell-window fogging, the results are difficult to interpret in terms of rod performance. The average amount was of the order of 0.7 mil thick, that, is 1.42 mg/cm^2. This gave an order of magnitude of the phenomenon to be studied.

A preliminary theoretical study was performed to analyse the sodium-evaporation phenomenon, but many difficulties were encountered. Even if one could have some confidence in the relationship proposed, for example, by Boelter[2] or Luikov,[3] the physical values of the parameters to be used are not well-known; this is particularly true for the mass diffusion coefficient of sodium in argon. Also, the exact definition of the location where each parameter should be taken (bulk, wall, or film value for example) has much influence.

The result of this theoretical study showed that an order of magnitude of the time for drying a fuel rod unloaded from a 1000-MWe faster breeder 75 hr after the reactor shutdown would be around 1.5 min with a wall temperature around 500°C. It was then decided that only experiments could give information about the sodium draining and evaporation phenomena, and the erection of a test loop was decided.

2. Description of the Test Loop

The test loop (see Fig. 1) is made of three parts: a sodium loop, an argon loop, and a movable platform with a balance.

The *test section* includes the dip tank in the sodium loop, connected through a gate valve with the argon test tube (of pyrex glass or quartz, depending on the operating temperature). The rod to be tested is hung from the platform, which enables a simulation of an unloading operation. The rod is immersed for a definite time in sodium, then lifted into the argon.

The *sodium loop* is equipped with heater and cooler to stabilize the temperatures and obtain a small natural circulation. The sodium purity can be maintained by regularly dumping the sodium at relatively high temperature into the lower tank and filling the loop again at low temperature through a sintered metal filter.

The *argon loop* is composed of a diaphragm pump, flowmeter, sodium vapor traps, heater, and cooler.

The *movable platform* can lift the rod at two different velocities without shocks to the balance. The rod can be either connected to the balance, in which

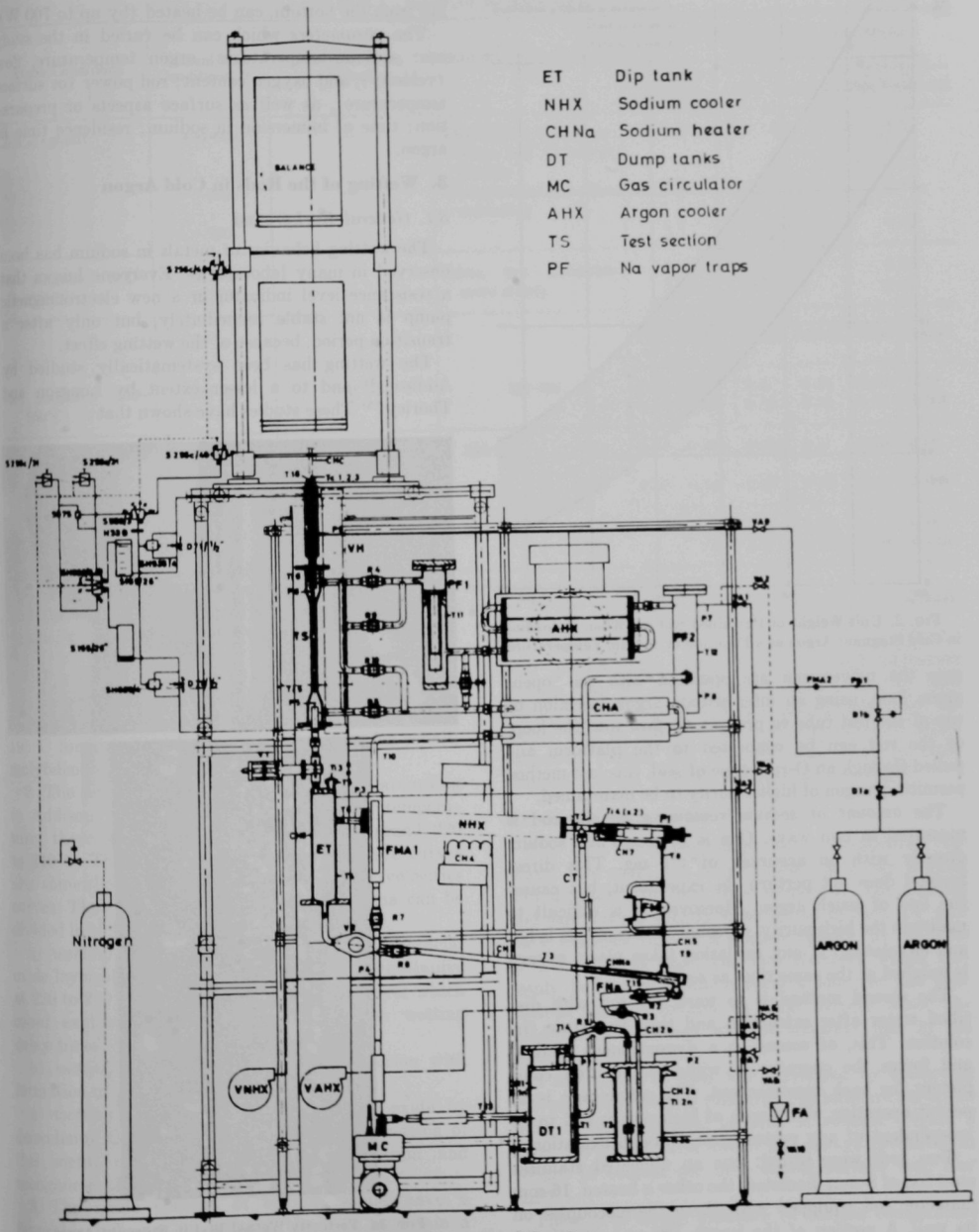

FIG. 1. Diagram of Test Loop.

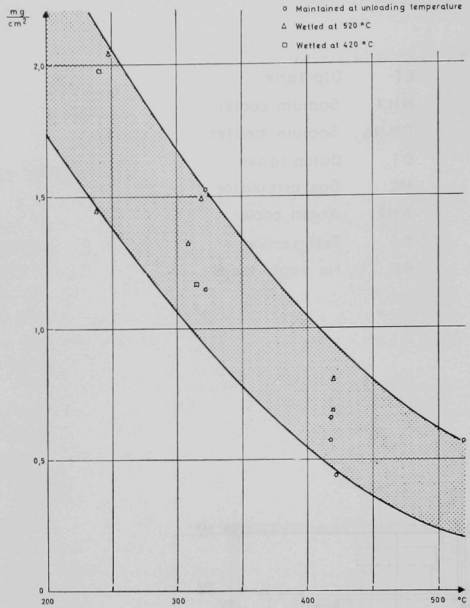

FIG. 2. Unit Weight of Entrained Sodium When Unloading in Cold Stagnant Argon as a Function of Sodium Temperature.

case the movements are operated with an "open" argon loop, using an intermediate argon injection on top of the test tube to prevent air flow into the loop; or the rod can be connected to the platform and pulled through an O-ring type of seal, this last method permitting argon of higher purity to be maintained.

The *amount of sodium remaining* on the rod is measured in two ways. One is to weigh the sodium directly with an accuracy of ±1 mg. This direct method does not perturb the experiment, but causes the loss of much argon. Moreover, it is difficult to maintain the high purity, especially if this argon is hot and circulating. If any oxidation takes place, oxygen is weighed at the same time as sodium.

The second method is to wash the rod with distilled water after extraction and then to titrate the solution. This, of course, is a discontinuous method and forces the operator to withdraw the rod completely for each measurement. The advantage is to permit operation with argon of high purity and to be independent of any perturbation through oxidation.

Two *rods* were tested: one an unheated stainless steel rod of 8-mm diameter; the other a heated, 16-mm diameter rod equipped with three thermocouples on its wall. A portion of the length (30 cm), starting 1 cm from the bottom, can be heated (by up to 700 W).

The *parameters* which can be varied in the study are: sodium temperatures; argon temperature, flow (velocity), and oxygen content; rod power (or surface temperature), as well as surface aspects or preparation; time of immersion in sodium; residence time in argon.

3. Wetting of the Rods in Cold Argon

3.1. General Background

The wetting behavior of metals in sodium has been observed in many laboratories. Everyone knows that a resistance level indicator or a new electromagnetic pump is not stable immediately, but only after a transition period, because of the wetting effect.

The wetting has been systematically studied by Addison[4] and to a lesser extent by Longson and Thorley.[5] These studies have shown that:

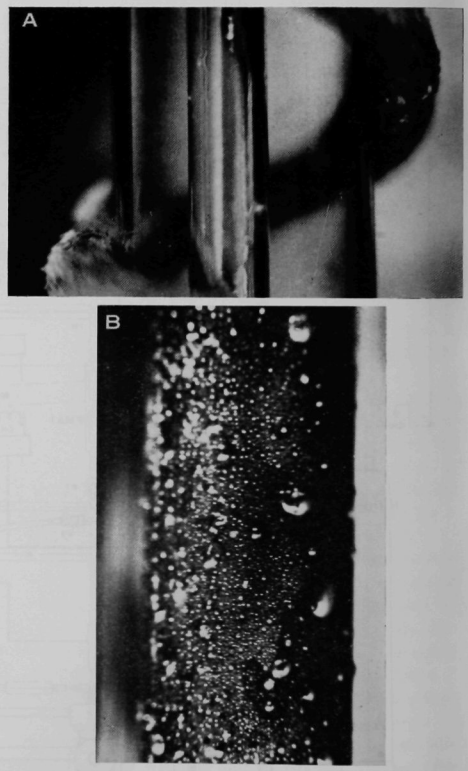

FIG. 3a. Perfectly Wetted Rod in Stagnant Argon.
FIG. 3b. Nonwetted Rod with Local Sodium Drops.

TABLE 1. SUMMARY OF TEST RESULTS

Argon Conditions	Sodium-tank Conditions, °C	Rod Heat Flux, W/cm²		Rod Wall Temperature, °C		Unit Weight of Sodium Remaining on Rod, mg/cm²					
						Average		Max Accidental		Min Accidental	
Cold stagnant	400–500	—		Identical to that of sodium, but decreases rapidly		0.6		0.8		0.4	
	~300	—		Change with time after unloading		1.35		1.55		1.15	
	~220	—				1.8		2.05		1.45	
Hot stagnant (100–250°C)	>270	—		*Idem*, but decreases more slowly		0.55		0.95		0.35	
	≤270	—				1.1		1.95		0.4	
						Total [a]	Lateral [b]	Total	Lateral	Total	Lateral
Hot stagnant (100–250°C)	320–370	0–2.66		330–555		0.35	0.18	0.5	0.24	0.25	0.14
						0.11	0.08	0.12	0.11	0.11	0.065
Hot circulating (100–250°C) ~15 m/s	320–370	0–2.66	<1.6	330–555	<450	0.22	0.075	0.375	0.2	0.08	0.03
			>1.6		>450	0.12	0.04	0.28	0.09	0.06	0.008
~4 m/s	320–370	0–2	<1.6	250–500	<450	0.29	0.085	0.49	0.15	0.15	0.04
			>1.6		>450	—	—	0.5	0.066	0.08	0.015

[a] "Total" means amount of sodium divided by total wetted surface (between 150 and 200 cm²).

[b] "Lateral" means amount of sodium measured on heated part of the rod (only lateral as no ends effects are incorporated) divided by this heated part surface (150 cm²).

1. For pure sodium, there is a value of temperature below which pure metal will not be wetted by sodium. This value varies from 140°C for pure iron to 195°C for nickel, with intermediate values for cobalt, molybdenum, and chromium.

2. The time required to obtain wetting, according to Addison, decreases with an increase of temperature; there is an observed discontinuity around 220 to 240°C. The aspect of the time-temperature curves are somewhat similar to surface-reaction velocities curves. Thus the wetting chemical phenomena can be divided in three groups:

a) *wetting obtained by* reduction of the superficial oxide layer of metals; for iron, there is a discontinuity at 220 to 240°C in the composition of this layer which could explain the similar discontinuity in wetting delay times;

b) *wetting obtained by* chemical interaction with formation of an intermetallic complex;

c) *wetting obtained by* metals forming oxide by deoxidizing the sodium, in which case the wetting of this metal oxide is the problem (zirconium and manganese, for example).

3. The oxide content of sodium would have a favorable influence on wetting, the time to obtain a zero contact angle being shorter for oxide-saturated sodium than for cold-trapped sodium. This has been particularly shown by Longson and Thorley. For example, iron at 250°C is wet after one hour in oxide-saturated sodium but not wet after 3 hr in cold-trapped sodium (120°C plugging temperature).

3.2. Experiments in the Test Loop

The tests were performed in oxide-saturated sodium; this could not be prevented, as many loading and unloading of rods were necessary. The theories and experiments shortly summarized in Sect. 3.1. give some evidence that in a nuclear reactor, at the time of unloading at least, the fuel elements would certainly be wet and thus entrain a more or less continuous film of sodium on their surface when unloaded. The problem was to simulate this in the shortest possible time.

A first series of tests was performed by extracting the unheated rod into cold argon to measure an upper limit of the entrained amount of sodium. Figure 2 gives the results. The values are always presented in weight of sodium per unit wetted surface (mg Na/cm²).

There is a strong influence of sodium temperature

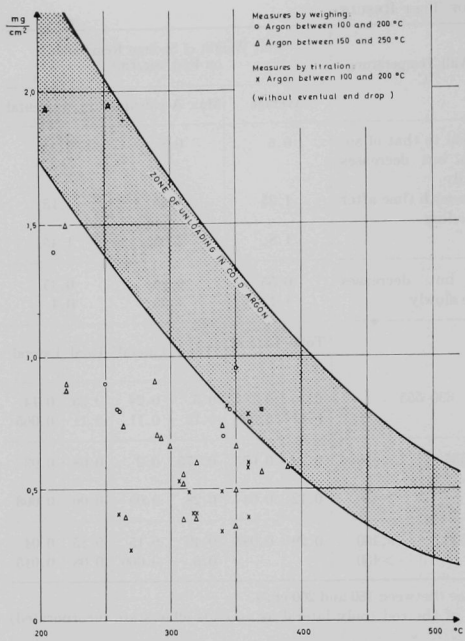

FIG. 4. Unit Weight of Entrained Sodium When Unloading in Hot Stagnant Argon as a Function of Sodium Temperature.

at the time of unloading, but the temperature history has no significant effect on the entrained amount. The sodium temperature only reduces the wetting time (between 30 min at high temperature, i.e., 400°C and more, and a few hours at lower temperatures).

The surface preparation has a strong effect: any type of pollution such as alcohol cleaning, traces of grease, or acetone degreasing increase the wetting delay. The best method to obtain a short-time wetting was polishing with emery cloth followed by a simple Kleenex cloth cleaning.

Figures 3a and 3b show pictures taken after unloading in argon. Figure 3a shows a perfectly continuous shiny film corresponding to approximately 0.8 mg/cm²; Fig. 3b shows a rod that is nonwetted apart from very local spots.

Table 1, which summarizes all results, shows that the amount of sodium varies with temperature from 0.6 to 1.8 mg/cm² average with a maximum value of 2 mg/cm².

4. Wetting of the Rods and Draining in Hot Argon

It seemed to the operator that the unloading in cold argon perturbed the wetting to a certain extent for after some time the sodium froze on the rod. Thus operations were started with hot stagnant argon. It was hoped that some sodium would drain as a result of the high temperature.

This was not the case for the amount of sodium that, at the higher temperatures (see Fig. 4) did drain, but simply accumulated as a drop at the bottom. This drop never grew to a sufficient volume to fall off. The amount remaining on the side surface of the rod, excluding this bottom drop, is scattered between 0.35 and 2 mg/cm² (see Table 1). But one can observe that above 270°C, the average value is around 0.55 mg/cm² and the values are far less scattered, with an accidental maximum of 0.95 mg/cm². The values are usually lower than during unloading in cold argon.

This wetting step around 270°C was also apparent in the behavior of the sodium. A continuous film is easily obtained above 300°C, but was practically never really obtained below 250°C; the sodium wetted only locally, showing dry spots, but the total amount was much higher than for a continuous film.

After these two sets of experiments, it was decided

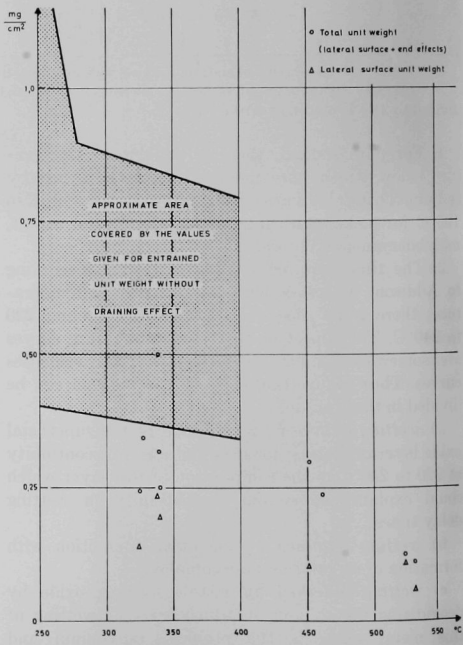

FIG. 5. Effect of the Draining and Evaporation of Sodium on Unit Entrained Weight as a Function of Rod Wall Temperature (Stagnant Gas). Sodium in wetting pot maintained between 320 and 360°C.

FIG. 6a. Aspect of the Rod at an Intermediate State of Evaporation at Wall Temperature of 450°C.
FIG. 6b. Completely Dried Rod (After Evaporation at Wall Temperature of 550°C.)

that for the simulation of reactor unloading, the sodium would be maintained between 320 and 370°C, to obtain a good continuous and reproducible film in about 1 hr.

5. Sodium Evaporation

5.1. Nonheated Rod in Circulating Argon

Up to now, the tests were performed with argon below 280°C. At this temperature, independently of the argon velocity, no evaporation was observed. In the near future, tests will be carried out at higher argon temperatures.

5.2. Heated Rod in Hot Stagnant Argon

Some experiments were performed with noncirculating hot argon (100 to 250°C) and a rod power up to 225 W, limited by surface temperature conditions (max 550 to 600°C).

The results are now presented as a function of rod-wall inside temperature; the sodium weights are lower than previously obtained because the temperature of the sodium on the wall is maintained at higher values, and thus improves the draining and the evaporation. It can be seen from Fig. 5 that the total value strongly decreases with temperature, and if one subtracts the amount remaining on the unheated portions of the rod (top and bottom), the uniformly covered side surface (called lateral surface in the figures and table) gives an even lower unit weight, down to 0.08 mg/cm² above 500°C.

5.3. Heated Rod in Hot Circulating Argon

In circulating argon, the power could be raised to 400 W, that is, a heat flux up to 2.66 W/cm², corresponding for a 6-mm-diameter fuel-element rod to about 5 or 6 W/cm. This is about 1% of the maximum power of a fast breeder fuel element and is a probable value of the residual power at the time of unloading. In fact, this limiting unloading power is

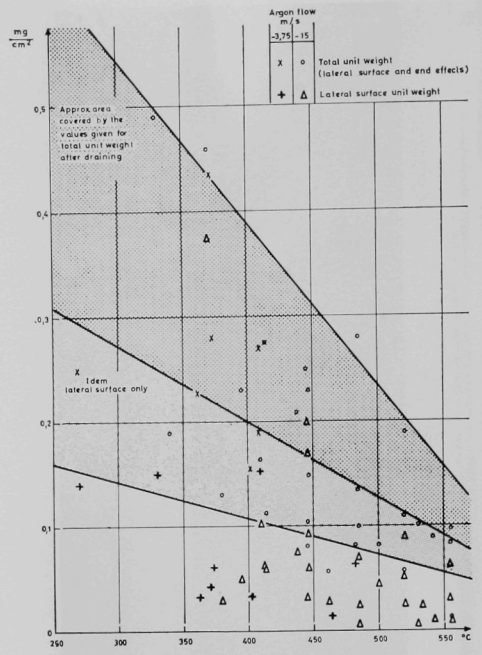

FIG. 7. Effect of the Draining and Evaporation of Sodium on Unit Entrained Weight as a Function of Rod Wall Temperature (Circulating Gas). Sodium in wetting pot maintained between 320 and 360°C.

strictly correlated with the maximum cladding temperature.

With hot circulating argon at a velocity of 4 or 15 m/s the side surface of the heated rod can be entirely dried at high temperature.

Evaporation is shown at an intermediate stage in Fig. 6a (at average wall temperature of 450°C) and a complete drying in Fig. 6b (wall temperature of around 550°C after a few minutes).

Observing the phenomena for a wall temperature above 450°C (1.6 to 2 W/cm²), one sees first the disappearance of practically the whole sodium film, except for some local droplets, in less than 2 or 3 min. Then, usually in about 10 to 15 min, these drops slowly evaporate until a complete drying is obtained.

There is not much influence of argon velocity, but its purity is important, as otherwise oxidation takes place before evaporation is obtained. The experiments were performed with argon containing less than 10 vpm O_2. The influence of this parameter will now be more accurately investigated.

As shown in Fig. 7 and in Table 1, above a wall temperature of 450°C the average amount remaining on the rod is an order of magnitude below the initial values: around 0.04 mg/cm², with accidental values up to 0.09 mg/cm². On the nonheated bottom and top portions of the rod (respectively 1 and 7 cm long) more sodium can remain; the conduction is not sufficient to enhance evaporation.

Between wall temperatures of 350 and 450°C, evaporation is often efficient, but accidental results can be much higher, even up to 0.2 mg/cm² on the heated surface.

Below a wall temperature of 350°C evaporation is efficient only accidentally, and high remaining quantity can often be observed.

6. Present Conclusions

It can be concluded from the results obtained up to now that:

1. Wetting will always be obtained in a sodium fast reactor, usually after a few hours except if the surface is strongly polluted. To obtain wetting for the experiments, a sodium temperature between 320 to 370°C gave good results in an immersion of about one hour.

2. The extraction of the rod from the dip tank to the test section takes about one minute; not much sodium draining is observed after this operation.

3. Evaporation is efficient for wall temperature above 350°C and permits a practically complete drying above a wall temperature of 450°C with very little risk of getting accidentally large amounts remaining on the rod. It does not seem there is a very sensitive influence of the velocity of the argon, but its purity should be good.

4. Nonheated parts such as bottom and top portions of the rods and grids, and holes between grids and rod, will be difficult to clean with this method.

A study of evaporation from a cluster of rods will now be undertaken, together with evaluation of the influence of argon purity and temperature (up to 500°C). It seems that one could rely on evaporation if the rod temperature is maintained above 450°C. If dismantling takes place before transport of irradiated elements to the reprocessing plant, it is possible that cleaning after evaporation would not be necessary at all.

Acknowledgments

This work has been performed under contract Association Euratom/Belgonucléaire.

The authors would like to thank also the members of the Belgonucléaire team who actively participated in performing these experiments and without whose

experimental skill no results would have been obtained.

REFERENCES

1. Horst, K. M., *SEFOR Development Program Quarterly Reports* (1 to 6) for 1964–1965, GEAP-4594, -4742, -4799, -4994.
2. Boelter, L. M. K., *et al.*, *Free Evaporation into Air of Water from a Free Horizontal Quiet Surface*, Ind. Eng. Chem., **38** (June 1946).
3. Luikov, A. V., "Heat and Mass Transfer in Capillary Porous Bodies," in *Advances in Heat Transfer, 1*. Academic Press (1964).
4. Addison, C. C., *et al.*, *The Role of Ozide Films in the Wetting of Iron, Cobalt and Nickel by Liquid Sodium*, J. Chem. Soc **1962**, 2699. This is Part VI of a series of papers on the same subject in the same journal.
5. Longson and Thorley, *The Wetting Behaviour of Some Alloys Based on Iron, Nickel and Chromium in Liquid Sodium*, TRG Rep. 1291, Risley, UKAEA (1966).

Discussion

Mr. Matte (APDA): Did the argon flow up or down?

Mr. Michel: We have tried both directions; in fact, the loop was designed to do this. It was reported that by up-flow we could prevent draining and thus see only evaporation, but when doing this, we had some trouble with the lower drops, which went to the side tube. As a result, we decided to do all our experiments with down-flow of argon. This is the most realistic way, because the purpose is to clean.

Mr. Pfahler (LMEC): Would you give your views on this technique for other components?

Mr. Michel: It's difficult to answer now. In the reported work we had a heat flux from the inside of the tube to the outside, so that the heat flux and the mass transfer were both in the same direction. I don't say that this is an important feature, I am just guessing, but the next step in our experiments is to work with hot argon, and, as we have seen it, it is necessary to go above a wall temperature of 400–450°C to have evaporation. I can't say now whether it will work with unheated parts. It could, but it certainly won't work with very difficult shapes. If you have indented shapes it will be difficult, and take longer times. It's a little like the distillation that we thought would always work if the argon were not diluted in time. Once you have obtained oxidation, it's finished, it's over—and at low temperature that's what happens.

Mr. Lindhe (AB Atomenergi): Did you investigate the residue on the rods after the sodium had evaporated?

Mr. Michel: We tried, but this is a rather difficult analytical technique. In most cases the residue was sodium oxide to a large extent. We tried to separate sodium oxide and sodium peroxide. Sometimes we appeared to have obtained sodium peroxide, but I couldn't guarantee it.

Mr. Lindhe: Do you know if the oxide comes from argon or from the sodium melt in the pot?

Mr. Michel: It comes from the argon, because mostly when we had oxidation it occurred through some faulty operation. If someone opened up a ring to weigh and mount, and if the pressure went up right at that moment, we had an inlet of air. This prevented any evaporation.

Mr. Brachet (EDF): Do you think that the smoothness or roughness of your rod is an important parameter? If it is, did you make measurements using this parameter?

Mr. Michel: We first tried to have the fastest wetting possible and so we tried different surface aspects. The fastest wetting was obtained by just cleaning the rod with water after one operation, putting it on the machine to polish it with very fine emery cloth, and then doing nothing more after that—just drying it with Kleenex or something like that. This is because we observed that if we worked, let's say a Friday evening, the next Monday morning it would take a much longer time, because of reoxidation of the surface, to obtain wetting again. Now from the point of view of surface roughness, I would say it has some influence insofar as products are held in the areas of roughness. When we tried to clean with acetone or with alcohol, many times we had trouble with adhering acetone or alcohol. In this case it would take a long, long time to obtain wetting, but we didn't try to heat it very strongly.

Mr. Shannon (BNWL): What was the purity of the argon that you used, particularly as regards water and oxygen content?

Mr. Michel: In the bottle, argon was below 5 ppm water, 5 ppm oxygen, a very small amount of nitrogen, and practically nothing else, as far as I can rely on the guarantee of the manufacturer. We tried to work with a Hirsch cell. Although it did work, it was only an indicative measurement as we had some trouble with calibration, but that's another story. It did give results between 5 and 10 ppm when the operation was good. Increasing above 1000 ppm we had trouble with the evaporation, oxidation being faster at this condition. This is just an order of magnitude; I wouldn't guarantee these numbers.

Mr. Harde (Interatom): Have you investigated the influence of the argon pressure in these tests?

Mr. Michel: We have been asked to, but we haven't had time up to now. That's what we will do next year.

Water Cleaning and Air Storage Effects on Sodium-exposed Fuel Clad Alloys, 304 and 304L Stainless Steel

F. A. Smith, E. L. Kimont, and L. H. Bohne

Argonne National Laboratory
Argonne, Illinois

(PRESENTED BY F. A. SMITH)

Introduction

EBR-II fuel-reprocessing operations feature a moist-air and water rinse followed by air storage of spent fuel before disassembly and reprocessing. Some EBR-II fuel may be stored in a NRTS water fuel-storage facility for relatively long periods of time. Also, some fuel pins of various experimental irradiation programs may be returned to the reactor one or more times after only relatively short periods of air storage after water cleaning. It is desirable to determine if out-of-reactor environmental effects on fuel clad exist. These effects, if real, may be separated from neutronic environmental effects on fuel clad.

The purpose of this paper is to present data related to water cleaning and air or water storage of a prototypic fuel clad alloy which has been exposed to one specific nonradioactive sodium source.

The principal alloy considered for evaluation is Type 304L stainless steel EBR-II driver core clad, MK-B-37. Type 304 stainless steel has also been compared with Type 304L stainless steel tubing for several reasons:

a. to have available direct data to compare Type 304L with Type 304 under similar conditions of specific sodium exposure;

b. to complement other data[1] already developed which featured sodium exposure and effective electrical-resistivity measurements primarily related to Type 304 stainless steel;

c. to promote a better understanding of how austenitic alloys may be affected by sodium exposure, air storage, or water storage, and re-exposure to sodium.

Conclusion

Several conclusions have been developed from one series of nonradioactive sodium exposures of Types 304 and 304L stainless steel fuel clad materials.

Conclusions are stated before presentation of the laboratory data as follows:

a. Re-exposure to sodium of previously water-cleaned and stored Types 304 and 304L stainless steel fuel clad results in accelerated deterioration* of fuel clad microstructure as the sodium-exposure and water-cleaning steps are repeated.

b. Dry, static air storage ($CaSO_4$ desiccated) compared to normal air storage of water-cleaned specimens provides evidence of unreacted subsurface sodium. This "stored" sodium can then react with any aqueous solution to produce adverse effects on clad microstructure.

c. Type 304L stainless steel is not affected as much by repeated sodium exposure, water cleaning, and air or water storage as is a comparable Type 304 stainless steel-clad specimen.

d. The presence of sodium causing the evidence of the increasing effects of repeated sodium exposure is not clearly known.

e. Until the mechanism of retention of sodium by a structural alloy is better established, the effect of sodium cleaning of irradiated fuel and subsequent storage environments should be examined carefully for each separate sodium reactor environment.

The work was completed in four chronological steps or phases, and the data are presented in the same sequence.

The general plan of evaluation of the effects of sodium exposure, storage, and recycle to sodium of fuel clad specimens is as follows:

A number of specimens were exposed in a sodium loop. This sodium exposure is the starting point for subsequent exposure of specimens to air storage and recycle to sodium.

In Phases I, II, and III, effective electrical-resistivity measurements were made at two different time intervals. Electrical-resistivity measurements were first made immediately after sodium exposure and specimen cleaning of residual sodium. Measurements made at this time are called "Tests A." Specimens were also subjected to a Strauss reagent and electrical resistivity of the specimens again measured for specific periods of time of specimen exposure to Strauss reagent. These measurements are called "Tests B." Following any given Strauss reagent test, the specific specimens tested are discarded.

Additional specimens for the next phase were

* Deterioration is defined as a microstructure change indicated by an increase in the measured effective electrical resistivity of the fuel clad alloy following a Strauss test.

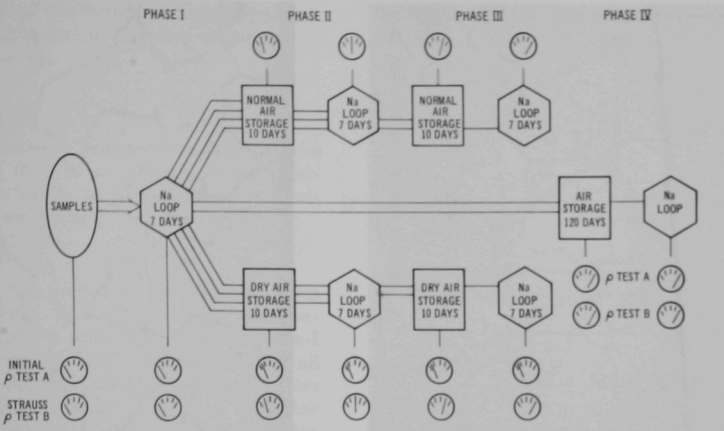

FIG. 1. Test and Exposure Flow Diagram.

stored in air for ten days. Following ten days of air storage, the specimens were then subjected to Strauss reagent and their effective electrical-resistivity values were again measured.

By comparing the effective electrical-resistivity values (in each case after Strauss test) before air storage and after air storage, the measured quantitative effects of air storage were evaluated.

Phase IV differs from Phases I–III in length of time of air storage. In Phase IV the specimens received the same initial sodium exposure as all other specimens. However, Phase-IV specimens were air stored for 120 days after the first sodium exposure and sodium cleaning. Electrical-resistivity measurements were made after the 120-day storage period. By comparing the electrical-resistivity values before and after 120 days of air storage, the effects of long-time air storage were evaluated.

This general plan of evaluation of the effects of air storage and sodium recycle is shown in Fig. 1.

The separate phases are defined and discussed in the following.

Phase I

Definition of Phase I

In Phase I, a specimen is exposed for seven days at 1100°F, the sodium removed from the specimen, and the electrical resistivity measured before and after exposure to Strauss[2] reagent.

Discussion of Phase I

Specimens of Types 304 and 304L stainless steel tubing were exposed to flowing sodium in a dynamic loop at 1100°F for seven days. The loop and the bases for a 7-day exposure to sodium is described and discussed in a recent IAEA paper.[1]

TABLE 1. PHASE-I TESTS A OF SODIUM-TREATED TYPES 304L AND 304 TUBING

(8 specimens for each group tested)

Treatment	Effective Electrical Resistivity, μΩ-cm
None, as-received Type 304L SS	70
Type 304L SS after sodium exposure and cleaning	71.5
Type 304 SS after sodium exposure and cleaning	68.5

After removal of specimens from the loop, the specimens were allowed to oxidize in air for one hour. This period of air oxidization of residual surface sodium was chosen as representative of the possible air-oxidation time allowable for removal of a reactor fuel element such as exists at EBR-II. Specimens were dry steam-cleaned for 15 min, immersed in demineralized water for 45 min, and air-dried.

Measurements of electrical resistivity of specimens were made soon after air drying. Techniques of specimen preparation and electrical-resistivity measurement are described in reference 3. Eight electrical-resistivity specimens of each type of tubing were prepared to provide the statistical basis for the results presented in Table 1.

Photomicrographs of the sodium-exposed Types 304 and 304L tubing, before Strauss test, are shown in Fig. 2.

The above sodium-exposed and cleaned specimens

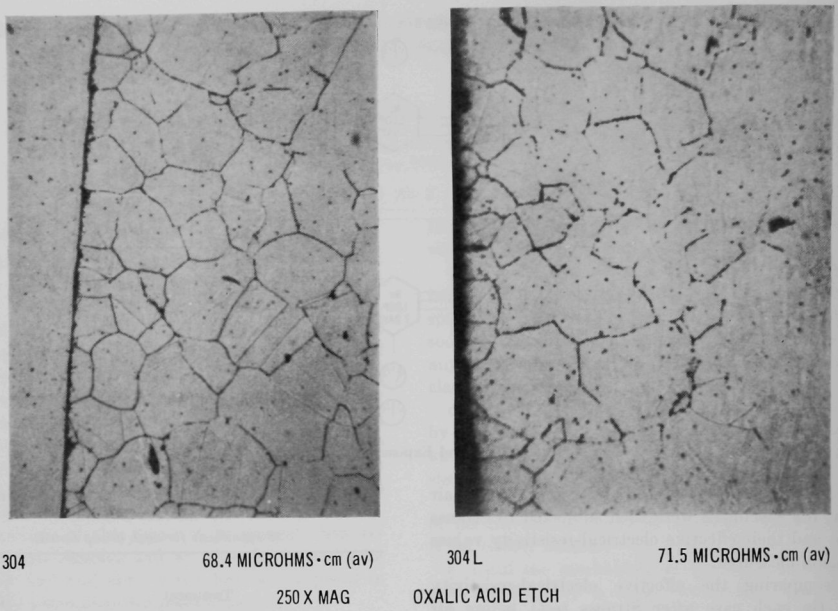

FIG. 2. Photomicrographs of Sodium-exposed Stainless Steel Tubing before Strauss Test.

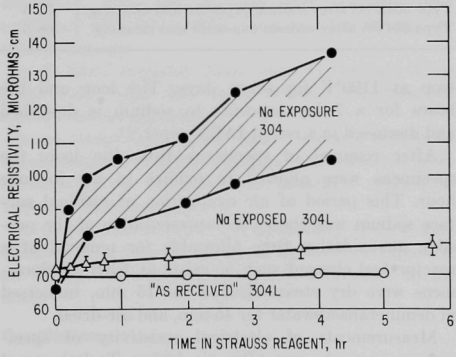

FIG. 3. Phase I, Test B. Rates of Attack of Strauss Reagent after Sodium Exposure.

were next subjected to a Strauss reagent test for various times of reagent exposure. The statistical data from eight Type 304 and eight Type 304L specimens are shown in Fig. 3. The data for Type 304L specimens indicate only a modest increase in effective electrical-resistivity values, with a narrow range of data spread for any given period of time of exposure to Strauss reagent. In contrast the Type 304 specimens indicate large increases in effective electrical values. Data spread of resistivity values of Type 304 stainless steel for a given time in Strauss reagent is large. Of some importance is that all minimum resistivity values of Type 304 specimens are considerably higher than the maximum values associated with Type 304L specimens.

The data of Fig. 3 included exposure to Strauss reagent for up to 6 hr. The less-affected Type 304L specimens were then exposed to longer-time Strauss tests, for up to 40 hr. The data from the longer exposures to Strauss reagent are shown in Fig. 4. It is noted that 40 hr of Strauss reagent exposure of Type 304L is required to produce a resistivity value of about 105 $\mu\Omega$-cm. In contrast only a 4.0-hr exposure of Type 304 stainless steel to Strauss reagent produces an effective electrical-resistivity value of about 105 $\mu\Omega$-cm (see Fig. 3).

Conclusion of Phase I

Phase-I data indicate that Type 304L stainless steel is only modestly affected by a single specific exposure to sodium. Type 304, compared to Type 304L, exposed to the same sodium environment under similar conditions of temperature, time, and flow,

exhibits increased effective electrical-resistivity values after a given exposure to a Strauss reagent.

Phase II

Definition of Phase II

Phase II consists of storage of sodium-exposed specimens for 10 days in air and re-exposed specimens for 10 days in air, and re-exposing the specimens to sodium a second time.

Discussion of Phase II

Phase-II work was limited to Type 304L stainless steel specimens only. Phase-II specimens were exposed to sodium at the same time that the Phase-I specimens were exposed. After sodium exposure, all specimens, including Phase-II specimens, were cleaned as discussed in Phase I. Half of all specimens were exposed in laboratory static air. The remaining half of all specimens were stored in a desiccator containing $CaSO_4$. Air-storage period for both groups of specimens was 10 days. Desiccated specimens were evaluated in an attempt to simulate the dry air environment of Idaho compared to the nominal humid air of Argonne. The tests were conducted at Argonne.

After the ten days of air storage, eight normal and eight desiccated specimens were set aside for testing. The results of effective electrical-resistivity measurements are shown in Table 2.

Table 2 indicates that some small changes in effective electrical resistivity had taken place because of 10-day air storage. Metallographic inspection of these specimens after 10-day air (normal and dry) storage showed no essential difference from the structures shown in Fig. 2.

The above specimens were exposed to a Strauss reagent and electrical-resistivity measurements made at various time intervals. Data for these measurements are shown in Fig. 5 along with a comparison for similar data for Phase I.

Of special interest is the observation that desiccated Type 304L stainless steel specimens, compared to normal air-stored specimens, show a lower initial electrical resistivity, but exhibit a sharper increase of electrical resistivity, a narrower statistical spread of data, and a slightly higher ultimate effective resistivity.

The balance of all specimens for the remainder of Phase-II and Phase-III work was returned to a sodium loop for a second sodium exposure.

Following the second 7-day, 1100°F sodium exposure, eight normal and eight desiccated specimens were set aside. Metallographic inspection of the Type

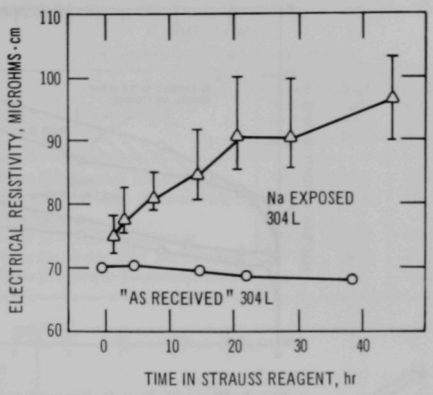

FIG. 4. Phase I, Test B. Long-term Rates of Attack of Strauss Reagent after Sodium Exposure.

TABLE 2. PHASE-II TESTS A OF SODIUM-TREATED TYPE 304L TUBING

(8 specimens for each group tested)

Phases Tested	Low Resistivity, μΩ-cm	High Resistivity, μΩ-cm	Average Resistivity, μΩ-cm
Phase II: 10-day Air Storage at Room Temp	68.4	72.0	70.3
Phase II: 10-day Storage in Desiccator with $CaSO_4$	67.5	68.6	67.9
Phase I: Sodium Treatment Only	—	—	71.5

304L stainless steel specimens after 10-day air storage and a second exposure to sodium is shown in Fig. 6. Item (B) in this figure illustrates a sensitized grain structure as a result of the second sodium exposure. One can observe that the microstructure of Type 304L after a second sodium exposure is significantly different than the microstructure of Type 304L after a single exposure to sodium [see Item (A)]. Item (C) shows Type 304 for only one sodium exposure and is to be compared to Item (B), which had two exposures to sodium.

Next, the normal and desiccated air-stored specimens, after their second exposure to sodium, were subjected to the Strauss reagent for various periods of time. Electrical-resistivity data for these tests are shown in Fig. 7. These data indicate that desiccated specimens after a second sodium exposure with 10-day air storage have effective electrical-resistivity values which exhibit a narrow spread in statistical data and fall within the statistical values for normal (humid) air-stored specimens.

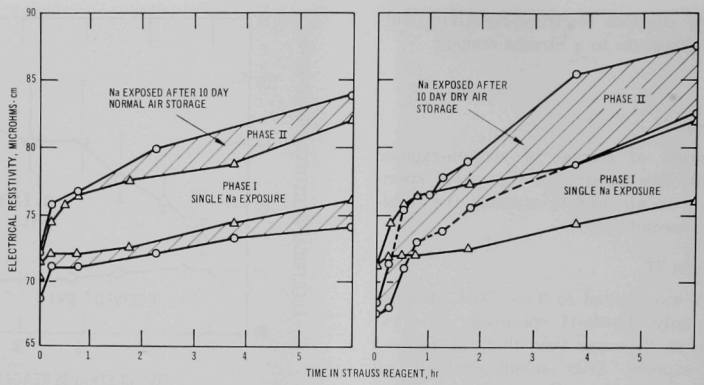

FIG. 5. Phase II, Test B. Rates of Attack of Strauss Reagent after Sodium Exposure.

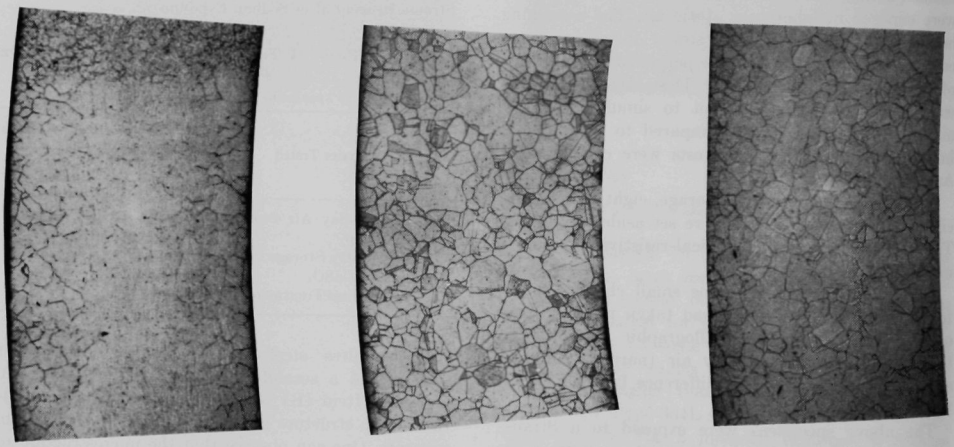

FIG. 6. Photomicrographs of Sodium-exposed Stainless Tubing.

Conclusions of Phase II

Type 304L tubing stored for 10 days in humid air or in dry air does undergo small changes in effective electrical resistivity. These small changes do not show up as marked changes in microstructure. A Strauss test shows that (normal or dry) air storage has only a small increasing effect on the effective electrical resistivity.

However, re-exposure to sodium for a second time after 10-day air storage does produce a significant change in microstructure. Data spread, in general, is believed to be a direct result of environmental exposure.

Phase III

Definition of Phase III

In Phase III, a second 10-day air (normal and dry) storage of specimens occurred after a second sodium exposure. Following the second 10-day storage period, specimens were exposed to sodium for the third time.

Discussion of Phase III

Following a second exposure to sodium, all specimens were stored for a second 10-day air (normal-dry) storage period. Eight normal and eight dry air-stored specimens were removed from the balance of available specimens. The effective electrical resistivities of these specimens were measured, with results noted in Table 3. For comparison, Table 3 repeats data taken from Phases-I and -II studies. To be noted is a slight increase in electrical resistivity of both "dry" and "normal" air-stored specimens above the respective values measured in Phase II.

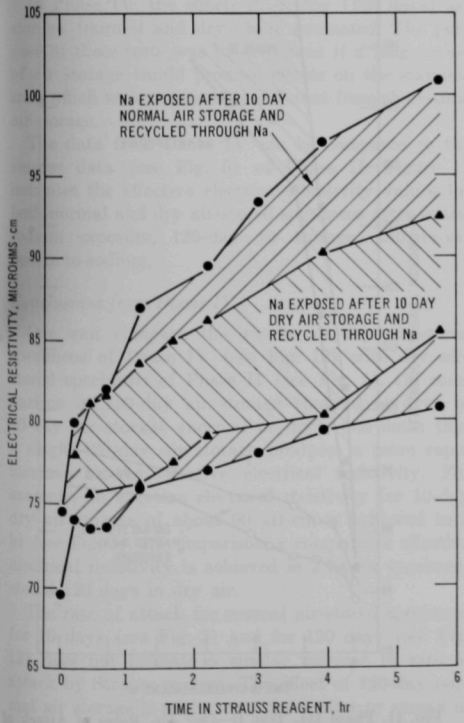

FIG. 7. Phase II, Test B. Rates of Attack of Strauss Reagent after Second Sodium Exposure.

TABLE 3. PHASE-III TESTS A OF SODIUM-TREATED TYPE 304L TUBING

(8 specimens for each group tested)

Phases Tested	Low Resistivity, μΩ-cm	High Resistivity, μΩ-cm	Average Resistivity, μΩ-cm
Phase III: Normal Air Storage	70.3	74.1	72.0
Phase II: 10-day Normal Air Storage	68.4	72.0	70.3
Phase III: Dry Air Storage	69.8	74.1	71.1
Phase II: 10-day Dry Air Storage	67.5	68.6	67.9
Phase I: Sodium Treatment Only	—	—	71.5

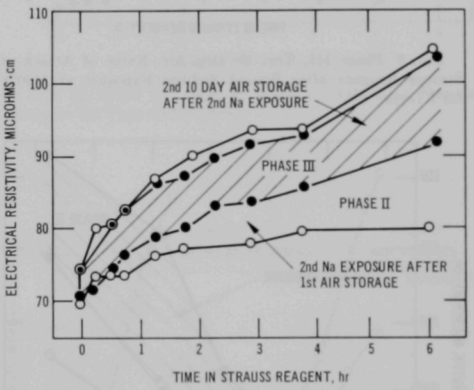

FIG. 8. Phase III, Test B—Normal Air. Rates of Attack of Strauss Reagent after Second Sodium Exposure at 1100°F for 7 Days.

Again, as in Phase II, there was no marked change in microstructure of Type 304L stainless steel due to the environmental exposures associated with Phase-III Tests A.

Eight additional "dry" and "normal" air-stored specimens were exposed to Strauss reagent and effective electrical resistivities were measured. Figure 8 indicates results of the second 10-day normal air storage after a second sodium exposure. Also Phase III is compared to Phase II. Figure 9 indicates similar data for the "dry" air-stored specimens.

Remaining specimens from Phase III were exposed for a third time to the sodium loop. After the third sodium exposure, the effective electrical resistivities of the specimens were measured. Results for the "normal" air-stored specimens is shown in Fig. 10. One can note that all data points for Phase III are higher than the highest effective electrical-resistivity values measured in Phase II.

Figure 11 shows results of Phase-III measurements

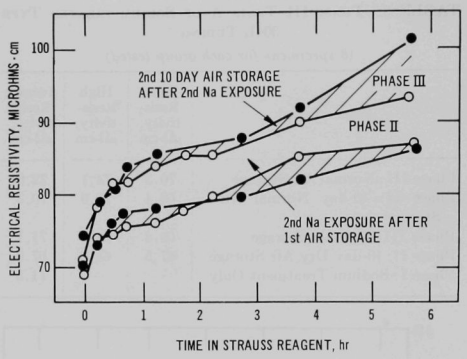

FIG. 9. Phase III, Test B—Dry Air. Rates of Attack of Strauss Reagent after Second Sodium Exposure at 1100°F for 7 Days.

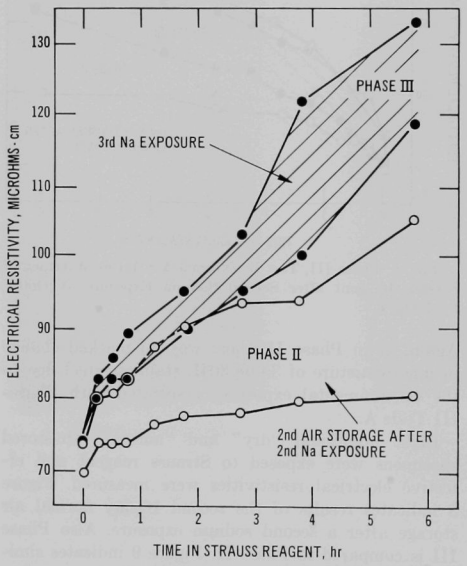

FIG. 10. Phase III, Test B—Normal Air. Rates of Attack of Strauss Reagent after Third Sodium Exposure at 1100°F for 7 Days.

of the dry air-stored specimens. One can note the large increase of effective electrical-resistivity values for the dry air-stored specimens. Comparing Phase-III normal air storage (see Fig. 10) with comparable data for the dry air-stored specimens of Fig. 11, one can note that high effective electrical resistivities of the "dry" air-stored specimens is achieved in less than one hour of exposure to Strauss reagent. The normal air-stored specimens require up to 6 hr of exposure to Strauss reagent to achieve similar resistivity values.

Conclusions from Phase III

Data from Phase III indicate that Strauss reagent is more aggressive in attack of dry air-stored specimens than in attack of normal air-stored specimens. A speculative model for high attack rates for the dry-stored specimens is developed from these laboratory data. Any residual subsurface sodium not removed by the cleaning procedure remains available to react with any available moisture during a given air-exposure period. During a normal air exposure (humid air) subsurface sodium could react with available moisture. Reaction with moist air would leave less unreacted subsurface sodium available to react with Strauss reagent after the moist air-storage

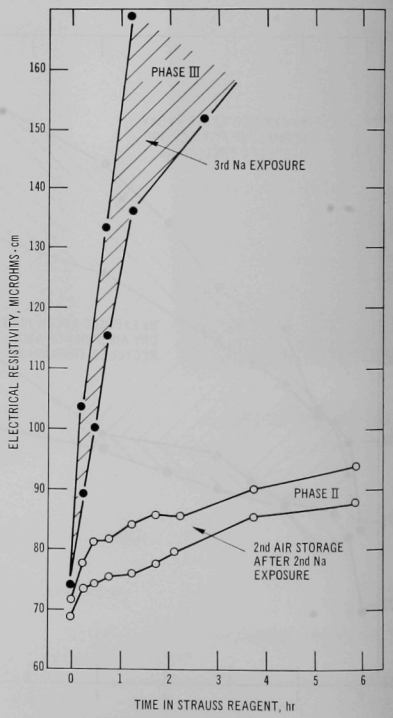

FIG. 11. Phase III, Test B—Dry Air. Rates of Attack of Strauss Reagent after Third Sodium Exposure at 1100°F for 7 Days.

cycle. In contrast, dry air-stored specimens have a limited amount of moisture available to the specimens during their storage time. A larger quantity of sodium would then be available to react with the Strauss reagent at the end of the dry air-storage period. These observations support the conclusions of earlier work [1] which indicates that, under certain incompletely understood conditions, sodium does penetrate stainless steel grain boundaries.

Phase IV

Definition of Phase IV

In Phase IV effective electrical resistivities of specimens placed in sodium 7 days at 1100°F and air-stored (normal and dry) for 120 days were measured. Another group of specimens, also sodium-treated and air-stored, were re-exposed to sodium a second time.

Discussion of Phase IV

In Phase IV, the effects of a long (120 days) air storage (normal and dry) were evaluated. The purpose of these tests was to determine if a long period of air storage would produce effects on the stainless steel which were measurably different from short-time air storage.

The data from Phase IV can be compared to the similar data (see Fig. 5) of Phase II. Figure 12 indicates the effective electrical-resistivity values for both normal and dry air-stored specimens after initial sodium exposure, 120-day air storage, and re-exposure to sodium.

Conclusions from Phase IV

One can compare the results of dry air-stored specimens of Phase IV (see Fig. 12) with dry air-stored specimens of Phase II (see Fig. 5). On comparison of 120-day air storage (normal or dry) to 10-day air storage (normal or dry), one notes that a single 120-day air storage produces a more rapid increase in the effective electrical resistivity. For example, an effective electrical resistivity for 10-day dry air storage of about 90 $\mu\Omega$-cm is achieved in 5 hr (see Fig. 5). In comparison, a comparable effective electrical resistivity is achieved in 2 hr for specimens stored 120 days in dry air.

The rate of attack for normal air-stored specimens for 10 days (see Fig. 5) and for 120 days (see Fig. 12) does not indicate a similar increase in rate of attack by Strauss reagent. The effect of 120-day normal air storage is to decrease the scatter or spread in measured resistivity values for any given time of exposure to Strauss reagent.

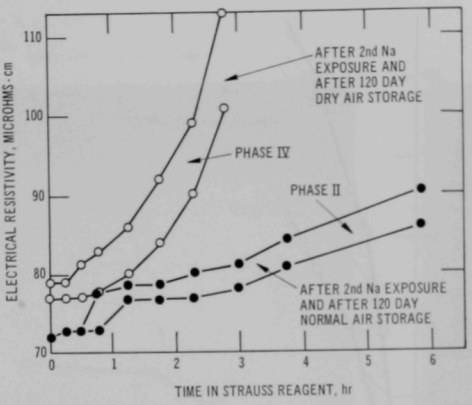

FIG. 12. Phase IV, Test B. Rates of Attack of Strauss Reagent for Type 304L Tubing.

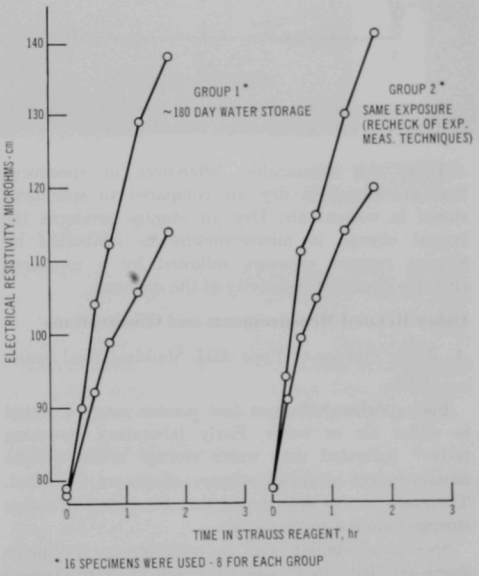

FIG. 13. Statistical Check of Type 304L Tubing after Single Sodium Exposure and Water Storage.

From the data of Phase IV, it is concluded that the variable of the length of time of air exposure, 10 days or 120 days, does not produce as large a change in resistivity or microstructure as does the variable of repeated cyclic exposures of the specimens to sodium and sodium cleaning after each sodium exposure.

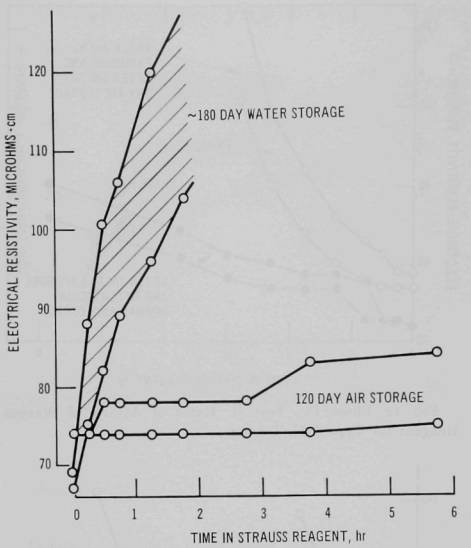

FIG. 14. Comparison of Dry Air Storage to Water Storage of Type 304L Tubing after Single Sodium Exposure.

There are measurable differences in specimens that are stored in dry air compared to specimens stored in normal air. Dry air storage produces the largest change in microstructure as evaluated by Strauss reagent exposure followed by a measured effective electrical resistivity of the specimen.

Other Related Measurements and Observations

A. Water Storage of Type 304L Stainless Steel Specimens

Fuel specimens from a fast reactor may be stored in either air or water. Early laboratory screening tests[4] indicated that water storage under specific circumstances produces adverse effects on fuel clad. Therefore, it was anticipated that the effects of water storage required further study.

Specimens similar and in addition to specimens discussed above in Phases I through IV were exposed to a sodium loop. Sodium treatment and removal of sodium from the surface were identical to techniques reported above. Two additional rinses of 1000 ml of distilled water were provided before the specimens were stored in 500 ml of distilled water. The second rinse indicated a pH reading of "neutral." These sodium-treated and -cleaned specimens were then stored in water for ~180 days at room temperature in a closed glass container.

After water storage was complete, the specimens were divided into two groups of 8 specimens each, selected at random. Rates of attack of Strauss reagent are compared in Fig. 13. Good agreement between the statistical results of both random groups can be noted.

Electrical-resistivity data for the comparison of water storage to dry air storage, from previous Phase-IV tests, are shown in Fig. 14. Comparisons of water storage to normal air storage from previous Phase-IV tests are shown in Fig. 15.

For the water-stored specimens a macro inspection of the OD surface showed visual evidence of pitting with a number of surface holes. Macro inspection of a pitted region indicated that pitting is about 0.005 in. deep. Etching of the specimen revealed that pitting was actually a loss of grains at the surface of the tube, as illustrated in Fig. 16. From these observations it is estimated that water penetration during water storage is up to 0.0005 in. There is evidence from photomicrographs that sodium treatment and water storage can produce grain boundary effects up to 0.001 in. deep.

B. Sodium and Loop Pipe Analysis

Because of concern for possible contamination of sodium by carbon from loop components, tests have

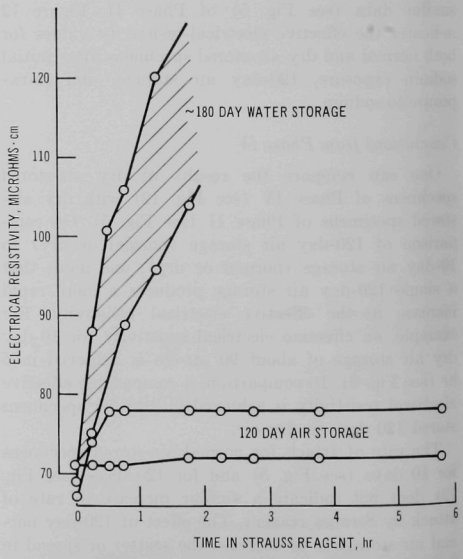

FIG. 15. Comparison of Normal Air Storage to Water Storage of Type 304L Tubing after Single Sodium Exposure.

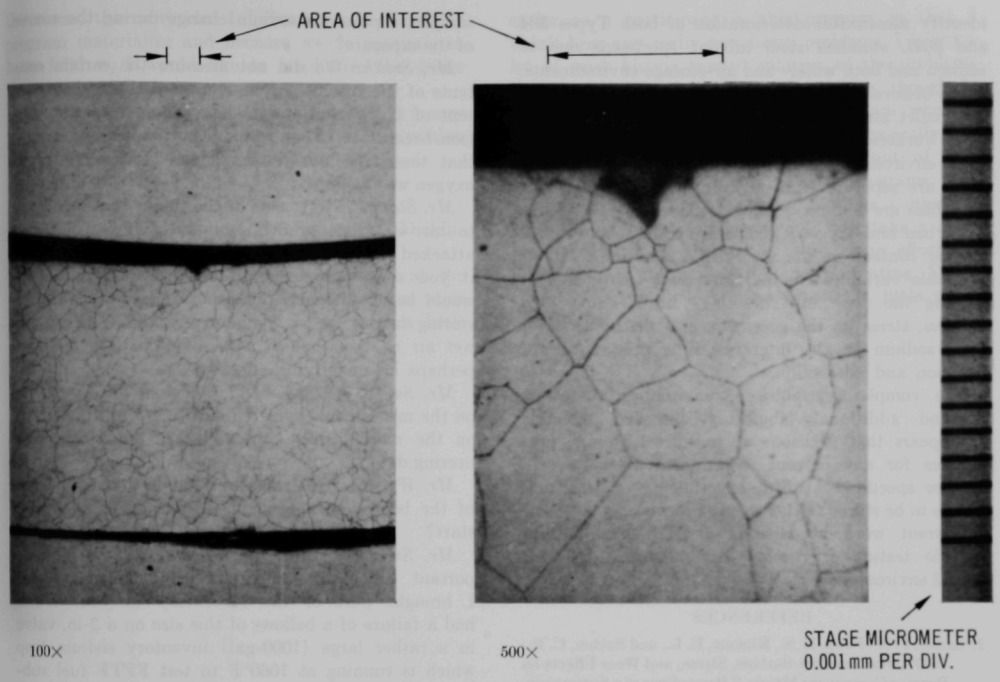

FIG. 16. Sodium-exposed Type 304L Tubing after 180-day Water Storage.

been conducted to measure loop sodium chemistry and to identify the composition of all loop components. The results of sodium analysis from specimens removed from the loop are shown in Table 4.

Sodium specimens were taken in a ½-in.-OD flow-through specimen tube at 1100°F. The oxygen value was obtained by determining the sodium content of the residue from a known amount of specimen. The sodium in the residue was assumed to exist as sodium oxide. The value reported in Table 4 was calculated on the basis that sodium oxide residue remains after sodium distillation.

An examination of each loop component has been made to determine if a length of pipe, fitting, or component could inadvertently contain high carbon steel. This analysis was conducted using an *in situ* nondestructive testing device called a "thermorator."[5] This instrument is sensitive to especially small changes in carbon content of steels. It has been determined that all loop components are Type 304 stainless steel.

TABLE 4. ANALYSIS OF LOOP SODIUM

Impurity	ppm
O	35
Ni	6.4
Cr	2.8
Cu	4.3
Fe	9.0
C	19.0

C. Generalized Conclusions

We have presented data related to the use of an engineering materials loop which is composed of Type 304 stainless steel and has logged over 21,000 hr of service in the range from 900 to 1550°F.

We wish to recommend the reader of this paper to an awareness of the current evolution of other data relating structural materials effects to sodium and other environments. Work in this current field is in progress and reported upon by General Electric Company, Mine Safety Appliance Company, Stanford Research, Atomics International, ORNL, and Argonne National Laboratory.

We have shown data from one specific engineering loop. For our conditions of sodium exposure we can

identify measurable deterioration of both Types 304 and 304L stainless steel tubular specimens due to sodium and both water- and air-storage environments.

We believe that these data, falling short of a model to predict structural-materials behavior, do serve to alert workers in the field to the possibility of structural environmental effects. These environmental effects are separate from neutronic effects. Important variables are sodium quality (especially with respect to carbon and oxygen), temperature, time, and initial carbon content of the steel being evaluated. Other probable variables can be prior heat treatment, including the tube mill drawing and cleaning procedures, stress on the specimen, and the influence of total sodium on the intercrystalline process of absorption and adsorption.

The complex variables of environmental testing demand additional laboratory-controlled research. It appears that decisions as to correct storage procedures for any current sodium-cooled reactor will require specific controlled experiments relating materials to be stored to their environments.

Current work at EBR-II[6] is directed toward specific testing of reactor clad materials in their actual environment.

REFERENCES

1. Smith, F. A., Sowa, E. S., Kimont, E. L., and Sutton, C. R., "650°C Sodium Free-Surface, Stress, and Wear Effects on Reactor Component Metals," *Proceedings of a Symposium, Alkali Metal Coolants*, IAEA Publication, Vienna (1967), Paper SM-85/22, pp. 231–245.
2. Rutherford, J. J. B., Aborn, R. H., and Kearny, N. J., "A Quantitative Method for the Estimation of Intercrystalline Corrosion in Austenitic Stainless Steels," American Institute of Mining and Metallurgical Engineers **100** (1932).
3. Bohne, L. H., Kimont, E. L., and Smith, F. A., "Electrical Resistivity Measurement Technique: A Tool for Sodium Exposed Materials Evaluation," Trans. ANS, **10**, 143 (June 11–15, 1967).
4. *Reactor Development Program Progress Report for February 1967*, ANL-7308, pp. 5–7.
5. D. E. Walker, Metallurgy Division, ANL, unpublished.
6. *Reactor Development Program Progress Report for August 1968*, ANL-7487, p. 56.

Discussion

Mr. Shannon (BNWL): I assume you've run some control specimens through comparable heat treatments, but not exposed to sodium. Do they behave the same or differently?

Mr. Smith: This information can be found in one of the references to our paper. Other work for other environments for these materials is contained in Reference 1.

Mr. Shannon: Did the carbon contents of the samples exposed to sodium change during the course of the exposure?

Mr. Smith: We did not measure the carbon contents of the specimens; we measured the carbon content of the loop. I should have given that information because it is important. The analysis of carbon that these specimens were exposed to is 19 ppm; oxygen was 35 ppm.

Mr. Stern (UNC): One of the things that stood out to me was that in Strauss reagent Type 304 was attacked more than Type 304L. I would expect that, if you store either one of them in wet air, they would be less attacked by Strauss reagent than after storing in dry air. I would expect that because the wet air is somewhat of a passivation agent. Is this perhaps an underlying effect?

Mr. Smith: It may be; I don't want to speculate on the mechanisms involved. There is work underway on the mechanisms. Our data are empirical engineering data.

Mr. Wensch (Chairman): What is the significance of the bellows you brought in as an exhibit at the start?

Mr. Smith: I think the bellows is extremely important. I couldn't invite you to our laboratory, so I brought part of the laboratory to you. We've had a failure of a bellows of this size on a 2-in. valve in a rather large (1000-gal) inventory sodium loop which is running at 1060°F to test FFTF fuel subassemblies. The loop was started 2 years before we did the work that I reported on today. When this loop was fabricated, there were 5 drain valves. Four drain valves were purchased new and one had previously been used in other experimental work at the Laboratory. Now comes my intelligence quiz. I'd like to ask you people which valve do you think broke? One of the new valves or the valve that had been exposed to sodium for a long period (sodium, air, and water)? The answer is obvious: the bellows that failed is exactly like this and it had been used in other experimental loops at the Laboratory. That dawned on me after I had written this paper. I wanted some way to get this information to you because I will admit that use of a Strauss solution is about as tricky, I think, as Kolodney's work, reported yesterday, in a mathematical sense. We have a practical experience where a previously used component has really failed. I think it's important to get a little bit serious, and I'd like to address a comment to Glen Wensch and Bob Dickinson. I heard about a year ago of efforts to establish a failure analysis program for failures that occur in the sodium programs as part of the LMEC work. These failures were to be documented and reported on—the nature,

the cause, the cure, etc. I haven't really seen this program materialize and because we do continue to have failures, I would like to emphasize the desire that this LMEC program be activated.

Mr. Wensch: If this effect is confirmed, if it is new in nature, I should like to suggest that consideration be given to calling it the "Smith Effect."

Mr. Wensch, Chairman: I have asked Bob Dickinson to summarize the session for us.

Mr. Dickinson (LMEC): I am impressed at the amount of data coming from the very excellent work by both the US and foreign groups. I feel a little easier as a participant in this program in that I didn't hear any really new nasty problems. I heard a lot of work hitting toward solution of the problems that we felt did exist. My last impression, though, is that we're really in a long-range program whether we like it or not. I think this is sort of generally acknowledged. There's a tremendous amount of empirical work going on in a number of programs, certainly not all of them. I wonder, more as a question than a summary, whether we could just take a deep breath once in a while and spend some effort on understanding the models that we're creating. Don't stop the experimenting, but try to do a little more understanding.

SESSIONS ON SODIUM TECHNOLOGY

SESSION ST-VA

Saturday Morning, November 9, 1968

Chairman: J. R. Humphreys, Jr.
Argonne National Laboratory

Secretary: F. A. Cafasso
Argonne National Laboratory

An Evaluation of Carbon Activity Sources in Sodium

JOHN M. MCKEE* AND WAYNE H. CAPLINGER

United Nuclear Corporation
Elmsford, New York

(PRESENTED BY J. M. MCKEE)

ABSTRACT

The carbon activity produced in sodium by various additives was explored in a series of 25 capsule tests at 1400°F. The carbon flux through the iron capsule wall into a stream of decarburizing gas was taken as a measure of the carbon activity. Very high carbon activity was produced in sodium by unstable carbides and by graphite plus large amounts of oxygen. Stable carbides, sodium cyanide, and graphite without oxygen produced low but significant activities.

Introduction

During the development of an on-line carbon meter for sodium systems,[1, 2] a modification of the carbon-meter concept was used to compare the carburizing potentials produced in sodium by various carbon-bearing additives. The immediate objective was to develop ways of holding the carbon activity of sodium in Type 316 stainless steel (SS) loops at controlled levels well above the normal value. It was also hoped that the results might yield some insight on the carbon-transfer mechanisms operating at normal activity levels.

In the carbon-meter sensor, carbon diffuses through a thin iron tube-wall from sodium on the outside to decarburizing gas on the inside. Conditions are arranged so that the carbon content thus produced in the gas stream is a useful measure of the carbon activity in the sodium.

For the tests reported here, it was convenient to place the sodium inside the tube and the gas stream outside, reversing the direction of carbon flow. The sodium "system" thus became a small static capsule. This geometry afforded some significant advantages over sodium loops or pots in testing additives. Damage to the sodium containment by the additive was not an operating problem, and cleanup of previous additives was not required, since a new capsule was used for each test. Providing an excess of additive in the sodium was mechanically simple. Integration with time of the carbon flux leaving the capsule permitted a mass balance for carbon in the sodium. The capsule-test concept was well adapted to the program objective of exploring numerous additives with a modest effort.

* Now at Argonne National Laboratory, Argonne, Illinois.

Test Procedure

A typical capsule cross section is shown in Fig. 1. The ½-in.-OD Armco iron tube was honed to 0.460-in. ID and then turned on a mandrel down to a 10-mil wall thickness over the 1-in. active length, taking care to avoid machining grooves on either surface. Type 316 SS was used for the ¼-in.-thick end plugs except where noted, because it was easy to weld and eliminated carbon flux out of the capsule ends.

Before assembly the capsule parts were thoroughly cleaned, finishing with ultrasonic agitation in an acetone-alcohol bath. Assembly was performed in a glovebox filled with high-purity argon. The bottom end plug was TIG welded to the capsule tube. A weighed amount of the carbon-bearing additive and an Armco iron control tab were placed in the capsule. Aged and filtered sodium, previously cast into an extrusion cylinder, was extruded at room temperature, trimmed to the desired weight, and inserted in the capsule. The sodium weight was calculated to bring the sodium level at 1400°F to ⅛ in. below the top end plug. The carbon in the additive generally amounted to 5 to 10% of the sodium weight, so that the sodium would remain saturated amply long even with a high carbon flux out of the capsule.

A top end plug containing a ⅛-in.OD SS evacuation tube was TIG welded into the top end of the capsule. A valve was coupled to the evacuation tube and closed for removal from the glovebox. The valve was then coupled to a vacuum system, and the argon was evacuated from the capsule. When outgassing was complete with the capsule warm, the evacuation tube was clamped shut, cut, and welded before releasing the clamp. Sealing under vacuum was necessary because any buildup of internal pressure on heating would bulge the thin iron wall at the test temperature.

For the test, the capsule was positioned vertically in a SS furnace tube as shown in Fig. 1. The furnace tube ID was machined to provide[1] a narrow annulus for gas flow past the capsule to minimize the gas transit time, and[2] a thick tube wall to minimize hydrogen loss and axial temperature variations. The test temperature and the gas composition, flow rate, and analysis train were the same as for carbon-meter sensors. The capsule was held at 1400°F (760°C) by

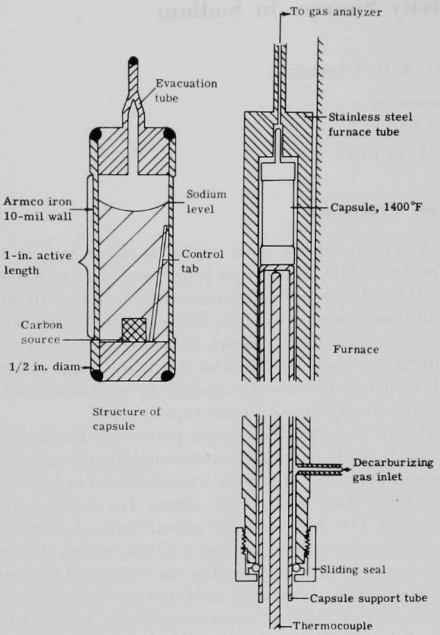

FIG. 1. Capsule Test Apparatus.

a 12-in.-long, Nichrome-wound, tube furnace. The decarburizing gas was argon + ½% water vapor + 5% hydrogen, flowing at 12½ cm³/min and essentially atmospheric pressure. Carbon diffusing to the outer surface of the capsule wall reacted with the moisture to form carbon monoxide, which was then converted to methane in a low-temperature catalytic converter and continuously measured in a flame ionization detector (FID). The calibration of the FID was checked periodically with analyzed gas mixtures and found to be quite stable. The accuracy of the carbon-flux measurements was limited to ±5% by the gas flowmeter rather than the FID.

The 5% hydrogen in the gas protected the iron capsule wall from oxidation by the water but did not protect the SS furnace tube. The steady-state carbon content of the gas with an empty control capsule in place was equivalent to 0.004 μg/cm²-min, mainly from carbon released by slow oxidation of the furnace tube. All of the additives tested produced carbon fluxes substantially higher than this background level. Calibration gases containing methane and carbon monoxide did not change their carbon content during passage through the empty furnace tube at 1400°F.

Results

The test conditions and results for 24 capsules are listed in Table 1. Figure 2 shows the patterns of carbon flux vs. time observed for some typical additives. The normal carbon content of the iron (0.015%) produced an initially high flux which dropped rapidly and ideally should approach a constant value. This was reasonably true for capsules in the shaded band of Fig. 2, which produced carbon fluxes of 0.3 μg/cm²-min or less. High fluxes were produced by some additives, and these tended to vary appreciably with time, probably owing to slow physical processes proceeding inside the capsule. The steep drop in flux from these capsules after two or three days was due to complete consumption of the carbon source.

The two capsules, plotted in Fig. 2, which contained sodium carbonate both developed leaks, apparently due to strongly corrosive decomposition products. Although concentrated at the bath line, the corrosion was in the form of uniform surface removal rather than intergranular attack.

The carbon fluxes produced by the various additives are visually displayed in Fig. 3. The range of flux values measured after the capsule reached a reasonably steady state and before depletion of the source took effect is shown in this figure as a flux band for each capsule.

The first tests were made with a small right cylinder of spectrographic-grade graphite, approximately of ¼-in. diameter, added to the sodium. Such a cylinder produced a much lower carbon flux than had been expected from previous tests[1] of carbon-meter probes in static sodium pots containing excess graphite. Since the sodium in the static pots had picked up considerable oxygen compared to that in the capsules, oxygen was added in various concentrations and forms to the sodium in seven capsules each containing a cylinder of graphite. An addition of 500 ppm (0.05%) oxygen produced no significant effect on the carbon flux, but 10% oxygen produced a very high carbon flux, averaging 4.9 μg/cm²-min. Intermediate oxygen concentrations produced intermediate fluxes more or less in proportion to the oxygen added. Oxygen appeared to be equally effective in the form of sodium peroxide, sodium hydroxide, and iron oxide, but less so in the form of sodium carbonate.

Sodium carbonate was shown to be capable of producing a high carburizing potential in the absence of graphite or other carbon surces in capsules 3 and 19, by resorting to very large concentrations. This is not surprising, since substantial decomposition into sodium oxide and some carbon-rich material would be expected above 850°F (450°C).

Iron oxide and sodium oxide were added to capsule

TABLE 1. CAPSULE-TEST CONDITIONS AND RESULTS

Capsule No.	Carbon Source		Oxygen Source		Sodium Weight, g	Carbon Flux, g/cm²-min
	Material	Weight, g	Material	Weight, g		
1	None	—	None	—	1.8	Low; run to test the vacuum sealing procedure.
2	Graphite	0.113	None	—	1.825	Dropped rapidly to 0.11.
3	Na_2CO_3	0.430	None	—	1.825	Rose to 1.75 at 20 hr, then dropped below 0.13. Wall penetrated by sodium at gas interface.
4	NaCN	0.500	None	—	1.818	Rose to 0.33 at 19 hr, then dropped below 0.16.
5	Graphite	0.280	None	—	1.832	Dropped rapidly to 0.35.
6	Graphite	0.310	None	—	1.830	Weld failure leaked sodium (Armco iron end plugs).
7	CaC_2	0.115	None	—	1.830	Dropped rapidly below 0.05.
8	Mo_2C	0.623	None	—	1.854	Dropped rapidly below 0.05.
9	SiC	0.300	None	—	1.847	Dropped from 0.7 to 0.3 in 7 hr, thence rapidly to 0.007. Leak in weld after 10 hr.
10	Graphite	0.193	Na_2O_2	0.002	1.809	Dropped rapidly below 0.04.
11	Graphite	0.167	Na_2O_2	0.019	1.807	Maximum of 3.3 at 4 hr, dropped slowly to 2.5 at 62 hr, then dropped below 0.27.
12	Quik-Lite[a]	2.45	Carbonates	—	None	Ruptured by gas pressure on heating.
13	Graphite	0.130	Na_2CO_3	0.090	1.810	Rose to 3.6 at 32 hr, held there until 72 hr. Wall penetrated by sodium corrosion at gas interface.
14	Graphite	0.125	Fe_2O_3	0.060	1.812	Produced 3.5 for about 60 hr, dropped rapidly thereafter due to source depletion. Wall penetrated by sodium at gas interface.
15	Graphite	0.167	NaOH	0.090	1.815	Produced 4.5 for about 60 hr, dropped rapidly thereafter due to source depletion.
16	Na_2C_2	0.430	None	—	1.520	4.0 down to 3.0 in 4 hr, quenched from 2.85 at 26 hr.
17	Fe_3C	2.530	None	—	1.715	5.1 ± 0.5 for 5 hr, quenched from 3.1 at 13 hr.
18	Graphite	0.137	NaOH	0.020	1.700	1.5 ± 0.2, quenched from 1.5 at 13 hr.
19	Na_2CO_3	1.370	None	—	1.530	3.8 ± 0.8, quenched from 3.8 at 12 hr.
20	NaCN	0.694	Na_2O_2	0.017	1.675	4.5, dropping rapidly to 0.7 at 13 hr.
21	Mo_2C	2.62	Na_2O_2	0.016	1.611	Dropped to 0.82 in 7 hr, stable at 0.26 after 30 hr.
22	Graphite	0.160	Na_2O and Fe_2O_3	0.352 / 0.308	1.605	4.9 ± 0.2 for 30 hr. Dropped to 0.007 when catalytic converter was by-passed.
23	Graphite sleeve	2.23	None	—	0.968	$1.9^{+1.3}_{-0.3}$ for 15 hr.
34	CO	1 atm	None	—	0	0.7 for 16 hr, dropping to near zero by 24 hr.

Note: All capsules are Armco iron, 0.460-in. ID × 10-mil wall × 1-in. active length, with SS end plugs, tested at 1400°F in probe gas containing 0.5% H_2O, 5% H_2, balance argon flowing at 12.5 cc/minute, unless otherwise noted.

[a] Commercial pack carburizing compound.

22 in amounts calculated to form the ferrate compound postulated by Horsley.[3] The high carbon flux observed gave no evidence that the oxygen availability had been reduced by formation of any stable compound.

Two graphite cylinders added to capsule 5 produced a significantly higher flux than a single cylinder, indicating that carbon diffusion through the iron wall was not completely rate-limiting in the overall carbon-transfer chain from the graphite to the gas. When the entire inner surface of capsule 23 was lined with a close-fitting graphite sleeve, a fairly high carbon flux was produced, as shown in Fig. 3A and Table 1, even though no oxygen was added to the sodium and the graphite had been thoroughly outgassed at 1600°F before insertion.

The highest carbon flux measured was produced by

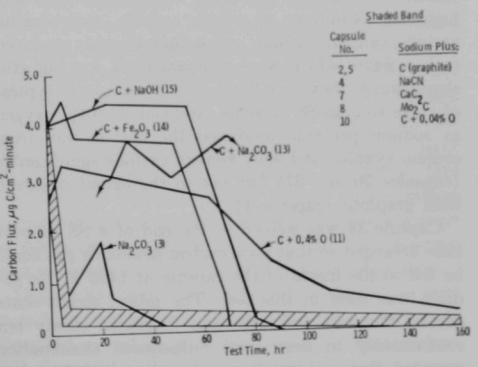

FIG. 2. Carbon Flux from Capsules *vs* Time.

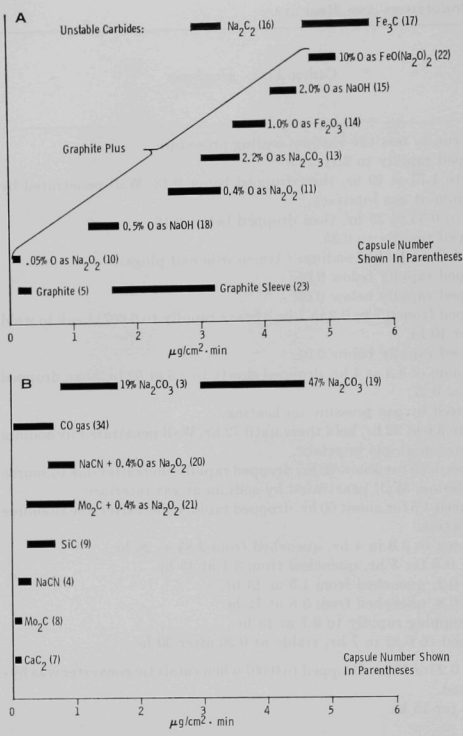

FIG. 3. Typical Carbon-flux Ranges Produced by Various Additives.

addition of iron carbide, which is quite unstable at the test temperature. Addition of sodium carbide, the stability of which is uncertain, also produced a fairly high flux. Additions of silicon carbide, molybdenum carbide, calcium carbide, and sodium cyanide produced carbon fluxes which were comparatively low but still significantly above the 0.007-$\mu g/cm^2$-min level typical of clean sodium-SS systems. Addition of 0.4% oxygen as sodium peroxide increased the carbon flux from sodium cyanide and molybdenum carbide significantly (capsules 20 and 21) but not to the extent observed with graphite (capsule 11).

Capsule 34 was welded to the end of a SS support tube arranged so that pure carbon monoxide gas could be fed to the inside of the capsule at 1400°F. No sodium was used in this test. The initial steady-state carbon flux was not large and decreased slowly but continuously to near zero. Subsequent examination revealed that a dense layer of carbon had deposited uniformly over the inner surface of the capsule wall.

A solid graphite rod, tested in place of a capsule at 1400°F, produced no detectable carbon content in the decarburizing gas stream. Although the gas reacts rapidly with carbon dissolved in iron, it is apparently inert to massive graphite.

Most of the capsule wall and control tabs were sectioned and examined metallographically. Capsules in which tests were terminated at a low carbon-flux level showed the normal ferrite structure at the top of Fig. 4. Capsules which were quenched from 1400°F at a high carbon flux showed a pearlite layer at the sodium side, as seen at the bottom of Fig. 4. The 8-mil-thick iron control table from capsule 17 was completely transformed to gamma iron after 13 hr at 1400°F in sodium with a high carbon activity, but only over the bottom ¼ in. of its length. The transition zone from gamma to alpha iron farther up the tab is seen in the top half of Fig. 5. The 20-mil-thick control tab from capsule 15 exhibited a strikingly flat grain boundary (see Fig. 5, bottom), located near its midplane and parallel with the faces. Presumably it was formed by the meeting of gamma-iron fronts advancing from both faces during the 60 hr of high carbon activity in the sodium. When the activity dropped owing to exhaustion of the carbon source, the tab decarburized and transformed back to alpha iron.

Significance of Results

The capsule test technique did reveal substantial differences in the carburizing potential produced in sodium by the various additives tested. Addition of iron carbide to capsule 17 produced readings of carbon flux up to 5.5 $\mu g/cm^2$-in. The maximum carbon flux theoretically attainable through a 10-mil iron wall at 1400°F is 5.9 $\mu g/cm^2$-min, based on 161 ppm as the solubility and 1.98×10^{-6} cm^2/sec as the diffusivity of carbon in alpha iron at the temperature. Transformation to gamma iron increases the carbon solubility to 8600 ppm but decreases the diffusivity to 8×10^{-9} cm^2/sec at 1400°F, resulting in a net decrease in theoretical carbon flux to 1.2 $\mu g/cm^2$-min through a 10-mil wall. Published data indicate that at 1400°F this transformation occurs at a carbon activity of about 0.67, referred to graphite. Substantially higher carbon activities must have been present in the sodium in the high-flux capsules to maintain the layer of gamma iron observed at the inner surface. Iron carbide is known to have a carbon activity higher than that of graphite at 1400°F and apparently can maintain a similarly high carbon activity in sodium in the face of a significant rate of drain. Sodium carbide produced the same effect, lending substance to the possibility that it is the principal form of carbon produced in sodium by iron carbide.

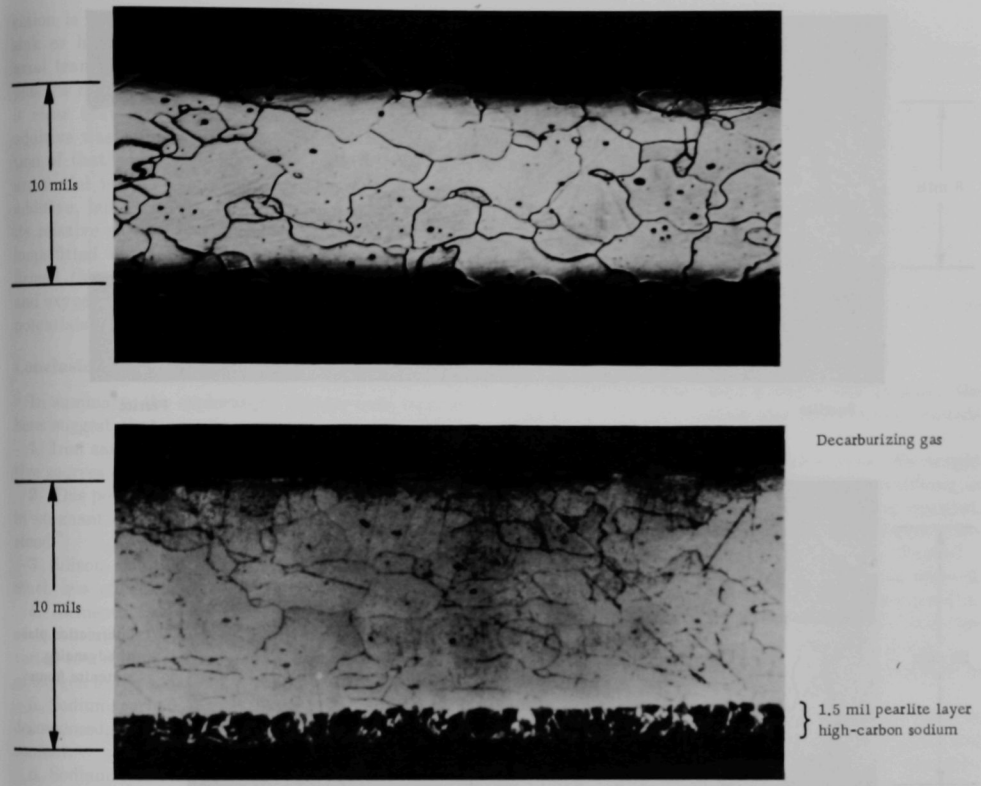

FIG. 4. Microstructure of Armco Iron Capsule Walls. Top: Low carbon flux, normal ferrite structure. Bottom: High carbon flux (5 μg/cm^2-min), pearlite layer on the sodium side (Capsule 17).

The ability of oxygen to enhance the carburizing effectiveness of elemental carbon in sodium cannot be called surprising, although the mechanisms involved are uncertain. Oxygen in some form has long been recognized as essential for efficient carburizing of steel parts. Russian workers[4] noted the important effect of oxygen in studies of carbon transfer by sodium reported in 1962. In the capsule tests reported here, the enhancement effect of oxygen on carburizing potential generally increased with the amount of oxygen added, up to 10 w/o, which was about the same atom fraction as the carbon present. Luner[5] has shown that elemental carbon is extremely insoluble in pure sodium. Perhaps oxygen exerts its effect by reacting with the carbon in sodium to form compounds that can then enter readily into carburizing reactions. Although the oxygen concentrations used in these capsule tests were much higher than will exist in reactor coolant systems, the carburizing potentials produced were also much higher than could be tolerated. There is no reason as yet to expect that oxygen-carbon interactions are likely to produce damaging carburization at concentration levels more typical of practical sodium systems. The capsule tests serve only to show qualitatively that such interactions can occur. One would expect that injection of oxygen into a sodium system containing excess carbon would produce a surge of carburizing potential, and this has been observed with a carbon meter probe in a stainless steel loop.

Carbon has been found by other workers[6] to exist in sodium in at least five forms, which may be loosely identified as carbide, cyanide, carbonate, hydrocarbon, and elemental carbon. Considerable practical interest attaches to the question of which, if any, of these forms

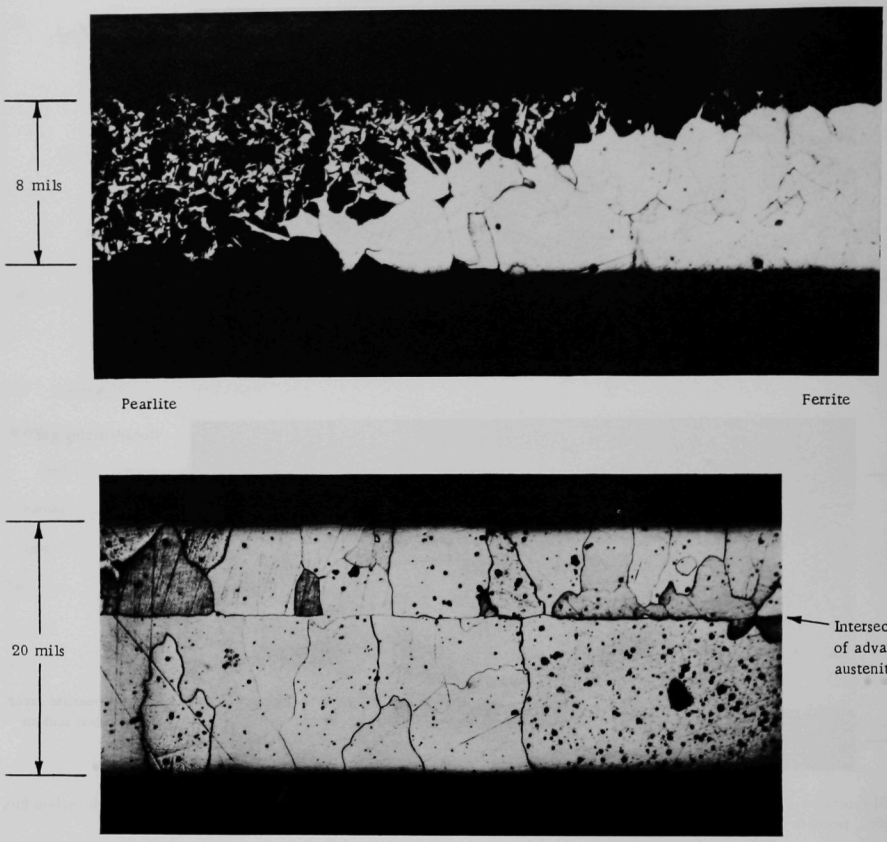

FIG. 5. Microstructure of Armco Iron Control Tabs. Top: Transition between high and low zones of carbon activity (Capsule 17). Bottom: After carburization to austenite and decarburization back to ferrite (Capsule 15).

accounts for the carbon transfer observed in sodium coolant systems at LMFBR temperatures. The capsule tests described here cannot answer the question directly but do permit a few speculations. Acetylide-bonded (carbide) carbon in sodium could be a highly effective transfer agent. Cyanide carbon, although probably less effective than carbide, could still be a significant source over long periods of time. Carbonate carbon is probably an effective source when it decomposes but not until then. Hydrocarbons were not tested as additives but are expected to have formed within the capsules and built up to a low pressure in equilibrium with excess carbon and the 0.74-psia hydrogen pressure from the decarburizing gas, thus nullifying the depression of carbon activity in sodium which hydrogen was shown to exert in earlier pot tests.[1] Elemental carbon is probably less effective as a direct source than when converted into other forms by interaction with oxygen or other impurities.

Several indications were observed, both in the capsule tests and in related pot tests, that the carburizing potential decreased rapidly with distance from the source in stagnant sodium. Since all of these indications were associated with a continuous carbon flux from the source, a final test was run duplicating capsule 17 (iron carbide addition) but substituting pure argon for the decarburizing gas. Metallographic examination after 8 hr at 1400°F showed that only the bottom ½ in. of the control tab had been converted to gamma iron, essentially the same as in capsule 17. The impli-

cation is that some mechanism other than a carbon sink or hydrogen interaction was operating to limit axial transfer of carbon in the capsule. This finding, plus the results obtained from capsules 5 and 23, make it clear that the carbon flux measured for a given additive was a function of the physical size and location of that additive in the capsule. Thus, the results are useful not as an absolute measurement for each additive, but rather as an approximate indication of its relative carburizing effectiveness. Additions to SS loops fitted with carbon meters have subsequently confirmed the ability of carburized iron and of carbon and oxygen in combination to produce high carburizing potentials in circulating sodium.

Conclusions

In summary, the exploratory capsule tests reported here suggest that:

1. Iron carbide and sodium carbide are highly effective sources of carburizing potential in sodium.
2. This potential is exerted over a rather short range in stagnant sodium, for reasons that are not understood.
3. Silicon, molybdenum, and calcium carbide are much less effective sources.
4. Elemental carbon is a comparatively poor source of carburizing potential in pure sodium, but is converted to a strong source by addition of large amounts of oxygen to the sodium in any of several forms.
5. Sodium carbonate can be a strong source when decomposed, as would be expected from its oxygen content.
6. Sodium cyanide is a comparatively weak source, but could be significant over long periods of time.
7. These results should be regarded as exploratory and qualitative.

Acknowledgments

This work was performed as part of a carbon-meter development program sponsored at the United Nuclear Corporation by the USAEC under contract AT(30-1)-3665. The authors were assisted by M. Kolodney and G. Stern in theoretical discussions, and by S. Lukasik and S. Skeckowski in carrying on the experimental work in the laboratory.

REFERENCES

1. J. M. McKee, W. H. Caplinger, and M. Kolodney, *Continuous Carbon Meter for Sodium Systems*, Nucl. Applications, **5**(4), 236–246 (1968).
2. W. Caplinger and G. Stern, *Engineering Development and Performance of the UNC Carbon Meter*, THIS CONFERENCE.
3. G. W. Horsley, *Corrosion of Iron by Oxygen Contaminated Sodium*, J. Iron Steel Institute (London), **182**, 43–48 (Jan 1956).
4. V. S. Lyashenko and B. A. Nevsorov, "The Mechanism of Carbon Transfer in Liquid Sodium," *Corrosion in Reactor Materials*, **2**, IAEA Conference, Vienna (1962).
5. C. Luner *et al.*, "Solubility of Carbon in Sodium," p. 171, *Alkali Metal Coolants*, IAEA, Vienna, 1967.
6. D. Dutina *et al.*, *Carbon Impurities in Sodium System Cold Traps*, THIS CONFERENCE.

Discussion

Mr. Yannopoulos (W): I would like to know the purity of the iron carbide and molybdenum carbide that you used.

Mr. McKee: In a word, we don't know. We bought the iron carbide from a supply house specializing in this compound. It was a crystalline-looking material. I don't believe we ever analyzed it. Is Wayne Caplinger here? Can you answer the question, Wayne?

Mr. Caplinger (UNC): It was claimed to be 99.9+% pure by the manufacturer, but we never analyzed it.

Mr. Yannopoulos: I would like also to know the source of the iron carbide. Where did you get it?

Mr. McKee: I think the name of the company is Research Inorganic Chemical Company.*

Mr. Yannopoulos: The reason I'm asking is that we requested some carbide from the same company, and X-ray examination showed that the bulk of the material was just iron and carbon despite the claim of the catalog that it was pure iron carbide.

Mr. McKee: I regard it as entirely possible that it was not all Fe_3C; that's hard to make. Nevertheless, I think there was enough there to demonstrate that iron carbide produces a very strong carburizing potential in sodium. The sodium carbide, incidently, was even harder to get than Fe_3C. It was part of a few grams produced for the AEC by Atomics International, and we knew equally little about its purity. I think that it sufficed for our purposes, which were exploratory.

* Sun Valley, California

Carbon Impurities in Sodium System Cold Traps*

D. Dutina, J. L. Simpson,

General Electric Company
Pleasanton, California

AND

R. S. Young

General Electric Company
Sunnyvale, California

(PRESENTED BY D. DUTINA)

1. Introduction

It is well recognized that in a bimetallic system bridged by sodium or potassium, carbon is transferred from low alloy ferritic steels at low temperature to high alloy austenitic steels at high temperature. Recent observations also show that carbon moves from the hot to the cold leg of systems made of all stainless steel.[1, 2]

Despite much interest, concern, and investigation, an understanding of the mechanisms of carbon transfer, and consequently of methods of control, is yet to be attained. The current approach to the problem is to seek carbon species in the sodium in hopes of deducing from their nature the mechanism of carbon movement, that is, the existence of carbon species in deposits in regions of sodium systems which differ in temperature can reflect the interaction of various solutes in sodium and thus provide clues to the process of carbon transfer.

Over the past half-dozen years, a considerable body of information has been accumulated about carbon species in sodium. Lyashenko and Nevzorov[3] deduced from electrolytic experiments that carbon and oxygen linkages exist in sodium containing these elements. Sabol *et al.*[4] concluded, from the chromatographic analyses of gases released during the aqueous dissolution of sodium and treatment of this solution with dilute acid, that at least three forms of carbon were present: those producing hydrocarbon gases; carbonates; and those which were refractory to these reagents, probably elemental carbon or heavy metal carbides. In 1965 Hobart and Bjork[5] demonstrated that cyanide was stable in sodium, and could be formed in this medium from carbon and nitrogen in any of a variety of forms. Cafasso[6] has recently reported solubility data for cyanide in sodium. Sinclair and coworkers[7] obtained preliminary data which indicated that carbonate, carbide, graphite, and carbonyl may exist in sodium. Luner *et al.*[8] have reported the solubility of carbon to be less than 0.005 ppm at 450°C, much lower than the value obtained in an earlier study. They also found that reactor-grade sodium contains a large fraction of its carbon in what is presumably the elemental form and that carbonate is present in appreciable quantities. In addition, a trace of carbon as CH_4, $NaCH_3$, or metal carbide was also seen. Grundy and Hamer[9] reported that the hydrolysis and acidification of deposits remaining after sodium removal by amalgamation evolved hydrocarbons and CO_2. From this they inferred the presence of sodium alkyls, sodium carbide, and sodium carbonate.

In 1967 the present authors[10] found at least 5 forms of carbon in a cold trap which had seen long service in a high-temperature sodium system fabricated of ferritic steel. Both the cyanide and carbonate anions were observed, and it was also inferred that carbides, elemental carbon, and a methane-yielding species were present. In the same period, Wildeman *et al.*[11] showed that acetylene, carbon dioxide, and hydrogen cyanide were released from the dissolution and acidification of cold-trap residues, and postulated that the precursors of these gases were Na_2C_2, Na_2CO_3, and NaCN.

In a continuation of our study, a second trap, this time from an austenitic steel loop, has been examined. A description of this experimental work and the results which pertain to the deposition of carbon and its compounds is the subject of this report. A comparison of the data obtained for the two systems provides some insight into the questions of carbon activity and transport.

2. Description of the Sodium Systems

The cold traps had been used to maintain sodium purity in two systems (loops) through which high-temperature sodium was pumped. The loops were operated by General Electric for the USAEC as part of a program† to study mass transfer. The systems, experimental programs, and some of the results obtained

* Work performed for the U. S. Atomic Energy Commission under Contract AT(04-3)-189, Project Agreement No. 15.

† Contract AT(04-3)-189, Project Agreement No. 15.

have been described in the project literature.[12] For convenience, a few pertinent details will be repeated.

The ferritic loop studied, Project Loop 5, was made of 2¼ Cr-1 Mo alloy steel; the austenitic loop, Project Loop 1, was fabricated of AISI Type 316 stainless steel. During the test runs maximum temperatures were generally 1200°F; the Type 316 loop was also run at 1300°F. The maximum temperature differential, from the hottest to the coldest sodium, in the loop was 500°F. Soduim velocity ranged up to 25 ft/sec. Sodium purity was maintained at plugging temperatures of either 450°F (believed to correspond to 50 ppm oxygen) or 300°F (believed to correspond to 10 ppm oxygen). Each loop operated for a total of about 20,000 hr.

3. Description of the Trap and Dismantling Procedure

The cold traps are stainless steel cylinders, 4½ in. in diameter and 15 in. long. The central four-fifths of the volume is packed with Type 316 stainless steel mesh. The sodium content of the trap is about 3 liters. Sodium temperature at the inlet of the trap varied between 600 and 900°F, and the coldest temperature corresponded to the plugging values listed above.

After removal from the system, the traps had been stored with all openings welded shut. The first steps in the examination were to clean the surface of the trap and saw off the ends, which were then discarded. The body of the trap was next transferred to an inert-atmosphere box (helium containing <1 ppm by volume each of H_2O and O_2) to complete the dismantling process. The exposed surfaces (ends) were scraped free of the oxide that had formed when the ends had been removed. The newly exposed surfaces had the typical metallic luster and the softness of sodium. This was surprising in that a fairly large buildup of oxide of considerable hardness had been anticipated and was most fortunate in that the remainder of the sampling procedure was simplified. Subsequent analyses confirmed that only minor amounts of sodium oxide, no more than 3%, were present in the regions of greatest deposition.

The contents of the trap were removed in one piece by heating the cylinder sufficiently to just melt the sodium at the walls while pushing on one end. The cylinder of sodium so obtained was cut transversely to provide five sub-samples (see Fig. 1). These sections, except for periods of subsampling, were kept in sealed containers and stored in the glovebox.

Sub-samples for the various analyses were obtained by cutting and gouging with spatulas. Although gross amounts of mesh were removed before these analyses, it was not possible to free the sample completely of this material.

4. Analytical Techniques and Results

It was found at the outset that the impurities were concentrated in a fairly narrow zone, about 4 in. above the inlet of the trap. In consequence, the work was focused on this area, and the results presented are in terms of concentration based on the weight of sample removed from this section.

Although the precision of the individual analytical methods to be discussed is considered to be better than ±10% (relative standard deviation), the analyses reported below are less precise by a factor of two due to inhomogeneity of the deposited material.

4.1. Determination of Total Carbon

A wet combustion procedure was used to measure total carbon.[4] The method also enables distinguishing between those carbon species which are converted to gases by the addition of water and dilute acid (e.g., carbonate, cyanide, methanides, and acetylides) from those which require oxidation to effect the transformation to a gas (e.g., elemental carbon and refractory carbides). The results appear in Table 1.

The following techniques were used to further characterize the carbon impurities.

4.2. Separation and Nondestructive Examination

The impurities were concentrated by removing sodium by means of vacuum distillation, amalgamation, or liquid ammonia.[13] The residues so obtained were analyzed by X-ray diffraction and by infrared spectroscopy. Care was taken to avoid atmospheric contamination. Evidence of carbonate, cyanide, and acetylide linkages were noted, but the high concentrations of sodium oxide, hydride, and hydroxide comprising the bulk of the sample prevented definitive identification of specific compounds.

4.3. Analysis of Decomposition Gases

Next, it was attempted to deduce the composition of impurities separated from sodium by amalgamation, distillation, and the action of liquid ammonia from the identity of the volatile species evolved during the hydrolysis and acidification of these residues. The gases evolved were identified and the amounts estimated by gas chromatography. Water addition yielded traces of ethane, methane, and appreciable quantities of acetylene in the case of the ferritic loop deposits. The results expressed in terms of carbon concentration are designated as "carbide" carbon in Table 2. Within the limits of detection, these gases were not found when the austenitic loop residues were treated similarly.

FIG. 1. Sectioned Contents of the Loop 1 Cold Trap.

TABLE 1. CONCENTRATION OF CARBON (ppm) IN COLD-TRAP SODIUM

	Austenitic Loop	Ferritic Loop
Volatilized by water and acid	90	640
Volatilized by oxidation	220	280
Total	310	920

Acidification of both solutions yielded carbon dioxide. The presence of carbonate was confirmed by means of a titrimetric method. The data obtained are shown in Table 2.

4.4. Determination of Cyanide

A re-examination by X-ray diffraction of the material remaining after the hydrolysis and acidification steps clearly showed the presence of complex metal cyanides. It was presumed that they resulted from the reaction in solution of sodium cyanide and the metallic elements present. Consequently, separate samples of sodium were analyzed for the cyanide anion. The procedure involved dissolution, distillation of HCN from the acidified solution, followed by spectrophotometric determination of cyanide in the distillate using p-phenylene diamine for color production.[14] Again, the data are presented in Table 2.

TABLE 2. FORMS OF CARBON IN COLD-TRAP DEPOSITS

Form of Carbon	Austenitic System (Carbon, ppm)	Ferritic System (Carbon, ppm)
"Carbide" (acetylene production)	Not detected (<1)	25
Evolved upon heating (largely CH_4)	10	25
Carbonate	50	350
Cyanide	45	280
"Elemental" [a]	220	280

[a] Repeated from Table 1.

4.5. Measurement of Gases Evolved upon Heating

During amalgamation separations, it was noted that methane was evolved along with hydrogen during the

initial, heat-producing reaction between mercury and the sample. To verify this observation, a separate sample from the cold trap was heated just above the melting point in a vacuum system. Analyses of the off-gases confirmed the presence of methane. Trace amounts of other hydrocarbons were also noted. These results, too, are shown in Table 2.

5. Discussion of Results

5.1. Sources of Carbon Species

There are, evidently, at least five separate forms of carbon deposits present in the trap. It seems valuable to discuss their probable sources and to provide information wherever it is available that supports or discounts the possible existence of the observed compounds in the hot sodium.

5.1.1. Carbonate

Carbonate has been detected regularly in samples from these loops, and thus identification of this anion in the cold trap is not surprising. The most likely source is the reaction of sodium with atmospheric carbon dioxide that enters the system while it is open for sample removal. A less probable source is the oxidation of carbides by Na_2O. It is expected that carbonate would be reduced in the system according to the reaction

$$Na_2CO_3 + 4Na = 3Na_2O + C.$$

Its persistence in the hot sodium is thus surprising. This may be due to slow kinetics for the decomposition or may represent a balance between rates of introduction by the means just suggested and its removal by decomposition and precipitation.

It should be noted that there was no evidence for carbonyl species.

5.1.2. Cyanide

Based on the work of Hobart[5] it is clear that cyanide can be formed in the hot leg of the mass-transfer loops—nitrogen is available in the cover gas or by permeation through the walls; carbon is ubiquitous. The solubility of cyanide should be of the order of several hundred ppm in the hot leg and virtually zero at the cold-trap temperature; thus deposition in the trap is not at all surprising. It should be noted that the analysis of a sodium sample taken at 750°F from a loop presently in operation contained 1.0 ± 0.2 ppm. This is also in reasonable agreement with the recently published solubility data and supports the hypothesis that cyanide is probably deposited to an appreciable extent in piping preceding the cold trap.

5.1.3. Carbides

The release of acetylene and other hydrocarbons upon hydrolysis of the separated impurities from the ferritic loop samples indicates the presence of carbides. Acetylene is known to be evolved when water is added to a metal or alkaline earth carbides (acetylides); a mixture of hydrocarbons is obtained when the carbides of the transition metals (Fe, Cr, Mn) are attacked by water and dilute acids.

Since acetylene is the predominant gas identified, the acetylides are the most likely precursors. It should be noted that calcium at concentrations of several hundred ppm was found in deposits from both loops. Wildeman[11] appears to favor the acetylides, specifically sodium carbide, as the source of acetylene he observed in cold-trap examination. Based on thermodynamic stabilities, calcium carbide is an even more likely source.

It should be emphasized, however, that no direct evidence for either calcium or sodium carbide has been obtained. Complex metal carbides of the $M_{23}C_6$ type have been observed on corrosion specimens[15] exposed to 1000°F sodium. Small amounts of these complex, heavier metal carbides thus may also be present in the trap and be the source of the traces of hydrocarbon gas detected.

5.1.4. Methane

The source of methane evolved on heating is unknown. Grundy and Hamer,[9] attempting to explain a similar observation, postulated the presence of sodium alkyl. However, one cannot argue with their comment that it is not clear how an alkyl compound could exist in high-temperature sodium and yet decompose at the relatively low temperatures of amalgamation.

Alternatively, the authors suggest that methane, released from steel, may dissolve in sodium. Were this the case, it would be expected that methane would find its way into the loop cover gas. With only a few exceptions, this was not the case for the two loops under investigation. On the other hand, methane is detected regularly in the gases involved during the amalgamation of sodium sampled at about 1000°F from our present systems and, recently, fairly high concentrations (1000 ppm) of the gas have appeared as an impurity in the cover gas of one of these loops.

A third proposed method of formation is suggested by the large amount of sodium hydride found in the traps. There may be a reaction of this compound with carbon according to the equation

$$4NaH + C = 4Na + CH_4.$$

However, the reverse reaction is favored thermodynamically, and thus this possibility is not strong.

5.1.5. Elemental Carbon

It is believed that a large portion of the carbon that requires oxidation to volatilize it is elemental carbon. The reduction of sodium carbonate yields carbon, and the nature of the production process for reactor-grade sodium is such as to yield the element as an impurity. In addition, the low solubility of carbon would preclude efficient cleanup in the cold trap, though it appears that some is removed in this manner—possibly due to a settling effect.

It is believed that some complex metal carbides would also require severe treatment for complete dissolution, and thus such species could make a small contribution to the fraction of carbon which was deposited in a relatively inert form.

5.2. Relationship to the Mechanism of Carbon Transport

The data presented in Table 1 show that the total amount of carbon deposited in the trap from the ferritic loop was three times that found in the deposits in the stainless steel system. The difference is due primarily to the increased amount of complex carbon forms in the ferritic-loop deposits. The greatest relative change is in the acetylene-producing fraction, which is essentially absent in the deposits of the Type 316 system.

A possible explanation for these observations lies in the interaction of carbon with potential carbide-forming solutes in the systems. Consider, for example, that chromium, calcium, and sodium all form carbides, but that the formation of the chromium compound is favored thermodynamically. In the stainless steel system the chromium activity should be high and the formation of carbides of this element is expected. It has been noted[15] that complex metal carbides were found in corrosion products deposited in the 800 to 1000°F temperature region of a stainless steel system. Therefore, it appears likely that the chromium carbides would precipitate before they reached the trap and thus lead to the observed reduction in the amount of carbon in the trap.

In the ferritic system the chromium activity is relatively low, and it seems reasonable that more carbon will be available for precipitation as alkali metal or alkaline earth carbides or as cyanides. In addition, if these species have an appreciable solubility at loop temperatures, larger quantities may be expected to reach the cold trap. The results in Table 2 show qualitative agreement with these hypotheses. The absence of the acetylene-producing species, almost surely calcium or sodium carbide, in the austenitic deposits may be attributed to the greater stability of the cyanide relative to the acetylides. Thus, in the system with lower carbon activity, the cyanide would tend to be formed preferentially.

The treatment of the data is qualitative; it is obvious that in multicomponent systems the interactions between various species becomes quite complex. The presentation is made, nevertheless, to indicate that the search for carbon species is a useful tool in the investigation of mechanisms of carbon transport. It argues for additional effort. Specifically, other potential deposition zones should be investigated to determine the nature of the precipitated material. Solubility studies of observed compounds should be continued as should investigations of the reaction of carbon with hydrogen, oxygen, and nitrogen.

Acknowledgment

The authors express their appreciation to Dr. P. Roy for a critical review of this report and for his suggestions in the interpretation of the data.

REFERENCES

1. Semmel, J. W., Jr., Engel, L. B. Jr., Frank, R. G., and Harrison, R. W., "Carbon Mass Transfer in Multimetallic Systems Containing Potassium," in *Alkali Metal Coolants*, IAEA, Vienna (1967).
2. Roy, P., Wozadlo, G. P., and Comprelli, F. A., *Mass Transport and Corrosion of Stainless Steels in Flowing Sodium Systems at 1300°F*, THIS CONFERENCE.
3. Lyashenko, V. S., and Nevzorov, B. A., "The Mechanism of Carbon Transport in Liquid Sodium," in *Corrosion of Reactor Materials*, **2**, pp. 373-406, IAEA, Vienna (1962). U. S. Translation-AEC Tr 5408.
4. Sabol, W. W., Dutina, D., Rey, D. E., and Simpson, J. L., *Sodium Mass Transfer: XIII. The Determination of Total Carbon in Sodium*, GEAP-4540 (June 1964).
5. Hobart, E. W., and Bjork, R. G., *Formation of Cyanide in Liquid Sodium*. Nuclear Applications **1**, 490 (1965).
6. Cafasso, F. A., "Solubility of NaCN in Liquid Sodium," in the *Reactor Development Progress Report for March 1968*, ANL-7445 (March 1968).
7. Sinclair, V. M., Drummond, J. L., and Smith, A. W., *The Analysis of Carbon in Sodium*, TRG Report 1185 (1966).
8. Luner, C., Cosgarea, A. Jr., and Feder, H. M., "Solubility of Carbon in Sodium," in *Alkali Metal Coolants*, IAEA, Vienna (1967).
9. Grundy, B. R., and Hamer, A. N., *A Study of Non-Metallic Impurities in Sodium by Amalgamation Coupled with Mass Spectrometry*, TRG Report 1227 (R) (1967).
10. Dutina, D., Simpson, J. L., and Young, R. S., *Determination of Impurities in a Sodium System Cold Trap*, Trans. ANS, **10**(1), 145, Annual Meeting, San Diego (June 11-15, 1967).
11. Wildeman, T. J., Palladino, C. A., and Rodgers, S. J., *Chemical Forms of Carbon Impurities in Sodium Cold Traps*, Anachem Conference, Detroit (Oct 3-5, 1967).

12. Rowland, M. C., Plumlee, D. E., and Young, R. S., *Sodium Mass Transfer: XV. Behavior of Selected Steels Exposed in Flowing Sodium Test Loops*, GEAP-4831 (March 1965).
13. Dutina, D., and Simpson, J. L., *Sodium Mass Transfer: XXIV Methods for Separation and Identification of Sodium Impurities*. GEAP-5020 (March 1967).
14. Bark, L. S., and Higson, H. G., *Investigation of Reagents for the Colorimetric Determination of Small Amounts of Cyanide—II*. **11**, 621–631 (1964).
15. Young, R. S., *et al. Sodium Components Development Program: Mass Transfer Investigation in Liquid Metals Systems*. Quarterly Program Report No. 5, GEAP-5148 (March–May 1968).

Discussion

Mr. Humphreys (Chairman): Was any examination made of the ferrite-loop materials for carbon depletion?

Mr. Dutina: Yes. That loop saw almost 30,000 hr of operation, and it was examined in detail—at least the main part of the loop was. What we found was decarburization generally in the areas of higher temperature. We didn't find out where the carbon was going. It wasn't extensive, but it was very definitely noticed.

Mr. Andrews (MSA): Did you eventually come up with a number for total oxygen in the two cold traps?

Mr. Dutina: Yes, the total oxygen was roughly the same in the two traps, within the uncertainty of the kind of analysis you can do on a trap like this. Looking at the most concentrated zones (and the distribution was about the same for both), the oxygen concentration in the ferritic-system trap was around 0.2%, and that for the austenitic system was about 0.3%.

Mr. Feder (ANL): I'm very pleased to see this kind of analysis of cold traps to get clues as to the species. I'm a little puzzled, however, and I think I'm expressing the puzzlement of others here. It would seem as though those species that would be the most carburizing would be gettered by the stainless steel system and thus the least likely to show up in the trap. Conversely, those that are indifferent to the steel might be expected to show up in the trap. Your results seem opposite to this.

Mr. Dutina: I don't really know how to answer. We know that there is movement of carbon. If it's moving we may also see some of it moving to the trap, and this may be an indication of that movement. That's about the best I can say.

Mr. Rodgers (MSA): When we have heated our cold trap, we have seen an increase in carburization of the monitoring tabs, and we've also seen an increase in the output of our carbon meter. Apparently we are concentrating carburizing species in the cold trap at the same time we carburize stainless steel.

Mr. Jansson (W): If one assumes that carburization occurs solely through a species in the solution, then one would expect that the high carburization rates would correspond to high levels of that particular species. If nearly everything in the cold trap comes out of a solution, this would fit very well with the notion that you would have high concentration of those particular species in the cold trap, too. However, it certainly isn't proved because their solubilities could be high and they could still remain in solution.

Mr. Zitek (ComEd): It seems as though there was a terrific amount of carbon in your ferritic loop. Was any attempt made to balance out the amount of carbon that came from decarburization with the amount of carbon that was found in the cold trap?

Mr. Dutina: What we showed was the amount that was deposited in the trap. As far as the carbon in the sodium went, if you were to analyze, as we did, grab samples from the loop proper (in either of the loops), the numbers all look about the same. They ran from 25–50 ppm, which is typical of most system loops.

Mr. Zitek: I guess my question was not clear. You say that the steel was decarburized in that loop. Was any attempt made to balance the amount of carbon that was obtained by decarburization of the steel with the amount of carbon seen in the cold trap?

Mr. Dutina: No. I don't know if we could have. Tabs were put in and taken out of the system over the course of a fairly extensive program. I don't think that could have been easily done.

Mr. Goldberg (ORNL): You have to remember that although you do lose carbon from the ferritic steel in some areas, you deposit it in other areas. You don't necessarily find it all in the sodium inventory and in the cold trap.

Mr. Zitek: I am aware of both carburization and decarburization. In the ferritic loop, however, there was so much carbon found that it seemed possible to come up with an approximate mass balance. But, if you were putting in other samples, then I'll admit it would have been difficult to do.

Mr. Goldmann (UNC): The wire mesh which was in your cold trap was made out of stainless steel. It could have picked up the tremendous amount of carbon that Mr. Zitek perhaps was talking about. I was wondering whether you made any analysis of the stainless steel to see how much carbon it picked up?

Mr. Dutina: Because of our method of sampling, we have no clear indication of the amount of carbon in the occasional bits of stainless steel mesh that occurred in the samples.

Mr. Weeks (BNL): The temperature was far too low to expect much carbon to diffuse into the steel. Do

you think the relative amounts of cyanide from the two systems is attributable to the relative chemical activities of nitrogen in the ferritic as opposed to the stainless steels?

Mr. Dutina: I have no comment.

Mr. Andrews: We agree that the temperature was too low to carburize the wire mesh. At one time we had temperature excursions in our cold traps; that is why Rodgers could find it in his, whereas you might not find it in yours.

Carbon Transport in Liquid Sodium

CHARLES LUNER, H. M. FEDER, AND F. A. CAFASSO

Argonne National Laboratory
Argonne, Illinois

(PRESENTED BY C. LUNER)

1. Introduction

It has been established that various metals may be significantly carburized or decarburized when in contact with liquid sodium. This phenomenon presents a potentially serious problem concerning the use of sodium in nuclear reactors because undesirable changes in the mechanical properties of structural materials, such as steel, can result from small changes in their carbon content. Various mechanisms of carbon transport in liquid sodium have been proposed; for example, Lyashenko and Nevzorov[1] postulated transport of carbon through sodium by carbon monoxide, whereas Flint[2] suggested transport by sodium carbide. Neither postulate has received experimental support. Clearly, identification of the carbon-bearing species undergoing transport is needed. This would provide an insight into the mechanism of carbon transport and could lead to effective methods for its control.

Previous investigations of carbon transport have been hampered by uncertainties as to the origin of the migrating carbon-bearing species. To overcome this difficulty, beta-active carbon-14 ($T_{1/2}$ = 5730 yr) was used to trace the migration of carbon between materials exposed to liquid sodium. In this manner, the transported carbon could be distinguished from contaminant carbon, and the sensitivity of the experiments was enhanced. The identity of the transported species was deduced from the nature of the ^{14}C-labeled products obtained on dissolution of the sodium in water. Sinclair *et al.*,[3] using a similar tracer technique, found that carbonate, carbide, graphite, and carbonyl were present in sodium at the parts per million level or less, but they reached no firm conclusion as to the species transported.

2. Experimental

2.1. Materials

A ferritic, labeled, iron-carbon alloy (0.030 wt % C, specific activity ~2650 dpm/μg C) was prepared by melting high-purity iron (>99.95% Fe) with amorphous carbon tagged with carbon-14. The alloy was remelted several times in an outgassed alumina crucible under a helium atmosphere to promote homogeneity. It was then rolled to a thickness of 18 mils and annealed at 750°C. Combustion analyses for total carbon in different sections of the sheet showed that the carbon was uniformly distributed. Also, beta-activity surveys of the surface as successive layers were ground off showed a uniform distribution of the carbon throughout its 18-mil thickness.

A single batch of United States Industrial Chemical Co. Reactor Grade sodium, stored molten at 120°C in a stainless steel (SS) container, was used for all experiments. The oxygen content of the sodium was 20 ppm; the carbon content, 10 ppm.

2.2. Apparatus and Procedure

A cylindrical crucible (of ~15-ml volume) with matching lid was fabricated from the labeled iron-carbon alloy and loaded with either molten sodium alone or with molten sodium in which was suspended a coupon of the austenitic alloy 316 SS (ferritic-to-austenitic area wetted ≃2.4). The crucible was welded shut and enclosed in a secondary nickel or Type 304 SS capsule, which was also welded shut. The capsule and contents were heated to 650°C for 120 hr, cooled, and then cut open. The operations of filling, welding, and opening, and the sampling of the crucible and its contents were all done in a helium-atmosphere glovebox.

The sodium in the opened crucible was dissolved outside the glovebox by placing the crucible in a quartz tube, evacuating the tube, and adding deaerated distilled water dropwise from a side arm. The condensable evolved gases were collected in a liquid-nitrogen-cooled silica-gel trap. Deaerated sulfuric acid was next added to acidify the solution, and the additional off-gas was passed through the same trap. The silica-gel trap was then removed from the apparatus and attached to the inlet of a combined gas chromatograph/proportional counter system in which the gases were identified and assayed. The solution and the filterable, finely divided, black particles resulting from the dissolution were also analyzed.

2.3. Analytical

(a) *Off-gas:* A radiogas chromatograph similar to that of Wolfgang and Rowland[4] was used to separate the trapped gases and assay their activities. Calibration experiments indicated that mixtures containing

TABLE 1. Carbon Content of Alloys Exposed to Liquid Sodium

	With Type 316 SS Coupon		Without Coupon	
	Initial, wt %	Final, wt %	Initial, wt %	Final, wt %
Ferritic crucible	0.030	0.006	0.030	0.016
Type 316 SS coupon	0.065	0.165	—	—

as little as 5×10^{-9} mole each of CH_4, C_2H_2, C_2H_4, C_2H_6, and CO_2 could be separated with a 6-ft column of Porapak R* and the components identified. A silica-gel column was required for separation and identification of CO. The relative error of the analysis for CO_2 was determined by adding known quantities of $^{14}CO_2$ to the radiogas chromatograph. This error, which includes the errors of both the mass and activity measurements, was about 6% and is assumed to be the same for the other gases.

(b) *Solution:* The filtered aqueous solution was assayed for its ^{14}C content as follows. It was refluxed with a strong oxidant, $K_2S_2O_8$, and the evolved gases were passed over CuO at 800°C. The carbon dioxide thus formed was absorbed in Hyamine,† a liquid scintillator‡ was added, and the resultant solution was counted in a Packard Tri-carb Model 2211 Liquid Scintillation Spectrometer. The procedure was tested with microgram to milligram amounts of ^{14}C present as benzoic acid-1-^{14}C dissolved in sodium sulfate solution. Oxidation was essentially complete, as indicated by the conversion of 90–100% of the ^{14}C to $^{14}CO_2$.

(c) *Fe-^{14}C alloy:* The specific activity of the carbon in the iron-carbon alloy was determined by dissolving the alloy in deaerated dilute sulfuric acid, collecting the hydrocarbon off-gases, and determining their masses and activities by radiogas chromatography. The specific activity of carbon in each off-gas (methane, ethane, and ethylene) was similar to that in the alloy, namely, 2650 ± 200 dpm/μg C.

3. Results

3.1. Alloy Analyses

The analyses for total carbon in the ferritic and austenitic alloys, before and after exposure to liquid sodium, are given in Table 1. They show that decarburization of the ^{14}C-labeled ferritic crucible occurred whether the Type 316 SS coupon was present or not. The extent of the decarburization, however, was considerably greater in the presence of the coupon.

The increase in the carbon content of the Type 316 SS coupon is attributed to carbon originating from the ferritic alloy, since the coupon became highly radioactive. These observations are consistent with the concept[5, 6] that the driving force for the transport of carbon through liquid sodium is a carbon activity rather than a carbon concentration gradient.

3.2. Sodium Analyses

Analytical results for the sodium, after being dissolved in water and acidified, follow.

3.3. Off-gas

Table 2 gives the results of the off-gas analysis of typical experiments with and without the Type 316 SS coupon. For the experiment without the coupon, acetylene was the major ^{14}C-labeled gas, and its specific activity was close to that of the carbon in the ferritic iron-carbon alloy. The ethylene and ethane found in small amounts are believed to originate from hydrogenation of acetylene during dissolution. The similarity of their specific activities is consistent with this contention. The minor amount of CO_2 found and its very low specific activity indicate that it originated from a carbonate impurity originally present in the sodium.

The corresponding results from the transport experiment with the Type 316 SS coupon show that, again, acetylene was the major ^{14}C-labeled gas; however, its concentration and that of ethylene plus ethane (and, therefore, of their precursor) were drastically reduced. This result is consistent with the frequent observation that austenitic steels in liquid sodium behave as sinks for carbon supplied by ferritic alloys. Note also that the specific activities of the hydrocarbons are about 30% lower than that of the source carbon in the ferritic crucible. This decrease is most likely due to dilution by inactive carbon

TABLE 2. Radiogas Chromatographic Analysis of Gases from Aqueous Dissolution of Sodium

Gases Evolved	With Type 316 SS Coupon		Without Coupon	
	C in Na, ppm	Specific Activity, dpm/μg C	C in Na, ppm	Specific Activity, dpm/μg C
C_2H_2	0.34	1910	18	2740
C_2H_4 and C_2H_6[a]	0.19	1750	2.2	2600
CO_2	3.7	15	1.8	28

[a] Average of C_2H_4 and C_2H_6; traces of methane also observed.

* Registered trademark of Waters Associates, Inc.

† Registered trademark of Rohm and Hass, Inc.

‡ 4.90 g of 2-5-diphenyloxazole (PPO) and 0.10 g of 1,4-bis-2-(5-phenyloxazolyl)-benzene (POPOP) diluted with toluene to one liter.

originating from the Type 316 SS coupon or to exchange with the carbon in the stainless steel.

Carbon monoxide was sought but not found, which contradicts Lyashenko and Nevzorov's hypothesis[1] that it is the migrating species responsible for carbon transport.

3.4. Solutions

The radiocarbon contents of filtered solutions from experiments with and without the Type 316 SS coupon were similar, indicating ~0.1 ppm C in the sodium.

3.5. Solids

X-ray powder diffraction analysis of the finely divided black particles from the sodium dissolution proved unsuccessful. However, the result of an entirely separate experiment is relevant and worth mention at this point. A coupon of an iron-carbon alloy of composition similar to that used in the present experiments, but containing 0.11 rather than 0.030 wt % carbon, was immersed in sodium at 650°C for 120 hr inside a tantalum crucible. The coupon was cleaned in alcohol, and a layer of black particles was removed from the surface and identified as graphite. It is believed that the unidentified black particles obtained in the present experiments were also graphite, and that these particles did not form as a reaction product of the sodium dissolution. Instead, the particles were already present in the sodium prior to the dissolution as a result of having been dislodged from the graphitized surface of the alloy. This type of graphitization of ferritic steels in sodium has been observed by others.[1, 7]

In the following discussion, it is assumed that transport by graphitic particles is negligible, an assumption currently being tested in this Laboratory.

4. Discussion

A direct identification of the precursor of acetylene was not feasible, and therefore its identity was deduced. Only acetylides (salts of $C_2^=$) yield acetylene as their principal hydrolysis product. The most likely precursor of acetylene in these experiments is therefore sodium carbide, Na_2C_2. Calcium carbide, formed from a calcium impurity in the sodium, was ruled out as the precursor when it was found that acetylene production was unaffected by reducing the calcium content of sodium from 20 to 5 ppm.

The evolution of considerably less acetylene from the sodium with the carbon sink than without strongly suggests that the precursor, sodium carbide, partook in the carbon transport. Recent observations at other laboratories seem to support this suggestion. For example, acetylene was evolved on hydrolysis of deposits from the cold traps of sodium loops in which carbon transport had occurred.[8, 9] In another investigation[10] sodium carbide was found to produce a high carbon flux in a diffusion-cell type of carbon meter.

Insight into the mechanism of formation of sodium carbide may be obtained from the literature on lithium-steel systems. Several investigators[11-13] have proposed that the corrosion of carbon steels in lithium proceeds according to the reaction

$$2\,\mathrm{Li(l)} + 2\,\mathrm{Fe_3C(s)} \rightarrow \mathrm{Li_2C_2(s)} + 6\,\mathrm{Fe(s)}, \quad (1)$$

which is thermodynamically possible.[11] Moreover, it is known that carbon in steel and in pure cementite is quantitatively converted to Li_2C_2 by reaction with lithium at 700°C.[12, 14] Thus, there is ample evidence that decarburization of steels in lithium proceeds according to reaction 1. By analogy, the decarburization of ferritic alloys in liquid sodium may proceed by formation of sodium carbide:

$$2\,\mathrm{Fe_3C(\text{solid soln in Fe-C alloy})} + 2\,\mathrm{Na(l)} \rightarrow \mathrm{Na_2C_2(s)} + 6\,\mathrm{Fe(s)}. \quad (2)$$

Formation of sodium carbide and its involvement in carbon transport were recently suggested by Flint,[2] whose calculations indicated that reaction 2 is thermodynamically possible. The calculation was approximate because the existing values[15, 16] for the free energy of formation of Na_2C_2 are unreliable. Our observation, that acetylene is evolved on aqueous dissolution of sodium that has reacted at 650°C with cementite (manganese stabilized), provides indirect evidence for the validity of reaction 2. In view of the importance of sodium carbide, measurement of its thermodynamic properties has been started.

In summary, our results support the hypothesis that sodium carbide is the species responsible for carbon transport in liquid sodium. However, before details of the transport mechanism can be put on a firm basis, information is needed on sodium carbide's stability, solubility, and tendency to carburize steels in sodium. These studies are now under way.

Acknowledgment

We wish to acknowledge the technical assistance of J. Althoetmar and the editorial assistance of M. Ader.

REFERENCES

1. Lyashenko, V. S., and Nevzorov, B. A., Proc. Conf. on Corrosion of Reactor Materials, Vol. II, pp. 373–405, IAEA, Vienna (1962). English translation AEC-TR-5408.
2. Flint, O., AERE-M 1522L (1965).
3. Sinclair, V. M., Drummond, J. L., and Smith, A. W., TRG Report 1185(D) (1966).
4. Wolfgang, R., and Rowland, F. S., Anal Chem. **30**, 903 (1958).
5. Hayes, W. C., and Shepard, O. C., NAA-SR-2973 (Dec 1, 1958).

6. Baenlecken, E., Lorenz, K., and Kranz, E., in *Alkali Metal Coolants*, p. 145, IAEA, Vienna (1967).
7. Brown, A. F., and Hayes, D. J., J. Nucl. Materials **27**, 187 (1968).
8. AEC Research and Development Report, General Electric Co., GEAP-5648 (July 1968).
9. Rodgers, S. J., Palladino, C. A., and Wildeman, T. J., MSA Research Corporation Topical Report No. 9., MSAR 67-203 (Dec 1967).
10. McKee, J. M., Caplinger, W., and Kolodney, M., Nucl. Appl. **5**, 236 (1968).
11. Beskorovainyi, N. M., Ivanov, V. K., and Znev, M. T., in *High-Purity Metals and Alloys*. Edited by V. S. Emel' Yanov and A. I. Evstyuklin. Translated from Russian by Consultants Bureau, New York (1967).
12. Beniere, M., Chemla, M., Aucouturier, M., LaCombe, P., and Roques-Carmes, C., Corrosion **24**[4], 83 (1968).
13. Hoffman, E. F., ORNL-2924 (1960).
14. Hobart, E. W., and Bjork, R. G., Anal. Chem. **39**, 202 (1967).
15. Guernsey, E. W., and Sherman, M. S., J. Amer. Chem. Soc. **48**, 140 (1926).
16. Richardson, F. D., J. Iron and Steel **175**, 3 (1953).

Discussion

Mr. Newman (BNL): Did you measure the specific activity of the elemental carbon?

Mr. Luner: Not yet. We are in the process of doing this. From preliminary results it appears that it is close to that of the original material.

Mr. Yannopoulos (W): You mentioned in the last portion of your paper that you reacted pure cementite. What was its purity? I would like to mention that we agree with your analysis of the uncertainty of the free energy of formation of sodium carbide. The way the free energy was obtained makes it very unreliable. Therefore the reaction is quite possible and this has been shown by us.

Mr. Luner: X-ray diffraction shows that it was pure cementite. Chemical analysis showed the carbon and iron to be in the right proportions. I must add, however, that we did not use pure Fe_3C since, as you probably know, it is very difficult to isolate from an iron matrix. Instead, we used a preparation that was given to us by U. S. Steel, which was Fe_3C with 6 at. % manganese added to stabilize the cementite. The manganese here was in solid solution. Hence one wouldn't expect any change as far as the products of the reaction are concerned. The kinetics of the reaction, however, may be much slower.

Mr. Yannopoulos: In that stable ternary compound, the free energy would be changed and it could not lead to sodium carbide formation, that is, it might not lead to sodium carbide formation as such because of the higher stability of this ternary compound.

Mr. Luner: Well, it did, and at 650°C.

Mr. Hiltz (MSA): I'm in agreement with the fact that cementite can be dissociated by sodium. Fortunately, however, in the structural materials that are being considered for LMFBR, the carbide is a chromium compound—M_7C_3—and the ferritics are $M_{23}C_6$ compounds. The austenitics, I feel strongly, on the basis of Darken's and other people's thermodynamic data, cannot be dissociated by sodium at the temperatures you're talking about. So I wonder what the relationship to understanding carbon transport in the actual system is here?

Mr. Luner: In this research we wanted to so simplify the situation that we would be reasonably assured of getting some idea of the species involved in transport. Once we understand what we think is the more simple system we expect to go on to more complicated systems.

Mr. Hiltz: Let me ask the question again. Do you expect to dissociate alloy carbides with sodium?

Mr. Luner: In some preliminary experiments in which we heated Type 316 stainless steel with sodium at 650°C and then hydrolyzed the sodium, small but significant amounts of acetylene were found. While this result is very preliminary, it shows that it may be possible.

Mr. Hobdell (BNL): Some time ago we did some simple qualitative experiments on pure sodium acetylide, or sodium carbide as you call it. And it appeared to decompose as low as 200°C in the presence of sodium or in vacuum. The white material went black when sodium was collected on a cold finger. I think the dissociation starts as low as 200°C.

Mr. Luner: This is possible, but I think those results were based on visual observations, and not on chemical evidence.

Mr. Hobdell: The residue remaining after the dissociation at 200°C was a black residue that was insoluble and which we have assumed was carbon.

Mr. Luner: Was this material on the surface of the sodium or did you sample the sodium?

Mr. Hobdell: We took a white pellet of sodium acetylide and heated it at 200°C. It turned black, and there was an insoluble black residue after treatment with water.

Mr. Lemke (DuPont): I would like to add a little to the confusion concerning the stability of sodium carbide, Na_2C_2. I'm amazed to hear the remarks of the gentleman from Brookhaven that he found decomposition of sodium carbide at 200°C. This may well be. Let me just say that we ran some tests quite a few years ago that may bear on this subject. I must hasten to point out that we did not identify sodium carbide by X-ray or any other similar techniques, but only by the evolution of acetylene on the addition of water. In one type of experiment we found that we could react carbon monoxide gas with sodium in the temperature range

from about 650 to 850°C and produce products containing large amounts, 30 or 40%, of a species which on hydrolysis would evolve acetylene. The other component in the reaction product was primarily soda ash. So much for that. I submit that in these tests and at these temperatures, the species which evolved acetylene was at the temperature for substantial periods of time, of the order of 8, 10, 15 min in most cases, and was quite clearly not decomposed.

In other experiments, we reacted carbon in the form of finely divided petroleum coke with anhydrous fused sodium hydroxide at temperatures of 750 to 950°C. In these experiments we made sodium, which was largely evolved from the apparatus at these temperatures. We found residues left in the retort which, by the way, was nickel, and contained very little carbon. We found in the residues a substantial amount of a species which would on hydrolysis evolve acetylene. When I say substantial amounts—I'm talking now from memory that goes back a fair number of years—our residues were several hundred grams and they contained the species, calculated as sodium carbide, Na_2C_2, to an extent ranging from about 3% to something over 10%, depending on the particular conditions we used. Again I submit that it is safe to assume that the species here being discussed is Na_2C_2, and that it was remarkably stable in this environment at these high temperatures. Now the other components in the residue were some unreacted carbon and the bulk was soda ash. There was always some alkalinity which could not be accounted for as sodium carbide or soda ash, and this was probably Na_2O. It may also have been NaH—there are a lot of possibilities here—but the bulk of the alkalinity was soda ash.

A Study of Reactions between Oxygen and Impurities in Sodium*

H. S. Isaacs, B. Minushkin, and F. J. Salzano

Brookhaven National Laboratory
Upton, New York

(PRESENTED BY B. MINUSHKIN)

Introduction

The reactions of oxygen with metals and nonmetals in sodium are being studied at Brookhaven National Laboratory to obtain a more detailed understanding of corrosion mechanisms and the chemistry of impurities in sodium. The emphasis in this investigation is on identifying those species that react with oxygen in sodium and determining their free energies and kinetics of formation. Such information is necessary in order to predict the effect of these impurities on the operation of sodium-coolant systems.

Some results of reactions in Na-O-stainless steel and Na-O-Cr systems at temperatures between 350 and 500°C are presented.

Reactions between oxygen and other materials in sodium are accompanied by changes in the partial molar free energy or activity of oxygen in solution. Measurement of the oxygen activity in solution provides a means for detecting and studying these reactions. In this investigation the oxygen activity in sodium at high temperature was measured by the solid-electrolyte galvanic cells[1, 2] shown symbolically in Fig. 1. Similar solid-electrolyte galvanic cells have been used to investigate free energies of formation of oxides,[3, 4] activities of metals in solids and liquid alloys,[5] solubility of oxygen in metals,[6] and, in general, free energy changes for a number of chemical reactions and phase changes.

The cell consists of three major components: an oxygen reference electrode, the sodium, and a solid electrolyte. The oxygen reference electrode maintains a fixed oxygen activity at a given temperature. In this work mixtures of Cu, Cu_2O or Na, Na_2O were used as reference electrodes. The sodium solution containing dissolved oxygen in the second electrode. The electrolyte is an ionically conducting ThO_2-Y_2O_3 ceramic tube which separates the two electrodes and is impermeable to sodium. It has been shown that for an ideal electrolyte the emf developed by this cell is given by

$$E_{cell} = E_T^o - \frac{RT}{2f} \ln a_o, \qquad (1)$$

where a_o is the activity of oxygen dissolved in the sodium, E_T^o is the standard electrode potential, R is the gas constant, f is the Faraday constant, and T is the absolute temperature. The cell emf is determined solely by the difference between the activity of oxygen in the sodium and at the chosen reference electrode. Thus for a given cell, changes in emf reflect changes in the activity of oxygen in the sodium.

Experimental Technique

The basic experimental technique was to add or remove oxygen or other reactants to the sodium and observe the changes in potential (emf) of the oxygen electrode. It was thereby possible to titrate impurities in sodium potentiometrically. The technique is analogous to a potentiometric pH titration in aqueous systems.

The apparatus is shown in Fig. 2. Sodium was in a container supported on a pedestal within a 4½-in.-diameter stainless steel tank. The ThO_2-Y_2O_3 tube containing the reference electrode was located at the top of the tank and was immersed approximately 1 in. below the sodium surface. The tank was equipped with a gas lock through which oxygen or other materials was introduced or removed from the sodium. Provisions were included for stirring and for measuring the sodium temperature. All materials contacting the sodium were fabricated of the same material as the container.

Reactor-grade sodium was purified by aging and filtering through a 1-micron porous stainless steel frit. In some cases the sodium was gettered by zirconium foil at 650°C.

Oxygen was added to the sodium in the form of pellets of high-purity Na_2O or as Fe_2O_3. Uranium foils were used to remove oxygen from the system[7] quantitatively. It has been shown that the weight gain of the foil after exposure to sodium was equal to the amount of oxygen removed from the system. If no sources or sinks for oxygen were present in the system, the weight gain would be proportional to the change in oxygen concentration. Successive gettering steps were performed in which the time of contact of the uranium foil with sodium was controlled to give equal

* Work performed under the auspices of the U. S. Atomic Energy Commission.

changes in oxygen-meter potential. Under these conditions it can be shown that

$$C_o = \frac{\Delta C_1^2}{\Delta C_1 - \Delta C_2}, \qquad (2)$$

where C_o is the initial unknown oxygen concentration in sodium, and ΔC_1 and ΔC_2 are the changes in oxygen concentration in successive steps; these were obtained by measuring the increase in weight of the uranium foils after successive equipotential gettering steps. This procedure provided a convenient method of calibrating the oxygen meters.

Results and Discussion

Initial tests were conducted in stainless steel systems at temperatures between 300 and 400°C using a commercial oxygen meter with a Cu, Cu_2O reference electrode. An example of the results obtained are shown in Fig. 3. This test was conducted at 362°C in a Type 304 stainless steel container. Uranium foil was immersed in the sodium at time zero. The cell potential initially increased (oxygen activity decreased) at a linear rate as oxygen was slowly removed from solution by oxidation of the uranium foil. The cell potential, and thus the oxygen activity, then remained constant at about 1.152 V for 2 hr while the uranium foil continued to remove oxygen. Subsequently, the cell potential increased to 1.158 V and again remained constant. After removal of the uranium foil the cell potential was constant for about two days. Iron oxide, equivalent to approximately 100 ppm oxygen, was then added. The cell potential proceeded to decrease, and potential arrests were evident at essentially the same values observed during oxygen removal. These arrests suggest that one or more substances present in this stainless steel system reacts with oxygen and tends to buffer the oxygen activity (i.e., keep it constant) while oxygen is added to or removed from the system.

Tests were also conducted with a reference electrode of Na, Na_2O which replaced the Cu, Cu_2O electrode in the commercial oxygen meter. The change in reference electrode was necessary because of the limitation in operating temperature of the commercial meter. The

oxygen reference electrode	solid electrolyte	sodium solution
Cu_s , Cu_2O_s or Na_l , Na_2O_s	ThO_2-Y_2O_3	Na_l , O_d

$$E_T = E_T^\circ - \frac{RT}{2f} \ln a_o$$

FIG. 1. Schematic Representation of Solid-electrolyte Galvanic Cell.

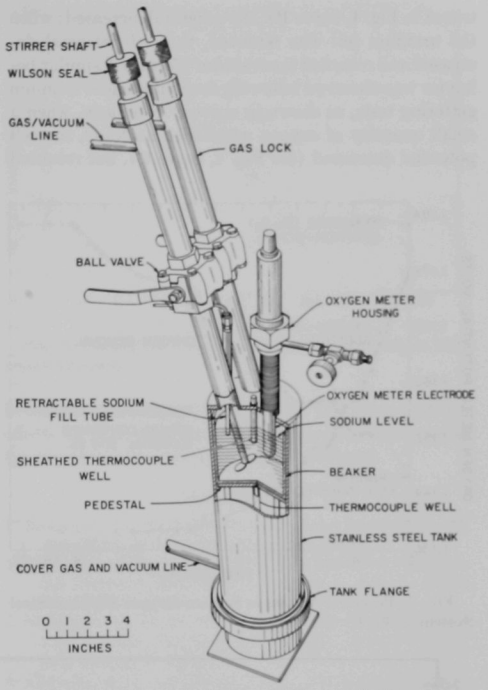

FIG. 2. Experimental Apparatus Used in Sodium-Oxygen Reaction Studies.

Na, Na_2O reference electrode can be used at temperatures to 550°C. Furthermore, it appears to be more reversible, less subject to atmospheric contamination than the Cu, Cu_2O reference electrode, and is not affected by normal variations in ambient temperature. However, the ceramic tubes (electrolyte) survived only a few weeks of operation at 500 or 550°C.

Figure 4 illustrates the data for potential vs time obtained with a Na, Na_2O reference electrode at 500°C during removal and addition of oxygen. In these tests approximately 2 g of chromium and chromium oxide (Cr_2O_3) were added to the sodium, which was contained in a heavily oxidized zirconium container. The results shown in Fig. 4 were selected to illustrate the behavior of the Na-O-Cr system at 500°C.

When the system was heated to 500°C and allowed to stabilize, a cell potential of approximately 154 mV was observed. This potential appeared to be characteristic of the system, i.e., the cell potential tended to return to this value following disturbances. If the system was altered by immersing uranium foil in the sodium to remove a small amount of oxygen (as illus-

trated in Fig. 4, curve B), the potential increased; when the uranium foil was removed, the cell potential decreased and returned to a value of 154 mV. A similar behavior was observed following four subsequent uranium gettering tests, as shown in curve B. Similarly, when a small quantity of oxygen was added as Na_2O, the cell potential decreased (see Fig. 4, curve C), but returned to a value of 154 mV when the Na_2O pellet was removed.

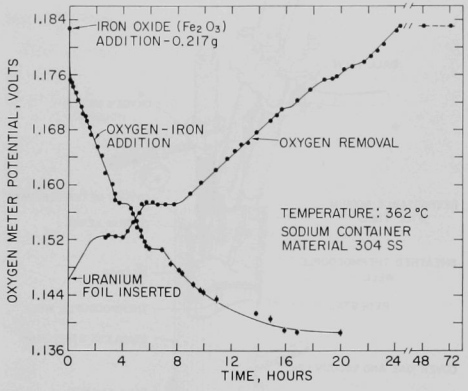

FIG. 3. Potential Arrests in Sodium-Oxygen-Stainless Steel System at 362°C.

This behavior suggest that a material existed in the system which could act as either a source or sink for oxygen and tended to maintain the system at a constant oxygen activity (buffered system) equivalent to 154 mV. Since a large quantity of chromium and chromium oxide was present during these tests, it is probable that the buffering action involved an equilibrium between a reduced and oxidized chromium-oxygen compound. It was found that when additional Cr_2O_3 was immersed in the sodium the equilibrium potential did not change. Tests established that the oxidized zirconium beaker was not a source or sink for any significant quantities of oxygen under these conditions.

Curve A illustrates the behavior of the system when the oxygen activity was initially high (Na_2O was added). Upon immersion of uranium, the cell potential increased at a linear rate. After 30 min the uranium was removed. When the uranium was reinserted the potential again increased at a linear rate and became approximately constant at a value of 232 mV. However, when the uranium was removed, the potential decreased and the weight gain of the uranium was anomalously high. This suggests the presence of an additional source of oxygen in the system. The arrest at 232 mV, therefore, was not due to a true thermody-

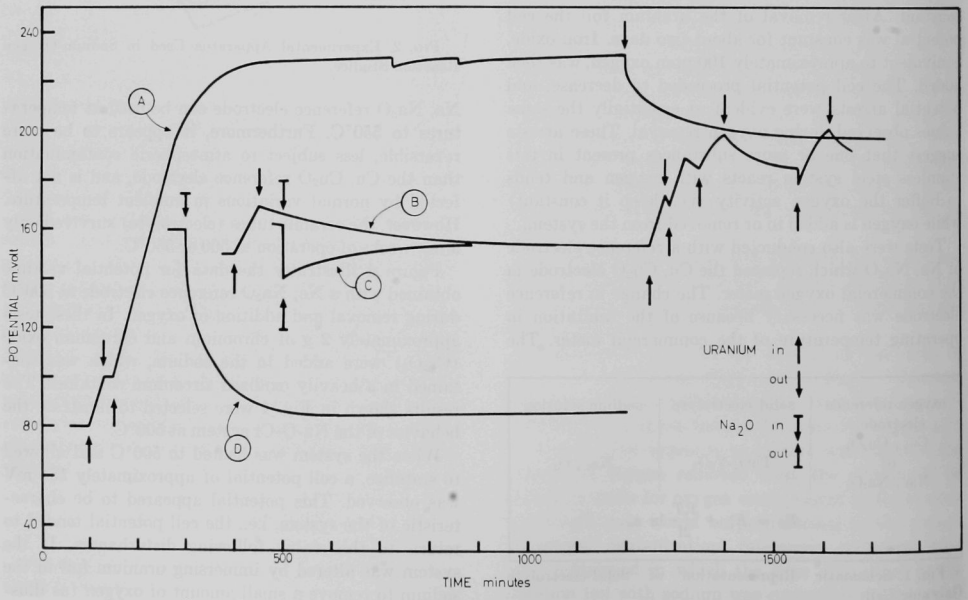

FIG. 4. Behavior of a Sodium-Oxygen System Containing Cr and Cr_2O_3 at 500°C.

namic equilibrium, but represented a dynamic steady-state situation in which the rate of gettering (oxidation of uranium) was equal to the rate at which oxygen was available from the source.

Curve D illustrates the behavior when large Na_2O additions were made. The potential dropped rapidly to a minimum, and then increased slightly, indicating the presence of a sink for oxygen. The increase in potential corresponded to a loss of 10 ppm oxygen.

The uranium-gettering data were used to obtain calibration curves for oxygen meters at temperatures to 550°C. The results for two cells at 500°C are shown in Fig. 5. The calibration points shown are for cell NA6 and were determined as previously described. At high oxygen concentrations a straight line was obtained, suggesting that the uranium weight gains are equivalent to the change in oxygen concentration. At lower concentrations, however, a break in the curve was observed. This suggests that the buffering reaction which occurs can mask the true calibration when one uses results obtained in the vicinity of the potential arrest.

The potential arrests shown in Fig. 4 were observed at 154 mV at 500°C for cell NA6 and at 161 mV for cell NA4. Based on the extrapolated calibration curve, the equilibrium oxygen concentration for the buffering reaction is tentatively set at 17 ppm oxygen at 500°C.

The above results have shown that if a substance capable of reacting with oxygen is added to sodium, the oxygen activity can be controlled by an equilibrium between the added material, its oxide, and dissolved oxygen. The variation of the cell potential with oxygen content depends on the nature of the reaction and its equilibrium constant.

Conclusions

The results show that reactions occur between the components of stainless steel and oxygen in sodium. These reactions can act to buffer the oxygen activity in the system. At 500°C it is probable that chromium is one of the metals which react with oxygen. The buffering action suggests that the reaction involves an equilibrium between a reduced and oxidized chromium-oxygen compound, and that two solid phases are present in the system. The equilibrium oxygen concentration for this reaction at 500°C is tentatively set at 17 ppm. Above this concentration chromium can getter oxygen from sodium, and below this concentration the oxidized species can supply oxygen to the system.

Acknowledgment

The authors acknowledge the invaluable discussions with Drs. D. H. Gurinsky, L. Newman, and J. R. Weeks as well as with other members of the staff of Brookhaven National Laboratory. The conscientious efforts of W. Becker and V. C. Williams in performing the experimental work is greatly appreciated.

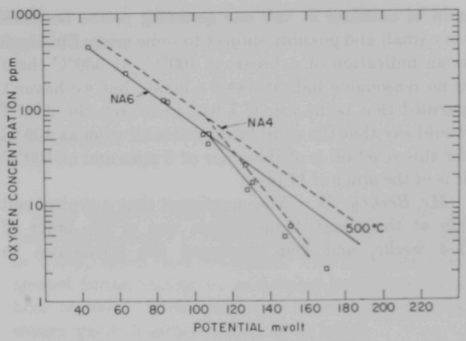

FIG. 5. Calibration Curves for Sodium-Sodium Oxide Reference Electrode.

REFERENCES

1. Kröger, F. A., *The Chemistry of Imperfect Crystals*, Ch. 22, John Wiley & Sons, Inc., New York (1964).
2. Minushkin, B., and Kolodney, M., *Development of a Continuous Electrochemical Meter for Oxygen in Sodium*, UNC-5131 (Dec 15, 1967).
3. Markin, T. L., Bones, R. T., and Wheeler, V. J., *Galvanic Cells and Gas Equilibration Techniques*, British Ceramic Soc. Proc. **8**, 51 (1967).
4. Charette, G. G., and Glengas, S. N., *Thermodynamic Properties of the Oxides of Fe, Ni, Pb, Cu and Mn, by EMF Measurements*, J. Electrochem. Soc. **115**(8), 796 (1968).
5. Kubic, A., and Alcock, C. B., *A Thermodynamic Study of Solid Iron-Gold and Cobalt-Gold Alloys by the Use of Solid Oxide Electrolytes*, Metal Science Journal **1**, 19 (1967).
6. Rapp, R. A., "Mixed Conduction in Solid Oxide Electrolytes," in *Thermodynamics of Nuclear Materials, 1967*, Proc. of a symposium, Vienna, Sept. 4–8, 1967, p. 559, IAEA.
7. Isaacs, H. S., *The Determination of Oxygen Concentration and Mass Transfer Coefficients in Sodium Using Uranium*, THIS CONFERENCE.

Discussion

Mr. Biery (LASL): Why did you not observe the break in the curves at 400 and 550°C?

Mr. Minushkin: We did not pursue the break in that region. The purpose of those experiments was strictly to calibrate the electrodes. I must admit it is very tenuous, but the data do suggest that down at a concentration of the order 2-3 ppm, we are beginning to see a break. The problem is that at low temperatures and low oxygen concentrations, the oxidation rate of uranium becomes very slow; to continue the experiment in this range requires many long tedious hours of gettering and regettering. You also face the problem that the weight

gain of uranium at any one gettering period becomes very small and possibly subject to some error. But there is an indication of a break at 400°C. At 550°C there is no reasonable indication of a break, but we haven't pursued that point yet. If I had to stretch the data I would say that the equilibrium concentration at 400°C for this reaction is of the order of 3 ppm and at 500°C it is of the order of 17 ppm.

Mr. Berkey (W): You mentioned that a typical cell life at these high temperatures was of the order of 3–4 weeks, and you attributed the breakdown to thermal shock. Does this mean that you thermally cycled several times?

Mr. Minushkin: No, I should have said thermal stress. There was no thermal shock; these electrodes would fail without any apparent temperature changes. Perhaps the cause arises from temperature fluctuations in the surface (if it's thermal stress), because there is a sharp temperature gradient at the interface between the sodium and the gas. There is an alternative possibility: the electrolyte may be attacked by solid sodium oxide.

The Determination of Oxygen Concentration and Mass-transfer Coefficients in Sodium Using Uranium*

H. S. Isaacs

Brookhaven National Laboratory
Upton, New York

Uranium has been found to react rapidly with oxygen in sodium. Although uranium oxide formed over long periods of contact with sodium was usually nonadherent,[1] weight gains were noted at low oxygen concentrations[2, 3] and showed that the nature of the oxide was also a function of temperature.[3] In addition to temperature and oxygen concentrations, either the time[4] or oxide thickness[3] also plays a part in obtaining fully adherent oxide layers.

Investigation using an electrochemical oxygen meter to monitor the oxygen activity showed that the potential of the meter increased linearly with time when uranium was used as an insoluble oxygen getter. This linear behavior indicated that the rate of reaction between oxygen in sodium and the uranium was proportional to the oxygen concentration.

These observations suggested that uranium could be used to determine the oxygen concentration in sodium. This work presents the experimental results and possible applications of this method.

Experimental

The apparatus was an externally heated stainless steel container holding nominally 14 kg of sodium under a helium cover gas. The pressure of the helium was maintained at 10 psi above atmospheric pressure. A vertical tube with a ball valve acted as a gas lock. The volume above the valve could be evacuated and filled with helium when the specimens were loaded.

The uranium specimens were approximately 0.002-in.-thick foils, $\frac{3}{8}$ in. wide and 6 in. long. The areas of the specimens were measured to within 3 %. Two $\frac{1}{32}$-in. holes were drilled, each about $\frac{3}{8}$ in. from the ends, through which wire was passed to attach them to the specimen holder. The surfaces of the specimens were electropolished in equal volumes of ethanol and phosphoric acid (85 w/o) at 7.5 to 15 V. Samples which had thick oxide layers were polished at the higher voltages, which assisted in removing the oxide. Electropolishing with a chromic acid and acetic acid solution[5] gave the same results within experimental error. After polishing, the specimens were washed in a large volume of water, dried, and weighed to ± 0.03 mg.

After removal from sodium the samples were immersed in methanol to remove adhering sodium, washed in water, dried, and reweighed. The specimens were treated before testing by immersion in sodium for an hour at 500°C. If this procedure was not adopted, the weight gains observed tended to be lower.

The specimen holder consisted of a $\frac{1}{16}$-in. stainless steel rod, about $3\frac{1}{2}$ ft long, with two rings welded on the rod to keep the specimens about $\frac{3}{32}$ in. away from the rod. The rings were about 5 in. apart. Holes were drilled in the rod, and wire was used to attach the specimens to the specimen holder.

The additions of oxygen to the sodium were made in the form of sodium oxide (Na_2O). The oxide was loaded in a stainless wire basket attached to a $\frac{1}{16}$-in. rod which fitted into a detachable gas lock and immersed in the sodium for 16 hr.

Results

The results were obtained by immersing two electropolished uranium specimens in sodium for one-hour periods and recording the weight gains. After additions of sodium oxide the weight gains increased in proportion to the amount of oxygen added. The analysis did show a trend, but the scatter was too large to show any significant dependence. However, the rates at which the uranium gained weight and the quantity of oxygen added to the sodium did show a definite relationship. The oxygen concentrations were therefore calculated by keeping an account of the weight of oxygen added to the sodium and removed by the uranium.

Up to about 1 ppm oxygen, the rates observed at 400 to 500°C were similar. Above 1 ppm the rates at 400°C were apparently lower than those at higher temperatures. The rates at 440 and 500°C were similar up to about 10 ppm, but above this concentration rates at 440°C were lower than at 500°C. Specimens which gave rates lower than those at 500°C also showed a nonadherent, fine, brown powder after washing in water.

Figure 1 shows the normalized results for experiments at 500°C. In one series of tests, the oxygen concentration had been initially increased to a calculated value of 16.6 ppm. After each test the oxygen concentration in the vessel was corrected by the weight gains of two

* Work performed under the auspices of the U. S. Atomic Energy Commission.

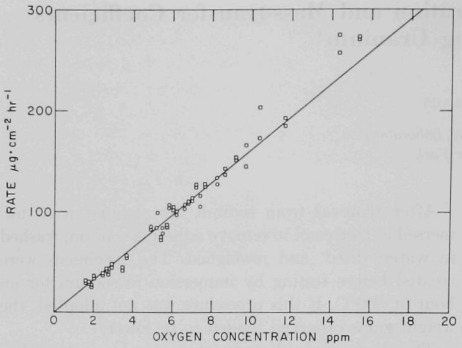

FIG. 1. The Dependence of the Rate of Uptake of Oxygen by Uranium on the Corrected Oxygen Concentration in Sodium after Two Sodium Oxide Additions. □ corrected by 1.1 ppm; ○ corrected by an additional 1.8 ppm.

TABLE 1. EXAMPLE: RESULTS FROM GETTERING AT 500°C FOR ONE HOUR

Weight gain, mg	Δ, ppm	Rate, $\mu g\text{-}cm^{-2}\text{-}hr$	Calculated oxygen concentration, ppm	Remarks
2.51 2.56	0.362	104 102	7.206	
2.06 2.07	0.295	84.7 85.5	6.844	After 2 days
1.78 1.82	0.257	71.2 74.0	6.549	
10.41 9.31	1.410	431 383	6.292	Specimens rotated at 240 rpm
1.29 1.40	0.192	52.5 56.0	4.882	
1.08 1.09	0.155	43.9 43.6	4.690	

uranium specimens, since this should be equal to the weight of oxygen removed from the sodium. Table 1 shows an example of the data from these experiments giving the weight gains, the calculated change in oxygen concentration (Δ ppm), the rate of weight gain per unit area, and the calculated oxygen concentrations. The table also includes data from an experiment in which the sample holder was rotated at 240 ± 10 rpm. The weight gains for these specimens were markedly greater than for those simply immersed in sodium.

The results plotted in Fig. 1 were normalized by subtracting 1.1 ppm from the calculated oxygen concentration. The other set of data plotted in Fig. 1 was normalized by an additional 1.8 ppm, after the oxygen concentration had been increased by a calculated value of 8.8 ppm. The normalization was necessary as oxygen was apparently lost from the sodium as a result of chemical reactions which remove oxygen from sodium.[4]

Two elements besides oxygen were considered as possible contributors to the weight gain, viz., hydrogen and carbon. A fraction of hydrogen produced during the removal of adhering sodium in methanol could enter the uranium and give rise to increased weight gains. This process was not studied because of the low weight gains observed of $1 \pm \frac{1}{2}$ $\mu g\text{-}cm^{-2}\text{-}hr^{-1}$ after zirconium gettering. These low rates indicated that any effects due to hydrogen were negligible compared with the higher rates observed at higher oxygen concentrations. Carbon was analysed for, in thick oxide films formed, using an electron-microprobe analyser. It was concluded that less than 1% carbon was present in the oxide layer.

Discussion

The results in Fig. 1 gave a linear relation between oxygen concentration and the rate of uptake of oxygen by uranium. These results are also in accord with those obtained using an oxygen meter to monitor oxygen concentrations.[4] The slope of the curve in Fig. 1, 16.3 $\mu g\text{-}cm^{-2}\text{-}hr^{-1}\text{-}ppm^{-1}$, represents the reaction rate constant at 500°C.

The rate constant is sufficiently high to be accounted for by diffusion of oxygen in the sodium to the surface of the uranium specimen. In addition, there was no apparent temperature dependence, and the rates at which oxygen reacted with the uranium increased markedly with velocity, as shown in Table 1. All these observations are consistent with a model involving the mass transfer of the oxygen in the sodium to the uranium. The apparent reaction constant is therefore equivalent to the mass-transfer coefficient.

Mass-transfer coefficients in nominally static liquids are usually found to be highly erratic, as convection currents are present. The small scatter of results in Fig. 1 therefore suggests that well-defined convection currents are present, which would depend on the positioning of the external heaters on the containers and the insulation.

Diffusion across the oxide formed on the uranium is extremely rapid, and oxide thicknesses up to 40 microns did not show any deviation from the calculated behavior. The uranium oxide layer did not show any signs of being wetted by the sodium after removal from the liquid metal, and penetration of any pores by sodium

does not appear likely. No calculations are at present possible to determine at what thickness diffusion through the oxide becomes rate determining, but future work at higher velocities should clarify this problem.

The lower rates at lower temperatures, e.g., at oxygen concentration above 1 ppm at 400°C or above 10 ppm at 440°C, when compared with those at higher temperatures could result from diffusion in the oxide becoming the rate-controlling step in the process. The change in the adherence of the oxide would also show apparent decreases in rates, and from the results available the two possibilities cannot be separated and may also be related.

Results obtained in other experiments[4] have shown that at 500°C uranium could be used to determine oxygen concentrations up to 200 ppm. Although these results were carried out under conditions different from those reported here, they suggest that uranium can be used to determine oxygen concentrations at much higher concentrations than those shown in Fig. 1.

Possible Applications

Equations relevant to the following discussions have been derived in the appendix. The parameters considered are: the relevant weight of sodium (W_{Na}), the initial weight of oxygen dissolved (W_o^I), the area of the uranium specimens used (A), and its weight gain (ΔW_o), the time t during which the uranium was immersed in the sodium, and the rate constant or mass-transfer coefficient k.

The dimensionless parameter

$$\varphi = Akt/W_{Na} \tag{1}$$

determines the possible applications of this method. The basic equation used is

$$\Delta W = W_o^I [1 - \exp(-\varphi)], \tag{2}$$

and an accuracy of 95% will be assumed.

Three cases are considered: (a) $\varphi < 0.5$, (b) $0.5 < \varphi < 3$, (c) $\varphi > 3$. Case (a) refers to conditions in which the change in the oxygen concentration resulting from the oxygen taken up by the uranium is negligible compared to the total amount of oxygen present; case (b) refers to conditions in which changes in the oxygen concentration of a system are significant; case (c) refers to those conditions in which the uranium extracts up to 95% of the oxygen originally present. It should be noted that a system could be changed from case (a) to (c) on changing φ by a factor of 6.

Case (a): Large Systems. In large systems the application of this method will require a knowledge of the value of k and the relevant equation is given by Eq. 11A in the appendix, which can be expressed as

$$R = kC \ \mu g/cm^2\text{-hr}.$$

The value of k may be obtained by knowing the oxygen concentration in one instance. If the oxygen concentration cannot be determined or the value of k roughly calculated, the method may be used to determine relative changes in oxygen concentration. Under conditions of case (a) the time of specimen is immersed should not influence the results except for very long periods when either spalling of the oxide results or case (a) is no longer applicable. Changes in the surface area should also have no effect when these changes do not influence the geometry and the value of the mass-transfer coefficient k. For this reason it may be necessary in systems of unusual geometry to standardize on the surface area and all other factors which would be expected to influence the mass-transfer coefficient, such as velocity or positioning of the uranium test specimens.

Case (b): Intermediate Systems. In this case Eq. 2 must be used. Nevertheless, if the same values of A, W_{Na}, k, and t are used to standardize the variables which influence the method, the weight gain is then proportional to the oxygen present prior to the determination:

$$\Delta W = K \frac{W_o^I}{W_{Na}} = KC_I,$$

where

$$K = \frac{1}{W_{Na}} [1 - \exp(-\varphi)]. \tag{3}$$

The oxygen concentration after testing (C_F) will be given by

$$C_F = \frac{W_o^I - \Delta W}{W_{Na}}. \tag{4}$$

This case also suggests a simple method for determining the value of k and C_I when two successive gettering steps are employed and all other conditions are standardized. If ΔW_1 and ΔW_2 are the weight gains observed, then, from Eq. 2 for the first getting,

$$\Delta W_1 = W_o^I [1 - \exp(-\varphi)]$$

and

$$\Delta W_2 = (W_o^I - \Delta W_1)[1 - \exp(-\varphi)] \tag{5}$$

for the second gettering step. Then

$$W_o^I = \frac{\Delta W_1^2}{\Delta W_1 - \Delta W_2}. \tag{6}$$

From the now known value of W_o^I the value of k can be determined from Eq. (1) and (2).

In systems in which case (b) applied it is possible to obtain the overall mass-transfer coefficient for a complicated geometry which either cannot be calculated or

TABLE 2. APPLICATION

Case	Applicable Equation	Value of ϕ, % Accuracy	Parameter Standardized of	Application
a	$\frac{\Delta W}{A t} = k \frac{W_o}{W_{Na}}$	<0.5	k	Determine oxygen concentration in reactor systems and k when oxygen concentration is known.
b	Rate = k (concentration) $\Delta W = W_I \left(1 - \exp \frac{-Akt}{W_{Na}}\right)$	$0.5 < \phi < 3$	A,k,tW_{Na}	Determine oxygen concentration. Oxygen chemistry studied. Determine mass-transfer coefficients.
c	Rate = K (concentration) $\Delta W = W_I$	>3		Sodium purification (hot traps). Determination of oxygen concentration.

in which calculations require experimental confirmation.

Case (c): Small Systems. When the system is small, the uranium getters 95 % or more of the oxygen present in the sodium. Specifically, only one condition will be considered here, viz., a large area A and other conditions are such that case (c) still applies.

When a large surface area of uranium is present in a system, the uranium will act as a highly efficient hot trap. The temperature of the hot trap need only be 500°C, which may be advantageous. The uranium replaces zirconium, which normally requires preheating of the sodium to a temperature in the neighborhood of 650°C. The calculations of the most economic size of a uranium hot trap would be very much simpler than one containing zirconium, as the variation of rate of oxygen gettering by zirconium will depend on its previous history. However, the possibility of the spalling of the uranium oxide formed must also be considered in a reactor coolant; such spallation would be a major disadvantage to the use of uranium hot traps under these conditions.

Conclusions

1) The rate at which uranium getters oxygen from sodium is proportional to the concentration of oxygen in sodium.

2) This method has a number of possible applications which are given in Table 2, and may be summarized as

a. a rapid method for the determination of oxygen concentrations in sodium;
b. a method for determining mass-transfer coefficients of oxygen in sodium;
c. a process for studying the chemistry of sodium systems.

Acknowledgments

The author wishes to thank D. H. Gurinsky, under whose general direction this work was carried out, and J. R. Weeks for their helpful council. Thanks are also due to W. W. Becker and J. C. Spira for their assistance, R. F. Doering for preparing the sodium oxide, J. Sadofsky for the electron microprobe analysis, and L. Newman and coworkers for the chemical analysis.

Appendix

It was observed that when uranium was inserted in sodium with an immersed electrochemical oxygen meter the potential E of the meter at constant temperature increased linearly with time t, i.e.,

$$\frac{dE}{dt} = \text{const} = K_1. \tag{1A}$$

The potential may be expressed as

$$E = E_o + \alpha \ln \frac{1}{C}, \tag{2A}$$

where E_o is a constant, and it is assumed that α is independent of concentration C at constant temperature.

Substitution of (2A) in (1A) gives

$$-\frac{dC}{dt} = \frac{1}{\alpha} C K_1, \tag{3A}$$

in which the change in concentration of oxygen results from the gettering action of uranium.

The concentration may be assumed to be given by $C = W_o/W_{Na}$, where W_o is the weight of oxygen dissolved in sodium and W_{Na} is the weight of sodium in which the weight of oxygen is considered to be dissolved.

The rate of gettering of oxygen (dW_o/dt) is considered to be proportional to the weight of oxygen dissolved in sodium, the surface area A of the uranium, and inversely proportional to the weight of sodium:

$$-\frac{dW_o}{W_{Na}} = k \frac{W_o A}{W_{Na}}. \tag{4A}$$

Integration of Eq. (4A) between $W_o = W_o^I$ at $t = 0$ to $W_o = W_o$ at $t = t$ gives

$$-\ln \left(\frac{W_o}{W_o^I}\right) = \frac{kA}{W_{Na}} t, \tag{5A}$$

which may be expressed as

$$\Delta W = W_o^I\left(1 - \exp\left\{-\frac{kA}{W_{Na}}t\right\}\right), \qquad (6A)$$

where

$$\Delta W = W_o^I - W_o \qquad (7A)$$

and ΔW is the oxygen reacted with uranium.

Equation (6A) can be expanded to

$$\Delta W = W_o^I\left\{\frac{kA}{W_{Na}}t - \frac{1}{2}\left(\frac{kA}{W_{Na}}t\right)^2 + \frac{1}{6}\left(\frac{kA}{W_{Na}}t\right)^3 + \cdots\right\}. \qquad (8A)$$

If kAt/W_{Na} is sufficiently small so that only the first term in Eq. (2A) need be considered, then

$$\Delta W = W_o^I kAt/W_{Na} \qquad (9A)$$

or

$$\frac{\Delta W}{tA} = k\frac{W_o}{W_{Na}}, \qquad (10A)$$

i.e., rate of uptake per unit area $= R = kC$. (11A)

If the value of the exponent in Eq. (6A) is large, then

$$\Delta W = W_o. \qquad (12A)$$

REFERENCES

1. J. H. Stang, E. M. Simons, J. W. DeMastry, and J. M. Genco, *Compatibility of Liquid and Vapor Alkali Metals with Construction Materials*, DMIC Report 227 (April 1966).
2. C. Tyzack, *Symposium on Advances in Materials*, Inst. Chem. Eng., p. 151, Pergamon Press (1966).
3. H. S. Isaacs, unpublished.
4. H. S. Isaacs, B. Minushkin, and F. J. Salzano, THIS CONFERENCE.
5. M. H. Cornett, *Metallography of Uranium: Procedure and Standards*, NLCO-954 (March 1966).

Discussion

Mr. Cheng (ANL): Have you correlated results of your method of determining oxygen against sodium oxide solubility?

Mr. Isaacs: No, because at high oxygen concentrations and for reasonable periods of time the actual oxide breaks down. The oxygen breakdown—that means that we no longer have an adherent oxide layer—results from a number of causes. The method cannot be used at low temperatures; in fact, the higher the temperature the better. There also is the chance that the oxide might spall off at high concentrations, because one gets tremendous thicknesses. We've measured it up to about 40 microns, and it still didn't show any deviations from the expected behavior. But we haven't really tried that, and I wouldn't say that it would work at extremely high concentrations, let's say about 500 ppm.

Mr. Feder (ANL): Why is material being chosen that forms a film of oxide rather than a soluble oxide, which would not create this difficulty?

Mr. Isaacs: It doesn't really create a difficulty; it facilitates the measurements. This work actually developed from our studies of oxygen chemistry using the oxygen meter. If one wants to extract a certain amount of oxygen, it is more simple if one can just put a tab into the sodium, reweigh it afterwards, and correlate that with the amount of oxygen that had been extracted. If one actually puts the soluble getter in, one is changing the chemistry of the system, and this is not advantageous.

Mr. Feder: I'm sorry I did not make myself clear. I had not meant a soluble getter, but a solid metal in which the oxide is soluble, such as titanium, and which still allows itself to be weighed, of course.

Mr. Isaacs: Well, the major advantage of using uranium in this case is that the rate is so extremely high. If one tries to use titanium or zirconium at 500°C, the times that are required to make the measurements are extremely large. Also, there is no direct relationship between oxygen concentration and the uptake of oxygen by any of the refractory metals. It's extremely surprising that uranium can be used in this way, and it indicates that there are tremendous diffusion coefficients in the oxide that is formed.

Mr. Jansson (W): I'd like to comment on the question of the break which Dr. Minushkin found in comparison to these results. Uranium is a very strong oxide former. It is so strong that it will take the oxygen from whatever species in which it exists. It is therefore something which measures the availability, which is the concentration available in the vicinity of the specimen. It therefore says that, in this case, the actual concentration of oxygen follows a sort of straight line, an extrapolation of the high-concentration curve. But, of course, the oxygen meter measures the activity or chemical potential for oxygen, and a break like that could be explained if you consider an interaction in the sodium between oxygen and, for example, hydrogen. That would give exactly this type of behavior. One more thing about uranium oxidation. You said that this points at a very high diffusion rate. I'd like to suggest that this probably isn't diffusion rate, but that the uranium oxide that forms is extremely porous and does not form a continuous film.

Mr. Isaacs: Your argument about the porous film is not really applicable here as it is in the case of gaseous corrosion environments. In this case, if there were empty pores when the specimen was extracted from the sodium, it would mean that the sodium hadn't pene-

trated the pores. If it had penetrated the pores and had been squeezed out, I would imagine that the surface was still wetted. That answers your second point.

In reply to your first point, we had hydrogen present in one case, but didn't see any major break (at 500°C). If the hydrogen is associated with the oxygen it doesn't change the diffusion coefficient very markedly.

Mr. Jansson: With your technique, the gettering rate would not be affected by the presence of any interacting element in the sodium. As for the uranium oxide again, did you look at the oxide as it forms?

Mr. Isaacs: Let me say that one can use about three or four different methods of calibrating oxygen. If one uses uranium at that particular potential where the two curves intersect, there is no indication at all that there is a break in the curve. If one uses uranium methods to calibrate, standardizing on conditions and using a given mass-transfer coefficient, then there is no break in the curve at that point at all. The actual break that we get results from the method that we are using to calibrate. We are not using concentrations as we would like to do; we are using a mass balance. If there is any deviation in the actual amount that is taken out and if this isn't reflected in changes in concentration, then we would expect to get these breaks. This is what we believe is happening.

Mr. Jansson: I think there could be several reasons. About the uranium oxide—did you look at it; does it perhaps crack open and expose new surface all the time; does the oxide stay on?

Mr. Isaacs: The actual film is fully adherent. It reveals whatever surface one had in the metal—one is actually just forming a replica of the metal with the oxide. The oxide does look slightly columnar, which might suggest that there were pores in it, but really I don't think that penetration of these pores by sodium is very likely.

Oxygen Transport in Sodium*

CHARLES C. McPHEETERS AND JOHN C. BIERY

Los Alamos Scientific Laboratory
Los Alamos, New Mexico

(PRESENTED BY C. C. McPHEETERS)

1. Introduction

Cold traps for removal of impurities from large sodium systems must be designed to provide adequate rates of system cleanup and impurity-holding capacity, and be of the simplest and least expensive design that will meet the requirements of the system. An understanding of the mechanisms of impurity collection and the rates of mass transfer of impurities to cold traps is required for intelligent design of cold traps. The purpose of this phase of the study was to determine overall mass-transfer coefficients for the collection of oxygen in a cold trap of simple geometry and the effects of Reynolds number, temperature, and concentration on the mass-transfer coefficient as calculated with use of a suitable mathematical model.

With an accurate understanding of the mechanism of deposition of a given impurity (oxygen, in particular) in cold traps and the mass-transfer coefficients involved, the rate of cleanup of a sodium system can be predicted. Disposition of the deposited oxide can be predicted as a function of the stage of the cleanup operation, and adequate volumes can be provided to prevent plugging of the cold trap during all phases of the cleanup. Also, system operating procedures can be established with use of the rate data to provide optimum programs for cold trapping.

2. Mathematical Model

A mathematical model to simulate the operation of a cold trap must begin with some assumptions concerning the mechanisms involved. If it is assumed that oxide crystals nucleate and grow in the liquid phase independent of solid surfaces, the mathematical analysis must include nucleation and growth rates as a function of temperature and agitation. Stokes' law is utilized to determine the smallest particle size that will settle to the bottom. Filtration is then used to remove smaller particles from the exit stream. The expected distribution of particle size is estimated and this information used to calculate the oxide-removal rate.

However, early cold-trap designs based on this assumption of liquid-phase nucleation and growth were unsuccessful.[1-3] In general, plugging occurred in entrance regions where the sodium passed through small annuli or in filters designed to retain suspended particles. It would appear, then, that liquid-phase nucleation and growth is not the only possible mechanism for impurity precipitation.

Based on experience at Los Alamos Scientific Laboratory and of others[1-4] concerning plugging of cold traps and ordinary piping with oxide, oxide deposition appears to involve mainly the nucleation and growth of crystals on cool solid surfaces, i.e., cold-trap walls and packing or pipe walls. A mathematical model can be developed from this assumption by postulating the growth of crystals from solution on solid surfaces to proceed at a rate proportional to the degree of supersaturation of the liquid, the crystal surface area, and a mass-transfer coefficient or proportionality constant. This rate of growth is expressed by

$$\frac{dm}{dt} = kaA(C - C_e), \qquad (1)$$

where m is mass of oxygen in pounds, t is time in hours, k is the mass-transfer coefficient in units of lb O/ft^2-hr-ppm, a is the surface area of the precipitate per unit area of cold-trap surface, A is the cold-trap surface area in ft^2, C is the concentration of oxygen in the sodium, and C_e is the saturation concentration at the temperature of the crystal. Crystal growth rate is assumed to be reversible. If C is less than C_e, the crystal will dissolve according to the same equation.

For a computer analysis of the cold trap by means of eq. 1, the cold trap is divided into a number of equal segments. Equation 1 is modified to

$$\Delta m_i = (ka)_i A_i (C_i - C_{e_i}) \Delta t, \qquad (2)$$

where Δm_i is the amount of oxygen deposited in the ith segment during a finite time step Δt. The time step is that time required to transfer the sodium from one segment to the adjoining downstream segment. The saturation concentration in segment i, C_{e_i}, is determined from the solubility curve[5] and the wall temperature of the ith segment, which is calculated from bulk sodium temperature data. Oxygen concentration in the ith segment, C_i, is taken as the concentration in segment $(i - 1)$ minus the amount of "concentration"

* Work performed under the auspices of the U. S. Atomic Energy Commission.

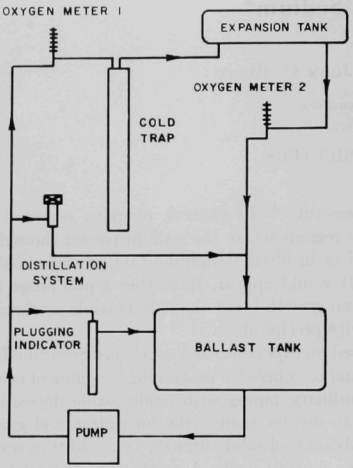

FIG. 1. Simplified Flow Diagram of Cold-trap Test Loop.

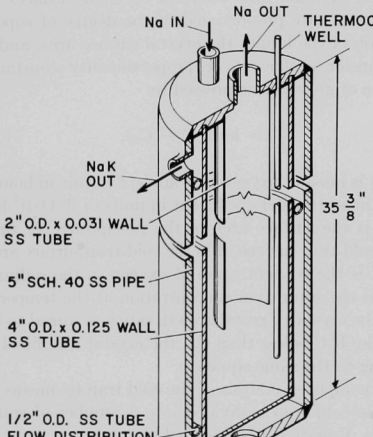

FIG. 2. First Packless Cold-trap Design.

equivalent to the mass deposited in segment $(i - 1)$. The mass of oxygen deposited in each segment is stored in computer memory. If the bulk sodium concentration C_i falls below C_{e_i} in the warmer segments of the cold trap, the deposited oxide dissolves according to eq. 2 until no more oxide remains on the wall.

Some fraction (called the mixing factor) of sodium leaving the cold trap is mixed with sodium in the system. (Experimental runs indicated that the system was very poorly mixed in most cases.) The computer program output includes bulk system oxygen concentration as a function of time. Experimental measurements also consist of oxygen concentration as a function of time.

3. Experimental Procedure

Figure 1 is a simplified flow diagram of the cold-trap test loop. The loop is a 60-gal, forced-convection, isothermal sodium system on which three types of analytical devices are installed. These include a vacuum distillation system, UNC oxygen meters,[6] and a plugging meter. The plugging meter was operated in the partially plugged mode[7] so that some solid or crystalline impurity material was kept in equilibrium with the impurities in solution. An equilibrium temperature is determined rather than a normal plugging temperature, which can be affected by operating parameters, orifice geometry, and by nucleation and growth difficulties in the plugging orifice.

The cold trap used in this series of runs is shown in Fig. 2. This line drawing illustrates the packless, regenerative type of cold trap which was used because of the relative simplicity with which the flow patterns and surface areas could be simulated mathematically. Sodium flow proceeded down the annular space and up the central tube. Cooling was accomplished by NaK flow into the bottom and up the outer annulus. The NaK heat was dumped to air.

Cold-trap runs were initiated by rapidly changing the initial cold-trap temperature to the run temperature. Oxygen concentration was measured at approximately 30-min intervals until 80 to 90 % of the total change had taken place. Both dissolution and precipitation runs were made. Cold-trapping runs were made at sodium flow rates from 0.25 to 1.5 gpm. Cold-trap temperatures from 120 to 180°C were tested for precipitation runs, and from 160 to 210°C for dissolution runs.

Oxygen concentrations were converted to dimensionless or fractional concentrations, $(C - C_e)/(C_0 - C_e)$, where C is the system oxygen concentration at any time, C_e is the final or equilibrium concentration, and C_0 is the initial concentration. The log of dimensionless concentration was plotted vs time for each run.

Figure 3 shows a typical cold-trap run. In this case (Run 1–20), C_0 was 10.1 ppm and C_e 3.6 ppm. The circles in the figure are concentration data determined with the plugging indicator and the Rutkauskas oxygen-solubility curve,[5] and the line represents the computer simulation. In this run, as in approximately one-third of all the runs, an oxygen concentration spike was detected after some period of cold trapping. These concentration spikes were attributed to oxide breakaway in

the packless cold trap. The oxide particles which were carried into the higher-temperature system dissolved and caused an increase in the oxygen concentration.

Cold-trap run data including cold-trap temperatures, sodium flow rate, NaK flow rate, NaK and sodium inlet temperatures, expected tank-mixing factor, and the value of dimensionless concentration at a specific time were put into the computer program. Through an iterative scheme, the mass-transfer coefficient ka was varied until the simulated dimensionless concentration fit the experimental value at the specified time. In this manner, the value of ka was determined, and the entire cold-trap run was simulated.

4. Results and Discussion

A total of 16 runs was made to determine the effect of sodium velocity (or Reynolds number) and temperature on the mass-transfer coefficient. The run conditions and the calculated mass-transfer coefficient for each run are shown in Table 1.

4.1. Velocity Effect

The effect of Reynolds number Re on the calculated overall mass transfer coefficient is shown in Fig. 4. The open circles are the data points from precipitation runs; the solid circles are data from dissolution runs. In general, the mass-transfer coefficient increases proportionally to the first power of the Reynolds number up to $Re \simeq 1200$. At that point, a discontinuity occurs and the mass-transfer coefficient increases greatly. The first-power relationship between k and the Reynolds number would not be expected in the laminar range. In turbulent flow, the relationship should involve approximately the 0.8 power of the Reynolds number. This first-power increase with Reynolds number is thought to be due to a certain amount of mixing or cross flow in the cold trap due to poor entrance conditions. Sodium enters the cold

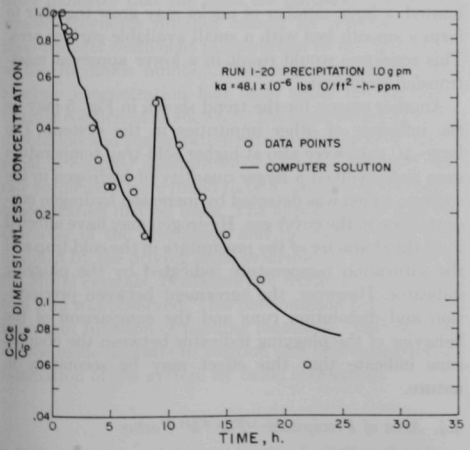

FIG. 3. Precipitation Runs Number 1-20 Showing an Oxygen Concentration Spike.

TABLE 1. SUMMARY OF COLD-TRAP RUNS

Run No.	Minimum Cold-trap Temp (°C)	Type of Run	Sodium Flow Rate (gpm)	Calculated Mass-transfer Coefficient, (lb O/ft²-hr-ppm) × 10^6
1-18	182	Precipitation	1.5	131
1-19	208	Dissolution	1.5	281
1-20	168	Precipitation	1.0	48
1-21	212	Dissolution	1.0	55
1-22	168	Precipitation	0.5	24
1-23	210	Dissolution	0.5	23
1-24	170	Precipitation	0.25	13.5
1-25	211	Dissolution	0.25	9.9
1-26	149	Precipitation	0.5	13.5
1-27	203	Dissolution	0.5	22.5
1-28	130	Precipitation	0.5	23.8
1-29	180	Dissolution	0.5	27.7
1-30	122	Precipitation	0.5	44.6
1-31	122	Precipitation	0.5	39.6
1-34	121	Precipitation	0.5	47.4
1-35	160	Dissolution	0.5	35.0

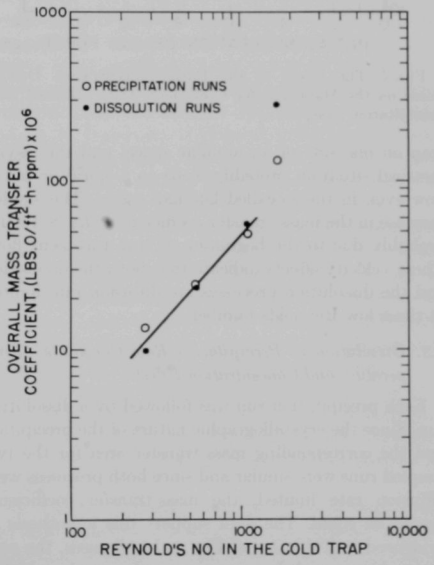

FIG. 4. The Effect of Reynolds Number on the Overall Mass-transfer Coefficient.

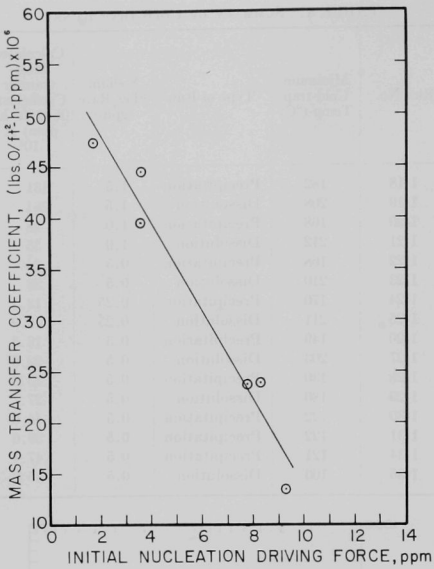

FIG. 5. The Effect of the Initial-concentration Driving Force on the Mass-transfer Coefficient. Data obtained from precipitation runs.

trap on one side of an annular space, and this asymmetrical situation probably leads to a spiral or mixed flow even in the so-called laminar region. The sudden increase in the mass-transfer coefficient at $Re \simeq 1600$ is probably due to the beginning of true turbulent flow. These velocity effects indicate that both the deposition and the dissolution processes are diffusion rate limited at these low Reynolds numbers.

4.2. Dissolution vs Precipitation Rate Constants—Temperature and Concentration Effect

Each precipitation run was followed by a dissolution run. Since the crystallographic nature of the precipitate and the corresponding mass-transfer area for the two coupled runs were similar and since both processes were diffusion rate limited, the mass-transfer coefficients should be equal. The data support this hypothesis as evidenced in Table 1 and Fig. 4. In all cases, the constants from coupled runs were nearly equal or highly correlated. No trend was established as to which constant was bigger if a difference occurred. The dissolution constant was larger in four cases and smaller in four other runs. This result also implies that there is little if any temperature or absolute concentration effect since the cold-trap temperatures and equilibrium concentrations for the coupled runs were significantly different.

Good agreement between mass-transfer coefficients calculated from precipitation and dissolution runs also supports the initial assumption of nucleation and growth of crystals only on solid surfaces. This agreement implies that the same mechanism is operative for both processes. It is highly probable that the mechanism in effect during the dissolution process is the dissolving of solid crystals and the diffusion of the material into the moving fluid stream. Therefore, with the agreement of mass-transfer coefficients the reverse process would be expected during precipitation runs, i.e., diffusion through a stagnant film and deposition of the material on crystals growing on the solid surface. If homogenous nucleation occurred significantly, a higher precipitation mass-transfer coefficient would be found in the event that the particles settled to the bottom of the trap, and a lower mass-transfer coefficient if the particles were carried back into the system. It is, therefore, concluded that for the conditions studied homogenous nucleation is insignificant in comparison to heterogeneous nucleation on solid surfaces.

4.3. Initial Concentration-difference Effect

In Fig. 5 are plotted the mass-transfer coefficients ka from the 0.5-gpm runs vs the concentration driving force at the beginning of the precipitation run. The plot clearly show an effect of increasing rate constant with decreasing initial ΔC. The reason for the effect is not clear. However, the influence of the initial driving force may be its effect on the number of crystals initially nucleated on the cold trap surface. The larger the ΔC, the larger is the number of crystals nucleated. However, since the area for lateral growth of the crystals is limited, a large number of nuclei may grow together to form a smooth bed with a small available surface area. This condition would result in a lower apparent mass-transfer coefficient.

Another reason for the trend shown in Fig. 5 may be the influence of other impurities in the system. The large-ΔC runs were also at higher cold-trap temperature runs and involved a larger quantity of hydrogen in the sodium, which was detected by increased hydrogen concentration in the cover gas. Hydrogen may have affected both the character of the precipitate in the cold trap and the saturation temperature indicated by the plugging indicator. However, the agreement between precipitation and dissolution runs and the comparison of the behavior of the plugging indicator between the coupled runs indicate that this effect may be secondary in nature.

4.4. Area of Precipitate—The "a" Factor

As indicated above, the "a" factor, area of precipitate per unit area of trap, appears to be a function of the

operating condition. Additional evidence that the area of crystals can be affected by operations was shown when extended periods of time were allowed between the coupled precipitation and dissolution runs. In two runs previously reported,[4] in which this delay period occurred, the dissolution mass-transfer coefficients were significantly lower than those obtained from the corresponding precipitation runs at similar flow rates. The implication is that the crystals were given a chance to recrystallize and produce less area per unit cold-trap surface area. When the delay time was not allowed, as in the runs reported here, the k_a coefficients were comparable and no change in area occurred.

4.5. Precipitate Breakaway

The concentration spikes which were observed in many of the cold-trap runs were thought to be due to breakaway of oxide in the cold trap. This observation points out an important function of packing in cold traps. Wire mesh or Raschig ring packing can support the fragile crystals of oxide and prevent them from being carried back into the system. The extended surface area of packing material also provides many nucleation and growth sites for the depositing oxide, and it shortens the distance between oxygen in solution and the growing crystals.

5. Summary

The cold-trapping experiments indicated that increased Reynolds number had a profound effect on the rate of removal of oxygen from the system. This velocity effect indicates that the rates are diffusion limited. Increased Reynolds number caused an increase in the mass-transfer coefficient proportional to the first power of the Reynolds number. Cold-trap temperature and absolute concentration had little effect on the mass-transfer coefficient as shown by the observation that the dissolution and precipitation rate constants were nearly equal in coupled constant-velocity runs. However, the rate coefficients were found to be a function of the initial concentration driving force. The implication is that the character of the precipitate and its specific area were modified by the driving force available for nucleation of the initial crystals. Breakaway of oxide deposits in the cold trap was observed. This phenomenon points out an important function of packing materials—that of holding the oxide deposits in position and preventing recontamination of the system by oxide breakaway.

REFERENCES

1. McDonald, J. S., *Analysis of Results of a Sodium Cold Trap Experiment*, NAA-SR-6801 (July 30, 1962).
2. I. J. Gray, R. J. Neal, and B. G. Voorhees, "Control of Oxygen in Sodium Heat Transfer Systems," in *Liquid Metal Technology*, Part I, Vol. 53, (1957).
3. J. A. Bray, "Experience on the Removal of Impurities From Liquid Metal Systems by Cold Trapping," *European Atomic Energy Society Symposium on Liquid Metals*, (Sept 1963).
4. McPheeters, C. C., *Mass Transfer of Oxygen in Sodium Cold Traps*, LA-3936 (May 1968).
5. Rutkauskas, V. J., *Determination of the Solubility of Oxygen in Sodium Using the Vacuum Distillation Analytical Techniques*, LA-3879-MS (1968).
6. Minushkin, B., and Kolodney, M., *Development of a Continuous Electrochemical Meter for Oxygen in Sodium*, UNC-5131 (Dec 1967).
7. McPheeters, C. C., and Biery, J. C., *The Dynamic Characteristics of a Plugging Indicator for Sodium*, Accepted for publication in Nuclear Applications (1968).

Discussion

Mr. Epstein (ANL): I'd like to congratulate Dr. McPheeters on this study, which has been badly needed for a long, long time. Cold-trap design has been something of an empirical art, and up until now we have had very little data of this kind. I'd like to make two comments about your observation that the kinetics of precipitation and of solution appear to check. This immediately suggests that phenomena of supersaturation, on which a lot of people have speculated, do not occur to any very great extent. Your observation of this checks a statement that was made by the Russians, specifically Prof. M. N. Ivanovsky of Obninsk at the Vienna Alkali Metals Meeting, about two years ago. He said he got the same results, namely, that the two rates were the same, indicating no evidence of supersaturation.

Mr. Feder (ANL): It's amazing how different people can look at the same data and come to different conclusions. I would, perhaps mistakenly, have hastened to the conclusion that since you did not see homogeneous nucleation, supersaturation was indeed an important phenomenon, and that it was only heterogeneous nucleation you saw because its rate was controlling.

Mr. McPheeters: I thought the same thing when Dr. Epstein started talking. Since we do get only heterogeneous nucleation, I would expect large supersaturations in some cases. You could have large undersaturations as well during dissolution.

Mr. Epstein: I simply remarked that if there were very large amounts of supersaturation this would lead to a difference between the rate of solution and the rate of deposition.

Mr. McPheeters: Not necessarily. You could have large undersaturations as well as large supersaturations, so the concentration driving force could be the same.

Mr. Biery (LASL): Actually there is confusion here. The rates are not the same; it is the mass-transfer coefficient that is the same for these processes. That is the more critical part—that you have different driving

forces. Certainly in this case you must have supersaturation for the precipitation process to occur.

Mr. Lemke (DuPont): It seems to me that yesterday I heard a paper in which someone pointed out that plugging indicators didn't tend to work very well until you had an initial deposit on the plug. This would seem to me to indicate that there must be supersaturation in a nice clean system. I don't see how you can avoid it.

Mr. McPheeters: Yes, I certainly think supersaturation occurs.

Calculated Hydrogen-Oxygen Equilibria in Liquid Sodium

PETER VILINSKAS

Argonne National Laboratory
Argonne, Illinois

1. Introduction

The hydrogen and oxygen in sodium solution may react to form the hydroxide. There is some experimental evidence[1, 2] that supports such a hypothesis. In addition, it is possible to predict and calculate the extent of such a reaction by the use of chemical thermodynamics. It follows that it is quite possible that the hydroxide in sodium figures quite prominently in the corrosive properties of sodium metal and that perhaps the discrepancies in the solubility data for hydrogen[3-6] and for oxygen[7] in sodium can be related to hydroxide formation. Further, the difficulties encountered with the use and calibration of in-line instruments in large sodium systems are sometimes also being ascribed to hydroxide formation.[8, 9]

The purposes of this paper are to present the results of the thermodynamic calculation for the hydrogen-oxygen equilibria in sodium, and to consider and predict some of the effects of this equilibria on measurements of hydrogen and oxygen solubility and the output of some in-line instruments.

2. Calculated Equilibrium Constant

The following equation formed the basis of the calculation:

$$NaOH(c) + Na(c) \rightleftarrows Na_2O(c) + \tfrac{1}{2}\,H_2(g). \quad (1)$$

The decomposition products of this reaction are assumed to be sodium oxide and hydrogen gas, even though at times the actual reaction probably goes to form the sodium hydride which then decomposes to give the hydrogen gas. The hydrogen gas in this system is assumed to be in equilibrium with the sodium hydride in solution, and therefore eq. (1), whether written with sodium hydride or hydrogen gas as the decomposition product, can be shown to be equivalent for our purposes. It is further assumed that an excess of sodium metal is always present, and therefore the equilibrium hydrogen pressure cannot ever exceed the measured dissociation pressure of the sodium hydride.

Equation (1) has been written for the equilibria at 298°K. At higher temperatures it is modified to take into account phase transformations such as the melting of sodium, the α to β sodium hydroxide transformation, and the melting of sodium hydroxide.

The equilibrium calculation was carried out with a computer. The following equation[10] formed the basis for the calculation:

$$\int_{K_1}^{K_2} d \ln K = \int_{T_1}^{T_2} \frac{\Delta H}{RT^2} dT, \quad (2)$$

where K is the equilibrium constant of the reaction given by eq. (1), ΔH is the enthalpy of the reaction expressed as a function of temperature T, and R is the gas constant. The change in enthalpy with temperature data were taken from a compilation by Kelly,[11] and the standard free energy and enthalpy data were taken from the Liquid Metals Handbook.[12] Table 1 lists the results of the thermodynamic calculation.

3. Discussion

3.1. Effect of Hydroxide Formation on Solubility Measurements of Sodium Oxide and Hydrogen Gas in Sodium.

The equilibrium constant for eq. (1) is defined by

$$K = \frac{A_{Na_2O} A_{H_2}^{1/2}}{A_{Na} A_{NaOH}}, \quad (3)$$

where A is the activity. Since the activity of sodium is unity and the activity of hydrogen gas is represented by its partial pressure,

$$K = \frac{A_{Na_2O}}{A_{NaOH}} P_{H_2}^{1/2}. \quad (4)$$

We may derive expressions which can be used to determine the effect of hydroxide formation on the solubility measurements. Let

C_{OH} = Concentration of the hydroxide in sodium solution expressed in mols/liter;
C_O = Concentration of the oxide in sodium solution expressed in mols/liter;
$C_{(O+OH)}$ = Concentration of the oxide plus the hydroxide;
$C_{(H+OH)}$ = Concentration of the hydride plus the hydroxide;
γ_{OH}, γ_O = The activity coefficient of the hydroxide and oxide, respectively.

Substituting concentrations and activity coefficients for activities in eq. (4) we obtain

$$K = \frac{C_O \gamma_O}{C_{OH} \gamma_{OH}} P_{H_2}^{1/2}; \quad (5)$$

$$K\frac{\gamma_{OH}}{\gamma_O} = \frac{[C_{O+OH} - C_{OH}]}{C_{OH}} P_{H_2}^{1/2}; \quad (6)$$

$$\frac{K(\gamma_{OH}/\gamma_O)}{P_{H_2}^{1/2}} = \frac{C_{(O+OH)}}{C_{OH}} - 1; \quad (7)$$

$$\frac{C_{OH}}{C_{(O+OH)}} = \frac{1}{1 + K(\gamma_{OH}/\gamma_O)P_{H_2}^{1/2}}. \quad (8)$$

If we multiply eq. (8) by $C_{(O+OH)}/C_{(H+OH)}$ we obtain

$$\frac{C_{OH}}{C_{(H+OH)}} = \frac{C_{(O+OH)}}{C_{(H+OH)}}\left[\frac{1}{1 + K(\gamma_{OH}/\gamma_O)P_{H_2}^{1/2}}\right]. \quad (9)$$

Likewise, the oxide content as a mol fraction of the total oxygen is given by

$$\frac{C_O}{C_{(O+OH)}} = \frac{1}{1 + P_{H_2}^{1/2}(\gamma_O/\gamma_{OH})K}. \quad (10)$$

If we assume some residual oxygen concentration in sodium, the error associated with the terminal hydrogen-solubility measurement if the hydroxide formation is ignored can be estimated using eq. (9). Table 2 gives such an estimate for several different oxygen concentrations. It has been assumed that for the low total oxygen concentrations $\gamma_O = \gamma_{OH} = 1$.

If we assume some residual hydrogen concentration in sodium, the error associated with measurements of sodium oxide solubility if the formation of hydride is ignored can be estimated using eq. (8). Table 3 gives such an estimate for several hydrogen activity levels (as represented by the partial pressure of hydrogen). It should be noted that in this instance, unlike the case of measurements of hydrogen solubility, Table 3 at best represents an estimate only, since at, or near, oxygen saturation γ_O and γ_{OH} do not equal unity. The given estimates are good if, however, $\gamma_O = \gamma_{OH}$.

TABLE 1. Calculated Results for the Equilibrium Given by Equation (1)

Temp, °C	ΔF, cal	K, atm$^{1/2}$	K^2, atm
50	572	0.411	0.169
98	444	0.548	0.300
100	442	0.551	0.304
150	378	0.638	0.407
200	307	0.722	0.521
250	232	0.800	0.640
293	169	0.860	0.740
300	178	0.855	0.731
305	185	0.852	0.725
319	203	0.841	0.708
350	326	0.769	0.591
400	528	0.674	0.454
450	735	0.600	0.360
500	944	0.541	0.293
550	1154	0.494	0.244
600	1364	0.456	0.208
650	1573	0.424	0.180
700	1779	0.398	0.159
750	1983	0.377	0.142

TABLE 2. Mol Percent Hydroxide of the Total Hydrogen in Sodium for Given Oxygen Concentrations

Mol Percent Hydroxide at Selected Oxygen Concentrations (ppm by weight)

Temp, °C	5 ppm	10 ppm	20 ppm	50 ppm	100 ppm
200	1.03	2.05	4.10	10.3	20.5
300	0.331	0.664	1.33	3.32	6.64
350	0.141	0.282	0.56	1.41	2.82
400	0.0434	0.0868	0.18	0.435	0.868
450	0.0106	0.0212	0.042	0.106	0.212

3.2. Stability of Sodium Hydroxide as a Separate Phase in the Presence of Sodium.

In a sodium system that is saturated with sodium oxide, $A_O = \gamma_O C_O^s = 1$, where C_O^s is the saturated concentration (solubility) of the oxide in sodium. Therefore $\gamma_O = 1/C_O^s$; likewise, $\gamma_{OH} = 1/C_{OH}^s$, where C_{OH}^s is the solubility of sodium hydroxide in sodium. The postulated solubility for the hydroxide will correspond to a physically measurable value only under conditions for which the hydroxide is stable in the presence of sodium metal.

Substituting these values into eq. (8) we obtain

$$\frac{C_{OH}}{C_{(O+OH)}} = \frac{1}{1 + \dfrac{K}{P_{H_2}^{1/2}}\dfrac{C_O^s}{C_{OH}^s}}; \quad (11)$$

$$\frac{1}{1 + \dfrac{C_O}{C_{OH}}} = \frac{1}{1 + \dfrac{K}{P_{H_2}^{1/2}}\dfrac{C_O^s}{C_{OH}^s}}; \quad (12)$$

$$\frac{C_O}{C_{OH}} = \frac{K}{P_{H_2}^{1/2}}\frac{C_O^s}{C_{OH}^s}. \quad (13)$$

Rearranging terms, we get

$$\frac{C_O}{C_O^s} = \frac{K}{P_{H_2}^{1/2}}\frac{C_{OH}}{C_{OH}^s}. \quad (14)$$

When $K/P_{H_2}^{1/2} = 1$, then $C_O/C_O^s = C_{OH}/C_{OH}^s$, and the actual concentrations equal the saturation concentrations. If $K/P_{H_2}^{1/2} > 1$, then C_{OH}/C_{OH}^s must be smaller than C_O/C_O^s to satisfy eq. (13). It follows that either $C_{OH} < C_{OH}^s$ or $C_O > C_O^s$, but since by definition C_O can only be equal to or less than C_O^s, then it must be that $C_{OH} < C_{OH}^s$ and the actual hydroxide concentration cannot reach saturation.

Likewise, if $K/P_{H_2}^{1/2} < 1$, then C_{OH}/C_{OH}^s must be greater than C_O/C_O^s. Therefore either $C_{OH} > C_{OH}^s$ or

$C_O < C_O^*$. Since by definition C_{OH} cannot be greater than the saturation value of C_{OH}^*, then it must be that $C_O < C_O^*$ and therefore the oxide cannot be brought up to saturation.

We must also take into consideration the formation of solid sodium hydride and thus assume that the hydrogen pressure in our system will not exceed the dissociation pressure of sodium hydride. By comparing the dissociation pressure of sodium hydride to K^2 (see Fig. 1), we may deduce that the system can be saturated with respect to the sodium oxide and hydroxide only at one temperature ($T = 400°C$; $P_{H_2} = 0.4$ atm) where $P_{NaH} = K^2$, and that below 400°C, $K^2 > P_{NaH}$, and the hydroxide cannot exist as a separate phase. Above 400°C, where $K^2 < P_{NaH}$, the sodium oxide cannot exist as a separate phase. The dissociation pressure of NaH was taken from the work by Keyes,[13] which agrees fairly well with work by others.[14]

It has been observed experimentally[1, 2] that a mixture of sodium hydroxide and sodium follows the dissociation pressure of sodium hydride up to a temperature of approximately 400°C at which a change in the slope of P_{H_2} vs. temperature is observed, indicating the formation of a new hydrogen-bearing compound (sodium hydroxide). This behavior is consistent with the calculation presented here (see Fig. 1).

3.3. Effect of Hydroxide Formation on the Calibration of In-line Instruments.

The in-line instruments that are currently in use, or are being tested, for impurity monitoring in large sodium systems consist of the plugging meter,[15] the electrochemical oxygen meter,[16] the electrical conductivity meter,[17] and the hydrogen chromatograph. The calibration procedure that is generally employed consists of a comparison of the meter output with the chemical analysis of a sample of sodium. The chemical analysis usually yields a measurement of total hydrogen and total oxygen, whereas the particular meter output is related proportionally and sometimes selectively to oxygen, hydrogen, and hydroxide concentrations. In addition, the analysis is usually performed with solid sodium at room temperature, whereas the instruments are usually read at about 300°C. Values from those two sources can be compared if it is known that significant change has not occurred in the hydroxide equilibrium and that segregation effects have been eliminated. Under the usual reactor operation conditions (~300°C and cold-trapped sodium) very little hydroxide will be present, as can be judged from Tables 2 and 3, and therefore the comparison of the sodium-instrument output and the chemical analysis is straightforward. The concentrations of oxygen and hydrogen in sodium above which the presence of the hydroxide should be taken into account may be determined from the following expressions:

TABLE 3. Mol Percent Hydroxide of the Total Oxygen in Sodium for Given Hydrogen Activity Levels (Assuming $\gamma_O = \gamma_{OH}$)

Mol Percent Hydroxide at Selected Hydrogen Pressures (ppm by vol.)

Temp, °C	$P_{H_2} = 10$ ppm	100	1,000	10,000	P_{NaH}
200	0.44	0.99	0.99	0.99	0.99
300	0.37	1.15	3.57	10.5	10.7
350	0.41	1.28	3.96	11.5	27.2
400	0.46	1.46	4.50	12.9	50.3
450	0.52	1.64	5.00	14.3	71.1

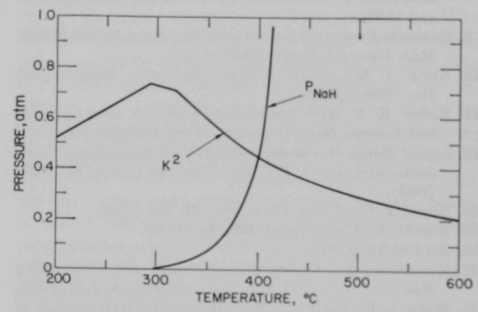

Fig. 1. Comparison of the Dissociation Pressure of Sodium Hydride (P_{NaH}) with the Equilibrium Constant Squared (K^2) for Reaction (1).

1. the plugging indicator should not be affected by hydroxide formation (see Sect. II.B);
2. the electrochemical oxygen meter by eq. (8);
3. the hydrogen chromatograph by a combination of eq. (9) and Sievert's Law:

$$C_{(H+OH)} = P_{H_2}^{1/2} K_H + \frac{C_{(O+OH)}}{1 + \frac{K}{P_{H_2}^{1/2}} \frac{\gamma_{OH}}{\gamma_O}}, \qquad (15)$$

where K_H is Sievert's law constant;

4. the electrical resistivity measurements by

$$\rho_T = \frac{C_{(O+OH)}}{\left(P_{H_2}^{1/2} + K \frac{\gamma_{OH}}{\gamma_O}\right)} \left(\rho_{OH} \rho_{H_2}^{1/2} + \rho_O K \frac{\gamma_{OH}}{\gamma_O}\right) + \rho_H K_H P_{H_2}^{1/2}, \qquad (16)$$

where ρ_T is the overall specific resistivity, and ρ_{OH}, ρ_O, and C_H are the specific resistivities of sodium due to hydroxide, oxide, and hydrogen in sodium.

REFERENCES

1. Williams, D. D., NRL Memo Report No. 33 (1952).
2. *Quarterly Technical Progress Report on AEC-Sponsored Activities, Sept. 15–Dec. 15,* APDA-195 (1966) p. 11.22.
3. Compare, E. L., and Savolainen, J. E., Nuc. Sci. Eng. **28** (1967).
4. Addison, C. C., Pulham, R. J., and Roy, R. J., J. Chem. Soc., 116 (1965).
5. McClure, D. W., and Halsey, G. D. Jr., J. Phys. Chem. **69,** 3542 (1965).
6. Williams, D. D., Grand, J. A., and Miller R. R., J. Phys. Chem. **61,** 379 (1957).
7. *Liquid Metals Handbook,* TID 5277 (July 1955), p. 8.
8. *Quarterly Technical Progress Report on AEC-Sponsored Activities, March 15–June 15,* APDA-206 (1967), p. 11.24 and 11.19.
9. *Quarterly Progress Report, April–May–June,* MSAR 67-213, MSA Research Corp. (1967) p. 34.
10. Klotz, I. M., *Chemical Thermodynamics,* Prentice-Hall Inc. (1958), p. 125.
11. Kelley, K. K. *High Temperature Enthalpy, Heat Capacity and Entropy Data,* Bureau of Mines Bulletin 584.
12. *Liquid Metals Handbook, Sodium NaK Supplement,* C. B. Jackson ed., 3rd ed., U. S. Atomic Energy Comm. TID-5277 (1955).
13. Keyes, F. G., J. Am. Chem. Soc. **34,** 779 (1912).
14. Harold, A., Compt. rend. **228,** 686 (1949).
15. See Ref. 12, p. 103.
16. Minushkin, B., *Electrochemical Oxygen Meter Operating Manual,* UNC-5113 *United Nuclear Corp.* (Aug. 31, 1965).
17. Blake, L. R., *Resistivity Meter to Indicate Oxide Content of Sodium,* Paper No. 3278M Institute of Electrical Engineers, August 1960.

Discussion

Mr. Jansson (W): I agree very much with your conclusions about the various relations and the general tendency that you are going to get with regard to the concentrations of hydroxide, oxide, and hydride and their species in solution. As for the treatment, I was surprised to see that you used in your first equation sodium hydroxide, sodium, sodium oxide, and hydrogen, because really this isn't right. Below 400°C you cannot have coexistence of sodium hydroxide, sodium, and sodium oxide. That was your final conclusion but I think that you could have arrived at this much sooner.

Mr. Vilinskas: Well, I didn't know whether that was going to be so or not. Basically what I've done is to write the equation for a reaction more or less as one would in freshman chemistry, and then see if it goes or not.

Mr. Jansson: This is an example, I think, of where it is dangerous to go in and take free energy values and expect to get the right results from such an approach. It has been done in several other cases too. You really have to go through the system and see what phases are going to be important; only then can you tell what the reactions are going to be. Do you agree with that?

Mr. Vilinskas: I certainly agree with you. Experimentation is the best thing.

Mr. Jansson: You really don't need experiments to do this. The free energy values themselves will tell you this right away if you just compare them.

Mr. Feder (ANL): Fortunately in this case there are very good experiments—the phase diagram study of the sodium hydroxide-sodium system by some Russian authors whose names at the moment I can't recall. [Ed. note: B. A. Shikhov, Russ. J. Inorg. Chem. **12,** 545 (1967)]. There are two papers which clearly delineate the phase diagram and you can tell at any given temperature or mixture what phases are present. I think this would be a more efficient starting point for any thermodynamic investigation.

Mr. Hill (APDA): I believe that the Russian article that you are referring to is that by V. I. Subbotin *et al.* (P/461)—his Vienna paper. I recommend that everyone that is interested in hydrogen-oxygen equilibria study it, because it is one of the finest pieces of experimental evidence of what really does happen in the sodium oxide and hydrogen system.

Some Effects of Hydrogen Compounds in Sodium Loops*

J. L. Simpson, D. Dutina, and L. E. Pohl

General Electric Company
Sunnyvale, California

(PRESENTED BY J. L. SIMPSON)

1. Introduction

In most sodium-loop operations a plugging meter is used as the most reliable means of indicating the relative level of oxide impurity. The impurity level of a loop is usually reported as a plugging temperature which, in practice, is correlated to a solubility curve for sodium oxide. This is backed up with periodic laboratory analyses done either by amalgamation or distillation procedures. The determination of these plugging temperatures is at times interfered with by the precipitation of other unknown compounds causing significant flow reductions at higher temperatures (300–600°F)[1] and partial or complete obscuring of the lower (oxide impurity) plug. The multibreak phenomenon has also been observed in many other loop installations.

Although there has been much speculation concerning the identity of the material causing early flow stoppage, only limited experimental work can be found in the literature. One explanation is found in the fact that the solubility of oxygen can change significantly due to the presence of solute elements in sodium. The presence of chromium, iron, and hydrogen will increase the saturation solubility of oxygen at a particular temperature due to the existence of stable compounds such as $NaCrO_2$ and $(Na_2O)_2FeO$. This may indicate a higher total oxygen concentration as determined by chemical analysis than would be determined by a "plugging temperature" based on an impurity-free system.

The operation of systems based on cold traps and plugging indicators with backup from chemical samples appears adequate for engineering purposes. However, on-line instrumentation for oxygen, carbon, and hydrogen is an eventual goal for convenient continuous indication and control. For oxygen, electrochemical cells are being developed for direct measurement of oxygen activity. Although the results so far are encouraging, the attainment of reproducible calibration and long-term stability requires further development. The oscillating mode of plugging-meter operation offers some potential for improved precision in determining plugging temperatures, but is still subject to drift as compounds with higher saturation temperatures, or slower rates of re-solution, build up in the orifices.

Plugging temperatures of 900–950°F have been observed in carbon-saturated sodium systems at Mine Safety Appliance,[2] where the oxide concentration was apparently in the range from 5 to 35 ppm. The high-temperature plugging was attributed to the presence of dissolved and particulate carbon. Oak Ridge National Laboratory[3, 4] reported observing multiple breaks in flow through the plugging indicator throughout their NaK corrosion program. Although the cold traps were operated at temperatures as low as 100°F, this only lowered the temperature at which precipitation occurred from 500 to 300°F, but did not completely remove the material causing the high-temperature flow stoppage.

Early attempts in this program at identifying the material causing flow stoppages in plugging indicators consisted of determining elemental impurities such as carbon, hydrogen, and calcium in sodium sampled from loops with widely varying plugging profiles. However, no correlation could be made between pronounced high-temperature breaks and the elemental analyses. This suggested that a more direct approach was necessary to identify the species causing the early flow reduction. A preliminary investigation led to the conclusion that the high-temperature precipitants were predominantly hydrogen-containing compounds.[5] Confirmation of these findings was made by altering the concentration of these species while following the plugging runs.

2. Experimental

2.1. Design of Plugging Collector

The first concern was for a means to collect the high-temperature precipitating species so that identification could be made. An early attempt at collection was made through use of the orifices in a normal plugging meter. The sensitivity of existing methods of analysis was insufficient to characterize reliably the few micrograms of material that were deposited in the small orifices of the plugging plate.

A special device called a plugging compound collector (PCC) (see Fig. 1) was then designed to collect

* Work performed for the U. S. Atomic Energy Commission under Contract AT(04-3)-189, Project Agreement No. 15.

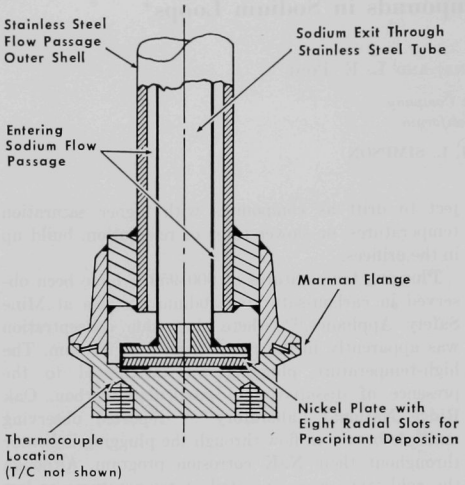

FIG. 1. Plugging Compound Collector.

larger amounts of the precipitating species. The PCC is quite similar to the plugging indicator. The sodium passes through an economizer in which the entering sodium is cooled in the outside passage. The cooled sodium flows through the collector plate and returns to the main loop through an inner tube, where it is reheated. Thermocouples were located in the collector-plate housing to give the plugging temperature. Aside from the collector plate, the entire PCC was constructed of Type 304 stainless steel. The essential difference lies in the substitution of a nickel plate, with eight radial slots for precipitant deposition for the normal plugging plate. The opening of each slot (a $\frac{1}{16}$-in.-diameter semicircular slot) is similar in diameter to the orifices of the plugging plate (each a $\frac{1}{32}$-in.-diameter hole) to simulate the plugging conditions. However, the greater depth of the slots affords a larger zone for deposition. The nickel collecting plate is in the form of two discs, which are held together by four welded nickel straps.

2.2. Sampling with Plugging Compound Collector

To collect the material causing the higher-temperature break, the PCC was installed on the loop-sampling manifold, preheated, and evacuated before sodium flow was initiated. Flow was maintained through the collector for about 48 hr at 800°F to clean the collector walls and the plugging plate. A plugging run was then made using the normal loop plugging indicator (PI) to obtain a temperature-flow profile and determine at which temperature precipitation of material began, as indicated by the first flow stoppage. Figure 2 shows the normal plugging-indicator trace with a high-temperature break occurring at about 400°F and the oxide break in the neighborhood of 300°F. The temperature in the plugging indicator is initially in the 700–750°F region, and sodium is flowing at a rate of 0.12 gpm.

Cooling rates while making the plugging runs were 10°F/min until approximately 50°F before the anticipated oxide break. The cooling rate was then reduced to 1½°F/min.

Once the PI run was completed, the temperature was increased and the flow recovered. Temperatures around the PI circuit were held above 700°F to eliminate any effect it might have while operating the PCC. Based on the PI information as a basis for temperature adjustment, the collector-plate temperature was cooled, in steps, to induce and maintain plugging. Collection of the precipitant proceeded until the flow through the collector decreased to <20% of the original value, at which time the collector was valved off and the contents frozen.

2.3. Opening the Plugging Compound Collector; Analytical Technique

The PCC was removed from the system and transferred to an inert-atmosphere (helium or argon) glovebox which contained less than 1 ppm of oxygen and moisture.

In the inert glovebox, the Marman flange was removed and the plugging plate exposed. The four welded straps were broken loose, and the discs were separated. Figure 3 shows the separated plugging plate and the precipitated material. The deposit was scraped from the channels, and samples were analyzed for total hydrogen by a hot extraction technique.[6] Hydride hydrogen was measured by amalgamating the material with mercury in vacuum and heating the amalgam to 200°C until all gas evolution ceased. The gas was collected, and the amount of hydrogen released was measured by chromatography. The material deposited in one of the channels was placed on a clean, dried glass slide, which was then positioned in a controlled-atmosphere sample holder (see Fig. 4) and analyzed for crystalline material by X-ray diffraction. The holder served to protect the sample during analysis from atmospheric contamination. The slide on which the sample had been placed was clamped to the back of the holder, and a back plate was then attached. A Viton-A gasket was used to seal the back plate to the body of the holder. Welded to the holder were two arms which were terminated by vacuum bellows valves. The arms, the body, and the valves were of stainless steel. The

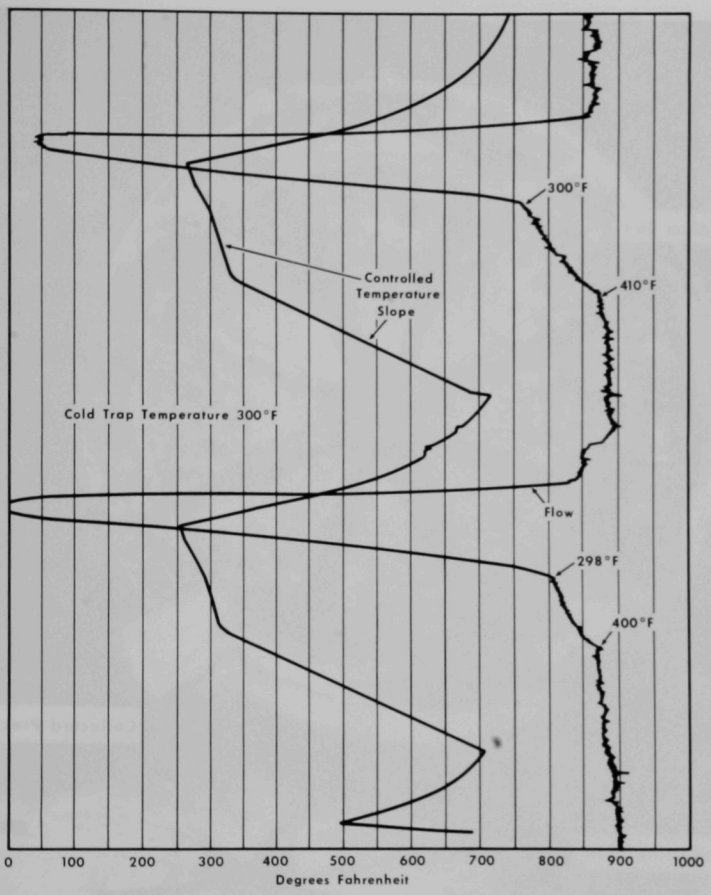

FIG. 2. Normal PI-operation Double Break.

holder had a beryllium window to permit passage of the incident and diffracted beams with only an approximate 15% loss of intensity. The sample can be analyzed with the holder, either under vacuum or filled with helium.

3. Identification of Deposits

Five experimental runs were made in which the collecting temperature was varied. To provide a range of conditions, the cold trap was not operated in two of the runs. The experimental conditions and the data obtained in each run are shown in Table 1.

In each of the first four runs, appreciable concentrations of sodium hydride and sodium hydroxide were observed. Because of the ease with which sodium can be contaminated with moisture to produce sodium hydroxide, the validity of the sampling and analytical procedures was tested. A number of samples of sodium, known to contain only traces of hydrogen (2–5 ppm), were processed in a manner analogous to that used for the PCC deposits; handling periods, sampling sizes, and delay between sampling and X-ray analysis were equivalent. In no case was sodium hydroxide or sodium hydride observed. Confirmation of the freedom from contamination was obtained fortuitously in one experiment in which the sampling device separated during the test, permitting sodium to flow between the discs rather than through

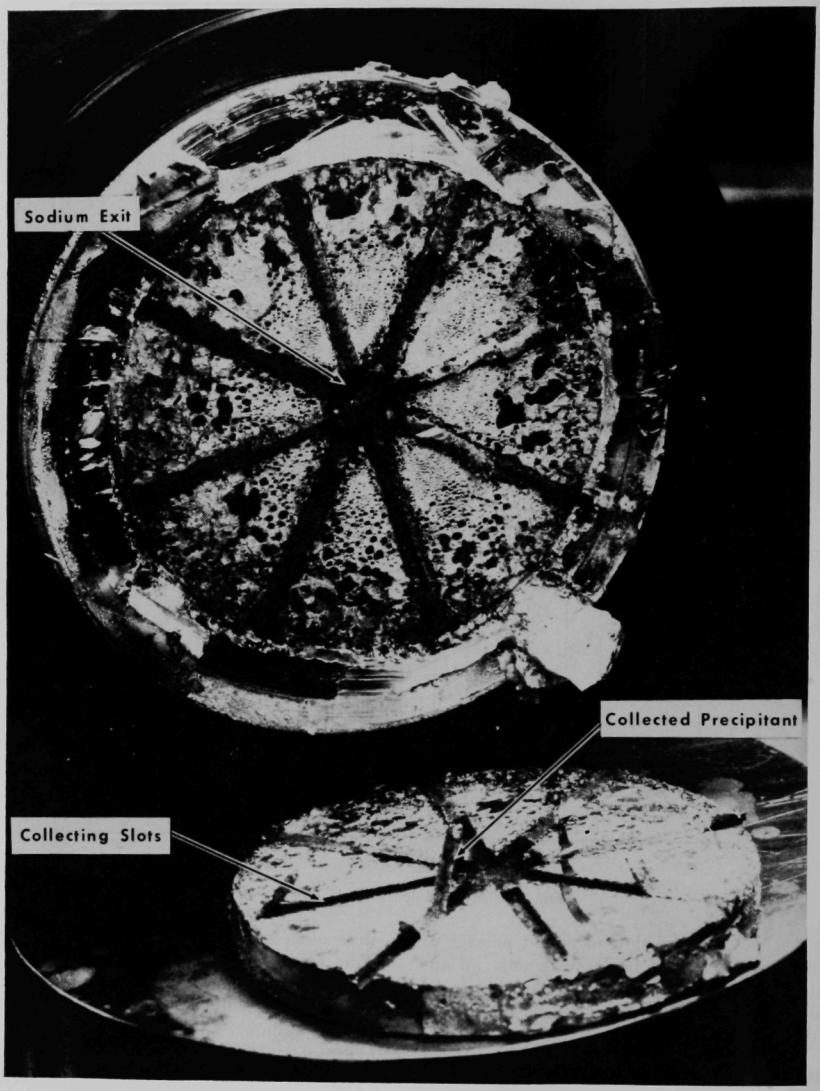

FIG. 3. Plugging Plate after Disassembly in Glovebox.

the orifices. No collection of precipitants occurred, and the subsequent analysis showed a negligible blank.

Analyses for elemental contaminants were also performed for some of the scrapings to ensure no major contaminant had escaped detection by X-ray diffraction. Metallic impurities were determined by emission spectrography, and total carbon by a wet

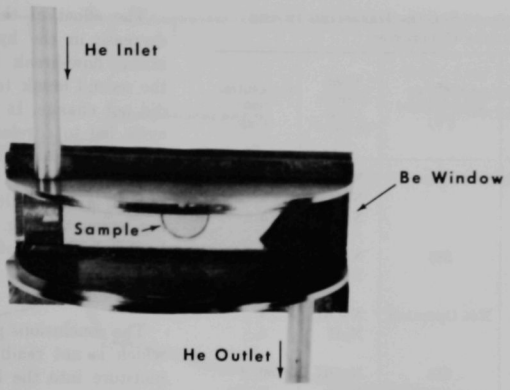

Photograph with Cutaway Beryllium Window

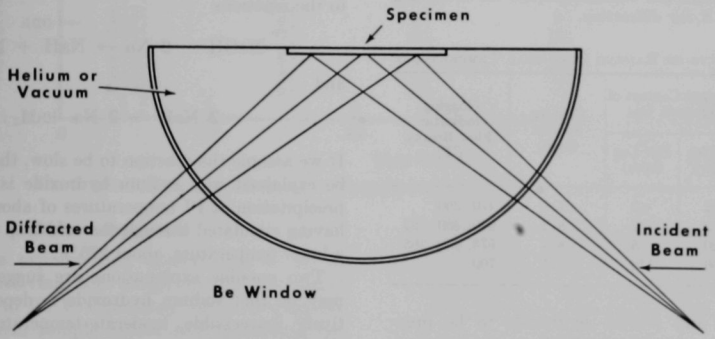

FIG. 4. Controlled-atmosphere Sample Holder for Diffractometer.

combustion technique. Although there was some apparent concentration of several elements over what is normally observed in the system, none of those detected exceeded 100 ppm; thus, it is not believed that they could have caused obstruction to the sodium flow. Sodium oxide was observed in only the first sample. However, this sample required prolonged manipulation to open, and some contamination by the glovebox atmosphere may have occurred. If this were so, the sodium hydroxide value may also be suspected. The sodium hydride value, however, is considered valid in any event. Oxygen was not detected in the remaining sample by X-ray diffraction.

In summary, the only species found at appreciable levels in the PCC deposits were those containing hydrogen. It was concluded that sodium hydroxide and sodium hydride were responsible for the high-temperature breaks. The data were examined to determine whether the ratio of these two impurities was a function of the collection temperature. There were insufficient data to reach any conclusion.

4. Effects of Hydrogen Addition and Removal

Hydrogen was deliberately added to the loops in an attempt to obtain direct corroboration of the conclusions reached in the study just described. This was accomplished by warming up the cold trap in incremental steps from 275 to 400°F. Previous examinations of cold-trap deposits have shown both

TABLE 1. ANALYSIS OF SPECIES DEPOSITED IN THE SOLIDS COLLECTOR

Run Number	Collecting Temperature (°F)	Cold-trap Temperature (°F)	Compounds Collected[a]	Concentration (%)
1	325–310	275	NaOH	>5
			NaH	5
			Na_2O	>5
2	460–300	285	NaOH	4
			NaH	0.5[b]
3	600–585	Not Operated	NaOH	>5
			NaH	4
4	405–360	318	NaOH	50, 5
			NaH	0.1[b]
5	460–300	285	—	—
			—	—

[a] The bulk of the deposit was sodium.

[b] By amalgamation-gas chromatography. All remaining concentrations by X-ray diffraction.

TABLE 2. EFFECTS OF RAISING COLD-TRAP TEMPERATURE

Cold-trap Temperature (°F)	Hydrogen Content of Surge-tank Gas		Cold-leg Sodium (ppm)	Plugging-indicator Flow Breaks (°F)
	Cold leg (vpm)	Hot Leg (vpm)		
275	<2	<2	7.1	470, 260
315	2	<2	8.2	640, 460, 355
350	120	5	8.3	675, 430, 365
400	660	110	14.3	700

sodium hydride and sodium hydroxide to be present.[7] The data, presented in Table 2, show that as a result of heating the cold trap, the hydrogen in the surge-tank argon cover gas and the total hydrogen in the sodium increased. It is also evident that the temperature of the initial flow break in the PI runs also increased. Since other species may have been released from the trap as a result of warming the trap, the argument that increasing hydrogen and increasing initial plugging temperature are directly related is not conclusive. An additional experiment was performed. The cold trap was kept at 400°F until the hydrogen concentration of the gas and the PI readings stabilized. The cold trap was then isolated. Next, the surge-tank gas was diluted with pure argon by partial evacuation and backfilling. The effects on the hydrogen and on the flow-break temperature are shown in Fig. 5.

The effect of the purging cycles is seen to be a decrease in the hydrogen concentration and in the initial flow-break temperature. The temperature of the second break (attributed to oxygen), as expected, did not change. It was noted that the initial purging cycle led to a release of hydrogen. This was attributed to contact between hydrogen deposits on the cooler portion of the surge-tank wall and the hot sodium as a result of change of sodium level during argon venting. The results again show a correlating plugging profile and hydrogen content.

5. Discussion

The conclusions proposed above present an anomaly which is not readily explained. The introduction of moisture into the loops during the insertion and removal of corrosion specimens is the most probable source of hydrogen in the loop. However, after a period of operation the presence of sodium hydroxide is not expected. In the high-temperature sections of the loop, this compound should decompose according to the reactions

$$NaOH + 2\ Na \rightarrow NaH + Na_2O$$

and

$$2\ NaH \rightarrow 2\ Na + H_2 .$$

If we assume the reaction to be slow, then it must yet be explained why sodium hydroxide is available for precipitation at PI temperatures of about 400°F after having circulated through the cold trap maintained at a lower temperature, about 275°F.

Two possible explanations are suggested. First, it may be that sodium hydroxide is deposited in relatively inaccessible, moderate-temperature regions of the system (the surge-tank walls, for example). Thus, a gradual leaching may occur as hot sodium reaches these areas, resulting in a slow introduction of the compound. Although thermodynamically unlikely, the reaction of Na_2O with hydrogen provides an alternate explanation, e.g., $Na_2O + H_2 \rightarrow NaOH + NaH$.

Regardless of the explanation, the results obtained in this study indicate that hydrogen compounds are potential precipitants in a sodium system. They can obscure determination of a plugging temperature as related to sodium monoxide. More important, the hydrogen can lead to potentially serious fast reactor coolant problems, such as channel blockage, hydriding of material, degradation of neutron spectrums, and confusion of water leaks. Thus, continued study of their behavior, detection, and content is mandatory.

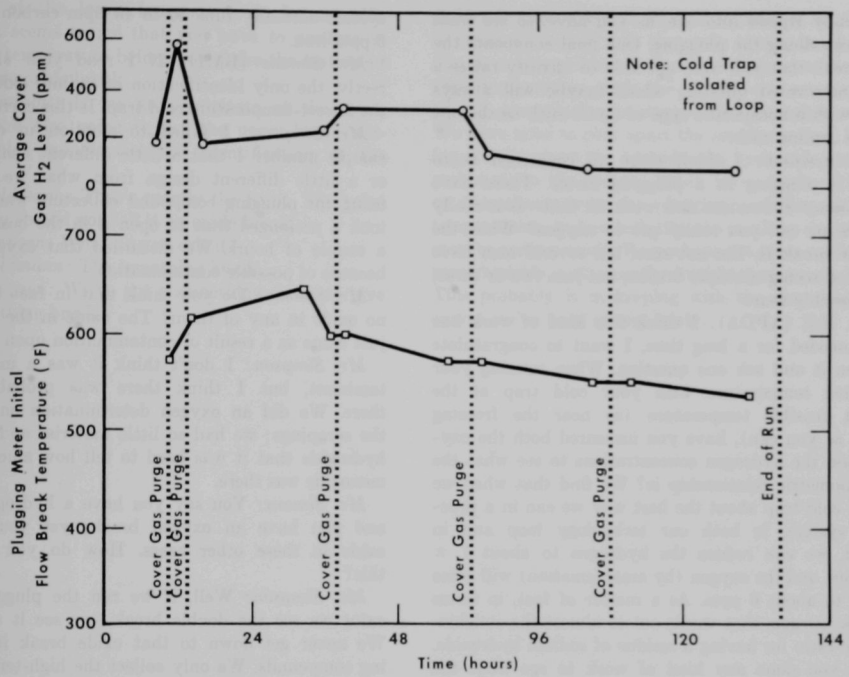

FIG. 5. Effect of Hydrogen Removal on Plugging-meter Initial Flow-break Temperature.

Acknowledgment

The authors express their appreciation to R. C. Blair for conceiving the design of the compound collector, and to W. V. Cummings for developing the X-ray diffraction sample holder and performing the X-ray analyses.

REFERENCES

1. Lockhart, R. W., *Sodium Mass Transfer XXI-1964 Test Run Report*, GEAP-4837.
2. MSA Research Corporation, *Effects of High Temperature Sodium on Austenitic and Ferritic Steels, Physical Properties of Materials, USAEC Report*, MSAR-64-30 (March 20, 1964).
3. Savage, H. W., *et al.*, *SNAP-8 Corrosion Program, Quarterly Progress Report for Period ending May 31, 1964*, ORNL-3671 (July 1964).
4. Savage, H. W., *et al.*, *SNAP-8 Corrosion Program, Quarterly Progress Report for Period ending February 28, 1965*, ORNL-3823 (June 1965).
5. Young, R. S., *et al.*, *Sodium Components Development Program Mass Transfer Investigations in Liquid Metal Systems. Quarterly Progress Report No. 2*, GEAP-5546 (June–Aug 1967).
6. Dutina, D., and Simpson, J. L., *Sodium Mass Transfer: XVII. The Determination of Hydrogen in Loop Sodium and Cover Gas*, GEAP-4833 (June 1965).
7. Dutina, D., Simpson, J. L., and Young, R. S., *Determination of Impurities in a Sodium System Cold Trap*, Trans. ANS, **10**(1), 145. Annual Meeting, San Diego (June 11–15, 1967).

Discussion

Mr. Rodgers (MSA): You stated what your cold-trap temperature and collecting temperatures were. What was the system temperature, and sodium loop temperature?

Mr. Simpson: We had a ΔT of 500° and we ranged from 800 to 1300°F.

Mr. Berkey (W): You've raised some questions as to why a plugging meter should, in fact, never be used in a sodium system. If the decision is to use a plugging indicator of some sort, you have certainly convinced me that you need an additional monitor of the plugging meter; in fact, you need two instruments: one to tell you what's doing your plugging, and one to tell you when it's being plugged. I'm delighted to see this because I think one great problem with plugging indicators has been that nobody

has really ripped into one, as you have, to see what has been doing the plugging. One final comment: the one break that you were not able to identify raises a yet unanswered question which maybe will always arise with a nonspecific type of meter such as the one you're dealing with.

Mr. Simpson: I think we're all concerned as to what is plugging in a plugging meter. There have been many discussions this week on that—is it really oxygen or can you really get to oxygen? What the middle break is, I'm not sure, but several men have reported seeing multiple breaks, not just two or three, but possibly four.

Mr. Hill (APDA): I think this kind of work has been needed for a long time. I want to congratulate you on it and ask one question. When running your plugging temperature with your cold trap at the lowest feasible temperature (as near the freezing point as you can), have you measured both the oxygen and the hydrogen concentrations to see what the stoichiometric relationship is? We find that when we run a cold trap about the best way we can in a practical system, in both our technology loop and in Fermi, we can reduce the hydrogen to about 1 ± 0.2 ppm, and the oxygen (by amalgamation) will come down to about 6 ppm. As a matter of fact, in terms of true oxygen, that works out to almost the stoichiometric ratio for having a residue of sodium hydroxide. Have you done any kind of work to see what the stoichiometry is?

Mr. Simpson: No, we have tried to maintain our cold-trap temperatures so that we give a plugging temperature corresponding to 10 ppm, using Klaxton's solubility curve. Therefore, we haven't cold-trapped all the way down, and I'm not sure we have made any stoichiometry measurements.

Mr. Hill: What is the lowest hydrogen concentration that you find?

Mr. Simpson: I think about 2–3 ppm. I must indicate that we don't always see the double break too. We can't explain why, and we don't know what we do differently when we don't.

Mr. Holden (UNC): In this system did you have any appreciable amounts of any constituents other than sodium, hydrogen, and oxygen; if not, can you reconcile the presence of three solid phases plus sodium with the phase rule?

Mr. Simpson: To answer the second part, no. To answer the first part, we looked at the deposition area for other compounds and we saw some increase. I would say carbon was in the range of 50–75 ppm. Iron was, as I recall, about 10 ppm. Carbon and iron were the greatest of the contaminants. Our sodium system normally runs 30 to 40 ppm carbon and 2 to 5 ppm iron.

Mr. Simons (BMI): If I read your slides correctly, the only identification of sodium oxide was in the lowest-temperature cold trap. Is this correct?

Mr. Simpson: I failed to mention in explaining sample number 1 that a little different configuration or a little different design from what we are now using for plugging compound collectors was used. It took a prolonged time to open it in the box, perhaps a couple of hours. We discarded that oxygen result because of possible contamination.

Mr. Simons: Do you think that in fact there was no oxide in any of them? The oxide in the first case just came as a result of contamination upon handling.

Mr. Simpson: I don't think it was a major contaminant, but I think there was probably oxide there. We did an oxygen determination on some of the scrapings; we had so little material and so much hydroxide that it was hard to tell how much sodium monoxide was there.

Mr. Simons: You say you have a hydrogen break and you have an oxygen break; yet you find no oxide in these other cases. How do you reconcile this?

Mr. Simpson: Well, if we run the plugging indicator we see the double break—we see it at 300°C. We never get down to that oxide break in collecting compounds. We only collect the high-temperature sample.

Mr. Simons: That's the answer I was looking for.

Mr. F. A. Smith (ANL): We're having considerable difficulty manually operating a cold trap on a large system for a period of about 1000 hr. This week, during the conference, some visitors from an architect-engineering firm asked me an embarrassing question. They asked if this process can be completely automated. Therefore, I wonder if you'd take a crack at that question from your experience with cold-trap operation. Do you see any hope for complete automation with no manual control or no human intelligence to manage a large inventory of sodium?

Mr. Simpson: Our operations man, Larry Pohl, is here—he may be able to answer that question.

Mr. Pohl (GE): We can put a cold trap on-line with a device that will control its temperature automatically.

Mr. Goldmann (UNC): I had problems similar to Simons' in interpreting the table. As I understand it now, you have analyzed only samples that were precipitated at the higher breaking temperature, but you have not analyzed any samples at the lower breaking temperatures. If that is right, why do you

say that at the lower temperature it is an oxide break? It seems to me that you have to analyze at the lower temperature before you make the statement that it is an oxide break.

Mr. Simpson: If we do precipitate at the lower break we're also going to get the upper-break material, which complicates the identification of the oxide.

Mr. Goldmann: That's exactly the point. The point is that you should not call it an oxide break.

Mr. Simpson: What do you call it?

Mr. Goldmann: The something break.

Mr. Simpson: We've got a something meter to give us a something break.

Mr. Dutina (GE): I think like most of us that it is incorrect to call that the oxide break, but I think like most of us—when we're somewhere near the cold-trap temperature with the break—we assume that what's precipitating is oxygen. It's probably wrong. We have tried to pick apart the amalgamation, knowing a little about the hydride, the hydroxide, and the carbonate in the system. When we're down at 275°F or thereabouts with the plugging and the cold-trap temperatures, it does look like the smallest constituent may be sodium oxide. We perhaps get more carbonate, more hydride, and more hydroxide than we do Na_2O. This probably is in keeping with the new solubility curves we've been seeing lately.

The Reaction of HCl with Liquid Sodium and a Sodium-Barium Alloy*

M. R. Hobdell and L. Newman

Brookhaven National Laboratory
Upton, New York

(PRESENTED BY M. R. HOBDELL)

Abstract

This paper describes the reaction of HCl with (i) pure sodium and (ii) sodium containing dissolved barium. In both cases the reaction took place in two separate steps:

(1) $HCl \rightarrow \frac{1}{2}H_2 + Cl^-$;

(2) $\frac{1}{2}H_2 \rightarrow H^-$.

The effect of barium was to decrease the rate of hydrogen production (1), while increasing that of hydrogen uptake (2).

The formation of molecular hydrogen was controlled by processes of a physical nature. The rate-determining step for hydrogen absorption, however, apparently involved the adsorption and dissociation of hydrogen molecules at the metal surface.

1. Introduction

The work described here forms part of an investigation of simple inorganic reactions of liquid sodium. Thermodynamically, such basic sodium chemistry is usually well established; kinetic information, however, is scarce.

One class of reaction exhibited by sodium is the displacement of hydrogen from gaseous compounds in which the hydrogen atom is linked to a more electronegative atom or group: H—X + Na → $\frac{1}{2}H_2$ + NaX. The reaction of hydrogen chloride with sodium falls in this category. One reason for studying this reaction was to investigate the mechanisms and rate-determining steps involved in (1) hydrogen displacement and (2) the formation of molecular hydrogen, both in the presence of liquid sodium.

The interaction of HCl with sodium was also considered from the standpoint of liquid-metal reactivity. It has recently been shown, for example, that dissolved barium stimulates sodium reactivity towards such compounds as nitrogen,[1] hydrogen,[2] and ethylene.[3] Since alkaline earth metals may find use as soluble getters in sodium systems, it was of interest to consider their effect on the chemical behavior of sodium. The reaction of HCl with sodium containing dissolved barium has therefore been studied and compared to that of pure sodium.

The interaction of a gas with a liquid metal is a heterogeneous process, and the initial step will involve adsorption of gas molecules at the metal surface. As the reaction proceeds, its overall rate may feasibly depend on (1) the initial adsorption or some chemical process or (2) the rate at which reactive species are transported across a product surface layer. Should the physical process (2) prevail, the nature of the reaction will depend largely on the properties of the reaction product. A study of the kinetic aspects of liquid-metal chemistry requires a situation for which this is not the case. An effort was therefore made in the present work to arrange conditions so that reaction products would not inhibit the reaction.

In the experiments described, a fixed volume of hydrogen chloride was reacted with a large excess of vigorously stirred liquid sodium or sodium-barium alloy. The course of the reaction was followed by measuring pressure change as a function of time.

2. Experimental

2.1. Apparatus

The apparatus used was similar to that previously described[3, 4] and is shown in Fig. 1. The reaction vessel, constructed from Pyrex glass, consisted of two concentric cylindrical vessels, A and B, which could be independently isolated. The former was an inner reservoir for HCl; the latter contained the sodium. The entire unit could be connected to a simple mercury manometer (of negligible volume compared to B) and a vacuum line. The vessel was heated by immersion in a silicone oil bath, whose temperature was carefully controlled (±1°C). When molten, the sodium could be vigorously stirred over an internal baffle by means of the external rotating magnet C.

2.2. Procedure

The important features of the technique employed were as follows:

(1) The sodium surface was observed throughout the reaction.

(2) Pure HCl from A was allowed into B (after pre-

* Work performed under the auspices of the U. S. Atomic Energy Commission.

vious evacuation); then A was quickly isolated. The reactants were at the same temperature when brought into contact, and pressure changes due to thermal expansion were eliminated. The use of capillary tubing outside B reduced the volume of gas at room temperature to a negligible minimum.

(3) All HCl in B was available for reaction; hydrogen produced could not prevent its access to sodium.

(4) The induced "eddy" currents set up in the liquid metal by the rotating magnet caused vigorous stirring over the internal baffle; agitation of the metal surface was expected to prevent the formation of protective-product layers and to expose fresh metal continuously.

In a typical experiment, the volume B (see Fig. 1) was ~140 ml. When ~40 g of sodium were used there remained a fixed volume of reacting gas of ~100 ml. Pressure values were measured to the nearest 0.5 mm Hg.

3. Results: Pure Sodium

3.1. The Reaction Curves

The variation of pressure P with time for successive additions of HCl to the same sodium sample at 160°C is shown in Fig. 2a. Each pressure-time curve exhibited a sharp discontinuity at a pressure P', after which the pressure fell slowly to zero (not shown).

A golden film, darkening with time, was formed on the metal surface on contact with HCl. Despite vigorous stirring, this film remained continuous in each case as the pressure fell from its initial value P^0 to P'. At the stage corresponding to P' the surface-product layer became mobile and would break up, exposing clear metal. Continued stirring would cause the surface products to coagulate behind the baffle, thus exposing a similar metal surface area prior to each HCl reaction.

The reaction of the first addition of HCl (see Curve 1 of Fig. 2a) exhibited an initial slow stage after which

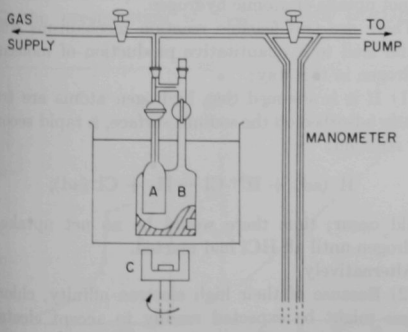

Fig. 1. Apparatus for Reaction of Gases with Excess Liquid Sodium.

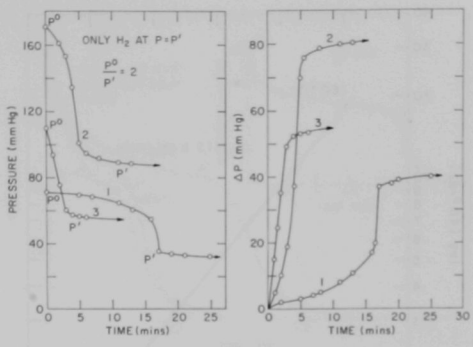

Fig. 2. Na + HCl Reaction at 160°C.

the reaction rate steadily increased (to P'); this behavior was found to a slight extent with the second addition also (see Curve 2 of Fig. 2a). However, the third addition at 160°C (see Curve 3 of Fig. 2a) gave rise to an initially rapid but constant reaction rate. Thereafter, successive HCl reactions produced identical linear P-t curves. (In Fig. 2a only one curve, namely Curve 3, is shown.) Linear P-t curves were also obtained when the same sodium was further reacted at a series of temperatures in the range 106–160°C.

The variation of pressure change, ΔP (i.e., $P^0 - P$), with time for the curves of Fig. 2a is shown in Fig. 2b. Here the first and subsequent HCl reactions are more conveniently compared. The slope of a ΔP vs. t curve is a measure of the overall reaction rate for the $P^0 \rightarrow P'$ stage; in Fig. 3 the variation of log $(d\Delta P/dt)$ with $1/T(°K)$ for the linear "reproducible" reaction stage is shown. An apparent activation energy of ~13 kcal/mole was obtained from the slope of this line.

In Table 1 values of initial pressures P^0 and "break" pressures P' are listed along with values for the ratio P^0/P'; in every case $P^0/P' \sim 2$. Hence the sudden decrease in reaction rate took place when the pressure was reduced to one-half its initial value.

Other experiments were conducted in which the gas phase was sampled after arresting the reaction at P'. Analysis by mass spectroscopy failed to detect any HCl; the gas phase consisted entirely of hydrogen.

3.2. The Initial Accelerating Stage

After the first HCl reaction, the sodium surface always contained some reaction products, so the absence of the accelerating stage in subsequent reactions could have feasibly been attributed to the presence of NaH or NaCl. Alternatively, the initial reaction of HCl could have been inhibited by trace impurities

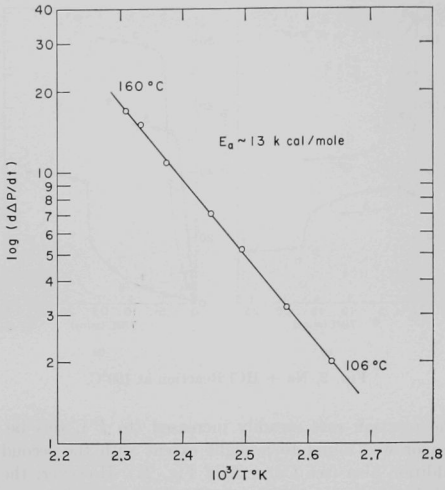

FIG. 3. Variation of Na-HCl Reaction Rate with Temperature.

TABLE 1. BREAK PRESSURES FOR Na-HCl REACTION

Temp (°C)	P^0 (mm Hg)	P' (mm Hg)	P^0/P'
106	126	63	2.0
117	135	70	1.92
128	130	67	1.94
136	118	60	1.96
148	134	69	1.94
156	86	43	2.0
160	110	57	1.92
160	72	36	2.0
160	171	89	1.9

(e.g., Na_2O) on the metal surface. In separate experiments, therefore, HCl was reacted with stirred sodium whose surface contained visible layers of (i) NaH, (ii) Na_2O, and (iii) NaCl. The following observations were made:

(i) NaH had no measurable effect, indicating that HCl had reacted preferentially with the sodium. (Complete reaction with NaH, namely, $NaH + HCl \rightarrow H_2 + NaCl$, would have produced no overall pressure change.) An initial accelerating stage was observed and $P^0/P' = 2$.

(ii) The presence of Na_2O gave rise to an extremely rapid initial reaction (a transient red glow appeared on the surface) and no accelerating stage; in addition, $P^0/P' > 2$. This suggested that the reaction $Na_2O + HCl \rightarrow NaOH + NaCl$ had initially predominated, eliminating the initial slow stage, and preventing some hydrogen from appearing as H_2 at P'.

(iii) The presence of NaCl eliminated the initial accelerating stage and gave rise to curves (at 160°C) identical to Curve 3 in Fig. 2.

These simple experiments suggested that the difference between the first and subsequent HCl reactions was associated with the presence of NaCl rather than of NaH or absence of Na_2O.

4. Discussion: Pure Sodium

4.1. Hydrogen Production

The results showed that each HCl reaction took place in two separate steps:

$$(1) \qquad Na + HCl \rightarrow \tfrac{1}{2}H_2 + NaCl;$$

$$(2) \qquad Na + \tfrac{1}{2}H_2 \rightarrow NaH.$$

In the first step, where $P^0 \rightarrow P'$, HCl reacted with sodium to produce gaseous hydrogen. The second step, where $P^0 \rightarrow 0$, was due to the reaction of hydrogen to produce sodium hydride, which had a negligible dissociation pressure at the temperatures involved. The fact that P^0/P' was always close to two (see Table 1) indicated that reaction (1) proceeded effectively to completion before step (2) took place, i.e., all hydrogen appeared in the gas phases as H_2 prior to sodium hydride formation.

This observation was of interest since:

(1) In the process: H-Cl $\xrightarrow{Na}$ $\tfrac{1}{2}$H-H + Cl^-, "reactive" hydrogen intermediates (e.g., $H^\bullet$) would be formed in contact with, or in the vicinity of, the sodium surface.

(2) The stable form of hydrogen was the hydride ion, H^- (as sodium hydride).

In view of its slow reaction rate, negligible uptake of molecular hydrogen was to be expected during the time taken for complete HCl reaction (step 1); the results further indicated, however, that there was also no net uptake of atomic hydrogen.

There are two feasible reaction mechanisms which would lead to a quantitative production of molecular hydrogen in this way:

(1) If it is assumed that hydrogen atoms are transiently adsorbed on the sodium surface, a rapid secondary reaction:

$$H^-(ad) + H^{\delta+}\text{-}Cl \rightarrow H_2 + Cl^-(ad),$$

could occur; thus there would be no net uptake of hydrogen until all HCl had reacted.

Alternatively,

(2) Because of their high electron affinity, chlorine atoms might be expected readily to accept electrons from the metal surface to form an adsorbed chloride layer:

$$HCl + e \rightarrow Cl^-(ad) + H^\bullet,$$

and then $2H^\bullet \rightarrow H_2$. The metal surface would be rendered inactive to released hydrogen atoms (until chlorine was desorbed as NaCl), i.e., the process $H^\bullet + e \rightarrow H^-$ would be inhibited. If the initial adsorption of HCl (via Cl) is assumed to be more rapid than that of hydrogen, then again there could be no net hydrogen uptake until all HCl had been consumed.

4.2. The Rate-determining Step

The shape ("concave upwards") of the ΔP-t curve for the first HCl addition (see Curve 1 of Fig. 2b) strongly suggested that the reaction was autocatalytic. An initial accelerating stage is characteristic of a heterogeneous reaction in which the rate-controlling step involves the formation and growth of product nuclei at a phase boundary.[5] The absence of further information obviously prevents any firm conclusions in the present case. The implication is, however, that the reaction rate of HCl, i.e., rate of hydrogen production, is controlled by the formation and growth of NaCl crystals on the metal surface. This was also suggested by the observed effect of NaCl on the form of the reaction curves described above.

In Fig. 4, Curve 1 from Fig. 2b is reproduced together with the corresponding log ΔP-t curve for comparison. The latter is linear over the initial region, indicating an exponential increase in reaction rate with time.

4.3. Reaction Model

A possible reaction scheme might involve the following sequence of steps:

(1) adsorption of HCl molecules to produce a chloride layer and hydrogen gas;

(2) the formation and growth of a thin, protective film of amorphous NaCl;

(3) the precipitation of nonprotective crystalline NaCl; this is considered to be the rate-determining step.

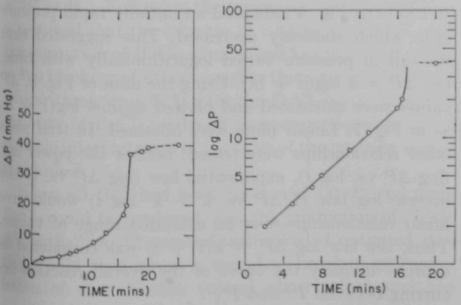

FIG. 4. Na + HCl Initial Reaction at 160°C.

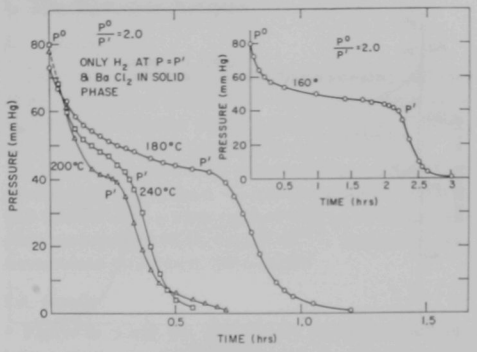

FIG. 5. Na-Ba + HCl Reaction.

The smallest pressure change measured (0.5 mm Hg) would correspond to the formation of a uniform NaCl layer $\sim 10^3$ Å thick. Hence, HCl absorption due to steps (1) and (2) would not be detected. Initially, the reaction rate, controlled by step (3), would be expected to increase steadily. Eventually, however, the rate at which the protective amorphous layer is consumed via step (3) would become equal to its rate of formation by steps (1) and (2) (for a given surface area). At this stage, the overall reaction rate would become constant, producing linear reaction curves.

5. Results: Sodium-Barium Alloy

5.1. The Reaction Curves

Typical pressure-time curves are shown in Fig. 5 for the reaction of HCl with sodium containing ~4 at % barium. In all cases a break in the curve (at P') again occurred when the pressure had fallen to one-half its initial value.

5.2. The Reaction Products

In separate experiments, the gas phase was sampled at the stage corresponding to P' (see Fig. 5) and only hydrogen was detected (mass spectroscopy). After evacuation and cooling to room temperature, the solid product was carefully removed from the metal surface, and remaining traces of free sodium and barium removed by repeated mercury washing. The residue was analyzed (by atomic absorption) for barium and sodium; an atom ratio for barium to sodium of 5 was found, i.e., the product appeared to contain some 83 % $BaCl_2$. The amount of barium consumed during the experiments was negligible compared to the total

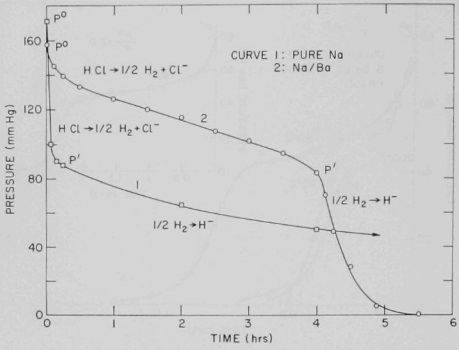

FIG. 6. HCl Reaction with Na and Na-Ba at 160°C.

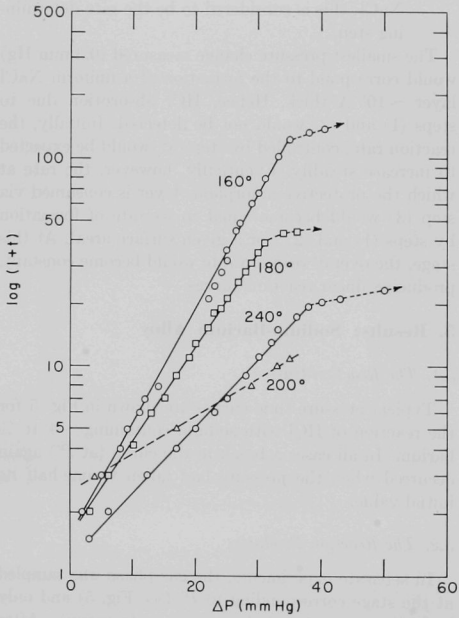

FIG. 7. Na-Ba + HCl Reaction: ΔP *vs* $\log(1 + t)$; t in min.

amount available, so that the alloy composition remained effectively constant throughout.

6. Discussion: Sodium-Barium Alloy

6.1. Comparison with Pure Sodium

The reaction again took place in two quite separate steps:

$$(1) \qquad HCl \rightarrow Cl^- + \tfrac{1}{2}H_2 ;$$

$$(2) \qquad \tfrac{1}{2}H_2 \rightarrow H^-.$$

Again all hydrogen appeared in the gas phase as H_2 prior to subsequent reaction. In this case, however, the rate of the second stage ($P' \rightarrow 0$) at 200–240°C was comparable to the rate of the first ($P^0 \rightarrow P'$), and at 160–180°C was even more rapid than the first stage (see Fig. 5).

Comparison of typical reaction curves at 160°C produced by pure sodium and sodium containing 4 at% barium is made in Fig. 6. The effect of barium is clearly illustrated. The uptake of HCl was markedly retarded, but the reaction with hydrogen was considerably enhanced. In other words, the effect of barium was to decrease the rate of hydrogen production while increasing that of hydrogen uptake.

These experiments with barium made it readily apparent that the reaction of molecular hydrogen (as well as atomic) was inhibited in some way in the presence of unreacted HCl (i.e., prior to P'). As the first stage of the reaction ($P^0 \rightarrow P'$) neared completion, the partial pressure of hydrogen would greatly exceed that of HCl, but in spite of its potentially rapid reaction rate none reacted. This implied that hydrogen was not produced by the reaction

$$H^-(ad) + HCl \rightarrow H_2 + Cl^-.$$

It was also unlikely that solid reaction products would physically restrict access of hydrogen, since they were still present as the reaction proceeded beyond P'. The implications were that (1) the initial adsorption of HCl was far more rapid than that of $H^\bullet$ or H_2 and (2) only initially formed chloride prevented electron transfer to hydrogen ($H^\bullet$ or H_2) to form hydride (H^-). The presence of unreacted HCl effectively prevented the reaction of any form of hydrogen.

6.2. Analysis of the Reaction Curves

The shape of the pressure-time curve from P^0 to P' at 160°C in Fig. 5 indicated an initially rapid pressure drop which suddenly decreased. This suggested that the fall in pressure varied logarithmically with time, i.e., $\Delta P = k \log(a + bt)$. Using the data of Fig. 5, ΔP values were calculated and plotted against $\log(1 + t)$, as in Fig 7. Linear plots were obtained. In trial plots other relationships were tested: neither the power law ($\log \Delta P$ vs. $\log t$), exponential law ($\log \Delta P$ vs. t) nor inverse log law ($1/\Delta P$ vs. $k - k' \log t$) would give linear relationships over an extended range of values. Thus, the law $\log \Delta P = k(1 + t)$ was considered to express uniquely the curve of the overall reaction occurring between P^0 and P'.

Laws of this type are met in kinetic studies of the

oxidation of metals,[6–8] but most models proposed to explain them involve transport of reactive species across a very thin oxide film (<100 Å). It is highly unlikely that such models would provide an explanation in the present case, which involves chloride layers approximating to 10^4 Å thick. However, Evans[6] and Harrison[9] have discussed oxidation mechanisms which will allow for a logarithmic oxidation law in which thick films (>1000 Å) are involved. The present results will be considered in this light.

6.3. Proposed Reaction Model

As indicated earlier, the main reaction is

$$\text{Na-Ba} + 2\text{HCl} \rightarrow \text{BaCl}_2 + \text{H}_2 .$$

Presumably the same basic steps will take place as in the case of pure sodium:

(1) adsorption of HCl on the metal surface with the formation of chloride ions and liberation of hydrogen;
(2) formation of amorphous $BaCl_2$;
(3) the growth of a layer of crystalline $BaCl_2$.

However, in this case the crystalline $BaCl_2$ layer is considered to be protective since: (1) the volume ratio (molecular volume of $BaCl_2$ to atomic volume of barium) for $BaCl_2$ on barium or sodium-barium alloy is greater than unity; (2) ionic conduction in $BaCl_2$ takes place via Cl^- migration,[5] so that a growth of a continuous $BaCl_2$ layer might be expected to occur by diffusion of Cl^- inward to the metal surface.

None of the above three steps is therefore considered to be rate controlling. (In practice, when the metal was not stirred, no pressure change was detected, although the surface did acquire a visible film.)

However, because of the stirring, external work was being done on the system. It is proposed that this causes the continuous formation of "leakage paths" [6, 9] (e.g., cracks and pores) in the surface layer. The reaction of HCl is considered to take place only at leakage points, and as discussed above does so at the expense of $H^\bullet$ or H_2 . Following the treatment by Evans,[6] if it is assumed that the increase in volume associated with the formation of $BaCl_2$ at each leakage point can result in the blocking of others nearby, then one can arrive at a logarithmic growth law for the $BaCl_2$ layer. Since the quantity of $BaCl_2$ produced was proportional to ΔP, a possible interpretation of the form of the reaction curves is obtained.

When all HCl had been consumed (at P') no more $BaCl_2$ could be produced, and the production of "leakage paths" would proceed unchecked. Continued stirring would then cause a complete breakup or coagulation of the chloride (visual observation) and the reaction of H_2 would take place.

7. The Hydrogen Reaction

7.1. Introduction

The reaction of hydrogen with liquid sodium and the effect of dissolved barium have been the subject of a separate investigation by the present authors.[2] Only a brief discussion will therefore be presented here.

A similar apparatus and technique was employed as described above. A fixed volume of hydrogen (75 ml) was reacted with a large excess (~50 g) of stirred sodium and sodium containing 5 at. % barium in the temperature range from 100 to 250°C.

7.2. Results

Figure 8a shows the variation of reaction rate with pure sodium as a function of pressure. The rate was directly proportional to hydrogen pressure, indicating a first-order process:

$$-\frac{dP_{H_2}}{dt} = k_1 P_{H_2} ,$$

where k_1 is the first-order rate constant.

The variation of reaction rate with temperature (see Fig. 8b) indicated an apparent activation energy of ~10 kcal/mole for this reaction.

The presence of 5 at. % barium markedly increased the rate of hydrogen uptake, and in this case it was convenient to measure pressure changes directly as a function of time. Linear plots of $\log_{10} P_{H_2}$ vs. time were obtained (see Fig. 9a), which again showed that the overall reaction was of first-order:

$$-\frac{dP_{H_2}}{dt} = k_1' P_{H_2} .$$

Integration gives

$$\log_{10} P_{H_2} = \text{constant} - \frac{k_1' t}{2.303} ,$$

where k_1' is the first-order rate constant in the presence of barium. The variation of k_1' with temperature (see Fig. 9b) again indicated an activation energy of ~10 kcal/mole.

From the data of Figures 8a and 9a one obtains $k_1'/k_1 \sim 100$ at 200°C. Thus the presence of 5 at. % barium increased the reaction rate by two orders of magnitude, but left the pressure dependence and apparent activation energy unchanged.

7.3. Discussion

The overall process in both cases was

$$\tfrac{1}{2}H_2(g) + e \rightarrow H^-(s).$$

An explanation of the results was proposed[2] in which the rate-controlling step was considered to be the

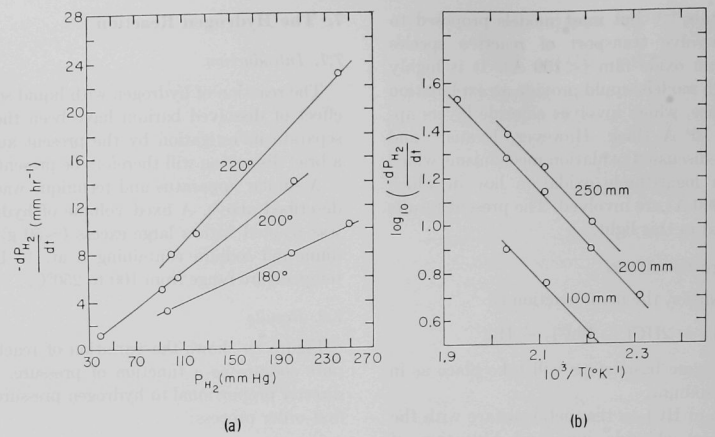

FIG. 8. Na-H_2 Reaction.

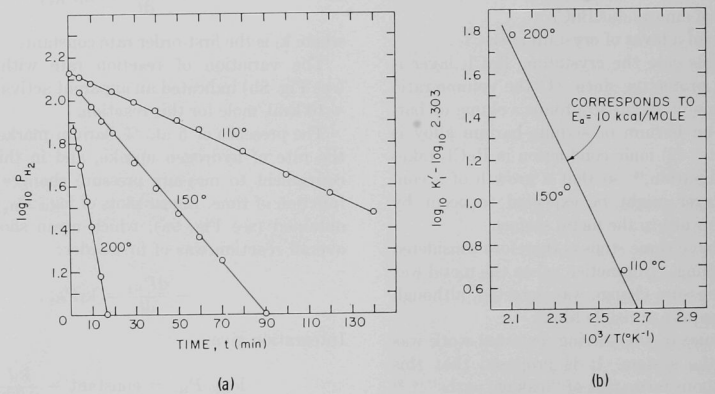

FIG. 9. Reaction of Na-Ba with H_2.

initial adsorption and dissociation of hydrogen molecules at the metal surface:

$$\tfrac{1}{2}H_2(g) + e \rightarrow H^-(ad).$$

The addition of barium to sodium was considered to modify the electron energy distribution at the metal surface. It was postulated that the observed increase in reaction rate with barium was due to an increase in the number of electrons with sufficient energy to bring about the dissociation of the H—H bond.

8. Conclusions

The results of this investigation indicate that the overall reaction of HCl with liquid sodium and a sodium-barium alloy takes place in two separate steps:

$$(1) \quad HCl(g) \rightarrow \tfrac{1}{2}H_2(g) + Cl^-(s);$$

$$(2) \quad \tfrac{1}{2}H_2(g) \rightarrow H^-(s).$$

The reaction of HCl (step 1) appears to be controlled by processes of a physical rather than a chemical nature, i.e., the reaction reflects the properties of the reaction products rather than the reactants. Thus the study of this reaction provides no insight into the nature of factors governing liquid-metal reactivity. This contrasts with the behavior of hydrogen under the same conditions. Hence an explanation is provided for the apparently slow HCl reaction (i.e., hydrogen production) in the presence of barium, which at first sight might seem incompatible with the effect of barium on the reaction of hydrogen.

The absence of any hydrogen reaction during step (1) is explained by assuming that whenever reactive surface is available, HCl molecules are preferentially chemisorbed. This would imply that in a "dynamic system" in which HCl was being continuously added, no hydride would ever be formed.

REFERENCES

1. C. C. Addison, B. M. Davies, R. J. Pulham, and D. P. Wallace. *The Alkali Metals*, special publication 22, The Chemical Society, London (1967), p. 290.
2. M. R. Hobdell and L. Newman. J. Inorg. Nucl. Chem., in press.
3. M. R. Hobdell. Unpublished work, Ph.D. Thesis, Nottingham, England (1967).
4. C. C. Addison, M. R. Hobdell, and R. J. Pulham, *The Alkali Metals*, special publication 22, The Chemical Society, London (1967), p. 270.
5. W. E. Garner. *Chemistry of the Solid State*, Butterworths Scientific Publications (1955).
6. U. R. Evans. *The Corrosion and Oxidation of Metals*, Edward Arnold, Ltd., London (1961).
7. O. Kubaschewski and B. E. Hopkins. *Oxidation of Metals and Alloys*, Butterworths Scientific Publications, London (1962).
8. P. Kofstad. *High Temperature Oxidation of Metals*, J. Wiley and Sons, Inc. (1966).
9. P. L. Harrison. J. Electrochem. Soc. **112**, 235 (1965).

Discussion

Mr. Draley (ANL): Concerning the reaction of HCl and sodium, in all the cases that I have had the occasion to learn the explanation for curves with that shape, they turned out to be associated with temperature increase during the course of the reaction. Have you examined the things that you have to examine to determine whether there are at least local temperature increases that correspond to your reaction?

Mr. Hobdell: Yes, of a sort. I didn't monitor the temperature at the metal surfaces of these reactions. I would say that I had a large, excessive amount of sodium metal, which we know is a good heat-transfer liquid. Possibly the sodium would rapidly dissipate any local heating; there is, however, another way of rationalizing it.

Mr. Draley: I'm sure there are other ways of rationalizing, but that doesn't answer the question. The first time it came to my attention was in the reaction of hydrogen with uranium. Uranium is not a wonderful heat-transfer agent. Yet the temperature of a somewhat massive piece of uranium rose some 80 or 90°C in the course of the first 10 or 15 minutes of reaction, which is pretty substantial. It was insulated somewhat from the gaseous environment. The metal itself didn't all reach that temperature, but the entire metal was heating pretty rapidly.

Mr. Hobdell: The first curve shows that the initial reaction of HCl with the sodium was a very slow reaction. In the case of barium, the hydrogen was lingering around in the gas phase for several hours in spite of its potentially rapid reaction rate. I would have expected even on the basis that you suggested that some hydrogen at least would have gone in, but it didn't.

Mr. Epstein (ANL): I presume that your HCl was very dry. Did you by any chance ever examine the effect of trace amounts of moisture on the kinetics of this reaction?

Mr. Hobdell: No, I haven't done that, but in this particular case, I would say that water vapor would react in a similar way. In other words, I would expect similar curves for water vapor under these conditions.

Mr. Epstein: What I was really thinking of was some experiments I remember, done years and years ago, on the reaction of sodium with oxygen at various levels in the gas state. It was found that exactly the same kind of rather slow rate initially was observed unless you had just a smidgen of moisture in the system, and then it went very rapidly.

Mr. Hobdell: The fact that I got a slow rate indicates I must have pure stuff.

Mr. Waber (Northwestern U.): You made an interpretation in terms of your rate curves involving crystallization. What kind of film thicknesses are you talking about?

Mr. Hobdell: From the uptake of the hydrogen chloride I should have films of the order of 10^3 to 10^4 Å.

Mr. Waber: The normal size of nuclei which one finds in reactions such as you're talking about are of the order of, perhaps, 50 Å thick, or something like that, but the crystallization process would not be expected to lead to your thicknesses. The development of space charges will give you the same kind of reaction kinetics. Have you considered this possibility?

Mr. Hobdell: I'm not familiar with space-charge relaxation. All I was saying really was that perhaps after the absorption of chlorine one gets an amorphous layer which is protective.

Mr. Waber: Of what?

Mr. Hobdell: Of sodium chloride. This layer is very thin. The nuclei appear and grow in this thin layer to produce three-dimensional crystalline sodium chloride, and with the stirring I am assuming that that layer is protective. Really, what I'm measuring is the rate at which the protective layer goes to a nonprotective layer.

Mr. Waber: Do you have any evidence that the film is really amorphous?

Mr. Hobdell: Well, yes. It is certainly protective because in the case of barium it stops the hydrogen from going in as well. I did a couple of the pressure curves with visual observations on the sodium surface, and I

noticed that at the stage where the break occurred I couldn't see any shiny metal. There was what appeared to be a cohesive layer on the surface. At a point, the effect disappeared and I could actually see clear metal. With each of the successive additions of hydrogen chloride I was exposing a similar subsurface area of metal.

Mr. Waber: I think that the interpretation that Dr. Draley raised about temperature rises might have an influence here in the interpretation of the observation which was made, namely, that when you started to get a fresh surface, your reaction could go up and the temperature increase could become much more substantial. In other words, you've said you have a temporary protection and a breakdown of protection. When there is a breakdown of protection, then the temperature can rise very rapidly.

Mr. Hobdell: On that basis, wouldn't you expect some sort of incremental drop as you're breaking and making this protective layer?

Mr. Waber: It may well happen. I don't know whether you've carried on the experiment long enough.

Mr. Hobdell: Well, certainly the curves look smooth.

Mr. Draley: Such a curve would result from progressive increase in the area where the fast reaction occurs, no matter what the causes of the faster and slower reactions. It doesn't mean, however, that it happened.

Mr. Isaacs (BNL): There is an exponentially increasing rate only for the initial addition; on subsequent additions the rate remains constant. This suggests that something is happening only on the first addition. If they were self-heating, it would apply to subsequent additions, too.

Mr. Draley: That depends on the film!

Mr. Isaacs: As I understood Dr. Hobdell, the initial film is protective. Very possibly, NaCl crystals nucleate and grow on that film. A reasonable explanation, one that I prefer, is that growth on the nucleated crystals is rapid; after the surface is covered with growing crystalline material, the rate remains constant (and rapid).

SESSIONS ON SODIUM TECHNOLOGY

SESSION ST-VB

Saturday Morning, November 9, 1968

Chairman: R. W. Dickinson
Liquid Metal Engineering Center

Secretary: R. A. Jaross
Argonne National Laboratory

Design of FFTF Closed Loops*

M. A. Vogel

Battelle Memorial Institute
Pacific Northwest Laboratory
Richland, Washington

(PRESENTED BY R. G. BAUMGARTEL)

One of the main objectives of the Fast Test Reactor (FTR) is to provide reliable closed-loop irradiation test facilities. These test facilities are to be responsive to the national Fast Breeder development needs beyond 1974. Support capabilities are being provided for six closed loops, with plans to install at least three prior to reactor startup.

The ranges of testing capabilities of the sodium-cooled closed loops are summarized in Table 1. In addition to the testing capabilities therein outlined, the closed loops provide:

- a controlled, independent sodium-coolant environment capable of being maintained at less than 20 ppm carbon and less than 5 ppm oxygen with either argon or helium as cover gas;
- full test instrumentation including temperature, pressure, flow, and flux monitors located both in the flowing coolant or attached to the test item;
- a means of exposing "high risk" tests to a fast breeder environment; such tests may include vented and intentionally defected fuels as well as advanced structural or control-rod materials;
- a means of testing fuels and materials under off-normal or peak conditions such as at elevated coolant temperatures or in sodium containing high impurity levels.

Other major irradiation test facilities which will be provided at the Fast Flux Test Facility include the open test positions and the short-term irradiation facility.

Open test positions provide a controllable, fully instrumented reactor sodium environment for the experimenter. Test conditions available are comparable to those experienced by the driver fuel.

The short-term facility permits controlled exposure of materials for less than one reactor cycle. Both trail cable-type and rabbit facilities were considered. The initial facility to be provided will be a trail cable-type arrangement providing full test instrumentation. Such a facility can be designed and constructed for a lower cost, and will serve a larger segment of FBR development needs than would a rabbit facility. These facilities will not be further discussed in this paper.

The closed-loop system which is required to satisfy the testing capabilities outlined in Table 1 consists of three subsystems. These are the in-reactor tube to contain the experiment, the primary radioactive heat-transport system to transfer heat from the irradiation experiment to the sodium coolant, and the secondary heat-transport system which receives heat from the primary system and dumps it to the atmosphere. The in-reactor tube is located in the reactor vessel, the primary heat-transport system is contained in a shielded cell within the containment vessel, and the secondary heat-transport system will be located in an equipment building external to containment.

Figure 1 is a simplified system-flow schematic. The major components in the primary circuit are the in-reactor tube to contain instrumented test assemblies; the intermediate heat exchanger to transfer heat from the primary to the secondary sodium system; two 100% capacity, variable-speed centrifugal, free-surface circulating pumps; one emergency standby electromagnetic decay cooling pump; and a loop heater to maintain loop temperature independent of reactor operation and to provide fine control of experiment inlet temperature. Other components which provide supporting roles to the primary system include a 200% loop volume, sodium-storage, fill and drain tank; an out-of-reactor materials test chamber in parallel with

TABLE 1. Ranges of Testing Capabilities of Sodium-cooled Closed Loops

Neutron flux	7×10^{15} n/cm²-sec (min)
Usable test diameter	2.5–3.0 in.
Tube bulk temperature at inlet, T_{In}	500–1200°F
Tube bulk temperature at outlet, T_{Out}	500–1200°F
Bulk ΔT	Isothermal to 400°F
Test-section temperature at outlet, T_{Out}	1400°F (max) with bypass flow
Test-section ΔP	90 psig (max)
Heat removal	0.7–6.0 MW
Coolant pressure	250 psi (max)
Coolant flow	30–600 gpm

* Based on work performed under U. S. Atomic Energy Commission Contract AT(45-1)-1830.

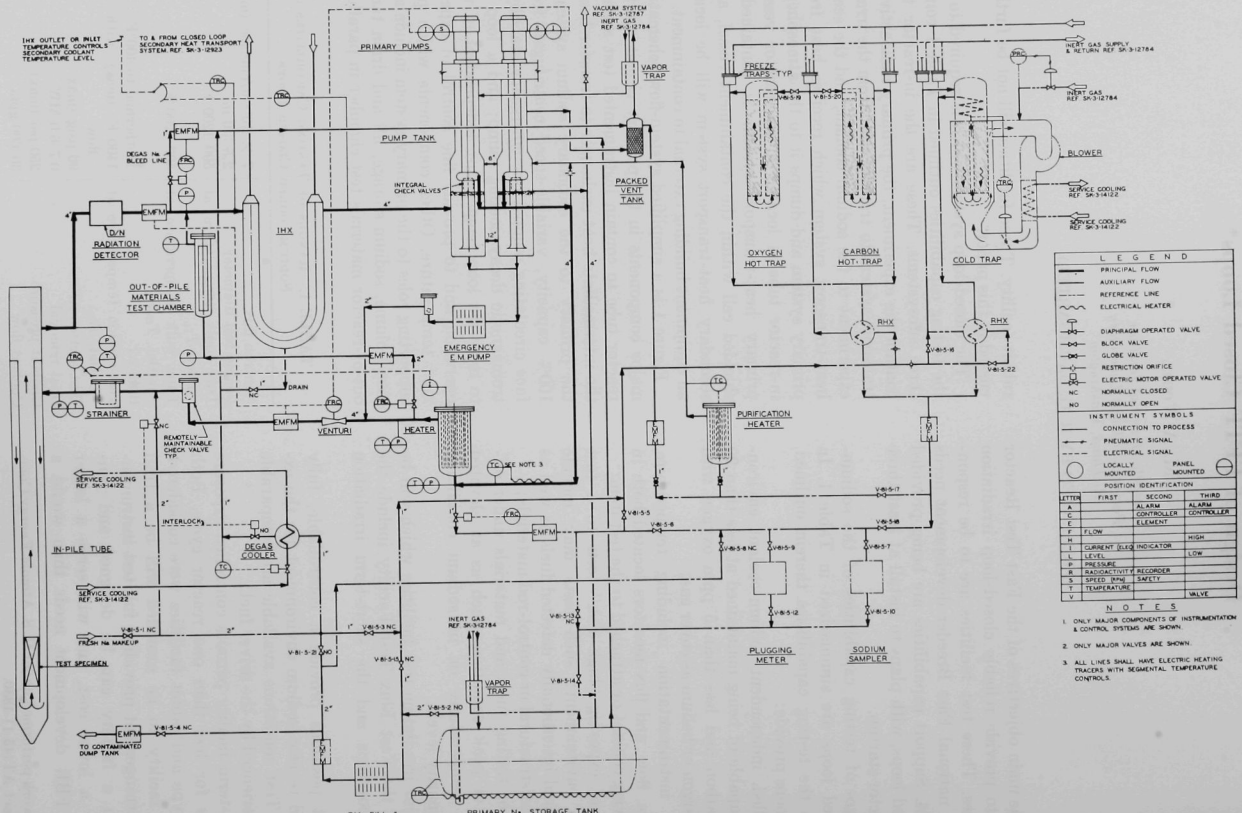

Fig. 1. Closed-loop Primary System.

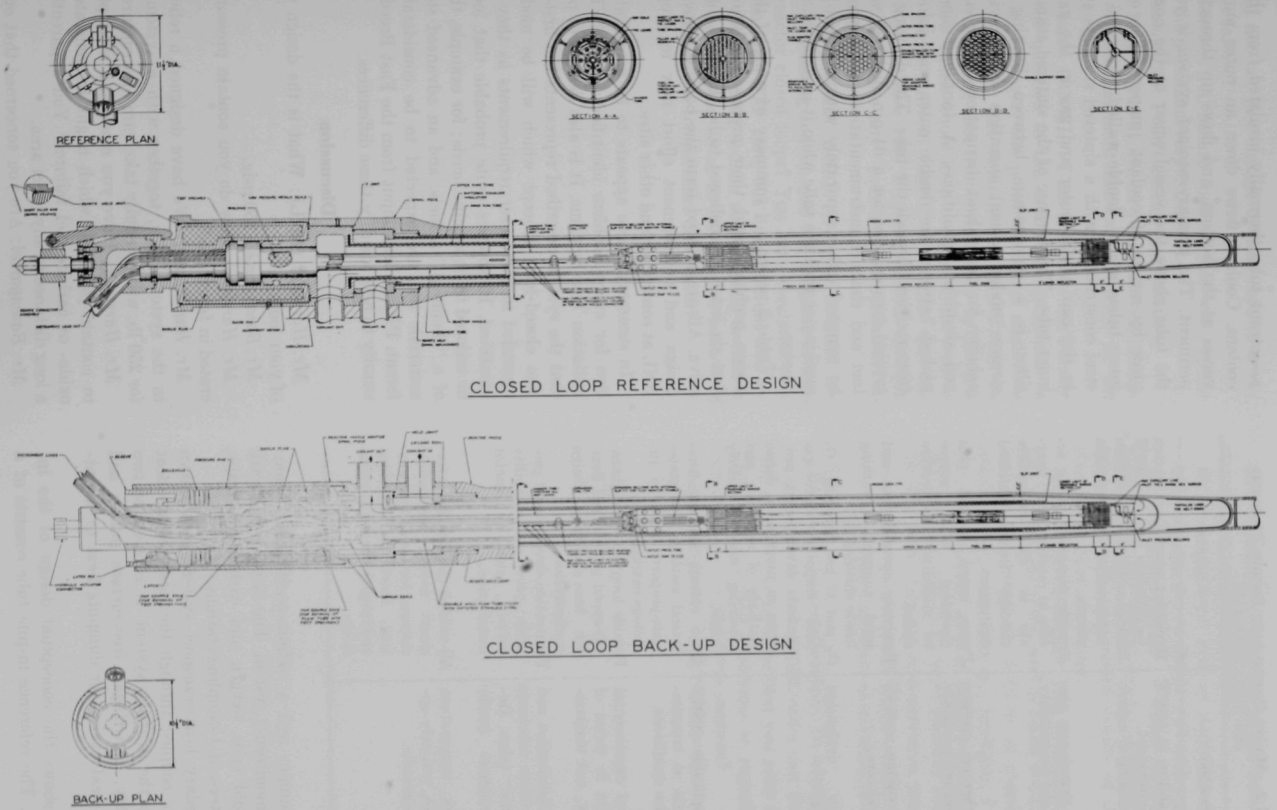

Fig. 2. Closed-loop In-reactor Tube.

TABLE 2. Major Closed-loop Design Problems and Their Solutions

Problem	Solution
Testing capability in 1400°F sodium environment.	Bypassing around test section to maintain loop at 1200°F
Emergency cooling of experiment	Backup coolant provided from independent nondrainable source.
Closed-loop branch-arm piping space and accessibility.	Provide dispersed nozzle access at reactor cover; operate in air atmosphere through locally shielded equipment.
Transient thermal stresses due to rapid reactor power reduction.	Pump speed control plus electrical heat source to minimize temperature cycles.
Radioactive sodium component maintenance.	Remotely operated cut and weld equipment working inside shielded cell.
Sodium-purity evaluation and control.	O_2 and C hot trapping; O_2 cold trapping; cover-gas control; development program in progress to define methods of sampling and attaining selected purity levels.
Lack of applicable ASME code criteria at temperature-pressure conditions.	Must extend existing analytical methods and materials-property data by judicious extrapolation.
Wide range of experimental requirements in terms of power, flow, and temperature.	Provide loop heater, adjustable-speed pumps, and flexible heat-exchange design configuration.
In-core tube fabrication and operation. Close tolerances of "long thin" tubes. Mechanical support inside reactor.	Fabrication-development program; proof and reliability testing prior to reactor installation.
Reliable high temperature and pressure, remotely operable sodium seals.	All-welded closures for infrequent access. Mechanical closures for lower temperature, inert gas interface and frequent access applications.

the main pumps; and a sodium-purification, -sampling, and -monitoring system. The latter system will include a cold trap, oxygen and carbon hot traps, plugging meters, and sampling stations.

The secondary heat-transport system (not shown in Fig. 1) is coupled through the intermediate heat exchanger to the primary system. It consists of two 100% capacity, centrifugal, free-surface pumps and an air-blast heat exchanger dumping heat to the atmosphere.

Figure 2 shows the conceptual design of the in-reactor tube. The reference in-pile tube consists of a re-entrant tube thermally insulated from the reactor coolant. Coolant flows down an outer annulus, reverses at the bottom, and flows up through the experiment. The primary-coolant system is coupled to the tube above the vessel cover at the nozzle spool piece by means of coolant jumpers. The outer and inner tubes are of double-walled, type 316 stainless steel construction with a sintered stainless steel filler in the gap of the outer and gas in the gap of the inner tube. The purpose of the sintered stainless steel filler is a compromise between limiting thermal stresses under normal operation and providing capability for decay-heat dissipation during emergency and shutdown conditions. A tantalum liner sandwiched between the double outer wall inhibits fuel from melting through the tube. The drawing shows a typical arrangement for a 61-pin fuel test with contact and channel instrumentation. Experiments may be removed either separately with the fuel-handling machine or with the tube when it is removed from the reactor.

Table 2 presents a summary of some of the major design problems and their proposed solutions. The first six listed are believed to be the most difficult to solve. All areas listed form the basis of concentrated design and development effort now in progress at PNL at contractor and other sites.

In summary, there appears to be a workable solution for every problem identified for the FFTF Irradiation Test Systems. It is also desired to point out that the system described represents the first-generation closed-loop concept which will be modified or upgraded to meet user requirements as they become identified. It appears quite probable that loops will be tailored to fit specific needs; for example, the needs of a "chemical," a fuels, and an advanced structural materials test are expected to be considerably different. PNL solicits input from the Fast Breeder community to help identify these differences.

Discussion

Mr. Harrison (ANL): What is the design pressure of your loops?

Mr. Baumgartel: 250 psig.

Mr. Harrison: How do you contain pressures generated in failed fuel?

Mr. Baumgartel: We have designed a relief valve in the system. This, together with a system design for 250 lb, will hopefully take care of a rupture.

Mr. Harrison: Have you made any attempt to try to contain pressures which might be generated with oxide- or carbide-fuel failures? You apparently have a long distance to any relief area.

Mr. Baumgartel: Are you concerned that our relief

valve will not act fast enough to take care of a catastrophic failure?

Mr. Harrison: A failure such as this was experienced in the plutonium recycle reactor.

Mr. Baumgartel: I can't answer that question.

Voice: May I have figures on your judicious extrapolation of the maximum allowable stresses in the wall of the loop?

Mr. Johnson (BNWL): I am afraid we can't really answer the question to the extent the gentleman is requesting. However, one point should be made: we have indicated the test capability of 1400°F, but we anticipate reaching this temperature only by using a bypass flow which would keep the rest of the loop at a design temperature of 1200°F. We realize that one cannot hope to have 1400°F operation with stainless steel and still have any "judicious extrapolation" as per ASME codes.

Mr. Soenen (CEN-MOL): Do you insulate between the incoming sodium and the outgoing sodium in the reactor closed loops? You have insulated your loop from the FFTF core, but have you not also insulated your incoming sodium and outgoing sodium in the reactor test loop so as to have better control of the temperatures or temperature differences?

Mr. Baumgartel: Yes, you would have some heat transfer, but you would insulate.

Mr. Soenen: What kind of insulation do you use?

Mr. Johnson: It is a double wall with a gas gap.

Mr. Rothman (ANL): I would like to know the total integrated fluxes during operation and what type of activity you would expect of the stainless steel under these conditions.

Mr. Brehm (BNWL): The saturation concentration of isotopes in the steel is about 2 Ci/cc of stainless steel of cobalt-60; 3 Ci/cc of stainless steel of chromium-51, both from n-γ reactions, I believe; 10 Ci/cc of stainless steel of manganese-54 with a 300-day half-life, and 31 Ci/cc of stainless steel of cobalt-58. The latter two are transmutation products; both have half-lives in excess of 70 days, so it will be a long time before the saturation is attained. But it will be pretty hot.

Mr. Reid (Aerojet-General): In relationship to the comment on lack of ASME codes and the extrapolation on the analytical end that you refer to as a solution, what are your intentions as regards an elastic extrapolation for long-term analysis?

Mr. Baumgartel: I can't answer that.

Liquid Sodium Technology Development (II). Sodium Loop Components and Related Techniques

KAZUO FURUKAWA, KEN YAMAMOTO, ISAO NIHEI, AND MITSURU KAMEI

Japan Atomic Energy Research Institute
Tokai, Ibaraki-ken, Japan

(PRESENTED BY K. FURUKAWA)

1. Introduction

The Mother and Daughter Test Loop System outlined in the preceding report[1] has been largely extended by adding many daughter loops. We have used about 1 m^3 of sodium and an electric power of 300 kW. At present, there are 11 daughter test loops:

mass-transfer test loops No. 1, 2, and 3;
impurity-behavior test loop;
heat-transfer test loop;
flowmeter-calibration bypass;
pump-test loop;
sodium-sampling and vacuum distillation bypass;
valve-test bypass;
fuel-assembly-assurance test loop;
fuel-assembly flow-test section.

The general view and schematic are shown in Figs. 1 and 2.

Although comparatively complex in construction, the system has been successfully operated for three years. It has provided savings of space, fabrication expense, construction time, and man power in the first stage of our sodium technology research and development program.

This report describes some results obtained in the development of several test loop components, instrumentations, and subsidiary sodium technology.

2. Electromagnetic Pumps

The connecting part of the electrodes to the duct of an AC Faraday-type electromagnetic pump is one of the weakest points, for its construction requires the brazing of different materials which form the sodium duct and electrodes.

We have developed a new method of connecting electrodes.[2]

At each connecting point a stainless steel case is TIG-welded to the stainless steel duct, as shown in Fig. 3. In this case the silver was of 99.9% purity.

Another end of the case was brazed to the end of the copper electrodes. Silver was selected because of its nonmagnetic properties so as to avoid a magnetic flux leakage, its high melting point, its high electric and thermal conductivities, and its similar coefficient of expansion to stainless steels.

In this method, only the welding between same materials and the brazing in the lower-temperature region are included, and no special fabrication technique is required.

The newly designed electromagnetic pumps can be used in higher-temperature sodium because a specific distance is kept between the duct and copper electrode. It can be easily fabricated and may be subjected to less severe thermal stress due to the nondirect contact of different metals at the part of electrode.

3. Canned-motor Pumps

A simple and compact canned-motor type of centrifugal pump applicable to a sodium system has been developed in collaboration with the Teikoku-Denki Co.[3]

As shown in Figs. 4 and 5, this pump mainly consists of a vertical shaft, an impeller incorporated with a rotor, and a stator isolated by a sealing diaphragm from the sodium. Conventional 3-phase, 200-V AC power is supplied to the motor.

Sodium comes upward from the inlet nozzle of the lowest position, flows through the impeller, and exits from the outlet nozzle.

The stator is cooled by forced air and is sealed by the diaphragm welded to the pump casing. The diaphragm is lined with mica and aluminum plates which serve as a thermal shield.

All parts wetted by sodium are made of Type 304 stainless steel except the journals and the bearings.

When rotating, the rotor is held in a floating state by the balance of the attractive force of the stator and the high sodium pressure in the cylinder. Radial and thrust bearings are both lubricated hydraulically. When the pump stops, the rotor drops by gravity. The clearance between the thrust bearings broadens, and the grooved paths on the shaft are open to allow for sodium drainage and to prevent plugging by Na_2O and other foreign materials.

The preheating of the internal parts of the pump is accomplished by applying single-phase power to the stator coils.

Tests were performed in the Pump Test Loop.

The prototype model No. 1 (1 kg/cm^2; 150 l/min) has journals of Meteco 32C and a bearing of

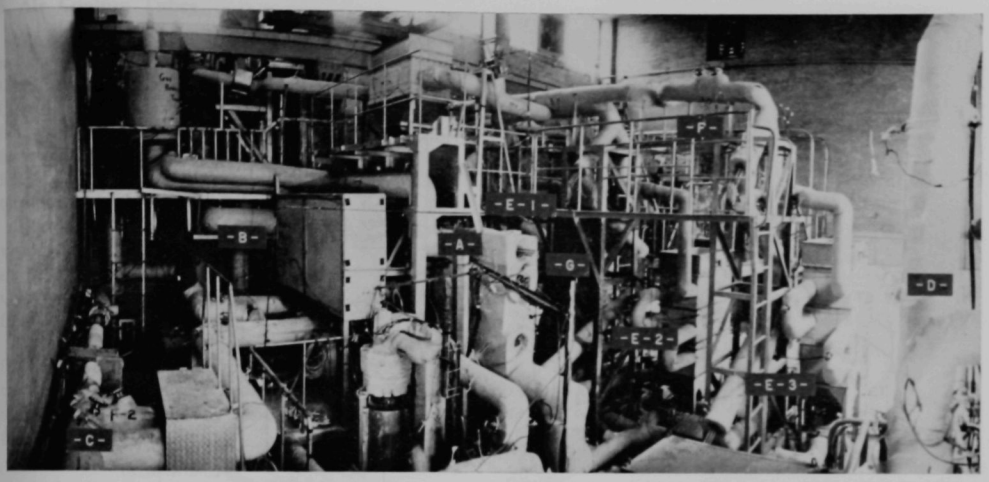

-A- Mother Loop
-B- Heat transfer test Loop
-C- Flowmeter calibration Loop
-D- Pump test Loop
-E- Mass transfer test Loop (1, 2, 3)
-F- Impurity behavior test Loop
-G- High temp. assurance test Loop

FIG. 1. General View of the Mother and Daughter Test Loop System.

tungsten carbide. After 50 hr of operation, the bearing was cracked. The modified No. 1 model had a bearing fixed to the cartridge by shrinkage fitting instead of by key; after 200 hr of successful operation a loosening of the bearing occurred as a result of a design mistake.

Model No. 2, in which the radial bearing material of the cylinder is of Stellite No. 1, is being tested, successfully thus far.

Compared with the ordinary electromagnetic pumps, our pump had a very low fabrication cost, a simple and compact design, and a high efficiency of more than 50%. It is possible to make a larger model of 3-kg/cm² head and 200-l/min capacity, or 1-kg/cm² head and 700-l/min of capacity, using the same design. Further modifications are planned.

4. Valves

4.1. Diaphragm Seal Valves

In our sodium-coolant system, bellows seal valves are widely applied. However, bellows still have a low reliability due to their poor resistance against frequent or abnormal bending or buckling.

The design in which edge-welded bellows are adopted is useful to get a shorter valve stem, but the narrow welded ends are apt to be attacked by crevice corrosion of the residual sodium contaminated by leaked air. We cannot recommend the use of this type of bellows.

To avoid these weaknesses, we developed a new valve in which we used as a shaft seal a diaphragm several times thicker than an ordinary bellows.

New one-inch diaphragm valves have been fabricated in collaboration with Kishikawa Valve Co. The most important characteristics of this design are its simplicity, firmness, compactness, and therefore its high reliability.

As shown in Fig. 6, the inner and outer edges of the corrugated stainless steel diaphragm disc, 0.6 mm in thickness, are welded to the surface of valve stem and to the inside of the bonnet, respectively.

The profile of the inside surface of the bonnet is shaped to fit the diaphragm, so that the diaphragm is

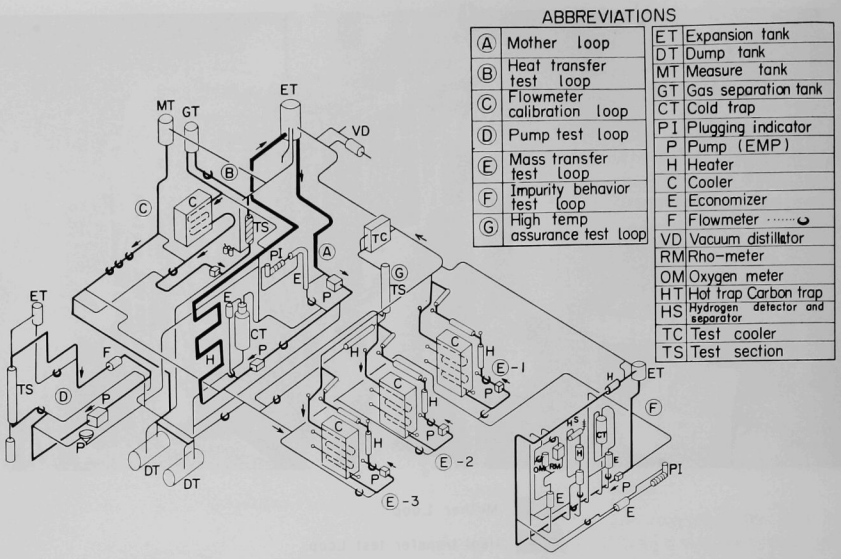

FIG. 2. The Mother and Daughter Test Loop System.

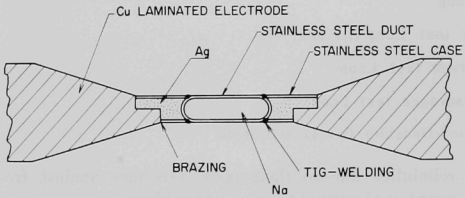

FIG. 3. Cross Section of Electrode Welding Part of an Electromagnetic Pump.

protected by a close contact to this surface. The diameter-reducing part of the stem is also fitted to the same surface so as to be able to seal in case of the diaphragm failure. Further, a back-up seal with graphitized asbestos packing is provided.

To relieve any air-pressure change in the space enclosed by the diaphragm and the bonnet due to the stem displacement, an air chamber is provided, as shown in Fig. 6.

This one-inch diaphragm valve was made of austenitic stainless steel except for the stellite disc and sheet, and tested in our Mother loop. With either no leakage or no change in handle-operating torque, a satisfactory result was obtained.

It is easily possible to fabricate 3-in. valves of the same design. The possibility of further scale-up is being investigated.

4.2. Freeze-seal Valves

An improvement was also made in freeze-seal valves.[4] Air-cooled fin cylinders, cut into two or three sections vertical to the stem axis, were attached to the stem cylinder. By this means the temperature gradient along the hollow stem was enlarged to suppress the shift of the sodium freezing point in this direction following operational changes. At the same time, a diminution of heat loss was achieved.

5. Nonwelded Pipe Joints

The development of the nonwelded pipe joint of high reliability in liquid sodium systems was done in collaboration with Kishikawa Valve Co.[5]

As shown in Fig. 7 this joint consists of stainless steel flanges, a nickel gasket, and a clamping mechanism made of three pieces. One of the clamping bolts has an elongated shaft. A spring is set on the low-temperature part of this bolt shaft so that the spring gives a constant clamping force regardless of the temperature change.

Pipe joints of this type, 3 in. in diameter, have been successfully used in our loops up to 700°C.

More compact and economical pipe joints with a nickel-plated, flat copper gasket or stainless steel O-ring seal are also applicable, depending on the severity of requirements.

6. Air Cooling Tubes

For the air cooling of high-temperature sodium, we have used an aluminum fin tube fabricated by the Furukawa Electric Co. in collaboration with Clamet and Hecla in the USA. This fin tube is fabricated by extrusion of aluminum alloy tube fitted on an inner stainless steel tube. The shaping of fins and the adhesion of a fin tube to a stainless steel tube are achieved at the same time.

This tube has a higher performance, a lighter weight, and a lower fabrication cost compared with stainless steel fin tubes. Therefore we can expect advantages of smaller size and less construction expense from its application to large air-cooling components.

We have already used this type of cooling tubes. As the coolers of the Mass Transfer test loops, these fin tubes of 19-mm ID were used up to 600°C for more than 4000 hr without any detectable change in performance.

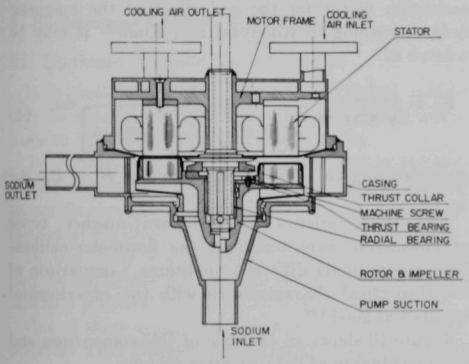

FIG. 4. Schematic of Canned-motor Pump.

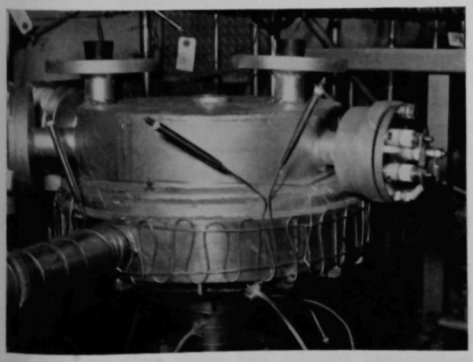

FIG. 5. The Canned-motor Pump.

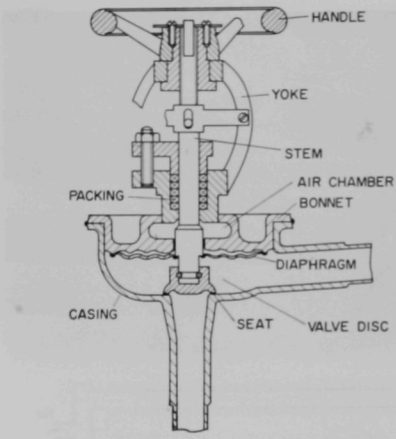

FIG. 6. Diaphragm Seal Valve.

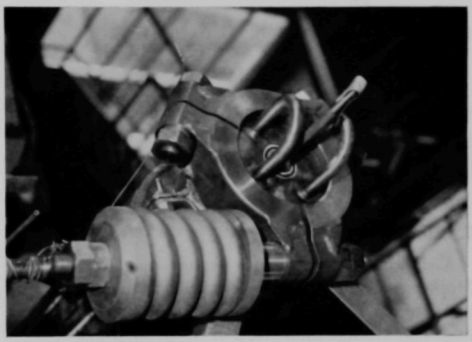

FIG. 7. Nonwelded Joint.

To pursue the cooling characteristics and the change of thermal resistance more precisely, a bypass was built and an endurance test of 450 hr was performed with test tubes of 21.4-mm-ID inner stainless steel tubes as shown in Figs. 8 and 9.[6] Test conditions were 620°C for the sodium inlet temperature, and 300 to 400°C for the outlet temperature, natural air convection being employed. We measured the change of the temperature distribution in flowing sodium along the tube axis corresponding to the same sodium inlet temperature. No change in the cooling characteristics was noticed over the entire cooling tubes.

By metallographic inspection of a surface of an aluminum-fin section, recrystallized structure was observed, but this does not affect the performance.

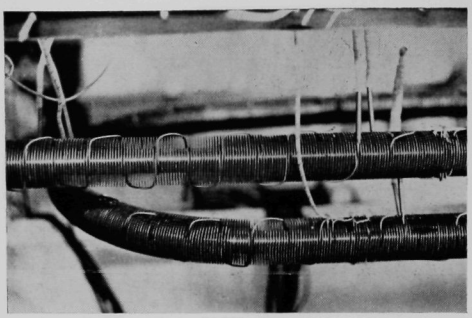

FIG. 8. Air Cooling Tube.

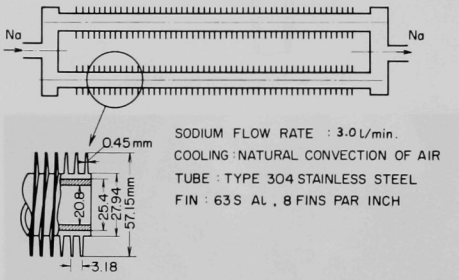

FIG. 9. Schematic of Air Cooling Tube.

7. Flowmeters

A flowmeter-calibration bypass attached to the Mother loop was built. It consists of a measure tank, test section of 1-in.-diameter piping, and a dump tank (the storage tank No. 2 of the Mother loop).

Several flowmeters were calibrated by measuring the volume change of the measure tank. The flow rate was calculated from the indications of seven level gauges. The upper limit was 73 l/min with an accuracy of more than 1%.

7.1. Permanent-magnet flowmeters

To get higher accuracy and stability of flow measurements, many problems remain to be solved, for example:

unknown electromotive force at zero flow;

influence of temperature on the flow indication;

correction for end effect of the magnetic field.

As regards the end effect of the magnetic field, comparison of theoretically corrected values and experimental data gave good agreement.

The theoretical electromotive force E may be written as

$$E = 2B\bar{v}aK_1K_2K_3,$$

where B is a magnetic flux density, $\bar{v}$ is an average flow rate of sodium, and 2a is an inner diameter of pipe. The factor K_1 corrects for the drop of output voltage due to a short-circuit current in the piping wall; as given by Elrod and Fouse[7] it is

$$K_1 + \frac{2\left(\frac{a}{b}\right)}{1 + \left(\frac{b}{a}\right)^2 + \frac{\sigma_w}{\sigma_f}\left\{1 - \left(\frac{a}{b}\right)^2\right\}}, \qquad (2)$$

where 2b is the outer diameter of the pipe, and σ_w and σ_f are the electric conductivities of pipe and of liquid sodium, respectively. K_2 is a correction factor for the drop of magnetic flux density with increase of the magnet temperature and is written as

$$K_2 = 1 + \alpha(T - 25), \qquad (3)$$

where T is the magnet temperature (°C). K_3 is a correction factor for the end effect of the magnetic field. According to Kobayasi and Kudo[8] it may be written as

$$K_3 = \frac{1}{\sqrt{a^2\gamma\pi}} \int_0^\infty \frac{e^{-\alpha^2/4\gamma} \cdot \tanh\alpha a}{a\left[1 + \left(\alpha \frac{\sigma_w}{\sigma_f} t\right) \cdot \tanh\alpha a\right]} d\alpha, \qquad (4)$$

corresponding to a flux distribution of $B = B_0 \exp(-\gamma z^2)$.

The characteristics of permanent-magnet types of flowmeters were tested in the flowmeter-calibration bypass under different conditions. Comparison of the theoretical characteristics with the experimental results was good.[9]

Figure 10 shows an example of this comparison and the contribution of the correction factors.

7.2. Coil-type Electromagnetic Flowmeter

A new type of electromagnetic flowmeter has been developed in collaboration with the Meidensha Electric Mfg. Co.

As shown in Fig. 11 this flowmeter mainly consists of a pair of magnetizing coils attached on the outer surface of thermal insulator of sodium piping, so that a magnetic field directed vertically to the pipe axis is produced by DC current. A pair of electrodes is welded on a stainless steel piping wall.

The advantageous features of this type of flowmeter are: (a) usability of conventional, noncladded fine wire for the coil, since the ambient temperature is low, (b) ease of generation of a strong magnetic field, especially for smaller sodium piping, (c) ease of maintenance, transfer, and repair, with no need for dismantling insulator and preheater, (d) negligible

influence of sodium temperature, (e) compactness and light weight, (f) flat magnetic field along the pipe axis, (g) possibility of multiple measurements with one set of circuit.

Alumina-formed aluminum wires were used as the coil material, and a new shape of coil, which is solid and easy to adapt to the insulator surface, was designed.

The performance of this type of flowmeter was tested in a test section of 1½-in. diameter. The results showed good linearities between the output voltage and flow rate and between the output voltage and magnetizing current, to an accuracy of 2% in each case. Little influence of sodium temperature was noticed.

This type of flowmeter is easily applicable to a larger piping with little modification, presenting a large economical advantage, although less economical for a piping of size as small as 1 in.

8. Sodium-purification Techniques

8.1. Hydrogen Detector and Separator

It is well-known that hydrogen in liquid sodium may be separated and detected by permeating into a vacuum through a thin metal plate or tube.

To improve the detecting performance, a bellows-shaped membrane, which is mechanically stable, easy to handle, and has large surface area, was employed instead of the plate or the tube.

It has been reported[10, 11] that this apparatus may be applicable not only as hydrogen detector, but also as a practical device for hydrogen removal.

One of these apparatus was placed in the Impurity-behavior Test Daughter Loop to determine the effect of interaction of oxygen, carbon and nitrogen with hydrogen. The utility of this apparatus has been proved for measurement of the hydrogen equilibrium

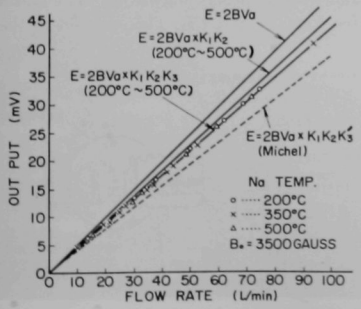

Fig. 10. The Relation between Flow Rate and Electromotive Force of a Permanent-magnet Flowmeter.

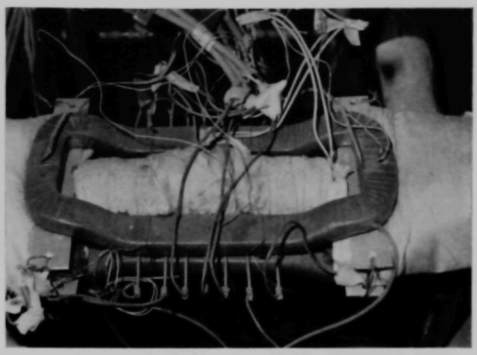

Fig. 11. Coil-type Electromagnetic Flowmeter.

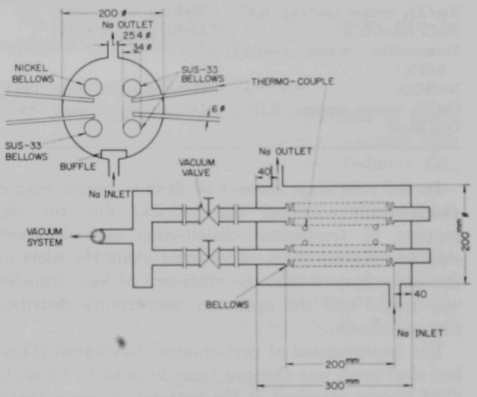

Fig. 12. Schematic of Hydrogen Detector and Separator.

pressure and as a device for hydrogen charging and removal.

As shown in Fig. 12 and 13, the apparatus now in operation consists of four bellows of 36-mm OD, 27.5-mm ID, 0.15-mm average thickness, and 200-mm length; each has a surface area of about 850 cm.^{2} Three were made of Type 316L stainless steel and one of nickel.

For the Type 316L stainless steel bellows, the hydrogen-removal rates were 0.053 and 0.159 cc(STP) mm/hr-cm^2-atm$^{1/2}$ at 600°C and 700°C, respectively; for the nickel bellows the rate was 2.3 times larger.

8.2. Cold Trapping

The cold trap and the cold finger described in the preceding report[1] have successfully served for the sodium purification in the Mother loop. Some modifications were made.

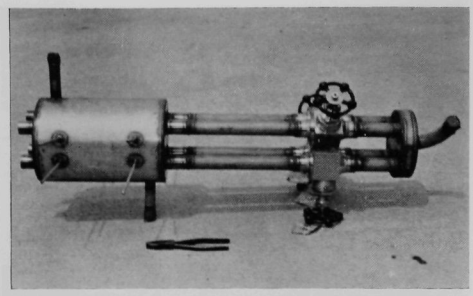

FIG. 13. Hydrogen Detector and Separator.

TABLE 1. SODIUM-FIRE EXTINGUISHERS

Na_2CO_3 (water content: 0.4%)	Melting temp, 860°C
NaCl (Met-L-X)	Melting temp, 800°C
Vermiculite (water content: 0.07%)	
$NaHCO_3$	Decomposition temp, 100°C
$CaCO_3$ (water content: 0.17%)	Decomposition temp, 900°C
Dry Sand	

In the cold trap, instead of flexible heater wound (horizontally) around the vertical fins for the purpose of temperature-distribution control, short sheathed heaters were set in series along the roots of the same fins, so that the efficiency of heat transfer was raised and the optimum temperature distribution was chosen.

For improvement of performance, the waved stainless steel mesh was changed from 30 mesh to 15 mesh. Cold fingers attached at the bottoms of dump tanks were very useful, elongating the life of the loop cold trap. They also served as a sink for debris or rubbish.

It is intended to employ this nonwelded joint (cf. § 5) for the connection of the cold finger and the dump tank to replace the degraded cold finger easily.

9. Sodium-fire Extinguishers

We have previously reported on sodium-fire extinguishers.[1] Recently we have recommended [12] the use of some powder extinguishers based on our tests and experiences (see Table 1). Their effectiveness depends greatly on the actual circumstances. However, their main characteristics are as follows.

(1) Dry sand: This is found useful only for fighting small fires. Although sand has a large heat capacity, it is heavy, difficult to keep dry, and may itself be inflammable in a violent fire.

(2) $CaCO_3$: This is a readily available material. Its ability to extinguish fires depends on the release of CO_2. It is difficult to treat with water after use.

(3) $NaHCO_3$: This material is the most popular powder extinguisher, and is useful even when an organic fire coexists. For large fires, NaCl or Na_2CO_3 is better.

(4) Vermiculite: This is the only material which floats on sodium and thus has a high suffocation extinguishability. However, once chemical reactions commence, it is not sufficiently effective.

(5) NaCl (Met-L-X): This has a melting point of 800°C, so it absorbs heat from violently burning sodium (maximum temperature: 883°C, the boiling point). By forming a crust it has good suffocating effect. In addition it is inert to sodium. However, NaCl is not so desirable because of its corrosive effects on apparatus.

(6) Na_2CO_3 (water contents 0.4%): The melting point of this material is likely to be 860°C, so it shows very good extinguishability by half-melting in contact with burning sodium. Further, it is easy to remove after the fire because of its high solubility in water.

In conclusion, dehydrated and dampproof-treated Na_2CO_3 may be the best extinguisher for fire fighting.

We have also developed a special blanket[13] for sodium fires. This is fabricated from three sandwiched layers: the two outer layers are graphite-fibre cloths about 1 mm thick; the inner one is nickel metal foil 0.1 mm thick.

The blanket, 1 by 1.5 m, is effective for fighting large sodium fires.

10. Miscellaneous

In order to obtain sodium samples for chemical analysis of oxygen and carbon, we fabricated a vacuum distillation apparatus made of Type 304 stainless steel and with a special nonwelded joint and a glove-box (see Figs. 14 and 15). This was set in the return

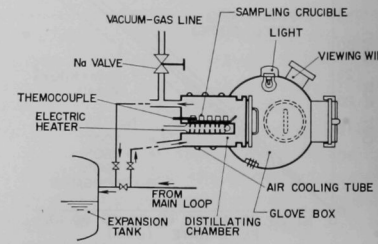

FIG. 14. Schematic of Sodium-sampling and Vacuum Distillation Apparatus.

line to the expansion tank of the Mother Loop. Operations have been successful.

Precleaning is done by sodium flowing at 2 l/min and 400°C for 24 hr. After the sodium is drained the sodium in the ten capsules is distilled at 200°C, as measured by a thermocouple inserted in one capsule.[14]

Several other techniques have been adopted.

Mineral Glass Black Fibre is employed as a thermal insulator in newly built daughter loops instead of Silicalite (SiO_2: 40% and CaO: 35%) which has been usually used. The new insulating materials consists of an inner, thin layer of thermal resisting material, such as Blue Felt (max, 650°C) or Fineflex (Al_2O_3: 54% and SiO_2: 45%; max, 1100°C), a second, main layer of Mineral Glass Black Fibre and asbestos paper, and an exterior layer of glass cloth.

In comparison with Silicalite, Mineral Glass Black Fibre has several merits: lighter weight, relative incombustibility in case of sodium leakage (because only a small quantity of solid material contacts the sodium), good elasticity (so that this insulator fits any thermal expansion of the piping), easy construction (especially for a complex-shaped part), and good economy of space (a result of the good insulation). On the other hand, the material releases tiny floating flakes that are irritating to skin and has a little higher cost.

Several types of MgO-insulated, stainless steel-sheathed heaters have been adopted. For preheating, flexible heaters of 3.2-mm or 4.8-mm diameter are attached to the whole system. Power density is only 2 W/cm².

As a main heater, an immersion type is employed. To replace a heater for exchange or repair easily, a cartridge type has been developed. This consists of a heater of 20-mm OD inserted in a sleeve tube of 21-mm ID; no special medium is used to fill the annular space. Good and lasting performance has been shown up to a limit of 5 W/cm² in power density of heater surface.

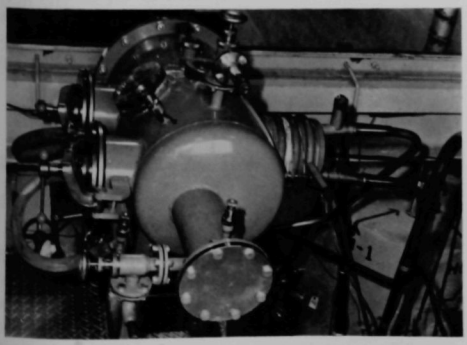

FIG. 15. Sodium-sampling and Vacuum Distillation Apparatus.

11. Conclusions

Our many technical problems concerned with the construction and the best use of our Mother and Daughter Test Loop System have been solved. Our further researches and development of sodium technology have been easily carried on, including components, instrumentation, and subsidiary technology developments such as pumps, valves, joints, flowmeters, air cooling tubes, cold traps, hydrogen separators, vacuum distillators, fire extinguishers, thermal insulators, and heaters.

The detailed description of these works will be published as separate reports.

Acknowledgments

We would like to express our gratitudes to many engineers of several companies who cooperated with us, including Mitsubishi Atomic Power Industry Co., Nippon Atomic Industry Groups, Daia Vacuum-plant Fab. Co. and Nippon Dry Chemical Co., apart from those mentioned in this report.

Furthermore, this work was made possible by the technical assistances of all members of the Sodium Technology Laboratory, especially Mr. E Yamada, Mr. Y. Fukaya, Mr. K. Takeda, Mr. T. Sudo, and Mr. I. Sumiya.

REFERENCES

1. Furukawa, K., Yamamoto, K., Nihei, I., and Iguchi, Y., *Liquid Sodium Technology Development (I) Test loops, Purification methods and Supplementary techniques*, JAERI 1129 (March 1967).
2. Furukawa, K., and Fukaya, Y., *On the Repair of Sodium Systems*, presented at Annual Meeting of the Atomic Energy Society of Japan (March 1968).
3. Furukawa, K., Sato, T., and Sudo, T., *Canned-motor Pumps for Liquid Sodium Systems*, unpublished.
4. Furukawa, K. *et al.*, *A Study on Freeze Sealing*, presented at Annual Meeting of the Atomic Energy Society of Japan (March 1968).
5. Furukawa, K. *et al.*, *Non-welded Pipe Joints*, presented at Annual Meeting of the Atomic Energy Society of Japan (March 1968).
6. Furukawa, K., Nihei, I., Sudo, T., Yamamoto, K., and Suita, S., *Air Coolers for Liquid Sodium Systems*, unpublished.
7. Elrod, H. G., Jr., and Fouse, R. R., *An Investigation of Electromagnetic Flowmeters*, Trans. ASME **74**, 589 (1952).
8. Kobayasi, K., and Kudo, A., *Electro-magnetic Flowmeter (I), A Theoretical Study on the End-Effect of the Magnetic Field*, presented at Autumn Meeting of the Atomic Energy Society of Japan (November 1968).

9. Kobayasi, K. *et al.*, *Electro-magnetic Flowmeter (II), Experiments*, presented at Autumn Meeting of the Atomic Energy Society of Japan (November 1968).
10. Furukawa, K. *Supplement to "Sodium Technology in Japan"* Int. Symp. Fast Breeder Reactor, London 5B/2 (May 1966).
11. Furukawa, K. *et al.*, *Hydrogen Behavior in Liquid Sodium*, presented at Anual Meeting of the Atomic Energy Society of Japan (March 1968).
12. Furukawa, K., Kitagawa, T., Kambe, R., and Yamada, E., *Protectors and Extinguishers for Sodium Fires*, presented at Discussion Meeting of Safety Chemistry of Japanese Society of Chemistry (February 1965).
13. Furukawa, K., Tsukahara, Y., and Yamada, E., *On the Fire-Fighting for Sodium Fires*, presented at Autumn Meeting of Atomic Energy Society of Japan (October 1966).
14. Furukawa, K. *et al.*, *Direct Type Vacuum Distillating and Analysing Apparatus*, presented at Annual Meeting of Atomic Energy Society of Japan (March 1968).
15. Furukawa, K. and Takeda, K., *Thermal Insulators for Liquid Sodium Systems*, unpublished.

Discussion

Mr. Probert (B&W): On your mother and daughter loops, does the same sodium circulate through the mass-transfer loops as circulates through the pump test and so on?

Mr. Furukawa: Yes, except if we perform maintenance on the loop, such as installing a new pump. Actually, we use the same sodium in both loops.

Mr. Pfahler (LMEC): You mentioned you do flowmeter calibration. This is for EM flowmeters?

Mr. Furukawa: Yes.

Mr. Pfahler: How do you actually perform the calibration? Do you use the weight or volume method?

Mr. Furukawa: We use a volumetric measuring tank and observe level change. We can calibrate up to a maximum of 70 l/min.

Mr. Pfahler: Have you tried any other flowmeters besides EM meters, for example, Venturi-type flowmeters?

Mr. Furukawa: No, not yet.

Mr. Pfahler: Do you intend to do any Venturi-flowmeter calibrations?

Mr. Furukawa: I have plans to do this, but I hope it will not be necessary. Hopefully, the EM flowmeters will suffice.

Mr. Van Gasselt (TNO, Netherlands): I would like to know what bearing material you use in your mechanical sodium pump?

Mr. Furukawa: We are now testing several materials in this pump bearing. Tungsten carbide and Stellite have been used successfully.

Voice: What kind of materials do you use in the casing and seating parts of your bellows valves?

Mr. Furukawa: We use Stellite 6, I believe.

Mr. Pfahler: I would like to ask a question about the coolers that you showed. You mentioned that you have operated these for 4,000 hr. Have you noticed any gapping between the aluminum and the steel because of differential expansion?

Mr. Furukawa: We are not able to dismantle and examine the coolers, but we have not observed any change in their operating conditions. Apparently nothing has changed.

Mr. Pfahler: What kind of cycle life have you applied? Has there been a large number of increases and decreases of temperature?

Mr. Furukawa: Yes.

Voice: In your cold trap you have the possibility to achieve a temperature gradient. Have you performed any experiments with this device? What oxide distributions were obtained?

Mr. Furukawa: Our purpose in changing the temperature distribution was not experimental, but only to accommodate the loop conditions. If we have a high sodium oxide concentration we would apply a steep temperature gradient in order to avoid plugging. But if we have a clean condition in the sodium loop, we would use a flatter temperature distribution. We are actually applying this flatter temperature distribution, thereby keeping a large effective cold-trap area.

Status of Sodium Components Technology in Italy

G. Fogagnolo, F. Pierantoni, and A. Tarantini

Comitato Nazionale per l'Energia Nucleare
Bologna, Italy

(PRESENTED BY A. TARANTINI)

1. Introduction

CNEN has undertaken the development of the main components of a sodium-cooled fast nuclear plant, with the aim of promoting, in the national industry, the study of general and specific problems connected with the design and construction of components for use in sodium. CNEN's attention converged particularly on intermediate heat exchangers, steam generators, and reheaters. The research and development program for sodium heat exchangers pass through these principal steps:

to find the functional schemes to be developed;
to define plant characteristics;
to develop the preliminary project from the functional schemes chosen;
evaluation, from economic and safety point of view, of the preliminary design that will be built as prototypes;
working experience relative to prototypes;
choice, design, and construction of heat exchangers for the power plant.

Besides this main line, other supporting activities are to be experimentally tested in a sodium-water loop and in a sodium-component-test installation. These include research in the sodium-water reaction and other technological, thermal, and hydraulic tests.

The execution times of the program are as follows:

selection of conceptual type of components of which the prototype has to be constructed (by 1970);
prototype testing and selection of definitive conceptual type (1974);
full-scale component construction (1976).

2. Sodium Heat Exchangers

2.1. Introduction

At the beginning of the project, many preliminary designs of all kinds of sodium heat exchangers existing in sodium-cooled fast breeder reactor power plants were studied. Steam generators also, because of design difficulties, were studied with particular care. From these designs some conceptual types of intermediate heat exchangers, steam generators, and reheaters were selected. Designs of the following units are now being studied;

a straight tube-bundle intermediate heat exchanger studied for a loop solution of the primary system;
a helical coiled-tube-bundle intermediate heat exchanger studied for a pool solution of the primary system;
a straight tube-bundle steam generator;
a helical coiled-tube-bundle steam generator;
a coiled-tube-bundle steam generator;
a helical coiled-tube-bundle reheater.

The intermediate heat exchangers now designed have a capacity of 182 MWt (see Table 1). The steam generators have a capacity of 153 and 306 MWt. The reheater has a capacity of 29 MWt.

For at least one type of intermediate heat exchanger and for some types of steam generators a 50-MWt prototype will be designed, built, and tested in a sodium-component-test installation. The results of experience with these prototypes, together with the results of the research and development program and of economic and safety evaluation, will permit the choice of the heat exchangers that will be built for the power plant.

2.2. Intermediate Heat Exchanger

2.2.1. Introduction

In both designs (see Fig. 1) primary sodium flows in the shell side of heat exchangers while the secondary sodium flows inside the tubes at a slight overpressure. In both designs it is possible to remove the tube bundle for inspection and repair, and to drain the lower head. In both designs the upper tube sheets are out of the direct contact with sodium, but the lower tube sheets are completely immersed in sodium.

It is necessary to note that because of the low pressure existing in the unit, the tube sheets are not very thick, and thermal transients are reduced because by the time the primary sodium encounters the lower tube sheets it has crossed all the tube bundles.

In the design of intermediate heat exchangers special attention has been required by the following points:

TABLE 1. 182-MWt Intermediate Heat Exchangers

	Straight Tubes	Helicoidal Tubes
Shell Side		
Primary sodium flow, ton/hr	3.46×10^3	3.46×10^3
Inlet temperature, °C	590	590
Outlet temperature, °C	439	439
Pressure, kg/cm²	4	2
Sodium velocity between tubes, m/sec	0.6	0.8
Pressure drop, kg/cm²		0.19
Total height, mm	16,200	13,500
Outside diameter, mm	2,100	2,000
Material	AISI 304	AISI 304
Tubes Side		
Heat-transfer surface, m²	1,040	767
Secondary sodium flow, ton/hr	2.60×10^3	2.60×10^3
Inlet temperature, °C	379	379
Outlet temperature, °C	580	580
Sodium velocity in the tubes, m/sec	2	5.8
Pressure drop, kg/cm²		2.7
Number of tubes	2,000	945
Size of tubes, mm	18×1	15.875×1
Material	AISI 304	AISI 304
Weights		
Weight of tube bundle, kg	9,000	5,500
Total weight of empty unit, kg	55,000	30,000

vibration;
tube-to-tube-sheet welded joints;
expansion of the various parts of the exchanger;
thermal shocks.

2.2.2. Straight-tube Intermediate Heat Exchanger

A straight-tube, floating-head, counter-flow type was studied for a loop solution of the primary system. The secondary sodium enters the shell at the top of the heat exchanger and flows downward through the pipe that is in the center of the unit, across the lower tube sheet, and then flows upward inside the tubes that are arrayed in concentric circles around the central pipe. At the upper end of the tubes the sodium flows into a header and then away from the unit.

The primary sodium enters into a distributor placed around the unit, and then flows downward in the annulus between the shell and the central pipe where the tubes are arrayed. The primary sodium flows out of the heat exchanger by means of a collector placed around the bottom of the unit.

The particular problem of this unit is the design of the expansion elbow that must be large enough to permit extensive expansion between the tubes, and between the tubes and central pipe to avoid excessive stress in the tubes-to-tube-sheet welded joints.

2.2.3. Helical-tube-bundle Intermediate Heat Exchanger

The main difference between this heat exchanger and the previous one is the type of tube bundle. This heat exchanger has been studied because of the compactness that it is possible to achieve using the helical tube bundle. It is possible in fact to adopt a sodium velocity significantly higher inside the tubes with only small increase in the length of the tube bundle. The outer diameter remains the same because, for the same tube diameter, using a significantly higher sodium velocity, the number of the tubes is reduced. These two characteristics are very useful for intermediate heat exchangers employed in a pool solution of the primary system.

In this heat exchanger there are no problems arising from the expansion between tubes and between tubes and central pipe because of the high elasticity of this type of tube bundle.

The particular problem in the design is to have a good primary sodium distribution in the annulus and to have a small pressure drop.

The choice between those two solutions will be made when the economic and safety aspects have been evaluated.

2.3. Steam Generators

2.3.1. Introduction

Because the steam generator is the more important sodium heat exchanger, particular care has been taken in the choice of conceptual design. Many functional schemes have been examined.

A preliminary design has been made from every scheme for the same condition of heat capacity, inlet and outlet temperatures of the fluids, and so on. Comparison of safety and functional properties has been made among them, and those with the best characteristics have been chosen.

All steam generators now studied are once-through, single-wall tubes, of counter flow and vertical type. The points that required particular attention during the design have been:

sodium-water reaction;
good flow distribution;
vibration;
transient thermal stresses;
tube-to-tube and tube-to-tube-sheet welded joints;
structural material.

2.3.2. Straight-tube-bundle Steam Generator

The straight-tube steam generator was designed for 153 MWt and 306 MWt (see Table 2 and Fig. 2).

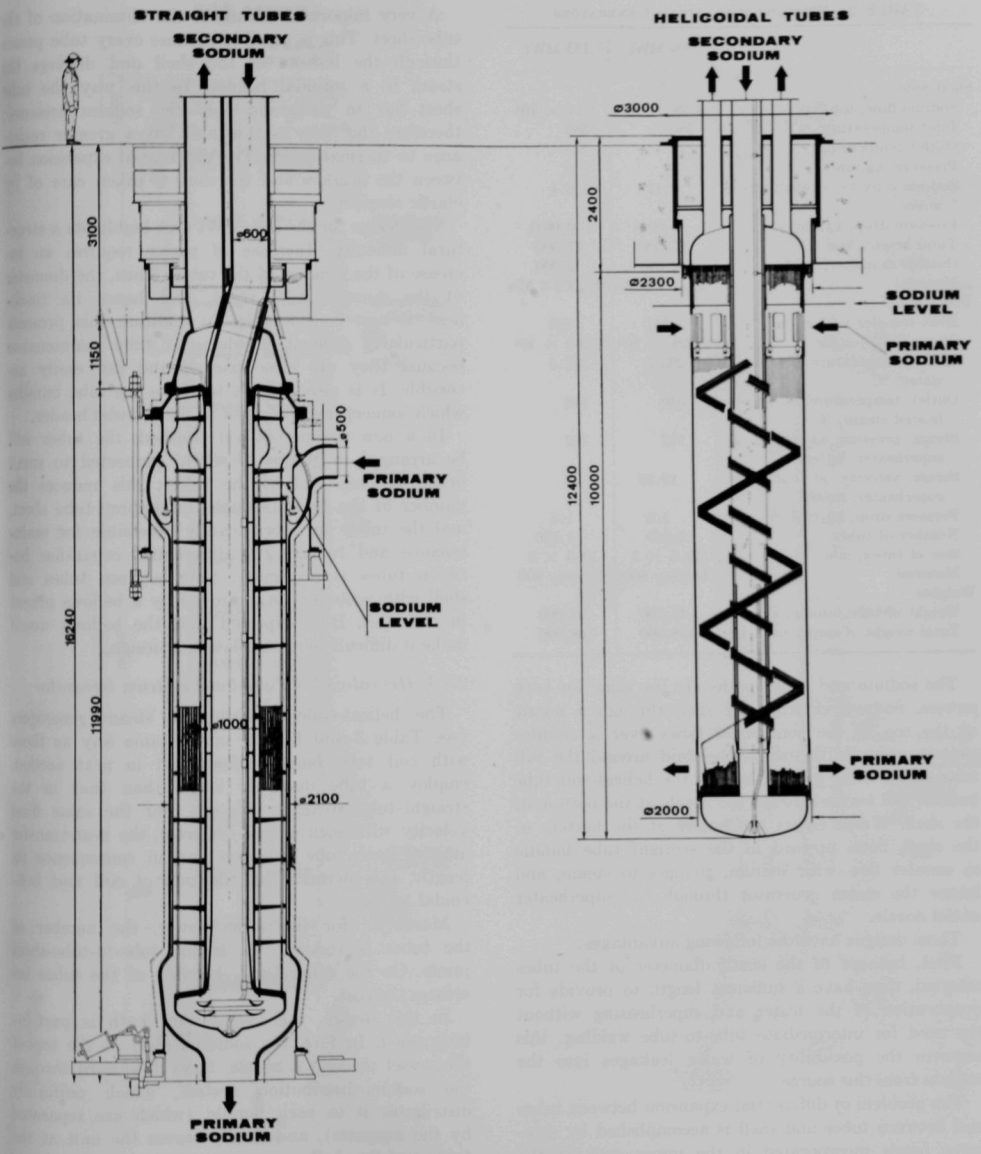

Fig. 1. 182-MWt Intermediate Heat Exchangers.

TABLE 2. STRAIGHT-TUBE STEAM GENERATORS

	306 MWt	153 MWt
Shell Side		
Sodium flow, ton/hr	4.28×10^3	2.14×10^3
Inlet temperature, °C	580	580
Outlet temperature, °C	375	375
Pressure, kg/cm²	3	3
Sodium velocity between tubes, m/sec	0.42	0.4
Pressure drop, kg/cm²	0.0041	0.0041
Total height, mm	17,500	17,500
Outside diameter, mm	2,340	2,000
Material	2¼ Cr-1 Mo	2¼ Cr-1 Mo
Tubes Side		
Heat-transfer surface, m²	1,557	842
Steam flow, ton/hr	0.528×10^3	0.263×10^3
Inlet temperature of feed water, °C	293.5	293.5
Outlet temperature of superheated steam, °C	540	540
Steam pressure at outlet of superheater, kg/cm²	172	172
Steam velocity at outlet of superheater, m/sec	19.30	20
Pressure drop, kg/cm²	1.6	1.6
Number of tubes	2,940	1,530
Size of tubes, mm	13.5 × 3	13.5 × 3
Material	Incoloy 800	Incoloy 800
Weights		
Weight of tube bundle, kg	47,700	23,000
Total weight of empty unit, kg	158,300	68,000

The sodium and water paths are the same for both powers. Sodium entering the shell through a nozzle at the top of the component flows over a circular weir in order to distribute the fluid around the full area of the unit, passes through the helical-coil tube bundle, and leaves through the nozzle at the bottom of the shell. Water enters the heater at the bottom of the shell, flows upward in the straight tube bundle in counter flow with sodium, changes to steam, and leaves the steam generator through the superheater outlet nozzle.

These designs have the following advantages:

First, because of the small diameter of the tubes adopted, they have a sufficient length to provide for evaporation of the water and superheating without the need for intermediate tube-to-tube welding; this removes the possibility of water leakages into the sodium from this source.

The problem of differential expansion between tubes and between tubes and shell is accomplished by sine-wave bends incorporated in the upper ends of the tubes. In the central part of the unit there is a large pipe which backs up the tube guide system. At the bottom of the shell there is a hole for the rapid draining of the unit in an emergency.

A very important feature is the elimination of the tube sheet. This is possible because every tube passes through the bottom of the shell and delivers the steam to a toroidal header. In this way the tube sheet has to withstand only the sodium pressure; therefore the plate is thin and has a greater resistance to thermal stress. The differential expansion between the headers and the shell is taken care of by elastic elements.

The design for the 306-MWt unit highlights a structural difficulty. Increase of power requires an increase of the number of the tubes. Thus, the diameter of the dummy tube sheet, and hence its thickness, is now considerable. In addition this presents particularly difficult problems of tube maintenance because they are close packed and not easily accessible. It is also difficult to make the tube bundles which connect the tube sheet to the toroidal header.

In a new design not yet finished, the tubes will be arranged in groups of seven, connected to small heads at each end of the tubes; this reduces the number of the holes through the dummy tube sheet, and the tubes are more readily accessible for maintenance and repair. The differential expansion between tubes is negligible; that between tubes and shell with probably be improved by a bellows placed in the shell. It is expected that the bellows would make it difficult to extrapolate this design.

2.3.3. Helical-coiled Tube-bundle Steam Generator

The helical-coiled tube-bundle steam generators (see Table 3 and Fig. 3) in the same way as those with coil tube bundles illustrated in next section, employ a tube diameter larger than that in the straight-tube steam generators. For the same fluid velocity with such a tube diameter, the heat-transfer area of each tube increases and in consequence its length; this permits the adoption of coil and helicoidal tubes.

Moreover, for the same power, the number of the tubes is reduced, as is the tube-to-tube-sheet joints. On the other hand, bending of the tubes increases the cost.

In this design, the sodium flow path is particularly good. In fact, the sodium enters at the top of the vessel through a nozzle, flows downward through the sodium-distribution system, which uniformly distributes it to each bundle (which are separated by the supports), and finally leaves the unit at the bottom of the shell.

Feedwater flows downward in downcomer tubes arranged in a central space without heat exchange, then turns and flows upward in the helical-coil tube bundle, where steam is produced. The superheated

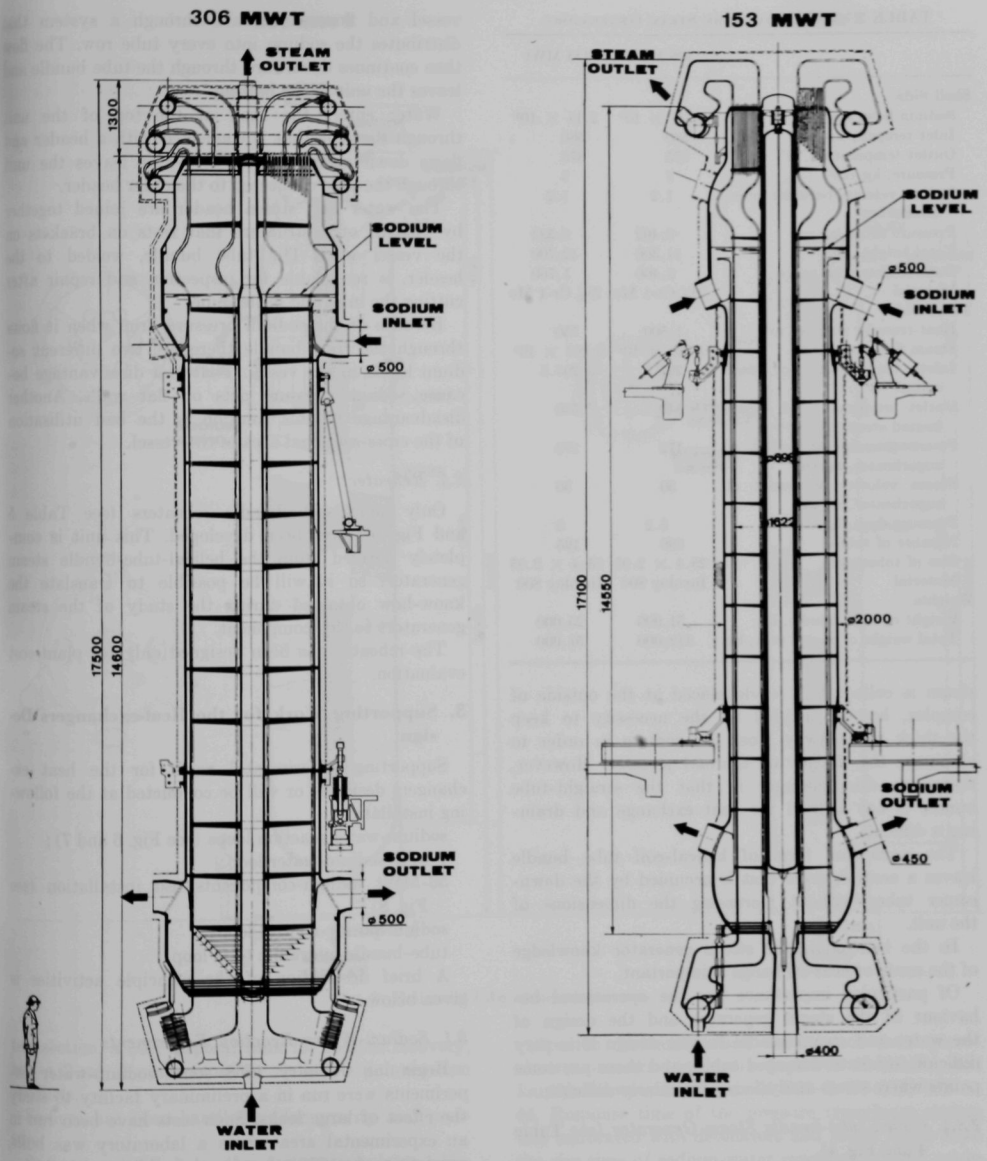

FIG. 2. Straight-tube Steam Generators.

TABLE 3. HELICOIDAL-TUBE STEAM GENERATORS

	306 MWt	153 MWt
Shell Side		
Sodium flow, ton/hr	4.28×10^3	2.14×10^3
Inlet temperature, °C	580	580
Outlet temperature, °C	375	375
Pressure, kg/cm²	3	3
Sodium velocity between tubes, m/sec	1.2	1.2
Pressure drop, kg/cm²	0.492	0.533
Total height, mm	14,300	12,700
Outside diameter, mm	2,400	1,760
Material	2¼ Cr-1 Mo	2¼ Cr-1 Mo
Tubes Side		
Heat-transfer surface, m²	1,500	750
Steam flow, ton/hr	0.528×10^3	0.263×10^3
Inlet temperature of feed water, °C	293.5	293.5
Outlet temperature of superheated steam, °C	540	540
Steam pressure at outlet of superheater, kg/cm²	172	172
Steam velocity at outlet of superheater, m/sec	30	30
Pressure drop, kg/cm²	5.2	5
Number of tubes	390	195
Size of tubes, mm	25.4 × 2.95	25.4 × 2.95
Material	Incoloy 800	Incoloy 800
Weights		
Weight of tube bundle, kg	51,000	25,000
Total weight of empty unit, kg	112,000	57,000

steam is collected in heads placed at the outside of complex, but is justified by the necessity to keep the thick tubes away from the sodium in order to eliminate the danger of thermal stresses. However, there are disadvantages in that the straight-tube bundle is not utilised for heat exchange and draining is difficult.

The particular form of helical-coil tube bundle leaves a central space that is occupied by the downcomer tubes without increasing the dimensions of the unit.

In the helicoidal-tube steam generator knowledge of the mode of heat exchange is important.

Of particular importance are the operational behaviour of the steam generator and the design of the water and steam heads. In this design it is very difficult to locate damaged tubes, and there are some points where stress analysis is particularly difficult.

2.3.4. Coiled-tube-bundle Steam Generator (see Table 4 and Fig. 4).

This design is particularly interesting because, unlike the helical tube bundle, it is possible to change a damaged group of tubes for a new one.

The sodium enters the shell at the top of the vessel and flows downward through a system that distributes the sodium into every tube row. The flow then continues downward through the tube bundle and leaves the unit at the bottom.

Water enters the shell at the top of the unit through the pipe that is connected with a header and flows down inside the tubes. Water leaves the unit through the pipe connected to the other header.

The water and steam header are joined together by means of a structure that rests on brackets on the vessel wall. The tube bundle, welded to the header, is removable for inspection and repair after cutting the inlet and outlet pipe.

Because of the sodium pressure drop when it flows through the tube bundle there are two different sodium levels in the vessel. That is a disadvantage because sodium pressure acts on flat walls. Another disadvantage of this solution is the bad utilisation of the cross-sectional area of the vessel.

2.4. Reheater

Only helical-tube-bundle reheaters (see Table 5 and Fig. 5) have been developed. This unit is completely derived from the helical-tube-bundle steam generator, so it will be possible to translate the know-how obtained during the study of the steam generators to this component.

The reheater has been designed only for plant-cost evaluation.

3. Supporting Work for the Heat-exchangers Design

Supporting experimental work for the heat exchangers design is or will be conducted at the following installations:

sodium-water reaction loops (see Fig. 6 and 7);
1-MW sodium-water loop;
50-MWt sodium-components test installation (see Fig. 8);
sodium-purity-control loop;
tube-bundle hydraulic tests loop.

A brief description of the principle activities is given below.

3.1. Sodium-Water Reaction Experiments

Beginning January 1968 some sodium-water experiments were run in a preliminary facility to study the effect of large leaks. Such tests have been run in an experimental area where a laboratory was built, consisting of a 250-m³ support building with a control room, as well as a mechanical and an electronic workshop, a 6-m-high test hut, and a 50-m³ concrete cubicle for sodium disposal.

The facility consists of a 50-l buffer tank, a 15-l

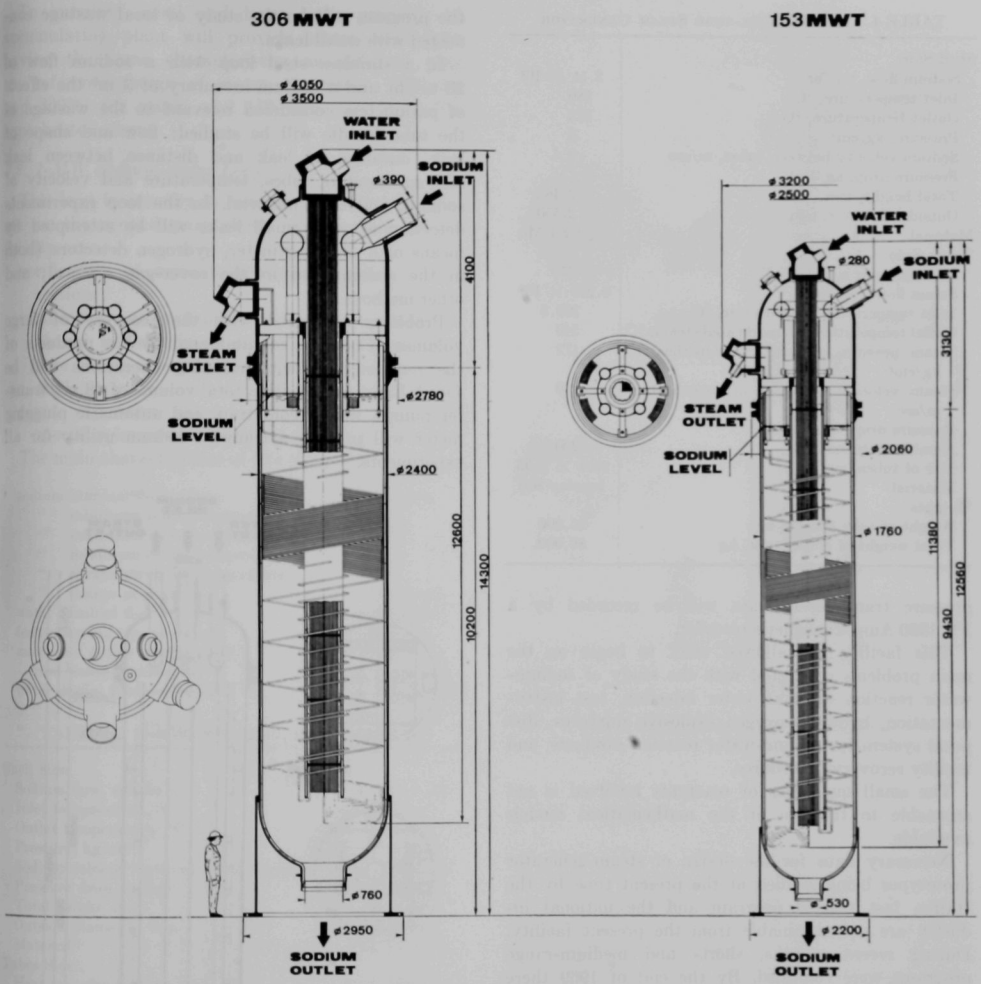

FIG. 3. Helicoidal-tube Steam Generators.

test section, a 50-l disposal tank for sodium recovery, and a 2-m³ disposal tank for sodium-water reaction products.

Sodium has been handled under gravity and pressure.

Sodium, solidified in the test-section inlet pipe, provides tightness during reaction.

In the test section, up to 1.5 kg of water were injected in 10 kg of sodium. Water was injected at room temperature at a pressure of 200 atm in 0.2 sec.

Specific instrumentation consists of four piezoelectric pressure tranducers, type 701 H Kistler, and four thermocouples, Conax K SS6 G T3 MK 062-A-44. Response time of the pressure transducer system was calibrated with detonators and found faster than the rise time of sodium-water reaction-pressure peaks rise time.

Data were recorded by a Galileo RS 14b photographic recorder with a 2-m/sec paper speed.

In the future tests will be run with strain-gauge

TABLE 4. 153-MWt Coil-tube Steam Generator

Shell Side	
Sodium flow, ton/hr	2.14×10^3
Inlet temperature, °C	580
Outlet temperature, °C	375
Pressure, kg/cm²	3
Sodium velocity between tubes, m/sec	0.4
Pressure drop, kg/cm²	
Total height, mm	12,460
Outside diameter, mm	2,550
Material	2¼ Cr-1 Mo
Tubes Side	
Heat-transfer surface, m²	770
Steam flow, ton/hr	0.263×10^3
Inlet temperature of feedwater, °C	293.5
Outlet temperature of superheated steam, °C	540
Steam pressure at outlet of superheater, kg/cm²	172
Steam velocity at outlet of superheater, m/sec	30
Pressure drop, kg/cm²	
Number of tubes	200
Size of tubes, mm	25.4 × 2.95
Material	Incoloy 800
Weights	
Weight of tube bundle, kg	26,000
Total weight of empty unit, kg	86,000

pressure transducers. Data will be recorded by a FR 1300 Ampex magnetic recorder.

This facility has allowed work to begin on the main problems connected with the study of sodium-water reaction, such as water injection, fast instrumentation, hydrogen-oxygen explosive mixtures, disposal system for sodium-water reaction products, and facility recovery procedures.

The small quantities of reactants involved is not amenable to the use of the mathematical models available.

Necessary data for the design of steam-generator prototypes being studied at the present time by the Italian fast reactor program and the national industry are not obtainable from the present facility. During recent months, short- and medium-range programs were compiled. By the end of 1969 there are anticipated a substantial increase of the experimental area and the construction of steam-generator models with maximum dimensions of 15-m height and 1-m diameter, in which to simulate the effects of large leaks corresponding to the rupture of at least one tube.

Models of tube bundles will be located in the test sections. Sodium will be mostly stagnant, but for smaller models provision will be made for sodium circulation. Inside the tubes there will be gas or naturally circulating water. Another major point of the program will be the study of local wastage connected with small leaks.

In a stainless steel loop with a sodium flow of 20 m³/hr and a sodium inventory of 3 m³ the effects of parameters considered relevant to the wastage of the tube bundle will be studied: flow and shape of leak, duration of leak and distance between leak and surrounding tubes, temperature and velocity of sodium, and tube material. In the loop experiments detection of very small leaks will be attempted by means of a plugging meter, hydrogen detectors (both in the sodium and in the cover-gas system), and other methods.

Problems connected with the recovery of large volumes of sodium contaminated by the products of the reaction and with cleaning operations will be faced. Eight tanks with a total volume of 48 m³, transfer pumps, filters, cold trap, and automatic plugging meter will provide a common sodium utility for all experiments.

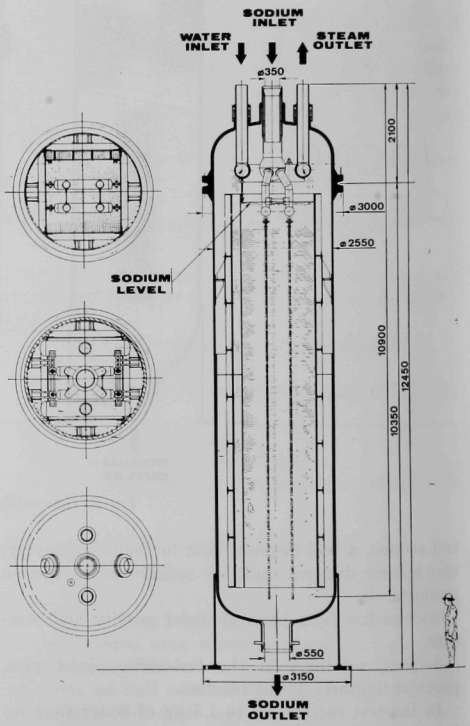

Fig. 4. 153-MWt Coil-tube Steam Generator.

To simulate small and large leaks properly an accumulating plant will provide steam and water having the same characteristics as obtained from the reference design of steam generators: 200 atm and 350°C for water, and 170 atm and 540°C for superheated steam.

3.2. 1-MW Sodium-water Loop

This loop is actually in construction and will operate in the second part 1969. Main scopes of the facility are:

- verification of some technological details of test sections;
- verification of calculations concerning heat-exchange surfaces in all operating conditions, pressure drops, thermal-hydraulic instability, stress analysis;
- plant experience of a sodium-water loop with special reference to safety conditions.

The main characteristics of this plant are:

sodium nominal flow	12500 kg/hr
" minimum inlet temperature	250°C
" maximum inlet temperature	450°C
" minimum outlet temperature	350°C
" maximum outlet temperature	650°C
" design pressure	10 kg/cm²
water nominal flow	1750 kg/hr
feedwater inlet temperature	25°C
maximum outlet temperature from water preheater	350°C
water design pressure	200 kg/cm²

TABLE 5. 29-MWt Helicoidal-tube Reheater

Shell Side	
Sodium flow, ton/hr	0.460×10^3
Inlet temperature, °C	580
Outlet temperature, °C	400
Pressure, kg/cm²	3
Sodium velocity between tubes, m/sec	0.3
Pressure drop, kg/cm²	0.02
Total height, mm	10,300
Outside diameter, mm	1,846
Material	2¼ Cr-1 Mo
Tubes Side	
Heat-transfer surface, m²	360
Steam flow, ton/hr	0.214×10^3
Inlet temperature, °C	332
Outlet temperature, °C	540
Steam pressure at outlet of reheater, kg/cm²	40
Steam velocity at outlet of reheater, m/sec	60
Pressure drop, kg/cm²	5.2
Number of tubes	234
Size of tubes, mm	25.4 × 1.47
Material	2¼ Cr-1 Mo
Weights	
Weight of tube bundle, kg	6,000
Total weight of empty unit, kg	25,000

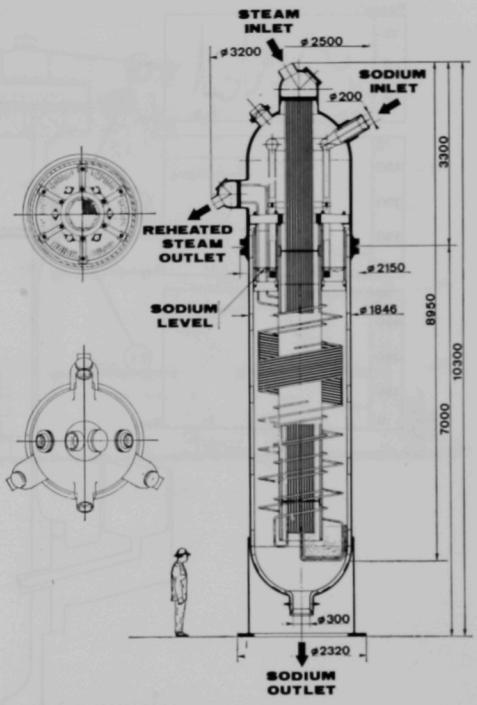

Fig. 5. 29-MWt Helicoidal-tube Reheater.

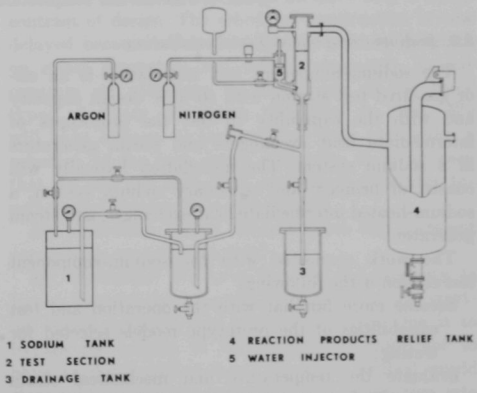

Fig. 6. Sodium-Water Reaction Preliminary Test Loop.

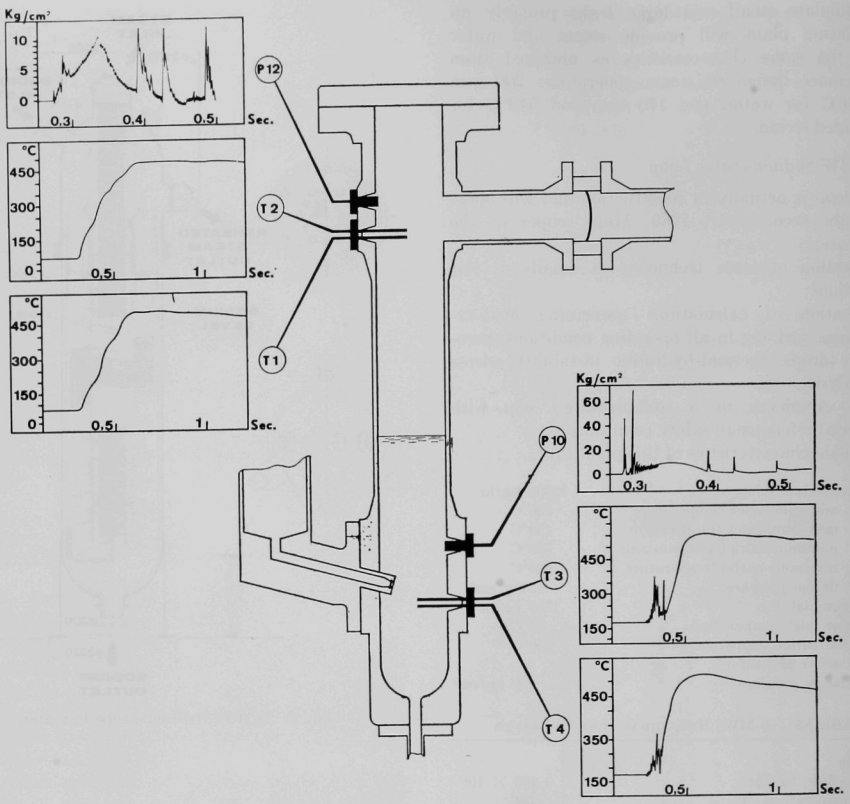

FIG. 7. Pressure and Temperature Profiles for Sodium-Water Reaction.

3.3. Sodium-component Test Installation

The sodium-component test installation is an oil- or gas-fired test station with 50-MW design capacity and with the capability to test the prototypes of intermediate heat exchangers and steam generators in a sodium system. The installation basically will consist of primary and secondary sodium system, a sodium-heated intermediate heat exchanger, and steam generator.

The work connected with the sodium-component test station is the following:

become more familiar with the operation and test capabilities of the prototype models selected for testing;

evaluate the temperature and mechanical strain data to determine the stress levels arising from both static and dynamic conditions;

evaluate all thermal and hydraulic performance and data, both steady-state and dynamic, resulting from the test programs.

Construction of this station will begin in 1970.

3.4. Other Problem Areas

Other areas of interest are as follows:

material selected must be suitable for both the sodium and water-steam environments, while resisting stress corrosion attack on the water side and mass transport on the sodium side;

heat transfer, effect on heat transfer and two-phase flow of coiled tubes;

procedure for welding tubes to the sodium face of the tube sheet and inspection of these welds;

distribution of sodium over tube bundles;

system stability and control.

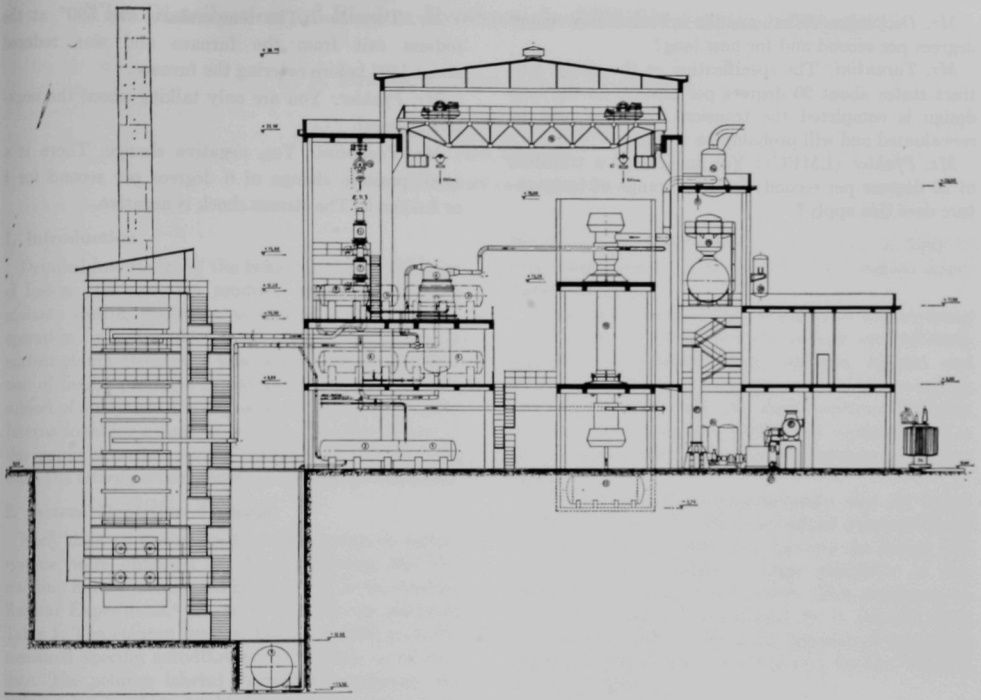

FIG. 8. 50-MWt Sodium-component Test Installation.

The research and development program directed toward solving these problems will be initiated in a very short time.

Discussion

Mr. Chamberlain (APDA): In your sodium-water reaction work, were you doing large or small leaktesting?

Mr. Tarantini: Up to this time we have done only large leaktesting. In 1969 tests will be performed in a unified facilities building with both large and small leaks.

Mr. Chamberlain: Was there any wastage of material observed in the large leaktesting that you have done?

Mr. Tarantini: In the preliminary test we have not sought to examine wastage of materials. The aim of this preliminary test was to gain experience with instrumentation and equipment operation. It was only a preliminary test that had no mathematical study or material-testing aim.

Mr. Dickinson (LMEC): What is the status of your sodium-component test installation? Have you purchased any of the parts yet, such as the heater? Have you ordered parts or is it still under design?

Mr. Tarantini: At this stage we have only a study contract of design. The scheduled construction is now delayed because we are engaged in a study program on steam generators and other components. In our program we will have to choose one of the three types of steam generators we chose in 1964. We will have 3 years to perform our tests and make a selection of the best steam generator. It is foreseen that we can test both IHX and steam generator together, and separately, in this facility.

Mr. Dickinson: What thermal shock and transient capabilities are you planning?

Mr. Tarantini: We have foreseen the necessity to have a thermal shock capability. A study is now starting which considers two possible methods. One is to bypass the sodium to the furnace in order not to have available cold sodium. The other method would store cold sodium in a large tank for introduction into the loop.

Mr. Dickinson: What are the criteria? How many degrees per second and for how long?

Mr. Tarantini: The specification of the study contract states about 20 degrees per second. As the loop design is completed the transient condition will be reevaluated and will probably be reduced.

Mr. Pfahler (LMEC): You mentioned a transient of 20 degrees per second; for what range of temperature does this apply?

Mr. Tarantini: The temperature was 590° at the sodium exit from the furnace and was reduced about 150° before entering the furnace.

Mr. Pfahler: You are only talking about the negative change?

Mr. Tarantini: Yes, negative change. There is a small positive change of 6 degrees per second for 4 or 5 seconds. The stream shock is negative.

The Distribution of Fission Products in LMFBR Sodium Systems*

G. B. Zwetzig, J. Guon, and M. Silberberg

Atomics International
A Division of North American Rockwell Corporation
Canoga Park, California

(PRESENTED BY G. B. ZWETZIG)

1. Introduction

Detailed knowledge of the behavior and distribution of fission and corrosion products released to reactor coolants during operation is needed for the design, operation, maintenance, and safety evaluation of nuclear plants. Because of this importance, the distribution of fission products in sodium systems has been a subject of analytical and experimental study at Atomics International for a number of years. The first section of this paper describes some highlights of earlier work, while the latter portion describes our current activities.

2. System Depletion Concept

Early data on fission product distribution in sodium systems were obtained by Hart following the fuel cladding failure incident which occurred in the Sodium Reactor Experiment.[1] Some of his data are shown in Table 1. The column headed August 2, 1959 gives the measured specific activities in the sodium as of that date. The column labeled "predicted" indicates the activity levels that would have been expected on October 31, 1959 based on removal of the indicated isotopes exclusively by radioactive decay. The column labeled "actual" indicates the activity levels which were measured on October 31. Since the values in these latter two columns are different, it is apparent that mechanisms in addition to radioactive decay were operative in reducing the contamination levels in the sodium. These mechanisms are evidently related to processes occurring within the primary loop, since circulation and cold-trapping of the primary sodium were maintained during this three-month interval.

Kunkel and Berger[2] postulated that this added removal could be represented by an exponential system depletion factor, analogous and in addition to the radioactive decay constant. The numerical value of the system depletion factor was estimated by taking the difference between the total depletion constant and the radioactive decay constant as shown in Table 2.

If the system depletion constant were dependent on chemical and physical properties, one would expect it to be the same for all isotopes of a given element. For the limited data available for preparation of Table 2, this, indeed, seems to be the case (e.g., cesium, strontium, and cerium).

Using these system depletion constants and assuming that isotopes removed from the coolant are uniformly deposited on primary-system surfaces, Kunkel and Berger developed a preliminary, and as yet unverified, method for estimating the post-shutdown radiation levels of primary-system piping and equipment. It is one of our present objectives to improve upon this method.

It should be noted parenthetically that all fission product data from the SRE fuel-failure incident should be accepted with reservations, because the failure was caused by the presence of large quantities of carbonaceous materials in the coolant. This carbonaceous material, which was introduced by a tetralin leak, could have greatly modified the behavior of the fission products in the coolant by acting as a "getter." This is shown by Table 3.

3. Early Experiments

A considerable number of investigations of the behavior of fission products in sodium have been performed at Atomics International in the past, and the results from most of these have been reported by Kunkel *et al.*[3, 4] More recent work, however, includes investigations of cesium and iodine vaporization from sodium and preliminary scoping experiments on cold-trapping of cesium. The work on cesium and iodine vaporization is reported in another paper[5] presented at this conference. The scoping experiments on cesium cold-trapping will be briefly described here.

These experiments were intended to investigate the apparent high efficiency of cold traps in removing cesium from the sodium coolant, as observed in the SRE.[6] One postulated mechanism was the adsorption of the cesium on deposited sodium oxide. To investigate this, experiments were performed in the small stainless steel loop shown in Fig. 1 using a ^{134}Ce tracer in stable cesium. The cold trap, which was air-cooled, is at the lower left corner of the loop. A shielded sodium iodide scintillation detector was used to monitor the radiation level in the cold trap.

* Based on studies conducted for the U. S. Atomic Energy Commission under Contract AT(04-3)-701.

TABLE 1. Decrease of Fission Product Contamination in Primary Sodium

Isotope	Fission Product Contamination (μCi/g Na)		
	August 2, 1959	October 31 (Predicted)	October 31 (Actual)
^{137}Cs	1.26	1.26	0.45
^{134}Cs	0.02	0.02	0.006
^{90}Sr	0.97	0.97	0.060
^{89}Sr	19.0	5.8	0.25
^{131}I	0.42	0.00019	0.00012
^{141}Ce	3.7	0.54	0.000088
^{144}Ce	5.1	3.9	0.00031
^{95}Zr–^{95}Nb	13.0	5.2	0.0067
^{103}Ru	0.85	0.19	0.0045

TABLE 2. Total and System Depletion Constants for SRE System

Isotope	Total Depletion Constant ($days^{-1}$)	Radioactive Decay Constant ($days^{-1}$)	System Depletion Constant ($days^{-1}$)
^{137}Cs	1.16×10^{-2}	6.3×10^{-5}	1.15×10^{-2}
^{134}Cs	1.35×10^{-2}	9.1×10^{-4}	1.26×10^{-2}
^{90}Sr	3.14×10^{-2}	6.6×10^{-5}	3.13×10^{-2}
^{89}Sr	5.05×10^{-2}	1.37×10^{-2}	3.68×10^{-2}
^{131}I	9.07×10^{-2}	8.61×10^{-2}	0.46×10^{-2}
^{141}Ce	1.18×10^{-1}	2.13×10^{-2}	9.67×10^{-2}
^{144}Ce	1.08×10^{-1}	2.43×10^{-3}	10.6×10^{-2}
^{95}Zr–^{95}Nb	8.40×10^{-2}	1.07×10^{-2}	7.33×10^{-2}
^{103}Ru	5.81×10^{-2}	1.73×10^{-2}	4.08×10^{-2}

TABLE 3. Radioactivity Analysis of Typical Sample of Carbonaceous Material from Primary-sodium Sample

Isotope	Activity of Carbonaceous Material[a] (μCi/g of particles)[b]	Activity of Filtered Sodium (μCi/g Na[b])
^{137}Cs	1.1×10^{3}	0.45
^{134}Cs	2.9×10^{1}	0.006
^{141}Ce	2.3×10^{2}	0.0007
^{144}Ce	2.9×10^{2}	0.00039
Zr–^{95}Nb	2.2×10^{2}	0.018

[a] Obtained from Reactor 10-31-59.
[b] As of 7-26-59.
(From Reference 1)

The results obtained for a cesium concentration of 65 ppm and three different oxygen concentrations are shown in Fig. 2. The theoretical solubility limits for the three oxide concentrations are also shown. Thus, for temperatures above (that is, to the left of) these limits there should be no oxide precipitation. Inspection of the data, however, reveals that there is cesium deposition with decreasing temperature even before the limits of oxide solubility are reached. To explain this, one might postulate that cesium adsorption on stainless steel occurs in this temperature region. In this case, the validity of the assumption of cesium adsorption on precipitated sodium oxide would require an increase in the slope of the curves in Fig. 2 when the sodium temperature fell below the oxide solubility limit. Such a change in slope is not discernible, however. There is, nevertheless, sufficient scatter in the data points that this mechanism cannot be ruled out. What is clearly apparent from the data is that cesium deposition is not exclusively dependent on precipitated Na_2O, though increased concentration of the oxide does appear to enhance deposition.

The scoping experiments with this small loop were useful in providing basic qualitative information on cesium behavior, and in providing operational information useful in the design of the AI Fission Product Behavior Loop (FPBL), which has recently commenced operation.

4. Current Experimental Studies

The Fission Product Behavior Loop which is presently in operation is shown in Figures 3 and 4. The loop consists of two deposition test sections in series with associated heating and cooling units at the ends

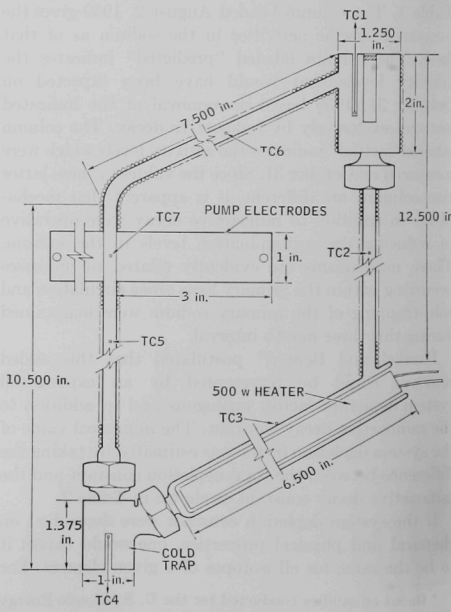

Fig. 1. Schematic Diagram of Cold-trapping Apparatus.

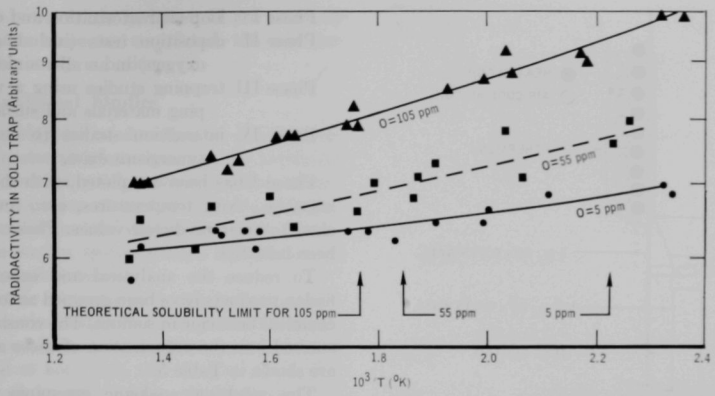

FIG. 2. Radiation Level in Cold Trap *vs* Cold-trap Inverse Temperature for Various Oxide Concentrations (65 ppm Cesium).

of each test section. It also includes a pump, a surge tank, a flowmeter, a level gauge, a bypass cold trap, and three bypass sampling lines. The loop is constructed entirely of Type 304 stainless steel except the valves, which are of Type 316 stainless steel. The loop tubing diameter is $\frac{3}{8}$ in. A detailed view of a deposition test section and the adjacent heating and cooling units is given in Fig. 5. Here it is seen that the test section consists of an enlarged annular region which for the first series of experiments is packed with Type 304 stainless steel mesh. The integral electrical heating and air-cooling units at the entrance and exit of the test sections permit wide flexibility in the operation of the loop so that the test sections may be operated in a variety of modes.

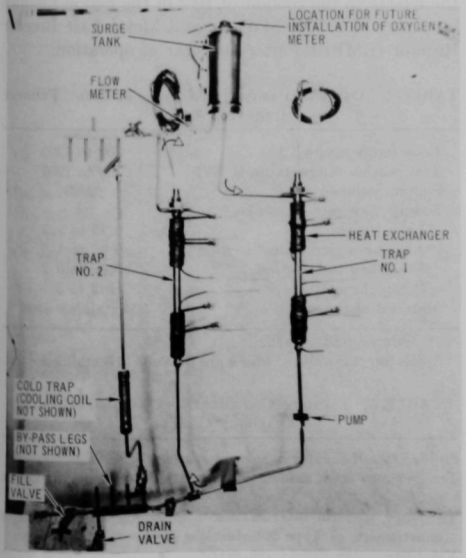

FIG. 3. Fission Product Behavior Loop.

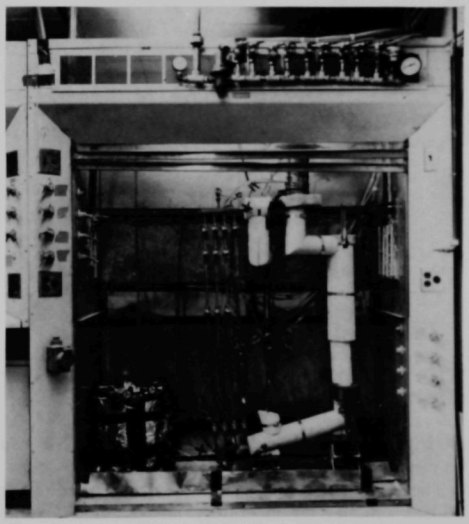

FIG. 4. Fission Product Behavior Loop in Hood.

Scintillation detectors capable of traversing the lengths of the test sections are used to measure *in situ* deposition or removal. A scintillation detector also monitors the radioactivity level in the surge tank.

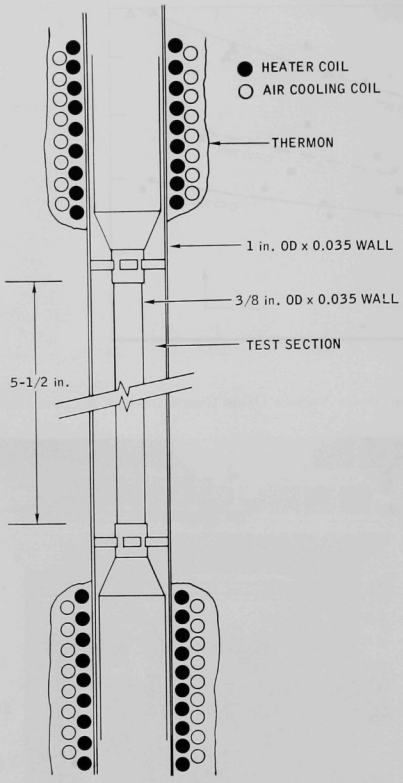

FIG. 5. Deposition Test Section of Fission Product Behavior Loop.

Both single and multichannel spectrum analyses can be performed.

The sample bypass lines are used for withdrawing coolant samples for laboratory analysis and for the introduction of radioactive tracers into the loop.

Some of the design parameters of the FPBL are given in Table 4.

The objectives of the FPBL tests are to provide information on:

1) the plating tendencies of various fission products on Type 304 stainless steel;
2) the effect of fission product and oxygen concentration on deposition;
3) suitable materials and conditions for the trapping of fission products.

It is planned that this program will be carried out in four phases:

Phase I loop characterization and calibration;
Phase II deposition tests (including the effect of oxygen) in an all-stainless steel system;
Phase III trapping studies using a variety of trapping materials and surfaces;
Phase IV interaction studies to determine if any synergisms exist.

Phase I has been completed, with the loop performance, i.e., flow, temperatures, etc., found to be very close to their predicted values. Phase II has recently been initiated.

To reduce the analytical and experimental effort, fission products have been grouped as to their predicted chemical behavior in sodium. The considerations which entered into the organization of these analogue groups are shown in Table 5.

The resulting analogue groupings are shown in Table 6. Also shown are the selected representative isotopes for each group and the expected fate of the isotope in the Phase II tests.

Calculations have been performed to determine the specific activities of the radioisotopes required for various detection levels. Based on these, the lower limit of radioisotope concentration in the sodium for adequate counting statistics is about 100 ppb. Because of several simplifying, pessimistic assumptions used in these calculations, the actual lower limit may be 10 ppb. This is roughly the same level as produced by the release to the coolant of 10^{-5} of the fission product inventory of a 1000-MWe Liquid Metal Fast Breeder Reactor (LMFBR) after one year of operation.

TABLE 4. DESIGN PARAMETERS FOR FISSION PRODUCT BEHAVIOR LOOP

Loop temperature (°F)	300 to 1200
Test section temperature[a] (°F)	300 to 1200
Sodium volume (cc)	2000
Sodium flow rate (ft/sec)	
Loop tubing	0.15 to 1.5
Annular region of test section	0.15 to 1.5
Unpacked test section	0.02 to 0.2
Pump throat	0.3 to 3
Material of construction[b]	304 stainless steel

[a] Independently variable.
[b] Except for valves, which are of Type 316 stainless steel.

TABLE 5. FACTORS CONSIDERED IN ORGANIZATION OF ANALOGUE GROUPS

Similarity of behavior in solvent systems other than sodium
Tendency to form oxides that are stable relative to sodium oxide
Tendency to form intermetallic compounds with the major constituents of Type 304 stainless steel
Volatility
Solubility in sodium

Experiments with cesium in Phase II are currently under way. When these are completed, the next isotope planned for study is barium.

5. Current Analytical Studies

The final activity to be described is the development of a computer program to aid in the prediction of fission and corrosion product distributions throughout the primary system of an LMFBR. As indicated earlier, such predictions are needed for safety evaluation, economics studies, system design, and operational and maintenance planning.

By means of this computer code, calculations are performed to determine individual isotope inventories in the fuel, in the coolant, in deposits on system walls, in deposits in cold or hot traps, and in cover-gas spaces. In performing these calculations, the code has been programmed to consider up to 50 fission product mass chains consisting of up to 5 members per chain, 5 corrosion products, and ^{24}Na and ^{22}Na.

The corrosion products considered in the calculation along with their production reactions are listed in Table 7. In computing these corrosion product activities, the system is assumed to be constructed of Type 304 stainless steel of nominal composition and containing 0.05 wt % cobalt impurity. In each case, the cross sections for each production reaction are weighted by a "typical" LMFBR neutron spectrum having a mean

TABLE 6. Analogue Grouping and Expected Fate of Various Fission Products

Analogue Grouping	Representative Radioisotope	Expected Fate in Stainless Steel System
Cs	Cs-134	Volatilization or deposition as complex oxide
Ba, Sr	Ba-133	Deposition as oxide
Mo, Ru, Sb, Ag	Ru-103 Sb-124	Diffusion into stainless steel
Ce, La, Nd, Y, Zr	Ce-141	Deposition as oxide or diffusion into stainless steel
Nb	Ta-182	Deposition as oxide or diffusion into stainless steel
H^3, I, Te	Se-75	Vaporization or diffusion into stainless steel

TABLE 7. Corrosion/Erosion Products Calculated in the Source-term Program

Radioisotope	Production Reactions
27.8-d ^{51}Cr	$^{50}Cr(n,\gamma)$, $^{54}Fe(n,\alpha)$, $^{52}Cr(n,2n)$
300-d ^{54}Mn	$^{54}Fe(n,p)$, $^{55}Mn(n,2n)$
45.1-d ^{59}Fe	$^{58}Fe(n,\gamma)$
72-d ^{58}Co	$^{58}Ni(n,p)$, $^{59}Co(n,2n)$
5.3-y ^{60}Co	$^{59}Co(n,\gamma)$, $^{60}Ni(n,p)$

(1) $$\dot{N}_g^i = \epsilon^i(Ry^i + \lambda^{i-1}N_f^{i-1}) + \lambda^{i-1}N_g^{i-1} - (\lambda^i + L)N_g^i$$

N_g^i = Atoms of isotope i available for release to coolant
N_f^i = Atoms of isotope i in fuel
λ^i = Decay constant of i
L = Fractional leakage rate
ϵ^i = Fuel escape and availability factor
R = Total fission rate
y^i = Fission yield
i − 1 = Isotope preceding i in mass chain

(2) $$f_c(t) = f_{c1} + f_{c2}t + f_{c3}\exp\,(t/f_{c4}) + f_{c5}(t - t_r)$$

f_{c1} to f_{c4} = Constants
$f_{c5} = 0$ for $t \leq t_r$
$f_{c5} = f_{c3}$ for $t > t_r$

Fig. 6. Equations Used for Fission Product Release to Coolant.

fission energy of 170 keV. In discussing corrosion products, it should be noted that two types are being considered: (1) core materials which are activated and which subsequently corrode into the coolant stream, and (2) materials which corrode from primary-system surfaces and are subsequently activated as they pass through the reactor core.

In applying the program to an LMFBR the following regions are considered in computing radioisotope inventories:

1) fuel;
2) fuel-rod gas space;
3) coolant;
4) primary-loop surfaces, up to 10 regions;
5) bypass trapping loops, up to 5 in number;
6) cover-gas volumes, up to 5 in number.

In addition, the code is designed to accommodate a variable reactor-power history consisting of up to 5 different constant-power levels, and a final shut-down level. Printout of selected quantities may be provided at up to 20 specified times.

The fission product inventory in the fuel is calculated using the general equations developed by Harris[7] for fission product chains with direct fission yield plus generation by parent decay for each member of the chain. To simplify calculations, the short-lived precursors ($T_{1/2} < 20$ min) were eliminated from the chains and their cumulative yields were added to the first relatively long-lived member of the chain. Fission product yields were based on fast fission in plutonium as given by Anderson.[8]

Fission product release to the primary system is based on a two-factor model. The first factor is the total inventory of an isotope available for release to the coolant in the event of cladding failure, and the second is the fraction of the cladding that is defected. The inventory available for release to the coolant is calculated from the differential Eq. 1 in Fig. 6. The

Inventory	Addition Processes	Removal Processes
Coolant (fission products)	Cladding leakage Parent decay Tramp fuel fission Corrosion of plated deposits	Deposition Trapping Decay Vaporization
Surface	Deposition	Decay Corrosion
Trap	Precipitation Adsorption	Decay
Cover gas	Vaporization	Decay
Coolant (corrosion products)	Corrosion of activated structure Activation of corroded structure	Deposition Trapping Decay

FIG. 7. Processes Used in Calculating Inventories.

fraction of cladding failed at a given time is programmed by means of Eq. 2 of Fig. 6.

Once fission products have been released from the fuel cladding, the code accounts for the inventory of the various isotopes in other parts of the reactor system. The processes that are considered in calculating these various inventories are summarized in Figure 7.

The basic forms of the equations used for treating some of these processes are shown in Fig. 8. Directing our attention to Eq. 1, we see that the rate of loss of atoms of isotope i from the coolant by deposition is proportional to the difference between the chemical activity of i in the coolant in region k, namely, $N_c^i(V_c\sigma_k^i)$, and the surface activity of i in region k, namely, S_k^i/Δ_k^i. The unknowns are K_k^i and Δ_k^i, and in a number of cases, σ_k^i as well. The quantity Δ_k^i is the surface concentration of i in region k when the surface is saturated with i. It is a function of the chemical species, temperature, and deposition reaction involved. The rate constant K_k^i is a function both of the deposition process involved and of the temperature, flow, and, perhaps, surface conditions in that region. We hope to obtain estimates of the values of K_k^i and Δ_k^i from the experiments performed in the Fission Product Behavior Loop and elsewhere.

It should also be noted that the concentration of isotope i in the coolant, N_c^i, is assumed constant throughout the loop during a given time step. This implies that the fractional removal of i from the coolant is relatively small during such an interval. Although this assumption is probably not correct for some elements (e.g., the corrosion product chromium), it is considered a necessary simplification if the code is to accommodate long periods of reactor operation efficiently. At the same time, the exceptional elements can be treated by judicious assignment of reaction rates K_k^i to the various regions.

Equation 2 shows the general form of the trapping relationships. Two specific mechanisms are shown: (1) trapping by exceeding the solubility limit and (2) deposition by adsorption. As indicated in Fig. 8, the first term is operative only when the concentration of isotope i, namely, N_c^i/V_c, exceeds its solubility at the trap conditions. The second term, intended to represent the deposition process, is similar to Eq. 1 except that in the interest of mathematical simplification the surface-concentration effect is neglected. Because significant surface concentrations will be developed on trap surfaces, however, the validity of this simplification is currently being reviewed and alternative formulations are being studied. In this simplified model,

(1) Deposition: $$\dot{N}_c^i\big|_{dep} = \sum^{k} - K_k^i \left(\frac{N_c^i}{V_c \sigma_k^i} - \frac{S_k^i}{\Delta_k^i} \right) A_k \sigma_k^i$$

N_c^i = Atoms of isotope i in coolant
V_c = Coolant volume
σ_k^i = Solubility of isotope i in region k
S_k^i = Surface concentration of isotope i in region k
Δ_k^i = Surface concentration of isotope i in region k at saturation
K_k^i = Deposition rate constant in region k
A_k = Area of region k

(2) Trapping: $$\dot{N}_c^i\big|_{trap} = \sum^{m} - F_m \left\{ \left(\frac{N_c^i}{V_c} - \sigma_m^i \right) + \frac{N_c^i}{V_c} \left[1 - \exp\left(- P_m K_m^i \frac{Z_m}{F_m} \right) \right] \right\}$$

F_m = Flow rate in trap m
σ_m^i = Solubility of isotope i in trap m
P_m = Surface area per unit length of trap
K_m^i = Deposition rate constant in trap m
Z_m = Length of trap
$[(N_c^i/V_c) - \sigma_m^i]$ is restricted to positive values

(3) Vaporization: $$\dot{N}_c^i\big|_{vap} = - \frac{1}{\Delta t} (N_{v,eq}^i - \bar{N}_v^i)$$

$N_{v,eq}^i$ = Atoms of isotope i in vapor spaces at equilibrium (based on atoms of isotope i in coolant)
$\bar{N}_v^i$ = Average no. of atoms of isotope i in vapor spaces during preceding time interval
Δt = Time interval used in calculation
$N_{v,eq}^i$ is derived from distribution coefficient k_D

(4) Corrosion: $$\dot{N}_c^i\big|_{corr} = \sum^{k} \lambda_{c,k} A_k S_k^i$$

$\lambda_{c,k}$ = Corrosion constant for monolayer in region k
A_k = Surface area of region k
S_k^i = Surface concentration of isotope i in region k

FIG. 8. Forms of Equations Used in Computing Inventories.

however, the exponential form of the term reflects the effect of trap surface area and flowrate on completeness of trapping.

One problem that arises in several of these equations as presently formulated is that element-dependent (i.e., chemical) processes are being treated on the individual isotope level. This is particularly apparent and important in connection with the trapping model based on solubility. Solubility, of course, refers to the aggregate concentration of an element, based on all isotopes, radioactive and stable. To treat this process rigorously, then, would require computing the inventory for all the isotopes of an element, both stable and unstable. Since this would add to an already large computational effort, we are treating this problem through the use of partial solubilities assigned to each isotope on the basis of its estimated relative abundance in the coolant.

A similar problem is potentially present in the case of surface deposition, but only in case that the surface reaction or adsorption sites become saturated. So long as that does not occur, the individual isotopes of a given element may be expected to deposit approximately in proportion to their activity in the coolant, and this behavior will be provided by the current analytical model.

The method of accounting for vaporization in the computer code is rather involved and arbitrary. This is necessary because of the limited data on vaporization properties of fission product solutes in sodium and because of the even more limited data on rates of vaporization. Equation 3 shows the presently used basic relationship. Since Δt is the calculational time increment, this equation states that enough atoms of isotope i will reach the vapor spaces during the time interval to produce an equilibrium concentration. Actually, Eq. 3 says that even more atoms will leave the coolant. This is because the subtraction is made using the average number of atoms of i in the vapor space during the preceding time interval rather than the equilibrium value. The purpose of this construction is to account for the decay of atoms already in the vapor space; thus, more atoms must leave the coolant to achieve the assumed equilibrium concentration.

Finally, corrosion is accounted for by Eq. 4. Here we are concerned with the corrosion of isotopes which have previously been deposited on a surface. To treat this problem we have assumed that the deposit exists in an atomic monolayer. We have then introduced the concept of the corrosion constant, which is analogous to the radioactive decay constant and indicates the fraction of the thickness of monolayer that is removed per unit time. This, then, produces a corresponding introduction of isotopes back into the coolant stream.

The foregoing models for treating deposition, trapping, vaporization, and corrosion have been combined into a computer code which will significantly simplify the prediction of distributions of fission and corrosion products in LMFBR systems. The present limitation is the availability of the necessary chemical-behavior data. The code, by being applied to current experimental loops, however, may assist in the development of these data.

At the time of preparation of this paper, the computer program has been written, punched on cards, and compiled. We are now in the process of running our first test problem and de-bugging the code.

REFERENCES

1. R. S. Hart, *Distribution of Fission Product Contamination in the SRE*, NAA-SR-6890 (March 1962).
2. W. P. Kunkel and S. Berger, *Fission-Product Deposition in a Fast Breeder Reactor System Containing Failed Fuel Elements*, Trans. ANS, **10**(2), 496 (1967).
3. W. P. Kunkel, D. M. Elliott, and A. S. Gibson, *Inpile Experiments on Retention of Fission Products in 500°F Sodium*, NAA-SR-9163 (Jan 1964).
4. W. P. Kunkel, *Fission Product Retention in Sodium—A Summary of Analytical and Experimental Studies at Atomics International*, NAA-SR-11766 (Aug 1966).
5. B. D. Pollock, M. Silberberg, and R. L. Koontz, *Vaporization of Fission Products from Sodium*, THIS CONFERENCE.
6. A. I. Hansen, *The Effects of Long-term Operation on SRE Sodium System Components*, NAA-SR-11396 (Aug 31, 1965).
7. N. A. Harris, P. Kenfield, W. Lahs, and W. Sayer, *An Improved Method of Dose Calculation From Airborne Fission Products*, CONF-642-8.
8. C. W. Anderson, *Fission Product Yields from Fast (~1 MeV) Neutron Fission of Pu-239*, LA-3383 (1965).

Radioisotope Transport and Deposition in Flowing Sodium

W. F. Brehm, E. A. Kovacevich, and D. W. Shannon

Batelle Memorial Institute
Pacific Northwest Laboratory
Richland, Washington

(PRESENTED BY W. F. BREHM)

Abstract

Transport and deposition of radioisotopes released to flowing sodium from corrosion of irradiated stainless steel has been studied. Quantitative measurements of deposition can be made with sensitive counting techniques. The results of the study indicate that ^{51}Cr and ^{60}Co are transported primarily by isotopic exchange and do not rapidly migrate to lower-temperature regions of loop systems. However, ^{54}Mn is released in larger quantities to deposit throughout the test loops. Preferential deposition sites are (1) immediately downstream from the source, (2) at minimum-temperature locations, and (3) in oxygen cold traps. These results indicate ^{54}Mn is transported both by exchange and by solution-and-precipitation. Deposited ^{54}Mn migrated rapidly to the cold trap; deposited ^{51}Cr and ^{60}Co migrated slowly by exchange.

The rapid transport of large amounts of ^{54}Mn to low-temperature locations can create serious problems for reactor maintenance. Work is continuing better to define the factors which affect this deposition, and to develop methods for trapping out radioisotopes in preselected shielded low-maintenance locations.

Introduction

In a sodium-cooled fast reactor such as the FFTF, material will be lost from the stainless steel fuel cladding by the corrosive action of the flowing sodium coolant. Under ultimate operating conditions (1200°F bulk coolant temperature, 25-ft/sec sodium velocity, 10 ppm oxygen in sodium) the rate of metal loss is approximately 0.0005 in. (0.0013 cm) per year.[1, 2] For Type 300 series stainless steel at 1200°F, this rate of metal loss is acceptable from considerations of cladding integrity. More detailed information of all factors affecting metal loss rate is available.[2-4]

However, the material removed from the core will contain large amounts of radioisotopes produced from irradiation of the cladding. A typical inventory is the following:[5]

^{51}Cr, 27.8-day half-life—2 Ci/cm^3;

^{58}Co, 71-day half-life—31 Ci/cm^3;

^{60}Co, 1913-day half-life—2 Ci/cm^3;

^{54}Mn, 313-day half-life—10 Ci/cm^3.

A study based on typical FFTF operation under the conditions described above has shown that about 1100 cc of material will be lost from the core and transported to other parts of the heat-removal circuit in one year of operation. The isotope inventory will be approximately 10,000 Ci, and the radiation level near heat-removal-system components may exceed 100 R/hr depending upon deposition conditions.[6] Previous studies of transport and deposition of irradiated stainless steel in flowing sodium have shown that activity transport is not necessarily coincident with gross mass transport, and these data are very meager.[7, 8]

Our experimental objective is to study the effect of various reactor operating variables such as temperature, system temperature gradient (ΔT), velocity, flow perturbations, and impurity level on the transport and deposition of these isotopes in test loops. The ultimate aim of the program is to identify the mechanisms of transport and deposition, and to make a quantitative model to predict deposition behavior in a reactor system. A necessary byproduct of this study will be development of methods to control or trap the isotopes in a shielded preselected location(s).

Experimental Proceedings

Two types of sodium loop are used: a pumped loop called the Radioisotope Transport Loop (RTL), and small thermal convection (TC) loops. The RTL, constructed of Type 304 stainless steel, has a 2-gal/min capacity in the primary flow circuit. The primary contains a 40-kW direct-resistance heater, shielded specimen-loading port, isothermal velocity-change section in the hot leg, and air-blast heat exchanger. An 0.2-gal/min secondary circuit contains cold trap, plugging meter, and sample-removal lines. A schematic of the RTL is shown in Fig. 1. The sodium velocity in the primary varies from 0.5 ft/sec in the heat exchanger to 40 ft/sec at the irradiated specimen location.

The thermal convection loops are also made of Type 304 stainless steel, and are 15 in. high and 8 in. wide. Heat is supplied with a clamshell furnace and trace heating. An irradiated specimen is hung from a wire fastened to the loop cap. Typical velocity estimates are 0.2 to 0.8 ft/sec. A schematic TC loop is shown in Fig. 2.

Various irradiated stainless steel specimens are used. They fall into two categories: material irradiated in a thermal flux, containing ^{51}Cr, ^{60}Co, ^{59}Fe; and stock from EBR-II (fast flux), containing ^{54}Mn and small amounts of ^{58}Co. Typical specimen inventories are given in Table 1.

The use of radioactive specimens and the counting techniques give us a very powerful tool for observing migration of various elements in test loops. The loops are scanned either in place with a portable lead-shielded NaI crystal, or sections are cut from the loops and counted in a shielded well with a NaI crystal or a 20-cc lithium-drifted germanium diode. Counts are analyzed in a 4096-channel analyzer. Calibration by the first (in-place) method has been achieved by counting radioactive solutions of known inventory in pipes of the same size as loop piping; thus absolute quantities of radioactive material can be measured in many instances. Further advantages of the *in situ* method are these: counting can be done quickly and without elaborate preparations, the method is nondestructive, and loop tests can quickly be resumed. Disadvantages include low sensitivity (about 1500 disintegrations/count), poor resolution (10 keV/channel), and Bremsstrahlung generated in the pipe that interferes with low-energy gamma-ray detection. Counting in the well eliminates these problems, especially when the diode is used, but is more time consuming and requires either a tab specimen in the loop or a part of the loop which must then be replaced. Counting in the well is usually done to supplement and clarify the data from the more rapid in-place scanning.

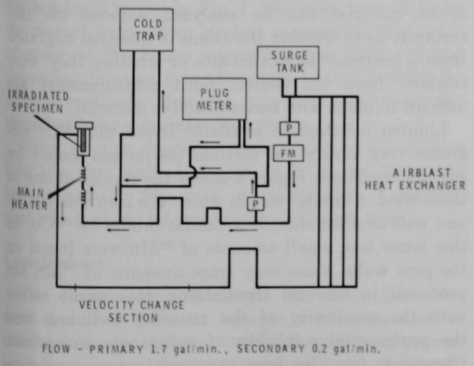

FIG. 1. Schematic Diagram of Radioisotope Transport Loop.

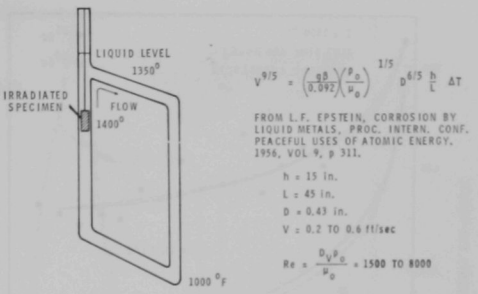

FIG. 2. Schematic Diagram of Thermal Convection Loop.

TABLE 1. TYPICAL SPECIMEN INVENTORIES

Hanford-irradiated stock
71-day ^{58}Co, 60 μCi/gram
1913-day ^{60}Co, 560 μCi/g
278-day ^{51}Cr, 2×10^5 μCi/g
45-day ^{59}Fe, 3×10^4 μCi/g
EBR-II stock, out of reactor 18 months
^{58}Co, 1000 μCi/g
^{60}Co, 600 μCi/g
313-day ^{54}Mn, 3×10^4 μCi/g

Results and Discussion

The first tests were run in the RTL and TC loops with a thermal-irradiated specimen. The results were similar; ^{51}Cr and ^{60}Co were released from the specimen but migrated only a short distance downstream, as shown in Fig. 3. No ^{51}Cr or ^{60}Co was found in the heat exchanger or cold trap of the RTL. The data of Figure 3 are not decay-corrected; the original chromium level was higher by two orders of magnitude. This is an example of radioisotope transport by isotopic exchange. Analysis of loop sodium showed ^{60}Co, ^{51}Cr, and traces of ^{54}Mn, indicating higher ^{54}Mn solubility. No ^{59}Fe has ever been identified on loop piping even though substantial amounts of ^{59}Fe are present in the source tab.

The first RTL run with an EBR-II irradiated specimen gave quite different results: the amount of manganese released was about 10 times the amount of chromium released in the other test, and ^{54}Mn was found all over the loop. High counting rates were obtained in the following regions immediately downstream of the specimen: the crossover pipe from heat-

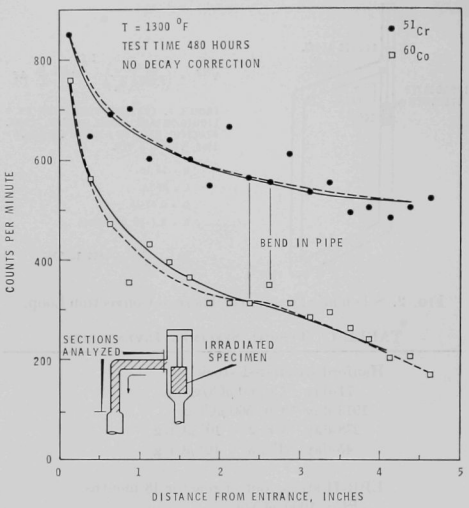

FIG. 3. Counting Rate in Original Radioisotope Loop Run.

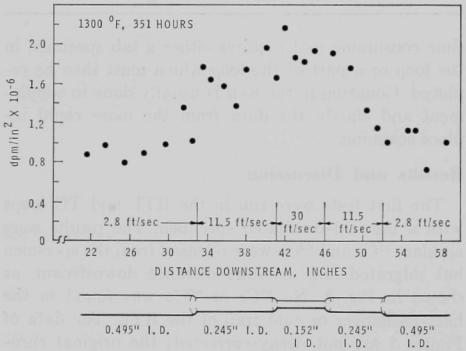

FIG. 4. Counting Rate of ^{54}Mn in Velocity Sections.

exchanger outlet to surge tank, and in the cold trap. This shows that some ^{54}Mn is transported by exchange, but the preferential deposition at lower-temperature regions suggests transport also occurs by solution and precipitation, possibly assisted in the cold trap by chemical reaction with the Na_2O to form $NaMnO_4$.[9] Specimens showed weight losses that were in approximate agreement with weight losses previously reported.[2]

Effect of Velocity on Deposition

Deposition of ^{54}Mn in the velocity-change section of the RTL varied as shown in Fig. 4. Note that the abscissa of the graph is dpm/in.^{2}; these measurements can be made with our calibrated counting technique. This part of the loop is isothermal at 1300°F, so the deposition is taking place by exchange. The higher deposition rate at the higher velocity suggests the rate-limiting step for deposition is diffusion through a boundary layer that decreases in thickness with increasing velocity. Similar indicative results were obtained in the cold leg of the RTL. ^{58}Co was not found.

Effect of Temperature and Delta-T (ΔT)

Tests in thermal convection loops with ^{54}Mn-bearing specimens gave the following indicative results.

In the absence of large temperature gradients (less than 200°F difference between maximum and minimum temperatures) in a TC loop, ^{54}Mn is also transported chiefly by isotopic exchange. However, at a larger ΔT (400°F) the segregation of ^{54}Mn to the cold side of the loop occurred (1400°F specimen temperature and a 1000°F minimum temperature). A comparison of the two cases is shown in Fig. 5. The ratio of counts at the minimum-temperature location to counts at maximum-temperature location in TCL #5 was 5.6; the ratio in another loop with 1230°F maximum and 1050°F minimum was 1.4. More than three times as much activity was released from the specimen at 1400°F as at 1225°F. These results show that both specimen temperature and loop ΔT affect the transport of ^{54}Mn. Work is in progress to attempt to define the affect of each variable separately.

Activity Migration

One of the most interesting aspects of our work concerns the migration of deposited activity. When the irradiated specimen is removed from the loop and sodium flow resumed, transport of the deposited radioactive material can be analyzed without the uncertainty as to whether the atoms in question migrated from a previous deposition site or whether they were released from the source. Such measurements are difficult to make with nonradioactive material.

Limited information available shows that ^{51}Cr migrates very slowly (in thermal convection loops) by isotopic exchange. Figure 6 shows the results of one of these tests. A similar test in which the loop was cut up and well-counted showed a similar profile for ^{60}Co. In this latter test, small amounts of ^{54}Mn were found on the pipe walls. Since only trace amounts of ^{54}Mn are produced in thermal irradiations, this result shows both the sensitivity of the counting technique and the preferential solubility of manganese in sodium. Chromium has also been reported to have preferential (with respect to iron and cobalt) solubility in sodium, but chromium migration similar to that observed has also been reported.[10]

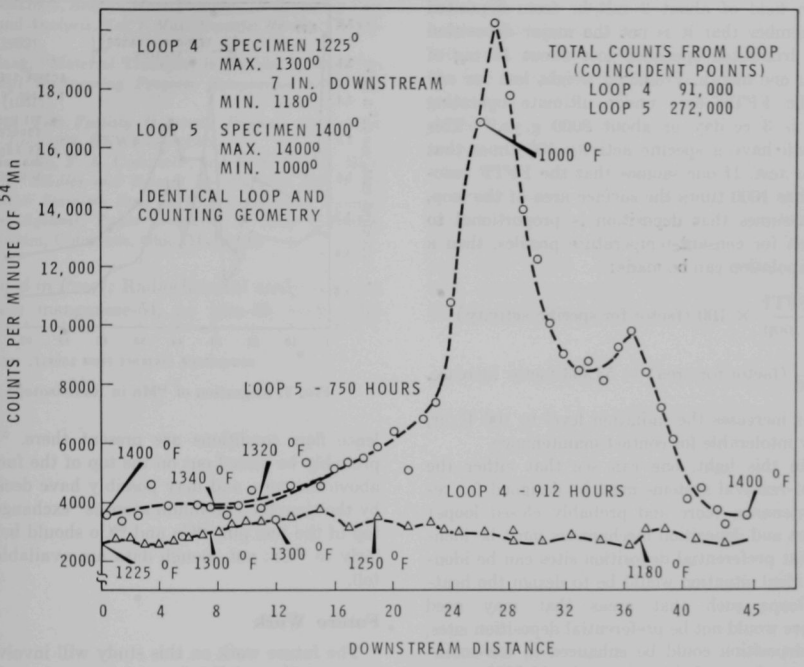

FIG. 5. Comparison of Activities in Loops 4 and 5.

The migration of ^{54}Mn in the RTL for two more runs produced a steady decrease in ^{54}Mn activity throughout most of the primary system, and an increase in activity in the cold trap. These results are presented in Table 2. A graph of ^{54}Mn migration in the hot leg is shown in Fig. 7. The peak near 31 in. in the restart data (open circles) is probably the result of some of the atoms migrating from their original deposition location near the source to that location by isotopic exchange. However, note that everywhere else there has been a decrease in activity.

Some of the deposited radioactive atoms diffuse into the pipe wall. Diffusion of ^{51}Cr and ^{54}Mn has been observed. The rate of penetration is roughly that which would be predicted by diffusion theory.

Conclusions

The obvious conclusions one can draw from this work are that different isotopes are transported in sodium loops by different processes, and each process is dependent on flow, temperature, and chemistry. Much more to the point, however, is a consideration of the implications the results of this work will have on reactor operation. The heat exchanger in the RTL has

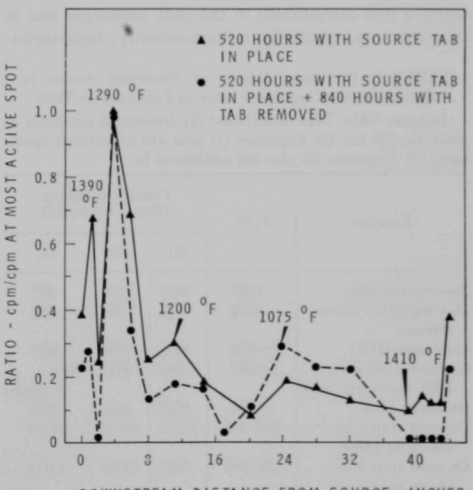

FIG. 6. Comparison of Activity Distribution in TC Loop #1 before and after Running Loop without Source Tab. Active species—^{51}Cr, 30-min counts.

a radiation field of about 2 mR/hr from deposited ^{54}Mn (remember that it is not the major deposition site). The irradiated specimen lost about 15 mg of material in one month. Predicted weight loss for one year in the FFTF core under ultimate operating conditions is 3 cc/day or about 8000 g/yr.[6] This material will have a specific activity 100 times that used in our test. If one ssumes that the FFTF reactor vessel has 1000 times the surface area of the loop, and also assumes that deposition is proportional to surface area for consant-temperature profiles, then a crude extrapolation can be made:

$$\frac{8000 \text{ g in FFTF}}{0.015 \text{ g in loop}} \times 100 \text{ (factor for specific activity)}$$

$$\times \frac{1}{1000} \text{ (factor for area)} = 53{,}333 \text{ factor increase.}$$

This factor increases the radiation level to 106 R/hr, completely intolerable for contact maintenance.

Taken in this light, one can see that either the FFTF heat-removal systems must be designed for remote maintenance (core and probably closed loops) or transport and deposition mechanisms must be identified so that preferential deposition sites can be identified. An ideal situation would be to design the heat-removal loops such that areas that may need maintenance would not be preferential deposition sites, and that deposition could be enhanced in low-maintenance areas that could be adequately shielded.

The results of our study show that ^{54}Mn would be trapped just downstream of the heat exchanger and in the cold trap, especially if high-velocity, high-turbulence flow conditions are present there. ^{51}Cr would probably be plated out on the top of the fuel pins just above the core, and may possibly have decayed away by the time the chromium atom is "exchanged" off the top of the fuel pin. ^{58}Co and ^{60}Co should behave similarly to ^{51}Cr; not enough data are available to really tell.

TABLE 2. Counting Rates at Selected Areas in Radioisotope Transport Loop as Function of Time

Isotope: ^{54}Mn. Test conditions: (1) Irradiated specimen in place for 351 hr; (2) Exposure (1) plus 416 hr without specimen; (3) Exposure (2) plus 384 additional hr.

Location	T, °F	Counts per Minute (Decay Corrected)		
		(1)	(2)	(3)
Specimen holder	1300	5218	3102	897
Hot leg 20 in. downstream	1300	944	704	589
Cold-side IHX	~850	3078	2859	3051
Crossover between IHX and surge tank	~800	7482	5047	Not counted
On surge tank	~800	4084	5016	4621
On cold trap 1 in. above entrance	250–300	13771	15416	27951
On cold trap 5 in. above entrance	250–300	3697	13563	12112
On heater	1300–1350	812	715	Not counted

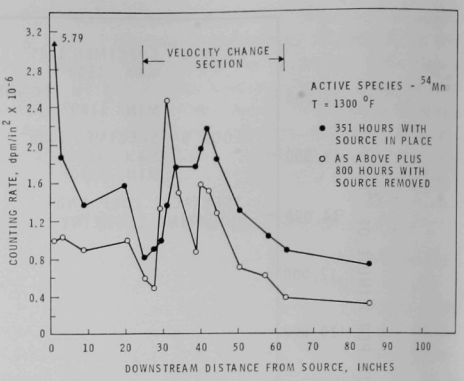

FIG. 7. Migration of ^{54}Mn in Radioisotope Loop.

Future Work

The future work on this study will involve redesign of the RTL and TC loops for insertion of more tab and ring specimens to take advantage of the strong points of both counting techniques. The RTL redesign will incorporate coplanar tubing for better detector positioning, and series-flow exchanger and cold trap for better determination of isotope concentration *vs.* temperature profiles. A high-cobalt stainless steel is being irradiated to introduce enough ^{60}Co into the loops for easier detection.

REFERENCES

1. P. T. Nettley *et al.*, "Problems in the Selection and Utilization of Materials in Sodium Cooled Fast Reactors," in *Fast Breeder Reactors*, Pergamon Press, Oxford (1966).
2. M. C. Rowland *et al.*, *Sodium Mass Transfer. XV. Behavior of Selected Steels Exposed in Flowing Sodium Test Loops*, GEAP-4831 (1965).
3. E. G. Brush, *Sodium Mass Transfer. XVI. The Selective Corrosion Component of Steel Exposed to Flowing Sodium*, GEAP-4832 (1965).
4. *Alkali Metal Coolants*, Proceedings of Symposium in Vienna, Nov–Dec 1966, International Atomic Energy Agency, Vienna (1967).
5. D. W. Shannon, *Fast Reactor Corrosion and Chemistry, Interim Technical Progress Report No. 1*, BNWL-483 (1967).
6. W. F. Brehm, *Radioactive Mass Transport in FFTF Primary Piping*, BNWL-808 (1968).

7. R. W. Lockhart, *Sodium Mass Transfer. II. Screening Test Data and Analysis. Vol. I. Mass Transfer Results*. GEAP-3726 (1962).
8. F. G. Haag, "Material Transport in Sodium Systems" in *Chemical Engineering Progress Symposium Series* **20**, 43-50 (1957).
9. *Fast Flux Test Facility Quarterly Progress Report for April-June 1968*, BNWL-880 (1968).
10. G. P. Wozadlo, F. A. Comprelli, and R. S. Young, *Mass Transfer Studies and Related Metallurgical Effects for Austenitic Stainless Steel in High-temperature Pumped Sodium Systems*, Paper presented at AEC Corrosion Symposium, Columbus, Ohio, May 1968.

Note added in Proof: Radiochemical analysis of our sodium gave manganese-54, no iron-59, very little cobalt-60, some chromium-51. This is when the cobalt and chromium were present. We also found silver-110 and antimony-124, which could have come from the fact that the EBR-II material was not completely cleaned out of the fission products. The antimony might have come from the fact that the material was used in a solder joint at one time. It just goes to show when you use radioactive material you find all kinds of strange things in your sodium. There was some discussion yesterday which prompted me to think of this. Everybody finds antimony and silver in their sodium, and the initial spectroscopy yielded manganese, iron, cobalt, chromium, and nickel, all in the less-than-one-part-per-million range.

Fission Product Vaporization from Sodium Systems*

A. W. Castleman, Jr. and I. N. Tang

Brookhaven National Laboratory
Upton, New York

(PRESENTED BY A. W. CASTLEMAN, JR.)

1. Introduction

A knowledge of the factors governing the rate and extent of fission product vaporization from liquid sodium is important in both operational and safety considerations of fast reactors. As regards normal reactor operation, this information is needed to determine the distribution in the coolant, on surfaces, and in cold traps of the fission products either intentionally or accidentally released to the primary system. Thermochemical data are also required in the design of coolant-stream cleanup systems employed during reactor operation. In considering the consequence of a reactor accident, the rate and extent of fission product release has a direct bearing on the engineered safeguard devices to be deployed in the event of a release as well as on the siting criteria which form a basis for reactor location with respect to populated areas.

The results of both analytical and experimental studies of the thermodynamic properties and transport behavior of some fission products in sodium are presented in this paper. Since the chemical states and relative volatility of the fission products are related to their thermochemical properties, this aspect of the work is covered first. Next, the transport properties are considered together with the limiting case of maximum release. Finally, the application of these results to the calculation of fission product partial pressures above sodium, as well as their relative extent of vaporization, is discussed.

Generally, only the limiting concentration region of infinite dilution is of interest since the total quantity of fission products dissolved in the sodium coolant is usually very small. However, because of the potential buildup of fission products in the sodium thermal bond of high-burnup fuel elements, regions of higher concentration are also of practical interest. Therefore, thermodynamic data are given for regions of high fission product concentration as well as those approaching infinite dilution.

2. Thermodynamics

The chemical potential or the "escaping tendency" of a solute from a solution is directly related to its fugacity f. At moderate pressures, the fugacity may be equated to the partial pressure of the solute, P, by the expression

$$f_i \cong P_i = P_i^0 \gamma_i x_i , \qquad (1)$$

where subscript i denotes the particular solute under consideration, P^0 the vapor pressure of the pure solute, γ its activity coefficient in solution, and x its mole fraction. The activity coefficient is, in turn, related to the partial molar excess free energy of mixing, $\overline{\Delta F}^E$, via the usual equation

$$\overline{\Delta F}_i^E = \overline{\Delta F}_i^M - RT \ln x_i = RT \ln \gamma_i , \qquad (2)$$

where $\overline{\Delta F}^M$ is the partial molar free energy of mixing, R the gas-law constant, and T the absolute temperature.

The free energy of mixing is needed not only in calculating the fission product partial pressures but also in determining the states of the fission products in solution. This follows from the fact that the standard free energy change of a reaction, ΔF_r^0, is given by

$$\Delta F_r^0 = RT \ln \frac{\prod_j a_j}{\prod_k a_k} , \qquad (3)$$

where a is the activity of a component in solution, and subscripts j and k refer to the products and reactants, respectively. The activities of the components of the solutions are related to their activity coefficients and compositions by the equation

$$a_i = \gamma_i x_i , \qquad (4)$$

where the pure liquids are chosen as the standard state.

Consequently, the main task at hand is to determine, either experimentally or analytically, the partial molar excess free energies of mixing. This section is primarily concerned with deducing these values.

Excess free energies of mixing are difficult to measure in very dilute systems and few methods are applicable. We have employed both a Rayleigh distillation technique and Knudsen cell vaporization experiments during the course of this work. In the absence of experimental data, there are several calculational methods

* Work performed under the auspices of the U. S. Atomic Energy Commission.

available for estimating the excess free energies of mixing from a phase diagram.[1-3] These methods were used to obtain many of the values given in this paper.

2.1. Iodine

As a result of its relatively high fission yield and its biological significance, the behavior of fission product iodine-131 is of great concern to reactor safety engineers. Previous studies[3, 4] by the present authors have shown that at the low concentrations expected in reactor coolant streams, iodine will react with sodium instead of fission product cesium. Consequently, considerable effort has been devoted to a measurement of the partial molar excess free energies of mixing of sodium iodide in sodium solutions.

Experimental measurements of the thermodynamic values at infinite dilution were made over the temperature range from 796 to 1103°K employing the Rayleigh method. A value of 15.9 kcal/mole was obtained for the heat of mixing, $\overline{\Delta H}$, and 6.8 eu for the partial molar excess entropy of mixing, $\overline{\Delta S}^{E}$. These values are in good agreement with an experimental measurement made at one temperature by Clough[5] and those calculated from the phase diagram[6] using various empirical methods.

Pitzer[7] employed a one-parameter expression to relate free energies across the NaI-Na immiscibility gap. His expression for $\overline{\Delta F}^{E}$ in terms of composition leads to values for $\overline{\Delta H}$ and $\overline{\Delta S}^{E}$ at infinite dilution of 14.2 kcal/mole and 6.0 eu, respectively. Extending his procedure with a two-parameter series expression, we deduced the corresponding values of 15.3 kcal/mole and 7.0 eu.

Various power series can be used to obtain estimates of the $\overline{\Delta F}^{E}$ values at higher concentrations from the phase diagram. A combination of the two-parameter expression with the experimental values obtained at infinite dilution leads to a self-consistent set of thermodynamic values. This is accomplished in the following manner.

Assuming that component 1 (the sodium) obeys an equation of the form

$$\frac{\overline{\Delta F}_1^{E}}{RT} = Ax_2^2 + Bx_2^3, \tag{5}$$

where subscript 2 refers to the sodium iodide, and A and B are constants which depend on temperature. The Gibbs-Duhem equation can be employed to obtain the corresponding power series for the other component:

$$\frac{\overline{\Delta F}_2^{E}}{RT} = Ax_1^2 + B\left(\frac{3}{2}x_1^2 - x_1^3\right) = \ln \gamma_2. \tag{6}$$

Since equilibrium exists along each solubility tie-line, it follows that

$$a_i^{I} = a_i^{II}, \tag{7}$$

where I and II represent the two phases in equilibrium across the immiscibility gap. Combination of Eqs. (4), (6), and (7) leads to the following expression relating constants A and B:

$$\left[Ax_1^2 + B\left(\frac{3}{2}x_1^2 - x_1^3\right) + \ln x_2\right]^{I} = \left[Ax_1^2 + B\left(\frac{3}{2}x_1^2 - x_1^3\right) + \ln x_2\right]^{II}. \tag{8}$$

Another equation involving A and B is obtained by combining the experimental values with Eq. (6). This leads to the equation

$$\overline{\Delta F}_2^{E}/RT = A + \frac{1}{2}B = \frac{8002.01}{T} - 3.42. \tag{9}$$

The constants A and B are evaluated by solving these two equations simultaneously. By use of these constants, $\overline{\Delta F}_2^{E}$ can be calculated at specified values of composition as a function of temperature, from which $\overline{\Delta H}$ and $\overline{\Delta S}^{E}$ can be deduced for each composition. These values are tabulated in Table 1.

TABLE 1. THERMODYNAMIC PROPERTIES OF NaI-Na SOLUTIONS

x_{NaI}	$\overline{\Delta H}_{NaI}$, kcal/mole	$\overline{\Delta S}_{NaI}^{E}$, eu
0	15.95	6.8
0.001	15.65	6.6
0.002	15.45	6.5
0.005	15.00	6.2
0.01	14.35	5.8
0.02	13.32	5.2
0.04	11.25	4.0
0.06	9.76	3.2

2.2. Cesium

Due to the relatively high volatility of metallic cesium, as well as the long half-life (30 yr) and the relatively high fission yield of the isotope of mass number 137, the thermodynamic properties of sodium-cesium solutions are of considerable interest. Earlier, Castleman, Tang, and Mackay[3] deduced the free energy of mixing of an infinitely dilute solution of cesium in sodium by assuming the solutions to be regular, i.e., $\overline{\Delta S}^{E} = 0$. In this paper, the cesium-sodium system is reconsidered over the entire range of concentrations without the assumption of a regular solution.

The cesium-sodium phase diagram[8] shows the presence of a simple eutectic at a composition of 75 mole %

TABLE 2. PARTIAL MOLAR QUANTITIES FOR LIQUID Na-Cs ALLOYS

x_{Na}	$\Delta\bar{H}_{Na}$, cal/mole	$\Delta\bar{S}^{E}_{Na}$, eu	$\Delta\bar{H}_{Cs}$, cal/mole	$\Delta\bar{S}^{E}_{Cs}$, eu
0.0	518	−1.24	0	0
0.1	515	−0.67	0.3	−0.03
0.2	498	−0.29	3.4	−0.09
0.3	464	−0.11	15	−0.15
0.4	411	−0.03	44	−0.20
0.5	340	0.00	103	−0.22
0.6	253	−0.02	209	−0.20
0.7	191	−0.01	325	−0.23
0.8	126	0.02	525	−0.30
0.9	48	0.02	987	−0.26
1.0	0	0	2019	0.15

TABLE 3. PARTIAL MOLAR QUANTITIES FOR LIQUID Na-Ba ALLOYS

x_{Na}	$\Delta\bar{F}^{E}_{Na}$, cal/mole	$\Delta\bar{F}^{E}_{Ba}$, cal/mole
0.0	1010	~0
0.1	1010	~0
0.2	1010	~0
0.3	1010	~0
0.4	1010	~0
0.5	1010	~0
0.6	1000	10
0.7	915	85
0.8	600	275
0.9	120	615
1.0	0	1700

cesium and a temperature of −29°C. Since the phase diagram shows that there is no solid solubility, the activity of each of the pure components is readily calculated by equating free energies along the tielines between the pure component and the respective liquidus curve. The resulting equation expresses the activity of either component i from the pure state up to the eutectic point or the first intersection of the pure component-liquidus tieline:

$$\ln a_i = \int_{T_m}^{T} \frac{(H_i^{(l)} - H_i^0) - (H_i^{(s)} - H_i^0)}{RT^2}\,dT, \quad (10)$$

where $H_i^{(l)} - H_i^0$ and $H_i^{(s)} - H_i^0$ are the enthalpy functions for the liquid and solid component i, respectively. Here the integration is carried out between the melting point of component i and temperature T at composition x_i on the liquidus curve. The partial molar free energies of mixing, computed from these data, are corrected to a reference temperature using available enthalpy data as discussed below.

Yokokawa and Kleppa[9] have reported heats of mixing for several alkali-metal systems. Guggenheim[10] has stated that a four-parameter power series is probably sufficient for representing the thermodynamic properties of all solutions. We found that the heats of mixing for the cesium-sodium system,[9] expressed as $\overline{\Delta H}/x_1x_2$, were best represented by a four-parameter equation for sodium concentrations greater than 50 mole %; a three-parameter equation was sufficient for lower concentrations. The continuity of the slopes of the two functions for heat of mixing was assured by also requiring that their first derivatives be equal at 50 mole %.

Utilizing the relationship

$$\overline{\Delta F}^{E} = \overline{\Delta H} - T\overline{\Delta S}^{E} \quad (11)$$

and the heats of mixing at each composition deduced from the above expressions, we evaluated a $\overline{\Delta S}^{E}$ using the free energies evaluated from the phase diagram, employing Eq. (10). These thermodynamic values are tabulated in Table 2. An extrapolation of the partial molar excess free energy for cesium to infinite dilution was accomplished using the power-series method discussed above for the correlation of the heats of mixing. The $\overline{\Delta F}^{E}$ value obtained by this method was 1963 cal/mole, which compares favorably with the value 2050 cal/mole reported earlier.[3]

2.3. Rubidium

The rubidium-sodium phase diagram[8] is very similar to that of the cesium-sodium system, showing a simple eutectic at 75.5 mole percent rubidium. Similar methods were used to deduce the thermodynamic properties of the rubidium-sodium system. A $\overline{\Delta F}^{E}$ of 1715 cal/mole was obtained at infinite dilution assuming the solutions to be regular. Yokokawa and Kleppa's heat of mixing data,[9] correlated with the power series discussed above, was used to calculate the free energies over the entire region of concentration without the simplifying assumption of a regular solution. A tabulation of the $\overline{\Delta H}$ and $\overline{\Delta S}^{E}$ values as a function of composition is given in Table 3.

2.4. Alkaline Earth Elements

Among the alkaline earth elements, strontium and barium are the most important. Roberts[11] reported a complex phase diagram showing several solid phases in equilibrium with different liquid compositions and pure strontium. In contrast, the diagram reported by Elliott[12] indicates the system to be a simple eutectic. No heats of mixing have been reported for this system, and the assumption of a regular solution was required to obtain $\overline{\Delta F}^{E}$ values from the phase diagram. However, the $\overline{\Delta F}^{E}$ values deduced from Roberts' phase diagram did not show a regular trend with compositions read along the liquidus curve, indicating that $\overline{\Delta S}^{E} \neq 0$. Since an assumption of a regular solution was required,

we used the phase diagram reported by Elliott[12] to obtain a very crude estimate[3] of $\overline{\Delta F}^E$ for strontium at infinite dilution (2885 cal/mole). Clearly, further experimental work is needed to obtain accurate thermodynamic values for this system.

The barium-sodium phase diagram reported by Kanda *et al.*[13] was used to calculate the excess free energy of mixing for this system. The solid solubilities of barium and sodium were considered in calculating the appropriate activities from the phase diagram. Again, the solution was assumed to be regular due to the absence of data on heat of mixing. Values of the $\overline{\Delta F}^E$ for sodium and barium were deduced from the phase diagram using the Bjerrum function. These are tabulated as a function of composition in Table 3. The $\overline{\Delta F}^E$ value for infinitely dilute barium concentrations is 1700 cal/mole.

2.5. Antimony and Tellurium

Regarding the elements of groups V and VI, antimony and tellurium are the fission products of major importance. The antimony-sodium phase diagram shows the existence of the stable compounds Na_3Sb and NaSb. Using Eq. (10) and the liquidus curve above 60.6 mole % antimony, we deduced $\overline{\Delta F}^E$ values for the antimony. These were divided by x_{Na}^2 and plotted vs. temperature. The resulting line, shown in Fig. 1, enabled us to calculate the temperature dependence of the free energy values so that it was not necessary to assume the solutions to be regular. A $\overline{\Delta F}^E$ of -6740 cal/mole was obtained for the infinitely dilute solutions of antimony. The thermodynamic values at higher composition are given in Table 4.

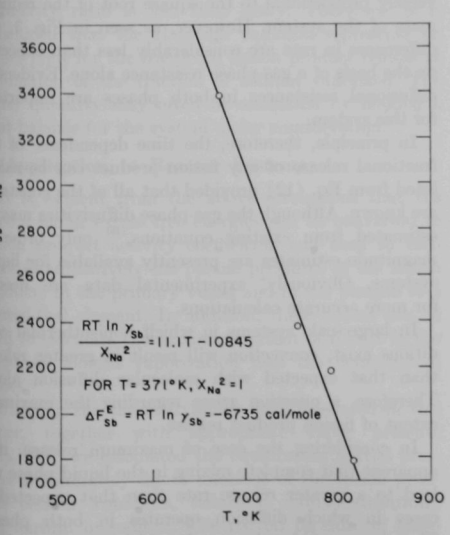

FIG. 1. Evaluation of ΔF_{Sb}^E from Na-Sb Phase Diagram.

TABLE 4. PARTIAL MOLAR QUANTITIES FOR LIQUID Na-Sb ALLOYS

x_{Na}	$\Delta\overline{H}_{Na}$, cal/mole	$\Delta\overline{S}_{Na}^E$, eu	$\Delta\overline{H}_{Sb}$, cal/mole	$\Delta\overline{S}_{Sb}^E$, eu
0.0	−10845	−11.1	0	0
0.1	−8790	−8.99	−108	−0.11
0.2	−6945	−7.10	−434	−0.44
0.3	−5310	−5.44	−976	−1.00
0.4	−3905	−4.00	−1736	−1.78
0.5	−2710	−2.78	−2710	−2.78
0.6	−1736	−1.78	−3905	−4.00
0.7	−976	−1.00	−5310	−5.44
0.8	−434	−0.44	−6945	−7.10
0.9	−108	−0.11	−8790	−8.99
1.0	0	0	−10845	−11.1

The tellurium-sodium phase diagram shows the existence of the compounds Na_2Te and $NaTe_3$. Values of $\overline{\Delta F}^E$ were again calculated from the phase diagram, employing Eq. (10). For this system, it was found that a plot of $\overline{\Delta F}^E/x_{Na}^2$ vs. x_{Te}/x_{Na} gave a straight line which could be extrapolated to zero mole percent tellurium (see Fig. 2). This is tantamount to correlating the data with a two-parameter power series in composition. The excess free energy at infinite dilution is -4050 cal/mole, assuming the solutions to be regular. Values of $\overline{\Delta F}^E$ for tellurium are given as a function of composition in Table 5.

These thermodynamic properties have a bearing on the transport of the fission products, their partial pressure, and extent of vaporization from solution, as well as their chemical states. Each of these aspects will be covered in the following sections.

3. Transport Considerations

In considering fission product transport, we concern ourselves with nonequilibrium vaporization, which is usually governed by diffusional resistances. Although the release of a species from a liquid solution into the vapor phase is often largely governed by a controlling resistance in one phase or the other, in some cases diffusion in both phases is important.

Consider the general case of release from a liquid of depth l, through a gas film of thickness b, and into a bulk gas phase. Fick's law can be solved for the fission product concentration gradient in each phase with appropriate boundary conditions. First, we assume the mass flux at the interface is continuous and that interfacial equilibrium exists. The partial pressure of the fission product adjacent to the interface is given by Eq. (1), where x_i is here taken to represent the

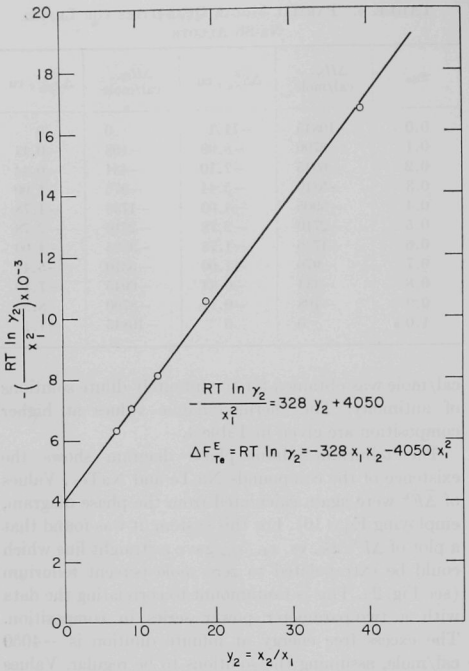

FIG. 2. Evaluation of $\Delta\bar{F}^E_{Te}$ from Na-Te Phase Diagram. The equation is only applicable for the concentration range $0.025 \leq x_1 \leq 1$.

TABLE 5. PARTIAL MOLAR QUANTITIES FOR LIQUID Na-Te ALLOYS

x_{Na}	$\Delta\bar{F}^E_{Na}$, cal/mole	$\Delta\bar{F}^E_{Te}$, cal/mole
0.1	−3475	−70
0.2	−2648	−214
0.3	−1989	−433
0.4	−1444	−727
0.5	−994	−1095
0.6	−632	−1537
0.7	−354	−2053
0.8	−156	−2645
0.9	−39	−3310
1.0	0	−4050

composition at the liquid surface. Next, the concentration in the bulk gas phase is assumed to be negligible compared to that at the gas-liquid interface. Solution of the differential equation for the case of a linear concentration gradient in the gas film leads to the following equation for the fractional fission product release, F:

$$F = 1 - \sum_{n=1}^{\infty} \frac{2L^2 \exp\left[-\beta_n^2 Dt/l^2\right]}{\beta_n^2(\beta_n^2 + L^2 + L)}, \qquad (12)$$

where

$$\alpha = \left(\frac{D_v}{b}\right)\left(\frac{P^0\gamma}{\rho RT}\right). \qquad (13)$$

ρ is the molar density of sodium, D_v is the diffusivity of the fission product in the gas phase, and D is the corresponding diffusivity in the liquid phase. The β_n's are the positive roots of

$$\beta \tan \beta = L, \qquad (14)$$

where $L = l/\alpha D$.

The release of cesium from liquid sodium into an inert gas stream was studied experimentally. Radioactive cesium-137 was dissolved in sodium to form an alloy with a very low cesium concentration. To carry out the transport experiment, the resulting alloy was melted in a crucible of known dimensions to form a liquid phase of known depth and a well-defined gas path above the liquid. The crucible was then heated to 730°K, and the rate of cesium release into a flowing gas was monitored continuously using a scintillation counter. The experimental details are given elsewhere.[14]

Both liquid depth and the molecular weight of the carrier gas were found to affect the release rate. The release into helium was faster than into argon, which may be expected since gas-phase diffusivities are inversely proportional to the square root of the reduced mass of the system. However, as seen in Fig. 3, the differences in rate are considerably less than expected on the basis of a gas-phase resistance alone. Evidently, diffusional resistances in both phases are important for this system.

In principle, therefore, the time dependence of the fractional release of any fission product can be calculated from Eq. (12) provided that all of the constants are known. Although the gas-phase diffusivities may be estimated from existing equations,[15] only order-of-magnitude estimates are presently available for liquid systems. Obviously, experimental data are needed for more accurate calculations.

In large-scale systems in which nonisothermal conditions exist, convection will result in greater release than that expected with molecular diffusion alone. Therefore, a question arises regarding the maximum extent of fission product release.

In considering the case of maximum release, it is apparent that complete mixing in the liquid phase will lead to a greater release rate than that expected in cases in which diffusion operates in both phases. Therefore, consider the case in which both the solvent

(Na) and the solute (fission product) diffuse through a gas film of constant thickness. It follows from the solution to Fick's law with appropriate boundary conditions that

$$\ln (1 - F_1) = -\frac{D_{v13} P_1^0}{RTb\rho} \frac{t}{l} \tag{15}$$

and

$$\ln (1 - F_2) = -\frac{D_{v23} P_2^0 \gamma_2}{RTb\rho} \frac{t}{l}, \tag{16}$$

where the subscripts 1, 2, and 3 refer to solvent, solute at infinite dilution, and carrier gas, respectively. Here F is the fraction vaporized, P^0 the vapor pressure, D_v the gas-phase diffusivity, ρ the molar density, and t the vaporization time.

Dividing the second equation by the first, one obtains

$$\frac{\ln (1 - F_2)}{\ln (1 - F_1)} = \frac{P_2^0 \gamma_2}{P_1^0} \left(\frac{D_{v23}}{D_{v13}} \right) = A\varphi \tag{17}$$

or

$$F_2 = 1 - (1 - F_1)^{A\varphi}. \tag{18}$$

When the ratio φ of the gas-phase diffusivities is unity, this equation reduces to the familiar Rayleigh equation[3] for the limiting case of equilibrium vaporization. Since gas-phase diffusivity is inversely proportional to the square root of the reduced mass of the system, in fission product-sodium systems the above diffusivity ratio is less than unity. Therefore, it is concluded that the Rayleigh equation represents an upper limit for the fractional fission product release as a function of the fraction of sodium vaporized. The latter quantity may often be estimated by making a heat balance for the system under consideration.

4. Application to Reactor Systems

It is evident from the above discussions that the partial molar excess free energies can be converted to fission product activity coefficients and used to estimate quantitatively the partial pressures of the fission products in the primary vessel and in the plenum of a vented-fuel element. In addition, these values can be used to calculate the maximum extent of release in the event of sodium vaporization into the containment vessel.

Utilizing the thermodynamic data presented in this paper, together with appropriate vapor pressure data,[16, 17] we calculated the equilibrium partial pressures for infinitely dilute solutions of the fission products cesium, rubidium, tellurium, iodine, strontium, and barium in sodium. The partial pressure of these fission products, per mole fraction, are plotted vs.

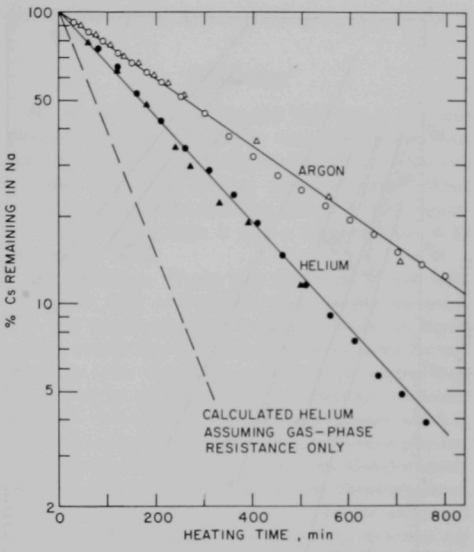

FIG. 3. Effect of Carrier-gas Molecular Weight on the Release Rate of Cesium from Liquid Sodium at 730°K.

reciprocal absolute temperature in Fig. 4. The solid curves were calculated using the $\overline{\Delta F^E}$ values given in this paper; the dotted curves, shown here for comparison, were calculated assuming ideal solution behavior. In some cases, the actual and ideal partial pressures differ by more than an order of magnitude. From the data given in Tables 1 to 6, one can readily calculate the partial pressures of NaI, Cs, Rb, Te, Sb, and Ba at higher fission product concentrations as well.

Although the chemical states of the other fission products are relatively well-established, the states of strontium and barium in solution are less certain. At high fission product concentrations strontium and barium are probably elemental and the above calculations are valid. However, at very low concentrations, the elements likely react with the dissolved oxygen present in reactor-grade sodium. Since the nature of even the oxygen species dissolved in sodium is not well-known, their interactions with the alkaline earth metals in solution is even less certain.

The equilibrium distribution of the potentially reactive species in a solution depends on their activities as shown by Eq. (3). Consequently, the free energies of mixing have a direct bearing on the extent of the individual species formed. Unfortunately, these quantities are unknown for sodium solutions of oxygen, SrO, BaO, and the respective alkaline earth hydroxides. However, since the vapor pressure of the alkaline earth

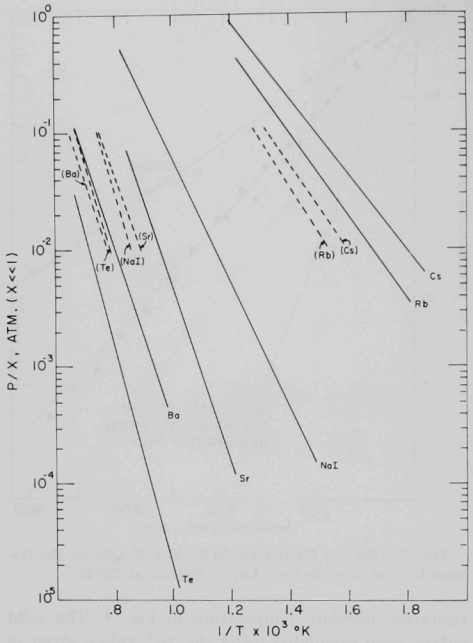

FIG. 4. Fission Product Partial Pressures over Liquid Sodium. The dotted curves, shown here for comparison, were calculated assuming ideal solution behavior.

TABLE 6. PARTIAL MOLAR QUANTITIES FOR LIQUID Na-Rb ALLOYS

x_{Na}	$\Delta\bar{H}_{Na}$, cal/mole	$\Delta\bar{S}^{E}_{Na}$, eu	$\Delta\bar{H}_{Rb}$, cal/mole	$\Delta\bar{S}^{E}_{Rb}$, eu
0.0	843	−0.37	0	0
0.1	781	0.15	4	−0.02
0.2	699	0.36	18	−0.06
0.3	602	0.37	51	−0.06
0.4	494	0.27	110	0.00
0.5	381	0.14	203	0.10
0.6	290	0.08	315	0.17
0.7	191	0.03	500	0.27
0.8	98	0.00	784	0.37
0.9	27	0.00	1188	0.39
1.0	0	0.00	1722	0.19

elements is higher than that of the respective oxides or hydroxides, the partial pressures given here probably represent the maximum values under practical conditions.

It is a well-known fact that the ratio of the differential vaporization of one component of a solution to that of another component is directly proportional to the ratio of their partial pressures:[18]

$$\frac{dn_1}{dn_2} = \frac{P_1}{P_2}. \qquad (19)$$

Here, dn represents a differential vaporization in terms of moles. Substituting from Eq. (1) and integrating leads to the Rayleigh Eq. (15) with $\varphi \equiv 1$. Consequently, the fraction of a fission product vaporized as a function of the sodium vaporized, for the limiting case of equilibrium vaporization, can be calculated with a knowledge of the A values. For any particular fission product, the constant A can be calculated from the vapor pressure and the data given here.

For dilute solutions, A is only a function of temperature:

$$A = a \exp(b/T).$$

Values of the appropriate constants a and b are given in Table 7 for Cs, Rb, Sr, NaI, Ba, Te, and Sb. A plot of the predicted fraction of Cs vaporized as a function

TABLE 7. CONSTANTS FOR CALCULATING THE EXTENT OF FISSION PRODUCT VAPORIZATION AS A FUNCTION OF THE SODIUM VAPORIZED

Fission Product	Temperature Range[b] °K	a	b
Cesium	700–900	0.121	5,073
Rubidium	700–900	0.213	4,184
Strontium	700–1000	5.41	−5,270
Iodine[a]	700–1200	0.37	−150
Barium	700–1100	1.73	−7,003
Tellurium	725–1100	2.81	−10,150
Antimony	1000–1100	2227	−21,989

[a] Present as NaI.

[b] a and b were evaluated employing vapor pressure data within this temperature range, but are not necessarily restricted to this range for practical use.

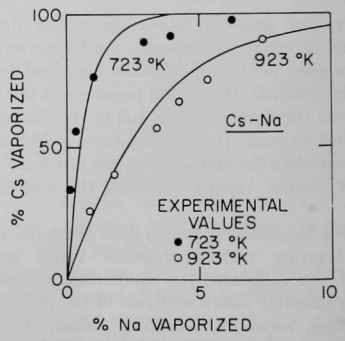

FIG. 5. Equilibrium Vaporization of Cesium from Sodium Solutions.

of the sodium vaporized is shown in Fig. 5. Also shown are some experimental points, which are seen to be in fairly good agreement with the theoretical predictions. The small discrepancies are undoubtedly due to the fact that the liquid-phase diffusional resistances were not completely absent in the vaporization cell employed in this study.

Acknowledgments

The authors acknowledge the invaluable assistance of Mr. Harry R. Munkelwitz and Mr. Steven Lewkowitz in performing many of the experiments and calculations.

REFERENCES

1. Wagner, C., *Thermodynamics of Alloys*, Addison-Wesley Publishing Co., Inc., Reading, Mass. (1952).
2. Kubaschewski, O., and Evans, E. *Metallurgical Thermochemistry*, Pergamon Press, New York (1958).
3. Castleman, A. W., Jr., Tang, I. N., and Mackay, R. A. in *Alkali Metal Coolants*, IAEA, Vienna (1967), pp. 729–42.
4. Castleman, A. W., Jr., and Tang, I. N., "Chemical Considerations in Fast Reactor Safety," *Proc. Conf. Safety, Fuels, and Core Design in Large Fast Power Reactors*, ANL-7120 (Oct 1965), 848–54.
5. Clough, W. S., Private communication.
6. Bredig, M. A., and Bronstein, H. R., *Miscibility of Liquid Metals with Salts. IV. The Sodium-Sodium Halide Systems at High Temperatures*, J. Phys. Chem. **64**, 64–7 (1960).
7. Pitzer, K. S., *Solubility and the Nature of Binding in Fused Alkali Halide-Metal Systems*, J. Am. Chem. Soc. **84**, 2025–8 (1962).
8. Hansen, M., *Constitution of Binary Alloys*, 2nd Ed., McGraw-Hill Book Co., Inc., New York (1958).
9. Yokokawa, T., and Kleppa, O. J., *Heats of Mixing in Binary-liquid-Alkali-metal Mixtures*, J. Chem. Phys. **40**, 46–54 (1964).
10. Guggenheim, E. A., *Applications of Statistical Mechanics*, Clarendon Press, Oxford, (1966), p. 98.
11. Roberts, W. O., *The Sodium-Strontium Equilibrium System*, Ph.D. Thesis, Syracuse University, Syracuse, N. Y. (1964).
12. Elliott, R. P., *Constitution of Binary Alloys, First Supplement*, McGraw-Hill Book Co., Inc., New York (1965), p. 651.
13. Kanda, F. A., Stevens, R. M., and Keller, D. V., *The Barium-Sodium Equilibrium System*, J. Phys. Chem. **69**, 3867–72 (1965).
14. Tang, I. N., Castleman, A. W., Jr., and Munkelwitz, H. R. "On the Transport of Fission-product Cesium from Sodium" in *Advances in Chemistry* (to be published).
15. Hirschfelder, J. O., Curtiss, C. F., and Bird, R. B. Molecular Theory of Gases and Liquids, John Wiley, New York 1964, 539.
16. Nesmeyanov, A. N., *Vapor Pressure of the Chemical Elements*. Elsevier Publ. Co., Amsterdam, London, New York (1963).
17. Stull, D. R., and Sinke, G. C. *Thermodynamic Properties of the Elements*, No. 18 of Advances in Chemistry Series, American Chemical Society, Washington, D. C. (1956).
18. McCabe, W. L., and Smith, J. C., *Unit Operations of Chemical Engineering*, McGraw-Hill Book Co., Inc., New York (1956).

Discussion

Mr. Genco (BMI): I thought that was a very fine piece of work, but I would be very interested in your rationale in the sodium-sodium iodide system when you consider Prigogine's average potential model. What was your rationale for selecting this model and expecting this to work, since it uses a Leonard-Jones 6–12 potential?

Mr. Castleman: If you look into what is now fashionable in solid state-liquids work, people are going into the pseudo-potential model for atoms in liquid metals. I think that if you would sit down as we did and calculate some Coulombic potentials in solution you would find the screening of the free electrons in solution will make this obey a pseudo-potential model, which is now what is becoming fashionable in solid-state physics. It is a pseudo-treatment, but we did find that it worked. Roughly what happens is that the free electrons screen the long-range Coulombic forces so that the atom acts like a pseudo-potential in a sea of electrons to screen out the long-range potential. You get something like a pseudo-Leonard-Jones potential even though that is probably not a very accurate potential in liquid metals. There isn't a better one available.

Mr. Soenen (CEN-MOL): Most of your released data were for free elements; when there are compound formations, how should the release be affected then?

Mr. Castleman: As I stated at the beginning of the talk, we have published elsewhere that the cesium and sodium iodide will exist as sodium iodide in cesium, that there will not be an interaction to form cesium iodide and sodium; in other words, even though the free energy of cesium iodide is more negative (because of the activities of the fission products in solution, their low concentration, and their activity coefficient), the equilibrium is shifted in the other direction so that there would be free cesium and sodium iodide. As I also mentioned for the case of strontium and barium, we plotted it as the free elements because it is the maximum case. It may end up as being hydroxide or oxides in solution, but we don't think there is really enough data to assess this accurately.

Mr. Johnson (BNWL): I would gather from your data that even though you are talking about regular solutions you are not approaching ideal solutions in liquid metals; at what concentration might you expect that you would approach ideal solutions?

Mr. Castleman: Actually, the ideal solution in the strict sense of the word is one where the activity coefficient is unity. Really you want to get that in a concentrated solution. It is the concentrated component

whose activity approaches a mol fraction. Sometimes people loosely call an ideal solution one which obeys a constant gamma and that is the Henry's law region, which would be extremely dilute. Probably for most of the systems we should be approaching that. I think the reason we are not at a sodium iodide-sodium system is that the solubilities are so very low that probably you would have to be quite low in concentration before you approach the Henry's law region. It's probably only valid right along the solubility line.

Vaporization of Fission Products from Sodium*

B. D. Pollock, M. Silberberg, and R. L. Koontz

Atomics International
A Division of North American Rockwell Corporation
Canoga Park, California

(PRESENTED BY M. SILBERBERG)

1. Introduction

Fission products released to the coolant during the operation of a Liquid Metal Fast Breeder Reactor (LMFBR) will be distributed between the sodium coolant, reactor cover gas, primary-system surfaces, and trapping devices in the system. Some volatile fission-product elements may be transported to the cover gas by vaporization from the liquid sodium. The presence of these radioisotopes in the cover gas may lead to subsequent problems in cover-gas storage, effluent disposal, or personnel exposure in the event of leakage from the top shield. The fission-product elements (other than the noble gases) which may vaporize significantly from sodium at LMFBR coolant temperature include: cesium, rubidium, iodine, and perhaps tellurium and strontium.

The purpose of this paper is to present the results of vaporization-equilibrium studies which were conducted to obtain relative volatility data for two volatile fission products, namely, cesium and iodine (present as NaI).

2. Analytical Studies

The equilibrium-vaporization behavior of a binary system is conveniently described by the relative volatility (or distribution coefficient), designated here by the symbol K_d and defined as the ratio of the mole fraction of the solute in the vapor, Y_2, to its mole fraction in the liquid, X_2, or $K_d = Y_2/X_2$. Experimentally this ratio may be determined using tracer techniques by determining the ratio of specific activity in the vapor to that in the liquid:

$$K_d = Y_2/X_2 = A_g/A_l, \tag{1}$$

where A_g and A_l are the specific activities (dpm of solute per gram of solvent) of the vapor and liquid, respectively.

We may note that at low solute concentrations

$$Y_2 = \frac{P_i}{P_i + P^0_{Na}} \cong \frac{P_i}{P^0_{Na}}, \tag{2}$$

where

P_i = partial pressure of the solute (fission product i);

P^0_{Na} = vapor pressure of pure sodium.

We may express P_i as a function of concentration:

$$P_i = \gamma X_i P^0_i, \tag{3}$$

where

γ = activity coefficient;

P^0_i = vapor pressure of pure fission product i;

X_i = mole-fraction of fission product i in sodium.

Substituting Equations 2 and 3 in Equation 1, we obtain

$$K_d = \frac{Y_2}{X_2}\frac{\gamma X_i P^0_i}{X_i P^0_{Na}} = \frac{\gamma P^0_i}{P^0_{Na}}. \tag{4}$$

2.1. Cesium in Sodium

The derivation of an analytical expression for K_d for cesium in sodium requires literature data for the vapor pressures of cesium and of sodium, and the activity coefficient for cesium in sodium, so that

$$K_d = \frac{\gamma_{Cs} P^0_{Cs}}{P^0_{Na}}$$

and

$$\text{Log } K_d = \text{Log } \gamma_{Cs} + \text{Log } P^0_{Cs} - \text{Log } P^0_{Na}. \tag{5}$$

By use of the data for monatomic cesium from Stull and Sinke,[1] it is possible to obtain the expression

$$\text{Log } P^0_{Cs} = (-3795/T) + 3.900. \tag{6}$$

The vapor pressure of liquid sodium is taken from Stull and Sinke.

To evaluate the activity coefficient (which incorporates departures from ideal solution behavior), one may express the activity coefficient in terms of the excess free energy of mixing:

$$\Delta F^E = \Delta H^E_{mix} - T\Delta S^E = RT \ln \gamma. \tag{7}$$

Yokokawa and Kleppa[2] have measured heats of mixing of cesium and sodium over the composition range by calorimetric means, at 111°C, and have stated that for cesium mole fractions less than about 0.5 the excess entropy of mixing is zero (i.e., the solutions are "regu-

* Work performed under U. S. Atomic Energy Commission Contract AT(04-3)-701.

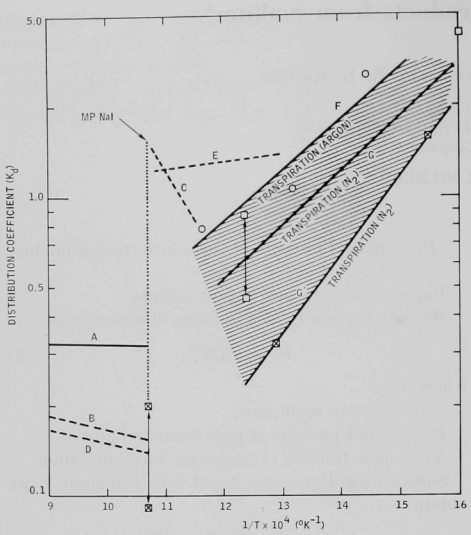

CURVE	SOURCE	EXPERIMENTAL METHOD
A	EXPL – CASTLEMAN[4]	DISTILLATION
B	PITZER[3] – KELLEY[6]	
C	PITZER[3] – COGIN[7]	
D	BREDIG[5] – KELLEY[6]	
E	BREDIG[5] – COGIN[7]	
F	○ EXPL – POLLOCK	ARGON TRANSPIRATION
GG′	⊠ EXPL – KOONTZ, et al[8]	N_2 – TRANSPIRATION

FIG. 1. Distribution Coefficients for Sodium Iodide-Sodium System.

lar"). An extrapolation of their data to zero mole fraction (infinite dilution) for cesium gives for the partial molar heat of mixing of cesium a value of approximately 1900 cal/mole. The activity coefficient for cesium should therefore be given by

$$\text{Log } \gamma_{Cs} = 1900/4.576T = 415/T. \qquad (8)$$

Combining the expressions for P_{Cs}, P^0_{Na}, and γ gives

$$\text{Log } K_d(Cs) = (1945/T) - 0.668. \qquad (9)$$

(A plot of this relation is shown later in Fig. 2.)

2.2. Sodium Iodide in Sodium

Determinations of excess free energy of mixing of NaI in sodium (ΔF^E) have been made by Pitzer[3] and Castleman.[4] Both evaluated the value of ΔF^E_{NaI} when the temperature of the solution was above the melting point of sodium iodide. Castleman[4] also determined the value of ΔF^E for NaI from measurements of the vaporization of NaI and sodium. He predicts

$$K_d = 0.37e^{-150/T} \qquad (10)$$

on the basis that ΔF^E_{NaI} is constant with temperature and equal to 9100 cal/mole.

Pitzer proposed the expression

$$\Delta F^E_{NaI} = 14{,}200 - 6T$$

from solubility data for NaI in sodium obtained from Ref. 5. Curves A and B in Fig. 1 show how K_d varies with temperature if it is computed from these two sources.

The vapor-pressure data for NaI and sodium was obtained from data of K. K. Kelley[6] and Stull and Sinke,[1] and the activity coefficient of Eq. 4 was computed from the relation $\gamma = \exp(\Delta F^E_{NaI}/RT) = e^{(14{,}200-6T)/RT}$, to obtain curve B of Fig. 1.

Vapor-pressure data for NaI below the melting point has been measured by Cogin and Kimball.[7] If their data are used with Pitzer's determination of ΔF^E one obtains curve C shown in Fig. 1.

One other estimation of K_d can be made from existing experimental data if one assumes that $\gamma = 1/X_2^0$, i.e., the activity coefficient is inversely proportional to the saturation solubility of NaI in sodium. Bredig, Johnson, and Smith[5] measured the solubility of NaI in sodium at temperatures both above and below the melting point of NaI. Their data combined with vapor-pressure data of Kelley and of Cogin and Kimball were used to compute K_d which is shown in curves D and E of Fig. 1. Thus as can be seen from Fig. 1, considerable variation exists in the estimation of K_d at temperatures above and below the NaI melting point.

3. Experimental Method

With the exception of a few trial experiments conducted with a very simple vapor-density apparatus, all vaporization experiments were performed with what proved to be a simplified version of a transpiration apparatus.

The transpiration apparatus used in both Cs-Na and Na-NaI studies is illustrated in Fig. 2. In this work, one of the concerns was that the solutions be adequately stirred in order to maintain uniform concentration. Otherwise, concentration gradients would be established which would give rise to a diffusion-limiting effect on one or another of the solution components and thus invalidate the results. The bubbler-tube design was therefore adopted in order to maintain good mixing.

The carrier gas was 99.999 % argon. Volume measurements could be made by the combination of the calibrated 3-liter stainless steel ballast tank and calibrated pressure gauge, or by the gas-collector burette; the results of both methods were in good agreement. A NaK bubbler was in the line to ensure carrier-gas purity.

To ensure establishment of the equilibrium vapor concentration in the carrier gas, the usual procedure was followed of making a series of runs at various flow rates. These runs showed that saturation with sodium occurred at least between 20 and 160 ml/min. At higher flow rates (260 ml/min), saturation also occurred but mechanical entrainment became a problem. In practice, flow rates between about 20 to 100 ml/min were used.

3.1. Cesium-Sodium System

In this work, the transpiration apparatus of Fig. 2 was operated with the furnace in a position slightly tilted from the horizontal. To agitate the liquid, the furnace was slightly rocked manually at frequent intervals.

To permit addition of a reasonably well-defined, but rather small, concentration of cesium (usually at mole fraction levels of 1.0×10^{-5}), a few grams of a "master batch" of cesium-sodium alloy in the atomic ratio of 1 to 10 was made up and stored in a plastic vial within an inert-atmosphere glovebox. This allowed use of pieces sufficiently large to permit easy handling and weighing on a small semi-micro balance kept within the glovebox. These small weighed samples, sufficient to dope about 175 to 200 g of sodium solution, were transported in sealed polyethylene vials and irradiated in the Shield Test and Irradiation Reactor (STIR) to a level corresponding to about 1 MWt-hr of reactor operation. The ^{24}Na was then allowed to decay over a period of several days before being brought back to the laboratory for incorporation in the main batch of sodium. After the activated alloy was added to the sodium, a sample was removed for analysis and determination of specific activity. Several transpiration cells were loaded with charges of about 23 g each. About 5 mg Na_2O_2 were added to provide an oxygen concentration of 125 ppm. Each cell was used for only a single run, to reduce concentration changes and to have well-defined specific activities of the liquid from run-to-run in a given series.

The runs were made in the temperature range from 650 to 900°K to simulate the expected range of reactor coolant temperatures. Carrier-gas volumes were selected to give approximately the same amount of condensed sodium in each run, i.e., 10 to 25 mg. The transported vapor was condensed in a water-cooled collector tube, and the amount of sodium content was determined by a titrimetric or flame photometric method. The cesium activity was determined with a scintillation-detector, pulse-height-analyzer system using the same geometry as for the liquid metal reference solution. Carrier-gas volumes were measured and theoretical sodium transports calculated for comparison with measured quantities as a check for gross experimental errors. The agreement was usually fairly good.

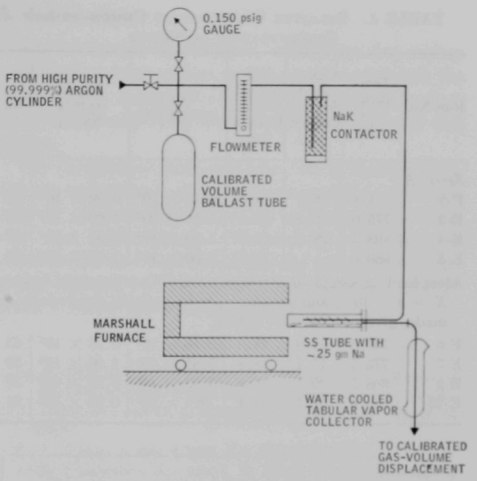

FIG. 2. Schematic of Transpiration Experiment.

3.2. Sodium Iodide-Sodium System

The furnace shown in Fig. 2 was used in a vertical position in runs with the sodium iodide-sodium system. To reduce the effect of surface absorption and exchange, a small quantity of carrier iodine, of the order of 1 to 2 atomic ppm, was added. Since sodium iodide is only slightly soluble in sodium, especially at the sampling temperatures that could be safely used in the glovebox, the following procedure was used to provide a sample that would be typical of a reactor coolant. About 10 mCi of ^{131}I, in the form of 1 ml aqueous sodium iodide, were washed into a small beaker using 0.5 mg of sodium iodide carrier and sufficient deionized water to give a total volume of about 25 ml. One ml was pipetted into a 100-ml volumetric flask, together with a few mg of sodium iodide, and was then diluted to the mark. Of the remaining iodide activity, 20 ml were then pipetted directly into the bubbler part of the transpiration apparatus; a drop of 5% NaOH was added to prevent loss due to oxidation, and the solution was then evaporated to dryness. The chamber or bubbler was then transferred to the glovebox, a weighed amount of sodium metal was added, and the apparatus was then assembled. In this way a known concentration of iodine was added to the sodium (usually 1 atom ppm).

In performing the iodine transpiration runs, the furnace was first brought to temperature, the bubbler was inserted, and, as soon as the sodium melted, a very low flowrate of gas was begun in order to prevent backflow

TABLE 1. Relative Volatility of Cesium at Low Concentration in Sodium

Run No.	Temperature (°K)	Calculated Sodium Carried (mg)	Observed Sodium Carried (mg)	Vapor (cpm/g Na)	Liquid (cpm/g $Na)_{avg}$	K_d
Series E						
E-1	731.8	18.2	19.8	6.45×10^6	0.99×10^5	65
E-2	775.0	16.5	21.3	5.18×10^6	1.00×10^5	52
E-4	868.5	28.8	34.7	3.65×10^6	0.99×10^5	37
E-5	680.0		14.7	7.60×10^6	1.00×10^5	76
After loading sample 5, 500 ppm normal Cs was added to give $X = 8 \times 10^{-5}$, and another specific-activity determination made, giving 0.92×10^5 cpm/g.						
E-6	736.5	18.9	28.0	6.16×10^6	0.98×10^5	63
E-7	773.5	15.1	18.4	5.85×10^6	1.00×10^5	59
E-9	868.5	30.1	31.8	3.82×10^6	0.99×10^5	39
E-10	684.0	16.3	19.1	9.1×10^6	0.99×10^5	93

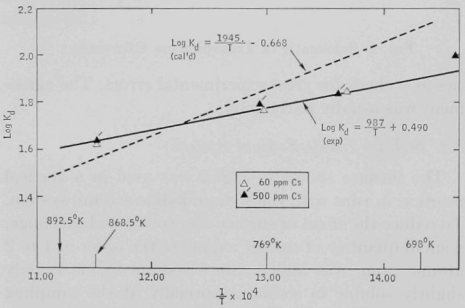

FIG. 3. Distribution Coefficient for Cesium-Sodium Systems.

of sodium and resultant plugging. When the sodium reached the desired experimental temperature, the flowrate was increased to 20 to 75 ml/min, until an estimated quantity of about 10 to 25 mg of sodium had volatilized. The flowrate was then reduced to the earlier value. The bubbler was then removed from the furnace and allowed to cool. When the system had cooled enough to handle, gas flow was stopped, and the cell with its collector and lead-in tube was removed. Sodium transport was determined with standard HCl, and the specific activity of the iodine counted and compared against the reference.

4. Experimental Results

4.1. Cesium-Sodium System

One of the difficulties encountered during much of the work with cesium was inconsistent liquid-metal specific-activity data. For example, on occasion the specific activity of the residue from a run might show a very substantially higher specific activity than found for the (apparent) initial specific activity. Part of the difficulty may have been due to inadequate mixing of the tracer batch; however, one definite source of trouble was traced to segregation during the freezing with the resultant appreciable inhomogeneities existing in the cesium-distribution activities. This effect was corrected by dissolving the entire sodium sample in butyl alcohol and taking an aliquot (instead of cutting and weighing a piece of the residue as before). When residues from a number of the runs were corrected for cesium-activity transport, the calculated initial activities agreed well (1 to 2%) with the measured initial activities.

Results of the transpiration runs at nominal oxygen levels of 125 ppm and cesium mole fractions of 1×10^{-5} and 8×10^{-5} are summarized in Table 1 and Fig. 3.

In computing the K_d values, the measured sodium transport was used in calculating specific activity of the vapor in order to reduce effects of gas-measuring and temperature errors. In addition, it should be noted that, although rather small fractional sodium transports were used, i.e., about 0.1%, the resulting changes in cesium activity (or concentration) in the liquid were sometimes as high as 15 to 20%. Accordingly, the average liquid-metal specific activity was calculated, based on the initial specific activities of the batches and transports during the run.

Least-squares treatment of the data in Fig. 3 gave the following relationship for relative volatility of cesium: Log $K_d = (+987/T) + 0.490$. Figure 3 shows the agreement between the two groups of runs, that is, the group with $X_{Cs} = 1 \times 10^{-5}$ and the group with $X_{Cs} = 8 \times 10^{-5}$. The latter fact is evidence that Henry's law is obeyed, as was expected.

4.2. Sodium Iodide-Sodium System

The results of the transpiration series, designated here as the iodine Series F, are summarized in Table 2 and plotted in Fig. 1.* The temperatures listed in the second column of Table 2 are average temperatures estimated from visual inspection of temperature-time data and are subject to uncertainty of 6 to 7°C. The difference between the observed and calculated sodium transports is in part the result of the temperature and gas-volume uncertainties, and in part the result of extraneous transport due to diffusion during the heating and cooling phases of the experiments. Such differences do not affect the results since the effects would apply to both sodium and iodide and would thus cancel each other. Because of the short half-life of I-131 as compared to

* Curve F.

TABLE 2. RELATIVE VOLATILITY OF SODIUM IODIDE IN SODIUM (SERIES F)

Run No.	Average Temperature (°K)	Sodium Transport (mg)			Measured Condensate (cpm)	cpm/47.5 mg Liquid Sodium	K_d
		Calculated	By Titration	By Flame Photometer			
F-2	754	9.1	16.2	16	82,720	229,200	1.06
F-3	863	31.8	41.0	44	156,800	229,200	0.79
F-4	695	5.9	10.4	11	123,400	224,600	2.50

Cs-134, it was necessary to count the reference solution at the same time as the experimental transports, and these counts are shown in the table. The values of K_d were calculated using the experimental values of sodium transports, for the same reasons as for the cesium work.

Some additional distribution coefficients were determined in another transpiration apparatus in this laboratory.[8] In this apparatus nitrogen gas was swept across the surface of a 1-in.-diameter pot. Flowrates of 25 to 100 cc/min were used. In this series of experiments the specific activity of the sodium (dpm NaI/g Na) was measured before and after an experiment. All of the material released into the gas stream was collected during a short time interval (less than 10 min). The collected material was than monitored for dpm of ^{131}I and sodium content. The sodium temperature was varied from 700 to 1200°F. The change in the specific activity of the liquid sodium during a series of tests was always less than 10%. A run at any one temperature involved only a very small fraction of sodium being vaporized and collected.

The Rayleigh equation $f_{NaI} = 1 - (1 - f_{Na})K_d$, which relates the fraction f of the solvent sodium and solute NaI vaporized, can be expanded to show that when $f_{Na} \ll 1$, then $f_{NaI}/f_{Na} = K_d$. This is also consistent with a transpiration experiment for the measurement of vapor pressure when equilibrium is reached.

The adequacy of mixing is not known, but there is a heater on the bottom of the pot that creates convective currents and therefore causes stirring. The apparatus can also be rocked gently during the test.

The data obtained with this apparatus are shown in Fig. 1, Curves G and G′. They can be compared to that obtained in the first apparatus when argon was used as the sweep gas (Curve F).

It was also observed that as sweep-gas flowrate is increased there is an increase in the value of K_d. Although it may not be correct to define the measurement at nonequilibrium condition as a distribution coefficient, it clearly shows that more activity is released as the flow is increased.

5. Conclusions

The computed distribution coefficients for cesium vaporization from sodium and those measured with the transpiration apparatus compare favorably. It is clear that K_d increases with decreasing temperature for this system.

The distribution coefficients for NaI in liquid sodium are not well-defined either experimentally or theoretically at temperatures below the melting point of NaI, and need further study. The need for such study is based on the fact that the maximum temperatures currently planned for the LMFBR are less than 1200°F, which is below the melting point of NaI.

REFERENCES

1. D. R. Stull and G. C. Sinke, *Thermodynamic Properties of the Elements*, Am. Chem. Soc., Washington, D. C. (1956).
2. T. Yokokawa and O. J. Kleppa, J. Chem. Phys., **40**, 46–54 (1964).
3. K. S. Pitzer, J. Am. Chem. Soc. **84**, 2025 (1962).
4. A. W. Castleman, Jr., and I. N. Tang, *Thermodynamics of Fission Product-Sodium Solutions*, BNL-11611 (Nov 1967).
5. N. A. Bredig, J. W. Johnson, and W. T. Smith, J. Am. Chem. Soc., **77**, 307–312 (1955).
6. K. K. Kelley, U. S. Bur. Mines Bull. 383 (1935).
7. G. E. Cogin and G. E. Kimball, J. Chem. Physics **16**, 1035 (1948).
8. R. L. Koontz, L. Baurmash, and C. T. Nelson, Atomics International, unpublished data.

Discussion

Mr. Castleman (BNL): I feel obligated to comment on the sodium-sodium iodide system. As we have said before, we believe that perhaps part of the reason for observation of higher distribution coefficients for the sodium-sodium iodide system is that the solubility limits are exceeded at the very low temperatures.

Mr. Silberberg: For our runs with carrier we thought so, too, and that is why we were concerned.

Mr. Castleman: Also, we do not see any break at the melting point of sodium iodide. Unfortunately, I didn't have my plot extending below the melting point. I think you did receive a report from us showing that it is continuous through the melting point. I still feel your problem is one of exceeding the solubility, in which case the chemical activity increases.

Mr. Silberberg: What about carrier-free runs? You will note that curve G′ in Fig. 1 was actually done carrier-free. I might mention that, although it hasn't been completely published, I understand from Cleff's results at 500°F that he varied the iodine concentration from carrier all the way up to 100 ppm, which is considerably below saturation.

Mr. Castleman: This is still below saturation. Incidentally, his point is plotted on that report I sent you and fell right on our line for the free energy.

Mr. Silberberg: He didn't mention the vapor pressure.

Mr. Castleman: We don't see a break at the melting points.

Mr. Silberberg: This is a good point. I thought originally, from your previous recommendations, that at the lower temperatures we had been getting a little bit outside of the dilute regime. That is why we have gone back and taken a look at some of the carrier-free data and still obtained a similar dependence. It has just confused us. We hoped that it would fall in the other direction and that would solve it, but for some reason it didn't. I might say that we had about 25 ppm of oxygen in the sodium iodide runs. Some work that has been done in England showed that the effect of oxygen was varied over a range up to 100–200 ppm and in some of these runs they found no dependence of the distribution coefficient on oxygen.

Mr. Genco (BMI): Could you tell me what is the precision in your experiments? On your carrier-free data, if your precision wasn't too good, you could have equally as well included that last point in your regression line.

Mr. Silberberg: Our precision is such that we do not want to do much least-squares work. We are really looking at something more than a trend, something which I think is definitive; the slopes, I think, are definitive. The accuracy is another question.

Mr. Brehm (BNWL): To get back on the oxygen-cesium business, could you expand on the effect of oxygen and the stainless steel container on the cesium-sodium partition?

Mr. Silberberg: We are doing some screening experiments at AI in which we have a full-flow cold trap in a very small loop. The loop was a forerunner of the loop that was described in Mr. Zwetzig's paper this morning. We had oxygen concentrations in sodium varying from 5 to 150 ppm, and we had about 60 ppm of cesium in solution. We found that as one decreased the temperature in the cold trap from 900°F, which is the isothermal condition at the start of the run, in general the activity in the cold trap increased. This occurred even though, according to our understanding of what the oxygen concentration was in the sodium at that time based upon the solubility data for oxygen and sodium, we believe we had not precipitated any oxygen in the cold-trap section. This would indicate that cesium was coming out in the cold trap even though we were really not depositing oxide. Whether there was a reaction between oxygen and cesium and the metal, etc., as other people have said at this meeting, we can only speculate. Until you really know the answer it is very nice to speculate, because you feel happy about it and no one can really prove to you that such is not the case. I think the real situation here certainly, as was explained yesterday, is not really known, but there appears to be a tendency for cesium to go to cold surfaces in a system containing oxygen without, shall we say, a precipitator or another phase of the oxide, solid phase. So I would think that this being the case, there is a possibility that as we decreased the temperature in succesive runs at 150 ppm oxygen, we could have been losing cesium from the solution to the walls, lowering its effective activity.

Behavior of Several Fission Products in the Atmosphere Surrounding Sodium-cooled Reactors in the Event of a Major Accident*

Cl. Descamps

Belgonucléaire
Brussels, Belgium

C. Beaudet and J. Rygaert

S.E.R.A.I.
Brussels, Belgium

(PRESENTED BY J. VAN DIEVOET)

1. Introduction

The different safety requirements which must be satisfied by a containment building for a nuclear reactor make it necessary to know all the consequences which might follow an accident occurring to the reactor. Different types of accidents can be considered. Nevertheless, it is usual to study the most credible accident in order to set up the basic parameters of the containment building.

We have followed the same method on an experimental basis, that is to say, we have simulated on a small scale a major accident of a sodium-cooled fast reactor. In such a reactor the most likely major accident is the rupture of fuel elements with simultaneous melting of the uranium oxide. This molten uranium oxide is brought into contact with the sodium coolant, which might be vaporized and, in case of rupture of the main circuit, violently react with the oxygen in the atmosphere of the containment building.

It is important to know the different consequences of the explosion resulting reaction from pressure, temperature, and contamination standpoints.

In fact, the object of the experimental tests reported hereafter was to study the behavior of several fission products in the aerosols formed during the sudden oxidation of sodium at high temperature in contact with molten irradiated uranium oxide. Previous studies in this field have been performed by our team and presented last year at the international conference at Aix-en-Provence.

During the first experiments the simulation was simplified by the fact that the irradiated uranium oxide and its spectrum of fission products was simply replaced by iodine, and it was the behavior of iodine in sodium oxide aerosol which was studied.

The results obtained during these experiments can be briefly summarized:

The temperature attained was between 1100 and 1300°C.

A maximum pressure of 2.6 kg/cm² absolute was reached in our vessel 2 sec after the start of the reaction.

There was practically no iodine in the gaseous phase of the vessel after the explosion.

In our present experiments we have approximated the simulated accident by using a real source of fission products, i.e., irradiated uranium oxide.

2. Experimental Conditions

Our work can be summarized the following way:

We want to simulate a major accident resulting from a sudden contact of sodium vapor contaminated by fission products with atmosphere.

This is achieved by breaking (by percussion) a capsule containing preheated sodium into a large vessel filled with atmospheric air, the released sodium being put at the same time in contact with molten irradiated uranium oxide.

For such an experiment the following conditions are required:

a) sodium heating in a sealed capsule;
b) melting of uranium oxide;
c) quick contact of sodium vapor, uranium oxide, and air;
d) collecting the evolved aerosols.

Three series of experiments have been performed. In each case the atmosphere of the vessel was ordinary air with a relative humidity of 50%. The aerosols produced came:

in the first series, from the reaction of air with radioactive sodium alone (^{24}Na: 5–6 g);

in the second series, from the reaction of air with natural sodium plus molten irradiated UO_2 (Na: 5–6 g);

in the third series, from the reaction of air with natural sodium plus unmolten irradiated UO_2 (same quantities as above).

* Work performed within the framework of the research programs of the Euratom/Belgonucléaire Association.

3. Experimental Device

The experimental device in which the explosions are produced (see Figures 1 and 2) is constituted of three parts:

a steel vessel containing the atmospheric air which reacts with the sodium vapor;

a sodium container in which the sodium is heated before put into contact with the air;

an uranium oxide melting device (see Fig. 3).

The steel vessel itself is made of three parts:

a) A steel cylinder (270 mm high, 250 mm in diameter, and 5 mm thick), clad on the inside with a foil of AISI 304 stainless steel. A 10-mm-thick glass scuttle allows us to make sure that the UO_2 is molten and to observe the explosion inside the cylinder. This cylinder is further fitted with:

a small-diameter tube for helium supply; it may be closed by a valve;

a Bourdon-type manometer to measure pressure variations (scale: $-1{,}000$ to $+2{,}000$ g/cm^2);

the uranium oxide melting device;

a high-flow valve (of ½-in. diameter) for evacuation and rapid air supply or sampling of the aerosols.

A deflector inside the cylinder prevents sudden cooling of the crucible by incoming cold air.

b) The stainless steel bottom (of 10-mm thickness).

c) The stainless steel cover bearing a tube (35 mm in diameter and 370 mm high) surrounded by a furnace to heat the sodium. The temperature of the furnace is read by means of two thermocouples placed outside the steel tube. The heating power required to reach 1,000°C is 750 W.

A punching device is fixed at the base of the tube; it is a bevel-edged tube of hardened steel that, at the moment of explosion, penetrates into the capsule. It is mounted on a strap and placed 25 mm above the crucible with molten UO_2, so that the stream of vaporized and liquid sodium is directed towards the crucible.

The device provided for moving the sodium container onto the punching rod is fixed on top of the tube.

Tightness is ensured by O-rings. The container-securing device is made of two parts, to avoid having O-rings placed in hot areas of the tube.

The cover and capsule-securing seals are cooled by water flowing through a copper spiral tube placed on top of the cover and extending over the upper part of the tube.

The sodium container is made of AISI Type 316 stainless steel. The bottom of the container has the shape of a cone frustum in order to ensure the complete ejection of sodium. The central part is 1 mm thick. Capacity is 25 ml. The container is closed by welding. The upper part of the container is fitted with a tube (of 2-mm inside diameter), the purpose of which is to counteract the excess pressure during welding and to ensure the clamping of the furnace.

The uranium oxide melting device is a crucible made of a spiral-shaped tungsten wire (ϕ 1 mm); the bottom of this crucible is made of alumina. The crucible is heated by passing electric current in the tungsten wire. The uranium oxide is brought to melting temperature by passing about 50 A at 20 V, which gives a power of about 1 kW. The melting of UO_2 is controlled visually through the scuttle.

In order to avoid oxidation of the tungsten at these high temperatures, melting is achieved under a 40-Torr pressure of helium, the current-supply connection being gastight.

4. Experimental Procedure

The experiment properly said is realized in four stages:

first stage: filling of the sodium capsule;
second stage: melting of UO_2;
third stage: explosion of sodium with air;
fourth stage: sampling of the aerosols for analysis.

Some details of the different stages of the experiments are as follows:

Filling the sodium container. Sodium (for analysis) purified by filtration under vacuum is admitted into the steel container under a slight helium pressure. After cooling under helium atmosphere the capsule is closed and welded.

Melting of UO_2. Natural uranium oxide irradiated in the BR-1 reactor to a neutron dose of about $5 \cdot 10^{16}$ nvt is introduced in the crucible. The cover of the chamber is replaced and the sodium furnace is heated to 1,000°C. When this temperature is reached, the sodium capsule is placed into the furnace and, the apparatus being leaktight, the air is evacuated. After several flushings with helium, a pressure of 40 mm helium is maintained, and the crucible is slowly heated by an electric current flowing through the tungsten wire which acts as a crucible for UO_2. Melting of the oxide is checked (above 2,700°C) through the scuttle; the current at that time is 50 A.

Explosion. Once the uranium oxide has melted, the current is brought to 70 A. Air is suddenly admitted into the apparatus and the air intake is closed. At the same time the capsule is perforated (by the percussing device) and the spiral tungsten wire is extended by means of an alumina rod. This provides a sound contact between the components. The jet of

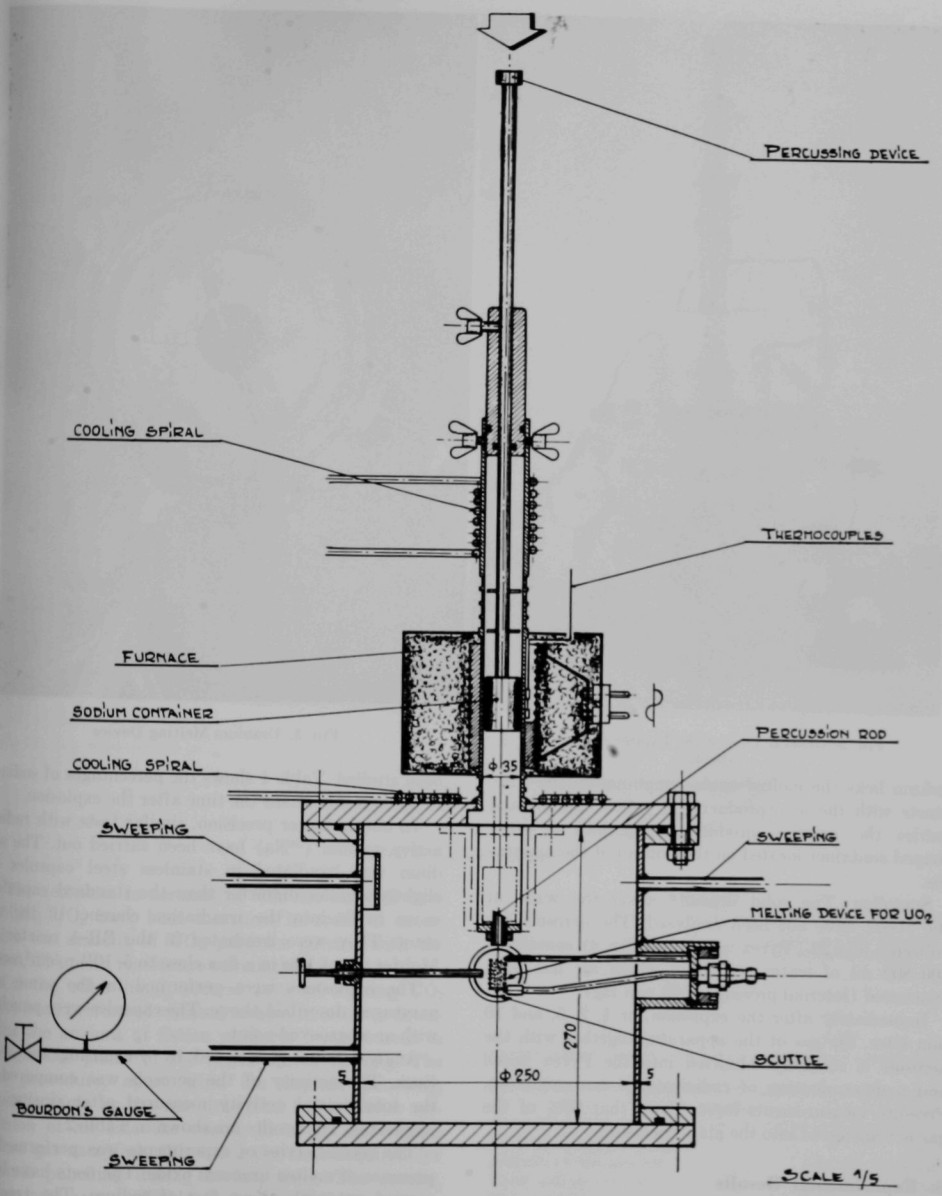

FIG. 1. Explosion Chamber.

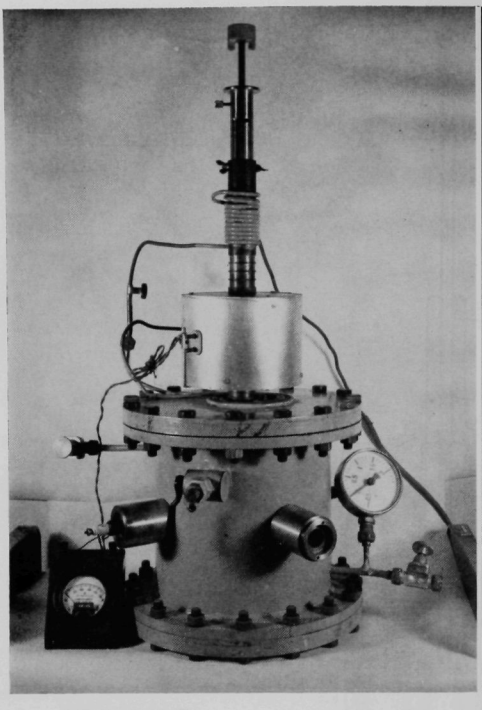

FIG. 2. General View of the Explosion Device.

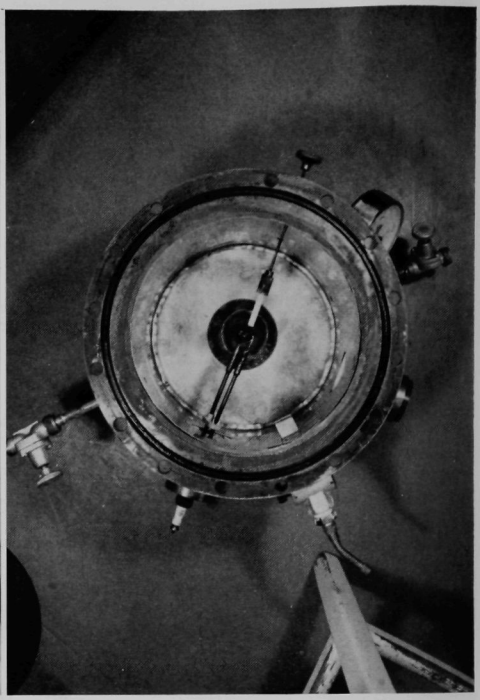

FIG. 3. Uranium Melting Device.

sodium licks the molten oxide remaining on the wire, reacts with the air (producing a yellow flame), and carries the reaction products along into a cone-shaped container located on the bottom of the apparatus.

Sampling. The solid deposits along the walls of the vessel have not been analysed. The aerosols are collected in a 20-l Pyrex vessel (see Fig. 4) containing 600–800 ml of water and from which air has been evacuated (internal pressure of 20 mm Hg).

Immediately after the explosion, or 1, 2, 5, and 10 min later, the gas of the apparatus together with the aerosols is suddenly admitted into the Pyrex vessel and a determination of radioisotopes is carried out. Pressure measurements have shown that 65% of the gas is transferred into the glass enclosure.

5. Experimental Results

In our first series of experiments the aerosols produced by the contact of air with sodium alone have been studied. Table 1 shows the percentages of sodium in the aerosols versus the time after the explosion.

To obtain better precision, similar tests with radioactive sodium (^{24}Na) have been carried out. The sodium was irradiated in stainless steel capsules of slightly smaller diameter than the standard capsules, so as to fit into the irradiation channel of the reactor. They were irradiated in the BR-1 reactor at Mol for about 1 hr in a flux close to $5 \cdot 10^{11}$ n/cm^2/sec.

The explosions were performed in the same apparatus as described above. The capsules were punched with an ungrooved point.

Analyses were performed by γ-counting the solutions. The activity of the aerosols was compared to the total initial activity measured after rinsing the apparatus. The results are shown in Table 2.

The second series of experiments was performed in presence of molten uranium oxide. The tests have been carried out with about 6 g of sodium. The tracked isotopes successively determined were: ^{131}I, ^{132}Te, ^{140}Ba, ^{89}Sr, $^{141+144}$Ce, and $^{103+106}$Ru.

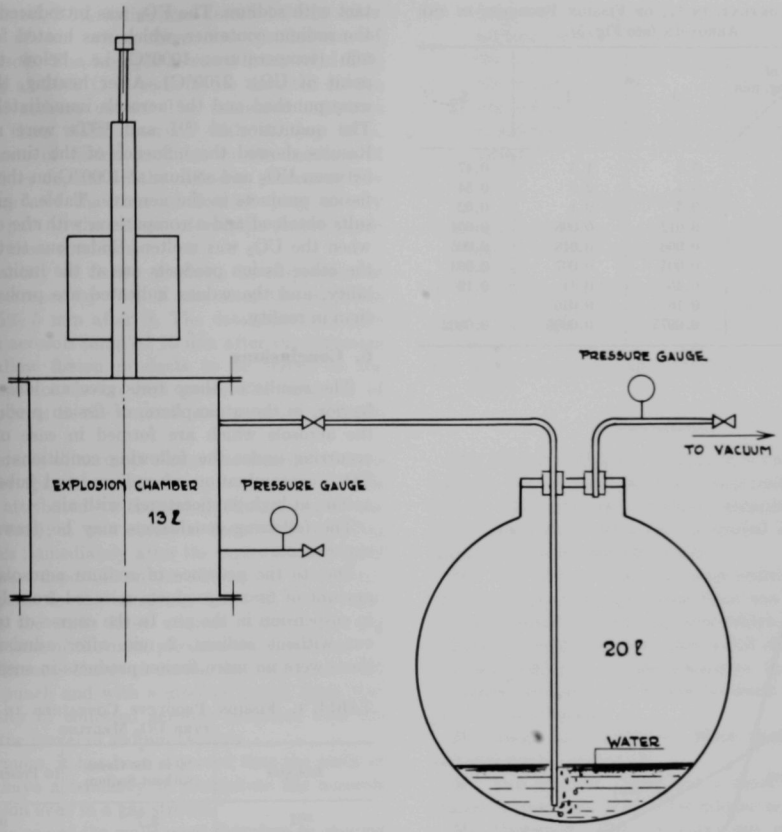

FIG. 4. Sampling Device.

The activities in aerosols of ^{95}Zr not released from melting UO_2 have been measured in order to determine the amount of UO_2 particles carried with the gases. The main results are summarized in Table 3.

On the other hand, several tests of melting UO_2 have been performed without sodium in order to determine the amount of fission products being present in the gaseous phase of the vessel during melting. The test procedure, apart from the capsule punching, was the same as the one described before. After admission of air into the vessel, 10 to 15 sec elapsed before gas sampling, this being the time required for capsule punching during normal tests. The results, as may be seen in Table 4, show that the quantities of radioisotopes in the atmosphere are much lower than those traced in the sodium oxide aerosols. By

TABLE 1.

Time after Explosion, min	% Sodium Initially Involved Recovered in Aerosol
0	5.6
2	1.5
5	0.47

TABLE 2. SODIUM CONTENT IN AEROSOLS, MEASURED BY γ ACTIVITY

Time after explosion, min	0	10
Activity of the aerosols	$3.57 \cdot 10^7$	$2.94 \cdot 10^5$
Total sodium activity	$1.27 \cdot 10^9$	$1.17 \cdot 10^9$
% in aerosols	2.8	0.025
Weight of sodium involved, g	5.5	5.1
Weight of sodium in the aerosols, mg	115	1.3

TABLE 3. Content, in %, of Fission Products in the Aerosols (see Fig. 5).

Time of Sampling, min / Isotope	0	2	5
Na	5.6	1.5	0.47
^{131}I	9.4	2.5	0.54
^{132}Te	0.5	0.1	0.02
^{140}Ba	0.012	0.008	0.001
^{89}Sr	0.066	0.018	0.005
^{141}Ce	0.005	0.007	0.003
^{137}Cs	0.45	0.34	0.19
^{103}Ru	0.16	0.046	
^{95}Zr	0.0075	0.0005	0.0002

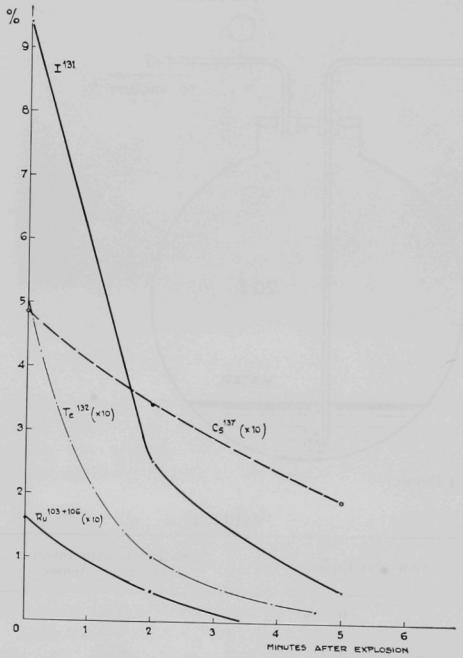

Fig. 5. Fission Products in Gases.

comparing the results of both series of tests (with and without sodium) it can be stated that the particles of sodium oxide capture the fission products and keep them in the gaseous phase, thus preventing their deposition on the walls of the vessel.

Finally, a third series of experiments was carried out. The single difference with those preceding was that the uranium oxide was not molten when in contact with sodium. The UO_2 was introduced directly in the sodium container, which was heated for 15 to 30 min (temperature: 1000°C, i.e., below the melting point of UO_2: 2700°C). After heating, the capsules were punched and the aerosols immediately sampled. The quantities of ^{131}I and ^{132}Te were measurable. Results showed the influence of the time of contact between UO_2 and sodium at 1000°C on the content of fission products in the aerosols. Table 5 gives the results obtained and a comparison with the experiments when the UO_2 was molten. Under our test conditions the other fission products are at the limit of detectability, and the values indicated are probably higher than in reality.

6. Conclusions

The results of these tests give an idea of the behavior, in the atmosphere, of fission products and of the aerosols which are formed in case of accidents occurring under the following conditions: melting of UO_2, contamination of sodium, and subsequent reaction, at high temperatures, with air.

The following conclusions may be drawn from the experiments:

Due to the presence of sodium aerosols, a certain amount of fission products released from UO_2 is kept in suspension in the air. In the course of tests carried out without sodium, 2 min after admission of air there were no more fission products in suspension. On

TABLE 4. Fission Products Contained in the Gases after UO_2 Melting

Isotopes	% in the Gases without Sodium	In Presence of Sodium
^{131}I	3.7	9.4
^{132}Te	0.75	0.5
^{140}Ba	0.10	0.012
^{89}Sr	0.05	0.066
^{141}Ce	0.013	0.005
^{137}Cs	0.06	0.45
^{95}Zr	0.008	0.0075

TABLE 5. Percentage of Fission Products in the Sodium Aerosols Produced from Solid UO_2 and from Molten UO_2

Isotopes	Without UO_2 Melting		With UO_2 Melting
	15-min Heating	30-min Heating	
^{131}I	0.012	0.052	9.4
^{132}Te	0.019	0.022	0.5
^{140}Ba	0.001	0.001	0.012
^{89}Sr	0.003	0.007	0.066
^{141}Ce	0.001	0.002	0.005

the other hand, 2.5% iodine was detected 2 min after admission of air when there was production of Na_2O aerosols. The isotopes released from solid UO_2 by heating at 1000°C in sodium are detected in the aerosols of sodium oxides. The measured activities are lower than those observed with melting UO_2. The amounts of fission products in the aerosols of sodium oxides depend on the diffusion processes. The temperature and the time of contact play a very important part in the release of volatile fission products under these conditions.

The quantity of fission products in suspension in the air decreased by 75% 2 min after the explosion and by 95% 5 min after it. The determinations performed on aerosols sampled 10 min after the explosion did not allow fission products to be traced in the gases except for fission rare gases. The amounts of fission products in the aerosols are reported in Table 3.

The amounts of aerosols versus the deposition times are smaller than those previously reported.[1-4] This could be attributed to the small dimensions of our reaction vessel; it was observed that when sampling the aerosols immediately after the explosion, the oxide particles were deposited on the walls of the tube carrying the gases to the sampling flask. It would thus seem that the walls have a great influence on the deposition time of the oxide particles in suspension.

The differences observed during the tests made with a normal punch and with a grooved punch show that the quantity of collected aerosols increases with the length of the travel of sodium vapours.

Furthermore, it has been observed that the walls of the flask have a tendency to precipitate the aerosols in suspension even in a gas stream.

The influence of the walls must therefore be studied in order to complete this series of works. Tests should be carried out in a greater apparatus with a view to determine:

1) the distance covered by the sodium vapours in the atmosphere before being cooled and collected by interposing a wall on their travel; these tests could be performed by increasing the height of the apparatus used for the tests described in the present report and by varying the travel of the sodium vapours by displacing the reception cone;
2) the influence of the wall surface, by increasing it artificially by the addition of baffles inside the vessel.

BIBLIOGRAPHY

1. J. Saroul, Conférence Internationale sur la sûreté des réacteurs à neutrons rapides VI/13, Aix-en-Provence, 19-2/9/1967.
2. H. A. Morewitz, R. L. Koontz, C. T. Nelson, M. A. Greenfield, and O. F. Hausknecht, *ibid.*, VI/5.
3. A. W. Castleman, Jr., I. N. Tang, and R. A. Mackay, SM-85/26.
4. J. R. Humphreys, Jr., 2nd UNICPUAE A/Conf. 15/P/1983 (1958).

Discussion

Mr. Lindsey (APDA): I know it is not your major interest, but what about the decontamination afterwards? Did you use ordinary decontamination of your apparatus or were you interested in driving off these things with heat afterwards?

Mr. Van Dievoet: No, we used ordinary methods. On the walls of the apparatus there was a solid mixture of sodium and the aerosols which was not too difficult to scrape out first; then a full cleaning operation was sufficient to decontaminate the equipment. Of course, working with fission products made it very easy for the analysis.

Mr. Dickinson (LMEC): Were these lightly irradiated fission products?

Mr. Van Dievoet: They had a short time of irradiation in order not to have too intense an activity.

Mr. Dickinson: Did you make any effort to scale in your volumes the relative volume of a reactor vessel and the core when you made your model of the center?

Mr. Van Dievoet: No, not yet. The reason for that is that we are working on the SNR project, and we will wait until we have the proper volumes to take into consideration.

SESSIONS ON SODIUM TECHNOLOGY

SESSION ST-VI

Saturday Afternoon, November 9, 1968

General Discussion

Chairman: J. E. Draley
Argonne National Laboratory

Secretary: C. E. Crouthamel
Argonne National Laboratory

Mr. Draley: Your presence this afternoon is testimony to your dedication and also to the strength of your constitutions. Summarizing a meeting is interesting and potentially valuable, but I thought it might be more valuable, and perhaps more interesting, if instead of summarizing only the meeting, we would try to be a little broader in our scope, and a little more ambitious, and address ourselves to the problems in sodium technology.

I've broken part of the subject of sodium technology into four areas: A) materials compatibility; B) analysis and monitoring; C) purification and control; D) basic chemistry. If you reflect, you will decide that that is not all of sodium technology but is a good bit of it, and these are the matters to which we have been addressing ourselves the most during the past three days. In order to find a way that the various speakers will address themselves to the same sorts of things, I have itemized a couple of questions. They are not really independent subjects, because they are related to each other.

1. Where are we with respect to LMFBR needs; how do we need to improve or what remains to be done?

2. How applicable to design needs are our present experimental results?

I have asked five people to serve as discussion initiators. I have asked each of them to talk no longer than 10 min. I will then solicit discussion addressed to the general topics. You may be critical of the discussion initiator; in fact, he has been encouraged to be a little controversial, but you may also address yourself to the general question.

The first discussion initiator will be Dr. Prodyot Roy, of the General Electric Co., on the topic, "Materials Compatibility." Then Mr. K. E. Horton, AEC-Washington will talk on the same topic before we have general discussion.

Mr. Roy (GE): The effect of long-term sodium exposure on the mechanical properties of reactor materials is not well established. Short-term tests carried out in both static pots and dynamic loops under isothermal conditions indicate that sodium has no effect on mechanical properties of materials. This observation is not too surprising, as one should not expect too much mass transport and microstructural changes under these conditions. Consequently, mechanical properties are not drastically affected.

However, relatively short-term experiments in a dynamic sodium loop with a ΔT have revealed that selective leaching of alloying elements in the hot leg causes serious changes in microstructures of materials. For example, it has been observed that carbon is transferred from the hot to the cold section of the loop. This observation implies that materials in the hot section will lose their strength and the materials in the colder regions will become brittle. This will create serious problems in actual reactor system.

I want to emphasize, therefore, that we must establish long-term mechanical-property behavior in dynamic loops with a ΔT. I would also like to point out that short-term tests of, say, 1000 to 3000 hr cannot be expected to establish that behavior, since it would be very difficult to predict the changes that would take place after 5 or 10 yr of operation from such tests.

As I stated earlier, carbon movement is perhaps the most important transport phenomenon to be considered in a dynamic system with a ΔT. In the last three days, we have heard much speculation about the mechanism and mode of carbon transport. At the present state of the art, it is unlikely that we will be able to control carbon movements in reactors in the near future. It seems to me that, apart from carrying out carbon-transport experiments with unstabilized materials, we should seek to use the most stable (carbon) materials. There are indications, for example, that carbon movement in stabilized alloys is lower than in similar but unstabilized alloys. Hence, I am proposing to introduce stabilized materials in our long-term test programs.

So far, I have stressed the importance of mechanical-properties testing, but we should not de-emphasize the study of an equally important effect of sodium exposure, that of corrosion and deposition. I definitely believe that carefully designed long-term mass-transfer experiments should be continued. The effect of sodium velocity, temperature, and apparent oxygen level in sodium on corrosion of stainless steel is not well established. Very little is known, for example, about the physicochemical properties of depositing materials. The effects of oxygen level and temperature on the nature and mode of deposition in a dynamic system have yet to be established.

The problems associated with these studies are not simple. For example, study of corrosion and deposition patterns based on plugging or cold-trap temperature is not sufficient to provide an understanding of the mass transport in a multicomponent system. On the other hand, none of the other oxygen-monitoring devices have been sufficiently developed for in-reactor use. We must therefore direct our attentions to perfecting these devices in small-scale dynamic systems,

concurrent with our studies of the fundamental effect of oxygen activity on corrosion and deposition.

The same thing, of course, applies to carbon activity and mode of carbon transport. These phenomena are even less clearly understood, yet are perhaps the most important from the standpoint of materials behavior in flowing sodium.

In conclusion, I would like to say that we are severely pressed for time. We are forced by the reactor designers to predict long-term materials behavior from the short-term experiments. So, let us coordinate and utilize the basic knowledge obtained from these experiments and, at the same time, design proper long-term experiments in reactor mock-up systems. Results from such carefully designed experiments will enable us to predict materials behavior during the lifetime of the reactors with more certainty. Furthermore, if we continue these efforts, we will eventually develop actual performance behavior of materials under conditions similar to that of a reactor.

Mr. Horton (AEC): This Thursday, John McKee addressed himself to the first question, when he said we were about 150 million dollars away from our LMFBR needs. I'm not going to go further in that area. I'm not going to try to give you a state of the art in two minutes. I have also found that if I ask the question "What remains to be done?" in a mixed audience like this, people are reluctant to part with ideas. They like to do so in the form of proposals. We've asked this question a number of times such that now I say, "Don't answer me now, send me a proposal." That's about the only way to get any ideas in that respect.

I would like to try to focus this discussion on sodium technology. These last three days you've been listening to papers on purification, solubility measurements, analytical techniques, and all sorts of scientific details. I'd like to tell you what the primary goal is in sodium technology. We are trying to develop the technology needed for LMFBR systems to assure long-term materials compatibility. I will state categorically that I don't care what the corrosion rate is, just as long as the sodium system remains structurally intact and I don't plug up my heat exchanger or transfer too much radioactive material downstream. Therefore, I could care less about the analysis and monitoring techniques, unless lack of monitoring, etc., resulted in loss of structural integrity. I really think the chemists, in particular, get confused as to what our true goal is. What I'd like to use this discussion period for is to have you people help me out with the question of loop sizing, since most of our contractors have sodium loops. Incidentally, it seems that our contractors believe they haven't made the big time until they have a forced-circulation loop. Now, I've noticed that our results at any given contractor are changing as a function of time. This may mean that the sodium itself is changing as a function of time. I've also noticed that results differ or conflict at various contractors, and between various countries for that matter. There may be many reasons for this, but one of the reasons may actually be the loops themselves, particularly the geometry of the loops. So the questions I want to ask are "Are we building the right kind of sodium loops? How big should we make our loops, or how small can we make them?" This morning Milton Shaw made the statement that we must demonstrate reliability in our test loops. He wasn't really talking about the sodium technology program. He was talking, I think, more about the sodium pump test facility, and things of that nature. But the statement is valid for our sodium program.

What I'd really like to know is how big should we make a loop such that we are fairly well assured that when we actually go in a large reactor we are going to get results that we predicted from our tests.

I've always believed (although I've gotten a lot of argument on this) that as long as we are going to be generating data in sodium technology, it may as well be useful data. It should be data that the designers can use. I say this over and over again, and I guess people are getting tired of hearing it. But I repeat, I'm firmly convinced that we can generate design data in our basic technology program. Therefore, I am most intent on generating data in sodium loops that produce effects similar to actual reactor environments.

May I have your comments?

Mr. Weeks (BNL): Since the question was just asked, and I'm sure there are a number of us who have various ideas on the interpretation, I question very strongly whether it is the size of the loop that is important, but rather whether or not the areas of the various materials and the temperature profiles are realistic in comparison with the overall reactor. I think this is what's important, not so much the size or the number of dollars spent, but how realistically can a loop be designed to yield the various surface area relationships which we suspect to be important, the various compositions of the materials which we expect to be important, the various temperature cycles and sodium purity aspects of the sodium which we expect to be important.

Mr. Horton: Does this mean then that it doesn't make any difference if we're going to study refractory alloys, whether or not we make our loop out of stabilized stainless?

Mr. Weeks: If we sincerely believe, and there is evidence to do so, that there is carbon transfer from

the unstabilized stainless steels to the refractory alloys, then we have to have the information for the designers to make this decision. If the designers make a decision that a refractory alloy fuel cladding is needed in the LMFBR then they have to know—can they avoid embrittlement of this alloy by using a stabilized stainless and therefore by reducing the carbon transfer?

Mr. Horton: Wouldn't it be nice if they also know if they could get away without using a stabilized stainless?

Mr. Weeks: Certainly. But, there is evidence that carbon does go quantitatively on a mass-balance calculation at the comparable temperatures.

Mr. Hiltz (MSA): Mr. Roy and I and some other people have been rather concerned about carbon mass transfer. The General Electric group have expressed this concern at this meeting; others of us are suddenly becoming aware that it may be real. However, General Electric and, I know, Babcock and Wilcox have talked about using downgraded 2¼ chrome on the ferritic side, which means you are now going to be transferring carbon in the other direction for some length of time. It's impossible to have both mechanisms operable, but where can you draw the line? The ferritic steel is not going to deliver carbon forever, and the cladding is going to come in and go out. It becomes rather difficult to try to design anything for a dynamic or an actual system. The only thing you can do is attempt to look at the possible combination. Designing a test loop which may combine all the things you expect to see over the lifetime of a reactor may be extremely difficult.

Mr. E. N. Pearson (LMEC): Just to address to the question of the size of a test loop, presumably there are two extremes one can go to: a full-scale developing test where one is interested in mechanics, and also a capsule test or screening type of operation that's a micro-miniature type of test. I think it depends upon the function that one wants to perform as to size of a test loop.

What I'd like to do is address myself to two general ideas that I've had regarding materials compatibility. Number one is corrosion testing; it's been interpreted also as erosion testing. Generally, all such tests have been somewhat limited in the sense that the flow direction in relation to the material sample has been parallel. Controlled experiments are needed, I believe, in which the flow is normal to the metal surface. I'm reminded of two events of the past six years in which a high rotational velocity resulted in a material loss that was quite severe. It was a vortex type of phenomenon that wasn't completely appreciated until after the event. Secondly, I think material-property tests ought to be expanded to include thermal-fatigue and thermal-shock tests. We heard a description yesterday about a proposed installation in Japan that was to do this. This is a unique characteristic of LMFBR plants because of the coolant. Water is not the same type of animal, nor are the temperature requirements, and temperature extremes in the hot and cold legs that we expect of these plants. Furthermore, there should be some attempt at setting specimen sizes that are comparable to pipes and valves and heat exchangers, etc., in other words, thermal fatigue compared to mechanical fatigue, thermal shock compared to impact.

Mr. Shannon (BNWL): I should comment that I'm working on the FFTF sodium technology development so my comments are in this context. With regard to the test loops that are being used to generate data, I'm reminded of a study that was done by one of the foremost management consultation firms in the US—it looked into what was good and what was bad about the research output of industrial concerns, and I think it's equally true here. The finding was that most research projects that failed did not fail due to technical ability, but failed because the output, the end product, wasn't relevant to the objectives of the corporation. I think it is true that in many cases we may have a loop generating very good scientific information which will produce a lot of very interesting results but will not be applicable to the LMFBR, which is their ultimate objective. Now, how does one design a loop such as this consistent with the objectives? There is a fair amount of effort and money being put into the 1000-MWe studies, and I want to examine very carefully all the documentation of those various reactors. Shortly after the first of the year the FFTF conceptual design will probably be fixed into preliminary design, and this will be another good example of the kind of a piping system that an LMFBR will represent for the first time. FFTF can be a very good example for all of you who are working in corrosion and materials to examine, see what velocities, surface-to-volume ratios, and temperature distributions are in those plants, and consider your research programs in that light. Is your loop relevant to those particular plants? If we can conclude that it is, then we're probably on the right track.

Mr. Draley: Thank you. That's very close to the kind of direction I wanted to use. I'd like for us not to be too specific about any one detail of the possible weakness in our testing, but to address ourselves to what are the things we have to do in order to be relevant. I would like to have you consider, for example, can you build a reactor on the basis of loop-test information? Do you have to know more than that about compatibility before you can build a reactor? Can you simulate irradiation effects? Can you

scale up? Are there size effects described quite differently than has been done in the words used today? There are sizes of sources and sinks, and these ought to be very important. I'd like to solicit statements relevant to what Don Shannon said. I want us to think out loud. What things do we have to do and which things can we not do without? Does anybody have any comment to make on that?

Mr. Young (GE): We have some observations that have been made and reported in this meeting that go a long way toward answering the question, "What kind of tests do we need, and what can't we do without?" I think we can't do without an environment for testing that in the best way we know how to make it simulates the reactor environment, both from physical and chemical standpoints. We've tried a couple of ways of getting at this, e.g., mocking up a 1000-MW design in terms of the corrosion products. The point is that you've seen examples of structural changes that have occurred in the materials over fairly short periods of time: 3, 4, and 5000 hours, although mostly 3000-hr tests. The point was made, I think by Jack DeVan yesterday, that you can see structural changes occur and you know that the long-term mechanical property must be affected by those changes that are produced by the sodium environment and we're just beginning to learn how to describe this environment. It may take a long time to describe it sufficiently so that you can mock up a really true environment or one that could be said to be representative of the full-size system. But until you do, you must at least pay attention to the material ratios between, for instance, a cold portion and a hot portion. Along with that you should pay attention to a mockup of a sodium environment that puts impurities in the system that are characteristic of the particular alloys you are testing and then proceed with long-term mechanical tests that are going to tell whether these materials will last in the reactor. The objective is to enter the stage of committing materials for construction with the highest level of confidence in the materials that you can possibly get in the time remaining. The only way of doing it is to do the compatibility tests and the mechanical-property tests in as long a period of time as you can with the best possible mockup of the environment. That's a corrosion mockup until we can get adequate tools to measure or detect types of impurities and enough chemistry work done to be able to precisely describe the environment.

Mr. Draley: I'd like to ask you a question pertinent to that. Can you be satisfied without demonstration that you mock up sufficiently well that you will see the right answer rather than the wrong answer in terms of success versus failure of materials? The alternative is that you would have to learn the effects of influential parameters; that the mockup will never do the job for you.

Mr. Young: If we can predict and begin to see some failures or bad performance in compatibility testing, then I'd say yes, we would have a fairly good idea or good confidence that the environment was OK. If we do not find anything failing in the sodium environments under which tests are run then this is a signal that the tests are not definitive.

Mr. McKee (ANL): You asked for general comments on what we need or don't need to satisfy the needs of the LMFBR in sodium technology. I think you know what my answer would be to that—it's written in WASH-1105. There is a program plan to accomplish these needs, and it has been agreed to by RDT as what's necessary, but it still needs the support of everybody who's going to do the work. If people here feel that, in fact, the plan is off the target and has called for work that isn't needed or doesn't call for work that is needed in sodium technology, I would like to hear about it. Aside from that, a more or less obvious comment. Dr. Roy brought up one point I thought we'd touch on a little bit. He called for introducing stabilized steels into the research program and Horton has talked about this several times. I certainly agree with him when he says that the only people we hear about this from are the National Laboratories, up until today when we heard from GE. Of course, who we would really like to hear this sort of suggestion from are the people who were going to make the steam generators or actual components out of these steels. What I'm wondering is: how does one go about introducing a new class of materials into the program in such a way that it really is meaningful and has everybody's support? I really don't know how to do that.

Mr. Shively (AI): I was sitting here thinking about Young's comments, and I think that what he had to say has a lot of merit, particularly with regard to large components in reactors, which in this country appear to be neglected. The other point I wanted to make is a plea from a metallurgist who is interested in sodium effects. I want to be sure that we understand that we should have a good control system upon which to make comparisons. So often the mistake has been made that the control test was the thing that was causing the effect and not what we were studying. In the sodium compatibility work I think we have to choose some baseline against which to compare, whether it be corrosion or some other effect.

Mr. Weeks: I think then the point is to ask yourself not what are these results after 1000 hr in sodium as against non-sodium environment, but what will

they be after 25 yr in a sodium and non-sodium environment.

Mr. Draley: The next topic is certainly an important part of the answer to the question about materials compatibility. That question will have to be answered in terms which include the requirement for proper and good analysis and monitoring. But the real basis on which I meant to develop this subject, and I hope that will turn out to be the one that our discussion initiator will employ, has to do with the development of analytical capability and monitoring capability as can be applied to systems.

Mr. Kovacic (APDA): If I could direct myself to a comment Ken Horton made about his interest being materials compatibility and that all these other aspects of sodium technology are support to it, I suggest that there are other problem areas that sodium technology is very much involved in that are not just related to materials compatibility: for example, fission product transport after fuel failure, sodium fires and aerosols, thermal and hydraulic aspects of sodium coolant systems, impurity behavior in cover-gas systems, leak detection for steam-generator leaks, to name just a few. I can see that if your main concern is for materials compatibility, you might begin to think that everything is directed in support of that activity. I doubt you meant that.

I am also going to take a speaker's prerogative and make a statement about a rather impassioned remark I made yesterday after Vince Rutkauskas gave his paper on vacuum distillation. After talking to several people in the corridors, I think I misled them and was in error. The point that was under discussion was the validity of the vacuum distillation analysis in reporting oxygen content in the sample as it is removed for the loop. In the amalgamation technique, if the oxygen is indeed there as hydroxide, and you titrate for the sodium and then report it as monoxide, you are going to be in error on the oxygen content by a factor of 2. In the vacuum distillation analysis I can see that if indeed the hydroxide that might be present is converted to monoxide during the distillation process, and you do the calculation on the basis it is monoxide, you do indeed get the right number of oxygen atoms. Another point I made which also ought to be clarified a bit: I said that we know in the Fermi system and in our loops we have sodium hydroxide in our cold-trapped sodium. We do know that sodium hydroxide is in the frozen samples, but in a cold-trapped system at 600°F, the hydroxide is not stable and is possibly dissociated as monoxide and hydride. Now I will get on with the topic I'm supposed to talk about.

I have a couple of observations which I'm going to make, just really to initiate discussion. They're not things that I feel really positive on, but I have questions on them. In the past two or three years there has been an extensive effort, three separate and independent efforts, to establish the status of sodium technology in the LMFBR program and to map out the direction in which we have to go. The most extensive and comprehensive effort, of course, is the one just completed by the Program Office at ANL. There are two other efforts, one of which is the Edison Electric Institute task force report which was published in April. The other was sponsored by the Analysis Branch in RDT, in which an industrial and National Laboratory group looked at the same thing; that report is not yet published. In all studies it was concluded that there is a real need in the LMFBR program to improve sampling and analysis methods and techniques, and to develop on-line purity-monitoring devices. One thing that has troubled me ever since I've been in this work, and I ask myself this about once a day, is what are we doing and why are we doing it? Some of the things I have been observing in the last year or two, and certainly have seen here again in this meeting, lead me to raise the question about what should be the proper near-term and intermediate-term priority on the development of improved analytical techniques and development of on-line monitoring devices. To me it's very noteworthy that we have operated a lot of sodium-cooled reactors in the past, and there are many being operated in the world now. By and large, there have not been any real serious problems that have come about because we don't have these improved devices and techniques that we say we will need in the long term. I can think of a couple of exceptions; I think the SRE meltdown might have been avoided if the tetralin leak could have been detected instantaneously by an on-line device. I know in Fermi the graphite out-gassing might have been detected and prevented some extensive damage, and the steam-generator leak might have been detected before it got as bad as it did. But I will emphasize *might* have been only if the devices had been so reliable and the operating procedure so stringent that when the meter registered, action would have been taken. I'm not sure that action would have been taken even if the devices had been there, because faith in the devices is an important consideration.

Another point that to me is very significant is this. As I hear the reports coming out from the various vendors on their demonstration plants and out of the European countries on the next generation of fast reactors, and hear what the development programs are, I fail to see at all, except in one or two cases, any effort going into the development of the chairman's Area B. To me that seems to indicate that the people

who are designing these plants and who hope to sell them must be quite confident that the present-day technology is going to be satisfactory for the conditions under which these plants have to operate. I have to give a lot of weight to that observation. Also, especially during the last couple of days, listening to the papers on the materials-compatibility properties and mass transfer, and reading the quarterly progress reports that come through, I get the distinct impression that for the conditions that we're going to see in the present reactors and in the next-generation demonstration plants the corrosion rates are going to be quite insignificant as far as fuel-clad performance is concerned, perhaps a mil per year under cold-trapped sodium conditions. In terms of mechanical properties, the diminution in the mechanical properties due to the sodium environment is really going to be insignificant compared to the change in properties due to the neutron environment. We really have to ask ourselves what priority should be put on area B considering the tremendous budget squeeze and the tremendous amount of problems.

The second observation I want to make has to do with the first point to which we were supposed to direct ourselves. It has to do with vendor participation in instrument development and sampling and analysis development as part of the industrial environment consistent with the American free enterprise system. Mr. Shaw, a couple of weeks ago here at Argonne, reiterated RDT's intention to fulfill the mandate that the LMFBR is to be developed within the industrial framework, and he said that there was a long way to go. I remember he specifically mentioned instrument development as an area where we hadn't even started. I make the observation that with one or two exceptions, notably with the exception of United Nuclear who has been in on the development end, I don't see any participation of the established instrument companies of the United States in this area. I think it's up to those of us who are in the development end to start getting these people involved, even if it means we stop doing some of the work we like to do. That's another observation.

The last point I'd like to make, and it's directed to the second question, is applicable to the evaluation of present experimental results. I find the status in our instrument development quite a "mish-mash." There's an awful lot of overlapping, and while at APDA we're saying the rhometer is looking good, reports are coming out of other facilities saying the rhometer is dead. It shows there's no communication or poor communication. I also see a lot of facilities working on the same devices. There seems to be a lot of duplication of effort, and the worst thing I see is that the evaluation of the performance of these devices is very qualitative and subjective in nature, i.e., "it's good," "it's not so good," "it's bad," etc. It's tough enough in life to have to believe in the things you have to have faith in because you can't prove them; but when we are dealing with technical things we shouldn't be believing and guessing; instead we should be finding out and knowing. I think in the area of instrument development we've got to do the same thing we've been doing in mass transfer and materials compatibility: tie it right down to quantitative things. What is the signal-to-noise ratio; what is the base-line drift; what is the response coefficient, today, next week, a year from now; what are the sodium temperature effects; what are the ambient temperature effects; what are the radiation effects, etc.? Let's list the number of tests, the average values, the standard deviation. Let's report the data in our quarterly reports, and let's get together once in a while and lay the data on the table.

Mr. Shannon: I think one major area of sampling, analysis, and monitoring work is hardly being looked at at all, and it may well be the most important one that we can consider. The objective of the LMFBR is to run reliably for 30 yr. For my money, the analysis and monitoring method that is needed the worst is the technique that you would apply to the plant after year 1, year 5, year 10, year 20, and year 30 to determine whether the plant is in its original condition, or at what rate it is degrading. Then you could have some advance warning of when you would have to replace a component. This is what I would call plant surveillance. I have personally had to go into two reactors after they were designed and built when something broke due to corrosion or metallurgy or some other effect, and then try to figure out ways to keep tabs on this particular phenomenon, to determine rates and magnitudes of the problems for future decisions. I would ask that we consider developing ways to monitor acceptable performance of materials in the plant.

Mr. Kovacic: I still am convinced that for long term, where we are talking about 1200°F sodium and possibly use of refractory metal clads, we definitely are going to have a need for this type of instrumentation. Also, in special situations like the FFTF closed loops. But I still question whether the people who are talking about demonstration plants believe they need this technology.

Mr. Draley: For area C, Purification and Control, I've asked Ross Humphreys to serve as a discussion initiator.

Mr. Humphreys (ANL): The main area of purification and control covered in these meetings concerned examination of precipitated residues, and the chemical states, interactions, and effects of carbon species in

sodium. In addition, the programs from AI, BNL, and BNWL investigating fission products distribution were reported in meetings this morning.

A number of papers touched on reaction processes which will be needed to develop purity-control levels. There is a great deal of study in the laboratory of sodium impurity effects which will further define allowable levels.

I think it can be concluded by surveying the experimental programs reported that the cold trap is considered sufficient at this stage to give the necessary control of system impurities.

There is one problem area that is being directly attacked in this area: basic nucleation and precipitation studies for the purpose of leading to optimization of cold-trap design. This work is being done at LASL, and was reported this morning in a paper by McPheeters and Biery.

The fission product studies have not yet reached the purification design stage. We are still developing the necessary information about general behavior.

Altogether, with the exception of the LASL work, purification areas in sodium technology are being treated mainly by programs having other objectives which need capability in the area to implement their other program objectives.

I think it is time we took an integrated look at the purification-system interactions and overall plant requirements. The present efforts are largely directed to meeting the needs of the LMFBR R&D program. We need programs directed to satisfy the design and operational requirements of large, radioactivity-contaminated LMFBR systems.

Now to answer the questions—where are we with respect to LMFBR needs; how do we need to improve; what remains to be done? First, a discussion of what these needs are.

The impurity-level requirements will be largely established in the materials-compatibility area. The types of impurities with which the LMFBR must deal fall into two general categories:

1) Bulk impurities—those with significant chemical concentrations and for whose removal the volume capacity of the removal device is a significant engineering and design consideration. These include, basically, the (a) atmospheric impurities: O, C, N, and H; (b) particulate impurities (carbon, Fe, Cr, Ni compounds, refractory metal oxide, alkaline earth oxides); (c) dissolved structural materials and their reaction products.

The second impurity category is:

2) Trace-concentration radioactive species. Here volume considerations in cold-trap design or reaction capacities for reaction removal methods are secondary to the shielding and heat-generation requirements for removal systems involving high concentrated collections of radionuclides. This class of impurities includes various spectra of fission products and radioactive corrosion products from the core region. Here, for LMFBR systems, I think we must assume vented fuel operation or operations permitting a small fraction of "defected" fuel elements to remain in the core as normal operations, say maybe up to 1% or some such number.

At the present stage it appears that LMFBR purification systems for both primary and secondary coolant systems will be based on the much used forced-convection cold trap, operating continuously and possibly supplemented by selective hot-trap or adsorption units to control specific impurities either unaffected by cold trapping or to levels below those corresponding to cold-trap saturation. These latter would be used for control of C, O, N, and H levels as needs for extended control of these impurities are developed and for fission product removal as the methods are developed.

The use of soluble getters for the chemical "trapping" of impurity species offers attractive economic and technological advantages. They are cheap; they maintain getter materials at the source of impurity contamination; they permit the control of certain impurities to much lower levels than cold trapping, or hot trapping too for that matter, if a discrete impurity source is present. However, sodium with dissolved materials is no longer sodium, and a very large and extensive materials program with such new media would be required before the required degree of confidence for LMFBR utilization could be met. This, coupled with the lack of a presently demonstrated clear need, makes the development of such systems for early LMFBR's unlikely.

The cold trap will probably remain the workhorse of purification systems. Design-limiting parameters may change from those we have been using. In the case of exposed-fuel operations it is likely that handling and shielding requirements may dictate geometries. Capacities in such cases will be limited by radiation and heat-generation level rather than bulk impurity capacities. Thus, traps will tend to be smaller, and designed for remote removal and replacement. In very large systems for which high flowrates are required, a multi-unit manifolded system of cold traps could be employed, with each unit being routinely replaced when given radioactivity levels are reached.

The most likely use of hot trapping, or more properly, solid-liquid reaction control, will be in the area of carbon control. In mixed austenitic-ferritic secondary systems, the maintenance of a critical carbon po-

tential in the sodium may be required to maintain acceptable carbon activities in both classes of structural material. A carbon sink may protect the austenitic steel in the IHX from carburizing, but it would tend to decarburize the ferritic steam generator with a significant effect on the mechanical properties of materials. Thus, a level control, one which won't carburize the austenitic steel too much or decarburize the ferritic steel, may be required.

The development of control systems for fission products is in a rather primitive stage. We know that some will plate out on metal surfaces, that some will wind up in the cold trap, and some in the cover-gas area; a few will stay in the sodium. Methods must be developed for the control of each of these groups, providing removable surface-adsorption and exchange columns.

Purification control of a cover gas includes the need to treat xenon, krypton, and their alkali-metal daughters. Possibly nitrogen and hydrogen control will also be needed.

Methods could include high-efficiency processes or a combination of dilution-low efficiency systems involving the additions of inactive xenon and krypton followed by a low-efficiency removal system. Fractional condensation, delay beds, membrane diffusion, adsorption, exchange columns, and decay storage are all methods under consideration for the removal of gaseous fission products. High heat-generation rates will probably necessitate the use of a dilution step in any process, such as fractional condensation, that tends to isolate relatively pure noble gas fractions. System designs will be limited by heat transfer and radiation level, and must be designed for ease of replacement and transportability.

In the area of cold traps, our present state of technology still leaves much to be done. We need more and better precipitation nucleation, as well as crystallization data for cold-trapped species in sodium. In addition to the oxides, this also includes the consideration of other dissolved interstitials, as well as metals and corrosion products. We need better system-design criteria to utilize crystallizer tank volume in nonradioactive systems and to prevent inlet plugging. We need to know more of what the effects are to a reactor system of a temperature excursion in the cold trap. We need to establish purification procedures for cleaning a system following a maintenance or other operation resulting in significant system contamination. We need to know more about fission products interaction in the heat economizer and crystallizer tank sections of a cold trap, as well as about coprecipitation or adsorption processes.

In hot-trap technology we need both technology development and the establishment of design criteria. Hot-trap systems will be needed in LMFBR R&D programs in which specific impurity levels are treated as independent variables. Materials interaction data and system kinetics are needed for getters specific to O, C, H, and N. For carbon traps which may be used in large, mixed-materials systems information on possible regeneration methods for trap material would be helpful.

Mr. Horton: The reason why the diffusion cold traps in Russia look so good, in fact look as good as our flow-through cold traps, is that we are probably running our flow-through cold traps completely opposite to the way they should be run. Los Alamos is studying cold-trap kinetics; they show that the driving force for precipitation of sodium oxide increases with sodium velocity. We are running flow-through cold traps with very low sodium velocity, and that's opposite to the way we should be running them.

Mr. Draley: Perhaps instead of precipitation, you meant precipitation and deposition.

Mr. Zitek (ComEd): I would like to commend Humphreys for his evaluation of the problems from an operational standpoint. I think you hit things on the head. I had come to the conclusion from listening to all the papers the last few days that we should just run the cold traps at their maximum capacity and take what we get. This might not be adequate for materials compatibility if we have ferritic and stainless steels in the overall system; we probably would have to maintain a certain carbon level to eliminate or minimize the decarburization and carburization. I would like some opinion as to whether my feeling is correct that if we put in more cold-trap capacity than is calculated and run continuously we might not need monitoring as close as we are attempting.

Mr. Humphreys: Until we develop more skill and more knowledge of the requirements, that is the only method available to us. I feel it will be preferable to run some things at controlled levels, after we learn to optimize.

Mr. Draley: Gentlemen, thanks very much. I would like to address our attention to the last area. If we didn't have any problems which would not yield quickly to short-term experimental tests, we probably wouldn't care about basic chemistry. It seems very important to know something about the basic chemistry of these systems, and Hal Feder will address himself to that.

Mr. Feder (ANL): I will right away violate the chairman's precept to stick to the subject. I think the subject should have been basic chemistry and *physics*.

Listening to the results of these three days, I was a little bit appalled because some of the physical properties of extreme importance haven't even been discussed; for example, the compression isotherms of sodium at pressures up to 200 megabars and temperatures up to 2000°C, which are essential kinds of information for the reactor safety people. Such measurements obviously haven't been reported, and I don't even know if they're being worked on. I cannot stress too much the importance of the physics of sodium; we should not be having sessions like this without any input in this area.

One further point about the physics of sodium. Because it's a rather unusual solvent, its physical properties—electrical conductivity, electronic and atomic structure—are very important to us and to the chemistry of the situation. I would venture to say that if we understood more in this area we would have less chemistry to do. For example, one of the symposium speakers reported on a physical model for the solubility of the inert gases in sodium; it would seem fairly obvious that we should test and apply the model. At this point I will issue a challenge to the gentleman who has proposed the physical model for the solubility of inert gases, Dr. Veleckis of this Laboratory, to predict the solubility of helium (which I believe he's going to measure), put the prediction in a sealed envelope, and see later if he has, in fact, got the right answer. I'm very hopeful that he will. If this kind of approach succeeds, then we can be hopeful that the solubility of zirconium, for example, or some other difficult-to-measure material in sodium, may yield more rapidly or more clearly or more completely to theoretical analysis than to the awful difficulties of measurement. Of course, this doesn't mean we shall not need to verify the predictions—we'll have to verify them—but I believe there's a great and important future in this area.

Now, with regard to the question Ken Horton raised, are we doing basic chemistry in a vacuum, so to speak, without regard to materials compatibility? Certainly, from the papers I heard these last three days, I'd say that is not the case. All the papers reporting in this area have a connection with the question of materials compatibility. Sometimes the connections seems a bit tenuous; but it may seem tenuous only because the experimenter is looking for phenomena which may *become* materials-compatibility-controlling upon long-term exposure. This is a perfectly reasonable and normal kind of research to do—and if we don't do it, in fact, we'll be in considerable trouble.

Next, let me address the questions that the chairman posed. How are we with respect to LMFBR needs, and what do we need to improve? If we consider the period since about 1951 as the period of modern, solid investigations in sodium technology and chemistry. I think we have moved to a very good position relative to where we were only in the past few years. In particular, I think that the acceleration of effort and the acceleration of obtention of useful results in the past two years has been remarkable. I think we need to maintain this accelerated pace for some time in order to meet the scheduled needs of LMFBR. Emphasis, it would seem to me, will have to shift from generalities to details. It is clearly not going to be desirable in the future to talk about total carbon in systems and to wave one's hands with respect to carburization potentials; rather, I believe, we will need to know precisely the rates at which various carbon-bearing species are formed from steels, precisely the rates at which they diffuse or transport through systems, precisely the rate at which the various species react with steels and carburize them or interact with other impurities, and so forth. The point I'm making is that we are in a period of breakthrough from the general to the specific in many areas, and this is an important notion to follow through on.

I would also make a special plea at this point for more qualitative observations. This may seem contradictory, but it's not meant to be, for occasionally it pays to give less attention to quantitative measurements and a great deal more attention to phenomenology. I think sodium technologists have been remiss in this area. It is a remarkable fact that after 18 years of looking at plugging meters, only this year has it been established that it's not always sodium oxide that plugs. There's pure phenomenology. It's a remarkable fact that after nearly 20 years of measuring the carbon content of sodium, we found only two years ago that when liquid sodium is sampled into a pipette its carbon content segregates. It's a remarkable fact that only recently have we become significantly aware that metallic mass transfer might be due to phenomena other than simple solution-crystallization cycles—that, in fact, film breakaways, oxide-particle transfers, surface diffusion and other things may be important. Phenomenology! I cannot stress enough how important it is that we examine all the possibilities, not just the naive and simplistic ones, in order to see what's going on, before we hasten to make measurements. Finally, insofar as there is a demand for data for design needs, all I can say is that we'll respond to the design needs only to the extent we understand the system. If we overlook important phenomenology, many of our measurements will have no bearing on design needs. If we understand the phenomena that the designers

are going to encounter in real systems, we can make the appropriate measurements.

Mr. Draley: I found those remarks valuable and thought-provoking, and as I listened to them I thought that they probably hit home to us quite a bit in sodium technology.

Mr. Zitek: I was glad to hear you make the statement that, considering that we have been looking at sodium since 1951, the technology has not moved as well as one would expect. I made this statement at a meeting in Cincinnati this spring, and there were quite a few people that sort of hit me on the head for doing it, but you have confirmed my feeling on the subject.

Mr. Draley: Since there is no further enthusiasm for discussion, let me thank you all for your participation in the meeting, tell you all how glad we have been to have you come and contribute to what has appeared to me a very valuable meeting (I hope you feel that way, too). The Conference on Sodium Technology is adjourned.

Attendees

Ackerman, J. P., Argonne National Laboratory
Ader, M., Argonne National Laboratory
Adler, F. T., University of Illinois
Aiello, P., CNEN-Bologna
Akin, R. J., Argonne National Laboratory
Allen, W. O., Jr., Atomics International
Ammon, R. L., Westinghouse Electric Corp.
Amorosi, A., Argonne National Laboratory
Anderson, C. A., Jr., Westinghouse Advanced Reactors Div.
Andrews, R. C., MSA Research Corp.
Arend, E., Luxatom
Aronstein, R. E., Atomics International
Ash, E. B., Atomics International
Askey, D. F., Battelle Memorial Institute
Avery, R., Argonne National Laboratory
Baker, L., Jr., Argonne National Laboratory
Barton, G. B., Battelle Northwest Laboratory
Baumgartel, R. G., Battelle Northwest Laboratory
Beaufrere, J., Electricité de France
Beckett, E. F., Westinghouse Advanced Reactors Div.
Behnke, W. B., Commonwealth Edison Co.
Benedict, M., Massachusetts Institute of Technology
Bennett, G. A., Argonne National Laboratory
Bennett, L. L., Union Carbide AECOP
Bergstresser, K. S., Los Alamos Scientific Laboratory
Berkey, E., Westinghouse Research Laboratories
Best, G., Los Alamos Scientific Laboratory
Biancheria, A., Westinghouse Advanced Reactors Div.
Biery, J. C., Los Alamos Scientific Laboratory
Bishop, A. A., Westinghouse Advanced Reactors Div.
Bishop, E. C., Westinghouse Electric Corp.
Blomberg, P. E., AB Atomenergi, Sweden
Bloom, G. R., Battelle Northwest Laboratory
Bogers, A. J., Metal Research Institute TNO, The Netherlands
Böhm, H., Karlsruhe
Bohmke, W., C. F. Braun & Co.
Boland, J. F., Argonne National Laboratory
Bolender, H. B., Interatom
Borgstedt, H. U., Karlsruhe
Bornstein, I., Argonne National Laboratory
Boyer, R., Babcock & Wilcox Co.
Brachet, A., Electricité de France
Bradley, H., General Electric Co.
Bray, J. A., UKAEA-Dounreay
Brehm, W. F., Jr., Battelle Northwest Laboratory
Bruzzi, L., CNEN-Bologna
Bunch, D., U. S. Atomic Energy Commission
Burelbach, J. P., Argonne National Laboratory
Burton, S. F., U. S. Atomic Energy Commission
Busch, J. S., Kaiser Engineers
Buschman, N. C., Argonne National Laboratory
Bush, S. H., Battelle Northwest Laboratory and ACRS
Butler, D. K., Argonne National Laboratory
Cafasso, F. A., Argonne National Laboratory
Caldwell, C. S., Nuclear Materials and Equipment Corp.
Callen, R. C., Atomic Power Development Associates
Campise, A. V., Argonne National Laboratory
Caplinger, W. H., United Nuclear Corp.
Carlsmith, R. S., Oak Ridge National Laboratory
Carmichael, B. M., Los Alamos Scientific Laboratory
Carter, J. C., Argonne National Laboratory
Casalini, P., CNEN-Bologna
Casey, D. F., Atomics International
Casey, D. J., U. S. Atomic Energy Commission
Castleman, A. W., Jr., Brookhaven National Laboratory
Cerchione, J. D., Argonne National Laboratory
Cervellati, A., CNEN-Bologna
Chamberlain, H. V., Atomic Power Development Associates
Champeix, L., CEA-CEN Saclay
Charak, I., Argonne National Laboratory
Charles, R. G., Westinghouse Research Laboratories
Chellew, N., Argonne National Laboratory
Cheng, C. F., Argonne National Laboratory
Clayer, M., Groupement Atomique Alsacienne Atlantique
Clifford, J. C., Los Alamos Scientific Laboratory
Cobb, E. C., The Nuclear Power Group Ltd., England
Cohen, K. P., General Electric Co.
Coleman, J. H., Atomic Power Development Associates
Collins, G. D., General Electric Co.
Comelli, O., CNEN-Bologna
Comprelli, F. A., General Electric Co.
Croft, M. W., Babcock & Wilcox Co.
Crothers, C. C., Argonne National Laboratory
Crouthamel, C. E., Argonne National Laboratory
Crowe, W. E., Los Alamos Scientific Laboratory
Cushman, R. A., Argonne National Laboratory
Cybulskis, P., Battelle Memorial Institute
Dalton, G. R., University of Florida
Davies, R., NASA Lewis Research Center
Davis, S. A., Argonne National Laboratory
Dee, R. W. R., Reactor Centrum Nederland
Deegan, G. E., Argonne National Laboratory
DeGrazia, A. R., U. S. Atomic Energy Commission
Denielou, G., CEA-CEN Cadarache

Detman, R., C. F. Braun & Co.
DeVan, J. H., Oak Ridge National Laboratory
Dickerman, C. E., Argonne National Laboratory
Dickinson, R. W., Liquid Metal Engineering Center
Dieckamp, H., Atomics International
Dimmick, G. R., Atomic Energy of Canada Ltd.
Dohm, A. J., Jr., U. S. Atomic Energy Commission
Draley, J. E., Argonne National Laboratory
Driscoll, M., Massachusetts Institute of Technology
Duffield, R. B., Argonne National Laboratory
Dutina, D., General Electric Co.
Eberhart, J. G., Argonne National Laboratory
Eichelberger, R. L., Atomics International
Emma, L., Brookhaven National Laboratory
Englemann, P., Karlsruhe
Epstein, L. F., Argonne National Laboratory
Ernst, R., Siemens AG
Etherington, H., Advisory Committee on Reactor Safeguards, USAEC
Falcinelli, G., CNEN-Bologna
Fauske, H. K., Argonne National Laboratory
Feder, H. M., Argonne National Laboratory
Fedor, P., Babcock & Wilcox Co.
Ferguson, R. L., U. S. Atomic Energy Commission
Fischer, J., AEG Kernenergie Versuchsanlage
Flagg, R. H., Aerojet-General Corp.
Fogagnolo, G., CNEN-Bologna
Foltz, J. R., Argonne National Laboratory
Fontana, M. H., Oak Ridge National Laboratory
Ford, J., Atomic Power Development Associates
Franke, I., Siemens AG
Fromm, L. W., Argonne National Laboratory
Furukawa, K., Japan Atomic Energy Research Institute
Gahn, R. F., NASA Lewis Research Center
Gardiner, D. M., U. S. Atomic Energy Commission
Gast, K. H. J., Karlsruhe
Gast, P. F., Argonne National Laboratory
Genco, J. M., Battelle Memorial Institute
George, J. A., Westinghouse Advanced Reactors Div.
Gibson, A. S., General Electric Co.
Gilbertson, J. C., Combustion Engineering, Inc.
Golan, S., Atomics International
Goldberg, J., Oak Ridge National Laboratory
Golden, G. H., Argonne National Laboratory
Goldmann, K., United Nuclear Corp.
Goodman, L., Atomics International
Goulding, B. J., Babcock & Wilcox Co.
Greenberg, S., Argonne National Laboratory
Griffith, D. G., Australian Atomic Energy Commission
Gunson, W. E., Westinghouse Advanced Reactors Div.
Guthmann, E., Interatom
Habersky, R., Curtiss-Wright Co.
Hall, R. S., Central Electricity Generating Board, England
Hallett, W. J., Argonne National Laboratory
Hannerz, K., ASEA, Sweden
Hannum, W. T., U. S. Atomic Energy Commission
Harbison, S. G., Aerojet-General Corp.
Harde, R., Interatom
Harms, W. O., Oak Ridge National Laboratory
Haroldsen, G. O., Argonne National Laboratory
Harrer, J. M., Argonne National Laboratory
Harrison, L. J., Argonne National Laboratory
Hartnett, J. P., University of Illinois—Chicago Circle, and AUA
Hendrie, J. C., Brookhaven National Laboratory and ACRS
Herbert, J., U. S. Atomic Energy Commission
Hickam, W. M., Westinghouse Research Laboratories
Hill, E. F., Atomic Power Development Associates
Hiltz, R. H., MSA Research Corp.
Hirons, T. J., Los Alamos Scientific Laboratory
Hobdell, M. R., Brookhaven National Laboratory
Hobson, R. G., Westinghouse Advanced Reactors Div.
Hoffman, E. E., General Electric Co.
Holden, R. B., United Nuclear Corp.
Honig, H., Babcock & Wilcox Co.
Hooker, H. H., Argonne National Laboratory
Hoover, J. A., Argonne National Laboratory
Hori, M., Japan Atomic Energy Research Institute, c/o APDA
Horton, K. E., U. S. Atomic Energy Commission
Hostetler, D. R., Babcock & Wilcox Co.
Hub, K. A., Argonne National Laboratory
Hummel, H. H., Argonne National Laboratory
Hummel, V. H., U. S. Atomic Energy Commission
Humphreys, J. R., Jr., Argonne National Laboratory
Hunter, R. A., U. S. Atomic Energy Commission
Hunze, J. O., U. S. Atomic Energy Commission
Hutter, E., Argonne National Laboratory
Impara, R. J., U. S. Atomic Energy Commission
Ireland, R. E., U. S. Atomic Energy Commission
Isaacs, H. S., Brookhaven National Laboratory
Isbin, H. S., University of Minnesota
Iwai, S., Mitsubishi Atomic Power Industries, Inc., Japan
Iwaki, T., Mitsubishi Atomic Power Industries, Inc., Japan
Ivins, R. O., Argonne National Laboratory
Jackson, M. E., U. S. Atomic Energy Commission
Jacobson, N. H., Argonne National Laboratory
Jahns, A., Institut für Reaktorsicherheit der TUV
Jansen, P., Karlsruhe
Jansson, S. A., Westinghouse Research Laboratories
Jaross, R. A., Argonne National Laboratory
Johnson, B. M., Battelle Northwest Laboratory

Johnson, K. P., Power Reactor Development Co.
Johnson, R. E., Argonne National Laboratory
Jones, R. H., U. S. Atomic Energy Commission
Joslin, M., Argonne Universities Association
Judd, A. M., Argonne National Laboratory
Judge, F., Knolls Atomic Power Laboratory
Kaden, W., Siemens AG
Kanamori, A., Tohoku Electric Power Co., Japan, c/o APDA
Kassner, T. F., Argonne National Laboratory
Kato, W. Y., Argonne National Laboratory
Kelber, C. N., Argonne National Laboratory
Kelly, J. C. R., Jr., Westinghouse Advanced Reactors Div.
Kelman, L. R., Argonne National Laboratory
Kendall, W. W., General Electric Co.
Kennedy, L., C. F. Braun & Co.
Keppler, J. G., U. S. Atomic Energy Commission
Kerr, W., University of Michigan and AUA
Kintner, E. E., U. S. Atomic Energy Commission
Kirchenmayer, A., AEG Kernenergie Versuchsanlage
Kirschler, L. H., MSA Research Corp.
Kitamura, H., Kyushu Electric Power Co., Japan, c/o APDA
Klueh, R. L., Oak Ridge National Laboratory
Knight, J., Atomic Power Development Associates
Koch, L. J., Argonne National Laboratory
Kohler, M., Interatom
Kolflat, R., Babcock & Wilcox Co.
Kolodney, M., United Nuclear Corp.
Kopchinski, N. L., Bechtel Corp.
Kovach, P., Babcock & Wilcox Co.
Kovacic, E. C., Atomic Power Development Associates
Kristianson, B., Argonne National Laboratory
Krumpelt, M., CEN-Mol
Kuczen, K. D., Argonne National Laboratory
Kuesters, H., Karlsruhe
Lagowski, J., Atomic Power Development Associates
Lancet, R. T., Atomics International
Larsen, R. P., Argonne National Laboratory
Latzko, D. G. H., University of Delft, The Netherlands
Lawroski, H., Argonne National Laboratory
Lawroski, S., Argonne National Laboratory
Leduc, J., CEA-CEN Saclay
Lee, P. K., Westinghouse Research Laboratories
Leitz, F. J., General Electric Co.
Lemke, C. H., E. I. duPont de Nemours & Co.
Lennox, D. H., Argonne National Laboratory
Leonard, B. H., Bechtel Corp.
Levenson, M., Argonne National Laboratory
Lewis, W., Battelle Northwest Laboratory
Lindhe, J. S., AB Atomenergi, Sweden
Lindsey, P. S., Atomic Power Development Associates
Lions, N., Commissariat a l'Energie Atomique
Litton, F., Los Alamos Scientific Laboratory
Loewenstein, W. B., Argonne National Laboratory
Longyear, A. B., Aerojet-General Corp.
Lorenzen, A. M., C. F. Braun & Co.
Lottes, P. A., Argonne National Laboratory
Luner, C., Argonne National Laboratory
Lutz, D. E., Argonne National Laboratory
McCarthy, J. E., Commonwealth Associates, Inc.
McCarthy, W. J., Detroit Edison Co.
McCown, J. J., Battelle Northwest Laboratory
McGoff, D. J., U. S. Atomic Energy Commission
McKee, J. M., Argonne National Laboratory
McMillan, K. W., Bechtel Corp.
McPheeters, C. C., Los Alamos Scientific Laboratory
McSorley, J. A., Westinghouse Electric Corp.
MacFarlane, D., Argonne National Laboratory
MacPherson, R. E., Oak Ridge National Laboratory
Madell, J. T., Argonne National Laboratory
Maffei, H. P., Battelle Northwest Laboratory
Mani, H. K., Ministry of Economic Affairs, The Hague
Marchaterre, J. F., Argonne National Laboratory
Margen, P. H., AB Atomenergi, Sweden
Marmonier, P., CEA-CEN Cadarache
Marshall, W. R., Jr., University of Wisconsin and AUA
Matte, J., III, Atomic Power Development Associates
Mausbeck, H., Interatom
Meadows, G. E., Los Alamos Scientific Laboratory
Melese, G., Gulf General Atomic
Meneghetti, D., Argonne National Laboratory
Meneley, D., Argonne National Laboratory
Menzel, G., Combustion Engineering, Inc.
Meshii, T., Mitsubishi Heavy Industries, Ltd., Japan, c/o APDA
Meyer, R. J., Argonne National Laboratory
Meyers, J. E., Atomic Power Development Associates
Michel, A., Belgonucléaire
Miki, R., Power Reactor and Nuclear Fuel Development Corp., Japan
Miles, C. C., Argonne National Laboratory
Miller, C. E., Argonne National Laboratory
Millhollen, M. K., Battelle Northwest Laboratory
Minogue, R. B., U. S. Atomic Energy Commission
Minushkin, B., Brookhaven National Laboratory
Mogard, H., AB Atomenergi, Sweden
Monson, H. O., Argonne National Laboratory
Moreau, J. C., Electricité de France
Morelle, J. M., Belgonucléaire
Morgenstern, G., General Electric Co.
Morikawa, S., Japan Gasoline Co., Ltd.
Morris, P. L., Battelle Memorial Institute

Morrison, W. C., Atomic Power Development Associates
Moser, R. M., U. S. Atomic Energy Commission
Moskowitz, S., Curtiss-Wright Co.
Mueller, R. E., Atomic Power Development Associates
Muenchow, H. O., Combustion Engineering, Inc.
Muramatsu, T., Ebara Mfg. Co., Ltd., Japan
Murphy, P. M., General Electric Co.
Nakagawa, H., Tokyo Electric Power Company
Natesan, K., Argonne National Laboratory
Newman, D., Curtiss-Wright Co.
Newman, L., Brookhaven National Laboratory
Nicholson, R. B., Argonne National Laboratory
Nijs, W. W., Reactor Centrum Nederland
Nilson, R., AB Atomenergi, Sweden
Noyes, R. C., Combustion Engineering, Inc.
Nozawa, M., Japan Atomic Energy Research Institute
Oakley, D. J., Battelle Northwest Laboratory
Odajima, K., Chubu Electric Power Co., Japan, c/o APDA
Oestmann, M. J., Argonne National Laboratory
Okrent, D., Argonne National Laboratory
Olson, W. H., Argonne National Laboratory
Ott, K., Purdue University
Parkman, M., Eimac Div., Varian Associates
Pearson, C. V., Argonne National Laboratory
Pearson, E. N., Liquid Metal Engineering Center
Pederson, E., Ralph M. Parsons Co.
Perkins, R. H., Los Alamos Scientific Laboratory
Persiani, P. J., Argonne National Laboratory
Peterson, R. E., Battelle Northwest Laboratory
Pfahler, S. J., Liquid Metal Engineering Center
Pierantoni, F., CNEN-Bologna
Pohl, L. E., General Electric Co.
Pomeroy, D. L., U. S. Atomic Energy Commission
Pouderoux, P., Stein & Roubaix, Paris
Probert, P. B., Babcock & Wilcox Co.
Purcell, J. J., U. S. Atomic Energy Commission
Ramachandran, T. P., Argonne National Laboratory
Razminas, R. B., Nuclear Materials and Equipment Corp.
Redding, A., Westinghouse Advanced Reactors Div.
Redman, W. C., Argonne National Laboratory
Redmond, R. F., Battelle Memorial Institute
Reid, R. K., Aerojet-General Corp.
Reynolds, A. B., University of Virginia
Rib, L. N., U. S. Atomic Energy Commission
Rice, R. E., Argonne National Laboratory
Richter, H., Metallgesellschaft AG
Robinson, L. C., Argonne National Laboratory
Rodgers, S. J., MSA Research Corp.
Rolf, W. F., Commonwealth Edison Co.
Romano, A. J., Brookhaven National Laboratory
Rosenberg, G. S., Argonne National Laboratory
Ross, F. J., E. I. duPont de Nemours & Co.
Rossin, A. D., Argonne National Laboratory
Rothman, A. B., Argonne National Laboratory
Roy, P., General Electric Co.
Royaards, R. v. E., N. V. KEMA, The Netherlands
Ruhle, M., Metallgesellschaft AG
Ruther, W. E., Argonne National Laboratory
Rutkauskas, V. J., Battelle Northwest Laboratory
Sagawa, M., Hitachi Ltd., Japan
Sangster, W. A., General Electric Co.
Sassoli, C., CNEN-Bologna
Scheuermann, C. M., NASA Lewis Research Center
Schubert, A. E., General Electric Co.
Sciacca, F., General Electric Co.
Scott, F. A., Battelle Northwest Laboratory
Scott, P. A., U. S. Atomic Energy Commission
Sesonske, A., Purdue University
Shackelford, M., Argonne National Laboratory
Shannon, D. W., Battelle Northwest Laboratory
Shaw, M., U. S. Atomic Energy Commission
Shearer, E. A, Aerojet-General Corp.
Shepard, R. L., Oak Ridge National Laboratory
Sherer, D. B., General Electric Co.
Shewmon, P. G., Argonne National Laboratory
Shiozuka, H., Nippon Atomic Industry Group Co.
Shively, J. H., Atomics International
Shreve, R. J., MSA Research Corp.
Shumaker, P. B., Atomic Power Development Associates
Siegel, S., Atomics International
Silberberg, M., Atomics International
Simmons, W. R., Argonne National Laboratory
Simons, E. M., Battelle Memorial Institute
Simpson, J. L., General Electric Co.
Smidt, D., Karlsruhe
Smiley, S. H., Nuclear Materials and Equipment Corp.
Smith, C. R., Westinghouse Advanced Reactors Div.
Smith, C. R. F., Battelle Northwest Laboratory
Smith, D. L., Argonne National Laboratory
Smith, F. A., Argonne National Laboratory
Smith, R. R., Argonne National Laboratory
Soenen, M., CEN-Mol
Soppet, C. K., Aerojet-General Corp.
Staker, W. P., Combustion Engineering, Inc.
Stepnewski, D., Battelle Northwest Laboratory
Stern, G., United Nuclear Corp.
Stevens, H. C., Argonne National Laboratory
Sturm, W. J., Argonne National Laboratory
Sutton, C. R., Argonne National Laboratory
Swain, R. K., Aerojet-General Corp.
Takahashi, J., Electric Mfg. Co., Ltd., Japan

Tang, I. N., Brookhaven National Laboratory
Tarantini, A., CNEN-Bologna
Taylor, G. R., Westinghouse Advanced Reactors Div.
Terasawa, S., Hitachi Ltd., Japan
Tessier, J. H., Argonne National Laboratory
Teyssedre, M., Babcock Atlantique, Paris
Thomas, K. C., Westinghouse Electric Co.
Thompson, D. H., Argonne National Laboratory
Till, C. E., Argonne National Laboratory
Toyoda, K. G., Battelle Northwest Laboratory
Trinko, J. R., Jr., Argonne National Laboratory
Ullrich, W., Institut für Reaktorsicherheit der TUV
Ulrich, A. J., Argonne National Laboratory
Valibus, L., Electricité de France
Van Dievoet, J., Belgonucléaire
Van Dorsser, A. H. de H., Central Technical Institute TNO, The Netherlands
Van Gasselt, M. L. G., Central Technical Institute TNO, The Netherlands
Van Kampen, F. A., Neratoom Ltd., The Netherlands
Van Meel, D. A., Central Technical Institute TNO, The Netherlands
Veleckis, E., Argonne National Laboratory
Venard, J. T., Argonne National Laboratory
Vilinskas, P., Argonne National Laboratory
Vissers, D. R., Argonne National Laboratory
Vogel, R. C., Argonne National Laboratory
Waber, J. P., Northwestern University
Wagener, H., Luxatom
Wajima, J. T., Hitachi Ltd., Japan
Walker, D. E., Argonne National Laboratory
Walker, R. A., Argonne National Laboratory
Warschauer, K. A., Central Technical Institute TNO, The Netherlands
Watts, M. J., UKAEA-Risley
Weeks, J. R., Brookhaven National Laboratory
Wensch, G. W., U. S. Atomic Energy Commission
Went, J. J., N. V. KEMA, The Netherlands
Werner, R. C., MSA Research Corp.
Williams, J. M., Los Alamos Scientific Laboratory
Williams, R. L., General Public Utilities, Parsippany, N.J.
Wincierz, P., Metallgesellschaft AG
Winkleblack, R. K., Argonne National Laboratory
Wirtz, K., Karlsruhe
Witt, A., Nuclear Materials and Equipment Corp.
Wolfe, B., General Electric Co.
Wyckoff, H. L., Commonwealth Edison Co.
Wykoff, W. R., Los Alamos Scientific Laboratory
Yaggee, F. L., Argonne National Laboratory
Yannopoulos, L., Westinghouse Electric Corp.
Yashin, D. A., International Atomic Energy Agency
Yiftah, S., Israel AEC
Yoshimi, H., Fuji Electric Co., Ltd., Japan
Young, R. S., General Electric Co.
Zambernard, M., Nuclear Materials and Equipment Corp.
Zebroski, E. L., General Electric Co.
Zegveld, W. C. L., Organization for Industrial Research TNO, The Netherlands
Ziegler, A., Siemens AG
Zinn, W. H., Combustion Engineering, Inc.
Zitek, C. B., Commonwealth Edison Co.
Zuromsky, G., Combustion Engineering, Inc.
Zwetzig, G. B., Atomics International

3 4444 00013316 5